


Active Volcanoes of the World

Ralf Gertisser · Valentin R. Troll ·
Thomas R. Walter ·
I Gusti Made Agung Nandaka ·
Antonius Ratdomopurbo *Editors*

Merapi Volcano

Geology, Eruptive Activity, and Monitoring of a
High-Risk Volcano



 Springer

Active Volcanoes of the World

Series Editors

Corrado Cimarelli, Section for Mineralogy, Petrology and Geochemistry,
Ludwig-Maximilians-University Munich, Department of Earth and
Environmental Sciences, München, Germany

Sebastian Muller, Mineralogisches Museum, Marburg, Hessen, Germany

About 500 active volcanoes presently exist on the Earth's surface, of which around 50 erupt each year. Volcanoes played a crucial role in the evolution of the planet and early life, and are constantly reshaping the morphology of Planet Earth. Many active volcanoes are located in dense settlement areas, with over 500 million people living in close proximity of still active or dormant volcanoes.

On one side, volcanoes provide valuable soil and rock basis for agriculture, but often the "mountains of fire" cause disastrous societal and economical disasters caused by ash clouds, lahars, lava flows, and pyroclastic flows. Eruptions are still difficult to predict, although volcanologists around the world are constantly working on new ways to understand the character and behavior of volcanoes.

Active Volcanoes of the World is an official book series of the International Association of Volcanology and Chemistry of the Earth's Interior (IAVCEI). The series aims to be a scientific library of monographs that provide authoritative and detailed reviews of state-of-the art research on individual volcanoes or a volcanic area that has been active in the last 10.000 years, e.g. the Teide Volcano or the Chiapas Region. The books in the series cover the geology, eruptive history, petrology and geochemistry, volcano monitoring, risk assessment and mitigation, volcano and society, and specific aspects related to the nature of each described volcano.

The Active Volcanoes of the World series contains single and multi-authored books as well as edited volumes. The Series Editors, Dr. Corrado Cimarelli and Dr. Sebastian Müller are currently accepting proposals and a proposal document can be obtained from the Publisher, Dr. Annett Buettner (annett.buettner@springer.com).

Ralf Gertisser • Valentin R. Troll •
Thomas R. Walter •
I Gusti Made Agung Nandaka •
Antonius Ratdomopurbo
Editors

Merapi Volcano

Geology, Eruptive Activity,
and Monitoring of a High-Risk
Volcano

Editors

Ralf Gertisser
School of Geography, Geology
and the Environment
Keele University
Keele, UK

Thomas R. Walter
GFZ German Research Centre
for Geosciences
Potsdam, Germany

Antonius Ratdomopurbo
Geological Agency
Ministry of Energy and Mineral
Resources
Bandung, Indonesia

Valentin R. Troll
Department of Earth Science
University of Uppsala
Uppsala, Sweden

I Gusti Made Agung Nandaka
Geological Agency
Center of Volcanology and Geological
Hazard Mitigation, BPPTKG
Yogyakarta, Indonesia

ISSN 2195-3589

ISSN 2195-7029 (electronic)

Active Volcanoes of the World

ISBN 978-3-031-15039-5

ISBN 978-3-031-15040-1 (eBook)

<https://doi.org/10.1007/978-3-031-15040-1>

© Springer Nature Switzerland AG 2023

This work is subject to copyright. All rights are reserved by the Publisher, whether the whole or part of the material is concerned, specifically the rights of translation, reprinting, reuse of illustrations, recitation, broadcasting, reproduction on microfilms or in any other physical way, and transmission or information storage and retrieval, electronic adaptation, computer software, or by similar or dissimilar methodology now known or hereafter developed.

The use of general descriptive names, registered names, trademarks, service marks, etc. in this publication does not imply, even in the absence of a specific statement, that such names are exempt from the relevant protective laws and regulations and therefore free for general use.

The publisher, the authors, and the editors are safe to assume that the advice and information in this book are believed to be true and accurate at the date of publication. Neither the publisher nor the authors or the editors give a warranty, expressed or implied, with respect to the material contained herein or for any errors or omissions that may have been made. The publisher remains neutral with regard to jurisdictional claims in published maps and institutional affiliations.

This Springer imprint is published by the registered company Springer Nature Switzerland AG
The registered company address is: Gewerbestrasse 11, 6330 Cham, Switzerland

Opening Letter: The Long Shadow of Merapi Volcano

Merapi Volcano—Geology, Eruptive Activity, and Monitoring of a High-Risk Volcano is a collection of 18 chapters that lead the reader through the development of volcano science and hazard mitigation at one of the world's most frequently active and hazardous volcanoes. Below, we provide our perspectives on the chapters in this impressive new book. Afterward, we reflect on how two crisis responses to eruptions at Merapi volcano contributed to the development of the Volcano Disaster Assistance Program (VDAP).

The **Foreword** to this book by Andiani, head of Indonesia's volcano hazards agency, describes how Indonesia's 127 active volcanoes are a "way of life" for the nation's people, posing an omnipresent hazard, but also offering natural resources and beauty. Andiani attributes Indonesia's success in mitigation not just to the nation's major internal investment in volcanology and mitigation, but also to contributions from international scientific and technical partnerships, such as those described in this book.

Gertisser and coauthors comprehensively review Merapi's scientific exploration and discovery in **Chap. 1**. They chronicle the abrupt disappearance of the formerly thriving eight- and ninth-century Mataram kingdom of central Java and the debated question of whether the fall of this kingdom was related to eruptions of Merapi volcano. They lead us through fascinating historical accounts of explorers and naturalists who visited Mount Merapi during the late nineteenth and early twentieth centuries. They also review the pioneering work of geologists and engineers during the Dutch colonial period and the establishment of the first volcanological agency in 1920. Whereas most "Merapi type" eruptions produce lava domes, they also range widely in explosivity. The authors attribute this range to variable gas content in magmas, differences in dynamics of magma ascent, extent of summit failure, and the degree of reaction between magma and limestone. This richly illustrated chapter highlights the hundreds of geological, geophysical, and geochemical studies that have been conducted at Merapi. With more than 350 references, the chapter is required reading for all future students of Merapi volcano.

Lavigne and coauthors explore the social aspects of crises at Merapi volcano in **Chap. 2**. They outline the use of hazard zones, danger maps, and warning levels and explain how these have been used to guide crisis responses and evacuations. A vivid example is the 2010 VEI 4 eruption during which 400,000 people were evacuated or displaced. They review the many costs and impacts of the 2010 eruption, and, expanding on their

previous work, they explain why so many returned to hazard zones. They also review the challenges communities face and how those communities were empowered to cope with crises. An outline of both positive and negative aspects of post-2010 mitigation policies illustrates the need to evaluate social, economic, and political factors over a long time period in order to understand people's vulnerability and their ability to cope with and recover from a disaster.

It is well known that effective communication of hazards and warnings is needed to prevent natural disasters. In **Chap. 3**, Holmberg shows how an understanding of culture, oral traditions, and long-held beliefs are also essential to such communication. At Mount Merapi, ancient Javanese traditions, beliefs, and rituals remain prevalent today and the volcano is personified as Mbah Merapi (an honorific title usually given to a grandparent). Holmberg guides us through the history of cultural beliefs and their intersection with science and technology. Holmberg shows us that at Merapi, as at many other volcanoes, an understanding of cultural beliefs contributes to improved crisis response and aids in the reduction of risk.

In **Chap. 4**, Harijoko and coauthors review the geological and tectonic settings of Merapi volcano, which lies above a trans-crustal magmatic system rooted in the mantle wedge above the subducting Indo-Australian Plate. Merapi is the southernmost of a northwest–southeast trending series of four volcanoes within the Central Java depression, a region that is cut by multiple fault zones. They note that Mount Merapi's eruptive products range from basalt to andesite and that the volcano has erupted at least 73 times in recorded history. The authors review the stratigraphy of central Java and suggest that the Kendang Zone, with its clastic turbidites, carbonates, and volcanoclastic rocks, is the likely basement to the volcano.

Lühr and coauthors (**Chap. 5**) review a variety of geophysical evidence concerning the plumbing system of Merapi volcano, revealing a remarkable three-dimensional image of the volcano and its hydrothermal and magmatic roots. The image synthesizes information from a series of large active and passive seismic experiments, along with gravity, tilt, GPS, electrical resistivity, and ambient noise tomography data, as well as earthquake locations. Surprisingly, Merapi and other active volcanoes in the region are not located above the central part of a broad seismic low-velocity anomaly below central Java; instead, they are situated above the contact between this anomaly and high-velocity forearc deposits to the south.

The comprehensive overview by Gertisser and coauthors (**Chap. 6**) subdivides Merapi volcano's history into Proto-, Old-, and New-Merapi and shows how the structure and stratigraphy of the volcano evolved. The authors also describe the two basaltic andesite types (medium-K and high-K) and their origins from a metasomatized magma source that differentiates and is contaminated during crustal transit.

Bronto and coauthors (**Chap. 7**) describe the history of debris avalanches on Mount Merapi, including the colossal (but heretofore undated) Godean debris avalanche. They discuss the deposits, unresolved aspects of their interpretation, and considerations for future catastrophic collapses and potential impacts on the surrounding communities.

In **Chap. 8**, Troll and Deegan characterize the petrology of Merapi lavas and the suite of inclusions found at the volcano. The latter include quenched basalts, coarse-grained intrusives, megacrysts, and calc-silicates. The authors combine petrographic, trace-element, and isotopic data to infer a story of a polybaric, trans-crustal magma system where crystallization, recharge, mixing, and assimilation occur repeatedly and at many scales.

Preece and coauthors (**Chap. 9**) look carefully at the textural characteristics of phenocrysts and microlites, with a goal of understanding the time-scale of crystallization and the interplay between crystallization and ascent rate. They discuss the implications for eruption mechanisms and explosivity at Merapi volcano.

Deegan and coauthors (**Chap. 10**) summarize evidence for assimilation, metasomatism, and metamorphism of limestones in Merapi magmas and how these processes impact the evolution and abundance of a CO₂-rich gas phase. Clear evidence of limestone assimilation is evident from carbon and other isotopic data, from analysis of calc-silicate xenoliths, and from the volcanic gases emitted from the volcano. The authors conclude that gas production through metamorphism increases the explosivity and consequently the hazards of Merapi's eruptions.

The history and evolution of studies of volcanic gas at Merapi are detailed in the paper by Nadeau and coauthors (**Chap. 11**). They characterize the bulk chemistry, isotopes, gas ratios, and gas flux, as well as volatile metal contents. They demonstrate that studies of gases at Merapi volcano provide critical additional insights into recent eruptions and generally improve understanding of magma ascent and evolution.

Subandriyo and coauthors (**Chap. 12**) cover the momentous VEI 4 eruption of Merapi volcano in 2010, the worst volcanic disaster at the volcano in 80 years. They comprehensively describe monitoring, inferred magma ascent and other volcanic processes, as well as eruption impacts, emergency response activities, and civil protection. The chapter is a broad and all-encompassing review of a seminal eruption.

Budi-Santoso and coauthors (**Chap. 13**) thoroughly document the history and current implementation of the monitoring system at Merapi volcano, which is the most modern and elaborate in Indonesia. The system includes seismic, geodetic, and gas monitoring equipment, as well as numerous cameras. Accordingly, the monitoring system offers wide reaching opportunities for visual and instrumental confirmation of anomalous behavior. Software facilitates data modeling, alarming, and state-of-the-art interpretation of volcanic processes. Open-conduit volcanoes like Merapi may lack or have only subtle precursors useful for early warnings, so innovative new developments are especially desirable here.

In **Chap. 14**, Walter provides a concise review of synthetic aperture radar (SAR) and interferometric SAR (InSAR) methods. Walter explains how Merapi has served as a "laboratory volcano," where these remotely sensed radar data have helped track deformation, estimate rates of lava dome extrusion, map and estimate volumes of pyroclastic deposits, detect eruption plumes, evaluate damage and assess risk. Looking to a future with more frequent observations, free access to data processing and assistance with

interpretation, Walter sees a world in which routine (operational) volcanic monitoring with SAR will become feasible, aiding in risk mitigation and enhanced understanding of volcanic processes.

In **Chap. 15**, Darmawan and coauthors review the use of unoccupied aircraft systems (UAS) at Mount Merapi. They describe how high-resolution imagery and photogrammetric structure-from-motion (SfM) analyses are used to interpret structural, hydrothermal, and magmatic phases of dome growth and explosions in the summit crater. This work highlights the value of UAS in documenting features that are too difficult or dangerous to access by other means.

Charbonnier and coauthors (**Chap. 16**) consider the hazards of pyroclastic density currents (PDCs)—the most deadly phenomena at Mount Merapi. They explain how these and other hazardous phenomena are represented in the maps used to reduce risk. They examine the success and the important uncertainties of both deterministic and probabilistic models of PDCs, with a focus on the challenging problems of simulating coignimbrite ash surges and overbank flowage into the highly populated interfluves between valleys at Mount Merapi. Their analysis includes development of a probabilistic approach, which utilizes a new database for the past 100 years of PDC activity. However, they caution the volcano hazards community about the importance of well-constrained geographic data, validation metrics, statistical approaches, and expert advice in the interpretation of models.

Thouret and coauthors give a comprehensive review of Merapi's lahars in **Chap. 17**. They explain that Mount Merapi is one of the most prolific producers of lahars in Southeast Asia because of its large volume of pyroclastic deposits, high frequency of eruptions, abundant rainfall, and steep and dense network of incising drainages. Although runout distances rarely exceed 20 km, hyperconcentrated flows and floods can extend farther across the volcano's ring plain and into Yogyakarta, together threatening at least 372,000 people. They describe physical characteristics of the lahars and their deposits at Mount Merapi, spatial and temporal distributions and flow regimes, as well as impacts, geophysical signals, and warning systems. The chapter also reviews the first use of FLO-2D computational lahar simulations for Mount Merapi and presents an innovative risk map, which depicts physical as well as socioeconomic factors for lahars and block-and-ash flows.

In **Chap. 18**, Nandaka and coauthors describe how Mount Merapi has served as a laboratory volcano for Indonesia and the world and how it may help to address fundamental scientific questions in volcanology and risk mitigation in the future. In addition to summarizing post-2010 activity and the unusual present growth of two lava domes at the summit, they explore longer term trends and examine what is needed to prepare for future eruptions, some of which could be stronger and longer lasting than that of 2010.

We close with a personal note about Merapi volcano and its role in the growth of the USGS-USAID Volcano Disaster Assistance Program (VDAP). VDAP has a long history of partnering with Indonesia's volcano hazards program (Center for Volcanology and Geologic Hazard Mitigation, CVGHM). In 2006, we responded in partnership with CVGHM to escalating unrest at Merapi volcano. During the event, our use of event trees became established as a routine procedure to implement with partners. We also used

lava extrusion rate as a proxy for conduit pressure. A tenfold increase in extrusion rate as compared to the long-term rate for Merapi suggested a 10 to 15% probability of a more explosive (1930-type) eruption (Newhall and Pallister 2014; Gertisser et al. 2023—Chap.1, this volume). During our response four years later in 2010, we tracked a hundred-fold increase in extrusion rate of the large-volume summit lava using satellite radar imagery (see Pallister et al. 2013 and Walter 2023—Chap.14, this volume). The extremely high extrusion rate (for Merapi volcano), along with increased seismicity and deformation on the night of November 4 and 5, 2010, raised the probability of a much more explosive eruption and resulted in the call for extended evacuations, saving thousands of lives (Surono et. al 2012; Mei et al. 2013; Pallister et al. 2013; Lavigne et al. 2023—Chap.2, this volume). Since then, we have expanded the use of radar satellite data (including InSAR) and now follow more than a hundred volcanoes worldwide using this technology, sharing observations with partners to ensure readiness.

In short, our VDAP responses to Merapi volcano have been instrumental in shaping the priorities and growth of our program and our collaborations with partners. Indeed, as reflected in the thorough and authoritative chapters in this book, Mount Merapi casts a long-shadow and has influenced the trajectory of volcanology all over the world.

John S. Pallister
Emeritus Scientist
USGS Cascades Volcano Observatory and
Past Chief of the USGS-USAID Volcano
Disaster Assistance Program (VDAP)

Jacob B. Lowenstern
Research Geologist
USGS Cascades Volcano Observatory and
Current Director of the USGS-USAID
Volcano Disaster Assistance Program (VDAP)

References

- Mei ETW, Picquout A, Lavigne F, Grancher D, Noer C, Sartohadi J, De Bézilal E (2013) Lessons learned from the 2010 evacuations at Merapi volcano. *J Volcanol Geotherm Res* 261:348–365
- Newhall CG, Pallister JS (2014) Using multiple data sets to populate probabilistic volcanic event trees. In: Shroder JF, Papale P (eds) *Volcanic hazards, risks and disasters. Hazards and disasters series*. Elsevier, Amsterdam, pp 203–232
- Pallister JS, Schneider DJ, Griswold JP, Keeler RH, Burton WC, Noyles C, Newhall CG, Ratdomopurbo A (2013) Merapi 2010 eruption-chronology and extrusion rates monitored with satellite radar and used in eruption forecasting. *J Volcanol Geotherm Res* 261:144–152
- Surono JP, Pallister J, Boichu M, Buongiorno MF, Budisantoso A, Costa F, Andreastuti S, Prata F, Schneider D, Clarisse L, Humaida H, Sumarti S, Bignami C, Griswold J, Carn S, Oppenheimer C, Lavigne F (2012) The 2010 explosive eruption of Java’s Merapi volcano—a ‘100-year’ event. *J Volcanol Geotherm Res* 241–242:121–135

Foreword

Indonesia is a country with many volcanoes. No less than 127 active volcanoes spread across the islands, making volcanoes an indispensable part of daily life for most Indonesians. The volcanoes bring benefits and harm like two sides of a coin. On the one hand, they bring blessings of soil fertility, clean water, geothermal energy, and sand mines, and the beautiful sceneries become tourist attractions. On the other hand, volcanoes can cause disaster by their eruptions. The risk of a volcanic eruption in Indonesia is high. Every year, on average five volcanoes are erupting or are at an alert level above “Normal.” Historical records show that the death toll from volcanic eruptions in Indonesia reached 200,000 people before 1980, while there were 450 deaths after 1980. In addition, after 1980, nearly 750,000 people had to be temporarily evacuated due to volcanic hazards and the high level of volcanic risk makes the existence of volcano monitoring institutions crucially important.

The history of volcano monitoring institutions in Indonesia has gone through three government eras, namely the Dutch colonial period from 1920 to 1942, the Japanese occupation from 1942 to 1945, and the Indonesian independence period after August 1945. The establishment of the *Vulkaan-bewakingsdienst* in 1920 is considered the birth of modern volcanology institutions in Indonesia. Through a long evolution, nowadays, the institution that takes care of volcanoes and geological hazards is *Pusat Vulkanologi dan Mitigasi Bencana Geologi* or, in English, the *Center for Volcanology and Geological Hazard Mitigation* (CVGHM), a unit of the Geological Agency under the Ministry of Energy and Mineral Resources of the Republic of Indonesia. The main task of CVGHM is to look for all possibilities and propose ways to minimize the impact of volcanic eruptions. Since establishing this national institution of volcanology, the mission to reduce the impact of volcanic eruptions has been the essential task and will remain at the core of its activity in the future.

The CVGHM is currently responsible for monitoring volcanoes for the safety of 5 million people living in disaster-prone areas. In addition, CVGHM performs the functions of research, investigation, engineering, and services in volcanology and geological disaster mitigation. In 2020, CVGHM celebrated 100 years of monitoring volcanoes in Indonesia. CVGHM’s headquarter is currently located in Bandung, in the same location of the office that was established in 1929. At present, 241 CVGHM staff are dealing with Indonesia’s volcanoes, including 197 volcano observers distributed over

74 observation posts at 69 volcanoes. This number of employees is 20 times higher than the number of employees of the Volcanological Survey during the early days of Indonesia's independence.

In addition, CVGHM plays an active role in the global world of volcanology and scientific volcanology meetings are held regularly in Indonesia. For instance, in 1995 and 1997, CVGHM organized a special workshop on Merapi volcano in Yogyakarta with the support of the International Association of Volcanology and Chemistry of the Earth's Interior (IAVCEI) and the United Nations Educational, Scientific and Cultural Organization (UNESCO). Then in 2000, CVGHM hosted the IAVCEI General Assembly, which was held in Bali. In 2014, IAVCEI assigned CVGHM to host the 8th Cities on Volcanoes (CoV) meeting in Yogyakarta. The international community has shown great appreciation of CVGHM's long journey of carrying out volcano disaster mitigation tasks, and at the 10th CoV meeting in Naples (Italy) in 2018, IAVCEI awarded CVGHM the "Volcano Surveillance and Crisis Management Award" for its outstanding achievements and contributions to mitigating volcanic hazards and risks in Indonesia.

One of the Indonesian volcanoes that has attracted much attention worldwide is Merapi. This unique volcano is located on the densely populated island of Java, right in the center of traditional Javanese culture. Based on its eruptive history, Merapi shows frequent activity, with sectoral pyroclastic density currents produced by the collapse of the active lava dome at the summit. Eruptions with a Volcanic Explosivity Index (VEI) of 1–2 occur every few years, while eruptions with a VEI of 3–4, which can impact larger areas, occur less frequently at decadal intervals, as was the case in 1872, 1930, and most recently in 2010. The average size of the eruptions of Merapi is therefore usually relatively small. Still, the risk is very high because nearly 185,000 people live in hazard-prone areas within a radius of less than 10 km from the eruption center. Since the sixteenth century, no less than 7000 people have been victims of eruptions and lahars at Merapi. Due to the high risk posed by an eruption, disaster mitigation measures must be taken to reduce the loss of life and property damage as much as possible.

Monitoring of Merapi volcano has been an inseparable part of the Indonesian volcanological institutions. Currently, Merapi is monitored by *Balai Penyelidikan dan Pengembangan Teknologi Kebencanaan Geologi* (BPPTKG) (English: Geological Disaster Technology Research and Development Center), which is the technical implementation unit of CVGHM, through which Merapi has a comprehensive and modern monitoring and early warning system. The Merapi monitoring system comprises five observation posts scattered across the volcano and a central office in Yogyakarta. The network of monitoring stations uses various seismic, deformation, visual, and geochemical methods, with the monitoring data sent by real-time telemetry from the field stations to the BPPTKG office in Yogyakarta for processing and analysis. The Yogyakarta office is equipped with modern laboratories for petrology, gas geochemistry, and volcanic water analyses and represents the heart of the surveillance effort at Merapi.

In the last decade, and especially after the extraordinary 2010 eruption, the monitoring system of Merapi volcano has improved significantly, supported by, for instance, close cooperation with universities and institutions at home and abroad. The latter includes collaborations with institutions and scientists in Japan, France, the USA, Germany, and, more recently, Singapore. The scope of cooperation includes scientific research, technical support, provision of monitoring equipment, methodological training, data analysis, and joint publications.

Data processing methods and techniques have changed dramatically from offline data processing to online analysis and modeling. In 2013, CVGHM installed a real-time modeling system “WebObs” at Merapi in collaboration with the Institut De Recherche Pour le Développement (IRD) France. Through this system, CVGHM can track model changes in real-time, particularly using ground deformation data. In 2014, CVGHM collaborated with Japan under the SATREP project to build a Support System for Decision Making (SSDM). The goal has been to make a multimodal assessment of volcanic hazards based on the volcanic products of a Merapi eruption. The output of this system is an eruptive hazard scenario map based on monitoring data input, particularly seismic energy data. In the same year, CVGHM, in collaboration with the Earth Observatory of Singapore (EOS), installed the “WOVOdat” system, a comprehensive volcano monitoring database for understanding eruption processes and forecasting, based on historical and monitoring data. At the same time, BPPTKG has built its own integrated collaborative work management system called “Cendana15.” The system, installed in 2019, includes, among others, a database, data visualization, graphical displays and network monitoring.

Researchers from various countries have conducted many studies on Merapi using different disciplines with diverse methodologies. New models have been tested analytically, numerically, and experimentally and subsequently compared with the occurring phenomena. Rich datasets allow better validation between models and empirical reality, which are leading to a steady stream of articles and scientific publications on Merapi. Similarly, many graduate students have completed their academic theses based on Merapi volcanism. An excellent special issue on Merapi was published in volume 100 of the *Journal of Volcanology and Geothermal Research* (JVGR) in 2000. This edition serves as a benchmark for Merapi, particularly for a very comprehensive synthesis of its geology and eruptive history. A special edition about the 2010 Merapi eruption was published in JVGR (Vol. 261) in 2013.

This new Springer book is a precious and up-to-date addition to previously published books and special journal issues about Merapi. The scope and scientific discussions are comprehensive, and it provides a new perspective on Merapi volcano from many different angles. We acknowledge the authors both from Indonesia and abroad who have contributed excellent articles to this book. My deep appreciation goes to the editors, authors, and reviewers who worked extra hard to complete this book amid the challenging

times of a global pandemic. This book will undoubtedly be a valuable reference for a better understanding of Merapi today and will pave the way for many further investigations in the future.

Andiani
Head of Center for Volcanology
and Geological Hazard Mitigation
Geological Agency
Ministry of Energy and Mineral Resources
Bandung, Republic of Indonesia

Acknowledgements

This book is the result of a long journey that started when we first discussed the idea for a Springer Merapi book with many colleagues at the 8th IAVCEI Cities on Volcanoes conference in Yogyakarta and with Springer editors in 2014. Now, the journey has been concluded and we can look back at the often windy and in places steep road, and we are delighted to hold a printed collection of chapters in our hands, summarizing the impressive pieces of research and development made at Merapi in the past decades. We are immensely grateful for all the help we received on this journey, and we are proud of this accomplishment.

Our gratitude is manifold, and first and foremost, we acknowledge the invaluable support toward this book from the Ministry of Energy and Mineral Resources of the Republic of Indonesia represented by the Center for Volcanology and Geological Hazard Mitigation (CVGHM) under the Geological Agency. In particular, we appreciate the support of Bapak Rudy Suhendar, the former Head of Geological Agency of Indonesia, and Bapak Eko Budi Lelono, the current Head of the Geological Agency of Indonesia. Furthermore, we gratefully acknowledge Bapak Kasbani, the former Head of CVGHM, for endorsing and supporting this book project from the beginning, and to Ibu Andiani, the current Head of CVGHM, who also provides the foreword to the book. We are full of gratitude toward our colleagues of the Balai Penyelidikan dan Pengembangan Teknologi Kebencanaan Geologi (BPPTKG) in Yogyakarta (informally also known as the Merapi Volcano Observatory), offering scientific, technical, and human support whenever feasible, and without whom this book would not have been possible. We, the editors, and many of the contributing authors, enjoyed year- to decade-long friendships and collaborations at BPPTKG through international, multidisciplinary projects such as MERAPI, MERAMEX, SUNDAARC, MIAVITA, SEDIMER, and DOMERAPI, and we hope this book will further cement the excellent collaborations with, and outstanding efforts of the BPPTKG and its associates.

Another very important address for us is the Gadjah Mada University (Universitas Gadjah Mada; UGM) in Yogyakarta, offering open scientific discussions, involving and proposing talented students to work on the volcano, and sharing information on many aspects of volcano and earthquake research. Shortly after initiating this book our career-long research, partner, Bapak Kirbani Sri Brotospito, sadly passed away. We will keep him in our most honourable memory.

We mention with gratitude that many of these larger collaborative projects were funded by international organizations and companies, such as the Deutsche Forschungsgemeinschaft (German Research Foundation), BMBF (Bundesministerium für Bildung und Forschung), the French National Research Agency (ANR), the European Research Council (ERC), and AXA, a leading multinational insurance firm. Numerous funding bodies have supported individual researchers that have contributed to this book, including the Natural Environment Research Council (UK), the Mineralogical Society of Great Britain and Ireland, and the Research Councils of the USA (NSF), Sweden (VR), New Zealand (NZCER), and many others that would be too many to mention here.

Our particular thanks go to all contributing authors who worked hard to complete this monumental publication in part amid the challenges of a global pandemic and the ongoing volcanic activity at Merapi and several other volcanoes in Indonesia and worldwide since this project commenced. We are grateful to John Pallister and Jake Lowenstern (United States Geological Survey) for providing the opening letter to this book, and to Jim Vallance, Tina Neal, and a USGS editor for their formal review of the letter. In addition, we thank all our colleagues who generously gave their time to provide us and the authors with thoughtful expert reviews of the individual book chapters. These include Alessandro Aiuppa, Nicolas Arndt, Andreas Auer, Amelia Bain, Lucia Capra, Sylvain Charbonnier, Amy Donovan, Richard Herd, Silvana Hidalgo, Philippe Jousset, Karim Kelfoun, Ben Kennedy, Franck Lavigne, Vern Manville, Chris Newhall, Ian Smith, Helen Smyth, Tod Waight, and Sri Widiyantoro.

A number of individuals are thanked for in depth and insightful discussions, which we found a true enrichment and a major contribution to our understanding of Merapi and particularly inspired our thinking of the geology, petrology, gas chemistry, geophysics, and monitoring of the volcano. These include, among many others, Anastasia Borisova, Shane Cronin, Alain Gourgaud, Claire Harnett, Michael Heap, Phillipe Jousset, Jean-Christophe Komorowski, Alexandra Kushnir, Gert Lube, Caroline Martel, John Pallister, Lothar Schwarzkopf, Ian Smith, Barry Voight, and Diana Wagner.

Institutional support for the editors is greatly acknowledged, in particular from Keele University (RG), Uppsala University and UNPAD (VRT), GFZ and the University of Potsdam (TRW), BPPTKG (IGMAN), and the Center for Geological Survey, Geological Agency of Indonesia (AR).

Last but not least, we wish to gratefully acknowledge the Springer publishing company, in particular Annett Buettner, Johanna Schwarz, and the series editors Corrado Cimarelli and Sebastian Müller for their invaluable support and patience during the long preparation phase and completion of this book. Their help and encouragement has been a great source of help and inspiration.

Terima Kasih!

Ralf Gertisser
Valentin R. Troll
Thomas R. Walter
I Gusti Made Agung Nandaka
Antonius Ratdomopurbo

Contents

| | | |
|----------|--|------------|
| 1 | The Scientific Discovery of Merapi: From Ancient Javanese Sources to the 21st Century | 1 |
| | Ralf Gertisser, Valentin R. Troll, and I Gusti Made Agung Nandaka | |
| 2 | Physical Environment and Human Context at Merapi Volcano: A Complex Balance Between Accessing Livelihoods and Coping with Volcanic Hazards | 45 |
| | Franck Lavigne, Estuning Tyas Wulan Mei, Julie Morin, Hanik Humaida, Annabelle Moatty, Edouard de Bézizal, Danang Sri Hadmoko, Delphine Grancher, and Adrien Picquout | |
| 3 | Merapi and Its Dynamic ‘Disaster Culture’ | 67 |
| | Karen Holmberg | |
| 4 | The Geodynamic Setting and Geological Context of Merapi Volcano in Central Java, Indonesia | 89 |
| | Agung Harijoko, Gayatri Indah Marliyani, Haryo Edi Wibowo, Yan Restu Freski, and Esti Handini | |
| 5 | Crustal Structure and Ascent of Fluids and Melts Beneath Merapi: Insights From Geophysical Investigations | 111 |
| | Birger G. Lühr, Ivan Koulakov, and Wiwit Suryanto | |
| 6 | Geological History, Chronology and Magmatic Evolution of Merapi | 137 |
| | Ralf Gertisser, Mary-Ann del Marmol, Christopher Newhall, Katie Preece, Sylvain Charbonnier, Supriyati Andreastuti, Heather Handley, and Jörg Keller | |
| 7 | The Godean Debris Avalanche Deposit From a Sector Collapse of Merapi Volcano | 195 |
| | Sutikno Bronto, Wartono Rahardjo, Pudjo Asmoro, Antonius Ratdomopurbo, Malia Adityarani, and Afrinia Permatasari | |
| 8 | The Magma Plumbing System of Merapi: The Petrological Perspective | 233 |
| | Valentin R. Troll and Frances M. Deegan | |

| | | |
|-----------|---|-----|
| 9 | A Textural Perspective on the Magmatic System and Eruptive Behaviour of Merapi Volcano | 265 |
| | Katie Preece, Froukje van der Zwan, Julia Hammer, and Ralf Gertisser | |
| 10 | Magma-Carbonate Interaction at Merapi Volcano, Indonesia | 291 |
| | Frances M. Deegan, Valentin R. Troll, Ralf Gertisser, and Carmela Freda | |
| 11 | Merapi Volcano: From Volcanic Gases to Magma Degassing | 323 |
| | Olivier Nadeau, Hanik Humaida, and Patrick Allard | |
| 12 | An Overview of the Large-Magnitude (VEI 4) Eruption of Merapi in 2010 | 353 |
| | Subandriyo, Ralf Gertisser, Nurnaning Aisyah, Hanik Humaida, Katie Preece, Sylvain Charbonnier, Agus Budi-Santoso, Heather Handley, Sri Sumarti, Dewi Sri Sayudi, I Gusti Made Agung Nandaka, and Haryo Edi Wibowo | |
| 13 | The Merapi Volcano Monitoring System | 409 |
| | Agus Budi-Santoso, François Beauducel, I Gusti Made Agung Nandaka, Hanik Humaida, Fidel Costa, Christina Widiwijayanti, Masato Iguchi, Jean-Philippe Métaixian, Indra Rudianto, Much Rozin, Sulistiyani, Ilham Nurdin, Karim Kelfoun, Svetlana Byrdina, Virginie Pinel, Ali Ahmad Fahmi, Antoine Laurin, Mochammad Husni Rizal, and Nabil Dahamna | |
| 14 | Radar Sensing of Merapi Volcano | 437 |
| | Thomas R. Walter | |
| 15 | Morphology and Instability of the Merapi Lava Dome Monitored by Unoccupied Aircraft Systems | 457 |
| | Herlan Darmawan, Raditya Putra, Agus Budi-Santoso, Hanik Humaida, and Thomas R. Walter | |
| 16 | Assessing the Pyroclastic Density Current Hazards at Merapi: From Field Data to Numerical Simulations and Hazard Maps | 473 |
| | Sylvain J. Charbonnier, Karim Kelfoun, Christina Widiwijayanti, Dewi Sri Sayudi, and Raditya Putra | |
| 17 | Merapi's Lahars: Characteristics, Behaviour, Monitoring, Impact, Hazard Modelling and Risk Assessment | 501 |
| | Jean-Claude Thouret, Nurnaning Aisyah, Susanna F. Jenkins, Edouard de Bélizal, Sulistiyani, Sylvain J. Charbonnier, Dewi Sri Sayudi, I Gusti Made Agung Nandaka, Guérolé Mainsant, and Akhmad Solikhin | |

| | |
|--|------------|
| 18 Merapi: Evolving Knowledge and Future Challenges | 553 |
| I Gusti Made Agung Nandaka, Ralf Gertisser, Thomas R. Walter, Valentin R. Troll, and Antonius Ratdomopurbo | |



The Scientific Discovery of Merapi: From Ancient Javanese Sources to the 21st Century

1

Ralf Gertisser, Valentin R. Troll,
and I Gusti Made Agung Nandaka

Abstract

Merapi is Indonesia's most active volcano and one of the most iconic volcanoes worldwide. Renowned for its almost continuous eruptive activity and its magnificent summit dome as well as the frequent occurrence of hazardous nuées ardentes (pyroclastic density currents; PDCs) produced by lava dome failure, Merapi has influenced the life of the Javanese people and local cultures since ancient times and attracted explorers and researchers from around the globe since the scientific enlightenment in the eighteenth century. This reverence and its

prominent role in volcano research, which continued throughout the Dutch occupation and up to the present time, have made Merapi the most intensely studied and best monitored volcano in Indonesia, and one of the best studied volcanoes in the world. Merapi has therefore played a crucial role in advancing not only the scientific understanding of the volcano itself but has also brought forward the discipline of volcanology with respect to understanding of dome-forming eruptions at andesite volcanoes and PDCs as well as regarding assessment and mitigation of associated hazards. This chapter summarises the journey of scientific discovery and volcano monitoring at Merapi, from ancient sources to modern day research efforts, and aims to highlight the major episodic advances in our knowledge and understanding of Indonesia's famous 'Mountain of Fire'.

R. Gertisser (✉)

School of Geography, Geology and the
Environment, Keele University, Keele, UK
e-mail: r.gertisser@keele.ac.uk

V. R. Troll

Department of Earth Sciences, Section for Natural
Resources and Sustainable Development, Uppsala
University, Uppsala, Sweden

Centre of Natural Hazards and Disaster Science,
Uppsala University, Uppsala, Sweden

Istituto Nazionale Di Geofisica E Vulcanologia,
Rome, Italy

Faculty of Geological Engineering, Universitas
Padjadjaran (UNPAD), Bandung, Indonesia

I G. M. A. Nandaka

Balai Penyelidikan Dan Pengembangan Teknologi
Kebencanaan Geologi (BPPTKG), Yogyakarta,
Indonesia

Keywords

Merapi · Research history · Scientific
discovery · Volcano monitoring

1.1 Introduction

Merapi has fascinated and stimulated local residents, explorers and scholars since ancient times. Towering almost 3,000 m above the dominantly agricultural lowlands surrounding Yogyakarta in

Central Java (Figs. 1.1 and 1.2), the volcano is probably best known for the frequent generation of small-volume pyroclastic density currents (PDCs) or block-and-ash flows that are produced when Merapi's viscous lava dome(s) collapse under gravity or due to small explosions. This phenomenon—referred to as 'Merapi-type' *nuées ardentes* (glowing clouds) in the classic volcanological literature (Fig. 1.3)—has made Merapi a household name among researchers and students in volcanology and lifted its status to one of the most iconic volcanoes on Earth. As one of the most frequently erupting and thus one of the most dangerous of Indonesia's active volcanoes, Merapi has influenced cultures and the inhabited surrounding area since ancient times. Testament to the thriving Mataram kingdom, a prosperous Hindu-Buddhist state in Central Java that flourished from the early eighth century, are the world-renowned temples of Borobudur and Prambanan, two among many ancient temples in the vicinity of the volcano. Built in the ninth century, they later fell into disrepair and became almost completely hidden until the eighteenth century beneath volcanic ash, rock, mud and sand from lahars, and vegetation. Stories, myths and legends about Merapi have also been handed down since ancient times and are well documented in early Javanese sources. Following on from these early accounts, naturalists and explorers of the late eighteenth and the nineteenth century, mostly from Europe, were the first to document their observations of the volcano and its eruptions in western accounts, bringing the knowledge about Merapi to an international audience. Since the second half of the nineteenth century, Dutch geologists and mining engineers started to systematically record the geology of the then Netherlands (or Dutch) East Indies, and descriptions of Merapi and its geology and eruptions were published in increasing numbers in the nineteenth and early twentieth century. In September 1920, the Netherlands East Indies administration founded the 'Vulkaanbewakingsdienst' (English: Volcano Surveillance Service) and at Merapi, then and now the most active Indonesian volcano, several

volcano observation posts were built. After Indonesia's independence in 1945, volcano monitoring became a national priority and today, the Center of Volcanology and Geological Hazard Mitigation (CVGHM; Indon.: Pusat Vulkanologi dan Mitigasi Bencana Geologi (PVMBG)) is the official Indonesian government agency responsible for monitoring the active volcanoes across Indonesia and for mitigating geological hazards. During these last seven decades, our understanding of Merapi and its activity has multiplied through the research conducted by CVGHM (including its preceding organisations) in collaboration with Indonesian academic scientists as well as through a series of international research programmes. Notably, a major leap in research was made in the 1990s, when Merapi was designated a 'Decade Volcano' by the International Association of Volcanology and Chemistry of the Earth's Interior (IAVCEI) as part of the United Nations' International Decade for Natural Disaster Reduction. This declaration focused several larger research efforts on Merapi that pushed our understanding forward. Subsequently, major eruptions, as in 2006 and 2010, have also led to a steep increase in both the scientific interest in Merapi and in the number of research outputs. As of 15 April 2021, the Scopus bibliographic database alone listed 718 research articles that have the term 'Merapi' in their title, abstract or as a keyword (Fig. 1.4), making Merapi the most intensively studied volcano in Indonesia. This chapter describes the development of scientific discovery at Merapi, from the myth and legends about the volcano in ancient Javanese sources to the research carried out in the twenty-first century, and provides a synopsis of the history of volcano monitoring at Indonesia's most active volcano. As such, it lays the foundations for the contributions in this book, which outline and review the detailed scientific progress that has been made to date, covering results from both the natural and social sciences and providing state-of-the-art information on geology, geophysics, geochemistry, petrology, volcano monitoring, volcanic hazards, and risk mitigation.



Fig. 1.1 Merapi, one of Indonesia's most active and dangerous volcanoes, towering above the dominantly agricultural lowlands surrounding Yogyakarta in Central Java. **a** Aerial view of Merapi, showing the active volcanic cone and the older Merapi edifice on the right (eastern) side in photo. Merbabu volcano can be seen immediately north of Merapi and Ungaran volcano is visible in the far distance (January 2008). Photo credit: Igan Sutawijaya, CVGHM. **b** View from the south (October 2006). **c** View from the southwest (May 2006). All photographs are from the BPPTKG (Geological Agency of Indonesia) archive

1.2 Merapi in Early Javanese Sources

The earliest mentions of Merapi date back to the time of the ancient Javanese Mataram kingdom, whose wealth was able to support the construction of many Hindu and Buddhist temples around Merapi (Fig. 1.5). Despite a time of immense cultural and political growth in the eighth and ninth century, the region and its temples were abandoned at around AD 1000 when the political power appears to have shifted to eastern Java (e.g. van Hinloopen Labberton 1921). Translation of an old Javanese stone inscription indicates a great flood and a series of related disasters on the island of Java in the year 928 or 929 in the Shaka calendar (i.e., AD 1006), when the whole of Java 'looked like one sea' and many people died. While some authors, such as Kern (as cited in van Hinloopen Labberton 1921), interpreted the stone inscription to relate to armed conflict or war, van Hinloopen Labberton (1921) advocated that a devastating eruption of Merapi turned Central Java into a wasteland, building on an idea first articulated by Ijzerman (1891) and Scheltema (1912). During this alleged massive eruption, the great temples of Borobudur, Mendut and Prambanan were buried under massive eruption and lahar products until their final rediscovery and excavation in the eighteenth century. The alleged eruption of Merapi in AD 1006 has become deeply engraved in the later literature, although the geological evidence for a major eruption at that time remains a matter of speculation (see Gertisser et al. 2023, Chap. 6).

The Pararaton ('Book of Kings'), a Javanese historical chronicle, and the Nagarakṛtāgama, a Javanese epic poem written in AD 1365, mention several eruptions in the fourteenth and fifteenth century, although none of these can be unequivocally ascribed to Merapi. Instead, these eruptions may have occurred at Kelud (Hartmann



Fig. 1.2 Map of the Indonesian archipelago showing active volcanoes (coloured circles) and the location of Merapi in Central Java. The Sunda arc is the part of the

Indonesian subduction zone system that stretches from Sumatra in the west to the Lesser Sunda Islands in the east (after Gertisser et al. 2011)



Fig. 1.3 ‘Merapi-type’ nuée ardente (glowing cloud) produced by gravitational dome collapse at the summit of Merapi on 15 May 2006. The photograph is from the BPPTKG (Geological Agency of Indonesia) archive

1935 a), as we now know that eruptions at Kelud, as most recently seen in 2014, can demonstrably impact the area around Merapi through e.g.,

regional earthquakes and particularly through heavy ashfall that is dispersed by active winds for many hundreds of kilometres.

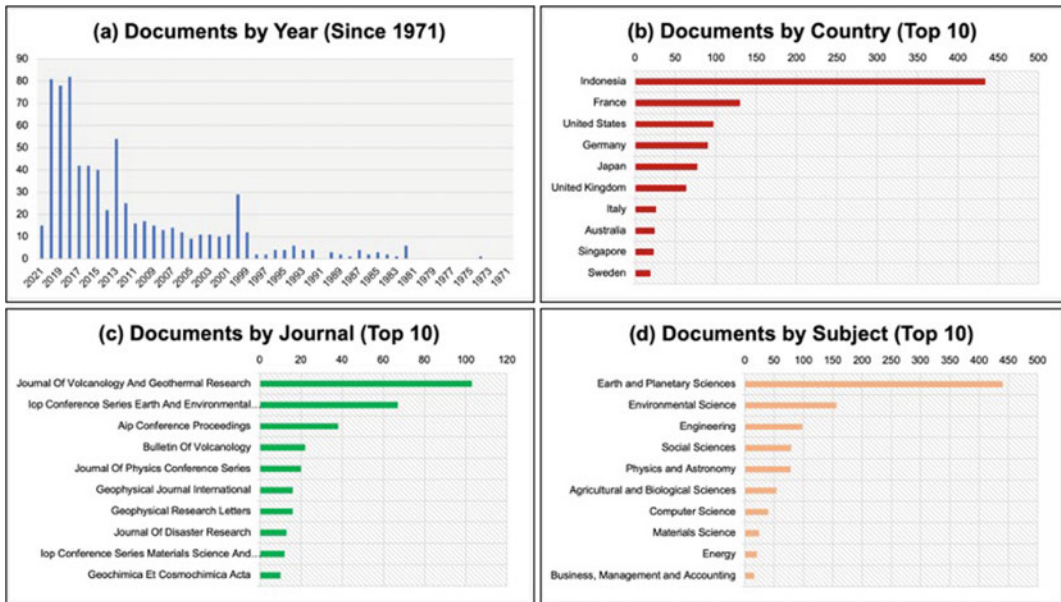


Fig. 1.4 Research outputs in the Scopus bibliographic database having the term ‘Merapi’ in the title, abstract or as a keyword (718 entries). **a** Documents published by year from 1 January 1971 to 15 April 2021, showing the fast-growing body of scientific publications on Merapi since the end of the twentieth century. **b** Documents

ranked by country (lead author affiliation). **c** Documents ranked by academic journal. **d** Documents ranked by subject area, illustrating the multidisciplinary nature of studies at Merapi. In **(b–d)**, only the top 10 entries are shown. The graphs are correct as of 15 April 2021

From the time of the Mataram sultanate, which lasted from the late sixteenth century to the beginning of the eighteenth century when the Dutch came to power in Indonesia, several historical documents exist that describe eruptions of Merapi. Among these is a document in the archive of the Kraton in Yogyakarta that indicates an eruption of Merapi in 1548. Other sources, including old Javanese chronicles, report on further eruptions in the sixteenth as well as in the seventeenth and eighteenth century (see Crawford 1820; Wichmann 1918; Neumann van Padang 1983). These descriptions are extremely helpful to establish the semi continuous activity at Merapi, although they differ in the detail recorded, making it difficult to derive a rigorous timeline or comparative framework of eruptive intensity for this specific period.

1.3 The Naturalists of the 18th and 19th Century

Javanese people were undoubtedly the first to climb Merapi, and local residents frequently travelled along old trade routes between the south and north side of the mountain via the Pasarbubar plain since ancient times. The first documented climb to the summit of Merapi by a European naturalist and explorer, in turn, was that of François van Boekhold in July 1786 (van Boekhold 1792). He arrived at Selo on the north side of Merapi at noon on 17 July 1786 and climbed the mountain in the evening of the same day or in the early hours of 18 July 1786. Following his descent from the mountain in the evening of 18 July, he travelled back to Salatiga



Fig. 1.5 Ancient Buddhist and Hindu temples (in-don. = candi) in the vicinity of Merapi volcano were constructed during the flourishing early Mataram culture (eighth–tenth century) in Central Java. Selected major temples are shown: **a** Borobudur. **b** Prambanan.

c Sambisari. **d** Plaosan. **e** Sari. **f** Kalasan. **g** Lumbung. Borobudur and Prambanan are UNESCO World Heritage Sites and count among the largest temple complexes of their kind in Southeast Asia. The photograph in **b** is from the BPPTKG (Geological Agency of Indonesia) archive

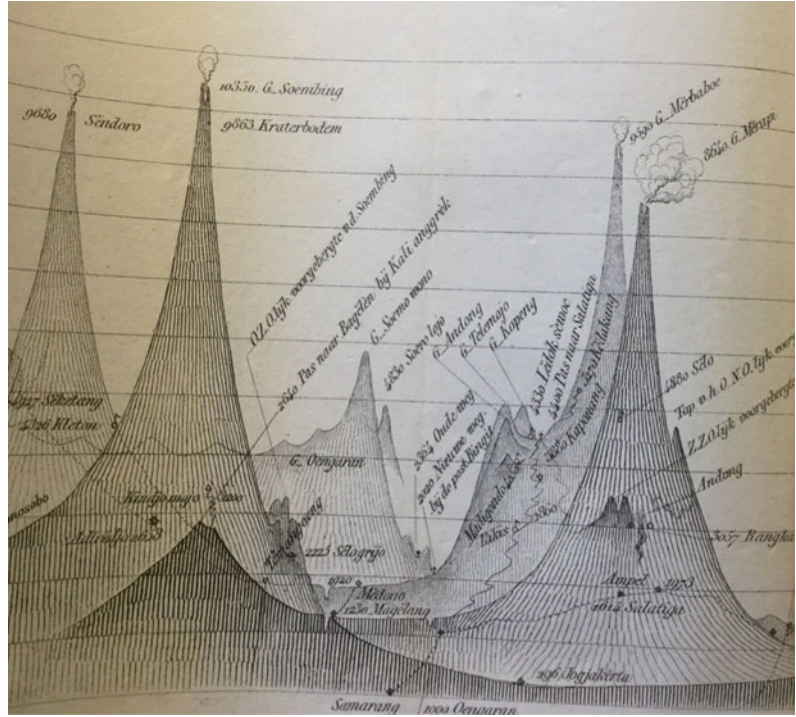
the following day. In van Boekhold's (1792) account, Merapi is described as the burning mountain ('Brandende Berg'), whose summit consisted of the Parabubar crater and an eccentric young lava dome, with abundant yellow, white and brown areas of burning sulphur and ongoing volcanic degassing of variable intensity. In his records we find that he was clearly captured by his experience, and he climbed Merapi again a few weeks later, on 10 August 1786.

The American naturalist Thomas Horsfield (1773–1859) studied the flora, fauna and entomology of Java but got also interested in geology, when he witnessed an eruption of Guntur volcano. He first travelled to Java in 1800 and returned the following year in October 1801 to settle for over a decade on the island. He subsequently published a number of essays on the geography, mineralogy, geology and botany of Java (e.g. Horsfield 1816a, b) as well as a mineralogical sketch of the island of Java (Horsfield 1812). As a doctor of the colonial army, he travelled frequently across Java, climbed many of its volcanoes and collected volcanic rock samples. His journeys brought him to Salatiga, Ampel and Boyolali, from where he explored and partly climbed Gunung Merbabu, located immediately north of Merapi, which was covered with abundant vegetation. He eventually climbed Merapi in 1805, two years after an alleged eruption in 1803 that was so violent that a sizeable part of its summit had collapsed. He found a large extinct crater thought to have been produced in 1803. In 1810, he climbed Merapi again (from Selo), making detailed observations of its summit crater (see Bastin 2019). Shortly after, William Thorn, a British army major, climbed the volcano in 1812/13 (Thorn 1815). Horsfield's studies and Thorn's expeditions were supported by Sir Thomas Stamford Raffles (1781–1826), Lieutenant-Governor of the Netherlands East Indies during the British Interregnum (1811–1815) and one of the first who expressed a scientific interest in Java and its history. In 1817, Raffles published 'The History of Java', in which he portrayed the island's history, geography, flora and fauna (Raffles 1817a, b). The two volumes are accompanied by a topographic map

(Raffles 1817b) that shows Java in unprecedented detail and contains several insets, including Horsfield's mineralogical sketch of the island published in 1812. Raffles (1817a) briefly mentions a "great" eruption of Merapi during which the mountain emitted "a sound louder than thunder, and flame which enlightened all Kérta Súra [Surakarta]". This was shortly followed by a second, "more violent eruption than the first [that] instantly rent the mountain asunder". The outbursts seemingly fell within the reign of Susúnan Mangkúrat Mas, who, according to Raffles (1817a), ruled the Mataram state from AD 1701 to AD 1704. However, as these eruptions are not reported elsewhere, they must be regarded as doubtful.

Further ascents to Merapi and vivid descriptions of its eruptions in 1560, 1664, 1678, 1768, 1822, 1832, 1837, 1846–47 and 1849—partly from hearsay and partly from personal observations—were documented by Friedrich Franz Wilhelm Junghuhn (1809–1864) in his monumental work published in Dutch 'Java: deszelfs gedaante, bekleeding en inwendige structuur' (Junghuhn 1850–1853), which was later expanded upon (Junghuhn 1853–1854) and translated into German (Junghuhn 1857). Junghuhn, a German botanist, was dispatched to the then Netherlands East Indies as a medical doctor and arrived in Batavia (now Jakarta) in October 1835. As a member of the Dutch 'Natuurkundige Commissie' (Commission of Natural History), founded in Leiden in 1820, he undertook many expeditions across Java and climbed 43 of the island's volcanoes. He documented his journeys in several books, maps and lithographs of his scientific work (Figs. 1.6, 1.7 and 1.8), including descriptions and maps of the then known active volcanoes of Java (e.g. Junghuhn 1845, 1850–1853, 1853–1854, 1855, 1856, 1857), making him "indubitably the greatest explorer ever of Java, for which he was deservedly given the epithet 'the Humboldt of Java'" (Bosma 2016). Although not a geologist by training, Java's volcanoes triggered a lifelong fascination for volcanology and a desire to draw a map of the island. By documenting the Tertiary limestones around Yogyakarta (Junghuhn 1850–1853,

Fig. 1.6 Vertically exaggerated sketch by Junghuhn of the Central Javanese volcanoes from Sindoro (Sundoro) on the left to Merapi on the right (Junghuhn 1853–1854)



1853–1854) (Fig. 1.8f), he added to Horsfield’s observations of the occurrence of limestone mostly in the southern part of Java (see Horsfield 1812), which, as we know now, has potentially important implications for the volcanic behaviour of Merapi (see Deegan et al. 2023, Chap. 10). Junghuhn died near Lembang on the slopes of the volcano Tangkuban Parahu north of Bandung in 1864, where a monument remembers him to this day.

Junghuhn visited Merapi for the first time in September 1836, approaching the mountain from the south from Yogyakarta, and again from 4 to 6 November 1836, when he proceeded from Selo on the north side. It was the first Javanese volcano he climbed and left a lasting impression on him (Fig. 1.8). In April 1837, a few months before the eruption of 10 August 1837, he spent eight days on the south side of the mountain. From 5 to 8 June 1838, he climbed the mountain again, this time in company of Dr Ernst Albert Fritze, chief medical officer in the East Indies and a botanist and volcano expert himself. He approached the volcano from Magelang via

Muntilan and Selo, describing the effects of the previous eruption on the crater area and its vegetation, particularly on the eastern crater wall, and in the Gandul river valley (Kali Gandul). Junghuhn (1850–1853, 1853–1854) neither mentions Horsfield’s climb to the summit of Merapi, nor those of William Thorn in 1812/13 and Arriens in 1839 (see Hartmann 1935a), but he reports on visits to the mountain by Pieter Mercus and Nahuys in September 1820, who provided a crude description of its topography and crater before the eruptions of 27–31 December 1822 and 25 December 1832. Based on accounts by others, including Raffles (1817a, b) and Crawford (1820), who also cited local chronicles, Junghuhn (1850–1853, 1853–1854) reported that the earlier of these two eruptions caused widespread ash fall and glowing clouds that destroyed eight villages on the western side of Merapi with only few survivors. Lahars and muddy stream floods (Indon. = banjir) occurred shortly after the eruption in January 1823 and continued at least until April 1823. Particularly large lahars occurred in the western and



Fig. 1.7 Junghuhn's map of the island of Java (Junghuhn 1855)

southwestern sectors of Merapi, where they occasionally overflowed valley margins and inundated villages, causing further casualties. Similar phenomena and effects were described from the 1832 eruption, which also caused inhabitants to abandon their villages, and loss of lives, particularly on the western side again (Junghuhn 1850–1853, 1853–1854).

In 1844–45, Junghuhn spent two months (December and January) in Selo, from where he examined the northern slopes of Merapi and carried out some temperature measurements below the surface, although not at the summit. In his later accounts, Junghuhn reported very minor changes in the summit area of Merapi caused by the eruption on 10 August 1837, despite the explosive nature of the eruption, producing a high, dark ash column visible above the volcano for a whole day that caused ash fall in the Magelang Regency, and PDCs that filled up, and temporarily blocked the drainage in the Blongkeng valley. He further described that the lava dome at the summit of Merapi continued to glow and produced rock falls until May 1838. By contrast, major changes were attributed to the large eruption of 1822 and the smaller event in 1832 described above, with destruction of vegetation all around the cone. Such effects, to a lesser degree, were also noted for the 1837/38 events.

Several years later, Junghuhn's (1850–1853, 1853–1854) account of an eruption that started on 2 September 1846 attests to a relatively long duration and intermittent explosive nature, with ash covering the entire mountain and PDCs mainly towards the Gendol and Woro river valleys in the south-southeast. The eruption ceased only in October 1847, with another significant explosion on 25 September 1847. Merapi's next eruption was short-lived but also explosive, occurring from 14 to 16 September 1849, and Junghuhn describes building destruction and considerable crop damage related to ash fall (Junghuhn 1850–1853, 1853–1854). Apart from these eruptions, Junghuhn (1850–1853, 1853–1854) also made remarks about earlier eruptions of Merapi and their effects in 1664, 1678 (19 August) and 1768 (17 July), based on accounts by others (e.g. Raffles 1817a, b; Crawford 1820).

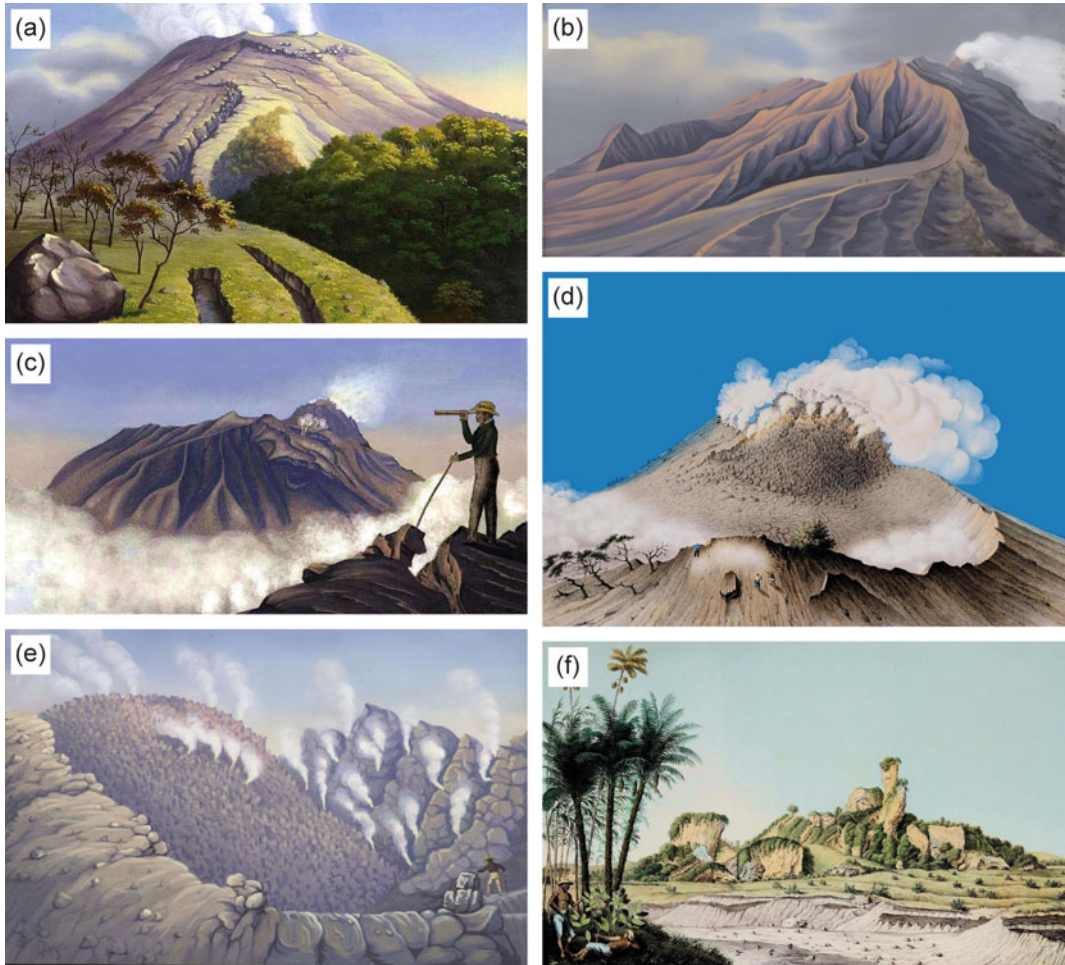


Fig. 1.8 Lithographs of Merapi and its surroundings after original drawings by Franz Wilhelm Junghuhn. **a** Merapi as seen from the south. **b** Merapi as seen from the north. **c** Merapi as seen from the upper slope of

Merbabu volcano. **d** The summit of Merapi. **e** The Merapi dome and inner crater wall. **f** Eocene limestone hills of Gunung Gamping near Yogyakarta. All files are reproduced from Junghuhn (1845, 1853–1854, 1856)

A great eruption in 1560, which threw out large quantities of ash and rock and caused lahars in low-lying areas, was attributed by Junghuhn (1850–1853, 1853–1854) to Merbabu volcano, although from today’s perspective, Merapi may have been a more likely source, as Merbabau has shown no signs of recent or historical eruptive activity.

A description of the contributions to Merapi by the early naturalists and explorers would be incomplete without mention of Raden Saleh (1811–1880), a pioneering Javanese painter and amateur naturalist from a noble family in

Semarang, who spent some 20 years in Europe. Saleh’s legacy includes two paintings of Merapi that show, one by day and one by night, the larger eruption of 1865 (Fig. 1.9). According to Kemmerling (as cited in Escher 1933a), the pictures depict a view of the volcano from the south from Gunung Plawangan. They record incandescent avalanches and glowing clouds covering the entire cone, although they may not have occurred simultaneously (Escher 1933a). This makes Raden Saleh one of the first to record what we term today ‘pyroclastic flows’ or ‘pyroclastic density currents’, which European

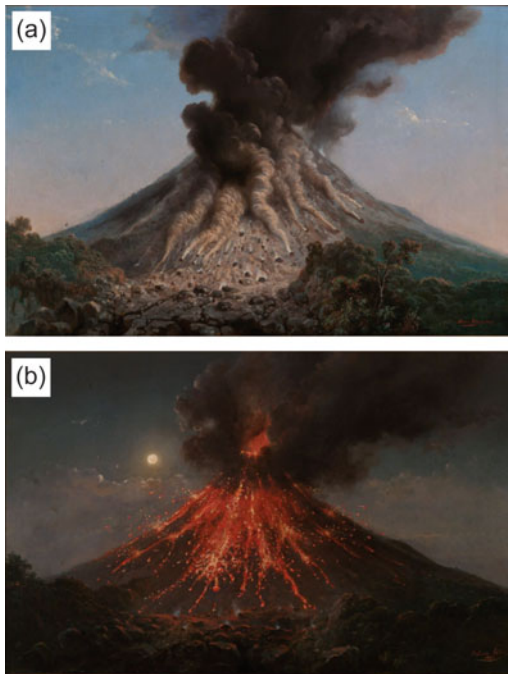


Fig. 1.9 Colour paintings of the eruption of Merapi in 1865 during the day (a) and at nighttime (b) by Raden Saleh. The original paintings are on display at the National Museum of Natural History (Naturalis Museum) in Leiden, The Netherlands

scientists only came to fully appreciate after the 1902 disaster at Mt. Pelée on Martinique through the work of Lacroix (e.g. Lacroix 1904, 1930).

1.4 Observations of Merapi and Its Eruptions in the Late 19th and Early 20th Century

In 1850, the first Dutch mining engineers set foot in Java and the ‘Dienst van het Mijnwezen’ was founded. Since then, increasing numbers of Dutch mining engineers and geologists started to study the geology of the region and created geological maps in the search for the possibly rich mineral resources of the then Netherlands East Indies. Of particular interest in the context of Merapi is the work of Rogier Verbeek, a mining engineer in the Netherlands East Indies from 1868 to the early twentieth century. To this day, Verbeek, one of the pioneers of regional

geological investigations in Indonesia, is perhaps best known for his seminal work on the 1883 eruption of Krakatau (Verbeek 1885), although his monograph ‘Geologische beschrijving van Java en Madoera’, published jointly with Reinder Fennema, was a milestone of Indonesian geology (Verbeek and Fennema 1896). This latter work provides a description of 32 Indonesian/Javanese volcanoes and contains both a geological map and cross-sections of the island, alongside descriptions, maps and cross-sections of the crater of Merapi in 1883 and 1885, and detailed accounts of its pyroxene andesite lava. In addition, Fennema and Verbeek climbed Merapi in 1880 and 1883, respectively, and left a record of their campaigns. Others who visited Merapi and documented their observations around this time were Wilson (1861), Arriens (1864), Hoogeveen (1865), van Dijk (1865), Blij (1871, 1873), Augustijns (1883), Rosenmeijer (1883), Cotteau (1884) and Stoop (1884) (see summary in Hartmann 1935a), adding greatly to an exponentially growing base of knowledge about the volcano and its summit activity in that period.

Increasingly more systematic volcanological investigations and descriptions of Merapi and its eruptions in the nineteenth and early twentieth century (Fig. 1.10) were mainly undertaken by Dutch and German geologists and frequently published in Dutch magazines. Since 1850, regular updates on the volcanoes, volcanic phenomena and volcanic activity in the Netherlands Indies archipelago were published in the ‘Naturkundig Tijdschrift voor Nederlandsch Indië’, and, since 1921, in the journal’s ‘Vulkanologische Berichten’. More detailed descriptions of volcanic investigations and eruptions were also given in several volumes of the ‘Vulkanologische en Seismologische Mededeelingen’ (1921–1940), a journal published by the ‘Dienst van het Mijnwezen’, which changed its name to ‘Dienst van den Mijnbouw’ in 1922. Since 1927, information on volcanic activity was recorded in the ‘Bulletin of the Netherlands East Indian Vulcanological Survey’ and later also in the ‘Bulletin of the Netherlands Indies Vulcanological Survey’ (1934–1941), with C.E. Stehn as chief editor. Many articles can also be found in journals,

including ‘De Ingenieur’, ‘De Mijningenieur’, ‘De Ingenieur in Nederlandsch-Indië’, ‘Leidsche Geologische Mededeelingen’ and ‘De Tropische Natuur’ as well as in reports of the Netherlands East Indies ‘Dienst van den Mijnbouw’ (see Neumann van Padang 1983 for further details). Among the most noteworthy contributions, which in some cases include personal observations of nineteenth and twentieth century eruptions and eruptive phenomena, are those of Brouwer (1928a, b), Escher (1931, 1933a, b), Grandjean (1931a, b, c), Hartmann (1933; 1934a, b; 1935a, b; 1936), Kemmerling (1921, 1930, 1932), Neumann van Padang (1931a, b, c, 1932, 1933), Petroschevsky (1943), Reck (1931, 1935), Stehn (1929, 1935a, b, 1939), Taverne (1925, 1933), van Bemmelen (1942, 1943), van Hinloopen Labberton (1921) and Wurth (1914). Several of these publications contain details of older, pre-nineteenth century eruptions (e.g. Hartmann 1935a), often compiled with reference not only to the accounts of the early naturalists such as Junguhn, but also to information in ancient Javanese sources, some of which was compiled and written down by authors such as Crawford (1820) and Wichmann (1918). A few of them also mention aspects of the eruptive history and structure of the volcanic edifice as well as the petrography of the eruptive products, but usually in passing only. A noteworthy pioneering study was that of van Bemmelen (1939) about Lake Toba, in which he describes the petrology of the volcanic products of the Toba region, concluding that both magma and magma (i.e., melts of palaeogenetic origin) produced the acid Toba tuffs. The work further compares Toba with the usual andesite volcanoes in Sumatra and Java and introduces the term ‘volcanotectonics’, marking the first steps into a now well-developed subdiscipline of volcanology. Moreover, a list or catalogue of eruptions of the Indonesian volcanoes between AD 1000 and 1941 was compiled by Petroschevsky (1943), a task currently performed for all eruptions worldwide by the Smithsonian Institution’s Global Volcanism Program (Global Volcanism Program 2013).

Given their frequent occurrence at Merapi, special attention was given to the problem of

what modern terminology refers to as pyroclastic density currents or PDCs (e.g. Branney and Kokelaar 2002). Terms used at the time comprised ‘glowing clouds’, ‘glowing avalanches’, and ‘nuées ardentes’, including the respective terms in the Dutch and German literature. Although all of these terms refer to this deadly volcanic phenomenon, specific names were given to particular types of currents and the eruptive processes producing them. Three types of ‘glowing clouds’ were described, often by drawing comparisons with eruptions at volcanoes such as Mont Pelée, La Soufrière on St. Vincent, and Kelud to place the activity of Merapi into a reference framework or context. The first type were the glowing clouds of the ‘Merapi-type’ (Escher 1933a, b), resulting from gravitational dome collapse. These were also termed ‘avalanches de pierres des volcans andésitiques du Japon et de Java’ and ‘nuées ardentes d’avalanche’ by Lacroix (1904, 1930). This type of activity has become synonymous with Merapi in the classic volcanological literature, and many of its eruptions during this period were of this type, including those of 1921–22 (Kemmerling 1921), where the phenomenon was originally recognised from Escher’s (1933b) interpretation of the eruptive events. This was cemented further in subsequent years, as the eruptions in 1930 and in 1942–43 (Fig. 1.10) were also of this type. The second type were the glowing clouds of the ‘St. Vincent-type’ (Escher 1933a), which result from an explosive eruption and the collapse of a vertical or near vertical eruption column or fountain. These correspond to the ‘nuées ardentes d’explosions vulcaniennes’ of Lacroix (1904, 1930) and the ‘explosion-type nuées ardentes’ of Neumann van Padang (1933). According to Hartmann (1935b), all explosive phases and associated glowing clouds during the 1934 eruption were of the ‘St. Vincent-type’, with other examples occurring during the eruptions in 1832–35, 1837–38 and 1846–47, as well as during the large eruption in 1872 (Hartmann 1934a). Independently, Grandjean (1931a, b, c), who lived in Yogyakarta and witnessed the catastrophic eruption in 1930 (Fig. 1.11), concluded that a third type occurred in this event.

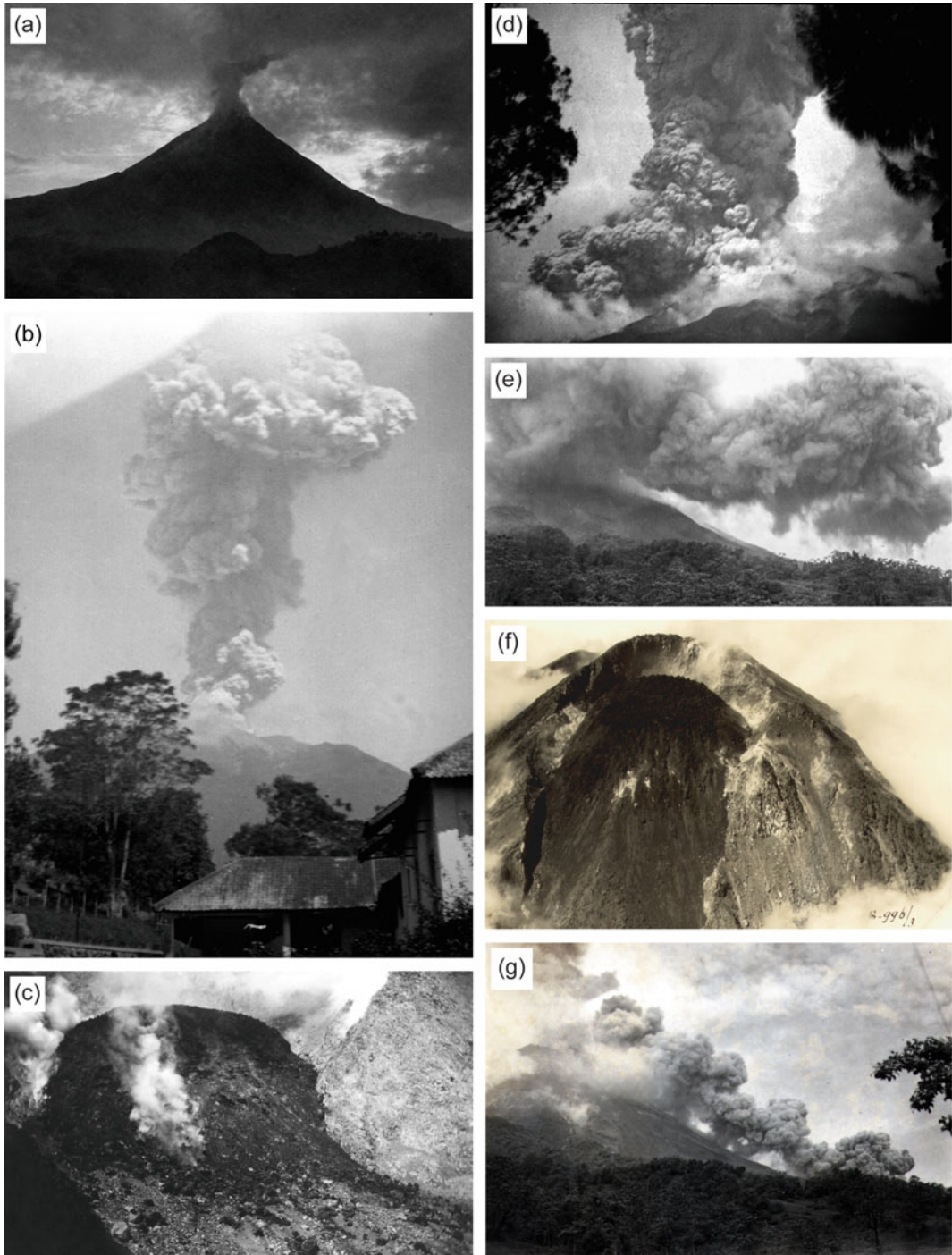
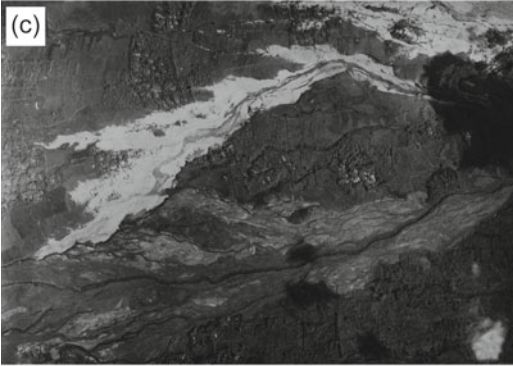


Fig. 1.10 Eruptive activity of Merapi in the early twentieth century. **a** 1920. **b** Explosive phase in 1930. **c** Summit lava dome in 1934. **d** Explosive phase in 1934. **e** Ash cloud in 1941. **f** Merapi summit and its lava dome as observed on 24 July 1941. **g** Observation of Merapi's

activity by van Bemmelen on 5 April 1943 during the Japanese occupation (1942–1945). All photographs are from the BPPTKG (Geological Agency of Indonesia) archive



◀ **Fig. 1.11** Impressions from the catastrophic eruption in 1930–31, during which pyroclastic density currents (PDCs) reached ~12 km from the summit on the western flank, destroying 42 villages and killing around 1369 people in one of Merapi's deadliest documented eruptions. **a** The western slopes of Merapi in 1930. **b** Close-up of Merapi's summit area in 1930. **c** Aerial image of PDC deposits (light grey in photograph) in Kali Poetih (Putih) and lahar deposits in Kali Batang (lower part of

photograph). The photograph was taken in 1930. **d** Hartmann inspecting eruption deposits (photograph from 14 March 1931). **e** Lahar deposits in Kali Blongkeng (photograph from 1931). **f** Houses in the village of Gedjoegang (Gedjugang) destroyed by PDCs (photograph from 1931). **g** Area affected by PDCs on Merapi's west flank near the village of Bendo (photograph from 1931). All photographs are from the BPPTKG (Geological Agency of Indonesia) archive

These glowing clouds of the 'Pelée-type' (Escher 1933a, b), or 'nuées peléennes d'explosion dirigée' (Lacroix 1904, 1930), envisaged to be generated by a horizontal dome explosion or directed blast, remained a controversial idea at Merapi. While the phenomenon was disputed by some at the time (e.g. Kemmerling 1932; Neumann van Padang 1933), Escher (1934b) mentioned the possible occurrence of glowing clouds of the 'Pelée-type' during the paroxysmal phase of the 1904 Merapi eruption as a result of initially directed PDCs that propagated down the Woro valley for approximately 6 km and, today, they are a well-recognised phenomenon at Merapi (see Sect. 1.7).

Attempts to understand and classify Merapi's activity were consequently made at that stage. In his work on the classification of central eruptions related the gas pressure of the magma and lava viscosity, Escher (1933b) associated the Merapi eruptions with those involving highly viscous lava. Glowing clouds of both the 'Merapi-type' and 'Pelée-type' were related to a lava plug at the top of the volcano. At low gas pressure, slow extrusion of new magma causes the lava plug to crumble down, producing glowing clouds of the 'Merapi-type', while those of the 'Pelée-type' occur when the lava plug blocks the vent completely, gas pressure builds up and is violently released in a horizontally or obliquely directed explosion. In case of the glowing clouds of the 'St. Vincent-type', there is no lava plug at the top of the volcano but a blocked vent under which gas pressure can build up. This may lead to a near-vertical or vertical explosion and collapse of the ejected rock fragments to produce glowing clouds that may descend in radial directions from the summit, a concept still discussed to this day (e.g. Newhall et al. 2000; Voight et al. 2000a; Drignon

et al. 2016; Preece et al. 2016; Heap et al. 2019). The most widely noted classification, which is occasionally still cited today, was that of Hartmann (1935a), who divided Merapi's activity into four groups (**A, B, C, D**) related to the gas content of the erupting magma. Eruption type **A** is characterised by the ascent of gas-poor magma, producing lava domes or coulées on steeper slopes. Rock falls and negligible explosions may accompany dome growth and resulting glowing clouds are insignificant. According to Hartmann (1935a), the lava dome of 1883–1885 and the formation of the western dome from 1909–1918 are related to this type of activity. Eruption type **B**, the most observed type at Merapi, begins with the ascent of a slightly more gas-rich magma forming a viscous lava dome at the summit. During the main eruption phase, a more gas-rich magma ascends, leading to limited gas overpressure and eruptions of the 'St. Vincent-type' that may destroy large parts of Merapi's summit area and produce glowing clouds, lava avalanches and rock falls. In a later phase, the degassed magma may form a lava dome or lava flow depending on the topography of the summit. Noted examples of this type of activity are the eruptions in 1930–31 and the earlier eruptive periods in 1862–1869, 1887–1889, 1891–1894, 1902–1908, 1920, 1921 and 1922 (Figs. 1.10 and 1.11). Eruption type **C** describes a moderately gas-rich magma that fragments in the uppermost conduit because of the release of the gases from the ascending magma to generate 'St. Vincent-type' and ash-rich glowing clouds (dilute PDCs or surges). In a later phase, lava domes or flows may form from the degassed magma, which may be destroyed again, leading to glowing clouds, as in eruption types **A** and **B**. Examples of this type of activity are the eruptions of 1832 to 1836, 1837/38,

1846/47 and 1933 to 1935 (Fig. 1.10). Eruption type **D** involves a gas-rich magma and is characterised by vigorous magmatic degassing at the beginning of the eruption, which is followed by a main eruption phase in which a high eruption column is produced. Glowing clouds are mainly of the ‘St. Vincent-type’, which develop from the onset of the eruption and the evolving destruction of the summit. Ash-rich glowing clouds and significant ash fall may occur during the main eruption phase. In a later phase, viscous lava may or may not extrude. A noteworthy example of this type of activity that included late-stage lava extrusion was the eruption of 1822, whereas those of 1849 and 1872 were not associated with lava extrusion. However, from today’s perspective we note that during some Merapi eruptions, transitions between these four types of activity were observed on a number of occasions and they may thus at least in part be gradational instead of resembling strictly independent endmember eruption styles or types.

The prehistoric eruptive history and structure of the volcanic edifice, in turn, received less attention during the late nineteenth and early twentieth century, although the two morphologically distinct parts—an old, heavily vegetated basal structure that forms a ring wall that is superimposed by the new cone—was already recognised by Kemmerling (1921), who further interpreted Gunung Pusunglondon in the east and Gunung Paseban in the north as small remains of the upper part of the old ring wall. Hartmann (1935a) argued that Merapi already existed at the time of the Hindu-Javanese kingdom of Mataram and speculated, as already hinted at in earlier works (e.g. van Hinloopen Labberton 1921), that the decline and disappearance of this ancient kingdom from the area was linked to a large eruption of Merapi at around AD 1006, which also buried Borobudur and other temples in the region by volcanic ash and lahars. He speculated further that the original crater (summit depression) of Merapi with a diameter of 3.5 km was a result of this large eruptions in AD 1006 and that remnants of this old depression include Gunung Djenggerlor, Djengger, Uto, Idjo, Kukusan, Kendil and Selokopo (see Gertisser et al. 2023,

Chap. 6). After AD 1006, a new cone grew inside this depression, whose summit was formed by the Pasarbubar crater. Moreover, Hartmann (1935a) expressed that in his view, which contrasts that of Kemmerling (1921), Gunung Pusunglondon and Gunung Paseban are remnants of the Pasarbubar crater of the new Merapi cone.

Similarly, while the importance of gas content and magma viscosity for the dynamics of Merapi’s eruptions was recognised (e.g. Escher 1933b; Hartmann 1935a), the petrography of the eruptive products is only briefly mentioned. Kemmerling (1921) described the Merapi eruptive products as hornblende-bearing andesites, with minerals of plagioclase, pyroxene, hornblende, olivine and ore. Similarly, Brouwer (1928a) noted that the summit lava dome of Merapi consists of pyroxene andesite, in which phenocrysts of zoned plagioclase occur alongside augite and less abundant hypersthene, joined by mostly resorbed and occasionally megacrystic amphibole and small amounts of olivine that are set in a groundmass of plagioclase, pyroxene, iron ore and a varying amount of glass (compare Troll and Deegan 2023, Chap. 8). In addition, he was among the first scholars to give a detailed petrographic description of xenoliths of metamorphosed limestone in the Merapi rocks (see Deegan et al. 2023, Chap. 10), which were collected by Kemmerling and during his own climb of Merapi in October 1923 (Brouwer 1928a), and to discuss the possible effect of carbonate assimilation on magma composition (Brouwer 1928b). Finally, Neumann van Padang (1933) emphasised the notable consistency of the hornblende-bearing augite-hypersthene andesite porphyries over the preceding 50 years of Merapi’s activity, which is a feature that is still relevant at present (e.g. Gertisser et al. 2023, Chap. 6; Troll and Deegan 2023, Chap. 8).

1.5 Into the Modern Era: Merapi Research After Indonesia’s Independence

In 1949, just at the very end of the Dutch colonial period, Dutch geologist Reinout Willem van Bemmelen published his *magnum opus* ‘The

Geology of Indonesia', the first volume of which is dedicated to the general geology of Indonesia and nearby archipelagos (van Bemmelen 1949). In this work, van Bemmelen provides a broad outline of the subvolcanic basement beneath Merapi, where presumably Cretaceous arc and ophiolite lithologies occur below a sequence of 8–11 km thick sediments of the Kendeng basin. This basin comprises Cretaceous to Cenozoic volcanoclastic sediments that are overlain by shallow marine limestones and marls (see Harijoko et al. 2023, Chap. 4), which are the source of abundant calc-silicate xenoliths in the Merapi lavas (see Deegan et al. 2023, Chap. 10). Building on observations and ideas communicated previously (e.g. Kemmerling 1921; Hartmann 1935a), van Bemmelen further elaborated on the overall structure of the volcanic complex of Merapi with its active stratocone that has grown on top of the remains of an older, partly destroyed and eroded edifice (van Bemmelen 1949, 1956). He thus reiterated the idea of a major eruption of Merapi in AD 1006 that destabilised the Mataram kingdom in Central Java and forced its migration to East Java (e.g. van Hinloopen Labberton 1921; but also see Holmberg 2023, Chap. 3). According to van Bemmelen, the “cataclysmic outburst” led to the collapse of the western side of the old Merapi edifice along a major listric fault zone, known as the Kukusan fault, leaving a horseshoe-shaped crater or ‘Somma rim’ on the northern and eastern flanks. In this context, the Gendol Hills, located ~20 km west-southwest of Merapi, were interpreted as folded units of the older edifice that formed during the gravitational collapse of Merapi’s western flank and the buttressing effect of the Menoreh Mountains further west (see Gertisser et al. 2023, Chap. 6). The broad stratigraphic framework established by van Bemmelen (1949) was later refined by Wirakusumah et al. (1980), whose work formed the basis for the publication of a 1:50,000 geological map of the volcano, including preliminary radiocarbon dates (Wirakusumah et al. 1989). The geological map, a simplified version of which is illustrated in Gertisser et al. (2023, Chap. 6), identifies an Old Merapi and a Young

Merapi edifice, as envisaged by van Bemmelen (1949, 1956), and distinguishes within the former, the older lavas of Gunung Turgo, Gunung Plawangan and Gunung Bibi from those that constitute the ‘Somma-Merapi’ in the northern and eastern parts of the volcanic complex (compare also Gertisser et al. 2023, Chap. 6).

The stratigraphy of Merapi remained the focus of further studies in the following decades and doubts started to be voiced over the timing of the disappearance of the Mataram kingdom in Central Java, which might have occurred almost a century prior to AD 1006 (i.e. in AD 928 or 929), but also about the evidence for a catastrophic (Somma rim-forming) eruption of Merapi in either AD 928–929 or AD 1006 (Djumarma et al. 1986). At the same time, petrological and geochemical investigations of the eruptive products of Merapi started to emerge, the results of which were often included in unpublished theses that appeared until the end of the 1980s (Kerinec 1982; Bahar 1984; Luais 1986; del Marmol 1989). Some of these, including the PhD thesis of Bahar (1984) and del Marmol (1989), combined stratigraphic investigations of either or both of the lava or pyroclastic sequences with petrological-geochemical analyses to shed light on petrogenetic processes (see also Troll and Deegan 2023, Chap. 8). Composite stratigraphic sections, constructed by C. Newhall and co-authors and included in del Marmol (1989), were the first detailed descriptions of the explosive eruptive activity of Old Merapi (see Gertisser et al. 2023, Chap. 6). Furthermore, building on the early Dutch accounts (see above), Clocchiatti et al. (1982) provided the first ‘modern’ petrographic account of the enclaves and calc-silicate xenoliths in the Merapi lavas and their mineralogical variety (compare Deegan et al. 2023, Chap. 10).

The recurrent eruptions of Merapi since the mid-twentieth century (Fig. 1.12) have continued to provide a focus for the investigation of eruptive phenomena, PDCs and the hazards associated with these. These more recent eruptions were systematically documented in frequent reports from the Volcanological Survey of Indonesia (see Kusumadinata 1979 and

references therein for a summary of the activity of the preceding decades) and, notably, a ‘Catalogue of the active volcanoes of the world’ was published in 1951, which contains a historical summary of the volcanoes of Indonesia and their eruptions, including Merapi (Neumann van Padang 1951). The types and characteristics of Merapi’s eruptions remained the focus of scientific investigations into the 1980s, with studies such as Zen et al. (1980) as well as Bardintzeff

(1984), who divided the ‘Merapi-type nuées ardentes’ into ‘Merapi-type’ sensu stricto, incorporating material from a fully solidified dome without any fresh glass, and ‘Arenal-type’, which is derived from a dome with a portion of the interior of the dome still being liquid. The measures taken by the authorities to safeguard the population from the consequences of volcanic eruptions in Indonesia, including those of Merapi and its PDCs, were also significantly

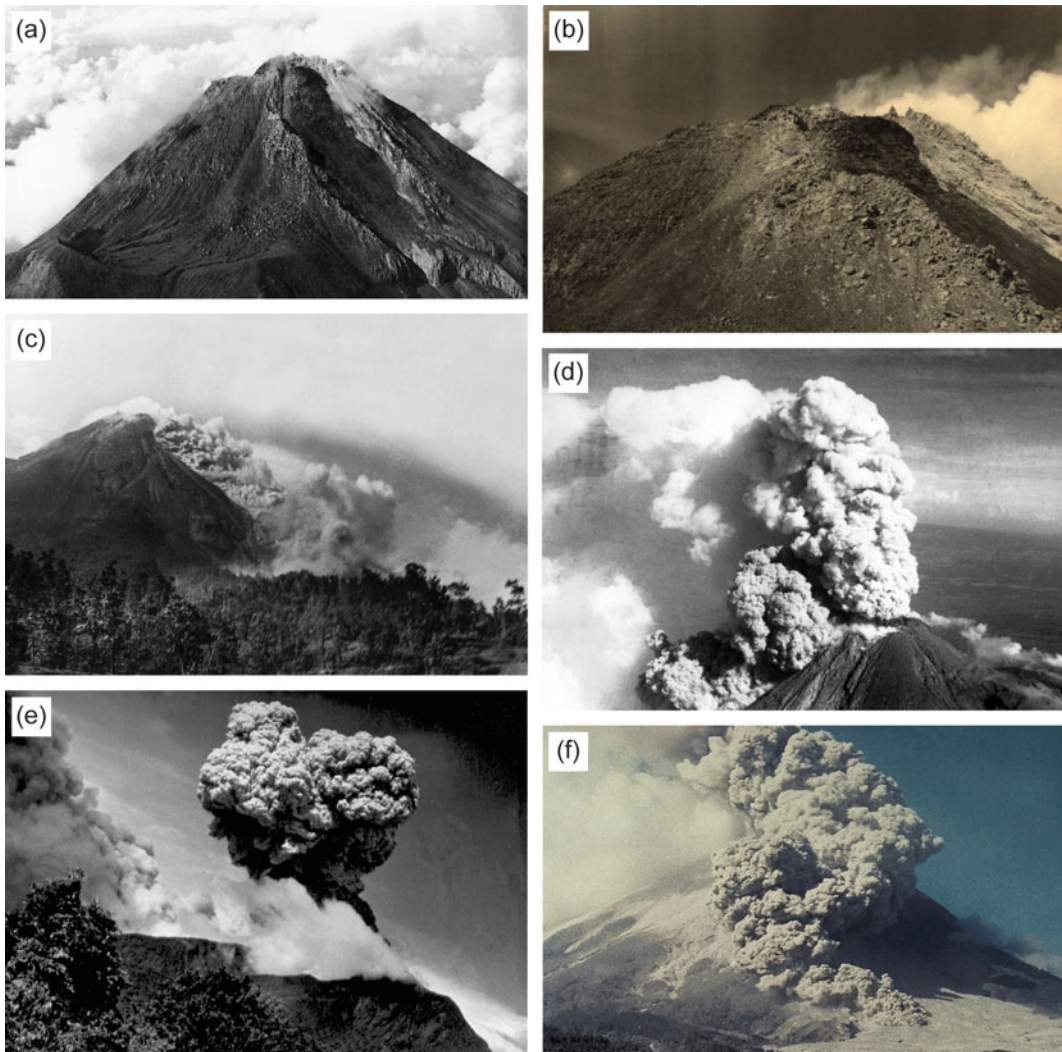


Fig. 1.12 Merapi and its activity after Indonesia’s independence. **a** Upper slopes of Merapi in 1954 as seen from the northwest. **b** Close-up of the summit area and 1954 lava dome (black). **c** 1957 pyroclastic density current (PDC). **d** Explosive eruption phase and PDC in

1960. **e** Vulcanian explosion in 1975. **f** PDC moving down Merapi’s southwest flank in 1984. All photographs are from the BPPTKG (Geological Agency of Indonesia) archive

advanced in this period, which was discussed by Neumann van Padang (1960), Suryo (1978) and Suryo and Clarke (1985), among others. At this stage, the first hazard map of Merapi was also published by Pardyanto et al. (1978), which formed the basis for further refinement and revisions of the actual hazard map of the most recent time (CVGHM 2002, 2011).

1.6 The United Nations International Decade for Natural Disaster Reduction and Merapi Decade Volcano

The 1990s were declared by the United Nations as the International Decade for Natural Disaster Reduction (IDNDR). Within this programme, the International Association of Volcanology and Chemistry of the Earth's Interior (IAVCEI) designated Merapi and fifteen other active volcanoes as 'Decade Volcanoes', which merited intensified study and public-awareness activities based on their history of destructive eruptions, recent geological activity, and proximity to populated areas.

Within the 'Decade Volcanoes' project, existing collaborative programmes between the Volcanological Survey of Indonesia and foreign institutions were strengthened and new collaborations were established at Indonesian volcanoes with partners from Japan, USA, France, the Netherlands, and Germany, among others. In two Merapi Decade Volcano International Workshops, held in Yogyakarta in October 1995 and December 1997, plans for international collaborations and initial results of these activities were presented. For example, in cooperation with the Volcanological Survey of Indonesia and other institutions in Indonesia and Germany, the GeoForschungsZentrum Potsdam initiated an interdisciplinary monitoring program at Merapi in 1994 that complemented other ongoing national and international activities at the volcano. The project MERAPI (Mechanism Evaluation, Risk Assessment, Prediction Improvement) aimed to contribute to the development of prediction and warning strategies for Merapi on different

timescales (see Luehr et al. 2023, Chap. 5). Investigations of the internal structure, magmatism, eruptive activity, and explosive history of the volcano formed the basis for a better understanding of the volcanic complex as a whole and led to improved hazard assessment and warning capabilities (e.g. Zschau et al. 2003). Results of the Indonesian-German collaboration at Merapi were also presented at two Merapi-Galeras Workshops held in Potsdam and Hannover, resulting in the publication of two special issues 'Decade Volcanoes under Investigation' of the DGG Mitteilungen (DGG = Deutsche Geophysikalische Gesellschaft; German Geophysical Society) in 1998 and 2000. Much of the international research carried out in this period culminated in a collection of landmark papers published in the 2000 special issue 'Merapi volcano' of the Journal of Volcanology and Geothermal Research (vol. 100) and numerous scientific contributions to the IAVCEI General Assembly held in Bali in July 2000 and the associated field trip to Merapi.

During the last decade of the twentieth century, significant eruptions occurred in 1992, 1994, 1997 and 1998 (Fig. 1.13) and considerable advances were made in many areas of research at Merapi during that time. Field studies of more recent eruptions and the associated PDC deposits focused on those of 1984 (Boudon et al. 1993) and 1994 (Abdurachman et al. 2000; Kelfoun et al. 2000), with further important contributions about the 1992, 1994 and 1998 eruption deposits published later (see Sect. 1.7). These studies provided new insights into the deposit architecture, emplacement mechanisms, and hazards of PDCs at Merapi. The latter also benefitted from the first two-dimensional numerical simulations that helped determine areas that could potentially be affected by PDCs (Itoh et al. 2000), studies of the dynamic pressure and emplacement temperature of the 1994 currents (Clarke and Voight 2000; Voight and Davis 2000) and considerations for a revised hazard assessment at Merapi (Thouret et al. 2000). An overview of the common lahar hazards at Merapi was given by Lavigne et al. (2000a), who showed that these hazards are high below about

450–600 m elevation in all of the thirteen major rivers that drain the volcano.

Summaries of Merapi's historical eruptions that synthesised information from many historical sources and publications from the late eighteenth to the late twentieth century (Berthommier 1990; Berthommier and Camus 1991; Voight et al. 2000a) and detailed stratigraphical and geochronological studies led to an improved understanding of the geological evolution of Merapi. The PhD thesis of Berthommier (1990) presented a geological history of Merapi, based on radiocarbon and U-Th disequilibrium ages and a $^{40}\text{K}/^{40}\text{Ar}$ age, which were complemented by whole-rock and mineral chemical data. Some of the results were published in Berthommier et al. (1990). Largely based on the PhD thesis of Andreastuti (1999), a more refined tephrostratigraphic framework at Merapi from 3000 to 250 years ago followed from that and was published in Andreastuti et al. (2000), identifying and dating by the radiocarbon method a series of important stratigraphic marker horizons around the volcano that are associated with moderate to large eruptions. The most recognisable tephra units were also included in the stratigraphic sections of Newhall et al. (2000), who presented a comprehensive stratigraphy and a large number of radiocarbon dates from pyroclastic deposits extending the record of the explosive activity of Merapi back to $\sim 10,000$ years ago. An alternative outline of the geological evolution of Merapi was presented by Camus et al. (2000). Drawing heavily on the PhD thesis of Berthommier (1990), the authors proposed a Mt. St. Helens-type edifice collapse, which occurred between ~ 6.7 ka and $2,200 \pm 160$ ^{14}C y BP and destroyed the older Merapi edifice, generating a debris avalanche now exposed as hummocks in the Gendol Hills. This interpretation was disputed by Newhall et al. (2000), who showed that the Gendol Hills are Upper Pliocene in age and therefore significantly older than Merapi. Furthermore, these authors found no other evidence of a large-scale debris avalanche deposit and suggested that it has probably been buried by younger deposits. The age of the latest of possibly several larger collapses of the old

Merapi edifice was inferred indirectly from the distribution of PDC deposits around Merapi and was reported to have occurred at $\sim 1,900$ ^{14}C y BP (see Gertisser et al. 2023, Chap. 6).

Although basic whole-rock geochemical and mineral chemical data of the eruptive products have been included and discussed in various theses and publications at the time (e.g. Berthommier 1990; Andreastuti 1999; Andreastuti et al. 2000; Camus et al. 2000), detailed investigations of the magma plumbing system, petrology and geochemistry of Merapi remained incomplete, but notable advances were made nevertheless. For instance, Siswawidjono et al. (1995) showed that despite wider monthly variations, the long-term magma output rate at Merapi has remained relatively constant over a century, culminating in more than 10^8 m^3 of lava discharged between 1890 and 1992. Insights into magma chamber and degassing dynamics were provided by Gauthier et al. (1999), who interpreted variations in ($^{210}\text{Pb}/^{226}\text{Ra}$) ratios in recently erupted lavas by phases of near-closed-system evolution shallow magma chamber evolution with continuous Rn degassing, and episodes of replenishment of this reservoir with undegassed magma from depth. Hammer et al. (2000) used quantitative textural analyses of the recent dome lavas to demonstrate a relationship between lava extrusion rates and groundmass crystal textures and compositions, providing a petrological tool to trace shallow magmatic and, particularly, conduit-style processes.

Technological advances at that time led to the increasing application of geophysical techniques to support the monitoring programme of the Volcanological Survey of Indonesia (see Sect. 1.8). These included self-potential measurements to gain insights into the internal structure and shallow hydrothermal system of the summit area (Aubert et al. 2000), magnetic monitoring that identified magnetic changes correlating with volcanic activity over different time scales (Zlotnicki et al. 2000), and monitoring of lahar dynamics using non-contact detection instrumentation installed on the slopes of the volcano, including real-time seismic amplitude measurement (RSAM), seismic spectral amplitude measurement (SSAM) and

acoustic flow monitoring (AFM) systems (Lavigne et al. 2000b). Ratdomopurbo (1995) and Ratdomopurbo and Poupinet (1995, 2000) analysed the seismicity of Merapi from 1983 to 1995 during which the volcano had two main eruptive episodes. They recognised that eruptions in 1984 and 1992 were both preceded by deep and shallow volcano-tectonic earthquakes, whereas the 1986 and 1994 eruptions were not, emphasising that important dome collapse events, such as those on 22 November 1994, may not be directly preceded by seismic precursors. They further pointed out that tremors may be observed but may not always precede a dangerous event. These were important realisations, although they showed the uncertainties of utilising monitoring to improve hazard predictions and forecasting. In addition, these authors identified an aseismic zone at a depth between 1.5 and 2.5 km below the summit, interpreted to signify a small shallow (intra-edifice) magma reservoir, where magmas are temporarily stored and blended prior to final eruption (see also Troll and Deegan 2023, Chap. 8).

1.7 Research in the 21st Century

Research interest in Merapi and research outputs continued to rise following the turn of the last century (Fig. 1.4). Notable increases in research activity occurred after the 2006 eruption, which was the first major eruption of Merapi in the twenty-first century after a smaller event in 2001. The 2006 eruption was followed soon after by the large-magnitude eruption of 2010 (Fig. 1.14), making these some of the best studied eruptions of Merapi. Significant advances were made during these events regarding the geological history of Merapi, PDC dynamics, petrogenetic processes and their impact on eruption dynamics, the deep structure and magma plumbing system of Merapi, volcano monitoring, and the environmental, sociological, economic and health impact of Merapi's eruptions.

Regarding the advances on the geological evolution of Merapi in the earliest years of the twenty-first century, important contributions were made by Gertisser (2001) and Gertisser and Keller

(2003a), who presented a large number of radiocarbon dates that extended the pyroclastic stratigraphy of Merapi back to $11,792 \pm 90$ ^{14}C y BP and challenged earlier views of a sector collapse of Old Merapi as young as 1900 ^{14}C y BP. Parallel research carried out in the Borobudur basin west of the volcano (Murwanto 2004) showed that the long sequence of lacustrine deposits, interpreted to have formed by recurrent impoundment of Kali Progo by debris avalanches or debris flows from Merapi to repeatedly establish an ancient Lake Borobudur, spanned at least 20,000 years from $22,040 \pm 390$ ^{14}C y BP. This timespan was later revised to $31,430 \pm 2070$ ^{14}C y BP (Murwanto 2014) and complemented by work on drill cores (Gomez et al. 2010) that shed further light on the activity of Merapi that affected more distal areas west of the volcano. Stratigraphic field data, additional radiocarbon dates, and several new $^{40}\text{K}/^{40}\text{Ar}$ and $^{40}\text{Ar}/^{39}\text{Ar}$ ages of the volcanic complex were published by Gertisser et al. (2012b) to provide a state-of-the-art synthesis of the geological history of Merapi (see Gertisser et al. 2023, Chap. 6). More recently, Bronto et al. (2014) discovered a large debris avalanche deposit approximately 30–35 km southwest of Merapi in the Godean area in the Sleman Regency, which was linked to a gigantic landslide of Merapi, termed herein the Godean debris avalanche. Although the age of the deposit and the associated sector collapse remain poorly constrained (Bronto et al. 2023, Chap. 7), this important finding may eventually cast new light on the long-standing debate about the destruction of the older Merapi edifice (Gertisser et al. 2023, Chap. 6). The burial of ancient temples in the vicinity of Merapi by volcanoclastic deposits was once more the focus of a recent study (Kusumayudha et al. 2019), confirming previous studies in proposing that volcanic disasters contributed to the demise of the Mataram kingdom in Central Java.

Several studies in the twenty-first century continued to be dedicated to the pyroclastic deposits of Merapi. Work on the 1992, 1994 and 1998 PDC deposits carried out in the 1990s and published in the early 2000s identified slickensided surfaces and partially melted pseudotachylite friction marks on blocks in block-and-



Fig. 1.13 Merapi during the last decade of the twentieth century. Significant eruptions occurred in 1992, 1994, 1997 and 1998. **a** Merapi summit and growing lava dome in 1992. **b** Small pyroclastic density current (PDC) during the 1992 activity. **c** 22 November 1994 PDC moving down Kali Boyong as seen from Kaliurang. **d** Explosion during

the 1997 activity. **e** The Merapi lava dome in 1998. **f** PDC on Merapi's southwest flank on 19 July 1998. **g** Merapi as seen from Kali Boyong to the south at the end of the twentieth century (1999). Photographs **a-f** are from the BPPTKG (Geological Agency of Indonesia) archive and the photograph in **g** is modified from Gertisser et al. (2011)

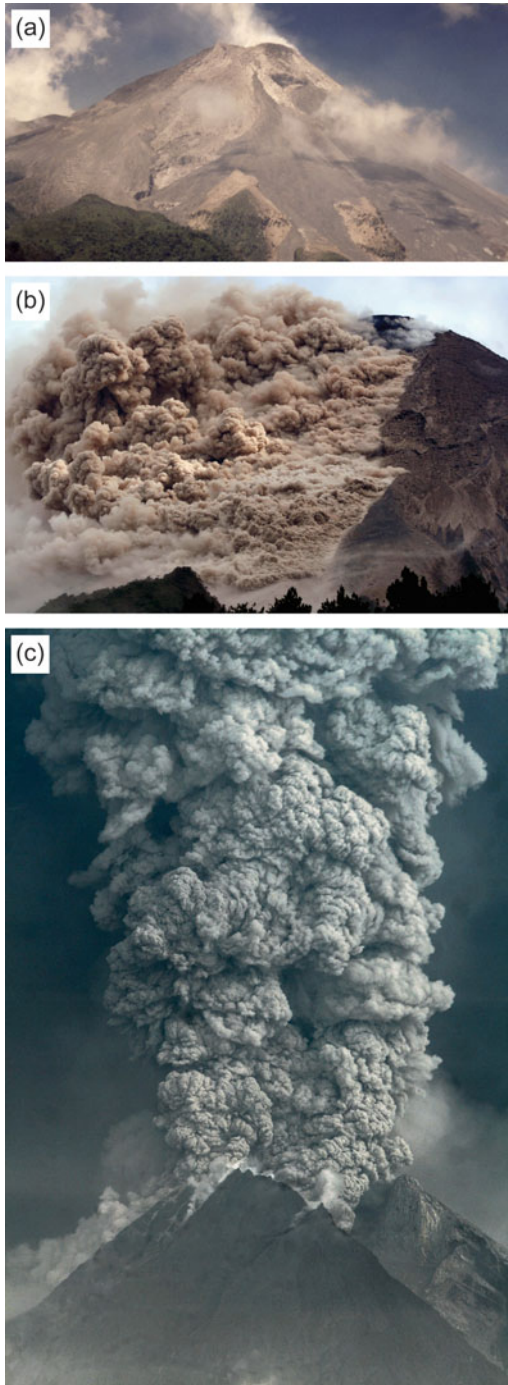


Fig. 1.14 Merapi's activity of the twenty-first century: **a** Merapi seen on 4 August 2001. **b** Pyroclastic density current (PDC) moving down the southern flank of Merapi during the 2006 eruption (photograph from 7 to June 2006). **c** Explosion phase on 6 November during the catastrophic 2010 eruption. All photographs are from the BPPTKG (Geological Agency of Indonesia) archive

ash flow deposits and substrate that was overridden by block-and-ash flows, which resulted from clast collision during transport of blocks in PDCs (Schwarzkopf 2001; Schwarzkopf et al. 2001). Other work postulated ash-cloud surge detachment from the dense basal current of the 1994 flows either relatively high on the volcano slope (Bourdier and Abdurachman 2001) or following passage over a steep cliff in Kali Boyong (Schwarzkopf 2001; Schwarzkopf et al. 2002), thus explaining the 1994 disaster at Turgo village, which furthermore helped to advance the conceptual facies model available for block-and-ash flows at Merapi (Schwarzkopf et al. 2005). These studies were punctuated by the devastating 2006 eruption, which brought a shift in focus to the 2006 dome-collapse PDCs, particularly those produced at the peak of the eruption on 14 June 2006. These, for the first time in a century, affected populated areas around Kali Gendol on Merapi's south flank and caused two fatalities in the village of Kaliadem (Charbonnier and Gertisser 2008, 2011; Donoghue et al. 2008; Lube et al. 2011; Gertisser et al. 2012a; Ratdomopurbo et al. 2013) (Fig. 1.15). The first geophysical mass flow simulations applied to Merapi, using the Titan 2D and VolcFlow codes, successfully reproduced the runout distance and valley over-spills of the 2006 PDCs and thus improved PDC hazard assessment (Charbonnier and Gertisser 2009, 2012). Detailed insights into the architecture of the 2006 valley-confined and overbank PDC deposits were obtained using ground-penetrating radar (Gomez et al. 2008, 2009; Gertisser et al. 2012a), complementing earlier outcrop-based studies of PDC deposits (e.g. Boudon et al. 1993; Abdurachman et al. 2000; Kelfoun et al. 2000; Schwarzkopf et al. 2005; Charbonnier and Gertisser 2008, 2011). An important observation from the 2006 eruption was the avulsion of the basal avalanche of block-and-ash flows from channels onto interflue areas, a process described in some of the early accounts about Merapi's activity, but not seen to such an extent during other recent eruptions, and probably enhanced by the presence of Sabo dams (Charbonnier and Gertisser 2008, 2011; Lube et al. 2011; Gertisser et al. 2012a). Furthermore,



◀ **Fig. 1.15** Impressions of the 2006 eruption, the first major eruption of Merapi in the twenty-first century. **a** Merapi and the growing 2006 summit lava dome as seen from Deles on the southeast flank of the volcano on 11 June 2006. **b** Valley-filling deposits of the 14 June 2006 dome collapse block-and-ash flows near their termination in the Gendol river valley ~ 7 km from the summit of Merapi. **c** Valley-filling and overbank pyroclastic density current (PDC) deposits around Kaliadem. Photo taken on 2 August 2006. **d** Overflow point of the 2006 PDCs above the Kaliadem Sabo dam in Kali

Gendol. Accumulation of large blocks characterises the valley-filling deposits below the overflow cliff that is covered by wedge-shaped, proximal overbank deposits. **e** Kaliadem before the 2006 eruption. **f** Houses in Kaliadem after the 2006 PDCs (view as in **e**). The village became partly buried and heavily damaged by avulsion of PDCs from nearby Kali Gendol (photo credit: Sylvain Charbonnier). **f** Detailed example of the damage caused to the built infrastructure in Kaliadem village. **h** Buried observation bunker in Kaliadem where two volcano observers died during the eruption



Fig. 1.16 Impact of the 6.4 Bantul earthquake south of Merapi on 27 May 2006. **a-c** Severe building damage in and around Yogyakarta. **d** Damage to Candi Prambanan. **e** Temporary shelters for earthquake victims near the village of Bantul. The earthquake caused more than 6,000

fatalities, left about 1.5 million people with desolated homes, and is thought to have triggered increased volcanic activity at Merapi in the weeks that followed the earthquake (see text for further information)

the eruption highlighted that during prolonged dome-forming activity, parts of Merapi's summit area may become unstable, resulting in small edifice collapses and, possibly, debris avalanches, as well as dramatic shifts in the areas affected by PDCs (e.g. Charbonnier and Gertisser 2008; Ratdomopurbo et al. 2013; Bronto et al. 2023, Chap. 7). Important results also included the demonstrable effect of the devastating regional magnitude 6.4 Bantul earthquake on 27 May 2006 (Fig. 1.16) on eruption intensity and lava extrusion rates, which both increased after the earthquake (Harris and Ripepe 2007; Walter et al. 2007, 2008). This increase coincided with a notable change in fumarole gas isotopic compositions, indicating considerable release of crustal CO₂ that may have intensified and sustained the eruption (Troll et al. 2012, 2013a, b). These aspects were among the key topics of an international workshop about Merapi and Merapi-type volcanoes held in Yogyakarta in September 2006, a few months after the 2006 eruption. The workshop reviewed the scientific experiments that have been conducted at Merapi during the past decade and focused on the 2006 eruption and related activity, hazards, volcano monitoring, Merapi's magma plumbing system and issues of hazard communication (Purbawinata et al. 2007).

In October and November 2010, Merapi's largest eruption in over 100 years (since 1872) drew both national and international attention because of its large-magnitude (VEI 4) and, in many respects, unusual character compared to the common dome-forming eruptions of the preceding decades (e.g. Surono et al. 2012; Subandriyo et al. 2023, Chap. 12). This extensive research effort gave rise to another special issue of the *Journal of Volcanology and Geothermal Research* in 2013 (vol. 261) that contains several contributions about the 2006 eruption and many describing early results about the 2010 eruption. One year later, in September 2014, the 8th Cities on Volcanoes (CoV) conference in Yogyakarta brought Merapi once more into the focus of the international volcanological community, bringing together geoscientists, emergency managers, social scientists, economists, city planners, engineers and educators to promote an exchange of

ideas and stimulate dialogue on the generation of volcanic hazards, the vulnerability of exposed communities and on mitigation of the resulting risks.

Notable highlights of that episode are the 2010 PDC deposits, which were discussed by several authors, including Charbonnier et al. (2013), Cronin et al. (2013), Jenkins et al. (2013), Komorowski et al. (2013), Preece (2014) and Preece et al. (2016), with discussions centred on the different types of PDCs generated, the unusually long runout distance of ~16 km of some of the currents, their generation mechanisms at the source and their environmental impact (see also Subandriyo et al. 2023, Chap. 12). An important contribution was made by Komorowski et al. (2013), who proposed the occurrence of directed dome explosions at the peak of the 2010 eruption generating blast-like, high-energy PDCs comparable to those postulated by Grandjean and Escher during the 1930 eruption. At this point, a significant step forward in the modelling of volcanic flows was made through the application of a new version of the VolcFlow code to the 2010 eruption. This improved code, which uses a new depth-averaged model of pyroclastic currents coupling concentrated and the dilute flow regimes, accurately reproduced the main field characteristics of the concentrated and dilute 2010 pyroclastic currents (Kelfoun 2017; Kelfoun et al. 2017; Charbonnier et al. 2023, Chap. 16), which implies that this model can be used as a predictive tool from now on to assess impacts of future eruptive scenarios. Further advances on the causes were made at this stage and the unusual size and intensity of the eruption were mainly attributed to a larger than normal influx of deep, volatile-rich magma that replenished the shallower magma system within the carbonate dominated upper crust beneath Merapi at relatively short time-scales. Transitions between explosive and effusive eruption phases were linked primarily to shallow-level magma ascent dynamics, enhanced by the presence of a plugged conduit (e.g. Surono et al. 2012; Borisova et al. 2013; Costa et al. 2013; Cronin et al. 2013; Jousset et al. 2013; Komorowski et al. 2013; Preece 2014; Genereau et al. 2015; Drignon et al. 2016; Kushnir et al. 2016,

2017; Preece et al. 2016; Handley et al. 2018; Carr et al. 2020; Li et al. 2021; Preece et al. 2023, Chap. 9; Subandriyo et al. 2023, Chap. 12).

In addition, a resurgence in petrological, geochemical and isotopic studies of the eruptive products of Merapi, often with a focus on the 2006 and, particularly, the 2010 eruption, led to significant advances in our understanding of the petrogenetic processes, the internal structure of Merapi's plumbing system, and the link between magmatic processes and eruption dynamics. The generation of primary magma at Merapi has been the subject of numerous studies that highlighted the depleted nature of the mantle source, overprinted by slab-derived components that have caused heterogeneous changes in the geochemical and isotopic composition of the mantle wedge beneath the volcano (Gertisser 2001; Turner and Foden 2001; Woodhead et al. 2001; Gertisser and Keller 2003b; Debaille et al. 2006; Deegan et al. 2016a, 2021; Handley et al. 2011, 2014, 2018). A variety of studies were devoted to magmatic differentiation in the arc crust. Early studies focused on the temporal evolution of Merapi's magma system, highlighting longer term cyclic magmatic variations during the past 2000 years of volcanic activity (Gertisser 2001; Gertisser and Keller 2003a), or dealt with various types of inclusions and the isotopic composition of plagioclase in the recent Merapi lavas, making a case for the importance of carbonate assimilation as a petrogenetic process (Troll et al. 2003; Chadwick et al. 2007). These initial efforts led to a revival of investigations of the processes of magma-carbonate interaction at Merapi and their role in magma genesis and in influencing eruptive behaviour (Deegan et al. 2010; 2016b; Troll et al. 2012, 2013a, b, 2015; Borisova et al. 2013; Blythe et al., 2015; Genareau et al. 2015; Whitley et al. 2019, 2020; Whitley 2020). Other studies addressed the issue of magmatic differentiation using geochemical and isotopic compositions of lavas and pyroclastic rocks and their constituent minerals (e.g. Gertisser 2001; Gertisser and Keller 2003a; Handley et al. 2014, 2018; Drignon et al. 2016; Peters et al. 2017; Deegan et al. 2021; Li et al. 2021), crystal

isotope stratigraphy (e.g. Chadwick et al. 2007; Borisova et al. 2016; Deegan et al. 2016a), igneous inclusion petrology (e.g. Chadwick et al. 2013; Troll et al. 2013a; van der Zwan et al. 2013), melt inclusion and glass analyses (e.g. Nadeau et al. 2013a; Preece 2014; Preece et al. 2014; Genareau et al. 2015; Drignon et al. 2016; Li et al. 2021), textural analysis (e.g. Innocenti et al. 2013a, b; van der Zwan et al. 2013; Preece et al. 2013, 2016; Preece 2014; Drignon et al. 2016; Kushnir et al. 2016, 2017), thermo-barometry and thermodynamic modelling (e.g. Gertisser 2001; Chadwick et al. 2013; Costa et al. 2013; Nadeau et al. 2013a; Erdmann et al. 2014; Deegan et al. 2016a; Preece et al. 2014, 2016; Peters et al. 2017; Li et al. 2021), phase equilibrium experiments (e.g. Erdmann et al. 2016), uranium-series disequilibria (e.g. Condomines et al. 2005; Handley et al. 2018) and detailed investigations of crustal xenoliths (e.g. Chadwick et al. 2007; Deegan et al. 2010; Troll et al. 2012, 2013b; Borisova et al. 2013; Whitley et al. 2019, 2020; Whitley 2020). Important results include the recognition of (1) a complex, trans-crustal magma storage and transport system beneath Merapi and the processes operating therein, (2) the importance of the assimilation of carbonate country rock on magma composition and CO₂ release potentially influencing the explosive nature of the Merapi eruptions, and (3) the influence of variations of magma ascent rates and associated pre-eruptive shallow magmatic processes and their timescales on eruptive behaviour (see Deegan et al. 2023, Chap. 10; Gertisser et al. 2023, Chap. 6; Preece et al. 2023, Chap. 9; Subandriyo et al. 2023, Chap. 12; Troll and Deegan 2023, Chap. 8).

Simultaneously, the deep structure and magma plumbing system of Merapi and the crustal and uppermost mantle structure beneath Central Java have been the subject of several large-scale geophysical and particularly seismic experiments, including the MERAMEX and DOMERAPI projects (e.g. Koulakov et al. 2007, 2016; Wagner et al. 2007; Luehr et al. 2013; Rohadi et al. 2013; Ramdhan et al. 2017; Widiyantoro et al. 2018). These have resolved

the three-dimensional seismic velocity structure beneath Merapi, identifying a large low velocity body that extends from the upper crust to the upper mantle beneath Central Java, have detected deep-seated tectonic features, and provided a structural image of the lithosphere and subduction zone beneath Central Java (see Luehr et al. 2023, Chap. 5).

The 2006 and 2010 eruptions and the post-2010 activity also provided a focus for several studies related to eruption monitoring in the wider sense. Ratdomopurbo et al. (2013) monitored lava dome growth during the 2006 eruption, arguing that deformation monitoring is crucial for eruption forecasting. Precursory signals, including a decrease in slope distances of the south and south-east baselines to the summit, as determined by electronic distance measurements (EDM) (Aisyah et al. 2018), signalling asymmetrical inflation of the summit area, an increase in seismicity, and a possible increase of SO₂ emissions followed by a more continuous period of inflation, were observed since mid-2005. Walter et al. (2013) used photographs to track dome growth and coulée flow following the peak of the 2006 eruption. Satellite remote sensing was an important volcano monitoring technique in 2010 employed to detect ground surface changes prior to the eruption (Saepuloh et al. 2013) and to monitor lava extrusion rates and dome growth as an eruption forecasting tool (Pallister et al. 2013). Satellite imagery was also used to calculate the volume of PDC deposits, delineate areas affected by these currents, estimate geomorphological changes of the volcanic edifice, and assess the risks emanating from the various volcanic hazards (e.g. Bignami et al. 2013; Charbonnier et al. 2013; Komorowski et al. 2013; Kubanek et al. 2015; Solikhin et al. 2015). The seismic phenomena before and during the 2010 eruption were analysed by Budi-Santoso et al. (2013), who showed that precursory seismic activity started about 6 weeks before the onset of the eruption and that the cumulative seismic energy released was approximately three times higher than that of preceding previous effusive eruptions. Volcano-tectonic earthquake hypocentres clustered at depths of

2.5–5 km and again at less than 1.5 km below the summit, confirming earlier results of an aseismic zone between approximately 1.5 and 2.5 km depth (Ratdomopurbo and Poupinet 2000), but were now interpreted differently and thought to represent a poorly consolidated layer of altered volcanic rocks. In another seismic study, Jousset et al. (2013) demonstrated the migration of long period seismic events towards the summit as the eruption progressed and linked this seismicity to the SO₂ flux of the eruption. As in 2006, eruption precursors included the asymmetrical inflation of the summit area, which was attributed to block movement that had been strongly controlled by topography, the presence of a hydrothermally weak zone and an underground gap near the summit between the west and east domes (Aisyah et al. 2018; Subandriyo et al. 2023, Chap. 12). Since 2010, further geophysical monitoring tools have become increasingly important monitoring tools, especially satellite remote sensing (Walter et al. 2015), surveys using unmanned aerial vehicles (Darmawan et al. 2018a, b), thermal, high-resolution visual imaging in stereoscopic configurations (Kelfoun et al. 2021), and combinations of visual video and seismic records (Darmawan et al. 2020). These methods are used to track volcanic activity, lava dome dynamics, including morphological and structural changes, dome growth and collapse, as well as rock falls, in ever increasing detail, thus providing increasingly vital information for hazard assessment and disaster mitigation (Darmawan et al. 2023, Chap. 15; Walter 2023, Chap. 14).

A longer perspective on the interpretation of multi-parameter volcano monitoring data was given by Nandaka et al. (2019). The authors evaluated data collected from 1992–2011 by the Volcanological Survey of Indonesia through BPPTKG (see Sect. 1.8) to show that explosive eruptions at Merapi had typically been preceded by an increase in volcano-tectonic earthquakes and increased CO₂ gas concentrations. By contrast, effusive eruptions were characterised by a significant rise in multiphase earthquakes correlating with SO₂ gas emissions, and fewer deep and shallow volcano-tectonic seismic events.

They further emphasised the significance of tiltmeter and EDM data for monitoring lava dome dynamics, and that of EDM slope distance for understanding eruption magnitude and variations thereof.

Studies of the physical environment and human context at Merapi, the sociological, economic and health impact as well as the effects of lahars, the most hazardous post-eruptive volcanic phenomenon at Merapi, also became popular over the last two decades (see Lavigne et al. 2023, Chap. 2; Thouret et al. 2023, Chap. 17). For instance, Donovan (2010) introduced the term ‘social volcanology’ to refer to the integration of social science research methods into the physical domain of volcanological research at Merapi (see Holmberg 2023, Chap. 3), exploring the influence of traditional cultural values and community reactions in relation to the 2006 volcanic crisis. Troll et al. (2015, 2021) argued that local folklore was used by earlier civilisations to describe and rationalise the complex interplay between geological processes such as volcanic activity and regional earthquakes at Merapi (Fig. 1.16), which may have not just influenced the 2006 eruption (see above) but similarly that in 2010 (Jousset et al. 2013) and conceivably earlier eruptions also, judging from accounts such as that of Wichmann (1918). In a study of the 2010 eruption, Mei et al. (2013) showed that the rapid onset, fast increase in intensity and unusually large size of the event posed major challenges for evacuations from the danger zone, which resulted in nearly 400,000 displaced people. While the evacuations were regarded as a success in terms of lives saved (e.g. Suroño et al. 2012), the need for continued hazard education and improved contingency planning using multiple eruption scenarios, and an adaptive governance system that strives to increase the capacity of institutions to coordinate relief operations, raise public awareness and implement risk reduction policies, were emphasised (Mei et al. 2013; Bakkour et al. 2015). Additionally, ancient legends have now also been successfully added to the hazard education at an increasing number of primary schools around Merapi, showing remarkable success in

hazard awareness and preparedness with students in these institutions (Atmojo et al. 2018). Moreover, the respiratory health hazard of ash emitted during the eruption was the focus of a study by Damby et al. (2013), who concluded that the health risk of inhaling volcanic ash was low for the general population. The greatest respiratory hazard was thought to be caused by the industrial scale mining of the volcanic deposits after the eruption, resulting in high occupational exposure to ash for sand miners (see Holmberg 2023, Chap. 3; Lavigne et al. 2023, Chap. 2; Subandriyo et al. 2023, Chap. 12). On the contrary, ash emissions during the 2010 eruption had a considerable impact on air traffic, with temporary closure of Adisucipto International Airport in Yogyakarta (Picquout et al. 2013). Given the large volume of pyroclastic material on the slopes of Merapi, post-eruptive lahars also posed a more severe hazard to the population compared to previous dome-forming eruptions. Both the number and frequency of lahar events during the 2010–2011 rainy season exceeded those of earlier eruptions, with lahar occurrences in almost all drainages reaching distances of more than 15 km from Merapi (de Bézilal et al. 2013). These recent efforts culminated in publication of the ‘Merapi Atlas’ published by Lavigne et al. (2015), which provides information about the volcano in an accessible format, ranging from the reconstruction of past eruptive activity and volcanic hazard assessment to the quantification of vulnerability and capacities. The atlas is targeted at a broad audience and thus provides a useful resource for planners and public officials involved in long-term development and risk assessment and crisis management at Merapi.

1.8 Volcano Monitoring at Merapi— A 100 Year History

Documented geological investigations and systematic volcano observation in Indonesia date back to the Dutch colonial era and began with the establishment of the ‘Dienst van het Mijnezuigen’ in 1850 and a ‘Commissie voor Vulkanologie’, which was established in the

Netherlands East Indies by the ‘Koninklijke Natuurkundige Vereeniging in Nederlandsch-Indië’ (KNV) in 1918 (Neumann van Padang 1960). After the catastrophic eruption of Kelud on 19–20 May 1919, KNV succeeded in urging the Netherlands East Indies government to establish a particular service for volcanic affairs, given the high frequency and effects of volcanic eruptions on the population. This led to the foundation of the ‘Vulkaanbewakingsdienst’ as part of the ‘Dienst van het Mijnwezen’ on 14 September 1920, the date that marks the beginning of institutional volcano surveillance in Indonesia. With a primary mission to seek all efforts and suggest ways to minimise the effects of volcanic eruptions, the task of the ‘Vulkaanbewakingsdienst’ was to investigate and monitor volcanoes, build volcano observation posts, determine dangerous areas, establish early warning and evacuation systems, and publish the scientific results obtained. In addition, it published guidelines about procedures for examining volcanoes, most of which are still relevant today. Following his work at Kelud, G.L.L. Kemmerling became the first head of the newly formed agency, which, in 1922, was renamed as ‘Vulkanologisch Onderzoek in Nederlandsch-Indië’. N.J.M. Taverne, head of the unit from 1922 to 1925, was aware of the importance of studying the nature of active volcanic eruptions and of understanding the signs that preceded an eruption as a basis for early warning. Accordingly, he carried out the first major aerial volcanic observation project in 1922–1924, which resulted in an unprecedented analysis of aerial photographs of Java’s active volcanoes. Kemmerling was reappointed as head of the ‘Vulkanologisch Onderzoek’ for the period from 1925–1926, and subsequently replaced by C.E. Stehn (1926–1940), M.E. Akkersdijk (1940–1941) and R.W. van Bemmelen (1941–1942). During the Japanese occupation (1942–1945), volcano surveillance was carried out by ‘Kazan Chosabu’, which operated under ‘Chishitsu Chōsajo’, a Japanese substitute for the ‘Dienst van het Mijnwezen’. If required, Dutch scientists such as van Bemmelen, were released from imprisonment to support Japanese experts and

carry out volcanological investigations, including, for example, observations of Merapi’s heightened activity in 1942 and 1943 (Fig. 1.10). After Indonesia’s declaration of independence in August 1945, the volcanological service operated under the Bureau of Mining and Geology and, in 1946, W.A. Petroeschevsky was appointed as its head until his departure in 1950. In 1952, the Bureau of Geology was formed and the volcanological service worked within this newly formed organisation. In 1976, the Sub-Directorate of Volcanology was formed, which, in 1978, became the Directorate of Volcanology, also known as the Volcanological Survey of Indonesia (VSI). In 2001, the Directorate of Volcanology became the Directorate of Volcanology and Geological Hazard Mitigation and then, in 2005, the Center for Volcanology and Geological Hazard Mitigation (CVHGM) under the Ministry of Energy and Mineral Resources. In 2020, the Volcanological Survey of Indonesia celebrated the 100th anniversary of volcano surveillance and monitoring in Indonesia. With its head office in Bandung, CVGHM currently employs 241 staff, of which 197 are volcano observers spread over 74 observation posts at 69 volcanoes. Volcano observers, who are primary residents, are on duty for 24 h a day, 7 days a week on a rotational basis. Their duties are to record and report on daily volcanic activity, oversee monitoring instruments, and assist local governments with ground truthed information for optimised management in case of volcanic crises.

Volcano observation, surveillance and monitoring at Merapi (Fig. 1.17) began soon after the launch of the ‘Vulkaanbewakingsdienst’, when the four volcano observation posts at Babadan, Maron, Ngepos, and Plawangan, and the subsidiary post at Krinjing were built on the slopes of the volcano between 1921 and 1942 (Fig. 1.18). Among these, the Maron post was destroyed during the 1930 eruption and replaced by the new post at Babadan. In 1954, two further observation posts were built in Jrahah and Selo, allowing now also to monitor the northern side of Merapi from the southern slopes of Merbabu volcano (Purbo-Hadiwidjojo 1961). Following

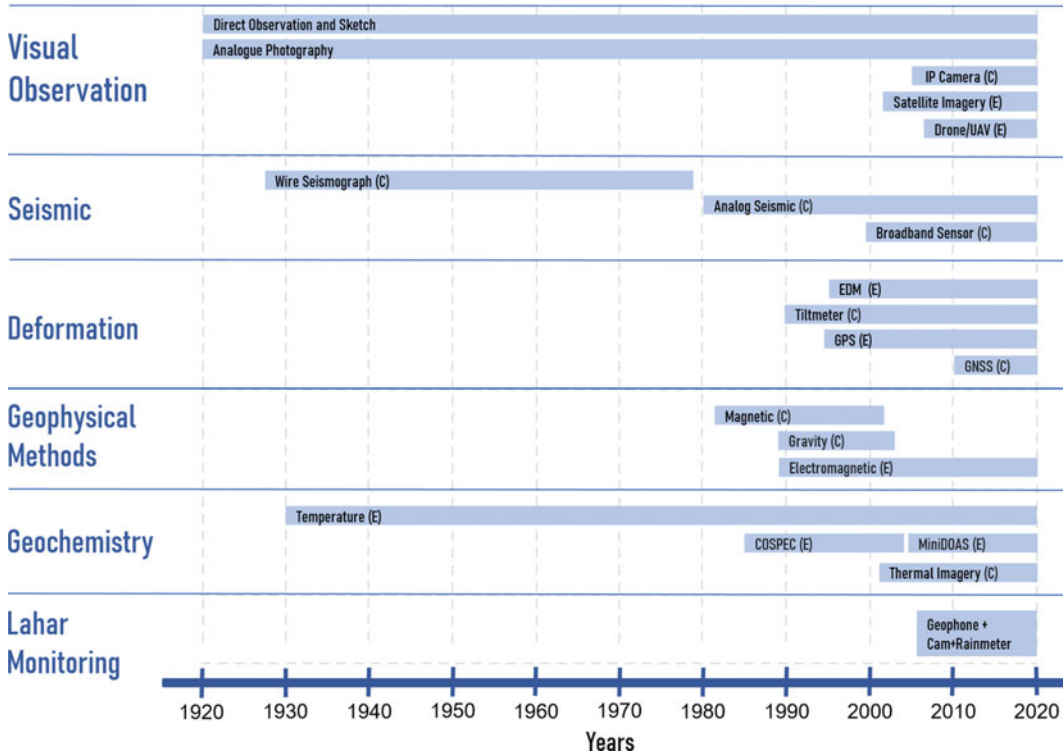


Fig. 1.17 Timeline of the development of the monitoring system at the Merapi Volcano Observatory from c. 1910 to the present. Since the early 1990s, there has been a rapid expansion of continuous (C) and episodic

(E) volcano monitoring at Merapi, culminating in the extraordinary success of forecasting and preventive measures in the run up to the 2010 eruption events

the 1994 eruption, the observation post on top of Gunung Plawangan was relocated to Kaliurang.

Additionally, a central office dedicated to Merapi volcano was created in Yogyakarta in 1945. In 1978, a volcano geochemistry and petrology laboratory was established, which was later renamed the ‘Merapi Monitoring Section’ or ‘Merapi Volcano Observatory’ (MVO). The duties of MVO were expanded in 1997, when it became a research centre for volcanoes called ‘Balai Penyelidikan dan Pengembangan Teknologi Kegunungapian’ (BPPTK) (English: Center for Research and Development of Volcano Technology). Since 2013, the unit is formally known as ‘Balai Penyelidikan dan Pengembangan Teknologi Kebencanaan Geologi’ (BPPTKG) (English: Center for Research and Development of Geological Disaster Technology) and the official technical implementing unit of CVGHM,

responsible for volcano monitoring and disaster mitigation. The unit currently employs 64 members of staff with its main headquarters in Yogyakarta.

The monitoring methods and techniques deployed at Merapi have evolved alongside scientific and technological advances. In the 1920s, the activities carried out consisted mainly of visual and morphological observations, meteorology, and in-situ gas and water sampling. Seismic monitoring at Merapi began with the installation of a Wiechert mechanical seismograph in 1924 that later helped Neumann van Padang to recognise the precursors of the November 1930 eruption (Ratdomopurbo 1995). A horizontal-component Omori seismograph was installed at the Maron observation post on Merapi’s southwest flank in 1927 but was destroyed during the 1930 eruptive events. Electromagnetic

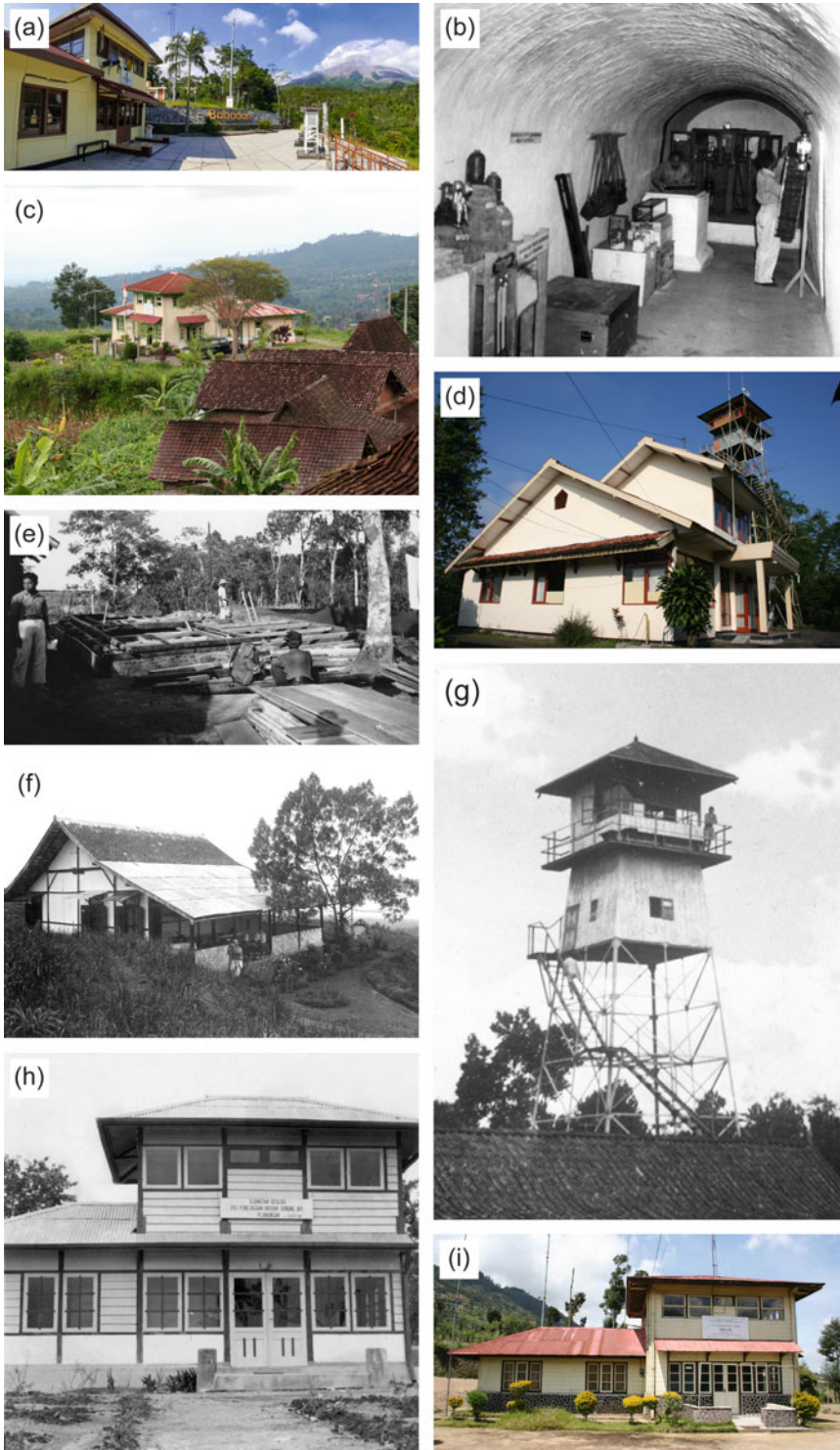


Fig. 1.18 Volcano observation posts at Merapi—past and present. **a** Babadan. **b** Escape tunnel at Babadan in 1955. **c** Jarakah. **d** Kaliurang. **e** Subsidiary post at Krinjing in 1935. **f** Maron (photograph from 1925). **g** Observation

tower at Ngepos in 1935. **h** Plawangan (photograph from 1954). **i** Selo. All photographs are from the BPPTKG (Geological Agency of Indonesia) archive

seismographs were temporarily installed in the 1960s. A classification scheme of seismic signals at Merapi was subsequently published by Shimozuru et al. (1969), who distinguished five distinct signal classes derived from a short-term seismological experiment in 1968. Real-time seismic monitoring, using radio transmission and allowing for precise hypocentre location, began in early 1982 in a collaboration between the Volcanological Survey of Indonesia and the United States Geological Survey (USGS). Seismic data recorded during the 1984 and later eruptions formed the basis for a new classification scheme for seismic signals at Merapi, consisting of volcano-tectonic, multiphase, low-frequency, tremor and rockfall types, as summarised in Ratdomopurbo (1995). Improvements of the seismic network and seismic survey campaigns were subsequently carried out in collaboration with French, German and American scientists, including the USGS Volcano Disaster Assistance Program (Fadeli 1992; Brodscholl et al. 2000; Hidayat et al. 2000; Voight et al. 2000a; Wassermann and Ohrnberger 2001).

In the late 1980s, routine deformation monitoring also began, using EDM measurements to detect ground displacement mechanisms both on the flanks and at the summit of Merapi. In the 1990s, a platform tiltmeter equipped with a telemetry system was implemented (Voight et al. 2000b; Young et al. 2000). Deformation monitoring using a Global Positioning System (GPS) monitoring network as well as gravity measurements began in the early 1990s and was used to monitor the evolution of surface displacements and modelling of the associated magmatic sources and flux (Beauducel and Cornet 1999; Beauducel et al. 2000; Jousset et al. 2000). Borehole tiltmeters, installed at 3–4 m depth, were first installed in 1995. These instruments have proved useful to minimise meteorological noise, particularly the influence of temperature variations (e.g. Rebscher et al. 2000), thus providing improved monitoring data for ongoing hazard assessment.

Detailed studies of sublimate and gas geochemistry of fumaroles were initiated by French scientists as early as the 1970s and are continued

to this day (e.g. Allard and Tazieff 1979; LeGuern and Bernard 1982; LeGuern et al. 1982; Symonds et al. 1987; Sayudi and Sulistiyo 1994; Sumarti and Suryono 1994; Allard et al. 1995; Troll et al. 2012; Nadeau et al. 2013a, b; Nadeau et al. 2023, Chap. 11). The routine measurement of SO₂ gas emissions began in the early 1990s, using a COSPEC instrument deployed from the Jrahah observation post located 6 km north of Merapi. Meanwhile, geochemical gas data, particularly H₂O and CO₂, were obtained from regular on-site sampling at the Gendol and Woro solfatara fields at the summit of Merapi until their destruction during the eruptions in 2006 and 2010. As a result, gas sampling by BPPTKG at present is conducted at a solfatara field located on the north-western slope of Merapi. CO₂ concentration and flux measurements were also carried during two inter-eruptive periods in 2002 and 2007 by Toutain et al. (2009), who related the spatial pattern of diffuse CO₂ degassing to the summit and wider edifice structure. They demonstrated that decreasing CO₂ concentrations are present with distance from the crater and that approximately 200–230 t day⁻¹ CO₂ degasses silently (diffusively) near the summit dome. A gas chromatograph for H₂O and CO₂, an alpha scintillation counter to measure ²²²Rn, and a temperature sensor ran successfully over several weeks in the high temperature fumaroles at Merapi's summit, documenting significant short-term variations in gas composition and temperature (Zimmer and Erzinger 2003). Several seismic events were found to correlate with fumarole temperature, an observation reported also by Richter et al. (2004), who linked the relation between the two parameters to magmatic degassing processes.

After the 2010 eruption, BPPTKG was forced to rebuild its monitoring network (see Budi-Santoso et al. 2023, Chap. 13). A significant increase in the scope of the monitoring system at Merapi was facilitated by dedicated national support and complemented by foreign cooperation with researchers from various countries conducting studies involving various disciplines and a variety of tested and novel methodologies. Current facilities and instruments include high-

sensitivity equipment consisting of 4 short period and 26 broadband seismometers, 10 Global Navigation Satellite Systems (GNSS), 13 electronic tiltmeters, 10 Ip cameras, and 1 thermal camera for temperature monitoring, some of which are installed in multi-parameter (GNSS, seismic, meteorological) volcano monitoring stations (Fig. 1.19a). In addition, a multi-gas instrument to monitor CO₂ emission and a Mini DOAS for SO₂ measurements (Fig. 1.17) complement routine manual gas sampling (Fig. 1.19b). Also, the use of unmanned aerial vehicles (UAVs) and LiDAR began to be implemented after 2010 for visual and deformation monitoring. Data from the field stations are sent to Yogyakarta in real-time using wireless transmission for further processing and analysis. Additional laboratories for petrology as well as for gas and water geochemistry are

available in the central office in Yogyakarta. Significant advances were made in the methods of data processing, which evolved from off-line data handling to online processing, analysis, and modelling. In 2013, the ‘WebObs’ modelling system was installed in collaboration with I.R.D France, which allows the real-time timeline of model changes from deformation, seismicity, or other monitoring data to be observed. In 2014, a system called ‘Support System for Decision Making’ (SSDM) began to be built in collaboration with Japanese scientists, which allows an assessment of volcanic hazards caused by eruptions. The output of this system is a map of hazards scenarios based on input monitoring data mainly from seismic energy. Meanwhile, in 2019 BPPTKG built its own Integrated Collaborative Work Management System, named ‘Cendana15’. This system includes, for example, a database, data visualisation, graphical displays, and network monitoring. Also, since 2014, the WOVODat platform (e.g. Newhall et al. 2017; Costa et al. 2019) has been installed at BPPTKG in collaboration with the Earth Observatory of Singapore.

Considering the developments over the last two decades, BPPTKG’s monitoring system is now at its most advanced in respect to monitoring in Java and the most modern one in all of Indonesia. At the same time, however, the vulnerability of the local population has increased due to increased agricultural use of the volcano’s flanks, higher levels of sand mining in the valleys, and through advancing urbanisation and technological developments. These aspects define Merapi as one of the most populated volcanoes with a Holocene record of $VEI \geq 4$ eruptions and Java as having among the highest volcano ‘Population Exposure Index’ in the world due to very high population densities in relatively close proximity to its active volcanoes (Brown et al. 2015). Therefore, continuous efforts by local authorities as well as national and international researchers will be required to keep the volcanic risk for people around Merapi as low as possible (Nandaka et al. 2023, Chap. 18). The aim to reduce the vulnerability of residents in the decades ahead will thus remain to be a challenge.

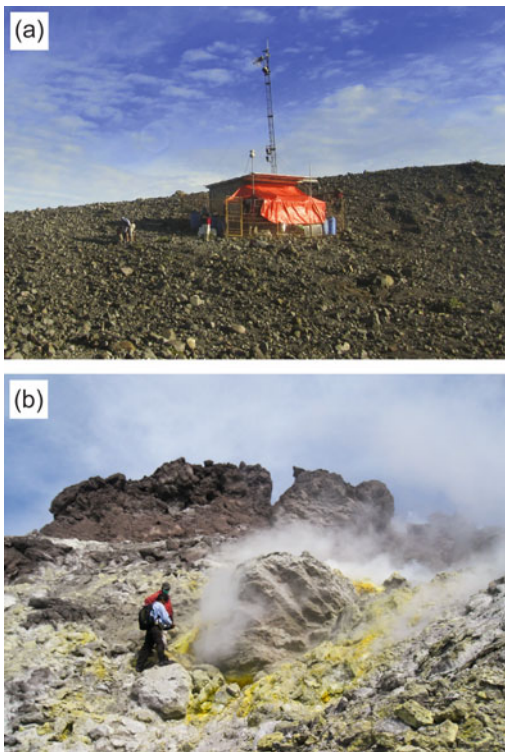


Fig. 1.19 **a** Multi-parameter (GNSS, seismic, meteorological) volcano monitoring station at the Pasarbubar crater near Merapi’s summit. **b** Gas sampling at the Woro fumarolic field at Merapi’s summit in 2007. Both photographs are from the BPPTKG (Geological Agency of Indonesia) archive

Acknowledgements We are grateful to the Center of Volcanology and Geological Hazard Mitigation (CVGHM) and BPPTKG (Balai Penyelidikan dan Pengembangan Teknologi Kebencanaan Geologi) for their support and for allowing us to use some of the historical photographs from the BPPTKG (Geological Agency of Indonesia) archive for this chapter.

References

- Abdurachman EK, Bourdier JL, Voight B (2000) Nuées ardentes of 22 November 1994 at Merapi volcano, Java, Indonesia. *J Volcanol Geotherm Res* 100:345–361
- Aisyah N, Iguchi M, Subandriyo BA, Hotta K, Sumarti S (2018) Combination of a pressure source and block movement for ground deformation analysis at Merapi volcano prior to the eruptions in 2006 and 2010. *J Volcanol Geotherm Res* 357:239–253
- Allard P, Carbonelle J, Dajlevic D, Metrich N, Sabroux J (1995) The volatile source and magma degassing budget of Merapi volcano: evidence from high-temperature gas emissions and crystal melt inclusions. *Merapi International Decade Volcano Workshop, UNESCO/Volcanological Survey of Indonesia, Yogyakarta*, pp 16–17
- Allard P, Tazieff H (1979) Phénoménologie et cartographie thermique des principales zones fumerolliennes du Mérapi (Indonésie). *C R Acad Sci Paris (sér D)* 288:747–750
- Andreastuti SD, Alloway BV, Smith IEM (2000) A detailed tephrostratigraphic framework at Merapi Volcano, Central Java, Indonesia: implications for eruption predictions and hazard assessment. *J Volcanol Geotherm Res* 100:51–67
- Andreastuti SD (1999) Stratigraphy and geochemistry of Merapi Volcano, Central Java, Indonesia: implication for assessment of volcanic hazards. Ph.D. Thesis, University of Auckland, Auckland, New Zealand
- Atmojo SE, Rusilowati A, Dwiningrum SIA, Skotnicka M (2018) The reconstruction of disaster knowledge through thematic learning of science, environment, technology and society integrated with local wisdom. *J Pendidik IPA Indon* 7:204–213
- Aubert M, Dana IIN, Gourgaud A (2000) Internal structure of the Merapi summit from self-potential measurements. *J Volcanol Geotherm Res* 100:337–343
- Bahar I (1984) Contribution à la connaissance du volcanisme indonésien: le Merapi (Centre Java); cadre structural, pétrologie, géochimie et implications volcanologiques. Ph.D. Thesis, Université des Sciences et Techniques du Languedoc, Montpellier, France
- Bakkour D, Enjolras G, Thouret JC, Kast R, MEI ETW, Prihatminingtyas B (2015) The adaptive governance of natural disaster systems: Insights from the 2010 mount Merapi eruption in Indonesia. *Intl J Disaster Risk Reduct* 13:167–188
- Bardintzeff JM (1984) Merapi Volcano (Java, Indonesia) and Merapi-type nuée ardente. *Bull Volcanol* 47:433–446
- Bastin J (2019) Sir Stamford Raffles and Some of His Friends and contemporaries: a memoir of the founder of Singapore. World Scientific Publishing Company Pte Limited, p 488
- Beauducel F, Cornet FH (1999) Collection and three-dimensional modeling of GPS and tilt data at Merapi volcano Java. *J Geophys Res Solid Earth* 104 (B1):725–736
- Beauducel F, Cornet F-H, Suhanto E, Duquesnoy T, Kasser M (2000) Constraints on magma flux from displacements data at Merapi volcano, Java Indonesia. *J Geophys Res Solid Earth* 105(B4):8193–8203
- van Bemmelen RW (1943) Merapi, no. 41. *Bull East Indian Volcan Survey* 95–98 (1941):69–78
- van Bemmelen RW (1949) The geology of Indonesia, Vol. 1A: General Geology. Government Printing Office, The Hague
- van Bemmelen RW (1956) The influence of geologic events on human history (an example from Central Java). *Verhand K Ned Geol Mijnbouw Genoot, Geol Serie*, pp 20–36
- Berthommier PC, Camus G (1991) Les éruptions historiques du Merapi (Centre Java, Indonésie). *Bull Sect Volcanol Soc Geol France* 23:1–11
- Berthommier PC, Camus G, Condomines M, Vincent PM (1990) Le Merapi (Centre Java): éléments de chronologie d'un strato-volcan andésitique. *C R Acad Sci Paris* 311:213–218
- Berthommier PC (1990) Etude volcanologique du Merapi (Centre-Java). Téphrostratigraphie et chronologie – produits éruptifs. Ph.D. Thesis, Université Blaise Pascal, Clermont-Ferrand, France
- Bignami C, Ruch J, Chini M, Neri M, Buongiorno MF, Hidayati S, Sayudi DS, Surono (2013) Pyroclastic density current volume estimation after the 2010 Merapi volcano eruption using X-band SAR. *J Volcanol Geotherm Res* 261:236–243
- Blythe LS, Deegan FM, Freda C, Jolis EM, Masotta M, Misiti V, Taddeucci J, Troll VR (2015) CO₂ bubble generation and migration during magma–carbonate interaction. *Contrib Mineral Petrol* 169:42
- van Boekhold F (1792) Relaa van een togt na den brandende berg, op Java. *Batavia Genoot Kunsten Wet*, pp 8–12
- Borisova AY, Martel C, Gouy S, Pratomo I, Sumarti S, Toutain J-P, Bindeman IN, de Parseval P, Metaxian J-P, Surono (2013) Highly explosive 2010 Merapi eruption: evidence for shallow-level crustal assimilation and hybrid fluid. *J Volcanol Geotherm Res* 261:193–208
- Borisova AY, Gurenko AA, Martel C, Kouzmanov K, Cathala A, Bohrson WA, Pratomo I, Sumarti S (2016) Oxygen isotope heterogeneity of arc magma recorded in plagioclase from the 2010 Merapi eruption (Central Java, Indonesia). *Geochim Cosmochim Acta* 190: 13–34

- Bosma U (2016) Franz Junghuhn's three-dimensional and transcendental Java. In: Arnez M, Sarnowsky J (eds) The role of religions in the European perception of insular and Mainland Southeast Asia: travel accounts of the 16th to the 21st century. Cambridge Scholars Publishing, pp 175–206
- Boudon G, Camus G, Gourgaud A, Lajoie J (1993) The 1984 nuée ardente deposits of Merapi volcano, Central Java, Indonesia: stratigraphy, textural characteristics, and transport mechanisms. *Bull Volcanol* 55:327–342
- Bourdier JL, Abdurachman EK (2001) Decoupling of small-volume pyroclastic flows and related hazards at Merapi volcano, Indonesia. *Bull Volcanol* 63:309–325
- Branney MJ, Kokelaar P (2002) Pyroclastic density currents and the sedimentation of ignimbrites. *Geol Soc Lond Memoirs* 27:143
- Brodtscholl A, Kirbani SB, Voight B (2000) Sequential dome-collapse nuées ardentes analyzed from broadband seismic data, Merapi Volcano, Indonesia. *J Volcanol Geotherm Res* 100:363–369
- Bronto S, Ratdomopurbo A, Asmoro P, Adityarani M (2014) Longoran rakasa Gunung Api Merapi Yogyakarta—Jawa Tengah (Gigantic landslides of Merapi volcano, Yogyakarta—Central Java). *J Geol Sumb Min* 15:165–183
- Bronto S, Rahardjo W, Asmoro P, Ratdomopurbo A, Adityarani M, Permatasari A (2023) The Gordean debris avalanche deposit from a sector collapse of Merapi volcano. In: Gertisser R, Troll VR, Walter TR, Nandaka IGMA, Ratdomopurbo A (eds) Merapi volcano—geology, eruptive activity, and monitoring of a high-risk volcano. Springer, Berlin, Heidelberg, pp 195–231
- Brouwer HA (1928a) Alkaline rocks of the volcano Merapi (Java) and the origin of these rocks. *Proc K Ned Akad Wet* 31:492–498
- Brouwer HA (1928b) Production of trachyte and phonolite from pyroxene andesitic magma associated with limestone. *J Geol* 36:545–548
- Brown SK, Auker MR, Sparks RSJ (2015) Populations around Holocene volcanoes and development of a population exposure index. In: Loughlin SC, Sparks RSJ, Brown SK, Jenkins SF, Vye-Brown C (eds) Global Volcanic hazards and risk. Cambridge University Press, Cambridge, pp 223–232
- Budi-Santoso A, Lesage P, Dwiyono S, Sumarti S, Subandriyo S, Jousset P, Metaxian J-P (2013) Analysis of the seismic activity associated with the 2010 eruption of Merapi Volcano, Java. *J Volcanol Geotherm Res* 261:153–170
- Budi-Santoso A, Beaucecel F, Nandaka IGMA, Humaida H, Costa F, Widiwijayanti C, Iguchi M, Métaxian J-P, Rudianto I, Rozin M, Sulistiyani, Nurdin I, Kelfoun K, Byrdina S, Pinel V, Fahmi AA, Laurin A, Rizal MH, Dahamna N (2023) The Merapi volcano monitoring system. In: Gertisser R, Troll VR, Walter TR, Nandaka IGMA, Ratdomopurbo A (eds) Merapi volcano—geology, eruptive activity, and monitoring of a high-risk volcano. Springer, Berlin, Heidelberg, pp 409–436
- Camus G, Gourgaud A, Mossand-Berthommier P-C, Vincent PM (2000) Merapi (Central Java, Indonesia): an outline of the structural and magmatological evolution, with a special emphasis to the major pyroclastic events. *J Volcanol Geotherm Res* 100:139–163
- Carr BB, Clarke AB, de' Michieli Vitturi M (2020) Volcanic conduit controls on effusive-explosive transitions and the 2010 eruption of Merapi Volcano (Indonesia). *J Volcanol Geotherm Res* 392:106767
- Chadwick JP, Troll VR, Ginibre C, Morgan D, Gertisser R, Waight TE, Davidson JP (2007) Carbonate assimilation at Merapi Volcano, Java, Indonesia: insights from crystal isotope stratigraphy. *J Petrol* 48:1793–1812
- Chadwick JP, Troll VR, Waight TE, van der Zwan FM, Schwarzkopf LM (2013) Petrology and geochemistry of igneous inclusions in recent Merapi deposits: a window into the sub-volcanic plumbing system. *Contrib Mineral Petrol* 165:259–282
- Charbonnier S, Gertisser R (2008) Field observations and surface characteristics of pristine block-and-ash flow deposits from the 2006 eruption of Merapi Volcano, Java, Indonesia. *J Volcanol Geotherm Res* 177:971–982
- Charbonnier S, Gertisser R (2009) Numerical simulations of block-and-ash flows using the TITAN2D flow model: examples from Merapi Volcano, Indonesia. *Bull Volcanol* 71:953–959
- Charbonnier S, Gertisser R (2011) Deposit architecture and dynamics of the 2006 block-and-ash flows of Merapi Volcano, Java, Indonesia. *Sedimentology* 58:1573–1612
- Charbonnier S, Gertisser R (2012) Evaluation of geophysical mass flow models using the 2006 block-and-ash flows of Merapi Volcano, Java, Indonesia: towards a short-term hazard assessment tool. *J Volcanol Geotherm Res* 231–232:87–108
- Charbonnier SJ, Germa A, Connor CB, Gertisser R, Preece K, Komorowski J-C, Lavigne F, Dixon T, Connor L (2013) Evaluation of the impact of the 2010 pyroclastic density currents at Merapi volcano from high-resolution satellite imagery, field investigations and numerical simulations. *J Volcanol Geotherm Res* 261:295–315
- Charbonnier SJ, Kelfoun K, Widiwijayanti C, Sayudi, DS, Putra R (2023) Assessing the pyroclastic density current hazards at Merapi: From field data to numerical simulations and hazard maps. In: Gertisser R, Troll VR, Walter TR, Nandaka IGMA, Ratdomopurbo A (eds) Merapi volcano—geology, eruptive activity, and monitoring of a high-risk volcano. Springer, Berlin, Heidelberg, pp 473–500
- Clarke AB, Voight B (2000) Pyroclastic current dynamic pressure from aerodynamics of tree or pole blow-down. *J Volcanol Geotherm Res* 100:395–412
- Clocchiatti R, Joron JL, Kerinec F, Treuil M (1982) Quelques données préliminaires sur la lave du dôme actuel du volcan Mérapî (Java, Indonésie) et sur ses enclaves. *CR Acad Sci Paris* 295:817–822
- Condomines M, Gauthier PJ, Tanguy JC, Gertisser R, Thouret JC, Berthommier P, Camus G (2005) ^{226}Ra or

- ²²⁶Ra/Ba dating of Holocene volcanic rocks: application to Mt. Etna and Merapi volcanoes. *Earth Planet Sci Lett* 230:289–300
- Costa F, Andreastuti S, Bouvet de Maisonneuve C, Pallister JS (2013) Petrological insights into the storage conditions, and magmatic processes that yielded the centennial 2010 Merapi explosive eruption. *J Volcanol Geotherm Res* 261:209–235
- Costa F, Widiwijayanti C, Nang TZW, Fajiculy E, Espinosa-Ortega T, Newhall C (2019) WOVodat—the global volcano unrest database aimed at improving eruption forecasts. *Disaster Prev Manag* 28:738–751
- Crawford J (1820) *History of the Indian archipelago: containing an account of the manners, art, languages, religions, institutions, and commerce of its inhabitants*. 3 volumes (with maps and engravings). A Constable and Co, Edinburgh
- Cronin SJ, Lube G, Dayudi DS, Sumarti S, Subrandiyo S, Surono (2013) Insights into the October–November 2010 Gunung Merapi eruption (Central Java, Indonesia) from the stratigraphy, volume and characteristics of its pyroclastic deposits. *J Volcanol Geotherm Res* 261:244–259
- CVGHM (Center of Volcanology and Geological Hazard Mitigation) (2002) *Merapi Volcano Hazard Map*. Bandung
- CVGHM (Center of Volcanology and Geological Hazard Mitigation) (2011) *Revised Merapi Volcano Hazard Map*. Bandung
- Damby DE, Horwell CJ, Baxter PJ, Delmelle P, Donaldson K, Dunster C, Fubini B, Murphy FA, Natrass C, Sweeney S, Tetley TD, Tomatis M (2013) The respiratory health hazard of tephra from the 2010 Centennial eruption of Merapi with implications for occupational mining of deposits. *J Volcanol Geotherm Res* 261:376–387
- Darmawan H, Walter TR, Brotopuspito KS, Subandriyo NIGMA (2018a) Morphological and structural changes at the Merapi lava dome monitored in 2012–15 using unmanned aerial vehicles (UAVs). *J Volcanol Geotherm Res* 349:256–267
- Darmawan H, Walter TR, Troll VR, Budi-Santoso A (2018b) Structural weakening of the Merapi dome identified by drone photogrammetry after the 2010 eruption. *Nat Hazards Earth Syst Sci* 18:3267–3281
- Darmawan H, Yuliantoro P, Rakhman A, Budi Santoso A, Humaida H, Suryanto W (2020) Dynamic velocity and seismic characteristics of gravitational rockfalls at the Merapi lava dome. *J Volcanol Geotherm Res* 404:107010
- Darmawan H, Putra R, Budi-Santoso A, Humaida H, Walter TR (2023) Morphology and instability of the Merapi lava dome monitored by unoccupied aircraft systems. In: Gertisser R, Troll VR, Walter TR, Nandaka IGMA, Ratdomopurbo A (eds) *Merapi volcano—geology, eruptive activity, and monitoring of a high-risk volcano*. Springer, Berlin, Heidelberg, pp 457–472
- de Bézal E, Lavigne F, Hadmoko DS, Degeai J-P, Gilang Dipayana A, Mutaqin BW, Marfai MA, Coquet M, Le Mauff B, Robin A-K, Vidal C, Cholik N, Aisyah N (2013) Rain-triggered lahars following the 2010 eruption of Merapi volcano, Indonesia: a major risk. *J Volcanol Geotherm Res* 261:330–347
- Debaille V, Doucelance R, Weis D, Schiano P (2006) Multi-stage mixing in subduction zones: application to Merapi volcano (Java island, Sunda arc). *Geochim Cosmochim Acta* 70:723–741
- Deegan FM, Troll VR, Freda C, Misiti V, Chadwick JP, McLeod CL, Davidson JP (2010) Magma-carbonate interaction processes and associated CO₂ release at Merapi volcano, Indonesia: insights from experimental petrology. *J Petrol* 51:1027–1051
- Deegan FM, Whitehouse MJ, Troll VR, Budd DA, Harris C, Geiger H, Hålenius U (2016a) Pyroxene standards for SIMS oxygen isotope analysis and their application to Merapi volcano, Sunda arc, Indonesia. *Chem Geol* 447:1–10
- Deegan FM, Troll VR, Whitehouse MJ, Jolis EM, Freda C (2016b) Boron isotope fractionation in magma via crustal carbonate dissolution. *Sci Rep* 6:30774
- Deegan FM, Whitehouse MJ, Troll VR, Geiger H, Jeon H, le Roux P, Harris P, van Helden M, González-Maurel O (2021) Sunda arc mantle source $\delta^{18}\text{O}$ value revealed by intracrystal isotope analysis. *Nat Commun* 12:3930
- Deegan FM, Troll VR, Gertisser R, Freda C (2023) Magma-carbonate interaction at Merapi volcano, Indonesia. In: Gertisser R, Troll VR, Walter TR, Nandaka IGMA, Ratdomopurbo A (eds) *Merapi volcano—geology, eruptive activity, and monitoring of a high-risk volcano*. Springer, Berlin, Heidelberg, pp 291–321
- Djumarma A, Bronto S, Bahar I, Suparban F, Sukhyar R, Newhall C, Holcomb RT, Banks NG, Torley R, Lockwood JP, Tilling RI, Rubin M, Del Marmol MA (1986) Did Merapi volcano (Central Java) erupt catastrophically in 1006 A.D.? Abstract, IAVCEI Intern Volcanol Congr 1986, Rotorua, New Zealand
- Donoghue E, Troll VR, Schwarzkopf LM, Clayton G, Goodhue R (2008) Organic block coatings in block-and-ash flow deposits at Merapi Volcano, central Java. *Geol Mag* 146:113–120
- Donovan K (2010) Doing social volcanology: exploring volcanic culture in Indonesia. *Area* 42:117–126
- Drignon MJ, Bechon T, Arbaret L, Burgisser A, Komorowski J-C, Martel C, Yaputra R (2016) Preexplosive conduit conditions during the 2010 eruption of Merapi volcano (Java, Indonesia). *Geophys Res Lett* 43:11595–11602
- Erdmann S, Martel C, Pichavant M, Kushnir A (2014) Amphibole as an archivist of magmatic crystallization conditions: problems, potential, and implications for inferring magma storage prior to the paroxysmal 2010 eruption of Mount Merapi Indonesia. *Contrib Mineral Petrol* 167:1016
- Erdmann S, Martel C, Pichavant M, Bourdier J-L, Champallier R, Komorowski J-C, Cholik N (2016) Constraints from phase equilibrium experiments on pre-eruptive storage conditions in mixed magma systems: a

- case study on crystal-rich Basaltic Andesites from Mount Merapi, Indonesia. *J Petrol* 57:535–560
- Escher BG (1933b) On a classification of central eruptions according to gas pressure of the magma and viscosity of the lava. *Leidsche Geol Med* 6:45–49
- Escher BG (1931) Over het vulkanisme van Java in verband met de uitbarsting van den Merapi. *De Ingenieur*, 11 Sept. 1931, 46e Jaarg., No. 37, blz. A. 357—A. 369
- Escher BG (1933a). On the character of the Merapi eruption in central Java. *Leidsche Geol Med* 6:51–58 (and 2 plates)
- Fadeli A (1992) Volcanic Earthquakes at Merapi (Central Java) During the Lava Dome Building Beginning in October 1986. In: Gasparini P, Scarpa R, Aki K (eds) *Volcanic seismology*. IAVCEI proceedings in volcanology, vol 3. Springer, Berlin, Heidelberg, pp 62–73
- Gauthier PJ, Condomines M (1999) ^{210}Pb - ^{226}Ra radioactive disequilibria in recent lavas and radon degassing: inferences on the magma chamber dynamics at Stromboli and Merapi volcanoes. *Earth Planet Sci Lett* 172:111–126
- Genereau K, Cronin SJ, Lube G (2015) Effects of volatile behaviour on dome collapse and resultant pyroclastic surge dynamics: Gunung Merapi 2010 eruption. *Geol Soc Lond Spec Publ* 410:199–218
- Gertisser R, Keller J (2003a) Temporal variations in magma composition at Merapi Volcano (Central Java, Indonesia): magmatic cycles during the past 2,000 years of explosive activity. *J Volcanol Geotherm Res* 123:1–23
- Gertisser R, Keller J (2003b) Trace element and Sr, Nd, Pb and O isotope variations in medium-K and high-K volcanic rocks from Merapi Volcano, Central Java, Indonesia: evidence for the involvement of subducted sediments in Sunda Arc magma genesis. *J Petrol* 44:457–486
- Gertisser R, Charbonnier SJ, Troll VR, Keller J, Preece K, Chadwick JP, Barclay J, Herd RA (2011) Merapi (Java, Indonesia): anatomy of a killer volcano. *Geol Today* 27:57–62
- Gertisser R, Cassidy NJ, Charbonnier SJ, Nuzzo L, Preece K (2012a) Overbank block-and-ash flow deposits and the impact of valley-derived, unconfined flows on populated areas at Merapi volcano, Java, Indonesia. *Nat Hazards* 60:623–648
- Gertisser R, Charbonnier SJ, Keller J, Quidelleur X (2012b) The geological evolution of Merapi volcano, Central Java, Indonesia. *Bull Volcanol* 74:1213–1233
- Gertisser R, del Marmol M-A, Newhall C, Preece K, Charbonnier S, Andreastuti S, Handley H, Keller J (2023) Geological history, chronology and magmatic evolution of Merapi. In: Gertisser R, Troll VR, Walter TR, Nandaka IGMA, Ratdomopurbo A (eds) *Merapi volcano—geology, eruptive activity, and monitoring of a high-risk volcano*. Springer, Berlin, Heidelberg, pp 137–193
- Gertisser R (2001) Gunung Merapi (Java, Indonesien): eruptionsgeschichte und magmatische evolution eines hochrisiko-vulkans. Ph.D. Thesis, Albert-Ludwigs-Universität Freiburg, Freiburg, Germany
- Global Volcanism Program (2013) *Volcanoes of the World*, v 4.9.4 (17 Mar 2021) Venzke E (ed) Smithsonian Institution. Downloaded 27 Apr 2021. <https://doi.org/10.5479/si.GVP.VOTW4-2013>
- Gomez C, Lavigne F, Lespinasse N, Hadmoko DS, Wassmer P (2008) Longitudinal structure of pyroclastic-flow deposits, revealed by GPR survey, at Merapi volcano, Java, Indonesia. *J Volcanol Geotherm Res* 176:439–447
- Gomez C, Lavigne F, Hadmoko DS, Lespinasse N, Wassmer P (2009) Block-and-ash flow deposition: a conceptual model from a GPR survey on pyroclastic-flow deposits at Merapi Volcano, Indonesia. *Geomorphology* 110:118–127
- Gomez C, Janin M, Lavigne F, Gertisser R, Charbonnier S, Lahitte P, Hadmoko SR, Fort M, Wassmer P, Degroot V, Murwanto H (2010) Borobudur, a basin under volcanic influence: 361,000 years BP to present. *J Volcanol Geotherm Res* 196:245–264
- Grandjean JB (1931a) Korte mededeeling over de uitbarsting van den Merapi op 18 December 1930. *De Mijningingenieur* 12(1):4–6
- Grandjean JB (1931b) De uitbarsting van den Merapi in 1930. *De Mijningingenieur* 12(4):47
- Grandjean JB (1931c) Bijdrage tot de kennis der Gloedwolken van den Merapi van Midden-Java. *De Mijningingenieur* 12(12):20–25
- Hammer JE, Cashman KV, Voight B (2000) Magmatic processes revealed by textural and compositional trends in Merapi dome lavas. *J Volcanol Geotherm Res* 100:165–192
- Handley HK, Turner SP, Macpherson CG, Gertisser R, Davidson JP (2011) Hf-Nd isotope and trace element constraints on subduction inputs at island arcs: limitations of Hf anomalies as sediment input indicators. *Earth Planet Sci Lett* 304:212–223
- Handley HK, Blichert-Toft J, Gertisser R, Macpherson CG, Turner SP, Zaennudin A, Abdurrachman M (2014) Insights from Pb and O isotopes into along-arc variations in subduction inputs and crustal assimilation for volcanic rocks in Java, Sunda arc, Indonesia. *Geochim Cosmochim Acta* 139:205–226
- Handley HK, Reagan M, Gertisser R, Preece K, Berlo K, McGee LE, Barclay J, Herd R (2018) Timescales of magma ascent and degassing and the role of crustal assimilation at Merapi volcano (2006–2010), Indonesia: constraints from uranium-series and radiogenic isotopic compositions. *Geochim Cosmochim Acta* 222:34–52
- Harijoko A, Marliyani GI, Wibowo HE, Freski YR, Handini E (2023) The geodynamic setting and geological context of Merapi volcano in Central Java, Indonesia. In: Gertisser R, Troll VR, Walter TR, Nandaka IGMA, Ratdomopurbo A (eds) *Merapi volcano—geology, eruptive activity, and monitoring of a high-risk volcano*. Springer, Berlin, Heidelberg, pp 89–109
- Harris AJL, Ripepe M (2007) Regional earthquake as a trigger for enhanced volcanic activity: Evidence from MODIS thermal data. *Geophys Res Lett* 34: L02304

- Hartmann M (1933) Bijdrage tot de kennis van gassen, sublimatie- en inkrustatieproducten en thermale wateren in de Merapiladoes. *Vulkanol Seismol Med* 12:1–135
- Hartmann M (1934a) Der grosse Ausbruch des Vulkanes G. Merapi (Mittel Java) im Jahre 1872. *Natuurk Tijdschr Nederl-Indië* 94:189–209
- Hartmann M (1934b) Die vulkanische Tätigkeit des Merapi Vulkanes (Mittel Java) in seinem östlichen Gipfelgebiete zwischen 1902 und 1908. *De Ing Nederl-Indië* 5:61–73
- Hartmann M (1935a) Die Ausbrüche des G. Merapi (Mittel-Java) bis zum Jahre 1883. *Neues Jahrb Mineral Geol Paläontol* 75:127–162
- Hartmann M (1935b) Die große Ausbruchperiode des Merapi im 2. Halbjahr 1934. *Zeitschr Vulkanol* 16:199–205
- Hartmann M (1936) Die Lavadomgebilde des Merapi (M.J.) nach dem grossen Ausbruch im Jahre 1930. *Zeitschr Vulkanol* 16:248–258
- Heap MJ, Troll V, Kushnir ARL, Gilg H, Collinson A, Deegan F, Darmawan H, Seraphine N, Neuberg J, Walter T (2019) Hydrothermal alteration of andesitic lava domes can lead to explosive volcanic behaviour. *Nat Commun* 10:5063
- Hidayat D, Voight B, Langston C, Ratdomopurbo A, Ebeling C (2000) Broadband seismic experiment at Merapi Volcano, Java, Indonesia: very-long-period pulses embedded in multiphase earthquakes. *J Volcanol Geotherm Res* 100:215–231
- Holmberg K (2023) Merapi and its dynamic ‘disaster culture’. In: Gertisser R, Troll VR, Walter TR, Nandaka IGMA, Ratdomopurbo A (eds) *Merapi volcano—geology, eruptive activity, and monitoring of a high-risk volcano*. Springer, Berlin, Heidelberg, pp 67–87
- Horsfield T (1812) Mineralogical sketch of the island of Java
- Horsfield T (1816a) On the mineralogy of Java—essay I. Hubbard AH, pp 141–173
- Horsfield T (1816b) Essay on the geography, mineralogy and botany of the western portion of the Territory of the native princes of Java. *Batavian Society of Arts and Sciences*, pp 1–183
- Ijzerman JW (1891) *Beschrijving der oudheden nabij de grens de Residentie’s Soerakarta en Djogdjakarta*. Batavia: Landsdrukkerij; ‘s Gravenhage: M. Nijhoff, 135 p
- Innocenti S, Andreastuti S, Furman T, del Marmol M-A, Voight B (2013a) The pre-eruption conditions for explosive eruptions at Merapi volcano as revealed by crystal texture and mineralogy. *J Volcanol Geotherm Res* 261:69–86
- Innocenti S, del Marmol M-A, Voight B, Andreastuti S, Furman T (2013b) Textural and mineral chemistry constraints on evolution of Merapi volcano, Indonesia. *J Volcanol Geotherm Res* 261:20–37
- Itoh H, Takahama J, Takahashi M, Miyamoto K (2000) Hazard estimation of the possible pyroclastic flow disasters using numerical simulation related to the 1994 activity at Merapi Volcano. *J Volcanol Geotherm Res* 100:503–516
- Jenkins S, Komorowski J-C, Baxter PJ, Spence R, Picquout A, Lavigne F, Suroño (2013) The Merapi 2010 eruption: An interdisciplinary impact assessment methodology for studying pyroclastic density current dynamics. *J Volcanol Geotherm Res* 261:316–329
- Jousset P, Dwipa S, Beauducel F, Duquesnoy T, Diamant M (2000) Temporal gravity at Merapi during the 1993–1995 crisis: an insight into the dynamical behaviour of volcanoes. *J Volcanol Geotherm Res* 100:289–320
- Jousset P, Budi-Santoso A, Jolly AD, Boichu M, Suroño DS, Sumarti S, Hidayati S, Thierry P (2013) Signs of magma ascent in LP and VLP seismic events and link to degassing: An example from the 2010 explosive eruption at Merapi volcano, Indonesia. *J Volcanol Geotherm Res* 261:171–192
- Junghuhn FW (1856) *Java-Album: landschaftsansichten von Java*. Arnoldische Buchhandlung, Leipzig, p 24
- Junghuhn F (1845) *Topographische und naturwissenschaftliche Reisen durch Java*. Verlag: E. Baensch, Magdeburg. 518 pages, 1 atlas (40 plates and maps)
- Junghuhn F (1850–1853) *Java, deszelfs gedaante, bekleeding en inwendige structuur* (3 volumes and atlas). PN van Kampen, Amsterdam
- Junghuhn F (1853–1854) *Java, zijne gedaante, zijn plantentooi en inwendige bouw* (4 volumes and atlas). CW Mieling, ‘s-Gravenhage [expanded edition of Junghuhn (1850–1853)]
- Junghuhn F (1855) *Kaart van het eiland Java*. CW Mieling, ‘s-Gravenhage
- Junghuhn F (1857) *Java, seine Gestalt, Pflanzendecke und innere Bauart*. Von Franz Junghuhn. Nach der zweiten verbesserten Auflage des holländischen Originals in’s Deutsche übertragen von J.K. Hasskarl. Arnoldische Buchhandlung, Leipzig
- Kelfoun K (2017) A two-layer depth-averaged model for both the dilute and the concentrated parts of pyroclastic currents. *J Geophys Res Solid Earth* 122:4293–4311
- Kelfoun K, Legros F, Gourgaud A (2000) A statistical study of trees damaged by the 22 November 1994 eruption of Merapi volcano (Java, Indonesia): relationships between ash-cloud surges and block-and-ash flows. *J Volcanol Geotherm Res* 100:379–393
- Kelfoun K, Gueugneau V, Komorowski J-C, Aisyah N, Cholik N, Merciecca C (2017) Simulation of block-and-ash flows and ash-cloud surges of the 2010 eruption of Merapi volcano with a two-layer model. *J Geophys Res Solid Earth* 122:4277–4292
- Kelfoun K, Budi-Santoso A, Latchimy T, Bontemps M, Nurdien I, Beauducel F, Fahmi A, Putra R, Dahamna N, Laurin A, Rizal MH, Sukmana JT, Gueugneau V (2021) Growth and collapse of the 2018–2019 lava dome of Merapi volcano. *Bull Volcanol* 83:8
- Kemmerling GLL (1921) *De hernieuwde werking van den vulkan G. Merapi (Midden Java) van den begin Augustus 1920 tot en met einde Februari 1921*. *Vulkanol Seismol Med* 3:1–30

- Kemmerling GLL (1932) De controverse uitgesloten gloedwolken (nuées ardentes d'explosion dirigée) of lawinen-gloedwolken (nuées ardentes d'avalanche). *De Ingenieur* 47:129–137
- Kemmerling GLL (1930) Beschouwingen over de hernieuwde werking van den Merapi der Vorstenlanden van December 1930. *Tijdschr. Kon. Ned. Aardrijkskundig Gen., 2e Serie, deel XLVIII, Afl. 4, Juli 1931, blz. 712–743*
- Kerinec F (1982) Le Merapi, volcan actif d'arc insulaire (Java): Petrographie et geochemie de matériaux solides; implications geotectoniques. Ph.D. Thesis (Thèse de Troisième Cycle), Université Paris-Sud, Orsay, France
- Komorowski J-C, Jenkins S, Baxter PJ, Picquout A, Lavigne F, Charbonnier S, Gertisser R, Preece K, Cholik N, Budi-Santoso A, Surono (2013) Paroxysmal dome explosion during the Merapi 2010 eruption: processes and facies relationships of associated high-energy pyroclastic density currents. *J Volcanol Geotherm Res* 261:260–294
- Koulakov I, Bohm M, Asch G, Lühr B-G, Manzanares A, Brotopuspito KS, Fauzi P, Purbawinata MA, Puspito NT, Ratdomopurbo A, Kopp H, Rabbel W, Shevkunova E (2007) P and S velocity structure of the crust and the upper mantle beneath central Java from local tomography inversion. *J Geophys Res* 112:B08310
- Koulakov I, Maksotova G, Jaxybulatov K, Kasatkina E, Shapiro NM, Luehr B-G, El Khrepy S, Al-Arifi N (2016) Structure of magma reservoirs beneath Merapi and surrounding volcanic centers of Central Java modeled from ambient noise tomography. *Geochem Geophys Geosyst* 17:4195–4211
- Kubaneck J, Westerhaus M, Schenk A, Aisyah N, Brotopuspito KS, Heck B (2015) Volumetric change quantification of the 2010 Merapi eruption using TanDEM-X InSAR. *Remote Sens Environ* 164:16–25
- Kushnir ARL, Martel C, Bourdier J-L, Heap M, Reuschlé T, Erdmann S, Komorowski J-C, Cholik N (2016) Probing permeability and microstructure: Unravelling the role of a low-permeability dome on the explosivity of Merapi (Indonesia). *J Volcanol Geotherm Res* 316:56–71
- Kushnir ARL, Martel C, Champallier R, Wadsworth FB (2017) Permeability evolution in variably glassy basaltic andesites measured under magmatic conditions. *Geophys Res Lett* 44:10262–10271
- Kusumadinata K (1979) Data Dasar Gunungapi Indonesia. *Volcanological survey of Indonesia*, Bandung, pp 250–280
- Kusumayudha SB, Murwanto H, Sutarto, Choiriyah SU (2019) Volcanic disaster and the decline of Mataram kingdom in the Central Java, Indonesia. In: Wasowski J, Dijkstra T (eds) *Recent research on engineering geology and geological engineering*. GeoMEast 2018. Sustainable Civil Infrastructures. Springer, Cham, pp 83–93
- Lacroix A (1930) Remarques sur les matériaux de projection des volcans et sur la genèse des roches pyroclastiques qu'ils constituent. *Livre Jubilaire Soc. Géol. De France 1830–1930. Tome II:431–472*
- Lacroix A (1904) *La Montagne Pelée et ses éruptions*. Paris, p 662
- Lavigne F, Thouret JC, Voight B, Suwa H, Sumaryono A (2000a) Lahars at Merapi volcano, Central Java: an overview. *J Volcanol Geotherm Res* 100:423–456
- Lavigne F, Thouret J-C, Voight B, Young K, LaHusen R, Marso J, Suwa H, Sumaryono A, Sayudi DS, Dejean M (2000b) Instrumental lahar monitoring at Merapi Volcano, Central Java, Indonesia. *J Volcanol Geotherm Res* 100:457–478
- Lavigne F, Morin J, Surono M (2015) *Atlas of Merapi volcano*. Laboratoire de Géographie Physique, Meudon, France, 58 color plates. Online Publication (hal-03010922)
- Lavigne F, Mei ETW, Morin J, Humaida H, Moatty A, de Bélizal E, Sri Hadmoko D, Grancher D, Picquout A (2023) Physical environment and human context at Merapi volcano: A complex balance between accessing livelihoods and coping with volcanic hazards. In: Gertisser R, Troll VR, Walter TR, Nandaka IGMA, Ratdomopurbo A (eds) *Merapi volcano—geology, eruptive activity, and monitoring of a high-risk volcano*. Springer, Berlin, Heidelberg, pp 45–66
- LeGuern F, Bernard A (1982) A new method for sampling and analyzing volcanic sublimates—application to Merapi volcano, Java. *J Volcanol Geotherm Res* 12:133–146
- LeGuern F, Gerlach TM, Nohl A (1982) Field gas chromatograph analyses of gases from a glowing dome at Merapi volcano Java, Indonesia, 1977, 1978, 1979. *J Volcanol Geotherm Res* 14:223–245
- Li W, Costa F, Nagashima K (2021) Apatite crystals reveal melt volatile budgets and magma storage depths at Merapi volcano, Indonesia. *J Petrol* 62:egaa100
- Luais B (1986) *Pétrologie et géochimie (éléments trace et rapports isotopiques du Sr) du magmatisme associé aux zones de subduction: Exemples du bassin méditerranéen (Santorin, Arc Egeen; Stromboli, Arc Eolien) et des îles de la Sonde (Merapi, Java)*. PhD Thesis (Thèse de Troisième Cycle), Université de Montpellier, Montpellier, France
- Lube G, Cronin SJ, Thouret J-C, Surono (2011) Kinematic characteristics of pyroclastic density currents at Merapi and controls on their avulsion from natural and engineered channels. *Geol Soc Am Bull* 123:1127–1140
- Luehr B-G, Koulakov I, Rabbel W, Zschau J, Ratdomopurbo A, Brotopuspito KS, Fauzi P, Sahara DP (2013) Fluid ascent and magma storage beneath Gunung Merapi revealed by multi-scale seismic imaging. *J Volcanol Geotherm Res* 261:7–19
- Luehr BG, Koulakov I, Suryanto W (2023) Crustal structure and ascent of fluids and melts beneath Merapi: Insights from geophysical investigations. In: Gertisser R, Troll VR, Walter TR, Nandaka IGMA, Ratdomopurbo A (eds) *Merapi volcano—geology, eruptive activity, and monitoring of a high-risk volcano*. Springer, Berlin, Heidelberg, pp 111–135
- del Marmol MA (1989) *The petrology and geochemistry of Merapi Volcano, Central Java, Indonesia*. Ph.D.

- Thesis, The Johns Hopkins University, Baltimore, USA
- Mei ETW, Lavigne F, Picquout A, de Bézilal E, Brunstein D, Grancher D, Sartohadi J, Cholik N, Vidal C (2013) Lessons learned from the 2010 evacuations at Merapi volcano. *J Volcanol Geotherm Res* 261:348–365
- Murwanto H, Gunnell Y, Suharsono S, Sutikno S, Lavigne F (2004) Borobudur monument (Java, Indonesia) stood by a natural lake: chronostratigraphic evidence and historical implications. *The Holocene* 14:459–463
- Murwanto H (2014) Penelusuran jejak lingkungan danau di sekitar Candi Borobudur dengan pendekatan paleogeomorfologi. S3 Dissertation, University of Gadjah Mada, Yogyakarta, Indonesia
- Nadeau O, Williams-Jones AE, Stix J (2013a) Magmatic-hydrothermal evolution and devolatilization beneath Merapi volcano. *Indonesia J Volcanol Geotherm Res* 261:50–68
- Nadeau O, Williams-Jones AE, Stix J (2013b) The behaviour of copper, zinc and lead during magmatic-hydrothermal activity at Merapi volcano, Indonesia. *Chem Geol* 342:167–179
- Nadeau O, Humaida H, Allard P (2023) Merapi volcano: From volcanic gases to magma degassing. In: Gertisser R, Troll VR, Walter TR, Nandaka IGMA, Ratdomopurbo A (eds) *Merapi volcano—geology, eruptive activity, and monitoring of a high-risk volcano*. Springer, Berlin, Heidelberg, pp 323–351
- Nandaka IGMA, Sulistiyani SY, Putra R (2019) Overview of Merapi volcanic activities from monitoring data 1992–2011 periods. *J Disaster Res* 14:18–26
- Nandaka IGMA, Gertisser R, Walter TR, Troll VR, Ratdomopurbo A (2023) Merapi: Evolving knowledge and future challenges. In: Gertisser R, Troll VR, Walter TR, Nandaka IGMA, Ratdomopurbo A (eds) *Merapi volcano—geology, eruptive activity, and monitoring of a high-risk volcano*. Springer, Berlin, Heidelberg, pp 553–572
- Neumann van Padang M (1931a) De Merapi (Midden Java). *Tropische Natuur* 6:99–103
- Neumann van Padang M (1931b) Een en ander over de uitbarsting van den Merapi in 1930. *Mijnningenieur* 12:20–25
- Neumann van Padang M (1931c) Der Ausbruch des Merapi (Mittel Java) im Jahre 1930. *Z Vulkan* 14:135–148
- Neumann van Padang M (1932) Over de Merapi-uitbarsting 1930 (een antwoord aan Kemmerling). *Tijds Kon Ned Aardr Genoot* 2(49):227–241
- Neumann van Padang M (1933) De uitbarsting van den Merapi (Midden Java) in de jaren 1930–1931. *Vulkanol Seismol Med* 12:1–117
- Neumann van Padang M (1960) Measures taken by the authorities of the vulcanological survey to safeguard the population from the consequences of volcanic outbursts. *Bull Volcanol* 23:181–192
- Neumann van Padang M (1951) Catalogue of the active volcanoes of Indonesia. *International Volcanological Association—Catalogue of the active volcanoes of the world, including solfatara fields*
- Neumann van Padang M (1983) History of the volcanology in the former Netherlands East Indies. *Scr Geol* 71:1–76 (4 plates)
- Newhall CG, Bronto S, Alloway B, Banks NG, Bahar I, Del Marmol MA, Hadisantono RD, Holcomb RT, McGeehin J, Miksic JN, Rubin M, Sayudi SD, Sukhyar R, Andreastuti S, Tilling RI, Torley R, Trimble D, Wirakusumah AD (2000) 10,000 years of explosive eruptions of Merapi Volcano, Central Java: archaeological and modern implications. *J Volcanol Geotherm Res* 100:9–50
- Newhall C, Costa F, Ratdomopurbo A, Venezky DY, Widwijayanti C, Win NTZ, Tan K, Fajiculay E (2017) WOVodat—An online, growing library of worldwide volcanic unrest. *J Volcanol Geotherm Res* 345:184–199
- Pallister PS, Schneider DJ, Griswold JP, Keeler RH, Burton WC, Noyles C, Newhall CG, Ratdomopurbo A (2013) Merapi 2010 eruption—chronology and extrusion rates monitored with satellite radar and used in eruption forecasting. *J Volcanol Geotherm Res* 261:144–152
- Pardiyanto L, Reksowirogo LD, Mitrohartono FXS, Hardjowarsito SH (1978) Volcanic hazard map. Merapi Volcano, Central Java. Geological Survey of Indonesia, Bandung (1 sheet, scale 1:100,000)
- Peters STM, Troll VR, Weis FA, Dallai L, Chadwick JP, Schulz B (2017) Amphibole megacrysts as a probe into the deep plumbing system of Merapi volcano, Central Java Indonesia. *Contrib Mineral Petrol* 172:16
- Petroeschevsky WA (1943) Preliminary historical register of volcanic activity in the East Indian Archipelago (1000 -1941 A.D.). *Bull East Indian Volcan Survey* 95–98 (1942):15–52
- Picquout A, Lavigne F, Mei ETW, Grancher D, Noer C, Vidal CM, Hadmoko DS (2013) Air traffic disturbance due to the 2010 Merapi volcano eruption. *J Volcanol Geotherm Res* 261:366–375
- Preece K, Barclay J, Gertisser R, Herd RA (2013) Textural and micro-petrological variations in the eruptive products of the 2006 dome-forming eruption of Merapi volcano, Indonesia: implications for subsurface processes. *J Volcanol Geotherm Res* 261:98–120
- Preece K, Gertisser R, Barclay J, Berlo K, Herd RA, Facility EIM (2014) Pre- and syn-eruptive degassing and crystallisation processes of the 2010 and 2006 eruptions of Merapi volcano Indonesia. *Contrib Mineral Petrol* 168:1061
- Preece K, Gertisser R, Barclay J, Charbonnier SJ, Komorowski J-C, Herd RA (2016) Transitions between explosive and effusive phases during the cataclysmic 2010 eruption of Merapi volcano, Java, Indonesia. *Bull Volcanol* 78:54
- Preece K, van der Zwan F, Hammer J, Gertisser R (2023) A textural perspective on the magmatic system and eruptive behaviour of Merapi volcano. In: Gertisser R, Troll VR, Walter TR, Nandaka IGMA,

- Ratdomopurbo A (eds) Merapi volcano—geology, eruptive activity, and monitoring of a high-risk volcano. Springer, Berlin, Heidelberg, pp 265–289
- Preece K (2014) Transitions between effusive and explosive activity at Merapi volcano, Indonesia: a volcanological and petrological study of the 2006 and 2010 eruptions. Ph.D. Thesis, University of East Anglia, Norwich, UK
- Purbawinata MA, Ratdomopurbo A, Surono, Pallister J, Luehr B, Newhall C (2007). Understanding Merapi-type Volcanoes. *Eos* 88(1, 2):5–6
- Purbo-Hadiwidjojo P (1961) The geological survey of Indonesia—a summary of its history. Unpubl Report—Geol Survey Indonesia
- Raffles TS (1817a) The history of Java (in two volumes). Black, Parbury and Allen, John Murray, London
- Raffles TS (1817b) A map of Java chiefly from surveys made during the British administration, constructed in illustration of an Account of Java by Thomas Stamford Raffles engraved by J Walker
- Ramadhan M, Widiyantoro S, Nugraha AD, Métaixian J-P, Saepuloh A, Kristyawan S, Sembiring AS, Budi Santoso A, Laurin A, Fahmi AA (2017) Relocation of hypocenters from DOMERAPI and BMKG networks: a preliminary result from DOMERAPI project. *Earthq Sci* 30:67–79
- Ratdomopurbo A, Poupinet G (1995) Monitoring a temporal change of seismic velocity in a volcano: application to the 1992 eruption of Mt. Merapi (Indonesia). *Geophys Res Lett* 22:775–778
- Ratdomopurbo A, Poupinet G (2000) An overview of the seismicity of Merapi volcano (Java, Indonesia), 1983–1994. *J Volcanol Geotherm Res* 100:193–214
- Ratdomopurbo A, Beauducel F, Subandriyo J, Nandaka IGMA, Newhall CG, Suharna SDS, Suparwaka H, Sunarta (2013) Overview of the 2006 eruption of Mt Merapi. *J Volcanol Geotherm Res* 261:87–97
- Ratdomopurbo A (1995) Etude sismologique du volcan Mérapi et formation du dôme de 1994. PhD Thesis, University of Joseph Fourier, Grenoble, France
- Rebscher D, Westerhaus M, Welle W, Nandaka IGMA (2000) Monitoring ground deformation at the decade volcano Gunung Merapi. Indonesia. *Phys Chem Earth* (part a) 25(9–11):755–757
- Reck H (1931) Der Merapi-Vulkan auf Java und sein Ausbruch im Dezember 1930. *Naturwiss* 19:369–373
- Reck H (1935) Der Ausbruchscyklus des Merapi in den Jahren 1933/34. *Naturwiss* 48:812–816
- Richter G, Wassermann J, Zimmer M, Ohrnberger M (2004) Correlation of seismic activity and fumarole temperature at the Mt. Merapi volcano (Indonesia) in 2000. *J Volcanol Geotherm Res* 135:331–342
- Rohadi S, Widiyantoro S, Nugraha AD, Masturyono (2013) Tomographic imaging of P- and S-wave velocity structure beneath central Java, Indonesia: joint inversion of the MERAMEX and MCGA earthquake data. *Int J Tomogr Stat* 24(3):1–16
- Saepuloh A, Urai M, Aisyah N, Sunarta WC, Subandriyo JP (2013) Interpretation of ground surface changes prior to the 2010 large eruption of Merapi volcano using ALOS/PALSAR, ASTER TIR and gas emission data. *J Volcanol Geotherm Res* 261:130–143
- Sayudi DS, Sulistiyo Y (1994) Variation in the chemical composition of volcanic gases of Merapi volcano, Central Java, Indonesia. Technical Report, The Fifth Field Workshop on Volcanic Gases in Indonesian Volcanoes. Volcanological Survey of Indonesia, Bandung, pp 65–77
- Scheltema JF (1912) Monumental Java. Macmillan and Co., Limited, London, p 302
- Schwarzkopf L, Schmincke HU, Troll V (2001) Pseudotachylite on impact marks of block surfaces in block-and-ash flows at Merapi volcano, Central Java, Indonesia. *Int J Earth Sci* 90:769–775
- Schwarzkopf LM, Schmincke H-U, Cronin SJ (2005) A conceptual model for block-and-ash flow basal avalanche transport and deposition, based on deposit architecture of 1998 and 1994 Merapi flows. *J Volcanol Geotherm Res* 139:117–134
- Schwarzkopf LW, Troll VR, Schmincke H-U (2002) Cliff-triggered surge generation: evidence from Merapi Volcano, Central Java, Indonesia. Abstract, IAVCEI 1902 Centennial Workshop, Mount Pelee, Martinique
- Schwarzkopf LM (2001) The 1994 and 1998 block-and-ash flow deposits at Merapi Volcano, Central Java, Indonesia: implications for emplacement mechanisms and hazard mitigation. PhD Thesis, Christian-Albrechts-Universität zu Kiel, Kiel, Germany
- Shimozuru D, Miyayaki T, Gyoda N, Matahelumual J (1969) Volcanological survey of Indonesian volcanoes: part 2. Seismic observation at Merapi volcano. *Bull Earthquake Res Inst Univ Tokyo* 47:969–990
- Siswowardjojo S, Suryo I, Yokoyama I (1995) Magma eruption rates of Merapi volcano, Central Java, Indonesia during one century (1890–1992). *Bull Volcanol* 57:111–116
- Solikhin A, Thouret J-C, Liew SC, Gupta A, Sayudi DS, Oehler J-F, Kassouk Z (2015) High spatial-resolution imagery helps map deposits of the large (VEI 4) 2010 Merapi Volcano eruption and their impact. *Bull Volcanol* 77:20
- Stehn CE (1929) Einige Mitteilungen über den vulkanologischen Dienst in Niederländisch Indien und seine Arbeiten. *Bull Volcanol* 3:13–20
- Stehn CE (1935a) 3. Merapi (C. Java). In: Volcanic phenomena during the months of October, November and December 1934. A. Regular observation stations. *Bull Neth Indies Volcan Survey*, 70(1934):120–131, pis
- Stehn CE (1935b) De Merapibewaking. Dienst Mijnw. Ned. Indie, Bandoeng, pp 1–12
- Stehn CE (1939) 4. Merapi (Central Java), No. 41. In: Volcanic phenomena during the months of January, February and March 1939. A. Regular observation stations. *Bull Neth Indies Volc Survey* 87:2–3
- Subandriyo, Gertisser R, Aisyah N, Humaida H, Preece K, Charbonnier S, Budi-Santoso A, Handley H, Sumarti S, Sayudi DS, Nandaka IGMA, Wibowo HE (2023) An overview of the large-magnitude (VEI 4)

- eruption of Merapi in 2010. In: Gertisser R, Troll VR, Walter TR, Nandaka IGMA, Ratdomopurbo A (eds) Merapi volcano—geology, eruptive activity, and monitoring of a high-risk volcano. Springer, Berlin, Heidelberg, pp 353–407
- Sumarti S, Suryono (1994) Chemistry model of Merapi Volcano. Technical Report, The Fifth Field Workshop on Volcanic Gases in Indonesian Volcanoes, Volcanological Survey of Indonesia, Bandung, p 96–111
- Surono JP, Pallister J, Boichu M, Buongiorno MF, Budisantoso A, Costa F, Andreastuti S, Prata F, Schneider D, Clarisse L, Humaida H, Sumarti S, Bignami C, Griswold J, Carn S, Oppenheimer C, Lavigne F (2012) The 2010 explosive eruption of Java's Merapi volcano—a '100-year' event. *J Volcanol Geotherm Res* 241–242:121–135
- Suryo I, Clarke MCG (1985) The occurrence and mitigation of volcanic hazards in Indonesia as exemplified at the Mount Merapi Mount Kelut, and Mount Galunggung volcanoes. *Q J Eng GeolHydrogeol* 18:79–98
- Suryo I (1978) Nuée Ardente at Merapi Volcano and precautionary measures against volcanic phenomena. In: Proceedings, Symposium on mudflows in Japan and Indonesia. Japan Public Works Research Institute Technical Memorandum no. 1407, pp 51–63
- Symonds R, Rose W, Reed M, Lichte F, Finnegan D (1987) Volatilization transport and sublimation of metallic and nonmetallic elements in high-temperature gases at Merapi Volcano, Indonesia. *Geochim Cosmochim Acta* 51:2083–2101
- Taverne NJM (1925) G. Merapi in 1924. *Natuurk Tijdschr Nederl-Indië* 85:137–149
- Taverne NJM (1933) De G. Merapi (Midden-Java) in 1922. *Vulkanol Ber XXI-XXIX*:2–26
- Thorn W (1815) Memoir of the conquest of Java; with the subsequent operations of the British Forces, in the oriental archipelago. To which is subjoined, a statistical and historical sketch of Java; being the result of observations made in a tour through the country; with an account of its dependencies. T Egerton, Military Library, Whitehall; R Wilks, London, p 369
- Thouret J-C, Lavigne F, Kelfoun K, Bronto S (2000) Toward a revised hazard assessment at Merapi volcano, Central Java. *J Volcanol Geotherm Res* 100:479–502
- Thouret J-C, Aisyah N, Jenkins SF, de Belizal E, Sulistiyani, Charbonnier S, Sayudi DS, Nandaka IGMA, Mainsant G, Solikhin A (2023) Merapi's lahars: Characteristics, behaviour, monitoring, impact, hazard modelling and risk assessment. In: Gertisser R, Troll VR, Walter TR, Nandaka IGMA, Ratdomopurbo A (eds) Merapi volcano-geology, eruptive activity, and monitoring of a high-risk volcano. Springer, Berlin, Heidelberg, pp 501–552
- Toutain J-P, Sortino F, Baubron J-C, Richon P, Surono SS, Nonell A (2009) Structure and CO₂ budget of Merapi volcano during inter-eruptive periods. *Bull Volcanol* 71:815–826
- Troll VR, Hilton DR, Jolis EM, Chadwick JP, Blythe LS, Deegan FM, Schwarzkopf LM, Zimmer M (2012) Crustal CO₂ liberation during the 2006 eruption and earthquake events at Merapi volcano Indonesia. *Geophys Res Lett* 39:L11302
- Troll VR, Deegan FM, Jolis EM, Harris C, Chadwick JP, Gertisser R, Schwarzkopf LM, Borisova AY, Bindeman IN, Sumarti S, Preece K (2013a) Magmatic differentiation processes at Merapi volcano: inclusion petrology and oxygen isotopes. *J Volcanol Geotherm Res* 261:38–49
- Troll VR, Chadwick JP, Jolis EM, Deegan FM, Hilton DR, Schwarzkopf LM, Blythe LS, Zimmer M (2013b) Crustal volatile release at Merapi volcano; the 2006 earthquake and eruption events. *Geol Today* 29:96–101
- Troll VR, Deegan FM, Jolis EM, Budd DA, Dahren B, Schwarzkopf LM (2015) Ancient oral tradition describes volcano–earthquake interaction at Merapi volcano, Indonesia. *Geografisk Ann: Series a, Phys Geograph* 97:137–166
- Troll VR, Deegan FM, Seraphine N (2021) Ancient oral tradition in Central Java warns of volcano–earthquake interaction. *Geol Today* 37:100–109
- Troll VR, Deegan FM (2023) The magma plumbing system of Merapi: The petrological perspective. In: Gertisser R, Troll VR, Walter TR, Nandaka IGMA, Ratdomopurbo A (eds) Merapi volcano—geology, eruptive activity, and monitoring of a high-risk volcano. Springer, Berlin, Heidelberg, pp 233–263
- Troll VR, Schwarzkopf LM, Gertisser R, Buckley C, Chadwick J, Zimmer M, Sulistiyono Y (2003) Shallow-level processes and their impact on the eruptive behaviour in arc volcanoes: evidence from recent Merapi lavas. *State-of-the-Arc, Mt. Hood, U.S.A.*, Aug 2003
- Turner S, Foden J (2001) U, Th and Ra disequilibria, Sr, Nd and Pb isotope and trace element variations in Sunda arc lavas: predominance of a subducted sediment component. *Contrib Mineral Petrol* 142:43–57
- van Bemmelen RW (1939) The volcano-tectonic origin of Lake Toba (North-Sumatra). *De Ing Nederl-Indië* 6–9:126–140
- van Bemmelen RW (1942) Report of the Merapi eruption of May 30, 1942. Bandoeng (unpublished report), Dienst Mijnb Ned Indië
- van Hinloopen LD (1921) Oud-Javaansche gegevens omtrent de vulkanologie van Java. *Natuurk Tijds Ned Indië* 81:124–158
- van der Zwan FM, Chadwick JP, Troll VR (2013) Textural history of recent basaltic-andesites and plutonic inclusions from Merapi volcano. *Contrib Mineral Petrol* 166:43–63
- Verbeek RDM (1885) Krakatau. Govt Press, Batavia, p 567
- Verbeek RDM, Fennema R (1896) Geologische beschrijving van Java en Madoera. Two volumes and a folio with maps and sections. J.G. Stemler, Amsterdam
- Voight B, Davis MJ (2000) Emplacement temperatures of the November 22, 1994 nuée ardente deposits, Merapi Volcano, Java. *J Volcanol Geotherm Res* 100:371–377

- Voight B, Constantine EK, Siswawidjono S, Torley R (2000a) Historical eruptions of Merapi volcano, Central Java, Indonesia, 1768–1998. *J Volcanol Geotherm Res* 100:69–138
- Voight B, Young KD, Subandrio HD, Purbawinata MA, Ratdomopurbo A, Suharna P, Sayudi DS, LaHusen R, Marso J, Murray TL, Dejean M, Iguchi M, Ishihara K (2000b) Deformation and seismic precursors to dome-collapse and fountain-collapse nuées ardentes at Merapi Volcano, Java, Indonesia, 1994–1998. *J Volcanol Geotherm Res* 100:261–287
- Wagner D, Koulakov I, Rabbel W, Luehr B-G, Wittwer A, Kopp H, Bohm M, Asch G, the MERAMEX Scientists (2007) Joint inversion of active and passive seismic data in Central Java. *Geophys J Int* 170:923–932
- Walter TR, Wang R, Zimmer M, Grosser H, Lühr B, Ratdomopurbo A (2007) Volcanic activity influenced by tectonic earthquakes: Static and dynamic stress triggering at Mt Merapi. *Geophys Res Lett* 34:L05304
- Walter TR, Ratdomopurbo A, Subandriyo AN, Brotopus-pito KS, Salzer J, Lühr B (2013) Dome growth and coulée spreading controlled by surface morphology, as determined by pixel offsets in photographs of the 2006 Merapi eruption. *J Volcanol Geotherm Res* 261:121–129
- Walter TR, Subandriyo J, Kirbani S, Bathke H, Suryanto W, Aisyah N, Darmawan H, Jousset P, Luehr BG, Dahm T (2015) Volcano-tectonic control of Merapi's lava dome splitting: the November 2013 fracture observed from high resolution TerraSAR-X data. *Tectonophysics* 639:23–33
- Walter TR, Wang R, Luehr B-G, Wassermann J, Behr Y, Parolai S, Angraeni A, Günther E, Sobiesiak M, Grosser H, Wetzel H-U, Milkereit, Sri Brotopus-pito PJK, Harjadi P, Zschau J (2008) The 26 May 2006 magnitude 6.4 Yogyakarta earthquake south of Mt. Merapi volcano: did lahar deposits amplify ground shaking and thus lead to the disaster? *Geochem Geophys Geosyst* 9:Q05006
- Walter TR (2023) Radar sensing of Merapi volcano. In: Gertisser R, Troll VR, Walter TR, Nandaka IGMA, Ratdomopurbo A (eds) *Merapi volcano—geology, eruptive activity, and monitoring of a high-risk volcano*. Springer, Berlin, Heidelberg, pp 437–455
- Wassermann J, Ohrberger M (2001) Automatic hypocenter determination of volcano induced seismic transients based on wavefield coherence—an application to the 1998 eruption of Mt. Merapi. *Indonesia. J Volcanol Geotherm Res* 110:57–77
- Whitley S, Gertisser R, Halama R, Preece K, Troll VR, Deegan FM (2019) Crustal CO₂ contribution to subduction zone degassing recorded through calc-silicate xenoliths in arc lavas. *Sci Rep* 9:8803
- Whitley S, Halama R, Gertisser R, Preece K, Deegan FM, Troll VR (2020) Magmatic and metasomatic effects of magma-carbonate interaction recorded in calc-silicate xenoliths from Merapi volcano (Indonesia). *J Petrol* 61:egaa048
- Whitley S (2020) Xenoliths as tracers of magmatic and intra-crustal processes at volcanic arcs. PhD Thesis, Keele University, Keele, UK
- Wichmann A (1918) Die Erdbeben des indischen Archipels bis zum Jahre 1857. *Verhandelingen Koninklijke Akademie van Wetenschappen; Tweede secite; Deel XX, No. 4*. Amsterdam, J Müller, p 193
- Widiyantoro S, Ramdhan M, Métaxian J-P, Cummins PR, Martel C, Erdmann S, Nugraha AD, Budi-Santoso A, Laurin A, Fahmi AA (2018) Seismic imaging and petrology explain highly explosive eruptions of Merapi volcano Indonesia. *Sci Rep* 8:13656
- Wirakusumah AD, Juwana H, Loebis H (1989) Peta Geologi Gunung Merapi. Jawa Tengah (geologic Map of Merapi Volcano, Central Java) 1(50):000
- Wirakusumah AD, Heriman AD, Hadisantono RD, Lubis H, Sutoyo (1980) Laporan kemajuan pemetaan geologi Daerah Gunung Merapi, Jawa Tengah. Unpublished Report – Volcanological Survey of Indonesia, Bandung
- Wurth T (1914) De G. Merapi (December 1904–June 1913). *Jaarverslag Topogr Dienst Nederl-Indië, Batavia*, pp 160–162
- Young KD, Voight B, Subandriyo S, Miswanto CTJ (2000) Ground deformation at Merapi Volcano, Java, Indonesia: distance changes, June 1988–October 1995. *J Volcanol Geotherm Res* 100:233–259
- Zen MT, Soeparto S, Djoharman L, Harto S (1980) Type and Characteristics of the Merapi eruption, vol I. *Bulletin Departemen Teknik Geologi Institut Teknologi, Bandung*, pp 34–46
- Zimmer M, Erzinger J (2003) Continuous H₂O, CO₂, ²²²Rn and temperature measurements on Merapi Volcano, Indonesia. *J Volcanol Geotherm Res* 125:25–38
- Zlotnicki J, Bof M, Perdereau L, Yvetot P, Tjetjep W, Sukhyar R, Purbawinata MA, Suharno (2000) Magnetic monitoring at Merapi volcano, Indonesia. *J Volcanol Geotherm Res* 100:321–336
- Zschau J, Sukhyar R, Purbawinata MA, Lühr BG, Westerhaus M (2003) The Merapi-Project—interdisciplinary monitoring of a high-risk volcano as a basis for an early warning system. In: Zschau J, Küppers A (eds) *Early warning systems for natural disaster reduction*. Springer, Berlin, Heidelberg, pp 527–532



Physical Environment and Human Context at Merapi Volcano: A Complex Balance Between Accessing Livelihoods and Coping with Volcanic Hazards

Franck Lavigne, Estuning Tyas Wulan Mei, Julie Morin, Hanik Humaida, Annabelle Moatty, Edouard de Bélizal, Danang Sri Hadmoko, Delphine Grancher, and Adrien Picquout

Abstract

Merapi is a two-sided, paradoxical volcano: on the one hand 1.8 million people live on its flanks. It is one of the most densely populated volcanoes on Earth, with population densities averaging 764 inhabitants per square kilometre within a 10 km radius from the summit. The main reasons for the high densities are land resources and associated livelihoods from agriculture, livestock, sand mining, and tour-

ism. On the other hand, Merapi is also one of the world's most active volcanoes. Dome-collapse pyroclastic density currents (PDCs) occur every few years (e.g. 1994, 2002, 2006), and more violent explosive episodes are generated with an average recurrence interval of several decades (e.g. 1872, 1930, 2010). Risk management at Merapi is based on volcanic hazard zonation (called KRB I, II, and III, from the less exposed to the most exposed), derived from its eruptive history. Since its first publication by the Volcanological Survey of Indonesia in 1978, the danger map has been updated twice, in 2002 and after the deadly eruption of Merapi in 2010. Most of the information is provided by scientists during the 'raising awareness program' phase and achieved in the framework of a Community-Based Disaster Risk Management (CBDRM), which empowers communities with self-developed ways of coping with crises due to natural hazards. In periods of emergency, the Center for Volcanology and Geological Hazard Mitigation provides four warning levels of volcanic activity. In 2010, Merapi produced its largest eruption since 1872, damaging around 12,000 buildings, claiming 367 lives, including 200 directly by PDCs, and triggering massive evacuations of up to 400,000 people, as counted in the evacuation camps.

F. Lavigne (✉) · A. Moatty · D. Grancher · A. Picquout

Laboratoire de Géographie Physique, Université Paris 1 Panthéon-Sorbonne, CNRS, Thiais, France
e-mail: franck.lavigne@univ-paris1.fr

E. T. W. Mei · D. S. Hadmoko
Fakultas Geografi, Universitas Gadjah Mada, Yogyakarta, Indonesia

J. Morin
Department of Geography, University of Cambridge, Cambridge, UK

H. Humaida
BPPTKG (Balai Penyelidikan dan Pengembangan Teknologi Kebencanaan Geologi), Yogyakarta, Indonesia

E. de Bélizal
Laboratoire Mosaïques, LAVUE, UMR 7218 CNRS, Université Paris-Nanterre, Paris, France

Keywords

Merapi · Vulnerability · Capacities · Land resources · Livelihoods · Risk and crisis management

2.1 Introduction: Merapi, a Highly Populated Volcano

Merapi is one of the most densely populated volcanoes on Earth (Brown et al. 2015), and also one of the most active. Therefore its flanks are categorised by the Center for Volcanology and Geological Hazards Mitigation (CVGHM) into 3 different danger zones (Fig. 2.1), based on eruptive history (Sayudi et al. 2010): (i) Hazard zone (KRB)-III: areas prone to frequent pyroclastic flows, surges, ballistics, ash falls, lava flows, and rock falls; (ii) KRB-II: areas prone to potential pyroclastic flows, surges, lava flows, and ash falls; (iii) KRB-I: areas prone to potential lahars, ash falls, and extended pyroclastic flows and lava flows.

Out of the 1.8 million people living on its flanks, more than half are at high risk in areas prone to pyroclastic flows, surges, and lahars. As buildings might be blasted, burnt and/or buried, and as it is unlikely to survive these hazards (Jenkins et al. 2013), the single option in case of an eruption is to evacuate these areas. However, people accept to live in these high-risk zones mostly because of the availability of material and immaterial land resources, first and foremost the rich volcanic soil.

Mapping population density around Merapi reveals a densification from the summit to the base of the volcano's flanks overall (Fig. 2.2). Within a 10 km radius from the summit, i.e. the most hazardous area should Merapi erupt (KRB III), the slopes of the volcano cone are steep and mainly covered by forest. However, population densities are very high, with an average of 764 inhabitants per square kilometre. Some highly populated villages (>1500 inhabitants/km²), settled within a 5 km radius area, are the most exposed to the volcanic hazards, as well as those located along the Gendol valley in the

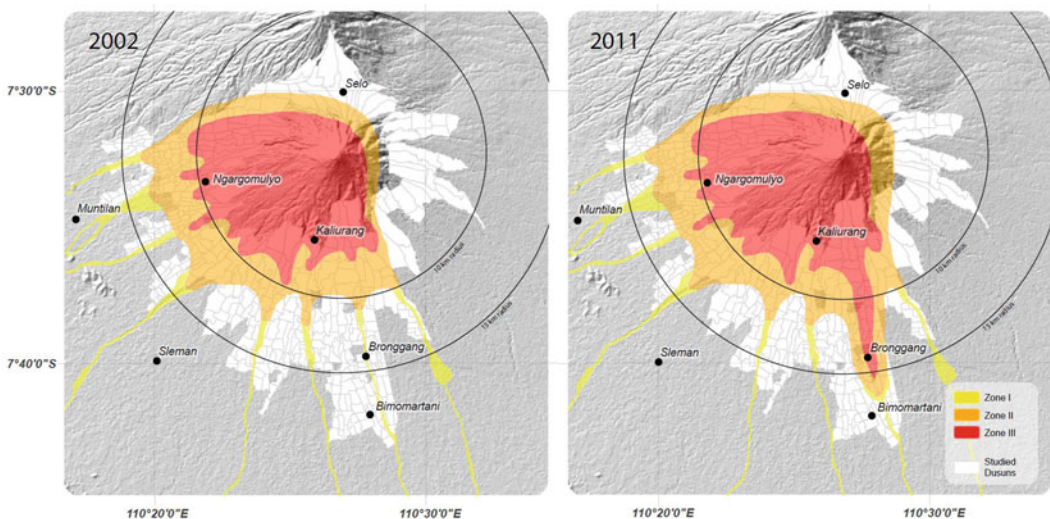


Fig. 2.1 Official danger zones at Merapi defined by the volcanology and geological hazard mitigation (CVGHM) in 2002, and revised in 2011. This map displays two zones threatened by PDC hazard: the zone III or KRB III (KRB stands for *Kawasan Rawan Bencana* in Indonesian or Hazard Prone Area in English) encompasses areas

located close to the summit, frequently affected by dome-collapsed pyroclastic flows, lava flows, rock falls and ejected rock fragments. The KRB II is affected by less frequent and longer runout pyroclastic flows, lahars, volcanic ash fall, and ejected rocks

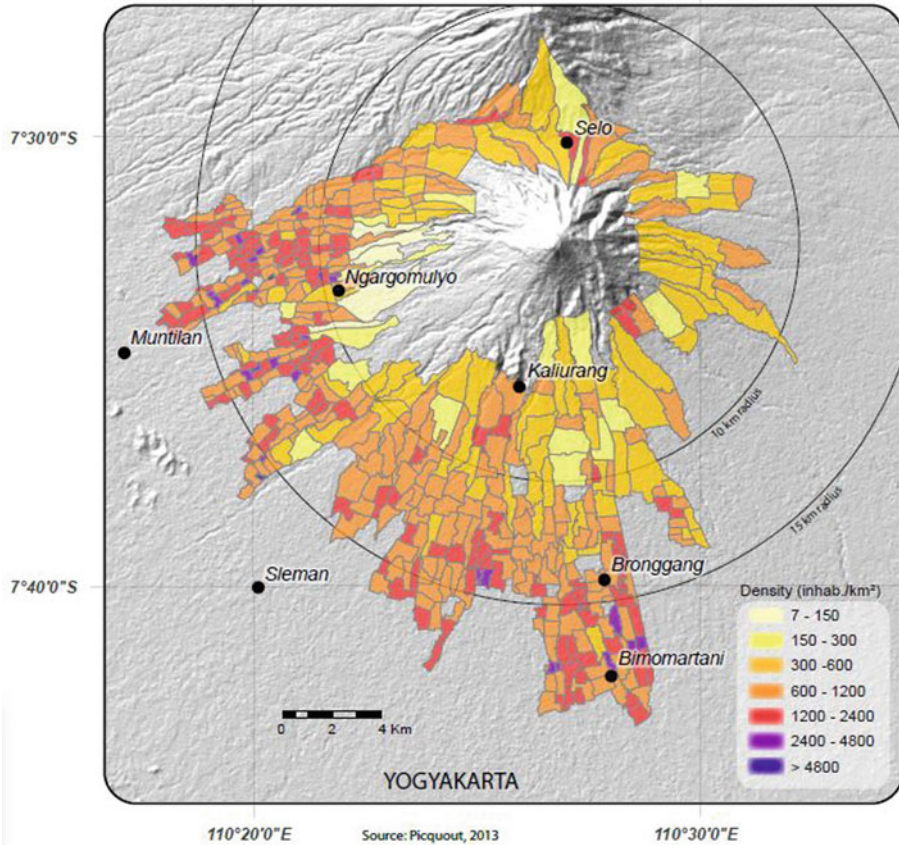


Fig. 2.2 Population density at Merapi volcano in 2009. *Source* MIAVITA WP5 Census, 2009 in Lavigne et al. (2015)

Cangkringan and Kemalang districts, Sleman Regency and Klaten Regency, respectively. Their vulnerability is increased because the local people must use steep and damaged roads as evacuation routes. Further south, population densities increase considerably between 400 and 200 m elevation, due to the attractive proximity of Yogyakarta.

The Yogyakarta urban area is located on the highly populated, fluvio-volcanic ring plain of Merapi. The city is the political, economic, social, and cultural centre of the Special Province of Yogyakarta. For 50 years, this city of over 1 million inhabitants has attracted people from the surrounding overcrowded rural areas. To preserve the productive tilled lands and irrigation networks around the city, the government has attempted to control urban growth. However, for

the last 30 years, thousands of migrants have settled within areas prone to floods due to heavy monsoon rainfall and lahars along the Code River. In 1995, about 13,000 people were already living at risk in the suburbs of Yogyakarta along the Code River with the population density exceeding 5600 inhabitants per km² (Lavigne 1999). In 2018, an estimated 96,500 people were living there (BPS 2018).

Besides the people being exposed to the directly lethal volcanic hazards, more than 2 million people are exposed to ashfall hazard around Merapi (Picquout 2013, based on a population survey in the framework of the MIAVITA EC Program). This includes the accumulation of ash on roofs that can trigger collapse of buildings, especially if the ash is saturated by rain (Blong et al. 2017). Medical

services can expect an increase in the number of patients with respiratory symptoms, eye or skin irritation during and after an ashfall event. In the worst cases, exposure to volcanic ash may result in acute respiratory morbidity (Damby et al. 2013), especially for those with pre-existing respiratory disease.

In addition, ash can cause severe disruptions of the terrestrial and aerial transportation networks, including when people have to evacuate with reduced-to-no visibility on slippery roads. It leads to motorcycle accidents, often worsened by potholes in the roads due to heavy traffic related to sand mining activity (Mei et al. 2013).

In this context, the aims of this chapter are to clarify: (i) the reasons of the high population densities around Merapi, with a focus on land resources; (ii) the capacity of people around Merapi to face eruptions, (iii) the crisis management and people's responses during the major 2010 eruption of the volcano, and (iv) the post-crisis and recovery process and the preventive measures that have been taken place after the 2010 eruption.

2.2 The Main Reason of High Population Densities: Land Resources and Associated Livelihoods at Merapi

2.2.1 A Climatic Context Suitable for Livelihoods

Java experiences a tropical monsoon climate, with annual rainfall ranges at various stations from 2000 mm to 4500 mm on the Merapi slopes. Exceptional rainfall can be as much as 466 mm/day recorded at Ngepos station on 25 November 1979. The latest exceptional rainfall on 27–29 November 2017 was due to a tropical cyclone named Cempaka, where the recorded rainfall was 286 mm/day in Yogyakarta. Between 1980 and 2000, rainfall exceeded 100 mm/h at least seven times on the slopes of Merapi (Lavigne et al. 2000). The role of rainfall is crucial for accessing livelihoods at Merapi. Combined with fertile soil, it allows high-

intensity agriculture. In addition, strong rainfalls remobilise volcanic material, triggering lahars (volcanic debris flows) whose deposits are exploited by people downstream.

2.2.2 Land Use, Agriculture and Livestock

The land use at Merapi can be described as high-intensity, low-technology, and subsistence tropical agriculture. Therefore, a very high population density is required, as this type of farming is very labour intensive since all work is done by hand. Merapi's surroundings are essentially rural. Rice fields represent the main land cover (36%), followed by settlements, grasslands and drylands (Fig. 2.3). All the land is exploited, except Merapi's steepest slopes, which are covered by forests protected by a National Park since 2004. Settlements also take up an important share of land use (25%), especially close to Yogyakarta. There is a contrast between Merapi's western flank, where rice fields are dominant, and its northern and eastern flanks, where dry lands are located. Unquestionably, and in direct relation with the foehn effect (a dry, warm, down-slope wind that occurs on the downwind side of the volcano), there is more rainfall on Merapi's western flank, providing the necessary conditions for rice production. As it requires a lot of workforces, the population density is generally higher on the western flank with more than 200 houses per hectare (ha), while the distribution of settlements is more diffuse on the eastern flank. Most rice farmers concentrate on small fields, modelling the landscape with terrace cultivation. Irrigation systems, widely developed in this area (41% of the cultivated area), associated with land fertility and the widespread use of fertilisers, contribute to the high productivity of rice fields.

Dry lands represent 23% of the cultivated area around Merapi. Most of them belong to the *Tegalan* type, i.e. dry fields that do not involve fire to enable cultivation on slopes as it is required for the *Ladang* type. Food crops are dominant (e.g. peanuts, cassava), but commercial

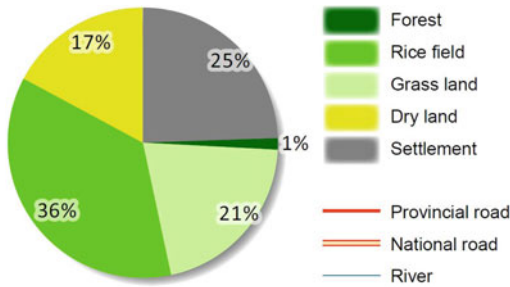


Fig. 2.3 Land use at Merapi volcano in 2009. *Source* MIAVITA WP5 Census, 2009 in Lavigne et al. (2015)

crops are also planted such as tobacco, chilli, or fruits like salak. Cultivation practices also include home gardens created within villages, providing families with extra food and income. The cultivation system is stratified and complex: cooking herbs, sweet potatoes, tomatoes and chilli cover the ground. Cassava plants provide roots and leaves that can both be eaten. Vines that produce beans, squash or edible berries are often cultivated on bamboo trellises around the edge, along with bananas. A few tall fruit trees provide protection or shade for the smaller plants.

The main volcanic hazard affecting agriculture at Merapi are tephra (ash) fall derived from convecting plumes rising off the block-and-ash flows from dome collapse events, and fallout from short-lived phreatic or vulcanian explosions. Farms in the direct path of pyroclastic density currents (PDCs) are frequently destroyed, e.g. in 2006 and 2010. Using ALOS PALSAR remote sensing data, Yulianto et al. (2013) estimated that the 2010 eruption destroyed around 92 ha of paddy fields, 235 ha of dry farming and 570 ha of plantations.

Livestock is considered more as a food livelihood than an economic resource, as it represents important food stocks for local communities on the Merapi slopes. Cows represent the main livelihood through milk production and sale. Cow stocks are mostly spread out along the slopes where they can graze freely (Dove 2008), while sheep and goat stocks can be found everywhere. Most bulls can be found on the western side of the volcano and are used as

workforce in rice fields. Pig stocks are not considered as they are very limited in the Merapi area. Merapi's eastern slopes display a high ratio of livestock per inhabitant, whereas the southern and south-western sides have a low ratio of livestock per inhabitant. Saving livestock during volcanic crises is a major concern for the inhabitants. Apart from the risk of immediate death, by voluminous ash fall or PDCs (KRB III and KRB II) or by lahars in KRB I, it is sometimes difficult to find clean grass and water for the cattle after ash fall events. Residents sometimes try to evacuate their livestock when they evacuate or before evacuating themselves. If necessary, they are ready to face the danger by feeding their livestock in the area evacuated by the people.

2.2.3 Block and Sand Mining in the Valleys: An Adaptation to Pyroclastic Density Currents and Lahars?

Block and sand mining is a widespread activity in the valleys around Merapi volcano (Fig. 2.4). The income of thousands of people depends on these activities (De Belizal et al. 2011, 2013). The activity remains highly informal and therefore the precise number of workers is hard to estimate: some people quarry for living, while others only quarry when needed to complete their income. In 2015, most workers in the Gendol River valley earned more than 100,000 IDR (10 USD) a day (Hoyos 2016). A full load of blocks and sand from the Gendol quarries was sold for between 600,000 and 800,000 IDR (60–80 USD) in Central Java shortly after the 2010 eruption. The high demand for building material made the price grow since 2011: in 2014, a load was sold for more than 1 million IDR (>100 USD) in Central Java. Therefore, sand mining plays a major role for the local economy; it does not only employ miners who dig out deposits. This activity is also the core of a small-scale economy in every quarry all around the volcano, which brings complementary income to farmers.

Fig. 2.4 Extensive block and sand mining in the Gendol valley in 2013. *Photo credit J. Morin*



Warung (small family-owned restaurant) keepers, or itinerant salesmen, who carry their shop on their scooters, provide food and refreshments for the workers. Teenagers, who fill the holes on the roads, and are paid by truck drivers, are also quite common near the quarries.

The location of quarries along the valleys follows the spatial distribution of pyroclastic and epiclastic (lahar) deposits. Until 2006, the main extraction basin at Merapi was located on the western slope of the volcano (Fig. 2.5), mainly along the Putih River. In 2006, dome-collapse block-and-ash flows occurred mainly in the

Gendol River (Charbonnier and Gertisser 2008; Gertisser et al. 2012), which therefore became the main extraction basin (Fig. 2.5). The high frequency of lahars following the voluminous 2010 eruption generated significant deposits on the western and southern flanks of the volcano (De Belizal et al., 2013). Many quarries opened, but since 2010 the main basin has remained located along the Gendol River. Having previously relied on manual methods of extraction (e.g., shovels), the introduction of excavators increased the truck traffic and the volume of extracted deposits and turned the industry from a

small, manual one into a large-scale industrial operation. In 2015, the estimated total volumetric rate of extracted materials reached $3.9 \times 10^6 \text{ m}^3/\text{year}$ (more than two and a half times more than extracted before 2010). The quarries located on the upstream Gendol River had the highest extracted volumetric rates, estimated at $8.8 \times 10^3 \text{ m}^3/\text{day}$, with more than 2200 trucks coming in and out every day, most of them in Kopeng, where a large quarry has been (re)activated since 2012 (Fig. 2.5).

At Merapi, Block and sand mining characterises the high adaptation of local communities to a natural hazard. People at Merapi are mostly farmers who do not necessarily own their lands, which constrain them to search for other sources of income. Young people are particularly concerned by unemployment. Sand mining is thus often perceived as a blessing, as it helps people to recover quickly after a crisis: those who may have lost their job due to the eruption can rapidly find a new job in the valleys. Those who struggle to find a job can finally get one easily. Lahars give people a way of keeping some substantial income because they occur up to years after an eruption: sand mining lowers the disturbance of a crisis and makes the communities resilient. Thus, people at Merapi have turned the frequent volcanic hazard into a livelihood, and therefore have taken advantage of this disturbance by exploiting the deposits. The resilience is not only economic, but also environmental: sand mining accelerates the erosion of the fresh pyroclastic deposits likely to be bulked into lahars. There are two main consequences: (1) it rapidly reduces the occurrences of future lahars, and (2) it recreates the pre-eruptive shape of the valleys and makes them ready to be filled again by the next eruption. Indeed, as shown by De Bézilal et al. (2013); Ville et al. (2015); Wibowo et al. (2015), the frequency of lahars decreased sharply two years after the 2010 eruption in 2012. When the upstream quarries of the Gendol River reopened, almost no lahars were reported anymore downstream. However, without regulation, the lack of

new materials provided by PDCs or lahars leads miners to exploit valley walls made of old, altered material subject to collapse. Therefore, landslide hazards –both natural and man-made– also need to be considered at Merapi.

Whatever the context of the quarrying activity is, the workers are exposed to lethal volcanic hazards (lahars, PDCs). The constantly changing topography of the channels due to the random excavations makes any emergency evacuation difficult, especially during the rainy season, when the roads are slippery. An unpublished field survey carried out in 2014 by Edouard De Bézilal and Anouk Ville in collaboration with the Universitas Gadjah Mada (UGM) has shown that 2000 trucks entered/exited the Kopeng quarry every day (Gendol River). As many as 20 trucks were queuing before being filled by the excavators in the valley at the busiest time of the day (end of the morning). The paths inside the valley floor were congested and any evacuation would have been impossible in case of an emergency. Unfortunately, the access to sand mining resources is not always available to local people, due to the inappropriate and unequal distribution of shared resources between investors, regulators, and local people. Usually, the investors coming from outside of the villages have more benefits than the local people: the latter work only on a daily basis and do not have any share of the total revenue obtained by the sand mining investors.

The lack of government regulation of the resources available in volcanoclastic materials generates high rates of mining: some quarries have already been closed since 2014 on the western flank due to the lack of fresh deposits. The workers have since remained unemployed. Sand mining, as it stands, does not seem to be an effective and sustainable answer to the long-term socioeconomic issues at Merapi. It may help the economic and environmental resilience immediately after an eruption, but it also endangers the workers physically (exposure to volcanic hazards), socially and economically (limited supply and lack of management).

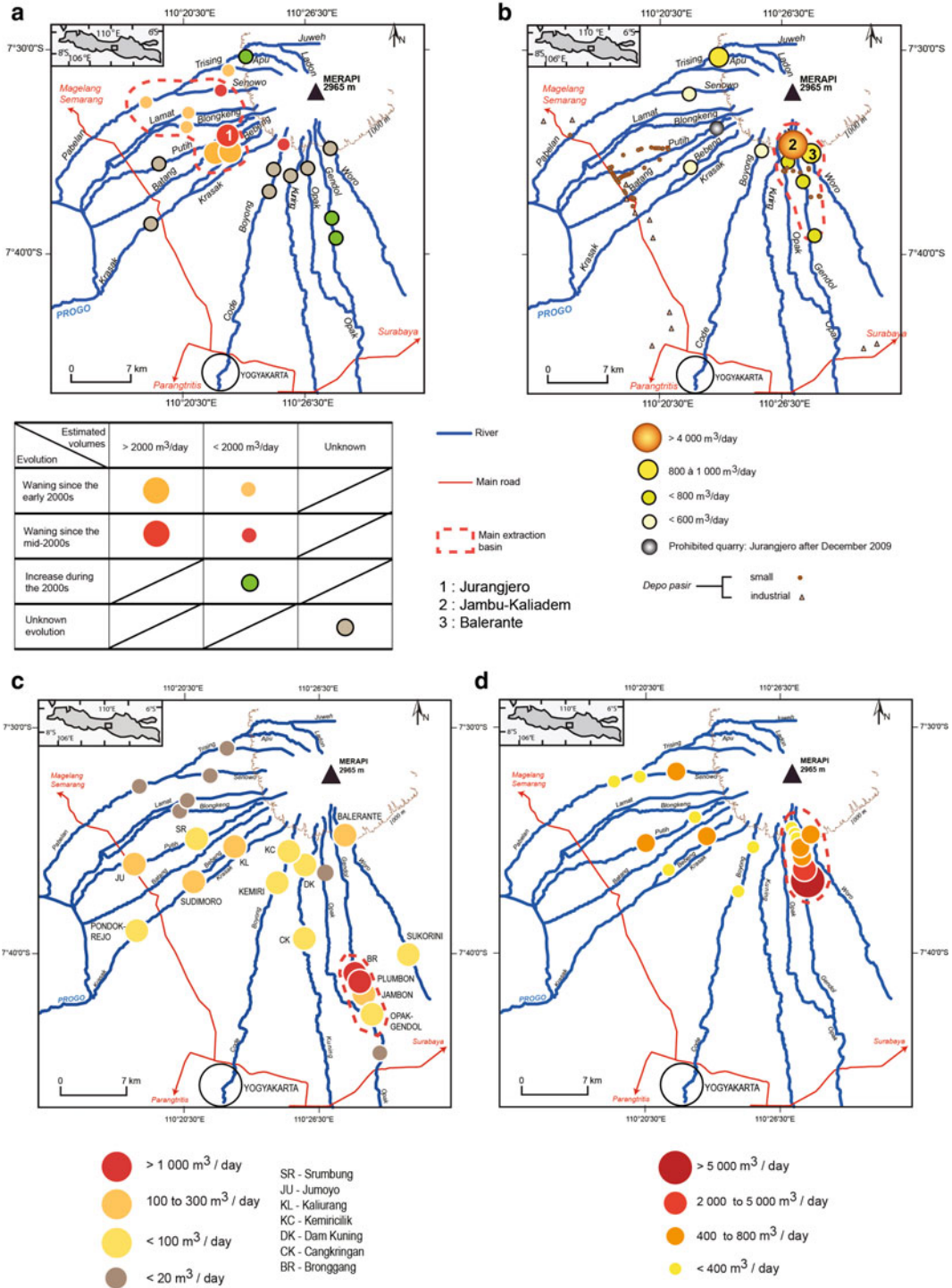


Fig. 2.5 Evolution of sand mining on Merapi volcano (De Belizal et al. 2013)

2.3 Capacities to Face High-Frequency/Low-Magnitude Eruptions at Merapi

For the past two centuries, the activity of Merapi has alternated regularly between long periods of viscous lava dome extrusion, and brief explosive episodes every few years, which generated dome-collapse pyroclastic flows and destroyed part of the pre-existing domes (Voight et al. 2000). More violent explosive episodes with an average recurrence of a few to several tens of years have generated pyroclastic flows, surges, tephra falls, and subsequent lahars (Thouret et al. 2000). The volcanic risk management has been based on impacts from such eruptions.

2.3.1 Volcanic Risk Management

The Ministry of Energy and Mineral Resources, through the Geological Agency and the Center for Volcanology and Geological Hazards Mitigation (CVGHM), is in charge of providing information services such as maps to the communities to reduce people's exposure to natural hazards. The first so-called hazard map (a map of the "official danger zones") was published at the 1:100,000 scale in 1978 by the Volcanological Survey of Indonesia (Pardiyanto et al. 1978). It was based on the lateral extent of the largest eruptions of the twentieth century (i.e., 1930, 1961, and 1969). This map was updated in 2002 (Fig. 2.1a; Hadisantono et al. 2002), in order to take into account situations that had not been considered before (e.g. eruptions in the central part of the summit, vertical ash columns). Made available online by CVGHM, this updated hazard map was used by local authorities as an input for contingency planning that took place in 2009 in each district surrounding the volcano. After the devastating 2010 PDCs, this map has been revised again (Fig. 2.1b), in order to consider a plinian or subplinian eruption scenario such as the one that occurred in 1872 (Sayudi et al. 2010). The maximum distance of the KRB II has been extended up to 17 km from the summit in the southern flank of the volcano.

Besides the scientific risk maps and zoning, the basic elements required for municipalities planning are information documents (at regional and local scale) gathering all the knowledge on hazards, elements at stake, prevention and emergency measures, or simplified hazard zonation. The most important information to be disseminated relates to the current activity of the volcano. There are five observatory posts at Merapi (namely Kaliurang, Babadan, Ngepos, Jrahah and Selo) which report routinely the instrumental and visual observational activity of Merapi to CVGHM's Volcano Investigation and Technology Development Office (*Balai Penyelidikan dan Pengembangan Teknologi Kebencanaan Geologi*; BPPTKG), which is then transmitted to CVGHM. Both CVGHM and BPPTKG provide real-time observations of the volcanic activity to the public, as well as closed-circuit video feeds on their website (<http://vsi.esdm.go.id/>). In addition, MAGMA Indonesia (<https://magma.vsi.esdm.go.id/>) also disseminates activities of all monitored volcanoes in Indonesia, including Merapi.

At Merapi, most of the information is provided during the 'raising awareness program' phase, a period of time corresponding to the pre-alarm phase, during which a great effort is put into informing people about the volcano and its activity. This raising awareness program is achieved in the framework of a Community-Based Disaster Risk Management (CBDRM), which empowers communities with self-developed ways of coping with crises due to natural hazards. At Merapi, the Obligatory Training for Volcano Eruption Disaster Countermeasure (OTVEDC or *Wajib latih*) for the communities located in zone KRB III is planned, prepared, and implemented by the community with the help of scientists and the government. It gathers together, among others, the PASAG Merapi (a 25-year-old community organisation on disaster preparedness) and the Merapi Forum (a government representation of disaster management around Merapi).

After the 1994 and 2006 eruptions, there were many programs related to volcanic disaster risk reduction conducted by government or

nongovernmental organisations. However, the programs were still conducted in fragmentary manners. This condition led some organisations to establish a partnership-based disaster risk mitigation network named Forum Merapi in 2006 (Mei and Lavigne 2012). It gathers local authorities from the Sleman, Klaten, Magelang and Boyolali districts, BPPTKG, several local, and international Non-Governmental Organisations, academic institutions, and representatives of local communities. The series of activities consist of workshops which aim: (i) to raise the awareness of the necessity of getting more advanced technology for the Mt. Merapi disaster monitoring system; (ii) to exchange views regarding the flow of Mt. Merapi disaster information; and (iii) to exchange views regarding the history and current position/performance of Forum Merapi. Community meetings (Focus group discussions or FGDs) are used to share experiences of past eruptions, identify problems during the crisis period, and ensure that everybody knows the emergency plan, evacuation procedure, location of meeting points, etc. This activity generates three features at the hamlet level: (i) disaster risk mapping, which fed the Merapi risk maps for lahar and PDCs drawn by CVGHM in 2012, (ii) standard operating procedures, and (iii) contingency plans. Jalin Merapi (*Jaringan Informasi Ligkar Merapi*) is a community-based information network around Merapi. It integrates various media to (i) quickly spread useful information about the volcano and (ii) support disaster response action during the Merapi eruptions (Justyna and Sulfikar 2016). At least four community radios (e.g. Radio Lintas Merapi at Deles, Klaten) are actively reporting information to their community, especially during volcanic crises. The Jalin Merapi website has interactive features such as an online messenger, a discussion forum, maps and databases (<https://jalinmerapi.net/>). Field updates are delivered by portable radios and SMS messages from mobile phones. Social media also play a key-role in disseminating information during volcanic crises, especially Twitter. This informational capital, a concept which aims to explain the interplay between social capital and information

technology in community-based disaster management, boosts the community capacity for disaster response (Justyna and Sulfikar 2016). After the 2010 eruption, young people from Yogyakarta and from settlements located along the rivers developed basic tools for helping dwellers to cope with the hazards related to repeated lahars. Observation posts were regularly installed and equipped with portable radios and mobile phones. When a lahar was reported upstream, the information could be instantly transmitted downstream. It allowed people living in areas where lahars were prone to spill over the channels to get away from the rivers, and helped sand miners to evacuate the quarries around 20–45 min before the lahars arrived (De B elizal et al. 2013).

Practicalities of risk management plans need to be thought of in advance, and plans need to encompass medical care. Horwell et al. (2019) highlight that a false sense of security might have been generated in the face of the ash fallout hazard in the Yogyakarta area. Indeed, during the ash fallout from the Kelud eruption in February 2014, public agencies distributed surgical masks as protections while the level of protection of these masks against volcanic ash has been unknown. Mapping local healthcare structures (e.g. public hospitals or medical centres locally called PUSKESMAS) and health-care providers is also an issue of great importance. The location of healthcare structures shows an irregular distribution around Merapi. Public hospitals are essentially located on the southern flank, close to main cities. Care centres and polyclinics are available in most villages. There are only a few doctors registered along the slopes of Merapi. Most of them are located more than 12 km away from the summit leaving the highest villages a doctor-free zone.

2.3.2 Crisis Management

Crisis management in Indonesia is based on a top-down hierarchical organisation (e.g. plate D.9. in the Atlas of Merapi Volcano, <http://lgp.cnrs.fr/spip/standard/index.html>). The Indonesian

National Coordinating Agency for Disaster Management (BAKORNAS) was founded in 1966. It became the Indonesian National Board for Disaster Management (BNPB) after the issuance of Law Number 24 of 2007 and Presidential Regulation Number 8 of 2008.

BNPB is a non-departmental body, which coordinates the implementation of planned, integrated and comprehensive disaster management activities. To implement disaster management duties in Province and District/City regions, Regional Disaster Management Agencies (BPBD) have been established. In the framework of the contingency plan approved in 2009, a scenario for an eruption at Merapi was prepared for each district, and the roles of each institution involved were defined (Mei and Lavigne 2012; Mei 2013).

2.3.2.1 Official and Traditional Warning Systems

The volcanic crisis management is based on the recommendations of the CVGHM, the institution in charge of assessing and monitoring volcanic activity in Indonesia. CVGHM provides four warning levels of volcanic activity. For each warning level, recommendations are provided to the people living on the volcano slopes: Level 1: No need for concern (*Normal*); Level 2: Caution or Stand by for technical direction issued by CVGHM (*Waspada*); Level 3: Prepare to evacuate (*Siaga*); Level 4: Evacuate because of imminent eruption (*Awas*). Information issued by volcano observatories are centralised at the Merapi central observatory based at the BPPTKG in Yogyakarta. This institution transfers the information to the local authorities (BPBD) in charge of disseminating the alert level to the public following the established communication protocol. Reports are sent daily for the “normal” (Level 1) status of Merapi, every 12 h for the level 2, and increased to every 6 h for the levels 3 and 4 statuses. This information is also reported to local governments. However, BPPTKG is allowed to directly alert the population in case of an imminent threat (Surono et al. 2012).

At Merapi, modern tools like sirens are increasingly used as “official” warning systems. As sirens allow wide-ranging warning, their

existence in a *dusun* (hamlet) is a real asset to broadcast alerts. In case of an imminent threat, Civil Defense authorities can trigger them to launch evacuation processes. Within communities, traditional means of alert are still available and used in case of a threat. The *kentongan* (traditional gong) is widely used for numerous purposes, including gathering local communities. When it is continuously activated, people know a danger is imminent and, following the authorities’ directives, gather themselves in a safe area. In 2002 at Merapi, over 70% of villagers thought that the traditional *kentongan* was an efficient system. However, only 46% of them were aware of the codes related to a volcanic eruption.

2.3.2.2 Organising the Evacuations: The Importance of Road Networks and Transportation Capacity

Coordination of evacuations is handled by one or more institutions: the Indonesian Department of Transportation, the Department of Public Works, and the Army. Official transport such as buses, trucks or cars are provided by the Indonesian Department of Transportation, Department of Health, Social Department, Army, Police, Sub-district Government, Non-Government Organisations (NGOs) and several other organisations and volunteers. In addition, private vehicles are used, preferentially trucks, because cars are more sensitive to the road conditions.

The road network is quite dense around Merapi. Main roads go straight up the volcano while secondary roads follow the volcano’s contours and connect the main roads. Provincial and district road conditions are generally good. Local roads linking each municipality are mostly asphalt and the roads in the southwestern part of the volcano are in the best conditions. In most villages, road conditions are inversely proportional to the altitude: the higher they are, the lower their quality (Mei et al. 2013). The tropical downpours contribute to fast degradation of the road network, especially of unpaved roads. In addition, roads covered by ash are very slippery. As a result, the efficiency of evacuation with vehicles is limited in many villages. The

maintenance of evacuation roads became a major issue for post-crisis management following the 2006 Merapi eruption (Mei and Lavigne 2013), and even more after the 2010 eruption (Mei et al. 2013). Because the conditions of the roads degrade with time, especially because of trucks hauling volcanic materials (De Belizal et al. 2011), local governments have worked to enhance the quality of roads by paving them with asphalt. In addition, the official evacuation roads are now forbidden to trucks, and are therefore subject to much lower degradation over time.

In Indonesia, the most common means of transport is the motorcycle, because of its low cost and its adaptation to mountainous small roads. On volcanoes, this phenomenon is accentuated because the population is poorer than the population of the big cities, where cars are mainly used by the middle and upper classes. The census conducted in 2010 and 2011 within the MIAVITA Project (<http://miavita.brgm.fr>), about the available means of local transport, recorded an average of one car per 43 inhabitants and one motorcycle per 5 inhabitants (Lavigne et al. 2015), which was clearly insufficient for mass evacuation. Nowadays, the situation is much better than in 2010: vehicles available locally are more numerous, especially motorcycles, and the Regional Disaster Management Agency (BPBD) prepares evacuation vehicles together with the chief of the village.

2.4 Crisis Management and Peoples' Responses During the 2010 Low-Frequency/High-Magnitude Eruption

In October and November 2010, Merapi did produce its largest eruption in a century, damaging around 12,000 buildings (Yulianto et al. 2013), claiming lives, triggering huge economic losses and massive evacuations (Mei et al. 2013), and resulting in daily life disruptions, such as loss of livelihoods, or disruption of schools for two months before the government succeeded to establish emergency schools (Rahman et al. 2016).

2.4.1 Crisis Management by the Authorities

Based on BNPB (Indonesian National Board for Disaster Management) data, 367 people were killed during the 2010 eruption, including 200 directly by PDCs that were emplaced on Merapi's southern flank. After the 1994 eruption, the main hazard-prone areas moved from westward to southward (Kali Boyong), for the first time since the 1969 eruption (Voight et al. 2000). In addition, 277 people were directly or indirectly injured by the 2010 eruption. Most of them were located on the southern and western flanks of the volcano, where the hazard was most intense: on the southern flank people were mainly wounded by burns from ash cloud surges, whereas those on the western flank were injured by ash fallout, due to the prevailing direction of the trade winds in early November. Jenkins et al. (2013) demonstrated that despite low structural damage along the path of surges, temperatures of 250–300 °C were not survivable by residents caught inside buildings because of the ease with which hot ash could infiltrate through ubiquitous ventilation openings. Slightly injured people located on the western flank were affected by respiratory issues due to their exposure to volcanic ash. A local NGO distributed around 1 million basic facemasks to inhabitants of the Special Region of Yogyakarta (Horwell et al. 2019) and the ash was rapidly washed away by monsoon rains (Damby et al. 2013). Since more than 1.1 million people inhabited the flanks of Merapi in 2009 (Lavigne et al. 2015), the evacuation process was considered successful by the authorities.

2.4.1.1 Evacuation Orders and Restricted Zones

Even though the 2010 eruption was much larger and longer than anticipated by contingency planners (Mei et al. 2013; Bakkour et al. 2015), the authorities were able to adapt the evacuation zones six times based on the evolution of volcanic activity (Fig. 2.6):

1. Period A: 25 October–2 November. According to the 2002 hazard zone map, CVGHM

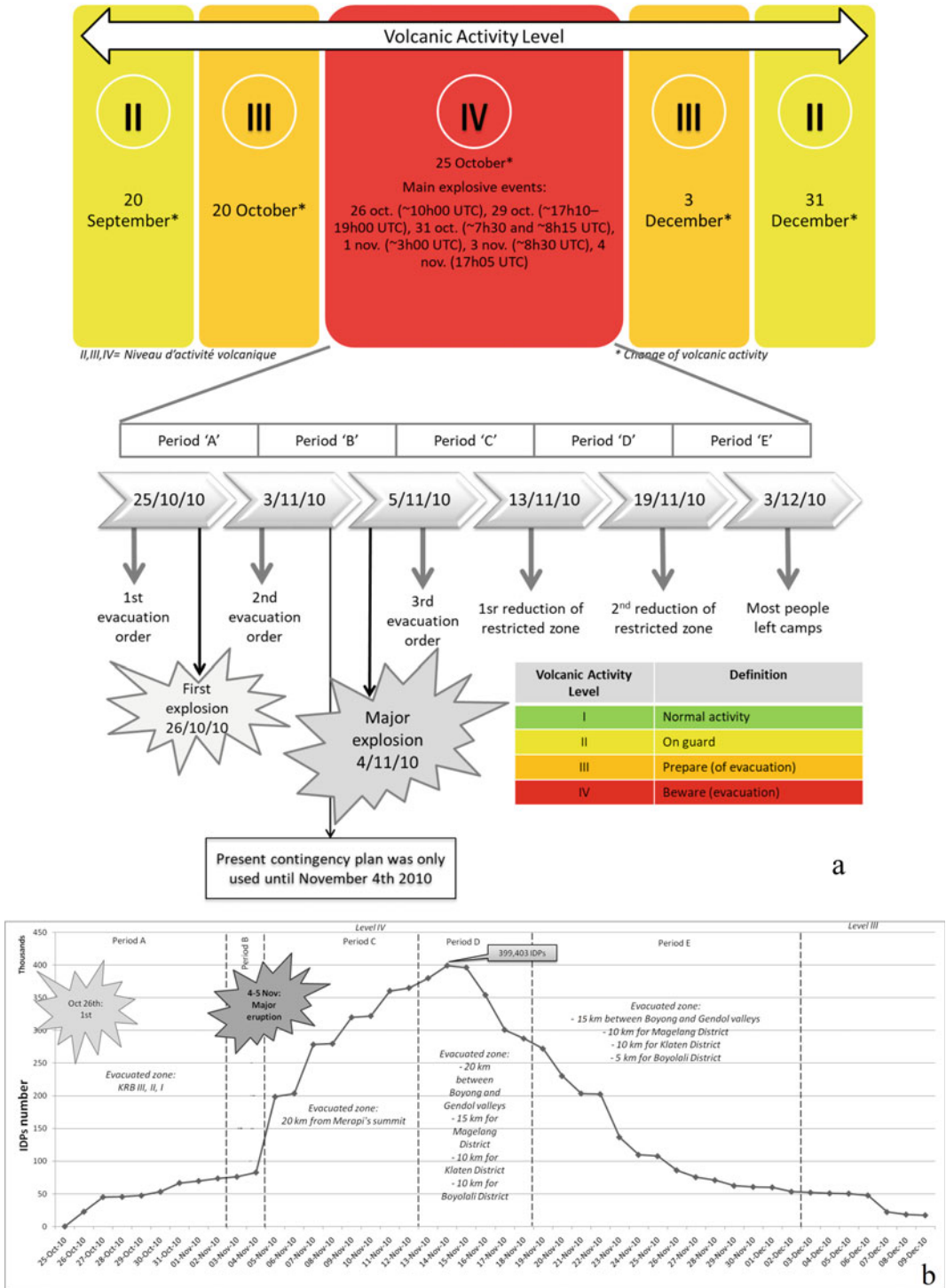


Fig. 2.6 Evacuation during the 2010 Merapi eruption. **a** Timeline of evacuation. **b** Population of Internally Displaced Person (IDP) camps over the course of the

2010 Merapi eruption. **c** Number of IDPs per District during evacuation period (Mei et al. 2013)

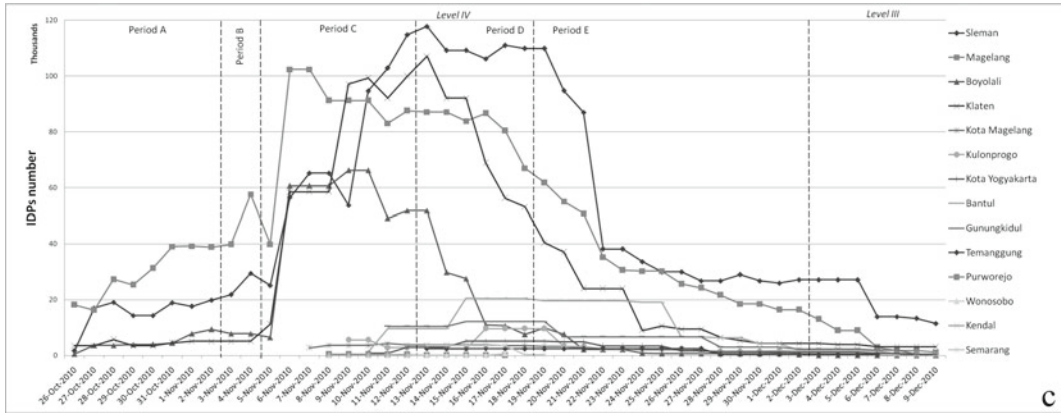


Fig. 2.6 (continued)

recommended the evacuation of 12 municipalities located in zone KRB III. Official shelters, such as schools or official buildings, were provided by the government. Local authorities recorded and registered the refugees during this period.

2. Period B: 3–4 November. CVGHM recommended the evacuation of 32 municipalities in the KRB III zone, abandoning the 2002 map for the benefit of new evacuation plans updated due to an increasing radius of the danger zone.
3. Period C: 5–13 November. Several hours before the paroxysmal eruption, CVGHM extended the restricted zone to 20 km from the summit and recommended immediate evacuation of people living within this radius. Based on a survey carried out among 1969 people in shelters during this eruption, only 16% of the people were warned by sirens before the PDCs entirely affected the southern flank of the volcano, whereas most people received evacuation alerts directly from the head of village (54%), or from neighbours (11%). The main reason for the limited use of modern tools was that the aerial distribution of sirens was not homogenous among each Merapi flank (Mei et al. 2013; Lavigne et al. 2017).
4. Period D: 14–19 November. A radius of 20 km for the restricted zone in the sector between the Boyong and Gendol rivers was

maintained. The radius was reduced to 15 km for the Magelang District and 10 km for the Klaten District and Boyolali District.

5. Period E: 19 November–3 December. The radius of the restricted zone was reduced to 15 km for the sector between the Boyong and Gendol rivers, 10 km for the rest of Sleman District, 10 km for the Magelang District and Klaten District and 5 km for the Boyolali District.

The wider extent of restricted zones to the south has been due to the morphology of the Merapi summit which consists of a horseshoe-shaped crater opened southward.

At the end of the 2010 eruption, about 400,000 people had been evacuated, some of them several times (Mei et al. 2013). This series of evacuations allowed saving between 10,000 and 20,000 lives (Suroño et al. 2012).

2.4.1.2 Crisis Management Related to Air Traffic

Volcanic eruptions that eject ash into the atmosphere represent a threat to the safety of air traffic. Tephra is very abrasive to the plane's cabin, and ash accumulates in the engines generating engine failure. On June 24th, 1982, a British Airways Boeing 747-236B flew through the ash cloud generated from the Mount Galunggung eruption (West Java), resulting in

the failure of all four engines. Since then, international rules restrict air traffic in case of a threat. The Darwin Volcanic Ash Advisory Center provides reports about volcanic plumes spreading over Southeast Asia. In parallel, CVGHM provides Volcano Observatory Notices for Aviation (VONA) to national and international stakeholders in the aviation sector, based on analysis of both monitoring networks and ground-based visual observations.

Under normal circumstances, 90 flights are scheduled every day at Adisucipto International Airport in Yogyakarta, with an average of 11,500 passengers per day. For the first time, the 2010 Merapi eruption triggered major air traffic disruptions in Yogyakarta, which resulted in a paralysis of the city's activities. During the volcanic crisis, about 2000 flights were cancelled, comprising 1350 flights during the closure of the airport for 15 days, and an additional 600 flight cancellations due to a lack of a sufficient number of reservations after its reopening (Picquout et al. 2013). Some companies like Garuda Indonesia suspended or transferred their flights to other airports, whereas the low-cost carriers like Lion Air continued to fly despite the risks involved. The eruption of Merapi was fatal to Mandala Airlines, which encountered financial problems since 2010 and declared bankruptcy on 13 January 2011 (Picquout et al. 2013).

2.4.2 Peoples' Response During the 2010 Eruption Crisis

People's behaviour in the face of volcanic crises at Merapi depends on a set of intricate factors (Lavigne et al. 2008). Because of the massive displacements of the population that took place during the 2010 crisis, we specifically focus on people's behaviour as observed in the face of the evacuation decisions and processes.

2.4.2.1 Shelter Attendance

When the restricted zone was extended soon before the main explosions on 4–5 November, the number of refugees exponentially increased while no refugee camps had been prepared

beyond the restricted radius of 20 km. Therefore, most of the evacuees were settled in emergency in three types of shelters: (i) public buildings (schools, hospitals, stadiums, village halls, and universities); (ii) community-based shelters provided by communities from other regions, as support and help were provided by NGOs and communities from beyond the area affected by the eruption; and (iii) relative-based shelters provided by individuals, mainly family members. Shelters provided by individuals after the evacuation were extended to a radius of 20 km. On 13 November, there were at least 600 camps registered by BNPB, scattered around Sleman, Magelang, Boyolali, Klaten and several other districts in the Central Java Province and the Yogyakarta Special Region Province (Fig. 2.7). Despite the evacuation order to clear the 20 km radius 10 days earlier, the highest number of refugees was reached on 14 November (399,403), due to insufficient preparedness in handling the evacuation and evacuees' movements from one camp to another (Mei 2013; Mei et al. 2013). The number of refugees then decreased significantly when the CVGHM decreased the radius of the restricted zone to 10 km on 18 November. People from villages that were still habitable went home for good. On 9 December, less than 20,000 people were still recorded in the refugee camps.

The community actively tried to self-organise and took initiative to the crisis response handled by the authorities. For instance, about 700 volunteers of Jalin Merapi were dispatched around the volcano to collect information about the evacuees' needs and help disseminate information and distribute the relief help (Saputro 2016).

2.4.2.2 Population Behaviour During the 2010 Eruption Crisis

Most inhabitants evacuated only when the first pyroclastic flows were reported on 26 October even though the evacuation order was given the day before on 25 October. This evacuation may be classified as "evacuation when hazard is imminent", a phenomenon that is common at Merapi in the context of dome extrusion which produces dome collapse pyroclastic flows

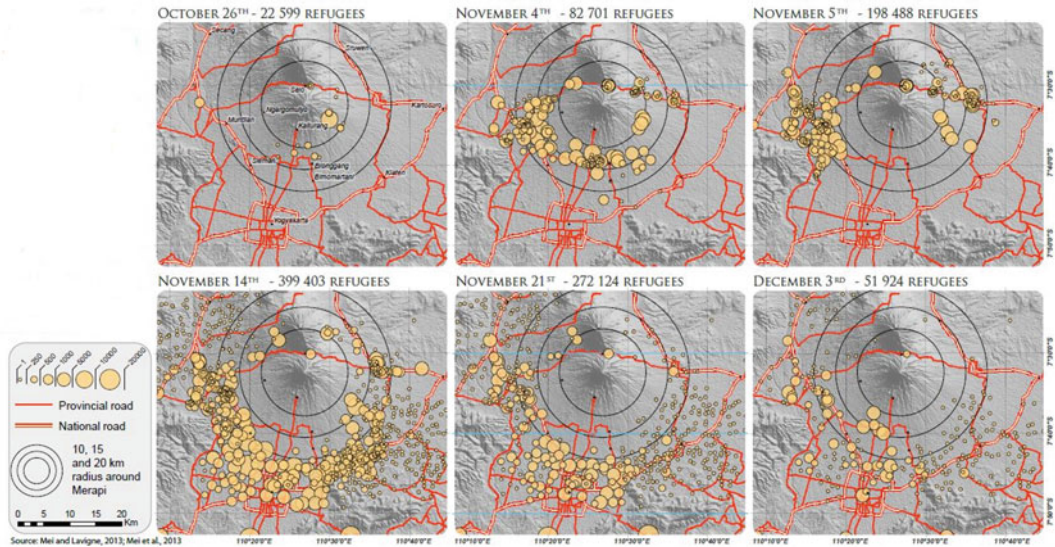


Fig. 2.7 Location and attendance of evacuation camps during and after the 2010 eruption. Modified from Mei et al. (2013)

(Mei and Lavigne 2012). As for the pre-2006 eruptions, people waited to evacuate until the first major pyroclastic flow or ash fall event had taken place, even though the government had previously informed them that the volcano was already at its highest warning level (Mei et al. 2013).

During the paroxysmal eruption on the night of 4–5 November 2010, people self-evacuated. Without detailed instructions, people tried to escape by themselves, but many did not know exactly where to go. In the village of Bronggang, approximately 13.5 km to the south of Merapi, 54 people, who were in the process of evacuating from the village a few hours before the 5 November paroxysm, were killed when PDCs entered the village (Mei et al. 2013). Despite a previous evacuation order, they were reluctant to evacuate because their village was not within the official danger zone of PDC hazard, and they felt safe.

Some people evacuated on time and attended a shelter, but they eventually came back home because of the lack of space and comfort in shelters (Mei and Lavigne 2013).

The majority of people partly evacuated, i.e. they tended to stay at home during the day and to

return to the evacuation shelters in the evening. This attitude concerned up to 68% of the local people at the beginning of the eruption, but still reached 52% after the paroxysmal eruption of 4–5 November (Mei et al. 2013). People took the risk to enter the successive forbidden zone during the eruption (Fig. 2.6) for various reasons that varied over time (Fig. 2.8). Before the paroxysmal eruption, most of the people returned home to feed the cattle (68%), which had not been evacuated. After the paroxysmal eruption, this proportion decreased to 24%, because the main reason to return home was to check the condition of their house (59%) or to take care of it (13%).

Despite evacuation orders and efforts of local authorities to evacuate people, some residents were reluctant to leave their villages. Refusal to evacuate was mostly due to people's perception of the volcano, cultural beliefs, and socio-economic conditions (Dove 2008; Donovan 2010). This refusal led to casualties, i.e. the evacuation refusal of Mbah Marijan (Merapi volcano's gatekeeper) and his followers led to the deaths of 38 people in the village of Kinahrejo (5 km from the summit). Along the southern flank of the volcano, evacuation refusals were mostly conditioned by trust in the gatekeeper and

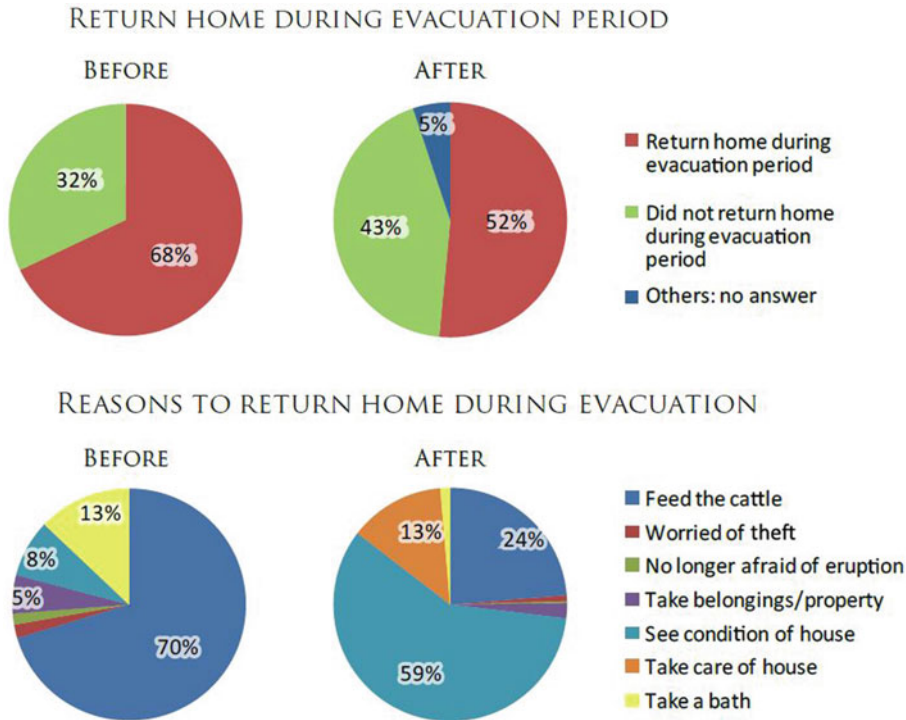


Fig. 2.8 Migration of affected people during evacuation period before and after the paroxysmal explosion of Merapi on 4–5 November 2010. **a** Proportion of people

who returned home ($n = 387$ before, and 1582 after 4 November). **b** Reasons to return home. *Source* Mei et al. (2013)

the feeling of being protected by his presence, even though Marijan suggested to people not to follow his decision to stay in the village. However, people living far away from the gate-keeper's village opted not to leave their house because of their poor understanding of volcanic processes (Picquout 2013). Others stayed in their village to look after their livestock. Jumadi et al. (2018) synthesised the behavioural variables observed during the 2010 evacuation to propose a model of the individual decisions leading to evacuation reluctance. Their most efficient model in simulating the real disaster events at Merapi was obtained considering the occurrence of an explosion as the most important motivation for evacuation. To improve future evacuations, Bakkour et al. (2015) proposed several solutions: (1) to better integrate disaster risk education at school, (2) to develop an updated disaster database including loss, (3) to improve facilities and their maintenance, (4) to better spread accurate

information, and (5) to elaborate multi hazards and multi scales scenarios including lahar scenarios at a local scale (village and hamlet). In addition, a key aspect to improve the evacuation process is the continuous community engagement and preparedness for volcanic hazards. The pitfalls met during the 2010 eruption reveal that communities, authorities and scientists should consider getting prepared for larger-than-usual volcanic hazards to reduce the risk of future volcanic disasters (Mei et al. 2013).

2.5 Post-Disaster Resilience and Adaptation at Merapi

A post-disaster analysis was conducted as part of the SEDIMER research project (*Sediment-related Disasters following the 2010 centennial eruption of Merapi Volcano, Java, Indonesia, 2012–2014*. PI: F. Lavigne. Funding: AXA

Research Fund). It was based on surveys addressing key issues of the recovery process such as timing of rehabilitation and reconstruction, human and financial resources implemented, difficulties faced by households and stakeholders in developing a “preventive reconstruction” adapted to their daily needs and constraints, and access to livelihoods before and after the disaster (Moatty 2015). The surveys (175 questionnaires) were conducted between 2013 and 2014 in two valleys located on the southern slope of Merapi: the Gendol valley (in the Special Territory of Yogyakarta) and the Putih valley (in Central Java). An additional survey based on 46 questionnaires and key informant’s interviews was made in 2015 in two sub-villages (Mei et al. 2016).

2.5.1 The Choice of Relocation

After the 2010 eruption, the Indonesian Government decided to relocate the affected people outside the hazard-prone areas, as delineated in the new hazard map (Fig. 2.1; Sayudi et al. 2010). Regarding the lahar hazard zone (KRB I), the Government also decided that a 300 m wide area from the riverbanks could not be built on anymore. All the households located in this area had the possibility to be relocated. To be eligible for resettlement centres, the households had to meet nine criteria: (1) they have lost their homes because of eruption and/or lahars, (2) the house is located in the hazard-prone area, (3) the house is destroyed or damaged but has not been repaired, (4) the house is the legal property of the household, (5) it is located on land whose owner has the right to use, (6) the household is not currently awaiting similar support provided by another funder, (7) the household is committed to not rebuild their “old house” (the one in their former hamlet) and to respect the risk zoning defined by the local government (i.e. Lahars (KRB I, KRB II, KRB III), (8) the household does not have any ability to rebuild his house even though it is not located in high-risk prone areas, (9) are also eligible households with building plots outside the hazard prone areas (Moatty 2015).

As a stimulus to recover, the Indonesian authority, through the *Rekompak (Rehabilitasi dan Rekonstruksi Pemukiman Berbasis Masyarakat / Community-based Housing Rehabilitation and Reconstruction)* program, gave each household who wanted to be relocated a 100 m² land and a 36 m² house outside the hazard-prone area. All the houses have been built earthquake resistant. Every household received the same lot regardless of the level of damage to the former house. To manage the construction of houses in the resettlement centres, households were gathered in units of 15–20 families and organised as a follow-up committee with a leader, a secretary, a treasurer, and controllers of the quality of materials and construction methods. *Rekompak* provided training to all households in each of these areas and held regular monitoring and support meetings using a team facilitator. The whole process, which involved about 4000 households, took on average three and a half years (Moatty et al. 2017).

2.5.2 Daily Challenges and Evolution of the Quality of Life

Both the village leaders and communities have identified many difficulties in the recovery process (Fig. 2.9). The people living in the red areas (Fig. 2.9) had to cope with disruptions of political stability, which has resulted in conflicts with local authorities. The post-disaster tensions revive preexisting conflict (Moatty 2017) between the hamlet leaders (*dusun* level) and the chiefs of villages (*desa* level) (Moatty 2015). Some village chiefs did not take on their role of assisting hamlet leaders in the administrative procedures, especially regarding the relocation process and issues. The hamlets leaders felt abandoned, and the departure of the media and NGO volunteers enhanced this feeling (Moatty et al. 2017).

The people living in the dark purple areas (Fig. 2.9) have experienced two kinds of funding problems: in the first case (the vast majority), the funds for the construction did not arrive fast enough compared to the work progress, and in the second case, the households faced difficulties with administrative procedures.

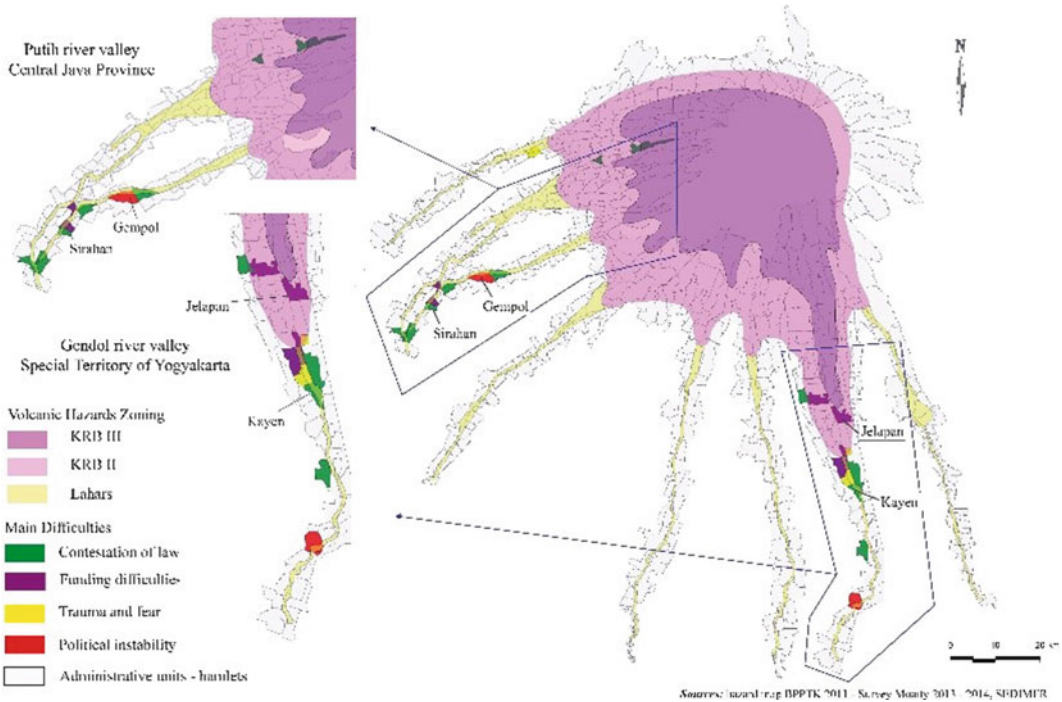


Fig. 2.9 Main difficulties in the recovery process. Modified from Moatty (2015)

The hamlets in the green areas (Fig. 2.9) have faced contestation of laws and regulations. They can be divided into two groups, based on governance policies. The first group is composed of territories where households and local authorities consider the seismic building standards as too expensive and unsuited for the needs of affected people, who would have preferred a bigger and more comfortable house located closer to their source of income (that is to say their fields in disaster-prone area). The second group is composed of hamlets where the strategy of relocation was strongly criticised, dividing communities into two, namely those who decided to leave and those who have remained. Critics focused on the fact that no effort was made to restore the villages and especially the agricultural sector. Finally, in the yellow areas (Fig. 2.9), the reconstruction was difficult and slowed down because of the trauma of the population struggling to recover.

A large majority of the respondents believe that their quality of life has declined because of lower income. This drop occurred between the

period they lived in the village and their new lives in the resettlement centre. Rahman et al. (2016) reported the same analysis and highlighted that it took a couple of years to normalise community livelihoods. The difficulties of access to everyday consumer products were related to the decrease of transportation means and the lack of road rehabilitation at that time. Facing those difficulties, about a third of the households began to rehabilitate their houses in the hamlet, therefore in the hazard-prone area.

The households staying in the resettlement centres had to diversify their livelihoods to compensate for the distance between their fields—and more broadly their livelihoods—and their new living space. NGOs such as Paluma (acting for women, children, the environment, industry and micro-industry agribusiness) facilitated their conversion offering training to develop home based businesses, such as the production of “candy tape” which are fermented cassava sweets produced in the resettlement centres and sold in markets or in stalls located at the roadside

(Moatty et al. 2017). Other groups diversified their livelihoods by developing post-disaster tourism in villages near the crater (such as Kinahrejo or Pentingsari) with jeep tours of the places affected by the eruption (Rindrasi 2018), or the visit of Marijan's house (Sagala et al. 2012). Even if the relocation program was globally successful, some conflict arose due to the inequity of the new situation: some households benefited from a new house in the relocation settlement, but also kept the former one because it was only slightly damaged. These inequalities deteriorated the social capital (defined as the family, professional and/or neighbourhood networks on which the household or social group can rely to recover more quickly) (Aldrich 2012; Aldrich and Meyer 2015; Moatty 2015, 2017; Moatty and Vinet 2016). This social capital, as a fundamental resource for recovery, is cyclically influenced by the socio-political and economic context on the Merapi slopes as in any other territory (Moatty et al. 2017).

2.6 Summary and Outlook

Like many other volcanoes in Indonesia and in the world, Merapi is densely populated. The high frequency of its eruption over the last century has led the population to adapt to a permanently changing environment and to cope with potentially lethal hazards. Volcanic hazards encompass dynamic processes, which will keep changing the environment where people live. Therefore, people need to have the capability to adapt and anticipate the potential hazards in the future. For example, the role of sand mining activity is highly controversial: on the one hand, it exposes workers to volcanic hazards, and increases conflicts between communities as it threatens the local agriculture, and on the other hand, it reduces the occurrence of future lahars by reducing the removable sediment volume. It also reduces the lahar's depth, velocity, and discharge by widening and deepening the natural valleys. Regarding the post-disaster period and the recovery process, the relocation program following the 2010 eruption has shown positive

aspects. However, it has produced inequities and conflicts likely to disrupt the traditional solidarity and social bounds among the villages surrounding Merapi. These conflicts are negative for the future resilience of the community because they induce a tendency to decreasing solidarity. The experience of the 2010 eruption in terms of crisis management and recovery process demonstrates the need to assess the social, economic, and political trajectories over a large period in order to understand people's vulnerability—which remains high—as well as their ability to cope with and recover from a disaster.

Acknowledgements This chapter brings together field data acquired in the framework of two successive scientific projects: (i) The MIA VITA Project (Mitigate and assess risk from volcanic impact on terrain and human activities; 2008–2013), financed by the European Commission under the 7th Framework Programme for Research and Technological Development, Area "Environment" (BRGM—Grant agreement no. 211393). (ii) The SEDIMER Project (Sediment-related Disasters following the 2010 centennial eruption of Merapi Volcano, Java, Indonesia), which was funded by the AXA Research Fund (2011–2015) and led by the Laboratoire de Géographie Physique (CNRS, France). Additional data on Merapi volcano can be found in the online 'Atlas of Merapi volcano' (F. Lavigne, J. Morin and Surono (Eds.), published in 2015). We are grateful to the LabEx Dynamite for its financial contribution to this work. The Center of Volcanology and Geological Hazard Mitigation and its local branch at Yogyakarta (BPPTKG) are acknowledged for their support and involvement in this work.

References

- Aldrich DP (2012) Building resilience: social capital in post-disaster recovery. The University of Chicago Press, Chicago, p 248
- Aldrich DP, Meyer MA (2015) Social capital and community resilience. *Am Behav Sci* 59:254–269
- Bakkour D, Enjolras G, Thouret JC, Kast R, Mei ETW, Prihatminingtyas B (2015) The adaptive governance of natural disaster systems: insights from the 2010 mount Merapi eruption in Indonesia. *Int J Disaster Risk Reduct* 13:167–188
- Blong RJ, Grasso P, Jenkins SF, Magill CR, Wilson TM, McMullan K, Kandlbauer J (2017) Estimating building vulnerability to volcanic ash fall for insurance and other purposes. *J Appl Volcanol* 6:2
- BPS (2018) Kecamatan dalam Angka. Yogyakarta, Biro Pusat Statistik (BPS)

- Brown S, Auken MR, Sparks RSJ (2015) Populations around Holocene volcanoes and development of a Population Exposure Index. In: Sparks S, Brown SK, Jenkins SF, Vye-Brown C (eds) Loughlin SC. *Global Volcanic Hazards and Risk*, Cambridge University Press, pp 223–233
- Charbonnier SJ, Gertisser R (2008) Field observations and surface characteristics of pristine block-and-ash flow deposits from the 2006 eruption of Merapi Volcano, Java, Indonesia. *J Volcanol Geotherm Res* 177:971–982
- Damby DE, Horwell CJ, Baxter PJ, Delmelle P, Donaldson K, Dunster C, Fubini B, Murphy FA, Nattrass C, Sweeney S, Tetley TD, Tomatis M (2013) The respiratory health hazard of tephra from the 2010 Centennial eruption of Merapi with implications for occupational mining of deposits. *J Volcanol Geotherm Res* 26:376–387
- De Bézal E, Lavigne F, Grancher D (2011) Quand l'aléa devient la ressource : l'activité d'extraction des matériaux volcaniques autour du volcan Merapi (Indonésie) dans la compréhension des risques locaux. *Cybergeo Eur J Geogr Environ Nat Pays* 525. <http://cybergeo.revues.org/23555>
- De Bézal E, Lavigne F, Hadmoko DS, Degeai JP, Dipayana GA, Mutaqin BW, Marfai MA, Coquet M, Le Mauff B, Robin AK, Cholik N, Nurnaning A (2013) Rain-triggered lahars following the 2010 eruption of Merapi Volcano, Central Java, Indonesia: a major risk. *J Volcanol Geotherm Res* 261:330–347
- Donovan K (2010) Cultural responses to volcanic hazards on Mt Merapi, Indonesia. PhD Thesis, University of Plymouth, Plymouth, United Kingdom
- Dove MR (2008) Perception of volcanic eruption as agent of change on Merapi Volcano, Central Java. *J Volcanol Geotherm Res* 172:329–337
- Gertisser R, Charbonnier SJ, Keller J, Quidelleur X (2012) The geological evolution of Merapi volcano, Central Java, Indonesia. *Bull Volcanol* 74:1213–1233
- Hadisantono RD, Andreastuti S, Abdurachman E, Sayudi D, Nurnasanto I, Martono A (2002) Volcanic hazard map of Merapi volcano, Central Java and Yogyakarta special province. Scale 1:50,000. Center for volcanology and geological hazard mitigation, Bandung, Indonesia
- Horwell CJ, Ferdiwijaya D, Wahyudi T, Dominelli L (2019) Use of respiratory protection in Yogyakarta during the 2014 eruption of Kelud, Indonesia: community and agency perspectives. *J Volcanol Geotherm Res* 382:92–102
- Hoyos L (2016) Sand mining at Merapi volcano, Indonesia: blessing or curse for miners' livelihoods? Masters Thesis, University of Innsbruck, Innsbruck, Austria
- Jenkins S, Komorowski JC, Baxter PJ, Spence R, Picquout A, Lavigne F, Suroño (2013) The Merapi 2010 eruption: an interdisciplinary impact assessment methodology for studying pyroclastic density current dynamics. *J Volcanol Geotherm Res* 261:316–329
- Jumadi J, Heppenstall A, Malleson N, Caryer S, Quincey D, Manville V (2018) Modelling individual evacuation decisions during natural disasters: a case study of volcanic crisis in Merapi. *Indonesia Geosci* 8 (6):196
- Justyna T, Sulfikar A (2016) Informational capital and disaster resilience: the case of Jalin Merapi. *Disaster Prev Manag* 25(3):395–411
- Lavigne F (1999) Lahars hazard micro-zonation and risk assessment in Yogyakarta city. *Indonesia GeoJournal* 49(2):131–138
- Lavigne F, Thouret JC, Voight B, Suwa H, Sumaryono A (2000) Lahars at Merapi volcano: an overview. *J Volcanol Geotherm Res* 100:423–456
- Lavigne F, De Coster B, Juvin N, Flohic F, Gaillard JC, Texier P, Morin J, Sartohadi J (2008) People's behaviour in the face of volcanic hazards: perspectives from Javanese communities, Indonesia. *J Volcanol Geotherm Res* 172:273–287
- Lavigne F, Morin J, Suroño M (2015) Atlas of Merapi volcano. Laboratoire de Géographie Physique, Meudon, France, 58 color plates. Online Publication (hal-03010922)
- Lavigne F, Morin J, Mei ETW, Calder ES, Usamah M, Nugroho U (2017) Mapping hazard zones, rapid warning communication and understanding communities: primary ways to mitigate pyroclastic flow hazard. In: Feamley CJ, Bird DK, Haynes K, McGuire WJ, Jolly G (eds) *Observing the volcano world. Advances in volcanology*. Springer, Cham, pp 107–119
- Mei ETW, Lavigne F (2012) Influence of the institutional and socio-economic context for responding to disasters: case study of the 1994 and 2006 eruptions of the Merapi Volcano Indonesia. *Geol Soc Lond Spec Publ* 361:171–186
- Mei ETW, Lavigne F (2013) Mass evacuation of the 2010 Merapi eruption. *Int J Emerg Manag* 9(4):298–311
- Mei ETW, Picquout A, Lavigne F, Grancher D, Noer C, Sartohadi J, De Bézal E (2013) Lessons learned from the 2010 evacuations at Merapi volcano. *J Volcanol Geotherm Res* 261:348–365
- Mei ETW (2013) Gestion des évacuations lors des crises volcaniques : étude de cas du volcan Merapi, Java, Indonésie. PhD Thesis, Université Paris 1 Panthéon-Sorbonne, Paris, France
- Mei ETW, Fajarwati A, Hasanati S, Meilyana IF (2016) Resettlement following the 2010 Merapi Volcano eruption. *Procedia Soc Behav Sci* 227:361–369
- Moatty A (2015) Pour une Géographie des reconstructions post-catastrophe: Risques, Sociétés et Territoires. PhD Thesis, Université Paul Valéry, Montpellier, France
- Moatty A, Vinet F (2016) Post-disaster recovery: the challenge of anticipation. *E3S Web Conf (3rd European Conference on Flood Risk Management—FLOODrisk 2016)* 7:17003
- Moatty A, Gaillard JC, Vinet F (2017) Du désastre au développement : Les enjeux de la reconstruction post-catastrophe. *Ann Géogr* 14(2):169–194

- Moatty A (2017) Post-Flood Recovery: an opportunity for disaster risk reduction? In: Vinet F (ed) *Floods*, vol 2. STE Press—Elsevier, pp 349–363
- Pardiyanto L, Reksowirogo LD, Mitrohartono FXS, Hardjowarsito SH (1978) Volcanic hazard map, Merapi volcano, central Java (1/100 000). Geol Survey of Indonesia, II, 14, Ministry of Mines, Bandung
- Picquout A, Lavigne F, Mei ETW, Grancher D, Noer C, Vidal CM, Sri Hadmoko D (2013) Air traffic disturbance due to the 2010 eruption of Merapi volcano. In: Jousset P, Pallister J, Surono (eds) *Merapi 2010 centennial eruption*. *J Volcanol Geotherm Res* 261:366–375
- Picquout A (2013) Impacts géographiques de l'éruption de 2010 du volcan Merapi, Java, Indonésie. PhD Thesis, Université Paris 1 Panthéon-Sorbonne, Paris, France
- Rahman MB, Nurhasanah IS, Nugroho SP (2016) Community resilience: learning from Mt Merapi eruption 2010. *Procedia Soc Behav Sci* 227:387–394
- Rindrasih E (2018) Under the volcano: responses of a community-based tourism village to the 2010 eruption of Mount Merapi. *Indonesia Sustainability* 10(5):1620
- Sagala S, Rosyidie A, Pratama A, Wimbardana R, Wijayanti A (2012) Promoting volcano tourism in hazard zone area for rebuilding local economy: case study of tourism in Cangkringan sub-district, Mt. Merapi, Yogyakarta. In: *International conference on sustainable built environment*, Yogyakarta, Indonesia, p 1–13
- Saputro KA (2016) Information volunteers' strategies in crisis communication: the case of Mt. Merapi eruption in Indonesia 2010. *Int J Disaster Resil Built Environ* 7 (1):63–72
- Sayudi DS, Aisyah N, Juliani Dj, Muzani M (2010) *Peta Kawasan Rawan Bencana Gunungapi Merapi, Jawa Tengah dan Daerah Istimewa Yogyakarta 2010 (Merapi Hazard Map, Central Java and Yogyakarta Special Region Provinces)*. Center for Volcanology and Geological Hazard Mitigation (CVGHM), Bandung
- Surono JP, Pallister J, Boichu BMF, Budisantoso A, Costa F, Andreastuti S, Prata F, Schneider D, Clarisse L, Humaida H, Sumarti S, Bignami C, Griswold J, Cam S, Oppenheimer C, Lavigne F (2012) The 2010 explosive eruption of Java's Merapi volcano-A '100-year' event. *J Volcanol Geotherm Res* 241–242:121–135
- Thouret JC, Lavigne F, Kelfoun K, Bronto S (2000) Toward a revised hazard assessment at Merapi volcano, Central Java. *J Volcanol Geotherm Res* 100:479–502
- Ville A, Lavigne F, Virmoux C, Brunstein D, De Bézilal E, Wibowo SB, Sri Hadmoko D (2015) Évolution géomorphologique de la vallée de la Gendol à la suite de l'éruption d'octobre 2010 du volcan Merapi (Java, Indonésie). *Géomorph Relief Process Environ* 21 (3):235–250
- Voight B, Constantine EK, Siswoidjyo S, Torley R (2000) Historical eruptions of Merapi Volcano, Central Java, Indonesia, 1768–1998. *J Volcanol Geotherm Res* 100(1–4):69–138
- Wibowo SB, Lavigne F, Mourot P, Métaixian JP, Zeghdoudi M, Virmoux C, Sukatja CB, Sri Hadmoko D, Mutaqin BW (2015) Analyse couplée d'images vidéo et de données sismiques pour l'étude de la dynamique d'écoulement des lahars sur le volcan Merapi. Indonésie *Géomorph Relief Process Environ* 21(3):251–266
- Yulianto F, Sofan P, Khomarudin M, Haidar M (2013) Extracting the damaging effects of the 2010 eruption of Merapi volcano in Central Java. *Indonesia Nat Hazards* 66(2):229–247



Merapi and Its Dynamic 'Disaster Culture'

3

Karen Holmberg

Abstract

The deep time depth of human life near Merapi volcano in Central Java and complex engagement of residents with a very dynamic and sometimes dangerous environment has produced a rich body of oral traditions linked to geological phenomena. Merapi is both a geophysical entity and a mythical one for those who live near it and plays an important cosmological role as part of a sacred axis that connects the volcano to the seat of power in the Yogyakarta palace (*kraton*) and the Southern Sea. Interdisciplinary research that entwines geosciences with social science considerations is important when considering any volcanic context but in the Merapi context it is requisite. The social importance of volcanism in Javanese contexts became increasingly relevant from the advent of modern scientific assessments beginning in the eighteenth century. These interpretations were at times catastrophism-tinged, however, and reliant upon an eruption date now interpreted as apocryphal. Advances through contemporary scientific studies convey nearly

real-time seismic data and webcam imagery to residents and use tomography, drone photogrammetry, and other new ways of visualizing and imaging volcanic processes, events, and structures. Contemporary scientific research is also increasingly explicit in acknowledging the importance of oral traditions as potential artifacts of carefully observed geological events that helped past people understand and mitigate hazards. These oral traditions, still prevalent, can also help convey information to local residents. The stories told about Merapi are not epiphenomenal to scientific understanding of it, but instead, they can aid culturally embedded communication to potentially prevent loss of human life.

Keywords

Merapi · Oral traditions · Social science · Disaster culture

K. Holmberg (✉)
New York University, Gallatin School of
Individualized Study, New York, USA
e-mail: kgh1@nyu.edu

3.1 Introduction

Awareness of the cultural embeddedness of risk has led to a widespread acceptance of the importance of interpretations, negotiations, experience, and creative adaptation to hazards when trying to analyse, intervene in, or mitigate disasters (Krüger et al. 2015). Interdisciplinary

research that entwines geosciences with social science considerations is important when considering volcanic contexts (e.g. Cronin and Cashman 2007; Cashman and Cronin 2008; Jenkins et al. 2013; Hayes et al. 2020). While this is true in the preparation for, response to, and recovery from any eruption it is especially true in contexts where traditional beliefs can aid culturally embedded communication and potentially prevent loss of human life. In this way, the stories told about a volcano are not epiphenomenal to scientific understanding of it. Merapi volcano, in particular, is both a geological entity and a mythical one for those who live near it. Understanding these components together—rather than separating them as the domain of different disciplines—helps create a more unified understanding of the volcano’s important role in the past and future and better convey scientific understandings of risk to the roughly one million people who currently live on Merapi’s flanks. Oral histories and ceremonial events can thus be exceptionally important components of risk reduction strategies that contribute to community resilience (Lavigne et al. 2008; Donovan 2010).

While other chapters in this volume very capably focus on specific components of the contemporary scientific understanding of Merapi, this chapter provides an overview of some ways in which Merapi was observed and viewed in traditional Javanese conceptions and how incorporating these understandings with scientific interpretations can benefit contemporary hazards communication. It also examines past and present scientific perceptions of Merapi’s role in Java’s cultural history—which are their own form of narrative or story—and new ways to ‘see’ Merapi. Modern descriptions of Merapi eruptions ‘have involved descriptions in six languages (Javanese, Indonesian, Dutch, German, French, and English) and have generated an ornate *batik* of terminology’ (Voight et al. 2000). The varied descriptions of Merapi also entail exceptionally varied and variegated cultural evocations, meanings, and interpretations that impact to this day the way scientific monitoring data and hazards forecasting are received.

3.2 The Role of the Past in the Present and Future of Merapi

The twenty-first century and its era of environmental changes in the Earth system make an improved understanding of the complex intersections between the geophysical world and human cultures of critical importance (e.g. Florindo and McEntee 2020). Studies of the past perceptions of Merapi as well as the impact the volcano has had on past human life in Central Java are by no means academic or antiquarian questions. Politics and human survival are fraught in any time period, but in early Java ‘they were played out in a physical environment that was both more fertile and more unstable than most’ (Wisseman Christie 2015). For this extremity alone, Merapi and human occupation in Central Java provide an important topic of study for any insight they may provide. Additionally, however, Merapi provides a remarkable, long-term example of the nature-culture entanglement as human occupation on Java is estimated to extend substantially into the prehistoric deep past (e.g. Kusumayudha et al. 2019).

Volcanoes are geological entities that are deeply incorporated into human social life in far more complex and social ways than the physical impacts of eruption (Holmberg 2007). When modern humans settled Java—roughly 40,000 years ago—they occupied the same territories formerly used by archaic members of the human family, *homo erectus*, who lived on the island from 1.5 million years ago until about 100,000 years ago (Fig. 3.1) and whose genetic material still exists in trace forms (Rizal et al. 2020). Humans and our earlier ancestors have had ample time to witness the various phases of Merapi, though data about them and their intersection with volcanism is fragmentary and only available via archaeology and palaeontology. Merapi has been observed by humans for an exceptionally long time period; Merapi literally ‘returned’ this gaze and observed (and continues to observe) humans, according to oral tradition (Dove 2008a, 2010).

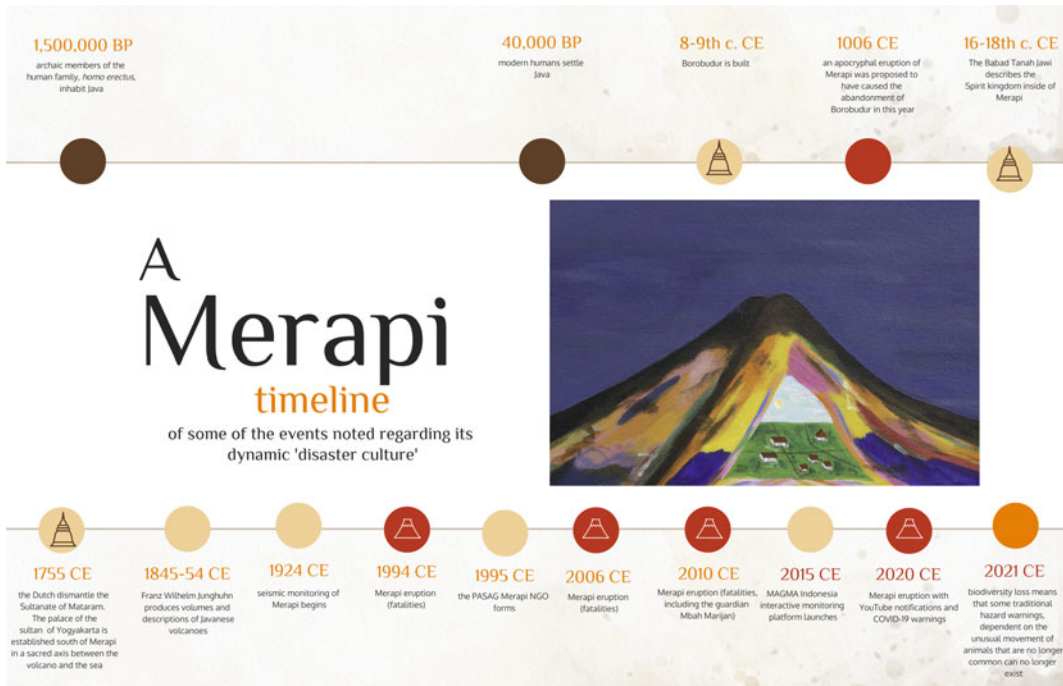


Fig. 3.1 Timeline of Merapi, illustrating some of the events noted in this chapter regarding its dynamic 'disaster culture'

Written records in the Merapi area, including descriptions of its volcanic activity, began a millennia ago. Modern scientific monitoring of Merapi is, comparatively, in its infancy. Understanding how past perceptions of the volcano shape the present has therefore important ramifications for how well scientific interpretations and understandings are communicated to communities at risk from future eruption events.

3.2.1 Misunderstandings of Past Intersections of Culture and Nature at Merapi

The impact of volcanic eruptions formed one of the earliest foci of social science investigation of environmental disasters in the mid-twentieth century and was a precursor of the important shift of scientific focus on equilibria to one that emphasises dynamic, historical, and only partly knowable intersections between the natural world and human life (Dove and Carpenter 2007a).

Scientifically, we now believe that a disaster is created through cultural choices, contexts, and information rather than existing as a simply geophysical event (e.g. Oliver-Smith 1996, 2013; Oliver-Smith and Hoffman 1999; Krüger et al. 2015; Kelman 2020). Contemporary studies acknowledge that Merapi eruptions only become 'disasters' through interaction with local social systems that have a temporal and geographic specificity (Muir et al. 2020).

This is apparent when, for instance, looking at the social role of volcanoes in Java in nineteenth and twentieth-century western literature that viewed volcanoes as prominent but in a less nuanced way than current understandings of the lived, experiential view of an animate volcano and its role in human life just noted. In *The History of Java*, British Governor-General Stamford Raffles (1817) cited numerous examples of volcanic eruptions that coincided with dynastic politics on Java and so natural disasters, in these interpretations, were prime movers of social and political change. The presence of

many archaeological sites covered by multiple lahar deposits (Fig. 3.2), still evident in the contemporary period, likely helped inspire these deterministic interpretations.

The overall shift of power and populations from Central Java to the east for several centuries after an unknown catastrophe was a topic of historical debate amongst western scholars of the colonial era. Suggestions of wars or pestilence as the root of the shift in the court's location were replaced by a theory that an eruption of Merapi prompted the depopulation and abandonment of the area (van Hinloopen Labberton 1921). This concept drew upon earlier work (Ijzerman 1891; Scheltema 1912) as well as an inscription in Sanskrit issued in 1041 CE by Airlangga and now referred to as the Pucangan charter. The inscription notes the year 1006 CE (or 1016 CE depending on translation) and a disaster (*pralaya*). This same artefact was also frequently referred to in colonial literature

as the Calcutta Stone, a name that stems from the fact that it was sent from central Java to Calcutta as a gift from Raffles to the British Governor-General of India.

Following examination of Merapi's form and evidence for what he believed was a catastrophic sector collapse and debris avalanche, Dutch volcanologist Reinout van Bemmelen declared that the volcanic *deus ex machina* hypothesis was accurate and that an eruption of Merapi in 1006 CE was one of the world's great 'volcanic outbursts'. This interpretation was part of a large body of work in which van Bemmelen focused on geological events in Indonesia and placed a specific interest in the importance of geological events like volcanic eruptions on societies (van Bemmelen 1949, 1956, 1971). One archaeological site in particular, Borobudur, became entrenched within these interpretations through its monumental architecture and enigmatic state of ruin and abandonment (Fig. 3.1).



Fig. 3.2 Archaeological site covered by multiple lahars. *Photo credit* Frances Deegan

3.2.2 The Colonial View of the Archaeological Site of Borobudur and Its Relationship to Merapi

Merapi and Borobudur are located within fairly close distance to one another (Fig. 3.3), yet their direct, catastrophic linkage a millennia ago is questionable. Archaeological interpretations of the Buddhist monument of Borobudur, built between the eight and mid-ninth centuries, became deeply linked in the colonial imagination of volcanic disaster (Fig. 3.1). Borobudur, like Pompeii, became a physical talisman of the relationship between large-scale geological events and human life.

The city of Pompeii, destroyed in 79 CE by an eruption of Vesuvius and rediscovered some 1500 years after the event, was foundational in shaping western ideas of how environmental events and human life intersect throughout the modern era (Holmberg 2013a). Borobudur became uncritically included within these Romanticism-tinged narratives of volcanic destruction by British and Dutch visitors to the site in the early nineteenth century. The monument, built during a period in which Buddhism was evolving rapidly, merits the attention it has received in hundreds of works, and anyone interested in beginning to study these should begin with the helpful annotated bibliography by Miksic (2012). Some of the best analyses of the monument, described in Javanese chronicles as a mountain with a thousand statues, are compiled by Gómez and Woodward (1981) while Frédéric (1996) provides photographs and descriptions of each of the 1460 reliefs on the monument. The eruption that prompted its abandonment, however, is apocryphal (but see Kusumayudha et al. 2019), and recent studies have argued against the AD 1006 ‘outburst’ theory proposed by van Bemmelen (see Gertisser et al. this 2023, Chap. 6, for a synthesis).

An unexplained disaster or event did occur in Central Java and prompted the site of Borobudur to be abandoned and never re-used. This may have been a political or military disaster, however, and was probably not related exclusively to

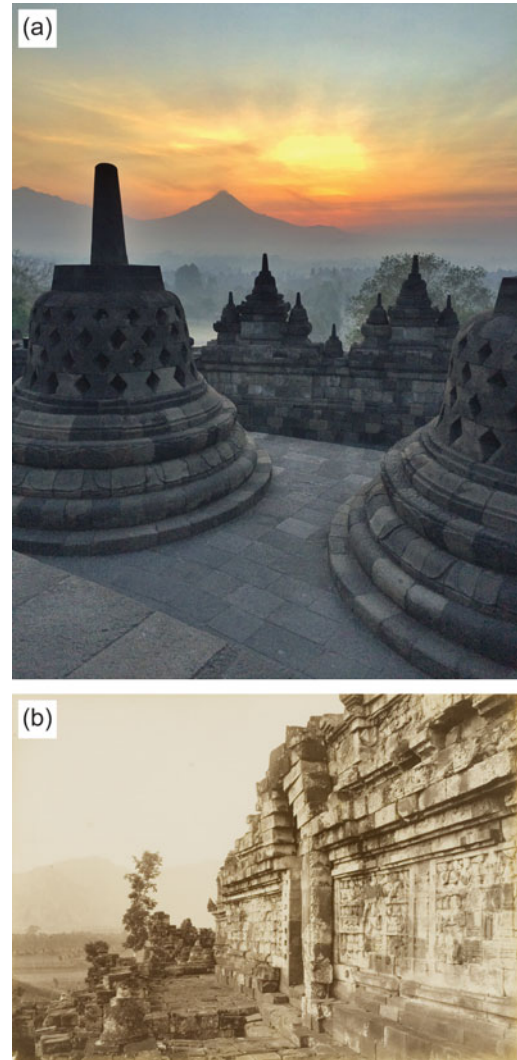


Fig. 3.3 Borobudur, with Merapi volcano in the background, as photographed in **a** 2014 and **b** 1890–91. *Photo credit a* K. Holmberg. *b* Kassian Cephas, Leiden University Library, KITLV, image 29,214 Collection page Southeast Asian, Public Domain. <https://commons.wikimedia.org/w/index.php?curid=40516381>

a volcanic eruption. Recent geological and archaeological data provide no evidence of this occurring because of a single eruption event or debris avalanche in 1006 CE (Murwanto et al. 2004; Purbawinata et al. 2007). Neither is there direct evidence of an eruption in 928 CE, which was the date of the last inscription at the site, though some researchers do still propose an eruption or series of relatively large eruptions at

around that time (Djumarma et al. 1986; Wisseman Christie 2015; Kusumayudha et al. 2019).

Archaeologically, the area around Merapi remained occupied continuously, though there was a shift from a centralised government with a unifying, monumental style of architecture to local government (de Casparis 1950; Dumarçay 1986; Newhall et al. 2000). Gomez et al. (2010) provided locations for 75 structures constructed in this time period, adding to the three well known temples in the Borobudur basin (Borobudur, Mendut, and Pawon). Satellite sites remained in use until the thirteenth century, long after Borobudur's abandonment (Newhall et al. 2000; Murwanto et al. 2004). The shift of the Mataram state is suggested to have been possibly prompted by waterborne diseases from an ancient lake whose existence or non-existence is debated (Murwanto et al. 2004). The often repeated and entrenched scientific mythology of Borobudur as a synecdoche for the destruction of Mataram state power in Central Java through a Merapi eruption, however, is not a unique solution and hence not founded on reliable scientific data.

3.2.3 The Non-Colonial View of Franz Wilhelm Junghuhn on Merapi

The work of Franz Wilhelm Junghuhn provides a notable exception to the colonial focus of early scientific inquiry on Java that viewed science as a means of extracting artefacts, collecting exotic specimens, or imposing Romantic-era interpretations of natural disaster (Fig. 3.4). Junghuhn produced many volumes of descriptions and images of Javanese volcanoes, including Merapi (e.g. Junghuhn 1845a, b, 1853–4) (Fig. 3.1). A humanist who was interested in expanding and sharing geological understanding through his many drawings and paintings of volcanic landscapes, he also sought to understand local communities through their own customs and cosmologies rather than imposing Western ones

upon them. Junghuhn's work would today fall within the field of landscape ecology, a term coined by geographer Carl Troll (Troll 1939). It serves as a sub-branch of geography and is already reflected in the German word *Erdkunde*, i.e. the study of the physical properties and contours of the Earth in a way that includes local human activity and action as well as remarkable natural events like volcanic eruptions (see Korintenberg et al. 2020). Junghuhn was prescient in foregrounding local, lived experience of Java's volcanic landscapes.

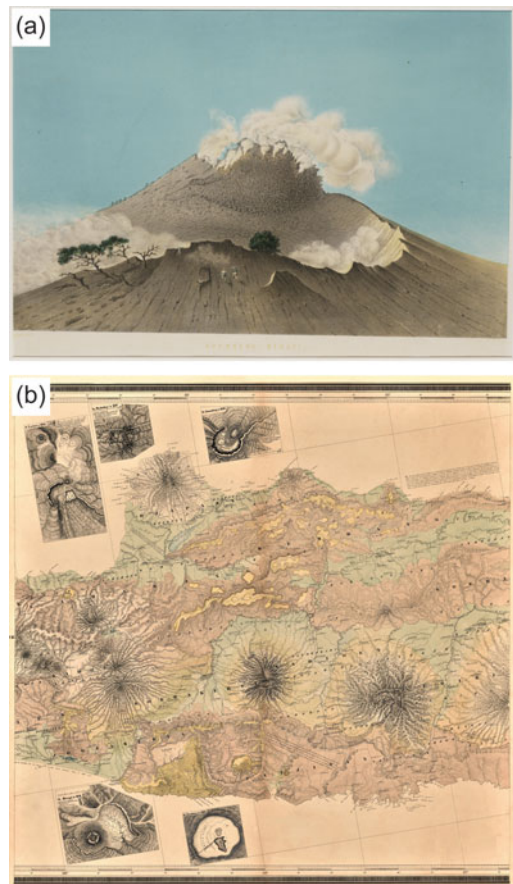


Fig. 3.4 Representations of Merapi by Junghuhn. *Photo credit a* Leiden University Library, KITLV, image 50H8 Collection page Southeast Asian, Public Domain, <https://commons.wikimedia.org>. *b* Nederlands: Kaart van het eiland Java, Public Domain, <https://commons.wikimedia.org/w/index.php?curid=48819655>

3.3 The Social Life of Merapi

Merapi is personified as *Mbah Merapi* in contemporary Java, using the honorific usually given to a grandparent. The living and lived presence of Merapi, however, is far more deeply embedded than this simple reference to animism or anthropomorphism. Contemporary Java has a complex and syncretic merging of Islamic, Hindu, Christian, Buddhist and earlier spiritualities that importantly temper the responses to volcanic eruptions (Schlehe 1996; Chester 2005). The main monotheistic religions, spirit cults, ancestor worship, spirit healing, shamanism, and mythical traditions all coexist within or despite the main monotheistic structures (Lavigne et al. 2015). In particular, the practice of *Kejawen*, an East Java and Central Java spiritual tradition with a focus on forecasting natural events, is important to understand not as a static religion but as a set of Central and East Javanese beliefs that can be described as ‘animist Islamic metaphysics with magic, witchcraft, and shamanic dimensions, in addition to influences from the Hindu-Buddhist Javanese sultanates’ (Bobbette 2018). These beliefs co-exist with ritual practices and a cosmological system, the admix of which colours how scientific information about Merapi and its hazards are received and hence they are important to understand (Troll et al. 2015, 2021; Martinez 2017, 2018, 2019; Bobbette 2018, 2020).

The first written accounts of Merapi’s incorporation into the social world is from the Sultanate of Mataram, dating to the sixteenth through eighteenth centuries, which was the last major independent Javanese kingdom prior to Dutch colonisation. The *Babad Tanah Jawi* (Fig. 3.1) chronicles Javanese legends, including descriptions of a spirit world within Merapi’s crater that formed when the arrival of humans caused the spirits to retreat into the volcanoes and other marginal places on Java (Geertz 1960). This powerful spirit kingdom (*kerajaan makhluk halus*) within Merapi mirrors that of the human world. It is populated by rulers, soldiers, farmers, and herders, and it draws humans into it through

their deaths when they are required as servants (Schlehe 1996, 2008; Zeilinga de Boer and Sanders 2002; Donovan 2010). Merapi’s eruptions are sometimes interpreted as the procession of spirit court members while lahars, ash, and gas clouds are sometimes interpreted as evidence of courtly house construction or cleaning (Schlehe 2008; Dove 2010). The spirit kingdom and physical landscape all exist within physical interaction of one another (Fig. 3.5).

When the Dutch dismantled the Sultanate of the Mataram in 1755, the palace (*kraton*) of the Sultan of Yogyakarta was established twenty kilometres south of Merapi (Fig. 3.1). The *kraton*, Merapi, and the sea are connected in a sacred axis (Karsono and Wahid 2008; Troll et al. 2015,

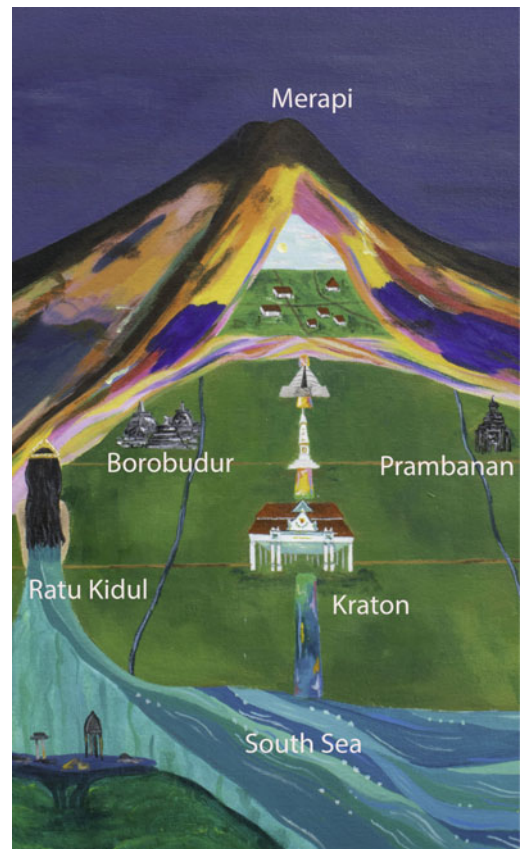


Fig. 3.5 The sacred axis between Merapi and the sea. *Illustration credit* Taylor Burkhead; adapted from Troll et al. (2015)

2021). In this axis, Merapi is literally the spike at the centre of the universe (*paku alam*) and hence extremely important (Dove 2007). Despite the volcano's importance, however, it is the goddess or Queen of the Southern Sea (the Indian Ocean), Ratu Kidul, who is the ruler of all of the spirits of Java (Wessing 1997). It is Ratu Kidul and her interaction with the other bookend of the sacred axis, Merapi, who play the key roles in creating balance (Fig. 3.6).

Ratu Kidul promised the sixteenth-century founder of the Mataram II kingdom, Senopati, protection from Merapi eruptions (Schlehe 1998, 2010). The present Sultan of Yogyakarta and the spiritual guardian (*Juru Kunci*) of Merapi perform rituals to this day that are connected to this mythical legacy. In particular, an elaborate annual ceremony called *Labuhan* (Fig. 3.7) occurs simultaneously at the south coast at Parangkusumo beach (near Parangtritis) where Ratu Kidul and Senopati first met as well as at Merapi to revitalise the relationship between the palace, the villages, the mountains, and the sea

(Schlehe 1998, 2008). Ritually prepared offerings include textiles, perfume, incense, money, and every eight years a saddle for a horse (Triyoga 1991). The spirits of people who were good in their lifetime enter the realm of Ratu Kidul in the South Sea or the Merapi kingdom before moving to paradise; 'like the spirits of the volcano, the spirits of the dead still maintain connections to the living' (Schlehe 1996). Ratu Kidul supports the Javanese sultans, and it is through her power that they hold state power (Jordaan 1984; Resnik 1997). The full mythology and role of Ratu Kidul is rich and worthy of discussion far beyond the scope of this chapter (see Wessing 1997; Troll et al. 2015).

3.3.1 A 'Disaster Culture'

Volcanoes and their eruptions are generally viewed through a lens of destruction and risk in western, scientific vantages that is antithetical to the traditional Javanese focus on lived

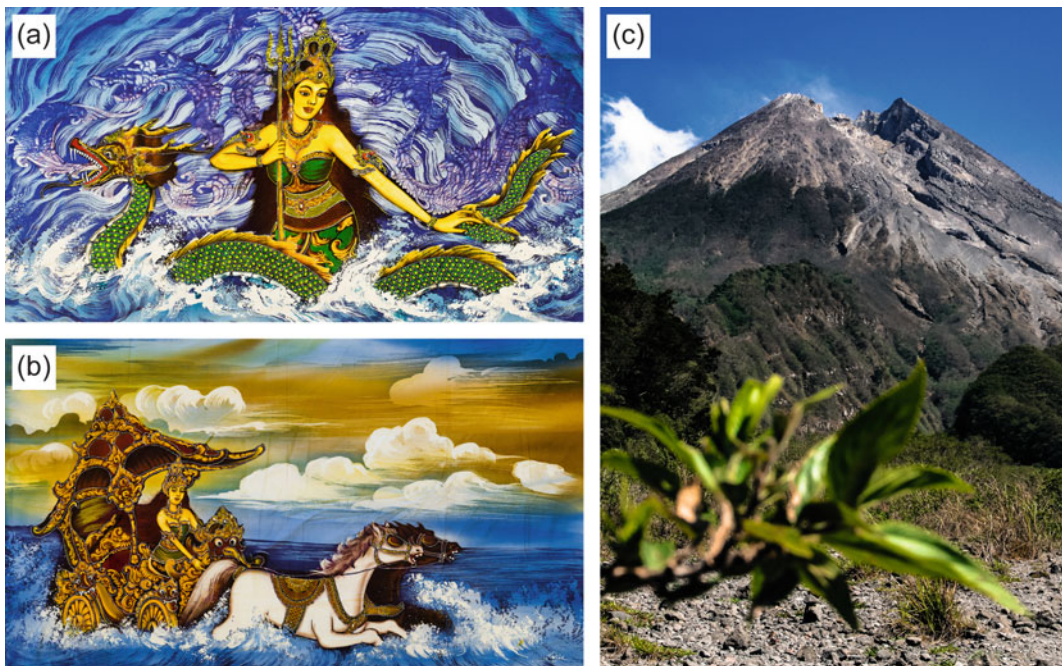


Fig. 3.6 Ratu Kidul and Merapi are the two end-members of the sacred balance. *Photo credit a, b* Valentin Troll, images of Ratu Kidul in batik from his personal

collection. *c* Merapi by Hildaniar Novitasari, CC BY-SA 4.0, <https://commons.wikimedia.org/w/index.php?curid=90747666>



Fig. 3.7 Images of the annual Labuhan ceremony. *Photo credit* a Tri Hand, CC BY-SA 4.0, <https://commons.wikimedia.org/w/index.php?curid=88221800>. b Arfani

M, CC BY-SA 4.0, <https://commons.wikimedia.org/w/index.php?curid=88155355>. c-d Flickr Commons

interactions with Merapi. In addition to the intercession that Ratu Kidul and the *Labuhan* ceremony allow to everyone, not just the sultan or guardian, residents acknowledge numerous benefits of Merapi’s presence. The 1994 eruption of Merapi (Fig. 3.1) killed several dozen people (Voight et al. 2000). Following this tragedy, however, a balance resumed through an ‘untroubled age’ (*jaman aiyem*) for people in the village of Turgo (Dove 2008b). This new age included changes in the agro-ecology that improved the villagers’ livelihoods through a shift from subsistence to market-oriented economy, particularly through the sale of milk produced by cows utilising grasslands. The high-

elevation grasslands, where fodder for the cattle is retrieved during the dry season, benefit from the periodic ash fall and the extensive below-ground root systems of the predominant grass there (*Imperata cylindrica*) permits it an adaptive advantage following pyroclastic flows (Dove 2007, 2008a; Dove and Carpenter 2007b). Block and sand mining of pyroclastic deposits and lahar-filled river beds (Fig. 3.8) also provide materials for construction and sculpture workshops (Lavigne et al. 2008, 2015). This mining, which removes sand and rock for cement in Singapore, mainland China, Bali, or Jakarta is linked into a complex political ecology of regional geopolitics and material flows. For those



Fig. 3.8 Example of block and sand mining of Merapi volcanic deposits taken at Kali Gendol and showing the mining of block-and-ash flow deposits from the 2006 eruption. *Photo credit* Sylvain Charbonnier

who believe in the Javanese spiritual tradition of *Kejawen*, treating the volcano as a resource for extraction is a cause of future disasters (Bobbette 2018, 2020).

The deep intersection of volcanic activity within social life near Merapi is sometimes referred to in the English-language literature as a ‘disaster culture’ (e.g. Troll et al. 2015) or ‘volcanic culture’ that requires social volcanology (e.g. Donovan 2010) to adequately address. This vantage refers to the very complex and phenomenological realities of living near active volcanoes (Blong 1984; Schlehe 1996, 2010; Chester 1998; Donovan 2010). Rather than a feeling of distinct threat, what scientists refer to as ‘hazard’ is perceived in the Merapi area as something quite different. This sense is instead described frequently in terms of being confused (*bingung*) or lost (*kesasar*) and while in this state of loss a female spirit (*wewe*) sometimes appears in the guise of relatives or close friends to lead them into the crater (Dove 2007, 2008a). The

stories of such states of confusion are described in ways that indicate both a familiarity and an ‘otherness’ to the volcano through stories of going to the market to buy rice cakes, for example, and realising that you actually bought flat rocks. When you are led to the crater in your confusion, you feel as though you are going to your own home. The ability to intercede in geological events through Ratu Kidul and ritual behaviour allows residents a sense that when disasters do occur—such as the eruption in 1994—the loss of life and property would have been higher without the ritual behaviour or that the losses will be compensated in some way in the long term (Dove 2007; Lavigne et al. 2008).

It is important to note that local cosmologies can have their own epistemological differences and peculiarities (Schlehe 2010). The same beliefs and perceptions are not shared universally even within the local area of Merapi, as Donovan (2010) points out in a discussion of the 2006 eruption (Fig. 3.1). What is commonly shared,

however, is the very personified idea of Merapi and the ability of the spiritual guardian (*Juru Kunci*) to communicate with the volcano. For this reason, the death of the guardian known as Mbah Marijan during the eruption in 2010 was a highly significant event (Fig. 3.1). Mbah Marijan was killed on 26 October 2010 when an explosive eruption began 35 h after an alert was issued that one was imminent. Remarkably, Mbah Marijan remained in the village of Kinahrejo, roughly six kilometres from the summit, along with 34 others who also refused to evacuate (Suroño et al. 2012; Subandriyo et al. 2023, Chap. 12).

Mbah Marijan was a symbol of traditional Javanese beliefs, masculinity, defiance of modern Muslim political power, and even an energy drink was using him through advertisements (Schlehe 2010). Despite the highest warning levels of volcanic activity, he refused to evacuate, prompting other villagers to follow his lead. This helped create a stark, exaggerated, and ultimately artificial division between traditional beliefs and modern science. It also exacerbated the frustrations of predominantly Muslim volunteers from West Java with local residents’ behaviour, as it seemed counter to scientific understanding and their own safety. Local volcano mythology regarding eruption precursors likely contributed to the reluctance to evacuate, although the socio-economic impact of losing livestock and hence livelihood as well as a lack of trust in the governmental disaster response may be the more important factors (Triyoga 1991; Schlehe 1996; Dove 2008a; Lavigne et al. 2008, 2015; Donovan 2010; Donovan et al. 2012; Mei and Lavigne 2012, 2013; Troll et al. 2015). As recent studies show (e.g. Mei et al. 2016), issues of livelihood and the adjustments required by resettlement are significant even for villagers who have positive responses to leaving their villages and recommendations on the basis of ancient legends or traditional beliefs that encourage not to evacuate may thus fall on fruitful ground, although being frequently counterproductive in respect to civil protection matters.

3.4 The Scientific Vision of Merapi

3.4.1 Modern Scientific Study of Merapi

Modern scientific observations and descriptions of Merapi began in the mid-eighteenth century. These include Dutch and German publications prior to World War II (e.g. Junghuhn 1853–1854; Verbeek and Fennema 1896) and more systematic observations in the first half of the twentieth century (see Voight et al. 2000 and references therein). The compiled genealogy of volcano science on Merapi by Voight et al. (2000) joins prior historical summaries (e.g. van Bemmelen 1949; Neumann van Padang 1951, 1983; Berthommier 1991). A shifting array of governmental organisations—often with multiple acronyms or names depending on the translations—have monitored, managed, or communicated information about Indonesian volcanoes throughout the twentieth century. Seismic monitoring of Merapi began in 1924 with one station located on the western slope roughly nine kilometres from the summit (VSI-ESDM 2020) and new forms of monitoring and new ways of disseminating data are continually evolving through new technologies (see Budi-Santoso et al. 2023, Chap. 13).

Merapi is currently monitored through five observation posts (Jrakah, Babadan, Selo, Kaliurang, and Ngepos; Fig. 3.9) which are located at distances of 5–10 km from the summit and operate under the supervision of the Research Development Center for Geological Disaster Technology (BPPTKG) in Yogyakarta (VSI-ESDM 2020; Lavigne et al. 2015). Current techniques for monitoring include: visual analyses (morphological changes and meteorological measurements using CCTV cameras, stereograph and thermal cameras); geological analyses of the summit and stratigraphic record, seismic (including four local short-period analog and five local broadband digital stations as well as a reference station some 40 km away for regional reference data); deformation (Electronic Distance Measurement reflector units, tiltmeter, real-time

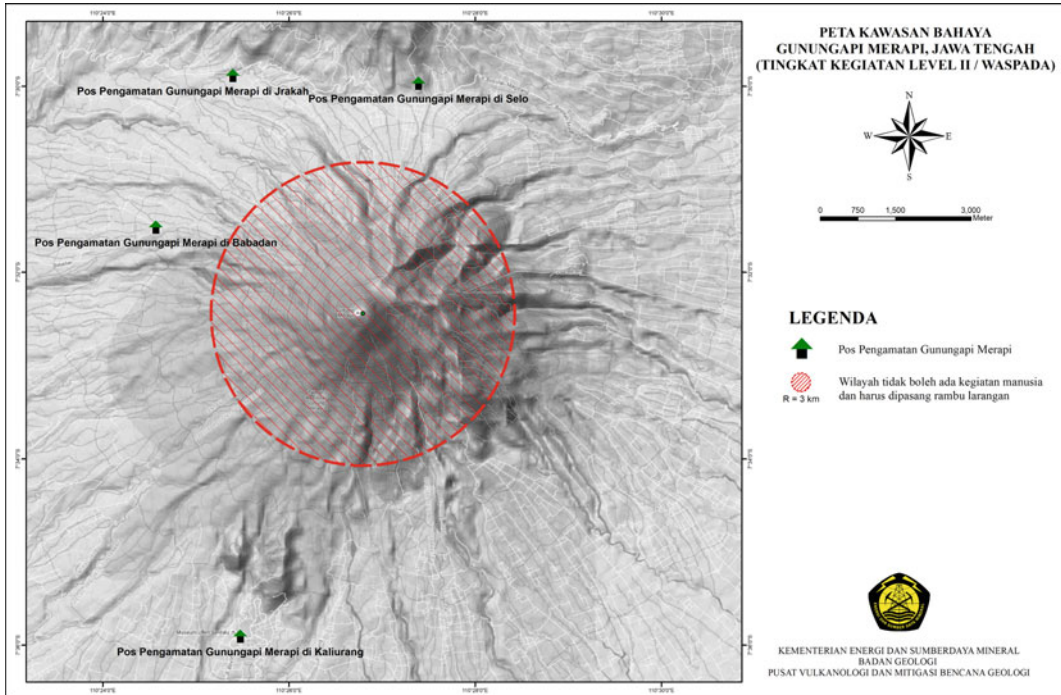


Fig. 3.9 Current volcano observation posts at Merapi. Note that the map only shows four of the observation posts as Ngepos is outside of the map view

GPS); and geochemical analyses of fumaroles using chromatography, spectrophotometry, and volumetry (VSI-ESDM 2020; Lavigne et al. 2015). Further information regarding volcano monitoring at Merapi, with particular reference to the 2010 eruption, can be found in Subandriyo et al. (2023, Chap. 12).

3.4.2 Collecting and Disseminating Data and Interpretations in the Twenty-First Century

The BPPTKG, a part of the Geological Agency (VSI), reports to the Center for Volcanology and Geological Disaster Mitigation (PVMBG). The BPPTKG is charged with Merapi disaster mitigation and monitoring and provides a website with current alert notifications, monitoring data, general information, and webcams from the monitoring stations (BPPTKG [access date: 8

June 2020]). When an eruption event occurs, as it did, for example, on 10 April 2020, the website records data such as the seismogram reading, duration, and height of the eruption column. A two-minute video of the event was immediately posted on YouTube and local residents were warned to watch for ash fall. Residents were told of the health problems the ashfall can cause (breathing difficulty, eye and skin irritation). Significantly, this information was placed within the context of the ongoing coronavirus pandemic and residents were informed that there is no evidence that ashfall can kill the virus that causes COVID-19 (Fig. 3.1). In addition to the website, the BPPTKG uses community radio stations, SMS updates, and Twitter to disseminate information during crises.

A new online and mobile phone platform launched in 2015, MAGMA Indonesia (Fig. 3.1), provides quasi-real time and interactive geological data, including live seismograph data (v2 Beta), via a dynamic digital map and

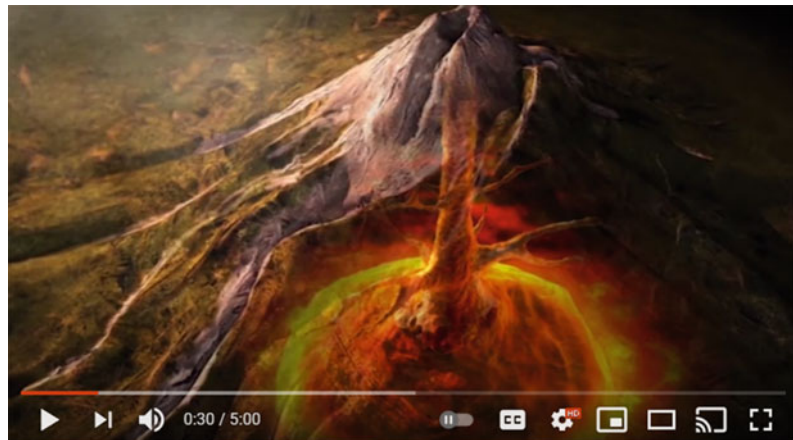
open-source technology (VSI-PVMBG 2020). MAGMA Indonesia (v0.1.3 Alpha) uses graphic indicators of different activities and risk levels for each volcano and other geological hazards such as tsunamis, earthquakes, and landslides. Users can zoom in to a three-metre resolution in the satellite imagery. The mobile application was last updated October 2019 and is available for phones with Android operating systems.

Videos on YouTube are important components of the MAGMA Indonesia outreach (Fig. 3.10). An animated introduction to MAGMA Indonesia, volcanic hazards, monitoring, and communication methods on its YouTube channel posted in September 2016 had over 18,000 views as of June 2020. Another representative video, titled ‘Top 40’ (posted in August 2017) uses computer-generated imagery to show magma rising through conduits to the

surface and a nighttime eruption while villagers run from houses before a pyroclastic density current inundates it. The video includes images of the monitoring stations and discussions with John Pallister from the Volcano Disaster Assistance Program of the United States Geological Survey.

It is worth noting that the dynamism of the Earth, which is what necessitates rapid sharing of information about volcanic hazards, is currently accompanied by the rapid transformation and dynamism of the technologies which we use to examine a volcano like Merapi. Seismology and deformation (Lühr et al. 2023, Chap. 5), gas emissions (Nadeau et al. 2023, Chap. 11), and petrology (Troll and Deegan 2023, Chap. 8) have long been used as ways of monitoring Merapi’s activity. The ‘hundred-year eruption’ in 2010 was the latest major eruption of Merapi to be

Fig. 3.10 MAGMA Indonesia screen captures from YouTube of its ‘Top 40’ video, https://www.youtube.com/watch?v=P_SX19Coefo, accessed 6 June 2021



forecast by those precursory signals as well as near-real-time satellite radar imagery (Surono et al. 2012). The 2010 pyroclastic deposits were mapped using dual-polarisation Synthetic Aperture Radar (Solikhin et al. 2015). Recent work provides new ways to ‘see’ Merapi through resistivity tomography (Byrdina et al. 2017), seismic tomography (Widiyantoro et al. 2018), drone photogrammetry (Darmawan et al. 2018), and numerical models to better understand its recent eruptive behaviour (Carr et al. 2020).

Simultaneously, while monitoring benefits from innovative technologies, new risks arise from our increasingly globalised and technological world and need to be considered. The wide-ranging effects of the Eyjafjallajökull eruption in Iceland in 2010 on the global economy through flight and commerce cancellations were striking. Flight disruptions such as those that occurred from Merapi’s relatively brief eruption in 2010 prompted the cancellation of roughly 2000 flights, paralysis of much activity in the city, the bankruptcy of one airline, and thwarted the Mecca pilgrimages of thousands of Muslims (Surono et al. 2012; Picquout et al. 2013). A much larger eruption could be a serious future threat (Newhall et al. 2000; Lavigne et al. 2015; Troll et al. 2015).

3.5 The Nature and Culture of Merapi in the Anthropocene

Volcanoes provide an important way to query how we as humans perceive the planet and the intersection of human life with the Earth system (Holmberg 2020). Merapi is one of the world’s most hazardous and one of the most important volcanoes for careful scientific research due to its frequent activity, long time depth of cultural resonance, and high population density. Additionally, Merapi is crucial through its inclusion in the Deep Earth Carbon Degassing Project (DECADE) as an initiative within the Deep Carbon Observatory. Study of Merapi is part of the study of a sustainable future globally and

directly contributes to our understanding of how anthropogenic carbon emissions relate to the overall carbon cycle (Deep Carbon Observatory 2019; Whitley et al. 2019, 2020).

The contemporary Merapi context is striking in its relationship to the past and to the volcanic landscape. Even with all of the technology available for communication, traditional means of alerting villagers are still used and important in times of crisis; these include the beating of a traditional gong (*kentongan*) as warning that a volcanic event is imminent and the community is in danger (Lavigne et al. 2015). A communication code in the pattern of sounds can convey messages such as ‘safe’, ‘major event’, ‘disaster,’ or ‘death’ in a way that to a westerner is discernible as a communication form similar to Morse code.

In this context, the sacred axis and the guardian’s intercession provide an ability to communicate with the spirit realm that Merapi is a part of according to traditional beliefs. In an extension of *Kejawen* to the contemporary era and scientific monitoring, some people now provide offerings to the seismic stations and meditate in the Babadan monitoring station at Merapi (Martinez 2017). Offerings of cooked rice grown on the volcano, shaped into a cone like the volcano (*tumpang*), and left at sand mining sites accentuate the link between the sustenance of the human body and the land that produces that sustenance, symbolising that both are deeply linked to the volcano with a deep appreciation for the gifts provided being expressed this way (Bobbette 2018, 2020). After the guardian of Merapi, Mbah Marijan, was killed in 2010, his son—Asih Lurah Surakso Sihono—became the new spirit guardian. He has expressed willingness to avert future disasters by serving as a liaison for the local volcano observatory (Troll et al. 2015). This willingness to merge traditional and scientific ways of understanding Merapi and the ability of different forms of knowledge to coexist is something to which the scientific community is also increasingly open (e.g. Schwartz-Marin et al. 2020).

3.5.1 Oral Traditions and Participatory Hazards Communication as a Bridge to Scientific Communication

Neither scientific understanding nor traditional beliefs are static narratives, however. Like all narratives, they are in constant revision, negotiation, and transformation. Computational methods of examining volcanic hazards in quantified terms are one important way to consider risk and social vulnerability and convey it to scientists (e.g. Maharani et al. 2016), yet a more qualitative engagement in which scientific interpretations are made understandable within an already existing cultural framework can be a better way to communicate with residents near the actual risk. Incorporating oral traditions within the Merapi context as a way to understand the actions of people who may distrust scientists or civil protection authorities is part of a growing body of important work that seeks to create a communication bridge (Dove 2008a; Lavigne et al. 2008; Donovan 2010; Schlehe 2010; Troll et al. 2015, 2021; Bobbette 2018, 2020).

These studies join a body of literature from other geographical regions that take the integration of local traditions into crisis management seriously (e.g. Cashman and Cronin 2008; Swanson 2008). Oral traditions may provide a means of understanding and communicating hazards but also ways of mitigating future harm by providing understanding of early warning signs. Examples of this include a lullaby created after a tsunami in 1907 that provided early warning and is credited with saving the lives of 78,000 people on Indonesia’s Simeulue Island by prompting them to run to higher ground when the sea receded (McAdoo et al. 2006; Syafwina 2014). Local tradition near Pinatubo volcano in the Philippines described a spirit of the sea who hid in the mountain and showered the land with rock, mud, dust and fire for three days while the earth shook (Rodolfo and Umbal 2008; Donovan and Suharyanto 2011). A Chamula story from pre-Columbian Mexico described a ‘boiling rain’ that poured out of El Chichón volcano; it rose to

the sky as clouds then poured down as fatal rain that helped make sense of a boiling mud flow produced by water trapped behind hot pyroclastic debris filled the valleys and villages below (Duffield 2001). In pre-Columbian Panamá, a Bribri story describes how the sea was a pregnant woman who was bitten by a poisonous snake and how her belly rumbled and swelled until a tree exploded from it and rose toward the sun, a story thought to incorporate observed eruptions of the Barú volcano (Holmberg 2013b).

Incorporating local communities in hazards observation, communication, and disaster prevention can have remarkably positive results. The long-term intersection of the scientific community and local communities near Tungurahua volcano in Ecuador is exemplary of what such integrated communication can accomplish (see Mothes et al. 2015). In the Merapi region, a non-governmental organisation, PASAG Merapi (PASAG is an abbreviation for *Paguyuban Sabuk Gunung*, or mountain chain association; this organisation formed in 1995; Fig. 3.1), has led communities in the creation of two-dimensional maps or models since the early 2000s (Lavigne et al. 2015). Following the 2010 Merapi eruption, a French non-governmental organisation, CCFD-Terre Solidaire, created a three-dimensional scale relief model for participatory community mapping of the eruption damage as well as the roads and routes utilised by residents to evacuate (Lavigne et al. 2015). For the scientific community, this would translate as a physical model of what a Geographical Information System represents, which is a layering of data. That same digital layering is not familiar necessarily to those in the Ngarmomulyo municipality on the western flank of Merapi, though, and hence the physical model is of far more utility in both obtaining and conveying information with local residents.

3.5.2 The Sacred Axis as Pre-Modern Observation

Data from pre-modern observation of Merapi’s behaviour is potentially reflected in the concept

of the sacred axis that connects Merapi to the *kraton* and the Southern Sea. Examination of the volcano-earthquake interaction along the Opak River fault line indicates that the geological phenomena is increasingly frequent in the contemporary context (Walter et al. 2007; Surono et al. 2012). The concept of the sacred axis between Merapi and the sea could be accrued knowledge of local seismic and eruptive events in the past, such as the volcano-earthquake interactions, that are renewing and cyclical (Troll et al. 2015, 2021). Use of this local tradition could help communicate hazards in ways that are understandable and memorable and alleviate a small portion of the friction that can often exist worldwide between government organisations, scientific institutions, and local communities.

A study by Atmojo et al. (2018) of primary school students near Merapi indicates that the inclusion of traditional stories in the educational process can result in quantifiably improved hazards awareness and ability to mitigate simulated volcanic hazards. The study draws upon recent Indonesian educational research focused on incorporating traditional knowledge within science studies (Rusilowati et al. 2015; Andriana et al. 2017; Setiawan et al. 2017). It also adds to recent investigations of how belief systems can aid disaster response and preparedness in Indonesia (e.g. Joakim and White 2015).

Another finding of the Atmojo et al. (2018) study worth highlighting is that some traditional hazard warnings of seismic or volcanic unrest at Merapi—such as the unusual movement of tigers, monkeys, lions, and deer—no longer exist in our current era of biodiversity loss (Fig. 3.1). The acknowledgement of anthropogenic destruction near Merapi requires ‘an ethics of dialogue and engagement’ (per Schlehe 2010) based not only on local understanding but the global transformations in which they are contextualised. Engaged scholarship should privilege constructions of the world that promote a just, accountable, egalitarian and democratic environmental future (Blaikie 1999; Dove 2008b). Scientific monitoring is very important, but social justice in the face of corruption—

particularly in the context of disaster assistance funds that feel more ephemeral than the spirits that live in Merapi’s crater for marginal residents—is as well (Dove 2007). In this sense, no less so now as in the past, geological disasters in the Merapi area are highly cultural events and not exclusively natural ones.

3.6 Engagement with Dynamic Pasts and Futures

The ritual forms that have developed possess deep roots in regional cultures across Indonesia; yet their contemporary importance shows not their timeless authenticity but, rather, their centrality in national projects and their local renegotiations (Tsing 1993).

Traditional beliefs regarding volcanic eruption cannot be seen only as remnants of the past as they are very much entwined in the contemporary world and future interactions. Javanese traditional conceptions, past and present, show a sense of dynamism as opposed to catastrophism. Eruptions were incorporated into Javanese cosmology as opposed to being something unusual or anomalous. An inscription from 824 CE prays for a king’s ascent to spiritual merit ‘so long as the underground fire breathing hot remains, as the wise see, unsuppressed through the openings which are in its control, so long as the earth remains also, and the Meru inhabited by the gods remains, also, so long as Vrta (Sun) of the sky scatters his own rays’ (Sarkar 1971; Newhall et al. 2000). The endemic instability of the Javan environment contributes to a complete inappropriateness of ‘environmental management policies based on assumptions of steady-state equilibria’ (Lavigne and Gunnell 2006; Dove 2008a). In fact, ‘the “normal” state of nature on Java is to be recovering from the last disaster, not equilibrium and repose’ (Lavigne and Gunnell 2006). To assume a generalised ecological harmony in the Javanese cosmology is a romanticised western construct of the manifold meanings and experiences that adhere to the volcanic landscape (Schlehe 2008).

A newspaper account of a visit to the new guardian of Merapi describes him in a context of

hawkers selling 'a Pompeiian collection of geological mementoes' such as mini-volcano key-chains or postcards of smoking volcanoes (Hodal 2012). The association of Pompeii and Merapi is pertinent to the western perception of the site of Borobudur as a site of nature overwhelming a vulnerable culture. The Merapi area, however, provides a far more complex study area for the intersection of human life and volcanism than this simplistic binary. The same newspaper article cites the new volcano guardian as saying, 'Merapi is really a special mountain with its own special character.... It's difficult to predict even using scientific methods. There are a few natural signs we can look out for, and I can use those, but I'm still quite new at this' (Hodal 2012). Modern volcanology is also a relatively new science, and this rightly prompts caveats such as 'there is currently no reliable method to anticipate whether Merapi will have an explosive event' (Newhall et al. 2000). There is a humility inherent in both of these statements, one from a traditional vantage and one from a scientific vantage, that is healthy. For those who live on Merapi's slopes, the ghosts, spirits, and shamans of *Kejawen* are important for predicting the future behaviour of the volcano but so are technology and scientific data (Bobbette 2018). New studies using samples from Merapi indicate that hydrothermal alteration of andesitic lava domes can lead to explosive behaviour and provide an important addition to real-time hazard assessment (Heap et al. 2019). With continued scientific research and innovative technologies available in the future we will hopefully continue to refine our capacity to forewarn residents on Merapi's flanks of eruption events. Overall, though, it is important to remember that we monitor Merapi, but the volcano simultaneously monitors and watches us (Dove 2010). Study of Merapi is a way of studying human culture and how we interact with the volcano as much as it is the geological world of natural phenomena that occur at Merapi.

Acknowledgements My genuine and heartfelt thanks to the editors of this volume for the remarkable patience and good spirits they had with the geological time that I spent

writing this chapter as well as their careful, thoughtful suggestions and guidance. The work is dedicated to the memory of Jelle Zeilinga de Boer, who was originally meant to be the primary author and whose loss I feel heavily. I give thanks to his wife Felicité de Boer, who thoughtfully mailed me his Merapi research materials in hopes I could continue some of the many projects and ideas Jelle had in progress. I gratefully thank Frances Deegan, Ralf Gertisser, John Miksic, Mary-Ann del Marmol, Ernesto Schwartz-Marin, Val Troll, Jay Wellick, and Jan Wisseman Christie for their helpful contributions and conversations. Brent Alloway gave much valued and very helpful feedback on an early draft, which is especially valued as Jelle admired his Merapi tephrochronology. I deeply appreciate conversations with Clive Oppenheimer and Øystein Lund Andersen about images and imagery of Merapi. Artist Taylor Burkhead contributed creative talent to the illustration of the sacred axis. The chapter is greatly improved by the always insightful and thoughtful comments given by Amy Donovan. I give, overall, unreserved gratitude to all those who have worked on or with Merapi and those who live amidst its dynamism and wonder.

References

- Andriana E, Syachuroji A, Alamsyah TP, Sumirat F (2017) Natural science big book with Baduy local wisdom base media development for elementary school. *J Pendidik IPA Indon* 6:78–80
- Atmojo SE, Rusilowati A, Dwiningrum SIA, Skotnicka M (2018) The reconstruction of disaster knowledge through thematic learning of science, environment, technology, and society integrated with local wisdom. *J Pendidik IPA Indon* 7:204–213
- Berthommier PC (1991) Les éruptions historiques du Merapi (Centre Java Indonésie). *Bull Sect Volcanol Soc Géol France* 23:1–11
- Blaikie P (1999) A review of political ecology: issues, epistemology and analytical narratives. *Z Wirtschgeogr* 43:131–147
- Blong R (1984) Some perspectives on geological hazards. In: McCall GJH, Laming DJC, Scott SC (eds) *Geohazards*. Chapman and Hall, London, pp 209–216
- Bobbette A (2018) Cosmological reason on a volcano. In: Bobbette A, Donovan A (eds) *Political geology: active stratigraphies and the making of life*. Springer International Publishing AG, Cham, Switzerland, pp 169–199
- Bobbette A (2020) Making a home on a volcano. In: Lenhard J, Samanani F (eds) *Home: ethnographic encounters*. Series: encounters: experience and anthropological knowledge. Routledge, London, pp 145–148
- BPPTKG research and development center for geological disaster technology (BPPTKG): Merapi's activity <http://www.merapi.bgl.esdm.go.id/>. Accessed 8 June 2020

- Budi-Santoso A, Beaucecel F, Nandaka IGMA, Humaida H, Costa F, Widiwijayanti C, Iguchi M, Métaxian J-P, Rudianto I, Rozin M, Sulistiyani, Nurdin I, Kelfoun K, Byrdina S, Pinel V, Fahmi AA, Laurin A, Rizal MH, Dahamna N (2023) The Merapi volcano monitoring system. In: Gertisser R, Troll VR, Walter TR, Nandaka IGMA, Ratdomopurbo A (eds) *Merapi volcano—geology, eruptive activity, and monitoring of a high-risk volcano*. Springer, Berlin, Heidelberg, pp 409–436
- Byrdina S, Friedel S, Vandemeulebrouck J, Budi-Santoso A, Suhari, Suryanto W, Rizal MH, Winata E, Kusdaryanto (2017) Geophysical image of the hydrothermal system of Merapi volcano. *J Volcanol Geotherm Res* 329:30–40
- Carr BB, Clarke AB, de' Michieli Vitturi M (2020) Volcanic conduit controls on effusive-explosive transitions and the 2010 eruption of Merapi volcano (Indonesia). *J Volcanol Geotherm Res* 392:106767
- Cashman K, Cronin S (2008) Welcoming a monster to the world: myths, oral tradition, and modern societal response to volcanic disaster. *J Volcanol Geotherm Res* 176:407–418
- Chester DK (1998) The theodicy of natural disasters. *Scott J Theol* 51(4):485–505
- Chester DK (2005) Theology and disaster studies: the need for dialogue. *J Volcanol Geotherm Res* 146:319–328
- Cronin S, Cashman K (2007) Volcanic oral traditions in hazard assessment and mitigation. In: Grattan J, Torrence R (eds) *Living under the shadow: cultural impacts of volcanic eruptions*. One World Archaeology Series. Left Coast Press, Walnut Creek, CA, pp 175–202
- Darmawan H, Walter TR, Troll VR, Budi-Santoso A (2018) Structural weakening of the Merapi dome identified by drone photogrammetry after the 2010 eruption. *Nat Hazards Earth Syst Sci* 18:3267–3281
- de Casparis JG (1950) *Inscripties uit de Çailendra-tijd* (Prasasti Indonesia I). Nix, Bandung, Indonesia
- Deep Carbon Observatory (2019) *Deep carbon observatory: a decade of discovery*. Washington, D.C. <https://deepcarbon.net/deep-carbon-observatory-decade-discovery>
- Djumarna A, Bronto S, Bahar I, Suparban F, Sukhyar R, Newhall C, Holcomb R, Banks N, Torley R, Lockwood J, Tilling R, Rubin M, del Marmol M (1986) Did Merapi volcano (Central Java) erupt catastrophically in 1006 A.D.? Abstract, IAVCEI Internat Volcanol Congr 1986, Rotorua, New Zealand
- Donovan A, Suryanto A, Utami P (2012) Mapping cultural vulnerability in volcanic regions: the practical application of social volcanology at Mt Merapi, Indonesia. *Environ Hazards* 11:303–323
- Donovan K (2010) Doing social volcanology: exploring volcanic culture in Indonesia. *Area* 42:117–126
- Donovan K, Suharyanto A (2011) The creatures will protect us. *Geoscientist* 21:12–17
- Dove M (2007) Volcanic eruption as metaphor of social integration: a political ecological study of Mount Merapi, Central Java. In: Connell J, Waddell E (eds) *Environment, development and change in rural Asia-Pacific: between local and global*. Routledge, London, pp 16–37
- Dove M (2008a) Perception of volcanic eruption as agent of change on Merapi volcano, Central Java. *J Volcanol Geotherm Res* 172:329–337
- Dove M (2008b) The view from the volcano: an appreciation of the work of Piers Blaikie. With Bambang Hidayana. *Geoforum* 39:736–746
- Dove M (2010) The panoptic gaze in a non-western setting: self-surveillance on Merapi volcano, Central Java. *Religion* 40:121–127
- Dove M, Carpenter C (2007a) Introduction: major historical currents in environmental anthropology. In: *Environmental anthropology. A historical reader*. Blackwell anthologies in social & cultural anthropology (ASCA). Blackwell, Malden, MA, pp 1–85
- Dove M, Carpenter C (eds) (2007b) *Environmental anthropology. A historical reader*. Blackwell anthologies in social & cultural anthropology (ASCA). Blackwell, Malden, MA, p 504
- Duffield W (2001) At least Noah had some warning. *Eos* (transactions, American Geophysical Union) 82:305–309
- Dumarçay J (1986) *The temples of java*. Oxford University Press, Singapore
- Florindo F, McEntee C (2020) The role of earth and space scientists during pandemics. *Eos* (Transactions, American Geophysical Union) 101
- Frédéric L (1996) *Borobudur*. Abbeville, New York
- Geertz C (1960) *The religion of java*. Free Press, Glencoe, IL
- Gertisser R, del Marmol M-A, Newhall C, Preece K, Charbonnier S, Andreastuti S, Handley H, Keller J (2023) Geological history, chronology and magmatic evolution of Merapi. In: Gertisser R, Troll VR, Walter TR, Nandaka IGMA, Ratdomopurbo A (eds) *Merapi volcano—geology, eruptive activity, and monitoring of a high-risk volcano*. Springer, Berlin, Heidelberg, pp 137–193
- Gomez C, Janin M, Lavigne F, Gertisser R, Charbonnier S, Lahitte P, Hadmoko SR, Fort M, Wassmer P, Degroot V, Murwanto H (2010) Borobudur, a basin under volcanic influence: 361,000 years BP to present. *J Volcanol Geotherm Res* 196:245–264
- Gómez LO, Woodward HW (eds) (1981) *Barabudur, history and significance of a Buddhist monument*. Distributed by Asian Humanities Press, Berkeley, CA, p 253
- Hayes JL, Wilson TM, Deligne NI, Lindsay JM, Leonard GS, Tsang SWR, Fitzgerald RH (2020) Developing a suite of multi-hazard volcanic eruption scenarios using an interdisciplinary approach. *J Volcanol Geotherm Res* 392:106763

- Heap MJ, Troll VR, Kushnir ARL, Gilg HA, Collinson ASD, Deegan FM, Darmawan H, Seraphine N, Neuberg J, Walter TR (2019) Hydrothermal alteration of andesitic lava domes can lead to explosive volcanic behaviour. *Nat Commun* 10:5063
- Hodal K (2012) Merapi volcano's 'spirit keeper' walks line between tradition and technology. *The Guardian*, 15 November 2021. <https://www.theguardian.com/world/2012/nov/15/merapi-volcano-spirit-guardian-tradition>
- Holmberg K (2007) Beyond the catastrophe: the volcanic landscape of Barú, western Panamá. In: Grattan J, Torrence R (eds) *Living under the shadow: cultural impacts of volcanic eruptions*. One World Archaeology series. Left Coast Press, Walnut Creek, CA, p 274–297
- Holmberg K (2013a) An inheritance of loss: archaeology's imagination of disaster. In: Davis M, Nkirote F (eds) *Humans and the environment: new archaeological perspectives for the 21st century*. Oxford University Press, Oxford, pp 197–209
- Holmberg K (2013b) The sound of sulfur and smell of lightning: sensing the volcano. In: Day J (ed) *Making senses of the past: toward a sensory archaeology*. Center for archaeological investigations occasional paper No. 40. Southern Illinois University, Carbondale, pp 49–68
- Holmberg K (2020) Landing on the terrestrial volcano. In: Latour B, Weibel P (eds) *Critical zones: the science and politics of landing on earth*. MIT Press, Cambridge, MA, pp 56–57
- Ijzerman JW (1891) *Beschrijving der oudheden nabij de grens de Residentie's Soerakarta en Djogdjakarta*. Batavia: Landsdrukkerij; 's Gravenhage: M. Nijhoff, p 135
- Jenkins S, Komorowski JC, Baxter P, Spence RJS, Picquout A, Lavigne F (2013) The Merapi 2010 eruption: an interdisciplinary impact assessment methodology for studying pyroclastic density current dynamics. *J Volcanol Geotherm Res* 261:316–329
- Joakim E, White R (2015) Exploring the impact of religious beliefs, leadership, and networks on response and recover of disaster-affected populations: a case study from Indonesia. *J Contemp Relig* 30:193–212
- Jordaen R (1984) The mystery of Nyai Lara Kidul, goddess of the southern ocean. *Archipel* 28:99–116
- Junguhn FW (1845a) *Bijdragen tot de geschiedenis der vulkanen in den Indischen archipel, tot en met het jaar 1842*
- Junguhn FW (1845b) *Die Topographischen und Naturwissenschaftlichen Reisen durch Java (Topographic and Scientific Journeys in Java)*
- Junguhn FW (1853–4) *Java Deszelfs Gedaante Bekleeding en Inwendige Structuur*. 2nd edn. Uitgave C. W. Mieling, 's Gravenhage
- Karsono B, Wahid J (2008) Imaginary axis as a basic morphology in the city of Yogyakarta-Indonesia. In: 2nd International Conference on Built Environment in Developing Countries (ICBEDC 2008), Universiti Sains Malaysia (USM), pp 187–195
- Kelman I (2020) *Disaster by choice: how our actions turn natural hazards into catastrophes*. Oxford University Press, Oxford, UK, p 192
- Korintenberg B, Libeskind R, Preusse R, Rau S (2020) Glossolalia: tidings from terrestrial tongues. In: Latour B, Weibel P (eds) *Critical zones: the science and politics of landing on earth*. MIT Press, Cambridge, MA, pp 318–325
- Krüger F, Bankoff G, Cannon T, Orłowski B, Schipper ELF, Schipper L (2015) *Cultures and disasters: understanding cultural framings in disaster risk reduction*. Taylor & Francis Group, London, UK, p 298
- Kusumayudha SB, Sutarto HM, Choiriyah SU (2019) Volcanic disaster and the decline of Mataram Kingdom in the Central Java, Indonesia. In: Wasowski J, Dijkstra T (eds) *Recent research on engineering geology and geological engineering: proceedings of the 2nd GeoMEast international congress and exhibition on sustainable civil infrastructures*, Egypt 2018, pp 83–93
- Lavigne F, De Coster B, Juvin N, Flohic F, Gaillard J-C, Texier P, Morin J, Sartohadi J (2008) People's behavior in the face of volcanic hazards: perspectives from Javanese communities, Indonesia. *J Volcanol Geotherm Res* 172:273–287
- Lavigne F, Gunnell F (2006) Land cover change and abrupt environmental impacts on Javan volcanoes: a long-term perspective on recent events. *Reg Environ Change* 6:86–100
- Lavigne F, Morin J, Surono (eds) (2015) *Atlas of Merapi volcano*. Laboratoire de Géographie Physique, Meudon, France, 58 color plates. Online Publication (hal-03010922)
- Lühr BG, Koulakov I, Suryanto W (2023) Crustal structure and ascent of fluids and melts beneath Merapi: insights from geophysical investigations. In: Gertisser R, Troll VR, Walter TR, Nandaka IGMA, Ratdomopurbo A (eds) *Merapi volcano—geology, eruptive activity, and monitoring of a high-risk volcano*. Springer, Berlin, Heidelberg, pp 111–135
- Maharani YN, Lee S, Ki SJ (2016) Social vulnerability at a local level around the Merapi volcano. *Int J Disaster Risk Reduct* 20:63–77
- Martinez A (2017) Understanding an active volcano: naturalism, analogism and animism in central Javanese society—societies and environments in Southeast Asia: Cosmic orders, knowledge systems and social relations. *OpenEdition Hypotheses*. <https://nature.hypotheses.org/368>
- Martinez A (2018) *Le volcan Merapi au carrefour du naturalisme et de l'analogisme - Réinstallation post-catastrophe et relations à l'environnement volcanique à Java centre, Indonésie*. Moussons: Soc Sci Res Southeast Asia 32:21–48
- Martinez A (2019) *Un espace social viable dans un environnement à risque? Réinstallation post-catastrophe et relations à l'espace sur le volcan Merapi (Java, Indonésie)*. Moussons: Soc Sci Res Southeast Asia 34:141–167

- McAdoo BG, Dengler L, Prasetya G, Titov V (2006) Smong: how an oral history saved thousands on Indonesia's Simeulue Island during the December 2004 and March 2005 tsunamis. *Earthq Spectra* 22:661–669
- Mei ETW, Lavigne F (2012) Influence of the institutional and socio-economic context for responding to disasters: case study of the 1994 and 2006 eruptions of the Merapi volcano, Indonesia. *Geol Soc Lond Spec Publ* 36:171–186
- Mei ETW, Lavigne F (2013) Mass evacuation of the 2010 Merapi eruption. *Int J Emerg Manag* 9:298–311
- Mei ETW, Fajarwati A, Hasanati S, Sari IM (2016) Resettlement following the 2010 Merapi volcano eruption. *Procedia Soc Behav Sci* 227:361–369
- Miksic JN (2012) Borobudur (an annotated bibliography). Oxford University Press, New York
- Mothes P, Yepes H, Hall M, Ramon P, Steele A, Ruiz M (2015) The scientific-community interface over the fifteen-year eruptive episode of Tungurahua Volcano, Ecuador. *J Appl Volcanol* 4:9
- Muir JA, Cope MR, Angeningsih LR, Jackson JE (2020) To move home or move on? Investigating the impact of recovery aid on migration status as a potential tool for disaster risk reduction in the aftermath of volcanic eruptions in Merapi Indonesia. *Int J Disaster Risk Reduct* 46:101478
- Murwanto H, Gunnell Y, Suharsono S, Sutikno S, Lavigne F (2004) Borobudur monument (Java, Indonesia) stood by a natural lake: chronostratigraphic evidence and historical implications. *Holocene* 14:459–463
- Nadeau O, Humaida H, Allard P (2023) Merapi volcano: from volcanic gases to magma degassing. In: Gertisser R, Troll VR, Walter TR, Nandaka IGMA, Ratdompurbo A (eds) *Merapi volcano—geology, eruptive activity, and monitoring of a high-risk volcano*. Springer, Berlin, Heidelberg, pp 323–351
- Neumann van Padang M (1951) Catalogue of the active volcanoes of Indonesia. International volcanological association—catalogue of the active volcanoes of the world, including solfatara fields
- Neumann van Padang M (1983) History of volcanology in the East Indies. *Scripta Geol* 71:1–76
- Newhall C, Bronto S, Alloway B, Banks N, Bahar I, del Marmol M, Hadisantono R, Holcomb R, McGeehin J, Miksic J, Rubin M, Sayudi S, Sukhyar R, Andreas-tuti S, Tilling R, Torley R, Trimble D, Wirakusumah A (2000) 10,000 years of explosive eruptions of Merapi volcano, Central Java: archaeological and modern implications. *J Volcanol Geotherm Res* 100:9–50
- Oliver-Smith A (1996) Anthropological research on hazards and disasters. *Annu Rev Anthropol* 25:303–328
- Oliver-Smith A (2013) Disaster risk reduction and climate change adaptation: the view from applied anthropology. *Hum Org* 72:275–282
- Oliver-Smith A, Hoffman S (eds) (1999) *The angry earth: disaster in anthropological perspective*. Routledge, New York, p 418
- Picquout A, Mei E, Grancher D, Cholik N, Vidal C, Hadmoko D (2013) Air traffic disturbance due to the 2010 eruption of Merapi volcano. *J Volcanol Geotherm Res* 261:366–375
- Purbawinata MA, Ratdompurbo A, Surono PJ, Luehr B, Newhall C (2007) Understanding Merapi-type volcanoes. *Eos (transactions American Geophysical Union)* 88:5–6
- Raffles TSS (1817) *The history of Java (in two volumes)*. Black, Parbury and Allen; John Murray, London, p 1817
- Resink G (1997) Kanjeng Ratu Kidul: the second divine spouse of the sultans of Ngayogyakarta. *Asian Folk Stud* 56:313–316
- Rizal Y, Westaway KE, Zaim Y, van den Bergh GD, Bettis EA, Morwood MJ, Huffman OF, Grün R, Joannes-Boyau R, Bailey RM, Sidarto WMC, Kurniawan I, Moore MW, Storey M, Aziz F, Suminto Z-x, Aswan SME, Larick R, Zonneveld J-P, Scott R, Putt S, Ciochon RL (2020) Last appearance of *Homo erectus* at Ngandong, Java, 117,000–108,000 years ago. *Nature* 577:381–385
- Rodolfo KS, Umbal JV (2008) A prehistoric lahar-dammed lake and eruption of Mount Pinatubo described in Philippine aborigine legend. *J Volcanol Geotherm Res* 176:432–437
- Rusilowati A, Supriyadi S, Widiyantoro S (2015) Pembelajaran Kebencanaan Alam Bervisi Sets Terintegrasi Dalam Mata Pelajaran Fisika Berbasis Kearifan Lokal. *J Pendidik IPA Indon* 11:42–48
- Sarkar H (1971) *Corpus of the Inscriptions of Java (Corpus inscriptionum Javanicarum)*, up to 928 A.D. Firma K.L. Mukhopadhyay, Calcutta, India
- Scheltema JF (1912) *Monumental java*. Macmillan and Co., Limited, London, p 302
- Schlehe J (1996) Reinterpretations of mystical traditions: explanations of a volcanic eruption in Java. *Anthropos* 91:391–409
- Schlehe J (1998) *Die Meereshkönigin des Südens, Ratu Kidul: Geisterpolitik im javanischen Alltag (German Edition)*. D. Reimer, Berlin, p 306
- Schlehe J (2008) Cultural politics of natural disasters: discourses on volcanic eruptions in Indonesia. In: Casimir M (ed) *Culture and the changing environment: uncertainty, cognition and risk management in cross-cultural perspective*. Berghahn Books, New York and Oxford, pp 275–300
- Schlehe J (2010) Anthropology of religion: disasters and the representations of tradition and modernity. *Religion* 40:112–120
- Schwartz-Marin E, Merli C, Rachmawati L, Horwell C, Nugroho F (2020) Merapi multiple: protection around Yogyakarta's celebrity volcano through masks, dreams, and seismographs. *Hist Anthropol*. <https://doi.org/10.1080/02757206.2020.1799788>
- Setiawan R, Innatesari DK, Sabtiawan WB, Sudarmin S (2017) The development of local wisdom-based natural science modules to improve science literacy of students. *J Pendidik IPA Indon* 6:49–54

- Solikhin A, Pinel V, Vandemeulebrouch J, Thouret J-C, Hendrasto M (2015) Mapping the 2010 Merapi pyroclastic deposits using dual-polarization synthetic aperture radar (SAR) data. *Remote Sens Environ* 158:180–192
- Subandriyo, Gertisser R, Aisyah N, Humaida H, Preece K, Charbonnier S, Budi-Santoso A, Handley H, Sumarti S, Sayudi DS, Nandaka IGMA, Wibowo HE (2023) An Overview of the Large-Magnitude (VEI 4) Eruption of Merapi in 2010. In: Gertisser R, Troll VR, Walter TR, Nandaka IGMA, Ratdomopurbo A (eds) *Merapi volcano—geology, eruptive activity, and monitoring of a high-risk volcano*. Springer, Berlin, Heidelberg, pp 353–407
- Surono JP, Pallister J, Boichu M, Buongiorno MF, Budisantoso A, Costa F, Andreastuti S, Prata F, Schneider D, Clarisse L, Humaida H, Sumarti S, Bignani C, Griswold J, Carn S, Oppenheimer C, Lavigne F (2012) The 2010 explosive eruption of Java's Merapi volcano—a '100-year' event. *J Volcanol Geotherm Res* 241–242:121–135
- Swanson D (2008) Hawaiian oral tradition describes 4000 years of volcanic activity at Kilauea. *J Volcanol Geotherm Res* 176:427–431
- Syafwina (2014) Recognizing indigenous knowledge for disaster management: smong, early warning system from Simeulue Island, Aceh. *Procedia Environ Sci* 20:573–582
- Triyoga L (1991) *Manusia Jawa dan Gunung Merapi: Persepsi dan kepercayaannya*. Gadjah Mada University Press, Yogyakarta, Indonesia
- Troll C (1939) Luftbildplan und ökologische Bodenforschung. *Zeitschr Gesellsch Erdkunde Berlin*:241–298
- Troll VR, Deegan FM (2023) The magma plumbing system of Merapi: the petrological perspective. In: Gertisser R, Troll VR, Walter TR, Nandaka IGMA, Ratdomopurbo A (eds) *Merapi volcano—geology, eruptive activity, and monitoring of a high-risk volcano*. Springer, Berlin, Heidelberg, pp 233–263
- Troll VR, Deegan FM, Jolis EM, Budd DA, Dahren B, Schwarzkopf LM (2015) Ancient oral tradition describes volcano–earthquake interaction at Merapi volcano, Indonesia. *Geografisk Ann: Series a, Phys Geograph* 97:137–166
- Troll VR, Deegan FM, Seraphine N (2021) Ancient oral tradition in Central Java warns of volcano-earthquake interaction. *Geol Today* 37:100–109
- Tsing AL (1993) In the realm of the diamond queen: marginality in an out-of-the-way place. Princeton University Press, Princeton, NJ, p 368
- van Bemmelen RW (1949) Report on the volcanic activity and volcanological research in Indonesia during the period 1936–1948. *Bull Volcanol* 9:3–30
- van Bemmelen RW (1956) The influence of geological events on human history (an example from Central Java). *Verh Kon Ned Geol Mijnbouw Genootschap* 16:20–36
- van Bemmelen RW (1971) Four volcanic outbursts that influenced human history: Toba, Sunda, Merapi and Thera. In: Kaloueropoulou A (ed) *Acta of the 1st international scientific congress on the volcano of Thera, Athens*, pp 5–50
- van Hinloopen LD (1921) Oud-Javaansche gegevens omtrent de vulkanologie van Java. *Natuurk Tijds Ned Indië* 81:124–158
- Verbeek RDM, Fennema R (1896) Two volumes and a folio with maps and sections. In: Stemler JG *Geologische beschrijving van Java en Madoera*. Amsterdam
- Voight B, Constantine EK, Siswoidjyo S, Torley R (2000) Historical eruptions of Merapi volcano, Central Java, Indonesia, 1768–1998. *J Volcanol Geotherm Res* 100:69–138
- VSI-ESDM (2020) Badan Geologi <https://vsi.esdm.go.id/>. Accessed 7 June 2020
- VSI-PVMBG (2020) MAGMA Indonesia <https://magma.vsi.esdm.go.id/>. Accessed 08 June 2020
- Walter TR, Wang R, Zimmer M, Grosser H, Lühr B, Ratdomopurbo A (2007) Volcanic activity influenced by tectonic earthquakes: static and dynamic stress triggering at Mt Merapi. *Geophys Res Lett* 34:L05304
- Wessing R (1997) A princess from Sunda: some aspects of Nyai Roro Kidul. *Asian Folkl Stud* 56:317–353
- Whitley S, Gertisser R, Halama R, Preece K, Troll VR, Deegan FM (2019) Crustal CO₂ contribution to subduction zone degassing recorded through calc-silicate xenoliths in arc lavas. *Sci Rep* 9:8803
- Whitley S, Halama R, Gertisser R, Preece K, Deegan F, Troll V (2020) Magmatic and Metasomatic Effects of Magma–Carbonate Interaction Recorded in Calc-silicate Xenoliths from Merapi volcano (Indonesia). *J Petrol* 61:egaa048
- Widiyantoro S, Ramdhan M, Métaxian JP, Cummins PR, Martel C, Erdmann S, Nugraha AD, Budi-Santoso A, Laurin A, Fahmi AA (2018) Seismic imaging and petrology explain highly explosive eruptions of Merapi volcano Indonesia. *Sci Rep* 8:13656
- Wisseman Christie J (2015) Under the volcano: stabilizing the early Javanese state in an unstable environment. In: Henley D, Nordholt HS (eds) *Environment, trade and society in Southeast Asia. A Longue Durée Perspective*. Brill, pp 46–61
- Zeilinga de Boer J, Sanders D (2002) *Volcanoes in human history: the far-reaching effects of major eruptions*. Princeton University Press, Princeton, NJ, p 320



The Geodynamic Setting and Geological Context of Merapi Volcano in Central Java, Indonesia

4

Agung Harijoko, Gayatri Indah Marliyani,
Haryo Edi Wibowo, Yan Restu Freski,
and Esti Handini

Abstract

Mount (Mt.) Merapi is a Quaternary stratovolcano situated on the active volcanic front in Central Java. It is a part of the active volcanic arc chain of Java Island formed by the Sunda-Banda subduction of the Indo-Australian oceanic plate beneath the Eurasian continental plate. The volcanic activity of Merapi shows a recurring pattern of eruptive events, with a background of frequent Volcanic Explosivity Index (VEI) 1–2 eruptions approximately every 4–5 years, interrupted by more violent (VEI 3–4) eruption episodes every few decades. As one of Indonesia's most active volcanoes, Mt. Merapi draws admiration and fear from many Indonesians and the world. The volcano plays a significant role in understanding the Quaternary volcanism in Java, as it has been continuously erupting since the historical records began. Located within the Central Java depression zone, Mt. Merapi is bound by the

Southern Mountains Zone to the south and the Kendeng and Rembang zones to the north. The basement of Mt. Merapi is composed of limestones of the Sentolo Formation and Tertiary volcanic and volcanoclastic rocks of the Nglanggran and Semilir formations. The region is dissected by several larger fault systems, namely the Progo Muria Fault and the Opak River Fault. Mt. Merapi and the Merbabu-Telomoyo-Ungaran volcanoes (located to the north of Merapi) follow a NW–SE-trend, similar in orientation to the regional fault systems, suggesting that geological structures control the emplacement of magma and its ascent to the surface. Tomographic studies underneath Mt. Merapi also indicate the presence of a NW–SE trending gravity anomaly that may represent a wider, more regional extent of the magma reservoir beneath the Merapi-Merbabu-Telomoyo-Ungaran volcanic chain.

Keywords

Merapi · Geodynamic setting · Regional geology · Sunda arc

A. Harijoko (✉) · G. I. Marliyani · H. E. Wibowo ·
Y. R. Freski · E. Handini
Department of Geological Engineering,
Faculty of Engineering, Universitas Gadjah Mada,
Yogyakarta, Indonesia
e-mail: aharijoko@ugm.ac.id

A. Harijoko · G. I. Marliyani · H. E. Wibowo ·
E. Handini
Center for Disaster Studies, Universitas Gadjah
Mada, Yogyakarta, Indonesia

4.1 Introduction

Being one of the most active volcanoes in Indonesia, Mt. Merapi attracts both admiration and fear among many Indonesians and globally.

Despite the danger of living in the volcano's proximity, many people occupy fertile land surrounding Mt. Merapi, risking exposure to pyroclastic flows and possible larger explosive eruptions (e.g. Lavigne 2004; Suroño et al. 2012; Troll et al. 2015). The volcano forms an impressive 2930 m high topographic relief over the Yogyakarta lowlands resulting from thousands of years of activity (Fig. 4.1). The eruptive history of Merapi was reconstructed from the historical record, stratigraphic investigations as well as radiocarbon, K–Ar, Ar–Ar, and U–Th dating. The historical record of Merapi's eruptive history ranges from AD 1548 to the present (Global Volcanism Program 2013). Radiocarbon dates extend from ~200 up to ~11,000 ¹⁴C years BP and are found in Gertisser et al. (2012) and references therein. Available K–Ar, Ar–Ar, and U–Th dating data span from 1.7 ± 1.7 ka for the recent Merapi cone (New Merapi) to 138 ± 3 ka for Gunung Turgo/Plawangan (Berthommier 1990; Camus et al. 2000; Gertisser et al. 2012). A K–Ar age of 670 ± 250 ka from G. Bibi (Fig. 4.1) was reported by Berthommier (1990) and Camus et al. (2000). However, the reliability of the age was later questioned by Newhall et al. (2000), who instead interpreted G. Bibi as a younger flank vent of Old Merapi (see Gertisser et al. 2023, Chap. 6). ⁴⁰Ar/³⁹Ar dating conducted by Gertisser et al. (2012) yielded an age of G. Bibi of 109 ± 60 ka (i.e. <170 ka).

Historical eruptive records from AD 1548 to 2010 show that Mt. Merapi erupted at least 73 times. The eruption scale of Mt. Merapi ranges from Volcanic Explosivity Index (VEI) 1 to 4, with VEI 1 (29%), VEI 2 (45%), VEI 3 (23%), and VEI 4 (3%) of the total number of events. Generally, Mt. Merapi is known to have a somewhat regular pattern of recurring moderate events with a VEI of roughly 1–2 that manifest themselves approximately every 4–5 years, interrupted by less frequent but more violent (VEI 3–4) eruption episodes every few decades (Voight et al. 2000). The compositions of the eruptive products range from basalt to andesite (~50–57 wt.%SiO₂) with basaltic andesite being predominant (e.g. Gertisser and Keller 2003a;

Gertisser et al. 2012). The volcanic rocks consist of a medium-K and a high-K series, and since 1900 ¹⁴C years BP, all erupted products have essentially been of high-K affinity (Gertisser and Keller 2003a; Gertisser et al. 2012). The variation of K₂O content for a given SiO₂ content has been shown to correlate with variations of Rb and Ba concentrations and Sr isotopic ratios, and was interpreted as a result of the variations in the deep source characteristics of primary magmas of the two magma types (Gertisser and Keller 2003b). Alternatively, changes in the volcano edifice configuration (see Gertisser et al. 2023, Chap. 6) or more pronounced carbonate assimilation may have been factors in these compositional variations (cf. Chadwick et al. 2007; Deegan et al. 2010; Troll et al. 2013).

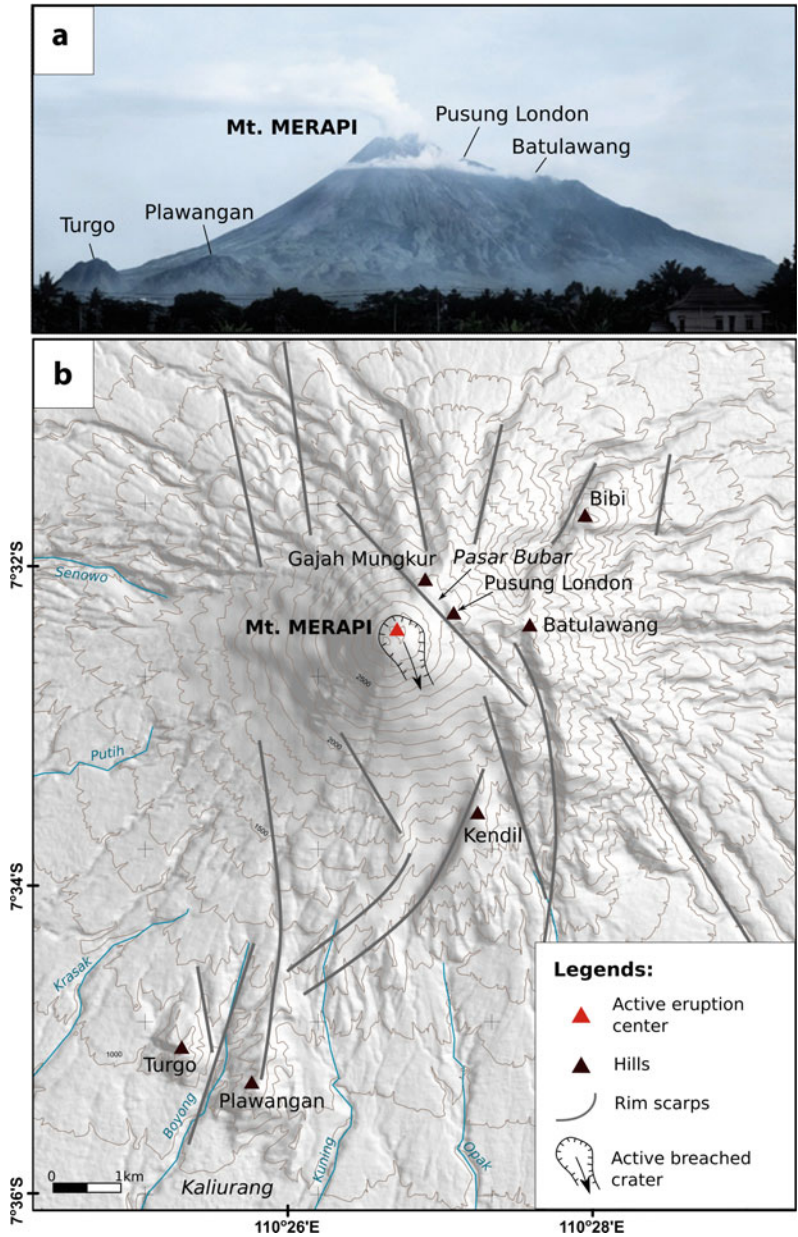
The geology of Mt. Merapi reveals essential information on the geodynamic processes of the Javanese arc and has been the subject of intensive study (e.g. Andreastuti et al. 2000; Camus et al. 2000; Newhall et al. 2000; Gertisser and Keller 2003a, b; Gertisser et al. 2011, 2012; Suroño et al. 2012; Costa et al. 2013; Jousset et al. 2013; Ratdomopurbo et al. 2013; Walter et al. 2015; Widiyantoro et al. 2018). Since it continuously ejects new volcanic material, the volcano holds a vital role in understanding the Quaternary volcanism in Java.

This chapter aims to provide an overview of the geodynamic setting and regional geology of Merapi and the surrounding area based on published data and field observations. These include a description of the underlying basement rocks, the regional structural setting that has influenced the volcano's location and emplacement of magma, and the geophysical characteristics of the surrounding area.

4.2 Geodynamic Setting

Mt. Merapi is a part of the active volcanic arc on Java Island. The volcanic arc results from the subduction of the Indo-Australian oceanic plate beneath the Eurasian continental plate at the southern edge of what is known as the Sundaland continent (Hamilton 1979; Tregoning et al. 1994;

Fig. 4.1 **a** View of Mt. Merapi from the southeast. **b** Topographic map of Merapi, showing the active crater, prominent hills and landmarks on its slopes, and prominent rim scarps or faults. DEM data is freely downloadable through (<http://tides.big.go.id/DEMNAS/>)



Tregoning 2002; Bird 2003; Hall and Smyth 2008). This subduction system is part of the Sunda-Banda subduction zone, which stretches from the Andaman Islands, passing the south of Sumatra and Java Island to the east, and ending at Flores Island. The age of the downgoing oceanic Indo-Australian Plate is ~80–140 Ma (Whitford

1975; Cloetingh and Wortel 1986; Packham 1996), while the Eurasian Plate is the amalgamated continental core of Southeast Asia constructed by accretion of continental blocks during the Triassic (Hall 2002; Hall and Smyth 2008; Metcalfe 2017). The crustal thickness decreases from West Java to Bali from c. 30 km to <20 km

(Wölbern and Rumpker 2016), and the oceanic-continent nature of the plate interaction along the Sunda-Banda subduction zone thus becomes more ocean-ocean like towards the East.

Based on a GPS campaign (from 1989 to 1993), Tregoning et al. (1994) estimated the convergence rate between the Indo-Australian Plate and the Eurasian Plate at the Java Trench at 6.7 ± 0.7 cm/year in the direction of N11°E. The deep foci earthquakes delineate the subducted slab below Java Island that extends down to a depth of c. 600 km (Hamilton 1979; Setijadji et al. 2006; Hayes et al. 2018). The earthquake data also indicate that the Java subduction zone has variable slab dip angles (Lühr et al. 2013). The earthquake distribution shows that the subduction angle is nearly horizontal for the first 150 km from the trench. The slab dip increases to $\sim 45^\circ$ from 150 to 350 km and to $\sim 70^\circ$ from 250 to 600 km (Figs. 4.2 and 4.3), yielding a steepening geometry with depth.

The Java subduction zone has existed at least since the Eocene, as shown by the formation of the Tertiary volcanic belt of the Southern Mountains (Soeria-Atmadja et al. 1994; Hall 2002; Hall and Smyth 2008). During the Early to Middle Miocene, the volcanic activity in Java decreased and then resumed at the end of the Middle Miocene due to the counterclockwise rotation of Borneo and Java (Hall and Smyth 2008). This rotation led to resumed volcanism and generated the modern volcanic arc located to the north relative to the Tertiary volcanic arc (Hall and Smyth 2008), including Mt. Merapi. Sediment thickness at the Java trench is ~ 300 m (Plank and Langmuir 1998), which is thinner than at the East Sunda and Sumatra segments (500 and 1400 m, respectively; Plank (2014)). The sediment is dominated by volcanic ash and pelagic clay with minor turbidites (Plank 2014). More recent estimates using seismic profiles suggest that the sediment volume in this arc segment is more carbonate-rich compared to the more organic-rich trench sediments further west, for example, off Sumatra (House et al. 2019). This further indicates intensive sediment scraping and frontal erosion in the Central Java

segment (Kopp et al. 2006; Kopp 2011). Subduction erosion at this arc segment is also indicated by onshore pullback of the trench and steepening of the lower trench slope (Kopp et al. 2006). The authors further suggested that continuing Roo Rise subduction into the trench uplifts the forearc and, consequently, narrows the forearc sedimentary basin.

Mt. Merapi is located ~ 300 km north of the Java trench. The subducted slab is located at around 150–200 km below Mt. Merapi (Fig. 4.2; Hamilton 1979; Wagner et al. 2007; Lühr et al. 2013). Wagner et al. (2007) proposed that partial mantle melting below Mt. Merapi occurs at a depth of about 100 km. The mineral textures, chemistry, and geothermobarometric data from Merapi volcanic rocks, supported by seismic tomographic images, indicate that the magma reservoirs beneath Mt. Merapi occur at multiple depths: a shallow reservoir or fluid-rich zone at less than 4 km depth, a primary reservoir at 10–20 km depth, and a deep reservoir at more than 25 km depth (e.g. Chadwick et al. 2013; Costa et al. 2013; Deegan et al. 2016; Peters et al. 2017; Widiyantoro et al. 2018; Whitley et al. 2020; Troll and Deegan 2023, Chap. 8). In addition to plutonic xenoliths and megacrysts of amphibole (e.g. Chadwick et al. 2013; Peters et al. 2017; Troll and Deegan 2023, Chap. 8), xenoliths of metamorphosed carbonate (calc-silicate) rock are also found in the Merapi products, representing the basement beneath Merapi (e.g. Camus et al. 2000; Chadwick et al. 2007; Deegan et al. 2010, 2011, 2023, Chap. 10; Troll et al. 2013; Whitley et al. 2019, 2020). The xenoliths are inferred to be derived from the Cretaceous-Tertiary marine limestones, marls, and volcanoclastic rocks that constitute the upper part of the arc crust (e.g. van Bemmelen 1949; Smyth et al. 2007; Whitley et al. 2019, 2020). The interaction of these lithologies with the magmas of Mt. Merapi may influence the explosivity of its eruptions, as it may alter the volatile budget of the magmatic system (e.g. Chadwick et al. 2007; Deegan et al. 2010, 2011, 2023, Chap. 10; Troll et al. 2012; Borisova et al. 2013; Costa et al. 2013; Whitley et al. 2019, 2020).

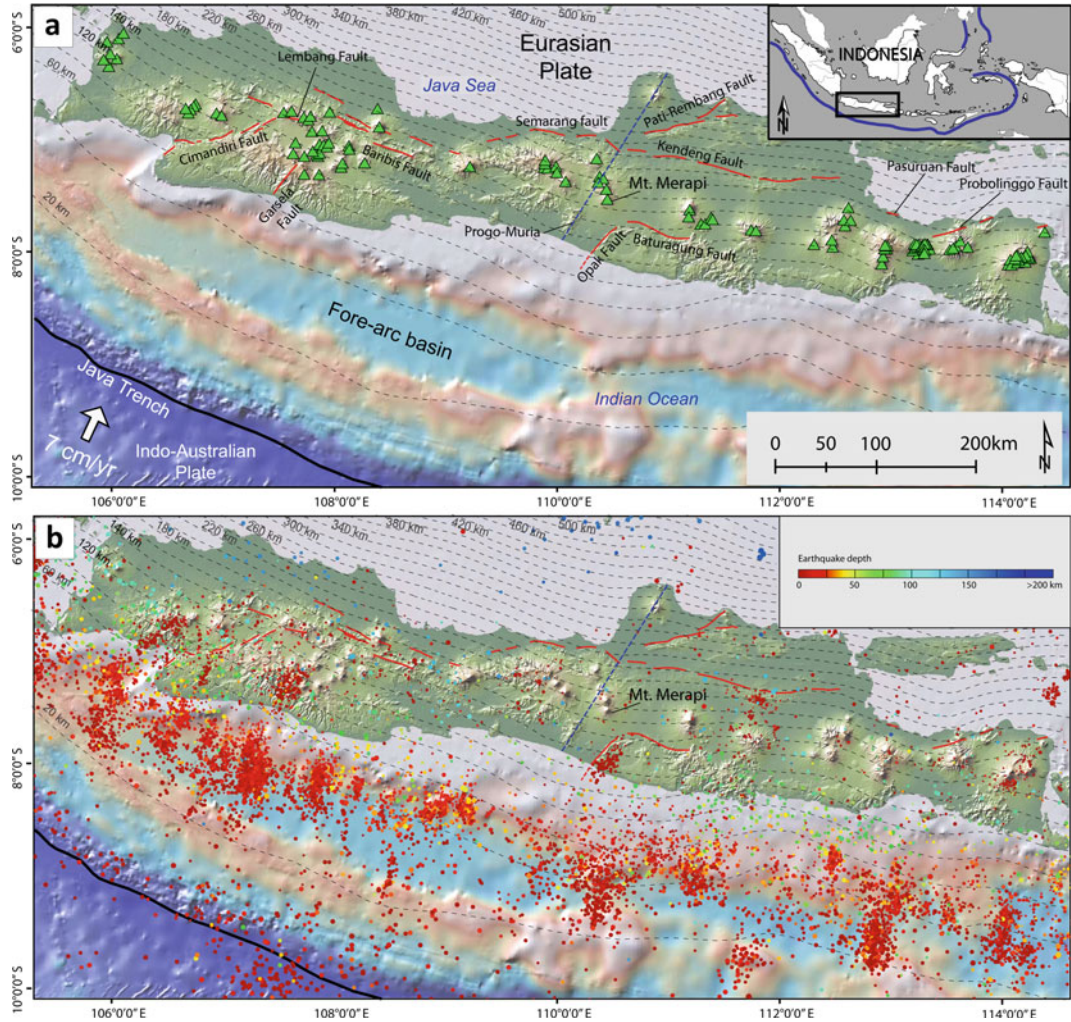


Fig. 4.2 **a** The geodynamic setting and distribution of Quaternary age volcanoes (green triangles) in Java (van Bemmelen 1949; Setijadji et al. 2006). Thin dashed lines indicate the contours of subducted slab depth (adopted from Hayes et al. 2018). Convergence rate adopted from Tregoning et al. (1994). Red lines are the inferred active structures of Java (adopted from Marliyani et al. 2016, 2019; Marliyani 2016; Supendi et al. 2018). The thick

black line is the megathrust of the Java subduction zone. Sediment thickness at the trench in this section is approximately 300 m (Plank and Langmuir 1998). **b** Distribution of seismicity in the Java region from 2009 to 2020 (catalogue BMKG; http://repogempa.bmkg.go.id/repo_new/repository.php). Figure made with GeoMapApp (www.geomapp.org) / CC BY

4.3 Geological Structure of Mt. Merapi

The alignment of volcanic edifices usually indicates the orientation of lithospheric or crustal-scale tectonic fractures and faults that may govern magma migration to the surface and can

probably also be used to estimate stress orientation at the time of their emplacement (cf. Nakamura et al. 1977; Pacey et al. 2013; Marliyani et al. 2020). Mt. Merapi and the nearby volcanoes Merbabu-Telomoyo-Ungaran follow a NW–SE trending lineament, a trend also observed at the nearby Dieng-Sindoro-Sumbing volcanoes (Fig. 4.4). Several researchers (Smyth

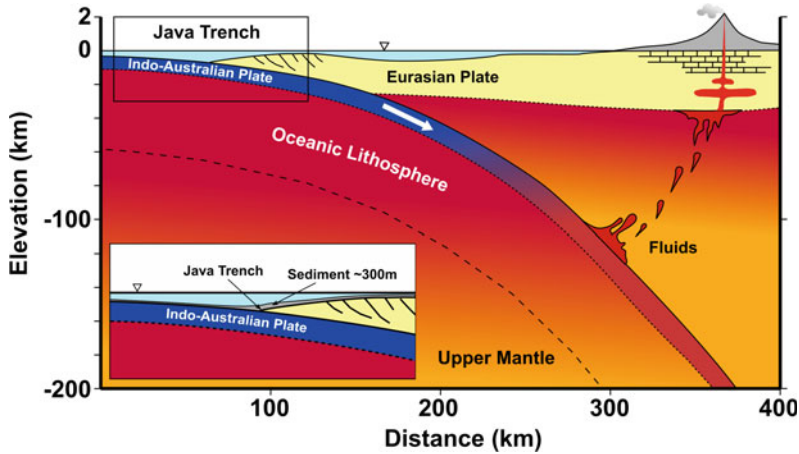


Fig. 4.3 Conceptual model of magma generation beneath Mt. Merapi, illustrating the increase of the slab dip angle at ~ 150 km depth. The inset diagram highlights the thickness of sediment at the Java trench (after Plank and Langmuir 1998). The model was compiled with results

from van Bemmelen (1949), Hamilton (1979), Camus et al. (2000), Wagner et al. (2007), Chadwick et al. (2007, 2013), Bohm et al. (2013), Costa et al. (2013), Lühr et al. (2013), Deegan et al. (2016), Peters et al. (2017), Hayes et al. (2018) and Widiyantoro et al. (2018)

et al. 2005, 2008; Clements et al. 2009) proposed a basement discontinuity running from the fore-arc through the Merapi area, Muria, and into the Java Sea, defined as the Muria-Progo Lineament. This feature is also indicated by changes in the seismic reflection of the deep crustal structure (Nugraha and Hall 2012) and would coincide with the boundary between the suture zone (Sevastjanova et al. 2011; Hall and Sevastjanova 2012), which underlies Mt. Merapi to the west, and continental crustal fragment to the east. However, gravity anomaly, density, and tomography results show no strong indication of this feature (Wölbern and Rumpker 2016), and instead highlight the NW–SE trend lineament beneath the Merapi-Merbabu-Ungaran volcanic complex (Tiede et al. 2005; Wagner et al. 2007; Lühr et al. 2013). Seismic evidence suggests that the crustal thickness beneath Central Java, measured as Moho depth, is 31 km beneath Mt. Merapi and 34 km on average (Wölbern and Rumpker 2016), slightly less than the crustal thickness north of Ungaran and at Dieng (37–38 km), but more than in East Java.

The 3D density model and gravity anomaly data analysed by Tiede et al. (2005) suggest the occurrence of an NNW-SSE density anomaly below the Merapi-Merbabu-Telomoyo-Ungaran

volcanic chain that may indicate the presence of a large intrusive body under these volcanoes. The NW–SE oriented lineament is also observed in seismic tomography data (Wagner et al. 2007; Lühr et al. 2013, 2023, Chap. 5; Koulakov et al. 2016). Wagner et al. (2007) identified a large negative velocity anomaly along the Merapi-Merbabu-Telomoyo-Ungaran alignment that extends to the Lawu volcano. They refer to this anomaly as the Merapi-Lawu Anomaly (MLA). They also identified a smaller area of a negative anomaly in the region between Merapi-Merbabu and Sumbing-Sindoro-Dieng (Fig. 4.5), which they interpreted as patches of molten material hosted by an array of rigid sediments. This structural configuration at the surface likely reflects the deep structural configuration of the arc crust in Central Java. We conducted a lineament analysis of the Merapi-Merbabu region to characterise the structural feature at the surface, using the 8 m resolution DEMNAS digital elevation model (freely downloadable at <http://tides.big.go.id/DEMNAS/>) as our base map. The lineament of this region is recognised through the linear arrangement of ridges, gullies, and scarps that indicate predominantly NW–SE trending, and some N-S oriented lineaments (Fig. 4.6).

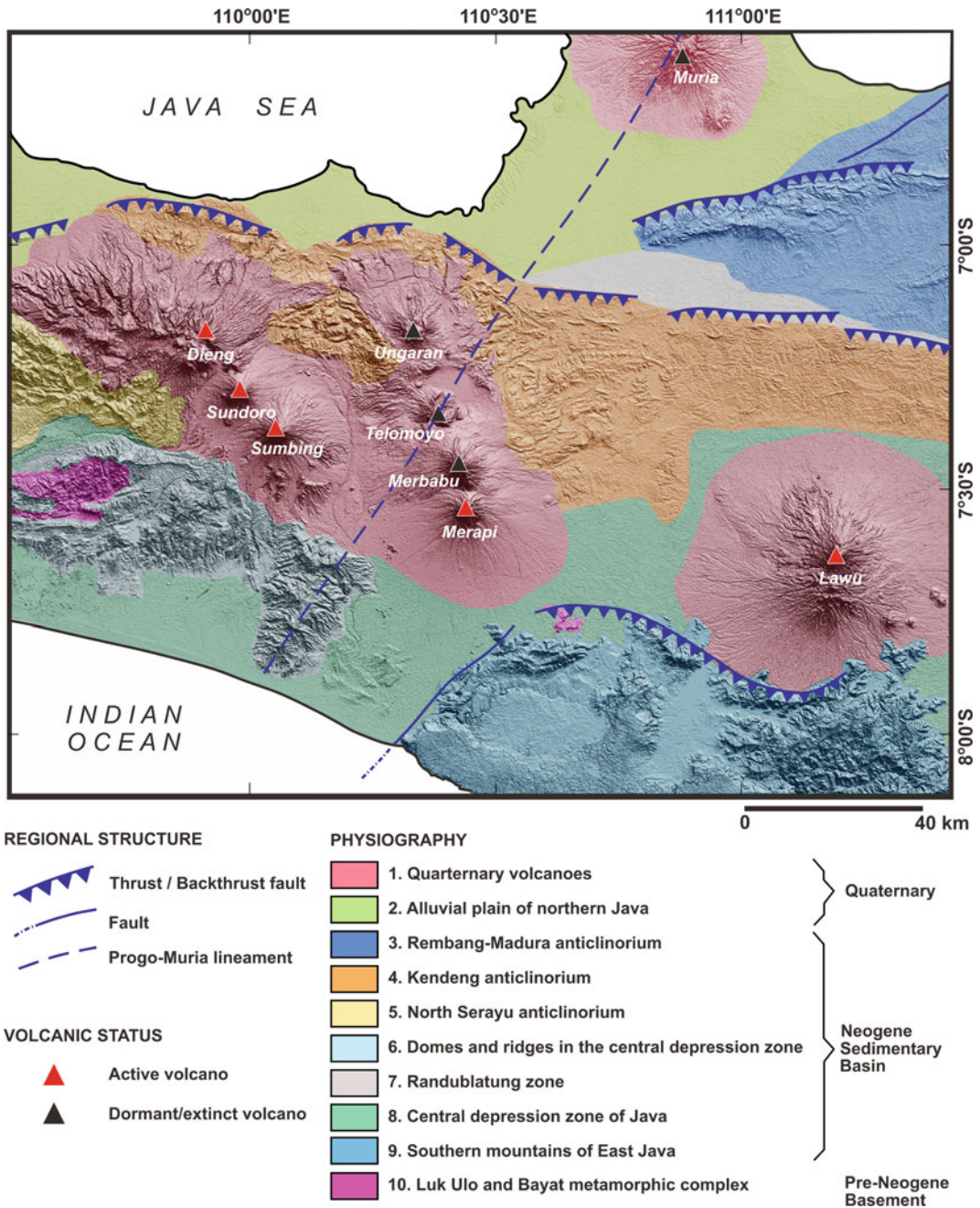


Fig. 4.4 Digital elevation model (DEM) with overlain physiographic zonation of Central and East Java (geological domain after van Bemmelen 1949). Faults shown are

presumably active; their locations are adapted from Irsyam et al. (2017). DEM data is freely downloadable through (<http://tides.big.go.id/DEMNAS/>)

The presence of a NW–SE trending regional structure of Mt. Merapi is also represented by the direction of newly formed fractures that dissect

the Merapi lava dome body at the top of the volcano and the southward opening of the Mt. Merapi summit amphitheatre (Walter et al. 2015;

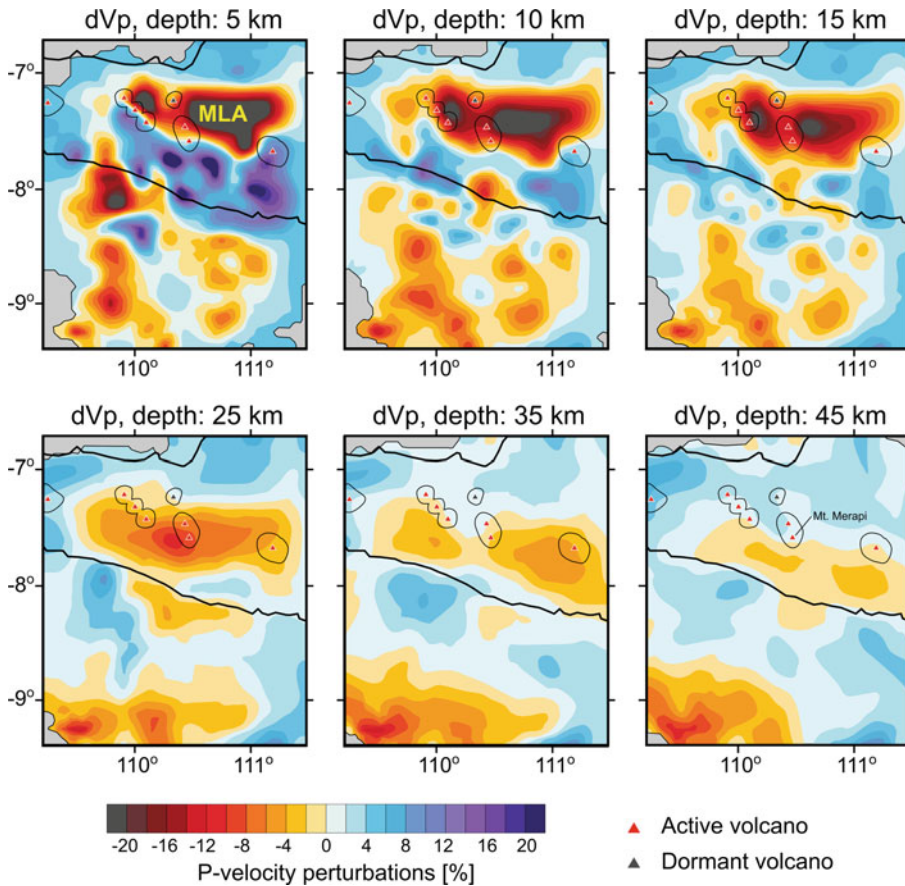


Fig. 4.5 Seismic velocity anomaly map of the Central Java region, showing a large negative velocity anomaly along Merapi-Merbabu-Telomoyo-Ungaran, referred to as the Merapi-Lawu Anomaly (MLA). The negative velocity

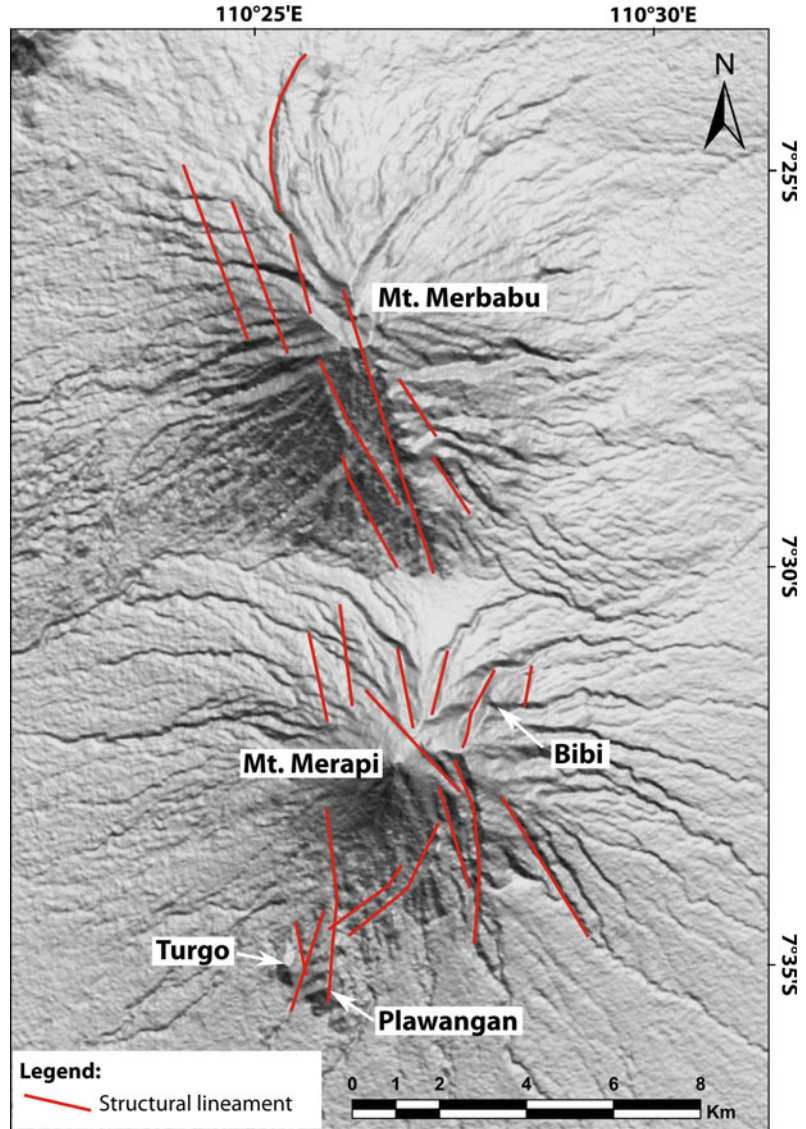
anomaly is interpreted as magma reservoirs or storage zones hosted by sedimentary rocks of the Kendeng stratigraphic sequence (after Wagner et al. 2007)

Darmawan et al. 2023, Chap. 15). The displacement in a NW–SE direction was also observed along the crater rim during the 1993–1997 eruption period (Beauducel et al. 2000) and could have been affected by the dome configuration at that time of the eruption.

To the south of Mt. Merapi, the NE–SW oriented Opak fault system (Fig. 4.7) and the E–W oriented Baturagung thrust fault dominate the structural configuration of the area (Fig. 4.2a). The Opak Fault is active; the most recent faulting event happened in 2006, when a M6.4 earthquake caused severe destruction and fatalities in Yogyakarta and nearby areas (e.g. Walter et al. 2008; Troll et al. 2012, 2015). The Baturagung

thrust shows no indication of recent seismic activity. The youngest stratigraphic unit displaced by this fault is the early Pliocene Wonosari limestone (Fig. 4.8; Surono et al. 1992), and it is considered an inactive fault. Another major structural feature in the region is the NE–SW trending Progo-Muria lineament, which follows the structural high in the Java forearc (Clements et al. 2009). This linear feature coincides with the centres of three Oligo-Miocene volcanoes in the West Progo Mountains (van Bemmelen 1949) and subsequent Quaternary volcanism (Mt. Merapi and Mt. Muria) that emerged along this lineament (Clements et al. 2009). Smyth et al. (2008) interpreted this lineament as the western

Fig. 4.6 The structural lineaments of Mt. Merapi and Mt. Merbabu drawn on 8 m resolution DEM based on linear arrangement of ridges, gullies, and scarps dominantly follow the regional NW–SE trend. DEM data is freely downloadable through (<http://tides.big.go.id/DEMNAS/>)



limit of an old continental basement, based on detrital zircon dates.

The largest tectonic stress affecting Java is mainly from the subduction of the Indo-Australian plate, with some local perturbation at some places (e.g. Pacey et al. 2013). The availability of local stress data near the Merapi region is limited; in the World Stress Map data (WSM, <http://www.world-stress-map.org/>), the only present stress data point in the vicinity of Merapi is

from the 2006 Yogyakarta earthquake event, indicating an orientation of maximum horizontal stress at $\sim N10^{\circ}E$, consistent with the present orientation of plate convergence. Marliyani et al. (2020) determined the Quaternary stress orientation in the Java arc based on a volcano morphology analysis, suggesting a generally N-S maximum horizontal stress orientation throughout Java, with some local stress perturbations. Near Merapi, these authors estimated a maximum

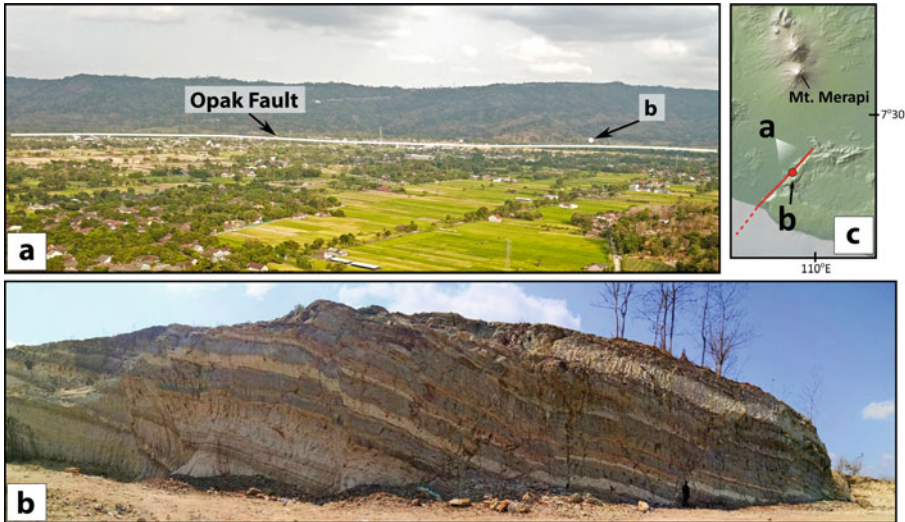


Fig. 4.7 a Oblique aerial photograph of the central part of the Opak fault system, showing a linear topographic break that marks the eastern boundary of the Yogyakarta depression. b Outcrop photograph of one of the faults within the fault zone, the fault zone is characterized by

reactivated normal fault, thrust fault and strike slip fault kinematics. c Index map of the outcrop locations. DEM data is freely downloadable through (<http://tides.big.go.id/DEMNAS/>)

horizontal stress orientation of $\sim N15^{\circ}E$, inferred mainly from the alignment of the Merapi-Merbabu-Telomoyo-Ungaran mountains.

4.4 Regional Stratigraphy of East-Central Java

It has long been considered that the pre-volcanic geological history might influence the high volcanic activity of Mt. Merapi compared to other volcanoes in the region (cf. Deegan et al. 2023, Chap. 10). As summarised by van Bemmelen (1949), East-Central Java is divided into ten physiographic zones, which, from north to south, are: (1) the Quaternary volcanoes; (2) the alluvial plain of northern Java; (3) the Rembang-Madura anticlinorium; (4) the Kendeng anticlinorium; (5) the North Serayu anticlinorium; (6) the domes and ridges in the central depression zone; (7) the Randublatung zone; (8) the central depression zone of Java; (9) the Southern mountains of East Java; and (10) the Luk Ulo and Bayat metamorphic complex (Fig. 4.4). Each zone resembles a unique depositional environment as reflected in its lithologies (Fig. 4.8).

4.4.1 Basement Rocks of East-Central Java

Wakita (2000) suggested that the East-Central Java basement rocks were formed during the Cretaceous when fragments of volcanic arc and ophiolitic material accreted in the southern part of Sundaland. There are no reports about the existence of continental basement rocks in East Java, either from drilling data or from surface outcrops. The Sundaland basement is suspected of having transitional characteristics: the northern and western parts showing continental features, whereas the eastern part, towards present-day Flores, shows oceanic features (Whitford 1975; Hamilton 1979). The composition of the deep crust beneath the modern arc is expected to be similar to the Cretaceous arc and ophiolitic fragments, as recognised from outcrops in Central Java (Smyth et al. 2007). Further refinements include the suggestion of a NE-SW oriented suture zone, which may represent terrane boundary beneath Mt. Merapi (Smyth et al. 2007; Sevastjanova et al. 2011; Hall and Sevastjanova 2012). A terrane boundary between the Cretaceous crust and the continental fragment of

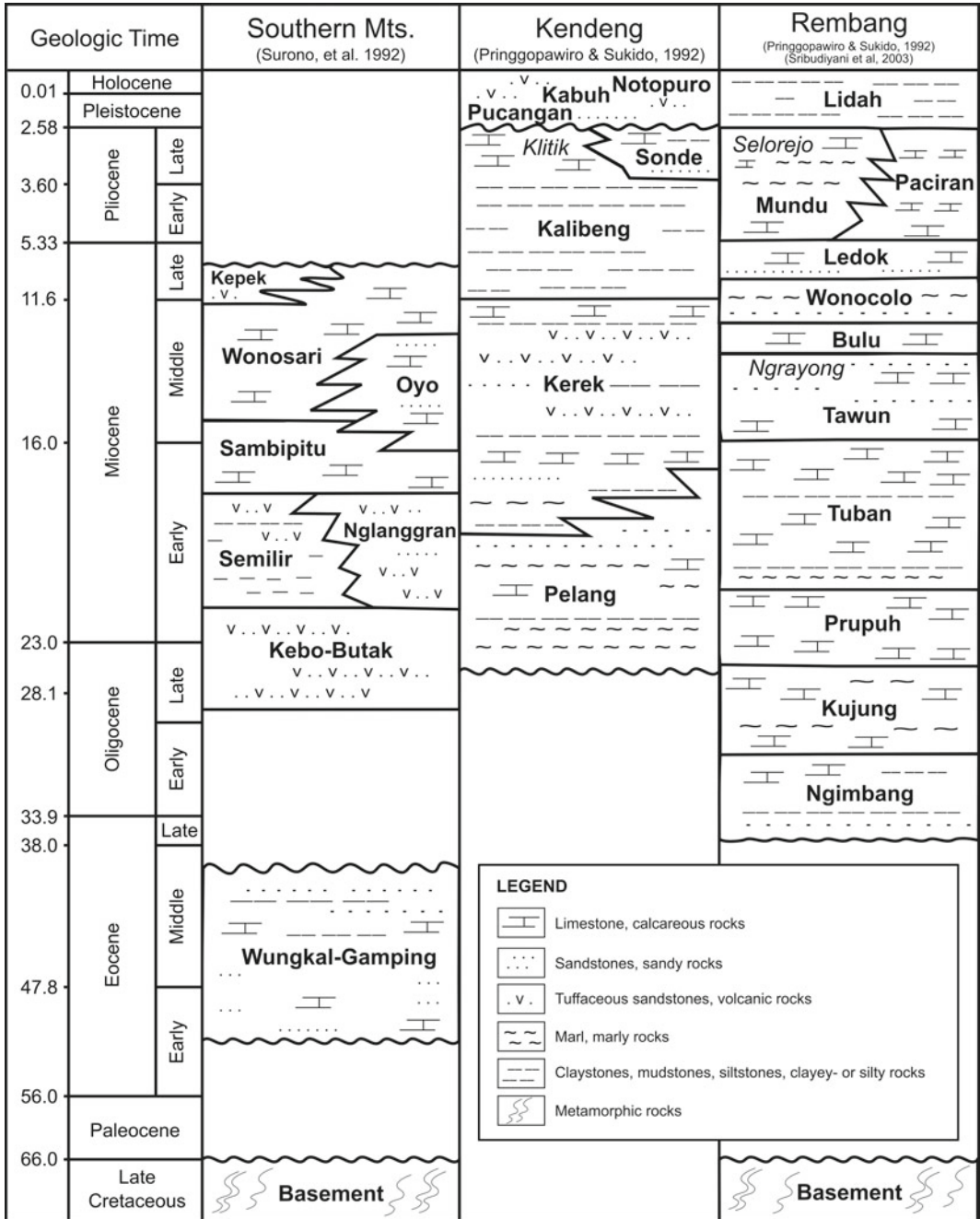


Fig. 4.8 Stratigraphy of the Rembang Zone (Pringgopawiro and Sukido 1992; Hartono and Suharsono 1997; Sribudiyani et al. 2003), the Kendeng Zone (Pringgopawiro and Sukido 1992), and the Southern Mountains Zone (Surono et al. 1992)

East Java has been postulated by several researchers (Smyth et al., 2007; Sevastjanova et al., 2011; Hall and Sevastjanova 2012), and

was proposed to be located along the Progo-Muria lineament. The boundary is further indicated by the absence of Cretaceous material

within the igneous rocks of the Southern Mountains arc to the east of Yogyakarta. It has been widely accepted that the crustal terrane beneath East Java and eastward is relatively young and has oceanic crust affinity (Whitford 1975; Hamilton 1979). However, new zircon dates of Miocene volcanism from the southern portion of East Java by Smyth et al. (2005, 2007) suggests the existence of a pre-Cretaceous continental crustal fragment derived from Australia beneath East Java.

4.4.2 The Rembang Zone

The Rembang Zone (Figs. 4.4 and 4.8) in the northernmost part of Java consists morphologically of several E-W oriented anticlines stretching from Purwodadi to Madura Island (van Bemmelen 1949; Fig. 4.4). The zone resembles the Palaeogene Sunda shelf deposition zone, as reflected by its lithological variation. The stratigraphy of the Rembang Zone reported by Pringgoprawiro and Sukido (1992), Hartono and Suharsono (1997), and Sribudiyani et al. (2003) is composed of twelve lithological formations, namely the pre-Tertiary basement formation, which is overlain by the Ngimbang, Kujung, Prupuh, Tuban, Tawun, Bulu, Wonocolo, Ledok, Mundu, Lidah, and Paciran formations (Fig. 4.8). Some rock formations, such as the Pre-Tertiary basement and the Ngimbang Formation, are not exposed at the surface and only reported through sub-surface data from various hydrocarbon exploration wells (Sribudiyani et al. 2003). The Kujung, Prupuh and Tuban formations are exposed in the eastern part of the Rembang zone in the Tuban area (Hartono and Suharsono 1997), whereas the Tawun, Bulu, Wonocolo, Ledok, Mundu, Lidah, and Paciran formation crop out slightly to the west in Bojonegoro area (Pringgoprawiro and Sukido 1992). Representative outcrops of the stratigraphic sequence of the Rembang Zone are shown in Fig. 4.9. Well data show that the pre-Tertiary basement comprises gabbro, ophiolitic material, metamorphic rocks, metavolcanic/volcanic rocks, and Cretaceous

sedimentary sequences of sandstone and shale with some cherts. These basement rocks are unconformably overlain by the Ngimbang Formation (Eocene), which can be separated into the Ngimbang clastic sequence, consisting of sandstone, siltstones, and shales, and the Ngimbang carbonate sequence. The Kujung Formation (Oligocene) is mainly composed of marl interbedded with fossiliferous sandstone and limestone. Overlying the Kujung Formation is the Prupuh Formation (Oligocene—Miocene), consisting of interbedded reef-type biocalcarenite, bio-calculutite, and marl, followed by the claystone and bioclastic limestone sequence of the Tuban Formation (Miocene). The oldest unit covering the Tuban Formation is the Tawun Formation (Miocene), which consists of claystone, marl, siltstone, and bedded quartz sandstone. The Bulu Formation (Miocene) comprises bedded grainstones and wackestones with reef build-ups in sparse areas. The Wonocolo Formation (Miocene), consisting of fossiliferous sandy marl intercalated with thin fossiliferous calcarenites, is overlain by the interbedded calcareous sandstones and sandy marls of the Ledok Formation (Miocene). The Mundu Formation (Miocene—Pliocene), composed of fossiliferous marl, interbedded fossiliferous calcarenite, and sandy marl, is followed by the deposition of the Pleistocene Lidah Formation, which comprises claystones and bedded marls with sandstone intercalations in the lower part, covered by mollusc-bearing layers in the upper part. The dominantly Pliocene Paciran Formation consists of chalky and reefal limestones, interfingers with the Mundu Formation and is overlain by the Lidah Formation.

4.4.3 The Randublatung Zone

The Randublatung zone (Fig. 4.4) is a depression bounded by the Kendeng Zone to the south and the Rembang zone to the north. The separation of this physiographic zone from the mountainous Kendeng and Rembang zones is mainly based on its distinctive lowland topography compared to

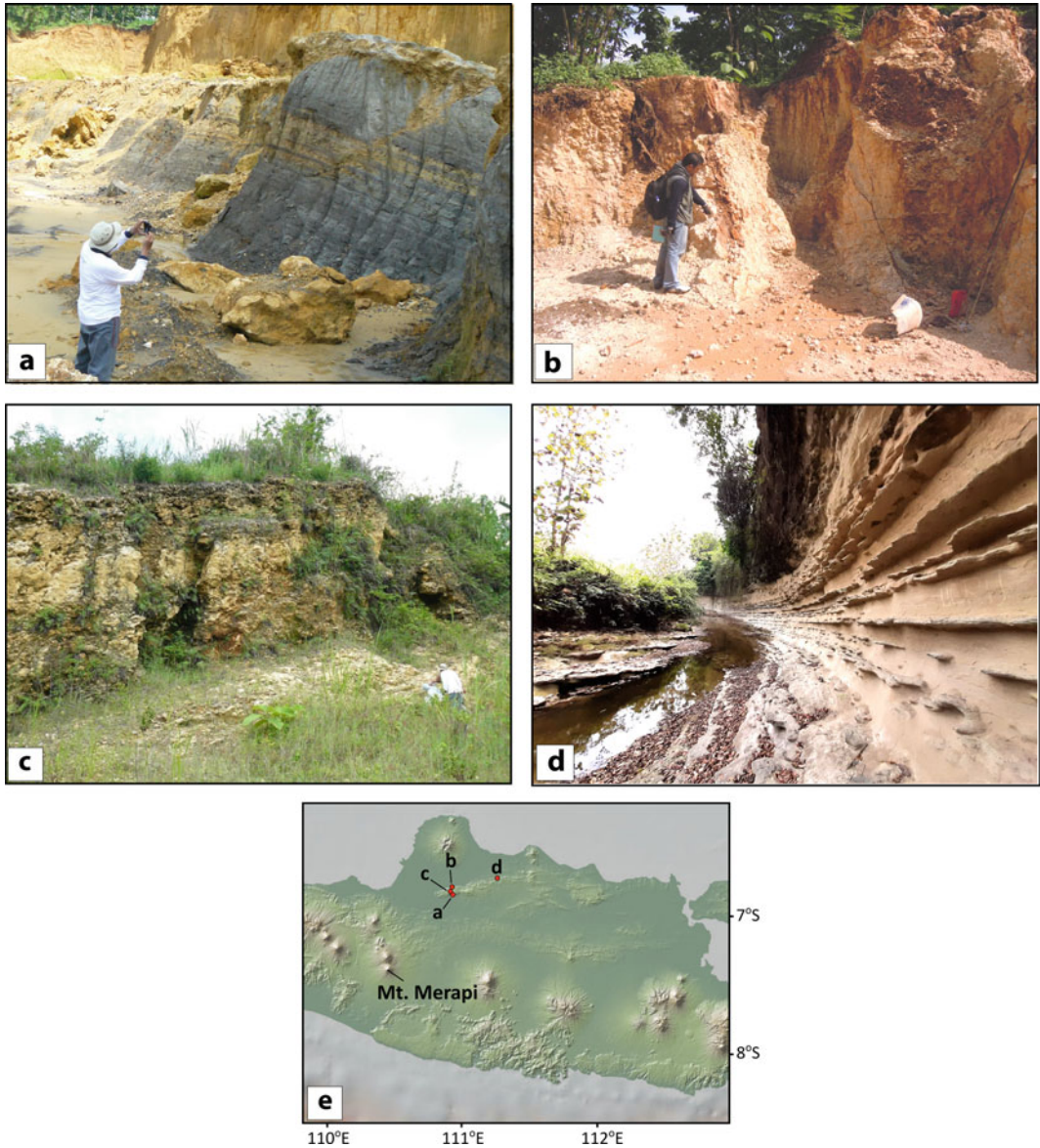


Fig. 4.9 Representative outcrops of the stratigraphic sequence of the Rembang Zone. **a** Shale of the Tawun (Ngrayong) Formation. **b, c** Calcareous sandstone of the Bulu Formation. **d** Calcareous sandstone and sandy marl

of the Ledok Formation. **e** Index map of the outcrop locations. DEM data is freely downloadable through (<http://tides.big.go.id/DEMNAS/>)

the surrounding region (van Bemmelen 1949). The depression is filled with the fluvial and alluvial deposits sourced from the Kendeng and Rembang mountainous regions. This fluvial and alluvial deposit is overlain by shallow marine sediments similar to the Kendeng and Rembang sequences (Pringgoprawiro and Sukido 1992).

4.4.4 The Kendeng Zone

The Kendeng Zone (Figs. 4.4 and 4.8) spans from the northeast of the Dieng volcanic complex to the east through the volcanoes of Merapi, Merbabu, Telomoyo, and Ungaran, and continues to extend eastward, mainly north of most of

the East Java volcanic front. Topographically, the zone is represented by a series of E-W oriented hills. The lithologies of the Kendeng Zone are dominated by marine sedimentary sequences of clastic turbidites, carbonates, and volcanoclastic rocks with a thickness of ~6 km (Untung and Sato 1978). Its subsurface part extends to the Madura Strait, as revealed by hydrocarbon exploration data (Sribudiyani et al., 2003).

The sedimentary rock sequence of the Kendeng zone resembles a gradual change from deep marine sediments to terrestrial deposits. The rock sequence (Fig. 4.8) can be grouped into seven formations (de Genevraye and Samuel 1972; Pringgoprawiro 1983; Pringgoprawiro and Sukido 1992), which, from the oldest to the youngest are: (1) the Pelang Formation (Late Oligocene—Middle Miocene), which is composed of marls, and bioclastic limestones; (2) the Kerek Formation (Middle to Late Miocene), comprising interbedded claystone, marls, calcareous tuffaceous sandstones, and tuffaceous sandstones, (3) the Kalibeng Formation (Late Miocene to Pliocene), composed of marls intercalated with volcanic sandstones, limestones, and claystones; (4) the Pucangan Formation, which consists of lahar deposits and black clay; (5) the Kabuh Formation, which is composed of sandstones, conglomerates, and tuffs; (6) the Notopuro Formation, which consists of lahar deposits; and (7) the Bengawan Solo terrace deposits that comprise polymictic conglomerates of fluvial origin. Field photographs of outcrops representing the stratigraphic sequence of the Kendeng Zone are shown in Fig. 4.10.

The proximity of the Kendeng physiographic zone with Mt. Merapi suggests that the stratigraphic sequence of this zone constitutes the basement of this volcano. This postulation is supported by seismic tomography data (Koulikov et al. 2007) and evidence for assimilation of calcareous sediments by the Merapi magmas (e.g. Chadwick et al. 2007; Deegan et al. 2010, 2023, Chap. 10; Troll et al. 2013; Whitley et al. 2019, 2020).

4.4.5 The Central Java Depression (Solo Zone)

The Central Java Depression (Solo Zone) is an ESE-WNW oriented open depression located in the middle of Java Island, stretching from Solo to Banyuwangi (Fig. 4.4). At present, this zone is an active fluvial sedimentary basin receiving sediment supply from the neighbouring active volcanoes, the Southern Mountains Zone in the south, and the Kendeng Zone in the north (Fig. 4.4).

4.4.6 The Southern Mountains of East-Central Java

The Southern Mountains of East-Central Java are an ESE-WNW-oriented mountainous highland region occupying eastern Java's southern part (Fig. 4.4). Van Bemmelen (1949) divided the western part of the Southern Mountains into three geomorphological units, which, from the south to the north are: (1) karst topography; (2) circular flat terrain; and (3) remnants of volcanic edifices. The stratigraphy of the Southern Mountains comprises Middle Miocene—Pliocene limestones overlying Eocene—Middle Miocene volcano-sedimentary rocks (Husein and Srijono 2007). Ten distinct rock formations have been distinguished (van Bemmelen 1949; Sumosusastro 1956; Suroño et al. 1992), which, from the oldest to the youngest, are (Fig. 4.8): (1) metamorphic basement rocks (Late Cretaceous—Palaeocene) consisting of phyllites, mica schists, calc-silicate schists, and marbles; (2) the Wungkal-Gamping Formation (Early to Middle Eocene) composed of quartz conglomerates, polymictic breccias, quartz sandstones, calcareous sandstones, calcareous siltstones, and intercalating nummulitic limestones; (3) the Kebo-Butak Formation (Middle Eocene—Early Miocene) composed of pebbly sandstones, siltstones, claystones, volcanic tuff, and shales with spotted basaltic pillow lavas and intrusions of diorite,

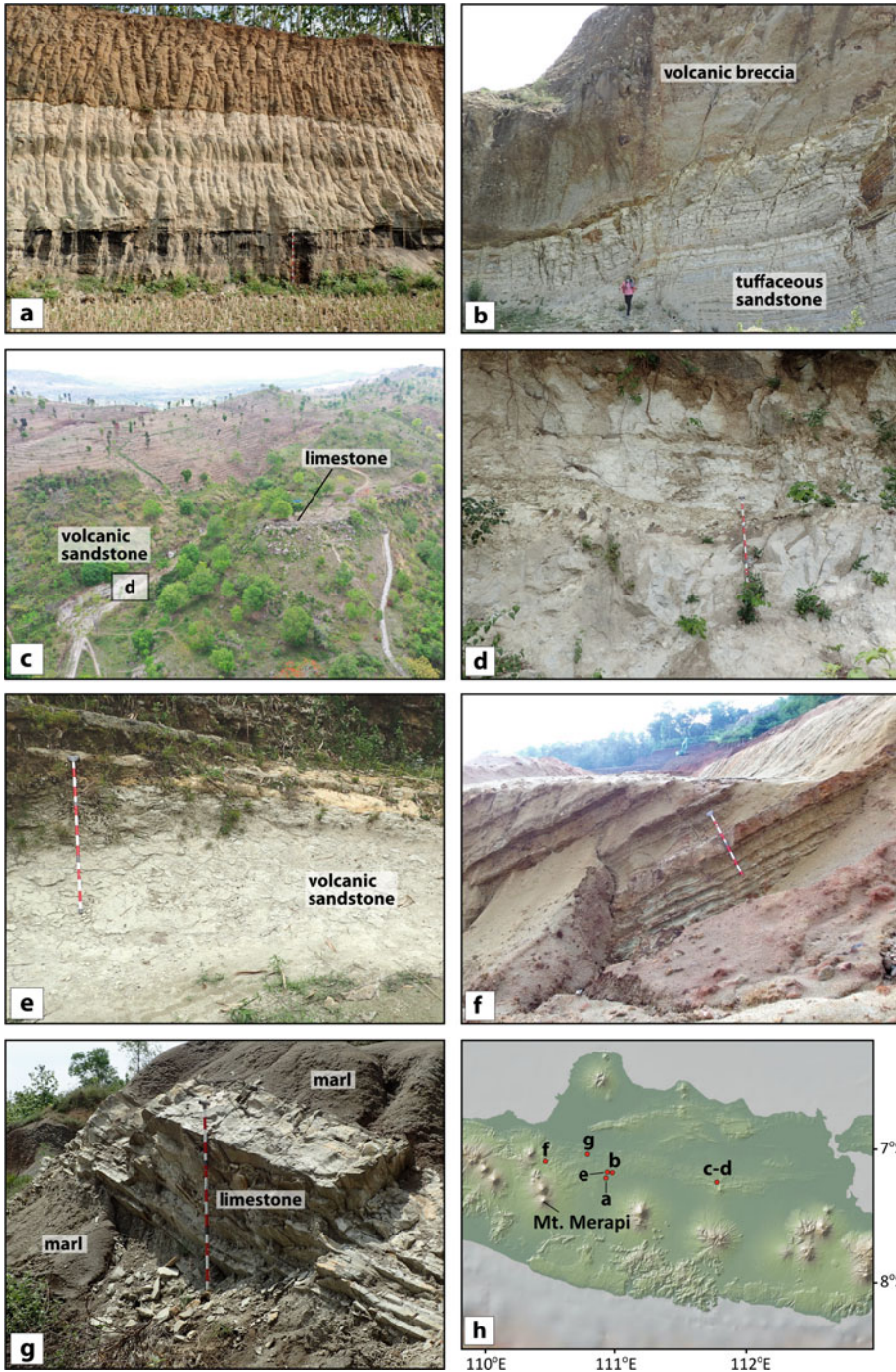


Fig. 4.10 Representative outcrops of the Kendeng Zone. **a** Fluvio-lacustrine deposits of the Kabuh Formation. **b** Volcanic breccia and tuffaceous sandstone of the Banyak Formation. **c** Volcanic sandstone of the Atasangin member of the Kalibeng Formation below limestone of the Klitik Formation. Location: Ngawi, East Java. **d** Volcanic sandstone resembling a turbidite sequence of the Kalibeng Formation. **e** Volcanic sandstone of the

Atasangin member of the Kalibeng Formation below limestone of the Klitik Formation. Location: Sragen, Central Java. **f** Tuffaceous sandstone of the Kerek Formation. **g** Limestone and marl intercalations of the Pelang Formation. **h** Index map of the outcrop locations. DEM data is freely downloadable through (<http://tides.big.go.id/DEMNAS/>)

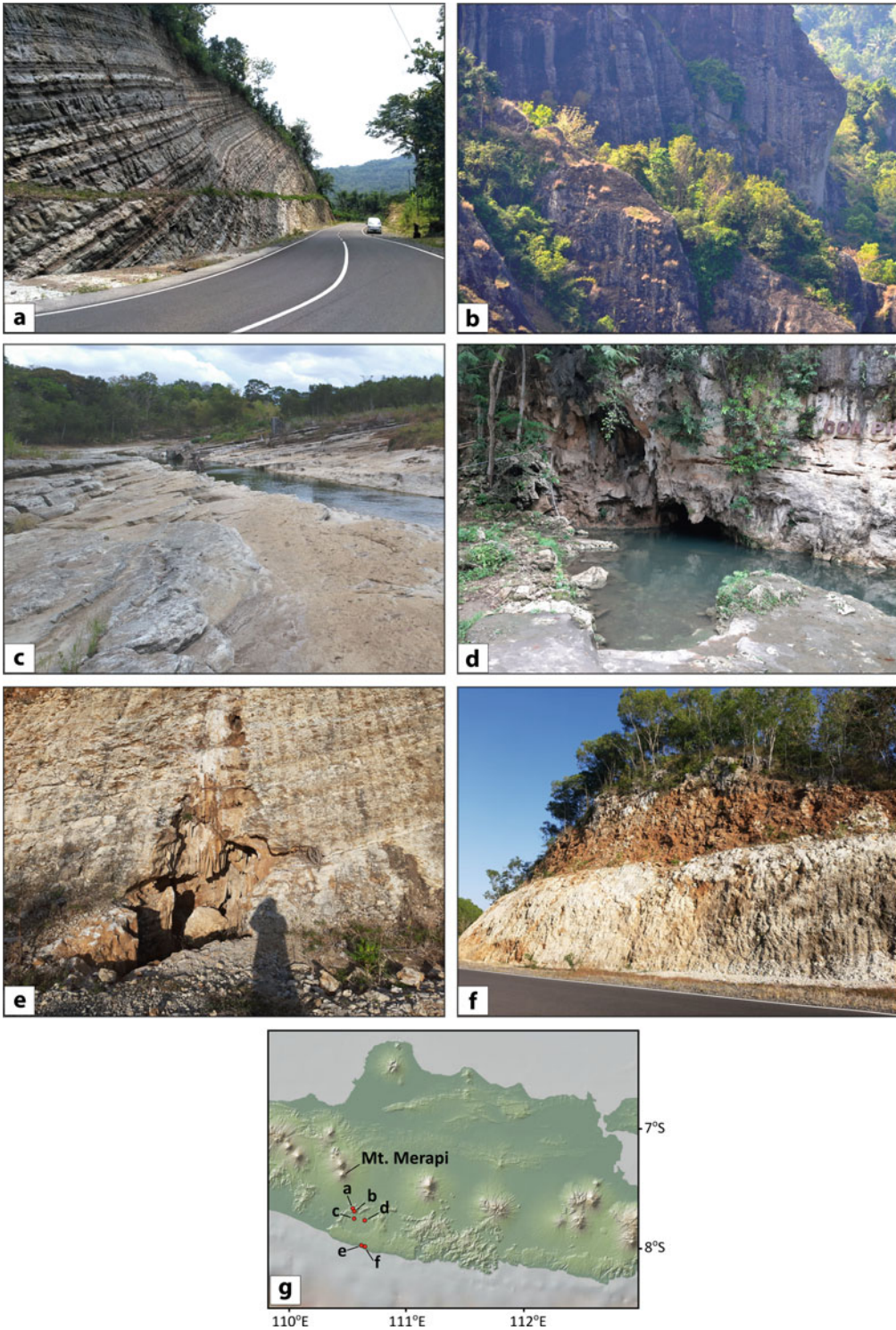


Fig. 4.11 Representative outcrops of the stratigraphic sequence of the Southern Mountains. **a** Volcaniclastic sandstone of the Semilir Formation. **b** Volcanic breccia of the Nglanggran Formation. **c** Calcareous sandstone of the

Oyo formation. **d–f** Limestone of the Wonosari formation. **g** Index map of the outcrop locations. DEM data is freely downloadable through (<http://tides.big.go.id/DEMNAS/>)

diabase, andesite porphyry, and basalt; (4) the Semilir Formation (Late Oligocene to Early Miocene; Fig. 4.11a), which is interfingering with the Kebo-Butak Formation and consists of lapilli tuff, tuffaceous sandstones, autoclastic breccias, polymictic breccias, and calcareous tuffaceous sandstones; (5) the Nglanggran Formation (Fig. 4.11b), which is interfingering with the Semilir Formation (Early Miocene) and comprises polymictic conglomerates, pebbly sandstones, tuffaceous sandstones, andesitic breccias, tuff, and basaltic lavas; (6) the Sambipitu Formation (Early Miocene) composed of calcareous sandstones, and tuffaceous siltstones; (7) the Oyo Formation (Early Miocene to Middle Miocene) consisting of limestones, calcareous sandstone, and tuffaceous sandstone (Fig. 4.11c); (8) the Wonosari Formation (Early Miocene to Late Miocene) composed of limestones and sandy limestones (Fig. 4.11d–f); (9) the Kepek Formation (Middle to Late Miocene), which is composed of tuffs, claystones and interlayered limestones; and (10) the Quaternary deposits of Pleistocene to recent fluvio-volcanic sediments from Mt. Merapi.

4.5 Summary

Mt. Merapi, an intermediate-composition volcano located in the active volcanic arc chain of Java Island, formed due to the subduction of the Indo-Australian oceanic plate beneath the Eurasian continental plate, widely known as the Sunda-Banda subduction zone. The subducted slab below Mt. Merapi is located at a depth of around 150–200 km, with a subduction convergence rate of $\sim 6.7 \pm 0.7$ cm/year in a N11°E direction. The subduction system in this arc segment is characterised by a downgoing slab consisting of the topographic high of the oceanic Roo Rise, with volcanic ash and pelagic clay sediment cover, and by subduction erosion, which is indicated by the trench and forearc geometry and may limit sediment supply. The magma storage zones beneath Mt. Merapi are suggested to occur at multiple depths and include a reservoir at shallow crustal depths, a

fluid-rich zone at less than 4 km depth, a main magma storage zone at 10–20 km, and a deep magma reservoir at more than 25 km. A NW–SE oriented deep structural configuration controls the emplacement of magma forming Mt. Merapi, as expressed in the surface structural configuration, including the orientation of neighbouring volcanic centres (Merapi-Merbabu-Telomoyo and Sumbing-Sundoro-Ungaran), the direction of newly formed fractures that separate the Merapi lava dome body at the volcano's summit; the trend of the Mt. Merapi amphitheatre, and the displacement of Mt. Merapi's crater rim during the 1993–1997 eruption period. The surface structures extracted from the Merapi-Merbabu region's lineament analysis also include similarly oriented NW–SE and N-S trending lineaments. Situated within the Central Java depression zone, Mt. Merapi is bordered to the south by the Southern Mountains Zone, and by the Kendeng and Rembang zones to the north. The basement of Mt. Merapi is most likely composed of a sedimentary sequence of clastic turbidites, carbonates, and volcanoclastic rocks of the Kendeng Zone. The interaction of the Merapi magmas with these basement rocks, particularly the carbonate lithologies, plays a crucial role in the petrogenesis of magma at Merapi and the explosivity of its eruptions.

Acknowledgements We would like to thank Ralf Gertisser, Helen Smyth and Valentin Troll for their significant input and constructive comments that greatly improved the presentation and contents of this chapter. We would also like to extend our thanks to Mradipta Lintang Alifcanta Mokitkanana for her assistance in preparing this manuscript.

References

- Andreastuti SD, Alloway BV, Smith IEM (2000) A detailed tephrostratigraphic framework at Merapi Volcano, Central Java, Indonesia: implications for eruption predictions and hazard assessment. *J Volcanol Geotherm Res* 100:51–67
- Beauducel F, Cornet F-H, Suhanto E, Duquesnoy T, Kasser M (2000) Constraints on magma flux from displacements data at Merapi volcano, Java Indonesia. *J Geophys Res Solid Earth* 105(B4):8193–8203

- van Bemmelen RW (1949) The geology of Indonesia, vol 1A: General geology. Government Printing Office, The Hague
- Berthommier PC (1990) Etude volcanologique du Merapi (Centre-Java). Téphrostratigraphie et chronologie—produits éruptifs. Ph.D. Thesis, Université Blaise Pascal, Clermont-Ferrand, France
- Bird P (2003) An updated digital model of plate boundaries. *Geochem Geophys Geosyst* 4:1027
- Bohm M, Haberland C, Asch G (2013) Imaging fluid-related subduction processes beneath Central Java (Indonesia) using seismic attenuation tomography. *Tectonophysics* 590:175–188
- Borisova AY, Martel C, Gouy S, Pratomo I, Sumarti S, Toutain J-P, Bindeman IN, de Parseval P, Metaxian J-P, Surono (2013) Highly explosive 2010 Merapi eruption: evidence for shallow-level crustal assimilation and hybrid fluid. *J Volcanol Geotherm Res* 261:193–208
- Camus G, Gourgaud A, Mossand-Berthommier P-C, Vincent P-M (2000) Merapi (Central Java, Indonesia): an outline of the structural and magmatological evolution, with a special emphasis to the major pyroclastic events. *J Volcanol Geotherm Res* 100:139–163
- Chadwick JP, Troll VR, Ginibre C, Morgan D, Gertisser R, Waight TE, Davidson JP (2007) Carbonate assimilation at Merapi Volcano, Java, Indonesia: insights from crystal isotope stratigraphy. *J Petrol* 48:1793–1812
- Chadwick JP, Troll VR, Waight TE, van der Zwan FM, Schwarzkopf LM (2013) Petrology and geochemistry of igneous inclusions in recent Merapi deposits: a window into the sub-volcanic plumbing system. *Contrib Mineral Petrol* 165:259–282
- Clements B, Hall R, Smyth HR, Cottam MA (2009) Thrusting of a volcanic arc: a new structural model for Java. *Pet Geosci* 15:159–174
- Cloetingh S, Wortel R (1986) Stress in the Indo-Australian plate. *Tectonophysics* 132:49–67
- Costa F, Andreastuti S, Bouvet de Maisonneuve C, Pallister JS (2013) Petrological insights into the storage conditions, and magmatic processes that yielded the centennial 2010 Merapi explosive eruption. *J Volcanol Geotherm Res* 261:209–235
- Darmawan H, Putra R, Budi-Santoso A, Humaida H, Walter TR (2023) Morphology and instability of the Merapi lava domemonitored by unoccupied aircraft systems. In: Gertisser R, Troll VR, Walter TR, Nandaka IGMA, Ratdomopurbo A (eds) Merapi volcano—geology, eruptive activity, and monitoring of a high-risk volcano. Springer, Berlin, Heidelberg, pp 457–472
- Deegan FM, Troll VR, Freda C, Misiti V, Chadwick JP, McLeod CL, Davidson JP (2010) Magma-carbonate interaction processes and associated CO₂ release at Merapi volcano, Indonesia: insights from experimental petrology. *J Petrol* 51:1027–1051
- Deegan FM, Troll VR, Freda C, Misiti V, Chadwick JP (2011) Fast and furious: crustal CO₂ release at Merapi volcano, Indonesia. *Geol Today* 27:63–64
- Deegan FM, Whitehouse MJ, Troll VR, Budd DA, Harris C, Geiger H, Hålenius U (2016) Pyroxene standards for SIMS oxygen isotope analysis and their application to Merapi volcano, Sunda arc, Indonesia. *Chem Geol* 447:1–10
- Deegan FM, Troll VR, Gertisser R, Freda C (2023) Magma-carbonate interaction at Merapi volcano, Indonesia. In: Gertisser R, Troll VR, Walter TR, Nandaka IGMA, Ratdomopurbo A (eds) Merapi volcano—geology, eruptive activity, and monitoring of a high-risk volcano. Springer, Berlin, Heidelberg, pp 291–321
- de Genevraye P, Samuel L (1972) The geology of Kendeng Zone (East Java). In: 1st Indonesian Petroleum Association Annual Convention. Indonesian Petroleum Association, Jakarta, pp 17–30
- Gertisser R, Keller J (2003a) Temporal variations in magma composition at Merapi Volcano (Central Java, Indonesia): magmatic cycles during the past 2000 years of explosive activity. *J Volcanol Geotherm Res* 123:1–23
- Gertisser R, Keller J (2003b) Trace element and Sr, Nd, Pb and O isotope variations in medium-K and high-K volcanic rocks from Merapi Volcano, Central Java, Indonesia: evidence for the involvement of subducted sediments in Sunda Arc magma genesis. *J Petrol* 44:457–486
- Gertisser R, Charbonnier SJ, Troll VR, Keller J, Preece K, Chadwick JP, Barclay J, Herd RA (2011) Merapi (Java, Indonesia): anatomy of a killer volcano. *Geol Today* 27:57–62
- Gertisser R, Charbonnier SJ, Keller J, Quidelleur X (2012) The geological evolution of Merapi volcano, Central Java, Indonesia. *Bull Volcanol* 74:1213–1233
- Gertisser R, del Marmol M-A, Newhall C, Preece K, Charbonnier S, Andreastuti S, Handley H, Keller J (2023) Geological history, chronology and magmatic evolution of Merapi. In: Gertisser R, Troll VR, Walter TR, Nandaka IGMA, Ratdomopurbo A (eds) Merapi volcano—geology, eruptive activity, and monitoring of a high-risk volcano. Springer, Berlin, Heidelberg, pp 137–193
- Global Volcanism Program (2013) Merapi (263250)—Volcanoes of the World, v. 4.10.1. Smithsonian Institution
- Hall R (2002) Cenozoic geological and plate tectonic evolution of SE Asia and the SW Pacific: computer-based reconstructions, model and animations. *J Asian Earth Sci* 20:353–431
- Hall R, Sevastjanova I (2012) Australian crust in Indonesia. *Aust J Earth Sci* 59:827–844
- Hall R, Smyth HR (2008) Cenozoic arc processes in Indonesia: Identification of the key influences on the stratigraphic record in active volcanic arcs. *Geol Soc Am Spec Paper* 436:27–54
- Hamilton WB (1979) Tectonics of the Indonesian region. *US Geol Surv Prof Paper* 1078:1–345
- Hartono, Suharsono (1997) Geological Map of Tuban Quadrangle, Jawa

- Hayes GP, Moore GL, Portner DE, Hearne M, Flamme H, Furtney M, Smoczyk GM (2018) Slab2, a comprehensive subduction zone geometry model. *Science* 362:58–61
- House BM, Bebout GE, Hilton DR (2019) Carbon cycling at the Sunda margin, Indonesia: a regional study with global implications. *Geology* 47:483–486
- Husein S, Sriyono (2007) Tinjauan Geomorfologi Pegunungan Selatan DIY/Jawa Tengah: telaah peran faktor endogenik dan eksogenik dalam proses pembentukan pegunungan. In: *Prosiding Seminar Potensi Geologi Pegunungan Selatan dalam Pengembangan Wilayah. Pusat Survei Geologi, Yogyakarta*
- Irsyam M, Widiyantoro S, Natawidjaja D, Meilano I, Rudiyanto A, Hidayati S, Triyoso W, Hanifa NR, Djarwadi D, Faizal L, Sunarjito (ed), Team for updating of seismic hazard maps of Indonesia 2017 (2017) Earthquake source and hazard maps of Indonesia 2017. National center for earthquake studies (PusGen), research center for housing and human settlement, directorate general for research and development, ministry of public works and people housing, ISBN 978–602–5489–01–3 (in Indonesian)
- Jousset P, Pallister J, Surono (2013) The 2010 eruption of Merapi volcano. *J Volcanol Geotherm Res* 261:1–6
- Kopp H (2011) The Java convergent margin: structure, seismogenesis and subduction processes. *Geol Soc Lond Spec Publ* 355:111–137
- Kopp H, Flueh E, Petersen C, Weinrebe W, Wittwer A, Scientists M (2006) The Java margin revisited: evidence for subduction erosion off Java. *Earth Planet Sci Lett* 242:130–142
- Koulakov I, Bohm M, Asch G, Lühr BG, Manzanares A, Brotopuspito KS, Fauzi P, Purbawinata MA, Puspito NT, Ratdomopurbo A, Kopp H, Rabbel W, Shevkunova E (2007) *J Geophys Res* 112(B8): B08310. <https://doi.org/10.1029/2006JB004712>
- Koulakov I, Maksotova G, Jaxybulatov K, Kasatkina E, Shapiro NM, Luehr B-G, El Khrepy S, Al-Arifi N (2016) Structure of magma reservoirs beneath Merapi and surrounding volcanic centers of Central Java modeled from ambient noise tomography. *Geochem Geophys Geosyst* 17:4195–4211
- Lavigne F (2004) Rate of sediment yield following small-scale volcanic eruptions: a quantitative assessment at the Merapi and Semeru stratovolcanoes, Java, Indonesia. *Earth Surf Process Landf* 29:1045–1058
- Lühr B-G, Koulakov I, Rabbel W, Zschau J, Ratdomopurbo A, Brotopuspito KS, Fauzi P, Sahara DP (2013) Fluid ascent and magma storage beneath Gunung Merapi revealed by multi-scale seismic imaging. *J Volcanol Geotherm Res* 261:7–19
- Lühr BG, Koulakov I, Suryanto W (2023) Crustal structure and ascent of fluids and melts beneath Merapi: Insights from geophysical investigations. In: Gertisser R, Troll VR, Walter TR, Nandaka IGMA, Ratdomopurbo A (eds) *Merapi volcano—geology, eruptive activity, and monitoring of a high-risk volcano*. Springer, Berlin, Heidelberg, pp 111–135
- Marliyani GI, Arrowsmith JR, Whipple KX (2016) Characterization of slow slip rate faults in humid areas: Cimandiri fault zone, Indonesia. *J Geophys Res Earth Surf* 121:2287–2308
- Marliyani GI, Arrowsmith JR, Helmi H (2019) Evidence for multiple ground-rupturing earthquakes in the past 4000 years along the Pasuruan Fault, East Java, Indonesia: documentation of active normal faulting in the Javan Backarc. *Tectonics* 38:1489–1506
- Marliyani GI, Helmi H, Arrowsmith JR, Clarke A (2020) Volcano morphology as an indicator of stress orientation in the Java Volcanic Arc Indonesia. *J Volcanol Geotherm Res* 400:106912
- Marliyani GI (2016) Neotectonics of Java, Indonesia: crustal deformation in the overriding plate of an orthogonal subduction system. Arizona State University
- Metcalfe I (2017) Tectonic evolution of Sundaland. *Bull Geol Soc Malaysia* 63:27–60
- Nakamura K, Jacob KH, Davies JN (1977) Volcanoes as possible indicators of tectonic stress orientation—Aleutians and Alaska. *Pure Appl Geophys* 115:87–112
- Newhall CG, Bronto S, Alloway B, Banks NG, Bahar I, Del Marmol MA, Hadisantono RD, Holcomb RT, McGeehin J, Miksic JN, Rubin M, Sayudi SD, Sukhyar R, Andreastuti S, Tilling RI, Torley R, Trimble D, Wirakusumah AD (2000) 10,000 years of explosive eruptions of Merapi Volcano, Central Java: archaeological and modern implications. *J Volcanol Geotherm Res* 100:9–50
- Nugraha AMS, Hall R (2012) Cenozoic history of the East Java Forearc. In: *Proceedings of the 36th annual convention of the Indonesian petroleum association, Jakarta*, pp 1–21
- Pacey A, Macpherson CG, McCaffrey KJW (2013) Linear volcanic segments in the central Sunda Arc, Indonesia, identified using Hough Transform analysis: implications for arc lithosphere control upon volcano distribution. *Earth Planet Sci Lett* 369–370:24–33
- Packham G (1996) Cenozoic SE Asia: reconstructing its aggregation and reorganization. *Geol Soc Lond Spec Publ* 106:123–152
- Peters STM, Troll VR, Weis FA, Dallai L, Chadwick JP, Schulz B (2017) Amphibole megacrysts as a probe into the deep plumbing system of Merapi volcano, Central Java Indonesia. *Contrib Mineral Petrol* 172:16
- Plank T (2014) The chemical composition of subducting sediments. *Treatise Geochem* 4:607–629
- Plank T, Langmuir CH (1998) The chemical composition of subducting sediment and its consequences for the crust and mantle. *Chem Geol* 145:325–394
- Pringgoprawiro H, Sukido (1992) *Geological Map of Bojonegoro Quadrangle, Jawa*
- Pringgoprawiro H (1983) *Biostratigrafi dan Paleogeografi Cekungan Jawa Timur Utara, Suatu Pendekatan Baru*. Dissertation, Institut Teknologi Bandung, Bandung, Indonesia
- Ratdomopurbo A, Beauceucel F, Subandriyo J, Nandaka IGMA, Newhall CG, Suharna SDS, Suparwaka H,

- Sunarta (2013) Overview of the 2006 eruption of Mt Merapi. *J Volcanol Geoth Res* 261:87–97
- Setijadji LD, Kajino S, Imai A, Watanabe K (2006) Cenozoic Island Arc Magmatism in Java Island (Sunda Arc, Indonesia): clues on relationships between Geodynamics of Volcanic Centers and Ore Mineralization. *Resour Geol* 56:267–292
- Sevastjanova I, Clements B, Hall R, Belousova EA, Griffin WL, Pearson N (2011) Granitic magmatism, basement ages, and provenance indicators in the Malay Peninsula: insights from detrital zircon U-Pb and Hf-isotope data. *Gondwana Res* 19:1024–1039
- Smyth HR, Hamilton PJ, Hall R, Kinny PD (2007) The deep crust beneath island arcs: Inherited zircons reveal a Gondwana continental fragment beneath East Java, Indonesia. *Earth Planet Sci Lett* 258:269–282
- Smyth HR, Hall R, Nichols GJ (2008) Cenozoic volcanic arc history of East Java, Indonesia: the stratigraphic record of eruptions on an active continental margin. *Geol Soc Am Spec Paper* 436:199–222
- Smyth HR, Hall R, Hamilton PJ, Kinny P (2005) East Java: Cenozoic basins, volcanoes and ancient basement. In: *Proceedings of the 30th IPA annual convention and exhibition of the Indonesian petroleum association*, Jakarta, pp 251–266
- Soeria-Atmadja R, Maury RC, Bellon H, Pringgoprawiro H, Polve M, Priadi B (1994) Tertiary magmatic belts in Java. *J Southeast Asian Earth Sci* 9:13–27
- Sribudiyani, Muchsin N, Ryacudu R, Kunto T, Astono P, Prasetya I, Sapiie B, Asikin S, Harsolumakso AH, Yulianto I (2003) The collision of the East Java microplate and its implication for hydrocarbon occurrences in the East Java Basin. *Proceedings of the 29th IPA annual convention and exhibition of the Indonesian petroleum association*, Jakarta, pp 1–12
- Sumosusastro S (1956) A contribution to the geology of the eastern Djiwo Hills and Southern Range in Central Java. *Indon J Nat Sci* 112:115–134
- Supendi P, Nugraha AD, Widiyantoro S (2018) Recent destructive earthquakes around Garut area, West Java, Indonesia: an unidentified fault? *AIP Conf Proc* 1987:020077
- Surono JP, Pallister J, Boichu M, Buongiorno MF, Budisantoso A, Costa F, Andreastuti S, Prata F, Schneider D, Clarisse L, Humaida H, Sumarti S, Bignami C, Griswold J, Carn S, Oppenheimer C, Lavigne F (2012) The 2010 explosive eruption of Java's Merapi volcano—a '100-year' event. *J Volcanol Geoth Res* 241–242:121–135
- Surono, Toha B, Sudarno I (1992) Geological map of Surakarta-Girintontro Quadrangle, Jawa
- Tiede C, Camacho AG, Gerstenecker C, Fernández J, Suyanto I (2005) Modeling the density at Merapi volcano area, Indonesia, via the inverse gravimetric problem. *Geochem Geophys Geosyst* 6:Q09011
- Tregoning P, Brunner FK, Bock Y, Puntodewo SSO, McCaffrey R, Genrich JF, Calais E, Rais J, Subarya C (1994) First geodetic measurement of convergence across the Java Trench. *Geophys Res Lett* 21:2135–2138
- Tregoning P (2002) Plate kinematics in the western Pacific derived from geodetic observations. *J Geophys Res Solid Earth* 107:ECV 7–1-ECV 7–8
- Troll VR, Hilton DR, Jolis EM, Chadwick JP, Blythe LS, Deegan FM, Schwarzkopf LM, Zimmer M (2012) Crustal CO₂ liberation during the 2006 eruption and earthquake events at Merapi volcano Indonesia. *Geophys Res Lett* 39:L11302
- Troll VR, Chadwick JP, Jolis EM, Deegan FM, Hilton DR, Schwarzkopf LM, Blythe LS, Zimmer M (2013) Crustal volatile release at Merapi volcano; the 2006 earthquake and eruption events. *Geol Today* 29:96–101
- Troll VR, Deegan FM, Jolis EM, Budd DA, Dahren B, Schwarzkopf LM (2015) Ancient oral tradition describes volcano–earthquake interaction at Merapi volcano, Indonesia. *Geogr Ann A* 97:137–166
- Troll VR, Deegan FM (2023) The magma plumbing system of Merapi: The petrological perspective. In: Gertisser R, Troll VR, Walter TR, Nandaka IGMA, Ratdomopurbo A (eds) *Merapi volcano—geology, eruptive activity, and monitoring of a high-risk volcano*. Springer, Berlin, Heidelberg, pp 233–263
- Untung M, Sato Y (eds) (1978) Gravity and geological studies in Jawa, Indonesia. Geological survey of Indonesia and geological survey of Japan—a joint research program on regional tectonics of Southeast Asia. *Spec Publ Geol Surv Indon* 6:207
- Voight B, Constantine EK, Siswoidjono S, Torley R (2000) Historical eruptions of Merapi volcano, Central Java, Indonesia, 1768–1998. *J Volcanol Geoth Res* 100:69–138
- Wagner D, Koulakov I, Rabbel W, Luehr B-G, Wittwer A, Kopp H, Bohm M, Asch G, the MERAMEX Scientists (2007) Joint inversion of active and passive seismic data in Central Java. *Geophys J Int* 170:923–932
- Wakita K (2000) Cretaceous accretionary–collision complexes in central Indonesia. *J Asian Earth Sci* 18:739–749
- Walter TR, Subandriyo J, Kirbani S, Bathke H, Suryanto W, Aisyah N, Darmawan H, Jousset P, Luehr BG, Dahm T (2015) Volcano-tectonic control of Merapi's lava dome splitting: the November 2013 fracture observed from high resolution TerraSAR-X data. *Tectonophysics* 639:23–33
- Walter TR, Wang R, Luehr B-G, Wassermann J, Behr Y, Parolai S, Anggraini A, Günther E, Sobiesiak M, Gresser H, Wetzel H-U, Milkereit, Sri Brotopuspito PJK, Harjadi P, Zschau J (2008) The 26 May 2006 magnitude 6.4 Yogyakarta earthquake south of Mt. Merapi volcano: did lahar deposits amplify ground shaking and thus lead to the disaster? *Geochem Geophys Geosyst* 9:Q05006
- Whitford DJ (1975) Strontium isotopic studies of the volcanic rocks of the Sunda arc, Indonesia, and their petrogenetic implications. *Geochim Cosmochim Acta* 39:1287–1302

- Whitley S, Gertisser R, Halama R, Preece K, Troll VR, Deegan FM (2019) Crustal CO₂ contribution to subduction zone degassing recorded through calc-silicate xenoliths in arc lavas. *Sci Rep* 9:8803
- Whitley S, Halama R, Gertisser R, Preece K, Deegan FM, Troll VR (2020) Magmatic and metasomatic effects of magma–carbonate interaction recorded in calc-silicate xenoliths from Merapi volcano (Indonesia). *J Petrol* 61:egaa048
- Widiyantoro S, Ramdhan M, Métaxian J-P, Cummins PR, Martel C, Erdmann S, Nugraha AD, Budi-Santoso A, Laurin A, Fahmi AA (2018) Seismic imaging and petrology explain highly explosive eruptions of Merapi volcano Indonesia. *Sci Rep* 8:13656
- Wölbern I, Rumpker G (2016) Crustal thickness beneath Central and East Java (Indonesia) inferred from P receiver functions. *J Asian Earth Sci* 115:69–79



Crustal Structure and Ascent of Fluids and Melts Beneath Merapi: Insights From Geophysical Investigations

5

Birger G. Lühr, Ivan Koulakov,
and Wiwit Suryanto

Abstract

The magma plumbing system of Merapi volcano is a key for understanding its eruptive activity and thus has received scientific interest for a considerable time. First detailed attempts to resolve the volcano's internal structure and alleged magma reservoir were carried out at the beginning of the 1990s and included measurements of electrical conductivity, material density, seismic velocities as well as geodetic parameters and surface deformations. Major questions addressed were: (1) where do the fluids and magmas come from; (2) what are the magma ascent paths; (3) where are fluids and partial melts stored; and (4) what is the size and geometry of the magma and fluid reservoirs and the volcanic conduit? Here we review experi-

ments and findings we made during various stages of investigation at Merapi volcano, and also discuss selected projects by other teams and projects. By using seismic methods different crustal zones could be identified with low-velocity values and high V_p/V_s ratios, which can be explained as fluid- and melt-hosting zones. Large-scale joint seismic experiments (MERAPI, MERAMEX and DOMERAPI) displayed seismic attenuation and scattering effects seen in the shallow portion of the edifice, revealed the presence of fluid percolation and subvertical fluid-magma transfer zones, and identified crustal and near-Moho magma reservoirs that are being off-centred to the north. The complementary results of these projects contributed to a new structural image and understanding of the deep structure of Merapi over a depth range of more than 100 km. These results are valid not only for Merapi but now serve as an important example of the crustal structure considered for subduction volcanoes elsewhere.

B. G. Lühr (✉)
Helmholtz-Zentrum Potsdam, Deutsches
GeoForschungsZentrum GFZ, Telegrafenberg,
14473 Potsdam, Germany
e-mail: ase@gfz-potsdam.de

I. Koulakov
Institute of Petroleum Geology and Geophysics,
SB RAS, Prospekt Akademika Koptyuga 3,
Novosibirsk 630090, Russia

W. Suryanto
Geoscience Research Group, Department of Physics,
Universitas Gadjah Mada, Sekip Utara Bulaksumur,
Yogyakarta 55281, Indonesia

Keywords

Crustal structure • Subduction zone • Merapi
magma plumbing system • Geophysical
investigations • Seismic tomography

5.1 Introduction

To understand a volcanic system like Merapi, unravelling the internal structures at crustal and mantle depths is important. However, investigating the internal geophysical and geochemical structure of an active stratovolcano with a sufficiently high resolution is challenging because of its heterogeneous construction. The alternation of lava beds, block-and-ash-flow layers, surge and lahar deposits as well as igneous intrusions, all overprinted by erosion, leads to a heterogeneous mixture of materials with contrasting physical properties, which makes them challenging for many geophysical investigations. Seismological investigations significantly contributed to the understanding of the internal and physical structure of the Merapi edifice (Ratdomopurbo 1995; Ratdomopurbo and Poupinet 1995). Specifically, the localisation of seismic events and the first classification of different seismic signals that could be distinguished from each other led to the detection of a zone with very low seismicity and anomalously high attenuation of seismic waves at depths of 1–2 km below the summit. This zone was interpreted as a shallow magma reservoir within the edifice, while the main magma reservoir was supposed to start at 4–5 km depth, where the volcanic seismicity fades out again (Ratdomopurbo 1995; Ratdomopurbo and Poupinet 1995). In this chapter, we provide an overview of selected major projects with a contribution from German institutions, highlighting a decade-long Indonesian-German collaboration, student graduation and exchange. These projects are also considered in context with other collaborators, laboratories, partners, and projects from several other countries.

One of the first systematic structural investigations of the Merapi cone were carried out during the Indonesian-German MERAPI project (Mechanism Evaluation, Risk Assessment, and Prediction Improvement) in the years 1997–2002 (Zschau et al. 2003) and complementing research activities of scientists from France, Japan, and the USA. In the framework of the MERAPI project, comprehensive geophysical structure

investigations were carried out to determine: (1) the density structure and mass distribution using gravity measurements; (2) volume changes based on tilt and GPS measurements; (3) the electrical conductivity structure using magnetotelluric (MT), long offset time-domain electromagnetic (LOTEM) and geoelectrical measurements; and (4) the seismic structure of Merapi using active and passive seismological experiments.

During the MERAPI project and later until 2004, efforts to resolve the crustal structure beneath Merapi were able to determine details of the physical parameters and information about the complex geological architecture of the volcano. Nevertheless, important questions related to the volcanic system with its supposed magma reservoir, the ascent path of fluids and partial melts, and the way Merapi is embedded in the subduction process remained poorly constrained. The finding that Merapi as a volcano at a subduction zone—the Sunda Arc—is fed through a complex ‘plumbing’ system, which involves not only shallow structures beneath the volcanic edifice but also deep structures and processes within the underlying crust and upper mantle, led to the design of the larger seismic experiment MERAMEX (MERapi AMphibious EXperiment) (Bohm et al. 2005). Essential scientific and logistical support, and an important student and scientific exchange programme, was realised together with the Volcanological Survey of Indonesia (VSI) in Bandung, the Volcanological Technology Research Centre (BPPTK) in Yogyakarta, the Gadjah Mada University (UGM) in Yogyakarta, the Institut Teknologi Bandung (ITB) and the Indonesian Meteorology, Climatology and Geophysical Agency (BMKG) in Jakarta.

During the MERAMEX project period from 2004 to 2007, we could image strong seismic velocity anomalies and interpret the fluid and magma ascent paths and storage regions down to >100 km depths. However, the final 10 kms to the surface could not be resolved in detail. This shallower portion was investigated in detail by the interdisciplinary DOMERAPI project (Budi-

Santoso and Lesage 2016; Byrdina et al. 2017; Widiyantoro et al. 2018). DOMERAPI commenced in 2013 as a four-year-long international scientific research project led by French scientists at the Institut de Physique du Globe de Paris (IPGP), with support from the Institut des Sciences de la Terre (ISTerre) at the Université Grenoble Alpes and in partnership with the Laboratoire Magmas et Volcans (LMV) at the Université Clermont-Auvergne, the Institut des Sciences de la Terre d'Orléans (ISTO), the Indonesian Center for Volcanology and Geological Hazard Mitigation (CVGHM), Badan Geologi (VSI), the Institut Teknologi Bandung (ITB), GFZ Potsdam (Germany) and the United States Geological Survey (USA). In the framework of DOMERAPI, a dense network of seismographs was installed from October 2013 to mid-April 2015, the collected data of which were combined with data from the permanent seismic network of BMKG.

While the data analysis of these three major projects (MERAPI, MERAMEX, DOMERAPI) continues, the results have already led to an advanced and fundamentally more comprehensive understanding of Merapi as a volcano-magma system within the Sunda arc subduction system. In the following sections, the different geophysical efforts from the outlined research projects and their key scientific achievements are described in further detail.

5.2 GPS, Tilt and Gravity Measurements

Volcano geodesy includes the basic techniques and key parameters of volcano activity monitoring, providing information about its status, structure and dynamical processes (e.g., Dzurisin 2007). Some twenty years ago, Indonesian researchers in cooperation with scientists from France, Japan and the United States focused deformation experiments mainly on the summit area of Merapi, recognising mass and volume changes related to the dynamic behaviour of the Merapi lava dome. Various methods and techniques were tested and applied, including:

- (1) visual observations of the dome with a telescope camera located at an observation post in 12 km distance (Purbawinata et al. 1996);
- (2) remote sensing techniques such as stereophotogrammetry using a kite (Kelfoun 1999);
- (3) electronic distance measurements on a trilateration network (Young et al. 2000);
- (4) first attempts with InSAR technology using corner reflectors and campaign GPS surveys (Nandaka 1999); and
- (5) the operation of uniaxial horizontal platform tiltmeters (Subandriyo et al. 1997). At two flank sites uniaxial horizontal platform tiltmeters were installed; one location with a single instrument and the other with 5 instruments installed within an area of about 20×30 m (Beauducel and Cornet 1999).

Within the MERAPI project several flank sites were chosen for permanent multiparameter stations equipped with GPS receivers, tiltmeters and seismometers to observe edifice changes related to dynamic internal processes. Seismic studies by Ratdomopurbo and Poupinet (1995) suggested that a small shallow magma reservoir is indicated by an aseismic zone within the edifice. The multiparameter stations were installed at altitudes of 1280–2020 m as a ring-profile-constellation in respect to Merapi, aiming to capture the largest flank deformation rates at these sites. Another aim was to observe displacements caused by inflation or deflation with continuous precise vertical tilt measurements by applying a new array technique with borehole tiltmeters in combination with a Differential Global Positioning System (DGPS) (Rebscher et al. 2000a). A variety of further sensors were added as supplements and, therefore, the stations were acting as multi-parameter stations. Horizontal and vertical displacements were observed by using four permanent deformation measurement sites at the flanks of Merapi. A fifth receiver served as a reference station located at BPPTK in Yogyakarta (100 m asl). This local differential GPS network was tethered in the regional GEODYS-SEA net (Wilson et al. 1998) via the GPS-point Butuh at 30 km distance to Merapi's summit and 27 km to Yogyakarta.

Tilt measurements were conducted at the four flank stations with arrays of three shallow biaxial

borehole tiltmeters (Applied Geomechanics TM722A and TM722B). The instruments of an array at each site had a nominal resolution of 0.1 μrad and 1.0 μrad , respectively, installed in boreholes at 3–4 m depths and distances of 50–90 m (Westerhaus et al. 1998; Rebscher et al. 2000a). The array technique provided the possibility to distinguish between local and regional tilt signals, and the installation in boreholes allowed the reduction of near-surface disturbances and biaxial quasi-continuous measurements with sampling intervals of 5 min, allowing adequate time resolution. This effort was required to recognise the relatively small volcanic tilt changes on the flanks compared to those obtained at the summit of Merapi. Unfortunately, soon after the project ended, the stations stopped functioning due to vandalism, theft and a lack of maintenance.

Because meteorological and hydrological records were required for the correct interpretation of the high precision deformation data, a variety of auxiliary sensors were installed to record local environmental parameters. These allowed the detection and correction of local disturbances in the recorded data (Westerhaus et al. 1998; Rebscher et al. 2000a), and provided meteorological data required for the interpretation of other measured parameters such as seismicity, electrical conductivity, chemistry and temperature of fumarole gases and hydrology.

Surprisingly, the GPS and tilt data collected on the mid and lower flanks of Merapi did not record any significant changes in horizontal or vertical axis or displacements (Rebscher et al. 2000b). During the volcanic crisis in January 1997 (eruptions on 14 and 17 January) and July 1998 (eruptions on 11 and 19 July) only minor tilt anomalies could be identified, with a tilt signal of maximum 1 μrad associated with the 14 January 1997 explosive event (Westerhaus et al. 1998). The loading of pyroclastic flows in 1998 produced a static tilt anomaly of $\sim 8 \mu\text{rad}$ in all tiltmeters. The lack of relatively large flank deformations associated with the volcanic activity did not support the existence of a large shallow magma reservoir inside the Merapi edifice. Accordingly, later related projects and

monitoring approaches concentrated on the notably deforming summit region (e.g., Budi-Santoso et al. 2023, Chap. 13).

In the summer of 1997, a gravity repetition network was established around Merapi (Gerstenecker et al. 1998a). The network consisted of 23 stations forming three loops around Merapi at different altitudes. The first loop connected altitudes of 100–500 m asl and the second one connected all stations at medium altitudes (1000–2000 m asl). The third loop was located at the crater rim at 2900–2970 m. All three loops were connected to each other along a gravity profile at the north flank of Merapi (Gerstenecker et al. 1998a). Gravity observations were carried out alongside GPS measurements, using geodetic 2-frequency receivers (Trimble 4000 SSE/SSI and Leica C322/RS299) to determine vertical crustal movements at the stations that influence secular gravity changes directly via the free air- or Bouguer-gradient. Gravity changes due to vertical crustal movement were eliminated for the estimation of the gravitational effect of mass movements in and outside of the volcano (Gerstenecker et al. 1998a). In each measurement campaign, four LaCoste&Romberg spring gravity metres were used. The calibration functions of the instruments and their changes in time were $\pm 5 \times 10^{-5}$. A change of the scale factor of 5×10^{-5} generates a virtual gravity change of about $38 \times 10^{-8} \text{ m/sec}^2$ (Gerstenecker et al. 1998a). The largest gravity difference amounted to $\sim 751 \times 10^{-5} \text{ m/s}^2$. Gravity differences at the installed network were observed four times at Merapi. Due to all limitations, the mean standard deviations of vertical crustal movements were $\pm 50 \text{ mm}$ (Gerstenecker et al. 1998a). The measured gravity and vertical crustal changes were, however, much smaller than expected before observed volcanic activity. Only near the crater rim, at altitudes of 2000–2970 m asl, a significant gravity increase (up to $100 \times 10^{-8} \text{ m/s}^2$) was detected and found to be associated with significant crustal subsidence in a range of up to -180 mm (Gerstenecker et al. 1998a). Gravity changes around the summit of Merapi increased during the campaign by $\sim 80 \times 10^{-8} \text{ m/s}^2$ (80 μgal), which may have been caused

by mass movements in- and outside of the volcano. Especially the changing topography of the dome in the immediate neighbourhood of the summit stations was thought to be responsible for these changes, further supported by observations from synthetic aperture radar (SAR) and photogrammetric images (Gerstenecker et al. 1998b). Gravity data inversion gave a mean density of 2241 kg/m^3 and an estimated porosity range of 10–20% (Tiede et al. 2005). Based on this mean density, Tiede et al. (2005) derived a subsurface 3-D density model of the Merapi and Merbabu region by the analysis of 443 campaign gravity points. Using a least-squares inversion approach, maximal density anomalies between -242 kg/m^3 and $+264 \text{ kg/m}^3$ were found relative to the mean density (Fig. 5.1), confirming relatively high rock porosities in the Merapi region (Tiede et al. 2005).

5.3 Electrical Resistivity Structure

The resistivity structure of Merapi was investigated using different electromagnetic methods. Applied methods, such as direct current electrical resistivity tomography (DC) and magnetotellurics (MT), were used to determine the spatial distribution of the electrical conductivity from natural geomagnetic and geoelectric field variations. Of these, the DC method has the highest spatial resolution but the smallest penetration depth, while MT has the largest penetration. The long-offset transient electromagnetic (LOTEM) method fills the gap between DC and MT (Telford et al. 1990).

The DC survey comprised two different approaches (Friedel et al. 1998), where benchmarks of resistivity were derived for pyroclastic material varying in saturation with air, meteoric water and solfataric water. These measurements

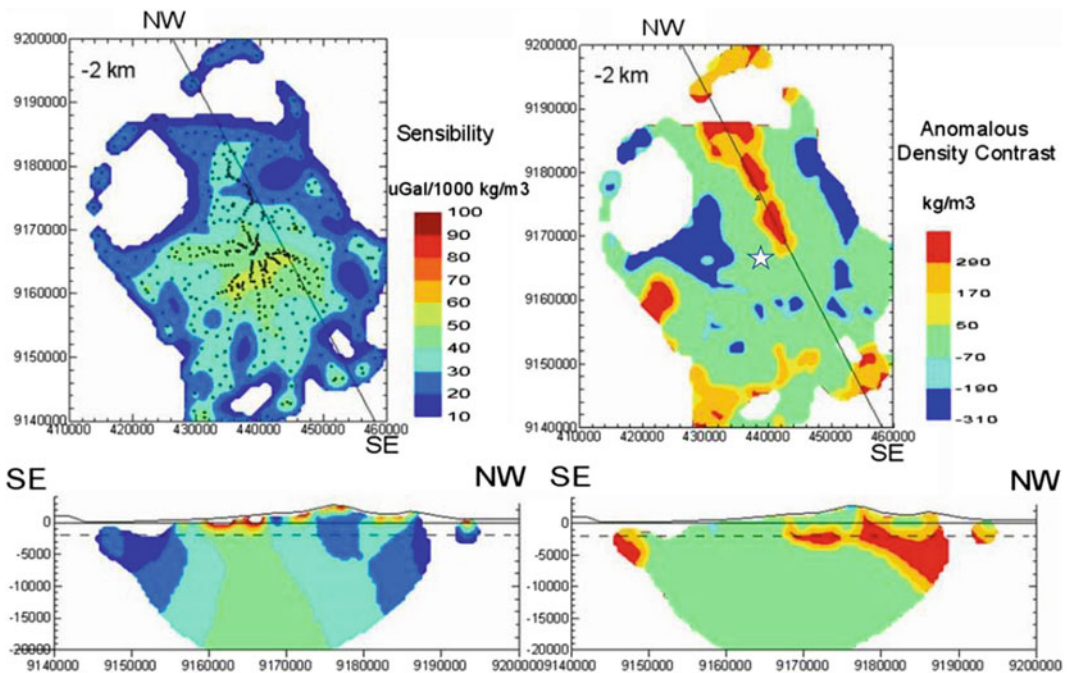


Fig. 5.1 Horizontal and vertical cross-sections of the 3-D anomalous density model (right) and gravity sensitivity distribution of the model (left). The vertical SE-NW profiles follow the 152°N course of an intrusive body. The sensitivity pattern corresponds to the station distribution

and the relative size and position of 20,000 cells. Maps are in UTM coordinates (after Tiede et al. 2005). The summit area of Merapi is marked on the right map by a white star and gravity measuring points are marked by black dots

were taken in quasi-homogeneous conditions at selected flank locations and at the Woro fumarole field near the summit, which was later destroyed by the 2006 and 2010 eruptions. LOTEM, which measures voltage decay curves with electric and magnetic receivers after a polarity reversion of a current (DC) in an electric dipole transmitter at several kilometres distance (Strack 1992), was used to resolve the structure of Merapi down to a depth of 800–1000 m below the surface by recording LOTEM data at 41 receiver locations on a 10 km W-E profile and a 15 km S-E profile. Signals were transmitted from a transmitter on the northern flank in SELO, two transmitters on the western flank (AGLI, BABA) and one transmitter on the southern flank (KINA) (Müller et al. 2002). Three dipole–dipole profiles with lengths of 2.3 km, 2.6 km and 3.6 km and dipole widths of 200 m were conducted along the west, north and south flanks, respectively (Müller et al. 2002).

Large scale MT measurements, which use natural time-varying electromagnetic fields that originated in the Earth's magnetosphere (Vozoff 1991), were carried out along a profile crossing Central Java with the aim to determine geomagnetic induction vectors (Müller and Haak 2004), recognise good conductors and detect striking faults. MT recordings were made at a total of 65 sites in a period range of 0.001–1000 s. The measurements took place at two different scales: 20 sites were set up to obtain information about the regional electric conductivity distribution (10 of them at a 130 km profile) (Ritter et al. 1998), while 40 locations were selected in the vicinity (i.e. within a 15 km radius) of Merapi. The best data quality was obtained at a site 50 km north of Java on an uninhabited island of the Karimunjawa archipelago.

At Merapi, the general resistivity structure was derived from LOTEM 1-D inversion and 3-D modelling (Müller et al. 1998; Müller 2000; Commer et al. 2005, 2006), DC 2-D inversion (Friedel et al. 1998, 2000; Byrdina et al. 2017) and MT 1-D inversion and the 3-D modelling (Müller 2004). For the northern part, a four-layer model could fit the data while for the southern

part a six-layer model best fitted the measured data curve (Fig. 5.2).

The main features of the combined model are as follows: on the western and southern flank, the soundings show electrical resistivities $>10,000 \Omega\text{m}$ within the first 200–300 m beneath the surface, which drop rapidly to values $<100 \Omega\text{m}$ and $10 \Omega\text{m}$, respectively, to a resolved depth of 800 m. DC results show that the top layer decreases in resistivity down the flanks of Merapi. The resistive layer is underlain by a conductive layer with resistivities of $10\text{--}30 \Omega\text{m}$. The conductor was identified by all three methods, and geometrically follows the topography of the volcano, as derived from induction vectors of the MT measurements (Müller 2004) and by the LOTEM data (Müller 2000). Further, a conductive feature was found 9 km south of the summit. A reanalysis of the LOTEM data (Kalscheuer et al. 2007) depicted again a layering that follows the topography of Merapi. At a depth range of 500–1000 m, the resistivity of the outward dipping layers decreases rapidly downwards into a good conductor with resistivities $<10 \Omega\text{m}$. For the deepest layer, the authors determined a resistivity of $0.4 \Omega\text{m}$, which is quantitatively explained with a combination of ion and electron conductivity caused by saline fluids and hydrothermally altered minerals. Furthermore, the final model supports a hypothesis from the interpretation of central-loop transient electromagnetic (TEM) data of an E-W oriented fault structure below Merapi's southern flank, ~ 7.3 km south of the summit. To the north of this structure, the top of this conductor is located at a shallow depth of 500–1000 m. Kalscheuer et al. (2007) hypothesised that this fault structure coincides with an ancient avalanche caldera rim or, alternatively, may be a structure generated on the slope by gravitational spreading caused by a flow of flank material on weak substrata due to volcanic loading (Delcamp et al. 2008).

Friedel et al. (2000) suggested that the increase of conductivity above values of 20 mS/m might indicate the contact zone of a hydrothermal system beneath the summit, rather than freshwater saturation of porous pyroclastic deposits. In the framework of the more recent

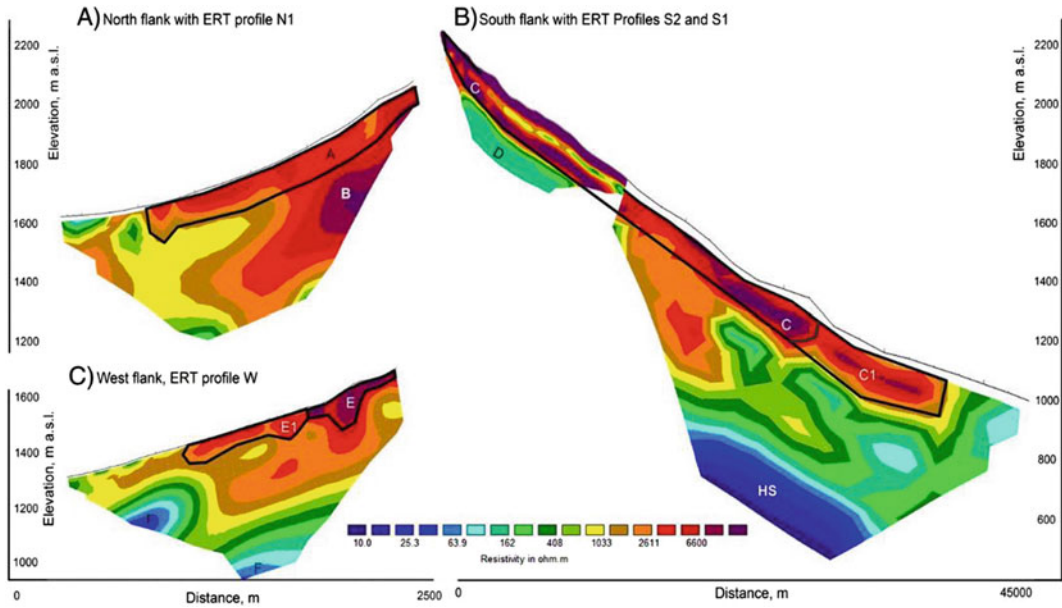


Fig. 5.2 Comparison of the resistivity structure at north and south flanks. Vertical elevation scale is common for north (A) and south (B) flanks. Conductive structures ‘HS’ with resistivity $< 10 \Omega\text{m}$ and ‘F’ with resistivities of $40\text{--}80 \Omega\text{m}$, probably representing a hydrothermal altered fluid-saturated layer or a hydrothermal system below the west and south

flank at a depth of 1000 m. At the surface, recent andesite lava flows below the south flank (unit ‘C’) are characterised by extremely high resistivities exceeding $100,000 \Omega\text{m}$. Units ‘A’, ‘C1’ and ‘E’ with resistivities of $1500\text{--}5000 \Omega\text{m}$ represent pyroclastic flow deposits of Old Merapi as well as lahar and airfall deposits (Byrdina et al. 2017)

DOMERAPI project, Byrdina et al. (2017) investigated the hydrothermal system of Merapi using electrical resistivity tomography (ERT), self-potential measurements and CO_2 flux mapping. Distinct low-resistivity bodies were interpreted as part of an interconnected hydrothermal system at the base of the south flank and in the summit area (Byrdina et al. 2017). In the summit area, a sharp resistivity contrast at the ancient crater rim of Pasarbubar separated a conductive hydrothermal system ($20\text{--}50 \Omega\text{m}$) from the resistive andesite lava flows and pyroclastic deposits ($2000\text{--}50,000 \Omega\text{m}$). The existence of preferential fluid circulation along this ancient crater rim was also indicated by self-potential data. In the vicinity of the active crater rim and close to the ancient crater rim of Pasarbubar, diffuse CO_2 degassing was observed with a median value of $400 \text{g/m}^2\text{d}$. The total CO_2 degassing mass rate across the accessible summit area with a surface of $140,000 \text{m}^2$ was around 20t/d , which equals to $\sim 10\%$ of the volume of

CO_2 estimated to have degassed before the 2010 eruption (Toutain et al. 2009).

On the southern flank of Merapi, the resistivity model shows a pronounced stratification. While recent andesite lava flows are characterised at the surface by resistivity values $>100,000 \Omega\text{m}$, resistivity values as low as $10 \Omega\text{m}$ have been encountered at a depth of 200 m at the base of the south flank, interpreted as reflecting the presence of the hydrothermal system (Byrdina et al. 2017). However, no hints for such a hydrothermal system were found on Merapi’s northern flank, which might be caused by the asymmetry of the heat supplying source of Merapi, whose activity is moving south, and/or by the asymmetry in topography caused by the presence of Merbabu volcano to the north. Thus, Byrdina et al. (2017) suggested that lithological layers on the south flank of Merapi separate the hydrothermal fluids with gaseous fluids rising through the crater rims, while liquids flow downwards to the base of the edifice.

At greater depth of ~ 1.5 km bsl, very low resistivity values of $<1\text{--}3 \Omega\text{m}$ were detected through MT data, extending as far as 15 km from the summit of Merapi. Results from a first regional campaign in 1997 (Hoffmann-Rothe et al. 1998; Ritter et al. 1998) showed that such low values can be found in the crust beneath Central Java but that partial melts are not likely to explain the conductive layers at Merapi at depths of ~ 1 km. The moderately conductive layer ($10\text{--}30 \Omega\text{m}$) covers a region of several 10 km^3 , while the high conductivity bottom layer ($<1\text{--}3 \Omega\text{m}$) could also be identified by MT measurements outside the area covered by Merapi down to 1800 m bsl (Ritter et al. 1998). Lloyd et al. (2007) investigated the hydrogeological situation in Central Java and described the presence of at least two aquifers, with the lower one often confined and saline. Commer et al. (2006) estimated a salinity range for the pore filling by applying conductivity measurements of NaCl solutions as a function of temperature and concentration (Keller 1988). For their model layers 1 and 2 (Commer et al. 2006), the maximal salinities of 0.2 and 0.7 eq. wt.% indicate a rather dilute solution. A low degree of salinity agrees with isotopic investigations at the summit of Merapi, showing that fumarolic water is mainly of meteoric origin, with only a small contribution of magmatic water (Zimmer et al. 2000). The deeper layers 3 and 4 (Commer et al. 2006) show increased salinities, and, while the salinity of seawater with a value of around 3.5 eq. wt.% falls well within the range of layer 3, the estimates for the bottom layer show a much higher concentration. Van Bemmelen (1949) pointed out earlier that the young Quaternary volcanoes of East Java are built upon a basement of plastic and not yet fully consolidated marine sediments. For weakly cemented marine rocks, usually Tertiary in age, the electrical conductivity can be very high because of a combination of ion and electron conductivity in claystones and micaceous clay. In this case, the low basement resistivities may well be explained by the intrusion of seawater beneath Java.

5.4 Active Seismic Measurements Explain Complex Earthquake Signals of a Stratovolcano

The influence of topography, the heterogeneous medium for propagating seismic waves and almost unknown source mechanisms lead to manifold difficulties in analysing and interpreting volcano-seismic signals. For locating and analysing natural seismic events within and beneath the edifice of Merapi—particularly for the separation of source, path and site effects—the seismic structure information is indispensable. Therefore, seismic profiles (Fig. 5.3) were already recorded through up to 30 three-component seismometers aligned radially to the volcano summit using a receiver spacing of 100 m in the framework of the MERAPI project in the late 1990s. Nearly 5 km away from the summit, in a radial fashion and at an altitude of about 1000 m asl, water basins were installed at three locations, and each filled with 40 m^3 water. In these basins, a 2.5 l mud gun was fired by an air pressure of 80–100 bar to generate well defined seismic source signals with high repeatability necessary to increase the signal energy by stacking up to 100 single shots and to improve the signal–noise ratio (Wegler et al. 1999).

Surprisingly, the recorded seismograms were characterised by unusually complicated wave fields that were difficult to explain by common standard seismic methods. Records near the source location showed a short and pulse-shaped waveform, while at greater distances, the signals spread out to longer wave trains. Only the p-phases showed, in traces, clear coherency, whereas later phases were mostly shear wave energy incoherent along the profile. Some of the coherent onsets were recognised with negative apparent velocities. They could be interpreted as refracted waves reflected at steeply dipping reflectors, while others may be backscattered surface waves, with some out of the profile lines (Luehr et al. 1998; Maercklin et al. 2000). Such complexity was later also identified at other volcanoes (Wegler 2003).

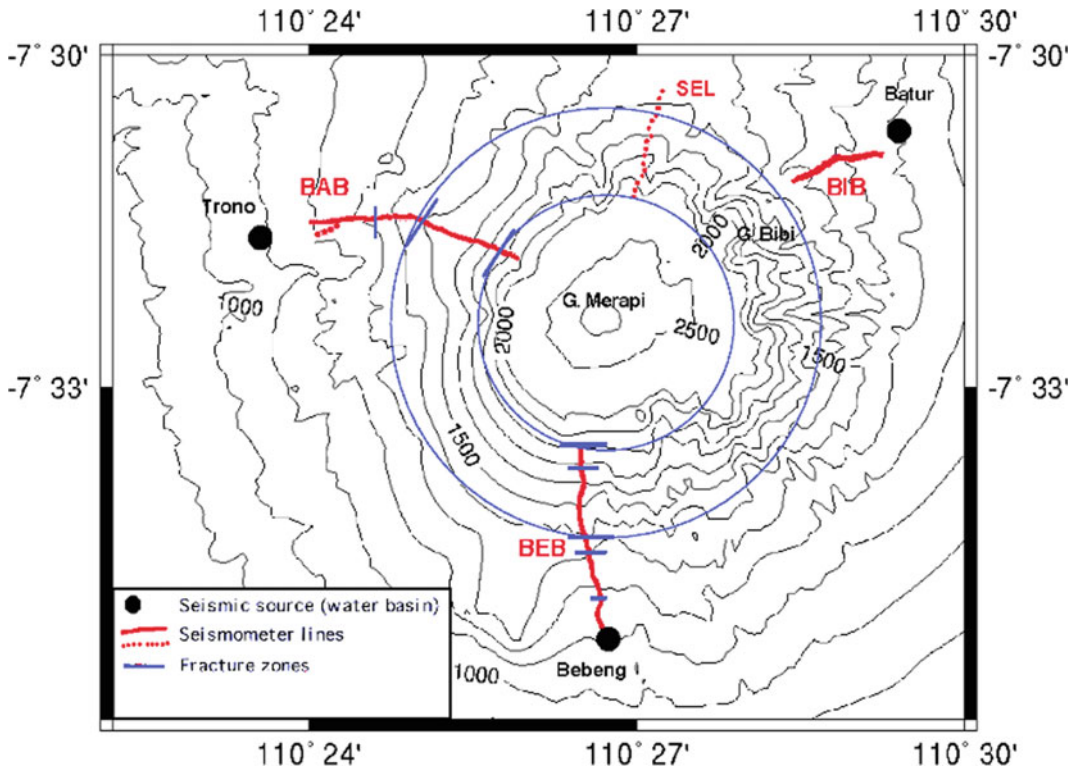


Fig. 5.3 Location of seismic lines measured in the frame of the MERAPI project in 1997, source points and mapped fracture zones. Profiles shown as dotted lines

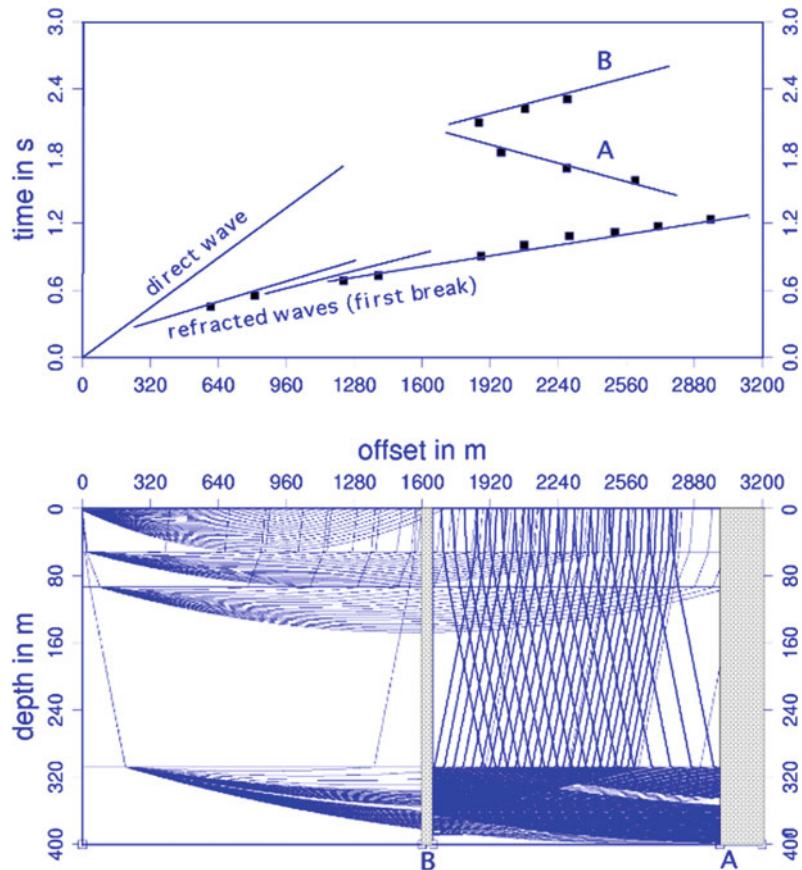
were not interpreted. Two circles mark the extent of possible weakness zones

Observed linear, coherent phases contained information on larger scale structures. To enhance these types of waves, all three spatial components were jointly processed using polarisation analysis (Maercklin et al. 2000). After processing, the first arrivals were recognisable up to 7.5 km distance, not far enough for penetrating the volcanic cone to the opposite side. Therefore, these records could not be applied for a travel time tomographic analysis. Direct S-waves were superimposed by the P-wave coda and only observable up to 1 km distance from the seismic source. 2-D ray-tracing supported the interpretation of first and later onsets. The resulting model is based on a layered 1-D depth profile of the P-wave velocity derived from first break travel times. The velocities range from some hundred m/s close to the surface to more than 3000 m/s at a maximum depth of ~ 300 m. As each model layer likely corresponded to

numerous different geological units, only an effective velocity was defined. With reflectors vertical to these layers, it was possible to fit the travel time curves of selected onsets. The model shown in Fig. 5.4 assumes a p- to s-wave conversion at reflector A, located ~ 3 km away from the source, to explain the lower apparent velocity of the reflected onsets A and B (Fig. 5.4).

The high impedance contrasts at both modelled reflectors were explained by structural heterogeneities (Maercklin et al. 2000). These fracture or weakness zones were mapped at Merapi using observed reflections on lines BEB and BAB (Fig. 5.3). The most prominent fracture zones on both profiles seem to be equidistant to the summit of Merapi and may belong to a larger, approximately circular zone of weakness with a diameter of ~ 4 km, which agrees well with the low resistivity zone found by electromagnetic

Fig. 5.4 Modelled ray paths and travel time curves for selected onsets of line BEB. The model is based on a simple 1-D velocity-depth function and reflectors perpendicular to the layers. Letters A and B denote reflectors and corresponding time curves; black boxes indicate measured travel times. The depth is defined in metres below the surface



measurements. White-coloured rocks and debris led to the speculation that the high-conductive anomaly detected at Merapi and the circular feature of low seismic velocity could be due to a hydrothermally altered zone surrounding the inner core or conduit of the volcano. Soil temperature and CO₂ gas flux measurements carried out at the summit from 2002 to 2007 (Toutain et al. 2009) support this idea. This study found degassing anomalies that appear to be controlled by structures identified as concentric historical crater rims (1768, 1872 and 1932), which may have undergone a hydrothermal self-sealing process that lowered permeability and porosity. Heap et al. (2019) showed that acid-sulphate alteration, common at Merapi and other volcanoes, can reduce the permeability at rock sample scale by up to four orders of magnitude as a result of pore- and micro-fracture filling mineral precipitation. Using these petrophysical data,

their calculations demonstrated that intense progressive alteration can reduce the equivalent permeability of a dome by two orders of magnitude, which is sufficient to increase pore pressure inside and beneath a dome such as that at Merapi.

A surprising observation in the recorded seismograms (Wegler and Luehr 2001a) was that the amplitude of the first onset decreases rapidly with increasing source-receiver distance, while the main part of seismic energy is included in the coda of the seismograms and shifted towards later travel times. The maximum energy of the coda waves moved with a group velocity of 200–400 m/s along the profiles. The coda waves were polarised horizontally but showed no preferred azimuths. This strange effect on the seismic signals can be explained physically by the inner structure of the volcanic cone, which is built up by alternating material of pyroclastic flow, lahar

and ash deposits. Big blocks and compact lava banks alternate with less intensively consolidated material. Layers vary in thickness and extension and were cut by erosion processes. These inhomogeneities with high acoustic impedance contrasts produce strong scattering effects which reduce the energy from the first onset so that it fades out after a distance of 7.5 km. For applying a travel time tomographic analysis, the first onset would have had to be detected up to 12 km distance. As this was not the case, the experiment was eventually discontinued.

Assuming that most of the energy in the seismograms was associated with multiple scattering and that S-waves dominated the coda, the observed waveform envelope was explained by the diffusion model (Dainty and Toksöz 1981). According to this model, the energy density as a function of time and space included the attenuation coefficients h_s and h_i as geophysical formation parameters. The parameter h_i described the energy loss of a seismic wave due to conversion to other forms of energy (e.g., heat) called intrinsic attenuation, while h_s denoted the energy loss due to scattering (Wegler et al. 2000; Wegler and Luehr 2001a, b). Interestingly, it was found that the resulting scattering attenuation was at least one order of magnitude larger than the intrinsic value. The frequency dependence of h_s was proportional to $f^{0.0}$, whereas h_i was proportional to $f^{1.6}$. At Merapi, the derived mean free path for generated airgun signals with an energy maximum of $\sim 7\text{--}8$ Hz was as low as $h_s^{-1} = 100$ m. This means that multiple scattering effects had to be considered for source-receiver distances greater than 100 m at Merapi, justifying the use of the diffusion model for source-receiver distances greater than several hundreds of metres. This result also explains the bad coherency of seismic traces with a chosen seismometer spacing of 100 m. No significant differences were found for the three different profiles in h_s . However, h_i of BAB on the west flank was 0.5 times smaller than h_i of BEB on the south flank and of BIB on the northeast flank, which might be correlated with the local geology (Wegler et al. 1999).

The natural seismicity of Merapi, particularly events located in the upper part of the volcano cone and called multiphase (MP) events, showed similar characteristics compared to airgun shot records. First onsets were weak and often difficult to recognise. The maximum energy of the wave trains was shifted by distance to later arrival times compared to small first onsets. Shear waves as body waves were nearly invisible.

5.5 Merapi's Magma Reservoir and Ascent Paths of Fluids and Partial Melts

After the first interpretation of the seismicity distribution, the main magma reservoir of Merapi was thought to be located at a depth of 4–5 km (Ratdomopurbo and Poupinet 1995), extending to a depth of 10 km or more because of the fade-out of the volcanic seismicity beneath 5 km below the summit. Later, the hypothesis of a main magma reservoir was supported by petrological data (Purbawinata et al. 1997). However, more recent petrological studies have shown that Merapi magmas are stored at multiple levels, ranging from the shallow conduit down to ~ 30 km (e.g. Chadwick et al. 2007, 2013; Costa et al. 2013; Preece et al. 2013; Deegan et al. 2016; Troll and Deegan 2023, Chap. 8).

Gossler (2000) analysed teleseismic event records at seismic monitoring stations located on the flanks of Merapi. Receiver functions (Yuan et al. 1997; Gossler et al. 1999) based on the analyses of P–S converted shear waves revealed structures in the crust, the Moho and the subsiding lithosphere plate. The application of the Receiver functions method allowed the properties and constitution of the deeper parts beneath Merapi down to the subducting slab to be inferred. However, the occurrence of strong multiple phases in the seismograms, interpreted as reverberations of the incoming waves between the down-going plate and the surface, impeded a detailed resolution of deeper structures. Moreover, a large magma reservoir could not be detected.

Besides, investigation of the polarisation of incident teleseismic waves showed an interesting effect depending on the analysed frequency band. Long-period waves above 10 s yield no significant differences between observed and theoretical calculated azimuths or incident angles, respectively, in which the incident angle represents a measure of the distance between a hypocentre of an earthquake and the receiver location. For higher frequencies with periods below 5 s, this changes dramatically. As a result of the polarisation analysis, the determined azimuths and incident angles of the incoming waves point towards the centre of Merapi, independent of the true location of an earthquake. This suggests that the hypocentres of the analysed earthquakes were located inside Merapi, a result interpreted as a topographic effect caused by the geometry of the cone-shaped volcanic edifice of Merapi (Gossler 2000).

Despite these geophysical studies, questions about the hypothesised magma reservoir, ascent paths of fluids and partial melts, and how Merapi is embedded in the subduction process, could not be answered. One reason for this was that all investigations were concentrated mainly on the edifice of Merapi, where, for instance, the small aperture of seismic stations in combination with the complex structure limited the retrieved information. The magma storage and complex feeding and plumbing system, which not only involves the shallow structures beneath the volcanic edifice but also deep structures and processes within the underlying crust and upper mantle, led to the design of the larger MERAMEX seismic experiment, which is further detailed below.

5.5.1 Deeper Structure Beneath Central Java

Regional-scale seismic tomography and the distribution of the Wadati-Benioff seismicity from the revised International Seismological Centre (ISC) bulletin constrains the subducting slab at the Sunda arc down to 1000 km depth (Lühr et al. 2013). A lack of robust data at shallow

depth can be compensated by using local earthquake data, which also provide more detailed information about the crustal structure and the volcanic plumbing system above the slab-related Wadati-Benioff zone beneath Central Java and Merapi. Results of the regional tomography suggest that the subducting slab cannot be represented by an oversimplified conveyor-type 2-D model. Considerable lateral and vertical variations in the slab thickness probably have effects upon the surface tectonics. In particular, the peculiar character of Merapi might be caused by a slab window that formed in the contact zone between two autonomously subducting oceanic plates (Koulakov et al. 2007).

Between May and October 2004, combined amphibious seismological investigations at 110°E were thus performed as part of the MERAMEX project (Reichert and Lühr 2005). A temporarily installed seismic network of 134 continuously recording stations (triangles in Fig. 5.5), 106 short-period Mark L4 seismometers, 14 broadband Guralp seismometers, 8 ocean bottom hydrophones (OBH) and 6 ocean bottom seismometers (OBS), covered a region of about 150 × 200 km. OBHs and OBSs were deployed during the RV SONNE cruise SO176 to extend the land network offshore to the south of Central Java. The average onshore station spacing was ~20 km. The spacing of ocean bottom instruments was ~40–90 km. The seismic instruments recorded both the natural local earthquakes as well as airgun-generated shots, the latter generated during a second cruise (SO179) in September and October 2004. The interpreted amphibious data consisted of 50,060 first arrival travel-time picks of airgun shots fired along three seismic wide-angle profiles and recorded also with the onshore MERAMEX network. Four to five local earthquake events could be recorded per day, in addition to regional and teleseismic events. The clearest signals were observed in the southern and northern coastal areas. In Central Java, north of Merapi and Lawu, the recorded shear wave phases were strongly attenuated. Thus, even a preliminary qualitative evaluation of the seismograms showed that there is a significant seismic anomaly located beneath Central Java.

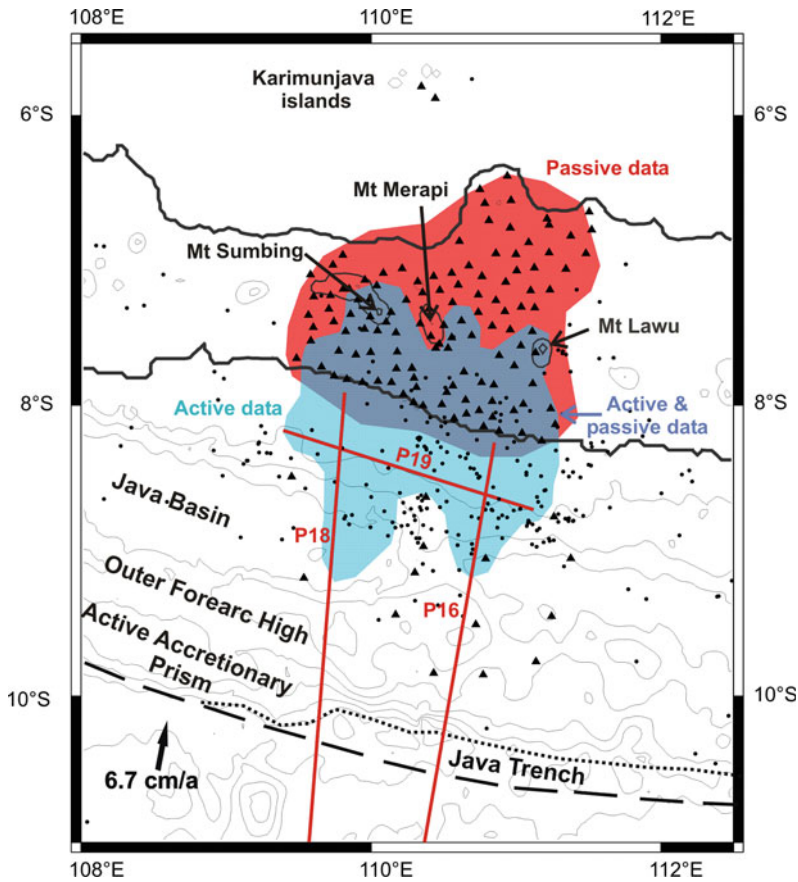


Fig. 5.5 Study area of the MERAMEX project, including the tectonic regime of the region. Triangles mark the temporary seismological network installed in 2004. Dots are recorded earthquakes collected in the MERAMEX catalogue. Red lines indicate seismic airgun profiles. The red coloured area in Central Java marks the area covered by passive seismic data, while the light blue and grey areas are covered by active seismic data and both data

For the earthquake data analysis, a total of 13,800 phases (8000 P- and 5800 S-phases) were selected for a simultaneous iterative source location and tomographic inversion. A detailed description of this study can be found in Koulakov et al. (2007, 2009b). The P velocity reference model down to a depth of 20 km was estimated based on results of an active seismic experiment performed in the offshore part of MERAMEX (Wagner et al. 2007a, b; Wittwer et al. 2010). For deeper parts, the velocity model was defined based on the global AK135 model

sets, respectively, in the uppermost 10 km depth layer. These areas are identified as areas with satisfactory recovery of 30 km size checkerboard anomalies at a depth of 5 km. The dotted line marks the current track of the Java trench, which is retreating northward from the normal curvature trend (dashed line) in front of Central Java (Wagner et al. 2007a)

(Kennett et al. 1995) because no reliable constraints were available for the range below 20 km depth. Derived final earthquake locations line up along the Wadati-Benioff Zone, but the events depict variable dipping angles of the slab. Looking to the north, for the first 150 km distance from the trench, the slab appears to be almost horizontal. From 250 to 450 km along profile P1–P2, the dip angle of the slab is about 45°, while in the depth interval from 250 to 600 km, the slab steepens to ~70° (Koulakov et al. 2007).

We developed new models of the anisotropic structure beneath central Java based on the local earthquake tomography (Koulakov et al. 2009b) (Figs. 5.6 and 5.7). Relative P (V_p) and S (V_s) velocity anomalies are illustrated in horizontal and vertical sections. The reconstruction of relative anomalies even in highly heterogeneous areas was fairly stable and found not to be significantly dependent on the chosen reference model (Koulakov et al. 2007). An interpretable spatial resolution could be achieved down to a depth of 150 km.

The first striking feature in the derived tomographic images is an almost perfect correlation of P and S wave anomalies in the crust. The most prominent feature in the crust is a strong low-velocity anomaly. This low-velocity anomaly is named Merapi-Lawu Anomaly (MLA), with a reduction in velocity up to 30% for the P-model, and up to 36% in case of the S-model. The MLA fills the areas within the main volcanic complexes

in Central Java. The largest part of this anomaly is located close to the volcanoes Merapi and Merbabu (briefly called “Merapi complex”), and extends to Lawu volcano at the eastern border of the investigation area. The second, smaller part lies between the Merapi complex and the volcanoes Sumbing, Sundoro and Dieng (briefly called “Sumbing complex”). Interestingly, these active volcanoes are not located above the central part of the anomaly but appear to be arranged surrounding it. In other words, the active volcanoes are found just above the contact region between the low-velocity anomaly and the high-velocity forearc. In vertical sections (Fig. 5.7), it is recognisable that the MLA is inclined southwards towards the subducting slab, extending into the upper mantle with decreasing intensity. The reliability of these models was tested comprehensively by Koulakov et al. (2007, 2009b).

Furthermore, the obtained seismic anomalies were compared with Bouguer gravity anomalies

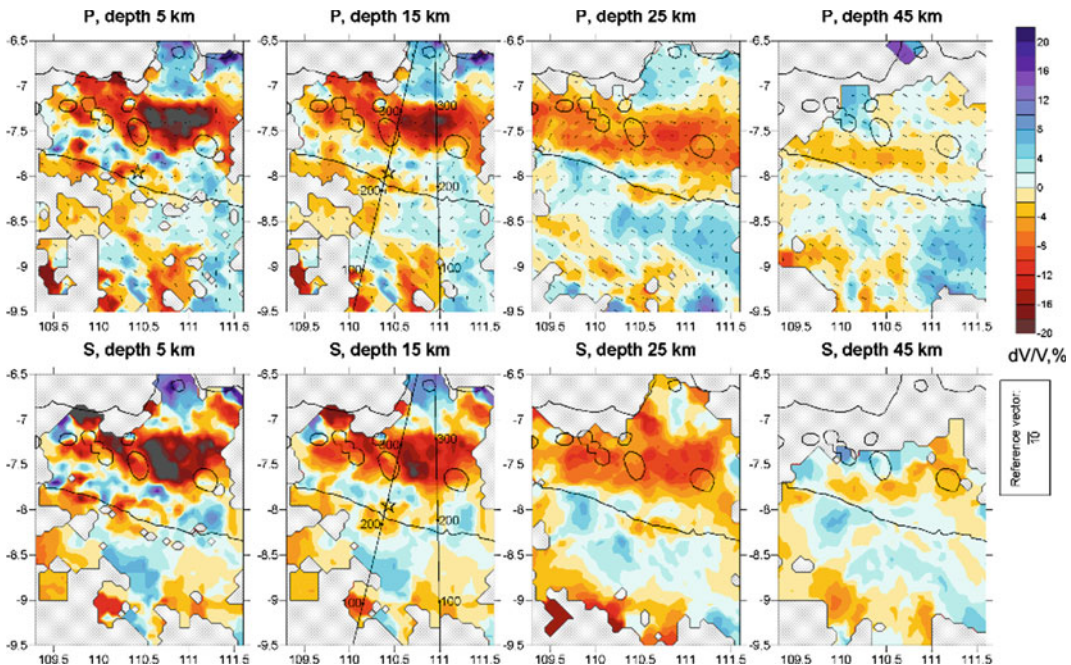


Fig. 5.6 Results of the anisotropic inversion after five iterations in horizontal sections. Colours indicate the isotropic velocity perturbations which are computed as an average of four anisotropic parameters in each point. Bars show directions of fast horizontal P velocities. The length of the bars reflects the difference between the fastest and

slowest horizontal velocities. The reference bar (10% of anisotropy) is shown in the right-bottom corner. Positions of two cross sections presented in Fig. 5.7 are marked in maps corresponding to 15 km depth. The star shows the hypocentre of the Bantul Mw = 6.4 earthquake on 26 May 2006 (UTC)

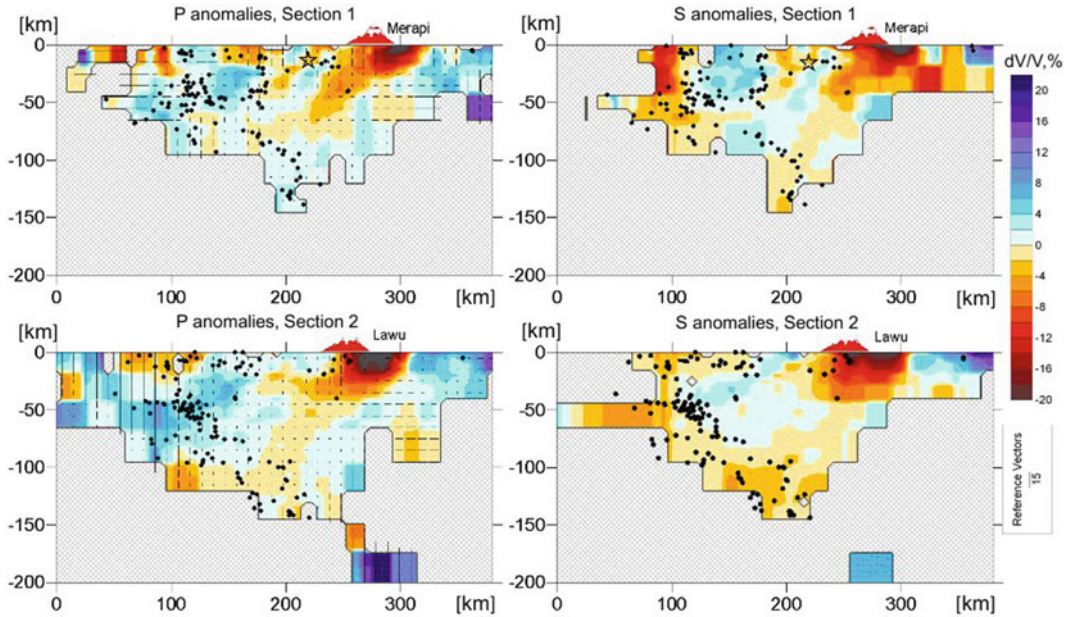


Fig. 5.7 Resulting anisotropic P and isotropic S models after five iterations in vertical sections. Positions of sections are shown in the map related to 15 km depth (Fig. 5.6). The anisotropy bars for the P model are vertical, if the vertical velocity variations are larger than

the average horizontal perturbations, and horizontal in the opposite case. The reference bar (6% of anisotropy) is shown in the left-bottom corner. The star shows the hypocentre of the Bantul Mw = 6.4 earthquake on 26 May 2006 (UTC)

(Sato 1978; Smith and Sandwell 1997), as illustrated in Fig. 5.8. It can be seen that the main features of gravity and seismic velocity models are consistent with each other. For example, the strong negative seismic anomaly located north of

the MLA corresponds to a negative gravity anomaly in the back-arc. Dominantly positive seismic anomalies in the forearc correspond to positive gravity anomalies. To quantify this link, we performed gravity modelling intended to

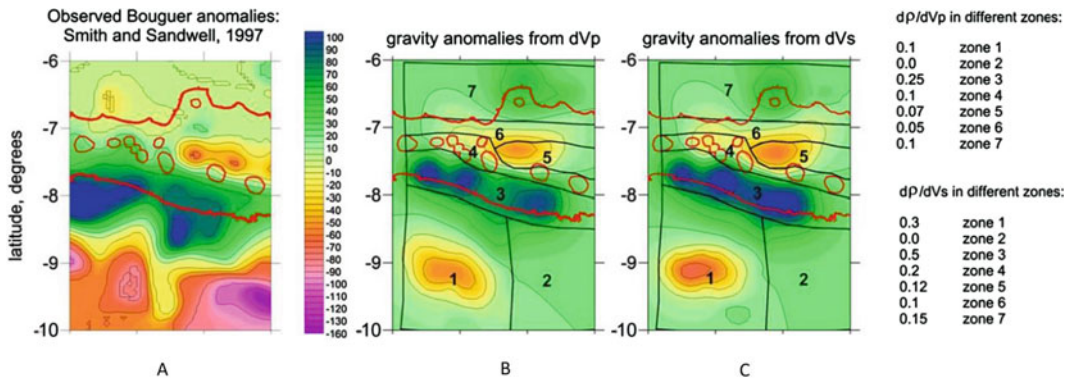


Fig. 5.8 Result of optimisation for dp/dv coefficients in the crust. The gravity map after Smith and Sandwell (1997) on the left and the calculated gravity values derived from Vp and Vs velocities (on the right) indicate a

strong negative gravity anomaly in Central Java, extending to the east. The gravity anomaly fits well with the Merapi-Lawu seismic velocity anomaly (centred at approximately 7°S, 111°E)

estimate values of dp/dv coefficients (anomalies of density over anomalies of seismic velocity) for different crustal zones.

For the gravity modelling, the crust was divided into several zones, representing main geological and geophysical features (Koulakov et al. 2007). The final computed gravity fields derived from the P- or S-velocity anomalies are shown in Fig. 5.8b, c. Although the derived coefficients determined by this modelling are not expected to be highly accurate, they provide semi-quantitative information concerning geological processes in the crust of Central Java. For the arc anomalies and the MLA, the calculated dp/dv values are found to be rather low (Koulakov et al. 2007, 2009b; Luehr et al. 2013).

Syracuse and Abers (2006) analysed the variations in vertical distance between arc volcanoes at the surface and the subducted slab at depth for nearly all subduction zones. They found that at subduction volcanoes, the average slab surface distance is ~ 100 km. Discrepancies were found only in a few cases, such as in Central Java, where the vertical distance from the surface to the slab is ~ 150 km. The authors attempted to explain such deviations from the average depth by calling on specific physical conditions. Another common feature of a subduction zone is that the earthquake hypocentre distributions show two maxima in depth. A shallow clustering at ~ 20 – 50 km is interpreted to be related to tectonic stress release. Another increase in the frequency of earthquakes can be detected at a depth range of ~ 100 km on average (International Seismological Centre 2001). These peaks in seismicity are also observable in the same depth ranges in the Sunda arc (Luehr et al. 2013; Halpaap et al. 2019).

The increase in seismicity in the range of 100 km depth can be explained by mineralogical phase transitions resulting in dehydration processes (e.g., Paulatto et al. 2017; Cooper et al. 2020) caused by de-serpentinisation, which leads to a volume decrease expressed by earthquakes (Davey and Ristau 2011).

Mineralogical investigations of Mierdel et al. (2007) demonstrated that the ratio of water saturation versus depth has a pronounced minimum

at depths between 100 and 200 km (Bolfan-Casanova 2007). Depending on the tectonic environment and temperature, the minimum solubility may be shallow, as in the case of the oceanic mantle, but deeper in the case of cold continental lithosphere. We propose that in the case of Central Java at a depth range near 100 km, where seismicity is increased, fluids (mainly water) are released from the subducted slab and begin to ascend into the overlying mantle wedge, leading to a reduction in melting temperature of the mantle rock (e.g., Poli and Schmidt 1995). The ascent path of upward migrating fluids released from the slab is imaged tomographically as a zone of low seismic velocity (Koulakov et al. 2007). In the case of Central Java, this path is not vertical but inclined at 45° and oriented towards the trench (Fig. 5.7). The ascending fluids cause decreasing viscosity and partial melting of the mantle. The melts then penetrate the arc crust and form magma reservoirs in the lower and middle crust and, in some cases, rise to the surface and cause volcanic eruptions.

As shown above, the most important feature of the MERAMEX tomographic models is an unusually strong low-velocity anomaly located in the backarc crust just north of the volcanoes Sumbing, Merapi and Lawu (Figs. 5.6 and 5.7). The main part of this anomaly extends for ~ 80 km from east to west and ~ 30 km from north to south, and to a depth of >50 km, from where it further extends as an inclined tongue with decreasing amplitude towards the slab pointing at a depth of ~ 100 km. The active volcanoes are located at the edge of this anomaly between high and low-velocity regions. Considering this geometry, it can be estimated that the low-velocity body has a volume of $>50,000$ km³ characterised by a reduction in velocity of up to 20% for the seismic P-wave model and up to 25% for the S-wave model (Koulakov et al. 2007, 2009b). Shear wave signals recorded above this zone are strongly attenuated compared to areas outside the anomaly volume. Furthermore, there is a good correlation between the distribution of velocity anomalies in the crust and gravity anomalies. High-velocity seismic

anomalies in the forearc correspond to gravity highs and the low-velocity MLA matches well with a distinct gravity low corresponding to the Kendeng Basin, which is located north of the MLA and parallel to the volcanic front of Central and East Java (Koulakov et al. 2007). The Kendeng Basin succession is not well exposed but contains much volcanic debris (see Harijoko et al. 2023, Chap. 4). The deposits have an estimated thickness of up to 10 km based on gravity modelling (Waltham et al. 2008). Consequently, we interpret this behind-the-volcanic-front anomaly as the combined product of a thick package of low-velocity sediments in the upper crust, and increased temperatures and magmatic fluids in the middle and lower crust. The very low P- and S-velocities within the shallowest part of the MLA could in part result from a high fluid (gas and liquid) content in the sediment layers. Mud volcanoes in northern Central Java (Satyana and Asnidar 2008), which actively release methane, favour this hypothesis. Synthetic tests (Koulakov et al. 2007) confirmed that the MLA cannot be explained simply and requires that the lower crust must also have low velocities, as confirmed by active seismic studies (Wagner et al. 2007b).

The velocity perturbations, attenuation of P- and S-waves, and high V_p/V_s ratio of the MLA, indicating a high Poisson's ratio of 0.3 and matching with a gravity low, suggest an area of increased temperature and reduced shear strength in the crust. Depending on the elastic modulus, a fluid and partial melt amount of 13–25% can be estimated for the MLA volume. Assuming that the region of the MLA beneath the sedimentary basin consists of a rigid matrix with cells filled with a magmatic crystal mush or near-molten material, the sediments may act as a seal for fluids from the mantle wedge just beneath the MLA to move vertically towards the surface. This hypothesis is indirectly supported by relatively strong, randomly looking travel time residuals after inversion (Koulakov et al. 2007). An explanation for this noise could be the existence of relatively small bodies of contrasting material, causing scattering (Luehr et al. 2013). These may affect the travel times of seismic rays

but cannot be resolved by the tomographic inversion. Considering realistic frequencies of seismic signals from natural sources, a significant scattering-induced effect on the travel time can be expected only for anomalies of a minimum diameter of 1–2 km. Anomalies of 15–20 km extension, for instance, would be resolved in the images clearly and would lead to more coherent signals. Therefore, the lower part of the MLA can be interpreted as a zone composed of a solid matrix or may be a 'reservoir' similar to a sponge structure that contains cells or sheeted sill structures of 2–15 km diameter filled with molten or partially molten material. This hypothesis is supported by petrological findings of magma storage and crystallisation at Merapi (e.g., Chadwick et al. 2013; Costa et al. 2013; Deegan et al. 2016; Preece et al. 2016; Peters et al. 2017; Troll and Deegan 2023, Chap. 8). Furthermore, Merapi magmas are contaminated by carbonates from the subvolcanic basement derived from depth of 3–11 km (e.g., Chadwick et al. 2007, 2013; Deegan et al. 2010, 2023; Chap. 10; Whitley et al. 2020). A significant contribution to the magmatic volatile budget via limestone assimilation may therefore influence the driving mechanism of eruptions at Merapi and other volcanoes sited on carbonate crust (e.g., Troll et al. 2012; Blythe et al. 2015; Deegan et al. 2023; Chap. 10).

The degree of velocity anomalies found beneath Central Java is exceptional, when compared to anomalies found at other subduction zones and large volcanic systems. For example, Toba volcano in northern Sumatra is the source of the largest eruption on Earth within the last two million years. The resulting caldera is 30×100 km wide and has a total relief of 1700 m. In one eruptive phase 75,000 year ago, Toba produced the Youngest Toba Tuff, which has an estimated volume of 2800 km^3 (e.g., Chesner and Rose 1991). Tomographic investigations of the Toba area (Koulakov et al. 2009a) derived a model that images patches of negative anomalies beneath Toba with velocity reduction values of no more than 15%. Such a velocity reduction appears to be typical for volcanic areas at subduction zones and is comparable to

anomalies found in the Andes (Schurr et al. 2003; Koulakov et al. 2005) and Kamchatka (Koulakov et al. 2011).

5.5.2 Shallower Structure Beneath Merapi

The resolution of our local earthquake tomography method using P- and S-body waves decreases with decreasing crustal depth. To improve the resolution in the shallower crust, especially in the uppermost 5 km, a tomographic inversion might be realised from the analysis of ambient noise data. Different levels of anomalies, which were previously blurred and indistinguishable in the Local Earthquake Tomography (LET) results (Koulakov et al. 2009b), can now be separated by applying the Ambient Noise Tomography (ANT) modelling method.

Results of ANT modelling for the MER-AMEX data in the Central Java area by Koulakov et al. (2016) show strong variations in the S-wave velocity, especially at shallow depths. Between the coastline and the volcanoes Merapi and Lawu, the authors found a strong high-velocity anomaly with an amplitude exceeding 25%. Beneath and to the south of Merapi, strong negative anomalies were revealed with amplitudes that reached -25% . Thus, the variations derived with this tomographic method are of the same order of magnitude as those of previous tomographic studies based on travel time tomography (Koulakov et al. 2007, 2009b). In Fig. 5.9, the ANT modelling results are compared with the results of the model derived from LET (Koulakov et al. 2009b). The main features, such as the high-velocity forearc and low-velocity anomalies surrounded by the volcanoes in Central Java, appear similar in both models. However, there are subtle differences. For example, in the LET results, the most prominent low-velocity anomaly has a high magnitude across the entire area between Merapi and Lawu, whereas in the ANT model, the eastern part of the anomaly in the vicinity of Lawu volcano is less pronounced. This difference can be partly explained by the lower resolution of the ANT

model in the eastern area of investigation and by some leakage of the amplitude of anomalies (Koulakov et al. 2016). Also, it has to be noted that the LET results were affected by significant vertical smearing, which suggests that some differences between the models may be caused by the projection of anomalies from different depths. For the vertical section (Fig. 5.9b, d), an overall fit of the main anomalies is observable in both the LET and ANT models. In the ANT model, an anomaly beneath the Merapi cone is apparent, whereas in the LET model, this shallow anomaly is not apparent. Interestingly, a large anomaly at the bottom-left corner of the ANT section is consistent with the inclined low-velocity anomaly in the LET model that links the volcano-related structures with the subducting slab. According to the results of the ANT model, the low-velocity anomaly beneath the northern flank of Merapi (section A1–B1; Fig. 5.9b) seems to be separated into two parts. Koulakov et al. (2016) suggested that the upper portion of this anomaly represents a thick layer of volcanoclastic sediments accumulated over a long period of time. Based on this model, the thickness of this layer may be greater than 1 km. A second strong low-velocity anomaly, detected at depths between 4 and 8 km beneath this volcanoclastic sediment layer, may be associated with a large, shallow felsic magma reservoir, as proposed by Koulakov et al. (2009b) based on the results of the LET model, and demonstrated by horizontally oriented anisotropy that may indicate a sill structure of this reservoir. A similar sill structure for a felsic magma reservoir at a similar depth range was identified beneath the Toba caldera (Jaxybulatov et al. 2014). However, it is notable that this structure appears to be separated from the upper crustal anomalies, although the ANT model tends to shift the deep boundaries higher. Consequently, the real location of this anomaly may be deeper than is indicated by these particular results.

A separation of two low-velocity layers is also found by the latest larger structure investigation project DOMERAPI. Within this project, a much denser seismic network of 46 broad-band seismometers was installed around Merapi between

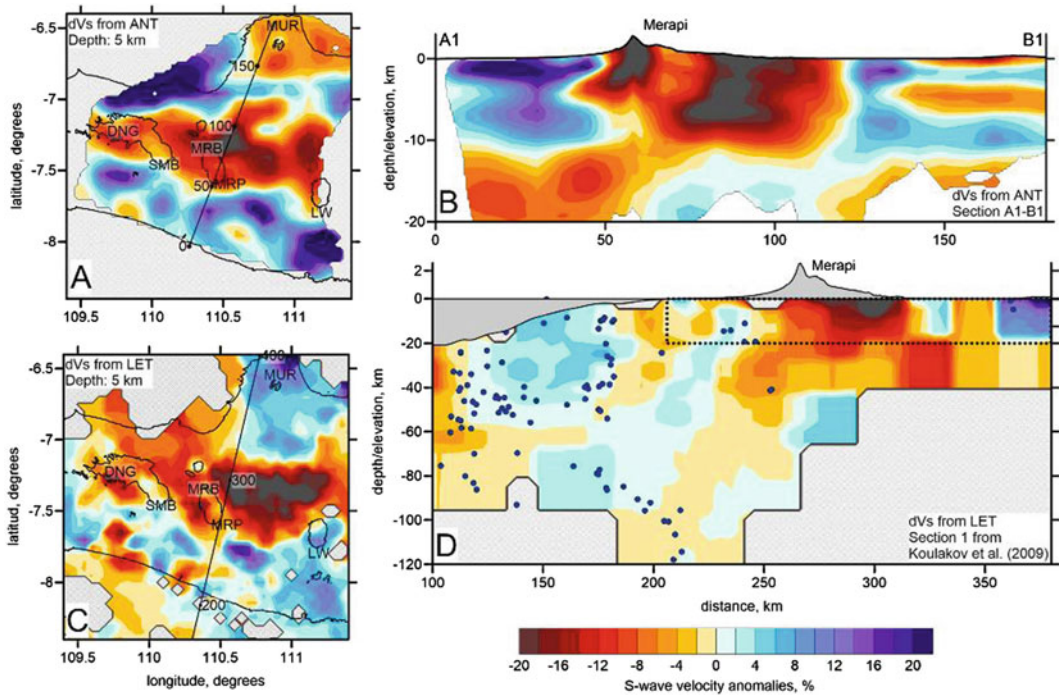


Fig. 5.9 Comparison of the ambient noise tomography (ANT) with the body wave local earthquake tomography model (LET). **a** and **c** are horizontal sections at 5 km depth of the ANT and LET model, respectively. Contour lines of topography at 1000 m altitude are shown with black lines. **b** and **d** are the vertical sections of the ANT and LET models along the profiles indicated in figures

a and **b**. In **b**, the vertical scale is twice exaggerated for positive altitudes. Blue points in **d** show earthquake hypocentres. The dotted line in **d** depicts the area corresponding to the section in **b**. The exaggerated topography for positive altitudes along the profiles is presented in images **b** and **d**

October 2013 and mid-April 2015 (Widiyantoro et al. 2018). The stations were deployed with an inter-station distance of ~ 4 km and the DOMERAPI data were combined with data of the permanent BMKG. All detected seismic events were relocated using a double-difference earthquake location algorithm. The jointly processed data produced a new, high-quality catalogue comprising 358 events for imaging the V_p and V_p/V_s structure below Merapi in exceptional detail, from below the volcano's summit to a depth of ~ 20 km below sea level. The P- and S-wave arrival time data with similar path coverage reveal a high V_p/V_s structure extending vertically from a depth of ≥ 20 km bsl up to the summit of Merapi. As mentioned by Koulakov et al. (2016) and Widiyantoro et al. (2018), their tomographic inversions reveal two pronounced anomalies beneath Merapi. One anomaly located

at <4 km depth was demonstrated by low V_p and very low V_s values as well as high V_p/V_s ratios. A second anomaly was found at ~ 10 – 20 km depth, with high V_p , very low V_s values and very high V_p/V_s ratios. Interestingly, their V_p/V_s tomograms suggests that another deeper anomaly may exist near the MOHO at ≥ 25 km depth with low V_p and low V_s values as well as high V_p/V_s ratios that match the findings of the MERAMEX project of a very large anomaly in Central Java with an estimated volume of more than $50,000$ km³ (Koulakov et al. 2007; Luehr et al. 2013). However, the most denoting feature in their tomographic images is a distinct sub-vertical high V_p/V_s anomaly. If this finding is correct, this sub-vertical, high V_p/V_s anomaly outlines a fluid-rich zone and, therefore, the last part of the magma ascent path from a depth of ~ 20 km up to the surface.

It is noteworthy that volcano edifices are typically associated with higher seismic velocities at the shallowest depths, representing the rigid properties of highly consolidated igneous rocks, whereas in areas between volcanoes, shallow seismic anomalies are generally negative. These negative anomalies can be explained by volcanoclastic deposits, eroded and transported down the volcano flanks by lahars and rivers. During the Bantul earthquake in May 2006, such deposits showed devastating effects, when strong resonant shaking with relatively high frequencies led to severe destruction of mainly smaller buildings and caused >5700 fatalities (e.g., Walter et al. 2008).

5.6 Summary

The past 25 years of investigation of the volcanism and magmatism of Merapi and the surrounding area in Central Java have brought geological and geophysical advances that greatly helped define the structure of the magma plumbing system and underlying magmatic processes. Direct current electrical resistivity (DC) tomography and magnetotelluric (MT, LOTEM) investigations as well as gravity measurements revealed the highly complex resistivity and density structure of the Merapi edifice and have provided many geophysical parameters that led to an improved understanding of the volcano's hydrological and hydrothermal system and its dynamics. The highly sensitive borehole tiltmeter array measurements on the flanks showed very small signal values related to Merapi's activity in 1997 and 1998 only, with a tilt signal of maximum $1 \mu\text{rad}$ associated with the 14 January 1997 explosive event. Many of the results obtained pertain to the large area between the subducting slab and the summit area and are not only valid for Merapi, but may also apply to other subduction zone volcanoes. A schematic cartoon illustrating the processes taking place beneath Central Java is shown in Fig. 5.10. As proposed by Luehr et al. (2013), an increased

level of subducted slab-related seismicity in Central Java can be observed at ~ 100 km depth, which likely represents dehydration and the release of hydrous volatiles from the slab (e.g., Peacock 1990; Maruyama and Okamoto 2007). When these volatiles pass through the mantle wedge, they react with the mantle rock and lower its melting temperature (e.g., Poli and Schmidt 1995) and the seismic velocity. In the case of Central Java, the ascent of fluids and partial melts is not vertical but inclined to the north. At the base of the crust at a depth of ~ 38 km (Wölbner and Rumpker 2016), a remarkable large negative velocity anomaly was detected by tomographic imaging, hinting at a large amount of partially molten rock and volatiles. Volcanoes at the surface in Central Java are located at the boundary of this anomaly. As suggested by Shapiro and Koulakov (2015), the continental crust may become a barrier for magmas from the mantle. Magma may ascend through the lower mafic crust but cannot propagate further into the upper felsic crust because of insufficient buoyancy. The low-velocity anomaly at ~ 20 km depth, which is separated from anomalies in the upper crust, may represent the top of the mafic magma pathway at the boundary between the lower and upper crust. Meanwhile, volatiles may continue to rise, providing substantial heat, partial melts and fluids from the mantle wedge, and may cause crustal assimilation in the upper crust (e.g., Deegan et al. 2023, Chap. 10). Fluids and partially molten material are inferred to form a complex system of reservoirs that feed Merapi's eruptions, as imaged by V_p/V_s ratio anomalies at depths <4 km and between 10 and 20 km. This derived geophysical image of the plumbing system of Merapi, with three main reservoirs along the magma ascent path is still simplified but consistent with petrological findings recorded in minerals as well as plutonic and crustal inclusions for the same depth ranges (Troll and Deegan 2023, Chap. 8) that also suggest the presence of significant portions of crystal mush.

For the Merapi edifice, a surprising result has been that seismic signals are affected by a strong

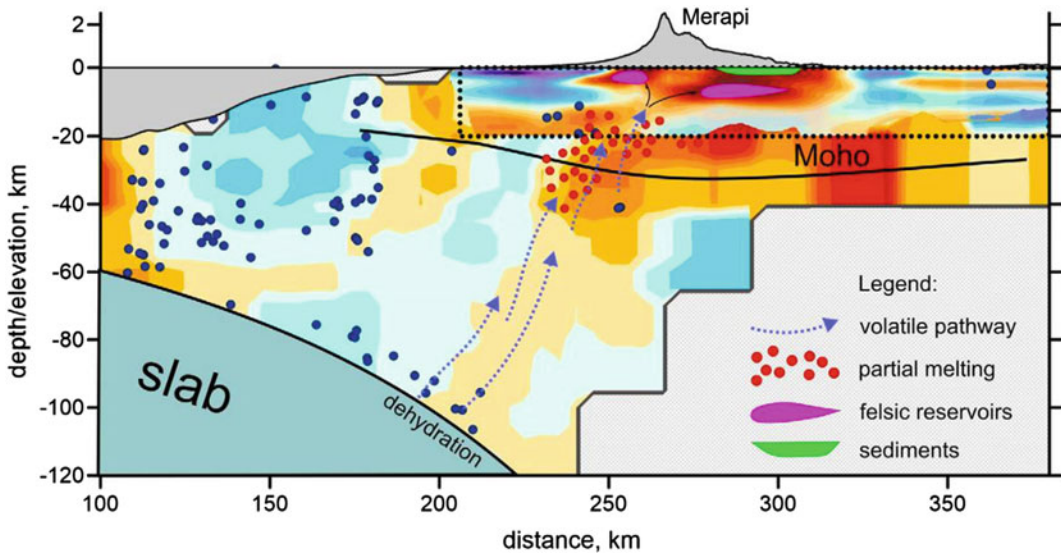


Fig. 5.10 Overlapped results of the LET and ANT models in a vertical section, as shown in Fig. 5.9d, and possible interpretation. Exaggerated topography is shown for positive altitudes. The Moho interface is schematically

indicated according to Wölbern and Rümpler (2016). Blue dots are earthquakes. The grey area depicts the subducting slab (after Koulakov et al. 2016)

scattering effect, caused by the heterogeneous construction of such a volcano. At Merapi, the mean free pathway for higher frequent signals is statistically only 100 m. This means that a generated signal will be affected by multiple scattering after travelling a distance of 100 m and, particularly, that the first onset amplitude is fading. Before the recent findings, seismic signals such as multiphase events were commonly explained by a complex seismic source mechanism of these volcanic earthquakes. However, as a result of this recent work, an alternative model has been established, highlighting those complex signals of volcanic earthquakes can also be explained by multiple scattering effects on their path within a stratovolcano. This effect on seismic waves is probably valid for many similar active volcanoes at subduction zones elsewhere. Moreover, inside this uppermost part of the Merapi edifice, a hydrothermal zone could be detected that surrounds the shallow volcanic conduit. The permeability of this zone up to the summit lava dome is not constant in time as recently shown by Heap et al. (2019). Highly mineralised fluids and gases that pass through

this zone lead to precipitation of sulphur and other minerals in pores and fractures that reduce the permeability of the host rock. This may result in a pressure increase in the conduit system with important implications for the eruptive activity and hazard assessment.

Acknowledgements The authors are grateful to get support for the different research projects by many colleagues and institutions. Funding was provided by the German Science Foundation (DFG), GeoForschungsZentrum Potsdam (GFZ) and the Volcanological Survey of Indonesia (VSI). Support by UNESCO, Deutsche Gesellschaft für Technische Zusammenarbeit (GTZ) and the International Bureau of German Federal Ministry for Education and Research (BMBF) is gratefully acknowledged. For scientific and logistical support, we are very grateful to our Indonesian partners from the former VSI in Bandung, Badan Meteorologi Klimatologi dan Geofisika (BMKG) in Jakarta, Gadjah Mada University (UGM) in Yogyakarta and the Institut Teknologi Bandung (ITB) in Bandung. Without the enthusiastic help of the Indonesian students these projects could not have been realised. We are also thankful that Ivan Kulakov could be supported by the RSF Grant #20-17-00075. Last but not least, the authors would like to thank the reviewers, especially Ralf Gertisser, Valentin Troll, Thomas Walter and Sri Widiyantoro. Their valuable help and guidance improved the quality of this chapter enormously.

References

- Beauducel F, Cornet FH (1999) Collection and three-dimensional modeling of GPS and tilt data at Merapi volcano. *Java. J Geophys Res* 104(B1):725–736
- van Bemmelen RW (1949) *The geology of Indonesia*, vol 1A. General Geology, Government Printing Office, The Hague, p 732
- Blythe LS, Deegan FM, Fred C, Jolis RM, Masotta M, Misiti V, Taddeucci J, Troll VR (2015) CO₂ bubble generation and migration during magma–carbonate interaction. *Contrib Mineral Petrol* 169:42
- Bohm M, Asch G, Fauzi F, Flüh ER, Brotopuspito KS, Kopp H, Luehr B-G, Puspito NT, Ratdomopurbo A, Rabbel W, Wagner D, MERAMEX Research Group (2005) The MERAMEX project—a seismological network in Central Java, Indonesia. *GEOTECHNOLOGIEN Science Report 5*, ‘Continental Margins—Earth’s Focal Points of Usage and Hazard Potential’, Potsdam, Germany
- Bolfan-Casanova N (2007) Fuel for plate tectonics. *Science* 315:338–339
- Budi-Santoso A, Beauducel F, Nandaka IGMA, Humaida H, Costa F, Widiwijayanti C, Iguchi M, Métaxian J-P, Rudianto I, Rozin M, Sulistiyani, Nurdin I, Kelfoun K, Byrdina S, Pinel V, Fahmi AA, Laurin A, Rizal MH, Dahamna N (2023) The Merapi volcano monitoring system. In: Gertisser R, Troll VR, Walter TR, Nandaka IGMA, Ratdomopurbo A (eds) *Merapi volcano—geology, eruptive activity, and monitoring of a high-risk volcano*. Springer, Berlin, Heidelberg, pp 409–436
- Budi-Santoso A, Lesage P (2016) Velocity variations associated with the large 2010 eruption of Merapi volcano, Java, retrieved from seismic multiplets and ambient noise cross-correlation. *Geophys J Int* 206:221–240
- Byrdina S, Friedel S, Vandemeulebrouck J, Budi-Santoso A, Suhari SW, Rizal MH, Winata E, Kusdaryanto (2017) Geophysical image of the hydrothermal system of Merapi volcano. *J Volcanol Geotherm Res* 329:30–40
- Chadwick JP, Troll VR, Ginibre C, Morgan D, Gertisser R, Waight TE, Davidson JP (2007) Carbonate assimilation at Merapi volcano, Java, Indonesia: insight from crystal isotope stratigraphy. *J Petrol* 48:1793–1812
- Chadwick JP, Troll VR, Waight TE, van der Zwan FM, Schwarzkopf LM (2013) Petrology and geochemistry of igneous inclusions in recent Merapi deposits: a window into the sub-volcanic plumbing system. *Contrib Mineral Petrol* 165:259–282
- Chesner CA, Rose WI (1991) Stratigraphy of the Toba Tuffs and the evolution of the Toba Caldera Complex, Sumatra, Indonesia. *Bull Volcanol* 53:343–356
- Commer M, Helwig SL, Hördt A, Tezkan B (2005) Interpretation of long-offset TEM data from Mount Merapi (Indonesia) using a 3D optimization approach. *J Geophys Res* 110:B03207
- Commer M, Helwig SL, Hördt A, Scholl TB (2006) New results on the resistivity structure of Merapi Volcano (Indonesia), derived from 3D restricted inversion of long-offset transient electromagnetic data. *Geophys J Int* 167:1172–1187
- Cooper GF, Macpherson CG, Blundy JD, Maunder B, Allen RW, Goes S, Collier JS, Bie L, Harmon N, Hicks SP, Iveson AA, Prytulak J, Rietbrock A, Rychert CA, Davidson JP, The VoiLA Team (2020) Variable water input controls evolution of the Lesser Antilles volcanic arc. *Nature* 582:525–529
- Costa F, Andreatuti S, Bouvet de Maisonneuve C, Pallister J (2013) Petrological insights into the storage conditions, and magmatic processes that yielded the centennial 2010 Merapi explosive eruption. *J Volcanol Geotherm Res* 261:209–235
- Dainty AM, Toksöz MN (1981) Seismic codas on the earth and the moon: a comparison. *Phys Earth Planet Inter* 26(4):250–260
- Davey FJ, Ristau J (2011) Fore-arc mantle wedge seismicity under Northeast New Zealand. *Tectonophysics* 509:272–279
- Deegan FM, Troll VR, Freda C, Misiti V, Chadwick JP, McLeod CL, Davidson JP (2010) Magma-Carbonate Interaction Processes and Associated CO₂ Release at Merapi Volcano, Indonesia: insights from experimental petrology. *J Petrol* 51:1027–1051
- Deegan FM, Whitehouse MJ, Troll VR, Budd DA, Harris C, Geiger H, Hålenius U (2016) Pyroxene standards for SIMS oxygen isotope analysis and their application to Merapi volcano, Sunda Arc, Indonesia. *Chem Geol* 447:1–10
- Deegan FM, Troll VR, Gertisser R, Freda C (2023) Magma-carbonate interaction at Merapi volcano, Indonesia. In: Gertisser R, Troll VR, Walter TR, Nandaka IGMA, Ratdomopurbo A (eds) *Merapi volcano—geology, eruptive activity, and monitoring of a high-risk volcano*. Springer, Berlin, Heidelberg, pp 291–321
- Delcamp A, Wyk V, de Vries B, James MR (2008) The influence of edifice slope and substrata on volcano spreading. *J Volcanol Geotherm Res* 177:925–943
- Dzurisin D (2007) *Volcano deformation: new geodetic monitoring techniques*. Springer-Verlag, Berlin, Heidelberg
- Friedel S, Jacobs F, Flechsig C, Reißmann C, Brunner I (1998) Large-scale DC resistivity imaging at Merapi Volcano. *DGG-Mitt Spec Issue III(1998):35–40*
- Friedel S, Brunner I, Jacobs F, Rücker C (2000) New results from DC resistivity imaging along the flanks of Merapi volcano. *DGG-Mitt Spec Issue IV/2000:23–29*
- Gerstenecker C, Heinrich R, Jentzsch G, Kracke D, Läufer G, Suyanto I, Weise A (1998a) Microgravity at Merapi Volcano: Results of the first two Campaigns. *DGG-Mitt Spec Issue III(1998):61–64*
- Gerstenecker C, Läufer G, Snilil B, Wrobel B (1998b) Digital Elevation Models for Mount Merapi. *DGG-Mitteilungen, Special Issue III(1998):65–68*
- Gossler J, Kind R, Sobolev SV, Kämpf H, Wylegalla K, Stiller M, TOR Working Group (1999) Major crustal

- features from the Harz Mountains to the Baltic Shield derived from receiver functions. *Tectonophysics* 314 (1–3):321–333
- Gossler J (2000) Teleseismic observations at Merapi Volcano, Indonesia. *DGG-Mitt Spec Issue IV/2000*:17–22
- Halpaap F, Rondenay S, Perrin A, Goes S, Ottemöller L, Austrheim H, Shaw R, Eeken TH (2019) Earthquakes track subduction fluids from slab source to mantle wedge sink. *Sci Adv* 5(4):eaav7369
- Harijoko A, Marliyani GI, Wibowo HE, Freski YR, Handini E (2023) The geodynamic setting and geological context of Merapi volcano in Central Java, Indonesia. In: Gertisser R, Troll VR, Walter TR, Nandaka IGMA, Ratdomopurbo A (eds) Merapi volcano—geology, eruptive activity, and monitoring of a high-risk volcano. Springer, Berlin, Heidelberg, pp 89–109
- Heap MJ, Troll VR, Alexandra RL, Kushnir ARL, Gilg HA, Collinson ASD, Deegan FM, Darmawan H, Seraphine N, Neuberg J, Walter TR (2019) Hydrothermal alteration of andesitic lava domes can lead to explosive volcanic behaviour. *Nat Comms* 10:5063
- Hoffmann-Rothe A, Mueller A, Ritter O, Haak V (1998) Magnetotelluric Survey at Merapi Volcano and across Java, Indonesia. *DGG-Mitt Spec Issue III(1998)*:47–52
- International Seismological Centre (2001) On-line Bulletin. <https://doi.org/10.31905/D808B830>
- Jaxybulatov KNM, Shapiro M, Koulakov I, Mordret A, Landes M, Sens-Schoenfelder C (2014) A large magmatic sill complex beneath the Toba caldera. *Science* 346:617–619
- Kalscheuer T, Commer M, Helwig SL, Hördt A, Tezkan B (2007) Electromagnetic evidence for an ancient avalanche caldera rim on the south flank of Mount Merapi, Indonesia. *J Volcanol Geotherm Res* 162:81–97
- Kelfoun K (1999) Processus de croissance et de déstabilisation des dômes de lave du volcan Merapi (Java centrale, Indonésie): Modélisations numériques des dômes, dynamique des écoulements pyroclastiques associés et surveillance par stéréo-photogrammétrie. PhD Thesis, Université Blaise Pascal Clermont-Ferrand II, Clermont-Ferrand, France
- Keller GV (1988) Rock and mineral properties. In: Nabighian MC (ed) *Electromagnetic methods in applied geophysics: vol 1, Theory*. Society of exploration geophysicists, pp 13–52
- Kennett BLN, Engdahl ER, Buland R (1995) Constraints on seismic velocities in the Earth from traveltimes. *Geophys J Int* 122:108–124
- Koulakov I, Sobolev SV, Asch G (2005) P- and S-velocity images of the lithosphere asthenosphere system in the Central Andes from local-source tomographic inversion. *Geophys J Int* 167:106–126
- Koulakov I, Bohm M, Asch G, Luehr B-G, Manzanares A, Brotospuspito KS, Fauzi PMA, Puspito NT, Ratdomopurbo A, Kopp H, Rabbel W (2007) P and S velocity structure of the crust and the upper mantle beneath central Java from local tomography inversion. *J Geophys Res* 112:B08310
- Koulakov I, Yudistira T, Luehr B-G, Wandono (2009) P, S velocity and VP/VS ratio beneath the Toba caldera complex (Northern Sumatra) from local earthquake tomography. *Geophys J Int* 177:1121–1139
- Koulakov I, Jakovlev A, Luehr B-G (2009) Anisotropic structure beneath central Java from local earthquake tomography. *Geochem Geophys Geosyst* 10:Q02011
- Koulakov I, Gordeev EI, Dobretsov NL, Vernikovskiy VA, Senyukov S, Jakovlev A (2011) Feeding volcanoes of the Kluchevskoy group from the results of local earthquake tomography. *Geophys Res Lett* 38:L09305
- Koulakov I, Maksotova G, Jaxybulatov K, Kasatkina E, Shapiro NM, Luehr B-G, El Khrepy S, Al-Arifi N (2016) Structure of magma reservoirs beneath Merapi and surrounding volcanic centers of Central Java modeled from ambient noise tomography. *Geochem Geophys Geosyst* 17:4195–4211
- Lloyd JW, Pim RH, Watkins MD, Suwara A (2007) The problems of groundwater assessment in the volcanic-sedimentary environment of Central Java. *Q J Eng Geol Hydrogeol* 18(1):47–61
- Luehr B-G, Maercklin N, Rabbel W, Wegler U (1998) Active Seismic Measurements at the Merapi Volcano, Java Indonesia. *DGG-Mitt Spec Issue III(1998)*:53–56
- Luehr B-G, Koulakov I, Rabbel W, Zschau J, Ratdomopurbo A, Brotospuspito KS, Fauzi P, Sahara DP (2013) Fluid ascent and magma storage beneath Gunung Merapi revealed by multiscale seismic imaging. *J Volcanol Geotherm Res* 261:7–19
- Maercklin NC, Riedel C, Rabbel W, Wegler U, Luehr B-G, Zschau J (2000) Structural Investigation of Mt. Merapi by an Active Seismic Experiment. *DGG-Mitt Spec Issue IV/2000*:13–16
- Maruyama S, Okamoto K (2007) Water transportation from the subducting slab into the mantle transition zone. *Gondwana Res* 11(1):148–165
- Mierdel K, Keppler H, Smyth JR, Langenhorst F (2007) Water solubility in aluminous orthopyroxene and the origin of Earth's asthenosphere. *Science* 315:364–368
- Müller A, Haak V (2004) 3-D modeling of the deep electrical conductivity of Merapi Volcano (Central Java): integrating magnetotellurics, induction vectors and the effects of steep topography. *J Volcanol Geotherm Res* 138:205–222
- Müller M, Hördt A, Neubauer FM (1998) The LOTEM survey at Merapi Volcano 1998. *DGG-Mitt Spec Issue III/1998*:41–46
- Müller M, Hördt A, Neubauer FM (2002) Internal structure of Mount Merapi, Indonesia, derived from long-offset transient electromagnetic data. *J Geophys Res* 107(B9):ECV 2–1–ECV 2–14
- Müller M (2000) *Elektromagnetik an Vulkanen*. PhD Thesis, Universität zu Köln, Köln, Germany
- Nandaka IGMA (1999) Étude des déformations d'un volcan actif à dôme. Application au Merapi. DEA Report, Institut de Physique du Globe de Paris, France

- Paulatto M, Laigle M, Galve A, Charvis P, Sapin M, Bayrakci G, Evain M, Kopp H (2017) Dehydration of subducting slow-spread oceanic lithosphere in the Lesser Antilles. *Nat Comms* 8:15980
- Peacock SA (1990) Fluid processes in subduction zones. *Science* 248:329–337
- Peters STM, Troll VR, Weis FA, Dallai L, Chadwick JP, Schulz B (2017) Amphibole megacrysts as a probe into the deep plumbing system of Merapi volcano, Central Java Indonesia. *Contrib Mineral Petrol* 172:16
- Poli S, Schmidt MW (1995) H₂O transport and release in subduction zones: experimental constraints on basaltic and andesitic systems. *J Geophys Res* 100:22299–22314
- Preece K, Barclay J, Gertisser R, Herd RA (2013) Textural and micro-petrological variations in the eruptive products of the 2006 dome-forming eruption of Merapi volcano, Indonesia: implications for subsurface processes. *J Volcanol Geotherm Res* 261: 98–120
- Preece K, Gertisser R, Barclay J, Charbonnier SJ, Komorowski J-C, Herd RA (2016) Transitions between explosive and effusive phases during the cataclysmic 2010 eruption of Merapi volcano, Java, Indonesia. *Bull Volcanol* 78:54
- Purbawinata MA, Ratdomopurbo A, Sinulingga IK, Sumarti S, and Suharno (eds) (1997) Merapi Volcano—a guide book. *Volcanol Surv Indon*, Bandung, Indonesia, p 64
- Ratdomopurbo A, Poupinet G (1995) Monitoring temporal change of seismic velocity in a volcano: application to the 1992 eruption of Mt. Merapi (Indonesia). *Geophys Res Lett* 22(7):775–778
- Ratdomopurbo A (1995) Etude sismologique du volcan Merapi et formation du dome de 1994. Ph.D. Thesis Université Joseph Fourier, Grenoble, France
- Rebscher D, Westerhaus M, Körner A, Welle W, Nandaka GM (2000a) Monitoring ground deformation at the Decade Volcano Gunung Merapi Indonesia. *Phys Chem Earth Int* 25(9–11):755–757
- Rebscher D, Westerhaus M, Körner A, Welle W, Subandriyo, Brodscholl A, Kumpel H-J, Zschau J (2000b) Indonesian-German multiparameters stations at Merapi Volcano. *DGG-Mitt Spec Issue IV/2000b*:93–102
- Reichert C, Luehr B-G (2005) High risk volcanism at the active margin of the SUNDA ARC -BMBF GEOTECHNOLOGIEN Science Report 5, 'Continental Margins—Earth's Focal Points of Usage and Hazard Potential.' Potsdam, Germany
- Ritter O, Hoffmann-Rothe A, Müller A, Dwipa S, Arsadi E, Mahfi A, Nurnusanto I, Byrdina S, Echternacht F, Haak V (1998) A magnetotelluric profile across Central Java Indonesia. *Geophys Res Lett* 25 (23):4265–4268
- Sato Y (1978) Gravity and geological studies in Java, Indonesia. Geological survey of Indonesia and geological survey of Japan joint research program on regional tectonics of Southeast Asia. Geological Survey of Indonesia, p 207
- Satyana AH, Asnidar (2008) Mud diapirs and mud volcanoes in depressions of Java to Madura: origins, nature, and implications to petroleum system. In: Proceedings of the 32nd annual convention and exhibition of the Indonesian petroleum association, IPA08-G-139
- Schurr B, Asch G, Rietbrock A, Trumbull R, Haberland C (2003) Complex patterns of fluid and melt transport in the central Andean subduction zone revealed by attenuation tomography. *Earth Planet Sci Lett* 215:105–119
- Shapiro NM, Koulakov IY (2015) Probing the underbelly of a supervolcano. *Science* 348:758–759
- Smith WHF, Sandwell DT (1997) Global seafloor topography from satellite altimetry and ship depth soundings. *Science* 277:1957–1962
- Strack K-M (1992) Exploration with deep transient electromagnetics (Methods in Geochemistry and Geophysics). Elsevier Science Ltd, p 374
- Subandriyo, Purbawinata MA, Igushi M, Ishihara K, Young KD, Voight B (1997) Characteristics of tilt changes associated with Merapi during the 1993–1997 eruption. Abstracts—Merapi Decade Volcano international workshop II, Yogyakarta, Indonesia, p 18
- Surono JP, Pallister J, Boichu M, Buongiorno MF, Budisantoso A, Costa F, Andreastuti S, Prata F, Schneider D, Clarisse L, Humaida H, Sumarti S, Chr B, Griswold J, Carn S, Oppenheimer C, Lavigne F (2012) The 2010 explosive eruption of Java's Merapi volcano—a '100-year' event. *J Volcanol Geotherm Res* 241–242:121–135
- Syracuse EM, Abers GA (2006) Global compilation of variations in slab depth beneath arc volcanoes and implications. *Geochem Geophys Geosyst* 7(5): Q05017
- Telford WM, Geldart LP, Sheriff RE (1990) Applied Geophysics (2nd edn), Cambridge University Press, p 770
- Tiede C, Camacho AG, Gerstenecker C, Fernandez J, Suyanto I (2005) Modeling the density at Merapi volcano area, Indonesia, via the inverse gravimetric problem. *Geochem Geophys Geosyst* 6(9):Q09011
- Toutain J, Sortino F, Baubron J, Richon P, Surono SS, Nonell A (2009) Structure and CO₂ budget of Merapi volcano during inter-eruptive periods. *Bull Volcanol* 71:815–826
- Troll VR, Hilton DR, Jolis EM, Chadwick JP, Blythe LS, Deegan FM, Schwarzkopf LM, Zimmer M (2012) Crustal CO₂ liberation during the 2006 eruption and earthquake events at Merapi volcano Indonesia. *Geophys Res Lett* 39:L11302
- Troll VR, Deegan FM (2023) The magma plumbing system of Merapi: The petrological perspective. In: Gertisser R, Troll VR, Walter TR, Nandaka IGMA, Ratdomopurbo A (eds) Merapi volcano—geology, eruptive activity, and monitoring of a high-risk volcano. Springer, Berlin, Heidelberg, pp 233–263
- Vozoff K (1991) The magnetotelluric method. In: Nabighian MN (ed) Electromagnetic methods in

- applied geophysics, vol 22, pp 1943–1961. <https://doi.org/10.1190/1.9781560802686.ch8>
- Wagner D, Koulakov I, Rabbel W, Luehr B-G, Wittwer A, Kopp H, Bohm M, Asch G MERAMEx Scientists (2007a) Joint inversion of active and passive seismic data in Central Java. *Geophys J Int* 170(2):923–932
- Wagner D, Rabbel W, Luehr B-G, Wassermann J, Walter TR, Kopp H, Koulakov I, Wittwer A, Bohm M, Asch G, the MERAMEx Scientists (2007b) Seismic structure of Central Java. In: Karnawati D, Pramumijoyo S, Anderson R, Husein S (eds) *The Yogyakarta Earthquake of May 27, 2006*. Star Publishing Company, Belmont, California, pp 1–2
- Walter TR, Wang R, Luehr B-G, Wassermann J, Behr Y, Parolai S, Anggraini A, Günther E, Sobiesiak M, Grosser H, Wetzler H-U, Milkereit C, Brotopuspito KS, Harjadi P, Zschau J (2008) The 26 May 2006 magnitude 6.4 Yogyakarta earthquake south of Mt. Merapi volcano: did lahar deposits amplify ground shaking and thus lead to the disaster? *Geochem Geophys Geosyst* 9(5):Q05006
- Waltham D, Hall R, Smyth HR, Ebinger CJ (2008) Basin formation by volcanic-arc loading. *Geol. Soc Am Spec Paper* 436:11–26
- Wegler U (2003) Analysis of multiple scattering at Vesuvius volcano, Italy, using data of the TomoVes active seismic experiment. *J Volcanol Geotherm Res* 128(1–3):45–63
- Wegler U, Luehr B-G (2001a) Scattering behaviour at Merapi volcano (Java) revealed from an active seismic experiment. *Geophys J Int* 145:579–592
- Wegler U, Luehr B-G, Ratdomopurbo A (1999) A repeatable seismic source for tomography of volcanoes. *Ann Geofis* 42(3):565–571
- Wegler U, Luehr B-G (2001b) Multiple scattering of seismic signals at Merapi Volcano (Java, Indonesia)—results of an active seismic experiment (extended abstract). *Tohoku Geophys J (Sci Rep Tohoku Univ Ser 5)* 36:295–296
- Wegler U, Luehr BG, Zschau J, Maercklin N, Riedel C, Rabbel W (2000) Multiple seismic scattering effect at Mount Merapi - active seismic measurements help to explain complex earthquake signals of a strato volcano. *DGG-Mitt Spec Issue IV/2000*:43–48
- Westerhaus M, Rebscher D, Welle W, Brodscholl A, Pfaff A, Körner A, Nandaka GM (1998) Deformation measurements at the Flanks of Merapi Volcano. *DGG-Mitt Spec Issue III(1998)*:93–99
- Whitley S, Halama R, Gertisser R, Preece K, Deegan FM, Troll VR (2020) Magmatic and metasomatic effects of magma-carbonate interaction recorded in calc-silicate xenoliths from Merapi volcano (Indonesia). *J Petrol* 61(4):egaa048
- Widiyantoro S, Ramdhan M, Métaixian J-P, Cummins PR, Martel C, Erdmann S, Nugraha AD, Budi-Santoso A, Laurin A, Fahmi AA (2018) Seismic imaging and petrology explain highly explosive eruptions of Merapi Volcano, Indonesia. *Sci Rep* 8:13656
- Wilson P, Rais J, Reigber C, Reinhart E, Ambrosius BAC, Le Pichon X, Kasser M, Suharto P, Dato' Abdul Majid, Dato' Paduka Awang Haji Othman Bin Haji Yaakub, Almeda R, Boonphakdee C (1998) Study provides data on active plate tectonics in southeast Asia region. Wilson, Patricia et al. "Study provides data on active plate tectonics in southeast Asia region. *Eos* 79:545–549
- Wittwer A (2010) Investigating the crustal and upper mantle structure of the central Java subduction zone with marine wide-angle seismic and gravity data. Ph.D. Thesis, Christian-Albrechts-Universität, Kiel, Germany
- Wölbner I, Rumpker G (2016) Crustal thickness beneath Central and East Java (Indonesia) inferred from P receiver functions. *J Asian Earth Sci* 115:69–79
- Young KD, Voight B, Subandriyo S, Miswanto CTJ (2000) Ground Deformation at Merapi Volcano, Java, Indonesia: distance changes, June 1988–October 1995. *J Volcanol Geotherm Res* 100(1–4):233–259
- Yuan X, Ni J, Kind R, Mechie J, Sandvol E (1997) Lithospheric and upper mantle structure of southern Tibet from a seismological passive source experiment. *J Geophys Res* 102:27491–27500
- Zimmer M, Erzinger J, Sulistiyo Y (2000) Continuous chromatographic gas measurements on Merapi volcano, Indonesia. *DGG-Mitt Spec Issue IV/2000*:87–91
- Zschau J, Sukhyar R, Purbawinata MA, Luehr B-G, Westerhaus M (2003) The Merapi-project—interdisciplinary monitoring of a high-risk volcano as a basis for an early warning system. In: Zschau J, Küppers A (eds) *Early warning systems for natural disaster reduction*. Springer, Berlin, Heidelberg, pp 527–532



Geological History, Chronology and Magmatic Evolution of Merapi

6

Ralf Gertisser, Mary-Ann del Marmol,
Christopher Newhall, Katie Preece,
Sylvain Charbonnier, Supriyati Andrestuti,
Heather Handley, and Jörg Keller

Abstract

This chapter provides a synthesis of the geological history, chronology and magmatic evolution of Merapi. Stratigraphic field and geochronological data are used to divide Merapi into three main evolutionary stages and associated volcanic edifices (Proto-, Old and New Merapi) and eight broad volcano-stratigraphic units to characterise the eruptive activity and structural evolution of the volcano through time. Complementary petrological, geochemical and isotopic data are used to characterise the eruptive products of Merapi and shed light on the geochemical evolution and petrogenetic processes. The data indicate that the eruptive products of Merapi are

mainly basaltic andesite of both medium-K and high-K type and support a two-stage petrogenetic model, where primary magmas are derived from a heterogeneous, Indian Ocean MORB-like mantle source metasomatised by slab-derived components. Subsequently, these magmas are modified during transfer through the crust by complex magmatic differentiation processes, including contamination by carbonate rocks of the local upper crust. The available data indicate that, since ~ 1900 ^{14}C y BP, the lavas and pyroclastic rocks of Merapi are essentially of the high-K type and that regular geochemical variations with systematic shifts in whole rock SiO_2 content occurred since at least the Late Holocene, although erupted magma

R. Gertisser (✉)
School of Geography, Geology and the
Environment, Keele University, Keele ST5 5BG,
UK
e-mail: r.gertisser@keele.ac.uk

M.-A. del Marmol
Department of Geology, Ghent University, 9000
Gent, Belgium

C. Newhall
Mirisbiris Garden and Nature Center, Sitio
Mirisbiris, 4508 Barangay Salvacion, Santo
Domingo, Albay, Philippines

K. Preece
Department of Geography, Swansea University,
Swansea SA2 8PP, UK

S. Charbonnier
School of Geosciences, University of South Florida,
Tampa, FL 33620-5201, USA

S. Andrestuti
Center for Volcanology and Geological Hazard
Mitigation, Geological Agency, Bandung 40122,
Indonesia

H. Handley
Department of Applied Earth Sciences, University of
Twente, 7514 AE Enschede, The Netherlands

School of Earth, Atmosphere and Environment, Monash
University, Clayton, VIC 3800, Australia

J. Keller
Institut für Geo- und Umweltwissenschaften,
Mineralogie-Petrologie, Albert-Ludwigs-Universität
Freiburg, 79104 Freiburg, Germany

compositions have remained broadly uniform since the mid-twentieth century.

Keywords

Merapi · Stratigraphy · Chronology · Petrology · Geochemistry · Isotope geochemistry · Petrogenesis · Magmatic evolution · Merapi-type volcanism

6.1 Introduction

Merapi, located 25–30 km north of the city of Yogyakarta in Central Java (Fig. 6.1), is one of Indonesia's most active and hazardous

volcanoes. Eruptions during the twentieth and early twenty-first century have mostly consisted of lava dome growth, typically lasting for weeks or months each time, and subsequent gravitational dome collapse to generate small volume pyroclastic density currents (PDCs) or block-and-ash flows, in the classic volcanological literature termed Merapi-type nuées ardentes. The well-recorded historical activity of Merapi (Voight et al. 2000 and references therein; Global Volcanism Program 2013), particularly since the late eighteenth century, indicates that eruptions have occurred every few years and have been dominated by effusive, lava dome-formation and intermittent short-lived explosive outbursts,

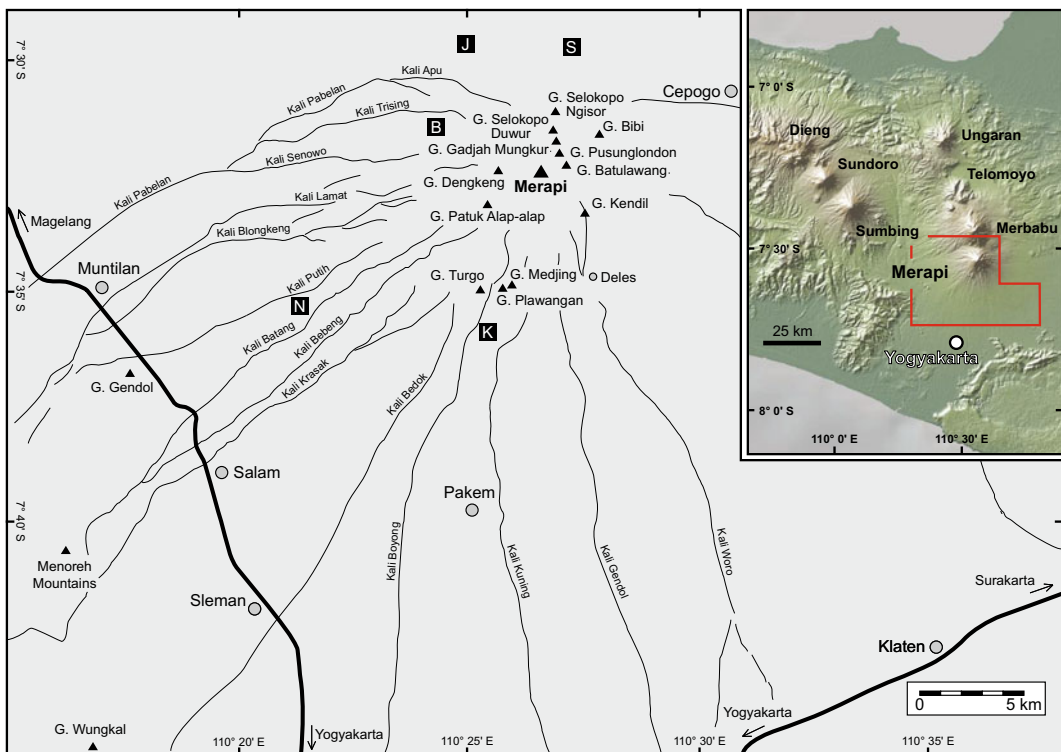


Fig. 6.1 Map of Merapi, showing locations referred to in the text. Major towns and villages are shown by filled circles, while volcano observation posts (K = Kaliurang; N = Ngepos; B = Babadan; J = Jrahah; S = Selo) are marked by black squares. The grey lines indicate main river valleys and the thick black lines show major roads.

The summit of Merapi and a series of hills (Indon. = Gunung (G.)) that rise from the volcanic complex or from the surrounding plain are indicated by black triangles. The three-dimensional inset map shows the location of Merapi north of the city of Yogyakarta and nearby Quaternary volcanoes in Central Java

producing PDCs. Stratigraphic and geochronological studies published since the 1980s have provided a detailed picture of Merapi's prehistoric activity, which was often explosive, as well as the overall structural and geological evolution of the volcanic complex. The results of these investigations, which built on earlier work of, for example, Kemmerling (1921), Hartmann (1935) and van Bemmelen (1949, 1956), are included in reports (e.g. Wirakusumah et al. 1980) and Ph.D. theses (Bahar 1984; del Marmol 1989; Berthommier 1990; Andreastuti 1999; Gertisser 2001), a collection of landmark papers published in a special issue 'Merapi volcano' of the *Journal of Volcanology and Geothermal Research* (Andreastuti et al. 2000; Camus et al. 2000; Newhall et al. 2000) and subsequent studies (e.g. Gertisser and Keller 2003a; Gertisser et al. 2012a; Bronto et al. 2014; Selles et al. 2015). A 1:50,000 geological map of Merapi was published by Wirakusumah et al. (1989). Complementary petrological, geochemical and isotopic studies of the eruptive products of Merapi have shed light on magma generation in the mantle wedge above the subducting Indo-Australian plate, magma storage and magmatic differentiation processes in the arc crust, and the magmatic evolution of Merapi in space and time. Such studies either focused on Merapi itself (e.g. Kerinec 1982; Bahar 1984; Luais 1986; del Marmol 1989; Berthommier 1990; Andreastuti 1999; Andreastuti et al. 2000; Camus et al. 2000; Newhall et al. 2000; Gertisser 2001; Gertisser and Keller 2003a, b; Gertisser et al. 2012a; Chadwick et al. 2013; Costa et al. 2013; Troll et al. 2013a; Deegan et al. 2016; Handley et al. 2018), or used rock samples from Merapi and other Indonesian volcanoes to discuss magma genesis on an arc-wide scale or in the global context of subduction zone magmatism (e.g. Whitford 1975a, b; Whitford and Nicholls 1976; Whitford et al. 1979, 1981; White and Patchett 1984; McDermott and Hawkesworth 1991; Turner and Foden 2001; Woodhead et al. 2001; Debaille et al. 2006; Handley et al. 2011, 2014; Deegan et al. 2021).

This chapter provides a synthesis of the geological history, chronology and magmatic evolution of Merapi, and discusses the underlying petrogenetic processes. Following a description of the geological evolution of Merapi, the compositional variations of the eruptive products are presented, including petrographical and mineral chemical information, major and trace element geochemistry as well radiogenic (Sr, Nd, Pb, Hf), stable (O) and uranium-series isotopic compositions of samples that span the entire geological history of the volcanic complex. The available petrological, geochemical and isotopic data are then placed into a stratigraphic framework, linked to the major evolutionary stages and associated edifices of the volcanic complex, to discuss the processes of magma genesis and magmatic differentiation at Merapi, and the geochemical variations through time.

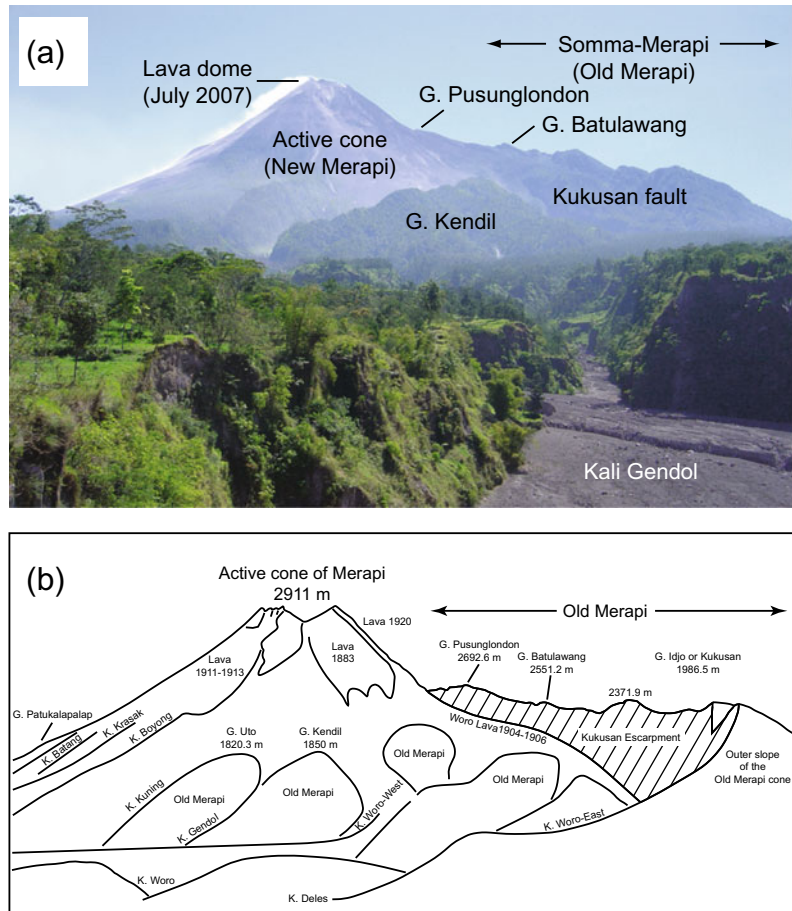
6.2 Geological Evolution of Merapi

6.2.1 Previous Research and the Development of Ideas

6.2.1.1 Early Work

Merapi is a volcanic complex consisting of an active stratocone which has grown on top of the remains of an older volcanic edifice, a structure mentioned by Kemmerling (1921) and Hartmann (1935), and elaborated upon by van Bemmelen (1949, 1956) (Fig. 6.2). Based on an idea first articulated by Ijzerman (1891) and Scheltema (1912), van Hinloopen Labberton (1921) advocated that a devastating eruption of Merapi in AD 1006 turned the surrounding area into a wasteland, buried the great temples of Borobudur, Mendut and Prambanan, and destabilised the Mataram Kingdom, a prosperous Hindu State in Central Java, forcing its migration to East Java. Both Hartmann (1935) and van Bemmelen (1949, 1956) expanded upon the idea of a major eruption of Merapi in AD 1006 and its effects on

Fig. 6.2 **a** View of the Merapi volcanic complex from the south, with the active cone of Merapi (New Merapi) on the left in the picture and Somma-Merapi, the remnants of Old Merapi, on the right (eastern) side. The Gendol river valley (Kali Gendol), filled with block-and-ash flow deposits from the 2006 eruption, is in the foreground. **b** Redrawing of the original sketch of van Bemmelen made at Deles, illustrating the morphology and structure of Merapi (after van Bemmelen 1956)



the structure of the volcano. Hartmann (1935) speculated that the oldest known crater (depression) of Merapi with a diameter of 3.5 km was a result of this eruption, while van Bemmelen (1949, 1956) suggested that the “cataclysmic outburst” led to the collapse of the western side of the old Merapi edifice along a major fault zone, known as the Kukusan fault, leaving a horseshoe-shaped crater or Somma rim on the northern and eastern flanks. In this context, Gunung (Indon. = hill or mountain) Gendol and nearby Gunung Sari, Gunung Ukir and several other hills located ~ 20 km west-southwest of Merapi, known collectively as the Gendol Hills, were interpreted as folded units of the older edifice, formed during the gravitational collapse of Merapi’s western flank and the buttressing effect of the Menoreh Mountains further

west (Fig. 6.3). The active Merapi cone started to grow soon after the assumed paroxysmal eruption in AD 1006 (Hartmann 1935; van Bemmelen 1949, 1956).

6.2.1.2 Research from 1980 to 2000

Since the early work of Kemmerling, Hartmann and van Bemmelen, more recent studies have built upon the idea of an Old and New Merapi, although the views are somewhat conflicting (Fig. 6.4). Hartmann’s and van Bemmelen’s catastrophic eruption in AD 1006 has been disputed by subsequent authors who have not found evidence for a catastrophic eruption of Merapi in AD 1006, even though this date has become deeply engraved in the literature. Consequently, the exact timing and process of what, in modern volcanology, is called a sector collapse or debris

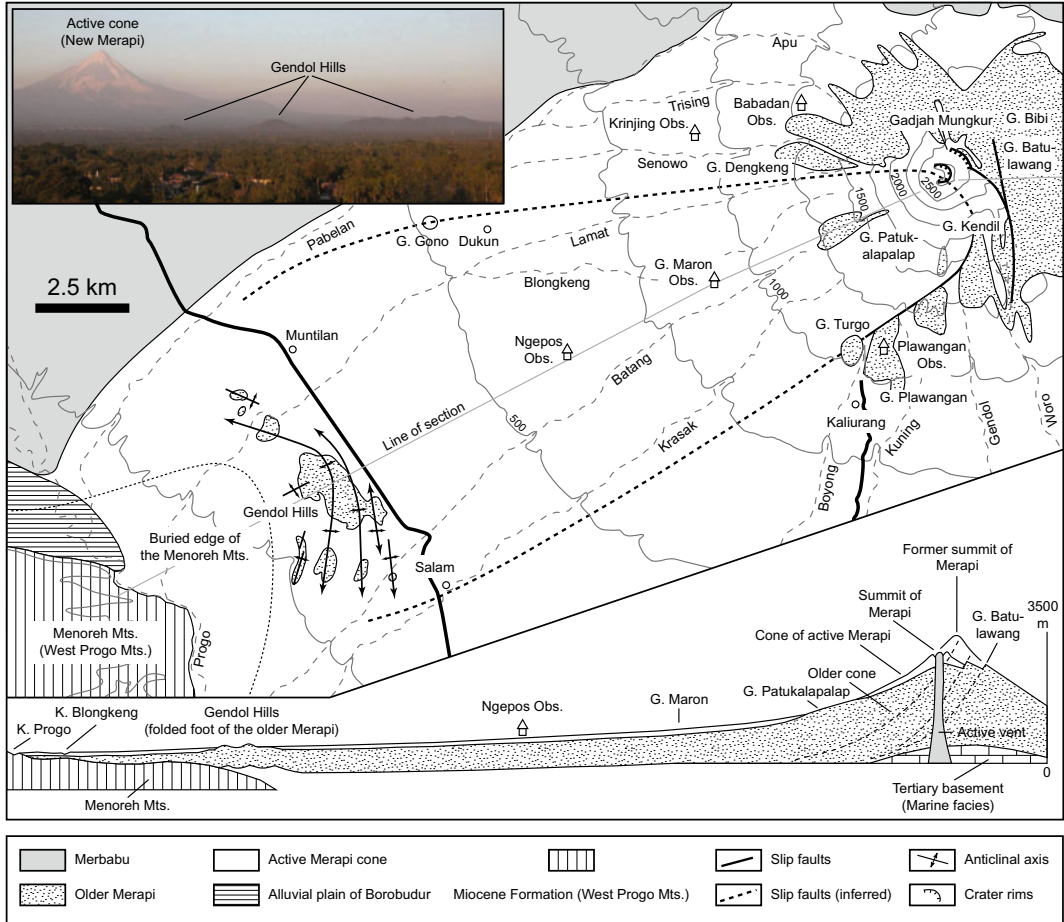


Fig. 6.3 Volcano-tectonic sketch map of Merapi and cross section through the western sector and foot of the volcanic edifice (after van Bemmelen 1949, 1956). The inset shows a field photograph of the Gendol Hills ~ 20

km west-southwest of Merapi, as seen from Candi (Indon. = temple) Borobudur. The active cone of Merapi can be seen in the background

avalanche failure of Old Merapi has remained controversial; an important new contribution by Bronto and co-workers is included in this volume (Bronto et al. 2023, Chap. 7). Additional details of the overall geological evolution of Merapi and its eruptive history, particularly over the past few millennia, have emerged from detailed field investigations. Considerable advances were made in the 1990s, when the volcano was designated a ‘Decade Volcano’ by the International Association of Volcanology and Chemistry of the Earth’s Interior (IAVCEI) as part of the United Nations’ International Decade for Natural Disaster Reduction.

The Ph.D. thesis of Bahar (1984) presented the geochemical compositions and stratigraphic relationships of the lava sequences of Merapi, distinguishing, based on the broad stratigraphic framework established by van Bemmelen (1949) and Wirakusumah et al. (1980), the ancient lavas of Gunung Plawangan that were followed by the units of Gunung Turgo and the parasitic cones of Gunung Bibi and Gunung Patuk Alap-alap, the younger lavas of the Batulawang Series, the recent and modern lavas of the Kali (Indon. = river) Kuning and Kali Selokopo Series (AD 1006–AD 1888), and those of the summit area (AD 1888–Present).

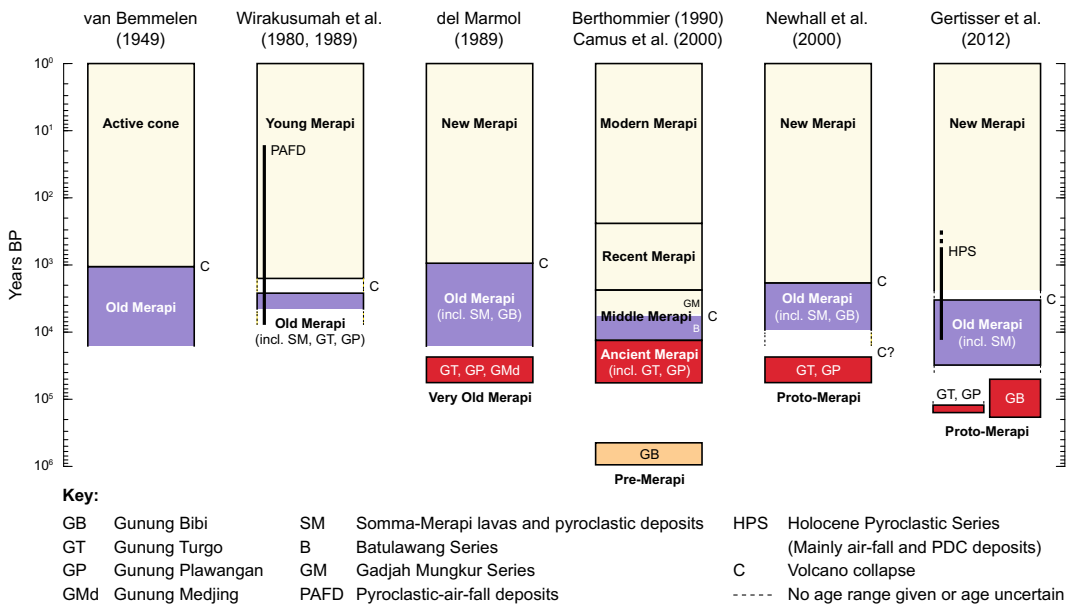


Fig. 6.4 Different interpretations of the stratigraphy and chronology of Merapi. Where available, the analytical uncertainty of the published dates was considered when

compiling the figure. A logarithmic time scale was chosen for clarity of presentation

Djumarma et al. (1986) quoted newly available archaeological evidence suggesting that the Mataram Kingdom left Central Java several decades earlier (i.e. in AD 928 or 929) than proposed by van Bemmelen (1949, 1956) and earlier studies. However, the authors did not find archaeological indications for a catastrophic, Somma rim-forming eruption of Merapi in either AD 928-929 or AD 1006, and argued that “the eruption of 1006 A.D. is a classic example of a reasonable speculation that has been transformed into a fact by uncritical repetition”. Instead, the authors suggested that the climactic eruption of the pre-Somma or Old Merapi according to van Bemmelen (1949, 1956) might have occurred up to three centuries before AD 1006, although no direct evidence was found for a westward directed landslide from Merapi and for a link between this eruption and the depopulation of the Mataram Kingdom of Central Java.

A key development in the history of geological research on Merapi was the publication of a 1:50,000 geological map of the volcano and preliminary radiocarbon dates by Wirakusumah

et al. (1989). Based on the earlier work of Wirakusumah et al. (1980), the geological map—a simplified version of which is shown in Fig. 6.5—identifies an Old Merapi and a Young Merapi edifice, as recognised by Kemmerling (1921), Hartmann (1935) and van Bemmelen (1949, 1956). Within Old Merapi, the authors distinguish the older lavas of Gunung Turgu, Gunung Plawangan and Gunung Bibi (their MI 1 lavas) from those that constitute the Somma-Merapi in the northern and eastern parts of the volcanic complex (their MI 2 lavas). Prehistoric lavas and those that erupted since AD 1888 (their MI 3 and MI 4 lavas, respectively) comprise Young Merapi. Based on the few available radiocarbon dates at the time, pyroclastic and lahar deposits on the slopes of Merapi dated back to ~ 4350 ^{14}C y BP. These deposits were produced by eruptions from both Old Merapi and Young Merapi, the transition of which was inferred to have occurred between ~ 2870 and 1700 ^{14}C y BP. The pronounced NE-SW curved escarpment at Merapi, shown as a tectonic (normal) fault on the geological map of Yogyakarta (Rahardjo et al.

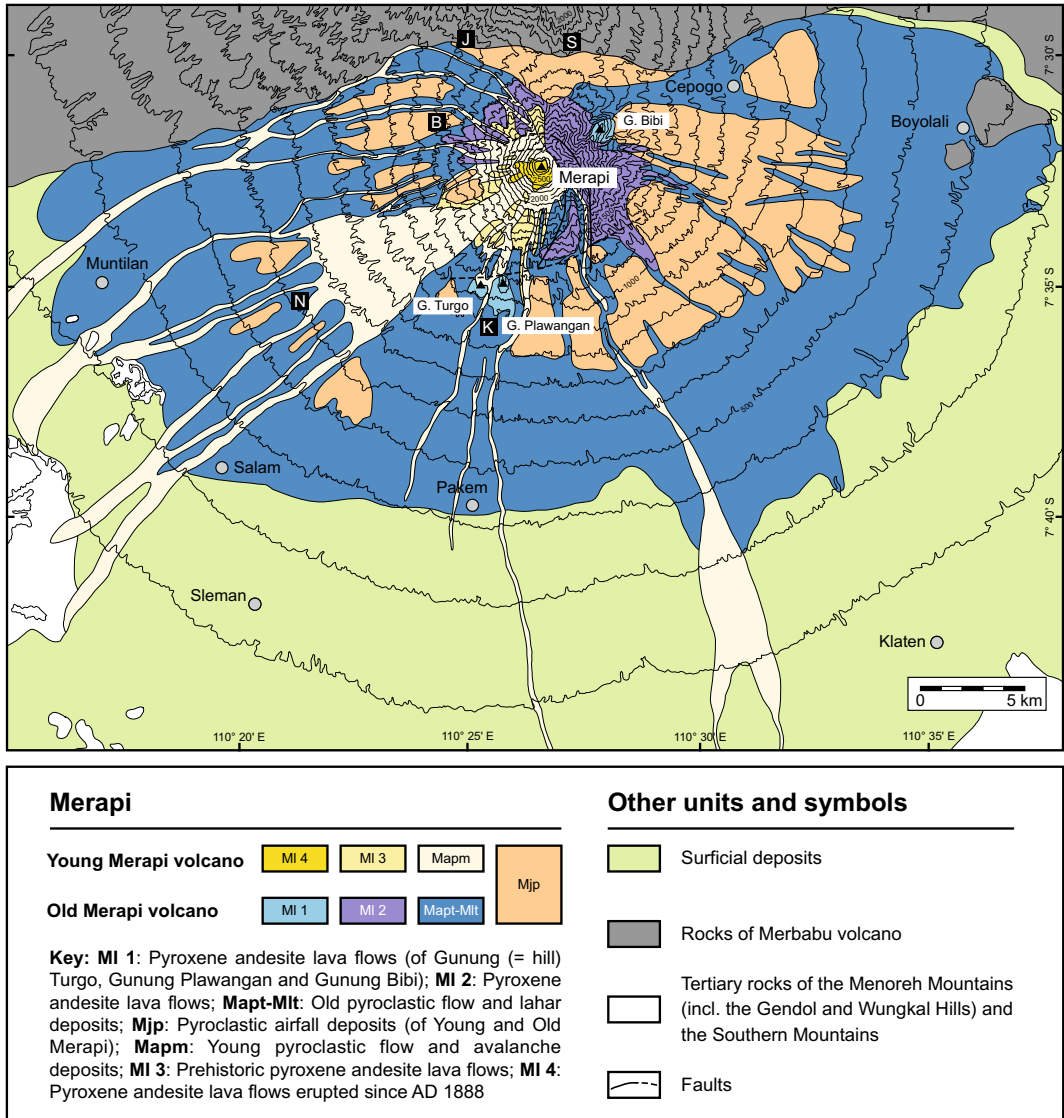


Fig. 6.5 Simplified version of the 1:50,000 geological map of Merapi published in 1989 (Wirakusumah et al. 1989), using the original terminology for the two major volcanic edifices distinguished and for the volcanic products of the different geological units. Some of the

original subdivisions were combined for clarity of presentation. Contours are shown in 100 m intervals. Other map symbols as in Fig. 6.1 (after Gertisser et al. 2012a)

1977), is marked as the Kukusan fault on the map of Wirakusumah et al. (1989).

Also in 1989, the Ph.D. thesis of del Marmol provided further detailed insights into the geology and petrology of Merapi, in particular its lavas. Like previous authors, del Marmol (1989) used the terms Old Merapi and New Merapi to

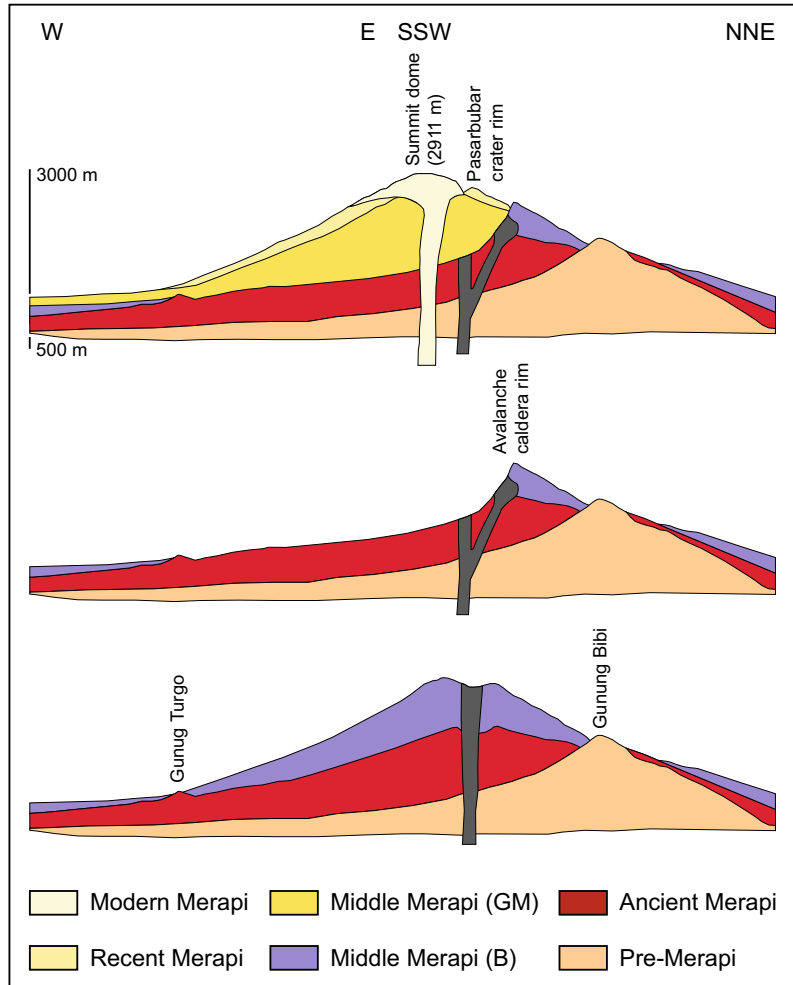
refer to the Somma-Merapi edifice and the active or young Merapi cone, respectively (Fig. 6.4). The author considered the rocks that were deposited before the inferred catastrophic sector collapse of the Somma-Merapi edifice, assumed to have occurred in AD 928, as part of Old Merapi with an ancestral part, referred to as Very

Old Merapi, and those that erupted afterwards as part of New Merapi. Very Old Merapi, according to del Marmol (1989), consists of Gunung Turgo and Gunung Plawangan, two steep-sided hills on Merapi's southern flank rising above the villages of Turgo and Kaliurang, as well as the lower part of Gunung Medjing (Figs. 6.1 and 6.4). Composite stratigraphic sections of the Somma-Merapi edifice, constructed by C. Newhall and co-authors and included in del Marmol (1989), were the first detailed descriptions of the explosive eruptive activity of Old Merapi, with representative sections in the Candi (Indon. = temple) Duwur and Candi Lumbung area as well as at Gunung Turgo-Kali Tritis. The lavas and pyroclastic deposits of the Batulawang Formation, as described by Bahar (1984), make up the main part of Old Merapi (del Marmol 1989). These were followed, in different sectors of the volcano, by the Selokopo, Gunung Gajah Munkur, Gunung Pusonglondon and Djengger Series, which were also thought to be from Old Merapi. According to del Marmol (1989), Gunung Bibi, a distinct hill situated on the northeast flank of Merapi, belongs to the Old Merapi stage or Somma-Merapi edifice, although an older age was not ruled out. Following the catastrophic eruption, New Merapi developed, consisting of the Kali Kuning Formation, the most recent eruptive products in the southwestern sector, and the lava dome complex (<AD 1883) of the summit area.

The Ph.D. thesis of Berthommier (1990), much of which formed the basis for a paper by Camus et al. (2000), presented a geological history of Merapi, supported by a few radiocarbon and U-Th disequilibrium ages, as well as a single $^{40}\text{K}/^{40}\text{Ar}$ age, and complemented by whole-rock and mineral chemical data. The thesis, as well as Camus et al. (2000), divided Merapi into four evolutionary stages (Ancient, Middle, Recent and Modern Merapi) and an older (pre-Merapi) volcanic structure (Fig. 6.4). Based on a $^{40}\text{K}/^{40}\text{Ar}$ date of 670 ± 250 ka, Gunung Bibi was attributed to remnants of a pre-Merapi structure. Ancient Merapi (40–14 ka) comprises Gunung Turgo and Gunung Plawangan, interpreted as parasitic structures, as well as the oldest

deposits of the Merapi cone *sensu stricto* (Fig. 6.6). Thus, Ancient Merapi corresponds to the Very Old Merapi or Proto-Merapi as well as part of the Old Merapi cone in the sense of van Bemmelen (1949, 1956) and del Marmol (1989). Middle Merapi (14.0–2.2 ka) consists of two thick andesitic lava sequences, namely the Batulawang Series, dated at ~ 6.7 ka using U-Th disequilibria, and the Gajah Mungkur Series, which comprises the lava sequences of Gunung Pusonglondon, Gunung Gajah Mungkur and Gunung Selokopo near the present-day summit of Merapi. Berthommier (1990) and Camus et al. (2000) postulated that during the time of Middle Merapi, a Mount St. Helens-type edifice collapse occurred between ~ 6.7 ka and 2200 ± 160 ^{14}C y BP, the oldest age obtained for pyroclastic deposits attributed to Recent Merapi (Fig. 6.6). They outlined an avalanche caldera open to the west and slightly wider than proposed by van Bemmelen (1949, 1956), with a northern limit that follows roughly the Senowo river valley and the Kukusan fault as the southern extension (cf. Figs. 6.1 and 6.3). Moreover, they interpreted the Gendol Hills as hummocks of a debris-avalanche deposit resulting from the inferred sector collapse, protruding from younger volcanoclastic deposits. A conspicuous, widespread and topography-controlled pyroclastic unit, consisting of a basal layer with moulds of bamboo, a middle layer with normal grading and tractional features and an upper layer of coarse grained, partly cross-bedded ash, was interpreted as a violent PDC or blast deposit emplaced at low temperature. Recent Merapi (2220 ± 160 ^{14}C years BP to AD 1786) and Modern Merapi (since AD 1786) overlie the lava sequences of Middle Merapi and are the main units that constitute the active Merapi cone or New Merapi (Fig. 6.6). Recent Merapi consists of lava flows and PDC deposits often produced by explosive eruptions and fountain collapse. Twice in the evolution of Recent Merapi, extended episodes of violent magmatic to phreatomagmatic eruptions occurred. These produced the widespread sub-Plinian and phreatoplilian deposits of the Gumuk ashes (2220 ± 160 to 1470 ± 140 ^{14}C y BP) that cover the entire edifice, as well as the overlying

Fig. 6.6 The geological evolution of Merapi after Camus et al. (2000). GM = Gajah Mungkur Series; B = Batulawang Series



Sambisari ashes on Merapi's southern slope that were emplaced by dilute PDCs and covered Candi Sambisari at the beginning of the fifteenth century (Berthommier 1990; Camus et al. 2000). Modern Merapi has been characterised by lava dome growth within the Pasarububar crater since AD 1786 and mostly gravitational dome failures that produced small-volume PDCs.

Newhall et al. (2000) provided a comprehensive stratigraphy and many radiocarbon dates of pyroclastic deposits extending the explosive activity of Merapi back to $\sim 10,000$ years ago. The paper questioned conclusions of Berthommier (1990) and Camus et al. (2000) regarding the edifice failure of Old Merapi and the

stratigraphic position of Gunung Bibi. Due to its weathered nature, Gunung Bibi was interpreted by the authors as a vent which built up on the flank of Old Merapi. For the latter, a date of 9630 ± 60 ^{14}C y BP, obtained for a PDC deposit on Merapi's east-northeast flank, marked the oldest age for an explosive eruption of Old Merapi (Fig. 6.4). Old Merapi was inferred to have collapsed one or more times, with hints for an early collapse event from impoundment of Kali Progo to form an early Lake Borobudur at 3430 ± 50 ^{14}C y BP. The latest sector collapse of Old Merapi was postulated to have occurred at ~ 1900 ^{14}C y BP based on their youngest PDC deposit found on the eastern side of the

volcano, if the Somma rim stopped all later PDCs from travelling in an easterly direction. In contrast to Berthommier (1990) and Camus et al. (2000), Newhall et al. (2000) argued that the Gendol Hills are Upper Pliocene in age and hence significantly older than Merapi. Furthermore, the authors found no other evidence of a large-scale debris avalanche deposit and suggested that it has probably been buried by younger deposits. New Merapi began to grow soon after ~ 1900 ^{14}C y BP (Fig. 6.4). Relatively large eruptions from New Merapi were significant enough to affect, destroy or bury many of the larger and smaller temples in the surrounding area, possibly contributing to the eastward migration of the Mataram Kingdom in AD 928 or 929. A smaller partial edifice collapse of New Merapi may have occurred after 1130 ± 50 ^{14}C y BP. Newhall et al. (2000) also coined the term Proto-Merapi (Fig. 6.4), which corresponds to the Very Old Merapi stage of del Marmol (1989) but without Gunung Medjing. The authors concluded that Gunung Plawangan and Gunung Turgo are erosional remnants of the earliest Proto-Merapi cone that precedes van Bemmelen's Old Merapi.

Largely based on the Ph.D. thesis of Andreastuti (1999), Andreastuti et al. (2000) established a detailed tephrostratigraphic framework at Merapi from 3000 to 250 years ago. Recognising important stratigraphic marker horizons around the volcano, some of which were dated by the radiocarbon method, Andreastuti (1999) and Andreastuti et al. (2000) identified a number of tephra units associated with moderate to large eruptions, which include, from old to young, the Sumber, Kadisepi, Bakalan, Jarak, Kujon, Tosari, Ngrangkah, Nglencoh, Tegalsruni, Temusari, Plalangan, Jarak, Selo, interregional marker (Muntilan), Deles, Selokopo, Kepuhharjo and Pasarubar tephra (Fig. 6.7). The most recognisable tephra units were included in the stratigraphic sections of Newhall et al. (2000) to link both stratigraphies. The Muntilan tephra has subsequently been correlated with the AD 1257 Samalas eruption on Lombok (Vidal et al. 2015).

6.2.1.3 Research in the Twenty-First Century

The Ph.D. thesis of Gertisser (2001) identified further stratigraphic marker horizons of moderate to large eruptions (Paten I, Paten II, Trayem, Jurangjero I, Jurangjero II tephra) that allowed tephra correlations from the south-eastern to the north-western sector of Merapi. A large number of radiocarbon dates extended the pyroclastic stratigraphy of Merapi back to $11,792 \pm 90$ ^{14}C y BP and challenged earlier views of a sector collapse of Old Merapi as young as 1900 ^{14}C y BP. Arguments against the latter included the recognition of a young dome-collapse PDC deposit on the eastern slopes of Merapi which suggested that the blockage of PDCs to the east—possibly caused by a westward directed sector collapse—became effective not until 1590 ± 40 ^{14}C y BP, or that by that time, the recent Merapi cone had already grown high enough for such currents to overflow the Somma rim. Some of the oldest dated deposits in the deeply incised valleys on the south-western flank hinted at the possibility of an early sector collapse more than 8380 ± 230 ^{14}C y BP. However, considering the results presented here, these deposits likely represent scattered outcrops of pre-sector collapse (Old Merapi) volcanoclastic units. The radiocarbon dates of Gertisser (2001) were published subsequently in a paper by Gertisser and Keller (2003a), which focused on the explosive activity of Merapi during the past 2000 years and the associated temporal evolution of the magma system.

Research carried out in more distal areas from Merapi in the Borobudur basin provided important new information about the geological history of Merapi. Murwanto (2004) showed that the long sequence of lacustrine deposits, interpreted to have formed by impoundment of Kali Progo to repeatedly establish an ancient Lake Borobudur, spanned at least 20,000 years from $22,040 \pm 390$ ^{14}C y BP. The timespan was subsequently extended with a maximum age of $31,430 \pm 2070$ ^{14}C y BP (Murwanto 2014), hinting indirectly at the occurrence of multiple debris avalanches or debris flows from Merapi which might have caused blockage of the Progo river (e.g. Newhall

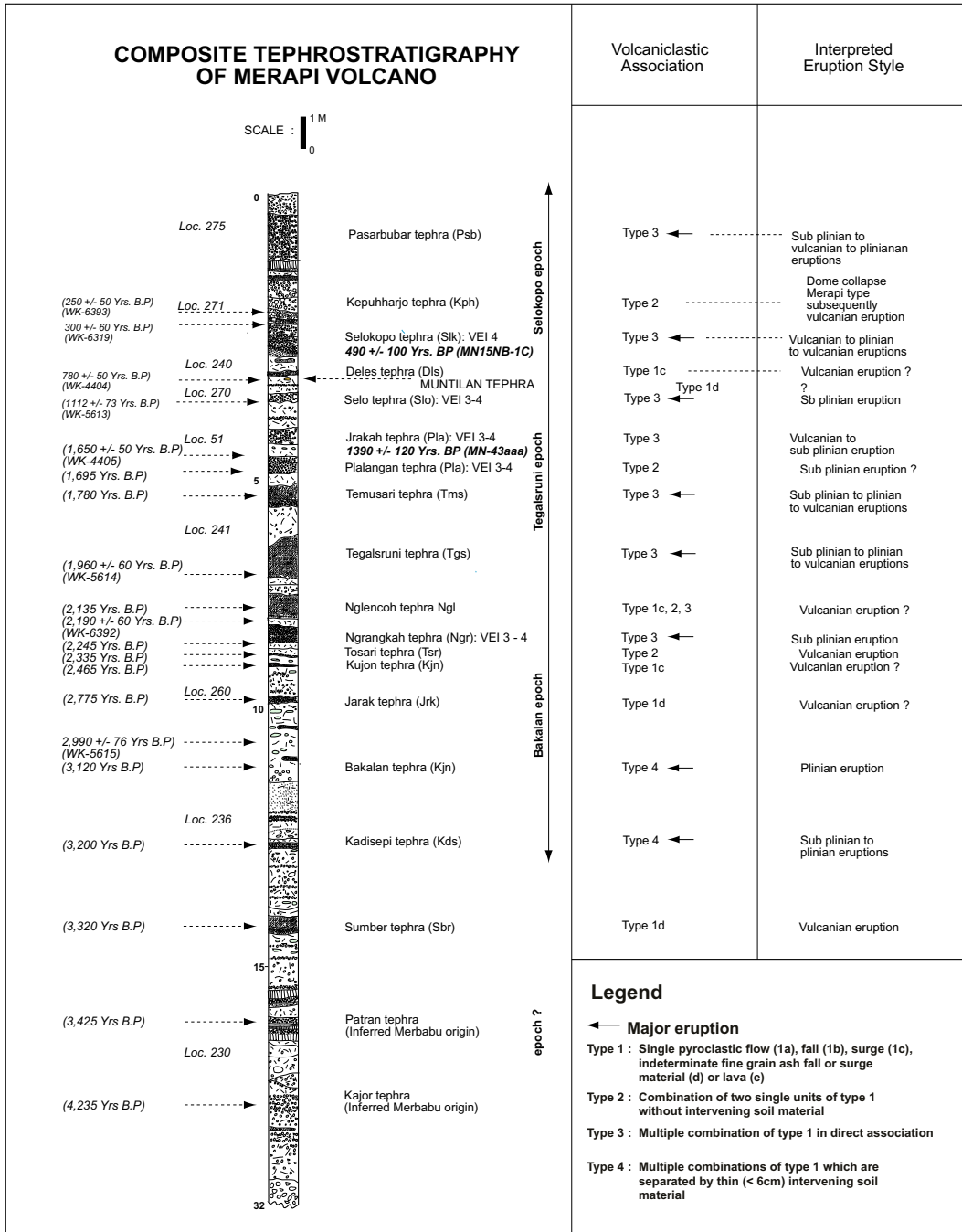


Fig. 6.7 Composite Late Holocene stratigraphy of Merapi volcano (after Andreastuti 1999; Andreastuti et al. 2000). Arrows point to the exact stratigraphic position where ¹⁴C dates were obtained. Estimated dates, assuming a constant rate of soil formation, are shown in italic letters

in brackets. Correlated ¹⁴C dates from Newhall et al. (2000) are shown in bold italic letters. Key locations, the stratigraphic range of geochemically defined cycles, typical volcanoclastic associations and interpretation of eruptive styles are also shown (Andreastuti 1999)

et al. 2000). Gomez et al. (2010) analysed material from two drill cores near Candi Borobudur and related these to possible sector collapse events at ~ 115 ka or 119 ka, and at $31,040 \pm 320$ ^{14}C y BP. The source of the older event remained elusive at the time, while the younger event was linked to a collapse of Ancient Merapi (Berthommier 1990; Camus et al. 2000) or Proto-Merapi (Newhall et al. 2000).

To reassess the geological evolution of Merapi, Gertisser et al. (2012a) published stratigraphic field data, new radiocarbon ages and amongst the first $^{40}\text{K}/^{40}\text{Ar}$ and $^{40}\text{Ar}/^{39}\text{Ar}$ ages of the volcanic complex (Fig. 6.8). The latter suggested that construction of the Merapi volcanic complex began < 170 ka ago. According to the authors, two earliest (Proto-Merapi) volcanic edifices—Gunung Bibi (109 ± 60 ka), and Gunung Turgo and Gunung Plawangan (138 ± 3 ka; 135 ± 3 ka)—predate the main Merapi edifice. The construction of Old Merapi,

a stratovolcano of basaltic andesite lavas and volcaniclastic rocks, began more than ~ 30 ka ago. The edifice was destroyed by one or, possibly, several sector collapses, the latest of which occurred some time after 4.8 ± 1.5 ka. The recent Merapi cone (New Merapi) started to grow afterwards and appears to have been almost continuously active, with periods of high eruption frequency interrupted by shorter intervals of apparently lower eruption frequency. The mostly basaltic andesite pyroclastic and epiclastic deposits of New Merapi cover the flanks of the entire volcanic complex, where they overlie similar deposits from eruptions of Old Merapi.

More recently, Bronto et al. (2014) discovered a large debris avalanche deposit in the Godean area in the Sleman Regency, approximately 30–35 km southwest of Merapi. The authors linked this deposit to a gigantic landslide of Merapi, although the age of the deposit and the associated sector collapse remained unconstrained. The authors estimated that the Godean debris

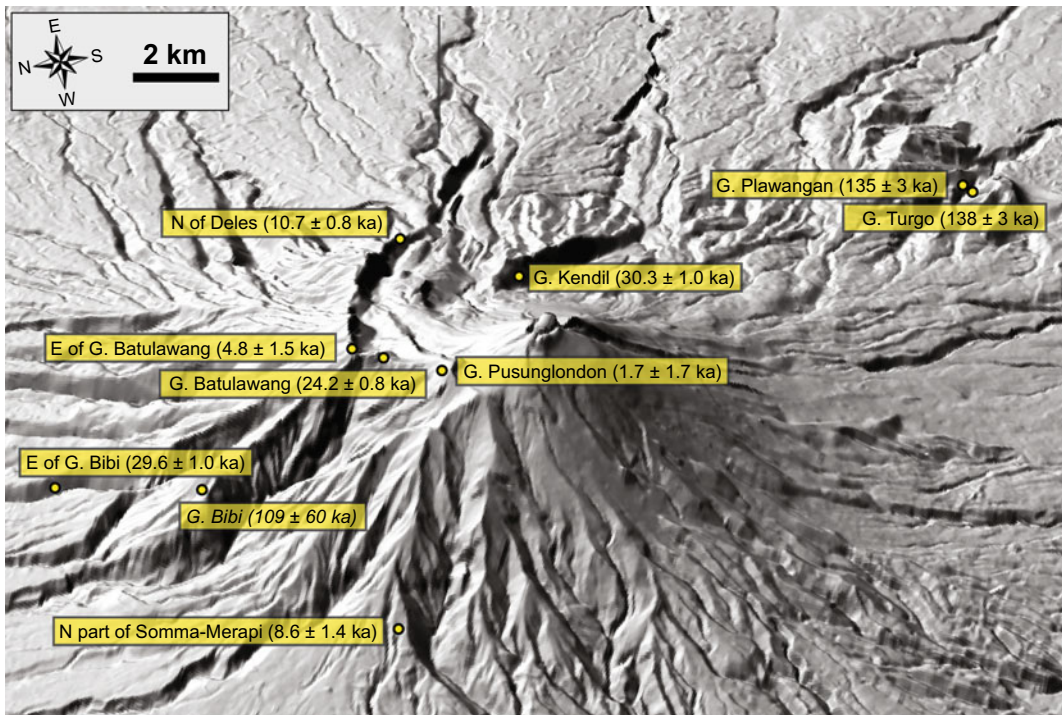


Fig. 6.8 Digital elevation model of Merapi showing the locations of lava samples dated using the $^{40}\text{K}/^{40}\text{Ar}$ and $^{40}\text{Ar}/^{39}\text{Ar}$ (shown in italic letters) techniques (Gertisser

et al. 2012a). Digital elevation model courtesy of Carl Gerstenecker (TU Darmstadt, Germany)

avalanche, as it is called in Bronto et al. (2023, Chap. 7), has a volume of $\sim 4.9\text{--}8.6\text{ km}^3$ and covers an area of $\sim 390\text{ km}^2$. It is characterised by a hummocky topography, and jig-saw-fractured blocks of pyroclastic material, lava flows and reworked deposits. The deposit becomes lahar-like at greater distances of up to 50 km to the south of Merapi. This first recognition of a large-scale debris avalanche from Merapi (Bronto et al. 2014) represents a milestone in the study of the volcano that may help shed light on the long-standing issue of the occurrence of sector collapse(s) at Merapi, and the nature and timing of the destruction of Old Merapi (van Bemmelen 1949, 1956; del Marmol 1989; Berthommier 1990; Camus et al. 2000; Newhall et al. 2000; Gertisser et al. 2012a). These issues are discussed in Sect. 6.2.2.2 and in Bronto et al. (2023, Chap. 7).

Selles et al. (2015) reconstructed the geological and geomorphological evolution of Merapi based on a detailed characterisation of the lithofacies, and the temporal and spatial evolution of the volcanoclastic deposits on the eastern slopes of the volcanic complex. The authors recognised a small debris avalanche and debris flow fan, tentatively linked to the Mount St. Helens-type edifice collapse of Berthommier (1990) and Camus et al. (2000) at the end of the Middle Merapi stage. The deposit is characterised by a volume of $2.2\text{--}3.1\text{ km}^3$ and covers an area of $\sim 45\text{ km}^2$ between 1000 and 400 m asl.

6.2.2 A Synthesis of the Geological History and Chronology of Merapi: Current Thinking

The synthesis of the geological history and chronology of Merapi presented here is centred on an updated version of the reinterpreted geological map of Wirakusumah et al. (1989), as presented in Gertisser et al. (2012a). A new version of this map, shown in Fig. 6.9 illustrates our current understanding of the geological evolution of Merapi, divided into eight main volcano-stratigraphic units, linked to three major

evolutionary stages or temporal volcanic edifices that have existed throughout the lifespan of the volcanic complex: Proto-Merapi, Old Merapi and New Merapi. Unit 1 (Lava flows of Gunung Bibi) and Unit 2 (Lava flows of Gunung Turgo, Gunung Plawangan and Gunung Medjing) are grouped together as part of Proto-Merapi. Old Merapi comprises Unit 3 (Lava flows of the Somma-Merapi) and the older deposits of Units 4/5 (Holocene Pyroclastic Series). The younger deposits of Units 4/5 (Holocene Pyroclastic Series), Unit 6 (Young (post-Somma-Merapi) lava flows) and Units 7/8 (Recent and historical pyroclastic density current and lahar deposits; Lava domes of the recent episode) constitute the recent Merapi cone or New Merapi. The eight main volcano-stratigraphic units are described in more detail in Sect. 6.2.2.1; structural modifications and edifice collapse in the history of Merapi are covered in Sect. 6.2.2.2.

6.2.2.1 Volcano-Stratigraphic Units

The eight main volcano-stratigraphic units of Merapi described in this section partly overlap in time and are linked to the geological map presented in Fig. 6.9.

Lava flows of Gunung Bibi (Unit 1) Gunung Bibi is a morphologically distinct, heavily forested cone- or dome-shaped hill 3.5 km to the northeast of the summit of Merapi (Fig. 6.10a). It consists of highly weathered lava flows and breccias that resemble the surrounding lavas of the Somma-Merapi (Old Merapi) edifice. A scoria fall and associated PDC deposit found nearby may have originated from Gunung Bibi (Newhall et al. 2000). Exposures at Gunung Bibi are rare and the hill remains a poorly known part of the Merapi volcanic complex. Based on the only published $^{40}\text{Ar}/^{39}\text{Ar}$ date of $109 \pm 60\text{ ka}$ on amphiboles (Gertisser et al. 2012a), Gunung Bibi is regarded as one of the oldest parts of Merapi. Despite the large uncertainty, which somewhat limits the value of this date, it is regarded more reliable than the earlier published $^{40}\text{K}/^{40}\text{Ar}$ whole-rock age of $670 \pm 250\text{ ka}$ (Berthommier 1990; Camus et al. 2000) due to the common problem of inherited argon in whole-rock dating. It suggests that Gunung Bibi is $< 170\text{ ka}$ old

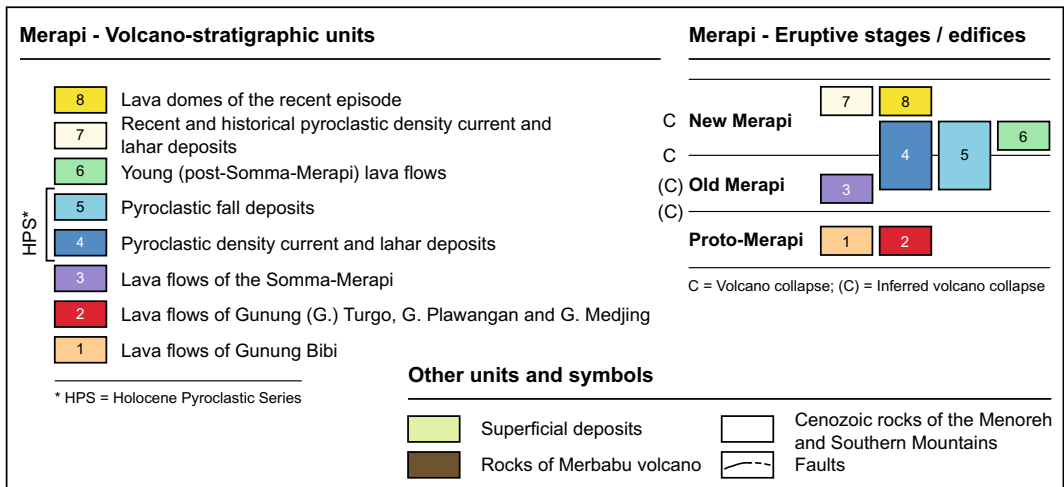
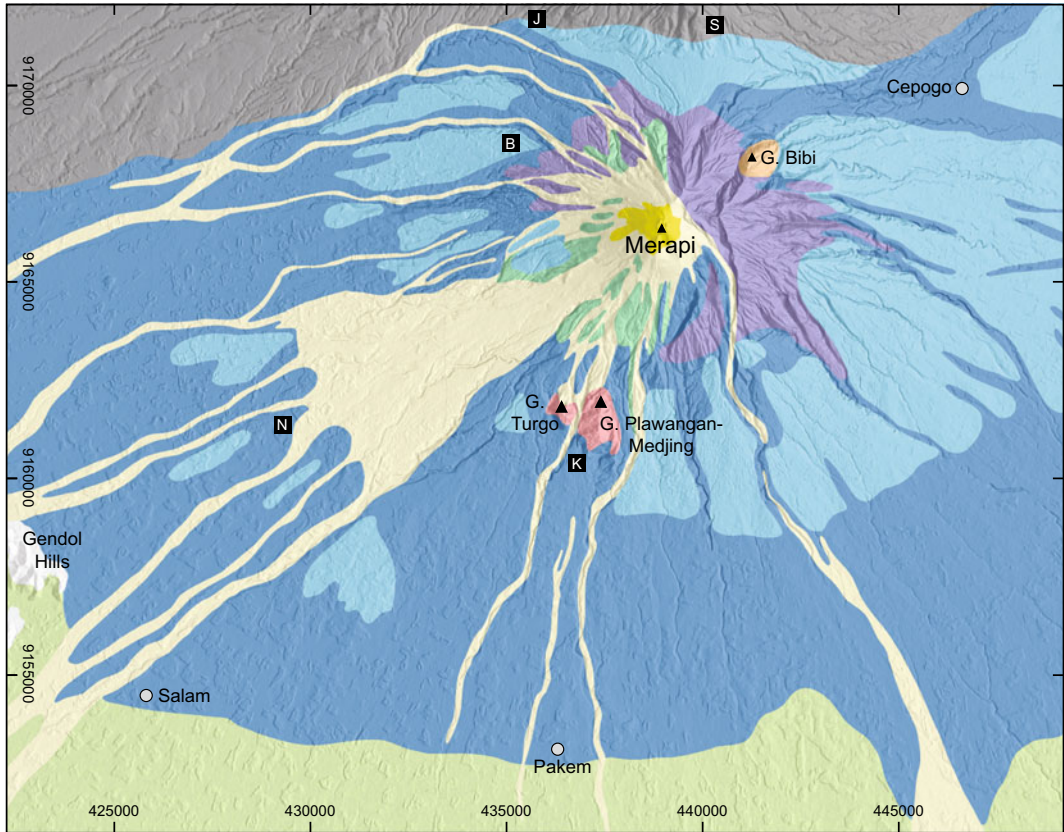


Fig. 6.9 Reinterpreted version of the geological map of Merapi (Wirakusumah et al. 1989), distinguishing eight main volcano-stratigraphic units linked to three main evolutionary stages or volcanic edifices—Proto-Merapi,

Old Merapi and New Merapi. Yogyakarta is located to the south of the map area. Map coordinates are in UTM metres, displayed map symbols as in Fig. 6.1 (adapted and updated from Gertisser et al. 2012a)

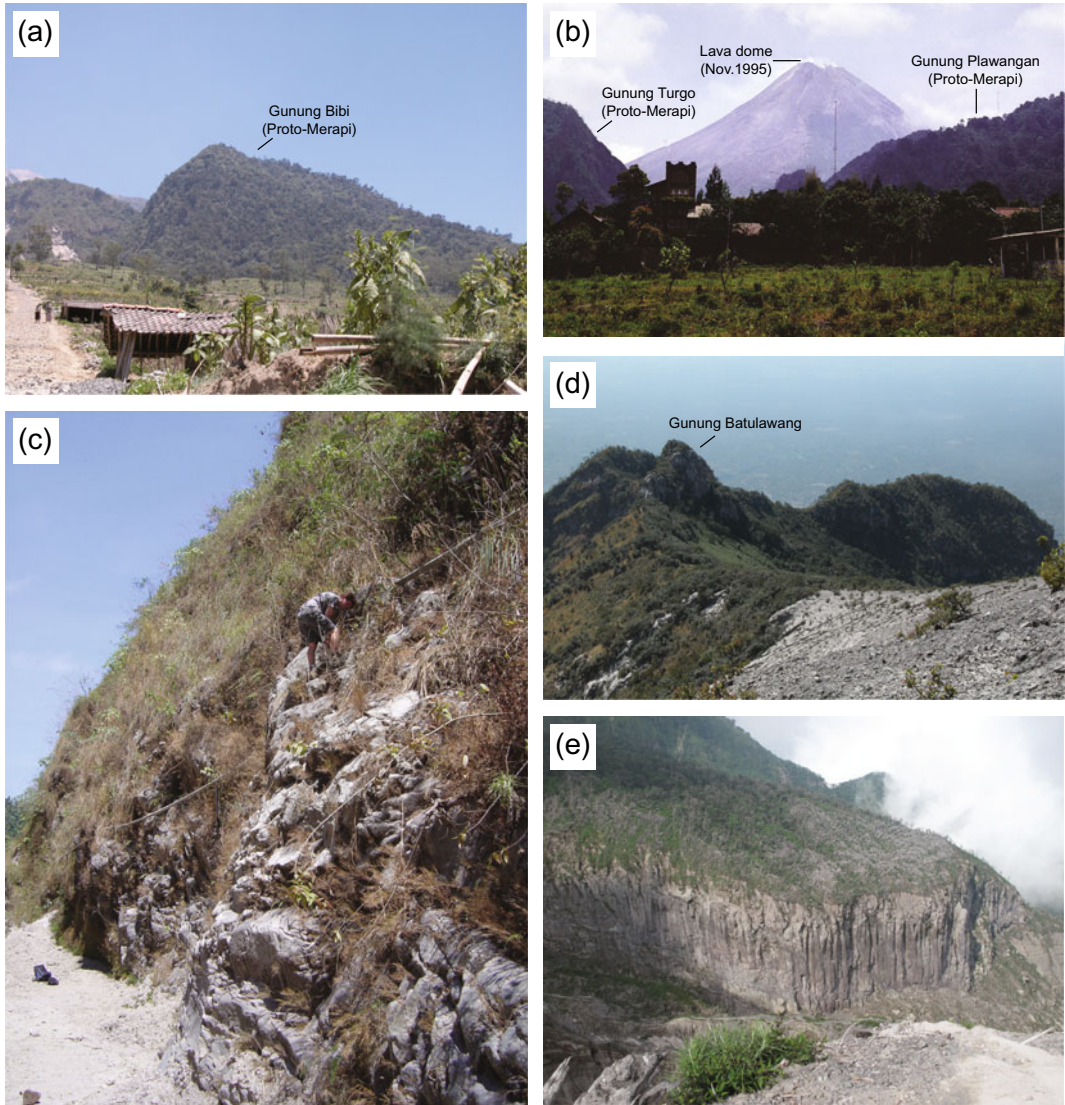


Fig. 6.10 Field photographs. **a** View of Gunung Bibi from the east. **b** Gunung Turgu and Gunung Plawangan, the erosional remnants of a Proto-Merapi edifice, as seen from the village of Kaliurang on Merapi's south slope. The active Merapi cone (New Merapi) is in the background. **c** The basaltic lava sequence exposed at the

foot of Gunung Turgu in the Boyong river valley (Kali Boyong). **d** View from Gunung Pusunglondon across to Gunung Batulawang and the Somma-Merapi (Old Merapi). **e** Thick, columnar jointed basaltic andesite lava flow of the Somma-Merapi (Old Merapi) in the upper Kali Woro

and, therefore, substantially younger than the only other available numerical date implies. The date of 109 ± 60 ka (i.e. $> \sim 50$ ka) further indicates that Gunung Bibi predates the lava sequences of the Somma-Merapi (Old Merapi) edifice (see below), in contrast to earlier views

that it may represent a volcanic plug (del Marmol 1989) or a vent that erupted through and built itself on the upper flank of the Somma-Merapi (Old Merapi) edifice (Newhall et al. 2000). Given the overlapping age range with Gunung Turgu and Gunung Plawangan as well as, by

inference, Gunung Medjing (see below), Gunung Bibi is regarded as an older, Proto-Merapi edifice (Gertisser et al. 2012a).

Lava flows of Gunung Turgo, Gunung Plawangan and Gunung Medjing (Unit 2)

Based on two new $^{40}\text{K}/^{40}\text{Ar}$ groundmass ages of 138 ± 3 ka and 135 ± 3 ka (Gertisser et al. 2012a) for lava flows from the basal successions of Gunung Turgo and Gunung Plawangan exposed in the Boyong valley (Fig. 6.10b, c), the two hills are now considered significantly older than inferred by previous authors based on debatable U-Th ages (Berthommier 1990; Camus et al. 2000). Both hills are ascribed to Proto-Merapi in the sense of Newhall et al. (2000) to which, in this contribution, the lavas of a nearby hill, Gunung Medjing, are added (del Marmol 1989). In agreement with del Marmol (1989) and Newhall et al. (2000), these hills are interpreted as ruins of an ancient volcano rather than flank vents of Old Merapi (van Bemmelen 1949). The northward dip of the lava sequences towards the recent Merapi cone suggests that the hills may be slightly tilted mega- or Toreva-blocks, possibly related to sector collapse (Berthommier 1990; Camus et al. 2000; Newhall et al. 2000).

Lava flows of the Somma-Merapi (Unit 3)

The thick succession of massive lava flows of the Somma-Merapi, exposed in the deeply incised valleys on the south-eastern, eastern and northern flanks of Merapi, and cut by the Kukusan fault, are part of Old Merapi (Fig. 6.10d, e). This succession constitutes the Batulawang Series of Berthommier (1990) and Camus et al. (2000). The beginning of Old Merapi was dated by Gertisser et al. (2012a) to $> 30.3 \pm 1.0$ ka ($^{40}\text{K}/^{40}\text{Ar}$), based on the oldest date obtained for a lava flow at the base of Gunung Kendil (Fig. 6.8). The youngest date for a Somma-Merapi lava flow near the summit of Gunung Batulawang is 4.8 ± 1.5 ka ($^{40}\text{K}/^{40}\text{Ar}$) (Fig. 6.8; Gertisser et al. 2012a). The growth of the Somma-Merapi edifice therefore ended less than 4.8 ± 1.5 ka, a date that provides a maximum age limit of New Merapi. In total, the age range of the Somma-Merapi lava flow succession is presently constrained by six lava groundmass $^{40}\text{K}/^{40}\text{Ar}$ ages (Fig. 6.8; Gertisser et al. 2012a).

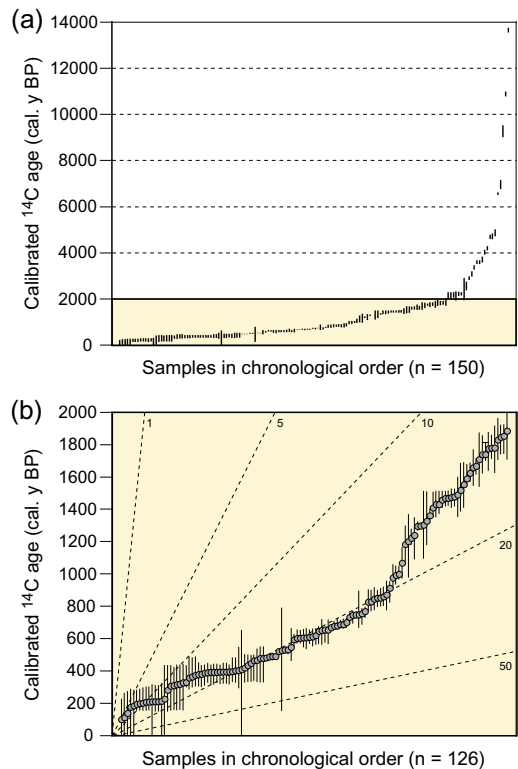


Fig. 6.11 The radiocarbon record of Merapi volcano (after Gertisser et al. 2012a). **a** Published radiocarbon dates plotted in chronological order (total number of analyses $n = 150$). All dates are shown as their maximum 1σ range in calibrated years BP (i.e., before 1950). **b** A close-up of figure (a) showing the subset of samples with calibrated ages < 2000 y BP (total number of analyses $n = 126$). Illustrated are the median probability and the maximum calibrated 1σ age range. The dashed lines indicate the gradients expected from the number of samples (as indicated) per 100 years. *Data sources* Andreastuti et al. (2000), Camus et al. (2000), Newhall et al. (2000), Gertisser and Keller (2003a) and Gertisser et al. (2012a)

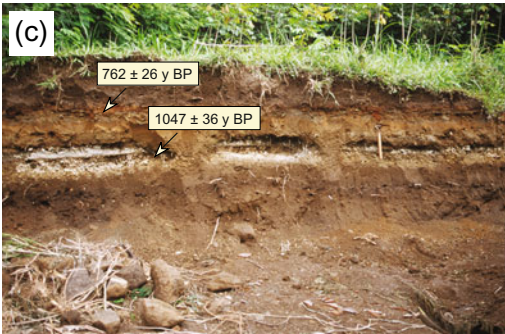
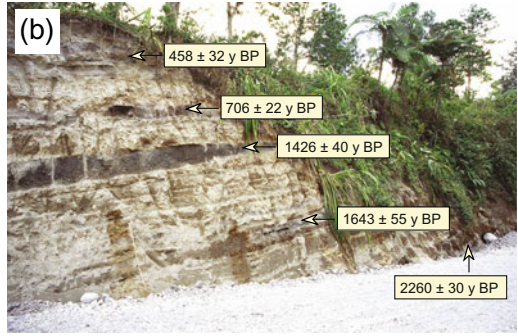
Holocene Pyroclastic Series (Units 4 and 5)

The pyroclastic and epiclastic deposits that cover the flanks of Merapi, constrained by ~ 150 radiocarbon ages to $< 11,792 \pm 90$ ^{14}C y BP (Fig. 6.11), belong to both Old Merapi and New Merapi. This means they either pre- or post-date the latest of several sector collapses of Old Merapi that left the prominent horseshoe-shaped avalanche caldera or Somma rim open to the west, marking the end of the Old Merapi stage (del Marmol 1989; Berthommier 1990; Camus

et al. 2000; Newhall et al. 2000; Gertisser et al. 2012a). These deposits, collectively termed the Holocene Pyroclastic Series (Gertisser 2001; Gertisser and Keller 2003a, b; Gertisser et al. 2012a), comprise all prehistoric volcanoclastic deposits, including the Gumuk and Sambisari ashes of Berthommier (1990) and Camus et al. (2000), the volcanoclastic successions described in del Marmol (1989), Andreastuti (1999), Andreastuti et al. (2000), Newhall et al. (2000), and the deposits on Merapi's eastern flank described by Selles et al. (2015). On interfluvial areas, the Holocene Pyroclastic Series comprises relatively thin PDC and reworked deposits, interbedded with numerous ash and lapilli fall layers and soil horizons. Prominent scoriaceous or pumiceous fall deposits, in many cases closely associated with PDC deposits, record large (VEI 3 and 4) sub-Plinian-type eruptions of Merapi during mid to late Holocene times (Andreastuti 1999; Andreastuti et al. 2000; Newhall et al. 2000; Gertisser 2001; Gertisser et al. 2012a). The sides of the valleys cut into the pyroclastic and epiclastic apron are dominated by thick sequences of intercalated valley-ponded PDC deposits, fluvial and laharc debris, and subordinate fall deposits and soils (Fig. 6.12a–c). Pyroclastic density current deposits include those of block-and-ash flows emplaced via dome collapse and other types that have been grouped according to dominant juvenile component lithology in the larger (lapilli to block size) clast range, including moderately vesicular breadcrust or cauliflower-textured bombs, and moderately to highly vesicular, light grey pumiceous clasts (Fig. 6.13). These latter types were related to fountain to eruption column collapse from Vulcanian- to sub-Plinian-type eruptions (Gertisser et al. 2012a). The base of the Holocene Pyroclastic Series is defined by a palaeosol in the northern sector of Merapi which underlies a succession of pyroclastic deposits from, presumably, both Merapi and Merbabu, the volcano immediately north of Merapi (Gertisser 2001; Gertisser and Keller 2003a; Gertisser et al. 2012a). The oldest direct date for an explosive eruption of Merapi currently remains at 9630 ± 60 ^{14}C y BP (Newhall et al. 2000). This suggests that most of

the lavas forming the bulk of the Old Merapi edifice are older and draped by pyroclastic and epiclastic deposits from dome-forming or explosive eruptions. In many of the deep river valleys in the southern to north-western sector of Merapi (Fig. 6.9), the volcanoclastic successions exposed in the valley walls and on adjacent interfluvial areas also comprise deposits belonging to the Holocene Pyroclastic Series. They date back to 2260 ± 30 ^{14}C y BP around Kali Batang and Jurangjero/Kali Putih and, in other places, back to 3868 ± 47 ^{14}C y BP (Kajangkoso-Kali Senowo) and 4153 ± 37 ^{14}C y BP (Candi Asu-Kali Trising). Comparatively old pyroclastic deposits up to 3453 ± 33 ^{14}C y BP and, as mentioned previously, 8380 ± 230 ^{14}C y BP are also exposed inside the valleys of the Bedok and Bebeng rivers, respectively (Gertisser 2001; Gertisser and Keller 2003a; Gertisser et al. 2012a). Despite such sporadic exposures of older volcanoclastic deposits, most of the presently available radiocarbon ages are within the last 2000 years (Fig. 6.11), indicating that the older eruption record is fragmented and that older deposits are comparatively rare due to burial by younger deposits. The radiocarbon record reveals that over the last 2000 years, the volcanic activity at Merapi has been persistent, with 126 ages documented, averaging one eruption every 15.9 years, under the assumption that each radiocarbon date represents a single eruption (Gertisser et al. 2012a). However, given the likely case that some eruptions be absent from the geological record, as may particularly be the case for phreatic and dome-building eruptions, or under-reported due to erosion, reworking or burial, the average eruption frequency would be higher and closer to that observed since the beginning of the nineteenth century.

Young (post-Somma-Merapi) lava flows (Unit 6) This unit constitutes the young lava flows that crop out near the summit of Merapi around the Pasarbubar crater (Gunung Selokopo Ngisor, Gunung Selokop Duwur, Gunung Gadjah Mungkur, Gunung Pusunglondon), high on the south-western and western flanks (Gunung Dengkeng, Gunung Patuk Alap-alap), and further downslope in the Kuning and Gendol river



◀ **Fig. 6.12** Field photographs. **a** Sequence of mainly thick pyroclastic density current (PDC) and epiclastic deposits exposed in the wall of the upper Kali Boyong north of Kaliurang. **b** Volcaniclastic succession at Jurangjero/Kali Putih on Merapi's southwest flank. The sequence, dated by the radiocarbon method, records more than 2000 years of intermittent explosive eruptions (Gertisser 2001; Gertisser et al. 2011). **c** Soil profile with intercalated widespread scoriaceous or pumiceous pyroclastic fall deposits near Krogowanan, approximately 11 km west-northwest of Merapi. The dated tephra layers correspond to the Trayem (older layer) and Jurangjero I (younger layer) tephra of Gertisser (2001) and Gertisser et al. (2012a). **d** Thick basaltic andesite lava flow forming the

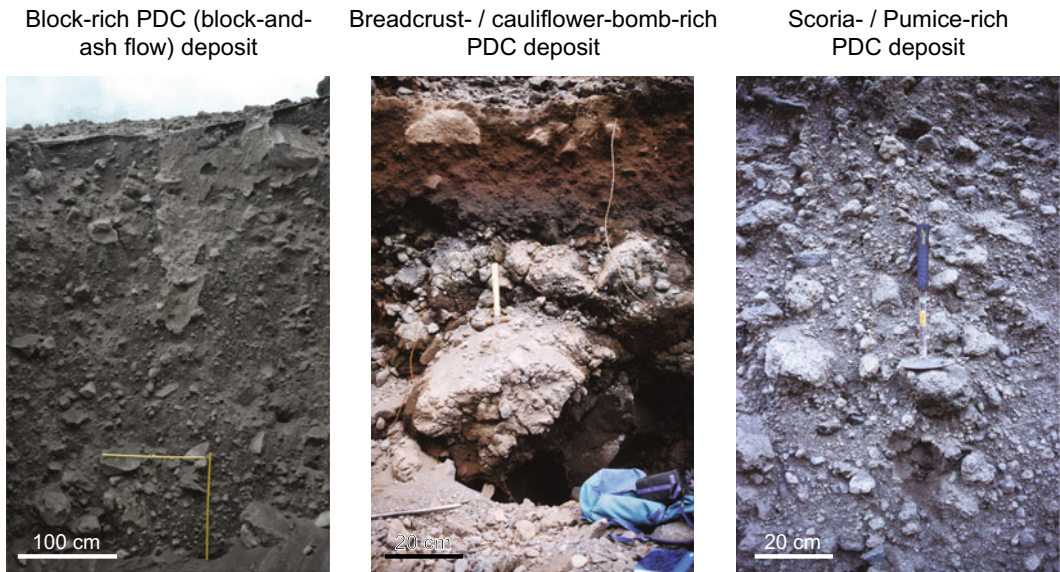
high point known as Gajah Mungkur high on Merapi's north flank. **e** Gunung Pusunglondon, a young post-collapse cone near the summit of Merapi. **f** Basaltic andesite lava flows on the southeast side of Gunung Pusunglondon unconformably overlie the older lavas of the Somma-Merapi (Old Merapi). **g** Massive young PDC deposits, separated by fluvially reworked deposits, on Merapi's south flank in a quarry west of Kali Opak near the Merapi golf course. Both PDC deposits are widespread on Merapi's south flank. The lower PDC deposits may be from a historical or prehistoric eruption. The radiocarbon dates are from Gertisser et al. (2012b). **h** Deeply incised, valley-confined 1954 PDC deposits in Kali Apu

valleys (Fig. 6.12d–f). Preliminary satellite image analysis also suggests the presence of prehistoric lava domes, such as on Merapi's upper NNW slope, which may be grouped into this unit (S. Bronto Personal Communication 2020). Based on the youngest age of the older Somma-Merapi lava flow succession, the lava sequences of this unit are considered younger than 4.8 ± 1.5 ka (Fig. 6.8). They constitute the Gajah Mungkur series of Berthommier (1990) and Camus et al. (2000), a sequence of lavas unaffected by, and therefore younger than the Kukusan fault, which we, in accordance with Berthommier (1990) and Camus et al. (2000), interpret as a structure related to sector collapse. As such, these lava sequences are part of New Merapi. A poorly constrained $^{40}\text{K}/^{40}\text{Ar}$ date of 1.7 ± 1.7 ka for a lava flow from Gunung Pusunglondon and another zero age for a flow from Gunung Gajah Mungkur (Gertisser et al. 2012a) are suggestive of the young ages of these lavas compared to those of the Somma-Merapi (Old Merapi) east of the Kukusan fault, although many of these lavas are not yet dated.

Recent and historical pyroclastic density current and lahar deposits (Unit 7) and lava domes of the recent episode (Unit 8) Given the difficulty of identifying the products of historical eruptions in the field, due to similarity of field characteristics, poor preservation potential, extensive reworking of primary deposits or lack of radiometric ages, the boundary between the youngest deposits of the Holocene Pyroclastic Series and the deposits of historical to recent

eruptions have remained difficult to determine in places (Fig. 6.12g). In general, the historical to recent volcaniclastic deposits consist of PDC and related deposits that are comparable to those of the Holocene Pyroclastic Series (units 4 and 5 above) and dominate the successions in the southern, western and north-western sectors up to 10 km (or occasionally more) from the summit (Figs. 6.12g, h and 6.14). In exceptional cases, PDCs reached up to 16 km from source (e.g. in 2010; Subandriyo et al. 2023, Chap. 12) and possibly further. In general, however, at greater distances downstream, the volcaniclastic successions are dominated by lahar and fluvial deposits in and around the main river valleys. The lava dome complex at the summit of Merapi (Fig. 6.15a) constitutes domes extruded after AD 1786 (Camus et al. 2000) within the larger Pasarububar crater. Reconstructions and maps of the dome complex were presented by del Marmol (1989), Berthommier (1990), Innocenti et al. (2013b) and Solikhin et al. (2015), among others. A schematic sketch map of the summit area and lava dome complex after the 2010 eruption (Solikhin et al. 2015) is shown in Fig. 6.15b. With a few possible exceptions, eccentric vents and flank eruptions are unknown in the historical eruption record of Merapi (Fig. 6.16), which suggests that there have been 29 eruptions or eruptive episodes in the nineteenth century (average of one eruption every 3.4 years) and 25 eruptions or eruptive episodes in the twentieth century (average of one eruption every 4 years). Most of the 78 historical eruptions or eruptive

Type of pyroclastic density current (PDC) deposit



Essential juvenile component



Dense to poorly vesicular andesite lava dome fragments, highly crystalline, but may contain glass, colour mainly reflects groundmass crystallinity, angular, occasional with prismatic cooling joints

Breadcrust bombs or bombs / clasts with cauliflower external morphology, typically dark- coloured (mafic), glass-rich, vesicular, subangular to rounded

Scoriaceous / pumiceous juvenile clasts, light coloured, glass-rich, highly vesicular, strongly rounded through abrasion during lateral transport

Eruptive mechanism

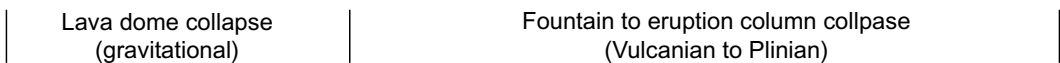


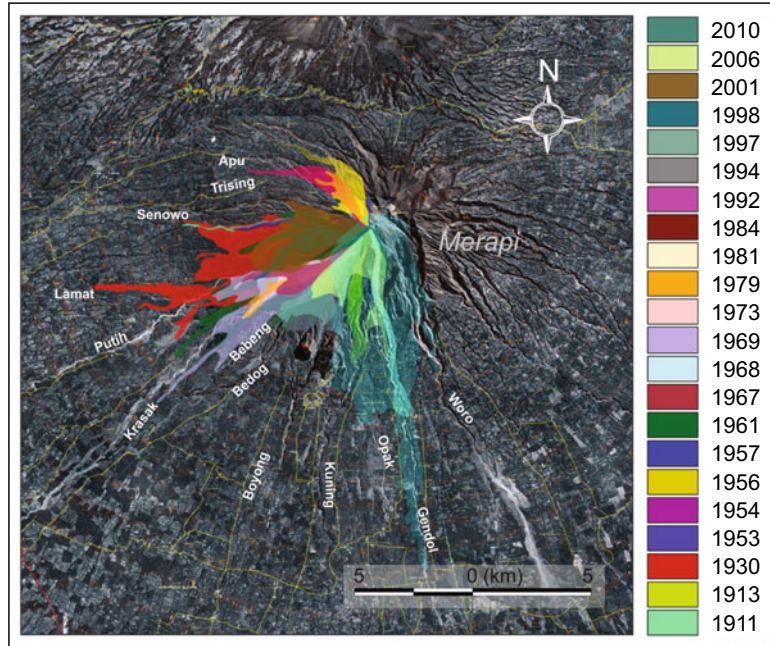
Fig. 6.13 Different types of pyroclastic density current deposits identified in the prehistoric and historical to recent geological record of Merapi based on the dominant

juvenile component they contain. Inferred flow generation mechanisms are also indicated (modified after Gertisser 2012a)

episodes were of VEI 1-3, with VEI 2 eruptions being most common. They erupted from central vents in Merapi's summit region, and produced lava domes or flows, explosions and PDCs. Approximately 20 eruptions or eruptive episodes caused damage to infrastructures and fatalities,

and 15 events produced syn- and/or post-eruptive lahars. It has been proposed that there was a shift in the style of activity from the nineteenth to the twentieth century, with explosive eruptions and some associated PDCs during the 1800s having been larger than any eruptions and PDCs

Fig. 6.14 Distribution of pyroclastic density currents of Merapi between 1911 and 2010. Map courtesy of I.G.M. A. Nandaka, Balai Penyelidikan dan Pengembangan Teknologi Kebencanaan Geologi (BPPTKG), Geological Agency of Indonesia



produced in the twentieth century (Newhall et al. 2000; Voight et al. 2000). However, such a pattern is less discernible from Fig. 6.16, and the large-magnitude eruption in 2010, which was preceded by a typical dome-forming eruption in 2006 and followed by a series of predominantly phreatic eruptions between 2012 and 2014 and in 2018, and renewed effusive (dome-forming) activity from 2018 onward (Global Volcanism Program 2013; Nandaka et al. 2023, Chap. 18; Fig. 6.17), shows that the size and intensity of eruptions at Merapi can change at relatively short timescales.

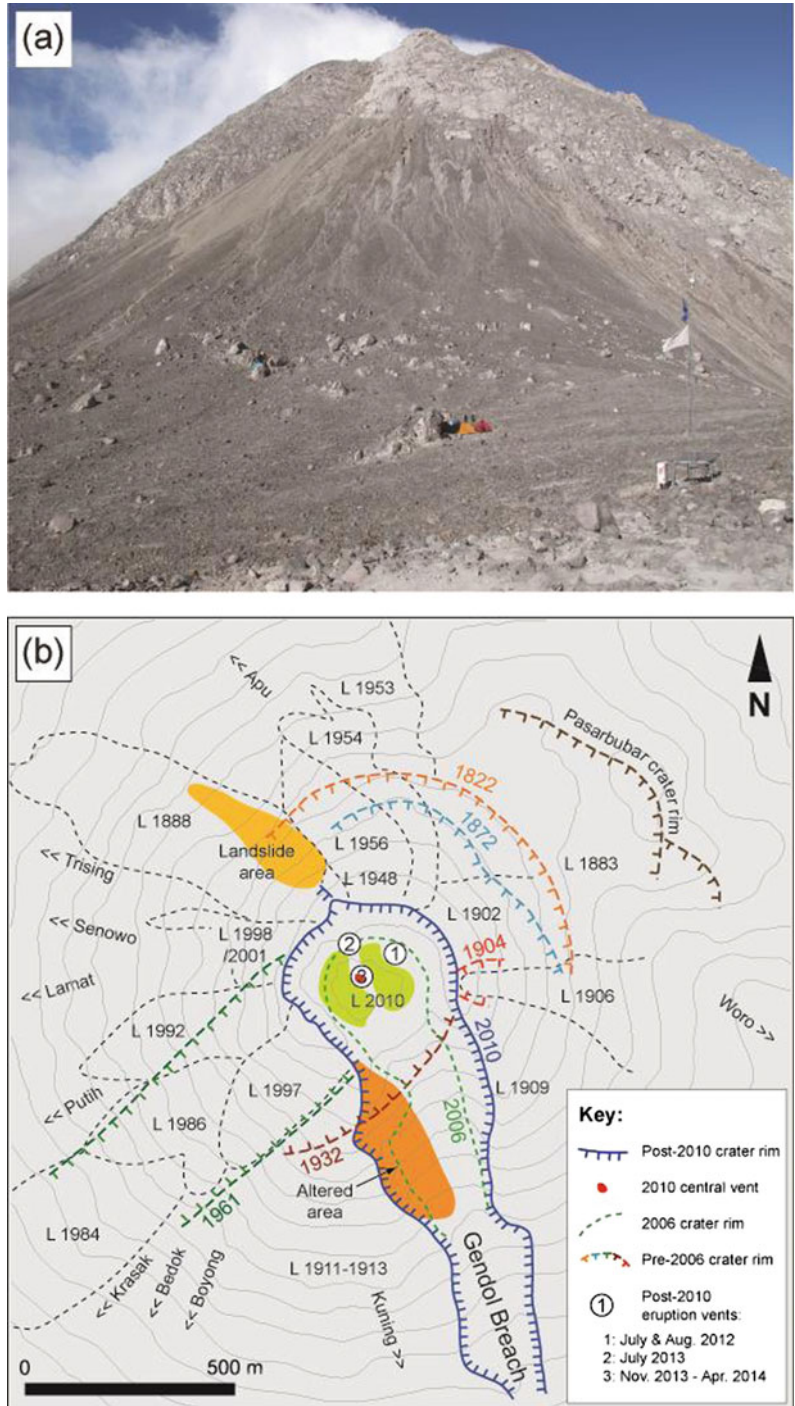
6.2.2.2 Structural Evolution and Volcano Collapse

Ever since the postulation of a collapse of the western flank of Merapi by van Bemmelen (1949, 1956), the issues of major structural modifications of the volcano and edifice collapse have remained debated topics. While there are still open questions about both the exact nature and timing of such events in Merapi's history, there has been significant progress since van Bemmelen's pioneering work. Evidence for edifice collapse at Merapi (Fig. 6.9) comes from

(1) the structure of the volcanic edifice, such as the presence of a segmented horseshoe-shaped crater, Somma rim or avalanche caldera that may have formed by one or more collapses, (2) indirectly from impoundment of Kali Progo west-southwest of Merapi to form lake deposits of an ancient, recurring Lake Borobudur, (3) analysis of rocks retrieved from drill cores in the Borobudur basin, and (4) the recognition of landslide or debris avalanche deposits, including the recent discovery of the Godean debris avalanche deposit, a large debris avalanche deposit in the Godean and surrounding area southwest and south of Merapi by Bronto and co-workers (e.g. Djumarna et al. 1986; del Marmol 1989; Wirakusumah et al. 1989; Berthommier 1990; Camus et al. 2000; Newhall et al. 2000; Gomez et al. 2010; Gertisser et al. 2012a; Bronto et al. 2014, 2023, Chap. 7; Murwanto 2014).

The earliest, and in many respects, least constrained volcano collapse may have occurred at the Proto-Merapi stage, leaving behind the prominent hills of Gunung Turgo, Gunung Plawanagan and Gunung Medjing on Merapi's south flank (Berthommier 1990; Camus et al. 2000; Newhall et al. 2000). To date, no deposits

Fig. 6.15 **a** The lava dome complex at the summit of Merapi above the plateau of the Pasarbubar crater (photo taken in August 2011). **b** Schematic sketch map of the Merapi summit area and lava dome complex after the 2010 eruption (after Solikhin et al. 2015)



of such a collapse are known. Considering the ages of 138 ± 3 ka and 135 ± 3 ka for the basal lavas of Gunung Turgo and Gunung Plawangan

(Gertisser et al. 2012a), it is possible that these hills are the source of mafic volcanoclastic material or blocks retrieved from drill cores in

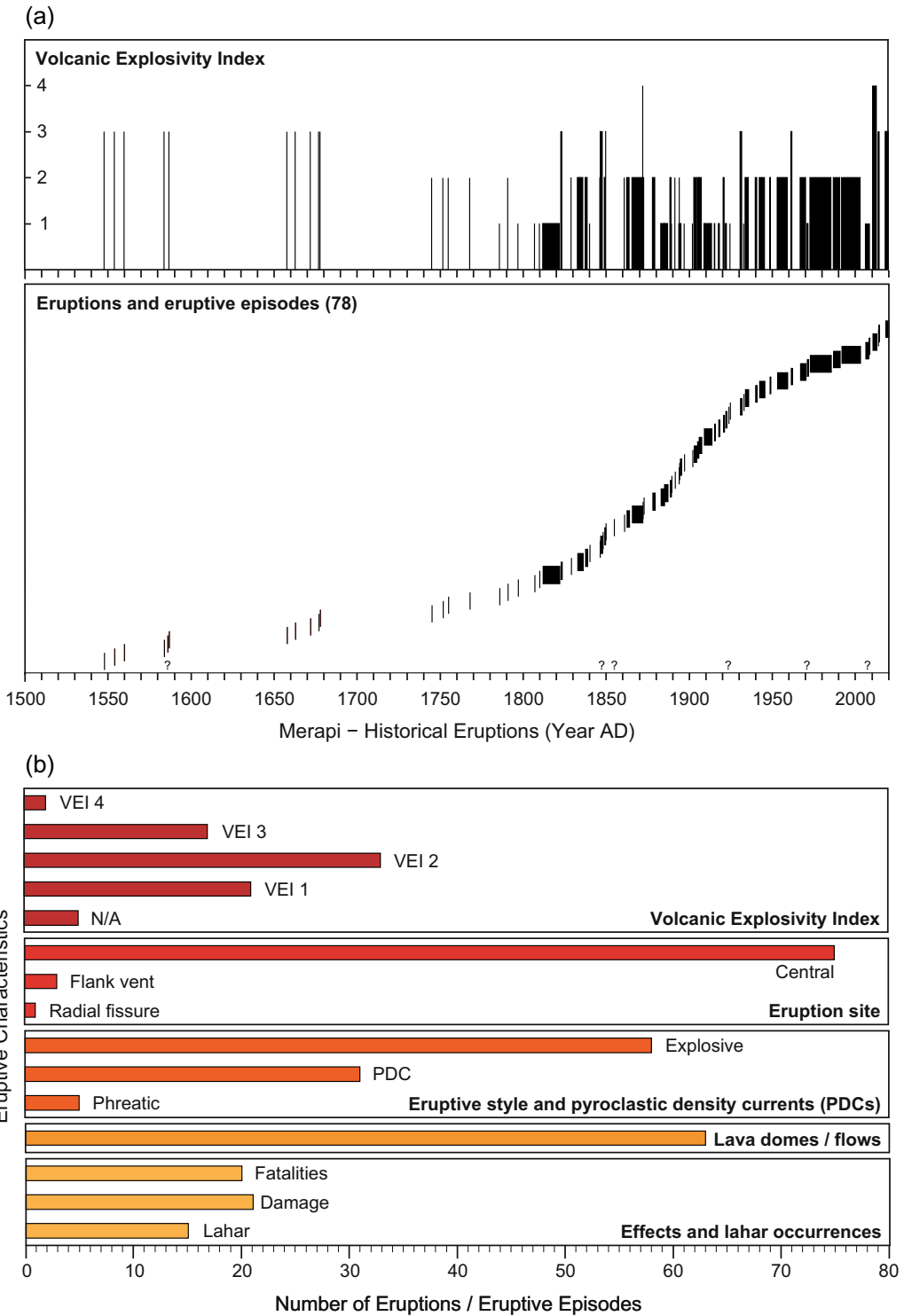


Fig. 6.16 Record of historical eruptions and eruptive episodes of Merapi compiled with data from Siebert et al. (2011) and the Global Volcanism Program (2013). The earliest historical observations date from AD 1584. **a** Eruptions and eruptive episodes and their Volcanic

Explosivity Index (VEI) designation (Newhall and Self 1982). The two VEI 4 eruptions are those in 1872 and 2010. **b** Eruptive characteristics: VEI, eruption site, eruptive style and occurrence of pyroclastic density currents, and effects and lahar occurrences

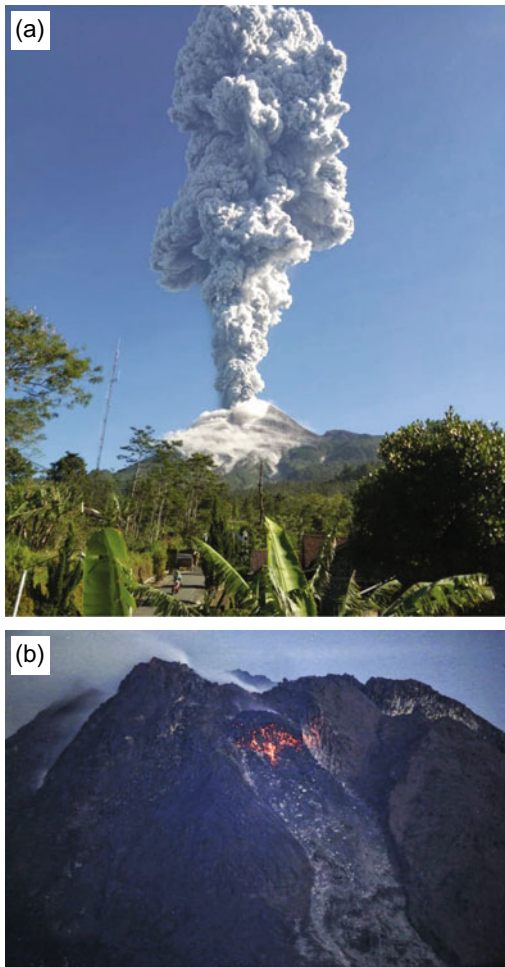


Fig. 6.17 Eruptive activity of Merapi after the 2010 eruption. **a** Ash plume rising at least 6 km above the summit during a short-lived phreatic explosion on 1 June 2018. **b** Lava dome in the western part of the summit as seen on 17 February 2021. The dome was first observed at the surface on 4 January 2021, marking the beginning of a new effusive eruption phase. *Photo credit* BPPTKG—CVGHM, Geological Agency of Indonesia

the southern part of the Borobudur basin, dated at 119 ± 2 ka or 115 ± 2 ka (Gomez et al. 2010). If correct, this would imply that the Proto-Merapi edifice, which comprises Gunung Turgo, Gunung Plawanagan and Gunung Medjing, existed until at least 115 ± 2 ka, after which it may have collapsed to generate a debris avalanche or debris flow that transported material

from the edifice to the Borobudur basin. This interpretation differs from that of Bronto et al. (2023, Chap. 7) and must be considered with caution, given (1) that the reported basaltic rocks at the respective depth(s) in the drill cores (see Table 2 in Gomez et al. 2010) could have possibly originated from either Merapi (Gunung Turgo, Gunung Plawanagan and Gunung Medjing) or Merbabu, and (2) a lack of more detailed petrological, geochemical and chronological investigations of the retrieved drill core material.

The post-Proto Merapi complex may have collapsed multiple times. Several volcano collapses can be linked to Old Merapi, leaving the pronounced avalanche caldera on the eastern and northern side of the volcano, and generating debris avalanches from edifice failure to the west (Newhall et al. 2000). The oldest date of $31,430 \pm 2070$ ^{14}C y BP for black lacustrine clay from an ancient Lake Borobudur (Murwanto 2014; Bronto et al. 2023, Chap. 7), which coincides with an age of $31,040 \pm 320$ ^{14}C y BP for dark grey volcanic ash in a drill core located at the confluence between the Elo and Progo river (Gomez et al. 2010), may hint at a collapse early in the evolution of Old Merapi, which, according to the latest dates, started to grow more than 30.3 ± 1.0 ka ago (Gertisser et al. 2012a). Younger dates from the long sequence of lacustrine deposits in the alluvial plain of Borobudur (Murwanto 2014; Bronto et al. 2023, Chap. 7), including a preliminary age of 3430 ± 50 ^{14}C y BP given by Newhall et al. (2000), may signify impoundment of Kali Progo by rapidly emplaced debris avalanches from Merapi, although we cannot exclude the possibility that they reflect other times in the history of Lake Borobudur not necessarily related to new blockages. Debris avalanche deposits associated with such events are not known at present. A younger and latest collapse of Old Merapi is widely considered to be the main Somma rim forming event, although the nature and date of this event have remained strongly debated (see Sect. 6.2.1 and Bronto et al. 2023, Chap. 7). We speculate that the Godean debris avalanche (Bronto et al. 2023,

Chap. 7) could possibly be related to this inferred major event in Merapi's geological history, although a lack of direct age constraints of the associated deposits precludes a definitive answer at present. This contrasts with Bronto et al. (2023, Chap. 7), who argue that the Godean debris avalanche is significantly older, linking it to the oldest of three collapse structures identified through satellite image analysis that separate Merapi into four evolutionary stages.

Volcano collapses have also affected New Merapi. Whether the youngest dates (660 ± 110 and 420 ± 50 ^{14}C y BP; Newhall et al. 2000; Bronto et al. 2023, Chap. 7) of lacustrine deposits from an earlier Lake Borobudur reflect a debris avalanche event from Merapi is poorly substantiated at present. However, a relatively small collapse did affect the New Merapi cone some time after 1130 ± 50 ^{14}C y BP (Newhall et al. 2000). This partial collapse event was the only one identified directly by a debris avalanche deposit, until the discovery of the much larger Godean debris avalanche (Bronto et al. 2014, 2023, Chap. 7). The deposit in Kali Boyong, exposed on the valley floor following the 1994 eruption, consists of megaclasts of brecciated lava clasts with typical jigsaw cracks and pyroclastic material in a finer grained matrix. From its limited exposure, no inferences could be made about the volume or extent of the event, although it is regarded a much smaller event compared with the latest collapse of Old Merapi (Newhall et al. 2000).

Like other steep-sided stratovolcanoes, New Merapi appears to have been affected by multiple larger or smaller flank or sector collapses throughout its lifespan. During the recent and historical period, small collapses of the uppermost, hydrothermally altered and weakened edifice, or older lava domes from the summit dome complex, have accompanied some of the eruptions. The collapsed material, however, has often been incorporated in PDCs of these eruptions rather than distinct debris avalanche deposits. Breaches at the top of the volcano or in the crater wall are a direct result of explosive activity or such collapses, removing small portions of the

uppermost volcanic edifice (e.g. Voight et al. 2000). The latest of these small collapses occurred during the 2006 and 2010 eruptions. Removal of part of the summit rim on 4 June 2006 led to a shift in the direction of dome-collapse PDCs from the southwest to the south during the 2006 eruption (Charbonnier and Gertisser 2008; Ratdomopurbo et al. 2013). Explosive activity and retrogressive summit collapses during the peak of the large-magnitude 2010 eruption on 5 November 2010 generated high-energy PDCs (Komorowski et al. 2013) and significantly enlarged the 'Gendol breach', which acted as the main pathway for subsequent rock-falls and dome-collapse PDCs, particularly in the later stages of the 2010 eruption and in 2019–2020, following another period of dome growth (Global Volcanism Program 2019, 2020). Small collapses of older parts of the summit are a potential future hazard that requires careful attention (Bronto et al. 2023, Chap. 7).

6.3 Compositional Variations of the Eruptive Products of Merapi

6.3.1 Rock Types and Classification

For the purpose of this chapter, 718 whole-rock major element analyses from the literature (Bahar 1984; Bardintzeff 1984; del Marmol 1989; Berthommier 1990; Boudon et al. 1993; Andreastuti, 1999; Andreastuti et al. 2000; Camus et al. 2000; Gertisser 2001; Gertisser and Keller 2003a, b; Debaille et al. 2006; Gertisser et al. 2012a; Chadwick et al. 2013; Preece 2014; this study) were grouped into the eight main volcano-stratigraphic units, and the major evolutionary stages or volcanic edifices of Merapi, based on information on sample location, sampled unit and/or sample age. Selected whole-rock data are presented in Tables 6.1 and 6.2; the complete dataset, including sample allocation to volcano-stratigraphic units, is available from the corresponding author upon request. Overall, the

Table 6.1 Selected whole rock major element oxide (wt.%) and trace element (ppm) data for Merapi

| Unit ^a | 1 | 2 | 2 | 2 | 3 | 3 | 3 | 3 |
|-----------------------------------|---------|---------|---------|---------|---------|---------|---------|---------|
| Geochemical affinity ^b | MK | HK | HK | HK | MK | MK | MK | MK |
| Sample | M96-175 | M95-028 | M96-050 | M96-052 | M95-026 | M96-056 | M96-071 | M98-047 |
| SiO ₂ | 56.49 | 50.20 | 50.37 | 50.30 | 55.50 | 55.41 | 56.60 | 55.58 |
| TiO ₂ | 0.72 | 1.03 | 1.09 | 0.92 | 0.78 | 0.76 | 0.73 | 0.79 |
| Al ₂ O ₃ | 18.71 | 19.78 | 18.68 | 19.17 | 18.33 | 18.69 | 18.75 | 18.45 |
| Fe ₂ O ₃ * | 7.45 | 9.53 | 10.12 | 9.90 | 8.33 | 8.07 | 7.51 | 7.79 |
| MnO | 0.17 | 0.13 | 0.14 | 0.17 | 0.17 | 0.18 | 0.16 | 0.17 |
| MgO | 2.58 | 3.19 | 4.28 | 4.91 | 3.41 | 3.17 | 2.26 | 2.56 |
| CaO | 8.09 | 9.72 | 9.26 | 10.24 | 8.44 | 8.43 | 8.01 | 8.08 |
| Na ₂ O | 3.59 | 3.19 | 3.18 | 3.11 | 3.43 | 3.59 | 4.00 | 3.67 |
| K ₂ O | 1.59 | 1.97 | 1.83 | 1.41 | 1.71 | 1.67 | 1.72 | 1.88 |
| P ₂ O ₅ | 0.29 | 0.28 | 0.28 | 0.21 | 0.21 | 0.22 | 0.24 | 0.32 |
| LOI | 0.71 | 1.14 | 1.40 | -0.08 | 0.10 | 0.29 | 0.49 | 1.03 |
| Total | 100.40 | 100.16 | 100.62 | 100.26 | 100.41 | 100.47 | 100.49 | 100.33 |
| Ba | 428 | 474 | 584 | 437 | 451 | 454 | 430 | 434 |
| Ce | 38.2 | 23.3 | 28.7 | 19.4 | 29.1 | 28.2 | 31.7 | 38.0 |
| Co | 14.6 | 31.0 | 28.1 | 29.3 | 21.4 | 19.1 | 13.3 | 17.0 |
| Cr | 10.4 | 124.1 | 34.3 | 49.0 | 11.2 | 6.2 | 7.1 | 5.9 |
| Dy | 3.77 | 2.88 | 3.49 | 2.57 | 2.94 | 3.14 | 3.25 | 3.56 |
| Er | 2.31 | 1.69 | 1.99 | 1.49 | 1.59 | 1.72 | 1.67 | 1.94 |
| Eu | 1.43 | 1.10 | 1.33 | 0.94 | 1.00 | 1.19 | 1.14 | 1.34 |
| Gd | 4.13 | 3.15 | 3.91 | 2.69 | 3.03 | 3.43 | 3.31 | 4.03 |
| Hf | 2.77 | 1.67 | 1.93 | 1.31 | 2.01 | 2.31 | 2.35 | 2.64 |
| Ho | 0.739 | 0.606 | 0.723 | 0.527 | 0.544 | 0.616 | 0.680 | 0.737 |
| La | 18.9 | 11.6 | 14.3 | 10.0 | 14.4 | 14.4 | 15.3 | 19.2 |
| Lu | 0.366 | 0.249 | 0.331 | 0.227 | 0.281 | 0.326 | 0.302 | 0.325 |
| Mo | 0.68 | 0.74 | 0.93 | 0.57 | 0.82 | 0.89 | 0.70 | 1.12 |
| Nb | 4.49 | 2.02 | 2.42 | 1.52 | 2.63 | 2.95 | 3.62 | 4.65 |
| Nd | 20.0 | 12.1 | 15.5 | 10.6 | 13.7 | 14.7 | 15.6 | 18.7 |
| Ni | b.d | 43.1 | 16.4 | 19.0 | 4.5 | 2.1 | 2.0 | 2.7 |
| Pb | 25.4 | 16.6 | 18.3 | 14.9 | 14.8 | 15.3 | 18.3 | 17.3 |
| Pr | 4.78 | 2.84 | 3.57 | 2.48 | 3.32 | 3.43 | 3.68 | 4.51 |
| Rb | 37.8 | 23.9 | 36.2 | 20.9 | 46.1 | 38.3 | 42.7 | 47.7 |
| Sm | 4.22 | 3.10 | 3.82 | 2.65 | 3.06 | 3.33 | 3.58 | 4.35 |
| Sr | 529 | 568 | 467 | 642 | 496 | 519 | 519 | 520 |
| Ta | 0.38 | 0.15 | 0.20 | 0.12 | 0.21 | 0.23 | 0.30 | 0.36 |
| Tb | 0.603 | 0.473 | 0.557 | 0.403 | 0.469 | 0.513 | 0.476 | 0.592 |
| Th | 5.68 | 4.91 | 5.46 | 4.21 | 6.27 | 5.52 | 5.87 | 6.16 |
| Tm | 0.326 | 0.258 | 0.297 | 0.243 | 0.254 | 0.299 | 0.262 | 0.343 |
| U | 1.35 | 0.84 | 1.08 | 0.62 | 1.31 | 1.16 | 1.29 | 1.53 |
| V | 151 | 331 | 298 | 316 | 243 | 213 | 150 | 189 |
| Y | 22.4 | 18.0 | 21.1 | 16.3 | 17.9 | 20.9 | 20.1 | 21.1 |
| Yb | 2.11 | 1.61 | 1.98 | 1.47 | 1.70 | 1.87 | 1.91 | 2.09 |
| Zr | 114 | 64 | 68 | 48 | 88 | 92 | 102 | 113 |

(continued)

Table 6.1 (continued)

| | | | | | | | | |
|-----------------------------------|---------|---------|---------|---------|----------|---------|---------|---------|
| Unit ^a | 3 | 4/5 | 4/5 | 4/5 | 4/5 | 4/5 | 4/5 | 4/5 |
| Geochemical affinity ^b | MK | MK | MK | MK | MK | HK | HK | HK |
| Sample | M98-107 | M96-073 | M96-137 | M96-163 | M98-0532 | M96-075 | M96-102 | M96-164 |
| SiO ₂ | 55.70 | 54.50 | 54.12 | 51.40 | 54.39 | 53.87 | 51.87 | 51.86 |
| TiO ₂ | 0.69 | 0.86 | 0.80 | 0.73 | 0.82 | 0.71 | 0.81 | 0.84 |
| Al ₂ O ₃ | 18.54 | 18.85 | 18.77 | 21.46 | 18.59 | 18.87 | 20.44 | 19.31 |
| Fe ₂ O ₃ * | 7.44 | 8.28 | 8.47 | 7.56 | 7.87 | 8.13 | 8.24 | 8.48 |
| MnO | 0.15 | 0.20 | 0.18 | 0.17 | 0.19 | 0.19 | 0.20 | 0.20 |
| MgO | 2.28 | 2.75 | 3.17 | 2.56 | 2.68 | 3.03 | 2.47 | 3.02 |
| CaO | 8.04 | 8.50 | 8.75 | 7.69 | 8.28 | 8.55 | 8.86 | 9.30 |
| Na ₂ O | 3.97 | 3.77 | 3.61 | 3.09 | 3.81 | 3.43 | 3.35 | 3.36 |
| K ₂ O | 1.73 | 1.71 | 1.61 | 1.25 | 1.77 | 2.04 | 1.74 | 1.82 |
| P ₂ O ₅ | 0.24 | 0.28 | 0.27 | 0.25 | 0.27 | 0.29 | 0.31 | 0.29 |
| LOI | 1.14 | 0.30 | 0.38 | 4.24 | 1.77 | 1.06 | 1.63 | 1.46 |
| Total | 99.90 | 100.00 | 100.14 | 100.40 | 100.45 | 100.17 | 99.91 | 99.93 |
| Ba | 458 | 478 | 445 | 411 | 439 | 525 | 364 | 477 |
| Ce | 41.1 | 35.3 | 33.5 | 31.5 | 33.6 | 38.0 | 33.4 | 36.0 |
| Co | 22.2 | 16.3 | 18.7 | 18.3 | 16.6 | 17.1 | 22.9 | 18.9 |
| Cr | 7.2 | 5.6 | 5.5 | 6.2 | 3.3 | 9.2 | 6.0 | 24.5 |
| Dy | 3.85 | 3.90 | 3.55 | 3.25 | 3.71 | 3.62 | 4.48 | 3.86 |
| Er | 2.30 | 2.29 | 2.18 | 1.96 | 2.17 | 2.15 | 2.52 | 2.14 |
| Eu | 1.42 | 1.40 | 1.39 | 1.18 | 1.44 | 1.33 | 1.40 | 1.35 |
| Gd | 4.29 | 4.20 | 3.89 | 3.73 | 4.29 | 3.85 | 4.74 | 4.17 |
| Hf | 2.66 | 2.54 | 2.45 | 2.23 | 2.74 | 2.23 | 2.88 | 2.21 |
| Ho | 0.805 | 0.845 | 0.749 | 0.718 | 0.769 | 0.780 | 0.926 | 0.791 |
| La | 20.0 | 16.5 | 16.1 | 15.6 | 16.3 | 18.7 | 16.3 | 18.0 |
| Lu | 0.338 | 0.385 | 0.349 | 0.339 | 0.371 | 0.358 | 0.416 | 0.358 |
| Mo | 1.11 | 0.93 | 1.12 | 0.95 | 1.00 | 1.14 | | 1.04 |
| Nb | 4.62 | 4.17 | 3.65 | 3.38 | 4.12 | 3.31 | 4.35 | 2.92 |
| Nd | 19.3 | 17.6 | 18.0 | 16.4 | 18.1 | 18.1 | 20.0 | 18.9 |
| Ni | 5.2 | 1.6 | 1.6 | 1.7 | 2.8 | 2.3 | 7.0 | 3.3 |
| Pb | 15.7 | 13.0 | 19.6 | 15.1 | 14.7 | 19.6 | 14.9 | 18.9 |
| Pr | 4.91 | 4.41 | 4.16 | 4.00 | 4.20 | 4.38 | 4.552 | 4.53 |
| Rb | 49.0 | 42.5 | 40.6 | 38.7 | 44.0 | 50.3 | 24.6 | 45.2 |
| Sm | 4.40 | 4.22 | 4.24 | 3.92 | 4.12 | 4.01 | 4.72 | 4.68 |
| Sr | 573 | 532 | 552 | 533 | 547 | 570 | 533 | 611 |
| Ta | 0.36 | 0.34 | 0.31 | 0.25 | 0.31 | 0.27 | 0.31 | 0.22 |
| Tb | 0.622 | 0.624 | 0.577 | 0.536 | 0.615 | 0.584 | 0.759 | 0.600 |
| Th | 6.20 | 5.92 | 5.98 | 5.35 | 5.07 | 7.61 | 5.27 | 7.33 |
| Tm | 0.330 | 0.382 | 0.353 | 0.322 | 0.358 | 0.345 | 0.391 | 0.341 |
| U | 1.42 | 1.29 | 1.28 | 1.06 | 1.34 | 1.57 | 1.06 | 1.35 |
| V | 239 | 200 | 199 | 194 | 197 | 193 | 259 | 224 |
| Y | 22.3 | 24.1 | 22.3 | 21.2 | 24.6 | 22.1 | 25.0 | 23.4 |
| Yb | 2.10 | 2.24 | 2.16 | 2.00 | 2.34 | 2.12 | 2.54 | 2.06 |
| Zr | 112 | 107 | 99 | 95 | 115 | 90 | 104 | 90 |

(continued)

Table 6.1 (continued)

| | | | | | | | | |
|-----------------------------------|---------|---------|---------|----------|---------|---------|----------|---------|
| Unit ^a | 4/5 | 4/5 | 4/5 | 4/5 | 4/5 | 4/5 | 4/5 | 4/5 |
| Geochemical affinity ^b | HK | HK | HK | HK | HK | HK | HK | HK |
| Sample | M96-167 | M97-021 | M97-031 | M97-0392 | M97-053 | M97-077 | M97-0781 | M98-030 |
| SiO ₂ | 54.41 | 52.85 | 55.62 | 52.86 | 54.12 | 52.45 | 53.24 | 52.13 |
| TiO ₂ | 0.75 | 0.88 | 0.71 | 0.87 | 0.74 | 0.78 | 0.75 | 0.78 |
| Al ₂ O ₃ | 18.72 | 18.57 | 18.63 | 18.80 | 18.92 | 18.96 | 19.35 | 19.02 |
| Fe ₂ O ₃ * | 8.31 | 9.09 | 7.37 | 8.78 | 8.19 | 8.89 | 8.31 | 8.49 |
| MnO | 0.18 | 0.18 | 0.19 | 0.19 | 0.19 | 0.20 | 0.20 | 0.20 |
| MgO | 2.94 | 3.51 | 2.37 | 3.20 | 2.91 | 3.27 | 2.82 | 2.80 |
| CaO | 8.39 | 9.41 | 7.79 | 8.94 | 8.49 | 9.18 | 8.88 | 8.72 |
| Na ₂ O | 3.57 | 3.36 | 3.80 | 3.48 | 3.47 | 3.32 | 3.43 | 3.39 |
| K ₂ O | 2.30 | 1.98 | 2.38 | 2.14 | 2.15 | 1.91 | 2.03 | 1.99 |
| P ₂ O ₅ | 0.27 | 0.25 | 0.25 | 0.24 | 0.30 | 0.31 | 0.32 | 0.31 |
| LOI | 0.16 | 0.42 | 1.34 | 0.55 | 1.08 | 0.91 | 0.73 | 2.07 |
| Total | 99.98 | 100.49 | 100.45 | 100.05 | 100.56 | 100.18 | 100.05 | 99.90 |
| Ba | 533 | 531 | 602 | 515 | 512 | 457 | 486 | 291 |
| Ce | 36.2 | 33.1 | 40.4 | 31.6 | 36.2 | 35.7 | 38.6 | 37.0 |
| Co | 20.0 | 23.6 | 16.9 | 21.9 | 18.8 | 19.2 | 18.8 | 11.3 |
| Cr | 8.3 | 12.6 | 9.2 | 8.9 | 6.6 | 5.7 | 6.0 | 2.4 |
| Dy | 3.26 | 3.56 | 3.54 | 3.41 | 3.30 | 3.54 | 3.68 | 4.82 |
| Er | 1.95 | 1.92 | 2.00 | 2.01 | 1.98 | 2.08 | 2.13 | 2.73 |
| Eu | 1.14 | 1.31 | 1.37 | 1.31 | 1.27 | 1.30 | 1.31 | 1.53 |
| Gd | 3.36 | 3.58 | 3.49 | 3.37 | 3.70 | 3.69 | 3.84 | 5.13 |
| Hf | 2.13 | 2.06 | 2.45 | 2.12 | 2.01 | 2.17 | 2.58 | 3.95 |
| Ho | 0.678 | 0.741 | 0.767 | 0.701 | 0.722 | 0.739 | 0.785 | 1.006 |
| La | 18.7 | 16.8 | 20.3 | 15.6 | 18.4 | 17.9 | 18.8 | 16.9 |
| Lu | 0.326 | 0.312 | 0.352 | 0.345 | 0.325 | 0.339 | 0.360 | 0.467 |
| Mo | 1.16 | 0.83 | 1.26 | 1.19 | 0.97 | 0.92 | 0.98 | |
| Nb | 2.77 | 2.85 | 3.27 | 2.73 | 2.85 | 3.18 | 3.55 | 6.28 |
| Nd | 17.1 | 17.0 | 18.6 | 16.2 | 16.8 | 18.3 | 19.1 | 23.4 |
| Ni | 2.3 | 4.6 | 3.0 | 2.9 | 1.4 | 0.1 | 0.1 | 2.2 |
| Pb | 15.7 | 24.3 | 13.8 | 18.2 | 17.6 | 16.7 | 19.6 | 21.3 |
| Pr | 4.08 | 4.07 | 4.74 | 3.91 | 4.40 | 4.27 | 4.63 | 5.288 |
| Rb | 58.1 | 49.4 | 64.5 | 48.7 | 52.7 | 44.1 | 48.0 | 20.5 |
| Sm | 3.93 | 4.17 | 4.40 | 4.15 | 4.19 | 4.27 | 4.70 | 5.39 |
| Sr | 600 | 555 | 614 | 569 | 586 | 588 | 624 | 544 |
| Ta | 0.20 | 0.21 | 0.25 | 0.20 | 0.21 | 0.22 | 0.26 | 0.47 |
| Tb | 0.519 | 0.568 | 0.526 | 0.606 | 0.570 | 0.581 | 0.615 | 0.832 |
| Th | 6.91 | 6.56 | 8.91 | 6.68 | 6.86 | 6.94 | 8.26 | 8.18 |
| Tm | 0.304 | 0.322 | 0.319 | 0.358 | 0.282 | 0.337 | 0.348 | 0.428 |
| U | 1.44 | 1.37 | 1.71 | 1.49 | 1.22 | 1.22 | 1.56 | 1.11 |
| V | 229 | 249 | 186 | 272 | 207 | 205 | 206 | 152 |
| Y | 22.7 | 22.5 | 22.3 | 22.4 | 22.6 | 22.5 | 23.3 | 26.9 |
| Yb | 1.93 | 2.02 | 2.17 | 2.10 | 1.99 | 2.01 | 2.10 | 2.84 |
| Zr | 89 | 83 | 99 | 85 | 88 | 89 | 94 | 144 |

(continued)

Table 6.1 (continued)

| Unit ^a | 4/5 | 4/5 | 4/5 | 6 | 6 | 7/8 | 7/8 | 7/8 |
|-----------------------------------|---------|---------|---------|---------|---------|---------|---------|---------|
| Geochemical affinity ^b | HK | HK | HK | HK | HK | HK | HK | HK |
| Sample | M98-031 | M98-066 | M98-096 | M07-001 | M07-044 | M95-011 | M96-142 | M97-068 |
| SiO ₂ | 51.70 | 53.06 | 53.29 | 54.77 | 53.23 | 52.88 | 55.88 | 51.85 |
| TiO ₂ | 0.84 | 0.81 | 0.78 | 0.84 | 0.87 | 0.80 | 0.69 | 0.87 |
| Al ₂ O ₃ | 18.77 | 18.97 | 18.64 | 18.68 | 18.21 | 18.61 | 19.05 | 18.53 |
| Fe ₂ O ₃ * | 8.38 | 8.95 | 8.55 | 7.88 | 9.30 | 9.32 | 7.45 | 9.65 |
| MnO | 0.20 | 0.20 | 0.20 | 0.18 | 0.19 | 0.20 | 0.18 | 0.21 |
| MgO | 3.09 | 3.23 | 3.22 | 2.59 | 3.05 | 3.50 | 2.44 | 3.90 |
| CaO | 9.23 | 9.23 | 8.86 | 8.32 | 8.96 | 9.39 | 8.13 | 9.58 |
| Na ₂ O | 3.35 | 3.41 | 3.45 | 3.86 | 3.75 | 3.30 | 3.76 | 3.20 |
| K ₂ O | 1.90 | 2.05 | 2.05 | 1.92 | 1.98 | 2.00 | 2.25 | 1.98 |
| P ₂ O ₅ | 0.26 | 0.30 | 0.29 | 0.28 | 0.25 | 0.29 | 0.31 | 0.29 |
| LOI | 2.49 | 0.27 | 0.81 | -0.13 | -0.17 | 0.07 | 0.24 | 0.31 |
| Total | 100.21 | 100.48 | 100.14 | 99.18 | 99.61 | 100.35 | 100.37 | 100.36 |
| Ba | 307 | 506 | 535 | 476 | 455 | 439 | 522 | 431 |
| Ce | 33.8 | 36.4 | 36.5 | 35.7 | 36.2 | 34.5 | 39.0 | 34.6 |
| Co | 13.0 | 20.4 | 19.8 | 15.5 | 24.4 | 21.6 | 14.2 | 27.8 |
| Cr | 2.5 | 4.9 | 9.7 | | | 11.7 | 8.2 | 16.0 |
| Dy | 4.49 | 3.77 | 4.07 | 4.04 | 4.06 | 3.46 | 3.88 | 3.45 |
| Er | 2.49 | 2.12 | 2.21 | 2.3 | 2.54 | 2.11 | 2.32 | 1.93 |
| Eu | 1.45 | 1.37 | 1.40 | 1.18 | 1.24 | 1.34 | 1.38 | 1.36 |
| Gd | 4.77 | 3.96 | 4.00 | 4.54 | 4.12 | 4.13 | 4.20 | 3.65 |
| Hf | 3.62 | 2.24 | 2.32 | 3 | 2.6 | 2.15 | 2.74 | 2.14 |
| Ho | 0.932 | 0.732 | 0.747 | 0.88 | 0.76 | 0.708 | 0.837 | 0.724 |
| La | 14.8 | 18.4 | 19.0 | 16.3 | 18 | 17.2 | 20.2 | 17.3 |
| Lu | 0.431 | 0.323 | 0.338 | 0.400 | 0.350 | 0.325 | 0.379 | 0.330 |
| Mo | | 1.05 | 1.03 | 0.7 | 0.6 | 1.05 | 1.22 | 0.92 |
| Nb | 5.63 | 3.10 | 3.25 | 4.3 | 4.5 | 3.30 | 4.06 | 2.94 |
| Nd | 21.0 | 18.8 | 19.1 | 16.2 | 14.2 | 17.8 | 19.9 | 18.0 |
| Ni | 2.1 | 3.1 | 4.1 | 1.3 | 2.3 | 3.1 | 0.8 | 2.6 |
| Pb | 20.0 | 18.5 | 18.9 | 3.5 | 2.6 | 15.7 | 19.8 | 14.8 |
| Pr | 4.736 | 4.24 | 4.37 | 4.24 | 4.47 | 4.18 | 4.79 | 4.28 |
| Rb | 20.7 | 47.4 | 50.8 | 42.3 | 42.2 | 46.8 | 52.4 | 45.7 |
| Sm | 4.97 | 4.37 | 4.27 | 3.95 | 3.73 | 4.34 | 4.57 | 4.33 |
| Sr | 531 | 565 | 584 | 564.2 | 594.6 | 600 | 546 | 603 |
| Ta | 0.41 | 0.24 | 0.25 | 0.4 | 0.3 | 0.23 | 0.34 | 0.21 |
| Tb | 0.773 | 0.595 | 0.636 | 0.63 | 0.62 | 0.588 | 0.622 | 0.627 |
| Th | 7.14 | 6.77 | 6.68 | 5 | 5.9 | 7.23 | 8.04 | 6.16 |
| Tm | 0.395 | 0.361 | 0.340 | 0.38 | 0.32 | 0.314 | 0.386 | 0.318 |
| U | 1.09 | 1.51 | 1.46 | 1.3 | 1.2 | 1.29 | 1.43 | 1.02 |
| V | 169 | 220 | 211 | 196 | 284 | 222 | 156 | 249 |
| Y | 24.7 | 22.1 | 22.3 | 23.8 | 20.6 | 23.0 | 23.9 | 22.8 |
| Yb | 2.59 | 2.16 | 2.12 | 2.2 | 2.63 | 2.22 | 2.35 | 2.01 |
| Zr | 133 | 87 | 91 | 108 | 107 | 86 | 107 | 83 |

^a Volcano-stratigraphic unit (see text and Fig. 6.9); ^b Geochemical affinity: MK = medium-K; HK = high-K. Other symbols and abbreviations: Fe₂O₃* = total Fe as Fe₂O₃; b.d. = below detection. Data sources: Gertisser (2001), Gertisser and Keller (2003a, b), Handley et al. (2011, 2014), Gertisser et al. (2012a) and previously unpublished data by the authors (shown by italic font), produced in the same laboratories and with the same methods as described in Gertisser (2001), Gertisser and Keller (2003a, b) and Handley et al. (2011, 2014)

Table 6.2 Whole rock isotopic data for Merapi

| Unit ^a | Geochemical affinity ^b | Sample | ⁸⁷ Sr/ ⁸⁶ Sr | ¹⁴³ Nd/ ¹⁴⁴ Nd | ²⁰⁸ Pb/ ²⁰⁴ Pb | ²⁰⁷ Pb/ ²⁰⁴ Pb | ²⁰⁶ Pb/ ²⁰⁴ Pb | ¹⁷⁶ Hf/ ¹⁷⁷ Hf | δ ¹⁸ O (‰ SMOW) |
|-------------------|-----------------------------------|----------|------------------------------------|--------------------------------------|--------------------------------------|--------------------------------------|--------------------------------------|--------------------------------------|----------------------------|
| 1 | MK | M96-175 | 0.705105 | 0.512752 | 39.070 | 15.674 | 18.740 | 0.283185 | +7.7 |
| 2 | HK | M95-028 | 0.705793 | 0.512729 | 39.219 | 15.703 | 18.823 | 0.283146 | +6.4 |
| 2 | HK | M96-050 | 0.705539 | 0.512742 | 39.189 | 15.693 | 18.807 | 0.283160 | +7.7 |
| 3 | MK | M95-026 | 0.705260 | 0.512727 | 39.130 | 15.693 | 18.769 | 0.283146 | +6.4 |
| 3 | MK | M96-056 | 0.705275 | 0.512765 | 39.170 | 15.709 | 18.771 | 0.283131 | +6.6 |
| 3 | MK | M98-047 | 0.705014 | 0.512712 | 39.110 | 15.689 | 18.740 | 0.283144 | +6.9 |
| 3 | MK | M98-107 | 0.705169 | 0.512722 | 39.215 | 15.715 | 18.781 | 0.283144 | +6.9 |
| 4/5 | MK | M96-073 | 0.705392 | 0.512774 | 39.134 | 15.692 | 18.755 | 0.283157 | +6.3 |
| 4/5 | MK | M96-137 | 0.705277 | 0.512758 | 39.139 | 15.695 | 18.759 | 0.283148 | +6.8 |
| 4/5 | MK | M96-163 | 0.705155 | 0.512754 | | | | | +8.3 |
| 4/5 | MK | M98-0532 | 0.705353 | 0.512759 | | | | 0.283160 | +7.3 |
| 4/5 | HK | M96-102 | 0.705515 | 0.512753 | | | | | +6.9 |
| 4/5 | HK | M96-167 | 0.705696 | 0.512701 | 39.117 | 15.684 | 18.766 | | +6.0 |
| 4/5 | HK | M97-021 | 0.705741 | 0.512712 | 39.125 | 15.685 | 18.769 | 0.283138 | +6.7 |
| 4/5 | HK | M97-031 | 0.705625 | 0.512711 | 39.098 | 15.678 | 18.760 | 0.283141 | +7.0 |
| 4/5 | HK | M97-0392 | 0.705663 | 0.512714 | 39.130 | 15.688 | 18.763 | 0.283137 | +6.2 |
| 4/5 | HK | M97-053 | 0.705658 | 0.512678 | | | | | +7.0 |
| 4/5 | HK | M98-030 | 0.705704 | 0.512732 | | | | | +7.1 |
| 4/5 | HK | M98-031 | 0.70554 | 0.512746 | | | | 0.283141 | +7.5 |
| 4/5 | HK | M98-066 | 0.705826 | 0.512675 | 39.175 | 15.699 | 18.780 | | +6.6 |
| 4/5 | HK | M98-096 | 0.705643 | 0.512686 | 39.156 | 15.697 | 18.771 | 0.283147 | +6.5 |
| 6 | HK | M07-001 | 0.70536 | 0.512774 | | | | | |
| 6 | HK | M07-044 | 0.705284 | | | | | | |
| 7/8 | HK | M95-011 | 0.705687 | 0.512695 | | | | | |
| 7/8 | HK | M96-142 | 0.705737 | 0.512723 | 39.195 | 15.714 | 18.773 | 0.283128 | +6.7 |
| 7/8 | HK | M97-068 | 0.705711 | 0.512671 | 39.141 | 15.694 | 18.763 | 0.283128 | +6.3 |

^a Volcano-stratigraphic unit (see text and Fig. 6.9); ^b Geochemical affinity: MK = medium-K; HK = high-K. Data sources: Gertisser (2001), Gertisser and Keller (2003a, b), Handley et al. (2011, 2014), Gertisser et al. (2012a) and previously unpublished data by the authors (shown by italic font), produced in the same laboratories and with the same methods as described in Gertisser (2001), Gertisser and Keller (2003a, b) and Handley et al. (2011, 2014)

lavas and pyroclastic rocks that constitute the eight main volcano-stratigraphic units display notable mineralogical, geochemical and isotopic variations, with variations in whole rock SiO₂ content between 48.3 and 61.4 wt% (recalculated to 100 wt%, volatile-free). In the chemical classification using TAS (total alkali–silica diagram) (Le Maitre et al. 2002; Fig. 6.18a), the Merapi rocks straddle the boundary between basalt/trachybasalt, basaltic andesite/basaltic trachyandesite and andesite/trachyandesite. Variations in K₂O content (Fig. 6.18b) divide the eruptive products of Merapi into medium-K and high-K types (Le Maitre et al. 2002). In the classic K₂O versus SiO₂ classification of Pecerillo and Taylor (1976), these types correspond to the calc-alkaline and high-K calc-alkaline suite of rocks, respectively. Basaltic andesite/basaltic trachyandesite (high-K basaltic andesite) is by far the dominant rock type of Merapi, which may therefore be classed as a basaltic andesite volcano. Basalt/trachybasalt (high-K basalt) and andesite/trachyandesite (high-K andesite) are subordinate.

Merapi lavas, including recent domes (e.g. 1984, 1994, 1998, 2006, 2010), and pyroclastic rocks may contain a range of igneous inclusions, including mafic and felsic plutonic fragments and co-magmatic, occasionally highly crystalline, enclaves (e.g. del Marmol 1989; Chadwick et al. 2013; Troll et al. 2013a; van der Zwan et al. 2013; Preece, 2014; Troll and Deegan 2023, Chap. 8), which range from 40.2 to 53.4 wt% SiO₂ and 48.8–55.0 wt% SiO₂ (recalculated to 100 wt%, volatile-free), respectively (Chadwick et al. 2013; Preece 2014).

Material derived from the subvolcanic crustal basement is frequently found as thermally metamorphosed (calc-silicate) xenoliths, less abundant metasedimentary or volcanoclastic rock fragments, and rare xenoliths of buchite (pyrometamorphic, glass-rich rock) within the eruptive products (Clocchiatti et al. 1982; del Marmol 1989; Berthommier 1990; Camus et al. 2000; Gertisser 2001; Gertisser and Keller 2003b; Chadwick et al. 2007, 2013; Deegan et al. 2010, 2023, Chap. 10; Troll et al. 2012, 2013a, b; Whitley et al. 2019, 2020; Whitley 2020).

6.3.2 Mineralogy and Petrography

6.3.2.1 Mineralogical and Petrographical Characteristics

Merapi volcanic rocks contain variable amounts of plagioclase, clinopyroxene, orthopyroxene, olivine, titanomagnetite and amphibole as major (> 5 vol%) or minor (1–5 vol%) mineral phases. Apatite is a common accessory phase (< 1 vol%). Rare chrome spinel occurs as inclusions in some olivine crystals, and similarly uncommon pyrrhotite has been identified within titanomagnetite, amphibole and clinopyroxene hosts. Alkali feldspar, cristobalite and biotite occur in the groundmass of a few Merapi samples (e.g. Bahar 1984; del Marmol 1989; Berthommier 1990; Andreastuti 1999; Camus et al. 2000; Hammer et al. 2000; Gertisser 2001; Gertisser and Keller 2003a, b; Deegan et al. 2010; Preece et al. 2013, 2016; Preece 2014; Peters et al. 2017; Li et al. 2021). Irrespective of the potassium content, and reflecting the relative restricted range of whole rock SiO₂ compositions, the mineralogical characteristics of the Merapi rocks are often similar, although differences between the basaltic, and basaltic andesitic to andesitic rock types are notable (Fig. 6.19).

Lavas and scoriaceous and pumiceous clasts in volcanoclastic deposits (Fig. 6.20) exhibit porphyritic textures with phenocryst contents typically up to ~ 60% of the total rock volume (e.g. Bahar 1984; del Marmol 1989; Berthommier 1990; Camus et al. 2000; Gertisser 2001). Phenocrysts (> 0.3 mm), microphenocrysts (0.03–0.3 mm) and crystal clots (glomerocrysts) are enclosed within a fine-grained or glassy groundmass (< 0.03 mm). The latter gives rise to a vitrophyric texture in quickly cooled magmas or lavas. In many cases, small, lath-shaped plagioclase microlites, which have grown before complete solidification of the quenched magmas or lavas, lead to a hyalopilitic texture. In more viscous lavas, the plagioclase microlites may be flow-aligned.

In all Merapi volcanic rocks, plagioclase and clinopyroxene are ubiquitous and typically dominate the phenocryst assemblage, with

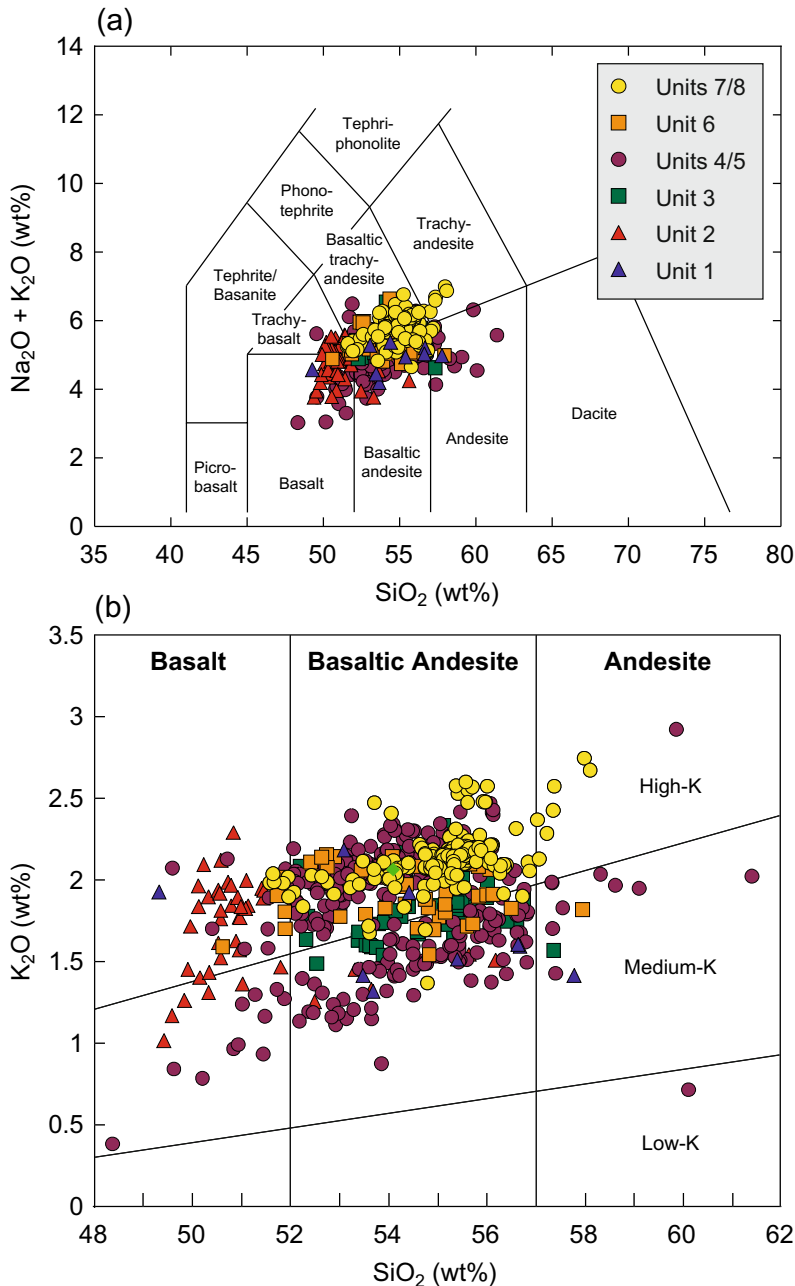


Fig. 6.18 **a** Total alkali versus SiO₂ (TAS) and **b** K₂O versus SiO₂ classification diagrams (Le Maitre et al. 2002) for Merapi lavas and pyroclastic rocks. All analyses are recalculated to 100 wt%, free of volatiles. Symbols (key as in Fig. 6.9): Unit 1 = Lava flows of Gunung Bibi; Unit 2 = Lava flows of Gunung Turgo, Gunung Plawangan and Gunung Medjing; Unit 3 = Lava flows of the Somma-Merapi; Units 4 and 5 = Pyroclastic deposits of the Holocene Pyroclastic Series; Unit 6 = Young (post-

Somma-Merapi) lava flows; Units 7 and 8 = Recent and mostly historical pyroclastic density current and lahar deposits as well as lava domes of the recent episode. *Data Sources* Bahar (1984), Bardintzeff (1984), del Marmol (1989), Berthommier (1990), Boudon et al. (1993, Andreastuti (1999), Andreastuti et al. (2000), Camus et al. (2000), Gertisser (2001), Gertisser and Keller (2003a, b), Debaille et al. (2006), Gertisser et al. (2012a), Chadwick et al. (2013), Preece (2014) and this study

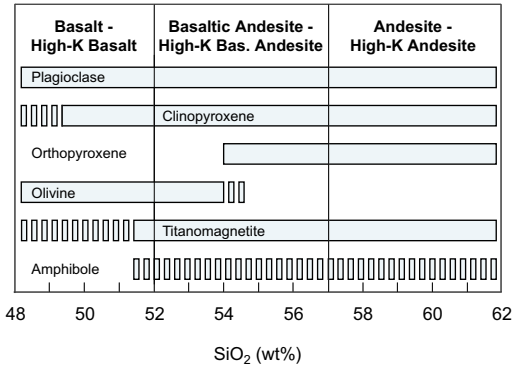


Fig. 6.19 Typical major and minor phenocryst and microphenocryst phases for Merapi lavas and pyroclastic rocks (after del Marmol 1989; Gertisser 2001)

plagioclase always prevailing (e.g. Bahar 1984; del Marmol 1989; Berthommier 1990; Gertisser 2001). In the basaltic rocks, especially those of Gunung Turgo, Gunung Plawangan and Gunung Medjing (Fig. 6.20b), olivine may appear as a major mineral phase and can replace clinopyroxene as a common phenocryst phase alongside plagioclase (del Marmol 1989). Therefore, clinopyroxene phenocrysts can be rare or even absent in the oldest basaltic lavas of Merapi, a phenomenon that was also observed in a lava flow located in Kali Kuning at the foot of Gunung Plawangan (del Marmol 1989). In the basaltic rocks of the younger periods, plagioclase and clinopyroxene dominate over olivine, which occurs as an accessory phase in some samples but is often absent in the lavas of the Somma-Merapi. Orthopyroxene occurs at the expense of olivine as phenocrysts or microphenocrysts in more SiO₂-rich volcanic rocks only and is an important index mineral to distinguish basaltic from basaltic andesitic and andesitic rock types. Occasionally, phenocrysts or microphenocrysts of olivine and orthopyroxene coexist in rocks with 52–55 wt% SiO₂. In relatively rare cases, both olivine and orthopyroxene are absent, resulting in basaltic andesite or andesite with only clinopyroxene. Except for the basalts of Gunung Turgo, Gunung Plawangan and Gunung Medjing, amphibole may occur as an accessory, minor or major mineral phase (Fig. 6.20). Titanomagnetite is the only primary magmatic

Fe–Ti oxide phase in the Merapi rocks. It is usually more abundant in the younger and more SiO₂-rich eruptive products and occurs only sporadically and as a minor phase in the basalts of Gunung Turgo, Gunung Plawangan and Gunung Medjing. Apatite is present as an accessory phase in nearly all Merapi volcanic rocks where it occurs as microphenocryst or as inclusion in plagioclase, pyroxene or amphibole. Furthermore, rare Cr-spinel has been observed as inclusions in olivine in the basalts of Gunung Turgo, Gunung Plawangan and Gunung Medjing (del Marmol 1989; Gertisser 2001). The groundmass mineral assemblages in the microcrystalline rock varieties are dominated by plagioclase, clinopyroxene, orthopyroxene and titanomagnetite, although alkali feldspar, cristobalite and biotite have been described in a few samples, with cristobalite also occasionally filling pore space (Hammer et al. 2000; Gertisser 2001; Costa et al. 2013; Preece et al. 2013, 2016). Glomerocrysts, consisting of plagioclase, clinopyroxene, minor amounts of orthopyroxene or, alternatively, olivine, titanomagnetite and, in some cases, amphibole, are often present in the Merapi rocks. Brownish glass may occur in interstitial spaces between larger crystals giving rise to an intersertal texture.

Igneous inclusions in the Merapi lavas consist of highly crystalline basaltic andesites, comagmatic enclaves, plutonic crystalline rocks, often characterised by a magmatic cumulate texture, and amphibole megacrysts up to several centimetres in length (del Marmol 1989; Camus et al. 2000; Chadwick et al. 2013; Troll et al. 2013a; van der Zwan et al. 2013; Preece 2014; Peters et al. 2017; Troll and Deegan 2023, Chap. 8). The light grey dense igneous inclusions in the 2010 lava dome are akin to the highly crystalline basaltic andesite inclusions. They were interpreted as fragments of a plug of cooled, rigid magma that resided at shallow depth within the magmatic system and was partially re-heated, fragmented and incorporated into the juvenile 2010 magma (Preece 2014; Preece et al. 2016; Subandriyo et al. 2023, Chap. 12). The igneous inclusions ubiquitously contain plagioclase, pyroxene and titanomagnetite, almost always amphibole, which can be a major

mineral phase in some inclusions, and various proportions of glass or groundmass depending on inclusion type (Camus et al. 2000; Chadwick et al. 2013; Troll et al. 2013a). Preece (2014) additionally identified alkali feldspar, cristobalite and biotite in the light grey inclusion material in the 2010 eruptive products.

The abundant calc-silicate xenoliths in the Merapi lavas were grouped into magmatic skarns, which contain evidence of formation within the magma, and exoskarns, which represent fragments of crystalline, metamorphosed wall-rocks (Deegan et al. 2010; Whitley et al. 2019, 2020; Whitley 2020). They are often dominated by wollastonite and diopside but may also contain plagioclase, augite, ferrian aluminian diopside or augite (fassaite), hedenbergite, tremolite, grossular-andradite or uvarovite garnet, quartz, magnetite, chromite, spinel, melilite, epidote, leucite, biotite, apatite, titanite, scapolite, prehnite, bustamite, cuspidine, fluorite, spurrite and a wadalite-phase, amongst others. Traces of texturally distinct calcite were also observed in several of the samples. In addition, magmatic skarns may contain Ca-enriched glass, which is largely absent in the exoskarn xenoliths (Clocchiatti et al. 1982; Kerinec 1982; Camus et al. 2000; Chadwick et al. 2007, 2013; Deegan et al. 2010, 2023, Chap. 10; Troll et al. 2012, 2013a, b; Preece 2014; Whitley et al. 2019, 2020; Whitley 2020). Buchites contain abundant (> 70 vol%) quartz or other SiO₂ polymorphs with interstitial glass around the crystal borders, and minor small interstitial clinopyroxene, plagioclase and wollastonite (Whitley 2020; Whitley et al. 2020).

6.3.2.2 Mineral Textures and Compositions

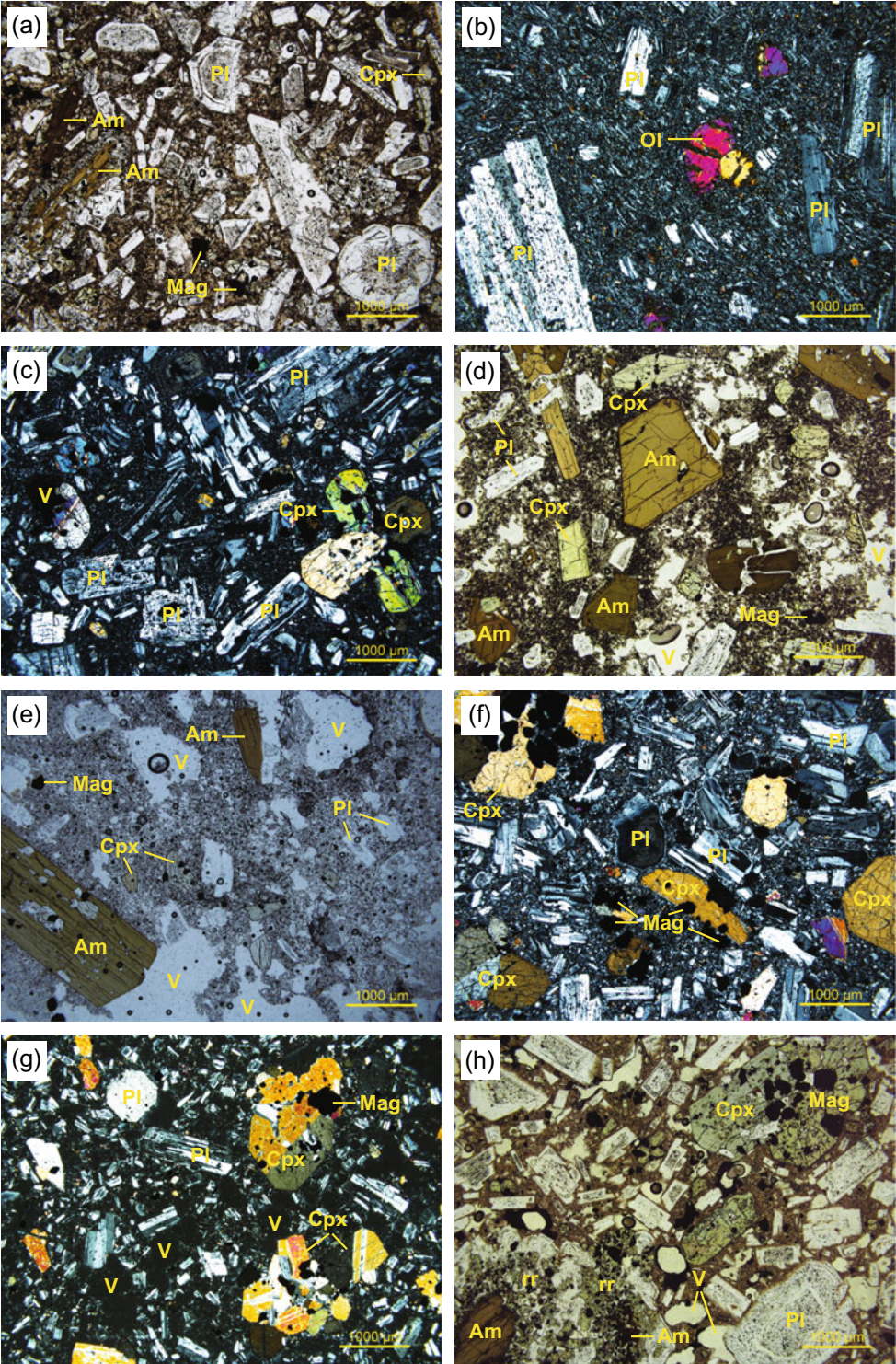
Detailed descriptions of mineral textures and compositions at Merapi, including extensive datasets of mineral analyses, can be found in

unpublished Ph.D. theses (e.g. Bahar 1984; del Marmol 1989; Andreastuti 1999; Berthommier 1990; Gertisser 2001; Preece 2014; Whitley 2020); other accounts are given in published work (e.g. Camus et al. 2000; Hammer et al. 2000; Gertisser and Keller 2003a, b; Chadwick et al. 2007, 2013; Costa et al. 2013; Nadeau et al. 2013; Preece et al. 2013, 2014, 2016; van der Zwan et al. 2013; Erdmann et al. 2014; Deegan et al. 2016; Peters et al. 2017; Whitley et al. 2000). The range of mineral (phenocryst and microphe-nocryst) compositions in the lavas and pyroclastic rocks of the main volcano-stratigraphic units are summarised below together with the main mineral textural characteristics. A subset of representative analyses is shown in Fig. 6.21.

Feldspar (Fig. 6.21a) is always present in the Merapi volcanic rocks as phenocrysts, microphenocrysts, inclusions in pyroxene and amphibole, and groundmass microlites; it is also a main constituent of crystal aggregates or glomerocrysts. Phenocrysts and microphenocrysts are ubiquitously plagioclase up to a few millimetres in size. Larger plagioclase crystals (up to 6 mm long), which are typically zoned, multiply twinned and fractured, and contain melt inclusions arranged in certain crystal zones, are occasionally found in the oldest basaltic lavas of Gunung Turgo, Gunung Plawangan and Gunung Medjing. This plagioclase type may be recognised in younger Merapi rocks as crystals, so-called antecrysts, that are typically smaller, complexly zoned, broken, rounded and mantled by more albitic feldspar (del Marmol 1989). Overall, plagioclase crystals at Merapi may be euhedral, rounded or resorbed, broken, twinned or sieve-textured, and frequently contain inclusions of brown glass and other minerals. They can be unzoned, but commonly display normal, reverse or oscillatory zoning. In rare cases, plagioclase phenocrysts may have rims of alkali feldspar

Fig. 6.20 Photomicrographs of volcanic rocks from the main volcano-stratigraphic units of Merapi (cf. Fig. 6.9). **a** Lava block of Gunung Bibi (Unit 1). **b** Lava flow of Gunung Plawangan (Unit 2). **c** Old Merapi lava flow near Deles (Unit 3). **d** Clast in PDC deposit in Kali Juweh in the north-western sector of Merapi (Unit 4). **e** Scoriaceous or pumiceous clast from the sub-Plinian Jurangjero I

tephra (Gertisser 2001; Gertisser et al. 2012a) (Unit 5). **f** Selokopo lava (Unit 6). **g** Breadcrust bomb from young PDC deposit on Merapi's south flank (Unit 7). **h** 1994 lava dome (Unit 8). Abbreviations: Am = amphibole; Pl = plagioclase; Cpx = clinopyroxene; Ol = olivine; Mag = magnetite; V = vesicles; rr = reaction (break-down) rim around amphibole



(Camus et al. 2000). Overall, plagioclase phenocryst and microphenocryst compositions range from An₂₅ to An₉₆ (del Marmol 1989; Andreastuti 1999; Camus et al. 2000; Preece 2014), with variations within a single sample and individual crystals up to 60 mol% and more than 40 mol% anorthite (An), respectively (Gertisser 2001). In some samples, clear and inclusion-free plagioclase phenocrysts are characterised by large homogeneous, anorthite-rich cores (> ~ An₉₀) and thin rims of more albitic compositions. Such crystals typically constitute only a small proportion of the plagioclase population of a sample but may occur in the basaltic and more evolved rock types, spanning the entire geological history from the oldest units through to the recent eruptive products (del Marmol 1989; Gertisser 2001; Chadwick et al. 2007, 2013; Preece 2014). A rare group of mostly fairly albitic (An₅₅₋₆₀), untwined, inclusion-free and anhedral crystals up to 0.5 mm in size is present primarily in the basalts (del Marmol 1989). Plagioclase microlites are generally more albitic in composition than phenocrysts and microphenocrysts (Camus et al. 2000), however they may contain up to ~ 84 mol% An (Preece 2014). In some of the recent dome rocks and pyroclastic material, plagioclase microlites are often mantled by alkali element-rich rims of anorthoclase and more K-rich alkali feldspar (sanidine) with up to 58 mol.% orthoclase (Camus et al. 2000; Hammer et al. 2000; Preece 2014; Preece et al. 2023, Chap. 9).

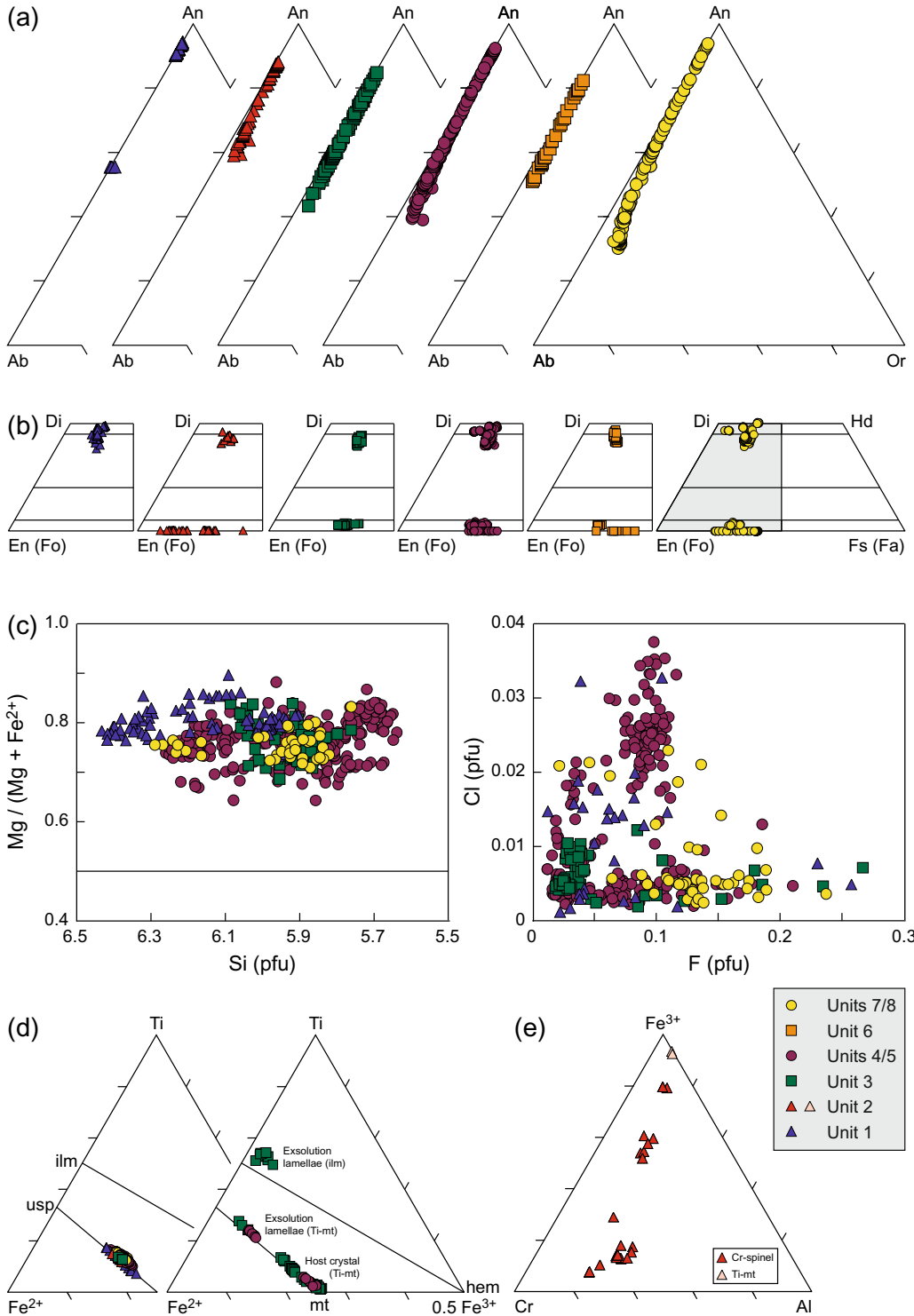
Clinopyroxene (Fig. 6.21b) occurs in essentially all Merapi volcanic rocks as phenocrysts, microphenocrysts and groundmass microlites. Phenocrysts are typically euhedral to subhedral, unzoned or only weakly zoned with continuous changes in composition, and often host silicate melt (glass) inclusions, as well as inclusions of magnetite, plagioclase and apatite (Gertisser 2001; Preece 2014). Some clinopyroxenes are

discontinuously zoned with abrupt compositional changes between core regions and outer zones. In a few samples, clinopyroxene can be found as overgrowth rims on earlier formed orthopyroxene crystals. The clinopyroxene phenocrysts of Merapi are augite (< 45 mol% wollastonite (Wo)) and diopside (> 45 mol% Wo) with a range of Wo₃₉₋₅₁En₃₄₋₅₀Fs₄₋₁₉, following the classification scheme of Morimoto (1988) (Fig. 6.21b). Al₂O₃ concentrations vary between 0.4 and 8.9 wt%; magnesium numbers (Mg# = $100 \times \text{Mg}/\text{Mg} + \text{Fe}^{2+}$ (molar)) between 73 and 85 (Andreastuti 1999; Camus et al. 2000; Gertisser 2001; Costa et al. 2013; Preece 2014; Deegan et al. 2016). High-Al compositions, which may also be enriched in Cr, occur as corroded, xenocrystic cores in abruptly zoned clinopyroxene crystals (Gertisser 2001). Clinopyroxene microphenocrysts and microlites analysed in the 2010 eruptive products are also usually augite and diopside (Wo₄₀₋₅₀En₃₅₋₄₅Fs₁₃₋₂₁), with 0.8–7.6 wt% Al₂O₃ and Mg# 65–81, with most between Mg# 70–80 (Preece 2014). However, several crystals with higher Fe content also occur and are classed as hedenbergite (Wo₄₉₋₅₀En₈₋₂₁Fs₂₉₋₄₁), with 1.2–2.6 wt% Al₂O₃ and Mg# 19–47 (Fig. 6.21b). These crystals were exclusively found in the 2001 dome rocks near a calc-silicate xenolith (Preece 2014).

Orthopyroxene phenocrysts and microphenocrysts (Fig. 6.21b) are homogeneous in composition or slightly normally zoned with higher Fe/Mg ratios towards the rims. With an overall compositional range of En₆₀₋₇₁Fs₂₆₋₃₆Wo₁₋₈, they may be classified as enstatite or, if the Wo component exceeds 5 mol%, formally as pigeonite in the Morimoto (1988) scheme (Gertisser 2001; Preece 2014). The Mg# of the orthopyroxenes varies between 66 and 76 and is always lower than that of clinopyroxenes in the same sample (Gertisser 2001).

Fig. 6.21 Mineral (phenocryst and microphenocryst) compositions in volcanic rocks from the main volcano-stratigraphic units of Merapi. **a** Feldspars (Ab-An-Or). **b** Pyroxenes (Wo-En-Fs) and olivine (Fo-Fa). **c** Amphiboles: (Mg/Mg + Fe²⁺) versus Si (pfu) plot for calcic amphiboles in the classification scheme of Leake et al. (1997); Cl (per formula unit; pfu) versus F (pfu) in Merapi

amphiboles. **d** Homogeneous and exsolved titanomagnetites in the system Fe²⁺-Fe³⁺-Ti. **e** Cr-rich spinels and titanomagnetite in lavas from Gunung Turgo, Gunung Plawangan and Gunung Medjing in the system Cr-Al-Fe³⁺. Symbols keyed to Fig. 6.9. *Data Source* Gertisser (2001)



Olivine phenocrysts and microphenocrysts (Fig. 6.21b) have forsterite (Fo) contents ranging from 56 to 88 mol%. Olivines with more than 80 mol% Fo are largely restricted to the basalts of Gunung Turgo, Gunung Plawangan and Gunung Medjing, where they occur as individual crystals or, more often, in crystal clots, while the more Fe-rich olivines (< Fo 65) are found in the younger eruptive products (del Marmol 1989; Gertisser 2001; Camus et al. 2000). In rare cases, phenocrysts exhibit reaction rims of orthopyroxene. Olivine is either unzoned or normally zoned with gradational changes from Mg-rich cores to more Fe-rich rims, and variations in Fo content up to 20 mol% in individual crystals. In the Gunung Turgo, Gunung Plawangan and Gunung Medjing basalts, zoned crystals with Mg-rich cores (Fo ~ 87–88) and thin, Fe-rich rims (Fo ~ 70) occur together with randomly distributed, unzoned olivines of Fo ~ 70 (del Marmol 1989; Gertisser 2001). The high-Mg olivine crystals or crystal cores are interpreted as xenocrysts that crystallised from a near-primary basaltic melt and were subsequently incorporated into a more differentiated magma.

Amphibole (Fig. 6.21c) in the Merapi volcanic rocks occurs as phenocrysts and microphenocrysts but is absent in the groundmass. It can be a major constituent of glomerocrysts and magmatic cumulate inclusions, and is found occasionally as megacrysts up to several centimetres long (e.g. Peters et al. 2017; Troll and Deegan 2023, Chap. 8). Euhedral amphiboles in equilibrium with the surrounding melt typically occur in pumiceous or scoriaceous clasts from pyroclastic fall or PDC deposits associated with larger explosive eruptions (Gertisser 2001; Gertisser et al. 2011), although fresh amphiboles without or with only minimal breakdown textures also occur in some recent dome lavas, e.g. in the 2010 lava dome (Preece 2014). Where amphibole is not in contact with glass, such as in magmatic cumulates, it also lacks a reaction rim. In most Merapi volcanic rocks, however, amphibole crystals are surrounded by reaction rims composed of small plagioclase, pyroxene (or olivine) and titanomagnetite, corresponding to the gabbroic type of

Garcia and Jacobson (1979). In several lava samples, amphibole breakdown rims of the black type occur, i.e. those without plagioclase (Garcia and Jacobson 1979). In cases where the amphibole has completely reacted, only amphibole relicts or pseudomorphs composed of titanomagnetite remain. The gabbroic type is considered as a result of slow magma ascent from depth during effusive eruptions, whereas the black type is thought to originate from oxidation, dehydrogenation and cooling during or after lava or dome extrusion. Compositionally, all Merapi amphiboles are calcic amphiboles (Leake et al. 1997), which, depending on the assumed ferric iron content, can be classified as either magnesiohastingsite ($Al^{VI} < Fe^{3+}$) or pargasite ($Al^{VI} > Fe^{3+}$) (Camus et al. 2000; Gertisser 2001; Preece 2014; Peters et al. 2017; Fig. 6.21c). Crystals are either homogeneous in composition or, occasionally, normally or reversely zoned, with rims containing either lower or higher Mg/Fe ratios than the cores. Where zoning is present, it can be either continuous or characterised by abrupt compositional changes. Core-rim variations are also observed with respect to Al_2O_3 , which ranges from 10.3 to 14.3 wt% in total. The Mg# of the amphiboles varies between 57 and 84 (Gertisser 2001; Preece 2014). Available data for Cl and F concentrations in Merapi amphiboles suggest the presence of both Cl- and F-dominated varieties (Gertisser 2001; Fig. 6.21c).

Titanomagnetite microphenocrysts or inclusions in plagioclase, pyroxene and amphibole (Fig. 6.21d) are typically anhedral or irregularly shaped. They span a wide compositional range in ulvöspinel content between 12 and 85 mol%, although compositions are often more uniform in specific rock types (del Marmol 1989; Camus et al. 2000; Gertisser 2001; Preece 2014). Titanomagnetite is always present in moderate amounts in the basaltic andesites, whereas it is relatively rare, and occasionally absent, in the basalts of Gunung Turgo, Gunung Plawangan and Gunung Medjing (del Marmol 1989; Gertisser 2001). In some samples, titanomagnetite shows lamellar exsolution, a feature that is prevalent in the lavas of the Somma-Merapi and the recent domes, but commonly absent in the

products of larger explosive eruptions. In addition to these exsolved titanomagnetites, a homogeneous population may occur in the same samples, although perhaps more often, exsolution can affect all titanomagnetite crystals (Gertisser 2001; Preece 2014). Most exsolution lamellae are of the trellis type that consist of ilmenite lamellae parallel to the {111} planes of the titanomagnetite host and result from slow cooling of the lavas below the solidus with accompanying oxidation (Buddington and Lindsley 1964; Haggerty 1993). Rarely, exsolution of a spinel phase of the magnetite-ulvöspinel solid solution series occurs (Gertisser 2001; Fig. 6.21d).

Cr-spinel (Fig. 6.21e) forms rare inclusions in some of the Mg-rich (Fo ~ 87–88 mol%) olivines in the basaltic lavas of Gunung Turgo, Gunung Plawangan and Gunung Medjing. The Cr-spinels contain variable concentrations of Cr₂O₃ (6.0–44.4 wt%), Al₂O₃ (4.5–16.5 wt%), Fe₂O₃ (10.5–55.9 wt%) and MgO (2.3–11.4 wt%), with corresponding notable variations in molar Cr/(Cr + Al), Al/(Al + Cr + Fe³⁺), Fe³⁺/(Al + Cr + Fe³⁺) and Mg/(Mg + Fe²⁺) (Gertisser 2001), and a large compositional spread in a ternary Fe³⁺–Cr–Al diagram (Fig. 6.21e).

Apatite is present as anhedral inclusions within clinopyroxene, plagioclase and amphibole phenocrysts, and rarely as groundmass micro-lites. Apatite in the 2010 eruptive products contain 0.4–1.4 wt% Cl, 1.1 to 5.4 wt% F and 0.4–1.0 wt% H₂O (Preece 2014; Li et al. 2021).

Biotite has been noted as a late crystallising phase of likely magmatic origin in the light grey inclusion material of the 2010 lava dome (Preece 2014). Costa et al. (2013) also noted the presence of biotite in 2010 samples. Biotite contains between 11.9 and 15.6 wt% FeO, with Mg# between 63 and 70. Fluorine and Cl vary between 0.5 and 3.8 wt% and 0.1–0.3 wt%, respectively (Preece 2014).

Cristobalite also occurs in the inclusions in the 2010 dome rocks where it fills small vesicles and is pervasive within the groundmass, often with ‘fish-scale’ cracked morphology or a microbotryoidal texture (Preece 2014). However, cristobalite is not restricted to this lithology and has previously been noted as vesicle infill in

several lava samples of the Somma-Merapi and some lava dome clasts in PDC deposits of the Holocene Pyroclastic Series (Gertisser 2001). Analyses from the 2010 samples (Preece 2014) show that cristobalite contains small amounts of Al₂O₃ (up to 1.73 wt%) and Na₂O (up to 0.99 wt%).

6.3.3 Major and Trace Element Compositions

Whole-rock variation diagrams of selected major and trace elements vs SiO₂ for Merapi are shown in Fig. 6.22. In general, the rocks of medium-K and high-K character, identified in Fig. 6.18b, do not display significant differences in major element oxides other than K₂O. Discernible trends can be observed for most if not all major element oxides with SiO₂, although the data for some elements are rather scattered. Overall, TiO₂, Fe₂O₃*, MgO and CaO abundances decrease with increasing SiO₂ content, while Na₂O, despite considerable scatter, and Na₂O increases. Unusually low Na₂O concentrations are found in some samples of the Holocene Pyroclastic Series (HPS) and are thought to reflect low-temperature alteration of volcanic glass by meteoric water mobilising and removing sodium. The Al₂O₃ content of the rocks always exceeds 16 wt% and is scattered without any systematic correlation with SiO₂. Extremely high Al₂O₃ contents (> 21 wt%) occur only in highly altered samples with > 2.5 wt% loss on ignition (LOI) (Gertisser 2001; Gertisser and Keller 2003b). The trace element variations with SiO₂ are generally more scattered than the major element data but systematic trends are nevertheless apparent. Concentrations of incompatible trace elements, such as the large ion lithophile elements (LILE) Rb and Ba, increase systematically with increasing SiO₂ content, and the variations of these elements mirror that of K₂O, with higher Rb and Ba concentrations in the more K₂O-rich rocks. In accordance with other high field strength elements (HFSE), Zr increases systematically with increasing SiO₂ content, with some samples of the HPS plotting above the main Merapi trend.

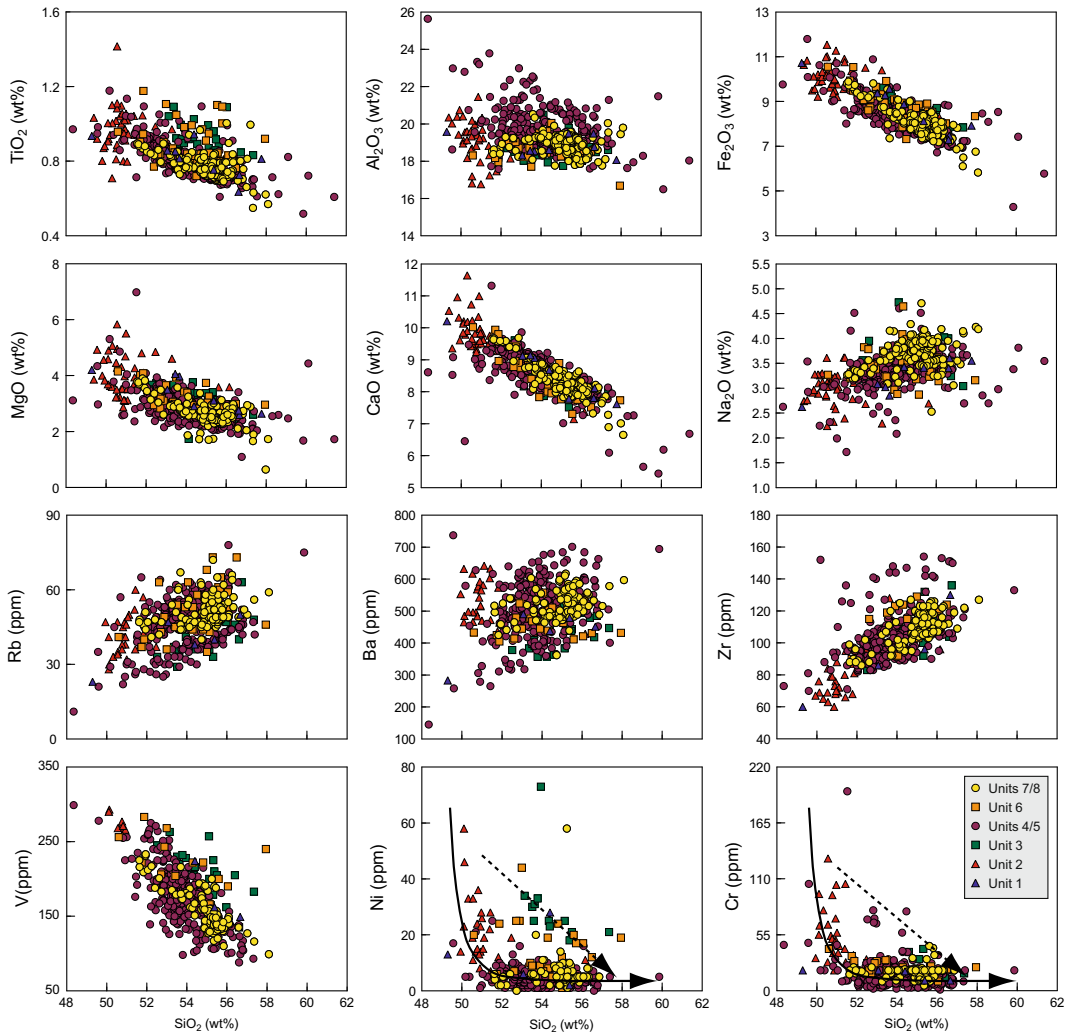


Fig. 6.22 Selected major and trace element variation diagrams vs SiO_2 for the Merapi volcanic suite. Major element analyses are normalised to 100 wt%, free of volatiles. General fractional crystallisation trends (solid

line) and magma mixing trends (dashed line) are shown in the Ni versus SiO_2 and Cr versus SiO_2 diagrams. Symbols keyed to Fig. 6.9. *Data Sources* as in Fig. 6.18

Among the transition elements, V shows near-linear negative correlation with SiO_2 , whereas both Ni and Cr display a main curvilinear trend of strongly decreasing abundance in the basalt range that becomes less pronounced in the more SiO_2 -rich rock types. Additionally, some samples of intermediate composition display anomalously high Cr and Ni contents and follow a linear trend of decreasing Ni and Cr abundances with increasing SiO_2 content. It should be noted,

however, that the lowest concentrations of both elements are at the analytical level of detection.

The trace element patterns of the Merapi volcanic rocks normalised to N-MORB are those typical of magmas from subduction-related tectonic settings. They are all remarkably similar, with enrichment in LILE, U and Th, a pronounced Pb peak in many samples and moderate enrichment in light rare earth elements (LREE) relative to the heavy rare earth elements (HREE) and the

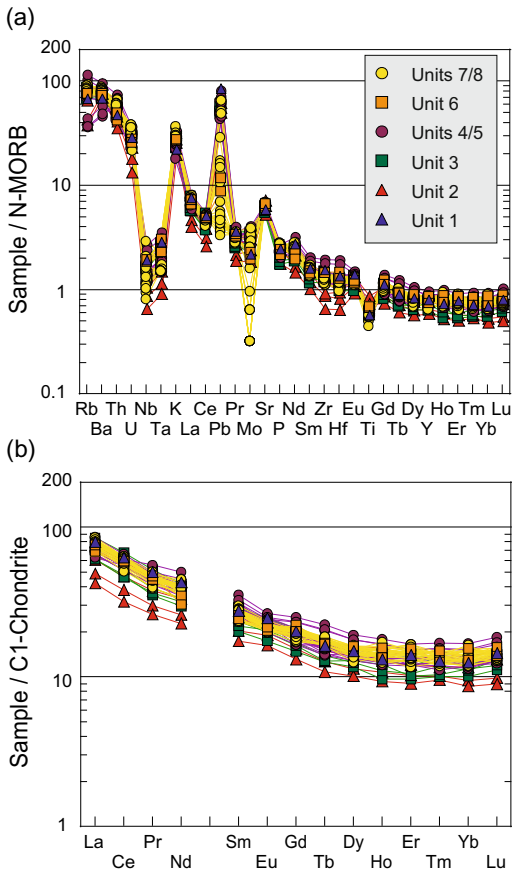


Fig. 6.23 **a** N-MORB-normalised trace element and **b** chondrite-normalised REE patterns for Merapi lavas and pyroclastic rocks. The normalising values are from Sun and McDonough (1989). Symbols keyed to Fig. 6.9. *Data Sources* Gertisser (2001), Gertisser and Keller (2003a, b), Handley et al. (2011); Gertisser et al. (2012a, b, c), Preece (2014) and this study

high field strength elements (HFSE). The elements Nb, Ta and Ti form distinct negative troughs in the trace element patterns, as does Mo in a few samples. In all rocks, the HREE are slightly depleted relative to N-MORB (Fig. 6.23a).

In a chondrite-normalised REE diagram (Fig. 6.23b), the Merapi volcanic rocks exhibit similar patterns, with fractionated LREE and relatively flat or slightly concave up HREE patterns, a typical feature of subduction-related volcanic rocks. However, there is a general lack of a pronounced Eu anomaly in all samples, or only a small negative or positive EU anomaly

present ($(\text{Eu}/\text{Eu}^* = 0.85\text{--}1.07)$). LREE (La) enrichment ranges from 42 to 86 times chondritic values, with $(\text{La}/\text{Sm})_{\text{N}} = 1.9\text{--}3.4$ and $(\text{La}/\text{Yb})_{\text{N}} = 4.1\text{--}7.0$. Middle rare earth elements (MREE) and HREE show unfractionated patterns ($(\text{Gd}/\text{Yb})_{\text{N}} = 1.3\text{--}1.7$), generally within 9–25 times chondritic values.

6.3.4 Isotopic Compositions

6.3.4.1 Radiogenic Isotopes

Sr, Nd, Hf and Pb isotopic ratios exist for whole rock samples spanning the entire geological history of Merapi, as well as a small number of magmatic minerals, plutonic inclusions, calc-silicate xenoliths and limestones from the local upper crust.

The $^{87}\text{Sr}/^{86}\text{Sr}$ ratios of the Merapi volcanic rocks (lavas and pyroclastic rocks) display significant variations between 0.70480 and 0.70594, while $^{143}\text{Nd}/^{144}\text{Nd}$ ratios range from 0.51267 to 0.51280 (Whitford 1975a, b; Whitford et al. 1981; White and Patchett 1984; del Marmol 1989; McDermott and Hawkesworth 1991; Gertisser 2001; Turner and Foden 2001; Woodhead et al. 2001; Gertisser and Keller 2003b; Debaille et al. 2006; Handley et al. 2011, 2014, 2018; this study). Systematic differences in Sr and Nd isotopic ratios are most pronounced between the rocks of medium-K and high-K type, with the latter typically characterised by higher $^{87}\text{Sr}/^{86}\text{Sr}$ and lower $^{143}\text{Nd}/^{144}\text{Nd}$ (Gertisser 2001; Gertisser and Keller 2003b). Variations in Sr and Nd isotopic ratios with whole rock SiO_2 content are negligible. $^{87}\text{Sr}/^{86}\text{Sr}$ ratios (0.70568–0.70627) of plagioclase phenocrysts in recent Merapi volcanic rocks may exceed those of the whole rocks (Chadwick et al. 2007; Troll and Deegan 2023, Chap. 8). Plutonic xenoliths have a comparatively narrow range of $^{87}\text{Sr}/^{86}\text{Sr}$ (0.70529–0.70575) and $^{143}\text{Nd}/^{144}\text{Nd}$ (0.51257–0.51272), largely within the range of the volcanic rocks. Generally higher $^{87}\text{Sr}/^{86}\text{Sr}$ (0.70567–0.70787) and lower $^{143}\text{Nd}/^{144}\text{Nd}$ (0.51215–0.51272) are reported for calc-silicate xenoliths, including xenolith-hosted plagioclase crystals, and the

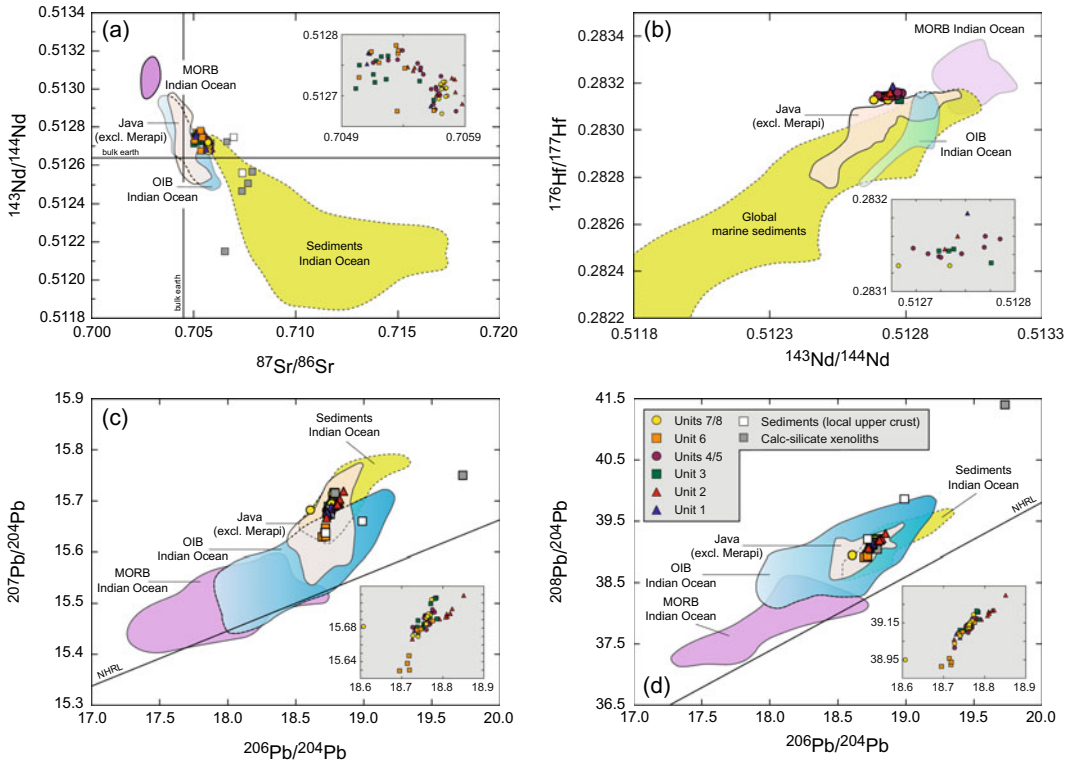


Fig. 6.24 Radiogenic isotope geochemistry of the main volcano-stratigraphic units of Merapi in relation to Indian Ocean MORB and OIB, volcanic rocks from Java and Indian Ocean marine sediments. Where available, isotopic data of sediments from the local upper crust and calc-silicate xenoliths in the Merapi lavas are also shown. **a** $^{143}\text{Nd}/^{144}\text{Nd}$ versus $^{87}\text{Sr}/^{86}\text{Sr}$ diagram. For *Data Sources*, see Gertisser et al. (2003b). Additional Sr and Nd isotopic data for Merapi are from Debaille et al. (2006), Handley et al. (2011, 2014, 2018) and this study; further calc-silicate xenolith data are from Chadwick et al. (2013). **b** $^{176}\text{Hf}/^{177}\text{Hf}$ versus $^{143}\text{Nd}/^{144}\text{Nd}$ diagram. The Merapi Hf isotopic data displayed are from Handley et al.

(2011). For *Data Sources* for the Indian Ocean MORB and OIB fields in Hf–Nd space, see Gertisser et al. (2012c). The Java field was compiled with data from White and Patchett (1984), Woodhead et al. (2001) and Handley et al. (2007, 2008, 2011). **c, d** $^{207}\text{Pb}/^{204}\text{Pb}$ and $^{208}\text{Pb}/^{204}\text{Pb}$ versus $^{206}\text{Pb}/^{204}\text{Pb}$ diagram. NHRL denotes the Northern Hemisphere Reference Line. Symbols of volcano-stratigraphic units keyed to Fig. 6.9. For *Data Sources*, see Gertisser et al. (2003b). Additional Pb isotopic data for Merapi are from Debaille et al. (2006) and Handley et al. (2014); further calc-silicate xenolith data from Chadwick et al. (2013)

local upper crust (Gertisser 2001; Gertisser and Keller 2003b; Chadwick et al. 2007, 2013; Troll et al. 2013a, b; Troll and Deegan 2023, Chap. 8). In the $^{143}\text{Nd}/^{144}\text{Nd}$ versus $^{87}\text{Sr}/^{86}\text{Sr}$ diagram (Fig. 6.24a), the Merapi eruptive products are broadly negatively correlated and form a cluster below the field for mid-ocean ridge basalt (MORB). The Merapi data plot between the field for MORB and sediments from the Indian Ocean, partly overlap the field of Indian Ocean island basalts and are displaced to somewhat higher $^{87}\text{Sr}/^{86}\text{Sr}$ at similar $^{143}\text{Nd}/^{144}\text{Nd}$ values compared

with many Javanese volcanoes. The upper crustal basement beneath Merapi and calc-silicate xenoliths plot near the unradiogenic end of the Sr isotopic spectrum of the Indian Ocean sediments, while $^{143}\text{Nd}/^{144}\text{Nd}$ is more scattered.

Hf isotopic data are available for a smaller whole rock sample set, with $^{176}\text{Hf}/^{177}\text{Hf}$ showing a compositional range between 0.28304 and 0.28319 (White and Patchett 1984; Woodhead et al. 2001; Handley et al. 2011) and no systematic variations with whole rock SiO_2 or K_2O content. In Hf–Nd isotopic space (Fig. 6.24b),

the Merapi rocks have amongst the highest Hf isotopic ratios of all Javanese volcanoes, plot near to, but are distinct from, the Indian Ocean MORB and OIB fields, and also fall outside the published range for global marine sediments.

$^{206}\text{Pb}/^{204}\text{Pb}$, $^{207}\text{Pb}/^{204}\text{Pb}$ and $^{208}\text{Pb}/^{204}\text{Pb}$ range from 18.601 to 18.851, 15.607 to 15.736 and 38.621 to 39.300, respectively (Whitford 1975a, b; del Marmol 1989; McDermott and Hawkesworth 1991; Gertisser 2001; Turner and Foden 2001; Woodhead et al. 2001; Gertisser and Keller 2003b; Debaille et al. 2006; Handley et al. 2014). In contrast to the Sr and Nd isotopic ratios, there are no apparent systematic variations in Pb isotopic ratios between rocks of medium-K and high-K type and with indices of magmatic differentiation (Gertisser 2001; Gertisser and Keller 2003b). Ratios of $^{206}\text{Pb}/^{204}\text{Pb}$ (18.706–18.849), $^{207}\text{Pb}/^{204}\text{Pb}$ (15.654–15.695) and $^{208}\text{Pb}/^{204}\text{Pb}$ (39.041–39.178) of plutonic xenoliths lie within the range of the volcanic rocks (Chadwick et al. 2013; Troll and Deegan 2023, Chap. 8). Calc-silicate xenoliths and the local upper crust show more pronounced variations in $^{206}\text{Pb}/^{204}\text{Pb}$ (18.720–19.728), $^{207}\text{Pb}/^{204}\text{Pb}$ (15.660–15.750) and $^{208}\text{Pb}/^{204}\text{Pb}$ (39.043–41.440) (Gertisser 2001; Gertisser and Keller 2003b; Chadwick et al. 2013; Troll and Deegan 2023, Chap. 8). Well-defined positive correlations can be observed in diagrams of $^{207}\text{Pb}/^{204}\text{Pb}$ and $^{208}\text{Pb}/^{204}\text{Pb}$ versus $^{206}\text{Pb}/^{204}\text{Pb}$ (Fig. 6.24c, d), where the Merapi data plot near and beyond the radiogenic $^{206}\text{Pb}/^{204}\text{Pb}$ end of the Indian Ocean MORB field. $^{207}\text{Pb}/^{204}\text{Pb}$ and $^{208}\text{Pb}/^{204}\text{Pb}$ ratios for Merapi are higher than typical Indian Ocean MORB values, and within the range of Java volcanic rocks and Indian Ocean marine sediments, which generally overlap with the field of the Merapi eruptive products in plots of $^{207}\text{Pb}/^{204}\text{Pb}$ and $^{208}\text{Pb}/^{204}\text{Pb}$ vs $^{206}\text{Pb}/^{204}\text{Pb}$. The Merapi rocks plot well above the Northern Hemisphere Reference Line (NHRL) and close to or within the field of Indian Ocean OIB field in diagrams of $^{207}\text{Pb}/^{204}\text{Pb}$ and $^{208}\text{Pb}/^{204}\text{Pb}$ versus $^{206}\text{Pb}/^{204}\text{Pb}$, respectively. Calc-silicate xenoliths and the local upper crust overlap with the field of the Merapi eruptive products or plot towards

more radiogenic Pb isotopic compositions, although $^{207}\text{Pb}/^{204}\text{Pb}$ values only marginally exceed those of the Merapi volcanics.

6.3.4.2 Oxygen Isotopes

A total of 44 whole rock oxygen isotope analyses are currently available for Merapi (Gertisser 2001; Gertisser and Keller 2003b; Troll et al. 2013a, b; Handley et al. 2014; Drignon et al. 2016). These are complemented by oxygen isotope data for magmatic crystals, plutonic and crustal xenoliths as well as sediments of the local upper crust (Gertisser 2001; Gertisser and Keller 2003b, Troll et al. 2013a; Deegan et al. 2016, 2021, 2023, Chap. 10; Whitley et al. 2019, 2020; Whitley 2020; Troll and Deegan 2023, Chap. 8).

$\delta^{18}\text{O}$ values in the basalt to andesite whole rocks range from +6.0‰ to +8.3‰ (SMOW) (Gertisser 2001; Gertisser and Keller 2003b). These values exceed typical mantle and basaltic oceanic crust values ($\delta^{18}\text{O} = +5.37$ to +5.81‰ (SMOW), average of 5.50‰; Eiler et al. 2000). Gertisser (2001) and Gertisser and Keller (2003b) observed the highest $\delta^{18}\text{O}$ values in pumiceous rocks and proposed that this reflects an increase in $\delta^{18}\text{O}$ by low-temperature alteration via hydration and oxygen exchange between the glassy groundmass and meteoric water. More recently, however, whole rock $\delta^{18}\text{O}$ values as high as +8.3‰ have also been measured in recent, unaltered basaltic andesites (Troll et al. 2013a). A similar range in oxygen isotope ratios was observed in medium-K and high-K rock varieties (Gertisser 2001; Gertisser and Keller 2003b). $\delta^{18}\text{O}$ values of phenocrysts range from +4.6‰ to +7.9‰ and 4.3‰ to +8.1‰ for plagioclase and pyroxene, respectively (Troll et al. 2013a; Borisova et al. 2016; Deegan et al. 2016, 2021; Troll and Deegan 2023, Chap. 8). Such values correspond to melt $\delta^{18}\text{O}$ values of up to +7.7‰ ($\delta^{18}\text{O}_{\text{plag}}$ (melt)) and up to +8.4‰ ($\delta^{18}\text{O}_{\text{pyx}}$ (melt)), assuming mineral-melt fractionation factors of +0.2 for plagioclase and -0.3 for pyroxene (Harris et al. 2005 and references therein). Plutonic xenoliths have $\delta^{18}\text{O}$ between +6.5‰ to +6.8‰, well within the range of the basaltic to andesitic whole rocks. Plagioclase and pyroxene within these xenoliths

display a narrow $\delta^{18}\text{O}$ range from + 5.4‰ to + 5.8‰ and 6.0‰ to + 6.2‰, respectively (Troll et al. 2013a; Troll and Deegan 2023, Chap. 8). Limestones from the local upper crust are characterised by $\delta^{18}\text{O}$ between + 18.9 and + 24.5, while calc-silicate xenoliths in the Merapi lavas generally have lower $\delta^{18}\text{O}$ between + 10.4‰ to + 14.2‰ (Gertisser 2001; Gertisser and Keller 2003b; Troll et al. 2013a), as a result of magma-carbonate interaction (e.g. Deegan et al. 2023, Chap. 10).

6.3.4.3 Uranium Series Isotopes

Disequilibria between short-lived radionuclides of the uranium decay chain are powerful indicators of magmatic processes and their time-scales (e.g. Bourdon et al. 2003). Short-lived uranium series isotopes were measured relatively frequently in Merapi whole rocks and in a few plagioclase crystals, mostly, but not exclusively, in recent eruptive products. Here, we summarise published ^{238}U – ^{230}Th – ^{226}Ra isotope data for Merapi (Gill and Williams 1990; McDermott and Hawkesworth 1991; Condomines and Sigmarsson 1993; Gauthier and Condomines 1999; Turner and Foden 2001; Condomines et al. 2005; Handley et al. 2018).

Most of the Merapi whole rock samples, as well as the few plagioclase separates analysed (Handley et al. 2018), show uranium excesses [$(^{238}\text{U}/^{230}\text{Th})$ activity ratios > 1], typical of subduction-related volcanic rocks. However, a small number of samples, including a clinopyroxene and a magnetite separate analysed, display small Th excesses [$(^{238}\text{U}/^{230}\text{Th})$ activity ratios < 1] (Gill and Williams 1990; Condomines et al. 2005; Turner and Foden 2001). ($^{230}\text{Th}/^{232}\text{Th}$) activity ratios range from 0.627 to 0.821, with some of the higher whole rock values coming from earlier studies which were mostly produced by alpha spectrometry (Fig. 6.25a). The vast majority of Merapi whole rock samples and plagioclase separates are also characterised by excess radium [$(^{226}\text{Ra}/^{230}\text{Th})$ activity ratios > 1], with most samples showing ($^{226}\text{Ra}/^{230}\text{Th}$) ratios between 3.0 and 3.4. The plagioclase separates from the 2006 and 2010 eruptions show similar ($^{226}\text{Ra}/^{230}\text{Th}$) ratios of 3.5–3.7, slightly higher

than the whole rocks (Handley et al. 2018). Whole rock Ra excesses comparable to those of the 2006 and 2010 eruptions are observed in other historical and recent eruptions (Gill and Williams 1990; Gauthier and Condomines 1999; Condomines et al. 2005), while significantly lower Ra excesses, or even small Th excesses, are reported for some older whole rock samples (Turner and Foden 2001; Condomines et al. 2005) (Fig. 6.25b).

6.4 Magma Genesis and Magmatic Differentiation at Merapi

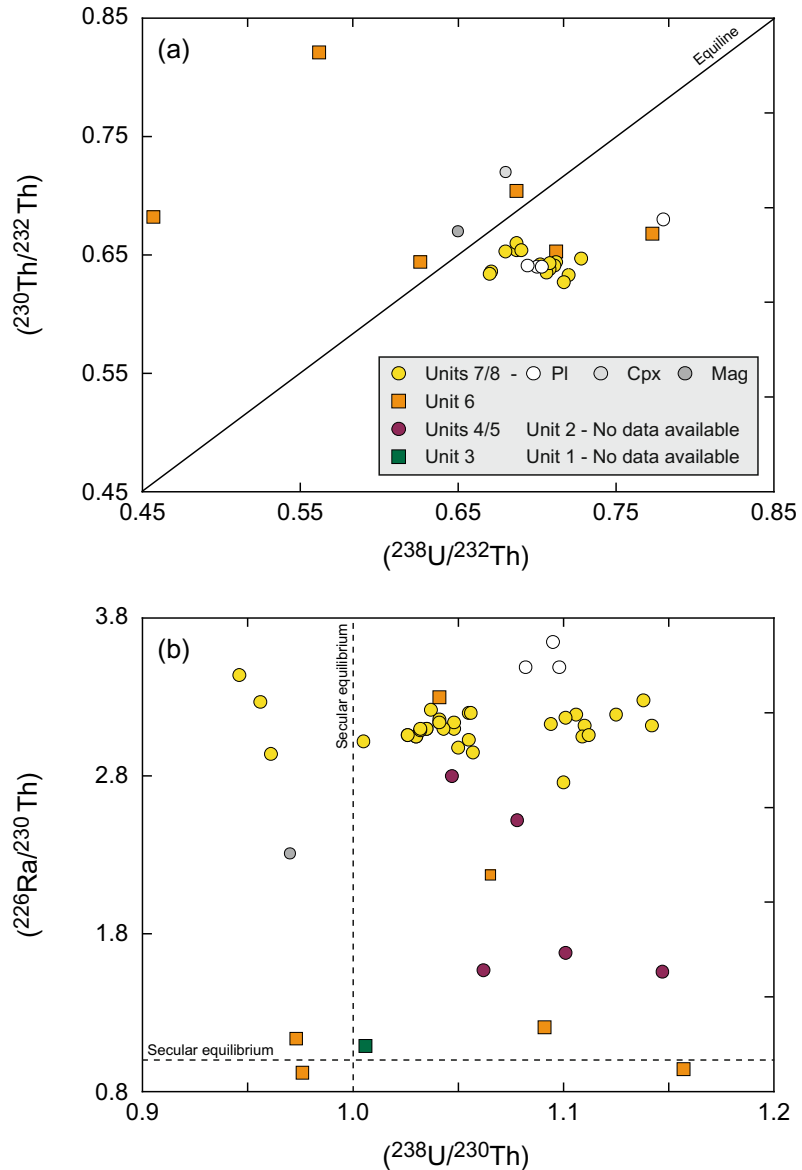
A broad petrogenetic model for Merapi involves the generation of primary magmas by partial melting of a heterogeneous, Indian Ocean MORB-like mantle source, metasomatised by slab-derived fluid and melt components of the Sunda arc subduction system, followed by complex magmatic differentiation processes during magma storage and ascent through the crust that have led to systematic geochemical variations, as detailed in the following sections.

6.4.1 Magma Generation

The generation of primary Merapi magmas in the mantle, the geochemical and isotopic characteristics of the mantle source and the nature of subducted slab-derived components have been the subject of numerous studies, including those of Whitford (1975a, b), Whitford and Nicholls (1976), Whitford et al. (1979, 1981), White and Patchett (1984), McDermott and Hawkesworth (1991), Gertisser (2001), Turner and Foden (2001), Woodhead et al. (2001), Gertisser and Keller (2003b), Debaille et al. (2006) and Handley et al. (2011, 2014, 2018), Deegan et al. (2016, 2021).

The mantle source of the Merapi magmas is thought to be similar to that of Indian Ocean mid-ocean ridge basalts (MORB), overprinted by slab-derived components that have caused heterogeneous changes in the geochemical and isotopic composition of the mantle wedge

Fig. 6.25 **a** ($^{238}\text{U}/^{232}\text{Th}$) versus ($^{230}\text{Th}/^{232}\text{Th}$) equiline diagram and **b** ($^{226}\text{Ra}/^{230}\text{Th}$) versus ($^{238}\text{U}/^{230}\text{Th}$) plot for Merapi whole-rocks (coloured symbols) and some mineral separates (PI = plagioclase, Cpx = clinopyroxene; Mag = magnetite). Symbols keyed to Fig. 6.9. *Data Sources* Gill and Williams (1990), McDermott and Hawkesworth (1991), Condomines and Sigmarsson (1993), Gauthier and Condomines (1999), Turner and Foden (2001), Condomines et al. (2005) and Handley et al. (2018)



beneath the volcano. This is illustrated in Fig. 6.24, where the displacement of Merapi (and other Javanese volcanoes) from the field of Indian Ocean MORB field in terms of Sr, Nd, Pb and Hf isotopic ratios has been related mainly to mantle source contamination (Gertisser 2001; Gertisser and Keller 2003b; Handley et al. 2011, 2014). Both fluids from the subducted mafic oceanic lithosphere and a subducted Indian Ocean sediment component have been identified in the mantle source of the Merapi magmas based

on trace element compositions and ratios as well as isotopic characteristics (del Marmol 1989; Gertisser 2001; Gertisser and Keller 2003b; Handley et al. 2011; Deegan et al. 2021). These include the LREE-enriched REE patterns, elevated LILE/HFSE, LREE/HFSE and Th/HFSE ratios compared with MORB, the negative Nb–Ta and Ti anomalies in multi-element normalised diagrams (Fig. 6.23a) and the Sr, Nd, Hf and Pb isotopic compositions (Fig. 6.24) that indicate the presence of a crustal component in the

Merapi magmas. This is further illustrated in the $\delta^{18}\text{O}$ versus $^{87}\text{Sr}/^{86}\text{Sr}$ diagram (Fig. 6.26), where the Merapi whole rock data plot in a narrow range towards the more radiogenic end of the Java field and are shifted from the MORB field to higher $^{87}\text{Sr}/^{86}\text{Sr}$. These features can be explained by variable degrees of mantle source contamination by a crustal component and suggest that a small percentage of sediment addition to the mantle wedge is sufficient to generate the Sr isotopic characteristics of primary magmas at Merapi (Gertisser 2001; Gertisser and Keller 2003b), a model that is consistent with oxygen isotopic compositions of Merapi pyroxenes (Deegan et al. 2021). Indicators of fluid addition from the slab to the mantle source also include the observed disequilibria between short-lived

radionuclides of the uranium decay chain in the Merapi eruptive products (Fig. 6.25). Most of the whole rock samples analysed (Gill and Williams 1990; Gauthier and Condomines 1999; Turner and Foden 2001; Condomines et al. 2005; Handley et al. 2018) show both uranium and radium excesses. These values may be used to constrain the timescales of slab dehydration to $< 375,000$ years and < 8000 years for the $^{238}\text{U}/^{230}\text{Th}$ and $^{226}\text{Ra}/^{230}\text{Th}$ disequilibria to be preserved. Gertisser (2001) and Gertisser and Keller (2003b) argued that the contrasts between the geochemical and radiogenic isotope (e.g. $^{87}\text{Sr}/^{86}\text{Sr}$) compositions of medium-K and high-K rock types, together with the similar oxygen isotope ratios within both suites can be reconciled with a model of variable source enrichment by subducted

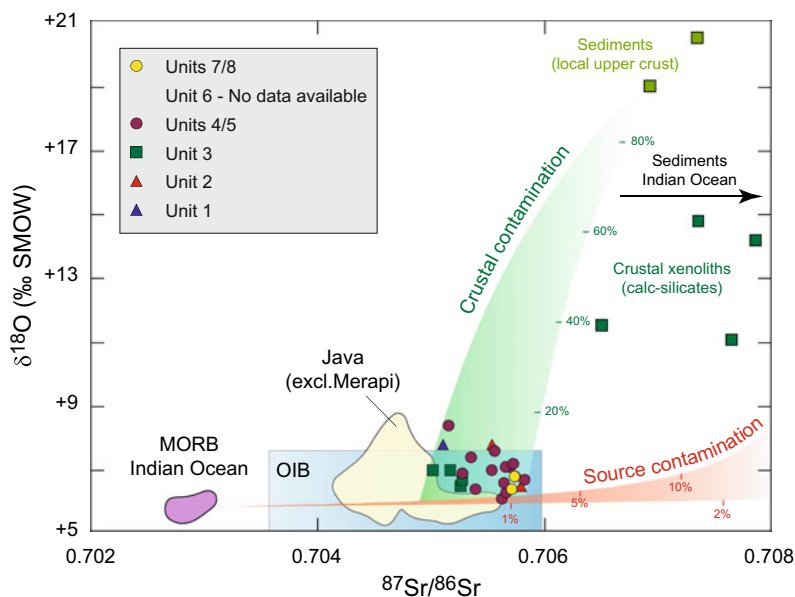


Fig. 6.26 $\delta^{18}\text{O}$ versus $^{87}\text{Sr}/^{86}\text{Sr}$ isotope diagram for Merapi whole rocks, Indian Ocean MORB and OIB, other volcanic rocks from Java, local upper crustal rocks, Merapi calc-silicate xenoliths and Indian Ocean marine sediments, visualising the effects of both contamination of the mantle source (source contamination) and magma contamination in the crust (crustal contamination) on magmatic compositions at Merapi. Because of higher Sr concentrations in the crustal component than in the mantle source, source contamination produces mixing curves that are strongly concave upward reflecting large changes in $^{87}\text{Sr}/^{86}\text{Sr}$ ratios at nearly constant $\delta^{18}\text{O}$ values produced

by relatively small amounts of contamination. By contrast, crustal contamination of magmas with initial Sr concentrations higher than those in the assimilated crustal material, more strongly affects $\delta^{18}\text{O}$ values than Sr isotope ratios (James 1981). Percentages of sediment or crust added are indicated along the mixing curves (after Gertisser and Keller 2003b). For *Data Sources*, see Gertisser et al. (2003b). The Java field has been updated with data from Handley et al. (2010); additional calc-silicate data are from Chadwick et al. (2013). Symbols keyed to Fig. 6.9. *Data Sources* for Merapi Sr isotopic data as in Fig. 6.24

sedimentary material (cf. Fig. 6.26). In their model, a slightly larger contribution from sediment-derived aqueous fluids and partial melts to the source of the high-K type compared to the medium-K magmas may account for the trace element and isotopic contrasts between the two suites, a compositional gap that coincides with the transition from the normal to the anomalous calc-alkaline association of the Sunda arc (Whitford 1975b). The contamination of a MORB-like mantle with sediments from the subducted slab has also been considered as an important process affecting the geochemical composition of the mantle source of other Quaternary volcanoes from Java and the Sunda arc in general (e.g. Turner and Foden 2001; Handley et al. 2010, 2014).

6.4.2 Magma Storage Conditions and Magmatic Differentiation

Magma storage conditions and magmatic differentiation processes affecting primary mantle-derived magmas during transfer through the crust and storage in crustal reservoirs were discussed in Bahar (1984), del Marmol (1989), Berthommier (1990), Andreastuti (1999), Gertisser (2001), Gertisser and Keller (2003a) and Handley et al. (2014, 2018) based on the geochemical and isotopic compositions of lavas and pyroclastic rocks and their constituent minerals. Additional studies addressed these issues using crystal isotope stratigraphy (e.g. Chadwick et al. 2007; Borisova et al. 2016; Peters et al. 2017), igneous inclusion petrology (e.g. Chadwick et al. 2013; Troll et al. 2013a; van der Zwan et al. 2013), melt inclusion studies (e.g. Nadeau et al. 2013; Preece et al. 2014), quantitative textural analysis (e.g. Innocenti et al. 2013a, b; van der Zwan et al. 2013), thermobarometry and thermodynamic modelling (e.g. Gertisser 2001; Chadwick et al. 2013; Costa et al. 2013; Nadeau et al. 2013; Erdmann et al. 2014; Preece et al. 2014, 2016; Deegan et al. 2016), phase equilibrium experiments (e.g. Erdmann et al. 2016) and detailed investigations of crustal xenoliths (e.g.

Deegan et al. 2010; Borisova et al. 2013; Whitley et al. 2019, 2020; Whitley 2020). These aspects are discussed in detail in Troll and Deegan (2023, Chap. 8), Deegan et al. (2023, Chap. 10) and Preece et al. (2023, Chap. 9) and therefore only a brief synopsis is provided here.

A consensus appears to emerge of the existence of complex crustal magma storage system beneath Merapi, where magmas are stored in magma storage zones or reservoirs at different levels throughout the crust from around the crust-mantle boundary at ~ 25 km depth (Katili 1975) to less than a kilometre below the summit of the volcano, where the magma system is interpreted to consist of highly interconnected magma reservoirs (Preece et al. 2014; Troll and Deegan 2023, Chap. 8). The presence of amphiboles without reaction rims in pumiceous or scoriaceous clasts from explosive eruptions and crystals with no or relatively thin breakdown rims in some of the recent and Holocene lava dome components indicate that magmas feeding these eruptions rise quickly through these near-surface magma reservoirs outside the amphibole stability field (Gertisser 2001; Gertisser et al. 2011; Chadwick et al. 2013; Costa et al. 2013; Preece et al. 2013; Preece 2014; Peters et al. 2017). Most lava domes, however, contain amphiboles with thick reaction rims indicative of temporary magma storage at shallow depth, slow magma ascent or a combination of both (Gertisser 2001; Gertisser et al. 2011; Costa et al. 2013; Preece et al. 2013; Preece 2014). Later studies on rock samples from recent eruptions corroborated these ideas, adding evidence from groundmass textural variations (Preece et al. 2013, 2016, 2023, Chap. 9; Preece 2014), clinopyroxene diffusion timescales (Costa et al. 2013) as well as ^{210}Pb isotopic data that indicate less efficient degassing related to faster magma ascent and vice versa (Handley et al. 2018). Mineral chemical data and phase equilibria based on the quartz–ulvöspinel–ilmenite–fayalite (QUILF) algorithm (Andersen et al. 1993) suggest magmatic temperatures between ~ 920 and 1050 °C and oxygen fugacities ($f\text{O}_2$) for the Merapi magmas between 0.6 and 2.2 logarithmic units above the FMQ oxygen buffer (Gertisser 2001), a

range not unusual for subduction-related volcanic rocks. These values are like those derived from amphibole compositions (Erdmann et al. 2014). Melt inclusion studies imply magmatic H₂O contents, based on the volatiles-by-difference method (e.g. Devine et al. 1995), of up to 6.4 wt % (Gertisser 2001), and between 0.2 and 4.8 wt % H₂O based on direct analysis of pyroxene-hosted melt inclusions by secondary ion mass spectrometry and attenuated total reflectance micro-Fourier transform infrared spectroscopy (Preece et al. 2014). The highest H₂O contents are preserved in melt inclusions from explosive eruption products rather than from dome lavas (Gertisser 2001; Preece et al. 2014).

Strong evidence for polybaric fractional crystallisation, magma replenishment and associated magma mixing or mingling, crystal mush remobilisation, crystal recycling and crustal contamination as important processes of magmatic differentiation is provided by petrological, geochemical and isotopic data. The forsteritic olivines and their inclusions of Cr-spinel in the basaltic lavas from Gunung Turgo, Gunung Plawangan and Gunung Medjing document the earliest stages of differentiation of primary, mantle-derived magmas at Merapi (del Marmol 1989; Gertisser 2001). Crystallisation at high pressure of Cr-spinel, Mg-rich olivine and Al-rich clinopyroxene before eruption of the most primitive Merapi magmas is regarded as an important process that determines the behaviour of ferromagnesian elements such as Ni and Cr in the residual melt and ultimately controls the relatively low concentrations of these elements in the least differentiated Merapi magmas (del Marmol 1989; Gertisser 2001). Continued fractional crystallisation is considered a feasible process in the evolution of magmas of both medium-K and high-K character, which were interpreted to represent discrete magma series or magma differentiation trends from distinct parental magmas (Gertisser 2001; Gertisser and Keller 2003b). Support for this interpretation comes from (1) the overall increase of the alkalis, LILE and HFSE, and the decrease of TiO₂, Fe₂O₃*, CaO, MgO and ferromagnesian trace elements with increasing SiO₂ (Fig. 6.22), and

(2) systematic changes in modal mineralogy, such as the occurrence of olivine as a major constituent exclusively in the basalts, the appearance of orthopyroxene at the expense of olivine in more evolved rock types, the increasing abundance of titanomagnetite with increasing SiO₂, and often late-stage crystallisation of amphibole. Collectively, the combined geochemical and petrographical characteristics indicate that magmatic differentiation at Merapi involves fractional crystallisation of a plagioclase-dominated mineral assemblage that includes clinopyroxene, olivine, orthopyroxene, titanomagnetite, amphibole and apatite. The absence of clinopyroxene in some of the basalts of Gunung Turgo, Gunung Plawangan and Gunung Medjing may suggest that olivine and plagioclase crystallisation precedes that of clinopyroxene (del Marmol 1989). Despite the important role of plagioclase fractionation, no significant Eu anomaly is observed in the Merapi rocks (Fig. 6.23b), likely due to the oxidised nature of the Merapi magmas (Gertisser 2001). The slightly concave up HREE patterns observed in some samples hint at amphibole fractionation at depth. Crystal clots and plutonic crystalline inclusions provide snapshots of these fractional crystallisation processes and provide unequivocal evidence for deep amphibole crystallisation, amphibole-bearing cumulate formation in the lower crust and crystal mush (cumulate) remobilisation (e.g. Chadwick et al. 2013; Erdmann et al. 2014; Peters et al. 2017; Troll and Deegan 2023, Chap. 8).

While fractional crystallisation appears to be a dominant magmatic differentiation process, there is compelling evidence for magma replenishment and associated mixing and mingling processes, typically accompanied by crystal recycling. These include the presence of complexly zoned crystals, in particular plagioclase and clinopyroxene (e.g. del Marmol 1989; Gertisser 2001; Chadwick et al. 2007; Borisova et al. 2016), mixed or bimodal mineral compositions (e.g. Erdmann et al. 2014) and clinopyroxene overgrowth rims around orthopyroxene (e.g. Gertisser 2001). Features of incomplete magma mixing or magma mingling, such as the presence of banded

pumiceous or scoriaceous clasts, exist but are less frequent (del Marmol 1989; Gertisser 2001; Gertisser and Keller 2003a; Troll et al. 2013a). Replenishment and mixing of primitive and more evolved magmas at Merapi may be responsible for intermediate compositions in the basaltic andesite range, characterised by Ni and Cr concentrations that are higher than those expected from fractional crystallisation (Fig. 6.22). The cyclical variations and gradual shifts towards more mafic compositions in the young tephra sequences of the Holocene Pyroclastic Series as well as during the historical to recent eruptions may therefore reflect magma mixing or mingling processes; these may result from continuous or periodic supply of primitive magma to a shallower magma storage zone, and progressive changes in the volume of intruding primitive to evolved magma residing at a shallower level (Gertisser and Keller 2003a). The relative monotony of magma compositions since the mid-twentieth century may imply the existence of a continuously active, small-volume, steady state magma reservoir where fractional crystallisation, magma recharge and eruption have been well balanced for erupting magmas to be essentially uniform in composition (Gertisser and Keller 2003a; Troll and Deegan 2023, Chap. 8).

Contamination and assimilation of crustal rocks during magma storage and ascent through the crustal basement at Merapi is best exemplified by the presence of predominantly calc-silicate crustal xenoliths in the eruptive products (Clocchiatti et al. 1982; del Marmol 1989; Camus et al. 2000; Gertisser and Keller 2003b; Chadwick et al. 2007, 2013; Deegan et al. 2010, 2023, Chap. 10; Troll et al. 2012, 2013a, b; Whitley et al. 2019, 2020; Whitley 2020). Magma-crust interaction is interpreted to be responsible for some of the isotopic variations within the Merapi suite, particularly the elevated $\delta^{18}\text{O}$ values up to 8.3‰ of Merapi compared to mantle values and above the MORB-sediment mixture in $\delta^{18}\text{O}$ versus $^{87}\text{Sr}/^{86}\text{Sr}$ space (Fig. 6.26), which can be reconciled by contamination of the parental magmas of the medium-K and high-K series rocks with crustal material compositionally similar to the

calcareous sediments of the local upper crust. Such a model is further supported by elevated oxygen isotopic compositions of pyroxenes relative to mantle values and inferred source contamination trends (Deegan et al. 2021), and evidence from carbon and uranium-series isotopes (Berthommier 1990; Handley et al. 2018; Whitley et al. 2019; Whitley 2020). However, crustal contamination by a classic assimilation and fractional crystallisation (AFC) process (DePaolo 1981) or bulk crustal contamination during the evolution of the Merapi magmas appears to be negligible, as, for example, Sr, Nd and Pb isotopic ratios remain relatively unchanged or vary unsystematically with increasing SiO_2 content in both medium-K and high-K series rocks (Gertisser and Keller 2003b).

6.4.3 Magmatic Evolution of Merapi: Temporal Geochemical Variations

The geochemical evolution of Merapi through time was described by Bahar (1984), del Marmol (1989), Berthommier (1990), Andreastuti (1999), Andreastuti et al. (2000), Camus et al. (2000), Gertisser (2001), Gertisser and Keller (2003a, b) and Gertisser et al. (2012a). First order observations include (1) long-term geochemical variations over the much of the life-span of the volcano, such as the general tendency of increasing SiO_2 content from the lavas of Gunung Turgo, Gunung Plawangan and Gunung Medjing to the younger units of the volcanic complex (Bahar 1984; del Marmol 1989; Berthommier 1990; Camus et al. 2000; Gertisser 2001; Gertisser and Keller, 2003a, b; Gertisser et al. 2012a), and the transition from an older medium-K to a younger high-K series (Andreastuti 1999; Gertisser 2001; Gertisser and Keller 2003a, b; Gertisser et al. 2012a); (2) medium-term variations over timescales up to several thousands of years, where cyclical trends of increasing and decreasing SiO_2 content through time were identified (Bahar 1984; del Marmol 1989; Berthommier 1990; Andreastuti 1999; Camus et al. 2000; Gertisser 2001;

Gertisser and Keller 2003a); and (3) short-term variations that occur within a single eruption or eruption cycle, such as those during larger Holocene eruptions (Andreastuti 1999) or during the historical to recent period (del Marmol 1989; Berthommier 1990; Andreastuti 1999; Andreastuti et al. 2000; Camus et al. 2000; Gertisser 2001; Gertisser and Keller 2003a).

The compositional variation of the eruptive products (K_2O vs. SiO_2 classification diagram; Le Maitre et al. 2002) of the main volcano-stratigraphic units is illustrated in Fig. 6.27. Most units, including, for example, the lava flows of Gunung Bibi (Unit 1), show considerable variations in SiO_2 and/or K_2O content, comprising medium-K and high-K type compositions or are dominated by high-K compositions only. Basaltic andesitic rocks are most common in all volcano-stratigraphic units except for the lava flows of Gunung Turgo, Gunung Plawangan and Gunung Medjing (Unit 2), which are, for the most part, basalts of both medium-K and high-K type, but also comprise a few basaltic andesites of medium-K variety (del Marmol 1989). Most whole-rock geochemical analyses exist for the Holocene Pyroclastic Series (Units 4 and 5), which comprises the extensive volcanoclastic apron on the flanks of Merapi apart from the recent and historical pyroclastic density current and lahar deposits (Unit 7). Samples of the Holocene Pyroclastic Series range from basaltic to andesitic compositions, and variations in K_2O content clearly divide its eruptive products into medium-K and high-K types (Gertisser 2001; Gertisser and Keller 2003a, b; Gertisser et al. 2012a). Based on their stratigraphic and chronological data, the authors showed that the volcanoclastic deposits younger than ~ 1900 ^{14}C y BP are distinctly more K-rich than the older deposits of the Holocene Pyroclastic Series, with the transition from medium-K to high-K type coinciding with the inferred date of the sector collapse at the end of the Old Merapi stage, as proposed by Newhall et al. (2000). The compositional change was attributed to deep processes at the magma source (Gertisser and Keller 2003b), leaving a temporal link between this collapse event and the high-K magmas that

erupted since ~ 1900 ^{14}C y BP unexplored. Similar shifts in magma compositions have been observed at other volcanoes such as Colima (Crummy et al. 2014), Bezymianny (Davydova et al. 2018), Stromboli (Francalanci et al. 2013) and Taranaki, a volcano that mirrors the geochemical variations observed at Merapi (Hatherton and Dickenson 1969; Stewart et al. 1996). Where these coincide with major structural modifications of the volcano, it was inferred that edifice instabilities were caused by injection of deep and compositionally distinct magma, or that edifice collapse led to subsequent changes in the composition of erupted magma through modifications of the architecture of the crustal magma plumbing systems. Such modifications may lead to enhanced decompression, opening of the system and increased magma flux rates, affect magma storage, ascent and differentiation processes, and provide a viable avenue for future structural, geochronological and petrological research at Merapi.

Based on their data, Gertisser (2001), Gertisser and Keller (2003a, b) and Gertisser et al. (2012a) included the lava flows of the Somma-Merapi (Unit 3) in their 'medium-K series', but the additional data presented here (Bahar 1984; del Marmol 1989; Berthommier 1990; Camus et al. 2000; Debaille et al. 2006) suggest that Somma-Merapi lavas contain higher K rock types also. By contrast, the picture of two distinct magmatic series and a shift from older medium-K to younger eruptive products of high-K type during the Late Holocene remains valid (Andreastuti 1999; Gertisser, 2001; Gertisser and Keller 2003a, b; Gertisser et al. 2012a). The young (post-Somma-Merapi) lava flows (Unit 6), the recent and historical pyroclastic density current and lahar deposits (Unit 7) and the lava domes of the recent episode (Unit 8) characteristically comprise volcanic products of high-K type, although subtle K_2O variations at a given SiO_2 content are apparent within the rocks of high-K affinity.

Furthermore, crude cyclical variations with systematic shifts in whole rock SiO_2 content have been identified in the young tephra sequences of the Holocene Pyroclastic Series

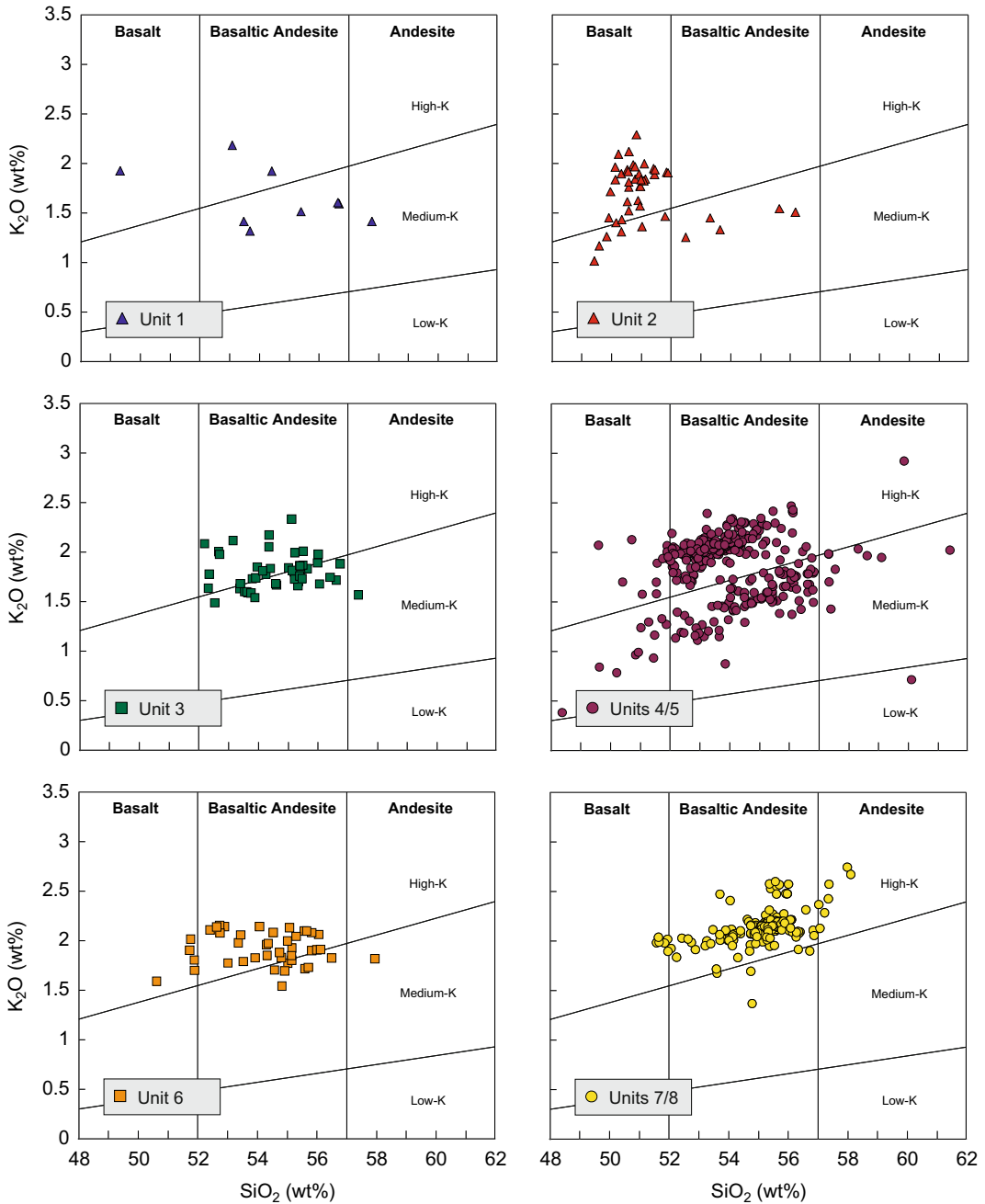


Fig. 6.27 K₂O versus SiO₂ variation diagrams (Le Maitre et al. 2002) for the main volcano-stratigraphic units of Merapi. Symbols keyed to Fig. 6.9. Data Sources as in Fig. 6.18

from as far back as ~ 3000 years ago. These are characterised by periods of decreasing SiO₂ content with changes from basaltic andesite (56–57 wt% SiO₂) to basalt (51–53 wt% SiO₂),

alternating with shorter periods of more abrupt SiO₂ increases. Trends towards more mafic compositions were recognised also within the historical to recent eruptions during the

nineteenth and early twentieth century, while magma compositions have remained largely uniform, and near the upper limit of the total whole rock SiO₂ range of Merapi, since the mid-twentieth century (Andreastuti 1999; Gertisser 2001; Gertisser and Keller 2003a).

6.5 Summary

Based on the available chronological data, the construction of the basalt to basaltic andesite volcanic complex of Merapi began after 170 ka. Remnants of the oldest parts of Merapi, Proto-Merapi, are preserved at Gunung Bibi, as well as at Gunung Turgo, Gunung Plawangan and Gunung Medjing. The main volcanic complex consists of an older edifice, Old Merapi, and the presently active stratocone, New Merapi. The evolution of Merapi has been governed by multiple gravitational sector collapses of various scales affecting the edifices of Proto-, Old and New Merapi. A major sector collapse or several successive sector collapses of Old Merapi produced the prominent remnant avalanche caldera open to the west, which has been subsequently filled by the growth of New Merapi. The eruptive products of Merapi are predominantly basaltic andesite. Basaltic and andesitic rock types are subordinate, although the lavas of Gunung Turgo, Gunung Plawangan and Gunung Medjing are principally basaltic. Variations in K₂O content divide the Merapi rocks into medium-K and high-K types. Geochemical and isotopic characteristics are consistent with a two-stage petrogenetic model, where primary magmas of both medium-K and high-K affinity are derived from a heterogeneous, Indian Ocean MORB-like mantle source metasomatised by components derived from the subducted oceanic slab and sediment cover. Magmas are subsequently modified during transfer through the crust by complex magmatic differentiation processes, including polybaric fractional crystallisation, magma replenishment followed by magma mixing or mingling, crystal mush remobilisation, crystal recycling and contamination by carbonate rocks of the local upper crust. Since ~ 1900 ¹⁴C y BP, all lavas and

pyroclastic rocks of Merapi are of the high-K type. Cyclical geochemical variations with systematic shifts in whole rock SiO₂ content have been identified in the Late Holocene to recent eruptive products, but magma compositions have remained broadly uniform since the mid-twentieth century.

Acknowledgements We gratefully acknowledge our colleagues from the Center of Volcanology and Geological Hazard Mitigation (CVGHM) and the Merapi Volcano Observatory (BPPTKG) in Yogyakarta for their generosity and support while conducting research at Merapi. Fieldwork at Merapi wouldn't have been possible without the generous help of our local guides and drivers, including Sutisna, Dedi, Budi, Sony, Biyanto and many others, who are gratefully acknowledged here. This synthesis has benefitted from stimulating discussions with many colleagues over many years, including Brent Alloway, Sutikno Bronto, Guy Camus, Alain Gourgaud, Antonius Ratdomopurbo, Dewi Sri Sayudi, Lothar Schwarzkopf, Ian Smith, Valentin Troll, Pierre Vincent and Barry Voight. Ian Smith and Valentin Troll are thanked for their constructive reviews and helpful suggestions.

References

- Andersen DJ, Lindsley DH, Davidson PM (1993) QUILF: a Pascal program to assess equilibria among Fe–Mg–Mn–Ti-oxides, pyroxenes, olivine and quartz. *Comput Geosci* 19:1333–1350
- Andreastuti SD (1999) Stratigraphy and geochemistry of Merapi Volcano, Central Java, Indonesia: implication for assessment of volcanic hazards. PhD Thesis, University of Auckland, Auckland, New Zealand
- Andreastuti SD, Alloway BV, Smith IEM (2000) A detailed tephrostratigraphic framework at Merapi Volcano, Central Java, Indonesia: implications for eruption predictions and hazard assessment. *J Volcanol Geotherm Res* 100:51–67
- Bahar I (1984) Contribution à la connaissance du volcanisme indonésien: le Merapi (Centre Java); cadre structural, pétrologie, géochimie et implications volcanologiques. PhD Thesis, Université des Sciences et Techniques du Languedoc, Montpellier, France
- Bardintzeff JM (1984) Merapi Volcano (Java, Indonesia) and Merapi-type nuée ardente. *Bull Volcanol* 47:433–446
- Berthommier PC (1990) Etude volcanologique du Merapi (Centre-Java). Téphrostratigraphie et chronologie – produits éruptifs. PhD Thesis, Université Blaise Pascal, Clermont-Ferrand, France
- Borisova AY, Martel C, Gouy S, Pratomo I, Sumarti S, Toutain J-P, Bindeman IN, de Parseval P, Metaxian J-P, Surono, (2013) Highly explosive 2010 Merapi

- eruption: evidence for shallow-level crustal assimilation and hybrid fluid. *J Volcanol Geotherm Res* 261:193–208
- Borisova AY, Gurenko AA, Martel C, Kouzmanov K, Cathala A, Bohrsen WA, Pratomo I, Sumarti S (2016) Oxygen isotope heterogeneity of arc magma recorded in plagioclase from the 2010 Merapi eruption (Central Java, Indonesia). *Geochim Cosmochim Acta* 190:13–34
- Boudon G, Camus G, Gourgaud A, Lajoie J (1993) The 1984 nuée ardente deposits of Merapi volcano, Central Java, Indonesia: stratigraphy, textural characteristics, and transport mechanisms. *Bull Volcanol* 55:327–342
- Bourdon B, Henderson GM, Lundstrom CC, Turner SP (eds) (2003) Uranium-series Geochemistry. *Min Soc Am, Rev Mineral Geochem* (Vol. 52)
- Bronto S, Ratdomopurbo A, Asmoro P, Adityarani M (2014) Longsoran rakasa Gunung Api Merapi Yogyakarta – Jawa Tengah (Gigantic landslides of Merapi volcano, Yogyakarta – Central Java). *J Geol Sumb Min* 15:165–183
- Bronto S, Rahardjo W, Asmoro P, Ratdomopurbo A, Adityarani M, Permatasari A (2023) The godean debris avalanche deposit from a sector collapse of Merapi volcano. In: Gertisser R, Troll VR, Walter TR, Nandaka IGMA, Ratdomopurbo A (eds) Merapi volcano—geology, eruptive activity, and monitoring of a high-risk volcano. Springer, Berlin, Heidelberg, pp 195–231
- Buddington AF, Lindsley DH (1964) Iron-titanium oxide minerals and synthetic equivalents. *J Petrol* 5:310–357
- Camus G, Gourgaud A, Mossand-Berthommier P-C, Vincent PM (2000) Merapi (Central Java, Indonesia): an outline of the structural and magmatological evolution, with a special emphasis to the major pyroclastic events. *J Volcanol Geotherm Res* 100:139–163
- Chadwick JP, Troll VR, Ginibre C, Morgan D, Gertisser R, Waight TE, Davidson JP (2007) Carbonate assimilation at Merapi Volcano, Java, Indonesia: insights from crystal isotope stratigraphy. *J Petrol* 48:1793–1812
- Chadwick JP, Troll VR, Waight TE, van der Zwan FM, Schwarzkopf LM (2013) Petrology and geochemistry of igneous inclusions in recent Merapi deposits: a window into the sub-volcanic plumbing system. *Contrib Mineral Petrol* 165:259–282
- Charbonnier SJ, Gertisser R (2008) Field observations and surface characteristics of pristine block-and-ash flow deposits from the 2006 eruption of Merapi Volcano, Java, Indonesia. *J Volcanol Geotherm Res* 177:971–982
- Clocchiatti R, Joron JL, Kerinec F, Treuil M (1982) Quelques données préliminaires sur la lave du dôme actuel du volcan Mériapi (Java, Indonésie) et sur ses enclaves. *CR Acad Sci Paris* 295:817–822
- Condomines M, Sigmarrsson O (1993) Why are so many arc magmas close to ^{238}U – ^{230}Th radioactive equilibrium? *Geochim Cosmochim Acta* 57:4491–4497
- Condomines M, Gauthier PJ, Tanguy JC, Gertisser R, Thouret JC, Berthommier P, Camus G (2005) ^{226}Ra or $^{226}\text{Ra}/\text{Ba}$ dating of Holocene volcanic rocks: application to Mt. Etna and Merapi volcanoes. *Earth Planet Sci Lett* 230:289–300
- Costa F, Andreastuti S, Bouvet de Maisonneuve C, Pallister JS (2013) Petrological insights into the storage conditions, and magmatic processes that yielded the centennial 2010 Merapi explosive eruption. *J Volcanol Geotherm Res* 261:209–235
- Crummy JM, Savov IP, Navarro-Ochoa C, Morgan DJ, Wilson M (2014) High-K Mafic Plinian Eruptions of Volcán de Colima, Mexico. *J Petrol* 55:2155–2192
- Davydova VO, Yu P, Plechov VD, Shcherbakov AB, Perepelov (2018) High-K basaltic trachyandesite xenoliths in pyroclastic deposits from the Bezmyianny volcano (Kamchatka). *Russ Geol Geophys* 59:1087–1099
- Debaille V, Doucelance R, Weis D, Schiano P (2006) Multi-stage mixing in subduction zones: Application to Merapi volcano (Java island, Sunda arc). *Geochim Cosmochim Acta* 70:723–741
- Deegan FM, Troll VR, Freda C, Misiti V, Chadwick JP, McLeod CL, Davidson JP (2010) Magma-carbonate interaction processes and associated CO_2 release at Merapi volcano, Indonesia: insights from experimental petrology. *J Petrol* 51:1027–1051
- Deegan FM, Troll VR, Gertisser R, Freda C (2023) Magma-carbonate interaction at Merapi volcano, Indonesia. In: Gertisser R, Troll VR, Walter TR, Nandaka IGMA, Ratdomopurbo A (eds) Merapi volcano—geology, eruptive activity, and monitoring of a high-risk volcano. Springer, Berlin, Heidelberg, pp 291–321
- Deegan FM, Whitehouse MJ, Troll VR, Budd DA, Harris C, Geiger H, Hålenius U (2016) Pyroxene standards for SIMS oxygen isotope analysis and their application to Merapi volcano, Sunda arc, Indonesia. *Chem Geol* 447:1–10
- Deegan FM, Whitehouse MJ, Troll VR, Geiger H, Jeon H, le Roux P, Harris C, van Helden M, González-Maurel O (2021) Sunda arc mantle source $\delta^{18}\text{O}$ value revealed by intracrystal isotope analysis. *Nat Commun* 12:3930
- DePaolo DJ (1981) Trace element and isotopic effects of combined wallrock assimilation and fractional crystallization. *Earth Planet Sci Lett* 53:189–202
- Devine JD, Gardner JE, Brack HP, Layne GD, Rutherford MJ (1995) Comparison of microanalytical methods for estimating H_2O contents of silicic volcanic glasses. *Am Mineral* 80:319–328
- del Marmol MA (1989) The petrology and geochemistry of Merapi Volcano, Central Java, Indonesia. PhD Thesis, The Johns Hopkins University, Baltimore, USA
- Djumarma A, Bronto S, Bahar I, Suparban F, Sukhyar R, Newhall C, Holcomb RT, Banks NG, Torley R, Lockwood JP, Tilling RI, Rubin M, del Marmol MA (1986) Did Merapi volcano (Central Java) erupt catastrophically in 1006 A.D.? Abstract, IAVCEI Internat Volcanol Congr 1986, Rotorua, New Zealand

- Drignon MJ, Bechon T, Arbaret L, Burgisser A, Komorowski J-C, Martel C, Yaputra R (2016) Preexplosive conduit conditions during the 2010 eruption of Merapi volcano (Java, Indonesia). *Geophys Res Lett* 43:11595–11602
- Erdmann S, Martel C, Pichavant M, Kushnir A (2014) Amphibole as an archivist of magmatic crystallization conditions: problems, potential, and implications for inferring magma storage prior to the paroxysmal 2010 eruption of Mount Merapi. Indonesia. *Contrib Mineral Petrol* 167:1016
- Erdmann S, Martel C, Pichavant M, Bourdier J-L, Champallier R, Komorowski J-C, Cholik N (2016) Constraints from Phase Equilibrium Experiments on Pre-eruptive Storage Conditions in Mixed Magma Systems: a Case Study on Crystal-rich Basaltic Andesites from Mount Merapi, Indonesia. *J Petrol* 57:535–560
- Eiler JM, Schiano P, Kitchen N, Stolper EM (2000) Oxygen-isotope evidence for recycled crust in the sources of mid-ocean-ridge basalts. *Nature* 403:530–534
- Francalanci L, Lucchi F, Keller J, De Astis G, Tranne CA (2013) Eruptive, volcano-tectonic and magmatic history of the Stromboli volcano (north-eastern Aeolian archipelago). In: Lucchi F, Peccerillo A, Keller J, Tranne CA, Rossi PL (eds) *The Aeolian Islands Volcanoes*. *Geol Soc London Mem* 37:397–471
- Garcia MO, Jacobson SS (1979) Crystal clots, amphibole fraction and the evolution of calc-alkaline magmas. *Contrib Mineral Petrol* 69:319–327
- Gauthier PJ, Condomines M (1999) ^{210}Pb - ^{226}Ra radioactive disequilibria in recent lavas and radon degassing: inferences on the magma chamber dynamics at Stromboli and Merapi volcanoes. *Earth Planet Sci Lett* 172:111–126
- Gertisser R (2001) *Gunung Merapi (Java, Indonesien): Eruptionsgeschichte und magmatische Evolution eines Hochrisiko-Vulkans*. PhD Thesis, Albert-Ludwigs-Universität Freiburg, Freiburg, Germany
- Gertisser R, Keller J (2003a) Temporal variations in magma composition at Merapi Volcano (Central Java, Indonesia): magmatic cycles during the past 2,000 years of explosive activity. *J Volcanol Geotherm Res* 123:1–23
- Gertisser R, Keller J (2003b) Trace element and Sr, Nd, Pb and O isotope variations in medium-K and high-K volcanic rocks from Merapi Volcano, Central Java, Indonesia: evidence for the involvement of subducted sediments in Sunda Arc magma genesis. *J Petrol* 44:457–486
- Gertisser R, Charbonnier SJ, Troll VR, Keller J, Preece K, Chadwick JP, Barclay J, Herd RA (2011) Merapi (Java, Indonesia): anatomy of a killer volcano. *Geol Today* 27:57–62
- Gertisser R, Charbonnier SJ, Keller J, Quidelleur X (2012a) The geological evolution of Merapi volcano, Central Java, Indonesia. *Bull Volcanol* 74:1213–1233
- Gertisser R, Cassidy NJ, Charbonnier SJ, Nuzzo L, Preece K (2012b) Overbank block-and-ash flow deposits and the impact of valley-derived, unconfined flows on populated areas at Merapi volcano, Java, Indonesia. *Nat Hazards* 60:623–648
- Gertisser R, Self S, Thomas LE, Handley HK, van Calsteren P, Wolff JA (2012c) Processes and timescales of magma genesis and differentiation leading to the great Tambora eruption in 1815. *J Petrol* 53:271–297
- Gill JB, Williams RW (1990) Th isotope and U-series studies of subduction-related volcanic rocks. *Geochim Cosmochim Acta* 54:1427–1442
- Global Volcanism Program (2013) *Volcanoes of the World*, v 4.9.4 (17 Mar 2021) Venzke E (ed) Smithsonian Institution. Downloaded 27 Apr 2021. <https://doi.org/10.5479/si.GVP.VOTW4-2013>
- Global Volcanism Program (2019) Report on Merapi (Indonesia). In: Krippner JB, Venzke E (eds). Smithsonian Institution — *Bull Global Volc Netw* 44:10
- Global Volcanism Program (2020) Report on Merapi (Indonesia). In: Bennis KL, Venzke E (eds). Smithsonian Institution — *Bull Global Volc Netw* 45:4
- Gomez C, Janin M, Lavigne F, Gertisser R, Charbonnier S, Lahitte P, Hadmoko SR, Fort M, Wassmer P, Degroot V, Murwanto H (2010) Borobudur, a basin under volcanic influence: 361,000 years BP to present. *J Volcanol Geotherm Res* 196:245–264
- Haggerty SE (1993) Oxide textures – a mini-atlas. In: Lindsley DH (ed) *Oxide minerals: petrologic and magnetic significance*. *Rev Mineral* 25:303–321
- Hammer JE, Cashman KV, Voight B (2000) Magmatic processes revealed by textural and compositional trends in Merapi dome lavas. *J Volcanol Geotherm Res* 100:165–192
- Handley HK, Macpherson CG, Davidson JP, Berlo K, Lowry D (2007) Constraining fluid and sediment contributions to subduction-related magmatism in Indonesia: Ijen Volcanic Complex, Indonesia. *J Petrol* 48:1155–1183
- Handley HK, Davidson JP, Macpherson CG (2008) Untangling differentiation in arc lavas: constraints from unusual minor and trace element variations at Salak Volcano, Indonesia. *Chem Geol* 255:360–376
- Handley HK, Macpherson CG, Davidson JP (2010) Geochemical and Sr-O isotopic constraints on magmatic differentiation at Gede Volcanic Complex, West Java, Indonesia. *Contrib Mineral Petrol* 159:885–908
- Handley HK, Turner SP, Macpherson CG, Gertisser R, Davidson JP (2011) Hf-Nd isotope and trace element constraints on subduction inputs at island arcs: limitations of Hf anomalies as sediment input indicators. *Earth Planet Sci Lett* 304:212–223
- Handley HK, Blichert-Toft J, Gertisser R, Macpherson CG, Turner SP, Zaennudin A, Abdurrachman M (2014) Insights from Pb and O isotopes into along-arc variations in subduction inputs and crustal assimilation for volcanic rocks in Java, Sunda arc, Indonesia. *Geochim Cosmochim Acta* 139:205–226

- Handley HK, Reagan M, Gertisser R, Preece K, Berlo K, McGee LE, Barclay J, Herd R (2018) Timescales of magma ascent and degassing and the role of crustal assimilation at Merapi volcano (2006–2010), Indonesia: constraints from uranium-series and radiogenic isotopic compositions. *Geochim Cosmochim Acta* 222:34–52
- Harris C, Pronost JJM, Ashwal LD, Cawthorn RG (2005) Oxygen and hydrogen isotope stratigraphy of the Rustenburg layered suite, Bushveld Complex: constraints on crustal contamination. *J Petrol* 46:579–601
- Hartmann M (1935) Die Ausbrüche des G. Merapi (Mittel-Java) bis zum Jahre 1883. *Neues Jahrb Mineral Geol Paläontol* 75:127–162
- Hatherton T, Dickenson WR (1969) The relationship between andesitic volcanism and seismicity in Indonesia, the lesser Antilles and other island arcs. *J Geophys Res* 74:5301–5310
- Ijzerman JW (1891) Beschrijving der oudheden nabij de grens de Residentie's Soerakarta en Djogdjakarta. Batavia: Landsdrukkerij; 's Gravenhage: M. Nijhoff, 135 p
- Innocenti S, Andreastuti S, Furman T, del Marmol M-A, Voight B (2013a) The pre-eruption conditions for explosive eruptions at Merapi volcano as revealed by crystal texture and mineralogy. *J Volcanol Geotherm Res* 261:69–86
- Innocenti S, del Marmol M-A, Voight B, Andreastuti S, Furman T (2013b) Textural and mineral chemistry constraints on evolution of Merapi volcano, Indonesia. *J Volcanol Geotherm Res* 261:20–37
- James DE (1981) The combined use of oxygen and radiogenic isotopes as indicators of crustal contamination. *Ann Rev Earth Planet Sci* 9:311–344
- Katili JA (1975) Volcanism and plate tectonics in the Indonesian island arcs. *Tectonophysics* 26:165–188
- Kemmerling GLL (1921) De hernieuwde werking van den vulkan G. Merapi (Midden Java) van den begin Augustus 1920 tot en met einde Februari 1921. *Vulkanol Seismol Med* 3:1–30
- Kerinec F (1982) Le Merapi, volcan actif d'arc insulaire (Java): Petrographie et geochemie de materiaux solides; implications geotectoniques. PhD Thesis (Thèse de Troisième Cycle), Université Paris-Sud, Orsay, France
- Komorowski J-C, Jenkins S, Baxter PJ, Picquout A, Lavigne F, Charbonnier S, Gertisser R, Preece K, Cholik N, Budi-Santoso A, Surono, (2013) Paroxysmal dome explosion during the Merapi 2010 eruption: processes and facies relationships of associated high-energy pyroclastic density currents. *J Volcanol Geotherm Res* 261:260–294
- Le Maitre RW (ed), Streckeisen A, Zanettin B, Le Bas MJ, Bonin B, Bateman P, Bellieni G, Dudek A, Efremova J, Keller J, Lameyre J, Sabine PA, Schmidt R, Sørensen H, Woolley AR (2002) Igneous rocks. A classification and glossary of terms. Recommendations of the International Union of Geological Sciences Subcommittee on the systematics of igneous rocks. University Press, Cambridge
- Li W, Costa F, Nagashima K (2021) Apatite crystals reveal melt volatile budgets and magma storage depths at Merapi volcano, Indonesia. *J Petrol* 62:egaa100
- Leake BE, Woolley AR, Arps CES, Birch WD, Gilbert MC, Grice JD, Hawthorne FC, Kato A, Kinsch HJ, Krivovichev VG, Linthout K, Laird J, Mandarino JA, Maresch WV, Nickel EH, Rock NMS, Schumacher JC, Smith DC, Stephenson NCN, Ungaretti L, Whittaker EJW, Youzhi G (1997) Nomenclature of amphiboles: report on the subcommittee on amphiboles of the International Mineralogical Association, Commission on New Minerals and Mineral Names. *Can Mineral* 35:219–246
- Luais B (1986) Pétrologie et géochimie (éléments trace et rapports isotopiques du Sr) du magmatisme associé aux zones de subduction: Exemples du bassin méditerranéen (Santorin, Arc Egeen; Stromboli, Arc Eolien) et des îles de la Sonde (Merapi, Java). PhD Thesis (Thèse de Troisième Cycle), Université de Montpellier, Montpellier, France
- McDermott F, Hawkesworth C (1991) Th, Pb, and Sr isotope variations in young island arc volcanics and oceanic sediments. *Earth Planet Sci Lett* 104:1–15
- Morimoto N (1988) Nomenclature of Pyroxenes. *Mineral Petrol* 39:55–76
- Murwanto H, Gunnell Y, Suharsono S, Sutikno S, Lavigne F (2004) Borobudur monument (Java, Indonesia) stood by a natural lake: chronostratigraphic evidence and historical implications. *The Holocene* 14:459–463
- Murwanto H (2014) Penelusuran jejak lingkungan danau di sekitar Candi Borobudur dengan pendekatan paleogeomorfologi. S3 Dissertation, University of Gadjah Mada, Yogyakarta, Indonesia
- Nadeau O, Williams-Jones AE, Stix J (2013) Magmatic–hydrothermal evolution and devolatilization beneath Merapi volcano, Indonesia. *J Volcanol Geotherm Res* 261:50–68
- Nandaka IGMA, Gertisser R, Walter TR, Troll VR, Ratdomopurbo A (2023) Merapi: evolving knowledge and future challenges. In: Gertisser R, Troll VR, Walter TR, Nandaka IGMA, Ratdomopurbo A (eds) Merapi volcano-geology, eruptive activity, and monitoring of a high-risk volcano. Springer, Berlin, Heidelberg, pp 553–572
- Newhall CG, Bronto S, Alloway B, Banks NG, Bahar I, Del Marmol MA, Hadisantono RD, Holcomb RT, McGeehin J, Miksic JN, Rubin M, Sayudi SD, Sukhyar R, Andreastuti S, Tilling RI, Torley R, Trimble D, Wirakusumah AD (2000) 10,000 years of explosive eruptions of Merapi Volcano, Central Java: archaeological and modern implications. *J Volcanol Geotherm Res* 100:9–50
- Newhall CG, Self S (1982) The volcanic explosivity index (VEI): an estimate of explosive magnitude for historical volcanism. *J Geophys Res* 87:1231–1238
- Peccerillo A, Taylor SR (1976) Geochemistry of Eocene calc-alkaline volcanic rocks from the Kastamonu area, northern Turkey. *Contrib Mineral Petrol* 58:63–81

- Peters STM, Troll VR, Weis FA, Dallai L, Chadwick JP, Schulz B (2017) Amphibole megacrysts as a probe into the deep plumbing system of Merapi volcano, Central Java, Indonesia. *Contrib Mineral Petrol* 172:16
- Preece K (2014) Transitions between effusive and explosive activity at Merapi volcano, Indonesia: a volcanological and petrological study of the 2006 and 2010 eruptions. PhD Thesis, University of East Anglia, Norwich, UK
- Preece K, Barclay J, Gertisser R, Herd RA (2013) Textural and micro-petrological variations in the eruptive products of the 2006 dome-forming eruption of Merapi volcano, Indonesia: implications for sub-surface processes. *J Volcanol Geotherm Res* 261:98–120
- Preece K, Gertisser R, Barclay J, Berlo K, Herd RA, Facility EIM (2014) Pre- and syn-eruptive degassing and crystallisation processes of the 2010 and 2006 eruptions of Merapi volcano, Indonesia. *Contrib Mineral Petrol* 168:1061
- Preece K, Gertisser R, Barclay J, Charbonnier SJ, Komorowski J-C, Herd RA (2016) Transitions between explosive and effusive phases during the cataclysmic 2010 eruption of Merapi volcano, Java, Indonesia. *Bull Volcanol* 78:54
- Preece K, van der Zwan F, Hammer J, Gertisser R (2023) A textural perspective on the magmatic system and eruptive behaviour of Merapi volcano. In: Gertisser R, Troll VR, Walter TR, Nandaka IGMA, Ratdomopurbo A (eds) *Merapi volcano—geology, eruptive activity, and monitoring of a high-risk volcano*. Springer, Berlin, Heidelberg, pp 265–289
- Rahardjo W, Sukandarrumidi, Rosidi HMD (1977) Geological Map of the Yogyakarta Quadrangle, Java, 1:100,000, Geol. Surv. of Indonesia, Ministry of Mines, Bandung
- Ratdomopurbo A, Beauducel F, Subandriyo J, Nandaka IGMA, Newhall CG, Suharna SDS, Suparwaka H, Sunarta, (2013) Overview of the 2006 eruption of Mt. Merapi. *J Volcanol Geotherm Res* 261:87–97
- Scheltema JF (1912) *Monumental Java*. Macmillan and Co., Limited, London, p 302
- Selles A, Deffontaines B, Hendrayana H, Violette V (2015) The eastern flank of the Merapi volcano (Central Java, Indonesia): architecture and implications of volcanoclastic deposits. *J Asian Earth Sci* 108:33–47
- Siebert L, Simkin T, Kimberly P (2011) *Volcanoes of the world*. University of California Press, Berkeley
- Solikhin A, Thouret J-C, Liew SC, Gupta A, Sayudi DS, Oehler J-F, Kassouk Z (2015) High-spatial-resolution imagery helps map deposits of the large (VEI 4) 2010 Merapi Volcano eruption and their impact. *Bull Volcanol* 77:20
- Subandriyo, Gertisser R, Aisyah N, Humaida H, Preece K, Charbonnier S, Budi-Santoso A, Handley H, Sumarti S, Sayudi DS, Nandaka IGMA, Wibowo HE (2023) An overview of the large-magnitude (VEI 4) eruption of Merapi in 2010. In: Gertisser R, Troll VR, Walter TR, Nandaka IGMA, Ratdomopurbo A (eds) *Merapi volcano—geology, eruptive activity, and monitoring of a high-risk volcano*. Springer, Berlin, Heidelberg, pp 353–407
- Stewart RB, Price RC, Smith IEM (1996) Evolution of high-K arc magma, Egmont volcano, Taranaki, New Zealand: evidence from mineral chemistry. *J Volcanol Geotherm Res* 74:275–295
- Sun SS, McDonough WF (1989) Chemical and isotopic systematics of oceanic basalts: implications for mantle composition and processes. In: Saunders AD, Norry MJ (eds) *Magmatism in the ocean basins*. *Geol Soc Lond Spec Publ* 42:313–345
- Troll VR, Deegan FM (2023) The magma plumbing system of Merapi: The petrological perspective. In: Gertisser R, Troll VR, Walter TR, Nandaka IGMA, Ratdomopurbo A (eds) *Merapi volcano—geology, eruptive activity, and monitoring of a high-risk volcano*. Springer, Berlin, Heidelberg, pp 233–263
- Troll VR, Hilton DR, Jolis EM, Chadwick JP, Blythe LS, Deegan FM, Schwarzkopf LM, Zimmer M (2012) Crustal CO₂ liberation during the 2006 eruption and earthquake events at Merapi volcano. Indonesia. *Geophys Res Lett* 39:L11302
- Troll VR, Deegan FM, Jolis EM, Harris C, Chadwick JP, Gertisser R, Schwarzkopf LM, Borisova AY, Bindeman IN, Sumarti S, Preece K (2013a) Magmatic differentiation processes at Merapi volcano: inclusion petrology and oxygen isotopes. *J Volcanol Geotherm Res* 261:38–49
- Troll VR, Chadwick JP, Jolis EM, Deegan FM, Hilton DR, Schwarzkopf LM, Blythe LS, Zimmer M (2013b) Crustal volatile release at Merapi volcano; the 2006 earthquake and eruption events. *Geol Today* 29:96–101
- Turner S, Foden J (2001) U, Th and Ra disequilibria, Sr, Nd and Pb isotope and trace element variations in Sunda arc lavas: predominance of a subducted sediment component. *Contrib Mineral Petrol* 142:43–57
- van Bemmelen RW (1949) *The geology of Indonesia, Vol. 1A: General Geology*. Government Printing Office, The Hague
- van Bemmelen RW (1956) The influence of geologic events on human history (an example from Central Java). *Verhand K Ned Geol Mijnbouw Genoot, Geol Serie*, p 20–36
- van der Zwan FM, Chadwick JP, Troll VR (2013) Textural history of recent basaltic-andesites and plutonic inclusions from Merapi volcano. *Contrib Mineral Petrol* 166:43–63
- Vidal CM, Komorowski J-C, Métrich N, Pratomo I, Kartadinata N, Prambada O, Michel A, Carazzo G, Lavigne F, Rodysill J, Fontijn K, Surono (2015) Dynamics of the major plinian eruption of Samalans in 1257 A.D. (Lombok, Indonesia). *Bull Volcanol* 77:73
- Voight B, Constantine EK, Siswawidjono S, Torley R (2000) Historical eruptions of Merapi volcano, Central Java, Indonesia, 1768–1998. *J Volcanol Geotherm Res* 100:69–138

- White WM, Patchett J (1984) Hf-Nd-Sr isotopes and incompatible element abundances in island arcs: implications for magma origins and crust-mantle evolution. *Earth Planet Sci Lett* 67:167–185
- Whitford DJ (1975a) Geochemistry and petrology of volcanic rocks from the Sunda arc, Indonesia: PhD Thesis, Australian National University, Canberra, Australia
- Whitford DJ (1975b) Strontium isotopic studies of the volcanic rocks of the Sunda arc, Indonesia and their petrogenetic implications. *Geochim Cosmochim Acta* 39:1287–1302
- Whitford DJ, Nicholls IA (1976) Potassium variation in lavas across the Sunda arc in Java and Bali. In: Johnson RW (ed) *Volcanism in Australasia*. Elsevier, Amsterdam, pp 63–75
- Whitford DJ, Nicholls IA, Taylor SR (1979) Spatial variations in the geochemistry of Quaternary lavas across the Sunda arc in Java and Bali. *Contrib Mineral Petrol* 70:341–356
- Whitford DJ, White WM, Jezek PA (1981) Neodymium isotopic composition of Quaternary island arc lavas from Indonesia. *Geochim Cosmochim Acta* 45:989–995
- Whitley S (2020) Xenoliths as tracers of magmatic and intra-crustal processes at volcanic arcs. PhD Thesis, Keele University, Keele, UK
- Whitley S, Gertisser R, Halama R, Preece K, Troll VR, Deegan FM (2019) Crustal CO₂ contribution to subduction zone degassing recorded through calc-silicate xenoliths in arc lavas. *Sci Rep* 9:8803
- Whitley S, Halama R, Gertisser R, Preece K, Deegan FM, Troll VR (2020) Magmatic and metasomatic effects of magma-carbonate interaction recorded in calc-silicate xenoliths from Merapi volcano (Indonesia). *J Petrol* 61 (4):egaa048
- Wirakusumah AD, Heriman AD, Hadisantono RD, Lubis H, Sutoyo (1980) Laporan kemajuan pemetaan geologi Daerah Gunung Merapi, Jawa Tengah. Unpublished Report – Volcanological Survey of Indonesia, Bandung
- Wirakusumah AD, Juwana H, Loebis H (1989) Peta Geologi Gunung Merapi. Jawa Tengah (geologic Map of Merapi Volcano, Central Java) 1(50):000
- Woodhead JD, Hergt JM, Davidson JP, Eggins SM (2001) Hafnium isotope evidence for ‘conservative’ element mobility during subduction processes. *Earth Planet Sci Lett* 192:331–346



The Godean Debris Avalanche Deposit From a Sector Collapse of Merapi Volcano

7

Sutikno Bronto, Wartono Rahardjo,
Pudjo Asmoro, Antonius Ratdomopurbo,
Malia Adityarani, and Afrinia Permatasari

Abstract

Debris avalanche deposits are products of large sector collapses of composite volcanic cones. Horseshoe-shaped craters open down-slope to a hummocky topography of the deposits. In the Godean area, Sleman District, Special Province of Yogyakarta, the deposit of a long-suspected large volcanic sector collapse of Merapi has been discovered, forming a hummocky topography north of the Godean palaeovolcanic hills. The exposed remnants of the Godean debris avalanche deposit cover an area of 2×2 km and the height of hummocks is < 30 m above the surrounding plain. The exposures are loose block facies composed of pyroclastics, lava flows and reworked deposits, highly fractured into jigsaw cracks and small-scale fault displacements. Andesitic

megablocks representing clasts of the matrix facies are widely distributed on the Sedayu plain south of Godean, from where the avalanche propagated southward until the confluence of the Bedog River and the Progo River. In its original form, the Godean debris avalanche flowed 50 km away from Merapi and covered an area of ~ 390 km². The gigantic landslide destroyed areas of the Magelang District, Central Java Province, as well as the Sleman, Bantul and the eastern part of the West Progo districts, Yogyakarta Special Province. The total volume of the deposit is estimated at 4.9–8.6 km³. Remnants of the Godean debris avalanche are preserved in the Godean and Sedayu areas because the avalanche hit, and was trapped by the north side of the Tertiary Godean palaeovolcanic hills. Southward, the debris avalanche was stranded on the north side of the wavy hills of the Tertiary Sentolo Formation. We suspect that the Godean debris avalanche was probably caused by the first stage of Merapi sector collapse (CE 1). However, this interpretation and the age of the event are still poorly constrained. To improve our understanding of past Merapi collapses, numerical dating studies, including tephra intercalations in black clay deposits of the ancient Borobudur and Gantiwarno lakes, are necessary. Merapi sector collapses range from small scales to large events like the Godean debris avalanche. In order to reduce volcanic risk from future

S. Bronto (✉) · P. Asmoro · A. Ratdomopurbo
Geological Agency, Ministry of Energy and Mineral
Resources, Bandung, Indonesia
e-mail: sutiknobronto@gmail.com

W. Rahardjo
Geological Engineering, University of Gadjah Mada,
Yogyakarta, Indonesia

M. Adityarani
Freelance Geologist, Bantul, Yogyakarta, Indonesia

A. Permatasari
Geological Engineering, University of Pembangunan
Nasional “Veteran” Yogyakarta, Yogyakarta,
Indonesia

sector collapses, a serious mitigation effort, focussing particularly on precursor phenomena, is suggested.

Keywords

Merapi · Godean · Debris avalanche · Sector collapse · Gigantic landslide · Yogyakarta

7.1 Introduction

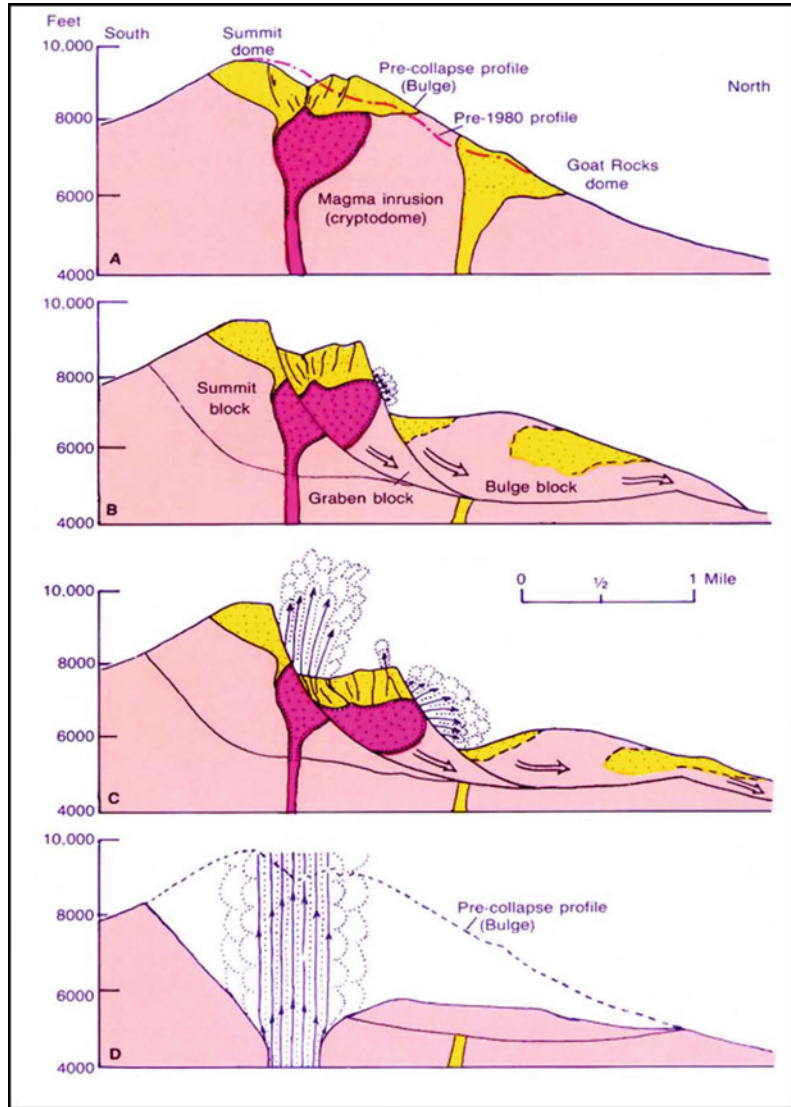
Volcanic sector collapses leave horseshoe-shaped craters and a hummocky topography downslope composed of volcanic debris avalanche deposits (e.g. Siebert 1984; Bronto 1989; Glicken 1996). The hummocks vary in height from 10 to 100 m above the surrounding plain and isolated depressions may be formed between them. Inside volcanic debris avalanche deposits, jigsaw cracks, highly fractured lavas and minor faults may be observed, and layered volcanic deposits may be drag-folded. In some cases, the horseshoe-shaped crater form may not be observed anymore due to cover by younger volcanic deposits or cones. Volcanic sector collapses may involve huge volumes ($> 0.1 \text{ km}^3$) of lavas, pyroclastic deposits and soil from their source volcanoes, and the affected area can be tens to hundreds of square kilometres in size. Previous workers have used various terms, such as volcanic dry avalanches (Ui 1983), rock-slide avalanches (Voight et al. 1981; Glicken 1996) and volcanic debris avalanches (Siebert 1984) to describe this phenomenon. In this chapter, we use the terms volcanic debris avalanche and gigantic landslide interchangeably to describe a mass movement of huge volume from a volcanic cone, sliding down the volcanic slope and onto adjacent plains. The term gigantic landslide is not a formal name, although indeed, it once was. It is used here as a more understandable term for the non-specialist reader.

During historical times, volcanic debris avalanches occurred at several volcanoes, such as Unzen (1792), Bandai (1888), Bezymianny (1956), Shiveluch (1964) and Augustine (1883)

(Siebert et al. 1987). Further studies of the Bandai volcanic debris avalanche deposits were carried out by, for example, Nakamura and Glicken (1997) and Ui (1997). In West Java, Indonesia, a gigantic landslide of Papandayan volcano occurred in 1772 (Neumann van Padang 1951). In prehistoric time, several well-known gigantic landslides occurred at Indonesian volcanoes, including Raung-Gadung in East Java (Neumann van Padang 1939; Siebert et al. 1997), and Gede (van Bemmelen 1949; Situmorang and Hadisantono 1992; Agustin and Bronto 2019) and Galunggung (Neumann van Padang 1951; Bronto 1989) in West Java. The hummocky topography of the Galunggung volcanic debris avalanche deposit is well known as ‘The Ten Thousand Hills of Tasikmalaya’, whereas that of Gede volcano is called ‘The 777 (Triple Seven) Hills of Cianjur’. Alloway et al. (2005) reported the stratigraphy, age and voluminous prehistoric debris avalanche events of Taranaki volcano in New Zealand. One of these debris avalanche deposits, the c. 25,000 y BP Pungarehu Formation, shows relatively unimpacted, a single flow deposit from proximal to distal facies, allowing a detailed characterisation of structural and textural features as indicators of transport and emplacement mechanisms (Roverato et al. 2015). Based on its chemical composition, Yoshida et al. (2006) published a study on the transport mechanism of a c. 24,000-year-old debris avalanche event at Asama volcano, Japan. A topographic control study of the Asama debris avalanche was conducted by Yoshida and Sugai (2007a), who also studied the magnitude of sediment transport of the Asama debris avalanche, whose volume totals ~ 4.9 to 5.4 km^3 (Yoshida and Sugai 2007b).

Understanding volcanic sector collapses and volcanic debris avalanches (or gigantic landslides) of volcanoes has improved dramatically among volcanologists after the eruption of Mount St. Helens on 18 May 1980 (Lipman and Mullineaux 1981). Due to an old lava dome plugging the summit, ascending magma was not able to move vertically, but intruded into the upper north slope, causing bulging and faulting on the north slope (Fig. 7.1). Eventually,

Fig. 7.1 Stages of the rock-slide avalanche process at Mount St. Helens, USA on 18 May 1980 (Lipman and Mullineaux 1981), as an example of partial volcanic cone collapse accompanied by explosive activity



oversteepening of the steep slope caused a gigantic landslide followed by a directed blast and vertical explosions. MacLeod (1989) introduced sector-failure eruptions in Indonesian volcanoes. Based on the experience working on active volcanoes, Bronto (1995, 2001) reported several volcanic debris avalanche deposits in Indonesia.

According to van Bemmelen (1949), a gigantic landslide of Merapi volcano occurred in AD 1006. This landslide was thought to be directed westward as far as 20 km and the deposit interpreted to form the Gendol Hills in

the Salam and Muntilan areas, Magelang District, Central Java Province. Newhall et al. (2000) argued that characteristics of a volcanic debris avalanche, such as jigsaw cracks, are not found in the Gendol Hills. In addition, there are some Hindu and Buddhist temples which were built in the seventh to ninth century on the summit of the hills. Radiometric dating of volcanic rocks of the Gendol Hills using the K–Ar method gave an age of 3.4 Ma, suggesting that the hills are significantly older than any deposit we know of the current Merapi volcano (e.g. Bronto 2016; Ger-tisser et al. 2023, Chap. 6). Furthermore, the age

of the Gendol Hills is much younger than the Tertiary volcanic rocks of the West Progo Mountains (12.6–29.6 Ma; Soeria-Atmadja et al. 1994; Ngkoimani 2005; Permanadewi et al. 2008) that lie further to the west. Based on these data, Bronto (2016) concluded that the Gendol Hills are a remnant of an *in situ* palaeovolcano.

The issue of gigantic landslides of Merapi resurfaced when we found a probable debris avalanche deposit from the volcano in the Godean area, Sleman District, Special Province of Yogyakarta. In order to trace the affected area and, possibly, the age of the event, available dates of ancient Lake Borobudur and ancient Lake Gantiwarno are discussed, which are located to the west, and at the south foot of Merapi. The Godean area lies about 35 km south–southwest of Merapi and 10 km west of Yogyakarta (Fig. 7.2).

This chapter builds on the previous Indonesian version (Bronto et al. 2014) by (i) adding important data from the area surrounding Merapi, such as ancient Lake Borobudur, (ii) describing the volcanological impact of the event, and (iii) providing a more detailed discussion of recommended future work.

7.2 Geological Setting and Previous Studies

Physiographically, Merapi is one of the active Quaternary volcanoes in the Central Zone of Java (van Bemmelen 1949; Harijoko et al. 2023, Chap. 4). To the northwest, the volcano is bounded by the volcanoes of Sumbing and Sindoro, whereas to the north there is a line of volcanoes consisting of Merbabu, Telomoyo and Ungaran. In the west, Merapi is limited by the West Progo Mountains, whereas to the south–southeast, it is bordered by the Jiwo Hills and the Southern Mountains. In the Jiwo Hills, pre-Tertiary metamorphic rocks are exposed (Suroño et al. 1992), whereas the West Progo and Southern Mountains are composed of Tertiary volcanic and sedimentary rocks. The Progo River forms from the convergence of several rivers north of Merapi.

Regionally, the geology of the Godean area was reported by Rahardjo et al. (1977) in the geological map of the Yogyakarta quadrangle (scale: 1:100,000). The oldest rock unit is the Nanggulan Formation, which is Palaeogene (Eocene–Oligocene) in age and composed of sandstones intercalated with lignites, sandy marls, claystones with limonite concretions, and tuffs. Palaeogene limestone is exposed in the Gamping area, west of Yogyakarta City. This rock unit is overlain by old andesite of the Bemmelen Formation that consists of intercalated andesitic breccias, tuffs, lapilli tuffs, agglomerates and lavas of Oligo-Miocene age. These two rock units were intruded by diorites and andesites in the Lower Miocene. Further to the south in the Bantul District, the Sentolo Formation is composed of limestones and marly sandstones of Neogene (Miocene–Pliocene) age.

Merapi volcanic products have been broadly divided into two rock units, namely Old Merapi volcanic deposits and Young Merapi volcanic deposits (Rahardjo et al. 1977; Wirakusumah et al. 1989; cf. Gertisser et al. 2023, Chap. 6). Both are composed of mainly basaltic to andesitic lavas, and pyroclastic, lahar and fluvial deposits. At the surface, most of the Godean area is covered by the Young Merapi volcanic deposits, particularly lahar and other reworked (fluvial) deposits.

7.3 Ancient Lake Borobudur

About 26 km west of Merapi there is the well-known Buddhist temple of Borobudur. The temple was built at the end of the eighth until the early ninth century (Murwanto 1996). Borobudur Temple was surrounded by an ancient Lake Borobudur (Murwanto et al. 2004; Murwanto 2012, 2014; Murwanto and Purwoarminto 2015) that had formed since the Late Pleistocene. Radiometric dating using the ^{14}C method of the oldest lake deposits gave ages between $31,430 \pm 2070$ ^{14}C y BP and 660 ± 110 ^{14}C y BP, although Newhall et al. (2000) reported an even younger age of 420 ± 50 ^{14}C y BP (Table 7.1).

Fig. 7.2 Black clay deposits of ancient Lake Borobudur (Murwanto 2014) overlain by **a** pyroclastic surge (?) deposits (location: Desa Sokorini), **b** tephra fall (?) deposits (location: Progo River) and **c** a Merapi lahar deposit (location: Progo River)

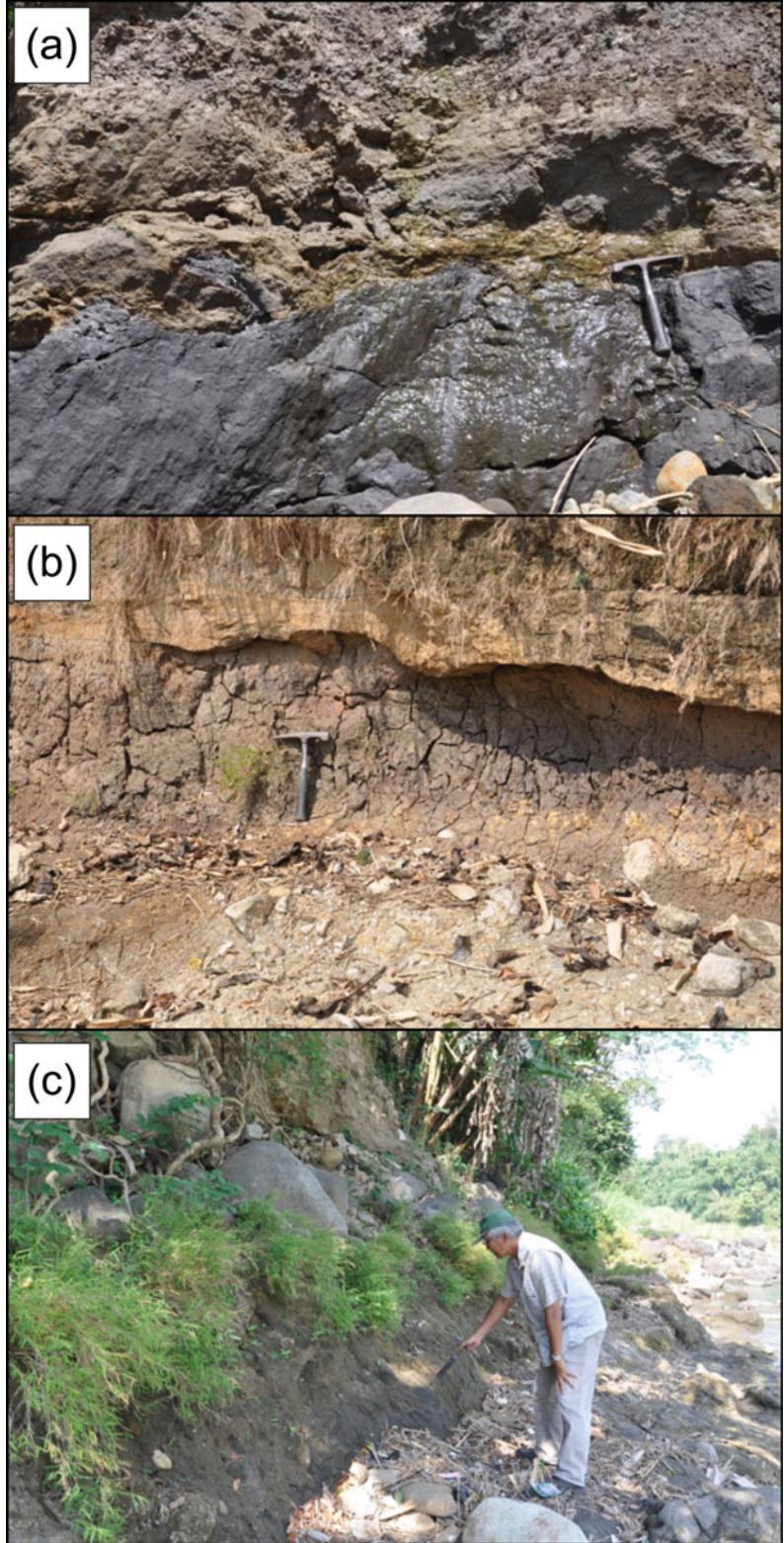


Table 7.1 ^{14}C ages in the Borobudur area

| No. | ^{14}C age (^{14}C y BP) | Explanation | Reference ^a |
|-----|--|---|------------------------|
| 1 | 420 ± 50 | Wood fragment in black clay, Sileng River | 2 |
| 2 | 660 ± 110 | Wood fragment in black clay, Progo River | 1 |
| 3 | 1700 ± 160 | Plant fossil in claystone in a drill core at 3 m depth, Desa (village) Ngaran | 3 |
| 4 | 3430 ± 50 | Wood fragment in black clay, taken in traditional well at 13.5 m depth | 2 |
| 5 | 4280 ± 100 | Wood fragment in black clay, Progo River, Desa Teluk | 3 |
| 6 | 6330 ± 130 | Black clay in Pacet riverbank, Desa Gatak | 4 |
| 7 | 13,300 ± 210 | Black clay, Desa Soko | 4 |
| 8 | 13,710 ± 540 | Plant fossil in black clay, in a drill core at 4 m depth, north of Borobudur Temple | 4 |
| 9 | 14,790 ± 230 | Black clay in the terrace of Progo River, Desa Kaliabon | 4 |
| 10 | 19,520 ± 340 | Black clay in a drill core at 7 m depth, Sileng River, Desa Soropadan | 3 |
| 11 | 22,130 ± 400 | Black clay in a drill core at 9 m depth, Sileng River, Desa Soropadan | 3 |
| 12 | 22,140 ± 390 | Black clay in riverbank, Desa Pakisaji | 4 |
| 13 | 23,640 ± 470 | Wood fragment in terrace of Progo River, south of Blondo bridge | 4 |
| 14 | 24,640 ± 530 | Black clay at 5 m depth in Progo riverbank, south of Sigug bridge | 4 |
| 15 | 25,110 ± 560 | Black clay in a river in Desa Soropadan | 4 |
| 16 | 27,070 ± 710 | Black clay in Progo riverbank at 12 m depth, east of Pawon Temple | 4 |
| 17 | 31,430 ± 2070 | Black clay in Progo riverbank at 7 m depth, north of Sigug bridge | 4 |

^a References 1 = Murwanto (1996); 2 = Newhall et al. (2000); 3 = Murwanto et al. (2001); 4 = Murwanto (2014)

The lower part of the ancient Lake Borobudur deposits is dominated by black clay with intercalations of river channel deposits consisting of silts, sands and gravels. In the upper part, the black clay deposits contain intercalated volcanic deposits, including tephra fall and other pyroclastic units of ash to lapilli size, lahar deposits and other reworked (fluvial) deposits (Fig. 7.2). Figure 7.2a shows fine to coarse grained volcanic deposits, with very angular fragments, reverse grading, and discontinued stratification or tongue structures. These characteristics may indicate directed blast or pyroclastic surge deposits, as discussed further below. In Fig. 7.2b, the volcanoclastic deposit shows bedding structures and presumably constitutes a tephra (ash) fall deposit. The source of the two volcanic deposits is presently uncertain. It is possible that they were derived from various Quaternary volcanoes, such as Sumbing and Sindoro in the north and Merbabu in the northeast, although, based on their proximity, they could be derived from Merapi.

Figure 7.2c clearly exhibits Merapi lahar deposits containing matrix-supported, subrounded boulders. Reworked volcanic material from Sumbing and Sindoro volcanoes would have had to be transported by the Tangsi and Progo Rivers, whereas material from Merbabu would have been transported by the Elo River, before joining the Apu, Batang, Putih and Krasak rivers to form the Progo River, which is considered less likely.

Murwanto et al. (2001) reported the results from two drill cores in terraces of the Elo and Sileng rivers, each reaching a depth of ~50 m. Names of volcanic deposits at the sites were based on descriptive lithological, not genetic terms. At Elo River, the lower part (38.5–41.5 m depth; 3 m thick) is composed of pumice lapilli tuffs that are interpreted as yet undated tephra deposits. In the middle to upper parts, there are four palaeosol layers, indicating temporary dry land or a dried lake that occurred several times due to renewed impoundment by volcanic deposits, possibly from Merapi. At

Sileng River, the lower part (21–50 m depth; 29 m thick) is composed of a fluvio-volcanic deposit consisting of andesitic gravels set in a very coarse sand matrix. The upper part up to 21 m depth is dominated by black clay with intercalated volcanic deposits. This study implies that ancient Lake Borobudur had a long existence as an impounded lake, interrupted occasionally by ‘subaerial’ spells. Thus, the lake formed, drained, re-formed and re-drained several times. Since ~400 or 600 ^{14}C y BP, the lake has disappeared completely (Murwanto 2014).

On the basis of palaeogeomorphology and the stratigraphy of clay deposits, the ancient Lake Borobudur has been divided into three periods of lake formation in the Late Pleistocene, in the Holocene and in recent time (~600 ^{14}C y BP) (Murwanto 2014). These dynamic reconstructions suggest that the lake had become narrower or smaller with time, with the first ancient lake being the widest. Gradually, the Borobudur Lake environment became dry when the accumulated material from volcanic eruptions reached a thickness of more than 10 m.

Murwanto (2014) also noted that Merapi volcanic deposits are more dominant than other

volcanic sources in the black clay deposits of the ancient Lake Borobudur. This conforms with the study of Gomez et al. (2010), who, based on analysis of two drill cores (drill cores 3 and 4) that reached depths of 70 and 111.5 m, suggested that the evolution of the Borobudur basin has been strongly influenced by volcanic activity. Core 3 was drilled from the lowest terrace of the Elo River at the confluence with the Progo River, whereas core 4 was located on a high western terrace of the Sileng River.

Based on the drill cores and dating using K/Ar and ^{14}C methods (Table 7.2), Gomez et al. (2010) concluded that the Borobudur area has been under volcanic influence since 361,000 y BP. During this time, two major volcanic events deposited volcanoclastic material up to tens of metres thick, and dated at ~119,000 y BP and ~31,000 y BP, in the southern part of the Borobudur basin. The source of the first major volcanic event remained unknown at the time, while the second event was loosely related to the collapse of the older Proto-Merapi edifice (Newhall et al. 2000), although derivation of the deposit from Merbabu volcano was also given as a possibility on geochemical grounds (Gomez et al. 2010).

Table 7.2 K/Ar and ^{14}C ages of volcanic material in the Borobudur area (Gomez et al. 2010)

| No. | Numerical age (^{14}C y BP) | Explanation |
|-----|---------------------------------------|---|
| 1 | 10,360 ± 25 | DC 4, charcoal lodged inside volcanic ash and sands, 13 m depth |
| 2 | 31,040 ± 300 | DC 3, wood fragment in 12 m thick of dark grey volcanic ash deposit on top of vesiculated blocks at 20–31 m depth |
| 3 | 80,000 ± 9000 | DC 4, 33.5 m depth, an andesitic block thicker than 1 m in a pyroclastic flow deposit at 38–30 m depth |
| 4 | 115,000 ± 2000 | DC 4, an andesitic block at 38.5 m depth |
| | 119,000 ± 2000 | DC 4, a single block andesite at 38 m depth |
| 5 | 158,000 ± 4000 | DC 3, more than 20 m thick of andesitic lava blocks down to the bottom of the core (70 m deep) |
| 6 | 161,000 ± 3000 | DC 4, a single block of andesite at 83 m depth |
| 7 | 361,000 ± 6000 | DC 4, more than 31 m thick massive andesitic unit down to the base of the core (111.5 m deep). This unit is composed of andesitic clasts and rounded pebbles, 5–15 cm in size. Dated sample is an andesite block, 80 cm in size |

Samples were taken from drill core (DC) 3 in the lowest terrace of the Elo River at the confluence with the Progo River and from DC 4 located on a high western terrace of the Sileng River. Charcoal and wood fragment samples were dated using the ^{14}C method, while dating of andesitic blocks used the K/Ar method

7.4 Ancient Lake Gantiwarno

South of Merapi, the plain between Prambanan and Klaten, bounded by the Southern Mountains, was previously also an ancient lake called Lake Gantiwarno (Rahardjo and Astuti 2000), as reflected by widespread black clay deposits in the Gantiwarno and adjacent areas. The palaeogeography of the ancient lake was studied in detail by Rahardjo and Astuti (2000), while the volcanic material intercalated with the black clay deposits has remained unstudied. Further to the west at the Opak River, about 30 km south of Merapi, a lacustrine pumice deposit from Merapi was found by S. Bronto in 1993 near the base of black clay deposits that overlie Tertiary volcanic rocks of the Semilir Formation (Surono et al. 1992). This lacustrine deposit, which is seemingly absent in the Lake Borobudur deposit, contains plant fossils dated at 6120 ± 110 ^{14}C y BP (Newhall et al. 2000).

7.5 Geology of the Godean Area

Referring to the regional geology of the Godean area, the Tertiary rocks were formed by the Godean palaeovolcano (Bronto 2016), whereas the Merapi products consist of volcanic debris avalanche, pyroclastic and lahar deposits.

7.5.1 Godean Palaeovolcano

Located ~ 10 km west of Yogyakarta (Fig. 7.4), the Godean plain has an elevation of 140 m asl in the north, decreasing to 100 m asl in the south. In the Godean plain, there are several hills aligned from north to south, including Gunung (G., Mount) Ngampon (222 m asl; Fig. 7.5), G. Gedang (193 m asl), G. Gede (218 m asl), G. Butak (154 m asl), and G. Berjo (175 m asl) (Fig. 7.6). In the central part of the plain, G. Patuk (231 m asl), G. Wungkal (187 m asl), G. Gede (218 m asl), and G. Siwareng (194 m asl) are aligned from southeast to northwest. Slightly separated in the western part is G. So (173 m

asl), located in Desa Sidorejo, Godean Subdistrict, while G. Ngampon, located at the most northern end of the Godean Hills, is part of Desa Margodadi, Seyegan Subdistrict, District of Sleman, Yogyakarta (Fig. 7.3).

The Godean Hills consist mainly of intrusive and pyroclastic rocks. Generally, hills consisting of intrusive rocks are higher than those made up of pyroclastic rocks. They are densely vegetated, and nearly all of the rocks are weathered to clay, which is utilised for making roof tiles and red bricks. Fresh outcrops are only found in some quarries. The intrusive rocks of the Godean Hills are porphyritic andesite and micro-diorite, most exhibiting spheroidal weathering with concentric shells 0.5–2 m in diameter (Fig. 7.5). A minor dark and aphanitic basaltic intrusion is observed on the northeastern slope of G. Gede ($07^{\circ} 44' 34.3''$ S– $110^{\circ} 16' 45.7''$ E). Gunung Gedang has recently been excavated for new residences, producing new exposures of a highly porphyritic andesite intruding into volcanic tuff (Fig. 7.7).

The intrusive rocks are grey to greenish grey due to the presence of chlorite, plagioclase-rich, and characterised by a porphyritic texture and a massive structure. Phenocrysts are plagioclase (20–30 vol%; 1–5 mm in size) and pyroxene (5–10 vol%; 0.5–1 mm in size) set in an aphanitic groundmass. Andesites and micro-diorites that form separated hills from G. Ngampon in the north to G. Berjo in the south are considered shallow intrusive bodies or subvolcanic intrusive rocks (Bronto 2013), representing magma chambers or storage zones beneath the local (Godean) palaeovolcano.

In the western part of the Godean Hills, an intrusive rock in form of a porphyritic andesite is exposed at G. So, Desa Sidorejo, Godean Subdistrict ($07^{\circ}44'15.1''$ S– $110^{\circ}15'58.7''$ E). Outcrops are spheroidally weathered, with rounded cores 1–3 m in diameter. The fresh andesite is light grey and massive. Phenocrysts are plagioclase (30 vol%), pyroxene (10 vol%) and hornblende (1 vol%), 1–3 mm in size, set in an aphanitic groundmass. Xenoliths composed of volcanic glass and other andesitic fragments are locally observed. The rocks are typically

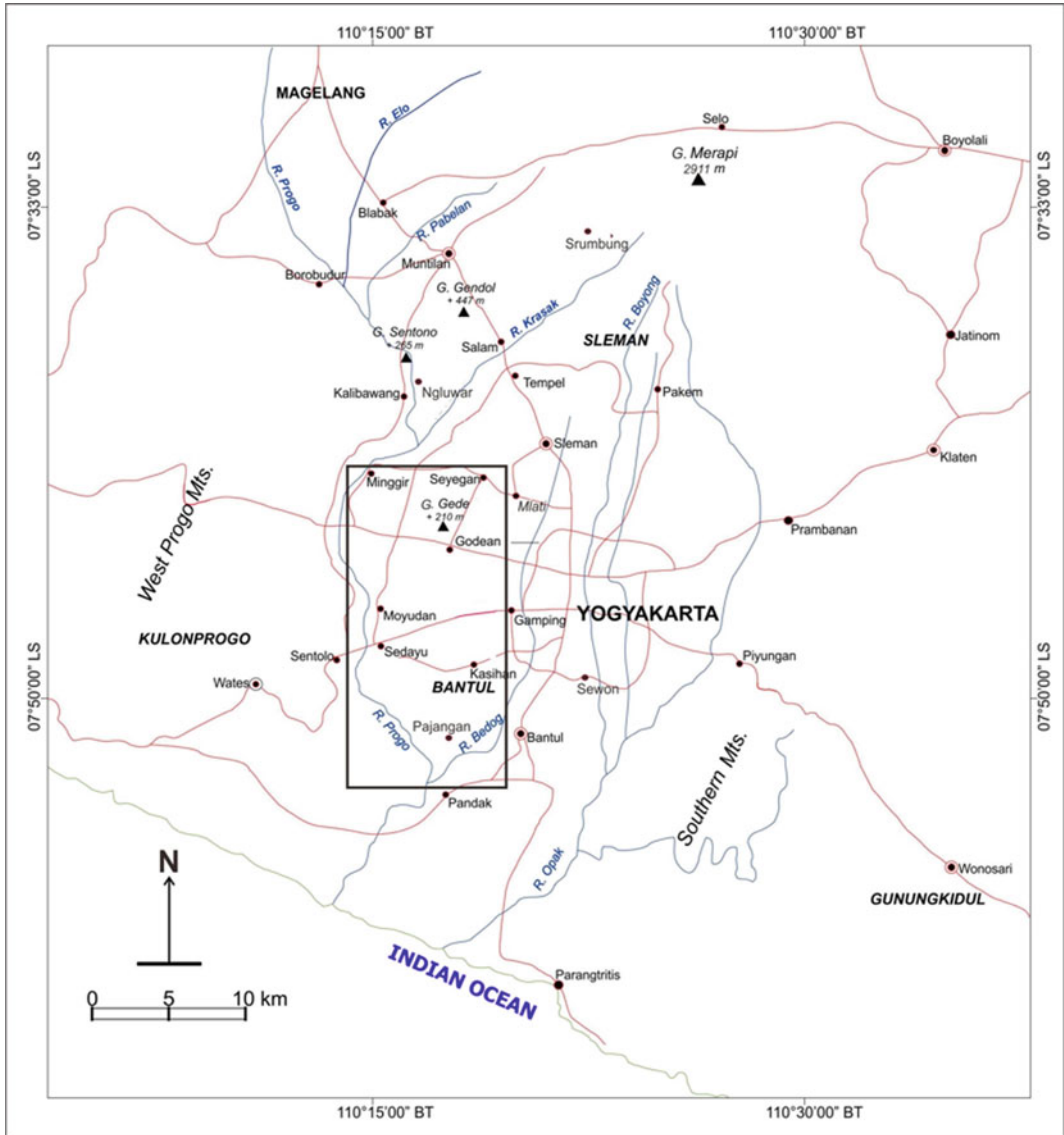


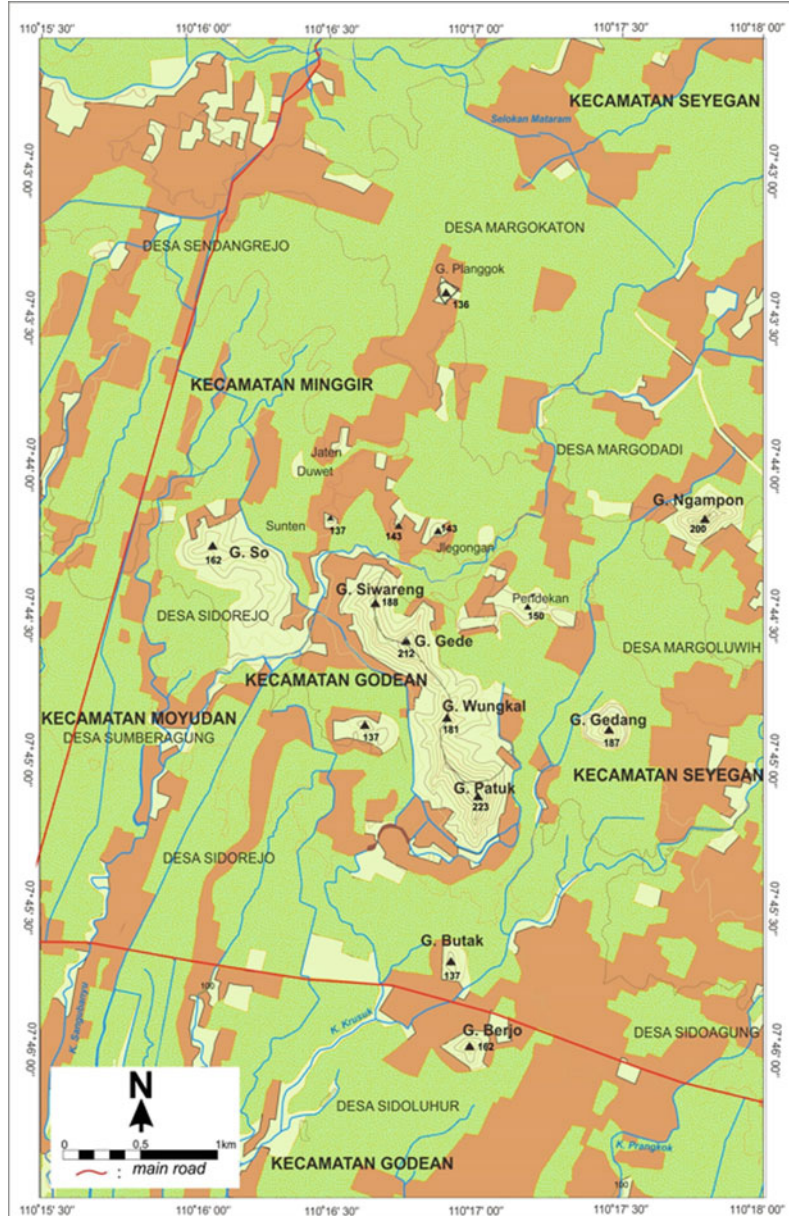
Fig. 7.3 Location map of the study area (black box), covering the Sleman and Bantul Districts, Special Province of Yogyakarta

hydrothermally altered, forming secondary silica, kaolinite, limonite and quartz veins or veinlets.

Pyroclastic rocks are predominantly weakly to strongly silicified, fine to coarse grained tuffs with pumiceous lapillistone intercalations. In the western part of the Godean area, a silicified bedded tuff is exposed in Dusun Celungan near G. So (07° 44' 45.4" S–110° 16' 09.6" E). In the eastern part of the Godean area, pyroclastic rocks

are exposed on the north side of Dusun Kandangan (at a hill 149 m asl), at G. Gedang (Fig. 7.7), and in Dusun Pendekan, Desa Margodadi, Sub-district of Seyegan. In the southern part, tuffs are also found at G. Wungkal (07°44'44.6" S–110°16'48.8" E), at a hill 153 m asl in Dusun Mloyorejo (07°44'54.1" S–110°16'44.4" E) and in Dusun Jomboran, Desa Sidorejo, Subdistrict of Godean. Fine tuffs are altered and oxidised,

Fig. 7.4 Map of the Godean Hills at Godean and the surrounding area, Sleman District. *Source* 1:25,000 topographic map, sheets 1408-223 (Yogyakarta) and 1408-241 (Sleman). Colours: residence areas (brown), rice fields (green), plantation (colourless) (BIG: Badan Informasi Geospasial, previously named Bakosurtanal)



varying in colour from white to grey, pinkish white and reddish brown, and containing secondary minerals, such as silica, kaolinite and iron oxides. At G. Wungkal, the tuffs have been replaced completely by quartz, resembling quartz sandstone. The name ‘wungkal’ (Javanese = sharpener) was based on the utilisation of the silicified tuffs as a sharpener. On the northeastern slope of G. Gede, tuffs are exposed as roof

pendants above an intrusive rock body, with some pieces incorporated into the intrusive rock as silicified xenolithic material (Fig. 7.8). At this location, a layer of baked, black silicified tuff is also observed.

In addition, an outcrop of blocky crystalline limestone has been found in the Pendekan area (Fig. 7.9). The blocky limestone is 1.3–1.5 m in diameter, very hard, and contains large carbonate

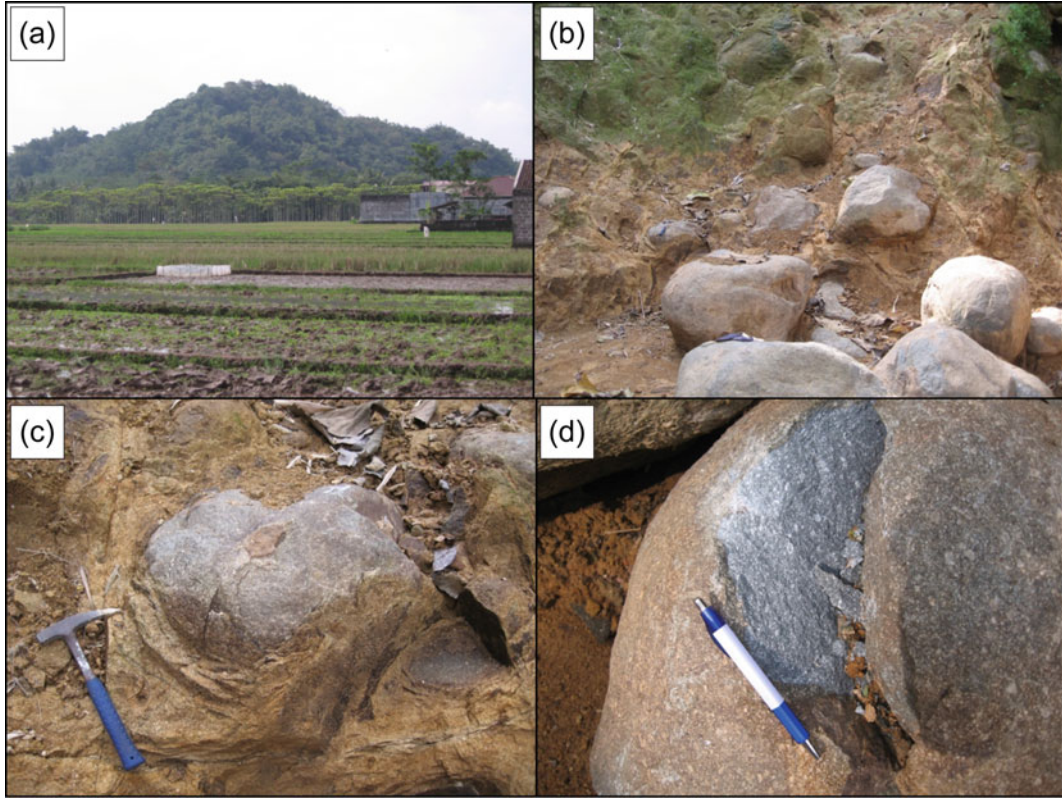


Fig. 7.5 **a** G. (Gunung, Mount) Ngampon, photo taken from the south side of the Godean—Seyegan main road (position: 07° 44' 34.8" S–110° 17' 43.3" E). **b** Andesite outcrop at Dusun Ngampon, Desa Margodadi, Seyegan

Subdistrict (position: 07° 44' 14.3" S–110° 17' 47.3" E). **c** Spheroidal weathering of andesitic intrusive rock. **d** Close-up of fresh andesite, showing a grey colour and porphyritic texture

crystals (0.5–3.0 cm in size). The presence of limestone in the Godean area has not been reported before and may represent either basement rock that correlates with Palaeogene limestone of the Nanggulan Formation exposed in the Gamping area south of Godean, or limestone that was originally the basement of Merapi (Wonosari Formation) and was brought here in the debris avalanche. The latter is suggested by the occurrence of limestone as blocks surrounded by weathered pumice-rich lapilli deposits.

In conclusion, the Tertiary volcanic rocks of the Godean palaeovolcano are composed of pyroclastic rocks intruded by andesite, micro-diorite and minor basalt. The faster cooling magma formed porphyritic andesite, while the slower cooling magma formed micro-diorite. Based on field evidence, there were at least three

intrusion stages during Godean volcanism (Bronto 2016). The oldest intrusive rocks are highly altered and occupy the line of the Gede hills. The second intrusion phase also occurred at G. Gede, represented by a basalt intrusion. The third and youngest intrusions formed G. Berjo, G. Butak, G. Gedang, G. Ngampon, G. So, G. Gede and a hill (153 m asl) south of G. Gede. In general, the third phase of intrusives have generally fresh relics of rock in the core of spheroidal weathering structures, which may allow numerical dating of these units.

Similar to the alignment of hills in Godean and the surrounding area, joints are oriented in a north–south direction, as observed at G. Ngampon, G. Gede and G. Butak. The general north–south pattern of joints and intrusive rocks may be controlled by normal faults in the Bantul-

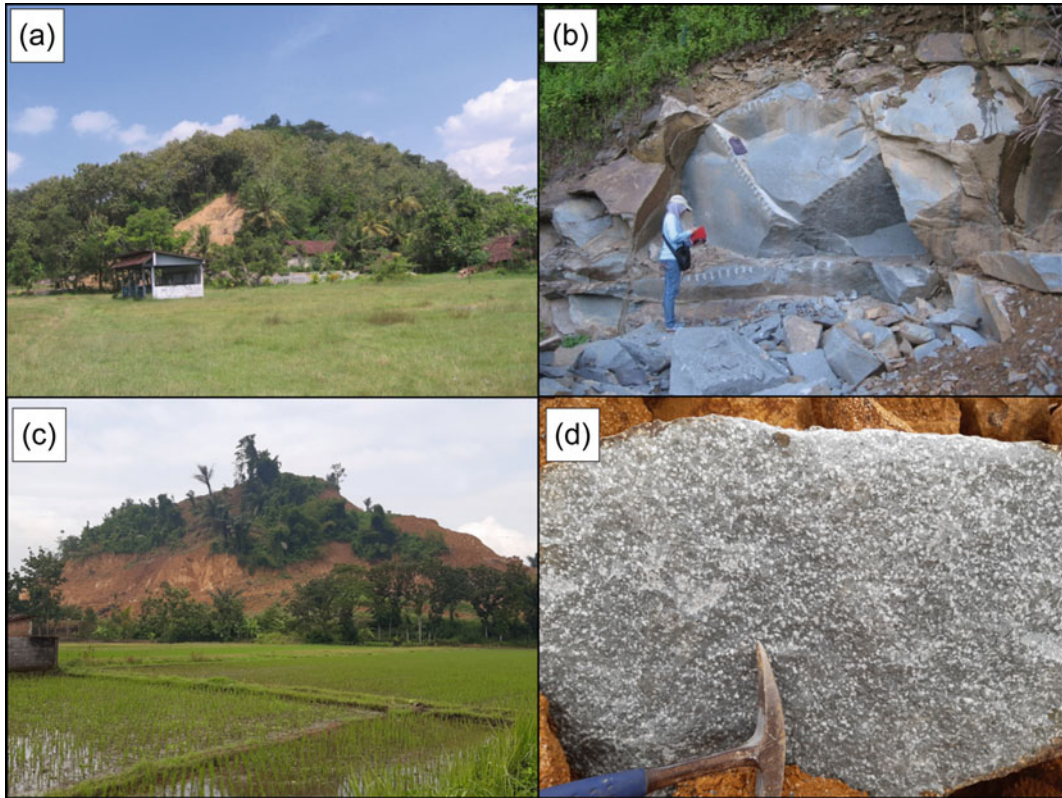


Fig. 7.6 **a** G. Berjo (175 m asl), photo taken from the Godean main road, camera facing southward. **b** Fresh fine grained and grey andesite with aphanitic to porphyritic texture exposed in a quarry on the eastern slope of G. Berjo, Dusun Berjo Wetan, Desa Sidoluhur, Godean

Subdistrict (position: 07°45'59.8" S–110°16'59.9" E). **c** G. Gedang being cleared for new housing, east of Dusun Kandangan, Desa Margodadi, Seyegan Subdistrict. **d** Close-up of slightly weathered andesite cropping out at G. Gedang

Yogyakarta graben structure (Bronto 2016). The distribution of the Tertiary rocks and Quaternary Merapi deposits in the Godean area (District of Sleman) and in the Sedayu area (District of Bantul, Yogyakarta), including the Godean debris avalanche deposit, is shown in Fig. 7.10.

7.5.2 Godean Debris Avalanche Deposit

Evidence of a gigantic Merapi landslide has been found in the Godean area, the type locality of what we herein call the Godean debris avalanche deposit. A large part of the debris avalanche deposit may have been transformed during flow or subsequently eroded to become lahars that are

exposed at several places in the districts of Sleman and Bantul, and westward at the Progo River in the District of Kulon Progo (West Progo), Yogyakarta. Physiographically, the Godean debris avalanche deposit forms low hills or a hummocky topography 142–146 m asl, but <30 m above the surrounding plain. Hummocks located in the northern part of the Godean Hills include the small hills (bukit—Bt.) of Jlegongan (145 m asl), Sunten (143 m asl) and Planggok (Fig. 7.11). In the eastern part, the hummocky topography is notable north of G. Gede (218 m asl), whereas in the western part it is visible north of G. So (173 m asl), both of which are part of the Godean palaeovolcano. The east–west distribution of the Godean hummocks extends over a distance of ~2 km from Dusun Pendekan and

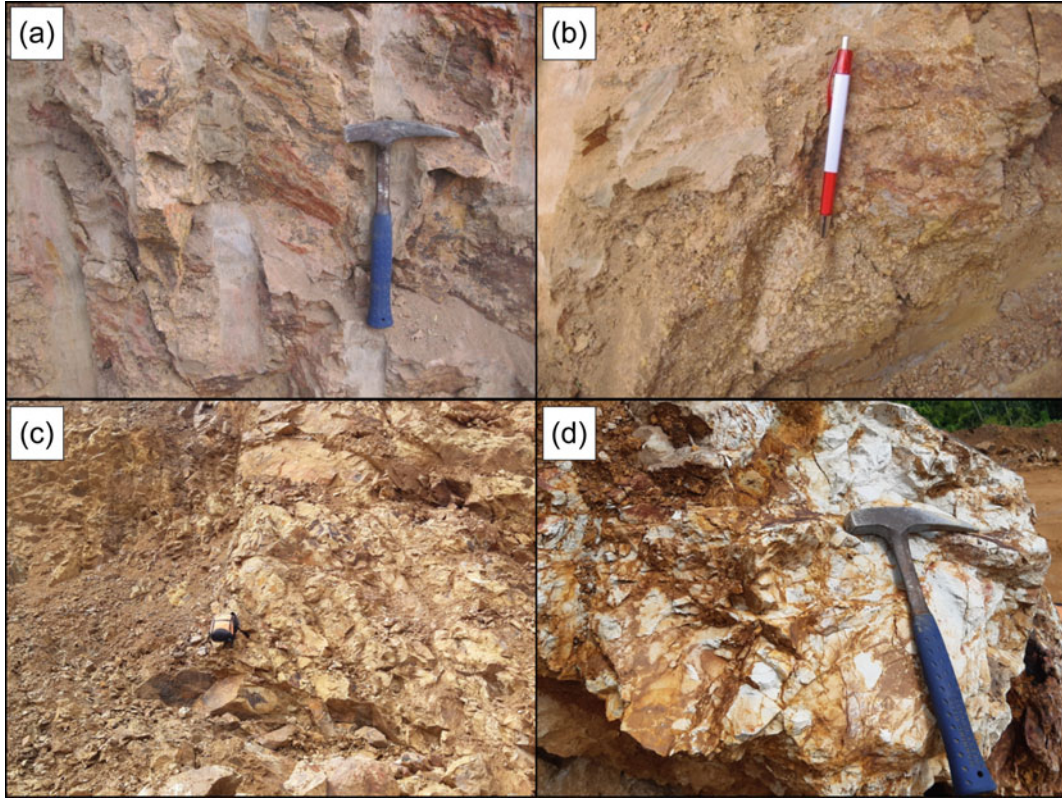


Fig. 7.7 **a** Tuff and **b** pumice lapillistone exposed in a quarry (hill 149 m asl), north of Dusun Kandangan, Desa Margodadi, Seyegan Subdistrict (position: 07°44'28.8" S–

110°17'16.3" E). **c** Tuff (right) intruded by andesite (left) at G. Gedang, east of Dusun Kandangan. **d** Close-up of the tuff exposure shown in (c)

Dusun Jlegongan (Desa Margodadi, Subdistrict of Seyegan) to Dusun Duwet, Dusun Jaten and Dusun Sunten (Desa Sendangrejo, Subdistrict of Minggir). Northwards, the hummocks can also be traced over a distance of 2 km to Dusun Plangkok (Desa Margokaton, Subdistrict of Seyegan).

Generally, fine grained material at the surface of the hummocks is deeply weathered soil, though andesitic blocks and (basaltic?) scoria bombs are still fresh and distributed randomly (Figs. 7.12 and 7.13). At the peak of a hummock in the Dusun Duwet area, an archaeological artefact (a *yoni*) was found. It proves that in the eighth to ninth centuries, this area had been occupied by Hindu society.

Outcrops of the fresh Godean debris avalanche deposit are found in quarries at Dusun

Duwet and Dusun Pendekan between two small, east–west oriented Tertiary hills. In the quarry of Pendekan, the Godean debris avalanche deposit shows intact strata of loose volcanoclastic deposits (Fig. 7.14), containing pyroclastics, reworked deposits and highly fractured lava. Former pyroclastic deposits are characterised by the presence of volcanic bombs, blocks and scoriae set in a poorly sorted ash to lapilli sized matrix. Coarse reworked deposits contain rounded boulders, while the fine-grained material occurs in discontinuous strata. The reworked deposits are interpreted as fluvial deposits on the volcano slopes that were incorporated into the landslide. Former lava flows were fractured during sliding and now appear as large andesitic blocks 1–2 m in diameter. The fractured lavas form a cataclastic texture, composed of fine to

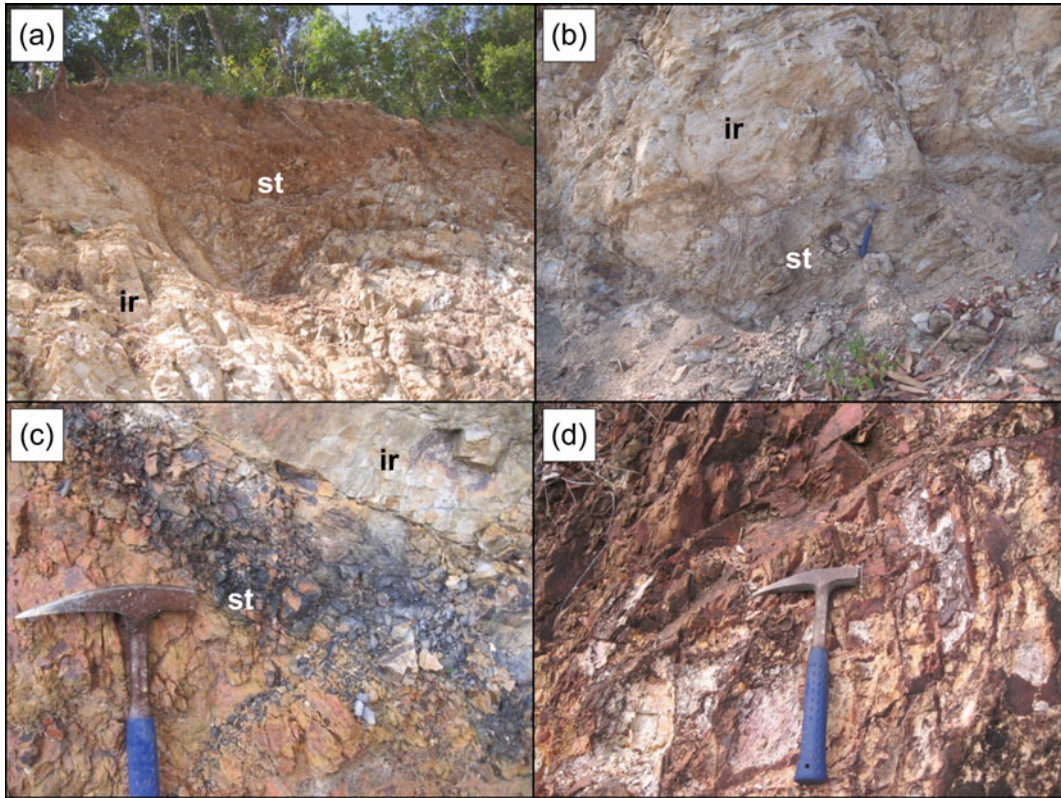


Fig. 7.8 **a** Silicified tuff (st) as a roof pendant above an igneous rock body (ir). **b** Xenolith of silicified tuff (st) in igneous rock (position: 07°44'34.3" S–110°16'45.7" E). **c** Baking effect of silicified tuff (black) at the contact between silicified tuff (st) and igneous rock (ir) (position:

07°44'30.9" S–110°16'46.7" E). **d** Hydrothermally altered tuffs with secondary quartz, kaolinite and limonite in a public resting place (position: 07°44'48.4" S–110°17'01.1" E). Pictures were taken on the southeastern slope of G. Gede, Dusun Pendekan, Desa Margodadi

coarse grained (ash to block sized) material. Jigsaw cracks and minor fault structures are found in the debris avalanche deposits.

The Godean debris avalanche deposit (Figs. 7.11, 7.12, 7.13 and 7.14) was preserved because the avalanche collided with, and got deposited on, the northern slopes and foot of remnant hills of the Tertiary Godean palaeovolcano. In general, the gravitational flow movement of the debris avalanche is shown by a north–south trend of the hummocky terrain extending from Dusun Planggok to Dusun Jlegongan. Locally, the avalanche was trapped by older, east–west oriented hills of the Godean palaeovolcano between Dusun Pendekan and the elevation points of 161 and 149 m asl at Dusun Kandangan. Minor fault structures, orientated at

N295°E/70° (Fig. 7.14i), also support the presence of strain or pressure from a NNE direction, caused by thrust faulting perpendicular to the strain during avalanche transport. Following deposition, the strain decreased or even reversed, causing normal minor faults striking in a NNW–SSE direction. Thus, the flow of the Godean debris avalanche from the north perpendicularly hit a line of small, east–west orientated hills.

The distribution of the Godean debris avalanche deposit in Godean and adjacent areas (Fig. 7.10) shows that to the east and west of the Godean Hills, the Godean debris avalanche may have been eroded, buried by subsequent sedimentation from Merapi or transformed into lahars. When a debris avalanche is deposited in a river valley, such as here in the Bedog River on



Fig. 7.9 Blocky crystalline limestone among weathered pumice lapilli deposits found behind Mr Sukarno's house, Dusun Pendekan, Desa Margodadi, Subdistrict of Seyegan

the eastern side and the Progo River in the west, erosion removes the avalanche deposit. By contrast, deposition on a convex apron like at Taranaki volcano (Alloway et al. 2005; Roverato et al. 2015) and also here at Merapi, may lead to subsequent overbank deposition or syn-transport transformation. North of Dusun Planggok, no hummocks are observed, but the main roads in this area connecting the small towns of the Minggir subdistrict in the west, and the Seyegan and Mlati subdistricts in the east have many bends. Possibly, construction of the main road was controlled by the subsurface distribution of debris avalanche and lahar deposits.

About 4–5 km south of the Godean and Moyudan subdistricts (District of Sleman), andesitic megablocks are widely distributed at the surface (Fig. 7.15) and overlie the wavy topography of the Sentolo Formation (Rahardjo

et al. 1977) in the Sedayu plain (70–80 m asl) in the areas of Desa Argomulyo and Desa Argosari (Sedayu Subdistrict, District of Bantul). Further to the south, the Sentolo Formation forms higher hills (> 100 m asl) than in the northern part.

In Desa Argomulyo, ~40 km from Merapi, the andesitic megablocks occur in many places, such as Dusun Panggang, Dusun Watu, Dusun Sengonmadinan and Dusun Rewulu. Westwards, the distribution of megablocks terminates at Desa Argosari (07°48'07.4" S–110°15'33.9" E), while to the east, it ends at Dusun Watu (07°48'01.9" S–110°17'05.8" E). The distance between the two locations is ~3–4 km. Based on information from local residents, this area was previously named Desa Watu, before it was changed to Desa Argomulyo. The term 'Watu' (Javanese, meaning stone or rock) probably matches with the abundance of andesitic megablocks in the area.

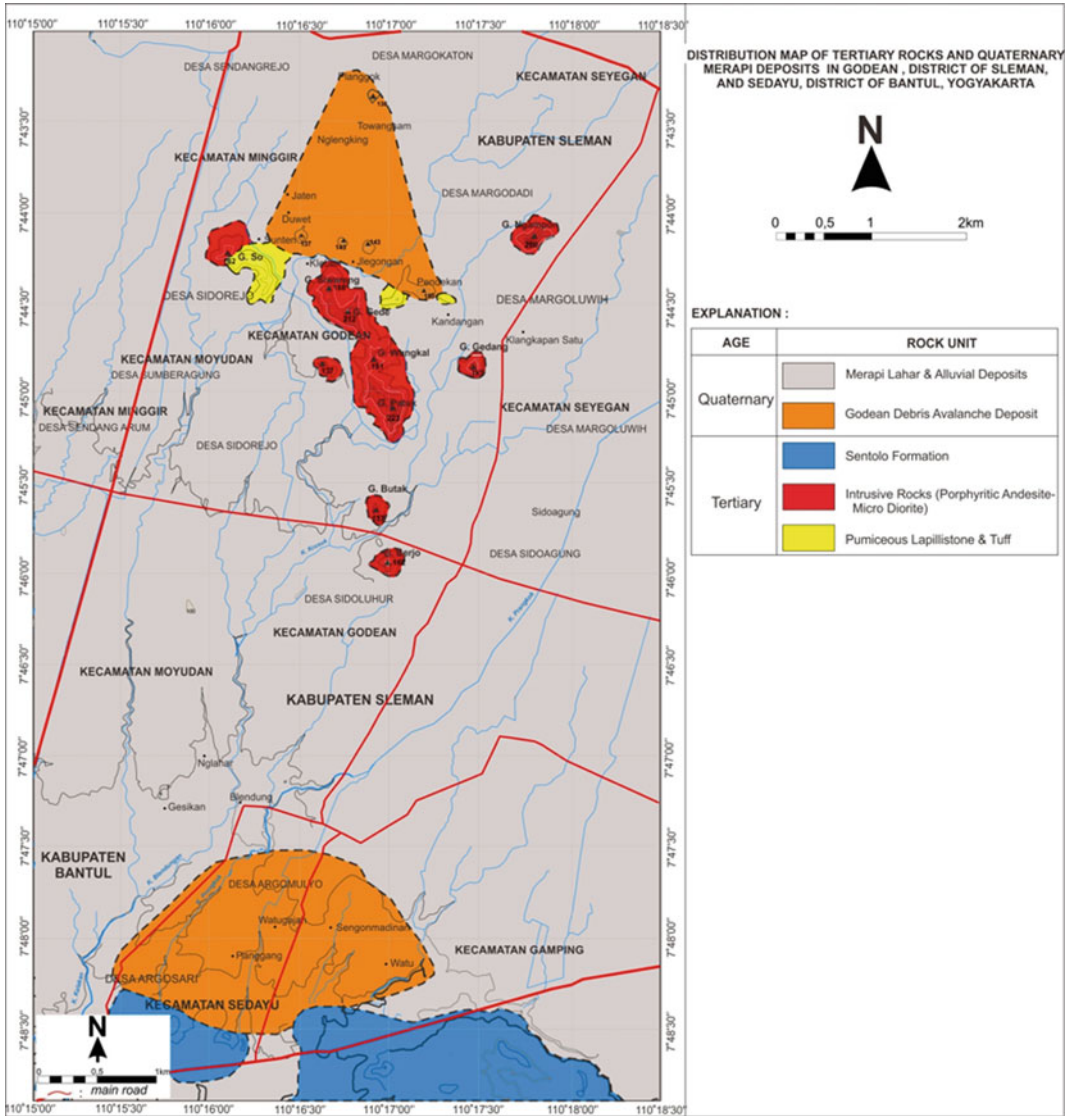


Fig. 7.10 Distribution map of Tertiary rocks and Quaternary Merapi deposits, including the Godean debris avalanche, in the areas of Godean (District of Sleman) Sedayu (District of Bantul, Yogyakarta)

Meanwhile, the name ‘Panggang’ means ‘toasted’, perhaps because at the time the area was very hot, with little vegetation but plenty of stones or rocks. Local residents also mentioned that during construction of the central gasoline station at Dusun Rewulu, the contractor excavated many big stones (megablocks).

The andesitic megablocks are 2.0–4.7 m in diameter and angular to subangular in shape. At Dusun Panggang, the large size of the andesitic

blocks led to two blocks being called ‘Watu Gajah’ or elephant stone (Fig. 7.15a, b). Another name for andesitic megablocks at Dusun Watu is ‘Watu Leter’ (flat stone, Fig. 7.15c, d) because of their flat surfaces. Andesitic megablocks are not limited to high land of gardens and residences, but are also scattered across graveyards, a resting place and in the middle of rice fields (Fig. 7.15e–g). Below the andesitic megablocks a slightly weathered matrix is often found (Fig. 7.15h),

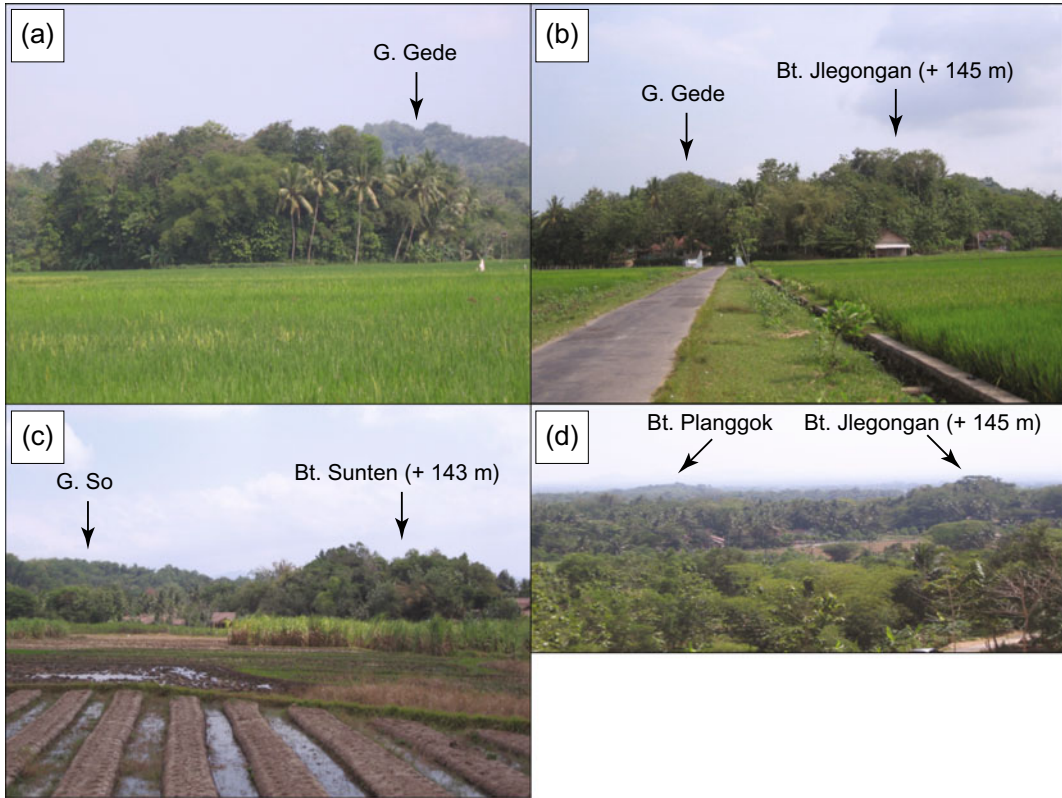


Fig. 7.11 Hummocky topography of the Godean debris avalanche deposit on the north side of remnant hills of the Godean palaeovolcano (G. Gede and G. So): **a** A small hill east of Dusun Jlegongan. **b** Jlegongan Hill (145 m asl) north of G. Gede. **c** Sunten Hill (143 m asl) north of

G. So (position: $7^{\circ} 44'10.7''$ S– $110^{\circ} 16'38.0''$ E). **d** Distribution of hummocky topography from Jlegongan Hill to Planggok Hill. Photo taken from the northern slope of G. Gede with the camera facing northward (position: $7^{\circ} 44'34.7''$ S– $110^{\circ} 16'45.1''$ E)

consisting of pebble-sized, angular to subangular and matrix supported andesitic fragments set in sandy granules to reddish brown clay soil.

Nearly all of the andesitic megablocks are still fresh, grey in colour, massive to vesicular, and characterised by porphyritic textures. Phenocrysts are predominantly plagioclase with additional pyroxene and rare amphibole set in an aphanitic groundmass.

The distribution of angular to subangular single megablocks, together with the presence of matrix supported angular to subangular andesitic fragments in the Sedayu area, indicates a more fluid downslope facies of the debris avalanche. Abundant megablocks distributed in this area are directly transformed from the upper slope facies, probably as disintegrated and fractured lavas, and

can be grouped into a clast-rich matrix facies (Roverato et al. 2015), i.e. a matrix facies enriched in clasts > 0.25 m. The large size of the megablocks requires transportation in a dense slurry (debris flow), which might have evolved directly from the groundwater-rich debris avalanche. Due to the loose and finer grained material, most of the matrix has been eroded with time. The andesitic megablock-rich (clast-rich) matrix facies of the debris avalanche was deposited in the Sedayu area because it was stranded by the wavy to hilly topography of the Sentolo Formation. Thus, the origin of the debris avalanche deposit in this area is similar to the presence of the debris avalanche deposit on the north side of the Godean Hills. Both were restrained, blocked or trapped by older, pre-existing hills at the time.



Fig. 7.12 **a** Exposure of the deposits of Jlegongan Hill (145 m asl), Dusun Jlegongan, Desa Margodadi, Seyegan Subdistrict. **b** Brown to dark brown, weathered topsoil, excavated for bricks and roof tiles. **c** Fresh (basaltic?) scoriaceous breadcrust bombs and volcanic blocks in the

weathered soil. **d** Exposure of the deposit showing slightly weathered matrix, but containing relatively fresh andesitic fragments (position: 07°44'13.3" S–110°16'52.0" E)

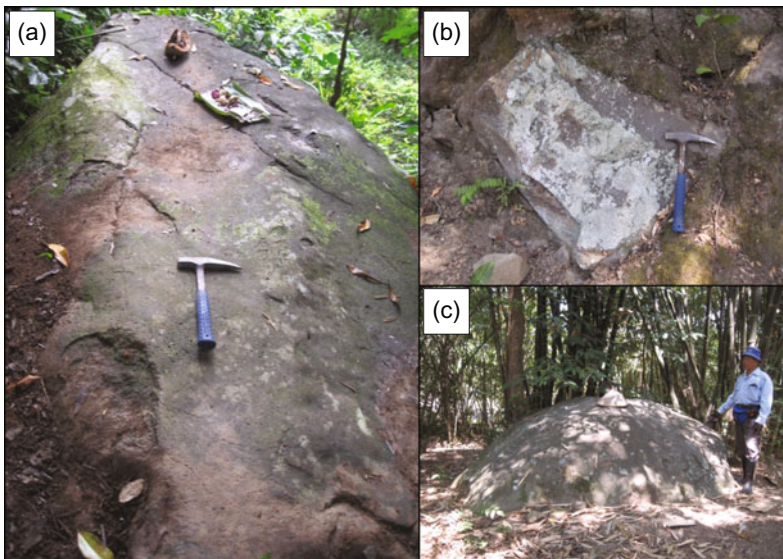


Fig. 7.13 Features of exposed megablocks in the Godean debris avalanche deposit: **a** Andesitic block, 8 m in length, near the + 145 m pole, Dusun Jlegongan, Desa Margodadi, Seyegan Subdistrict (position: 07°44'11.3" S–110°16'52.4" E). **b** Angular and sharp andesitic block at Dusun Sunten, Desa Sendangrejo, Minggir

Subdistrict (position: 7° 44'05.1" S–110° 16'34.1" E). **c** Subrounded andesitic block, 4.5 m in diameter, at the top of the Jaten hummock, located in Dusun Jaten, Desa Sendangrejo, Minggir Subdistrict (position: 7° 43'56.1" S–110° 16'28.9" E)

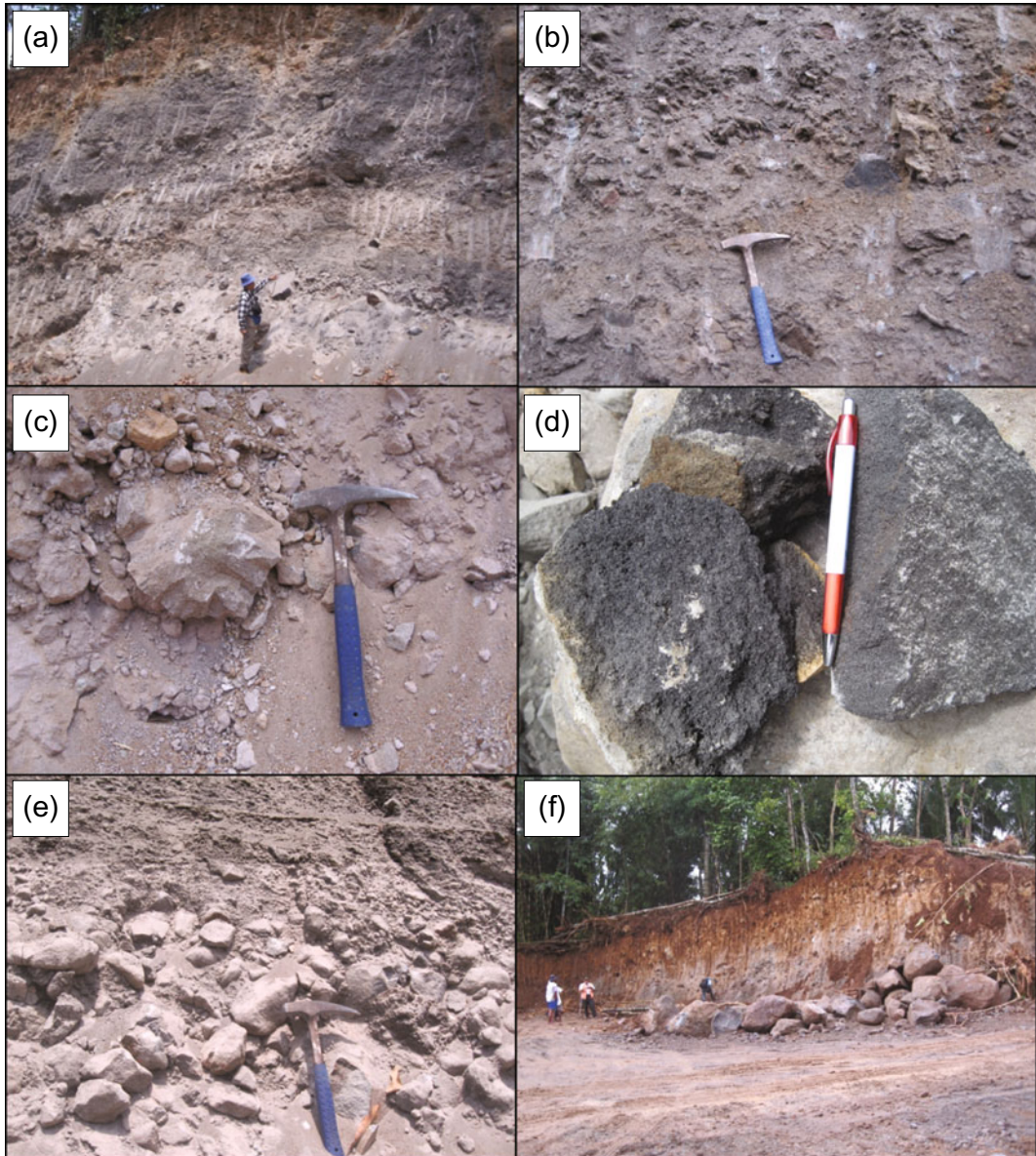


Fig. 7.14 Exposures of the Godean debris avalanche deposit in an excavation at Dusun Pendekan, Desa Margodadi, Seyegan Subdistrict, District of Sleman, Yogyakarta (position: 07°44'20.2" S–110°17'06.4" E): **a** Intact strata of pyroclastic and reworked deposits, and a fractured lava flow (at the base), all swept up and transported in the debris avalanche. **b** Contact of two highly fractured pyroclastic deposits in the intact strata. **c** A volcanic bomb (the biggest size) among small volcanic blocks in the pyroclastic deposit. **d** Dark grey (basaltic?) scoria of volcanic bombs in the pyroclastic deposit. **e** Reworked deposit, presumably a fluvial deposit on the Merapi slope before sliding, characterised by subangular to subrounded clasts with rough normally graded bedding, overlain by discontinuous fine grained

layers. **f** Blocks of fractured andesitic lava at the base of the excavation. **g** Close-up of the andesitic lava, characterised by a grey colour, a massive to fine vesicular structure, and a fine grained to porphyritic texture with phenocrysts of plagioclase, amphibole and pyroxene set in aphanitic groundmass. Occasionally, darker xenoliths are observed. **h** Jigsaw cracks in a block in the Godean debris avalanche deposit. **i** Minor fault (N295°E/70°) in the debris avalanche deposit. **j** Field visit with C. Newhall at the Pendekan exposure (from left to right: A. Ratdomopurbo, S. Bronto, C. Newhall and P. Asmoro). **k** Field visit with W. Rahardjo at the Pendekan exposure (from left to right: M. Adityarani, P. Asmoro, S. Bronto, W. Rahardjo and A. Ratdomopurbo)

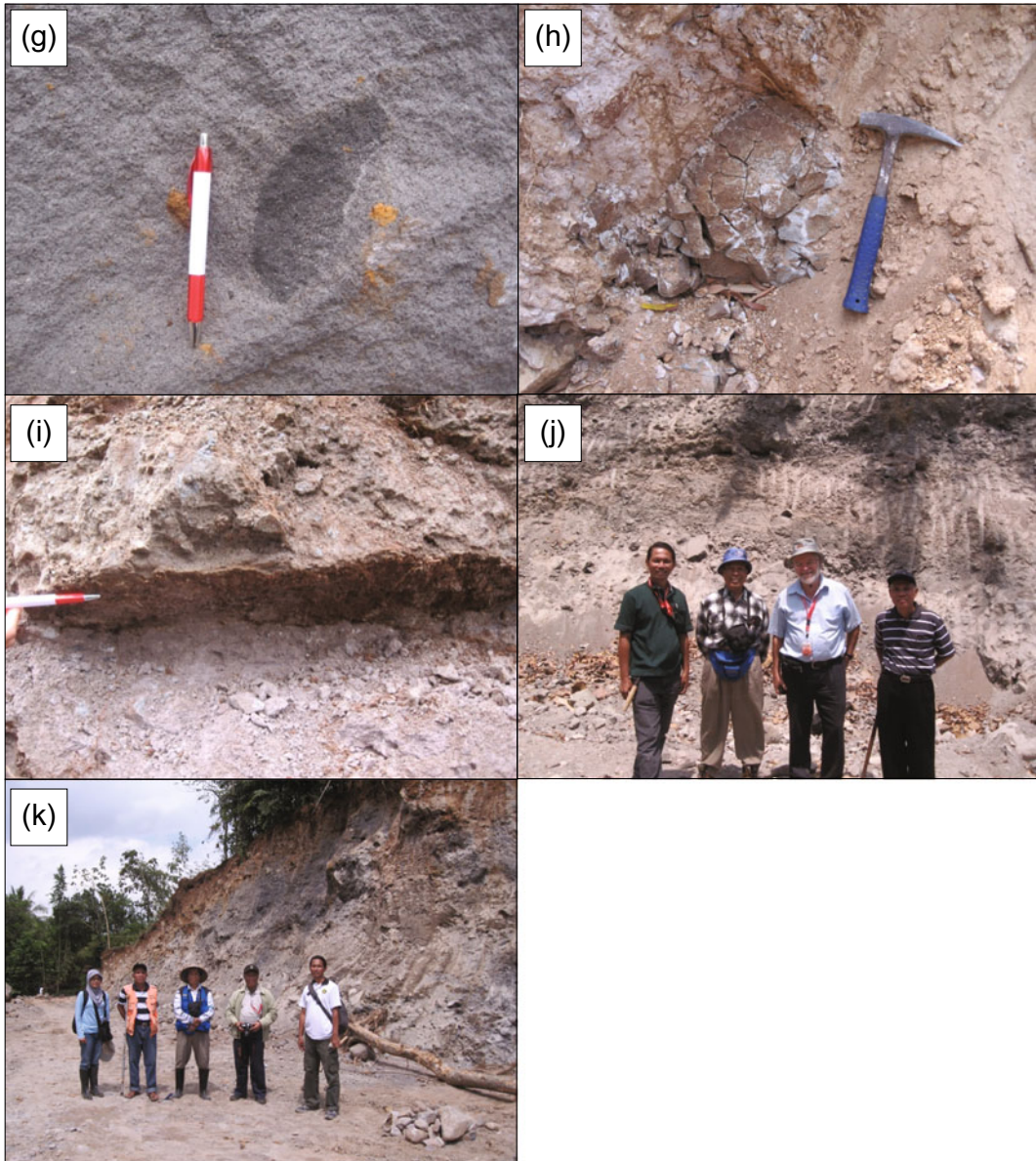


Fig. 7.14 (continued)

A fine grained volcaniclastic deposit is exposed in the Bedog riverbank (Fig. 7.16), situated ~ 10 km southeast of Sedayu and 50 km from Merapi. This location is positioned ~ 160 m north of the Bedog bridge connecting Desa Pendowoharjo, Subdistrict of Sewon in the east, and Desa Bangunjiwo, Subdistrict of Kasihan in the west. The deposit overlies the Sentolo Formation

and is covered by fluvial deposits. It is composed of small angular andesitic fragments set in a brown silty sand matrix, poorly sorted and structureless (Fig. 7.16a, b). Referring to investigations at Mount St. Helens (Glicken 1996) and Taranaki (Roverato et al. 2015), these characteristics may correspond to the matrix facies of the Godean debris avalanche deposit, which may also

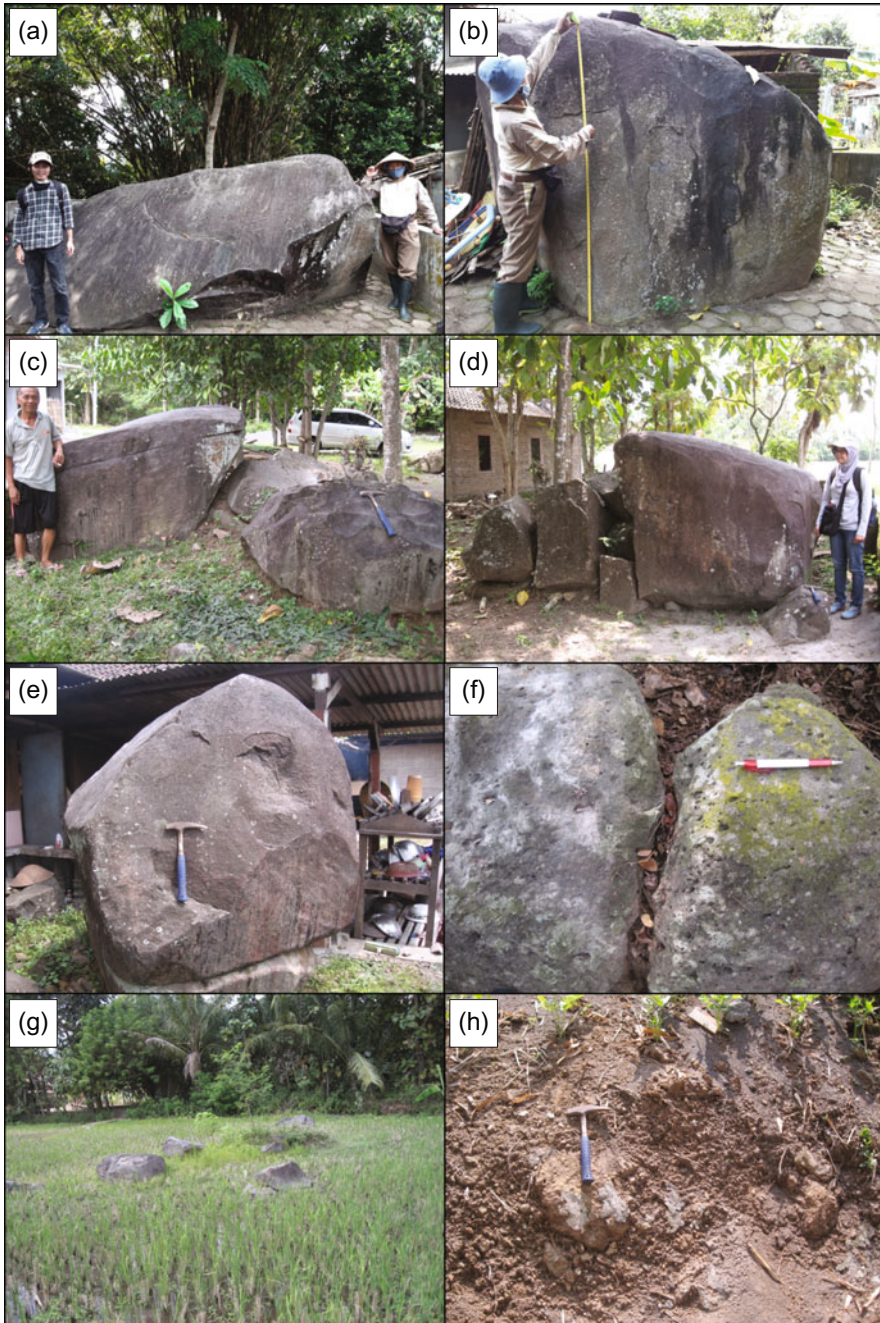


Fig. 7.15 Andesitic megablocks observed at Desa Argomulyo, Sedayu Subdistrict, District of Bantul, Yogyakarta: **a, b** Two of the ‘watu gajah’ (‘elephant stones’) at Dusun Panggang, 470 × 160 cm and 300 × 200 cm in size (position: 07°47’58.0” S–110°16’33.3” E.) **c, d** “Watu leter” (flat stone) in front of Mr Sumanto’s house, Dusun Watu (position: 07°48’01.9” S–

110°17’05.8” E). **e** Andesitic megablock in the yard of a house in Dusun Sengonmadinan (position: 07°48’17.4” S–110°16’43.9” E). **f** Andesitic megablocks in a resting place west of Dusun Panggang (position: 07°47’57.4” S–110°16’22.0” E). **g** Andesitic megablocks in a rice field south of Dusun Watu. **h** Weathered matrix of debris avalanche deposit in Dusun Panggang

be comparable to the marginal facies of the Okawa debris avalanche deposit at Taranaki (Alloway et al. 2005). A palaeosol of the Sentolo Formation is locally observed below the debris avalanche deposit (Fig. 7.16c). Towards the south, the area becomes flat until the coast of the Indian Ocean and is composed of fluvio-volcanic deposits of the Bantul plain. Due to the long distance (> 50 km) from Merapi, the location of the matrix facies in this area can be considered as a distal area of the Godean debris avalanche deposit. Based on the drainage pattern (Fig. 7.3), the Godean debris avalanche likely ended at the confluence of the Bedog River and the Progo River.

7.5.3 Pyroclastic Deposits

In the Dusun Pendekan area of Desa Margodadi, weakly consolidated pyroclastic deposits are exposed under the Godean debris avalanche deposit. The pyroclastic deposits are pumice-rich lithic breccias and lapilli deposits that are already weathered to a white to yellowish brown colour (Fig. 7.17) and reddish-brown soil. One outcrop contains a poorly sorted deposit of angular pumice and lithic fragments with grain sizes of 1–3 (max. 10) cm (Fig. 7.17a). The lithic fragments consist of dark grey, massive to finely vesicular andesite that varies from glassy to aphanitic and porphyritic textures. These deposits appear to be from pyroclastic density currents (Branney and Kokelaar 2002). The same pumice-rich lapillistone is also observed in Dusun Jering, Desa Sidorejo, Sub-district of Godean (Fig. 7.17c), although this deposit could be reworked, as indicated by the presence of predominantly well sorted, sub-rounded pumice clasts, and absence of contact with the Godean debris avalanche deposit.

In a previous publication (Bronto et al. 2014), all of the pumice lapillistones were considered to be of Tertiary age. In this chapter, however, some are thought to be of Quaternary age, based on a lack of hydrothermal alteration (no silicification), weak consolidation and, particularly in Dusun

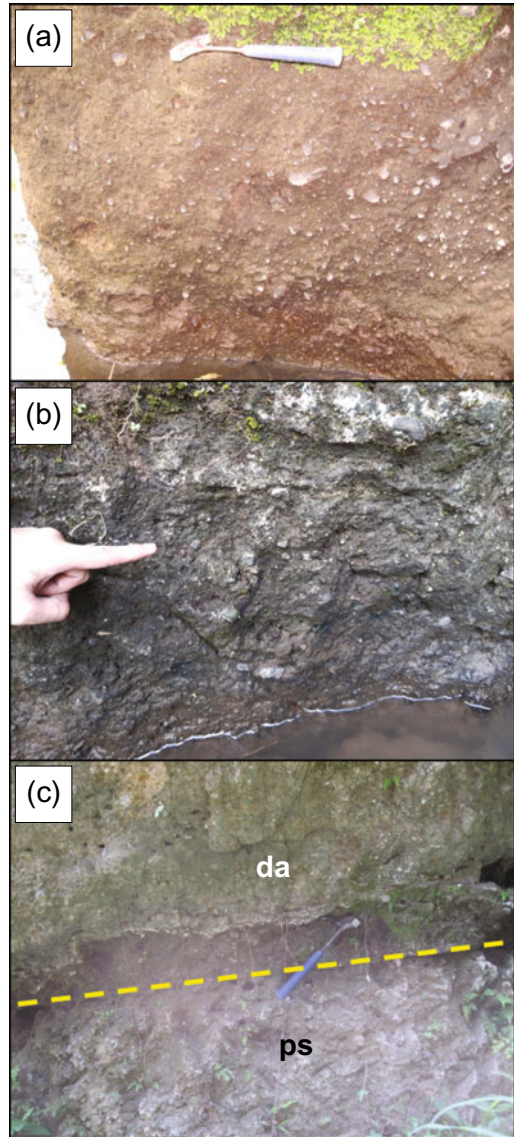


Fig. 7.16 The Godean debris avalanche deposit exposed in the Bedog riverbank ~160 m north of the Bedog bridge connecting Dusun Kalangan, Desa Bangunjiwo, Kasihan Subdistrict in the west and Dusun Rogoitan, Desa Pendowoharjo, Sewon Subdistrict in the east (position: 07°51'27.7" S–110°19'42.0" E): **a**, **b** Matrix facies of debris avalanche deposit, showing very angular small andesitic fragments in a brown silty sand matrix. The picture in **a** was taken in September 2014 (dry condition), the one in **b** in May 2020 (wet condition). **c** Weathered matrix facies of debris avalanche deposit (da) overlying a palaeosol (ps) of limestone of the Sentolo Formation (Rahardjo et al. 1977)

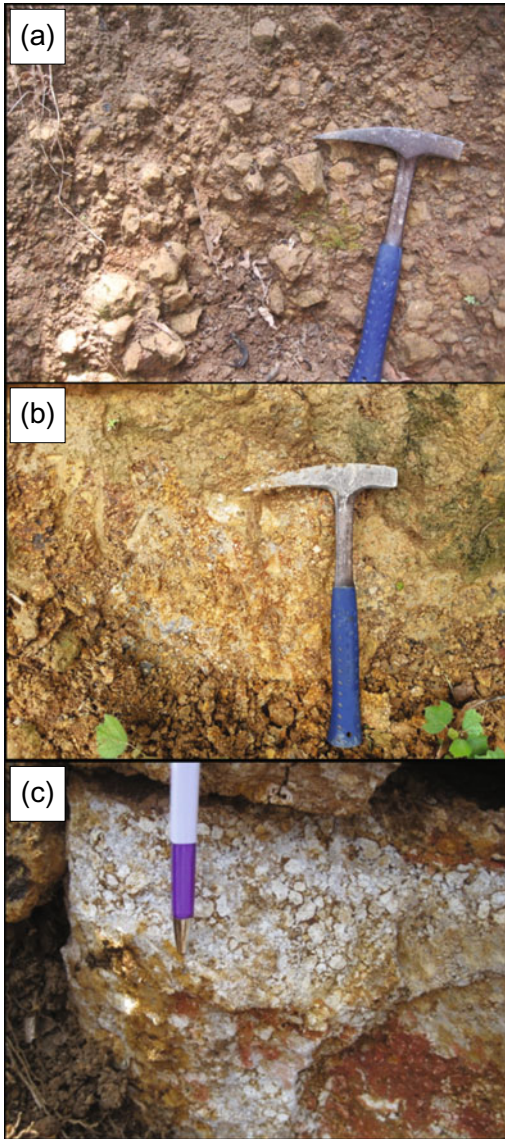


Fig. 7.17 Pyroclastic deposits that may have accompanied the Godean debris avalanche: **a** Pumice lithic (breccia?) deposit in Dusun Pendekan, Desa Margodadi, Seyegan Subdistrict (position: $07^{\circ}44'31.4''$ S– $110^{\circ}17'02.5''$ E). The lithic fragments are andesite and very angular in shape. **b** Weathered pumice-rich lapilli deposits with few lithic fragments near the site displayed in Fig. 17a. The two deposits (Fig. 17a, b) are located below the Godean debris avalanche deposit. **c** Pumice-rich lapilli deposit found in Dusun Jering, Desa Sidorejo, Godean Subdistrict (position: $07^{\circ}44'38.0''$ S– $110^{\circ}16'20.9''$ E). The deposit has no contact with the Godean debris avalanche deposit

Pendekan, their spatial association with the Godean debris avalanche deposit, although the exact contact relationships could not be established. Occasionally, distinguishing Tertiary and Quaternary pyroclastic deposits in the field is difficult due to the weathered condition of the material; a Quaternary age is favoured, if the outcrop is far away from Tertiary intrusive rocks, structureless and has no indication of hydrothermal alteration.

7.5.4 Lahar Deposits

Lahar deposits are exposed in river incisions of the Godean plain. One of the lahar exposures is found at the south gate of Padukuhan or Dusun Nglahar, Desa Sumbersari, Subdistrict of Moyudan, Sleman District ($07^{\circ}47'13.7''$ S– $110^{\circ}16'01.4''$ E) (Fig. 7.18a). It is likely that the name ‘padukuhan’ was related to lahar occurrences that destroyed the area in the past. As we know the term ‘lahar’ is originally Javanese, meaning mud overflow related to a volcanic explosion. The word ‘lahar’ is a noun that becomes a verb by adding the prefix ‘Ng’. Thus, ‘nglahar’ could mean ‘to go to’ (lahar area), ‘to become’ (lahar), ‘to do something with’ (lahar as an object) or ‘at’ (lahar location). Padukuhan Nglahar is located ~ 3 km southwest of Godean town and on the west side of the Blendung River, the downstream continuation of the Krusuk River that flows through Godean, where a lahar deposit is well exposed (Fig. 7.18b). Exposures of lahar deposits are located at an irrigation channel in the south corner of Padukuhan Nglahar and along the Blendung riverbank. At both locations, the lahar deposits are 1–2 m thick, grey to brown, and slightly weathered. Boulders of the lahar deposits are andesitic, subangular to subrounded in shape, with average diameters of 10–15 (max. 80) cm, set in a sand-granule size, and moderately consolidated, matrix. Another unique name nearby is Dusun Gesikan, which is situated on the south side of Padukuhan Nglahar. The Javanese word ‘gesikan’ denotes a place where



Fig. 7.18 Padukuhan (Dusun) Nglahar and lahar deposits exposed at the Blendung River and the Progo River: **a** The south gate of Padukuhan Nglahar, Desa Sumber-sari, Moyudan Subdistrict, District of Sleman (position: $07^{\circ}47'13.7''$ S– $110^{\circ}16'01.4''$ E). **b** Lahar deposit at the Blendung River on the southeast side of Padukuhan Nglahar. **c** G. Sentono, composed of (Merapi?) lahar

deposits, located on the west side of the Progo River and the Klangon bridge, Desa Banjaroyo, Kalibawang Sub-district, District of West Progo. **d** Lahar deposit (a laharic breccia) possibly from Merapi in the Progo River floodplain under the Klangon bridge (position: $07^{\circ}38'32.5''$ S– $110^{\circ}15'15.8''$ E)

sandy material is widely distributed, or a place composed of predominantly sand deposits, which may have originated from the sandy matrix of lahar or fluvial deposits.

Old lahar deposits along the Progo River that may be related to the Godean debris avalanche deposit are exposed at G. Sentono on the west side of Klangon bridge ($07^{\circ}38'32.5''$ S– $110^{\circ}15'15.8''$ E) (Fig. 7.18c, d). Here, the thickness of lahar deposits is over 20 m. The lahar fragments range in size from 30 to 50 (max. 150) cm, are angular to subrounded in shape, and set in light grey gravely tuff matrix. The lahar boulders are andesitic, with massive to vesicular structures, and aphanitic to

porphyritic textures. Phenocrysts, if present, are plagioclase, pyroxene and amphibole.

About 8 km southeast of the Sedayu area, finer grained lahar deposits are found in Dusun Lemahdadi ($07^{\circ}50'07.9''$ S– $110^{\circ}18'16.4''$ E) and Dusun Sembungan, Desa Bangunjiwo, Kasihan Subdistrict, District of Bantul. At Dusun Sembungan, located between the Bedog River in the east and G. Sempu in the west, fine grained (sand-granule size) lahar deposits are situated above the Tertiary Sentolo Formation (Fig. 7.19). In this location, lahar deposits are 3–5 m thick, moderately consolidated and preserved as conglomeratic breccias and sandstones.

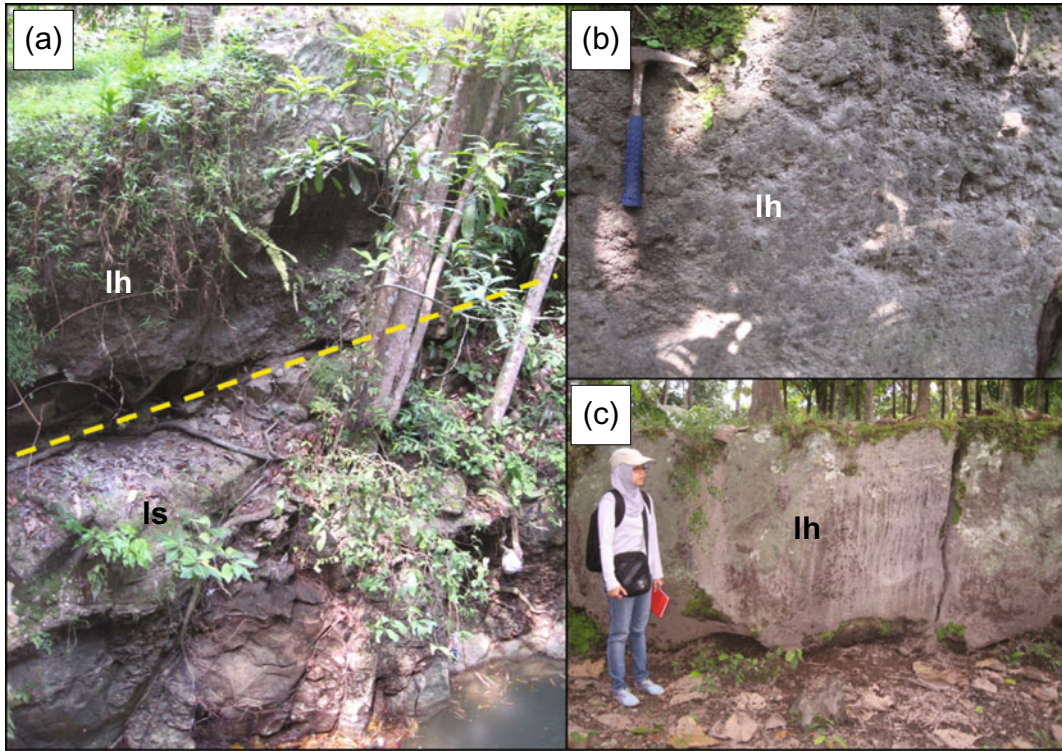


Fig. 7.19 Lahar deposits in Dusun Sembungan, Desa Bangunjiwo, Kasihan Subdistrict, District of Bantul: **a** Lahar deposit (lh) overlying limestone (ls) of the Sentolo Formation in a small riverbank between the

Bedog River in the east and G. Sempu in the west. **b** Lahar deposit (position $07^{\circ}50'02.4''$ S– $110^{\circ}20'23.3''$ E). **c** Lahar deposit (position $07^{\circ}50'07.1''$ S– $110^{\circ}20'23.7''$ E)

In historical records, Merapi lahars never struck the Padukuhan Nglahar District of Sleman and the Dusun Sembungan District of Bantul. Lahars flowing down rivers on the Merapi slopes have become much more fluid in the Progo River due to highly increased water input. So far, the direct contact between the Godean debris avalanche and lahar deposits has not been found. Exposures in the medial region of the Godean debris avalanche deposit are not syn-collapse lahars, but lahars that occurred after the deposition of the debris avalanche. They could have formed months to years later by overtopping, breakout and erosion, where the debris avalanche deposit blocked the Progo River. Another possibility is that these lahars are related to younger (but prehistoric) Merapi volcanism. Solving this problem would require dating of the Godean debris avalanche and lahar deposits.

7.6 Significance of the Tertiary Volcanic Rocks

The Tertiary volcanic rocks in the Godean area have been reported as remnants of the Godean palaeovolcano (Bronto 2016). Strong hydrothermal alteration created silicified tuff that resemble quartz-sandstone, particularly at G. Wungkal. This resemblance led van Bemmelen (1949) and Rahardjo et al. (1977) to falsely report that the Nanggulan Formation (in the Godean area) contains sedimentary quartz-sandstone, which urges revision to the geological map of the Yogyakarta quadrangle (Rahardjo et al. 1977).

The Tertiary Godean Hills are a ‘blocker’ (‘defender’ or ‘restrainer’) to the Godean debris avalanche so that a small part of the deposit is well preserved there. The Gendol Hills in the

Salam and Muntilan areas west of Merapi may have played a similar role, although remnant deposit(s) of a Merapi gigantic landslide in this area are presently unknown.

7.7 Emplacement, Area Covered and Volume of the Godean Debris Avalanche Deposit

Based on the results described above, the Merapi gigantic landslide collided with the Tertiary hills of the Godean palaeovolcano, so that its deposits were trapped and well preserved on the northern side of the Godean Hills. Intact strata of pre-collapse lithologies are still observed, consisting of pyroclastic deposits, lava flows and reworked deposits. However, these deposits are already highly fractured due to the sliding movement, with jigsaw cracks and minor faults (Fig. 7.14). These characteristics indicate that the Godean debris avalanche deposit in the Godean area is of block facies (Ui 1983, 1997; Glicken 1996; Nakamura and Glicken 1997). Further south, the block facies changes to a clast-rich matrix facies (Roverato et al. 2015) in the Sedayu area, as shown by the scattered distribution of andesitic megablocks (Fig. 7.15) stranded on the wavy Tertiary Sentolo Formation. The matrix facies is found further south (Fig. 7.16), which is considered to be the distal area of the Godean debris avalanche. The new discovery of the Godean debris avalanche deposit in the Godean area and District of Bantul proves the long-held inference from the morphology of Merapi that a gigantic landslide carried away the top of Old Merapi volcano to the southwest (e.g. van Bemmelen 1949; see Gertisser et al. 2023, Chap. 6). When it collided with the West Progo Mountains, the mass movement turned south through the Godean area and probably stopped at the confluence of the Bedog and the Progo River, ~50 km away from Merapi (Fig. 7.20). Deflection to the south occurred approximately in the Kalibawang area, where the West Progo high protrudes to the east and the Progo River channel turns south-eastward. This position is now occupied by the confluence of the Krasak and the Progo River.

West of Merapi, the Godean debris avalanche deposit covers an area of the Magelang District (Central Java Province) and dammed the Progo River to re-form the ancient Lake Borobudur upstream. Further to the south, the debris avalanche destroyed areas of the Sleman District, the eastern side of the West Progo District, and the western part of the Bantul District.

Estimating the volume of the Godean debris avalanche deposit is challenging, as it has been mostly eroded, with remnants only locally preserved. This differs from Taranaki, New Zealand (Alloway et al. 2005; Roverato et al. 2015) and Asama, Japan (Yoshida and Sugai 2006), where the debris avalanche deposits are relatively pristine and can be traced continuously from proximal to distal areas.

A rough volume estimate for the Godean debris avalanche deposit is made using several topographical maps (scale: 1:25,000) published by Badan Informasi Geospasial (Geospatial Information Agency). These include the sheets of Kaliurang, where the summit of Merapi is positioned (sheet number 1408-244), Muntilan (1408-243), Mungkid (1408-234), Sleman (1408-241), Sendangagung (1408-232), Wates (1408-214), Yogyakarta (1408-223) and Bantul (1408-221). The volume estimate is based on the following assumptions:

1. In the proximal area, the lateral distribution of the debris avalanche deposit forms a right-angled triangle with side lengths of 13 and 18 km, covering an area of 117 km². This triangle extends from the lower slope of Merapi (1000 m asl) in the Srumbung Subdistrict as the eastern corner, to the Progo River (230 m asl) in the Muntilan Subdistrict as the western corner; the southern corner is in the Ngluwar Subdistrict (140 m asl) at the confluence of the Krasak and the Progo River. Assuming an average thickness of 30 m, the subtotal volume is 3510 km³ (2340 km³ if the average thickness is assumed to be 20 m).
2. In the medial area, the lateral distribution of the deposit forms a 18 km long and 13 km wide rectangle that extends from the Minggir Subdistrict (120 m asl) in the northwest to the Sleman Subdistrict (200 m asl) in the

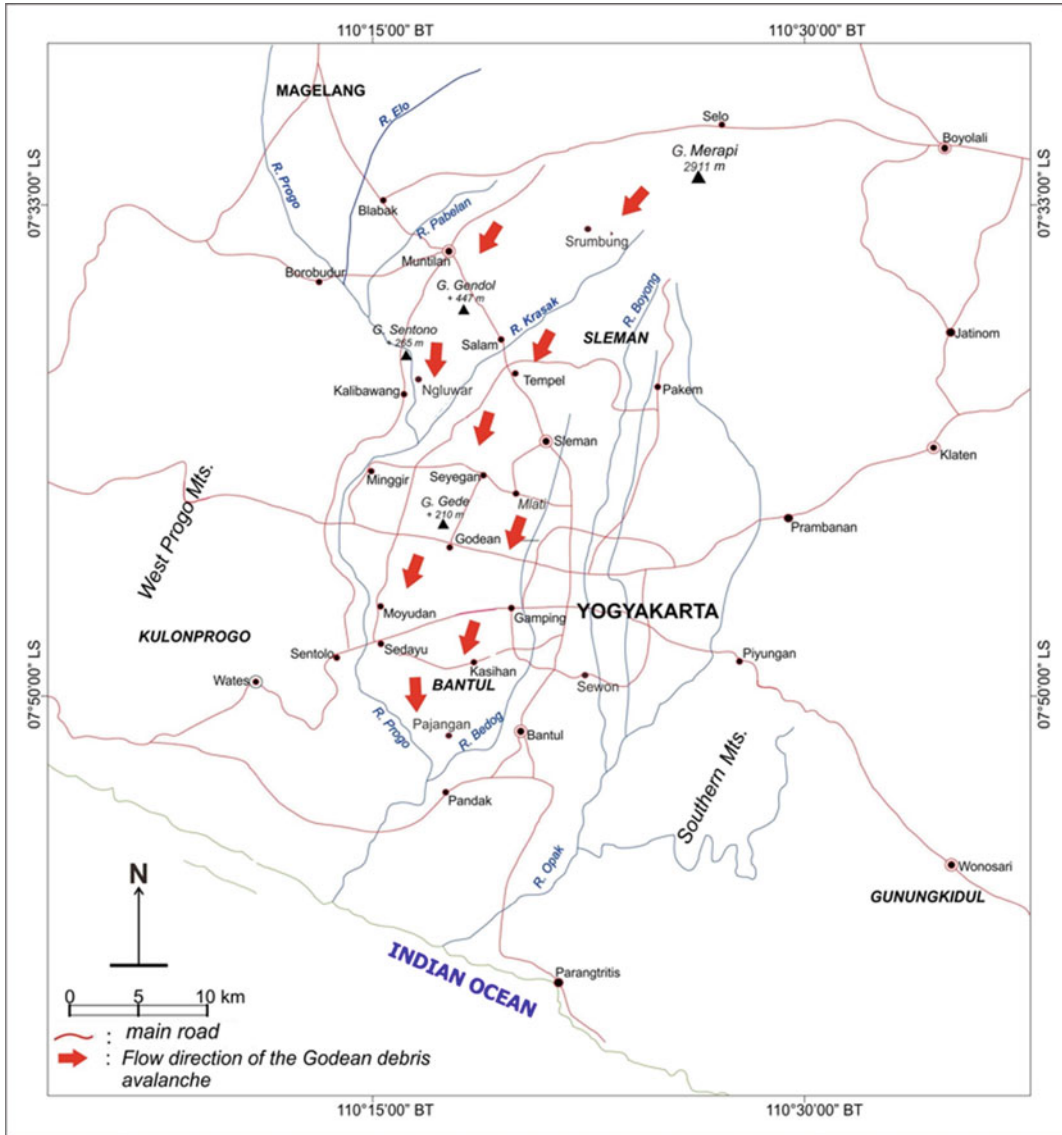


Fig. 7.20 Map showing the flow direction of the Godean debris avalanche. The avalanche flowed southwestward through the Magelang District (Central Java) and then continued southward to the Sleman District through the Godean area until the Bantul District, reaching the Sedayu and Kasihan areas. The avalanche possibly stopped at the

confluence of the Bedog River and the Progo River in the Pandakan area. The southward turn of the debris avalanche was caused by collision with the West Progo Mountains roughly in the Kalibawang area. The confluence of the Bedog River and Progo River is ~50 km from Merapi

northeast, the Sedayu Subdistrict (40 m asl) in the southwest and the Bantul Subdistrict (50 m asl) in the southeast. The Subdistrict of Godean is situated in the middle of this area, which is bordered by the Bedog River on the east side and the Progo River (east of the West Progo Mountains) on the west side,

covering an area of 234 km². Using an estimated average thickness of 20 m, the subtotal volume is 4680 km³ (2340 km³ if the average thickness is assumed to be 10 m).

3. In the distal area, the lateral distribution of the deposit also forms a right-angled triangle with side lengths of 7 and 11 km, covering areas of

the Pajangan Subdistrict (50 m asl) in the northwestern corner and of the Bantul Subdistrict (50 m asl) in the northeastern corner up to the confluence of the Bedog River (20 m asl) in the southern corner, and the Progo River in the Pandak Subdistrict. This end point of the Godean debris avalanche deposit is located ~ 50 km away from the Merapi. All these subdistricts are within the District of Bantul, covering an area of 38.5 km^2 . Using an estimated average thickness of 10 m, the subtotal volume is 0.385 km^3 (0.1925 km^3 if the estimated average thickness is 5 m).

Using the simple model above, the Godean debris avalanche deposit covers an area of 389.5 km^2 ($\sim 390 \text{ km}^2$) to a distance of up to ~ 50 km from Merapi, and ranges in volume between 4.8725 km^3 ($\sim 4.9 \text{ km}^3$) and 8.575 km^3 ($\sim 8.6 \text{ km}^3$), using the estimated minimum and maximum thicknesses, respectively. The huge deposit volume, long travel distance and very large buried area testify to a gigantic landslide of Merapi.

Referring to Ui et al. (1986) and considering the height of Merapi (2911 m asl), the elevation of the Godean and Bantul plains (20–100 m asl) as the base of vertical collapse, and a deposit volume that may approach 10 km^3 , the sliding distance could reach ~ 50 – 100 km away from the source. The Godean debris avalanche reached the minimum travel distance of ~ 50 km in the Pandak area, caused by several factors that slowed down the flow, including (1) the collision of the landslide with the West Progo Mountains, the biggest and the strongest barrier west of Merapi, that led to a velocity decrease when the avalanche turned southwards, (2) the presence of the Godean Hills that blocked some of the debris avalanche, and (3) the wavy to hilly terrain of the Sentolo Formation that caused andesitic megablocks to be stranded in the Sedayu area, with only the finer grained avalanche material capable of sliding down further to the Pandak area. Without such barriers, the Godean debris avalanche may have travelled significantly more than 50 km.

Voight et al. (1981) calculated a maximum rock-slide velocity of the Mount St. Helens debris avalanche event in 1980 between 180 and

288 km/h. Nakamura and Glicken (1997) and Ui (1997) proposed that the velocity of the Bandai sliding movement in 1888 was 180 km/h, while Siebert et al. (1997) estimated that the velocity of the Gadung-Raung gigantic landslide in East Java reached 360 km/h. Given the three factors that may have slowed down the Godean debris avalanche described above, its maximum velocity was probably < 200 km/h.

Topographically, in order to impound water forming the ancient Lake Borobudur upstream, the natural dam material of debris avalanche material blocking the Progo River should have a thickness of at least 50 m. This enables the natural dam to be of similar elevation to the West Progo Mountains (178 m asl), given that the Progo riverbed is located 120 m asl in the Kalibawang area. The Muntilan landscape surrounding the Gendol Hills forms a wide gentle slope towards Merapi, which means that a debris avalanche with a minimum thickness of at least 50 m could slide and be widely distributed across the Muntilan landscape before reaching the Gendol Hills. This differs from the Asama debris avalanche (Yoshida and Sugai 2007a, b) that moved down following a narrow river channel between Haruna and Akagi volcano. Consequently, and comparable to the Godean Hills, parts of the debris avalanche could have been plastered against the Gendol Hills. However, due to the dense vegetation, thick soil and the lack of quarries, the debris avalanche deposit has not been found yet in the Gendol Hills area. Geophysical investigations and core drilling would be required to reveal the Godean debris avalanche deposit in this area.

Siebert et al. (1987) defined two types of volcanic debris avalanches; a ‘Bezmyianny’ type, accompanied by a magmatic eruption, and a ‘Bandai’ type, which may only have phreatic or hydrothermal explosions, or may not be related with volcanic activity at all. The relation between pyroclastic deposits (pumice lithic breccias and pumice-rich lapilli deposits; Fig. 7.17a, b) and the Godean debris avalanche deposit is not clear enough to determine whether they are related or not. If the pyroclastics occurred syn-collapse, accompanying the avalanche, they may be associated with pyroclastic density currents (Branney

and Kokelaar 2002) that moved down much faster than the avalanche and were therefore deposited below the debris avalanche at Dusun Pendekan. Alternatively, the pyroclastic deposits may be older than the Godean debris avalanche and may have even come from a different volcanic source. In the ancient Lake Borobudur deposits, the pyroclastic deposits exposed at Dusun Pendekan may be related to a pumice lapilli tuff in the lower part (38.5–41.5 m depth) of a drill core at the Elo River terrace (Murwanto et al. 2001), although there are no dates at present to confirm such a correlation. In a deeper drill core (Gomez et al. 2010), which includes deposits of major volcanic events, the pumice-rich deposits are not found. Consequently, the Godean debris avalanche cannot be classified currently as either ‘Bezymianny’ or ‘Bandai’ type. Further studies are needed to clarify the relation between the Godean debris avalanche and the pumice-rich pyroclastic deposits exposed at Dusun Pendekan.

7.8 Merapi Sector Collapse(s) and the Relation to Old Merapi and New Merapi

Before the 1980s, volcanic structures such as sector collapses and horse-shoe shaped craters due to volcanic activity were essentially unrecognised in structural geology. Linear and curved escarpments in a volcanic edifice were regarded as faults generated by tectonic activity, including escarpments located on the upper slopes and summit areas of active volcanoes such as Merapi. This is why on the geological map of the Yogyakarta quadrangle (Rahardjo et al. 1977), which was reprinted in 1995 and 2012, the NE-SW curved escarpment at Merapi is shown as a normal (tectonic) fault. This has been cited on the geological map of Merapi volcano (Wirakusumah et al. 1980, 1989) as the Kukusan fault. However, from experience at many active Indonesian volcanoes, such as Galunggung, Guntur, Gede and Raung, the example of the Mount St. Helens eruption on 18 May 1980, and carefully considering the terms ‘volcano-tectonic

graben’ or ‘volcano-tectonic collapse’ (van Bemmelen 1949), we conclude that curved escarpments at active volcanoes may not always be tectonically generated faults, but possibly a result of a combination of tectonic activity and volcanism, or volcanic activity alone linked to a sector collapse. Below, we aim to identify curved escarpments at Merapi that are most likely not tectonically generated faults but related to volcanically generated sector collapse.

At Merapi, three curved escarpments (somma rims) are observed on the southeast and south slopes based on satellite image analysis (Fig. 7.21). There are two possibilities for the origin of these escarpments. First, they could have been caused by a single volcanic sector collapse that formed three blocks of curved escarpments, similar to block faulting or step faults in tectonics. Consequently, such activity could produce a single debris avalanche deposit, and possibly separate Old Merapi from New Merapi.

A second possibility, which is our preferred interpretation, is that these somma rims were produced by three cycles of collapse events (CE) of the Merapi cone to the west-southwest, namely CE 1, CE 2 and CE 3. In this context, the oldest Merapi volcanic activity or cone is referred to herein as M I. The first collapse (CE 1) was followed by a construction period of a second Merapi cone (M II) in the first horseshoe-shaped crater. The second Merapi volcanic cone then collapsed and formed a second horseshoe-shaped crater (CE 2), in which renewed volcanic activity formed a third Merapi volcanic cone (M III). Following the collapse of this third cone, the youngest Merapi volcanic cone (M IV) has grown in the third horseshoe-shaped crater (CE 3) until today. A long time before these collapses, a Proto-Merapi (Ancient Merapi) may have also collapsed and left Turgo and Plawangan hills on the southern slope of present-day Merapi (Berthomier 1990; Camus et al. 2000; Newhall et al. 2000, Gomez et al. 2010; cf. Gertisser et al. 2023, Chap. 6).

CE 1 is probably similar to a crater rim shown on the geological map of the Yogyakarta quadrangle (Rahardjo et al. 1977). CE 2 is the most

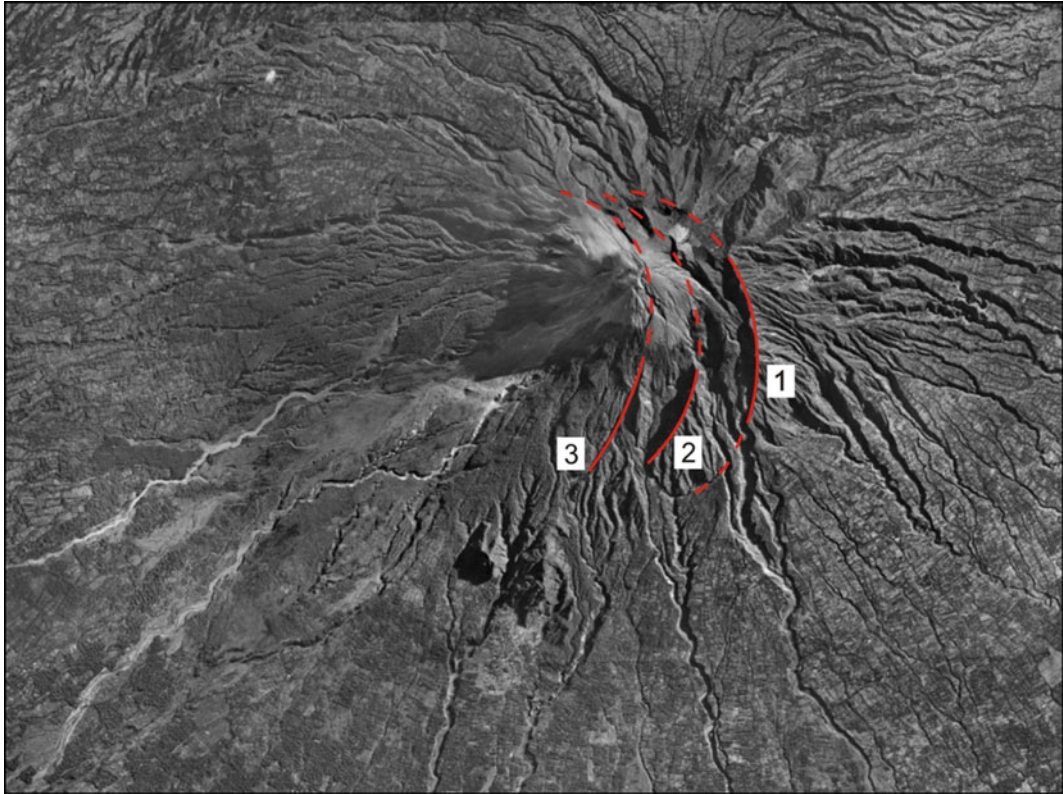


Fig. 7.21 Merapi satellite image showing three curved escarpments (1, 2 and 3) on the southeast and south slopes, presumably indicating features of horse-shoe shaped craters, caused by three southwest-directed

rockslides that developed from east to west. For reasons given in the text, we suspect that the curved escarpment 1 corresponds to the Godean debris avalanche. *Source Image BPPTKG Yogyakarta*

obvious, clearly observable from the Kaliadem campsite on the southern slope of Merapi and located at G. Watukendit in the headwaters of the Gendol River, extending northeastward through G. Kendil near the Woro River headwaters to the Pasarbubar scarp east of Merapi summit. On the geological map of the Yogyakarta quadrangle (Rahardjo et al. 1977) it is plotted as a curved normal fault, while on the geological map of Merapi volcano (Wirakusumah et al. 1989) it is called the Kukusan fault. The term ‘watukendit’ (Javanese: watu = stone; kendit = belt) was presumably given as it resembles, from a distance, a belt of the volcanic body of Merapi. The curved deep scarp on the slope of G. Kendil resembles the rim of a traditional cooking pot, called ‘kendil’, which may explain the name given to this topographic feature. There also appear to be two

further shorter escarpments between CE 1 and CE 2, which are already shown as parts of a crater rim on the geological map of the Yogyakarta quadrangle (Rahardjo et al. 1977) and regarded here as probable north-eastward extension of CE 2, but slightly shifted to the east. CE 3 is not clearly observed, as particularly on the east and the north side, it has been covered by younger Merapi products. As a matter of fact, the three Merapi collapses (CE 1, CE 2 and CE 3) and four volcanic cones (M I, M II, M III and M IV) are illustrated as two crater rims and one normal fault on the geological map of Rahardjo et al. (1977), differing only in the scarp direction. The first crater rim has a north-northeast direction that merges with the second crater rim towards the south, while the second rim has a northwest–southeast direction that also merges with the

normal fault at the northwest end. Although the third rim is plotted as a curved normal fault with a southwestern to northern trend on the Rahardjo et al. (1977) geological map, we believe it also relates to a volcanic collapse.

CE 1 seemingly is the largest sector collapse, likely producing the most voluminous debris avalanche deposit. The problem is that so far we have not found three distinct debris avalanche deposits. Were the two older deposits covered by the third one? Or had they been eroded away before the third one was deposited? This is discussed further below.

If the interpretation of four cycles of Merapi volcanism (M I–M IV), separated by three sector collapses (CE 1–CE 3) is correct, it follows that the division of Old Merapi and New Merapi (e.g. van Bemmelen 1949) becomes vague. We believe that this division was based on a general physiographic feature only, with Old Merapi characterised by a rough topography due to a very long time of erosion, and New Merapi forming a perfect volcanic cone with a smooth topography because of its younger age and active outpouring of eruptive material. In our view, the terms of Old Merapi and New Merapi have gone too far and have been applied too excessively by previous workers (e.g. del Marmol 1989; Berthomier 1990; Camus et al. 2000; Newhall et al. 2000; Gertisser et al. 2012, 2023, Chap. 6). It is worth noting that van Bemmelen (1949) did not consider detailed topographic analysis accompanied by numerical age data, as in the 1940s and before, satellite images were not available and numerical dating methods had not yet been developed.

In summary, we propose that the three curved escarpments (CE 1–CE 3) may indicate four cycles of construction phases of Merapi (M I–M IV) that are not clearly related to the division of Old Merapi and New Merapi. Consequently, we argue that there is no obvious relationship yet between a Merapi sector collapse and the division of Old Merapi and New Merapi (cf. Gertisser et al. 2023, Chap. 6). High-resolution satellite image analysis may help to clarify whether a sector collapse occurred once or several times at Merapi.

7.9 Ages of Merapi Sector Collapse(s) and the Godean Debris Avalanche

If the assumption of three Merapi sector collapses is correct, besides the oldest possibly linked to a Proto-Merapi (see Gertisser et al. 2022, Chap. 6, and references therein), CE 1 may represent the first major collapse event at Merapi. So far, there are no confirmed dates for the Merapi sector collapse(s) and the Godean debris avalanche deposit. Gomez et al. (2010) reported two major volcanic events at $119,000 \pm 2000$ y BP and $31,040 \pm 300$ y BP that deposited volcanoclastic material up to tens of metres thick in the southern part of the Borobudur basin. The nearest volcano is Merapi, having essentially basaltic compositions for Proto-Merapi and mainly basaltic andesitic compositions for the main Merapi edifice itself (e.g. Gertisser et al. 2023, Chap. 6). Although the authors stated that the origin of the $\sim 119,000$ y BP deposit is still unclear, based on the location and lithological composition, its source may be from Merapi. Megablocks of the Godean debris avalanche have a composition, which may be comparable with the compact unit in drill core 4 at 88 m depth that was dated at $119,000 \pm 2000$ y BP. Thus, one possibility is that the first major collapse event that corresponds to the Godean debris avalanche has an age of $\sim 119,000$ y BP.

The second major volcanic event at $31,040 \pm 300$ y BP results from dating wood remains in a 12 m thick dark grey, basaltic volcanic ash in drill core 3 at 8–20 m depth (Gomez et al. 2010). Figures 7.12b and 7.14d present dark grey (basaltic?) scoriaceous volcanic bombs in pyroclastic deposits of the Godean debris avalanche. This suggests that the sources of basaltic pyroclastic deposits are not limited to Proto-Merapi and Merbabu volcano but may also come from the main Merapi edifice (cf. Gertisser et al. 2023, Chap. 6). Therefore, a second possibility for the age of the Godean debris avalanche is $\sim 31,000$ y BP.

Murwanto (2014) reconstructed the dynamics of ancient Lake Borobudur, dividing it into three

periods (Upper Pleistocene ($> 11,700$ years), Holocene ($< 11,700$ years) and recent (600 y BP), and showing that the lake became smaller with time. This means that the first ancient lake was the largest and may have formed due to the Progo River being blocked by the huge volume of the Godean debris avalanche deposit. If correct, this may also support an age of $\sim 31,000$ y BP for the Godean debris avalanche.

For the ancient Lake Borobudur, Newhall et al. (2000) reported that the youngest black clay deposit is 420 ± 50 ^{14}C y BP, whereas Murwanto (2014) reported a slightly different youngest date of 660 ± 110 ^{14}C y BP, a difference that remains valid, if the calibrated ^{14}C ages are considered. However, the difference may also be due to possible inter-laboratory differences. If so, not only these two dates, but also the date of 1700 ± 160 ^{14}C y BP (Murwanto 2014) could be similar to the date of ~ 1900 ^{14}C y BP, the time, according to Newhall et al. (2000), when Old Merapi changed to New Merapi through sector collapse of its western part and inferred generation of a huge debris avalanche. With this in mind, the age of the Godean debris avalanche deposit could be as young as ~ 1900 ^{14}C y BP.

Thus, there are at least three possible ages for the Godean debris avalanche deposit: $\sim 119,000$ y BP, $\sim 31,000$ y BP, and ~ 1900 ^{14}C y BP. We consider the oldest age, linked to the first sector collapse (CE 1) as the most likely date of the Godean debris avalanche deposit, although further studies are needed to resolve this issue.

The first Merapi cone (M I) may have been an intact composite cone, larger than M II and M III, whose cone sizes may have been comparable to M IV. If we assume that the Godean debris avalanche deposit is the result of the first Merapi sector collapse (CE 1); where are the products of the second (CE 2) and third (CE 3) collapses? Due to smaller cone sizes, these two collapses are inferred to have been smaller and consequently should have smaller volumes. Their products could have possibly been deposited in river valleys only, had a much shorter travel distance (< 30 km?) or did not reach the Godean Hills, and may have been completely eroded or buried by younger fluvial deposits. On the other hand, the

arguably oldest (Godean) debris avalanche deposit is still well preserved because of its large volume, much longer travel distance (~ 50 km), and because some of the deposit was stranded in relatively high areas of the Godean Hills and the wavy to hilly topography of the Sentolo Formation in Sedayu.

Formation of CE 2 and CE 3 may correspond to the second (Holocene) and the third (~ 600 y BP) stage of ancient Lake Borobudur (Murwanto 2014). In this scenario, debris avalanche deposits resulting from CE 2 and CE 3 did not reach the Borobudur basin, but blocked the Progo River intermittently, causing a repeat occurrence of ancient Lake Borobudur. However, pyroclastic material that may have been associated with the two collapses probably entered and was deposited in the Borobudur basin. For instance, Gomez et al. (2010) reported that after the first major volcanic event, volcanic activity around Borobudur basin remained important, lasting at least until 80,000 years ago. Assuming that the age $\sim 119,000$ y BP for CE 1 is correct, one of these events may relate to CE 2.

Based on a field survey and drill core data, Murwanto (2014) reported the presence of palaeosol layers and intercalations of volcanoclastic deposits in the black clay lake deposits of ancient Lake Borobudur. This means that at certain times, parts of the lake area had become dry land where soil was formed, before the area was filled again by stagnant water to form a lake. The dry land in the area of ancient Lake Borobudur was formed because a part of its natural dike was eroded and lake water drained out, flowing downstream through the Progo River. The dry land and palaeosol were then covered by stagnant water forming a lake again and depositing younger black clay sediment above the palaeosol. How did the stagnant water reform in the Borobudur area? One possibility is that the debris avalanche deposits of Merapi sector collapses CE 2 and CE 3 re-dammed the Progo River to form new natural dikes. Volcanic activity is shown by the presence of intercalations of volcanoclastic deposits in the sequence of the black clay lake deposits (Murwanto 2014). Formation of palaeosol layers overlain by younger black clay

deposits indicates that ancient Lake Borobudur formed several times related to volcanic activity nearby, presumably from Merapi. The pyroclastic surge (?), ash fall and lahar deposits (Fig. 7.2) may also correspond to the formation CE 2 and CE 3. If the deposit shown in Fig. 7.2a is indeed a pyroclastic surge (or blast) deposit of almost 1 m thickness, it may have been associated with a very large pyroclastic current, corresponding, possibly, to a Merapi sector collapse. This hypothesis, however, requires a detailed study confirming the ages of both CE 2 and CE 3.

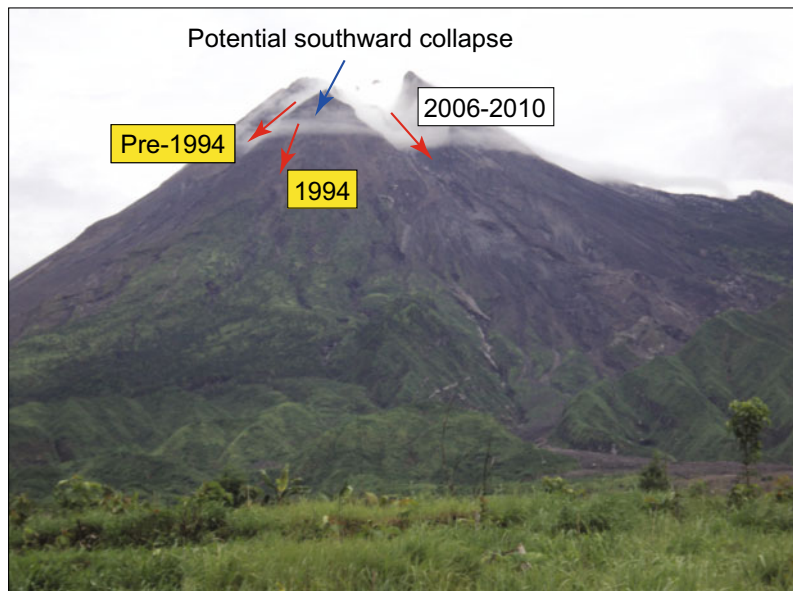
7.10 Future Hazards

Whether a Merapi sector collapse occurred once or several times in the past, the presence of the Godean debris avalanche deposit proves that the volcano had a major sector collapse in the past. If we agree that the Turgo-Plawangan hills are remnants of an Ancient or Proto-Merapi sector collapse, there were at least two major collapse events in the history of the Merapi volcanic complex. The recurrence of long-term sector collapse events on a composite volcanic cone is not uncommon. For example, Siebert et al. (1987) reported sector collapse occurrences at

Bandai volcano, Japan. In New Zealand, Alloway et al. (2005) reported several debris avalanches at Taranaki volcano, while in Indonesia, Bronto and Pratomo (1997) stated that prehistoric sector collapses occurred three times at the Guntur volcanic complex in West Java. This, together with the fact that Merapi has a perfect cone right now, implies that the volcano has the potential for a major sector collapse in the future. This urgently requires long term mitigation efforts, starting with research on the presence of volcanic debris avalanche deposits and probable indications of precursor activity.

Sector collapse and debris avalanche events on a volcanic cone may range from large to relatively small scales. Small scale debris avalanche deposits were found at Raung volcano in East Java (Siebert et al. 1997) and at Merapi, where such a deposit was discovered on the south slope (Newhall et al. 2000). During the 2006 eruption, the 1883 lava dome, situated at the southern summit and well-known as ‘Geger Boyo’ (Javanese, meaning crocodile’s back) collapsed. The collapse probably occurred because the lower part of the 1883 lava dome became weak or fragile due to intensive hydrothermal alteration. Consequently, during the 2006 and 2010 activity, magma easily intruded and erupted to open the

Fig. 7.22 Southern part of Merapi summit (blue arrow) between pre-1994 volcanic eruptions (west–southwest direction), and the 2006 and 2010 eruptions (south–southeast direction; red arrows) that may collapse to the south. It should be noted that such a collapse would be significantly smaller than the Godean debris avalanche



crater in a south-southeast direction. Figure 7.22 shows a possible small future partial collapse of the southern block of Merapi's summit to the south. This block is limited by activity directions before the 1994 eruption in the west and bordered in the east by the opening crater formed in 2010.

On the southern and southwestern slopes of Merapi, between the Sleman District in the west and the Klaten District in the east, widely distributed volcanic bomb-rich pyroclastic flow deposits are exposed, as examples of the products of explosive eruptions in the past (Bronto 2016). In the Sleman District, in the southwestern part of the Merapi slope, explosion-generated pyroclastic flow deposits are distributed from Dusun Turgo, Desa Purwobinangun ($07^{\circ}35'21.4''$ S– $110^{\circ}25'01.9''$ E) to roughly the Merapi Museum ($07^{\circ}37'18.5''$ S– $110^{\circ}25'14.5''$ E) in Dusun Tanen, Desa Candibinangun, Subdistrict of Pakem. On the southern slope, these pyroclastic flow deposits are distributed from the Kaliadem tourist resort or campsite up to the golf course at Desa Kepuharjo, Cangkringan Subdistrict. In the Klaten area, these deposits cover Desa Balerante and Desa Panggang, Subdistrict of Kemalang ($07^{\circ}36'36.6''$ S– $110^{\circ}28'22.6''$ E). Newhall et al. (2000) reported ^{14}C ages from explosion-generated (?) pyroclastic flows and surges, ranging from 1990 ± 140 ^{14}C y BP to 160 ± 30 ^{14}C y BP (AD 1740, 1674–1817) and 140 ± 30 ^{14}C y BP (AD 1730, 1680–1882) on the south slope of Merapi (see also Gertisser et al. 2012). The two youngest ages were obtained from charcoal taken from bomb-rich pyroclastic flow deposits at Kaliadem golf course and Desa Kinarejo. Such a wide distribution of explosion-generated pyroclastic flow deposits, some of which have relatively young ages and occurred in historical times, indicates that explosive eruptions have destroyed areas on the southwest-, south- and southeast sides of Merapi. The 2010 events (e.g. Subandriyo et al. 2023, Chap. 12) show that Merapi had an explosive eruption recently, although in 2018 it returned to effusive dome growth with sporadic short-lived explosions. This, together with the present crater opening to the south to southeast and the potential collapse shown in Fig. 7.22, means that

a future collapse and explosion of Merapi may threaten both the Sleman and Yogyakarta areas, and potentially cause serious fatalities and burial of the destroyed area for a long time (Bronto and Hartono 2002). Thus, although much smaller than the Godean debris avalanche event, a mitigation effort for such small potential collapses (accompanied by explosive eruptions) at Merapi should be carried out, focussing on past events and precursor phenomena leading towards either a small- or a large-scale collapse.

7.11 Summary and Outlook

The Godean debris avalanche deposit in the western part of the Yogyakarta plain is a new discovery and evidence for a gigantic landslide of Merapi, sliding down as far as 50 km from the volcano in a southwest direction until the confluence of the Bedog and the Progo River. The gigantic landslide covered and destroyed areas of the Magelang District (Central Java Province), and the Sleman, Bantul and eastern part of the West Progo districts (Yogyakarta Special Province). The total volume of the Godean debris avalanche deposit is estimated between 4.9 and 8.6 km³, covering an area ~ 390 km². Remnants of the Godean debris avalanche are preserved in the Godean and Sedayu areas because the avalanche hit and was trapped at the north side of the Tertiary Godean palaeovolcanic hills, while southwards, the avalanche stranded on the north side of the wavy hills of the Tertiary Sentolo Formation. The Godean debris avalanche may have been caused by the first sector collapse of Merapi (CE 1). However, this interpretation, together with the age of the event, requires further study. Numerical dating studies, including intercalations of volcaniclastic deposits in black clay deposits of the ancient Lake Borobudur and Lake Gantiwarno, are required to support the analysis of past Merapi collapse events. Merapi sector collapses range from small events to scales as large as the Merapi gigantic landslide or Godean debris avalanche. To reduce volcanic risk from future sector collapses, mitigation efforts, focussing particularly on precursor phenomena, is suggested.

Acknowledgements First and foremost, we would like to express our appreciation to Dr Chris Newhall who has worked on Merapi volcano since 1981, and was the first since van Bemmelen to investigate the evidence of a sector collapse of Merapi. After being shown the Merapi debris avalanche deposits in the Godean and Sedayu areas and reading the initial publication in Indonesian, he urged us to publish our new discovery in an international forum. We like to thank Dr Ralf Gertisser, who kindly invited us to publish our work in this book, and Dr Helmy Murwanto who provided important data on the ancient Lake Borobudur. Dr Didit H. Barianto, lecturer at the University of Gadjah Mada, has guided us to the andesitic megablocks in the Sedayu area and lahar deposits in Kasihan Subdistrict, Bantul. We are grateful to Ms Ir. Dewi Sayudi and Dr Subandrio MS, senior volcanologists at BPPTKG Yogyakarta, who organised a field trip to the Godean and Sedayu areas in order to introduce the Godean debris avalanche and old lahar deposits in the area to junior volcanologists. In addition, we thank Elisabeth Magdalena and Riza Fahmi Ma'rufi, geology students at the University of UPN "Veteran" Yogyakarta, who assisted during a recent field check. Finally, we would like to acknowledge the careful reviews by Dr Chris Newhall and Dr Ralf Gertisser.

References

- Agustin F, Bronto S (2019) Volkanostratigrafi Inderaan Jauh Kompleks Gunung api Gede dan sekitarnya, Jawa Barat. Indonesia. *J Geol Min Res* 20(1):9–16
- Alloway B, McComb P, Neall V, Vucetich C, Gibb J, Sherburn S, Stirling M (2005) Stratigraphy, age, and correlation of voluminous debris-avalanche events from an ancestral Egmont volcano: implications for coastal plain construction and regional hazard assessment. *J R Soc New Zeal* 35(1–2):229–267
- Branney MJ, Kokelaar P (2002) Pyroclastic density currents and the sedimentation of ignimbrites. *Geol Soc London Mem* 27:1–143
- Bronto S (1989) Volcanic geology of Galunggung, West Java, Indonesia. Ph.D. Thesis, University of Canterbury, Christchurch, New Zealand
- Bronto S (1995) Volcanic debris avalanches and lahars on Galunggung, Merapi and Kelut, Java, Indonesia. In: Proceedings of the workshop on debris avalanche and debris flow of volcano, Science and Technology Agency, Japan, 7–11 March 1995, pp 21–57
- Bronto S (2001) Volcanic debris avalanches in Indonesia. In: Proceedings of the 3rd Asian symposium on engineering geology and the environment (ASEGE), Yogyakarta, 3–6 September 2001, pp 449–462
- Bronto S (2013) Geologi Gunung Api Purba (Geology of palaeovolcanoes), 2nd edn. Geological Agency Ministry of Energy and Mineral Resources, Bandung, p 184
- Bronto S (2016) Pengembangan dan Terapan Geologi Gunung Api (Development and applied volcanic geology). Center for Geological Survey, Geological Agency, Bandung, p 370
- Bronto S, Hartono G (2002) Longoran gunung api dan bahayanya volcanic debris avalanches and their hazard. Simposium Nasional Pencegahan Bencana Sedimen, Sabo Technical Centre, Kerjasama Ditjend. Sumber Daya Air, Dept. Kimpraswil. dengan JICA, Maguwoharjo, Sleman, Yogyakarta, 12–13 Mar 2002, pp 413–426
- Bronto S, Pratomo I (1997) Endapan longoran gunung api dan implikasi bahayanya di kawasan G. Guntur, Kabupaten Garut, Jawa Barat (Debris avalanche deposits and their hazard implication in the Guntur volcanic area, District of Garut, West Java). In: Proceedings of the 25th annual convention meeting, Indonesian Geologists Association (IAGI), Bandung, 11–12 Dec 1997, pp 51–66
- Bronto S, Ratdompurbo A, Asmoro P, Adityarani M (2014) Longoran Raksasa Gunung Api Merapi Yogyakarta—Jawa Tengah (Gigantic landslides of Merapi Volcano, Yogyakarta—Central Java). *J Geol Min Res* 15(4):165–183
- Camus G, Gourgaud A, Mossand-Berthommier P-C, Vincent PM (2000) Merapi (Central Java, Indonesia): an outline of the structural and magmatological evolution, with a special emphasis to the major pyroclastic events. *J Volcanol Geotherm Res* 100:139–163
- Gertisser R, Charbonnier SJ, Keller J, Quidelleur X (2012) The geological evolution of Merapi volcano, Central Java, Indonesia. *Bull Volcanol* 74:1213–1233
- Gertisser R, del Marmol M-A, Newhall C, Preece K, Charbonnier S, Andreastuti S, Handley H, Keller J (2023) Geological history, chronology and magmatic evolution of Merapi. In: Gertisser R, Troll VR, Walter TR, Nandaka IGMA, Ratdompurbo A (eds) Merapi volcano—geology, eruptive activity, and monitoring of a high-risk volcano. Springer, Berlin, Heidelberg, pp 137–193
- Gomez C, Janin M, Lavigne F, Gertisser R, Charbonnier S, Lahitte P, Hadmoko SR, Fort M, Wassmer P, Degroot V, Murwanto H (2010) Borobudur, a basin under volcanic influence: 361,000 years BP to present. *J Volcanol Geotherm Res* 196:245–264
- Glicken H (1996) Rockslide-debris avalanche of May 18, 1980, Mount St. Helens Volcano. Washington. US Geol Surv Open-File Rep 96–677:1–90
- Harijoko A, Marliyani GI, Wibowo HE, Freski YR, Handini E (2023) The geodynamic setting and geological context of Merapi volcano in Central Java, Indonesia. In: Gertisser R, Troll VR, Walter TR, Nandaka IGMA, Ratdompurbo A (eds) Merapi volcano—geology, eruptive activity, and monitoring of a high-risk volcano. Springer, Berlin, Heidelberg, pp 89–109
- Lipman PW, Mullineaux DR (eds) (1981) The 1980 eruptions of Mount St. Helens Washington. US Geol Surv Prof Pap 1250:1–844
- MacLeod N (1989) Sector-failure eruptions in Indonesian volcanoes. *Geol Indon* 12(1):563–601

- Murwanto H (1996) Pengaruh aktivitas gunung api Kuarter terhadap perubahan lingkungan danau di daerah Borobudur dan sekitarnya, Jawa Tengah. S2 Thesis Geografi, University of Gadjah Mada, Yogyakarta, Indonesia
- Murwanto H (2012) Situs Danau di Sekitar Bukit Borobudur, Jawa Tengah. In: Santiko H (ed) 100 Tahun Pasca Pemugaran Candi Borobudur. Trilogi I Menyelamatkan Kembali Candi Borobudur, 2nd edn., Balai Konservasi Peninggalan Borobudur, Magelang 56553, Central Java, pp 141–161
- Murwanto H (2014) Penelusuran jejak lingkungan danau di sekitar Candi Borobudur dengan pendekatan paleogeomorfologi. S3 Dissertation, Prodi Geografi Program Pascasarjana—Fakultas Geografi, University of Gadjah Mada, Yogyakarta, Indonesia
- Murwanto H, Purwoarminto A (2015) Borobudur ancient lake site. In: Kiyoko K, Adishakti LT, Fatimah (Eds) Borobudur as cultural landscape. Kyoto Univ. Press and Trans Pacific Press, Kyoto–Melbourne, pp 79–92
- Murwanto H, Sutanto, Suharsono (2001) Kajian pengaruh aktivitas gunung api Kuarter terhadap perkembangan “Danau Borobudur” dengan bantuan Sistem Informasi Geografis. Laporan Akhir DCRG, Dept. Pendidikan Nasional, Indonesia
- Murwanto H, Gunnell Y, Suharsono S, Sutikno S, Lavigne F (2004) Borobudur monument (Java, Indonesia) stood by a natural lake: chronostratigraphic evidence and historical implications. *Holocene* 14 (3):459–463
- Nakamura Y, Glicken H (1997) Debris avalanche deposits of the 1888 eruption, Bandai volcano. In: Research Group for the Origin of Debris Avalanche (eds) Bandai volcano. Recent progress on hazard prevention. Science and Technology Agency, Japan, pp 135–147
- Neumann van Padang M (1939) Über die vielen tausend Hügel im westlichen Vorlande des Raoeng-Vulkans (Ost Java). *De Ing Nederl-Ind* 6(4):35–41
- Neumann van Padang M (1951) Catalogue of the active volcanoes of the world including Solfatara fields. Part I Indonesia. International Volcanology Association, Via Tasso 199, Napoli, Italia, pp 1–271
- Newhall CG, Bronto S, Alloway B, Banks NG, Bahar I, del Marmol MA, Hadisantono RD, Holcomb RT, McGeehin J, Miksic JN, Rubin M, Sayudi DS, Sukhyar R, Andreastuti S, Tilling RI, Torley R, Triple D, Wirakusumah AD (2000) 10,000 years of explosive eruptions of Merapi volcano, Central Java: archaeological and modern implications. *J Volcanol Geotherm Res* 100:9–50
- Ngkoimani LO (2005) Magnetisasi pada batuan andesit di pulau Jawa serta implikasinya terhadap paleomagnetisme dan evolusi tektonik. S3 Dissertation, Bandung Institute of Technology, Bandung, Indonesia
- Permanadewi S, Saefudin I, Siregar DA (2008) Kecepatan pergerakan magma dasit ke permukaan di daerah Purworejo dan sekitarnya, Jawa Tengah berdasarkan analisis penarikan jejak belah. *J Sumber Daya Geologi* 18(4):223–230
- Rahardjo W, Sukandarrumidi, Rosidi HMD (1977) Geological map of the Yogyakarta Quadrangle, Java, 1:100,000. Geol Surv Indonesia, Ministry of Mines, Bandung, Indonesia
- Rahardjo W, Astuti BS (2000) Tinjauan Geologi dan Paleogeografi Daerah Gantiwarno, antara Prambanan—Klaten, Jawa Tengah. In: Proceedings 2 of the 29th annual convention of the Indonesian Association of Geologists, Bandung, 21–22 Nov 2000, pp 70–75
- Roverato M, Cronin S, Procter J, Capra L (2015) Textural features as indicators of debris avalanche transport and emplacement. Taranaki Volcano. *Geol Soc Am Bull* 127(1–2):3–18
- Siebert L (1984) Large volcanic debris avalanches: characteristic of sources areas, deposits, and associated eruptions. *J Volcanol Geotherm Res* 66:367–395
- Siebert L, Glicken H, Ui T (1987) Volcanic hazards from Bezymianny- and Bandai type eruptions. *Bull Volcanol* 49:435–459
- Siebert L, Bronto S, Sutawidjaja IS, Mulyana R (1997) Massive debris avalanche from Raung Volcano, Eastern Java. Abstract, IAVCEI General Assembly, Puerto Vallarta, Mexico, 19–24 Jan 1997
- Situmorang T, Hadisantono R (1992) Geological map of Gede volcano, Cianjur, West Java, 1:50,000. Geol Surv Indonesia, Ministry of Mines, Bandung, Indonesia
- Soeria-Atmadja R, Maury RC, Bellon H, Pringoprawiro H, Polve M, Priadi B (1994) Tertiary magmatic belts in Java. *J Southeast Asian Earth Sci* 12:13–27
- Subandriyo, Gertisser R, Aisyah N, Humaida H, Preece K, Charbonnier S, Budi-Santoso A, Handley H, Sumarti S, Sayudi DS, Nandaka IGMA, Wibowo HE (2023) An overview of the large-magnitude (VEI 4) eruption of Merapi in 2010. In: Gertisser R, Troll VR, Walter TR, Nandaka IGMA, Radtomopurbo A (eds) Merapi volcano—geology, eruptive activity, and monitoring of a high-risk volcano. Springer, Berlin, Heidelberg, pp 353–407
- Surono, Toha B, Sudarno I (1992) Geological Map of the Surakarta—Giritontro Quadrangle, Java, 1:100,000. Geological Research and Development Centre, Bandung, Indonesia
- Ui T (1983) Volcanic dry avalanche deposits—identification and comparison with nonvolcanic debris stream deposits. *J Volcanol Geotherm Res* 22:163–197
- Ui T (1997) Characterization of debris avalanches associated with volcanic activity. In: Research Group for the Origin of Debris Avalanche (eds) Bandai volcano. Recent progress on hazard prevention. Science and Technology Agency, Japan, pp 149–154
- Ui T, Yamamoto H, Suzuki-Tamata K (1986) Characterization of debris avalanche deposits in Japan. *J Volcanol Geotherm Res* 29:231–243
- Van Bemmelen RW (1949) The geology of Indonesia, vol IA. Martinus Nijhoff, The Hague, p 732

- Voight B, Glicken H, Janda RJ, Douglass PM (1981) Catastrophic rockslide-avalanche of May 18 (Mount St. Helens). In: Lipman PW, Mullineaux DR (eds) *The 1980 eruptions of Mount St. Helens*, Washington. US Geol Surv Prof Pap 1250, pp 347–377
- Wirakusumah AD, Heriman AD, Hadisantono RD, Lubis H, Sutoyo (1980) Laporan kemajuan pemetaan geologi Daerah Gunung Merapi, Jawa Tengah. Unpublished report—Volcanological Survey of Indonesia, Bandung
- Wirakusumah AD, Juwana H, Loebis H (1989) Peta Geologi Gunungapi Merapi, Jawa Tengah (Geological map of Merapi volcano, Central Java), 1:50,000, Volcanol Surv Indonesia, Bandung, Indonesia
- Yoshida H, Sugai T (2007a) Topographical control of large-scale sediment transport by a river valley during the 24 ka sector collapse of Asama volcano, Japan. *Geomorphol* 13(3):217–224
- Yoshida H, Sugai T (2007b) Magnitude of the sediment transport event due to the Late Pleistocene sector collapse of Asama volcano, Central Japan. *Geomorphol* 86:61–72
- Yoshida H, Sugai T, Ohmori H (2006) Transportation mechanism of Debris Avalanche Event at 24ka of Asama Volcano, Central Japan, Interpreted from Chemical Composition of the Deposits. *The Quat Res (Daiyonki-Kenkyu)* 45(2):123–129



The Magma Plumbing System of Merapi: The Petrological Perspective

8

Valentin R. Troll and Frances M. Deegan

Abstract

Merapi volcano in Central Java is one of the most active volcanoes in the Sunda arc and poses a continuous threat to the local population. Basaltic-andesites from Merapi carry a voluminous crystal cargo and varied inclusion types, suggesting the presence of a complex subvolcanic plumbing system that feeds the volcano. Merapi basaltic-andesite lavas are dominated by a crystal assemblage of plagioclase with lesser pyroxene, Fe-oxides, and yet rarer amphibole phenocrysts. Inclusions in the lavas can be separated into four main groups, comprising (1) basaltic enclaves and highly crystalline basaltic-andesite inclusions, (2) plutonic inclusions, (3) amphibole megacrysts, and (4) calc-silicate crustal xenoliths.

Co-magmatic basaltic enclaves display chilled margins, whereas highly crystalline basaltic-andesite inclusions usually lack chilled margins, indicating mixing and mingling of compositionally variable magmas within the Merapi plumbing system. Holocrystalline plutonic inclusions comprise gabbro to diorite compositions and are generally coarse grained with occasional mineral layering. Mineral and isotope compositions of the plutonic inclusions largely overlap with those of recent Merapi lavas, defining them as cognate in origin. Mafic enclaves and amphibole megacrysts are isotopically more primitive and reflect deeper portions of the plumbing system. Geobarometry of plutonic inclusions, amphibole megacrysts, and pyroxene in lavas suggest a polybaric magma supply system beneath Merapi, likely with a larger basaltic storage reservoir at the base of the crust and a broadly andesitic one at mid crustal depth, plus several smaller pockets or chambers in the shallow upper crust. The shallow reservoir system is further supported by frequent contact-metamorphic calc-silicate xenoliths, which testify to intense magma-crust interaction in the upper crust. This is in line with elevated Sr, Pb, and O isotope data for the more evolved plutonic inclusions and in the rims of shallow-grown plagioclase crystals. The petrological evidence thus records crystallisation, crystal accumulation, magma mixing, mafic recharge, and assimilation

V. R. Troll (✉) · F. M. Deegan
Department of Earth Sciences, Section for Natural Resources and Sustainable Development, Uppsala University, Uppsala, Sweden
e-mail: valentin.troll@geo.uu.se

Istituto Nazionale Di Geofisica e Vulcanologia (INGV), Rome, Italy

Centre of Natural Hazards and Disaster Science (CNDS), Uppsala, Sweden

V. R. Troll
Faculty of Geological Engineering, Universitas Padjadjaran (UNPAD), Bandung, Indonesia

processes below Merapi and reflects considerable amounts of semi-molten crystalline mushes that are stored within the multi-tiered (polybaric) Merapi magma plumbing system. This implies that a considerable amount of potentially eruptible magma is currently stored beneath the volcano.

Keywords

Merapi · Magma plumbing system · Lava composition · Magmatic and plutonic inclusions

8.1 Introduction

In Indonesia, more than 197 million people live within 100 km of an active volcano. Merapi, on the island of Java, is one of the most hazardous volcanoes in the country and is characterised by periods of dome growth and intermittent explosive events. Merapi erupts frequently and usually erupts basaltic-andesite dome lavas and associated pyroclastic block-and-ash-flows and is believed to have caused upward of 7000 fatalities in the last 400 years (e.g. Andreastuti et al. 2000; Newhall et al. 2000; Thouret et al. 2000; Gertisser and Keller 2003a, b; Surono et al. 2012). To complement geophysical forecasting at active volcanoes like Merapi, which aims to detect active magma movement (e.g. via seismic and deformation data), an important contribution is to identify where magma is usually stored beneath Merapi and what processes typically occur within the plumbing system. A crucial first step in this respect is to investigate previous eruptive products for mineralogy, chemical composition and volatile concentrations, which, combined with phase-equilibrium experiments, can retrieve crucial information on magma compositions, magma storage levels, and magma ascent conditions. This information can assist forecasting of future eruptive scenarios by providing an interpretative framework (or catalogue) of possible to probable sub-volcanic processes that can help inform real-time geophysical monitoring efforts. Here we review recent petrological, and

geochemical data available on Merapi lavas and the inclusions contained within the eruptive products with the aim of unravelling the main magma storage levels beneath the volcano and to identify the key magmatic processes that operate within Merapi's magma plumbing system.

8.2 Geological Background

Merapi volcano (Fig. 8.1) is situated on the active volcanic front of the Sunda arc that extends > 3000 km from the Andaman Islands north of Sumatra to Flores island west of Bali. The Sunda arc is the result of the northward orthogonal subduction of the Indo-Australian plate, which forms a continuous slab beneath the Sunda plate (Hamilton 1979; Jarrard 1986; Tregoning et al. 1994; Wagner et al. 2007). Merapi volcano forms part of a cross volcanic arc chain, together with Ungaran, Telemoyo, and Merbabu (Camus et al. 2000) and rises from the lowlands of the Central Java Solo Zone (van Bemmelen 1949), a perpendicular depression to the strike of the arc that is infilled by a lithologically variable cover of alluvial deposits. Through seismic investigations, it has been determined that the deeper basement beneath Merapi consists of immature arc crust approximately 30 km thick (Curry et al. 1977; Jarrard 1986; Wölbern and Rumpker 2016; Lühr et al. 2023, Chap. 5), with the upper part of the crust comprising a thick Cretaceous to Tertiary limestone and marl-type sequence (e.g. van Bemmelen 1949; Smyth et al. 2005; Newhall et al. 2000; Deegan et al. 2010; Troll et al. 2013). The active Holocene arc in East to Central Java is bound to the south by the Southern Mountains Zone, remnants of the earlier Eocene to Miocene volcanic arc, and to the north by the Kendeng and Rembang Zones (Smyth et al. 2005; Harijoko et al. 2023, Chap. 4). The most northerly Rembang zone represents accreted crustal slivers joined up in the Cretaceous, while the Kendeng Zone is the main Cenozoic depocentre for the region, and is thought to contain between 8 and 11 km of sediment (De Genevraye and Samuel 1972;

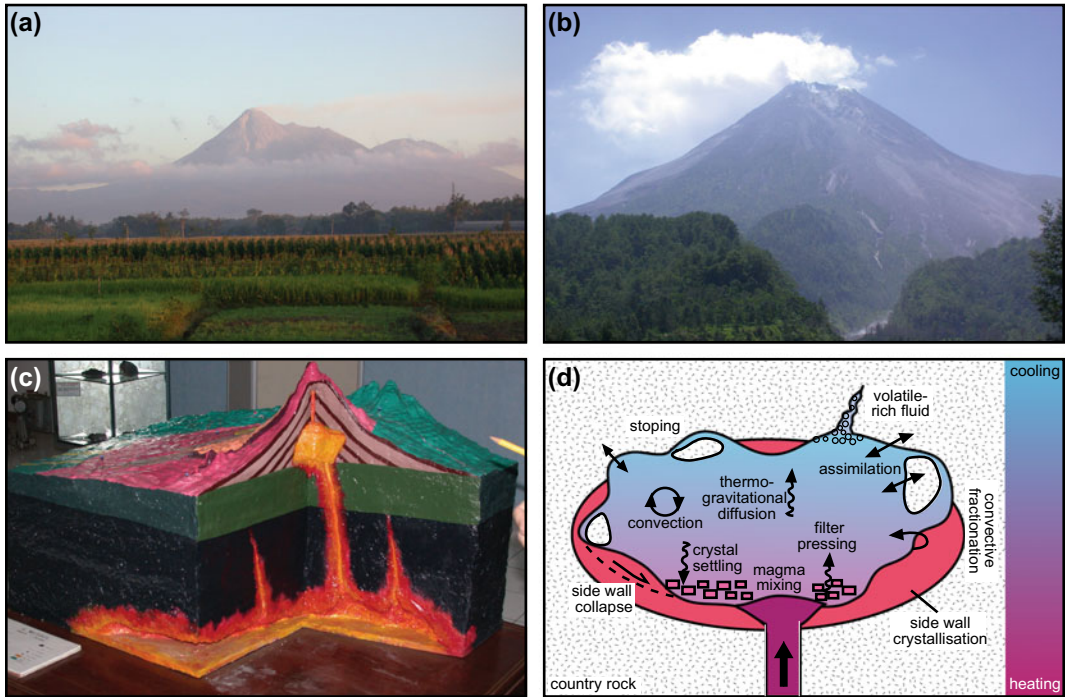


Fig. 8.1 a, b Views of Merapi volcano from the southeast and south. c Model of Merapi's plumbing system on display in the Merapi volcano Observatory (BPPTKG) in Yogyakarta, depicting a relatively simple

plumbing system with a deep crustal and a smaller mid-crustal reservoir that feeds the volcano. d Sketch of widely recognized magma chamber processes that may take place beneath Merapi volcano

Untung and Sato 1978; Smyth et al. 2005). This type of basement is also thought to make up the crust in the area below and immediately to the south of Merapi. Surface exposures of bedrock near Merapi comprise Cenozoic marine limestones and marls interlayered with in part extensive volcanoclastic sedimentary sequences (van Bemmelen 1949).

Merapi itself is a large Quaternary stratovolcano currently characterised by periods of active dome growth and intermittent explosive events. Due to its proximity (≤ 30 km) to the city of Yogyakarta (~ 0.5 million) and the Yogyakarta Special District (> 4 million inhabitants), Merapi poses a threat to the local population (Newhall et al. 2000; Suroño et al. 2012). Merapi's eruptive activity is characterised by dome growth, small-volume pyroclastic flows (block-and-ash flows, BAFs) and associated ash fall that is compositionally restricted to mainly basaltic-andesite with an SiO_2 content of ~ 51.5 to

56.5 wt. % (Gertisser and Keller 2003a, b). Dome growth episodes can last for several years but are frequently interrupted by shorter explosive events that last for hours to days (e.g. Andreastuti et al. 2000; Camus et al. 2000; Newhall et al. 2000; Voight et al. 2000). Merapi's long-term record suggests that frequent plinian, sub-plinian and vulcanian eruptions (up to ~ 0.3 km³ and VEI = 4) have occurred in the past and are likely to reoccur in the future (Andreastuti et al. 2000; Camus et al. 2000; Newhall et al. 2000; Gertisser and Keller 2003a, b; Gertisser et al. 2011, 2023, Chap. 6). Cyclicity lasting several hundred years, with at least three major cycles occurring in the past 2000 years, have been suggested and that Merapi might thus be at the beginning of a major phase of increased eruptive activity (Gertisser and Keller 2003a, b; Troll et al. 2015). If correct, this would pose formidable problems to risk assessment and disaster mitigation in the decades to come (e.g.

Andreastuti et al. 2000; Thouret et al. 2000; Charbonnier and Gertisser 2008; Gertisser et al. 2011; Darmawan et al. 2018). This is because central Java has amongst the highest population density in the world (c. 1121 people/km²) and, as a result of being close to Merapi volcano, the area has the highest volcano- population vulnerability index globally (Brown et al. 2015). In terms of human mortality, Merapi is one of the top ten deadly volcanoes worldwide, and a “disaster subculture”, i.e. a level of acceptance of volcanic risks, has developed in the region and is reflected in certain rituals and behaviours (e.g. Donovan and Suharyanto 2011; Troll et al. 2015; Holmberg 2023, Chap. 3). A particular problem at Merapi is its, at times, erratic behaviour. Although dome growth events are relatively long-lived and can be monitored, prediction of short-lived explosive events is usually more difficult. These may build up in only hours to days and precursor seismic signals at Merapi cannot always be directly translated into subsurface processes (e.g. Ratdomopurbo and Poupinet 2000; Richter et al. 2004; Budi-Santoso et al. 2013; Jousset et al. 2012; Surono et al. 2012; Darmawan et al. 2018). Longer periods of dome growth are generally associated with (mid- and upper- crustal) volcano-tectonic earthquakes but some short-lived pyroclastic eruptions seem to be associated with shallow hybrid seismic events and tremors only (Ratdomopurbo and Poupinet 2000; Voight et al. 2000; Surono et al. 2012; Troll et al. 2012; Budi-Santoso et al. 2013). The eruptions associated with deep earthquakes suggest magma recharge from depth into the plumbing system and ultimately into the shallow-level magma reservoirs and the volcanic edifice (e.g. Surono et al. 2012; Costa et al. 2013). Those eruptions that are, however, associated with shallow, near-surface hybrid earthquakes, multi-phase events, and tremors, point towards additional high-level, upper crust-hosted magma chamber(s) and reservoirs that can potentially erupt independently of deep magmatic processes (cf. Walter et al. 2008; Troll et al. 2012; Cassidy et al. 2016). An aseismic zone was recently identified beneath Merapi at a depth of about 2.5–3 km (e.g. Ratdomopurbo and Poupinet

2000), supporting the existence of at least transient shallow-crustal magma pockets or chambers beneath Merapi. This is consistent with recent petrological and mineral barometry studies that suggest a relatively high-level, quasi-steady state magma system beneath the volcano (e.g. Gertisser and Keller 2003b; Preece et al. 2013, 2014, 2016; van der Zwan et al. 2013).

8.3 Petrology of Merapi Lavas and Inclusions

8.3.1 The Basaltic-Andesite Lavas

The recent erupted products at Merapi volcano are broadly of basaltic-andesite composition and are medium to dark grey in colour. The basaltic-andesite lavas range from massive to mildly vesicular and contain up to 60% phenocrysts by volume dominated by plagioclase, typically complexly zoned, with additional clinopyroxene ($\leq 5\%$), minor orthopyroxene, Fe-oxides, and amphibole. The groundmass surrounding the crystals is microcrystalline to glassy with plagioclase and pyroxene as dominant microcrystals. The recent Merapi volcanics exhibit a high-K character and a relatively restricted spread in whole rock, radiogenic and stable isotope geochemistry (Hammer et al. 2000; Turner and Foden 2001; Gertisser and Keller 2003a, b; Chadwick et al. 2013; Troll et al. 2013; Deegan et al. 2016a, b). However, large compositional variations exist in plagioclase and pyroxene, and intra-crystal Sr and O isotope variations coupled with the presence of numerous inclusions of both igneous and meta-sedimentary origin in the recent deposits suggest a complex spectrum of magmatic processes are at play (e.g. Gertisser and Keller 2003a, b; Chadwick et al. 2007; Deegan et al. 2010, 2016a, 2021; Borisova et al. 2013, 2016; Chadwick et al. 2013; van der Zwan et al. 2013; Whitley et al. 2019, 2020). For instance, plagioclase crystals display complex, sometimes (reverse), zoning and dissolution features (e.g. sieve-textured cores or rims) that are often coupled with isotopic changes from core to rim (Chadwick et al. 2007; Borisova et al. 2016),

documenting a long and complex magmatic history with variable compositional influences. In addition to crystals, the inclusions found in Merapi's eruptive products are particularly varied and can be divided into five main groups: (1) highly crystalline basaltic-andesite inclusions and domains, (2) co-magmatic basaltic enclaves, (3) plutonic crystalline inclusions, (4) igneous megacrysts, and (5) true crustal skarn (calc-silicate) xenoliths of contact-metamorphic origin. Each of these is discussed in more detail below.

8.3.2 Highly-Crystalline Basaltic-Andesite Schlieren and Domains

“Highly-crystalline basaltic-andesite schlieren and domains” refer to samples with similar mineralogy to the host lavas, but with more abundant crystals (Chadwick et al. 2013). The crystalline basaltic-andesite inclusions (‘andesite in andesite’ texture) contain plagioclase crystal textures with similarly complex zoning as present in the basaltic-andesite host lava, but they usually occur as strung-out layers (schlieren) in the basaltic andesite lavas. Generally, they display sharp to lobate contacts, indicating a formerly fluid–fluid relationship with the host-basaltic-andesite, but they usually lack a chilled margin against the host lavas (Fig. 8.2), implying the host magma and the schlieren were of similar temperature at the time of mingling and incorporation (Chadwick et al. 2013; Troll et al. 2013). Their strung-out fluidal contacts, which support the concept of dynamic mixing and mingling processes, likely reflect recycling of semi-solidified crystal mushes, partly from reservoir walls and partly from remobilisation of semi-solidified magma pockets (Chadwick et al. 2013; van der Zwan et al. 2013). The schlieren are mineralogically and compositionally surprisingly similar to their host basaltic-andesite lavas, and only small differences in Ca content are observed between the whole rock composition of the schlieren and the host rock, likely the result of higher plagioclase content. Indeed, the highly-crystalline basaltic-andesite schlieren overlap

with the analysed 1994 and 1998 basaltic-andesite lavas (i.e. ~ 52 to 56 wt% SiO_2 and 2 to 4 wt% MgO ; Gertisser and Keller 2003a, b; Chadwick et al. 2013) (Figs. 8.3, 8.4).

8.3.3 Co-magmatic Basaltic Enclaves

Rare basaltic enclaves occur within the Merapi lavas that also show lobate to strung-out contacts against the host basaltic-andesites. The basaltic enclaves are generally restricted in size to a few centimetres across (Fig. 8.2) and frequently show a chilled granulated (fine-grained) margin, thus recording partial freezing of the enclave in the host lava and therefore a considerable temperature difference (Chadwick et al. 2013; Troll et al. 2013). They are finely crystalline, with < 1 mm crystals of plagioclase, pyroxene, and less frequent amphibole set in a glassy to microcrystalline groundmass. Clinopyroxenes are diopside to augite in composition and range from sub- to anhedral, frequently with simple zoning. Plagioclase crystals form relatively small elongate laths, which are usually normally zoned. Amphibole is present and often forms small laths with strong reaction rims (Chadwick et al. 2013). Plagioclase compositions in the basaltic enclaves show bimodal population trends (Fig. 8.3), with crystal rims and micro-crystals in the groundmass typically showing compositions of An_{49–65} (average An ~ 57 and 54 for rims and groundmass respectively), while crystal cores have more calcic compositions of An_{70–90} (average An ~ 82). Major element compositions of the basaltic enclaves range from 49 to 52 wt% SiO_2 and from 3 to 8 wt% MgO (Chadwick et al. 2013). Thus, they plot from close to the host basaltic-andesite field to more mafic compositions that link up along a fractionation trend (Fig. 8.4), likely reflecting the principal fractionation of the andesitic magma compositions from similar basaltic compositions. The REE patterns of the basaltic enclaves are, however, similar to those of the host basaltic-andesite patterns (Fig. 8.5), and the radiogenic isotope ratios of the enclaves consistently plot within the Merapi basaltic-andesite field (Fig. 8.6),

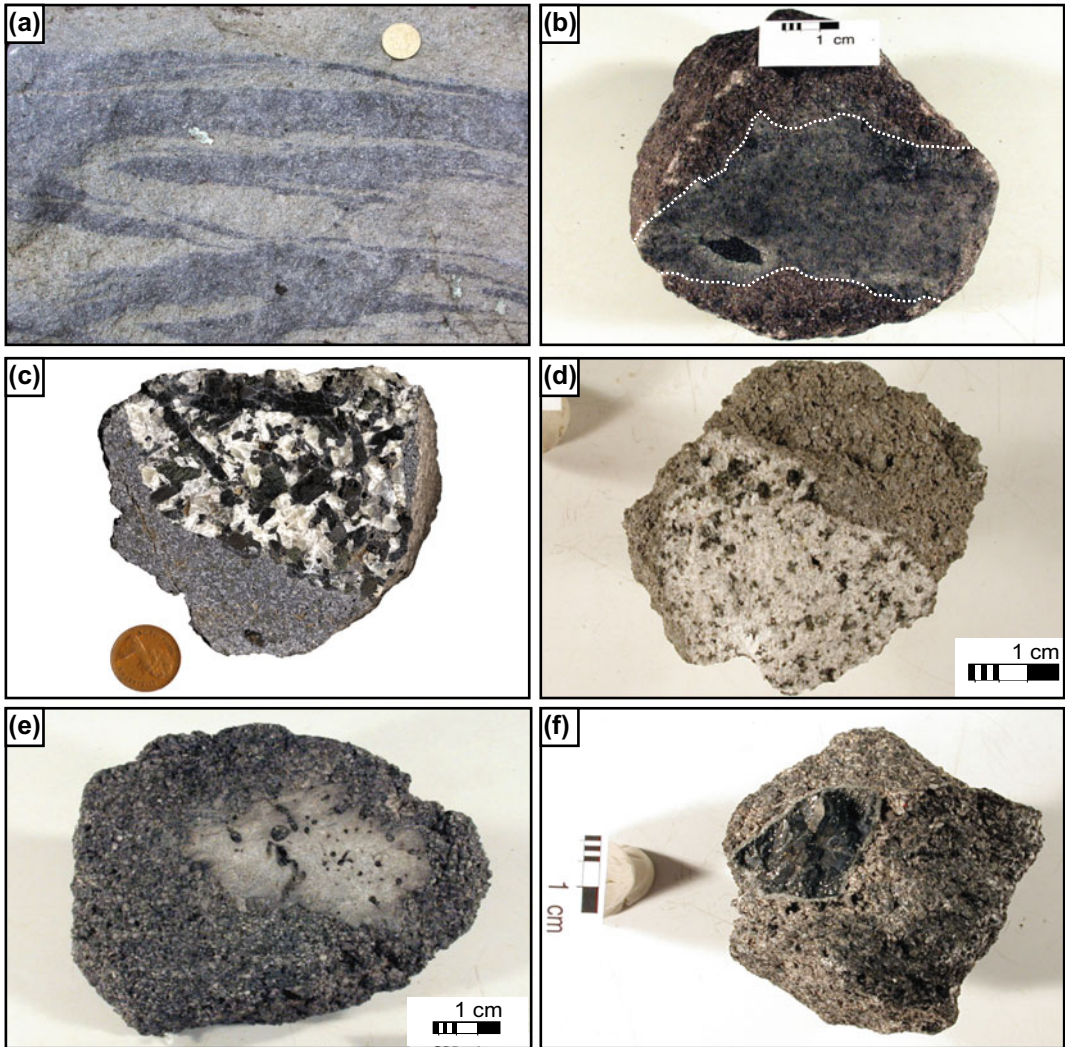


Fig. 8.2 Photographs of typical magmatic inclusions in recent Merapi lavas (after Troll et al. 2013). **a** Andesite in andesite schlieren. **b** Mafic (basaltic) enclave in basaltic andesite. Contact is highlighted in white. **c** Mafic plutonic (gabbroic) inclusion with pyroxene and plagioclase as

dominant minerals. **d** Felsic plutonic (dioritic) inclusion with plagioclase and minor pyroxene as the dominant mineral phases. **e** Partly resorbed dolerite/microgabbro in basaltic andesite. **f** Amphibole megacryst in basaltic andesite

confirming a genetic link between the basaltic enclaves and the host lavas (e.g. Chadwick et al. 2013; Troll et al. 2013). Basaltic enclaves in volcanic rocks are usually the products of recharge and mixing between coexisting liquids (i.e. co-magmatic) (e.g. Eichelberger et al. 1980; Bacon 1986; Coombs et al. 2003; Izbekov et al. 2004). Given the textural relationships and chilled contacts with the host basaltic andesite, the

Merapi basaltic enclaves are interpreted to indicate the result of mafic replenishments and magma mixing in the Merapi plumbing system.

In addition, angular to resorbed basaltic to intermediate inclusions (e.g. dolerites) with various degrees of thermal and hydrothermal alteration features, metamorphic recrystallization, and resorption textures are occasionally found. These likely reflect older igneous products of basaltic

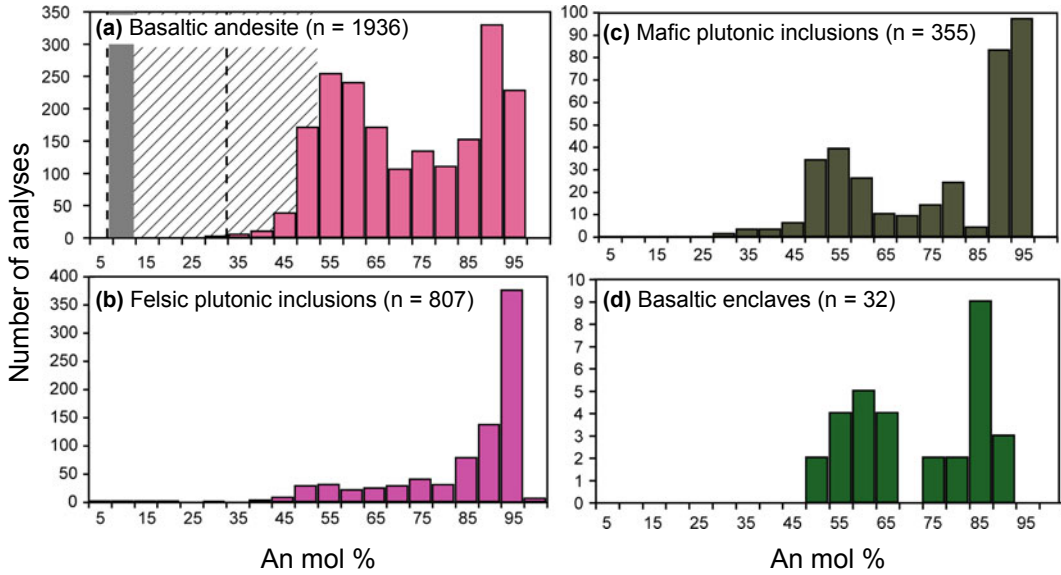


Fig. 8.3 Plagioclase compositions (An mol%) in Merapi lavas, basaltic enclaves and felsic and mafic plutonic inclusions (after Chadwick et al. 2013). **a** Plagioclase in host basaltic-andesite lava is shown in pink. For comparison, calculated equilibrium groundmass plagioclase compositions fall between the dashed vertical lines (calculated from CIPW norms based on groundmass/glass compositions of Hammer et al. (2000) and Schwarzkopf et al. (2001)). Observed microlite compositions from Hammer et al. (2000) fall into the oblique dashed area, with microlite rims usually showing the lowest An

composition (grey bar on the left). Plagioclase in **b** felsic plutonic inclusions, **c** mafic plutonic inclusions, and **d** comagmatic basaltic enclaves in recent Merapi lavas shows a wide range of An composition, ranging from high calcium to intermediate calcium contents. This reflects a range of mafic to intermediate parental liquids to be present in the Merapi plumbing system, consistent with the occurrence of mafic basaltic enclaves and variously evolved andesitic compositions. A fraction of high An plagioclase crystals is probably also derived from calcisilicate xenoliths

composition, such as dykes or other minor intrusions that were incorporated into the Merapi magmas during ascent, implying a longer history of mafic to intermediate compositions to be recorded in the plumbing system of the volcano.

8.3.4 Plutonic Crystalline Inclusions

Co-eruptive plutonic inclusions may preserve a record of magma differentiation processes that complements the information contained in the host magmas (e.g. Bacon 1986; Costa and Singer 2002). Plutonic inclusions in Merapi lavas comprise coarse- to medium-grained gabbro to diorite compositions (Fig. 8.2) with textures that range from massive to finely layered varieties (e.g. millimetre to centimetre thick modal mineral layers). The plutonic inclusions are typically

5–10 cm across, sub-rounded to angular, and resorption features are present in several examples, documenting that the plutonic inclusions are not always in equilibrium with their host lavas (Chadwick et al. 2013; Troll et al. 2013). The Merapi plutonic inclusions can be subdivided on the basis of modal mineralogy into mafic amphibole- and/or clinopyroxene-gabbros on the one hand and felsic leuco-gabbros, anorthosites and diorites on the other hand and where mostly cooled and crystallized before entrapment in the host lava (e.g. Chadwick et al. 2013). Contacts with the host basaltic andesite are typically sharp, often with an alignment of phenocrysts in the host lava along the contacts and often with concentrations of oxides along the margin of the inclusions. There is usually, however, no chilled domains in either the inclusions or the adjacent host basaltic-andesite (Fig. 8.2), indicating that

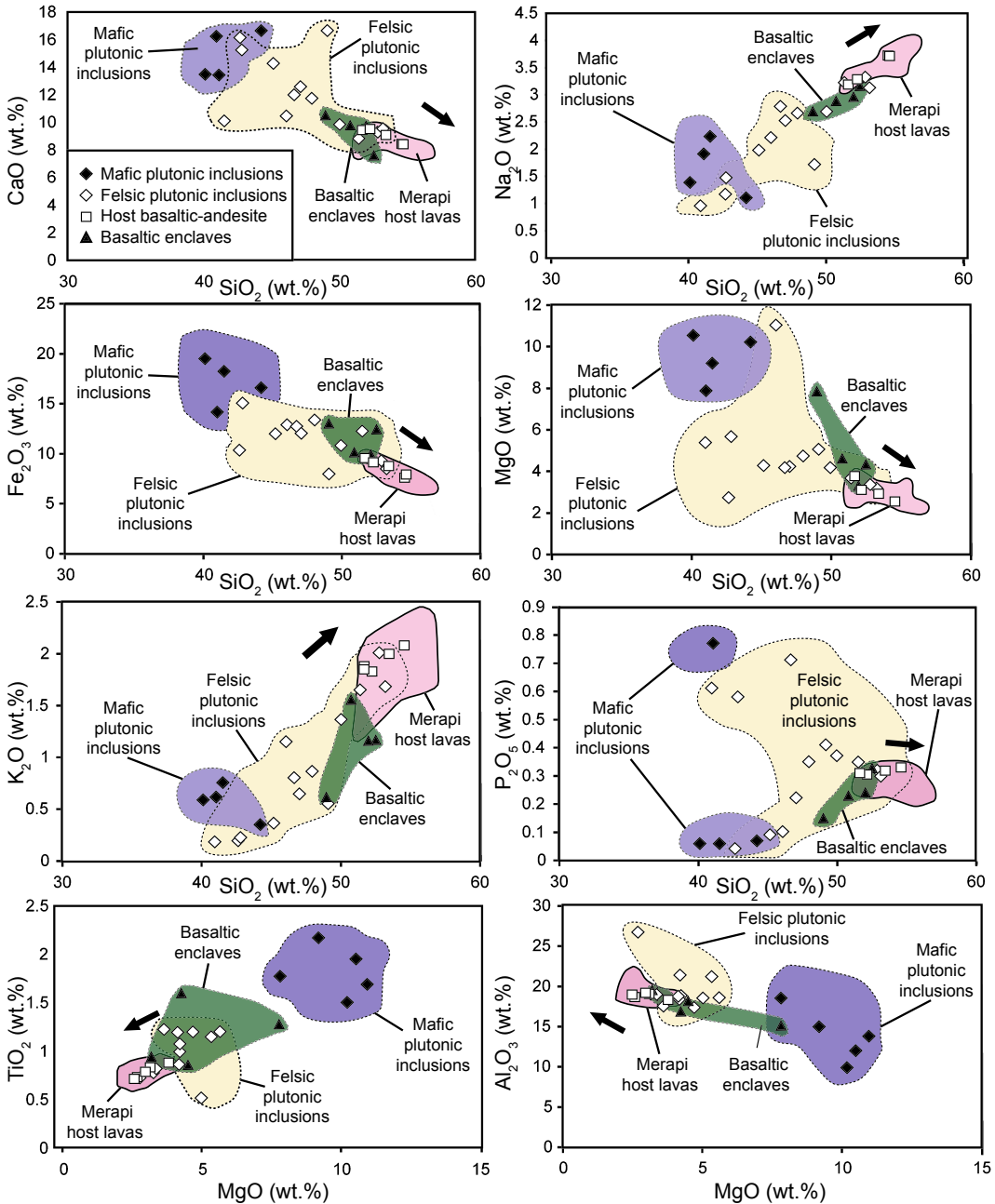


Fig. 8.4 Major element variation diagrams of recent Merapi lavas, basaltic enclaves, and mafic to felsic plutonic inclusions (after Chadwick et al. 2013). In

respect to major element compositions, lavas and plutonic inclusions show considerable overlap. Arrows indicate fractionation trends from Gertisser and Keller (2003a, b)

most plutonic inclusions were either abraded or incorporated into the host melt at elevated temperature. Some of the inclusions possess up to 10% vesiculated glass or micro-crystalline

groundmass, which may be taken as a partial melting texture in most of the cases (Chadwick et al. 2013; Troll et al. 2013). Rounded vesicles in the glassy portions indicate that vesiculation

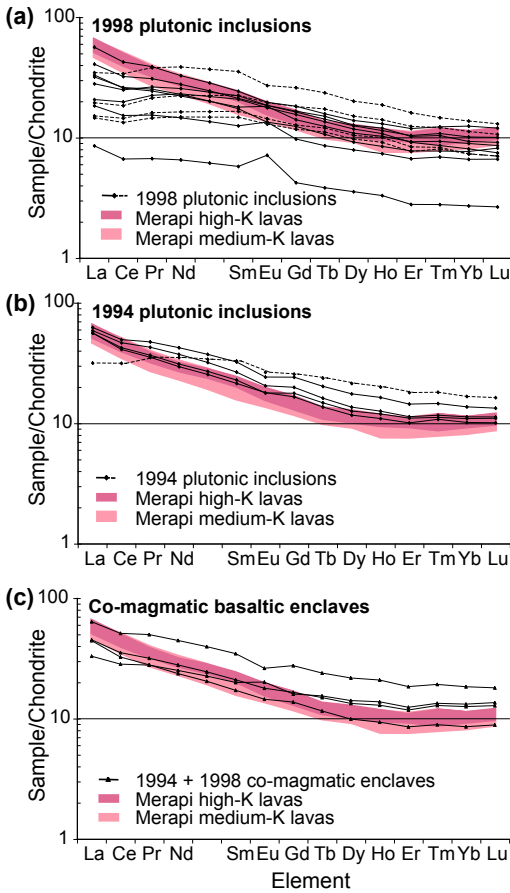


Fig. 8.5 Chondrite-normalised REE diagram for Merapi plutonic inclusions, co-magmatic basaltic enclaves and Merapi High- and Medium-K lavas. Dashed lines denote mafic plutonic inclusions, while the solid lines represent felsic ones (after Chadwick et al. 2013). Lava data are from Gertisser and Keller (2003a). The value for Pm was averaged between Nd and Sm

was a late process, perhaps even syn-eruptive. Crystals in these inclusions frequently show subsolidus textural re-equilibration along boundaries between plagioclase crystals and apparent dihedral angles of approximately 120° are common, implying high degrees of equilibration at a former (plutonic) state (cf. Holness et al. 2007a, b) prior to entrapment and partial re-melting.

Mafic plutonic inclusions are mineralogically dominated by amphibole and/or pyroxene with oxides (titanomagnetite, spinel, ilmenite), lesser plagioclase and rare apatite and titanite as accessories. The felsic inclusions display

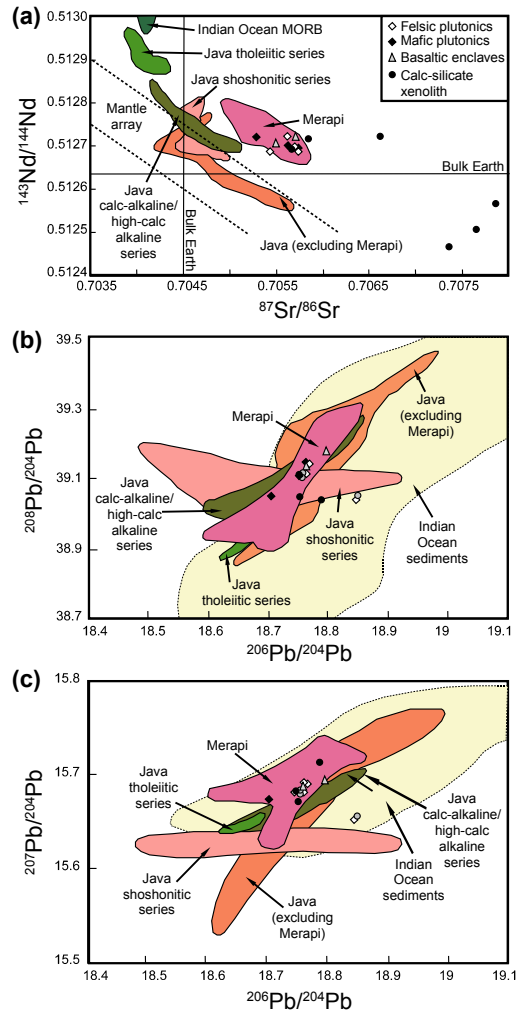


Fig. 8.6 Sr–Nd–Pb isotope relationships of recent Merapi lavas and plutonic inclusions (after Gertisser and Keller 2003a; Chadwick et al. 2013). **a** $^{143}\text{Nd}/^{144}\text{Nd}$ versus $^{87}\text{Sr}/^{86}\text{Sr}$ diagram, illustrating data from Merapi basaltic-andesite lavas, plutonic inclusions, basaltic enclaves and plutonic xenoliths relative to the mantle array, Indian Ocean MORB, and data from other Javanese volcanoes. **b** $^{208}\text{Pb}/^{204}\text{Pb}$ versus $^{206}\text{Pb}/^{204}\text{Pb}$ diagrams and **c** $^{207}\text{Pb}/^{204}\text{Pb}$ versus $^{206}\text{Pb}/^{204}\text{Pb}$ diagrams. Pb-isotopes show Merapi lavas, plutonic inclusions, basaltic enclaves and calc-silicate xenoliths (Gertisser and Keller 2003a; Chadwick et al. 2013) relative to other Javanese volcanoes, local upper crustal xenoliths and Indian Ocean sediment (additional data from Turner and Foden 2001 and references therein)

plagioclase as the dominant phase with lesser pyroxene, amphibole, oxides, but accessory quantities of apatite and titanite. In both sub-

groups, clinopyroxene of diopside to augite composition occurs, with anhedral to subhedral crystal shapes (Chadwick et al. 2013; Troll et al. 2013). Ca-rich clinopyroxene is present in the mafic inclusions only. Amphibole is commonly present as large laths > 5 mm, which are dominantly magnesio-hastingsite with some pargasite and hornblende. The amphibole laths may show reaction rims of oxides and finely crystalline pyroxene and plagioclase (Chadwick et al. 2013; Erdmann et al. 2014; Peters et al. 2017). Plagioclase crystals are typically concentrically zoned, subhedral and exhibit a broad range in An mol% from 4 to 95% (Fig. 8.3), but with two dominant domains at An 50–70 and An ~ 90. Late feldspar crystals in the groundmass and infilling cracks in mafic and felsic inclusions are of a more restricted compositional range An 52–58 (Chadwick et al. 2013). A small number of analyses fall in the Na-sanidine to anorthoclase fields, but appear to be the result of late alteration.

The plutonic crystalline inclusions display a relatively broad range in SiO₂ (40–55 wt%) and MgO (3–11%) with the mafic plutonic inclusions possessing MgO values of 9 to 11 wt %, whereas values recorded for the felsic inclusions range from 3 to 8 wt% MgO (Fig. 8.4). Fe₂O₃, MgO, and CaO contents decrease from mafic plutonic inclusions toward the felsic ones along broadly negative arrays when plotted against SiO₂ (Chadwick et al. 2013) and positive trends are observed between SiO₂ and Na₂O and K₂O (Fig. 8.4). P₂O₅ shows a positive and a negative array with increasing SiO₂ and when plotting MgO as index of differentiation against e.g. TiO₂ and Al₂O₃, a compositional gap between the mafic plutonic inclusions and the other samples, becomes apparent. Variations in modal mineral abundances (amphibole, plagioclase, apatite, and Fe-Ti oxides) are reflected by the whole rock variations producing with a degree of scatter in the data relative to Merapi basaltic-andesite host lavas (Fig. 8.4). Crystalline plutonic inclusions in arc magmas are usually considered fractionation residues that reflect magma solidification and differentiation processes (e.g. Beard and Borgia 1989; Burt et al. 1998; Costa

et al. 2002) and we consider this view to also apply to the Merapi plutonic inclusions, in line with available trace elements and isotope data (see below).

8.3.5 Amphibole Megacrysts

Amphibole megacrysts, up to several cm across, occur in the Merapi lavas, and appear to be out of equilibrium with the host lavas (Chadwick et al. 2013; Costa et al. 2013; Nadeau et al. 2013). Amphibole megacrysts at Merapi reach up to 8 cm in size, with internal zoning and pronounced reaction rims against the basaltic-andesite host (e.g. Erdmann et al. 2014; Peters et al. 2017). The reaction rims (Fig. 8.2) comprise fine-grained intergrowths of clinopyroxene, plagioclase and titanomagnetite and also occur along cleavage planes of many large amphiboles. These reaction textures are likely the result of late break-down and oxidation effects (cf. Garcia and Jacobson 1979; Davidson et al. 2007). The unaltered megacryst compositions define them as magnesio-hastingsite to ferro-edenite and thus they are of similar composition to the amphibole crystals observed in the lavas and mafic plutonic inclusions (e.g. Chadwick et al. 2013; Nadeau et al. 2013; Erdmann et al. 2014; Peters et al. 2017). The amphibole megacrysts crystallised probably from a more hydrous source within the deeper plumbing system of the volcano since the fine-grained reaction rims on the amphibole megacrysts and on many larger amphibole crystals are likely the result of ascent-related break-down and degassing during decompression and partial reheating (cf. Rutherford and Devine 2003), especially as petrographic evidence of reheating in the Merapi magma system exists, for example through the presence of basaltic enclaves and glass in crystalline plutonic inclusions (Chadwick et al. 2013; Peters et al. 2017). Reaction rims are not always well developed or are usually absent in the smallest amphibole phenocrysts contained within some Merapi ejecta, implying real phenocrysts of amphibole are present also (Gertisser et al. 2011; Costa et al. 2013; Nadeau et al. 2013; Preece et al. 2013;

Erdmann et al. 2014). The amphibole megacrysts are thus, most probably, from deeper and more hydrous portions of the Merapi plumbing system, consistent with their comparatively primitive Sr isotope compositions discussed in more detail below. Amphibole breakdown may represent one source of extra volatiles (H₂O) being added to the shallow magmatic system and could thus represent an independent eruption trigger.

8.3.6 Metasedimentary Calc-Silicate Inclusions (Crustal Xenoliths)

Abundant calc-silicate xenoliths occur in recent Merapi lavas, which are thermally metamorphosed limestones, partially infiltrated by basaltic-andesite and often with well-developed reaction rims (Chadwick et al. 2007; Deegan et al. 2010; Troll et al. 2012; Whitley et al. 2019, 2020). These calc-silicate inclusions are true crustal xenoliths and are composed of a characteristic diopside and wollastonite mineralogy with traces of quartz, tremolite and garnet in many samples (Chadwick et al. 2007; Deegan et al. 2010). Accessory Fe-oxides, titanite, apatite and exotic skarn minerals are usually also present (Whitley et al. 2019, 2020). Mineral determination by XRD indicates an increase in wollastonite content towards the cores of the inclusions (up to 74%) and a dominance of diopside and anorthite in the rims (diopside up to 60% in rims) (Chadwick et al. 2007; Troll et al. 2012), which reflects the conversion of an original limestone mineralogy to a gradually more “lava-like mineralogical composition” (cf. Bowen 1928; Fulignati et al. 2004; Jolis et al. 2015). Notably calc-silicate inclusions have also been found as small xenoliths in felsic plutonic inclusions and at direct magma–calc-silicate contacts, where the basaltic-andesite host is often extremely vesicular, indicating liberation of volatiles due to magma-carbonate interaction (cf. Deegan et al. 2010, 2011). Besides the notable calc-silicate inclusions, rare thermally overprinted siliciclastic and volcanoclastic inclusions also occur (Chadwick et al. 2007; Whitley et al. 2020), testifying to the

presence of some inhomogeneity within the upper crust beneath Merapi. Notably, the calc-silicate inclusions show elevated Sr and O isotope ratios relative to the Merapi lavas (Gertisser and Keller 2003a; Chadwick et al. 2007; Troll et al. 2013), and may be responsible elevated Sr and O isotopes in portions of the feldspar phenocrysts in recent Merapi lavas (e.g. Chadwick et al. 2007; Borisova et al. 2016). This may happen due to addition of calc-silicate crystalline materials to the Merapi magmas or result from crystallisation of feldspar from magma that assimilated limestone or calc-silicate material prior to feldspar crystallisation. Together with an at times high CO₂ output and elevated δ¹³C values in fumarole gas (e.g. Troll et al. 2012; Aiuppa et al. 2017; Carr et al. 2018), late stage crustal additions to mantle-derived magma is likely a relevant process at Merapi (e.g. Deegan et al. 2016a, b, 2021). In respect to magma plumbing, these calc-silicate xenoliths underline the notion of shallow-magma storage beneath Merapi volcano as limestone crust is restricted to ≤ 10 km depth beneath the volcano (e.g. Whitley et al. 2020). Furthermore, the crustal volatile additions from these xenoliths could represent an eruption trigger due to the potential to act as a sudden pressurisation agent to the shallowest parts of the magma storage system, possibly at times decoupled from magmatic recharge and or magmatic gas saturation due to crystal fractionation (Deegan et al. 2010; Troll et al. 2012, 2013; Blythe et al. 2015; Carr et al. 2018). Indeed, limited seismic precursors may be associated with this type of upper crustal eruption trigger, offering a potential explanation for the sometimes erratic behaviour observed at Merapi (Deegan et al. 2011; Troll et al. 2015).

8.4 A View into the Magma Plumbing System of Merapi

8.4.1 Evidence from Thermobarometry

A link between clinopyroxene crystal chemistry and pressure of crystallisation has been established by several authors (e.g. Nimis 1995, 1999;

Nimis and Ulmer 1998). According to Nimis and Ulmer (1998), Nimis (1995, 1999), pressure can be expressed as a linear function of the crystallographic unit cell volume and the M1 site volume. The standard error on prediction of pressure crystallisation values is generally around 140 MPa (Nimis 1999). Recent work on more hydrous and higher SiO₂ experimental compositions has highlighted inherent weaknesses in this model, which appears to slightly underestimate crystallisation pressures for more evolved and/or more hydrous systems (Putrika et al. 2003, Putrika 2008), but it should nevertheless provide a first order approximation for mafic to intermediate magmatic systems. A range of crystallisation temperatures from 920 to 1050 °C were provided for the Merapi basaltic-andesite lavas by various approaches such as oxide and pyroxene thermometry (Gertisser 2001; Chadwick et al. 2013) and thus an average temperature of 1000 °C has been used for geobarometric models.

The Nimis (1999) barometer as applied by Chadwick et al. (2013) to pyroxenes from basaltic-andesites and a variety of inclusions in the Merapi lavas yielded an overall range of pyroxene crystallisation pressures from ~ 100 to 1300 MPa and a concentration of values between 400 and 700 MPa was noted. Lavas range from 200 to 900 MPa with the bulk of pyroxene pressure data clustering between 400 and 500 MPa. Assuming reasonable densities for the Merapi edifice (2.6 g/cm³), the Javan crust (2.8 g/cm³), and the upper mantle (3.3 g/cm³), the bulk of pyroxenes in the basaltic-andesites are thought to have crystallised in mid- to deep crustal reservoirs (12–18 km) (Chadwick et al. 2013). Pyroxenes in felsic plutonic inclusions show crystallisation pressures between 65 and 720 MPa (2–25 km) and the lower pressure results are generally confined to the rims of these crystals, likely reflecting late storage in shallow parts of the plumbing system. The majority of the crystallisation pressures from pyroxene in felsic inclusions, however, clusters between 300 and 400 MPa (10–15 km), i.e. at mid crustal depth. Pyroxenes in mafic plutonic inclusions, in turn, have a similar range of crystallisation pressures

to the felsic inclusions, but with values clustering between 300 and 720 MPa. Co-magmatic basaltic enclave pyroxenes record the deepest crystallisation pressures, ranging from 300 MPa to 1300 MPa, consistent with magma storage extending well into the upper mantle (c. 45 km depth (see below).

More recent clinopyroxene barometry, using the updated approach of (Putrika 2008), was performed for pyroxenes from basaltic-andesite lava (Preece et al. 2014; Deegan et al. 2016a, b). The (Putrika 2008) formulation is a recalibration of the Nimis (1995) model, which improves the systematic error by incorporating a H₂O content. Assuming H₂O contents of 6 wt%, based on the clinopyroxene hygrometry of Weis et al. (2016), the thermobarometry results show a range of pyroxene crystallisation pressures from 250 to 600 MPa, with a frequency peak at 470 MPa (standard error of estimate = ± 260 MPa), and thus confirms a mid-crustal crystallisation level.

The available pyroxene barometry data from lavas and inclusions therefore suggests the presence of magma storage reservoirs (or regions) at multiple depths throughout the crust and into the lithospheric mantle beneath the volcano. Crystallisation and magma evolution thus takes place in several presumably larger chambers or reservoirs at the base of the crust, in the mid crust, and presumably in smaller reservoirs and pockets at relatively shallow crustal levels.

To complement pyroxene-based barometry estimates, amphibole- barometry (e.g. Ridolfi et al. 2010; Ridolfi and Renzulli 2012; Putrika et al. 2003) was carried out by Preece (2014), Peters et al. (2017). This approach suggests that the amphibole megacrysts crystallised at pressures of > 500 MPa, i.e. in the mid- to lower crust beneath Merapi, supporting a deep-seated magma storage level, below the main level of pyroxene crystallisation established by Chadwick et al. 2013; Preece et al. 2014; Deegan et al. 2016a). Rare-earth element concentrations, in turn, require the absence of magmatic garnet in the Merapi feeding system (see below) and, therefore, this places an uppermost limit for the pressure of amphibole crystallisation at c. 800 MPa, thus reflecting a total depth range

of $\sim 19\text{--}32$ km (lower crust and uppermost mantle) for crystallisation of the amphibole megacrysts.

8.4.2 Evidence from Phase-Equilibrium Experiments

Phase-equilibrium experiments make use of natural or synthetic rock and volatile compositions as starting materials and subject these to controlled pressure, temperature and oxygen fugacity in order to replicate the mineral phases in natural rock assemblages (e.g. Bowen 1928; Erdmann et al. 2016; Martel et al. 2017). With this approach, pressure, temperature, melt composition, and volatile content (H_2O , CO_2 , S, etc.) can be constrained and the crystallisation sequence of characteristic mineral assemblages for particular conditions can be established (e.g. Grove and Kinzler 1986; Scaillet and Pichavant 2003; Riker et al. 2015; Erdmann et al. 2016; Martel et al. 2017). This way, specific mineral compositions can be linked to certain pressure (depth) and temperature ranges, provided that P–T conditions change the resulting crystallisation assemblages. One limitation of this approach is that erupted rocks are often no longer a true reflection of original mineral and especially volatile contents due to crystal cargo, i.e. that older magmatic crystals (antecrysts) or crystals from the contact aureole and country rock (distinctly xenocrysts) can obscure the picture. Also, information from melt inclusions may no longer be representative of the initial volatile content, e.g. due to possible leakage or recrystallization (e.g. Baker 2008; Erdmann et al. 2016; Martel et al. 2017). This can lead to distortion of the resulting mineral assemblage relative to the pressure, temperature, and composition at which the natural assemblages have formed and considerable errors can be produced. For instance, Erdmann et al. (2014) performed phase equilibrium experiments at fixed crystallisation pressure and melt H_2O content to produce amphibole and then calculated pressure using barometric models (e.g. Ridolfi et al. 2010; Ridolfi and Renzulli 2012) from these crystals. They found that a large range of calculated

pressures was obtained from the experimental amphibole crystals (calculated pressures ranged from 200–800 MPa) and they concluded that pressure and temperature estimates largely reflect compositional variation in the crystallising magmas and only poorly reflect the pressure and temperature applied in the experiments. The authors thus argue that large calculated pressure variation for experimental amphibole from Merapi is indicative of thorough mixing of mafic to felsic magmas in the natural Merapi rocks and not strictly a reflection of crystallisation over a large depth range. Thus, the authors propose that bimodal pressure estimates obtained for natural Merapi samples, and other arc magmas, may reflect amphibole crystallisation from mafic and more evolved magmas, respectively (Erdmann et al. 2014, 2016). This, in turn, is however a good indication for at least two main reservoirs (a felsic and a mafic one) at variable depth beneath the volcano. Phase equilibrium experiments by Erdmann et al. (2016), using Merapi compositions, have been interpreted to show a pre-eruptive reservoir pressure of at $\geq 100\text{--}200 \pm 75$ MPa and thus at relatively shallow depths of c. ≥ 4.5 to ~ 9 km depth of magma storage. Magma temperatures of c. $925\text{--}950 \pm 25$ °C and melt H_2O contents of ~ 3 to 4 wt% were suggested with a vapour phase with $X_{\text{H}_2\text{O}}$ [$\text{H}_2\text{O}/(\text{H}_2\text{O} + \text{CO}_2)$] of $\sim 0.5\text{--}0.6 \pm 0.1$ (Erdmann et al. 2016). Following these authors, pre-eruptive (mafic) recharge magmas have temperatures of 950–1000 °C, and a higher melt H_2O content of ~ 4 to 5 wt% with a vapour phase of $X_{\text{H}_2\text{O}}$ of $\sim 0.8 \pm 0.1$.

8.4.3 Rare Earth Element Concentrations and Patterns

Whole rock REE data of Merapi lava possess a relatively elevated LREE but flat HREE distribution (e.g. Gertisser and Keller 2003a, b; Chadwick et al. 2013; Peters et al. 2017; Gertisser et al. 2023, Chap. 6). The co-magmatic basaltic enclaves have similar REE concentrations as the Merapi basaltic-andesites lavas,

however, a positive Eu anomaly is seen in most enclaves (Fig. 8.5). Some plutonic inclusions, in turn, show depletion in LREE and an enrichment in middle to HREE, relative to the Merapi lavas (Fig. 8.5), which is likely due to a higher abundance of accessory minerals relative to the lavas, while positive Eu anomalies in the plutonic inclusions result from their high plagioclase content. The REE patterns of the plutonic inclusions (Chadwick et al. 2013) dominantly overlap with those of the host basaltic-andesite (Fig. 8.5), however, there is a depletion in LREE relative to Merapi lavas in some sample specimens. This agrees with a low plagioclase/clinopyroxene modal ratio and low apatite and accessory content in these samples and or loss of interstitial liquid rich in REE is indicated. Flat to positive Eu anomalies in the plutonic inclusions, in turn, reflect plagioclase accumulation. Regarding the amphibole megacrysts, because of their comparatively low Dy/Yb ratios relative to the estimated compositions of the parent magmas (Peters et al. 2017), a significant amount of amphibole and/or clinopyroxene were likely fractionated at depth. Amphibole fractionation at depth is further supported by coupled variations of trace element ratios in the amphibole megacrysts, such as decreasing Zr/Hf and Th/U ratios with Dy/Yb (Peters et al. 2017). The low Th/U ratios relative to that of the host magma, implies that uranium in the megacrysts' parent magmas may have been present predominantly in the tetravalent state. This, in turn, suggests that magmatic fO_2 in the deep Merapi plumbing system increased from below the FMQ buffer in the mid-to-lower crust to above the FMQ buffer in the near surface environment, reflecting an increasingly oxidising environment for magmas ascending through the Merapi plumbing system (see also Deegan et al. 2010; Erdmann et al. 2014, 2016).

8.4.4 Radiogenic Isotopes

Sr, Nd and Pb isotope data for Merapi are plotted in Figs. 8.7 and 8.8. Merapi shows elevated $^{87}\text{Sr}/^{86}\text{Sr}$ values relative to other Sunda arc

volcanoes (cf. Turner and Foden 2001) and the radiogenic isotope data for Merapi enclaves and plutonic crystalline inclusions fall dominantly within the range defined by the erupted Merapi lavas (Turner and Foden 2001; Gertisser and Keller 2003a; Chadwick et al. 2013) (Fig. 8.6). Specifically, co-magmatic basaltic enclaves range from 0.7055 to 0.7057 for $^{87}\text{Sr}/^{86}\text{Sr}$ and from 0.51270 to 0.51272 for $^{143}\text{Nd}/^{144}\text{Nd}$, while plutonic inclusions show a $^{87}\text{Sr}/^{86}\text{Sr}$ and $^{143}\text{Nd}/^{144}\text{Nd}$ range of 0.7053–0.7058 and 0.51256 to 0.51272, respectively (Chadwick et al. 2013). The $^{206}\text{Pb}/^{204}\text{Pb}$ ratios for plutonic inclusions range from 18.71 to 18.75 and for co-magmatic basaltic enclaves from 18.76 to 18.80 (Fig. 8.6), while the $^{207}\text{Pb}/^{204}\text{Pb}$ and $^{208}\text{Pb}/^{204}\text{Pb}$ ratios for plutonic inclusions and basaltic enclaves range from 15.65 to 15.69 and 39.04 to 39.14 and 15.69 to 15.70 and 39.14 to 39.18, respectively. These compositions overlap with the published range for Merapi host lavas (cf. Turner and Foden 2001; Gertisser and Keller 2003a; Gertisser et al. 2023, Chap. 6). Sr and Nd and Pb isotopes for plutonic inclusions thus fall dominantly within the range of Merapi lavas (e.g. Gertisser and Keller 2003a; Gertisser et al. 2023, Chap. 6), highlighting their cognate nature (Figs. 8.6, and 8.7). In fact, Sr isotope ratios of plutonic inclusions show a stepwise progression from relatively nonradiogenic Sr ratios for the mafic inclusions and amphibole megacrysts to mildly higher values for felsic inclusions (Fig. 8.7), but are still less radiogenic than the available lava whole rock suite, and significantly lower than the available groundmass and plagioclase data (Chadwick et al. 2007, 2013; Peters et al. 2017) (Fig. 8.8). The amphibole megacrysts and mafic enclaves are thus the most primitive compositions at Merapi, providing us with an isotopic starting point to assess magma differentiation within the Merapi plumbing system.

With respect to mineral phases, variations in $^{87}\text{Sr}/^{86}\text{Sr}$ ratios amongst the cores and different zones of single plagioclase crystals have been recorded and variations have been attributed to crystal growth during assimilation of upper crust carbonate rocks (≤ 10 km depth), consistent with frequent calc-silicate xenoliths in the

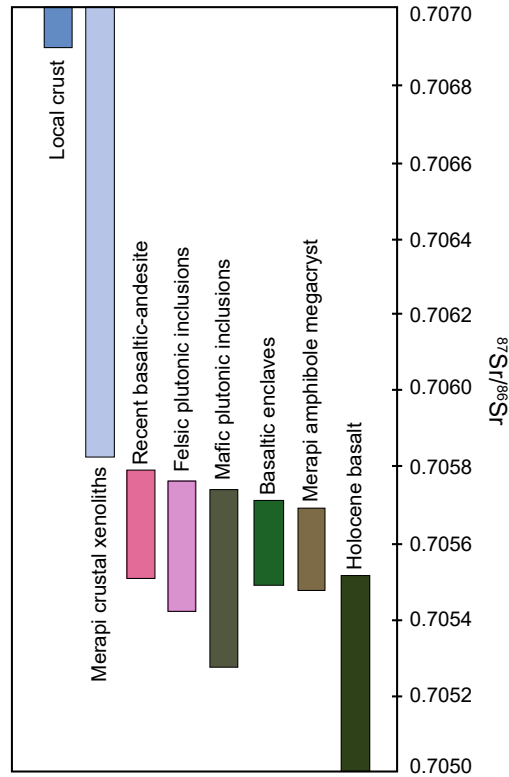


Fig. 8.7 Sr isotope bar chart (modified after Chadwick et al. 2013) for recent Merapi basaltic-andesite lavas, Holocene basalts, basaltic enclaves, amphibole megacrysts, and plutonic inclusions (lava data from Gertisser and Keller 2003a; amphibole data are from Peters et al.

2017). The compositional groups reflect a general increase of maximum Sr isotope values from mafic to increasingly felsic compositions, implying that crustal assimilation has become more important with increasing lifetime of the Merapi system

Merapi lavas (see above). In addition, these studies showed that some of the plagioclase cores were in fact xenocrysts derived from carbonates and their reaction products (calc-silicate skarns) (Chadwick et al. 2007). The elevated whole-rock and plagioclase Sr isotope ratios relative to the amphibole megacrysts and mafic enclaves, coupled with the barometry information, are strong indications of mixing of various mafic and evolved melts and their interaction with upper crustal materials during magma evolution. The lower $^{87}\text{Sr}/^{86}\text{Sr}$ ratios of most of the amphibole megacrysts and clinopyroxene compared to most plagioclase samples at Merapi (Fig. 8.8), support that amphibole and also clinopyroxene grew dominantly prior to the onset of upper crustal

sediment assimilation recorded in many plagioclase crystals (Chadwick et al. 2007; Borisova et al. 2013, 2016; Deegan et al. 2016a, b; Peters et al. 2017).

Realising that crustal (high-level) magma-carbonate interaction in the Merapi plumbing system is possibly widespread, we can hypothesise that Merapi's exceptionally dangerous and often erratic behaviour, at least compared to most other Javanese volcanoes, may be in part due to assimilation of upper crustal carbonates and associated crustal CO_2 added to the system (Deegan et al. 2010, 2011; Troll et al. 2012; Carr et al. 2018; Whitley et al. 2019). In this respect, Merapi is similar to other dangerous and erratic volcanoes located on a carbonate substratum

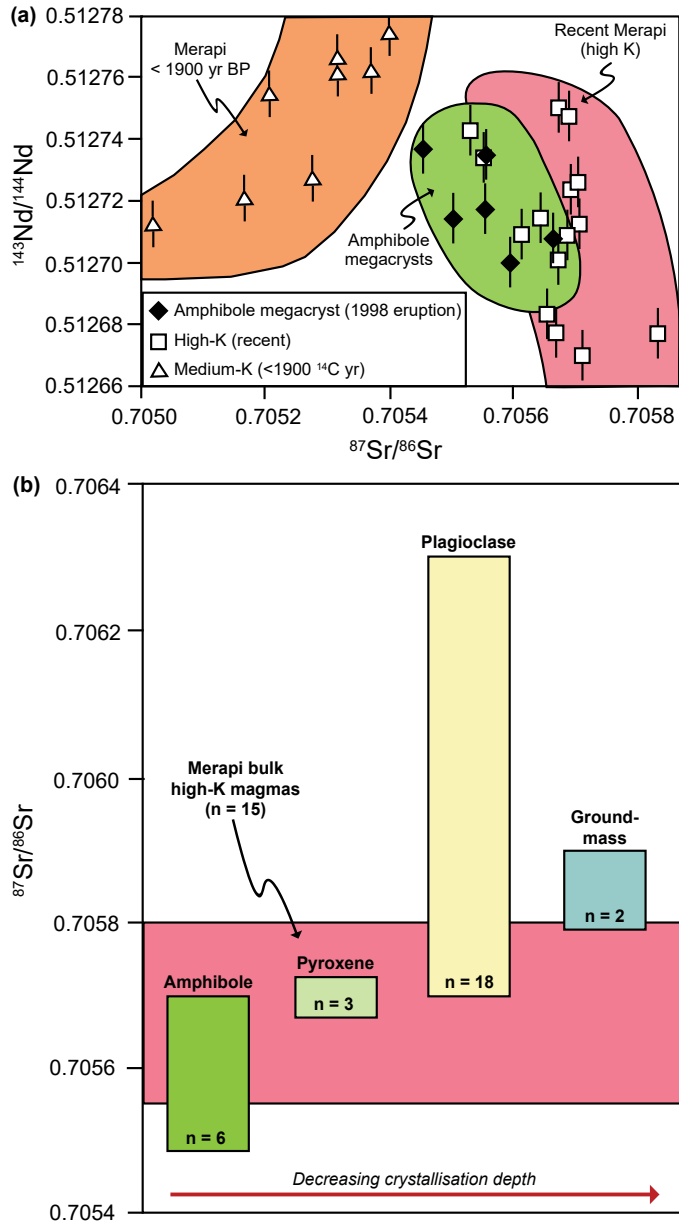


Fig. 8.8 **a** Sr–Nd diagram showing the values of amphibole megacrysts and recent and Holocene Merapi lavas. **b** Mineral phases in Merapi lavas, including amphibole megacrysts, relative to the groundmass and recent and Holocene Merapi lavas (after Peters et al. 2017). Note the shallow-grown plagioclase (plagioclase is only stable in to upper 25–30 km of the Earth’s crust) shows the strongest evidence for crustal assimilation processes, likely reflecting a proportion of xenocrysts to

be present (e.g. Chadwick et al. 2007; Whitley et al. 2020). Amphibole megacrysts are, in turn, least affected by crustal assimilation processes, offering a window into the early crystallisation processes of primitive Merapi magmas at depth. Pyroxene crystals seem to have largely formed below the sedimentary upper crust (c. top 10 km) and are thus also relatively unaffected by upper crustal assimilation

(e.g. Vesuvius and Popocatepetl). The details of this set of processes and their wider significance are treated in Deegan et al. (2023, Chap. 10) and are therefore not treated in detail in this account. The fundamental realisation in respect to the Merapi plumbing system is, however, that shallow crustal magma storage is likely a relevant phenomenon at Merapi that is documented through crustal xenoliths and the specific crustal contamination patterns in e.g. plagioclase crystals, strongly supporting prolonged magma-crust interaction and magma residence in the shallow upper crust beneath Merapi.

8.4.5 Oxygen and Deuterium Isotopes

Whole-rock basaltic-andesite $\delta^{18}\text{O}$ values range from + 5.6 ‰ to + 8.3 (±) 0.1‰ (Gertisser and Keller 2003a; Troll et al. 2013; Gertisser et al. 2023, Chap. 6), while feldspar and pyroxene crystal separates show $\delta^{18}\text{O}$ values from + 5.9 to + 7.9 ± 0.1 ‰ and from 5.1 to 7.2 ± 0.1‰, respectively (Jolis 2013; Troll et al. 2013; Deegan et al. 2016a). These values are higher than typical mantle values ($\delta^{18}\text{O}$ of average Indian Ocean type MORB = 5.7 ± 0.2 ‰; Ito et al. 1987) and most mafic arc melts ($\delta^{18}\text{O}$ = 5.2 to 6.2 ‰; e.g. Eiler 2001). Limestones from the local platform carbonate sequence have $\delta^{18}\text{O}$ between + 18.9 and + 24.5 ‰ (± 0.1 ‰) (Troll et al. 2013), whereas calc-silicate inclusions in the lavas show a range of $\delta^{18}\text{O}$ from ~ + 10.0 to + 15.0 (± 0.1 ‰) (Gertisser and Keller 2003a; Troll et al. 2013).

In situ measurements of oxygen isotope ratios in silicate minerals from Merapi by Secondary Ion Mass Spectrometry (SIMS) is to date limited to two studies that focus on plagioclase and pyroxene (Borisova et al. 2016; Deegan et al. 2016a). Recently erupted pyroxene crystals from Merapi yield $\delta^{18}\text{O}$ by SIMS with an overall range of $\delta^{18}\text{O}$ = 4.3 to 8.1 ‰ (average $\delta^{18}\text{O}$ = 5.8 ± 1.2 ‰, 2SD; n = 204, Deegan et al. 2016a). The bulk of the SIMS data overlap with

the $\delta^{18}\text{O}$ values of Merapi 2006 pyroxene crystals obtained by laser fluorination, which range from 5.1 to 5.8 ‰ (average $\delta^{18}\text{O}$ = 5.4 ‰, Troll et al. 2013; Deegan et al. 2016a). In turn, Merapi bulk pyroxene separates (representing 10 s to 100 s of crystals) have $\delta^{18}\text{O}$ values that range from 5.9 to 7.2 ‰ (n = 7, average $\delta^{18}\text{O}$ = 6.7 ‰, Troll et al. 2013). These bulk separates overlap with the Merapi whole-rock record (5.6 to 8.3 ‰, n = 32, average $\delta^{18}\text{O}$ = 6.9 ‰; Troll et al. 2013). We note that SIMS data are likely superior to determine true pyroxene $\delta^{18}\text{O}$ values as analyses are generally of pure pyroxene, i.e. in areas free from inclusions (see Deegan et al. 2016a, 2021). Bulk samples appear somewhat offset to higher $\delta^{18}\text{O}$ values, which likely reflects the presence of mineral and glass inclusions, while the in situ SIMS pyroxene data record a frequency peak at 5.8 ‰, which was used to constrain the $\delta^{18}\text{O}$ value of primitive mafic Merapi magma to be ~ 6.1 ‰ by using appropriate magma-mineral fractionation factors (Deegan et al. 2016a). This value is only mildly elevated from MORB-type mantle values globally reported (e.g. Eiler 2001).

Plagioclase $\delta^{18}\text{O}$ data by SIMS are at present limited to information from three crystals only and show lower $\delta^{18}\text{O}$ in Ca-rich cores (4.6–6.6 ‰) compared to rims (5.7–7.9 ‰) (Borisova et al. 2016). These authors advocate a two-stage model with Ca-rich plagioclase cores dominantly crystallising in the deeper plumbing system, partly interacting with high-temperature (low $\delta^{18}\text{O}$) crustal rocks to explain the sub-MORB values seen in their data. The Ca-poorer rims usually show higher $\delta^{18}\text{O}$ values, which following these authors reflect shallow crustal (4–9 km) assimilation of crustal carbonate. Intriguingly, no such “extra low” values as recorded in plagioclase cores have been observed in the much larger SIMS pyroxene data set of Deegan et al. (2016a). These unusually low values would thus need to be verified, especially since low $\delta^{18}\text{O}$ values in igneous rocks are not common in the latitudes around the equator (cf. Balsley and Gregory 1998; Budd et al. 2017).

Hydrogen (deuterium) isotopes (δD) are available from the amphibole megacrysts (Fig. 8.9). The data show a wide range of values (-107 to -11‰) that exceed the range of regular magmatic amphibole and suggest that the megacrysts experienced dehydrogenation (H_2 loss) and/or dehydration (H_2O loss). This is backed up by variable H_2O contents and Fe^{3+}/Fe^{2+} ratios in the megacrysts (Peters et al. 2017). Amphibole is not stable at low pressure and breakdown of amphibole during ascent to low pressure will release its originally crystal-bound volatile species (mainly water) into the shallow plumbing system. This phenomenon may play a role in respect to Merapi's explosive and often erratic eruptive behaviour as crystal-bound water may feed rapid development of a free vapour phase (and associated pressure-increase), especially at shallow crustal levels, i.e. in the top 2 km below the volcano (cf. Feeley and Sharp 1996; Davidson et al. 2007; Peters et al. 2017).

8.4.6 Constraints from Geophysics and Thermobarometry Approaches

Dome growth at Merapi is typically associated with deep and shallow earthquakes. Deep volcano-tectonic (VT) seismic events are believed to indicate magma migration in the plumbing system (Ratdomopurbo and Poupinet 2000; Surono et al. 2012; Budi-Santoso et al. 2013; Subandriyo et al. 2023, Chap. 12), while many pyroclastic and dome eruptions at Merapi are associated with shallow hybrid seismic events and tremors only (Ratdomopurbo and Poupinet 2000; Voight et al. 2000; Walter et al. 2008). The eruptions associated with shallow seismic activity indicate shallow eruption triggers in a high-level storage region (cf. Ratdomopurbo and Poupinet 2000; Deegan et al. 2011; Troll et al. 2012; Carr et al. 2018) and the identification of an aseismic zone at a depth of approximately

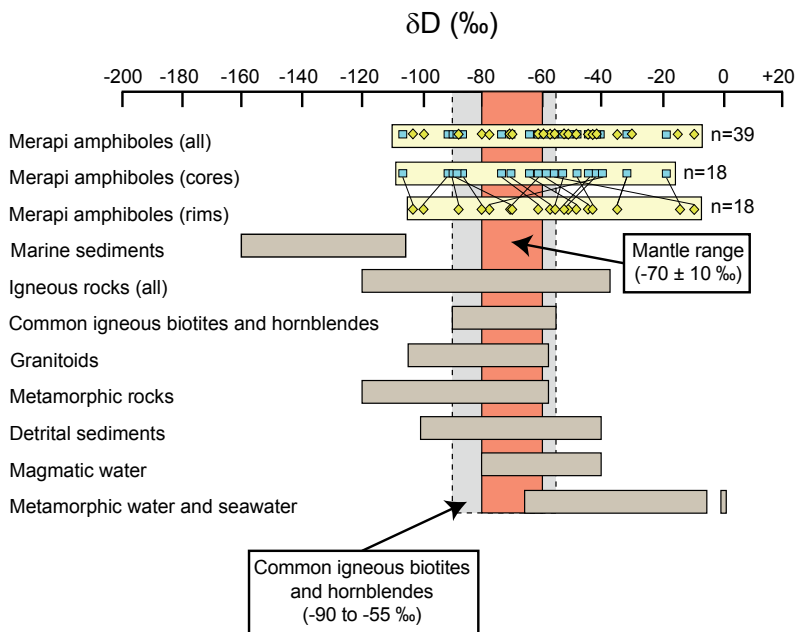


Fig. 8.9 Hydrogen (deuterium) isotopes from amphibole megacrysts in recent Merapi lavas (after Peters et al. 2017 and references therein). The extremely wide spread of recorded hydrogen isotope data is interpreted to reflect

originally magmatic amphiboles that crystallised at depth beneath Merapi, but experienced hydrogen loss and degassing during ascent and reheating within the polybaric Merapi plumbing system

1.5–2.5 km below the summit indicates the at least temporary existence of shallow magma storage pockets and reservoirs beneath Merapi (Wasserman et al. 1998; Ratdomopurbo and Poupinet 2000). In addition, recent tomographic efforts have identified a large reservoir anomaly in the crust and upper mantle beneath Merapi (Koulakov et al. 2007; Wagner et al. 2007; Widiyantoro et al. 2018), indicating that the magma supply system beneath the volcano is extensive. In particular, following the discussion in (Widiyantoro et al. 2018), an intermediate to high Vp/Vs anomaly is observed beneath Merapi in the upper to middle crust. This finding is broadly consistent with petrological information (Gertisser et al. 2011; Chadwick et al. 2013; Costa et al. 2013; van der Zwan et al. 2013; Erdmann et al. 2014, 2016; Borisova et al. 2016). Specifically, amphibole and clinopyroxene mineral barometry has been used to estimate the depth of Merapi's main pre-eruptive magma reservoirs (Chadwick et al. 2013; Costa et al. 2013; Nadeau et al. 2013; Preece et al. 2014; Deegan et al. 2016a; Peters et al. 2017). However, the reliability of some of these estimates has recently been questioned, especially those for amphibole megacrysts (Erdmann et al. 2014) and phase-equilibrium experiments (Erdmann et al. 2016) suggest that most magma erupted in 2010 (and possibly in other eruptions of the last ~ 100 years) was sourced from a depth of ~ 4 to 15 km. Unfortunately, these experiments suffer from uncertainties in pre-eruptive volatile content and the natural variations of exact starting compositions, and are thus associated with considerable uncertainties as well. For instance, although melt inclusion hygrometry and melt inclusion volatile contents imply magma storage depths of 6–14 km (e.g. Nadeau et al. 2013; Preece et al. 2014), pyroxene barometry and melt inclusion data in amphibole also show deeper values down to and even below 20 km depth (Nadeau et al. 2013; Preece et al. 2014; Deegan et al. 2016a). In contrast, GPS ground deformation data discussed in Widiyantoro et al. (2018) imply that the 1996–1997 eruptive magma was possibly sourced from a slightly shallower reservoir at c. 8.5 km below the

summit (cf. Beauducel and Cornet 1999; Widiyantoro et al. 2018). The main magma source depth inferred from petrological studies (4–6 and 10–20 km) thus partly overlaps with the uppermost part of the main tomographic anomaly at 10–20 km depth (e.g. Wagner et al. 2007; Widiyantoro et al. 2018; Lühr et al. 2023, Chap. 5), providing strong support for a main storage system in the mid-crust beneath Merapi. Notably, the clinopyroxene composition thermobarometry of Deegan et al. (2016a) puts the main mid-crustal reservoir at 9–21 km with a frequency peak at 16 km depth, in line with clinopyroxene compositional and melt inclusion barometry (Preece et al. 2014), and experimental approaches (Erdmann et al. 2016). A deeper reservoir has previously been suggested based on deep seated amphibole crystallisation pressures and inclusions in these amphiboles (Costa et al. 2013; Nadeau et al. 2013) and seems to coincide with a deep crustal/upper mantle reservoir system seen in tomographic data (Widiyantoro et al. 2018; Lühr et al. 2023, Chap. 5). This deep reservoir has recently been confirmed by the multi-method barometry approach on large amphibole megacrysts by (Peters et al. 2017), which imply that these crystals formed between 19 and 32 km and thus overlap with the deeper anomaly of (Lühr et al. 2013, 2023, Chap. 5; Widiyantoro et al. 2018).

8.5 Magma Storage and Origin of Inclusions and Xenolith Types

In subduction zone settings, primary mafic magma is generated in the mantle wedge (e.g. Sisson and Bronto 1998; Lühr et al. 2013) and initial modification of primary melts occurs in a MASH or deep crustal hot zones around the mantle-crust boundary (e.g. Hildreth and Moorbath 1988; Annen et al. 2006; Geiger et al. 2018). Following this stage, magma rises through a series of crustal arc reservoirs. In these crustal reservoirs, a number of magmatic processes take place, including magma mixing, degassing, (fractional) crystallisation and also crustal contamination (e.g. De

Paolo 1981; Gill 1981; Grove and Kinzler 1986; Hildreth and Moorbath 1988; Davidson and Tepley 1997; Izbekov et al. 2004; Davidson et al. 2007). Erupted enclaves, plutonic inclusions, and megacrysts are often used to provide a means to investigate the detailed processes and formation conditions of the varied crystallisation assemblages (Renzulli and Santi 1997; Dungan and Davidson 2004) and have frequently been identified as fractionation residues that reflect crustal residence and solidification processes (e.g. Beard and Borgia 1989; Costa and Singer 2002). Plutonic inclusions and megacrysts are often viewed as high-pressure crystallisation products from a range of pressure and temperature conditions that reflect earlier evolutionary episodes of erupted magmas at a particular volcano (e.g. Irving and Frey 1984; Dungan and Davidson 2004; Chadwick et al. 2013; Peters et al. 2017). These can thus provide us with a catalogue of evidence to establish sub-volcanic magma storage conditions and magmatic processes as well as magma-crust interaction processes that are operating in the Merapi plumbing system. Complemented by the crystal-rich nature of the Merapi lavas, we have a relatively detailed, albeit highly complex, record of crystallisation and crystal-liquid fractionation processes.

In simple terms, it appears that while large amphibole crystals and pyroxene in mafic enclaves originate dominantly in the upper mantle and lower crust, the dominant pyroxene growth occurs in the mid-crust (e.g. Preece et al. 2014; Deegan et al. 2016a). Plagioclase, in turn, forms in the mid to upper region of crust beneath Merapi and becomes the dominant mineral in the upper (sedimentary) portions of the crust directly beneath the volcano (e.g. Chadwick et al. 2013; Costa et al. 2013). In respect to the specific processes, “andesite in andesite” inclusions reveal mixing of variably crystallised basaltic-andesite magmas that mingled by either self-mixing within compositionally zoned reservoirs or pockets, e.g. mingling of different portions of a pocket (centre vs. rim) or by mixing and blending of andesitic magmas that evolved in different chambers or pockets (cf. Gertisser and Keller 2003a, b; Chadwick et al. 2013; Troll

et al. 2013; van der Zwan et al. 2013; Deegan et al. 2016a). Indeed, seismic and other geophysical investigations (see above) have by now identified several larger magma reservoirs or reservoir zones beneath Merapi and, moreover, raise the possibility of many smaller magma pockets and chambers at various levels beneath the volcano (cf. Widiyantoro and van der Hilst 1997; Ratdomopurbo and Poupinet 2000; Wagner et al. 2007; Nadeau et al. 2013; Widiyantoro et al. 2018; Lühr et al. 2023; Chap. 5). The basaltic enclaves, in turn, support mafic recharge processes, in line with the commonly complex zoning in feldspar crystals in the erupted basaltic-andesites. These show strong drops in Ca content between successive internal zones that are often associated with disequilibrium textures (e.g. Chadwick et al. 2007). The basaltic enclaves together with the complex plagioclase crystal zoning suggest mafic magma recharge even into the high-level plumbing system, and recharge thus appears as an integral process in Merapi’s sub-volcanic plumbing system (e.g. Gertisser and Keller 2003b; Chadwick et al. 2007; Costa et al. 2013). A key realisation from this is that fresh mafic magma is at times present beneath Merapi (cf. Chadwick et al. 2013; Troll et al. 2013; van der Zwan et al. 2013), although it may not erupt very frequently due to the density filter of the andesite-dominated plumbing system. The plutonic inclusions and amphibole megacrysts, in turn, support a major role of magma storage and crystal fractionation in several storage levels (or holding reservoirs) beneath the volcano. Notably, the pyroxenes in the plutonic inclusions and lavas are from broadly mid-crustal depths (e.g. Chadwick et al. 2013; Preece et al. 2014; Deegan et al. 2016a), whereas the amphibole megacrysts are from lower crustal regions of some 19–32 km depth (cf. Nadeau et al. 2013; Peters et al. 2017), i.e. in the lowermost crust and the uppermost mantle (see also Costa et al. 2013; Erdmann et al. 2014; Wölbern and Rumpker 2016), implying intense crystallisation of hydrous melts at variable depth. In this context, gabbros and diorites are dominantly lower to mid-crustal solidification products (Chadwick et al. 2013), in line with their magmatic isotope signatures. Although

megacrysts and plutonic inclusions clearly highlight deep crystal-liquid fractionation processes, they also underline an important role for recycling of previously solidified products within the Merapi plumbing system. This means that in addition to crystal growth in the basaltic-andesite magmas, a portion of crystals in Merapi lava is likely “crystal cargo”, i.e. antecrysts (earlier crystals) instead of true phenocrysts grown from the groundmass in which they reside (e.g. Beard and Borgia 1989; Davidson et al. 2005; Chadwick et al. 2007).

The non-igneous (meta-sedimentary) calc-silicate inclusions found in Merapi deposits are “true crustal xenoliths” and derive from the interaction of the sedimentary upper crust in the top 10 km beneath the volcano (see Deegan et al. 2023, Chap. 10). The relative abundance of skarn xenoliths amongst the erupted Merapi products suggests ongoing interaction between shallow magma batches and the limestone country rock that is found down to a depth of ca 10 km in the crust (see Chadwick et al. 2007). The common calc-silicate xenoliths also testify to intense crustal degassing (e.g. Deegan et al. 2010, 2011; Troll et al. 2012, 2013; Whitley et al. 2019), which appears to leave a compositional imprint on the host magmas as seen in, for example, elevated Sr and O isotopes in whole rock lavas and within plagioclase crystal zones, as well as in elevated C and He isotope ratios in high-T fumarole gas (e.g. Hilton and Craig 1989; Chadwick et al. 2007; Borisova et al. 2013, 2016; Troll et al. 2012, 2013; Aiuppa et al. 2017; Gertisser et al. 2023, Chap. 6). A realisation from the frequent calc-silicate inclusions in the Merapi lavas is that volatile constituents at Merapi may be highly variable at times, e.g. prior to or during an eruption (Deegan et al. 2011; Troll et al. 2012; Carr et al. 2018; Whitley et al. 2019). This is because reaction of limestone and magma to diopside + wollastonite assemblages releases CO₂ [CaCO_3 (limestone) + SiO₂ (silica) = CaSiO₃ (wollastonite) + CO₂] and the liberated CO₂ is not redissolved, but will temporarily modify the magmatic volatile budget (e.g. Deegan et al. 2010, 2023, Chap. 10; Troll et al. 2012).

8.6 An Integrated Model for Merapi’s Plumbing System

The petrography and geochemistry, and particularly the isotope data of the host lavas and igneous inclusions summarised above underline that most of the inclusions are petrogenetically linked to the Merapi magma system, i.e. they are for most parts cognate. It is therefore possible to use the intrinsic conditions of their formation to describe stages of evolution and levels of storage in Merapi’s magma supply system to complement the information recorded in the Merapi host lavas. Specifically, plutonic igneous inclusions in arc lavas have previously been interpreted to reflect residues of differentiation processes that have operated within the magma plumbing systems of such arc volcanoes (e.g. Beard 1986; Beard and Borgia 1989; Costa and Singer 2002). While the bulk rock compositions of plutonic rocks vary significantly, e.g. due to crystal accumulation and melt migration, the mineral compositions present usually reflect their formation depth. Pyroxene from basaltic enclaves, and pyroxene and plagioclase from the plutonic inclusions largely plot within the compositional reference fields for Merapi basaltic-andesite crystals. The plutonic inclusions, however, possess a relatively large spread in plagioclase compositions, extending up to An₉₅ (e.g. Chadwick et al. 2013). This highly calcic feldspar may be a function of high H₂O contents in a deep crystalline mush (cf. Tepley et al. 2006), which is supported by the presence of significant amounts of amphibole in some of the plutonic inclusions. Alternatively, the high Ca in a portion of the plagioclase crystals may be due to a dominance of mafic liquids with high Ca/Na at depth within the Merapi plumbing system (e.g. Borisova et al. 2016). Finally, high Ca plagioclase xenocrysts from skarn xenoliths or grown from liquids contaminated by the carbonate country rock, may also be present (e.g. Chadwick et al. 2007; Deegan et al. 2010). The lower Ca plagioclase, in turn, reflects shallower growth and underlines the presence of more evolved magma compositions in the upper portions of the

Merapi system (mid and upper crust mainly; Chadwick et al. 2013; Costa et al. 2013; Preece et al. 2014). The shallow storage system likely consists of a plexus of potentially ephemeral, partly solidified, crystal-rich (semi-molten) and locally fully molten magma reservoirs and/or pockets (e.g. Ratdomopurbo and Poupinet 2000; Chadwick et al. 2013; Nadeau et al. 2013; Preece et al. 2013, 2016) with remnants of former crust in-between pockets (Troll et al. 2013). Intrusions of mafic magmas into more fractionated and partly crystalline magma and mush-filled pockets then results in frequent remobilisation of highly crystalline resident mushes and magmas and makes it possible for magmas to mingle, producing lavas with mafic enclaves and highly-crystalline “andesite in andesite” schlieren. Further support for magma mixing and mingling in the Merapi plumbing system is found in the plagioclase sieve textures in the basaltic-andesite host and magma recharge and reheating processes that play a crucial role in helping to initiate Merapi’s surface eruptions (e.g. Chadwick et al. 2007, 2013; Costa et al. 2013).

A comparison of the crystallisation pressures obtained in petrological studies (e.g. Chadwick et al. 2013; Costa et al. 2013; Nadeau et al. 2013; Erdmann et al. 2014, 2016; Preece et al. 2014; Deegan et al. 2016a; Peters et al. 2017) with geophysical (mainly seismic) data (e.g. Ratdomopurbo and Poupinet 2000; Koulakov et al. 2007; Wagner et al. 2007; Lühr et al. 2013; Widiyantoro et al. 2018; Lühr et al. this issue) shows a link between seismic anomalies in the mid- and shallow crust beneath Merapi and the dominantly mid-crustal crystallisation pressures obtained by various petrological studies. These results are complemented by a smaller number of shallower pressure estimates from melt inclusions (e.g. Nadeau et al. 2013; Preece et al. 2014) and from pyroxene in felsic plutonic inclusions (Chadwick et al. 2013). Consistent with the occurrence of mixed basaltic-andesite schlieren of highly variable crystallinities and the smaller number of low crystallisation pressures obtained, late (upper crustal) crystallisation likely occurs in many small, possibly ephemeral magma pockets in the shallow crust prior to eruption. However,

using the available geobarometric data range, and imaged as anomalous with geophysical methods beneath Merapi (Koulakov et al. 2007; Wagner et al. 2007; Costa et al. 2013; Lühr et al. 2013; Preece et al. 2014; Deegan et al. 2016a; Widiyantoro et al. 2018), the main magma storage system that will control larger eruptions is located at mid-crustal level, broadly from ~ 10 to 20 km. The geochemical, petrological, and geobarometric data combined with the geophysical constraints further support the presence of a mafic to ultramafic lower crustal reservoir or “deep crustal hot zone”, as megacrysts and mafic enclave lithologies found in the erupted lavas argue for gradual recycling of the deepest plutonic roots of the Merapi magmatic system (cf. Dungan and Davidson 2006; Davidson et al. 2007; Reubi and Blundy 2008; Nadeau et al. 2013; Peters et al. 2017).

Based on the combined results from petrology, mineralogy, major and trace element studies, isotope geochemistry, and geophysical constraints, we thus argue that Merapi is fed by a multi-level magma supply system that includes (i) a deep storage level in the upper mantle and lower crust (a deep crustal ‘hot zone’) located below 20 km depth, likely at 25 to 35 km below the summit (cf. Annen et al. 2006; Costa et al. 2013; Nadeau et al. 2013; Peters et al. 2017; Widiyantoro et al. 2018), (ii) a mid-crustal storage level, which represents the main volume of eruptible magma located at ca 10–20 km depth (e.g. Chadwick et al. 2013; Costa et al. 2013; Preece et al. 2014; Erdmann et al. 2016; Deegan et al. 2016a; Widiyantoro et al. 2018), and (iii) a shallow-level storage region or chamber in the upper arc crust at < 5 km, c. 2–4 km depth (a SHARC zone, cf. Ratdomopurbo and Poupinet 2000; Chadwick et al. 2013; Preece et al. 2013, 2014, 2016; Adam et al. 2016; Geiger et al. 2018; Deegan et al. 2019). The uppermost reservoir system is smaller in volume compared to the other two major storage reservoirs and likely comprises a series of transient smaller chambers or pockets (e.g. Chadwick et al. 2013; Nadeau et al. 2013; Widiyantoro et al. 2018).

This overall magma supply arrangement at Merapi likely plays a considerable role in

Merapi's propensity for sudden explosive behaviour. The multi-chambered, plumbing system that feeds Merapi has considerable long-term implications for hazard assessment. Although Merapi volcano may represent a relatively small surface expression, a much larger magmatic system is present at depth. Multiple chambered systems have recently been proposed for a number of subduction zone volcanoes in the wider region (e.g. Price et al. 2005; Jaxybulatov et al. 2011; Dahren et al. 2012; Cashman et al. 2017; Geiger et al. 2018; Deegan et al. 2019), and given the long-lived nature of Merapi volcanism, it is sensible to conclude that a significant mass of crystalline material has accumulated in the crust below the volcano. The varied mineral compositions and inclusions contained in the Merapi lavas demonstrate that this material is regularly recycled into ascending magmas and can thus indicate dormant magma can be mobilised by e.g. new recharge events (cf. Izbekov et al. 2004; Troll et al. 2013). Given the mid- to lower crustal level of large-volume magma storage at Merapi, indicated by the combined geobarometric and geophysical studies, it is integral that deep seismic activity is continuously and routinely monitored to better understand the relationships between primitive magma replenishment and eruptions to improve timely warning in case activity in the mid-crustal storage system is triggered. In conjunction with geophysical data, there is also strong petrological evidence for the presence of upper-crustal magma pockets and reservoirs that contain semi-molten crystalline mush, which can then also be activated due to activity from depth. This uppermost storage level has implications for magma chemistry and the volatile budget of the magma, as assimilation of mid- to shallow level carbonates may at times be significant when fresh magma enters 10 km of the crust (Deegan et al. 2011, 2023, Chap. 10; Whitley et al. 2019, 2020). Importantly, these shallow pockets can initiate smaller and largely unexpected, possibly explosive, eruptions without deep seismicity, e.g. through gas oversaturation in individual pockets, gas liberation from assimilated limestone basement, or from shaking

up by regional earthquakes (see Deegan et al. 2019).

8.7 Magma Storage Along the Java-Bali Segment of the Sunda Arc

Mineral barometry on plagioclase, pyroxene, and amphibole has recently become available from an increasing number of volcanic centres along the Java-Bali segment of the Sunda arc, including Anak-Krakatau volcano, Gede volcano, Merapi volcano, and Kelut volcano (e.g. Handley et al. 2010; Dahren et al. 2012; Chadwick et al. 2013; Jeffery et al. 2013; Geiger et al. 2018). These crystallisation depths inferred by petrological means can be compared to the results of geophysical investigations carried out in Java such as seismic, magnetotelluric and long-offset transient electromagnetic experiments (e.g. at Anak-Krakatau, Merapi and Lawu volcanoes). These latter studies imply frequent aseismic zones situated at 1.5–2.5 km depth at these volcanoes, indicating the existence of shallow magma reservoirs with likely regular magma supply from deeper levels (Ratdomopurbo and Poupinet 2000; Wegler and Lühr 2001; Müller et al. 2002; Müller and Haak 2004; Jaxybulatov et al. 2011). In addition, most recently, ground displacements via InSAR measurements on six volcanoes along the Sunda arc (Sinabung and Kerinci in Sumatra, and Slamet, Lawu, Lomongan on Java and Agung on Bali), detected shallow magma reservoirs at ~ 1 to 3 km depth (Chaussard and Amelung 2014), which the authors relate to extensional and strike-slip settings caused by the intra-arc stress regime. Shallow magma storage is hence increasingly detected with both petrological and independent geophysical methods along the Sunda arc (see Geiger et al. 2018; Deegan et al. 2019, 2021) and the available studies thus point to complex supply systems feeding these volcanoes, involving multi-stage magma storage in the crust prior to eruption at the surface (Fig. 8.10). This realisation is furthermore consistent with circumstantial geological and petrochemical information at Merapi, such as crystal size distribution (CSD), and melt inclusion

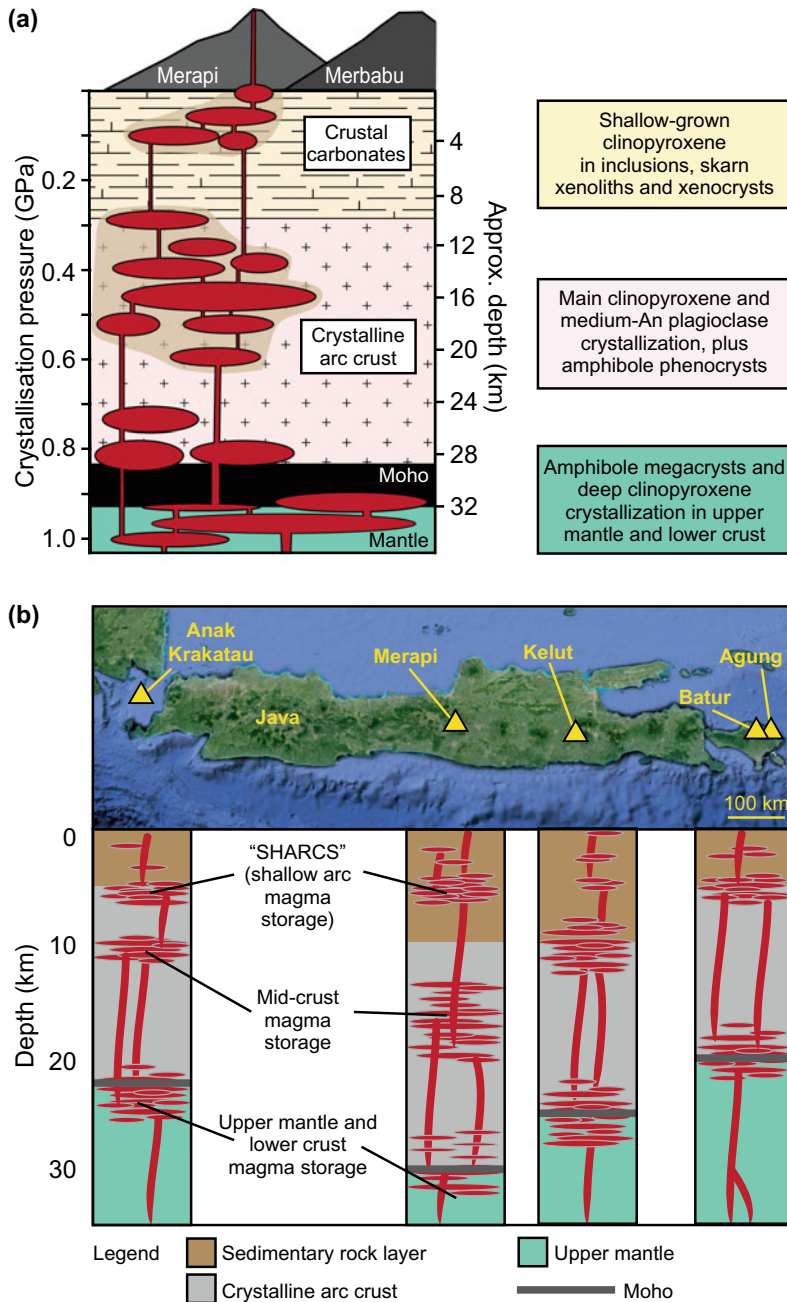


Fig. 8.10 **a** Schematic plumbing system of Merapi (modified after Deegan et al. 2016a). Shown is (i) a deep upper mantle/lower crustal storage area recorded through e.g. amphibole megacrysts, some deep clinopyroxene and perhaps some high An plagioclase cores, (ii) a mid-crustal storage region recorded through the bulk of the clinopyroxene crystals in lavas and inclusions and (iii) an upper crustal storage region documented through some shallow grown clinopyroxene in felsic plutonic inclusions, low An plagioclase with crustal signatures, and abundant calc-

silicate xenoliths. **b** Schematic illustration of magma plumbing in the Java and Bali region (modified after Deegan et al. 2019). Multi-level magma storage has recently been proposed for Anak Krakatau (Sunda Strait), Merapi (Central Java), Kelut (East Java), and Agung and Batur (Bali) based on petrological data and geophysical approaches (see also Geiger et al. (2018) and Deegan et al. (2019, 2021)). Notably, there seems to be ubiquitous shallow arc storage chambers (SHARCS) throughout the region

studies that indirectly support polybaric crustal magma storage (e.g. Innocenti et al. 2013; Preece et al. 2013, 2014, 2016; van der Zwan et al. 2013; Preece et al. 2023, Chap. 9).

The concept of polybaric storage beneath the Sunda arc volcanoes has thus led to recent propositions of ‘shallow crustal cold zones’ or ‘shallow arc storage’ (SHARCS; Deegan et al. 2019) as a major source of intermediate to felsic magmas in arcs (e.g. Gardner et al. 2013; Adam et al. 2016; Cashman et al. 2017; Deegan et al. 2019) in addition to the widely accepted deep crustal hot zones (e.g. Annen et al. 2006). Not only does it seem that such upper crustal storage zones are more widespread in arc settings than previously thought (Fig. 8.10), they are probably also critical for the final ‘eruptive conditioning’ of magma prior to eruption (Gardner et al. 2013; Adam et al. 2016; Cassidy et al. 2016; Geiger et al. 2018). Specifically, the consistency of results from diverse methods in favour of shallow-level storage in the Sunda arc provides a plausible link between magma ascent and the relatively widespread evidence for late-stage (shallow-level) crustal differentiation and assimilation in many Sunda arc volcanoes (Borisova et al. 2013, 2016; Innocenti et al. 2013; Gardner et al. 2013; Jeffery et al. 2013; Geiger et al. 2018). Shallow magma storage likely facilitates favourable conditions for magma differentiation, which in turn, drives magma evolution to more felsic compositions. These shallow storage or holding reservoirs may also act as sites for intense magma degassing due to, e.g. crystal fractionation, replenishing magmas that experience low volatile solubilities at shallow crustal levels, or from crustal volatile additions that cannot be dissolved in the magma at these low pressures (e.g. Deegan et al. 2019). The shallow depth of these reservoirs may provide limited advanced warning before eruption, as was recently the case for Kelut volcano in East Java in February 2014, or the outburst of Merapi in spring 2018. For instance, after only a few days of unrest, Kelut erupted violently from an upper crustal magma reservoir in early 2014 over the course of a few hours (Cassidy et al. 2016). The intensity of the 2014 Kelut eruption, with its

exclusively shallow and short-lived seismic warning interval, underlines the hazardous nature of shallow magma reservoirs in Sunda arc plumbing systems and is most probably relevant for many active Javanese stratovolcanoes.

8.8 Summary and Outlook

The petrology and geochemistry of magmatic enclaves, plutonic inclusions and megacrysts are useful for better constraining the petrogenesis within, and the structure of, the Merapi plumbing system. The plutonic inclusions, enclaves and schlieren provide evidence for a complex, multi-tiered, and open plumbing system feeding Merapi with mixing, mingling, crystallisation, crystal accumulation, crustal contamination, and periodical recharges, all being frequent processes at work. This record of magmatic evolution is only poorly preserved in the relatively homogenised host basaltic-andesite lavas, but is recorded in minerals and plutonic and crustal inclusions, and must be taken into account when assessing petrology at Merapi and elsewhere. Indeed, minerals and inclusions in recent Merapi lavas record a complex evolution that can only be fully explained by (i) a larger deep crustal reservoir, analogous to a crustal hot zone, (ii) a mid-crustal reservoir zone where most of the magma evolution from basalt to andesite takes place, and (iii) an upper crustal concentration of small chambers or pockets that may be regarded as an andesitic magma reservoir zone, where final differentiation through extensive plagioclase crystallisation takes place. These pockets likely contain large portions of crystal mush and appear to evolve somewhat independently from each other. Recharge with more mafic magma provides many opportunities to recycle the magmatic crystalline products of these pockets as well as provides the heat to interact with the surrounding crustal lithologies. These SHARC-type crustal reservoirs produce crystal-rich magmas with abundant crystal- and lithics-cargo (plutonic and crustal xenoliths and antecrysts and xenocrysts). As frequently seen in andesite-type stratovolcanoes elsewhere in Java and the Sunda

arc, multi-level (polybaric) plumbing systems are likely a common feature in Indonesian andesite volcanoes, posing risks for long-lived (weeks to months) eruptions fed from depth, but also for rapid and short-lived explosive events (days) that are conditioned by magma evolution and magma-crust interaction in upper crustal magma pockets, chambers, and smaller reservoirs.

Acknowledgements We are grateful to L.S. Blythe, A. Borisova, J.P. Chadwick, B. Dahrén, H. Damarvan, J. Gamble, R. Gertisser, H. Handley, H. Humaida, E.M. Jolis, I. Koulakov, B. Lühr, I. Made, L.M. Schwarzkopf, C. Martel, S. Peters, K. Preece, F. van der Zwan, T.R. Walter, and D. Wagner for constructive discussion on Merapi and its inner workings. We also thank N. Sharaf Aldeen, N. Seraphine and A. Pawar for help during preparation of the manuscript and R. Gertisser, T.E. Waight, and B. Lühr for thoughtful reviews of our manuscript. This work was supported by the European Research Council (ERC), the Swedish Research Council (VR), the Royal Swedish Academy of Science (KVA), and the Swedish Centre for Natural Hazards and Disaster Science (CNDS).

References

- Adam J, Turner S, Rushmer T (2016) The genesis of silicic arc magmas in shallow crustal cold zones. *Lithos* 264:472–494
- Aiuppa A, Fischer TP, Plank T, Robidoux P, Di Napoli R (2017) Along-arc, inter-arc and arc-to-arc variations in volcanic gas CO_2/S_T ratios reveal dual source of carbon in arc volcanism. *Earth Sci Rev* 168:24–47
- Andreastuti SD, Alloway BV, Smith IEM (2000) A detailed tephrostratigraphic framework at Merapi Volcano, Central Java, Indonesia: implications for eruption predictions and hazard assessment. *J Volcanol Geotherm Res* 100:51–67
- Annen C, Blundy JD, Sparks RSJ (2006) The genesis of intermediate and silicic magmas in deep crustal hot zones. *J Petrol* 47:505–539
- Baker DR (2008) The fidelity of melt inclusions as records of melt composition. *Contrib Mineral Petrol* 156:377–395
- Bacon CR (1986) Magmatic inclusions in silicic and intermediate volcanic rocks. *J Geophys Res (Solid Earth)* 91:6091–6112
- Beard JS (1986) Characteristic mineralogy of arc-related cumulate gabbros: implications for the tectonic setting of gabbroic plutons and for andesite genesis. *Geology* 14:848–851
- Beard JS, Borgia A (1989) Temporal variation of mineralogy and petrology in cognate gabbroic enclaves at Arenal volcano, Costa Rica. *Contrib Mineral Petrol* 103:110–122
- Beauducel F, Cornet FH (1999) Collection and three-dimensional modeling of GPS and tilt data at Merapi volcano, Java. *J Geophys Res (Solid Earth)* 104: 725–736
- Blythe LS, Deegan FM, Freda C, Jolis EM, Masotta M, Misiti V, Taddeucci J, Troll VR (2015) CO_2 bubble generation and migration during magma–carbonate interaction. *Contrib Mineral Petrol* 169:42
- Balsley SD, Gregory RT (1998) Low- $\delta^{18}\text{O}$ silicic magmas: why are they so rare? *Earth Planet Sci Lett* 162:123–136
- Borisova AY, Martel C, Gouy S, Pratomo I, Sumarti S, Toutain JP, Bindeman IN, de Parseval P, Métaxian JP, Surono (2013) Highly explosive 2010 Merapi eruption: evidence for shallow-level crustal assimilation and hybrid fluid. *J Volcanol Geotherm Res* 261:193–208
- Borisova AY, Gurenko AA, Martel C, Kouzmanov K, Cathala A, Bohrsen WA, Pratomo I, Sumarti S (2016) Oxygen isotope heterogeneity of arc magma recorded in plagioclase from the 2010 Merapi eruption (Central Java, Indonesia). *Geochim Cosmochim Acta* 190:13–34
- Bowen NL (1928) *The origin of igneous rocks*. Princeton University Press
- Brown SK, Auker MR, Sparks RSJ (2015) Populations around Holocene volcanoes and development of a Population Exposure Index. In: Loughlin SC, Sparks RSJ, Brown SK, Jenkins SF, Vye-Brown C (eds) *Global volcanic hazards and risk*. Cambridge University Press, Cambridge, pp 223–232
- Budi-Santoso A, Lesage P, Dwiyo S, Sumarti S, Subandriyo, Surono, Jousset P, Metaxian J-P (2013) Analysis of the seismic activity associated with the 2010 eruption of Merapi volcano, Java. *J Volcanol Geotherm Res* 261:153–170
- Burt RM, Brown SJA, Cole JW, Shelley D, Waight TE (1998) Glass-bearing plutonic fragments from ignimbrites of the Okataina caldera complex, Taupo Volcanic Zone, New Zealand: remnants of a partially molten intrusion associated with preceding eruptions. *J Volcanol Geotherm Res* 84:209–237
- Budd DA, Troll VR, Deegan FM, Jolis EM, Smith VC, Whitehouse MJ, Harris C, Freda C, Hilton DR, Halldórsson SA, Bindeman IN (2017) Magma reservoir dynamics at Toba caldera, Indonesia, recorded by oxygen isotope zoning in quartz. *Sci Rep* 7:40624
- Camus G, Gourgaud A, Mossand-Berthommier PC, Vincent PM (2000) Merapi (Central Java, Indonesia): an outline of the structural and magmatological evolution, with a special emphasis to the major pyroclastic events. *J Volcanol Geotherm Res* 100:139–163
- Carr BB, Clarke AB, Vitturi MDM (2018) Earthquake induced variations in extrusion rate: a numerical modeling approach to the 2006 eruption of Merapi Volcano (Indonesia). *Earth Planet Sci Lett* 482:377–387
- Cassidy M, Castro JM, Helo C, Troll VR, Deegan FM, Muir D, Neave DA, Mueller SP (2016) Volatile dilution during magma injections and implications for volcano explosivity. *Geology* 44:1027–1030

- Cashman KV, Sparks RSJ, Blundy JD (2017) Vertically extensive and unstable magmatic systems: a unified view of igneous processes. *Science* 355:3055
- Chadwick JP, Troll VR, Ginibre C, Morgan D, Gertisser R, Waight TE, Davidson JP (2007) Carbonate assimilation at Merapi Volcano, Java, Indonesia: insights from crystal isotope stratigraphy. *J Petrol* 48:1793–1812
- Chadwick JP, Troll VR, Waight TE, van der Zwan FM, Schwarzkopf LM (2013) Petrology and geochemistry of igneous inclusions in recent Merapi deposits: a window into the sub-volcanic plumbing system. *Contrib Mineral Petrol* 165:259–282
- Charbonnier SJ, Gertisser R (2008) Field observations and surface characteristics of pristine block-and-ash flow deposits from the 2006 eruption of Merapi Volcano, Java, Indonesia. *J Volcanol Geotherm Res* 177:971–982
- Chaussard E, Amelung F (2014) Regional controls on magma ascent and storage in volcanic arcs. *Geochem Geophys Geosyst* 15:1407–1418
- Costa F, Singer B (2002) Evolution of Holocene dacite and compositionally zoned magma, Volcán San Pedro, southern volcanic zone, Chile. *J Petrol* 43:1571–1593
- Costa F, Andreastuti S, de Maisonneuve CB, Pallister JS (2013) Petrological insights into the storage conditions, and magmatic processes that yielded the centennial 2010 Merapi explosive eruption. *J Volcanol Geotherm Res* 261:209–235
- Coombs ML, Eichelberger JC, Rutherford MJ (2003) Experimental and textural constraints on mafic enclave formation in volcanic rocks. *J Volcanol Geotherm Res* 119:125–144
- Curry JR, Shor GG, Raitt RW, Henry M (1977) Seismic refraction and reflection studies of crustal structure of the eastern Sunda and western Banda arcs. *J Geophys Res* 82:2479–2489
- Dahren B, Troll VR, Andersson UB, Chadwick JP, Gardner MF, Jaxybulatov K, Koulakov I (2012) Magma plumbing beneath Anak Krakatau volcano, Indonesia: evidence for multiple magma storage regions. *Contrib Mineral Petrol* 163:631–651
- Darmawan H, Walter TR, Troll VR, Budi-Santoso A (2018) Structural weakening of the Merapi dome identified by drone photogrammetry after the 2010 eruption. *Nat Haz Earth System Sci* 18:3267–3281
- Davidson JP, Tepley FJ (1997) Recharge in volcanic systems: evidence from isotope profiles of phenocrysts. *Science* 275:826–829
- Davidson JP, Hora JM, Garrison JM, Dungan MA (2005) Crustal forensics in arc magmas. *J Volcanol Geotherm Res* 140:157–170
- Davidson JP, Turner S, Handley H, Macpherson C, Dosseto A (2007) Amphibole “sponge” in arc crust? *Geology* 35:787–790
- Deegan FM, Troll VR, Freda C, Misiti V, Chadwick JP (2011) Fast and furious: crustal CO₂ release at Merapi volcano, Indonesia. *Geol Today* 27:63–64
- Deegan FM, Troll VR, Freda C, Misti V, Chadwick JP, McLeod CL, Davidson JP (2010) Magma-carbonate interaction processes and associated CO₂ release at Merapi volcano, Indonesia: insights from experimental petrology. *J Petrol* 51:1027–1051
- Deegan FM, Whitehouse MJ, Troll VR, Budd DA, Harris C, Geiger H, Hålenius U (2016a) Pyroxene standards for SIMS oxygen isotope analysis and their application to Merapi volcano, Sunda arc, Indonesia. *Chem Geol* 447:1–10
- Deegan FM, Troll VR, Whitehouse MJ, Jolis EM, Freda C (2016b) Boron isotope fractionation in magma via crustal carbonate dissolution. *Sci Rep* 6:30774
- Deegan FM, Troll VR, Geiger H (2019) Forensic probe of Bali’s great volcano. *Eos. Trans Am Geophys Union* 100:26–30
- Deegan FM, Whitehouse MJ, Troll VR, Geiger H, Jeon H, le Roux P, Harris C, van Helden M, González-Maurel O (2021) Sunda arc mantle source $\delta^{18}\text{O}$ value revealed by intracrystal isotope analysis. *Nat Commun* 12:3930
- Deegan FM, Troll VR, Gertisser R, Freda C (2023) Magma-carbonate interaction at Merapi volcano, Indonesia. In: Gertisser R, Troll VR, Walter TR, Nandaka IGM, Ratdomopurbo A (eds) *Merapi volcano—geology, eruptive activity, and monitoring of a high-risk volcano*. Springer, Berlin, Heidelberg, pp 291–321
- De Paolo DJ (1981) A neodymium and strontium isotopic study of the Mesozoic calc-alkaline granitic batholiths of the Sierra Nevada and Peninsular Ranges, California. *J Geophys Res (solid Earth)* 86:10470–10488
- Dungan MA, Davidson J (2004) Partial assimilative recycling of the mafic plutonic roots of arc volcanoes: An example from the Chilean Andes. *Geology* 32:773–776
- Donovan K, Suharyanto A (2011) The creatures will protect us. *Geoscientist* 21:12–17
- Eiler JM (2001) Oxygen isotope variations of basaltic lavas and upper mantle rocks. *Rev Mineral Geochem* 43:319–364
- Erdmann S, Martel C, Pichavant M, Kushnir A (2014) Amphibole as an archivist of magmatic crystallization conditions: problems, potential, and implications for inferring magma storage prior to the paroxysmal 2010 eruption of Mount Merapi, Indonesia. *Contrib Mineral Petrol* 167:1016
- Erdmann S, Martel C, Pichavant M, Bourdier JL, Champallier R, Komorowski JC, Cholik N (2016) Constraints from phase equilibrium experiments on pre-eruptive storage conditions in mixed magma systems: a case study on crystal-rich basaltic andesites from Mount Merapi, Indonesia. *J Petrol* 57:535–560
- Feeley TC, Sharp ZD (1996) Chemical and hydrogen isotope evidence for in situ dehydrogenation of biotite in silicic magma chambers. *Geology* 24:1021–1024
- Fulignati P, Marianelli P, Santacroce R, Sbrana A (2004) Probing the Vesuvius magma chamber–host rock interface through xenoliths. *Geol Mag* 141:417–428
- Garcia MO, Jacobson SS (1979) Crystal clots, amphibole fractionation and the evolution of calc-alkaline magmas. *Contrib Mineral Petrol* 69:319–327

- Gardner MF, Troll VR, Gamble JA, Gertisser R, Hart GL, Ellam RM, Harris C, Wolff JA (2013) Crustal differentiation processes at Krakatau Volcano, Indonesia. *J Petrol* 54:149–182
- Geiger H, Troll VR, Jolis EM, Deegan FM, Harris C, Hilton DR, Freda C (2018) Multi-level magma plumbing at Agung and Batur volcanoes increases risk of hazardous eruptions. *Sci Rep* 8:10547
- Gertisser R, Keller J (2003a) Trace element and Sr, Nd, Pb and O isotope variations in medium-K and high-K volcanic rocks from Merapi Volcano, Central Java, Indonesia: evidence for the involvement of subducted sediments in Sunda Arc magma genesis. *J Petrol* 44:457–489
- Gertisser R, Keller J (2003b) Temporal variations in magma composition at Merapi Volcano (Central Java, Indonesia): magmatic cycles during the past 2000 years of explosive activity. *J Volcanol Geotherm Res* 123:1–23
- Gertisser R, Charbonnier SJ, Troll VR, Keller J, Preece K, Chadwick JP, Barclay J, Herd RA (2011) Merapi (Java, Indonesia): anatomy of a killer volcano. *Geol Today* 27:57–62
- Gertisser R, del Marmol M-A, Newhall C, Preece K, Charbonnier S, Andreastuti S, Handley H, Keller J (2023) Geological history, chronology and magmatic evolution of Merapi. In: Gertisser R, Troll VR, Walter TR, Nandaka IGMA, Ratdomopurbo A (eds) Merapi volcano—geology, eruptive activity, and monitoring of a high-risk volcano. Springer, Berlin, Heidelberg, pp 137–193
- Gill JB (1981) What is “Typical Calcalkaline Andesite”? Orogenic andesites and plate tectonics. Springer, Berlin, Heidelberg 1–12
- Grove TL, Kinzler RJ (1986) Petrogenesis of andesites. *Ann Rev Earth Planet Sci* 14:417–454
- Handley HK, Macpherson CG, Davidson JP (2010) Geochemical and Sr–O isotopic constraints on magmatic differentiation at Gede Volcanic Complex, West Java, Indonesia. *Contrib Mineral Petrol* 159:885–908
- Hamilton WB (1979) Tectonics of the Indonesian region. US Govt. Print. Office No. 1078
- Hammer JE, Cashman KV, Voight B (2000) Magmatic processes revealed by textural and compositional trends in Merapi dome lavas. *J Volcanol Geotherm Res* 100:165–192
- Harijoko A, Marliyani GI, Wibowo HE, Freski YR, Handini E (2023) The geodynamic setting and geological context of Merapi volcano in Central Java, Indonesia. In: Gertisser R, Troll VR, Walter TR, Nandaka IGMA, Ratdomopurbo A (eds) Merapi volcano—geology, eruptive activity, and monitoring of a high-risk volcano. Springer, Berlin, Heidelberg, pp 89–109
- Hilton DR, Craig H (1989) A helium isotope transect along the Indonesian archipelago. *Nature* 342:906–908
- Hildreth W, Moorbath S (1988) Crustal contributions to arc magmatism in the Andes of central Chile. *Contrib Mineral Petrol* 98:455–489
- Holmberg K (2023) Merapi and its dynamic ‘disaster culture’. In: Gertisser R, Troll VR, Walter TR, Nandaka IGMA, Ratdomopurbo A (eds) Merapi volcano—geology, eruptive activity, and monitoring of a high-risk volcano. Springer, Berlin, Heidelberg, pp 67–87
- Holness MB, Tegner C, Nielsen TFD, Stripp G, Morse SA (2007a) A textural record of solidification and cooling in the Skaergaard intrusion, East Greenland. *J Petrol* 48:2359–2377
- Holness MB, Anderson AT, Martin VM, MacLennan J, Passmore E, Schwindinger K (2007b) Textures in partially solidified crystalline nodules: a window into the pore structure of slowly cooled mafic intrusions. *J Petrol* 48:1243–1264
- Innocenti S, Andreastuti S, Furman T, del Marmol MA, Voight B (2013) The pre-eruption conditions for explosive eruptions at Merapi volcano as revealed by crystal texture and mineralogy. *J Volcanol Geotherm Res* 261:69–86
- Irving AJ, Frey FA (1984) Trace element abundances in megacrysts and their host basalts: constraints on partition coefficients and megacryst genesis. *Geochim Cosmochim Acta* 48:1201–1221
- Ito E, White WM, Göpel C (1987) The O, Sr, Nd and Pb isotope geochemistry of MORB. *Chem Geol* 62:157–176
- Izbekov PE, Eichelberger JC, Ivanov BV (2004) The 1996 eruption of Karymsky volcano, Kamchatka: historical record of basaltic replenishment of an andesite reservoir. *J Petrol* 45:2325–2345
- Jarrard RD (1986) Terrane motion by strike-slip faulting of forearc slivers. *Geology* 14:780–783
- Jaxybulatov K, Koulakov I, Ibs-von Seht M, Klinge K, Reichert C, Dahren B, Troll VR (2011) Evidence for high fluid/melt content beneath Krakatau volcano (Indonesia) from local earthquake tomography. *J Volcanol Geotherm Res* 206:96–105
- Jeffery AJ, Gertisser R, Troll VR, Jolis EM, Dahren B, Harris C, Tindle AG, Preece K, O’Driscoll B, Humaida H, Chadwick JP (2013) The pre-eruptive magma plumbing system of the 2007–2008 dome-forming eruption of Kelut volcano, East Java, Indonesia. *Contrib Mineral Petrol* 166:275–308
- Jolis EM (2013) Magma-crust interaction at subduction zone volcanoes. Ph.D. Dissertation Uppsala University, Sweden, Acta Universitatis Upsaliensis
- Jolis EM, Troll VR, Harris C, Freda C, Gaeta M, Orsi G, Siebe C (2015) Skarn xenolith record crustal CO₂ liberation during Pompeii and Pollena eruptions, Vesuvius volcanic system, central Italy. *Chem Geol* 415:17–36
- Jousset P, Budi-Santoso A, Jolly AD, Boichu M, Surono, Dwiyono S, Sumarti S, Hidayati S, Thierry P (2013) Signs of magma ascent in LP and VLP seismic events and link to degassing: an example from the 2010 explosive eruption at Merapi volcano, Indonesia. *J Volcanol Geotherm Res* 261:171–192

- Koulakov I, Bohm M, Asch G, Lühr BG, Manzanares A, Brotopuspito KS, Fauzi P, Purbawinata MA, Puspito NT, Ratdomopurbo A, Kopp H, Rabbel W, Shevkunova E (2007) P and S velocity structure of the crust and the upper mantle beneath central Java from local tomography inversion. *J Geophys Res* 112:B08310
- Lühr BG, Koulakov I, Rabbel W, Zschau J, Ratdomopurbo A, Brotopuspito KS, Fauzi P, Sahara DP (2013) Fluid ascent and magma storage beneath Gunung Merapi revealed by multi-scale seismic imaging. *J Volcanol Geotherm Res* 261:7–19
- Lühr BG, Koulakov I, Suryanto W (2023) Crustal structure and ascent of fluids and melts beneath Merapi: Insights from geophysical investigations. In: Gertisser R, Troll VR, Walter TR, Nandaka IGMA, Ratdomopurbo A (eds) *Merapi volcano—geology, eruptive activity, and monitoring of a high-risk volcano*. Springer, Berlin, Heidelberg, pp 111–135
- Martel C, Brooker RA, Andújar J, Pichavant M, Scailliet B, Blundy JD (2017) Experimental simulations of magma storage and ascent. In: Gottsmann J, Neuberg J, Scheu B (eds) *Volcanic unrest. Advances in volcanology*, Springer, pp 101–110
- Müller A, Haak V (2004) 3-D modeling of the deep electrical conductivity of Merapi volcano (Central Java): integrating magnetotellurics, induction vectors and the effects of steep topography. *J Volcanol Geotherm Res* 138:205–222
- Müller M, Hördt A, Neubauer FM (2002) Internal structure of Mount Merapi, Indonesia, derived from long-offset transient electromagnetic data. *J Geophys Res (solid Earth)* 107:2187
- Nadeau O, Williams-Jones AE, Stix J (2013) Magmatic–hydrothermal evolution and devolatilization beneath Merapi volcano, Indonesia. *J Volcanol Geotherm Res* 261:50–68
- Newhall CG, Bronto S, Alloway B, Banks NG, Bahar I, del Marmol MA, Hadisantono RD, Holcomb RT, McGeehin J, Miksic JN, Rubin M, Sayudi SD, Sukhyar R, Andreastuti S, Tilling RI, Torley R, Trimble D, Wirakusumah AD (2000) 10,000 years of explosive eruptions of Merapi volcano, Central Java: archaeological and modern implications. *J Volcanol Geotherm Res* 100:9–50
- Nimis P (1995) A clinopyroxene geobarometer for basaltic systems based on crystal-structure modeling. *Contrib Mineral Petrol* 121:115–125
- Nimis P (1999) Clinopyroxene geobarometry of magmatic rocks. Part 2. Structural geobarometers for basic to acid, tholeiitic and mildly alkaline magmatic systems. *Contrib Mineral Petrol* 135:62–74
- Nimis P, Ulmer P (1998) Clinopyroxene geobarometry of magmatic rocks Part 1: an expanded structural geobarometer for anhydrous and hydrous, basic and ultrabasic systems. *Contrib Mineral Petrol* 133:122–135
- Peters STM, Troll VR, Weis FA, Dallai L, Chadwick JP, Schulz B (2017) Amphibole megacrysts as a probe into the deep plumbing system of Merapi volcano, Central Java, Indonesia. *Contrib Mineral Petrol* 172:16
- Preece K (2014) Transitions between effusive and explosive activity at Merapi volcano, Indonesia: a volcanological and petrological study of the 2006 and 2010 eruptions. Ph.D. Dissertation, University of East Anglia, United Kingdom
- Preece K, Barclay J, Gertisser R, Herd RA (2013) Textural and micro-petrological variations in the eruptive products of the 2006 dome-forming eruption of Merapi volcano, Indonesia: implications for subsurface processes. *J Volcanol Geotherm Res* 261:98–120
- Preece K, Gertisser R, Barclay J, Berlo K, Herd RA, EIMF (2014) Pre- and syn-eruptive degassing and crystallisation processes of the 2010 and 2006 eruptions of Merapi volcano, Indonesia. *Contrib Mineral Petrol* 168:1061
- Preece K, Gertisser R, Barclay J, Charbonnier SJ, Komorowski JC, Herd RA (2016) Transitions between explosive and effusive phases during the cataclysmic 2010 eruption of Merapi volcano, Java, Indonesia. *Bull Volcanol* 78:54
- Preece K, van der Zwan F, Hammer J, Gertisser R (2023) A textural perspective on the magmatic system and eruptive behaviour of Merapi volcano. In: Gertisser R, Troll VR, Walter TR, Nandaka IGMA, Ratdomopurbo A (eds) *Merapi volcano—geology, eruptive activity, and monitoring of a high-risk volcano*. Springer, Berlin, Heidelberg, pp 265–289
- Price RC, Gamble JA, Smith IEM, Stewart RB, Eggins S, Wright IC (2005) An integrated model for the temporal evolution of andesites and rhyolites and crustal development in New Zealand's North Island. *J Volcanol Geotherm Res* 140:1–24
- Putrika KD (2008) Thermometers and barometers for volcanic systems. *Rev Mineral Geochem* 69:61–120
- Putirka K (2016) Amphibole thermometers and barometers for igneous systems and some implications for eruption mechanisms of felsic magmas at arc volcanoes. *Am Mineral* 101:841–858
- Putrika KD, Mikaelian H, Ryerson F, Shaw H (2003) New clinopyroxene-liquid thermobarometers for mafic, evolved, and volatile-bearing lava compositions, with applications to lavas from Tibet and the Snake River Plain, Idaho. *Am Mineral* 88:1542–1554
- Ratdomopurbo A, Poupinet G (2000) An overview of the seismicity of Merapi volcano (Java, Indonesia), 1983–1994. *J Volcanol Geotherm Res* 100:193–214
- Renzulli A, Santi P (1997) Sub-volcanic crystallization at Stromboli (Aeolian Islands, southern Italy) preceding the Sciara Del Fuoco sector collapse: evidence from monzonite lithic suite. *Bull Volcanol* 59:10–20
- Reubi O, Blundy J (2008) Assimilation of plutonic roots, formation of high-K 'exotic' melt inclusions and genesis of andesitic magmas at Volcán de Colima, Mexico. *J Petrol* 49:2221–2243
- Richter G, Wassermann J, Zimmer M, Ohmberger M (2004) Correlation of seismic activity and fumarole temperature at the Mt. Merapi volcano (Indonesia) in 2000. *J Volcanol Geotherm Res* 135:331–342

- Ridolfi F, Renzulli A (2012) Calcic amphiboles in calc-alkaline and alkaline magmas: thermobarometric and chemometric empirical equations valid up to 1130°C and 2.2 GPa. *Contrib Mineral Petrol* 163:877–895
- Ridolfi F, Renzulli A, Puerini M (2010) Stability and chemical equilibrium of amphibole in calc-alkaline magmas: an overview, new thermobarometric formulations and application to subduction-related volcanoes. *Contrib Mineral Petrol* 160:45–66
- Riker JM, Cashman KV, Rust AC, Blundy JD (2015) Experimental constraints on plagioclase crystallization during H₂O- and H₂O–CO saturated magma decompression. *J Petrol* 56:1967–1998
- Rutherford MJ, Devine JD (2003) Magmatic conditions and magma ascent as indicated by hornblende phase equilibria and reactions in the 1995–2002 Soufriere Hills magma. *J Petrol* 44:1433–1453
- Scailliet B, Pichavant M (2003) Experimental constraints on volatile abundances in arc magmas and their implications for degassing processes. *Geol Soc Lond Spec Publ* 213:23–52
- Schindwein V, Wassermann J, Scherbaum F (1998) Spectral analysis of harmonic tremor signals at Mt. Semeru volcano, Indonesia. *Geophys Res Lett* 22:1685–1688
- Schwarzkopf L, Schmincke H-U, Troll V (2001) Pseudotachylite on impact marks of block surfaces in block-and-ash flows at Merapi volcano, Central Java, Indonesia. *Intern J Earth Sci* 90:769–775
- Sisson TW, Bronto S (1998) Evidence for pressure-release melting beneath magmatic arcs from basalt at Galunggung, Indonesia. *Nature* 391:883–886
- Subandriyo, Gertisser R, Aisyah N, Humaida H, Preece K, Charbonnier S, Budi-Santoso A, Handley H, Sumarti S, Sayudi DS, Nandaka IGMA, Wibowo HE (2023) An overview of the large-magnitude (VEI 4) eruption of Merapi in 2010. In: Gertisser R, Troll VR, Walter TR, Nandaka IGMA, Ratdomopurbo A (eds) *Merapi volcano—geology, eruptive activity, and monitoring of a high-risk volcano*. Springer, Berlin, Heidelberg, pp 353–407
- Surono, Jousset P, Pallister JS, Boichu M, Buongiorno MF, Budisantoso A, Costa F, Andreastuti S, Prata F, Schneider D, Clarisse L, Humaida H, Sumarti S, Bignami C, Griswold J, Carn S, Oppenheimer C, Lavigne F (2012) The 2010 explosive eruption of Java's Merapi volcano—a '100-year' event. *J Volcanol Geotherm Res* 241:121–135
- Smyth HR, Hall R, Hamilton J, Kinny PD (2005) East Java: Cenozoic basins, volcanoes and ancient basement. In: *Proceedings, Indonesian Petroleum Association. Thirtieth Annual Convention & Exhibition*, pp 251–266
- Tepley FJ, Lundstrom CC, Gill JB, Williams RW (2006) U–Th–Ra disequilibria and the time scale of fluid transfer and andesite differentiation at Arenal volcano, Costa Rica (1968–2003). *J Volcanol Geotherm Res* 157:147–165
- Thouret JC, Lavigne F, Kelfoun K, Bronto S (2000) Toward a revised hazard assessment at Merapi volcano, Central Java. *J Volcanol Geotherm Res* 100:479–502
- Tregoning P, Brunner FK, Bock Y, Puntodewo SSO, McCaffrey R, Genrich JF, Calais E, Subarya C (1994) First geodetic measurement of convergence across the Java Trench. *Geophys Res Lett* 21:2135–2138
- Troll VR, Hilton DR, Jolis EM, Chadwick JP, Blythe LS, Deegan FM, Schwarzkopf LM, Zimmer M (2012) Crustal CO₂ liberation during the 2006 eruption and earthquake events at Merapi volcano, Indonesia. *Geophys Res Lett* 39:L11302
- Troll VR, Deegan FM, Jolis EM, Harris C, Chadwick JP, Gertisser R, Schwarzkopf LM, Borisova AY, Binde-man IN, Sumarti S, Preece K (2013) Magmatic differentiation processes at Merapi volcano: inclusion petrology and oxygen isotopes. *J Volcanol Geotherm Res* 261:38–49
- Troll VR, Deegan FM, Jolis EM, Budd DA, Dahren B, Schwarzkopf LM (2015) Ancient oral tradition describes volcano–earthquake interaction at Merapi volcano, Indonesia. *Geografisk Ann: Series A, Phys Geograph* 97:137–166
- Turner S, Foden J (2001) U, Th, and Ra disequilibria Sr, Nd and Pb isotope and trace element variations in Sunda arc lavas: predominance of a subducted sediment component. *Contrib Mineral Petrol* 142:43–57
- van Bemmelen RM (1949) *The Geology of Indonesia, 1A, General Geology*. The Hague: Government Printing Office
- van der Zwan FM, Chadwick JP, Troll VR (2013) Textural history of recent basaltic-andesites and plutonic inclusions from Merapi volcano. *Contrib Mineral Petrol* 166:43–63
- Voight B, Constantine EK, Siswoidjyo S, Torley R (2000) Historical eruptions of Merapi volcano, Central Java, Indonesia, 1768–1998. *J Volcanol Geotherm Res* 100:69–138
- Voight B, Young KD, Hidayat D, Subandriyo, Purbawinata MA, Ratdomopurbo A, Suharna, Sayudi DS, LaHusen R, Marso J, Murray TL, Dejean M, Iguchi M, Ishikara K (2000) Deformation and seismic precursors to dome-collapse and fountain-collapse nuées ardentes at Merapi volcano, Java, Indonesia, 1994–1998. *J Volcanol Geotherm Res* 100:261–287
- Wagner D, Koulakov I, Rabbel W, Luehr BG, Wittwer A, Kopp H, Bohm M, Asch G, MERAMEX Scientists (2007) Joint inversion of active and passive seismic data in Central Java. *Geophys J Int* 170:923–932
- Walter TR, Wang R, Luehr BG, Wassermann J, Behr Y, Parolai S, Anggraini A, Günther E, Sobiesiak M, Grosser H, Wetzel HU, Milkereit C, Sri Brotopuspito PJK, Harjadi P, Zschau J (2008) The 26 May 2006 magnitude 6.4 Yogyakarta earthquake south of Mt. Merapi volcano: did lahar deposits amplify ground shaking and thus lead to the disaster? *Geochem Geophys Geosyst* 9:Q05006
- Weis FA, Stalder R, Skogby H (2016) Experimental hydration of natural volcanic clinopyroxene phenocrysts under hydrothermal pressures (0.5–3 kbar). *Am Mineral* 101:2233–2247

- Wegler U, Lühr BG (2001) Scattering behaviour at Merapi volcano (Java) revealed from an active seismic experiment. *Geophys J Int* 145:579–592
- Wölbern I, Rumpker G (2016) Crustal thickness beneath Central and East Java (Indonesia) inferred from P receiver functions. *J Asian Earth Sci* 115:69–79
- Whitley S, Gertisser R, Halama R, Preece K, Troll VR, Deegan FM (2019) Crustal CO₂ contribution to subduction zone degassing recorded through calc-silicate xenoliths in arc lavas. *Sci Rep* 9:8803
- Whitley S, Halama R, Gertisser R, Preece K, Deegan FM, Troll VR (2020) Magmatic and metasomatic effects of magma-carbonate interaction recorded in calc-silicate xenoliths from Merapi volcano (Indonesia). *J Petrol* 61:egaa048
- Widiyantoro S, van der Hilst R (1997) Mantle structure beneath Indonesia inferred from high-resolution tomographic imaging. *Geophys J Int* 130:167–182
- Widiyantoro S, Ramdhan M, Métaixian JP, Cummins PR, Martel C, Erdmann S, Nugraha AD, Budi-Santoso A, Laurin A, Fahmi AA (2018) Seismic imaging and petrology explain highly explosive eruptions of Merapi volcano, Indonesia. *Sci Rep* 8:13656



A Textural Perspective on the Magmatic System and Eruptive Behaviour of Merapi Volcano

Katie Preece, Froukje van der Zwan, Julia Hammer, and Ralf Gertisser

Abstract

Quantitative textural analysis of crystals, including their number density, shapes, sizes, overall abundance and size distribution can be used to shed light on magmatic processes and the timescales over which they operate. At Merapi, textural analysis of phenocrysts in dome lavas, lava flows, tephra, and in plutonic cumulates has revealed that open system steady state conditions prevail throughout the crustal magma plumbing system over short time periods, with non-steady state conditions prevailing over the longer term. Phenocryst crystallisation likely takes place over tens to hundreds of years prior to eruption. Quantitative textural analysis of feldspar microlites, in

conjunction with compositional data, elucidate magma ascent and degassing processes within the conduit during dome forming eruptions, and additionally reveal the driving forces behind transitions between effusive and explosive eruptive behaviour. For example, micro-lite textures from different stages of the 2010 eruption show that transitions between explosive and effusive activity in 2010 were driven primarily by the dynamics of magma ascent in the shallow conduit.

Keywords

Merapi • Quantitative textural analysis • Magmatic processes • Eruptive behaviour • Explosive-effusive eruption transition

K. Preece (✉)

Department of Geography, Swansea University,
Swansea SA2 8PP, UK

e-mail: k.j.preece@swansea.ac.uk

F. van der Zwan

Physical Sciences and Engineering Division, King
Abdullah University of Science and Technology
(KAUST), Thuwal 23955-6900,
Kingdom of Saudi Arabia

J. Hammer

Department of Earth Sciences, University of Hawai'i
at Manoa, Honolulu, HI 96822, USA

R. Gertisser

School of Geography, Geology and the
Environment, Keele University,
Keele ST5 5BG, UK

9.1 Introduction

Crystal textures provide important insights into volcanic and magmatic processes. The shape, size, abundance, size distribution, as well as evidence of chemical disequilibrium (e.g. mineral breakdown rims and zoned rims) can reveal information about the timescales of magma processes and magma ascent. By analysing a range of crystal populations and mineral phases, it is possible to build up a picture of the magmatic processes occurring throughout the magmatic plumbing system, spanning wide spatial and temporal ranges. For example, deep crustal

processes occurring at an early stage of magmatic evolution can be resolved via analysis of cumulates and phenocrysts (Fig. 9.1). Shallow, late-stage processes occurring on syn-eruptive timescales, can be resolved via textural investigation of microlite crystals and amphibole breakdown rims (Fig. 9.1). At Merapi, textural analysis has been used to probe the deep magmatic system, via plutonic inclusions and phenocrysts (van der Zwan et al. 2013), and processes occurring during magma storage in crustal reservoirs have been investigated using phenocryst phases (Innocenti et al. 2013a; van der Zwan et al. 2013). Magma ascent and effusive dome eruption processes (e.g. Hammer et al. 2000; Preece et al. 2013) and effusive-explosive transitions (Preece et al. 2016; Innocenti et al. 2013b) have been resolved using feldspar microlites textures and amphibole reaction rims.

This chapter provides a review of how quantitative textural analysis has been used to gain understanding of the Merapi magmatic plumbing system and processes occurring within it. In particular, the chapter synthesises and evaluates data from quantitative textural studies in order to interpret the processes and timescales operating within the crustal plumbing system, shallow-level magma ascent and degassing, and the driving forces behind effusive-explosive transitions.

9.2 Background

9.2.1 Eruptive Styles of Merapi

Over the last two centuries, eruptive activity at Merapi volcano has been dominated by effusive dome-forming eruptions, occurring every few years. These eruptions have typically consisted of prolonged periods of dome growth, followed by multiple gravitational dome collapses, to produce block and ash flows (BAFs) [see Voight et al. (2000) for a detailed summary]. This type of activity has become so synonymous with Merapi that small volume BAFs from gravitational dome collapse are often termed Merapi-type *nuées ardentes*. Looking further back in the geological record however, it is apparent that more varied

styles of activity have been commonplace at Merapi. Basaltic and basaltic andesite lava flows have erupted throughout Merapi's history (e.g. Bahar 1984; del Marmol 1989; Berthommier 1990; Camus et al. 2000; Newhall et al. 2000; Gertisser et al. 2012, 2023, Chap. 6). In addition, more explosive eruptions (up to VEI 4) have occurred, most notably in 2010 and in 1872, and were common in prehistorical time, as revealed by field studies over the past few decades (del Marmol 1989; Berthommier 1990; Andreastuti 1999; Andreastuti et al. 2000; Camus et al. 2000; Newhall et al. 2000; Gertisser 2001; Gertisser et al. 2012, 2023, Chap. 6). For example, pumice fallout and pyroclastic density current deposits have been identified in the geological record at Merapi and linked to past vulcanian and subplinian style activity (e.g. Andreastuti 1999; Andreastuti et al. 2000; Newhall et al. 2000; Gertisser 2001; Gertisser et al. 2012, 2023, Chap. 6). Together with the more common dome-forming eruptions of recent times, these more explosive eruptions should also be considered typical of Merapi. Variations in magma supply from depth, magma ascent rate, and volatile behaviour during ascent are thought to be important factors which control whether Merapi erupts effusively or explosively (e.g. Chadwick et al. 2007; Gertisser 2001; Deegan et al. 2010; Gertisser et al. 2011; Costa et al. 2013; Preece et al. 2013, 2014, 2016; Troll et al. 2012; Kushnir et al. 2016; Handley et al. 2018). Evidence for these processes is preserved in the crystals, making the processes resolvable via textural and chemical analysis of the crystal populations.

9.2.2 Merapi Magmatic System

The plumbing system of Merapi is demonstrated to consist of multiple magma storage and crystallisation regions, ranging over almost the entire thickness of the crust, although details are still controversial. Geobarometry of magmatic inclusions suggests that crystallisation at Merapi occurs over a wide range of depths, with the bulk of magma stored in the mid- to lower-crust (Fig. 9.1), and small pockets of magma stored in

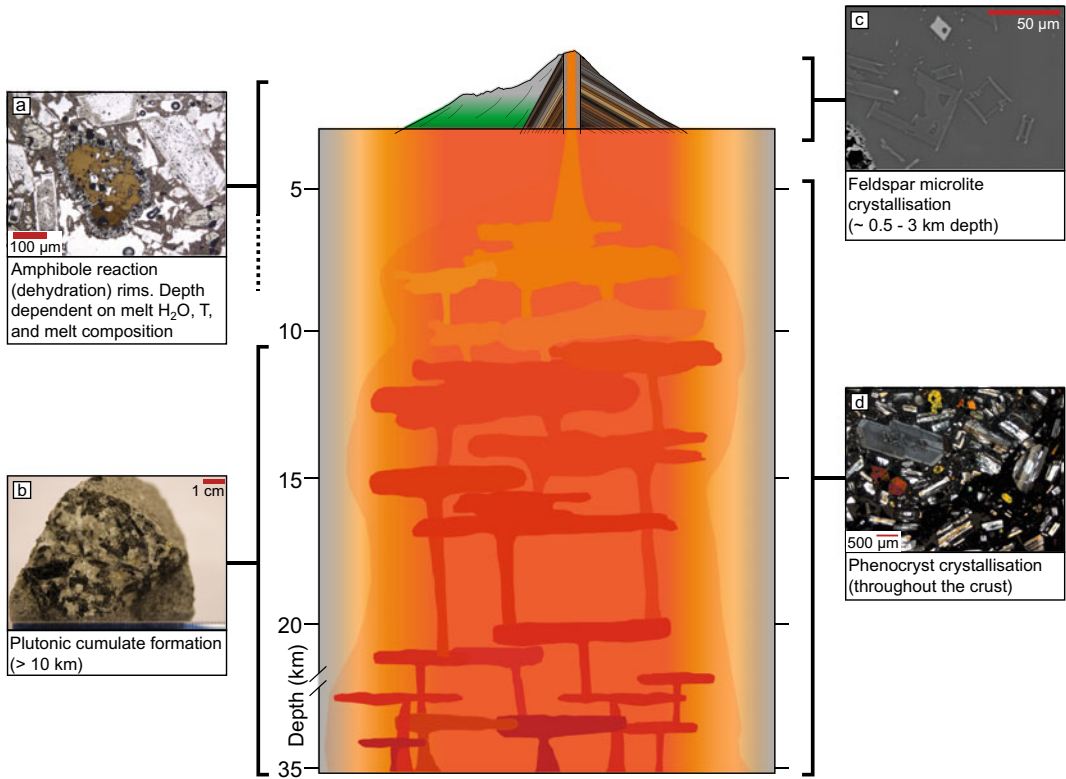


Fig. 9.1 Schematic diagram of Merapi magmatic system, and textural features that may be used to gain insight into magmatic and volcanic processes. Magma storage regions depths are based on petrological and geophysical studies (see main text for references). **a** Amphibole reaction (dehydration) rims formed via ascent related H₂O degassing, at depths dependent on melt H₂O content, temperature and chemical composition. **b** Plutonic

cumulate formation at Merapi is thought to take place at > 10 km depth (van der Zwan et al. 2013). **c** Feldspar microlites formed via degassing induced crystallisation in the top few km of the conduit (e.g. Preece et al. 2013; 2016). **d** Feldspar phenocrysts crystallise throughout the crust at Merapi (e.g. Chadwick et al. 2007; Costa et al. 2013; van der Zwan et al. 2013)

the top few kilometres of the crust (e.g. Chadwick et al. 2013; Troll and Deegan 2023, Chap. 8). Amphibole megacrysts (up to ~ 8 cm diameter) in basaltic andesite lava are thought to represent the deepest mineral phases, forming at ~ 500 to 800 MPa, equivalent to 19–32 km depth below the summit (Peters et al. 2017; Troll and Deegan 2023, Chap. 8). Phenocryst geobarometry in lavas and pyroclastic rocks reveal a major magma storage region throughout mid- to lower-crustal levels (14–19 km) (Gertisser 2001). The presence of a mid- to lower-crustal storage region is corroborated by data from clinopyroxene-hosted melt inclusions (Preece et al. 2014), as well as by calculated amphibole phenocryst crystallisation depths (Nadeau et al. 2013; Erdmann et al. 2014;

Preece 2014). Phase equilibrium experiments suggest a main storage region at 100–200 ± 75 MPa (> 4.5 to ~ 9 km), where magma temperatures are 925–950 ± 25 °C, with 3–4 wt.% H₂O (Erdmann et al. 2016). Clinopyroxene-hosted melt inclusions provide evidence for a major zone of crystallisation at ~ 11 to 15 km depth, with re-equilibration during shallower storage and/or ascent at 0.6–9.7 km depth, and inputs of fresh magma prior to eruption coming from deeper in the system (up to ~ 20 km) (Preece et al. 2014). In contrast, Costa et al. (2013) defined three zones of crystallisation based on thermobarometry and MELTS modelling: (1) a deep reservoir at 30 ± 3 km depth, evidenced by amphibole and high-Al clinopyroxene crystals,

which constitutes a region where the basaltic andesite is generated, probably by fractionation of a more primitive magma; (2) a mid-level zone at 13 ± 2 km recorded by amphibole, high-Al clinopyroxene and Ca-rich plagioclase; (3) a shallow (< 10 km depth) region where lower-Al plagioclase and low-Al clinopyroxene crystallise, along with orthopyroxene. This region is envisaged to be largely degassed and crystal-rich. Also at < 10 km depth, crustal carbonate assimilation is thought to occur, contributing to the volatile budget of the system, potentially intensifying and sustaining eruptions (Chadwick et al. 2007; Deegan et al. 2010, 2023, Chap. 10; Troll et al. 2012, 2013; Borisova et al. 2013; Whitley et al. 2019, 2020; Troll and Deegan 2023, Chap. 8).

Seismic tomographic imaging suggests an extensive fluid-magma zone from mantle to surface, including a deep magmatic region near the MOHO, a main pre-eruptive magma reservoir at ≥ 10 –20 km, as well as a zone of fluid percolation beneath the summit (Widiyantoro et al. 2018; Luehr et al. 2023, Chap. 5). GPS and tilt data indicate a magma storage region at 8.5 ± 0.4 km below the summit (Beauducel and Cornet 1999), which is broadly consistent with the depth of an aseismic zone observed by Ratdomopurbo and Poupinet (2000) at > 5 km below the summit. Ratdomopurbo and Poupinet (2000) also detected a shallow aseismic zone at a depth of 1.5–2.5 km below the summit, interpreted to represent a small shallow ephemeral magma reservoir into which magma is injected from greater depths and stored temporarily before eruption. Shallow storage region(s) have also been proposed based upon Bouguer gravity anomaly data (Saepuloh et al. 2010). However, a decrease in resistivity below the summit, near the conduit, has been attributed to the presence of saline fluids rather than melt (Müller et al. 2002; Commer et al. 2005) and the presence of a shallow brine phase has been corroborated by melt inclusion data (Nadeau et al. 2013; Preece et al. 2014). Tiede et al. (2005) reported a low-density body within the Merapi edifice, although could not confirm whether this can be attributed to a magmatic body. It is possible that if a

shallow storage region(s) exists, it is either too small or diffuse to be observed by certain techniques, or it is ephemeral with magma only stored there prior to an eruption.

A complex interplay of magmatic processes is thought to act at Merapi, including: the interaction between magma stored in various parts of the plumbing system (i.e. shallower, degassed magma and deeper, hotter, more volatile-rich magma) (Costa et al. 2013); mixing and mingling with a more mafic magma resulting in the remobilisation of the basaltic andesite (Gertisser and Keller 2003; Chadwick et al. 2013); mixing of distinct basaltic andesite magma batches (Chadwick et al. 2013); and contamination via assimilation of carbonate crustal rocks (e.g. Chadwick et al. 2007; Deegan et al. 2010, 2023, Chap. 10; Troll et al. 2012, 2013; Whitley et al. 2019, 2020; Gertisser et al. 2023, Chap. 6; Troll and Deegan 2023, Chap. 8).

9.2.3 Crystallisation: Nucleation, Growth and Equilibrium Effects

Crystal textures reflect their crystallisation environment and can preserve textural modification due to changing magmatic parameters. The magmatic conditions prevalent at the time of crystallisation control, and are therefore recorded by, the number, sizes and shapes of crystals, zoning/resorption patterns, as well as reaction/breakdown rims and exsolution lamellae of certain minerals. The majority of quantitative textural studies for volcanoes worldwide are carried out on feldspar crystals, as feldspar crystallisation is highly responsive to changes in temperature, pressure and water content in the melt, although other minerals such as pyroxene, olivine, amphibole and Fe-Ti oxides have also been used in igneous textural studies (e.g. Donaldson 1976; Cashman 1992; Armienti et al. 1994; Higgins and Roberge 2003).

Within the magma storage region, crystals begin to nucleate and grow once the magma cools past the mineral liquidus. The manner in which the crystallisation proceeds is largely

governed by the degree of undercooling (ΔT), defined as the difference between the temperature of the liquidus and the actual temperature of the magma. At small degrees of ΔT , growth of existing crystals is the dominant process, whereas nucleation of new crystals will dominate at larger ΔT . In a magma storage region, the degree of undercooling is low and therefore crystal growth will dominate over crystal nucleation, leading to the formation of relatively few and large crystals (i.e. phenocrysts). If the system is maintained close to the liquidus for prolonged periods of time and the driving force of crystallisation is low, e.g. temperature loss is buffered by the latent heat of crystallisation, then textural coarsening may occur. In this situation, the rock texture adjusts to minimise the overall energy of the system, and surface energy is minimised by small crystals dissolving at the same time as larger crystals growing, called Ostwald ripening. During this process, the nucleation rate is zero and growth is dominant. These effects are often found in plutonic rocks (e.g. Higgins and Chandrasekharam 2007; Higgins 2011).

A high, or rapid rate of ΔT (i.e. during fast ascent and degassing) favours nucleation of new crystals, leading to the formation of many smaller crystals. As magma ascends in the shallow conduit, decompression leads to volatile exsolution and degassing of H_2O . The H_2O loss from the melt results in an increase in the stability and the liquidus temperature of anhydrous minerals such as feldspar. As a consequence of the increase in liquidus temperature, there is an increase in the relative undercooling, causing the melt to crystallise (degassing-induced crystallisation). At very high undercooling, e.g. very fast ascent during explosive eruptions, low rates of diffusion due to high melt viscosity at low H_2O content (Hess and Dingwell 1996) mean that the magma does not crystallise microlites, but is quenched to glass upon eruption. Apart from affecting the crystal size and the crystal number density [commonly measured as the number of crystals per unit area (N_A) or volume (N_V)], crystallisation kinetics and ΔT also affect crystal morphology and crystallinity (Lofgren 1980; Kirkpatrick 1981; Swanson et al. 1989). Microlite

morphology is linked to ΔT , with tabular and equant crystals forming under conditions of lower ΔT , and hopper, swallowtail and acicular crystals forming at higher ΔT (e.g. Lofgren 1974; Donaldson 1976; Hammer and Rutherford 2002). Within this chapter, crystallinity is mainly discussed in relation to the groundmass. The groundmass crystallinity (ϕ) is the fraction of groundmass area that is occupied by, in this case, feldspar microlites. Groundmass crystallinity is a function of both crystal size and abundance, so that a sample with many small microlites or few larger microlites may have the same crystallinity.

In summary, the final rock texture is therefore the combined result of the often complex magma reservoir processes, magma ascent rate, the ascent path depth and style (continuous ascent vs. temporary stalling at one or several levels in the crust), as well as any post-extrusion crystallisation.

9.2.4 Crystal Size Distribution (CSD) Analysis

Crystal size distribution (CSD) analysis is a way to quantify the textural characteristics of a crystal population in volumetric space. In conjunction with detailed petrography, CSDs can help to resolve dynamic magmatic processes, such as magma mixing, and allows quantification of crystallisation timescales based on textural data. Crystal size distribution analysis was first developed to examine crystallisation in chemical engineering studies (Randolph and Larson 1971), before being applied to quantify crystallisation processes in igneous rocks (Cashman 1988; Marsh 1988; Cashman and Marsh 1988). The CSD of a rock may be defined as the number of crystals of a mineral per unit volume, within a series of defined size intervals (e.g. Cashman and Marsh 1988; Marsh 1988; Higgins 2000). A typical CSD plot considers the population density $ln(n)$ (a measure of the number of crystals per unit volume of the population), plotted against crystal size (L), where both parameters are a consequence of the crystal growth rate and crystal growth time (sometimes taken to be residence time) (Fig. 9.2a). If crystal growth rates are

known or can be approximated, then the slope of the CSD can be used to calculate growth times, or vice versa, where crystal growth times are known, growth rates can be calculated. The crystal nucleation density is the zero-size intercept (Fig. 9.2a). Marsh (1988) proposed that a continuously erupting volcano approximates a steady-state system, where magma is injected into the magma chamber from below, and partial crystallisation takes place in the chamber, before an equal quantity of magma is withdrawn from the chamber during eruption. Under steady state conditions, the number of crystals in each size interval does not change, as growing crystals move out of one specific interval and into the next largest, theoretically producing a log normal crystal size distribution, and thus, a straight line CSD (Fig. 9.2a). However, in reality, open-system processes such as magma mixing and mingling, assimilation and fractionation, as well as changes in temperature, volatile content and undercooling, force the CSD to deviate from a straight line and instead produce a curved or kinked CSD pattern (Fig. 9.2).

The CSD data presented in this chapter from Innocenti et al. (2013a, b) have been calculated using crystal shape correction methods from Higgins (1996), whilst van der Zwan et al. (2013) and Preece et al. (2013, 2016) used *CSDSlice* (Morgan and Jerram 2006) to calculate the crystal shape correction. Crystal size distributions of Merapi products presented in this chapter have all been calculated using the *CSDCorrections* software (Higgins 2000).

9.3 The Crustal Plumbing System and Magmatic Processes Revealed Through Textural Analysis

9.3.1 Coarse Plutonic Inclusions and the Deep Plumbing System

Textural analysis reveals insights into Merapi's current plumbing system, and the evolution throughout its geological history (Innocenti et al.

2013a, b; van der Zwan et al. 2013). The deep (mid to lower crustal) plumbing system can be probed by examining phenocrysts, as well as plutonic material brought up during eruptions as inclusions. Both mafic and felsic plutonic inclusions occur at Merapi as coarse-grained (up to ~ 7 mm) intergrowths of feldspar, amphibole, pyroxene, oxides and accessory phases such as apatite (Chadwick et al. 2013; Troll and Deegan 2023, Chap. 8) (Fig. 9.3). Few plutonic inclusions have been studied texturally, but quantitative textural analysis of two felsic, feldspar-dominated plutonic inclusions enclosed in 1994 and 1998 andesite dome magma preserve evidence of a range of processes occurring within the deeper portions of the Merapi plumbing system (van der Zwan et al. 2013). Strontium isotope ratios of these plutonic inclusions indicate that crystallisation took place prior to crustal carbonate assimilation within the limestone crust (Chadwick et al. 2007, 2013; Deegan et al. 2010). As the limestone crust underlies Merapi to depths of ~ 10 km (van Bemmelen 1949), it is considered that the plutonic inclusions form at depths > 10 km in the mid- to lower crust (van der Zwan et al. 2013).

The limited textural observations and CSD analysis of feldspar crystals of the two cumulates (Fig. 9.4) are suggestive of multiple processes modifying the crystal population, including pressure solution, crystal coarsening by textural equilibration (i.e. annealing or Ostwald ripening) and resorption (van der Zwan et al. 2013). One of the plutonic inclusions (Fig. 9.4a; 8-P-5), hosted in basaltic andesite from the 1998 deposits, preserves evidence of feldspar accumulation, with closely packed crystals of feldspar and clinopyroxene, a lack of interstitial glass, a positive Eu anomaly, and a higher number density of the largest plagioclase crystals ($> \sim 2$ mm) compared to CSDs of the lava (Chadwick et al. 2013; van der Zwan et al. 2013). The second studied plutonic cumulate (Fig. 9.4b; 4-P-2), contained in basaltic andesite erupted in 1994, has plagioclase crystals intergrown with abundant amphibole ($\sim 20\%$), indicating that crystal growth took place at hydrous conditions, probably within the mid to deep crust. Smaller crystals of

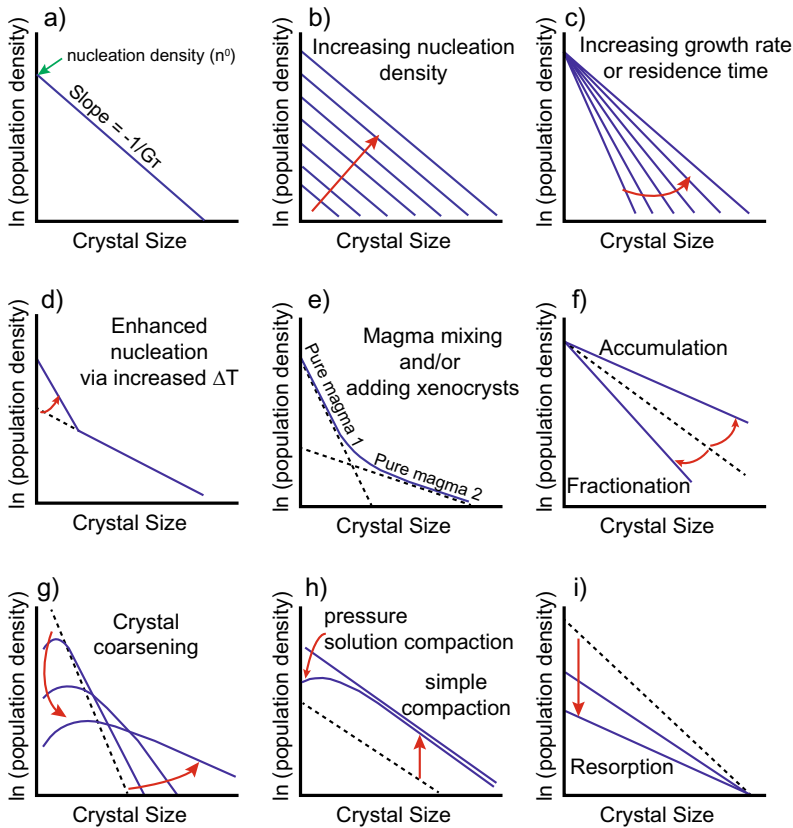


Fig. 9.2 Schematic CSD plots, based on Higgins (2006) and references therein, showing how various magmatic processes affect the shape of a CSD: **a** Straight line CSD theoretically produced under steady-state conditions. **b** If the residence time is constant but the nucleation density gradually increases, then subsequent CSDs will be parallel with but with increasing nucleation density (y-axis intercept). **c** If the residence time or growth rate increases but the nucleation density stays constant, the subsequent CSDs will pivot around a fixed point on the y-axis. **d** A burst of nucleation during crystallisation, e.g. via increased ΔT , results in an increased number of small crystals and an upturn in the CSD slope at small sizes, assuming time is available for the nuclei to develop into observable crystals. **e** Mixing of different magmas and

crystal populations leads to a curved or kinked CSD, with the original slopes preserved for small and large crystal populations. **f** As crystals accumulate or fractionate, e.g. via gravity settling in response to density differences, the number of larger crystals will first increase or decrease respectively, leading the CSD to swing up or down, with a fixed point on the y-axis. **g** Textural coarsening results in a loss of small crystals and growth of larger ones, leading to gradually shallowing CSDs with gradually lower population densities. **h** Simple compaction increases all population density values evenly, whereas pressure-solution compaction results in preferential absorption of small crystals, creating a downturn at small sizes and similarities with coarsening processes. **i** Resorption leads to a progressive reduction in nucleation density and slope

feldspar ($< \sim 2$ mm) in both studied cumulates have lower population densities than expected for a log normal distribution of simple crystallisation (Fig. 9.4c), suggesting that either crystal growth was inhibited or that crystals were subsequently modified by processes which broke down the crystals (Fig. 9.2). It is possible that these crystals were modified by pressure solution

and coarsening by textural re-equilibration and/or resorption (van der Zwan et al. 2013), whilst stored for a period of time at temperatures close to the plagioclase liquidus. The smallest crystal population (< 0.8 mm) in the amphibole-rich cumulate displays steep CSD slopes (Fig. 9.4c), indicating that these crystals were not affected by coarsening processes, and instead represent a

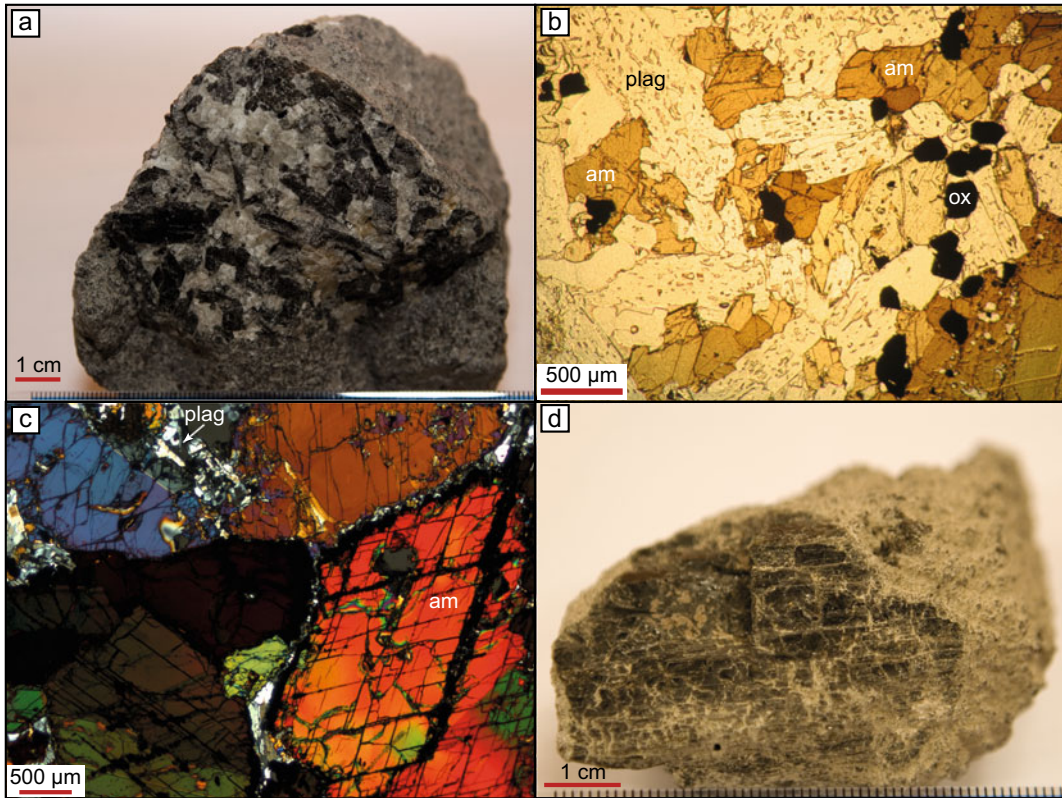


Fig. 9.3 Features of the deep Merapi system, formed early in the magmatic evolution: **a** Feldspar-amphibole cumulate inclusion in 2006 dome lava. **b** Photomicrograph of cumulate inclusion in PPL, predominantly formed of

amphibole (am) and plagioclase (plag). **c** Photomicrograph of cumulate inclusion in XPL, predominantly formed of amphibole (am) and plagioclase feldspar (plag). **d** Amphibole megacryst in 2006 dome lava

renewed crystallisation phase. The CSD slope of the small crystals is similar to that found in the basaltic andesite (Fig. 9.4c), and therefore these crystals are perhaps related to the infiltration of the host basaltic andesite at a shallower storage level within the system (van der Zwan et al. 2013). Based on CSD analysis, crystallisation times for plagioclase within plutonic inclusions were calculated at between 20 and 310 years, assuming constant growth rates of 10^{-10} and 10^{-11} cm s $^{-1}$, respectively (van der Zwan et al. 2013). However, given that these crystals were modified by pressure solution coarsening and/or resorption, as well as the possibility that cumulate material may reside for periods without significant crystallisation, assuming a constant growth rate is not appropriate and any calculated

crystallisation times must be taken as a first-order minimum approximation only.

9.3.2 Phenocrysts: Crustal Magma Storage System and Its Evolution Through Time

Textural analysis of phenocrysts can be used in order to gain information about the magmatic processes operating in the crustal magma plumbing system and the timescales over which these processes occur. Feldspar phenocrysts in eruptive products from Merapi display a wide compositional range (between \sim An $_{25}$ and An $_{95}$) (e.g. del Marmol 1989; Berthommier 1990; Andreastuti 1999; Gertisser 2001; Costa

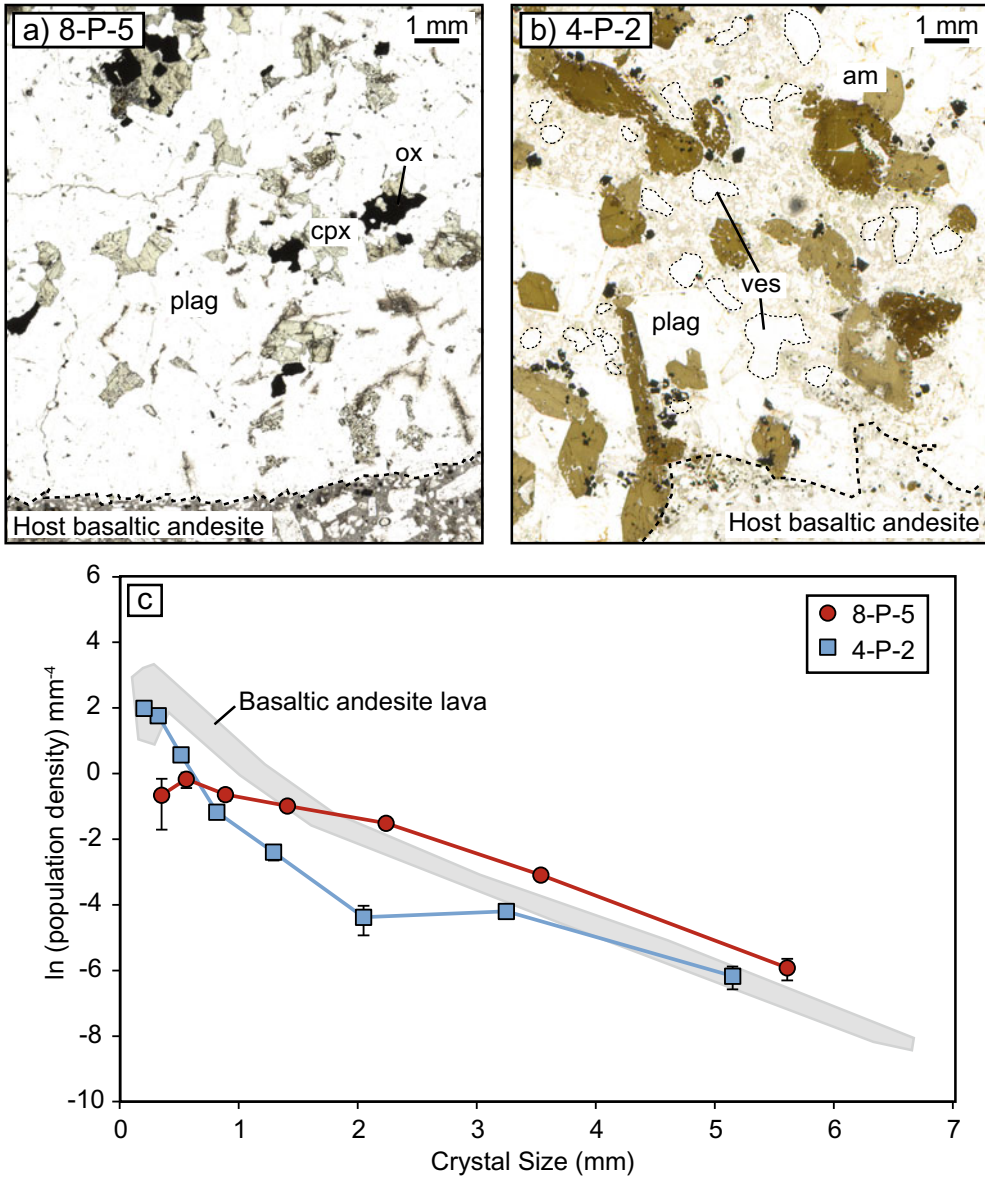


Fig. 9.4 Plutonic cumulate inclusion textures: **a** Photomicrograph of cumulate 8-P-5, hosted in basaltic andesite from the 1998 eruption. Note closely packed plagioclase (plag), clinopyroxene (cpx) and Fe-Ti oxides (ox). **b** Photomicrograph of cumulate 4-P-2, hosted in basaltic andesite from the 1994 eruption. Note plagioclase

intergrowth with amphibole (am) and presence of vesicles (ves). **c** Crystal size distributions (CSDs) of plagioclase in plutonic cumulate inclusions. For comparison, the grey field outlines the CSD data of plagioclase phenocrysts from the host basaltic andesite lava. Data from van der Zwan et al. (2013)

et al. 2013; Preece 2014; Gertisser et al. 2023, Chap. 6) and exhibit a range of textures, which preserve a record of the magmatic conditions they formed in. The variety of feldspar phenocryst zoning types (oscillatory, normal,

reverse, sieve-textured, high-An cores) represents evidence of dynamic open-system processes occurring within the Merapi magmatic system (e.g. Chadwick et al. 2007; Costa et al. 2013). In conjunction with detailed petrographic studies

and chemical compositional information, quantitative textural analysis of phenocrysts from recent and historical eruptions can provide an insight into this dynamic magmatic system. Plagioclase phenocrysts and microphenocrysts from basaltic andesite dome lavas erupted over approximately the last century (1888–1998), display concave-upwards curved CSD patterns (Fig. 9.5a). The difference between the population density of small crystals in the studies of Innocenti (2006) compared to van der Zwan et al. (2013) is probably an artefact resulting from not all small crystals being counted in van der Zwan et al. (2013) (Fig. 9.5a). Disregarding this artefact, similar slopes and population densities across dome lava samples from different eruptions, reflect the stability of the magma system throughout the twentieth century (Innocenti 2006; Innocenti et al. 2013b; van der Zwan et al. 2013). This textural indication of similar crystallisation conditions during Merapi's recent history is consistent with generally uniform bulk rock chemical compositions over the same time period (e.g. del Marmol 1989; Berthommier 1990; Andreastuti 1999; Gertisser 2001; Gertisser and Keller 2003; Gertisser et al. 2023, Chap. 6). These unvarying chemical and textural features are remarkable, considering that a host of processes such as recharge and mixing with a more primitive magma, fractional crystallisation, and crustal contamination, are all invoked to play a major role in the magmatic evolution at Merapi (e.g. Camus et al. 2000; Gertisser and Keller 2003; Chadwick et al. 2007; Costa et al. 2013). Gertisser and Keller (2003) suggest that in order to maintain uniform magma compositions over decadal time periods, a continuously active magma reservoir is maintained in a quasi-steady state by balanced fractional crystallisation, recharge and eruption. Mineral chemical compositions combined with CSDs suggest initial crystallisation at > 10 km depth (Innocenti et al. 2013a; van der Zwan et al. 2013), followed by a period of residence in a reservoir that is steady state over the long-term, but is pulsed on the shorter-term (Innocenti et al. 2013a). Two crystal populations are often evident in the plagioclase phenocryst CSDs from Merapi dome lavas,

which has been interpreted to be a result of processes such as magma mixing, a change in the undercooling conditions and/or assimilation of crystals from carbonate crustal material (van der Zwan et al. 2013; Innocenti et al. 2013a, b). Residence times for dome lava phenocryst populations have been calculated to be between 20 and 240 years (Innocenti et al. 2013a; van der Zwan et al. 2013). However, given that the phenocrysts often display resorption textures, a constant growth rate cannot be assumed and therefore these values should be taken as minimum values only. The crystal number densities of clinopyroxene phenocrysts from recent dome basaltic-andesites (Fig. 9.5b) are lower than the plagioclase number densities, and the size distributions are concave up and unkinked, so that individual crystal populations cannot be accurately identified. The gradual CSD slopes may be due to the effect of gradual modifications of crystallisation conditions or partial re-equilibration after a slope changing event such as magma mixing, increased crystallisation due to undercooling, or pyroxene xenocryst addition (van der Zwan et al. 2013).

Plagioclase phenocrysts in tephra produced during explosive (VEI 3–4) eruptions in Merapi's past (~ 1960 y BP to ~ 1650 y BP) display more variable phenocryst CSD patterns (Innocenti et al. 2013b), when compared to the consistent effusive dome lava CSDs (Fig. 9.5a, c). It has been suggested that the magma which is eventually erupted as either dome lava or tephra undergoes a similar early-stage of crystallisation in the mid-crustal storage reservoir, including magma mixing and open-system crystallisation, before then following a different ascent path to the surface which affects the final eruptive style (Innocenti et al. 2013b). However, in comparison to dome lavas, the pumice CSDs generally have smaller maximum crystal sizes and lower population densities for a given size (Fig. 9.5a, c). Considering these differences, it is possible that compared to the dome lavas, the magma that erupted as pumice resided for less time in the magma reservoir(s) and erupted before as many crystals had time to grow. Calculated residence times for the plagioclase phenocryst populations in the pumice range from

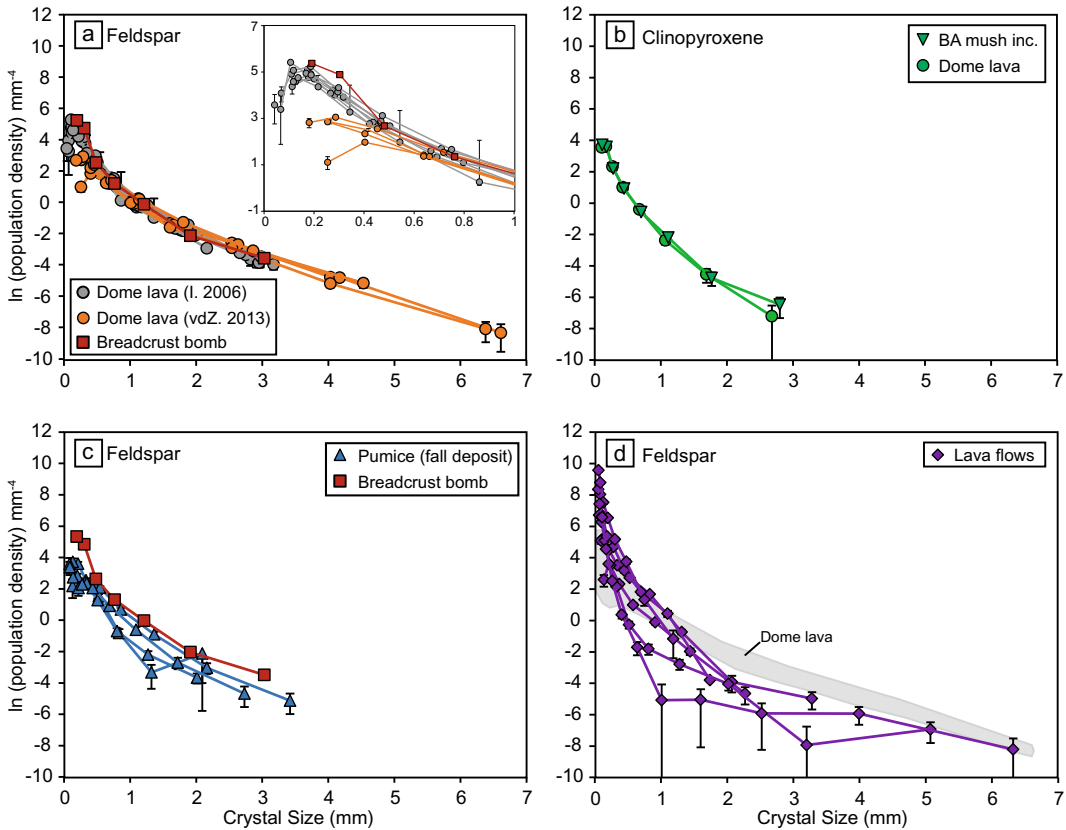


Fig. 9.5 Crystal size distributions (CSDs) of Merapi phenocrysts: **a** Feldspar phenocrysts from dome lavas and Kepuharjo breadcrust bomb, data from Innocenti (2006) and van der Zwan et al. (2013) with inset showing a close-up view of smaller crystal sizes. **b** Clinopyroxene phenocrysts in dome lava and a basaltic andesite mush inclusion, data from van der Zwan et al. (2013).

c Feldspar phenocrysts in pyroclastic fall deposits and Kepuharjo breadcrust bomb, data from Innocenti (2006). **d** Feldspar phenocrysts from basaltic and basaltic andesite lava flows, data from Innocenti (2006). For comparison, grey field outlines CSD data of plagioclase phenocrysts from dome lava plotted in part A

approximately 130–290 years for the largest crystal sizes and between 30 and 100 years for smaller (micro)phenocrysts, assuming the validity of constant growth rate (Innocenti et al. 2013b). In comparison, a vulcanian breadcrust bomb from the Kepuharjo tephra, deposited on the southern flank of Merapi ~ 250 y BP (Andreastuti et al. 2000), has a similar CSD to dome lavas (Innocenti et al. 2013b) in terms of slope and population density, but with an elevated number of small sized crystals (Fig. 9.5a, c). This suggests that vulcanian explosive products may share a similar residence-zone crystallisation history with the dome lavas, differing in only the shallow-conduit overprint of late stage crystallisation.

Basaltic and basaltic andesite lava flows from Proto, Old and New Merapi (Gertisser et al. 2023, Chap. 6), produce CSDs that have different intercepts, slopes and population densities from each other (Fig. 9.5d), suggesting they formed in a non-steady state system (Innocenti et al. 2013a). For example, the multiple pronounced kinks in the lava flow CSDs could be produced by the mixing of magma batches with different prior crystallisation histories, or by multi-step crystallisation. It is likely that crystals resided for a prolonged period of time in a chamber > 10 km depth, followed by shorter and shallower nucleation and growth (Innocenti et al. 2013a).

Based on the differences between the lava dome and lava flow CSD data, it has been suggested that multiple physical scenarios exist in which Merapi magmas have been stored during Merapi's history, and that magmatic storage over the last century may differ from that which preceded earlier eruptions (Innocenti et al. 2013a). The lava dome samples erupted over the last century show evidence for open system steady state behaviour (mass inflow and outflow are approximately equal), whereas the lava flows indicate non-steady state (unequal mass inflow and outflow) conditions (Innocenti et al. 2013a). However, it should be noted that the lava dome samples only provide a snapshot of the magmatic system over a relatively short time period (approximately 100 years between 1888 and 1990) compared to the Proto-, Old- and New Merapi lava flow samples, which span a time period of $\sim > 7000$ years. Long-term non-steady state variations occurring over longer periods of time may therefore only be visible in the lava flow samples and not in the dome lava, as a consequence of differing time spans represented by the samples.

9.4 Shallow Conduit Processes Revealed Through Textural Analyses

Textural analysis has been used to provide a window into the shallow magmatic system and processes occurring within the conduit at Merapi. Most commonly, shallow processes at Merapi have been investigated via quantitative analysis of feldspar microlite textures (Hammer et al. 2000; Preece et al. 2013, 2016). In addition, amphibole reaction rims can be useful indicators of magma ascent rates and ascent paths.

9.4.1 Amphibole Reaction Rims

Amphibole is a common mineral phase in rocks from many eruptions at Merapi and is present as both phenocrysts and microphenocrysts but is absent as groundmass microlites (see Gertisser et al. this volume for more details about

amphibole in Merapi rocks). Amphibole is a hydrous mineral (hornblende contains ~ 2 wt. % H_2O in its crystal structure) and is therefore only stable when coexisting melts contain H_2O . For example, at 900°C , the amphibole stability field requires ~ 4 wt. % H_2O to be dissolved in the coexisting melt (Merzbacher and Eggler 1984; Rutherford and Hill 1993). As magma ascends to the surface from depth, the decrease in pressure leads to H_2O degassing from the melt, causing any amphibole to leave its stability field. Once out of the stability field for a long enough period of time ($> \sim 4$ days; Rutherford and Hill 1993), amphibole begins to break down, forming a reaction rim of stable anhydrous minerals including plagioclase, pyroxene and Fe-Ti oxides (Fig. 9.6a), and releasing H_2O into the magmatic system. The thickness of the rim can be related to the time the crystal spent out of the stability field (i.e. the magma ascent duration). However, if magma ascends quickly from the storage region to the surface in less than a few days, amphibole crystals remain pristine and without a reaction rim (Fig. 9.6b). At Merapi, amphibole reaction rims are present in many, but not all, of the effusive dome lavas. For example, in the 2006 dome lavas, the extent of breakdown is variable between eruption stages, with amphiboles in dense material taken from 14 June 2006 BAFs (peak of 2006 eruption) showing minimal breakdown textures compared to all other 2006 samples (Preece et al. 2013). This is indicative of faster magma ascent to the surface during periods of higher dome extrusion rates and larger dome collapse and BAF generation, demonstrating that even during low-VEI effusive activity, magma can ascend to the surface in less than a few days. High magma ascent rates during the 2010 eruption are also confirmed by the lack of amphibole reaction rims on many of the phenocrysts and microphenocrysts (Fig. 9.6b), even in effusive dome samples (Preece et al. 2016). In older plinian deposits, amphiboles are pristine and display no reaction rims, consistent with rapid magma ascent prior to explosive eruptions (Gertisser 2001; Gertisser et al. 2023, Chap. 6).

Calculating ascent rates based on the thickness of amphibole reaction rims is possible, if the

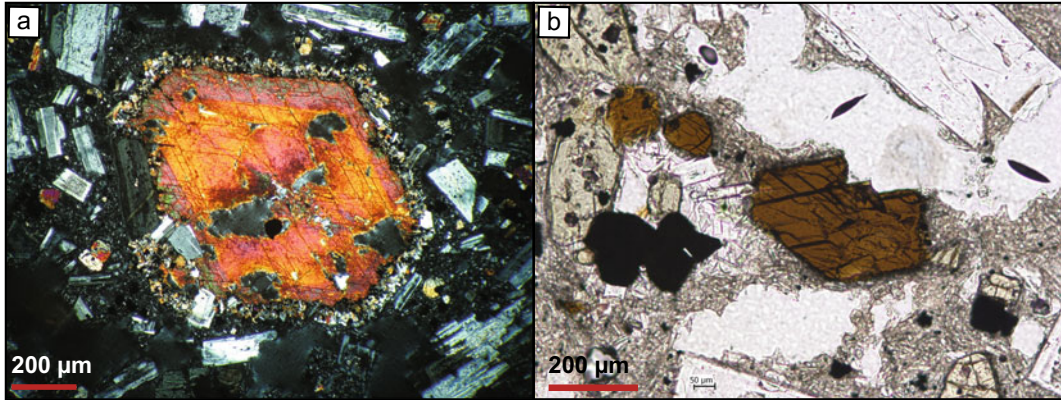


Fig. 9.6 **a** Amphibole phenocryst with dehydration reaction rim from 1994 dome lava. **b** Pristine amphibole with no reaction rim, from 2010 dome lava (Stage 4 of Komorowski et al. 2013)

amphibole stability field (i.e. the depth at which the amphibole begins to break down) is known. However, experiments to characterise this for Merapi have not been published, therefore the exact depth at which the amphibole at Merapi begins to break down during ascent is not known. Water saturated melting experiments carried out on basaltic andesite from Mexico show that the amphibole stability field changes rapidly between 975 and 1075 °C, with breakdown occurring at ~ 0.9 and 3 kbars respectively (Moore and Carmichael 1998). Temperatures for Merapi magma during ascent are at the lower end of this experimental range, if not lower (Erdmann et al. 2014; Preece 2014); therefore, amphibole is likely to break down within a few km of the surface, although this is highly dependent upon melt water content. Decompression experiments tailored to Merapi, in terms of starting composition and intensive variables, would enable the comparison of experimental amphibole reaction rims to those from natural samples and allow for the calculation of amphibole breakdown depths and ascent speeds.

9.4.2 Feldspar Groundmass Microlite Textures

To gain insight into the shallower regions of the plumbing system, it is necessary to use groundmass microlite crystals, rather than phenocrysts which reflect the deeper processes. Quantitative textural studies of microlites can be used to shed

light on magma ascent dynamics and elucidate the magmatic and volcanic processes that took place in the conduit over hours to weeks prior to magma eruption. It can be a powerful tool, especially when paired with information about chemical compositions of the microlite crystal population. Variations in magma ascent affect microlite compositions, with anorthite content increasing with increasing water pressure and temperature (e.g. Couch et al. 2003). The microlite chemical composition can therefore be indicative of the extent of degassing over time.

9.4.2.1 Feldspar Microlite Textures in Effusive Dome-Forming Eruptions

Quantitative textural analysis of groundmass microlites has been used in several studies to reveal conduit processes occurring during recent effusive dome-forming activity at Merapi (Hammer et al. 2000; Preece et al. 2013, 2016). Microlite textural analysis at Merapi was first carried out on a series of dome lavas extruded during the 1986–88, 1992–93, 1994 and 1995 effusive periods (Hammer et al. 2000). Although the relative ages of many of the samples are incompletely constrained within each effusive period, the 1995 dome (which grew after the November 1994 collapse), was sampled at intervals down-flow from the vent, providing relative information about the extrusion timing of each sample, with lava younging up-flow. Samples from the 1995 dome eruption (Fig. 9.7a, b)

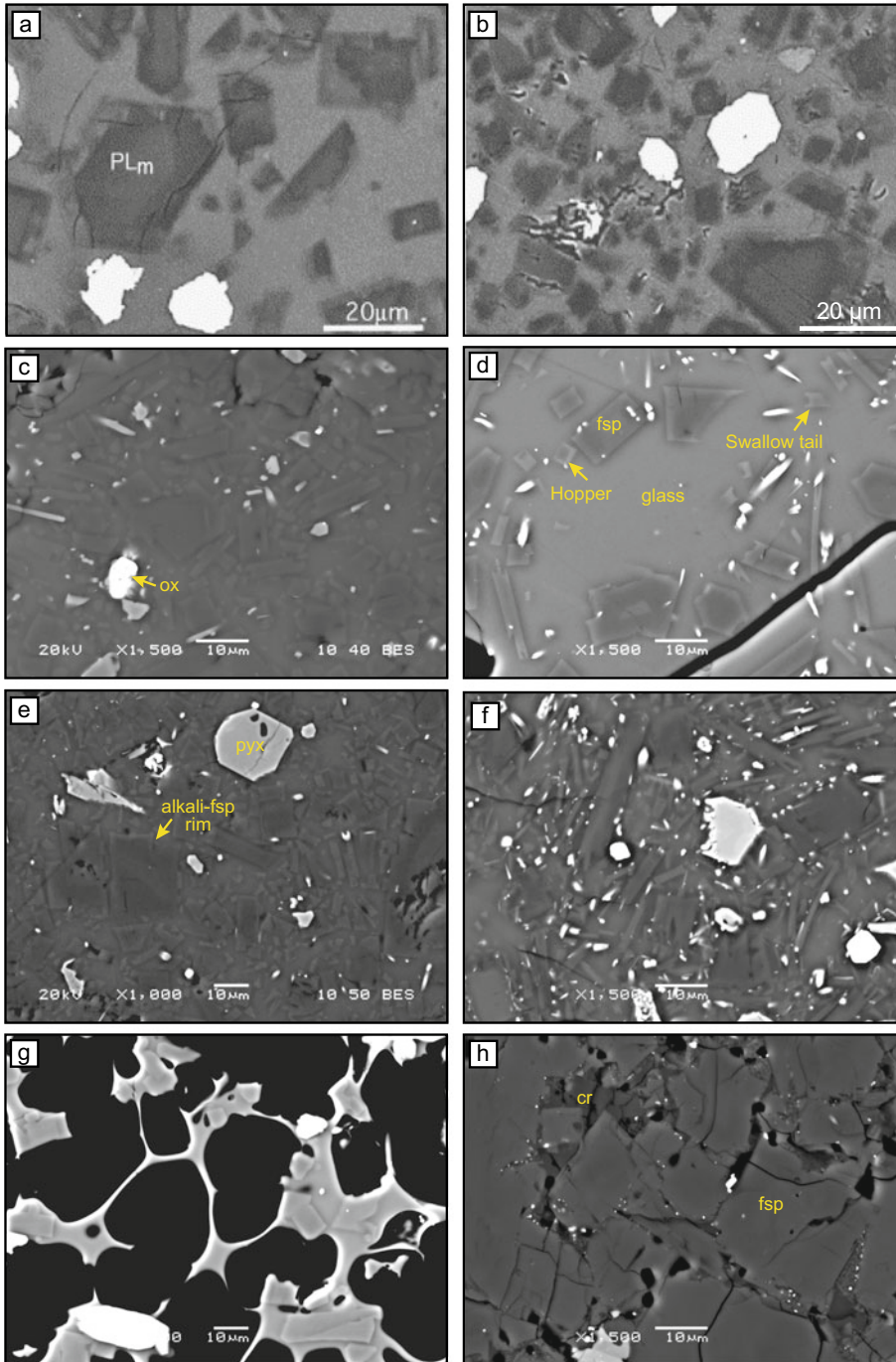


Fig. 9.7 Backscattered electron images of groundmass textures from recent Merapi eruptions: **a, b** Textural end-members of the 1995 dome from Hammer et al. (2000), showing a higher N_A in b. **c** 2006 dense dome lava erupted during peak effusion rates and emplaced in 14 June 2006 BAFs (Lobe 1 of Charbonnier and Gertisser 2008; Preece et al. 2013). **d** Post-14 June 2006 dome lava (Lobe 4 of Charbonnier and Gertisser 2008; Preece et al. 2013). **e** Remnant 2006 dome, collected from summit in 2008

(Stage IV of Preece et al. 2013). **f** 2010 dome which was destroyed by lateral blasts on 5 November (Stage 4 of Komorowski et al. 2013). **g** 2010 white pumice from subplinian activity on 5 November (Stage 6 of Komorowski et al. 2013). **h** Light grey inclusion material found within 2010 dome lava. Abbreviations are as follows: plagioclase microlite (PL_m), feldspar (fsp), pyroxene (pyx), Fe-Ti oxides (ox), cristobalite (cr)

all exhibit similar crystallinity (ϕ), suggesting that throughout this eruptive period similar microlite growth conditions (temperature and PH_2O) prevailed. However, there are textural differences in 1995 samples (Fig. 9.7a,b), with microlite N_A increasing and microlite sizes decreasing with distance from the vent, indicative of progressively decreasing ΔT throughout the 1995 eruption, potentially caused by decreasing ascent rates (Hammer et al. 2000). Comparison of the 1995 dome lavas to those erupted throughout 1992–93 and 1994 showed similarities in the microlite textures and chemical compositions, suggesting that the ΔT rates, determined by effusive flux, are cyclical at Merapi (Hammer et al. 2000).

The well-documented 2006 effusive dome-forming eruption has been studied texturally to investigate the shorter timescale (> 3 -month duration) variations of shallow magma ascent and conduit processes during a single dome-forming eruption cycle at Merapi (Preece et al. 2013). The detailed monitoring record (Ratdomopurbo et al. 2013) and comprehensive field descriptions (Charbonnier and Gertisser 2008) allowed samples to be related directly to the eruptive activity during the 2006 episode. Preece et al. (2013) divided 2006 samples into four stages linked to eruptive activity, as follows: Stage I relates to the onset of BAF emplacement on the SW flanks from 11 May until 1 June 2006; Stage II includes the 14 June 2006 BAF, which can be considered as the peak of the eruption following the highest dome growth rates; Stage III is the period from 15 June 2006 to 2007, when overlapping BAFs were emplaced from a new dome that grew at slower rates; Stage IV samples are remnant 2006 dome collected at the summit in 2008. The chronologically controlled sampling enabled textural features to be related to differences in magma ascent processes and their control on eruptive mechanisms and behaviour (Preece et al. 2013). Although peak effusion rates were an order of magnitude larger in 2006 compared to other recent effusive dome eruptions ($3.3 \text{ m}^3 \text{ s}^{-1}$ pre-14 June 2006, Ratdomopurbo et al. 2013; compared to $0.32 \text{ m}^3 \text{ s}^{-1}$ estimated maximum extrusion rate in 1994, Hammer et al.

2000), values of N_A (number of feldspar microlites per mm^2) are similar to the previous eruptions. This implies that nucleation conditions were similar despite the higher extrusion rate. Crystallinity values (ϕ) are lower for a particular N_A than in previous eruptions, signifying that crystal growth was less dominant in 2006 than in the previous eruptions, due to differing ΔT . Textural changes with time throughout the 2006 eruption (Fig. 9.7c–e) (Preece et al. 2013) are also in contrast with those seen in 1995 (Hammer et al. 2000), with no clear correlation between effusion rate and N_A . This therefore suggests that although ascent rate contributes to the degree of ΔT and N_A , other factors influencing undercooling, such as magma ascent path and source depth also play a part in controlling the final ground-mass texture during dome-forming eruptions at Merapi and are variable over relatively short (intra-eruption) timescales (Preece et al. 2013). Textural analyses of the 2006 dome lavas also provide an insight into the evolution of the Merapi plumbing system during this single eruption. For example, samples from the peak of the eruption (Stage II, 14 June 2006) preserve textural evidence (Fig. 9.7c) of rapid magma ascent from a magma storage region at depths within the amphibole stability field (highest N_A and ϕ , and smallest average microlite size of all 2006 samples, as well as pristine amphiboles with few breakdown rims) (Preece et al. 2013). Near the end of the 2006 eruption (Stages III and IV), effusion rates decreased from $3.3 \text{ m}^3 \text{ s}^{-1}$ to $\sim 1.2 \text{ m}^3 \text{ s}^{-1}$ (Pallister et al. 2013), but seemingly paradoxically, microlite textures display gradually increasing N_A and decreasing areal sizes, reflecting increasing degrees of ΔT (Preece et al. 2013) (Fig. 9.7d,e). Slower magma ascent compared to the peak of eruptive activity is evidenced by the presence of amphibole reaction rims in these samples. In addition, feldspar microlite compositions for these samples have lower anorthite contents compared to other stages of the eruption, often An_{30-40} , suggestive of crystallisation at 25–50 MPa, or 1–2 km depth (Preece et al. 2013). These textural and chemical features can be reconciled if the magma stalled at shallow depths, allowing for degassing and an increase in

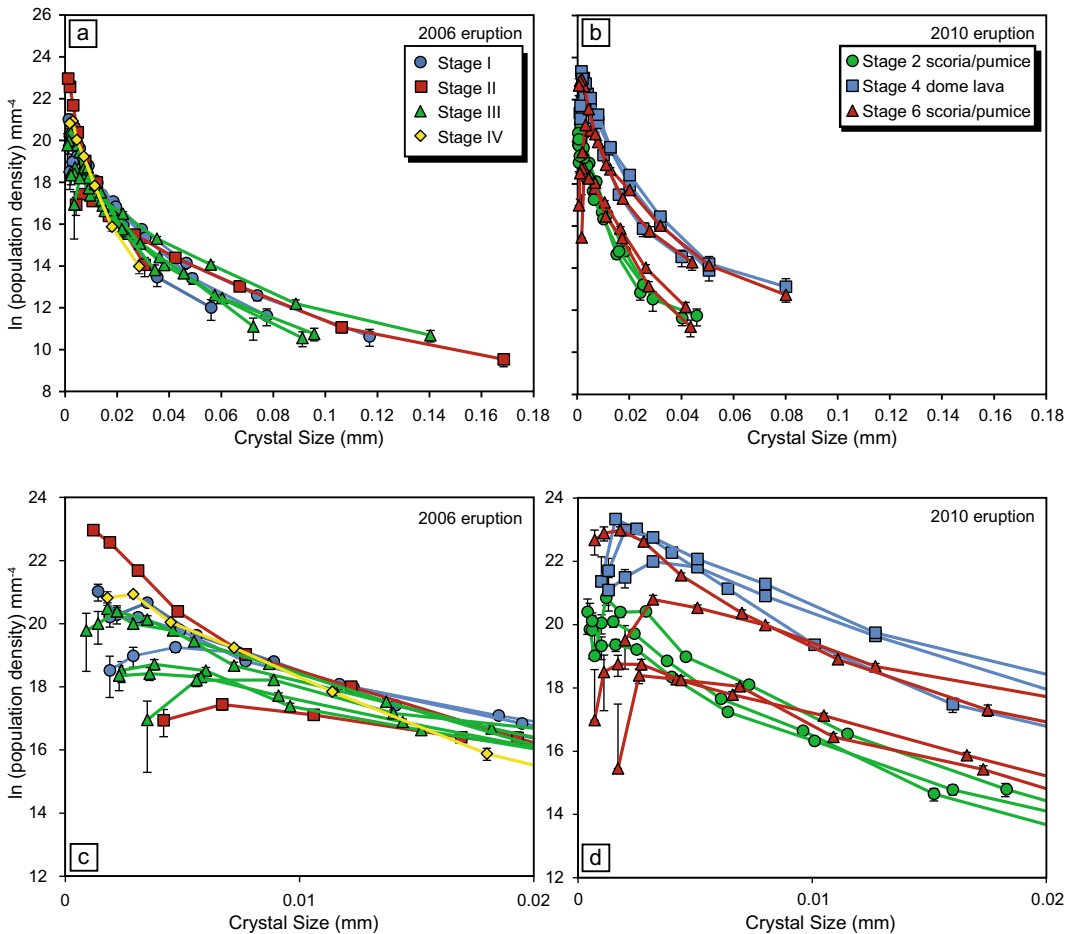


Fig. 9.8 Crystal size distributions (CSDs) of feldspar microlites in recent Merapi eruptive products: **a** 2006 dome lavas from Stage I to Stage IV (Preece et al. 2013). **b** 2010 eruptive products, including scoria and pumice

from Stage 2, dome lava from Stage 4, and scoria and pumice from Stage 6 (Preece et al. 2016). **c** Close-up view of smaller crystals shown in panel a. **d** close-up view of smaller crystals shown in panel b

ΔT . These depths agree with the previously proposed shallow ephemeral storage region, where magma is temporarily stored as it migrates from the deeper reservoir(s) before eruption (Ratdompurbo and Poupinet 2000). Older dome lavas also display amphibole reaction rims and are thought to have stagnated at shallow levels during ascent (Innocenti et al. 2013b).

CSD analyses of the 2006 dome lavas presented in Preece et al. (2013), display curved lines approximated by 2–3 segments, reflecting changes in microlite growth and nucleation rates and ratio, during magma ascent as a function of changing ΔT (Fig. 9.8a). Different microlite sizes

reflect magmatic conditions at different depths, for example, growth of existing crystals is dominant in the lower conduit, whereas nucleation begins to dominate in the shallower system, leading to steeper slopes for smaller crystal sizes (Melnik et al. 2011; Preece et al. 2013). Calculated microlite crystallisation times for the largest microlites in early erupted samples (based on the shallowest segments of the CSDs and a growth rate of $10^{-8} \text{ mm s}^{-1}$), range from 16 to 23 days (Preece et al. 2013), possibly reflecting the time period observed in the monitoring record when the movement of magma to shallow levels began to cause summit deformation (Ratdompurbo

et al. 2013). The five-day period between 26 April and 1 May 2006, when magma moved from inside the edifice to the surface based on real-time seismic amplitude measurement (RSAM) signals (Ratdomopurbo et al. 2013), is similar to calculated crystallisation times of the smallest microlites (based on the steepest slopes), for early erupted samples, which range from ~ 4 to 6 days (Preece et al. 2013). The apparent correspondence between calculated crystallisation times and estimated ascent rates based on the monitoring data suggests that microlite crystallisation occurred at shallow depths, within the edifice. It also indicates that differently sized microlites may preserve evidence of different stages of magma ascent, with the larger microlite population within a sample revealing information about early ascent and the smaller crystals within a sample revealing evidence of crystallisation conditions at the latest stages of ascent. However, given uncertain crystal growth rates, this relation must be viewed with caution. Decompression experiments tailored to Merapi would allow comparison of experimental microlite textures to those from natural samples, in order to provide more robust estimates of microlite growth rates specific to this volcanic system.

9.4.2.2 Effusive—Explosive Transitions at Merapi: Textural Evidence

Transitions between effusive and explosive activity are commonly observed at many subduction zone volcanoes. Worldwide, it has been estimated that 95% of dome eruptions are associated with an explosive component (Newhall and Melson 1983; Ogburn et al. 2015). The style of magma ascent and syn-eruptive degassing during ascent plays a large role in determining the style of eruption of compositionally similar magmas. For example, open-system degassing, where magma degasses freely during ascent, typically results in a less explosive eruption compared to a partly closed system, where gas is prevented from escaping, more often resulting in explosive activity (e.g. Westrich et al. 1988; Stix et al. 1993). Degassing also influences the rheological properties of magma by affecting the

permeability, viscosity and crystallinity, which in turn affect the style of eruption (e.g. Eichelberger et al. 1986; Mastin 2005; Edmonds and Herd 2007; Hale et al. 2007). Textural analysis of microlites, formed by degassing-induced crystallisation, therefore provides an ideal way to gain a better understanding of magma ascent and degassing processes, especially when combined with other petrological observations and linked to the monitoring record.

The 2010 Merapi eruption (VEI 4) was the largest since 1872. In contrast to other recent eruptions, the 2010 eruption began with explosions rather than lava dome effusion and displayed remarkably high extrusion rates when dome growth did later occur (Surono et al. 2012; Pallister et al. 2013; Ratdomopurbo et al. 2013). The 2010 eruption was divided into eight stages (Komorowski et al. 2013; Preece et al., 2016), based on transitions between eruptive styles (see Subandriyo et al. 2023, Chap. 12). Feldspar microlite textures coupled with chemical compositional data for eruptive products from the 2010 eruption have been used to examine the driving forces for this larger than ‘usual’ eruption and for transitions in eruptive style throughout the eruption. Quantitative comparison of microlite textures from scoria, pumice and dome lava from different stages of 2010 revealed that initiation and cessation of the 2010 eruption were predominantly driven by magma flux at depth, with transitions between explosive and effusive activity in 2010 driven primarily by the dynamics of magma ascent in the shallow conduit (Preece et al. 2016). Degassing and degassing-induced crystallisation during magma ascent in the conduit played a crucial role in influencing eruptive behaviour, via complex feedback mechanisms resulting in cycles of explosive and effusive activity (Preece et al. 2016). Microlites for different stages of the eruption vary in terms of shape, size and number density. For example, microlites within dome lava (Stage 4 of Komorowski et al. 2013) are small and acicular with high N_A (Fig. 9.7f) and crystallised at high ΔT during high ascent and extrusion rates leading to nucleation-dominated conditions. By contrast, pumice from the sub-plinian stage (Stage 6 of Komorowski et al. 2013) contains fewer,

larger, more equant-shaped crystals (Fig. 9.7g), which formed at lower ΔT under growth-dominated conditions, before a final rapid ascent to the surface which did not result in the nucleation of new crystals because it was too rapid (Preece et al. 2016).

Light grey coloured, dense, crystalline material is found as abundant inclusions within the 2010 deposits. These light grey inclusions have a high groundmass crystallinity, with low amounts of groundmass glass present, which is speckled in appearance probably due to phase separation and devitrification during shallow storage or slow extrusion (Fig. 9.7h). Cristobalite, which formed during late-stage vapour-phase crystallisation (Fig. 9.7h), is present within these inclusions, as previously observed for example in the Mount St. Helens cryptodome in 1980 and subsequent dome rocks (Hoblitt and Harmon 1993; Pallister et al. 2008). This inclusion material also contains biotite, which is very rare at Merapi and has not been previously observed in Merapi products before 2010. The biotite crystallised at a late magmatic stage from a more evolved residual melt (Preece et al. 2016). High groundmass crystallinity, low proportions of groundmass glass and the presence of cristobalite are indicative that the light grey inclusion material spent a prolonged period of time crystallising at shallow depths (< 50 MPa) within the magmatic system. The light grey dense material is therefore interpreted to originate from a plug of cooled, rigid magma that resided at shallow depth within the magmatic system and was partially re-heated, fragmented and incorporated into the juvenile 2010 magma (Preece 2014; Preece et al. 2016). In addition, basaltic andesite mush inclusions (van der Zwan et al. 2013) were found within other recent Merapi dome lavas. Based on CSD analysis of the mush phenocrysts (Fig. 9.5b), the mush inclusions likely originated from the same magma batch as the host lava but have experienced an extra crystallisation stage later in their evolution, probably due to shallow degassing. The mush inclusions were interpreted to represent side wall facies of an upper crustal magma storage zone at 1.5–3 km depth, such as that proposed by Ratdomopurbo and Poupinet (2000).

The feldspar microlites from the 2010 eruption have variable compositions ranging from $An_1Ab_{41}Or_{58}$ to $An_{84}Ab_{16}Or_{<1}$ (Preece et al. 2016), with a high proportion ($\sim 60\%$) of measured microlites from the dome (Stage 4) having high anorthite contents ($> An_{60}$), whereas pumice microlites (Stage 6) are generally more albitic. The light grey inclusion microlites display the widest compositional range, but $> 70\%$ of measured microlites are alkaline with $> Or_{20}$ (Preece et al. 2016). The plagioclase-liquid hygrometer of Waters and Lange (2015), gives similar H_2O content and pressure ranges for all juvenile 2010 material, corresponding to microlite crystallisation depths of 1.2–2.4 km, and shallower depths of 0.6–1.5 km for the microlites within the light grey inclusions. This suggests that magma decompression and resultant microlite crystallisation originated from similar depths throughout the 2010 eruption. As such, it is likely that the high-An microlites in the initial explosions and subsequent dome formed via the interaction with an influx of hotter magma, the presence of which is consistent with previous petrological work (Costa et al. 2013; Preece et al. 2014) and monitoring data from the 2010 eruption (Suroño et al. 2012). The Stage 6 white pumice microlites grew at low ΔT under growth-dominated conditions, suggesting the magma stalled in the conduit for a period of time, at depths of ~ 1.4 to 2.4 km. This indicates that the very fast final ascent and magma fragmentation before the explosive activity only occurred within the last kilometres of ascent, rather than by very fast ascent from greater depths. The subplinian stage (Stage 6) therefore may have been caused by rapid decompression and fragmentation driven by unloading after the 5 November 2010 dome explosions (Stage 4) and retrogressive summit collapse (Stage 5), leading to explosive behaviour. K-rich feldspar microlites and hygrometry results for the light grey inclusions are in accord with this material originating from a plug in the shallow conduit (Preece 2014).

Crystal size distribution analysis of 2010 microlites are concave-upwards curves, reflecting progressive changes in crystal growth and nucleation rates as a function of changing ΔT in

the system (Fig. 9.8). Average crystallisation rates may be calculated using known time constraints based on observations of the eruption chronology. For example, during 1–26 October 2010, an increase in seismic activity and summit deformation marked an ‘intrusive phase’ believed to reflect the movement of magma to shallower (< 5 km below the summit) regions in the volcano magma plumbing system (Budi-Santoso et al. 2013), likely inducing microlite crystallisation. Based on this observation, it is possible to calculate an average crystallisation rate for the first microlites grown in scoria and pumice erupted during initial explosions on 26 October (Stage 2), using the shallowest segment of the CSD (representing the largest microlites) and a crystallisation period of 26 days. This revealed a crystal growth rate of 9.5×10^{-9} mm s⁻¹ for the large Stage 2 scoria microlites and slower rates of $2.2\text{--}3.5 \times 10^{-9}$ mm s⁻¹ for Stage 2 pumice microlites (Preece et al. 2016). These calculated rates are close to the low end of the range of growth rates (10^{-6} to 10^{-8} mm s⁻¹) deemed appropriate for syn-eruptive plagioclase crystallisation based on experimental data (Brugger and Hammer 2010a). The fact that the calculated growth rates are at the slow end of this range may be expected for these early microlites, which formed deeper within the conduit during growth-dominated crystallisation conditions. Crystals formed later during ascent, at shallower levels within the conduit, may have faster growth rates (Preece et al. 2016).

Combining the microlite crystal textures, CSDs and microlite compositional data highlights that transitions between explosive and effusive activity in 2010 were driven primarily by the dynamics of magma ascent in the conduit, with degassing and crystallisation acting via feedback mechanisms, resulting in cycles of effusive and explosive activity. A large influx of hotter, possibly mafic magma from depth, likely triggered gas overpressure and faster magma ascent rates compared to those observed in 2006 (Preece et al. 2016). The presence of a plug in the conduit, coupled with fast ascent rates led to closed-system conditions, which pressurised the system and led to explosions on 26 October.

Initial explosions temporarily opened the system, allowing ascending magma to degas more freely, and extrude as a lava dome, representing the transition back to effusive activity. Open-system degassing led to rapid microlite nucleation and crystallisation, and the extrusion of a dense, degassed lava dome. This effectively resealed the system and closed-system degassing of the ascending magma began to prevail, leading to a build-up of gas overpressure, resulting in the cataclysmic dome explosions and sub-plinian stage on 5 November 2010. These explosions then enabled open-conduit conditions, facilitating the transition back to effusive activity, allowing for rapid extrusion and emplacement of a dome the following day. By this stage, the eruption was waning and, therefore, further explosive activity did not occur due to decreasing magma flux from depth (Preece et al. 2016).

Looking further back in Merapi’s eruptive history, textural analysis can provide clues about the driving forces behind historic explosive eruptions. Pumice clasts from VEI 3–4 eruptions over the past 200 years, breadcrust bombs from the 1822 or 1872 eruption, and dome lava samples investigated by Innocenti et al. (2013b) all share similar phenocryst textures, indicating similar early (phenocryst) crystallisation processes for each different eruptive style. In contrast, the small-sized crystal populations show textural differences related to variations in ascent rate and degassing during ascent. For example, microlite nucleation densities in pumice samples are lower compared to other lithologies, suggesting the magma erupted quickly before small crystals could form. Breadcrust bombs have high crystallinities, which would have formed a highly viscous magma which blocks gas escape from the conduit. The bomb textures provide evidence of a largely degassed, crystalline magma plug that resided in the upper conduit prior to explosion, which may have sealed the conduit and promoted conduit overpressure (Innocenti et al. 2013b).

The $N_A - \phi$ relationship of feldspar microlites (Fig. 9.9) shows differences between high- and low-intensity eruptions (Hammer et al. 2000; Preece et al. 2013, 2016). Generally, effusive dome eruptions, including the 2006 and 1986–

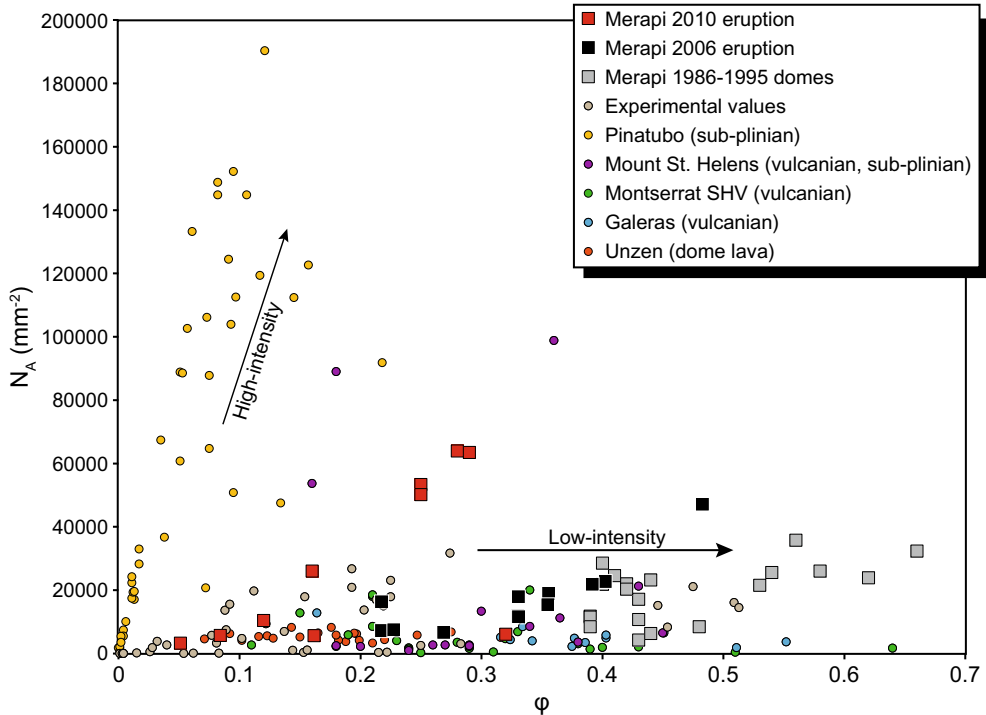


Fig. 9.9 $N_A - \phi$ relationship of feldspar microlites from Merapi 2010 eruption (Preece et al. 2016), Merapi 2006 eruption (Preece et al. 2013) and Merapi 1986–1995 domes (Hammer et al. 2000). For comparison, feldspar microlites from decompression experiments (Brugger and Hammer 2010b) are shown, in addition to feldspar microlites in natural samples from;

Pinatubo eruption (Hammer et al. 1999); Mount St. Helens summer 1980 vulcanian and sub-plinian products (Cashman and McConnell 2005); vulcanian products from Soufrière Hills volcano, Montserrat (Clarke et al. 2007); vulcanian products from Galeras (Bain 2019); dome lava from Unzen (Noguchi et al. 2008)

1995 eruptions of Merapi have relatively low N_A for a given ϕ , suggesting that crystallisation proceeded via nucleation and growth. In comparison, sub-plinian samples from Pinatubo and Mount St. Helens display higher microlite number densities due to crystallisation being more nucleation dominated, resulting from higher eruption intensity and higher decompression rates. Merapi 2010 samples are intermediate between the dome and sub-plinian samples, consistent with Merapi 2010 eruption intensity being intermediate between previous Merapi effusive dome-forming eruptions and sub-plinian activity. Vulcanian eruptions of Montserrat and Galeras have some of the lowest N_A values (Fig. 9.9), suggesting that microlite crystallisation was less nucleation-dominated and more growth-dominated compared to sub-plinian and

most dome samples. The vulcanian samples display textural characteristics typically associated with low-intensity eruptions and low ΔT conditions. This is perhaps due to rapid shallow ascent in these eruptions, which hindered crystal nucleation, so that the microlites which are present in these samples may only be reflecting the deeper conduit conditions.

9.5 Summary and Outlook

Although relatively few textural studies about Merapi have been published compared to other petrological techniques, the body of textural work has provided valuable insights into a variety of processes occurring throughout the magma plumbing system. Plutonic cumulate inclusions

formed at depths of > 10 km over a minimum of tens to hundreds of years and show evidence for textural coarsening, achieved via prolonged residence in a mid- to deep-crustal storage region (van der Zwan et al. 2013). Plagioclase phenocrysts from a variety of eruptive products provide evidence that similar steady-state crystallisation conditions prevailed within the Merapi magma storage region throughout the twentieth century. Quantitative textural analyses of phenocrysts (Innocenti et al. 2013a, b; van der Zwan et al. 2013) reveal that magma mixing and crustal carbonate assimilation occur within the magma storage region at Merapi, in agreement with other petrological and geochemical data. Minimum phenocryst crystallisation times are on the order of tens to hundreds of years. Older Merapi lavas differ from each other texturally, suggesting that a non-steady state system existed thousands of years ago. When comparing lava and pumice phenocryst textures, their similarity suggests that effusively and explosively erupted products share a common storage history, with the eruptive style therefore determined by processes occurring within the shallow magma system. This is in agreement with microlite textural analyses and amphibole textures, which show that effusive—explosive transitions at Merapi are governed by changes in magma ascent, degassing, and the rheological transformations associated with that.

Over the last century, activity at Merapi has been dominated by effusive (VEI 1-2) dome-forming eruptions, but explosive vulcanian and sub-plinian eruptions should all be considered for long-term hazard assessment at Merapi. Rapid transitions in behaviour are exemplified by recent activity. The 2006 and 2010 eruptions demonstrate the capacity for dome-forming periods at Merapi to transition to explosive behaviour, and the 2010 eruption demonstrates that future eruptions may begin explosively, with little warning time and without initial dome growth. Petrological evidence suggests that precursors to a large eruption in the future may include a pulse of gas-rich magma and a build-up of gas overpressure or rapid dome extrusion. Warning signs that these processes are occurring may be

monitored remotely via seismic networks, satellite monitoring, gas flux and ground deformation measurements. The fact that whole rock compositions were similar in recent effusive dome eruptions and the explosive 2010 eruption, means that Merapi magma is inherently capable of producing explosive (VEI 4 or potentially higher) eruptions and that a shift in magma composition was not responsible for a change in eruptive style. However, the 1872 eruption, which was the last VEI 4 eruption before 2010, has been tentatively linked to a prominent basaltic PDC deposit distributed up to a minimum of 11 km from the summit in valleys and interfluvial areas on the southern flanks of Merapi (Newhall et al. 2000; Gertisser et al. 2011, 2012). If indeed the 1872 eruption was basaltic, then magmatic parameters such as volatile content, viscosity and temperature, would have been unlike those in 2010, indicating that magmatic and eruption dynamics would have also been different during this explosive eruption. Further investigation into microlite textures from different styles of activity in Merapi's past could therefore elucidate magma ascent mechanisms at Merapi for varying eruption styles and aid future monitoring efforts.

To conclude, quantitative textural analysis is an important tool to elucidate processes occurring during magma storage and ascent, especially when combined with additional petrological and compositional information. Currently however, quantitative textural information cannot be used to numerically reveal an ascent rate or magmatic process and is still largely confined to providing only relative rather than absolute information. Advances in the technique are still needed before, for example, a specific crystal number density can be correlated to a particular ascent rate. In the future, advances may potentially be aided by further experiments and comparison of textural data with geophysical data. For example, decompression experiments to establish microlite growth rates, as well as phase equilibria experiments to determine the amphibole stability field at Merapi, would be valuable in order to resolve magma ascent rates and aid future hazard management plans more fully.

Acknowledgements We gratefully acknowledge our colleagues from the Center of Volcanology and Geological Hazard Mitigation (CVGHM) and from BPPTKG in Yogyakarta for their support of this work in Indonesia. KP and RG extend their special thanks to Biyanto for logistical help in the field. Amelia Bain is thanked for a timely and constructive review, which helped to improve this chapter. This is SOEST publication no. 10992.

References

- Andreastuti SD (1999) Stratigraphy and geochemistry of Merapi Volcano, Central Java, Indonesia: implication for assessment of volcanic hazards. Ph.D. Thesis, University of Auckland, New Zealand
- Andreastuti SD, Alloway BV, Smith IEM (2000) A detailed tephrostratigraphic framework at Merapi volcano, Central Java, Indonesia: implications for eruption predictions and hazards assessment. *J Volcanol Geotherm Res* 100:51–67
- Armienti P, Pareschi MT, Innocenti F, Pompilio M (1994) Effects of magma storage and ascent on the kinetics of crystal growth. The case of the 1991–93 Mt. Etna Eruption. *Contrib Mineral Petrol* 115:402–414
- Bahar I (1984) Contribution à la connaissance du volcanisme indonésien: le Merapi (Centre Java); cadre structural, pétrologie, géochimie et implications volcanologiques. PhD Thesis, Université des Sciences et Techniques du Languedoc, Montpellier, France
- Bain AA (2019) Eruption dynamics of cyclic vulcanian explosions from Galeras volcano, Colombia. Ph.D. Thesis, The University of Edinburgh, UK
- Beauducel F, Cornet FH (1999) Collection and three-dimensional modeling of GPS and tilt data at Merapi volcano, Java. *J Geophys Res* 104:725–736
- Berthommier PC (1990) Etude volcanologique du Merapi (Centre-Java): téphrostratigraphie et chronologie—produits éruptifs. Ph.D. Thesis, Université Blaise Pascal, Clermont-Ferrand, France
- Borisova AY, Martel C, Gouy S, Pratomo I, Sumarti S, Toutain JP, Bindeman IN, de Parseval P, Metaxian JP, Surono (2013) Highly explosive 2010 Merapi eruption: evidence for shallow-level crustal assimilation and hybrid fluid. *J Volcanol Geotherm Res* 261:193–208
- Brugger CR, Hammer JE (2010a) Crystal size distribution analysis of plagioclase in experimentally decompressed hydrous rhyodacite magma. *Earth Planet Sci Lett* 300:246–254
- Brugger CR, Hammer JE (2010b) Crystallization kinetics in continuous decompression experiments: implications for interpreting natural magma ascent processes. *J Petrol* 51:1941–1965
- Budi-Santoso A, Lesage P, Dwiyono S, Sumarti S, Subandriyo S, Jousset P, Metaxian JP (2013) Analysis of the seismic activity associated with the 2010 eruption of Merapi Volcano, Java. *J Volcanol Geotherm Res* 61:153–170
- Camus G, Gourgaud A, Mossand-Berthommier CP, Vincent PM (2000) Merapi (Central Java, Indonesia): an outline of the structural and magmatological evolution, with special emphasis to the major pyroclastic events. *J Volcanol Geotherm Res* 100:139–163
- Cashman KV (1988) Crystallization of Mount St. Helens 1980–1986 dacite: a quantitative textural approach. *Bull Volcanol* 50:194–209
- Cashman KV (1992) Groundmass crystallisation of Mount St. Helens dacite, 1980–1986: a tool for interpreting shallow magmatic processes. *Contrib Mineral Petrol* 109:431–449
- Cashman KV, Marsh BD (1988) Crystal size distribution (CSD) in rocks and the kinetics and dynamics of crystallisation II: Makaopuhi lava lake. *Contrib Mineral Petrol* 99:292–305
- Cashman KV, McConnell SM (2005) Multiple levels of magma storage during the 1980 summer eruptions of Mount St. Helens. *WA. Bull Volcanol* 68:57–75
- Chadwick JP, Troll VR, Ginibre C, Morgan D, Gertisser R, Waight TE, Davidson JP (2007) Carbonate assimilation at Merapi volcano, Java, Indonesia: insights from crystal isotope stratigraphy. *J Petrol* 48:1793–1812
- Chadwick JP, Troll VR, Waight TE, van der Zwan FM, Schwarzkopf LM (2013) Petrology and geochemistry of igneous inclusions in recent Merapi deposits: a window into the sub-volcanic plumbing system. *Contrib Mineral Petrol* 165:259–282
- Charbonnier SJ, Gertisser R (2008) Field observations and surface characteristics of pristine block-and-ash flow deposits from the 2006 eruption of Merapi volcano, Java, Indonesia. *J Volcanol Geotherm Res* 177:971–982
- Clarke AB, Stephens S, Teasdale R, Sparks RSJ, Diller K (2007) Petrologic constraints on the decompression history of magma prior to Vulcanian explosions at the Soufrière Hills Volcano, Montserrat. *J Volcanol Geotherm Res* 161:261–274
- Commer M, Helwig SL, Hördt A, Tezkan B (2005) Interpretation of long-offset transient electromagnetic data from Mount Merapi, Indonesia, using a three-dimensional optimization approach. *J Geophys Res* 110:B03207
- Couch S, Harford CL, Sparks RSJ, Carroll MR (2003) Experimental constraints on the conditions of formation of highly calcic plagioclase microlites at the Soufrière Hills volcano, Montserrat. *J Petrol* 44:1455–1475
- Costa F, Andreastuti S, de Maisonneuve CB, Pallister JS (2013) Petrological insights into the storage conditions, and magmatic processes that yielded the centennial 2010 Merapi explosive eruption. *J Volcanol Geotherm Res* 261:209–235
- Deegan FM, Troll VR, Freda C, Misiti V, Chadwick JP, McLeod CL, Davidson JP (2010) Magma-carbonate interaction processes and associated CO₂ release at Merapi Volcano, Indonesia: insights from experimental petrology. *J Petrol* 51:1027–1051

- Deegan FM, Troll VR, Gertisser R, Freda C (2023) Magma-carbonate interaction at Merapi volcano, Indonesia. In: Gertisser R, Troll VR, Walter TR, Nandaka IGMA, Ratdomopurbo A (eds) Merapi volcano—geology, eruptive activity, and monitoring of a high-risk volcano. Springer, Berlin, Heidelberg, pp 291–321
- del Marmol MA (1989) The petrology and geochemistry of Merapi volcano, Central Java, Indonesia. Ph.D. Thesis. The Johns Hopkins University, Baltimore, USA
- Donaldson CH (1976) An experimental investigation of olivine morphology. *Contrib Mineral Petrol* 57:187–213
- Edmonds M, Herd RA (2007) A volcanic degassing event at the explosive-effusive transition. *Geophys Res Lett* 34:L21310
- Eichelberger JC, Carrigan CR, Westrich HR, Price RH (1986) Non-explosive silicic volcanism. *Nature* 323:598–602
- Erdmann S, Martel C, Pichavant M, Kushnir A (2014) Amphibole as an archivist of magmatic crystallization conditions: problems, potential, and implications for inferring magma storage prior to the paroxysmal 2010 eruption of Mount Merapi, Indonesia. *Contrib Mineral Petrol* 167:1016
- Erdmann S, Martel C, Pichavant M, Bourdier JL, Champallier R, Komorowski JC, Cholik N (2016) Constraints from phase equilibrium experiments on pre-eruptive storage conditions in mixed magma systems: a case study on crystal-rich basaltic andesites from Mount Merapi, Indonesia. *J Petrol* 57:535–560
- Gertisser R (2001) Gunung Merapi (Java, Indonesia): Eruptionsgeschichte und Magmatische Evolution eines Hochrisiko-Vulkans. Ph.D. Thesis, Universität Freiburg, Germany
- Gertisser R, Keller J (2003) Temporal variations in magma composition at Merapi Volcano (Central Java, Indonesia): magmatic cycles during the past 2000 years of explosive activity. *J Volcanol Geotherm Res* 123:1–23
- Gertisser R, Charbonnier SJ, Troll VR, Keller J, Preece K, Chadwick JP, Barclay J, Herd RA (2011) Merapi (Java, Indonesia): anatomy of a killer volcano. *Geol Today* 27:57–62
- Gertisser R, Charbonnier SJ, Keller J, Quidelleur X (2012) The geological evolution of Merapi volcano, Central Java, Indonesia. *Bull Volcanol* 74:1213–1233
- Gertisser R, del Marmol M-A, Newhall C, Preece K, Charbonnier S, Andreastuti S, Handley H, Keller J (2023) Geological history, chronology and magmatic evolution of Merapi. In: Gertisser R, Troll VR, Walter TR, Nandaka IGMA, Ratdomopurbo A (eds) Merapi volcano—geology, eruptive activity, and monitoring of a high-risk volcano. Springer, Berlin, Heidelberg, pp 137–193
- Hale AJ, Wadge G, Mühlhaus HB (2007) The influence of viscous and latent heating on crystal-rich magma flow in a conduit. *Geophys J Intern* 171:1406–1429
- Hammer JE, Rutherford MJ (2002) An experimental study of the kinetics of decompression-induced crystallization in silicic melt. *J Geophys Res* 107:1–24
- Hammer JE, Cashman KV, Hoblitt RP, Newman S (1999) Degassing and microlite crystallization during pre-climactic events of the 1991 eruption of Mt. Pinatubo, Philippines. *Bull Volcanol* 60:355–380
- Hammer JE, Cashman KV, Voight B (2000) Magmatic processes revealed by textural and compositional trends in Merapi dome lavas. *J Volcanol Geotherm Res* 100:165–192
- Handley HK, Reagan M, Gertisser R, Preece K, Berlo K, McGee LE, Barclay J, Herd R (2018) Timescales of magma ascent and degassing and the role of crustal assimilation at Merapi volcano (2006–2010), Indonesia: Constraints from uranium-series and radiogenic isotopic compositions. *Geochimica Cosmochimica Acta* 222:34–52
- Hess KU, Dingwell DB (1996) Viscosities of hydrous leucogranite melts; a non-Arrhenian model. *Am Mineral* 81:1297–1300
- Higgins MD (1996) Crystal size distributions and other quantitative textural measurements in lavas and tuff from Egmont volcano (Mt. Taranaki), New Zealand. *Bull Volcanol* 58:194–204
- Higgins MD (2000) Measurement of crystal size distributions. *Am Mineral* 85:1105–1116
- Higgins MD (2006) Quantitative textural measurements in igneous and metamorphic petrology. Cambridge University Press, UK, p 265
- Higgins MD (2011) Textural coarsening in igneous rocks. *Int Geol Rev* 53:354–376
- Higgins MD, Roberge J (2003) Crystal size distribution of plagioclase and amphibole from Soufrière Hills Volcano, Montserrat: evidence for dynamic crystallisation-textural coarsening cycles. *J Petrol* 44:1401–1441
- Higgins MD, Chandrasekharam D (2007) Nature of sub-volcanic magma chambers, Deccan Province, India: evidence from quantitative textural analysis of plagioclase megacrysts in the Giant Plagioclase Basalts. *J Petrol* 48:885–900
- Hoblitt RP, Harmon RS (1993) Bimodal density distribution of cryptodome dacite from the 1980 eruption of Mount St. Helens. Washington. *Bull Volcanol* 55:421–437
- Innocenti S (2006) Lavas and tephra of Merapi volcano, Java, Indonesia: insights from textural analyses and geochemistry. Ph.D. Thesis, The Pennsylvania State University, USA
- Innocenti S, del Marmol MA, Voight B, Andreastuti S, Furman T (2013a) Textural and mineral chemistry constraints on evolution of Merapi volcano, Indonesia. *J Volcanol Geotherm Res* 261:20–37
- Innocenti S, Andreastuti S, Furman T, del Marmol MA, Voight B (2013b) The pre-eruption conditions for explosive eruptions at Merapi volcano as revealed by crystal texture and mineralogy. *J Volcanol Geotherm Res* 261:69–86
- Kirkpatrick RJ (1981) Kinetics of crystallization of igneous rocks. *Rev Mineral* 8:321–398
- Komorowski JC, Jenkins S, Baxter PJ, Picquout A, Lavigne F, Charbonnier S, Gertisser R, Preece K, Cholik N, Budi-Santoso A, Surono (2013) Paroxysmal

- dome explosion during the Merapi 2010 eruption: processes and facies relationships of associated high-energy pyroclastic density currents. *J Volcanol Geotherm Res* 261:260–294
- Kushnir ARL, Martel C, Bourdier JL, Heap MJ, Reuschlé T, Erdmann S, Komorowski JC, Cholik N (2016) Probing permeability and microstructure: unravelling the role of a low-permeability dome on the explosivity of Merapi (Indonesia). *J Volcanol Geotherm Res* 316:56–71
- Lofgren G (1974) An experimental study of plagioclase crystal morphology: isothermal crystallization. *Am J Sci* 274:243–273
- Lofgren G (1980) Experimental studies on the dynamic crystallization of silicate melts. In: Hargreaves RB (ed) *Physics of magmatic processes*. Princeton University Press, Princeton, United States, pp 487–551
- Luehr BG, Koulakov I, Suryanto W (2023) Crustal structure and ascent of fluids and melts beneath Merapi: insights from geophysical investigations. In: Gertisser R, Troll VR, Walter TR, Nandaka IGMA, Ratdomopurbo A (eds) *Merapi volcano—geology, eruptive activity, and monitoring of a high-risk volcano*. Springer, Berlin, Heidelberg, pp 111–135
- Marsh BD (1988) Crystal size distribution (CSD) in rocks and the kinetics and dynamics of crystallization I. Theory. *Contrib Mineral Petrol* 99:277–291
- Mastin LG (2005) The controlling effect of viscous dissipation on magma flow in silicic conduits. *J Volcanol Geotherm Res* 143:17–28
- Melnik OE, Blundy JD, Rust AC, Muir DD (2011) Subvolcanic plumbing systems imaged through crystal size distributions. *Geology* 39:403–406
- Merzbacher C, Eggler DH (1984) A magmatic geohygrometer: application to Mount St. Helens and Other Dacitic Magma. *Geology* 221:587–590
- Moore G, Carmichael ISE (1998) The hydrous phase equilibria (to 3kbar) of an andesite and basaltic andesite from western Mexico: constraints on water content and conditions of phenocryst growth. *Contrib Mineral Petrol* 130:304–319
- Morgan DJ, Jerram DA (2006) On estimating crystal shape for crystal size distribution analysis. *J Volcanol Geotherm Res* 154:1–7
- Müller M, Hördt A, Neubauer FM (2002) Internal structure of Mount Merapi, Indonesia, derived from long-offset transient electromagnetic data. *J Geophys Res* 107(B9):2187
- Nadeau O, Williams-Jones AE, Stix J (2013) Magmatic-hydrothermal evolution and devolatilization beneath Merapi volcano, Indonesia. *J Volcanol Geotherm Res* 261:50–68
- Newhall CG, Melson WG (1983) Explosive activity associated with the growth of volcanic domes. *J Volcanol Geotherm Res* 17:111–131
- Newhall CG, Bronto S, Alloway B, Banks NG, Bahar I, del Marmol MA, Hadisantono RD, Holcomb RT, McGeehin J, Miksic JN, Rubin M, Sayudi SD, Sukhyar R, Andreastuti S, Tilling RI, Torley R, Trimble D, Wirakusumah AD (2000) 10,000 Years of explosive eruptions of Merapi Volcano, Central Java: archaeological and modern implications. *J Volcanol Geotherm Res* 100:9–50
- Noguchi S, Toramaru A, Nakada S (2008) Relation between microlite textures and discharge rate during the 1991–1995 eruptions at Unzen, Japan. *J Volcanol Geotherm Res* 175:141–155
- Ogburn SE, Loughlin SC, Calder ES (2015) The association of lava dome growth with major explosive activity ($VEI \geq 4$): DomeHaz, a global dataset. *Bull Volcanol* 77:40
- Pallister JS, Thornber CR, Cashman KV, Clynne MA, Lowers HA, Mandeville CW, Brownfield IK, Meeker GP (2008) Petrology of the 2004–2006 Mount St. Helens lava dome—implications for magmatic plumbing and eruption triggering. *US Geol Surv Prof Paper* 1750:647–702
- Pallister JS, Schneider DJ, Griswold JP, Keeler RH, Burton WC, Noyles C, Newhall CG, Ratdomopurbo A (2013) Merapi 2010 eruption—chronology and extrusion rates monitored with satellite radar and used in eruption forecasting. *J Volcanol Geotherm Res* 261:144–152
- Peters STM, Troll VR, Weis FA, Dallai L, Chadwick JP, Schulz B (2017) Amphibole megacrysts as a probe into the deep plumbing system of Merapi volcano, Central Java, Indonesia. *Contrib Mineral Petrol* 172:16
- Preece KJ (2014) Transitions between effusive and explosive activity at Merapi volcano, Indonesia: a volcanological and petrological study of the 2006 and 2010 eruptions. Ph.D. Thesis, University of East Anglia, UK
- Preece K, Barclay J, Gertisser R, Herd RA (2013) Textural and micro-petrological variations in the eruptive products of the 2006 dome-forming eruption of Merapi volcano, Indonesia: implications for sub-surface processes. *J Volcanol Geotherm Res* 261:98–120
- Preece K, Gertisser R, Barclay J, Berlo K, Herd R, Facility EIM (2014) Pre- and syn-eruptive degassing and crystallisation processes of the 2010 and 2006 eruptions of Merapi volcano, Indonesia. *Contrib Mineral Petrol* 168:1061
- Preece K, Gertisser R, Barclay J, Charbonnier SJ, Komorowski JC, Herd R (2016) Transitions between explosive and effusive phases during the cataclysmic 2010 eruption of Merapi volcano, Java, Indonesia. *Bull Volcanol* 78:1–16
- Randolph AD, Larson MA (1971) *Theory of particulate processes*. Academic Press, New York
- Ratdomopurbo A, Poupinet G (2000) An overview of the seismicity of Merapi volcano (Java, Indonesia), 1983–1994. *J Volcanol Geotherm Res* 100:193–214
- Ratdomopurbo A, Beauducel F, Subandriyo J, Nandaka IGMA, Newhall CG, Suharna, Sayudi DS, Suparwaka H, Sunarta (2013) Overview of the 2006 eruption of Mt. Merapi. *J Volcanol Geotherm Res* 261:87–97
- Rutherford MJ, Hill PM (1993) Magma ascent rates from amphibole breakdown: an experimental study applied

- to the 1980–1986 Mount St. Helens Eruptions. *J Geophys Res* 98:19667–19685
- Saepuloh A, Koike K, Omura M, Iguchi M, Setiawan A (2010) SAR- and gravity change-based characterization of the distribution pattern of pyroclastic flow deposits as Mt. Merapi during the past 10 years. *Bull Volcanol* 72:221–232
- Stix J, Zapata JA, Calvache M, Cortés GP, Fischer TP, Gómez D, Narvaez L, Ordoñez M, Ortega A, Torres R, Williams SN (1993) A model of degassing at Galeras Volcano, Colombia, 1988–1993. *Geology* 21:963–967
- Subandriyo, Gertisser R, Aisyah N, Humaida H, Preece K, Charbonnier S, Budi-Santoso A, Handley H, Sumarti S, Sayudi DS, Nandaka IGMA, Wibowo HE (2023) An overview of the large-magnitude (VEI 4) eruption of Merapi in 2010. In: Gertisser R, Troll VR, Walter TR, Nandaka IGMA, Ratdomopurbo A (eds) *Merapi volcano—geology, eruptive activity, and monitoring of a high-risk volcano*. Springer, Berlin, Heidelberg, pp 353–407
- Surono JP, Pallister J, Boichu M, Buongiorno MF, Budisantoso A, Costa F, Andreastuti S, Prata F, Schneider D, Clarisse L, Humaida H, Sumarti S, Bignami C, Griswold J, Carn S, Oppenheimer C, Lavigne F (2012) The 2010 explosive eruption of Java’s Merapi volcano—a ‘100-year’ event. *J Volcanol Geotherm Res* 241–242:121–135
- Swanson SE, Naney MT, Westrich HR, Eichelberger JC (1989) Crystallization history of Obsidian Dome, Inyo Domes, California. *Bull Volcanol* 51:161–176
- Tiede C, Camacho AG, Gerstenecker C, Fernández J, Suyanto I (2005) Modeling the density at Merapi volcano area, Indonesia, via the inverse gravimetric problem. *Geochem Geophys Geosyst* 6:Q09011
- Troll VR, Deegan FM (2023) The magma plumbing system of Merapi: The petrological perspective. In: Gertisser R, Troll VR, Walter TR, Nandaka IGMA, Ratdomopurbo A (eds) *Merapi volcano—geology, eruptive activity, and monitoring of a high-risk volcano*. Springer, Berlin, Heidelberg, pp 233–263
- Troll VR, Hilton DR, Jolis EM, Chadwick JP, Blythe LS, Deegan FM, Schwarzkopf LM, Zimmer M (2012) Crustal CO₂ liberation during the 2006 eruption and earthquake events at Merapi volcano, Indonesia. *Geophys Res Lett* 39:L11302
- Troll VR, Deegan FM, Jolis EM, Harris C, Chadwick JP, Gertisser R, Schwarzkopf LM, Borisova AY, Bindeman IN, Sumarti S, Preece K (2013) Magmatic differentiation processes at Merapi volcano: inclusion petrology and oxygen isotopes. *J Volcanol Geotherm Res* 261:38–49
- van Bemmelen RW (1949) *The geology of Indonesia*, vol. 1A, General geology, Government Printing Office, The Hague, Netherlands
- van der Zwan FM, Chadwick JP, Troll VR (2013) Textural history of recent basaltic-andesites and plutonic inclusions from Merapi volcano. *Contrib Mineral Petrol* 166:43–63
- Voight B, Constantine EK, Siswoidjyo S, Torley R (2000) Historical eruptions of Merapi volcano, Central Java, Indonesia, 1768–1998. *J Volcanol Geotherm Res* 100:69–138
- Waters LE, Lange RA (2015) An updated calibration of the plagioclase-liquid hygrometer-thermometer applicable to basalts through rhyolites. *Am Mineral* 100:2172–2184
- Westrich HR, Stockman HW, Eichelberger JC (1988) Degassing of rhyolitic magma during ascent and emplacement. *J Geophys Res* 93:6503–6511
- Widiyantoro S, Ramdhan M, Métaxian JP, Cummins PR, Martel C, Erdmann S, Nugraha AD, Budi-Santoso A, Laurin A, Fahmi AA (2018) Seismic imaging and petrology explain highly explosive eruptions of Merapi Volcano, Indonesia. *Sci Rep* 8:13656
- Whitley S, Gertisser R, Halama R, Preece K, Troll VR, Deegan FM (2019) Crustal CO₂ contribution to subduction zone degassing recorded through calc-silicate xenoliths in arc lavas. *Sci Rep* 9:8803
- Whitley S, Halama R, Gertisser R, Preece K, Deegan FM, Troll VR (2020) Magmatic and metasomatic effects of magma-carbonate interaction recorded in calc-silicate xenoliths from Merapi volcano (Indonesia). *J Petrol* 61:egaa048



Magma-Carbonate Interaction at Merapi Volcano, Indonesia

10

Frances M. Deegan, Valentin R. Troll,
Ralf Gertisser, and Carmela Freda

Abstract

Merapi volcano, Indonesia, is a highly active arc volcano built upon a crustal succession that includes thick carbonate sequences. Calc-silicate (skarn) xenoliths are frequently found in Merapi's erupted products and constitute direct evidence for magma-carbonate interaction beneath the volcano. The xenoliths show mineral assemblages that allow them to be subdivided into two main groups: (1) magmatic skarns formed within the magma system and

(2) exoskarns formed of metamorphosed and metasomatised wall-rocks. Geochemical data including $^{87}\text{Sr}/^{86}\text{Sr}$ and $\delta^{18}\text{O}$ values in erupted rocks and minerals support a model involving magma-carbonate interaction in Merapi magma evolution, while elevated (crustal-type) $\delta^{13}\text{C}_{\text{CO}_2}$ values in fumarole gases have been recognised during recent eruptive events. Furthermore, experiments confirm that carbonate assimilation in Merapi-type magma can rapidly produce a voluminous C–O–H gas phase, which may at times place additional pressure on the magmatic system. The detection of extremely low $\delta^{13}\text{C}$ values in remnant calcite in Merapi xenoliths relative to unmetamorphosed limestone underscores the efficiency of carbonate and calc-silicate degassing during carbonate assimilation. Decarbonation of the arc-crust beneath Merapi may thus at times magnify the volcanic CO_2 output and potentially contribute to the volcano's notoriously erratic eruption behaviour. Magma-carbonate interaction at Merapi is therefore particularly well-studied and represents an archetypical locality for this process.

F. M. Deegan (✉) · V. R. Troll
Department of Earth Sciences, Section for Natural Resources and Sustainable Development, Uppsala University, Uppsala, Sweden
e-mail: frances.deegan@geo.uu.se

F. M. Deegan · V. R. Troll
Centre of Natural Hazards and Disaster Science (CNDS), Uppsala University, Uppsala, Sweden

F. M. Deegan · V. R. Troll · C. Freda
Istituto Nazionale di Geofisica e Vulcanologia (INGV), Rome, Italy

V. R. Troll
Faculty of Geological Engineering, Universitas Padjajaran (UNPAD), Bandung, Indonesia

R. Gertisser
School of Geography, Geology and the Environment, Keele University, Keele, UK

C. Freda
European Plate Observing System (EPOS)—
European Research Infrastructure Consortium (ERIC), Rome, Italy

Keywords

Merapi · Magma-carbonate interaction ·
Crustal assimilation · CO_2

10.1 Introduction

Crustal assimilation occurs when materials comprising the Earth's crust (e.g. sedimentary rock, volcanic deposits, crystalline igneous rocks, and their metamorphic equivalents) are physically and chemically incorporated into magma as it makes its way towards the surface. In his seminal work, Bowen (1928) dedicated a chapter to the role of crustal assimilation in magma genesis, but for several decades afterwards, closed system fractional crystallisation remained the favoured model to explain magmatic differentiation. More recently, discussion of the importance of crustal assimilation in magmatic evolution has undergone a "renaissance" (e.g. O'Hara 1998) and there is general consensus that magma that passed through continental crust (e.g. at continental subduction zones and large igneous provinces) possesses geochemical features that indicate variable amounts of crustal interaction (e.g. Large Igneous Provinces: Bédard et al. 2021; Callegaro et al. 2021; Subduction zones: Davidson et al. 2005; Price et al. 2005). At subduction zones in particular, detailed insight into the processes of magma recharge, assimilation, and fractionation in magma genesis and evolution have come primarily from the application of *in-situ* micro-analytical methods such as laser-based and micro-milling techniques for measurement of radiogenic isotope ratios, which have enabled a wealth of new chemical information to be extracted from individual crystals (e.g. Davidson and Tepley 1997; Tepley et al. 2000; Chadwick et al. 2007; Gardner et al. 2013). In their review paper, Davidson et al. (2005) refer to this new generation of petrology as "crustal forensics", a term which encapsulates the notion of utilising cutting-edge analytical technology to investigate crystal histories.

Magma-carbonate interaction is a sub-type of magma-crust interaction involving CO₃-bearing materials (e.g. minerals and rocks such as calcite, dolomite, limestone, and marl), that when heated by magma have the potential to liberate CO₂. The impact of this liberated CO₂ on volcanic

behaviour, the subduction carbon cycle, and climate can be profound (e.g. Lee et al. 2019). For these reasons, magma-carbonate interaction has been intensely studied at numerous carbonate-hosted volcanic systems such as Etna, Italy (Mollo et al. 2010; Chiodini et al. 2011), the Roman Magmatic Province, Italy (Freda et al. 1997, 2008, 2010; Conte et al. 2009; Dallai et al. 2004; Gaeta et al. 2009; Di Rocco et al. 2012; Gozzi et al. 2014), Vesuvius, Italy (e.g. Barberi and Leoni, 1980; Fulignati et al. 2000, 2004; Del Moro et al. 2001; Gilg et al. 2001; Piochi et al. 2006; Iacono-Marziano et al. 2009; Dallai et al. 2011; Jolis et al. 2013, 2015; Buono et al. 2020) and Popocatepetl, Mexico (e.g. Goff et al. 2001; Schaaf et al. 2005). In addition to these examples, studies have also been carried out on intrusive systems that interacted with carbonate (\pm evaporite) host rocks, such as the Bonanza arc, Canada (Morris and Canil 2022), the Hortavaer intrusive complex, Norway (Barnes et al. 2005, 2009), the Sierra Nevada batholith, USA (Ramos et al. 2020), the Siberian LIP (Pang et al. 2013; Callegaro et al. 2021), the Jinchuan and Panzhihua intrusions in N-central and SW China, respectively (e.g. Lehmann et al. 2007; Ganino et al. 2008, 2013), and the sill province associated with the Central Atlantic Magmatic Province (Heimdal et al. 2018). Numerous experimental studies have also been carried out on magma-carbonate interaction, which we will address further below.

Mount Merapi (*Gunung Merapi*) in Central Java, Indonesia, is a subduction zone (arc) volcano whose plumbing system intersects crustal sedimentary rocks with a large carbonate component (Fig. 10.1). Merapi is so well-studied that it has come to represent a text book locality for magma-carbonate interaction. Many workers have utilised modern analytical techniques to conduct "forensic" studies of Merapi's erupted products (e.g. Chadwick et al. 2007, 2013; Borisova et al. 2013, 2016; Nadeau et al. 2013; Prece et al. 2013, 2014, 2016; Troll et al. 2013a; van der Zwan et al. 2013; Deegan et al. 2016a, 2021; Peters et al. 2017; Handley et al. 2018; Whitley et al. 2019, 2020; Whitley 2020), some have

looked at the source of the CO₂ emitted by Merapi (e.g. Troll et al. 2012; Aiuppa et al. 2017) and others have performed direct experimentation to clarify reaction rates and pathways involved in magma-carbonate interaction (Deegan et al. 2010, 2016b; Blythe et al. 2015). In this chapter, we review the current state of knowledge regarding magma-carbonate interaction at Merapi, beginning with a brief outline of the geological context of Merapi including an overview of the variety of calc-silicate xenoliths reported from Merapi (Sect. 10.3), before moving on to the mineralogy of calc-silicate xenoliths at Merapi (Sect. 10.4), the geochemical record of magma-carbonate interaction at Merapi (Sect. 10.5), and advances made at Merapi employing experimental petrology (Sect. 10.6). We close with a summary of the volatile budget of the carbonate-hosted magmatic system at Merapi (Sect. 10.7).

10.2 A Brief History of Research on Magma-Carbonate Interaction

One of the most fundamental advances in our understanding of contact metamorphism (also often referred to as “thermal” or “pyro” metamorphism) was made by Victor Moritz Goldschmidt (1888–1947) in his 483-page doctoral monograph published in 1911, entitled “*Die Kontaktmetamorphose im Kristianiagebiet*” (“Contact Metamorphism in the Kristiania Region”; note that Kristiania was the name for Oslo, Norway until 1925). In this work, Goldschmidt studied contact phenomena in a range of intruded rock compositions, including limestones in the present-day Oslo region of Norway. Crucially, Goldschmidt (1911) produced a pressure–temperature curve for the contact metamorphic reaction that describes the transformation of limestone into wollastonite: $\text{CaCO}_3 + \text{SiO}_2 = \text{CaSiO}_3 + \text{CO}_2$. A related petrological term is “*skarn*”, which is a rock type characterised by calcium-rich mineral assemblages. The word “*skarn*” has its roots in the Scandinavian mining sector and in 1920, Arthur Holmes (1890–1965)

published his book “The Nomenclature of Petrology”, in which he defined skarn as:

An old Swedish mining term for the silicate gangue (amphibole, pyroxene, garnet, etc.) of certain iron ore and sulphide deposits of Archaean age, particularly those which have replaced limestone and dolomite. The term is used in this sense by Fennoscandian geologists, but it has been extended to cover analogous products of contact metamorphism in younger formations”. (Holmes 1920)

Another pioneering work in the field of magma-carbonate interaction is that by Eskola (1922), who reports extensive mineralogical observations on contact phenomena between limestone and gneiss in Western Massachusetts. Pentti Eskola (1883–1964) was a Finnish scholar and was accompanied by Norman L. Bowen (1887–1956), during the field campaign that led to his 1922 publication in which he writes:

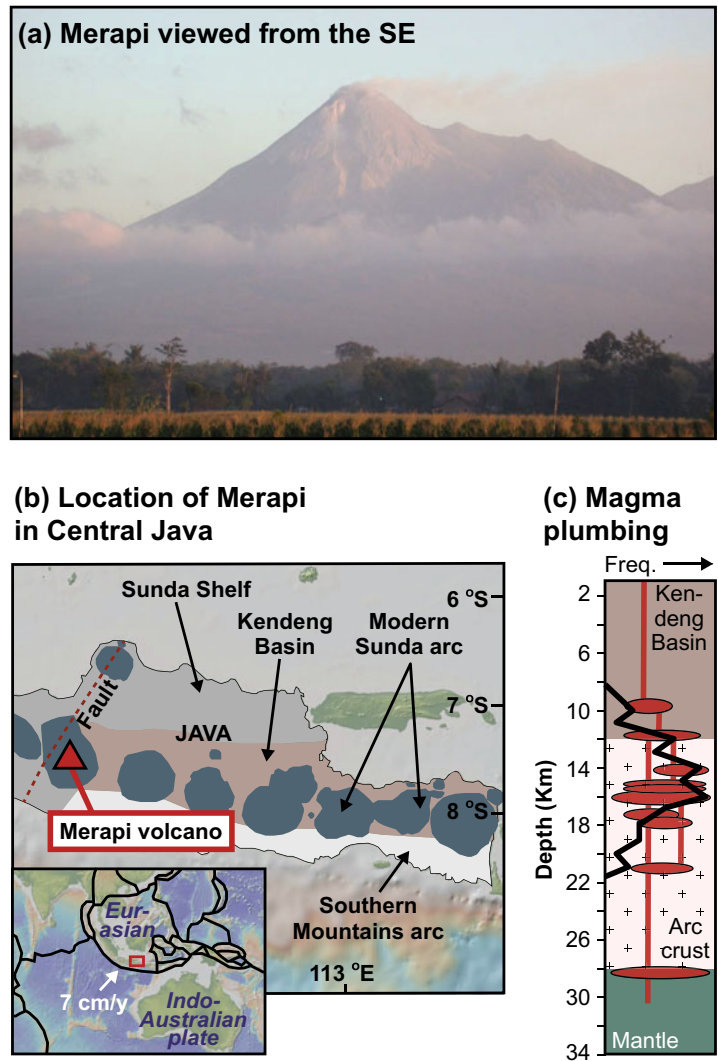
The writer believes that the mode of occurrence of the clinopyroxene gneiss around and near the occurrences of limestone included in the gneiss is in itself sufficient evidence that the gneiss has received its excessive amount of lime through assimilation of the limestone. (Eskola 1922)

Following the work by Eskola, in 1928, Dutch geologist H.A. Brouwer published a paper concerning magma-carbonate interaction at Merapi volcano, wherein he discusses the phenomena of limestone assimilation at Javanese volcanoes and offers, to the best of our knowledge, the earliest mineralogical description of a calc-silicate crustal xenolith at Merapi:

A large block (50 × 50 × 30) centimeters of metamorphosed limestone on the slope of the volcano Merapi has a zonal structure. In some zones wollastonite is the principal mineral; calcite and augite are often found associated with it, and sometimes plagioclase and augite are the predominating minerals. [...] Of course these observations have not the same value as that of an experiment on the effects of dissolving limestone in basaltic or andesitic melts. (Brouwer 1928)

Brouwer would go on to teach Reinout Willem van Bemmelen (1904–1983), who in turn mapped large parts of Java and Sumatra and witnessed the 1930s and 1940s activity of Merapi before publishing his seminal work “The Geology of Indonesia” in 1949.

Fig. 10.1 **a** Photo of Merapi volcano taken in 2014 with a visible open crater (after Troll et al. 2015). **b** Map of Central to East Java showing the location of Merapi and the Kendeng Sedimentary Basin. Inset shows the regional tectonic setting with Central Java shown in a red box (modified after Deegan et al. 2021). **c** Crustal structure and magma plumbing beneath Merapi. Black curve represents the frequency (“Freq.”) of crystallisation depths calculated from clinopyroxene mineral data (after Deegan et al. 2016a)



It is also worth mentioning here the important contributions to our current understanding of magma-carbonate interaction from Swiss volcanologist Alfred Rittmann (1893–1980). A major part of Rittmann’s early career focussed on Vesuvius volcano in Italy, where he demonstrated the role of limestone assimilation in controlling the compositional evolution of Vesuvian magmas. One of Rittmann’s most famous works was his textbook “*Vulkane und ihre Tätigkeit*”, originally published in the German language and later translated to English

(Rittmann 1962), which contains a summary of the role of crustal assimilation in generating magma diversity.

The recent scientific literature (since the 2000s) has seen a surge of publications addressing magma-carbonate interaction. Due to the continually unfolding wealth of petrological and geochemical information available on Merapi in particular (e.g. Gertisser and Keller 2003a, b; Chadwick et al. 2007, 2013; Deegan et al. 2010, 2016a, 2021; Troll et al. 2012, 2013a; Borisova et al. 2013, 2016; Costa et al. 2013;

Nadeau et al. 2013; Preece et al. 2013, 2014, 2016; van der Zwan et al. 2013; Erdmann et al. 2014, 2016; Aiuppa et al. 2017; Peters et al. 2017; Handley et al. 2018; Whitley et al. 2019, 2020; Whitley 2020), magma evolution and magma-carbonate interaction is particularly well-documented in this locality.

10.3 Geological Context of Merapi

The geodynamic context of Merapi is reviewed in detail by Harijoko et al. (2023, Chap. 4). In brief, Merapi is a large stratovolcano (c. 3000 m a.s.l.) located in Central Java, Indonesia, and constitutes part of the active volcanic front of the Sunda arc (Fig. 10.1a, b). The Sunda arc, in turn, is a ca. 5600 km long, mixed oceanic-continent arc system, which results from northward subduction of the Indo-Australian plate beneath Eurasia at a rate of about $6.5\text{--}7\text{ cm yr}^{-1}$ and extends from the Andaman Islands, through Sumatra, Java, Bali, and Flores (e.g. Curray et al. 1977; Hamilton 1979; Tregoning et al. 1994; Hall 2002; Smyth et al. 2008; Metcalfe 2011; see Fig. 10.1b).

In Central Java, subduction occurs beneath arc crust of c. 30 km thickness, however, the nature of the lower arc crustal basement is uncertain and sometimes referred to as “immature arc crust” (Curray et al. 1977; Hamilton 1979; Wölbern and Rümpler 2016). Regarding the upper arc crust, the currently active central Javan volcanic arc is partly sited on the Kendang sedimentary basin, of which estimates of the sediment thickness range from 8 to 11 km (de Genevraye and Samuel 1972; Untung and Sato 1978; Smyth et al. 2008; Fig. 10.1b, c). Beneath Merapi, the upper arc crustal succession consists of Cretaceous to Cenozoic limestone, marl, and volcanoclastic units (van Bemmelen 1949). Thick limestone packages can be observed in quarries on the outskirts of Yogyakarta (Fig. 10.2a) as well as on the beach at Parangtritis, south of Merapi, but good exposure is otherwise rare due to the young sedimentary fill of the Yogyakarta graben that results in dense vegetation and habitation in the area. The upfaulted cliffs at

Parangtritis (25–100 m) are part of the *Gunung Kidul*, a plateau that extends along the southern coast of Central and Eastern Java (Haryono and Day 2004). This topographic high is largely composed of Miocene carbonates of the Wonosari Formation, which consists of massive coral reef limestone in the south and bedded chalky limestone in the north (Balazs 1968; Waltham et al. 1983; Surono et al. 1992). In thin section, radiolarians, pollen or spores, and numerous foraminifera types, including e.g. *Globigerina* among others, can be identified (Fig. 10.2b). The total thickness of this limestone unit is estimated to be greater than 650 m but sedimentary units in the Central Java area extend to even greater depths.

The volcano-magmatic plumbing system at Merapi is reviewed in this volume by Gertisser et al. (2023, Chap. 6), Luehr et al. (2023, Chap. 5), and Troll and Deegan (2023, Chap. 8). To summarise briefly, magma generation is focused in the mantle wedge under Central Java leading to formation of a plexus of magma reservoirs first in the lower crust and then in the mid-crust (i.e. in the crystalline basement under the volcano) where magmas stall and crystallise (Fig. 10.1c). Petrological barometers as well as geophysical radar techniques have identified an additional magma storage region in the upper crust under Merapi at depths of 5 km or less (e.g. Ratdomopurbo and Poupinet 2000; Nadeau et al. 2013; Chadwick et al. 2013; Chaussard and Amelung 2014; Preece et al. 2014; Deegan et al. 2016a). These types of high-level reservoir systems have been termed “SHARCS” (Shallow Arc Storage Systems) by Deegan et al. (2019) and are the sites where arc magmas may come into contact with crustal carbonate whereupon the two may chemically and physically interact.

Recent volcanic deposits at Merapi are largely the result of extrusion of viscous lavas forming a dome complex in the summit area, producing block and ash flows due to gravitational instability and collapse of the dome area (see Voight et al. 2000 for an overview of the topic). Pyroclastic deposits are of basaltic andesite composition and contain abundant fragments of foreign material (xenoliths). These fragments may be

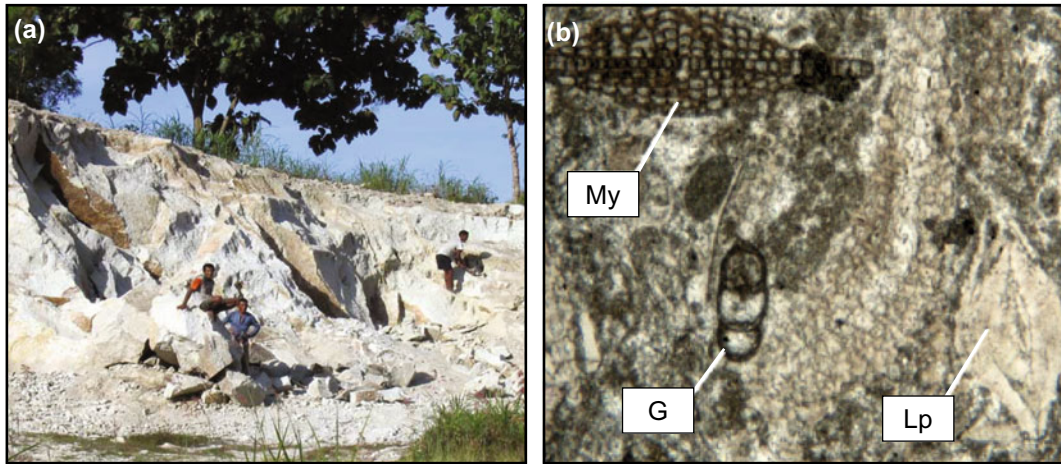


Fig. 10.2 **a** Limestone quarry in the western outskirts of Yogyakarta, Central Java, with quarry workers for scale. Image after Troll et al. (2013a, b). **b** Photomicrograph of Javanese limestone under plane polarised light, showing

in this case three types of foraminifera—Myogypsina (My), Lepidocyclina (Lp), and Globigerina (G). Field of view is approximately 2 mm. Image after Chadwick (2008)

broadly divided into two groups (Troll et al. 2013a) comprising (1) igneous inclusions such as mafic enclaves and crystalline cumulates and (2) variably metamorphosed calc-silicate xenoliths derived from thermal metamorphism of crustal carbonate rock, which frequently exhibit well-developed, skarn-type, vesicular reaction rims (Fig. 10.3). The presence of calc-silicate xenoliths points to high-level crustal processes, especially magma-carbonate interaction and volatile release. The occurrence of calc-silicate xenoliths at Merapi has been noted and described by several workers (e.g. Brouwer 1928; Clocchiatti et al. 1982; Kerinec 1982; Camus et al. 2000; Gertisser and Keller 2003a), and detailed geochemical and isotope analyses were subsequently presented by Chadwick et al. (2007), Deegan et al. (2010), Troll et al. (2013a), Borisova et al. (2016), Whitley et al. (2019, 2020), and Whitley (2020), which we summarise below.

10.4 Mineralogy of Merapi Calc-Silicate Xenoliths

Calc-silicate xenoliths are relatively frequent in Merapi basaltic-andesite deposits and tend to occur as white to green coloured, thermally

metamorphosed limestones with well-developed reaction rims that may be partially infiltrated by basaltic-andesite (Fig. 10.3). Merapi calc-silicate xenoliths are commonly up to several centimetres in size, but on rare occasions xenoliths several decimetres in size can be found (e.g. the sample in Fig. 10.3a and the sample described by Brouwer (1928). Besides calc-silicate xenoliths, rare thermally overprinted siliciclastic and volcanoclastic inclusions occur that testify to lithological inhomogeneity within the sub-Merapi sedimentary bedrock (Chadwick et al. 2007; Whitley et al. 2020). Calc-silicate inclusions have also been found as small, but rare, xenoliths within diorite inclusions in Merapi basaltic-andesite, suggesting their availability in the plutonic environment (Chadwick et al. 2013).

Merapi calc-silicate xenoliths were described by Chadwick (2008) as being dominated by diopside and wollastonite with traces of quartz, tremolite and garnet. Chadwick et al. (2007) carried out a core to rim mineralogical analysis of a large calc-silicate xenolith using X-ray diffraction (XRD) and the results indicate an increase in wollastonite content towards the xenolith core (up to 74%) and a dominance of diopside and anorthite in the rim (diopside up to 60% in rims) (Fig. 10.4). This mineralogy is

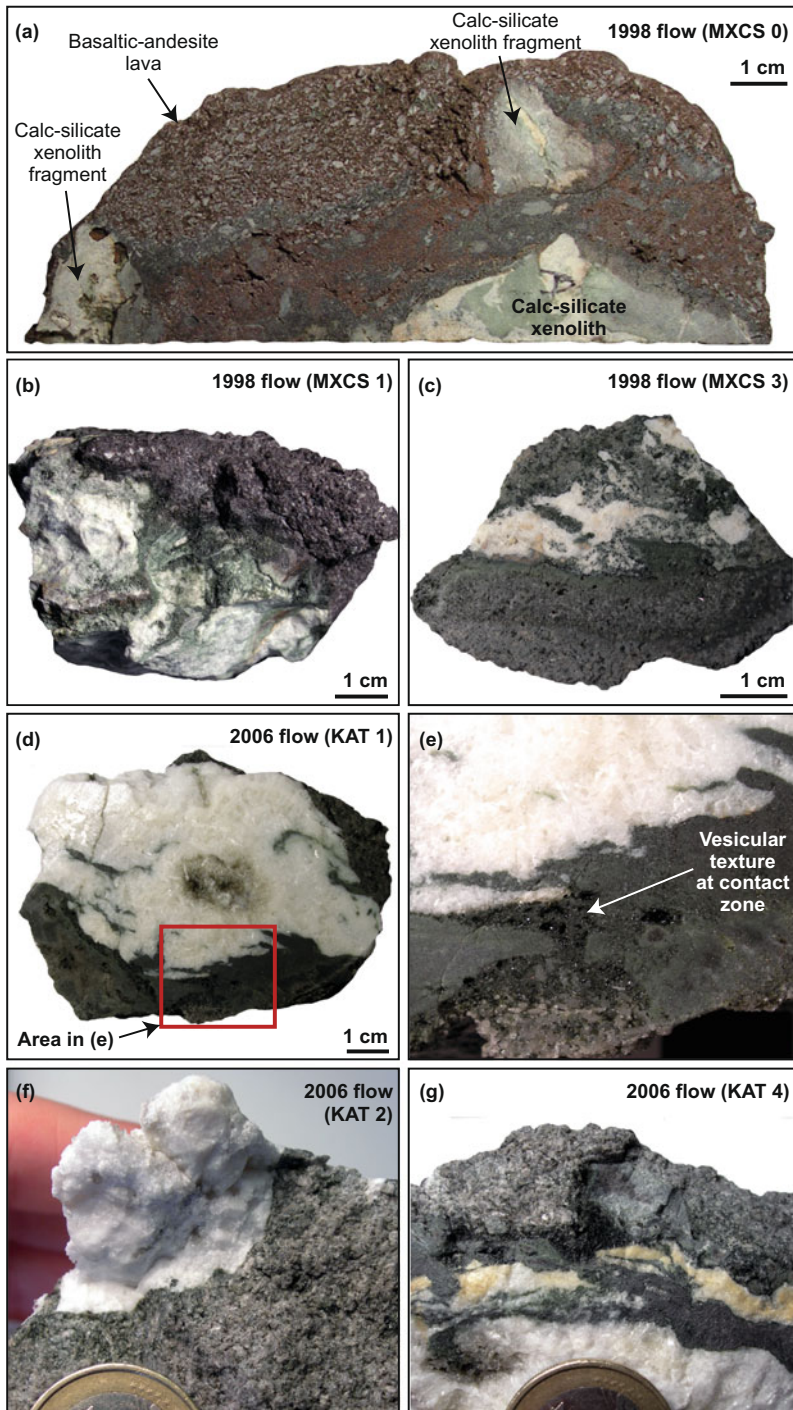
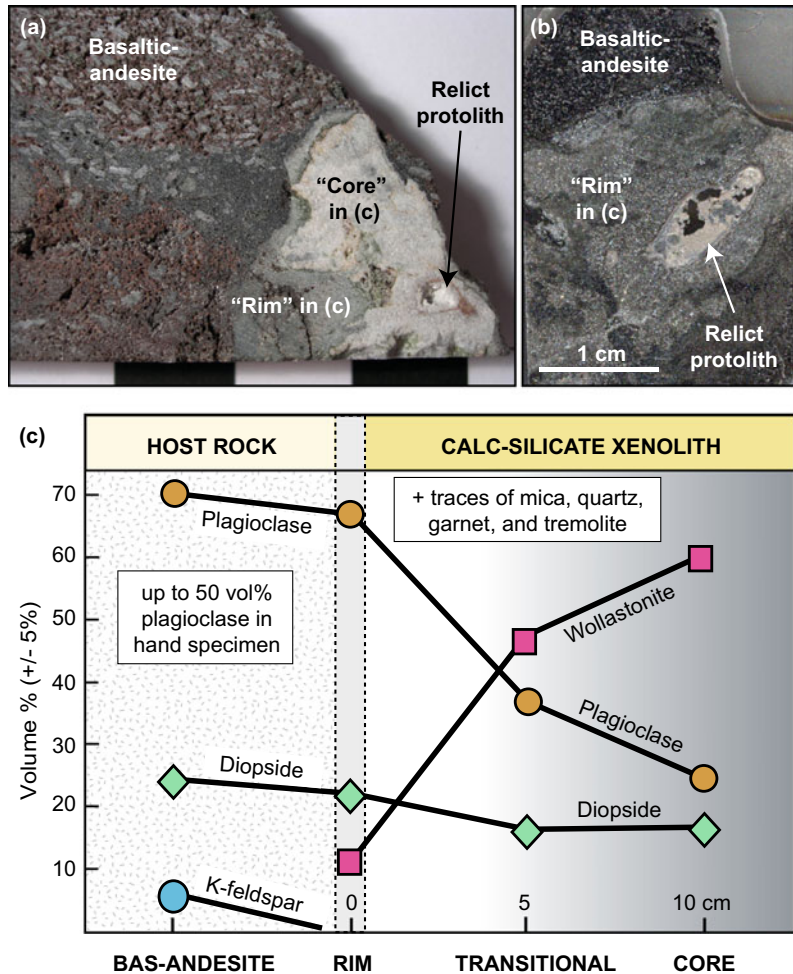


Fig. 10.3 a–g Examples of calc-silicate xenoliths from the 1998 (a–c) and 2006 (d–g) eruption deposits of Merapi volcano. While the textures are diverse, in all cases a pale coloured wollastonite-rich xenolith core is mantled by a green coloured diopside-bearing skarn-type mineral assemblage. Note the particularly vesiculated

texture at the contact zone in (e), which appears to be more vesiculated than the surrounding lava. These xenoliths are part of the sample collection of Chadwick et al. (2007), Deegan et al. (2010), and Troll et al. (2012, 2013a, b). Scale in (f) and (g) is provided by the top part of a €1 coin (23.25 mm diameter)

Fig. 10.4 **a** Slice through a representative wollastonite-bearing, light coloured calc-silicate xenolith mantled by a greenish reaction rim in contact with Merapi host basaltic-andesite (same sample as shown in Fig. 10.3a). **b** Close up of another slice through the same calc-silicate showing a relict fragment of carbonate surrounded by a finely crystalline, green hued reaction rim. **c** Mineralogical rim to core profile of this xenolith shows an increase in vol% wollastonite from rim to core accompanied by a concomitant decrease in plagioclase and diopside. These observations demonstrate that the xenolith was “caught in the act” of magma-carbonate interaction. Data in panel **c** replotted after Troll et al. (2012)



indicative of an advanced stage of magma-xenolith interaction, as it reflects the conversion of the original limestone to a higher-grade metamorphic rock through prograde thermo-metamorphic reactions (cf. Bowen 1928; Fulignati et al. 2004; Gaeta et al. 2009; Mollo et al. 2010). Element maps across the contact between a calc-silicate xenolith and its host lava are consistent with this process. For instance, the calc-silicate xenolith MXCS 3 (from the sample collection of Chadwick et al. 2007 and Deegan et al. 2010) is mantled by a finely crystalline (diopside-rich), green coloured reaction zone with a composition transitional between the xenolith and lava (Fig. 10.5).

More recently, a detailed appraisal of Merapi calc-silicate xenoliths was carried out by Whitley et al. (2019, 2020), who described both magmatic skarn xenoliths (formed within the magma) and exoskarn xenoliths (fragments of metamorphosed and metasomatised wall-rocks). According to Whitley et al. (2020), the magmatic skarn group comprises distinct compositional and mineralogical zones and contains Ca-enriched glass (up to 10 wt% relative to lava groundmass). The magmatic skarns are mineralogically dominated by clinopyroxene, plagioclase, and magnetite in the outer zones towards the host lava and by wollastonite, clinopyroxene, plagioclase, garnet, and quartz in xenolith cores. Whitley

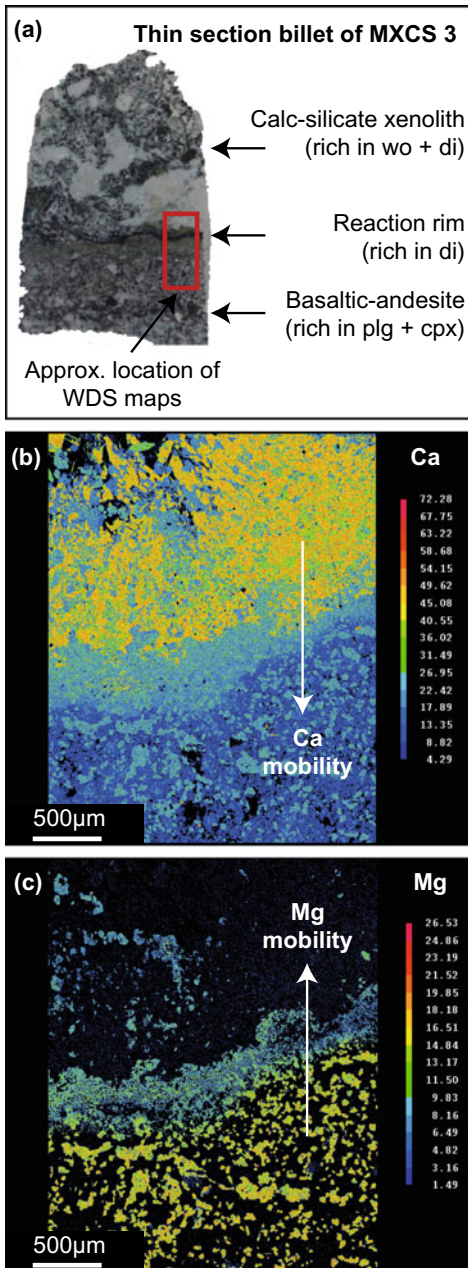
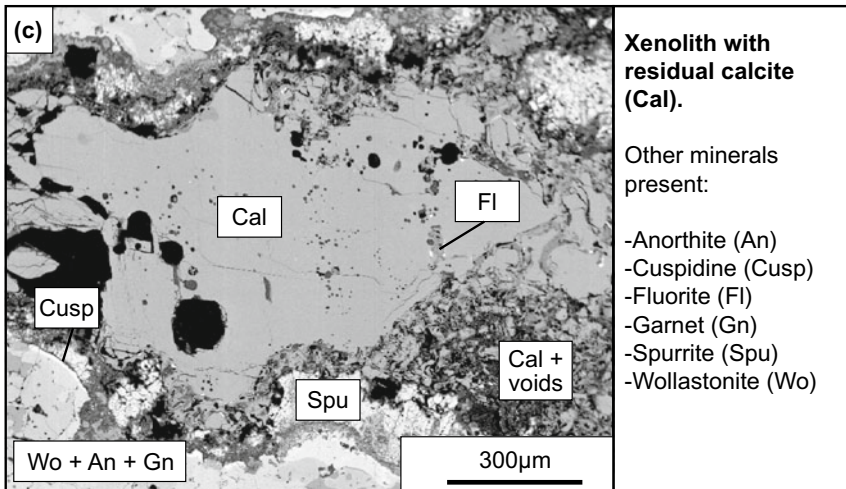
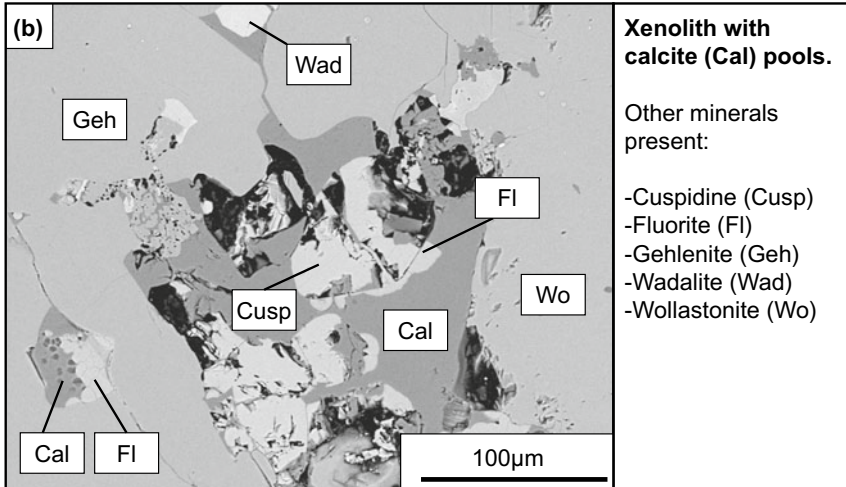
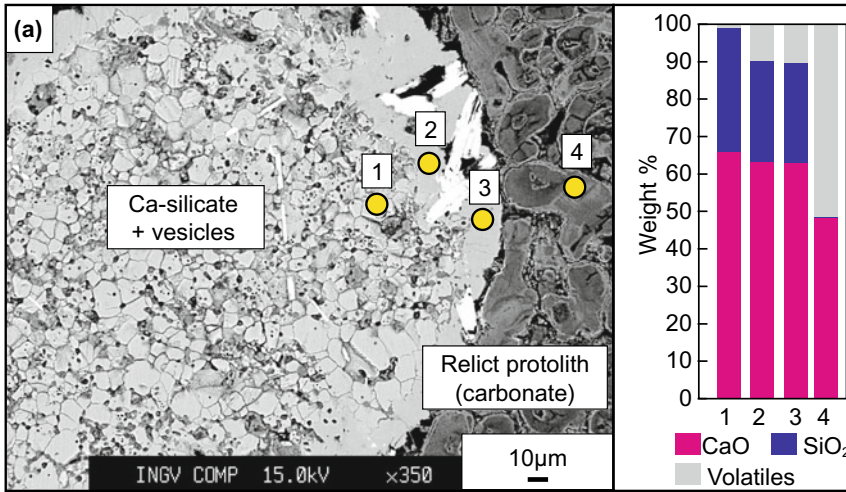


Fig. 10.5 **a** Photograph of a thin section billet prepared from xenolith MXCS 3 with a sharp reaction zone visible in the red box (MXCS 3 is part of the sample collection presented in Chadwick et al. (2007) and housed at Uppsala University, Sweden). **b, c** Electron microprobe X-ray maps of the area in the red box in **(a)** are shown in panel **(b)** for Ca and in panel **(c)** for Mg. Note that the contact between xenolith and host lava is demarcated by a finely textured zone of transitional Ca and Mg contents. X-ray maps were acquired at INGV Rome (see also Deegan et al. 2010). Abbreviations: wo = wollastonite; di = diopside; plg = plagioclase; cpx = clinopyroxene

et al. (2020) proposed that the distinct xenolith zones are controlled by Ca transfer from the limestone protolith to the magma and by transfer of magma-derived elements in the opposite direction, which is consistent with the X-ray maps presented in Fig. 10.5, where Ca can be seen to be transferred from the xenolith towards the host lava whereas Mg appears to be transferred in the opposite direction.

Exoskarns, on the other hand, do not display mineral zonation due to equilibration crystallisation at sub-solidus conditions. The major mineral assemblage in the exoskarn xenoliths includes wollastonite, garnet, Ca-Al-rich clinopyroxene, anorthite, and quartz, with variable amounts of either quartz or melilite and spinel (Whitley et al. 2020). These authors also carried out thermobarometric calculations, fluid inclusion microthermometry and oxybarometry to show that the studied magmatic skarn xenoliths formed at ca. 850 ± 45 °C, <100 MPa, and at oxygen fugacity between the NNO and HM buffer, whereas the exoskarn xenoliths formed at ca. 510–910 °C under oxygen fugacity conditions between NNO and air (Whitley et al. 2020). Furthermore, Whitley et al. (2019, 2020) demonstrated that Merapi calc-silicate xenoliths likely interacted with a halogen-bearing fluid, which can explain the occurrence of exotic, halogen-bearing mineral phases such as cuspidine ($\text{Ca}_4(\text{Si}_2\text{O}_7)(\text{F},\text{OH})_2$) in some of the xenoliths (Fig. 10.6).

Occasionally, remnants of unmetamorphosed calcium carbonate occur in the cores of calc-silicate xenoliths (Figs. 10.4a, b and 10.6; Deegan et al. 2010; Whitley et al. 2019). Where original carbonate is found in the xenoliths, it tends to be associated with Ca-enriched and volatile-bearing mineral phases and/or glass in close proximity (Fig. 10.6). Samples with original carbonate can be thought of as being “caught in the act” of magma-carbonate interaction and associated decarbonation (Deegan et al. 2010; Whitley et al. 2019). The key reaction involved in the Merapi calc-silicate xenoliths is CaCO_3 (limestone) + SiO_2 (silica) \rightarrow CaSiO_3 (wollastonite) + CO_2 . This reaction releases CO_2 and indeed, glassy zones within calc-silicate xenoliths in contact with



◀ **Fig. 10.6** **a** Back scattered electron (BSE) image of the core of the xenolith shown in Fig. 10.3a. Electron Probe Microanalysis (EPMA) analysis spots traversing carbonate and adjacent recrystallised calc-silicate show a progressive loss of volatiles and increase in CaO and SiO₂ (wt%) as carbonate is converted to calc-silicate (image and data after Deegan et al. 2010). **b** BSE image of a calc-silicate xenolith with calcite pools and fluorine-

bearing minerals such as fluorite (CaF₂) and cuspidine (Ca₄(Si₂O₇)(F,OH)₂). **c** BSE image of a calc-silicate with residual calcite, mantled by spurrite (Ca₅(SiO₄)CO₃) and wollastonite (CaSiO₃), among others. These images demonstrate the diverse assemblage of volatile-bearing minerals that can develop during magma-carbonate interaction. Images in panels (b) and (c) are modified after Whitley et al. (2019)

carbonate contain dissolved volatiles (Fig. 10.6a) whereas lava at direct magma–calc-silicate interfaces is often vesicular, probably due to degassing of volatiles from the magma (cf. Deegan et al. 2010; Troll et al. 2012; Fig. 10.3). The liberated CO₂ is added to the magmatic volatile budget and has been discussed in the literature as having the potential to impact the volcano’s gas chemistry and eruptive behaviour (e.g. Troll et al. 2012; Aiuppa et al. 2017; Carr et al. 2020).

10.5 Geochemical Evidence of Magma-Carbonate Interaction

At Merapi, there is strong geochemical evidence for assimilation of carbonate rocks during magma differentiation (e.g. Chadwick et al. 2007; Costa et al. 2013; Deegan et al. 2010, 2016a, 2021; Troll et al. 2012, 2013a, b; Borisova et al. 2013, 2016; Whitley et al. 2019, 2020; Whitley 2020). As we have so far reviewed, this process was initially recognised by the presence of partially metamorphosed and metasomatised calc-silicate xenoliths in Merapi’s erupted products. These xenoliths are coupled with geochemical features in the Merapi’s erupted products that permit detailed insight into assimilation processes, as described below.

10.5.1 Strontium Isotopes

Strontium isotope data obtained for Merapi erupted materials are summarised in Table 10.1 and Fig. 10.7a. Among the earliest reports of strontium isotope data for Merapi were the works by Whitford (1975), McDermott and Hawkesworth (1991), and Turner and Foden (2001).

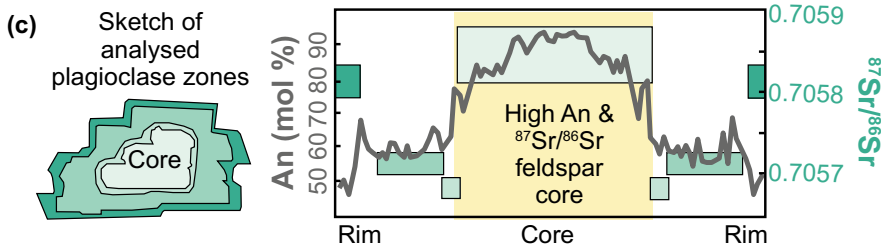
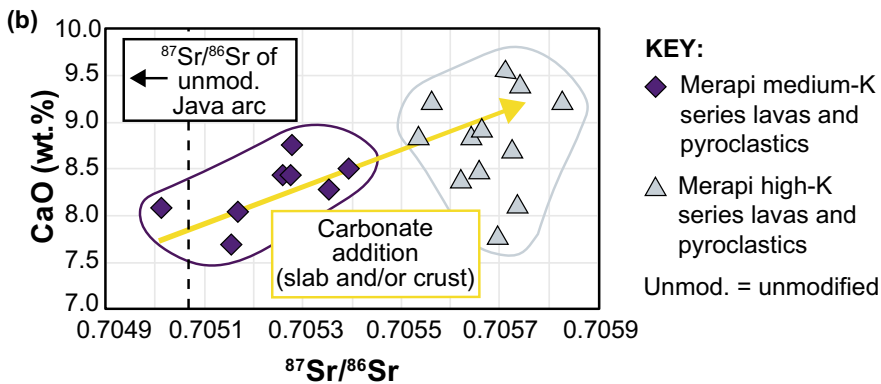
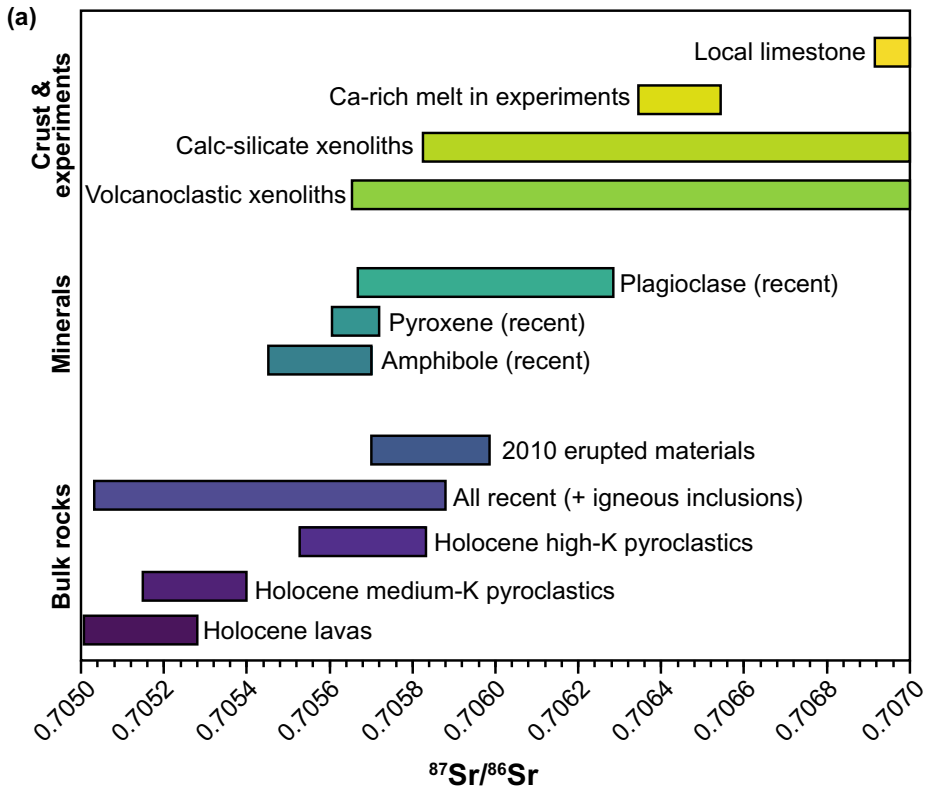
Following these pioneering efforts, the work by Gertisser and Keller (2003a) presented a comprehensive dataset of major and trace elements as well as Sr–Nd–Pb–O isotopic ratios for Holocene and recent Merapi erupted materials. Later work by Debaille et al. (2006), Borisova et al. (2013), Chadwick et al. (2013), Jolis (2013), Handley et al. (2018) and Deegan et al. (2021) added ⁸⁷Sr/⁸⁶Sr ratios for recent Merapi lavas and plutonic inclusions. The study by Gertisser and Keller (2003a) showed that Merapi high-K series rocks have overall higher ⁸⁷Sr/⁸⁶Sr than their medium-K counterparts, as well as being enriched in LILE and LREE and slightly depleted in HREE and HFSE compared with rocks from the medium-K series. In fact, the increase in K₂O among Merapi erupted products was found to be accompanied by a marked increase in ⁸⁷Sr/⁸⁶Sr and an overall decrease in ¹⁴³Nd/¹⁴⁴Nd, but not by systematic variations in oxygen isotope ratios. These geochemical patterns led the authors to focus their discussion on the involvement of subducted sediments with high ⁸⁷Sr/⁸⁶Sr ratios in magma genesis at Merapi. At that time, the available oxygen isotope data did not signal significant crustal assimilation and the study by Debaille et al. (2006) subsequently excluded crustal assimilation in the context of their isotopic mixing models. It should be noted, however, that later studies added considerably to the available oxygen isotope data pool for Merapi (including data for individual mineral phases) and the oxygen isotope data as a whole now permit a somewhat different perspective to what was possible prior to 2013 (see Sect. 10.5.2). We also highlight here that the relationship between CaO and ⁸⁷Sr/⁸⁶Sr in the dataset from Gertisser and Keller (2003a) might point to crustal additions from the arc crust (Fig. 10.7b), but looking at the data as a whole, it would appear that both

Table 10.1 Summary of strontium isotope data for Merapi volcano reported since the year 2000

| Analysed material | Min. $^{87}\text{Sr}/^{86}\text{Sr}$ | Max. $^{87}\text{Sr}/^{86}\text{Sr}$ | Reference(s) |
|---|---|---|--|
| <i>Lavas and ash (Holocene to 2010 eruption)</i> | | | |
| Holocene and recent | 0.705010 | 0.705830 | Gertisser and Keller (2003a) |
| Recent (since 1006 AD) | 0.705040 | 0.705349 | Turner and Foden (2001) |
| Recent | 0.705043 | 0.705876 | Debaille et al. (2006) |
| Recent (1998, 2006 eruptions) | 0.705598 | 0.705714 | Jolis (2013) |
| Recent (2006 eruption) | 0.705713 | 0.705727 | Deegan et al. (2021) |
| Recent (2006, 2010 eruptions) | 0.705290 | 0.705742 | Handley et al. (2018) |
| Recent (2010 eruption) | 0.705710 | 0.705980 | Borisova et al. (2013) |
| <i>Mineral data (minerals from recent eruptions, 1990s and 2000s)</i> | | | |
| Amphibole (single megacrysts) | 0.705459 | 0.705690 | Peters et al. (2017) |
| Plagioclase (individual mineral zones) | 0.705680 | 0.706270 | Chadwick et al. (2007) |
| Plagioclase (mineral separates) | 0.705697 | 0.705731 | Jolis (2013) |
| Pyroxene (mineral separates) | 0.705611 | 0.705711 | Jolis (2013) |
| <i>Igneous inclusions</i> | | | |
| Co-magmatic and plutonic inclusions | 0.705290 | 0.705740 | Chadwick et al. (2013) |
| <i>Experimental glass</i> | | | |
| Ca-enriched glass (limestone contaminated) | 0.706361 | 0.706532 | Deegan et al. (2010) |
| <i>Calc-silicate xenoliths</i> | | | |
| | 0.705842 | 0.707866 | Gertisser and Keller (2003a), Chadwick et al. (2007) |
| <i>Volcaniclastic xenoliths</i> | | | |
| | 0.705671 | 0.707361 | Chadwick et al. (2007, 2013) |
| <i>Java limestone</i> | | | |
| | 0.706932 | 0.707350 | Gertisser and Keller (2003a) |

Fig. 10.7 a Sr isotope variation diagram for Merapi bulk rocks and minerals in comparison to crustal materials and experimentally generated Ca-rich glasses. The bulk rock data display an overall stepwise progression towards more radiogenic isotope ratios from Holocene lavas to materials erupted from the explosive 2010 event. The mineral data also show a stepwise progression towards higher $^{87}\text{Sr}/^{86}\text{Sr}$ ratios from (relatively deep grown) amphibole to (relatively shallow grown) plagioclase. Both plagioclase and materials from the 2010 eruption overlap with the range of $^{87}\text{Sr}/^{86}\text{Sr}$ ratios for calc-silicate xenoliths and they approach the range of $^{87}\text{Sr}/^{86}\text{Sr}$ ratios for Ca-rich melts produced by experimental magma-carbonate interaction, which constitutes strong evidence for carbonate and/or calc-silicate assimilation at Merapi. Data sources are given in Table 10.1. **b** Plot of $^{87}\text{Sr}/^{86}\text{Sr}$ versus CaO wt% for Merapi medium-K and high-K lavas using data presented in Gertisser and Keller (2003a) demonstrating a correlation that hints at carbonate addition during magma genesis (note that there is

significant overlap in CaO contents of both groups of lavas, with the high-K group extending to higher CaO contents; this overlap in CaO content is not obvious here as only lavas with both CaO and $^{87}\text{Sr}/^{86}\text{Sr}$ data are plotted). Notably, regional values for Javanese arc magmas fall to the left of the vertical dashed line, implying that the elevated Sr isotope ratios in Merapi lavas are likely the result of crustal assimilation within the Merapi plumbing system rather than slab processes. **c** Example of mineral-scale $^{87}\text{Sr}/^{86}\text{Sr}$ data obtained on Merapi plagioclase (modified after Chadwick et al. 2007). This particular plagioclase crystal is strongly zoned and displays a high anorthite (thick grey line) core and high $^{87}\text{Sr}/^{86}\text{Sr}$ (green rectangles) core and outermost rim, demonstrating the dynamic nature of magmatic processes at Merapi, which may include crustal xenocryst recycling (high An core) and carbonate assimilation during subsequent crystal growth (medium An outermost rim). The height of the rectangles corresponds to 2σ uncertainty on the $^{87}\text{Sr}/^{86}\text{Sr}$ data



source and crustal contamination have a role to play in controlling the geochemistry of Merapi rocks (see also Gertisser et al. 2023, Chap. 6).

The advent of mineral-scale Sr-isotope investigations provided access to a wealth of new information regarding the question of carbonate assimilation at Merapi. Carbonate assimilation at Merapi is directly supported by a study of Sr isotopic zonation in Merapi plagioclase from the 1998 eruptive products based on micro-drilling (Chadwick et al. 2007). Significant zoning in $^{87}\text{Sr}/^{86}\text{Sr}$ (0.70568–0.70627) was identified to be related to crystal texture, with crystal rims often more radiogenic than their cores. Notably, the plagioclase zones with the highest $^{87}\text{Sr}/^{86}\text{Sr}$ values were also found to have the highest anorthite contents, necessitating crystallisation of plagioclase from a melt enriched in both radiogenic strontium and calcium (Fig. 10.7c). In addition, Chadwick et al. (2007) identified high strontium isotopic ratios in a number of high-anorthite crystal cores, which they postulated to represent non-magmatic crystal relicts (i.e. xenocrysts) from a sedimentary protolith (note that magmatic high-anorthite cores are characterised by less radiogenic values more aligned with regional magmatic values, cf. Turner and Foden 2001). Local crustal rocks record strongly radiogenic Sr isotope compositions of up to 0.70789 for calc-silicates (Chadwick et al. 2007) and up to 0.70735 for local Java limestone (Gertisser and Keller 2003a; Fig. 10.7a) and both were modelled as potential assimilants by Chadwick et al. (2007). Subsequently, the study by Borisova et al. (2013) reported $^{87}\text{Sr}/^{86}\text{Sr}$ values for bulk erupted materials from the explosive 2010 eruption that overlap the $^{87}\text{Sr}/^{86}\text{Sr}$ ratios of Merapi calc-silicate xenoliths, which led Borisova et al. (2013) to suggest an assimilation scenario involving extensive digestion of calc-silicate material and subsequent mixing between a calcium-enriched melt and a deeper sourced potassium-rich melt. Complementary to these isotope determinations, the petrological experiments of Deegan et al. (2010) confirmed that Ca-enriched silicate melts produced by magma-carbonate interaction involving Merapi basaltic-

andesite and local carbonate yield highly radiogenic, $^{87}\text{Sr}/^{86}\text{Sr}$ ratios (Fig. 10.7a), confirming that Ca-rich, high $^{87}\text{Sr}/^{86}\text{Sr}$ melts could be a viable contamination mechanism for the 2010 magmas. According to the modelling presented by Borisova et al. (2013), the pre-eruptive Merapi basaltic-andesite would have been required to assimilate between 15 and 40 wt% calc-silicate crustal material to explain the observed Sr-isotopic results. However, such high assimilation rates are not reflected in the major element compositions of Merapi eruptive products, which constitutes somewhat of a petrological conundrum, as discussed further below (see Sect. 10.5.4).

With respect to other common mineral phases at Merapi, $^{87}\text{Sr}/^{86}\text{Sr}$ ratios have been reported for amphibole (Peters et al. 2017) and plagioclase and pyroxene separates (Jolis 2013) (Fig. 10.7a). In the work by Peters et al. (2017), the authors point out that the considerably less radiogenic Sr-isotope compositions of amphibole and pyroxene compared to plagioclase is evidence that amphibole and pyroxene grew dominantly prior to the onset of high-level carbonate assimilation in the top ~10 km of the crust. This finding is in stark contrast to plagioclase which grew from mid-crustal to relatively shallow levels, and thus complements the record of high-level crustal assimilation relative to earlier grown phases.

10.5.2 Oxygen Isotopes

The available oxygen isotope data (reported as $\delta^{18}\text{O}$ values) for Merapi are summarised in Table 10.2 and Fig. 10.8. Some of the earliest $\delta^{18}\text{O}$ values reported for volcanic rocks from the Java segment of the Sunda arc were analyses of whole-rocks and mineral separates from Galunggung volcano (West Java) by Gerbe et al. (1992) and Harmon and Gerbe (1992). The acquisition of oxygen isotope data for Merapi volcano, however, began with the work by Gertisser and Keller (2003a) who reported $\delta^{18}\text{O}$ values for a suite of whole-rocks and plagioclase separates, as well as limestone and a calc-silicate xenolith. This work was followed by a dedicated

Table 10.2 Summary of available oxygen isotope data for Merapi volcano

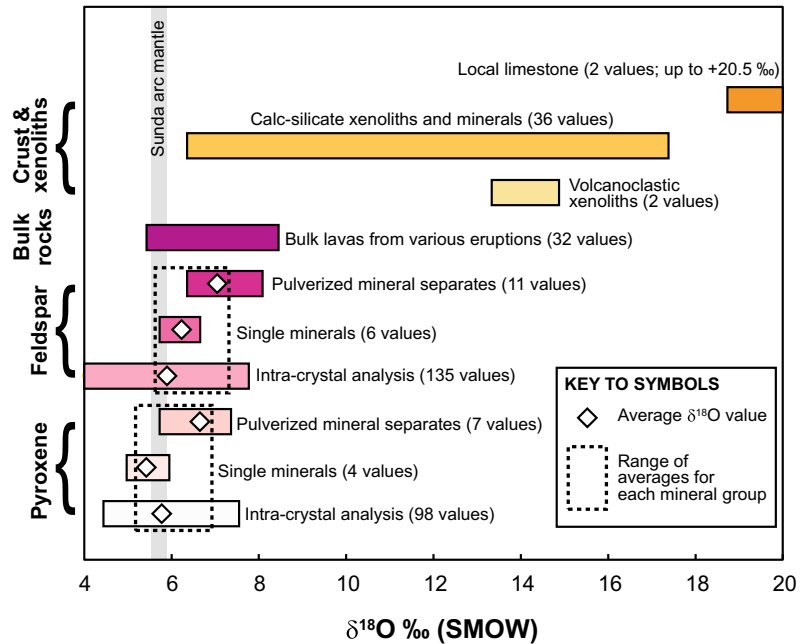
| | Number of analyses and sample information | Min. $\delta^{18}\text{O}$ (‰) | Max. $\delta^{18}\text{O}$ (‰) | Mean $\delta^{18}\text{O}$ (‰) | Reference(s) |
|---------------------------------|---|--------------------------------------|--------------------------------------|--------------------------------------|--|
| <i>Whole-rock lavas and ash</i> | | | | | |
| CF (except ash, analysed by LF) | 32 (Merapi-Somma, Holocene Pyroclastic Series, and recent and historical erupted materials including the 1998, 2006, and 2010 lavas and 2010 ash) | 5.6 | 8.3 | 6.9 | Gertisser and Keller (2003a), Borisova et al. (2013), Troll et al. (2013a) |
| <i>Plagioclase</i> | | | | | |
| SIMS | 135 (2010 erupted materials) | 4.1 | 7.6 | 5.9 | Borisova et al. (2016) |
| LF | 6 (2006 and 2010 erupted materials plus one cumulate sample) | 5.9 | 6.5 | 6.2 | Borisova et al. (2013), Troll et al. (2013a) |
| CF | 11 (Holocene Pyroclastic Series and the 1998 and 2006 erupted materials) | 6.5 | 7.8 | 7.0 | Gertisser and Keller (2003a), Troll et al. (2013a) |
| <i>Pyroxene</i> | | | | | |
| SIMS | 98 (2006 erupted materials) | 4.6 | 7.4 | 5.8 | Deegan et al. (2016a) and Deegan et al. (2021) |
| LF | 4 (2006 and 2010 erupted materials plus one cumulate sample) | 5.1 | 5.8 | 5.4 | Troll et al. (2013a) |
| CF | 7 (1998 and 2006 erupted materials) | 5.9 | 7.2 | 6.7 | Troll et al. (2013a) |
| <i>Plutonic inclusions</i> | | | | | |
| CF | 3 (whole-rock samples of plutonic inclusions found within the 1998 erupted products) | 6.5 | 6.8 | 6.7 | Troll et al. (2013a) |
| <i>Calc-silicate xenoliths</i> | | | | | |
| SIMS | 69 (calcite in magmatic skarn and exoskarn) | 9.9 | 25.6 | 19.0 | Whitley et al. (2019) |
| LF | 8 (crystal separates of wollastonite, grossular, anorthite, calcite, titanomagnetite, and combinations thereof) | 6.5 | 17.2 | 10.9 | Borisova et al. (2016) |
| CF | 8 (whole-rocks as well as xenolith core and rim samples) | 10.4 | 14.2 | 11.9 | Gertisser and Keller (2003a), Troll et al. (2013a) |
| <i>Volcanoclastic xenoliths</i> | | | | | |
| | 2 (whole-rocks) | 13.5 | 14.7 | 14.1 | Troll et al. (2013a) |
| <i>Java limestone</i> | | | | | |
| CF | 2 (whole-rocks) | 18.9 | 20.5 | 19.7 | Gertisser and Keller (2003a) |

Abbreviations *SIMS* Secondary Ionisation Mass Spectrometry; *LF* Laser Fluorination; *CF* Conventional Fluorination.

publication on oxygen isotopes a decade later by Troll et al. (2013a) who reported $\delta^{18}\text{O}$ values for a variety of materials at Merapi, including whole-rock samples of lava and inclusions, plagioclase and pyroxene mineral separates, and calc-silicate and siliciclastic xenoliths. Around the same time, Borisova et al. (2013) published a number of

$\delta^{18}\text{O}$ values for Merapi whole-rock and plagioclase separates from the 2010 eruption. Until this point, material analysed from Merapi consisted of either rock/mineral pulp whose oxygen was extracted by conventional fluorination (cf. Borthwick and Harmon 1982) or small-volume mineral separates (ca. 5 mg of material per

Fig. 10.8 Compilation of oxygen isotope data available for Merapi volcano for various sample types. Data sources are provided in Table 10.2. Note that the $\delta^{18}\text{O}$ values of bulk lava extend well beyond the range of values determined for the Sunda arc mantle source (Deegan et al. 2021), suggesting addition of material with high $\delta^{18}\text{O}$ values to the magmatic system at Merapi



analysis) whose oxygen was extracted by laser fluorination (cf. Harris and Vogeli 2010). The year 2016 saw publication of two papers that utilised Secondary Ionisation Mass Spectrometry (SIMS) to perform mineral-scale oxygen isotope analyses of plagioclase (Borisova et al. 2016) and clinopyroxene (Deegan et al. 2016a). Notably, these SIMS studies represent the first mineral-scale oxygen isotope analyses of plagioclase and pyroxene for the entire Javanese arc segment. Most recently, Whitley et al. (2019) presented SIMS oxygen and carbon isotope data for calcite in Merapi calc-silicate xenoliths (see also Sect. 10.5.3), which represented a great step forward for Merapi, but highlighted a need for future mineral-scale studies for other Javanese volcanoes (cf. Deegan et al. 2021).

In Fig. 10.8a, we have compiled the available Merapi oxygen isotope data and arranged them by sample type. In this chapter, we first discuss the $\delta^{18}\text{O}$ values of Merapi pyroxene with a view to constraining the $\delta^{18}\text{O}$ of parental magmas supplying the Merapi magmatic system. Pyroxene is a mafic, oftentimes early grown mineral phase and is therefore our best candidate for retrieving parental $\delta^{18}\text{O}$ values, particularly since

olivine is not present in Merapi's erupted materials (cf. Deegan et al. 2016a; González-Maurel et al. 2020). The SIMS pyroxene data reported in Deegan et al. (2016a) show a large spread of values for the 98 analysed crystals (4.6–7.4‰) with a mean value of 5.8‰ ($\pm 0.4‰$, 2σ), which agrees within analytical uncertainty with the values obtained by laser fluorination for four mineral separates, which range from 5.1 to 5.8‰ and have a mean of 5.4‰ ($\pm 0.2‰$, 2σ) (Fig. 10.8b). The pyroxene analysed by SIMS were extracted from a bulk rock sample with $\text{SiO}_2 = 55.5$ wt% (sample M-BA06-KA1 reported in Jolis 2013), which allows us to estimate the $\delta^{18}\text{O}$ value of the equilibrium melt by utilising the Si-dependent isotopic fractionation equations of Bindeman et al. (2004). To illustrate, a pyroxene $\delta^{18}\text{O}$ value of 5.8‰ (mean of the SIMS dataset) would yield a $\delta^{18}\text{O}$ melt value of 6.5‰. This is similar to the parental melt value estimated by Deegan et al. (2016a) of 6.1‰. Although a range of pyroxene $\delta^{18}\text{O}$ values exist, the implication is that Merapi pyroxene largely reflect a parental melt with $\delta^{18}\text{O}$ values somewhat higher than Sunda arc mantle-derived melts, which was recently established to be

$5.7 \pm 0.2\%$ (Deegan et al. 2021). Considering the thermobarometrical evidence for pyroxene crystallisation in the mid-crust under Merapi, we conclude that parental melts at Merapi interacted to a limited but measurable degree with high $\delta^{18}\text{O}$ crustal material (perhaps altered crystalline arc crust) during storage at mid-crustal depths.

Turning to plagioclase, SIMS $\delta^{18}\text{O}$ data for three crystals were reported by Borisova et al. (2016) and display a large spread of values (4.6–7.9‰; mean value of 5.9‰) that overlap with those obtained by laser fluorination of mineral separates (5.9–6.5‰; mean value of 6.2‰) (Fig. 10.8b). The SIMS plagioclase $\delta^{18}\text{O}$ values extend to values substantially lower than the corresponding laser fluorination data. A large range of data values is normal in SIMS analysis, potentially due to the SIMS method being capable of detecting very small length-scale (ca. 20 μm) compositional variations (see also Deegan et al. 2016a; Budd et al. 2017). The question is how representative some of these variations are, for instance it remains to be confirmed how representative the values on the “tails” of the data distribution are, especially as the Merapi plagioclase SIMS $\delta^{18}\text{O}$ dataset is restricted to three crystals. It is therefore conceivable that the mean $\delta^{18}\text{O}$ value obtained from the SIMS plagioclase dataset is weighted relatively low due to the presence of unusual, low $\delta^{18}\text{O}$ plagioclase. If taken at face value, the low $\delta^{18}\text{O}$ values obtained for plagioclase could reflect interaction between mafic melts and high temperature altered (low $\delta^{18}\text{O}$) crustal materials in the mid-crust beneath Merapi. The relatively high $\delta^{18}\text{O}$ values, in turn, were suggested by Borisova et al. (2016) to reflect magma-carbonate interaction in the upper arc crust.

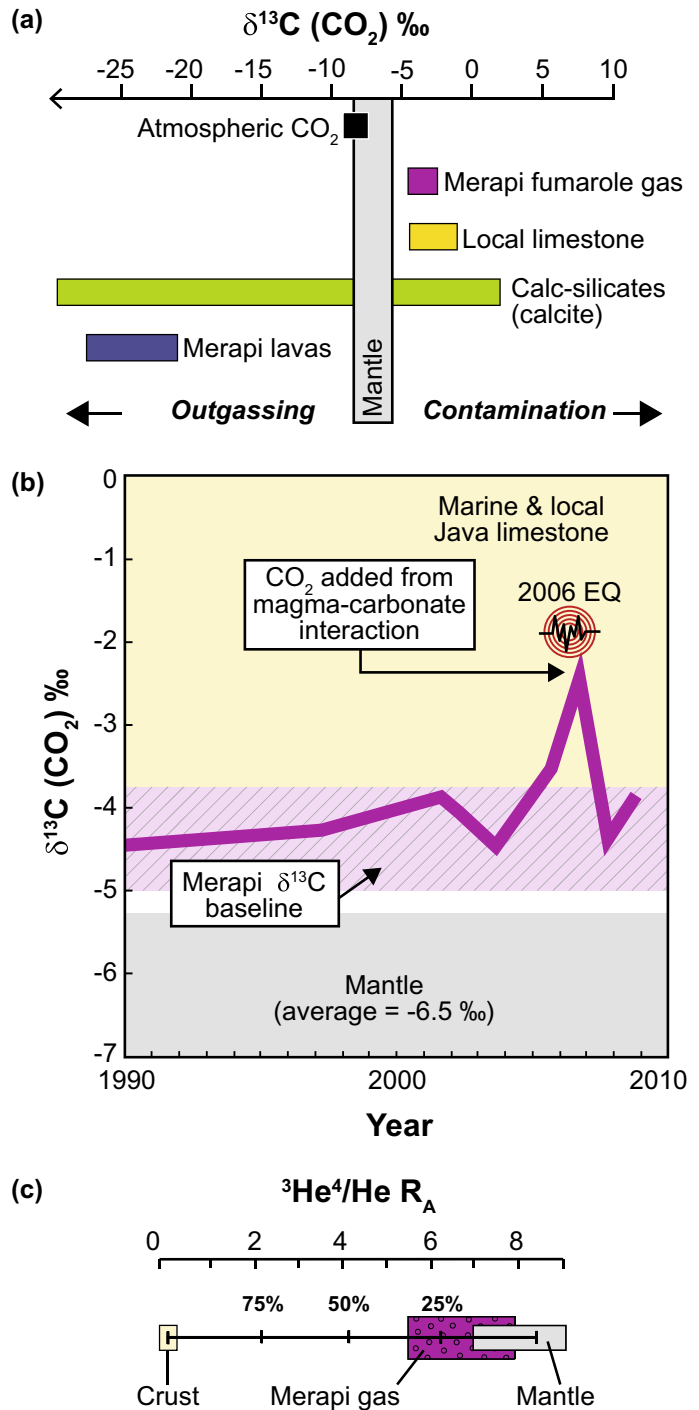
Overall, the relatively high $\delta^{18}\text{O}$ values recorded in Merapi bulk rocks, plagioclase and in a small portion of the pyroxene SIMS dataset provide compelling evidence for magma-carbonate interaction within the Merapi system. Calc-silicate xenoliths and local limestone have high $\delta^{18}\text{O}$ values, extending up to ca. 25‰ for calc-silicates and 20‰ for limestone (Table 10.2), making both lithologies possible crustal assimilants, as interaction of mafic magma with crustal

material with high $\delta^{18}\text{O}$ values would cause an increase in the $\delta^{18}\text{O}$ value of the magma. The study by Troll et al. (2013a) presented a model whereby Merapi mafic melts evolved to basaltic-andesite composition before assimilating a combination of calc-silicate and carbonate material during late-stage magma storage and solidification in the upper crust. These authors concluded that several 10's of wt% assimilation could have taken place, based on the presented oxygen isotope data. A subsequent study by Borisova et al. (2016) similarly concluded that the relatively high $\delta^{18}\text{O}$ values recorded in Merapi plagioclase reflect assimilation of up to 18 wt% calc-silicate material. Most recently, the study by Deegan et al. (2021) modelled source and crustal contamination at Merapi as a function of oxygen isotopes (in clinopyroxene) and Sr isotopes (in bulk lavas) and concluded that Merapi magmas assimilated between 10 and 20 wt% upper crustal sediments and calc-silicate xenoliths. Although the exact amount of carbonate assimilation proposed by previous workers may be discussed on the basis of which endmember compositions are chosen for the various model calculations, there is little doubt that magma-carbonate interaction has played a significant role in generating oxygen isotope heterogeneity in Merapi's erupted products.

10.5.3 Carbon and Helium Isotopes

Carbon isotopes were reported for CO_2 in Merapi fumarole gas by a number of workers since the 1980s, giving rise to a range of $\delta^{13}\text{C}$ values of ca. -4.3 to -3.9% (e.g., Allard 1983; Giggenbach 1997; Toutain et al. 2009). The work by Troll et al. (2012) added to this data repository, which extended the range of $\delta^{13}\text{C}$ values for Merapi fumarole gases to slightly higher values, from -4.4 to -2.4% . The highest values reported by Troll et al. (2012) overlap with the range of $\delta^{13}\text{C}$ values reported for local limestone near Merapi, with values between -0.8 and -4.2 (Troll et al. 2012, 2013a; Fig. 10.9a). Troll et al. (2012) argued that the highest $\delta^{13}\text{C}$ gas values at Merapi could not be produced by either open or closed system magmatic degassing alone (cf. Holloway

Fig. 10.9 **a** $\delta^{13}\text{C}$ values of Merapi fumarole gas compared to local limestone, andesite lavas and calcite in calc-silicates. Figure modified after Troll et al. (2013a) with additional data from Whitley et al. (2019). **b** Variation in $\delta^{13}\text{C}$ values in Merapi fumarole gas over time. The major crustal earthquake in 2006 is indicated and coincides with a sharp increase in $\delta^{13}\text{C}$ values in emitted CO_2 . Note that large magnitude earthquakes also occurred in 1994 and 2001, but these were deep slab events and do not appear to have impacted on the Merapi $\delta^{13}\text{C}$ baseline. Figure modified after Troll et al. (2012). **c** He isotope composition of Merapi fumarole gas compared to typical mantle and crustal values. The Merapi data can be explained by He input from a crustal source on the order of 25–30%. Figure modified after Troll et al. (2013a)



and Blank 1994) implying that an addition of a high $\delta^{13}\text{C}$ component is required. Allard (1983) was one of the first to point out that the somewhat elevated $\delta^{13}\text{C}$ values of Merapi fumarole gases (compared to mantle) may be caused by crustal decarbonation reactions associated with limestone assimilation. Crustal decarbonation would be expected to leave behind residual carbonate severely depleted in ^{13}C . Recent work by Whitley et al. (2019) confirmed this hypothesis by reporting $\delta^{13}\text{C}$ values of calcite in Merapi calc-silicates, which extend to values as low as -30% (Fig. 10.9a). These values are among the lowest reported in magmatic systems so far and combined with the fact that very little relict calcite is found in Merapi calc-silicate xenoliths (Deegan et al. 2010; Whitley et al. 2019), these extremely low $\delta^{13}\text{C}$ values demonstrate highly efficient remobilisation of CO_2 from crustal materials over geologically short timescales.

Notably, Troll et al. (2012) show that the highest $\delta^{13}\text{C}$ gas values thus far recorded for Merapi were measured shortly after the 2006 earthquake and during the final stages of the 2006 eruptive events (Fig. 10.9b). During passive degassing episodes prior to and also after the 2006 events, $\delta^{13}\text{C}$ values in Merapi fumarole gas fell within the Merapi $\delta^{13}\text{C}$ “baseline” (Fig. 10.9b). Troll et al. (2012) suggest that the 2006 earthquake (M6.4, hypocentres at 10–15 km depth) represented a major tectonic event that may have intensified magma-carbonate interaction for a short time. This sharp rise in $\delta^{13}\text{C}$ values after the earthquake and during the eruption of 2006 is consistent with considerable release of crustal CO_2 , which may have reached the surface via channels that were opened during seismic activity. Troll et al. (2012) suggested that this shallow crustal volatile input supplemented the mantle-derived volatile flux at Merapi, intensifying and sustaining the 2006 eruption (see also Carr et al. 2018). In line with this idea, Whitley et al. (2019) performed mass balance calculations to constrain the amount of CO_2 produced at Merapi and found that 24–56% of CO_2 emissions are crust-derived during quiescence, whereas a staggering 41–95% of CO_2 could be derived from crustal carbonates during eruptive periods.

Combining the elevated $\delta^{13}\text{C}(\text{CO}_2)$ values with available He isotope data, the relative contribution of the volatile sources may be further constrained (cf. Sano and Marty 1995; Hilton et al. 2002). The Earth’s mantle stores primordial He, and the average MORB-type mantle shows $^3\text{He}/^4\text{He}$ R_A of ca. 8 ± 1 , while the continental crust has $^3\text{He}/^4\text{He}$ R_A of 0.1 to 0.001. Subduction of oceanic crust and small portions of sediment does not seem to significantly affect mantle He signatures in island arc lavas, because most of the Pacific ring of fire yield generally mantle-like values. The regional values in Java range from $^3\text{He}/^4\text{He}$ $R_A = 8\text{--}9$ (Hilton and Craig 1989; Sano and Marty 1995; Goff et al. 1998; Fischer and Marty 2005), but Merapi shows comparatively low $^3\text{He}/^4\text{He}$ values of 5.5–6.5 (Hilton and Craig 1989; Varekamp et al. 1992; Giggenbach 1997; Sano et al. 2001; Hilton et al. 2002; Fig. 10.9c). This implies variable, but at times significant, radiogenic helium additions (potentially in excess of 25–30%) to the Merapi gas phase via a crust-derived gas (Fig. 10.9c), corroborating the crustal signature determined through carbon isotopes in Merapi fumarole gas.

10.5.4 A Major Element Conundrum?

From a mass balance viewpoint, magma-carbonate interaction adds calcium to the host magma and drives magma compositions towards lower silica contents. This phenomenon has been established at Italian volcanoes emplaced in carbonate crust, such as the Colli Albani (Alban Hills) volcanic system, whose erupted products have K-foiditic compositions and show unequivocal evidence of carbonate assimilation (e.g. Iacono-Marziano et al. 2007, 2008; Freda et al. 2008, 2010). These relationships are not as clearly developed at Merapi, and the limited whole-rock major element evidence for magma-carbonate interaction has been discussed as precluding significant amounts of carbonate assimilation at Merapi (Gertisser and Keller 2003a; Costa et al. 2013; Handley et al. 2014). Although the work by e.g. Costa et al. (2013) does not entirely discount carbonate assimilation at Merapi, these authors

argue that carbonate assimilation of more than just a few wt% is unlikely as it would result in marked bulk compositional changes that are not observed. This argument is at odds, however, with the large degree of magma-carbonate interaction recorded by multiple isotope systems, primarily in Merapi minerals and emitted gas (Chadwick et al. 2007; Troll et al. 2013a; Borisova et al. 2013, 2016; Deegan et al. 2021). It remains an open question at this stage as to why Merapi lavas do not show a greater bulk chemistry effect from carbonate assimilation, but Whitley et al. (2020) suggested that Ca shows relatively limited mobility in Merapi pre-eruptive melts compared to Sr and B. Isotopic analysis of petrological experimental products demonstrated that Sr and B are rapidly mobilised during magma-carbonate interaction (Deegan et al. 2010, 2016b), which would support the idea of Ca being decoupled from certain trace elements, with Ca being, at least in part, retained in calc-silicate materials (e.g. wollastonite, diopside). Moreover, Spandler et al. (2012) performed geochemical modelling of magma-carbonate interaction and confirmed that carbonate assimilation may not necessarily cause obvious major element changes to the magma, but rather magma-carbonate interaction may cause significant Sr addition to the magmatic system, as observed at Merapi and also at the nearby Sumbing volcano (Macpherson et al. 2019). While there is little doubt that magma-carbonate interaction is an important petrogenetic process at Merapi, the degree of major element compositional change may not always be prominent and metasomatic processes may also play a significant role in preferentially retaining Ca in the exoskarn (cf. Whitley et al. 2020).

10.6 Experimental Magma-Carbonate Interaction at Merapi

Carbonate assimilation in active volcanic systems has been the subject of a growing number of experimental studies over the last two decades.

Most of these have focussed on an individual or a group of closely related systems, with a strong focus on Italian carbonate-hosted volcanic systems at Vesuvius and the Alban Hills (e.g. Iacono-Marziano et al. 2007, 2008; Freda et al. 2008, 2010; Mollo et al. 2010; Jolis et al. 2013). Many of these experiments were conducted with the aim of characterising the effect of carbonate assimilation on phase relationships and magma evolution. The works by e.g. Iacono-Marziano et al. (2007, 2008) and Mollo et al. (2010) showed that clinopyroxene compositions are strongly affected by magma-carbonate interaction and they also showed that a substantial CO₂-rich fluid is generated by this process. Another experimental study focussed on Merapi volcano in Indonesia (Deegan et al. 2010) and some others have addressed specific aspects of magma-carbonate interaction at both Vesuvius and Merapi (Blythe et al. 2015; Deegan et al. 2016b). In addition to the above-mentioned publications, a number of studies have been performed looking in a more general way at magma-carbonate interaction, by utilising a range of magmatic (basalt, andesite, and dacite) and carbonate (calcite and dolomite) starting materials and by varying the experiment intensive parameters (Carter and Dasgupta 2015, 2016, 2018).

The following sections focuses on the magma-carbonate interaction experiments carried out using Merapi starting materials by Deegan et al. (2010), but many aspects of the other experimental studies mentioned above are applicable at Merapi too, such as those relating to clinopyroxene chemistry in skarns. The Merapi experiments comprise a suite of short-duration (0 to 300 s) piston cylinder disequilibrium experiments, wherein lithic fragments of Javan limestone were allowed to interact with basaltic-andesite melts at 0.5 GPa and 1200 °C (Fig. 10.10). These experiments were designed to replicate the onset of magma-carbonate interaction in the mid-crust beneath Merapi and to capture the rapid transformations occurring at magma-carbonate interfaces. The main features of these experiments are described below.

10.6.1 Volatile Degassing

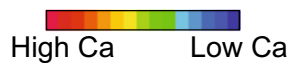
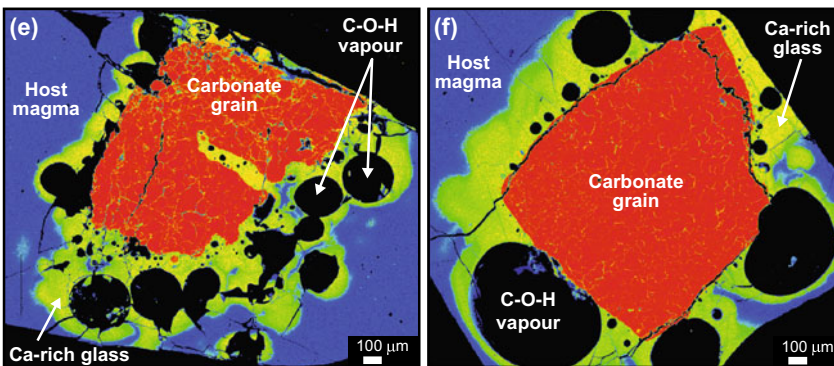
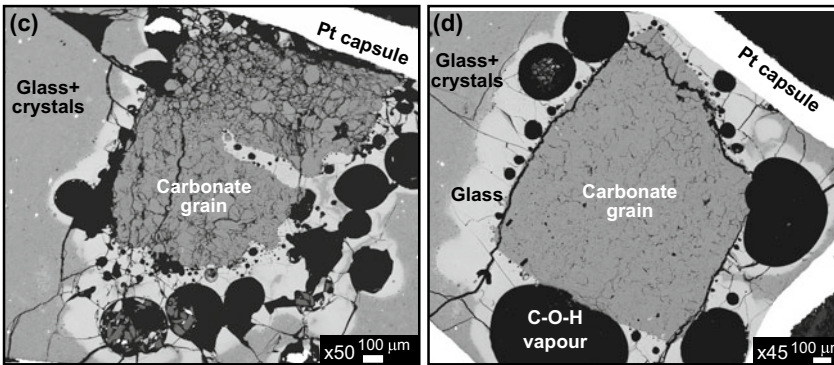
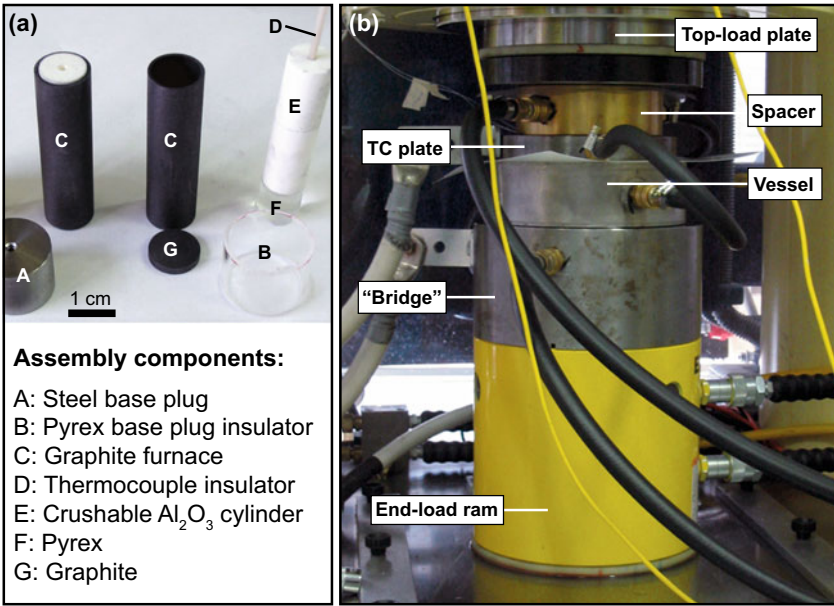
Perhaps the most significant outcome of the experiments by Deegan et al. (2010) was the realisation that carbonate can dissolve into magma over geologically extremely short time-scales. Under the simulated magmatic conditions, it was observed that carbonate dissolves into the surrounding magma and releases voluminous C–O–H volatile bubbles (Fig. 10.10c–f). The work by Blythe et al. (2015) added a detailed discussion of bubble nucleation and growth during this process and compared the Merapi experiments to similar experiments carried out employing magmatic and carbonate starting materials from Vesuvius (see also Jolis et al. 2013). Blythe et al. (2015) describe how the different compositions of melts at Merapi and Vesuvius result in different melt viscosities. The relatively low viscosity melts at Vesuvius facilitate efficient removal of volatiles from the reaction site resulting in continual carbonate-fuelled degassing, whereas the relatively higher viscosity melts at Merapi tend to inhibit volatile migration leading to volatile concentration at the reaction site that can cause local gas concentrations that may eventually trigger short-lived explosive outbursts. The key take-away point is that melt viscosity can exert a fundamental control on both carbonate assimilation rates and the style of CO₂-driven eruptions (see also Iacono-Marziano et al. 2009; Freda et al. 2010). The hazard potential of this process at Merapi was discussed by Deegan et al. (2011), who described the process as “fast and furious” in reference to the rapid decarbonation rate (seconds to minutes) as observed in experiments and the potential for vigorous bubble nucleation, temporary bubble arrest, and eventual blow out, which may contribute to volcano explosivity. Moreover, this process was considered to be a possible explanation for the at times erratic explosive behaviour of Merapi and, as discussed by Troll et al. (2012, 2015), magma-carbonate interaction could represent an even more important factor in volcano explosivity if accompanied by regional seismic activity, which could fracture the carbonate bedrock thus

creating more reaction surfaces and opening channel ways to the surface for CO₂ release.

10.6.2 Calcium-Contamination

Carbonate assimilation leads to the production of a silica-undersaturated, calcium enriched melts and diopside–hedenbergite–Ca-Tschemmak clinopyroxene solid solution reaction products (e.g. Iacono-Marziano et al. 2007, 2008; Freda et al. 2008, 2010; Gaeta et al. 2009; Deegan et al. 2010; Mollo et al. 2010; Di Rocco et al. 2012; Jolis et al. 2013; Carter and Dasgupta 2015; Whitley et al. 2020; Morris and Canil 2022). At Merapi, evidence for Ca-rich contaminated melts has been reported in the form of Ca-rich zones in plagioclase (Chadwick et al. 2007), Ca-rich melt inclusions and matrix glasses in volcanic products of the 2010 eruption (Borisova et al. 2013), and extremely Ca-rich zones in calc-silicate xenoliths (Deegan et al. 2010; Whitley et al. 2020). In order to investigate the compositions of Ca-contaminated melts in the Merapi experiments, several micro-analytical approaches have been adopted, making these experiments arguably the most intensely studied to date. The analytical techniques employed for the Merapi experiments include:

1. Scanning Electron Microscopy (SEM) and electron probe microprobe analysis (EPMA). This work revealed magma-carbonate interaction textures, bubble distribution patterns, as well as the major element composition of Ca-rich melts and their diffusive interfaces with Ca-normal melts (Fig. 10.10c–f; Deegan et al. 2010; Blythe et al. 2015). The major element profiles of the melt-melt interfaces in the experiments (as well as Sr and B isotope compositions – see below) provide evidence for dynamic exchange of both major and minor elements between carbonate and host melt (see also Whitley et al. 2020).
2. Micro-drilling and Thermal Ionisation Mass Spectrometry (TIMS). This work showed that Ca-rich melts have highly radiogenic Sr isotope ratios, overlapping with the composition



◀ **Fig. 10.10** **a** Components of an experiment assembly constructed to encase the experimental capsules in the piston cylinder device for the Merapi magma-carbonate interaction experiments. **b** The end-loaded piston cylinder at INGV Rome, Italy. The “vessel” is the steel pressure plate with a tungsten carbide core into which the sample assembly is inserted. The “bridge” houses the piston ram, which generates pressure on the sample. **c, d** Scanning electron microscopy (SEM) images of Merapi magma-carbonate interaction experiments (after Deegan et al.

2010). Experiments were run for 0 s **c** and 150 s **d** at 1200 °C and 0.5 GPa using Merapi basaltic-andesitic glass and Javanese limestone as starting materials. Large C–O–H vapour bubbles and Ca-rich glass surround the carbonate grains. **e, f** Ca-maps acquired at the electron microprobe at INGV Rome (Italy) of the same experiments shown in (c) and (d). These maps highlight the extent of the Ca-rich compositional boundary layers (Ca-contaminated melt – bright yellow/green) surrounding the carbonate grains (red).

of natural calc-silicate xenoliths (Fig. 10.7a; Deegan et al. 2010).

3. Secondary Ionisation Mass Spectrometry (SIMS). This work documented boron isotope variations in the experimental products and coupled B–CO₂ degassing in the experiments (Deegan et al. 2016b). The CaO-rich experimental glasses were found to have extremely low $\delta^{11}\text{B}$ values down to -41.5% , reflecting partitioning of ¹⁰B into the contaminated melt and transport of ¹¹B away from the reaction site via a B- and CO₂-rich fluid.

10.7 The Volatile Budget at Merapi

Magma-carbonate interaction at Merapi takes place in the mid to upper part of the magmatic plumbing system (Fig. 10.11) and has a strong impact on the carbon and helium isotopic composition of the gases released to the atmosphere (Sect. 10.5.3; Troll et al. 2012, 2013a). Carbon isotope ratios have been found to show a large spike towards crustal values during eruptive periods (Fig. 10.9b; Troll et al. 2012). This spike signals that a positive feedback loop is at play whereby carbonate bedrock can become fractured during seismic events and magma injections, leading to exposure of fresh reaction surfaces, opening of new channel ways to the surface, and intensified CO₂ liberation (Deegan et al. 2011; Troll et al. 2012; Carr et al. 2018). Magma-carbonate interaction is therefore a dynamic process which may intensify eruption flare-ups for short periods of time (e.g. Blythe et al. 2015). Calc-silicate xenoliths and experiments document snapshots of this process and

highlight that the timescales involved are short: (1) experiments have shown that addition of volatiles derived from crustal carbonates to a shallow magma reservoir would promote vesicle formation and growth in the melt on a timescale of seconds to minutes (Deegan et al. 2010; Blythe et al. 2015), and (2) using known growth rates of clinopyroxene, Whitley et al. (2020) calculated that compositionally distinct, non-magmatic, growth zones in clinopyroxene in calc-silicate xenoliths could have grown in just days to at most one year.

If we consider a scenario whereby hot, volatile-rich magma is supplied to the Merapi magmatic system from depth (this scenario could be applied to the VEI 4 2010 eruption of Merapi, e.g. Carr et al. 2020), the increased heat and volume would cause thermal stress, decarbonation, and fracturing of carbonate bedrocks at relatively shallow depths. The resulting volatile overpressure may lead to further carbonate fracturing, and greater amounts of magma-carbonate interaction due to increased reactive surface area, which could then lead to greater CO₂ release, calcic clinopyroxene crystallisation, and a heightened probability for CO₂-driven eruptions (Iacono-Marziano et al. 2007, 2008, 2009; Freda et al. 2008, 2010; Deegan et al. 2010; Mollo et al. 2010; Troll et al. 2012, 2013a, b; Carr et al. 2018, 2020). Faults and fractures in the crust would likely facilitate transfer of volatiles to the surface and this could be exacerbated by seismic activity (e.g. Troll et al. 2012). As well as explaining certain aspects of the 2010 eruption, a similar scenario has also been shown to be viable for the VEI 1 2006 eruption (Carr et al. 2018). Magma-carbonate interaction may thus be an important contributing factor in volcanological

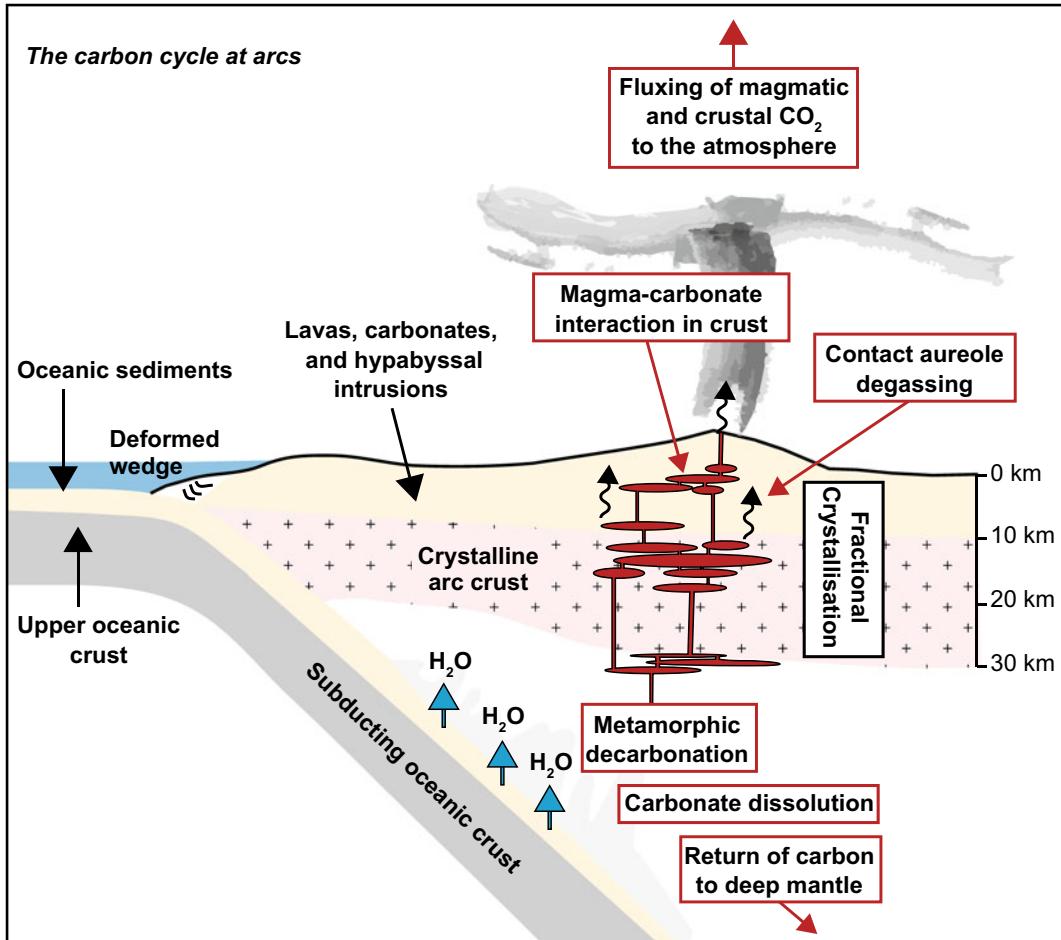


Fig. 10.11 Cartoon showing the possible sources and pathways of carbon in subduction zone systems emplaced into carbonate basement. Carbon in the subducting slab is bound as organic carbon and inorganic carbonate in sediments and as inorganic carbonate in the oceanic lithosphere. Carbon may be released from the slab by metamorphic decarbonation or fluid-mediated dissolution, or it may be returned to the deep mantle. During ascent through the crust, CO₂-rich fluids can be produced

through magma-carbonate interaction and/or degassing of contact aureoles surrounding sub-volcanic magmatic intrusions. The total CO₂-load of the system is a mixture of original magmatic CO₂ and CO₂ from carbonates and may outgas through eruption at the surface or via crustal structures such as faults. Figure is based on work by Mason et al. (2017) and Lee et al. (2018). The Merapi plumbing system is drawn based on the model presented in Deegan et al. (2016a)

hazard considerations at Merapi, especially when considering that, in addition to the scenario described above, decarbonation may cause volcanic edifice or dome weakening, which could be disastrous in terms of triggering dome collapse (cf. Mollo et al. 2012; Carr et al. 2018; Heap et al. 2019). Merapi is probably not unique in this sense and we note that magma-carbonate interaction has also been discussed as a potential

driving factor in eruptions at other carbonate-hosted volcanoes, including for instance the Alban Hills (Freda et al. 1997, 2008, 2010; Iacono-Marziano et al. 2007, 2008) and Vesuvius (Iacono-Marziano et al. 2009; Dallai et al. 2011; Jolis et al. 2015) in Italy, and Popocatepetl in Mexico (Goff et al. 2001; Schaaf et al. 2005).

To get a first order handle on crustal CO₂ released from volcanoes like Merapi, we need to

consider short time scale magmatic-carbonate interaction as described above, but also CO₂ that is released as a consequence of decarbonation reactions in thermal aureole(s) surrounding magma reservoirs in the upper arc crust (Fig. 10.11; see also Ganino and Arndt 2009; Svensen et al. 2018), thereby adding to the crustal volatile release around active volcanoes. Whitley et al. (2019) presented a calculation of the amount of CO₂ that could be derived from metamorphic aureoles in the crust beneath Merapi and found that up to 3.8×10^{13} kg of CO₂ could be emitted on the timescales of just thousands of years, assuming a magma reservoir and aureole similar in size to that of the 2010 eruption. These authors also note that although Merapi is currently considered a relatively low CO₂ emitter on a global scale (see Burton et al. 2013), crustal CO₂ liberation may be temporally variable with potentially large amounts released during eruptive episodes compared to periods of overall quiescence (cf. Troll et al. 2012, 2013b). It is entirely possible that carbonate intersecting arc volcanoes generally behave in this manner and have perhaps done so throughout geologic time. Indeed, several workers have recently advocated that crustal CO₂ release from volcanic arcs intersecting carbonate may have influenced the concentration of carbon dioxide in the atmosphere and contributed to climate warming during known greenhouse conditions on Earth, such as the Cretaceous “hot-house” period (e.g. Johnston et al. 2011; Lee et al. 2013; Aiuppa et al. 2017; Lee and Lackey 2015; Ramos et al. 2020). In this context, the sources of CO₂ in arc emissions and the role of non-mantle CO₂ (i.e. derived from crustal carbonate) has been discussed widely in terms of amplifying volcanic CO₂ output and also in terms of influencing eruptive dynamics, particularly during current and ancient subduction zone activity but also during larger magmatic events in Earth’s past (Fig. 10.11; see also Freda et al. 1997, 2010; Ganino and Arndt 2009; Iacono-Marziano et al. 2009; Dallai et al. 2011; Johnston et al. 2011; Di Rocco et al. 2012; Lee et al. 2013, 2019; Troll et al. 2012; Carter and Dasgupta 2015, 2016, 2018; Jolis et al. 2015; Aiuppa et al. 2017; Lee and Lackey 2015; Mason et al. 2017; Svensen

et al. 2018; Ramos et al. 2020). Merapi occupies an important place in this discussion, due to the depth of research that has been conducted on magma-carbonate interaction at this locality. Merapi thus provides us with a potentially unrivalled window on carbon cycling at arcs with which we may better assess Earth’s past and ongoing volcanic and crustal CO₂ emissions (see Fig. 10.11).

Acknowledgements We are grateful to C. Barnes, J.H. Bédard, L.S. Blythe, A. Borisova, J.P. Chadwick, L. Dallai, R. Dasgupta, J.P. Davidson, M. Gaeta, J. Gamble, H. Geiger, D.R. Hilton, R. Halama, C. Harris, H. Humaida, E.M. Jolis, C. Macpherson, V. Misiti, S. Mollo, O. Nadeau, K. Preece, A. Skelton, M.J. Whitehouse, and S. Whitley for constructive discussions over the years on magma-carbonate interaction both in a general sense and at Merapi in particular. S. Whitley and V. Misiti are acknowledged for providing display materials for Figs. 10.6 and 10.10, respectively. N.T. Arndt and A. Auer are thanked for their encouraging and constructive reviews which improved this chapter. Financial support was provided by the Swedish Research Council (*Vetenskapsrådet*), the Royal Swedish Academy of Science (*Kungl. Vetenskapsakademien*), and the Natural Environment Research Council of the United Kingdom.

References

- Aiuppa A, Fischer TP, Plank T, Robidoux P, Di Napoli R (2017) Along-arc, inter-arc and arc-to-arc variations in volcanic gas CO₂/S_T ratios reveal dual source of carbon in arc volcanism. *Earth Sci Rev* 168:24–47
- Allard P (1983) The origin of hydrogen, carbon, sulphur, nitrogen and rare gases in volcanic exhalations; evidence from isotope geochemistry. In: Tazieff H, Sabroux J (eds) *Forecasting volcanic events*. Elsevier, New York, pp 337–386
- Balazs D (1968) *Karst regions in Indonesia: Karszt-Es Barlangkutatas, V.5*. Globus nyomda, Budapest, Hungary, 61 p
- Barberi F, Leoni L (1980) Metamorphic carbonate ejecta from Vesuvius Plinian eruptions: evidence of the occurrence of shallow magma chambers. *Bull Volcanol* 43:107–120
- Barnes CG, Prestvik T, Sundvoll B, Surratt D (2005) Pervasive assimilation of carbonate and silicate rocks in the Hortavaer igneous complex, north-central Norway. *Lithos* 80:179–199
- Barnes CG, Prestvik T, Li Y, McCulloch L, Yoshinobu AS, Frost CD (2009) Growth and zoning of the Hortavaer intrusive complex, a layered alkaline pluton in the Norwegian Caledonides. *Geosphere* 5:286–301

- Bédard JH, Saumur BM, Tegner C, Troll VR, Deegan FM, Evenchick CA, Grasby SE, Dewing K (2021) Geochemical systematics of high arctic large igneous province continental tholeiites from Canada—Evidence for progressive crustal contamination in the plumbing system. *J Petrol* 62:egab041
- Bindeman IN, Ponomareva VV, Bailey JC, Valley JW (2004) Volcanic arc of Kamchatka: a province with high- $\delta^{18}\text{O}$ magma sources and large scale $^{18}\text{O}/^{16}\text{O}$ depletion of the upper crust. *Geochim Cosmochim Acta* 68:841–865
- Blythe LS, Deegan FM, Freda C, Jolis EM, Masotta M, Misi V, Taddeucci J, Troll VR (2015) CO_2 bubble generation and migration during magma-carbonate interaction. *Contrib Mineral Petrol* 169:42
- Borisova AY, Martel C, Gouy S, Pratomo I, Sumarti S, Toutain JP, Bindeman IN, de Parseval P, Métaixian JP, Surono (2013) Highly explosive 2010 Merapi eruption: Evidence for shallow-level crustal assimilation and hybrid fluid. *J Volcanol Geotherm Res* 261:193–208
- Borisova AY, Gurenko AA, Martel C, Kouzmanov K, Cathala A, Bohrsen WA, Pratomo I, Sumarti S (2016) Oxygen isotope heterogeneity of arc magma recorded in plagioclase from the 2010 Merapi eruption (Central Java, Indonesia). *Geochim Cosmochim Acta* 190:13–34
- Borthwick J, Harmon RS (1982) A note regarding ClF_3 as an alternative to Br_2F_5 for oxygen isotope analysis. *Cosmochim Geochim Acta* 46:1665–1668
- Bowen NL (1928) The evolution of the igneous rocks. Princeton University Press, Princeton, p 334
- Brouwer HA (1928) Production of trachyte and phonolite from pyroxene andesitic magma associated with limestone. *J Geol* 36:545–548
- Budd DA, Troll VR, Deegan FM, Jolis EM, Smith VC, Whitehouse MJ, Harris C, Freda C, Hilton DR, Halldórsson SA, Bindeman IN (2017) Magma reservoir dynamics at Toba caldera, Indonesia, recorded by oxygen isotope zoning in quartz. *Sci Rep* 7:40624
- Buono G, Pappalardo L, Harris C, Edwards BR, Petrosino P (2020) Magmatic stoping during the caldera-forming Pomici di Base eruption (Somma-Vesuvius, Italy) as a clue of eruption explosivity. *Lithos* 370–371:105628
- Burton MR, Sawyer GM, Granieri D (2013) Deep carbon emissions from volcanoes. *Rev Mineral Geochem* 75:323–354
- Callegaro S, Svensen HH, Neumann ER, Polozov AG, Jerram DA, Deegan FM, Planke S, Shiganova OV, Ivanova NA, Melnikov NV (2021) Geochemistry of deep Tunguska Basin sills, Siberian Traps: correlations and potential implications for the end-Permian environmental crisis. *Contrib Mineral Petrol* 176:49
- Camus G, Gourgaud A, Mossand-Berthommier PC, Vincent PM (2000) Merapi (Central Java, Indonesia): an outline of the structural and magmatological evolution, with a special emphasis to the major pyroclastic events. *J Volcanol Geotherm Res* 100:139–163
- Carr BB, Clarke AB, de' Michieli Vitturi M (2018) Earthquake induced variations in extrusion rate: a numerical modelling approach to the 2006 eruption of Merapi volcano (Indonesia). *Earth Planet Sci Lett* 482:377–387
- Carr BB, Clarke AB, de' Michieli Vitturi M (2020) Volcanic conduit controls on effusive-explosive transitions and the 2010 eruption of Merapi volcano (Indonesia). *J Volcanol Geotherm Res* 392:106767
- Carter LB, Dasgupta R (2015) Hydrous basalt-limestone interaction at crustal conditions: Implications for generation of ultracalcic melts and outflux of CO_2 at volcanic arcs. *Earth Planet Sci Lett* 427:202–214
- Carter LB, Dasgupta R (2016) Effect of melt composition on crustal carbonate assimilation: implications for the transition from calcite consumption to skarnification and associated CO_2 degassing. *Geochem Geophys Geosyst* 17:3893–3916
- Carter LB, Dasgupta R (2018) Decarbonation in the Ca–Mg–Fe carbonate system at mid-crustal pressure as a function of temperature and assimilation with arc magmas—Implications for long-term climate. *Chem Geol* 492:30–48
- Chadwick JP (2008) Crustal processes in volcanic systems: case studies from Northern Ireland, New Zealand, and Indonesia. Ph.D. thesis, Trinity College Dublin, Ireland
- Chadwick JP, Troll VR, Ginibre C, Morgan D, Gertisser R, Waight TE, Davidson JP (2007) Carbonate assimilation at Merapi volcano, Java, Indonesia: insights from crystal isotope stratigraphy. *J Petrol* 48:1793–1812
- Chadwick JP, Troll VR, Waight TE, van der Zwan FM, Schwarzkopf LM (2013) Petrology and geochemistry of igneous inclusions in recent Merapi deposits: a window into the sub-volcanic plumbing system. *Contrib Mineral Petrol* 165:259–282
- Chaussard E, Amelung F (2014) Regional controls on magma ascent and storage in volcanic arcs. *Geochem Geophys Geosystems* 15:1407–1418
- Chiadini G, Caliro S, Aiuppa A, Avino R, Granieri D, Moretti R, Parello F (2011) First $^{13}\text{C}/^{12}\text{C}$ isotopic characterization of volcanic plume CO_2 . *Bull Volcanol* 73:531–542
- Clochiatti R, Joron JL, Kerinec F, Treuil M (1982) Quelques données préliminaires sur la lave du dome actuel du volcan Merapi (Java Indonésie) et sur ses enclaves. *C R Acad Sci Sér A* 295:817–822
- Conte AM, Dolfi D, Gaeta M, Misi V, Mollo S, Perinelli C (2009) Experimental constraints on evolution of leucite-basanite magma at 1 and 10^{-4} GPa: implications for parental compositions of Roman high-potassium magmas. *Eur J Mineral* 21:763–782
- Costa F, Andreastuti S, de Maisonrouve CB, Pallister JS (2013) Petrological insights into the storage conditions, and magmatic processes that yielded the centennial 2010 Merapi explosive eruption. *J Volcanol Geotherm Res* 261:209–235
- Curry JR, Shor GG, Raitt RW, Henry M (1977) Seismic refraction and reflection studies of crustal structure of

- the eastern Sunda and western Banda arcs. *J Geophys Res* 82:2479–2489
- Dallai L, Freda C, Gaeta M (2004) Oxygen isotope geochemistry of pyroclastic clinopyroxene monitors carbonate contributions to Roman-type ultrapotassic magmas. *Contrib Mineral Petrol* 148:247–263
- Dallai L, Cioni R, Boschi C, D’Orlando C (2011) Carbonate-derived CO₂ purging magma at depth: influence on the eruptive activity of Somma-Vesuvius, Italy. *Earth Planet Sci Lett* 310:84–95
- Davidson JP, Tepley FJ III (1997) Recharge in volcanic systems: evidence from isotope profiles of phenocrysts. *Science* 275:826–829
- Davidson JP, Hora JM, Garrison JM, Dungan MA (2005) Crustal forensics in arc magmas. *J Volcanol Geotherm Res* 140:157–170
- Debaille V, Doucelance R, Weis D, Schiano P (2006) Multi-stage mixing in subduction zones: application to Merapi volcano (Java island, Sunda arc). *Geochim Cosmochim Acta* 70:723–741
- Deegan FM, Troll VR, Freda C, Misti V, Chadwick JP, McLeod J, Davidson JP (2010) Magma-carbonate interaction processes and associated CO₂ release at Merapi volcano, Indonesia: insights from experimental petrology. *J Petrol* 51:1027–1051
- Deegan FM, Troll VR, Freda C, Misiti V, Chadwick JP (2011) Fast and furious: crustal CO₂ release at Merapi volcano, Indonesia. *Geol Today* 27:63–64
- Deegan FM, Whitehouse MJ, Troll VR, Budd DA, Harris C, Geiger H, Hålenius U (2016a) Pyroxene standards for SIMS oxygen isotope analysis and their application to Merapi volcano, Sunda arc, Indonesia. *Chem Geol* 447:1–10
- Deegan FM, Troll VR, Whitehouse MJ, Jolis EM, Freda C (2016b) Boron isotope fractionation in magma via crustal carbonate dissolution. *Sci Rep* 6:30774
- Deegan FM, Troll VR, Geiger H (2019) Forensic probe of Bali’s great volcano. *Eos. Trans Am Geophys Union* 100:26–30
- Deegan FM, Whitehouse MJ, Troll VR, Geiger H, Jeon H, le Roux P, Harris C, van Helden M, González-Maurel O (2021) Sunda arc mantle source $\delta^{18}\text{O}$ value revealed by intracrystal isotope analysis. *Nat Commun* 12:3930
- de Genevraye P, Samuel L (1972) Geology of the Kendeng Zone (Central & East Java). In: *Proceedings, First Annual Convention. Indonesian Petroleum Association*, pp 17–30
- Del Moro A, Fulignati P, Marianelli P, Sbrana A (2001) Magma contamination by direct wall rock interaction: constraints from xenoliths from the walls of a carbonate-hosted magma chamber (Vesuvius 1944 eruption). *J Volcanol Geotherm Res* 112:15–24
- Di Rocco T, Freda C, Gaeta M, Mollo S, Dallai L (2012) Magma chambers emplaced in carbonate substrate: petrogenesis of skarn and cumulate rocks and implications for CO₂ degassing in volcanic areas. *J Petrol* 53:2307–2332
- Erdmann S, Martel C, Pichavant M, Kushnir A (2014) Amphibole as an archivist of magmatic crystallization conditions: problems, potential, and implications for inferring magma storage prior to the paroxysmal 2010 eruption of Mount Merapi, Indonesia. *Contrib Mineral Petrol* 167:1016
- Erdmann S, Martel C, Pichavant M, Bourdier JL, Champallier R, Komorowski JC, Cholik N (2016) Constraints from phase equilibrium experiments on pre-eruptive storage conditions in mixed magma systems: a case study on crystal-rich basaltic andesites from Mount Merapi, Indonesia. *J. Petrol* 57:535–560
- Eskola P (1922) On contact phenomena between gneiss and limestone in Western Massachusetts. *J Geol* 30:265–294
- Fischer TP, Marty B (2005) Volatile abundance in the sub-arc mantle: insights from volcanic and hydrothermal gas discharges. *J Volcanol Geotherm Res* 140:205–216
- Freda C, Gaeta M, Palladino DM, Trigila R (1997) The Villa Senni eruption (Alban Hills, central Italy): the role of H₂O and CO₂ on the magma chamber evolution and on the eruptive scenario. *J Volcanol Geotherm Res* 78:103–120
- Freda C, Gaeta M, Misiti V, Mollo S, Dolfi D, Scarlato P (2008) Magma-carbonate interaction: an experimental study on ultrapotassic rocks from Alban Hills (Central Italy). *Lithos* 101:397–415
- Freda C, Gaeta M, Giaccio B, Marra F, Palladino DM, Scarlato P, Sottili G (2010) CO₂-driven large mafic explosive eruptions: the Pozzolane Rosse case study from the Colli Albani Volcanic District (Italy). *Bull Volcanol* 73:241–256
- Fulignati P, Marianelli P, Santacroce R, Sbrana A (2000) The skarn shell of the 1944 Vesuvius magma chamber. Genesis and P-T-X conditions from melt and fluid inclusion data. *Eur J Mineral* 12:1025–1039
- Fulignati P, Marianelli R, Santacroce R, Sbrana A (2004) Probing the Vesuvius magma chamber-host rock interface through xenoliths. *Geol Mag* 144:417–428
- Gaeta M, Di Rocco T, Freda C (2009) Carbonate assimilation in open magmatic systems: the role of melt-bearing skarns and cumulate-forming processes. *J Petrol* 50:361–385
- Ganino C, Arndt NT (2009) Climate changes caused by degassing of sediments during the emplacement of large igneous provinces. *Geology* 37:323–326
- Ganino C, Arndt NT, Zhou MF, Gaillard F, Chauvel C (2008) Interaction of magma with sedimentary wall rock and magnetite ore genesis in the Panzhihua mafic intrusion, SW China. *Miner Deposita* 43:677–694
- Ganino C, Harris C, Arndt NT, Prevec SA, Howarth GH (2013) Assimilation of carbonate country rock by the parent magma of the Panzhihua Fe–Ti–V deposit (SW China): evidence from stable isotopes. *Geosci Front* 4:547–554
- Gardner MF, Troll VR, Gamble JA, Gertisser R, Hart GL, Ellam RM, Harris C, Wolff JA (2013) Crustal differentiation processes at Krakatau volcano, Indonesia. *J Petrol* 54:149–182

- Gerbe MC, Gourgaud A, Sigmarsson O, Harmon RS, Jouron JL, Provost A (1992) Mineralogical and geochemical evolution of the 1982–1983 Galunggung eruption (Indonesia). *Bull Volcanol* 54:284–298
- Gertisser R, Keller J (2003a) Trace element and Sr, Nd, Pb and O isotope variations in medium-K and high-K volcanic rocks from Merapi volcano, Central Java, Indonesia: evidence for the involvement of subducted sediments in Sunda Arc magma genesis. *J Petrol* 44:457–489
- Gertisser R, Keller J (2003b) Temporal variations in magma composition at Merapi volcano (Central Java, Indonesia): magmatic cycles during the past 2000 years of explosive activity. *J Volcanol Geotherm Res* 123:1–23
- Gertisser R, del Marmol M-A, Newhall C, Preece K, Charbonnier S, Andreastuti S, Handley H, Keller J (2023) Geological history, chronology and magmatic evolution of Merapi. In: Gertisser R, Troll VR, Walter TR, Nandaka IGMA, Ratdomopurbo A (eds) Merapi volcano—geology, eruptive activity, and monitoring of a high-risk volcano. Springer, Berlin, Heidelberg, pp 137–193
- Giggenbach WF (1997) Fifth field workshop on volcanic gases, Java, 18–29 July 1994: preliminary evaluation of analytical results II. *IAVCEI Commun Chem Volcanol Gases Newsl* 12:4–10
- Gilg HA, Lima A, Somma R, Belkin HE, De Vivo B, Ayuso RA (2001) Isotope geochemistry and fluid inclusion study of skarns from Vesuvius. *Mineral Petrol* 73:145–176
- Goff F, Janik CJ, Delgado H, Werner C, Counce D, Stimac JA, Siebe C, Love SP, Williams SN, Fischer T, Johnson L (1998) Geochemical surveillance of magmatic volatiles at Popocatepetl volcano, Mexico. *Geol Soc Am Bull* 110:695–710
- Goff F, Love SP, Warren RG, Counce D, Obenholzner J, Siebe C, Schmidt SC (2001) Passive infrared remote sensing evidence for large, intermittent CO₂ emissions at Popocatepetl volcano, Mexico. *Chem Geol* 177:133–156
- Goldschmidt, VM (1911) Die Kontaktmetamorphose im Kristianiegebiet. Kristiania: In kommission bei J. Dybwad, 483 p
- González-Maurel O, Deegan FM, le Roux P, Harris C, Troll VR, Godoy B (2020) Constraining the sub-arc, parental magma composition for the giant Altiplano-Puna Volcanic Complex, northern Chile. *Sci Rep* 10:6864
- Gozzi F, Gaeta M, Freda C, Mollo S, Di Rocco T, Marra F, Dallai L, Pack A (2014) Primary magmatic calcite reveals origin from crustal carbonate. *Lithos* 190–191:191–203
- Hall R (2002) Cenozoic geological and plate tectonic evolution of SE Asia and the SW Pacific: computer-based reconstructions, model and animations. *J Asian Earth Sci* 20:353–431
- Hamilton WB (1979) Tectonics of the Indonesian region. US Govt Print Office No. 1078
- Handley HK, Blichert-Toft J, Gertisser R, Macpherson CG, Turner SP, Zaennudin A, Abdurrachman M (2014) Insights from Pb and O isotopes into along-arc variations in subduction inputs and crustal assimilation for volcanic rocks in Java, Sunda arc, Indonesia. *Geochim Cosmochim Acta* 139:205–226
- Handley HK, Reagan M, Gertisser R, Preece K, Berlo K, McGee LE, Barclay J, Herd R (2018) Timescales of magma ascent and degassing and the role of crustal assimilation at Merapi volcano (2006–2010), Indonesia: constraints from uranium-series and radiogenic isotopic compositions. *Geochim Cosmochim Acta* 222:34–52
- Harijoko A, Marliyani GI, Wibowo HE, Freski YR, Handini E (2023) The geodynamic setting and geological context of Merapi volcano in Central Java, Indonesia. In: Gertisser R, Troll VR, Walter TR, Nandaka IGMA, Ratdomopurbo A (eds) Merapi volcano—geology, eruptive activity, and monitoring of a high-risk volcano. Springer, Berlin, Heidelberg, pp 89–109
- Harmon RS, Gerbe M-C (1992) The 1982–83 eruption at Galunggung volcano, Java (Indonesia): Oxygen isotope geochemistry of a chemically zoned magma chamber. *J Petrol* 33:585–609
- Harris C, Vogeli J (2010) Oxygen isotope composition of garnet in the Peninsula Granite, Cape Granite Suite, South Africa: constraints on melting and emplacement mechanisms. *S Afr J Geol* 113(4):401–412
- Haryono E, Day M (2004) Landform differentiation within the Gunung Kidul Kegelkarst, Java, Indonesia. *J Cave Karst Stud* 66:62–69
- Heap MJ, Troll VR, Kushnir ARL, Gilg HA, Collinson ASD, Deegan FM, Darmawan H, Seraphine N, Neuberg J, Walter TR (2019) Hydrothermal alteration of andesitic lava domes can lead to explosive volcanic behaviour. *Nat Commun* 10:5063
- Heimdal TH, Callegaro S, Svensen HH, Jones MT, Pereira E, Planke S (2018) Evidence for magma-evaporite interactions during the emplacement of the Central Atlantic Magmatic Province (CAMP) in Brazil. *Earth Planet Sci Lett* 506:476–492
- Hilton DR, Craig H (1989) A helium isotope transect along the Indonesian archipelago. *Nature* 342:906–908
- Hilton DR, Fischer TP, Marty B (2002) Noble gases in subduction zones and volatile recycling. *Rev Mineral Geochem* 47:319–370
- Holloway JR, Blank JG (1994) Application of experimental results to C–O–H species in natural melts. *Rev Mineral Geochem* 30:187–230
- Holmes A (1920) The nomenclature of petrology: with references to selected literature. Thomas Murby and Co., London, p 284
- Iacono-Marziano G, Gaillard F, Pichavant M (2007) Limestone assimilation and the origin of CO₂ emissions at the Alban Hills (Central Italy): constraints from experimental petrology. *J Volcanol Geotherm Res* 166:91–105

- Iacono-Marziano G, Gaillard F, Pichavant M (2008) Limestone assimilation by basaltic magmas: an experimental re-assessment and application to Italian volcanoes. *Contrib Mineral Petrol* 155:719–738
- Iacono-Marziano G, Gaillard F, Scaillet B, Pichavant M, Chiodini G (2009) Role of non-mantle CO₂ in the dynamics of volcano degassing: the Mount Vesuvius example. *Geology* 37:319–322
- Johnston FKB, Turchyn AV, Edmonds M (2011) Decarbonation efficiency in subduction zones: implications for warm Cretaceous climates. *Earth Planet Sci Lett* 303:143–152
- Jolis EM (2013) Magma-crust interaction at subduction zone volcanoes. Ph.D. Thesis Uppsala University, Acta Universitatis Upsalensis
- Jolis EM, Freda C, Troll VR, Deegan FM, Blythe LS, McLeod CL, Davidson JP (2013) Experimental simulation of magma-carbonate interaction beneath Mt. Vesuvius, Italy. *Contrib Mineral Petrol* 166:1335–1353
- Jolis EM, Troll VR, Harris C, Freda C, Gaeta M, Orsi G, Siebe C (2015) Skarn xenolith record crustal CO₂ liberation during Pompeii and Pollena eruptions, Vesuvius volcanic system, central Italy. *Chem Geol* 415:17–36
- Kerinec F (1982) Le Merapi, volcan actif d'arc insulaire (Java): pétrographie et géochimie des matériaux solides, implications géotectoniques. Thèse de III^{ème} cycle. Université de Paris Orsay, p 92
- Lee CTA, Shen B, Slotnick BS, Liao K, Dickens GR, Yokoyama Y, Lenardic A, Dasgupta R, Jellinek M, Lackey JS, Schneider T, Tice MM (2013) Continental arc-island arc fluctuations, growth of crustal carbonates, and long-term climate change. *Geosphere* 9:21–36
- Lee CTA, Lackey JS (2015) Global continental arc flare-ups and their relation to long-term greenhouse conditions. *Elements* 11:125–130
- Lee CTA, Erdman M, Yang W, Ingram L, Chin EJ, DePaolo DJ (2018) Sulfur isotopic compositions of deep arc cumulates. *Earth Planet Sci Lett* 500:76–85
- Lee CTA, Jiang H, Dasgupta R, Torres M (2019) A framework for understanding whole-earth carbon cycling. In: Orcutt BN, Daniel I, Dasgupta R (eds) *Deep carbon: past to present*. Cambridge University Press, pp 313–357
- Lehmann J, Arndt N, Windley B, Zhou MF, Wang CY, Harris C (2007) Field relationships and geochemical constraints on the emplacement of the Jinchuan intrusion and its Ni–Cu–PGE sulfide deposit, Gansu, China. *Econ Geol* 102:75–94
- Luehr BG, Koulakov I, Suryanto W (2023) Crustal structure and ascent of fluids and melts beneath Merapi: insights from geophysical investigations. In: Gertisser R, Troll VR, Walter TR, Nandaka IGMA, Ratdomopurbo A (eds) *Merapi volcano—geology, eruptive activity, and monitoring of a high-risk volcano*. Springer, Berlin, Heidelberg, pp 111–135
- Macpherson CG, Dempsey SR, Nowell GM, Ottley CJ, Thirwall MF, Hall R (2019) Carbonate assimilation by Sunda Arc magma at Sumbing volcano, central Java, Indonesia. *Goldschmidt Abstracts* 2019:2113
- Mason E, Edmonds M, Turchyn AV (2017) Remobilization of crustal carbon may dominate volcanic arc emissions. *Science* 357:290–294
- McDermott F, Hawkesworth C (1991) Th, Pb, and Sr isotope variations in young island arc volcanics and oceanic sediments. *Earth Planet Sci Lett* 104:1–15
- Metcalfe I (2011) Tectonic framework and Phanerozoic evolution of Sundaland. *Gondwana Res* 19:3–21
- Mollo S, Gaeta M, Freda C, Di Rocco T, Misiti V, Scarlato P (2010) Carbonate assimilation in magmas: a reappraisal based on experimental petrology. *Lithos* 114:503–514
- Mollo S, Heap MJ, Iezzi G, Hess KU, Scarlato P, Dingwell DB (2012) Volcanic edifice weakening via decarbonation: a self-limiting process? *Geophys Res Lett* 39:L15307
- Morris R, Canil D (2022) CO₂ transport at shallow depths in arc magmas: evidence from unique orbicular dikes in the Jurassic Bonanza arc, Vancouver Island, Canada. *Contrib Mineral Petrol* 177:6
- Nadeau O, Williams-Jones AE, Stix J (2013) Magmatic–hydrothermal evolution and devolatilization beneath Merapi volcano, Indonesia. *J Volcanol Geotherm Res* 261:50–68
- O'Hara MJ (1998) Volcanic plumbing and the space problem – thermal and geochemical consequences of large-scale assimilation in Ocean Island development. *J Petrol* 39:1077–1089
- Pang KN, Arndt N, Svensen H, Planke S, Polozov A, Polteau S, Iizuka Y, Chung SL (2013) A petrologic, geochemical and Sr–Nd isotopic study on contact metamorphism and degassing of Devonian evaporites in the Norilsk aureoles, Siberia. *Contrib Mineral Petrol* 165:683–704
- Peters STM, Troll VR, Weis FA, Chadwick JP, Dallai L, Schulz B (2017) Amphibole megacrysts as a probe into the deep plumbing system of Merapi volcano, Central Java, Indonesia. *Contrib Mineral Petrol* 172:16
- Piochi M, Ayuso RA, De Vivo B, Somma R (2006) Crustal contamination and crystal entrapment during polybaric magma evolution at Mt. Somma-Vesuvius volcano, Italy: Geochemical and Sr isotope evidence. *Lithos* 86:303–329
- Preece K, Barclay J, Gertisser R, Herd RA (2013) Textural and micro-petrological variations in the eruptive products of the 2006 dome-forming eruption of Merapi volcano, Indonesia: implications for sub-surface processes. *J Volcanol Geotherm Res* 261:98–120
- Preece K, Gertisser R, Barclay J, Berlo K, Herd RA, EIMF (2014) Pre- and syn-eruptive degassing and crystallization processes of the 2010 and 2006 eruptions of Merapi volcano, Indonesia. *Contrib Mineral Petrol* 168:1061

- Preece K, Gertisser R, Barclay J, Charbonnier SJ, Komorowski JC, Herd RA, (2016) Transitions between explosive and effusive phases during the cataclysmic 2010 eruption of Merapi volcano, Java, Indonesia. *Bull Volcanol* 78:54
- Price RC, Gamble JA, Smith IEM, Stewart RB, Eggins S, Wright IC (2005) An integrated model for the temporal evolution of andesites and rhyolites and crustal development in New Zealand's North Island. *J Volcanol Geotherm Res* 140:1–24
- Ramos EJ, Lackey JS, Barnes JD, Fulton AA (2020) Remnants and rates of metamorphic decarbonation in continental arcs. *GSA Today* 30:4–10
- Ratdomopurbo A, Poupinet G (2000) An overview of the seismicity of Merapi volcano (Java, Indonesia), 1983–1994. *J Volcanol Geotherm Res* 100:193–211
- Rittmann A (1962) *Volcanoes and their activity*. Wiley, New York, p 305
- Sano Y, Marty B (1995) Origin of carbon in fumarolic gas from island arcs. *Chem Geol* 119:265–274
- Sano Y, Takahata N, Nishio Y, Fischer TP, Williams SN (2001) Volcanic flux of nitrogen from the Earth. *Chem Geol* 171:263–271
- Schaaf P, Stimac J, Siebe C, Macías JL (2005) Geochemical evidence for mantle origin and crustal processes in volcanic rocks from Popocatepetl and surrounding monogenetic volcano, central Mexico. *J Petrol* 46:1243–1282
- Smyth HR, Hall R, Nichols GJ (2008) Cenozoic volcanic arc history of East Java, Indonesia: the stratigraphic record of eruptions on an active continental margin. *Geol Soc Am Spec Pap* 436:199–222
- Spandler C, Martin LHI, Pettke T (2012) Carbonate assimilation during magma evolution at Nisyros (Greece), South Aegean Arc: evidence from clinopyroxene xenoliths. *Lithos* 146–147:18–33
- Surono BT, Sudarno I, Wiryosujono S (1992) *Geology of the Surakarta-Girintoro Quadrangles, Java*. Geological Research and Development Center, Bandung, Indonesia, Scale 1:100,000, 2 sheets
- Svensen HH, Frolov S, Akhmanov GG, Polozov AG, Jerram DA, Shiganova OV, Melnikov NV, Iyer K, Planke S (2018) Sills and gas generation in the Siberian Traps. *Phil Trans R Soc A* 376:20170080
- Tepley FJ III, Davidson JP, Tilling RI, Arth JG (2000) Magma mixing, recharge and eruption histories recorded in plagioclase phenocrysts from El Chichón volcano, Mexico. *J Petrol* 41:1397–1411
- Toutain JP, Sortino F, Baubron JC, Richon P, Surono, Sumarti S, Nonell A (2009) Structure and CO₂ budget of Merapi volcano during inter-eruptive periods. *Bull Volcanol* 71:815–826
- Tregoning P, Brunner FK, Bock Y, Puntodewo SSO, McCaffrey R, Genrich JF, Calais E, Rais J, Subarya C (1994) First geodetic measurement of convergence across the Java Trench. *Geophys Res Lett* 21:2135–2138
- Troll VR, Hilton DR, Jolis EM, Chadwick JP, Blythe LS, Deegan FM, Schwarzkopf LM, Zimmer M (2012) Crustal CO₂ liberation during the 2006 eruption and earthquake events at Merapi volcano, Indonesia. *Geophys Res Lett* 39:L11302
- Troll VR, Deegan FM, Jolis EM, Harris C, Chadwick JP, Gertisser R, Schwarzkopf LM, Borisova A, Bindeman IN, Sumarti S, Preece K (2013a) Magmatic differentiation processes at Merapi volcano: inclusion petrology and oxygen isotopes. *J Volcanol Geotherm Res* 261:38–49
- Troll VR, Chadwick JP, Jolis EM, Deegan FM, Hilton DR, Schwarzkopf LM, Blythe LS, Zimmer M (2013b) Crustal volatile release at Merapi volcano; the 2006 earthquake and eruption events. *Geol Today* 29:96–101
- Troll VR, Deegan FM, Jolis EM, Budd DA, Dahren B, Schwarzkopf LM (2015) Ancient oral tradition describes volcano–earthquake interaction at Merapi volcano, Indonesia. *Geogr Ann A Phys Geogr* 97:137–166
- Troll VR, Deegan FM (2023) The magma plumbing system of Merapi: the petrological perspective. In: Gertisser R, Troll VR, Walter TR, Nandaka IGMA, Ratdomopurbo A (eds) *Merapi volcano—geology, eruptive activity, and monitoring of a high-risk volcano*. Springer, Berlin, Heidelberg, pp 233–263
- Turner S, Foden J (2001) U, Th and Ra disequilibria, Sr, Nd and Pb isotope and trace element variations in Sunda arc lavas: predominance of a subducted sediment component. *Contrib Mineral Petrol* 142:43–57
- Untung M, Sato Y (1978) *Gravity and geological studies in Java*, vol 6. Geological Survey of Indonesia and Geological Survey of Japan, Special Publication 6, 207 pp
- van Bemmelen (1949) *The geology of Indonesia*. Vol 1A: General geology. The Hague Government Printing Office, Netherlands
- van der Zwan FM, Chadwick JP, Troll VR (2013) Textural history of recent basaltic-andesites and plutonic inclusions from Merapi volcano. *Contrib Mineral Petrol* 166:43–63
- Varekamp JC, Kreulen R, Poorter RPE, van Bergen MJ (1992) Carbon sources in arc volcanism, with implications for the carbon cycle. *Terra Nova* 4:363–373
- Voight B, Constantine EK, Siswoidjoyo S, Torley R (2000) Historical eruptions of Merapi volcano, Central Java, Indonesia, 1768–1998. *J Volcanol Geotherm Res* 100:69–138
- Waltham AC, Smart PL, Friederich H, Eavis AJ, Atkinson TC (1983) The caves of Gunung Sewu, Java. *Cave Sci* 10:55–96
- Whitford DJ (1975) Strontium isotopic studies of the volcanic rocks of the Saunda arc, Indonesia, and their petrogenetic implications. *Geochim Cosmochim Acta* 39:1287–1302
- Whitley S (2020) *Xenoliths as tracers of magmatic and intra-crustal processes at volcanic arc*. Ph.D. Thesis, Keele University, Keele, UK
- Whitley S, Gertisser R, Halama R, Preece K, Troll VR, Deegan FM (2019) Crustal CO₂ contribution to subduction zone degassing recorded through calc-silicate xenoliths in arc lavas. *Sci Rep* 9:8803

-
- Whitley S, Halama R, Gertisser R, Preece K, Deegan FM, Troll VR (2020) Magmatic and metasomatic effects of magma-carbonate interaction recorded in calc-silicate xenoliths from Merapi volcano (Indonesia). *J Petrol* 61:egaa048
- Wölbern I, Rümpler G (2016) Crustal thickness beneath Central and East Java (Indonesia) inferred from P receiver functions. *J Asian Earth Sci* 115:69–79



Merapi Volcano: From Volcanic Gases to Magma Degassing

11

Olivier Nadeau, Hanik Humaida,
and Patrick Allard

Abstract

Volcanic activity at Merapi is characterised by continuous summit degassing, sustaining a volcanic plume both between and during eruptions. A considerable amount of data was obtained on these volatile emissions which, in complement to geophysical surveys, provides a sensitive understanding of the volcano dynamics. Direct sampling and analysis of high-temperature (400–870 °C) gases issued from the long-lived fumarolic fields of Gendol and Woro was initiated in the late 1970s, then operated for routine monitoring until the 2010 eruption. At the same time, the SO₂ plume output became regularly surveyed using remote UV spectroscopy (COSPEC then DOAS). Both types of measurements, plus isotopic investi-

gations and trace metal analysis, have provided important insight into the magmatic source of Merapi, the gas emission rates and their relationship with volcanic activity, and the compositional gas changes precursory to major eruptive events (e.g. the 2010 Plinian eruption). Moreover, the initial abundances and pressure-related behavior of volatile components in Merapi magma were determined from both microprobe analysis of natural samples (melt inclusions, crystal zoning) and petrologic experiments. Combined with volcanic gas data, such information allows constraining the magma supply rate and degassing budget, as well as the depth and dynamics of magma degassing processes controlling the volcanic activity. Finally, a specificity of Merapi is that its upper plumbing system intrudes thick carbonate sediments whose fragments are commonly entrained by the magma and whose metamorphism or even melting may contribute significant amounts of carbon dioxide to the volcano degassing budget. After reviewing this information, two synthetic models for Merapi volatile sources and emissions are proposed.

O. Nadeau (✉)

Department of Mineral Resources and Engineering,
Laboratory for Isotopes in Economic Geology and
Its Environment, School of Earth Resources, China
University of Geosciences, Wuhan, China
e-mail: nadeau.olivier@cug.edu.cn

H. Humaida

Balai Penyelidikan Dan Pengembangan Teknologi
Kebencanaan Geologi (BPPTKG), Jl.Cendana 15,
Yogyakarta 55166, Indonesia

P. Allard

Institut de Physique du Globe de Paris, Université de
Paris, UMR7154 CNRS, Paris, France

Keywords

Merapi · Volcanic gases · Magma degassing ·
Volatiles

11.1 Introduction

Gas emission is a characteristic manifestation of erupting and dormant volcanoes. Depending on the magma proximity and the level of activity, it can take a wide variety of forms, ranging from cold gases bubbling through surface waters, diffuse soil emanations, moderately hot fumaroles, up to high-temperature crater emissions strong enough to sustain a volcanic plume (e.g. Allard et al. 1991; Symonds et al. 1994). Amongst the several hundreds of Holocene volcanoes that are currently degassing subaerially on Earth (Siebert et al. 2015), about 120 are particularly active and remain major gas emitters even during quiescence. Merapi is one such continuously degassing volcano.

Volcanic gases are mainly composed of molecular combinations of H, O, C, S, Cl, F and N, amongst which H₂O, CO₂, SO₂ or/and H₂S usually are the dominant species (e.g. Symonds et al. 1994; Giggenbach 1996), associated with HCl, HF and a great variety of volatile compounds of minor and trace elements in the hottest gases. The chemical composition of volcanic gases varies drastically as a function of temperature, the depth of their sources, and the extent of mixing between magmatic- and other hydrothermal fluids from the volcanic basement (e.g. Symonds et al. 1994; Giggenbach 1996).

Monitoring volcanic gas emissions by combining fluid chemistry and geophysical surveys is of prime interest to detect precursory signals of volcanic unrest, and possibly forecast eruptions. This relies on the specific properties of magmatic volatiles such as H₂O, CO₂, S, Cl and F. Despite the minor concentrations of some of these volatiles, they play a major role in magmatic processes through their unique capability to form gas bubbles during magma decompression. Indeed, bubble nucleation and expansion strongly affect the density and viscosity of magmas, their crystallisation path, and hence the dynamics of their storage, ascent and eruption (e.g. Sparks 1978). Moreover, gas bubbles can rise faster than their host melts and reach the surface well ahead of magmas, carrying sensitive

thermochemical information about underground conditions. The chemistry of the magmatic volatile phase evolves gradually with decreasing pressure, from initially CO₂-rich at depth, to H₂O-halogens-rich near the surface, owing to the contrasted solubility behaviour of the volatile components (e.g. Blank and Brooker 1994; Holloway and Blank 1994; Baker and Alletti 2012). Therefore, under given temperatures and redox states, volcanic gas ratios have proven to be sensitive geobarometers. Monitoring the composition and the mass flux of volcanic gas emissions also allows assessing the amount of magma prone to erupting and, more broadly, the geochemical and environmental impacts of volcanism at both the local and global scales.

The chemistry of volcanic gases also varies drastically with the tectonic setting and the volatile contents of magmas. Volcanic gases from arc volcanoes such as Merapi are usually enriched in H₂O and halogens by comparison to gases from mid-ocean ridges basalts (MORB) and hot spots, which are relatively water- and halogen-depleted but enriched in CO₂ (e.g. Wallace et al. 2015). The origin of volatiles at arc volcanoes is further complicated by the fact that it involves the partial melting of a mantle wedge that was metasomatised by fluids released from the devolatilization of a subducted hydrothermally altered oceanic crust. While ascending through volcanic arcs across complex trans-crustal systems (Cashman et al. 2017), the generated silicate melts and fluids can interact with surrounding rocks and hydrothermal systems. These interactions are greater in continental arcs such as the Sunda arc, which are thicker and host extensive sedimentary successions (Aiuppa et al. 2017a, b). When magmas coexist with free CO₂-rich volatile phases at deep crustal levels, such as recently suggested (e.g. Edmonds and Woods 2018; Nadeau et al. 2018; Nadeau 2019), extensive mixing may occur between the magmatic volatile phase and other hydrothermal fluids circulating through the crust. Furthermore, magma-carbonate interaction (see Deegan et al. 2023, Chap. 10) is also prone to generate crustal-derived fluids that likely mix with the magmatic

volatiles, and Merapi is one typical volcano where this has been investigated extensively (Brouwer 1928, 1945; Chadwick et al. 2007; Deegan et al. 2010; Whitley et al. 2020). In summary, during its ascent towards the surface, the magmatic volatile phase experiences diverse interactions with hydrothermal fluids and crustal wall rocks which modify its chemical composition. Deciphering the origins of the different components of volcanic gases nevertheless remains feasible, by using a combination of petrographical observations (e.g. Brouwer 1928, 1945; Nadeau et al. 2010; Whitley et al. 2020), petrological information and experiments (e.g. Gertisser and Keller 2003a; Deegan et al. 2010, 2023, Chap. 10; Nadeau et al. 2013a, b; Preece et al. 2014), chemical and isotopic tracers (e.g. Allard 1983; Chadwick et al. 2007; Troll et al. 2012, 2013a; Gertisser and Keller 2003b; Mason et al. 2017), geophysical methods (e.g. Luehr et al. 2013; Koulakov et al. 2016; Byrdina et al. 2017) as well as thermodynamic modelling (e.g. Burgisser et al. 2015; Erdmann et al. 2016).

At Merapi, a considerable amount of data has been obtained on volatile emissions over the past four decades. Combined with petrological information, these data provide a sensitive understanding of the magmatic source of the volcano, the magma supply rate and degassing budget, the depth and dynamics of degassing processes controlling the volcanic activity, and the temporal changes in gas compositions and emission rates in relation with volcanic activity and major eruptive events. These data and their interpretations are reviewed below.

11.2 Early Analyses of Merapi Volcanic Gases

11.2.1 Major Gas Chemistry

Volcanic gases from Merapi were investigated for the first time during the 1977–1980 period within an Indonesian-French collaboration project. High-temperature gases emitted from two long-lived fumarolic fields located on the eastern summit rim of the volcano (Fig. 11.1), Woro

(430–645 °C) and Gendol (710–870 °C), were repeatedly sampled (NaOH-bearing glass bottles) or/and analysed in situ with a chromatographic tool (Le Guern et al. 1979; Allard 1980, 1983, 1986). Allard and Tazieff (1979) had mapped these fumarolic fields in detail, including their vent temperatures. Still hotter gases (901 °C) could also be directly sampled and analysed from the extruding andesitic lava dome. The molar composition of the hottest gases from Gendol and the lava dome was found to average 88.5% H₂O, 8.4% CO₂, 0.84% H₂, 0.67% SO₂, 0.65% H₂S, 0.55% HCl, 0.23% N₂, 0.0% CO and 0.017% HF (Allard 1986) (for a comparison, see the average composition of volcanic gases from both Gendol and Woro fields over the 1999–2010 period in Fig. 11.1 and Table 11.1). The equilibrium temperature and redox state of the volcanic gases were assessed by applying thermodynamic modelling to the field gas chromatograph data (Gerlach 1982) and the gas samples (Allard 1986). Equilibrium gas temperatures calculated from the H₂O–H₂, CO₂–CO and H₂S–SO₂ redox couples were found to systematically exceed (by >100 °C) the exit temperatures, implying a chemical ‘quenching’ of the gas phases under hotter conditions in the conduit during their final ascent towards the surface. Thermodynamic calculations, but also in situ electrochemical measurements of the oxygen fugacity in the volcanic gases (Gantes et al. 1983), revealed redox conditions ranging between the Quartz-Fayalite-Magnetite (QFM) buffer for the hottest gases and the Nickel-Nickel Oxide (NNO) buffer for the cooler Woro gases.

In 1978, a new method was applied to assess the metal load of Merapi volcanic gases: open silica tubes equipped with thermocouples and inserted into fumarolic vents allowed gradual sublimation, onto the inner wall of the tubes, of the metal-bearing volatile species of the flowing gases down the temperature gradients (Le Guern and Bernard 1982). A zoned mineral paragenesis was observed in the sublimated products, tracking the formation of cristobalite, magnetite, hercynite and molybdenite at high temperature, followed by acmite, halite and sylvite at medium temperature, then sphalerite, pyrite and galena at

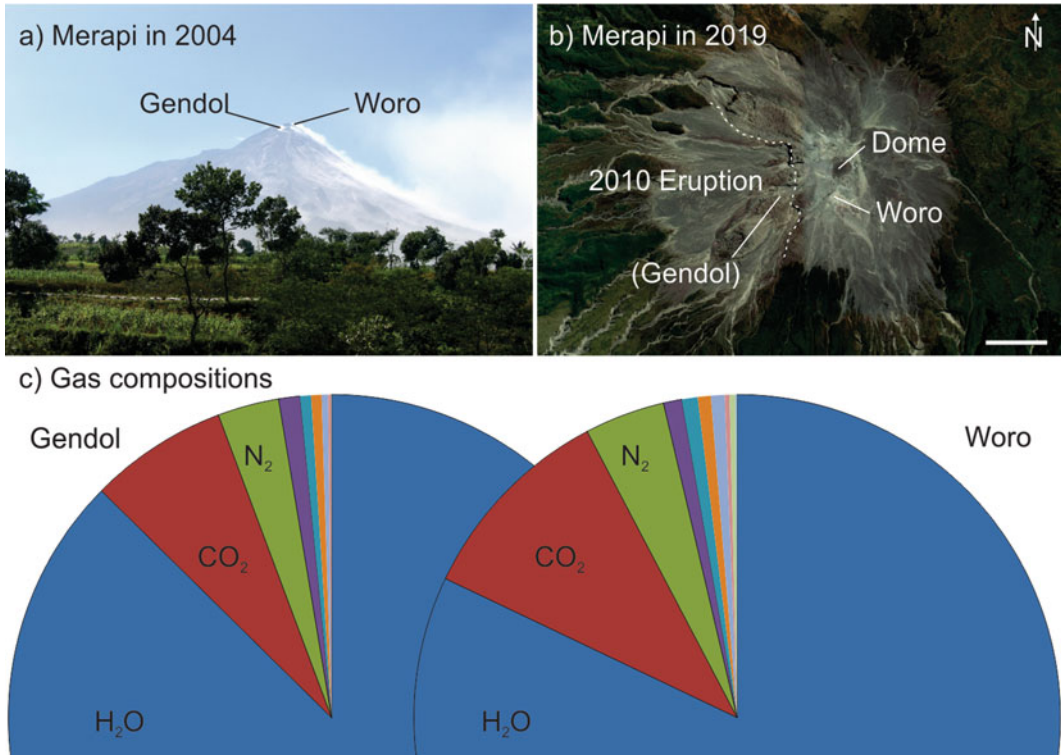


Fig. 11.1 Location of the Gendol and Woro fumarolic fields (a–b) and average composition of their volcanic gases (c). **a** North view of Merapi volcano in 2004 with Gendol and Woro fumarolic fields near the summit. **b** Satellite view of Merapi in 2019 with location of the Dome, Woro, and former Gendol fumarolic fields. Gendol was destroyed during the 2006 eruption. Scale bar is 500 m. **c** Average

composition of volcanic gases from Gendol and Woro fumarolic fields at Merapi summit, Indonesia. The data were collected by the Indonesian Center of Volcanology and Geological Hazard Mitigation (CVGHM) and compiled by Humaida et al. (2017). Data cover the period from May 1999 to October 2010 at Woro and from May 1999 to October 2005 at Gendol (see Table 11.1)

low temperature. These results revealed that, in addition to major species such as H₂O, CO₂ and SO₂, the volcanic gas phase transported major rock-forming elements such as Fe but also economic trace elements such as Mo, Zn and Pb.

11.2.2 Stable Isotope Tracing

Hydrogen and oxygen isotopes in 750–900 °C water vapor from the Gendol fumarolic field were analysed by Allard (1980, 1986) in 1978, 1979 and 1980, by Priatna and Kadarsetia (2007) in 1993–1995 and by Nadeau et al. (2010) in 2004. Most results plot within or close to the ‘Andesitic Magmatic Water’ box defined by Giggenbach (1992), indicating the predominant

emission of mantle-derived magmatic arc water variably mixed with local meteoric groundwater (Fig. 11.2). The δD and $\delta^{18}O$ (VSMOW) values reported for more peripheral Woro fumarolic gases (Allard 1986; Priatna and Kadarsetia 2007; Nadeau et al. 2010) evidence an enhanced meteoric dilution of the same magmatic component, in agreement with the lower temperature and higher oxidation state of these gases. By contrast, the carbon isotope ratio of CO₂ from both the lava dome and the Gendol and Woro fields was found to be spatially uniform and constant over time, with a $\delta^{13}C$ averaging $-3.9 \pm 0.3\%$ in 1978–1980 (Allard 1983, 1986) but also in subsequent decades (Allard et al. 1995, 2011; Troll et al. 2012; Allard 2013). A similar $\delta^{13}C$ composition was also found for

Table 11.1 Average composition of volcanic gases from the Gendol and Woro summit fumarolic fields of Merapi, Indonesia

| | Gendol | | Woro | |
|---------------------|---------|---------------|---------|---------------|
| | Average | (1 σ) | Average | (1 σ) |
| Temperature (°C) | 650 | 98 | 553 | 89 |
| H ₂ O | 87.4 | 6.7 | 82.5 | 18.6 |
| CO ₂ | 6.9 | 3.0 | 10.3 | 11.2 |
| N ₂ | 3.1 | 3.1 | 4.0 | 11.3 |
| HCl | 1.1 | 1.4 | 0.69 | 0.98 |
| SO ₂ | 0.56 | 0.30 | 0.80 | 0.73 |
| H ₂ S | 0.52 | 0.33 | 0.66 | 0.84 |
| H ₂ | 0.32 | 0.21 | 0.25 | 0.22 |
| O ₂ + Ar | 0.15 | 0.18 | 0.27 | 0.69 |
| HF | 0.014 | 0.010 | b/l | b/l |
| CO | 0.009 | 0.007 | 0.018 | 0.039 |
| NH ₃ | b/l | b/l | 0.92 | 0.87 |
| CH ₄ | b/l | b/l | 0.084 | 0.157 |

The data were collected and analysed by the Indonesian Center of Volcanology and Geological Hazard Mitigation (CVGHM) and compiled by Humaida et al. (2017). Data cover the period from May 1999 to October 2010 at Woro and from May 1999 to October 2005 at Gendol. All results are in mol%; b/l = below limit of detection. See also Fig. 11.1

diffuse carbon dioxide percolating through the upper volcanic edifice (Toutain et al. 2009). Such an isotopic signature, and its constancy, were interpreted to characterise a deep source mixing between 20% of mantle-derived carbon and 80% of subducted sedimentary carbon (Allard 1986, 2013; Allard et al. 2011). A mixed mantle-slab derivation of both sulphur and nitrogen in the same gases was also inferred from their isotopic composition (Allard 1983, 1986). However, Troll et al. (2012) measured a higher $\delta^{13}\text{C}$ value of -2.4% in Woro gases collected soon after the moderately explosive 2006 eruption, which led them to suggest a possible CO₂ release from shallow magma-limestone interaction in the crustal basement and a potential link between this interaction and explosive activity (see Sect. 11.6 and Deegan et al. 2023, Chap. 10).

11.2.3 Trace Elements

Following the first measurements by Le Guern and Bernard (1982), Symonds et al. (1987) demonstrated that Merapi volcanic gases are

enriched, by factors of 10^1 to 10^5 , in a variety of trace elements (Se, Re, Bi, Cd, Au, In, Pb, As, W, Mo, Cs, Sn, Zn, Rb, Cu, K, Na, Sb, Ni, Ga, V, Fe, Mn, Li). Combining SO₂/metal ratios in gas condensates with the SO₂ flux measured by the Volcanological Survey of Indonesia (VSI), they estimated average emission rates of 10–1000 kg/day for Al–Zn–Fe–K–Mg, 1–10 kg/day for Pb–As–Mo–Mn–V–W–Sr and <1 kg/day for Ni–Cu–Cr–Ga–Sb–Bi–Cd–Li–Co–U. Symonds et al. (1987) concluded that most of the metals originate from the incomplete degassing of shallow magma, even though some metals are influenced by reaction of the magmatic gases with the wall rocks. Comparing samples of gas condensates, silica tube sublimates and encrustations from around fumaroles, Bernard et al. (1990) highlighted a systematic enrichment of Fe, Mo, W and Re in Merapi gases. Sublimates of molybdenite (MoS₂) were enriched in Re up to 11.5 wt% and the powellite-scheelite solid solution (CaMoO₄–CaWO₄) was identified in fumarole encrustations. Thermodynamic calculations suggested that Mo–W were transported in the vapor phase as acids (H₂MoO₄ and H₂WO₄)

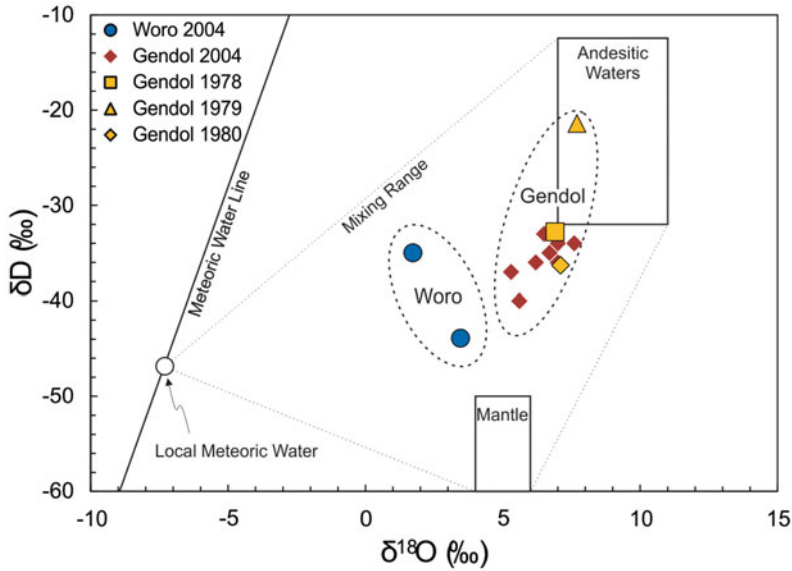


Fig. 11.2 Stable isotope composition of Merapi volcanic steam (gas condensates). The δD and $\delta^{18}O$ values are reported against VSMOW. Data from 1978–1980 are from Allard (1986) and those from 2004 are from Nadeau

et al. (2010). The ‘Andesitic Water’ box is from Giggenbach (1992). The Mantle box extends to lower δD values (Sheppard and Epstein 1970). Data for local meteoric waters are from BudhieWijatna et al. (2013)

at temperatures $>500\text{ }^{\circ}\text{C}$ under QFM to Hematite-Magnetite (HM) redox conditions, but that oxychlorides (MoO_2Cl_2 and WO_2Cl_2) were present in significant concentrations at $T < 400\text{ }^{\circ}\text{C}$ or at very high HCl fugacity. A scanning electron microscope study of tube sublimates showed a zonation of mineral types with decreasing temperature, similar to that reported by Symonds et al. (1987), but also a gradual change in the size and morphology of crystals formed along the temperature gradient from the hot to the cold ends of the tubes (Symonds 1993). This was thought to result from gradual supersaturation of the gases with respect to the minerals as temperature decreases, in agreement with thermodynamic inferences of ‘quenched’ gas compositions (Gerlach 1982; Allard 1986).

In summary, by around the mid-1980s it was understood that 600–900 $^{\circ}\text{C}$ Merapi volcanic gases (1) are, at most times, predominantly of magmatic derivation, (2) keep the thermodynamic record of underground equilibrium temperatures $\geq 1000\text{ }^{\circ}\text{C}$ and of redox conditions between the QFM and NNO buffer reactions, and (3) carry many major-to-trace metals, such as Fe,

Mo, Zn and Pb, which sublime as oxides or sulphides as the gases cool down upon emission. An important hope in the scientific community was also that compositional changes of Merapi volcanic gases could eventually be used to predict volcanic eruptions, in combination with geophysical surveys. However, detecting causal links between the volcanic gas composition and eruptive activity required a regular gas monitoring.

11.3 Routine Survey of Merapi Volcanic Gases

11.3.1 Gas Composition

Stimulated by the early research described above, the Merapi Volcano Observatory (MVO, hereafter referred to as BPPTKG) developed a routine survey of Gendol and Woro fumarolic gases starting in the mid 80 s, using field gas sampling and laboratory analyses in Yogyakarta. The large data set collected eventually revealed temporal changes in the volcanic gas composition in relation to eruptive activity, in particular a

relative increase of CO₂ (CO₂/SO₂ and CO₂/H₂O ratios) and of SO₂/HCl ratios prior to major dome-related pyroclastic flow events (e.g. Priatna and Kadasetia 2007; Sumarti et al. 2007). In July 1994, the 5th workshop of the Commission on the Chemistry of Volcanic Gases (CCGV) of the International Association of Volcanology and the Chemistry of the Earth's Interior (IAVCEI) offered the opportunity of simultaneous sampling and comparative analysis of Merapi volcanic gases by twenty-eight geochemists from Indonesia, New Zealand, Italy, Japan, Russia and the USA. The molar composition of gas emissions from Gendol (803 °C) and Woro (575 °C) averaged 89% H₂O, 6.3% CO₂, 2.0% N₂, 0.8% SO₂, 0.4% H₂S, 0.4% HCl and 0.4% H₂ (Giggenbach et al. 2001), quite similar to that of the hottest emissions measured in 1978–1980 (Le Guern et al. 1979; Allard 1986).

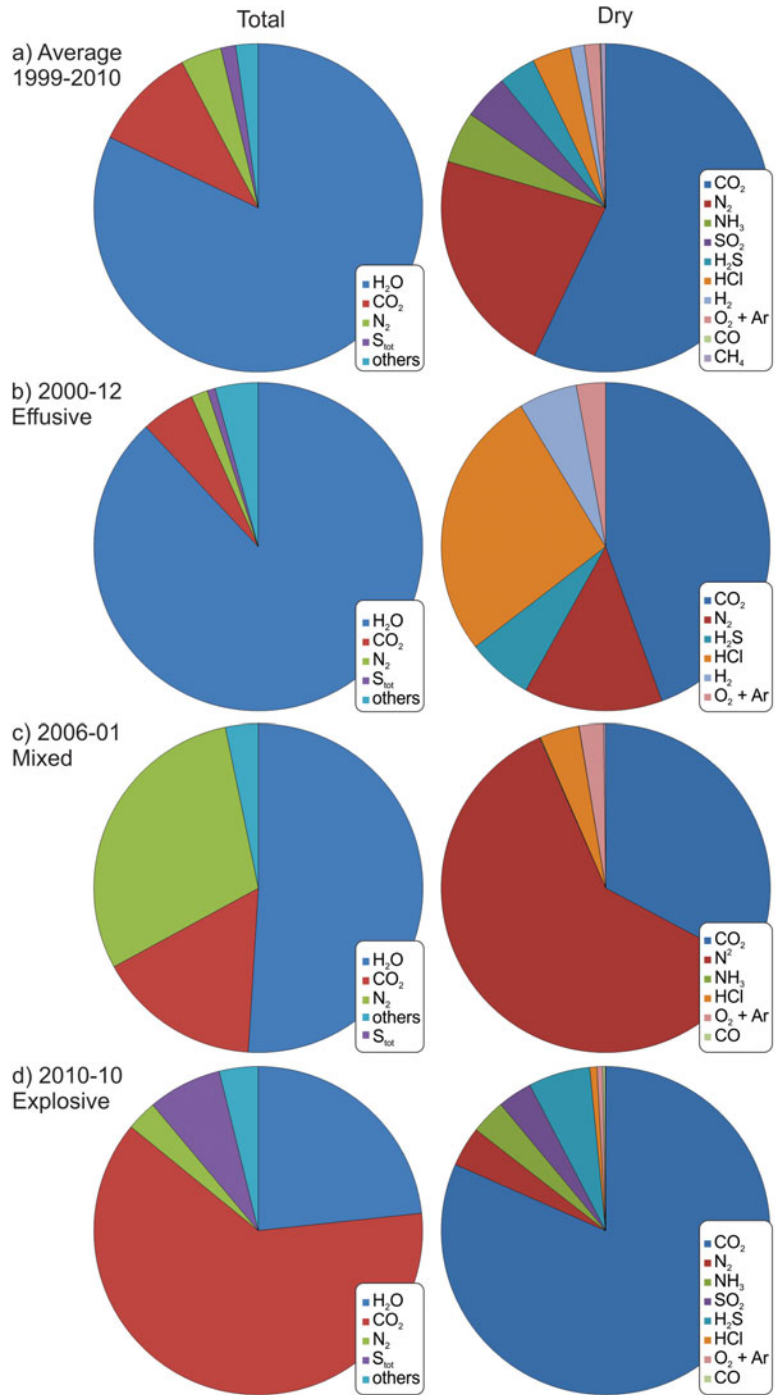
The most recent and exhaustive data compilation for Merapi volcanic gases was published by Humaida et al. (2017) and reports gas emissions from Gendol between May 1999 and October 2005 (the Gendol field was destroyed during the 2006 eruption) and from Woro between May 1999 and October 2010. Over these periods gas temperatures varied from 527 to 770 °C at Gendol and from 380 to 718 °C at Woro. Gas compositions were less variable at Gendol (72–93% H₂O, 3.5–13.2% CO₂, 0.17–0.96% SO₂, 0.12–1.16% H₂S and 0.18–4.64% HCl) than at Woro (18–96% H₂O, 1.9–62.6% CO₂, 0.01–3.02% SO₂, 0.058–4.7% H₂S and 0–4.28% HCl). However, the range at Woro (the single field monitored since 2005) (Fig. 11.3) includes the remarkable compositional changes that preceded the centennial 2010 eruption, especially the sharp increase of CO₂ (up to 62.6% of total gas) detected about two weeks before the cataclysm (Surono et al. 2012) (another remarkable change occurred prior to the 2006 eruption when N₂ reached up to 29.7 mol% but has remained unexplained). Otherwise, the compilation by Humaida et al. (2017) further verifies the chemical differences previously observed between Gendol and Woro gases. In agreement with isotopic data and thermodynamic modelling (see above), volcanic gases from Gendol, spatially the

closest to the volcano conduit, always preserved a more 'primary' magmatic signature than volcanic gases from the more peripheral Woro field, these latter being more affected by groundwater dilution, gas-rock interactions, and shallow oxidation. A greater effect of these secondary processes at Woro was further demonstrated by a continuous thermometric and chromatographic gas survey conducted in May–June 1997 and then 2000–2001 within an Indonesian-German collaboration (Zimmer and Erzinger 2003a, b). Apart from some rhythmic oscillations in T–CO₂–SO₂–H₂O observed to occur every 3–4 h in May 1997, attributed to possible pulsations in shallow magma degassing, the negative correlations systematically recorded between H₂O on one side and T–CO₂–SO₂ on the other side indicated a predominant effect of variable gas dilution by meteoric water. In fact, both increasing H₂O/CO₂–H₂O/SO₂ ratios and decreasing gas temperature were observed to follow periods of intensive rainfall, whereas higher temperatures and lower H₂O/CO₂–H₂O/SO₂ ratios coincided with the dry season.

11.3.2 Sulphur Dioxide Emission Rate

The rate of SO₂ degassing from Merapi was first measured in 1978–1979 using UV correlation spectrometry (COSPEC) during car traverses under the volcanic plume (Allard et al. 1984). The SO₂ flux during quiescent lava dome extrusion at that time was found to range between 150 and 330 tons/day. A routine COSPEC survey, performed in scanning mode from the Babadan Observation Post (4.9 km to the West of Merapi), was then developed by VSI, before being recently substituted by DOAS (Differential Optical Absorption Spectroscopy) monitoring. Humaida et al. (2017) compiled all COSPEC data obtained by the Indonesian Center of Volcanology and Geological Hazard Mitigation (CVGHM) from 1992 to 2011 (Fig. 11.4). Over 2200 measurements made on a daily basis show SO₂ flux variations from 11 tons/day (1995–09 and 1998–07) to 500 tons/day (on November 3 during the 2010 eruption). The

Fig. 11.3 Major molecular composition of volcanic gases from the Woro fumarolic field. **a** Average composition over the 1999–2010 period. **b–d** Compositions before the 2001 effusive eruption (**b**), the effusive and mildly explosive 2006 eruption (**c**), and the 2010 cataclysmic (VEI-4) eruption (**d**). Dry compositions on the right column means without H₂O



reported time averaged SO₂ flux is 123 ± 57 tons/day. Note, however, that this may be a minimal value only, as distal UV (COSPEC, DOAS) scanning of volcanic plumes frequently

involves significant signal dilution of the back-scattered solar radiation and therefore may lead to underestimation of computed SO₂ flux (e.g. Kern et al. 2012).

Complex relationships were observed between SO_2 flux changes and eruptive activity. Although the eruptions in 1992, 1994, 1997 and 1998 were generally accompanied by increases in SO_2 flux, the 2001 eruption was neither preceded nor accompanied by an increase in SO_2 flux (Fig. 11.4b). By contrast, the 2006 eruption was preceded by a rise in SO_2 degassing, from about 150 tons/day in March to nearly 300 tons/day during the peak of the eruption on 15 June 2006 (Fig. 11.4c). Prior to the November 2010 VEI-4 eruption, measurements resumed since 25 Oct. 2010 indicated a SO_2 flux rising from 100–200 tons/day, equivalent to that measured in early 2009, to a maximum of 500 tons/day on 3 Nov. 2010 (Fig. 11.4d). Note, however, that contemporaneous ground-based DOAS and space-borne Ozone Monitoring Instrument (OMI) remote sensing revealed much higher SO_2 flux levels, rising from a few hundred tons/day until 25 Oct. 2010 to several thousands of tons/day in

coincidence with explosions during the following week and to over 10^5 tons/day during the 4–5 Nov. 2010 paroxysm (Surono et al. 2012). Therefore, the time averaged SO_2 flux from Merapi may be significantly higher than inferred from routine UV measurements in the past decades. In summary, larger eruptive events at Merapi are usually accompanied, and sometimes preceded, by a significant increase in the SO_2 degassing rate that correlates with increased seismicity and can be ascribed to injections of new magma beneath the volcano (see below).

11.4 Degassing of Resident Magma in Shallow Feeding System

Magmatic gases emanating from the summit of Merapi are thought to commonly derive from degassing of a shallow magma feeding system connecting the volcano conduit to underlying

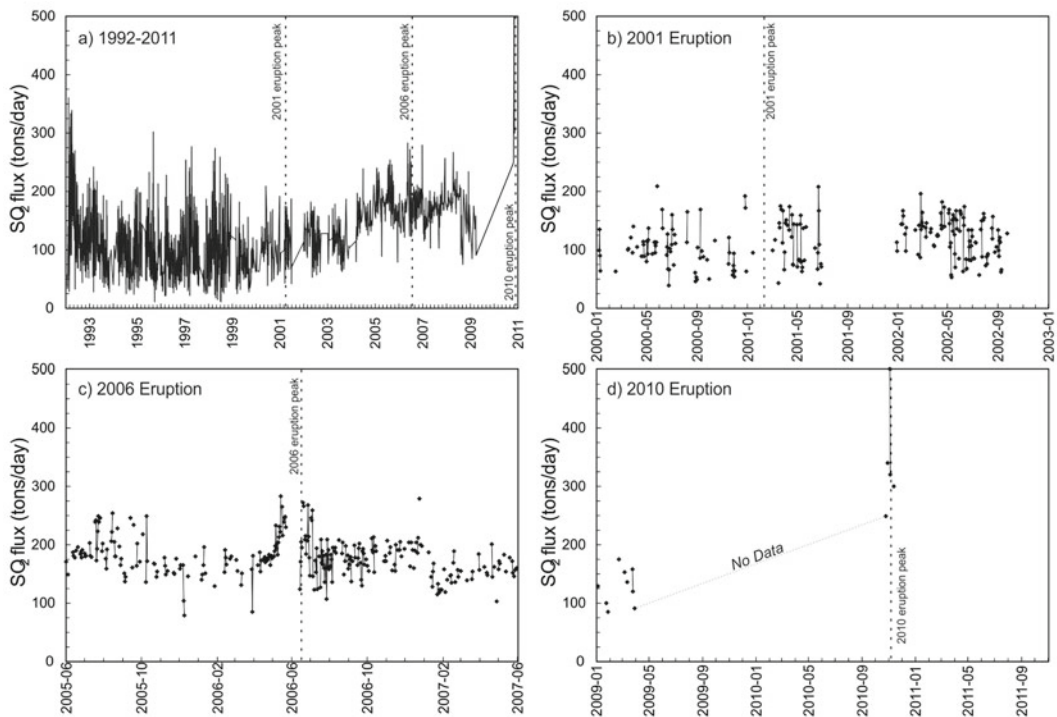


Fig. 11.4 SO_2 plume flux from Merapi measured by the Indonesian Center of Volcanology and Geological Hazard Mitigation (CVGHM) using correlation spectrometry (COSPEC) and later Differential Optical Absorption

Spectroscopy (DOAS). The data span from 21 January 1992 to 12 November 2010 (Humaida et al. 2017): **a** 1992–2011. **b** 2001 eruption. **c** 2006 eruption. **d** 2010 eruption

crustal reservoirs. Combined with rigorous observations by CVGHM staff, this feeding system was investigated through geophysical, geochemical and petrological approaches (see Troll and Deegan 2023, Chap. 8). Based on the volcanic seismicity recorded between 1983 and 1995, Ratdomopurbo and Poupinet (2000) identified the shallowest part of this magmatic system as an aseismic gap that extends from 1.5 to 2.5 km depth below the summit, i.e. within the edifice, between two active seismic zones. A 3D electromagnetic survey conducted in 1998 (Müller et al. 2002) confirmed the existence of a conductive layer corresponding to volatile-saturated magma (and possibly strata of hydrothermally altered rocks and fluids) at similar depths (0.5–2.5 km) beneath the volcano's south flank. Ratdomopurbo and Poupinet (2000) further showed that the explosive onsets of the 1984–1986 and 1992–1994 eruptive cycles were preceded by volcano-tectonic earthquakes occurring at 2.5–5 km depth, indicating seismogenic magma influx from a deeper reservoir. In fact, modeling of ground deformations in the same period (Beauducel and Cornet 1999) evidenced inflation/deflation of a sill-like ellipsoidal magma body emplaced at between 5 and 9 km depth below the volcano summit (2–6 km below sea level). Hence, the standard regime of magma extrusion and degassing of Merapi appears to be controlled by a connected two-stage magma storage system that extends from within the edifice itself down to 6 km depth in its crustal basement. However, as shown thereafter this shallow system is repeatedly replenished with deeper-derived magma rising from deeper crustal levels and the underlying mantle wedge (e.g. Gertisser and Keller 2003a; Costa et al. 2013; Nadeau et al. 2013b; Koulakov et al. 2016).

By studying $^{210}\text{Pb}/^{226}\text{Ra}$ radioactive disequilibrium in recent Merapi lavas, Gauthier and Condomines (1999) computed that the volcanic activity is sustained by steady-state degassing of a $16 \times 10^6 \text{ m}^3$ shallow magma reservoir. Deeper un-degassed magma is recurrently injected into this reservoir and mixes with the resident magma. Direct sourcing of the volcanic gases from that shallow reservoir is also supported by the

proportions of ^{210}Pb , ^{210}Bi and ^{210}Po radionuclides and SO_2 in the plume emissions, measured during the 1978–1995 period (Le Cloarec and Gauthier 2003). Combining $^{210}\text{Po}/^{210}\text{Pb}/\text{SO}_2$ ratios with the average SO_2 flux, Le Cloarec and Gauthier (2003) estimated the degassing of twice as much magma was erupted, even though gas interaction with brines and hydrothermal precipitation through water–rock interactions could also affect the radioactive isotopes. Allard et al. (1995, 2000, 2011) estimated an even higher ‘excess’ degassing factor of between 5 and 10, by directly normalising the time averaged SO_2 flux to the initial sulphur content ($\sim 0.1 \text{ wt}\%$) of Merapi andesitic magma, as determined by analysing melt inclusions trapped in pyroxene crystals, and by comparing with the magma extrusion rate over the past century (Siwawidjono et al. 1995) and recent decades (Allard and Tazieff 1979; Voight et al. 2000). These different estimates therefore suggest that, on a time-averaged basis, differential gas transfer across the shallow feeding system strongly determines the volatile budget of Merapi.

Further insight into the degassing of magma residing in the shallow plumbing system of Merapi was obtained via petrological methods. By investigating the chemical and physical properties of microlites of plagioclase and alkali feldspar in lava dome products and 1994 air fall tephra, Hammer et al. (2000) showed that the crystallisation of microlites was controlled by syn-eruptive water degassing and that the microlite compositions—either plagioclase or alkali feldspar—depend on the water saturation depth of the magma. While plagioclase prevalently formed during decompression crystallisation and degassing of dome-forming lava, its replacement by alkali feldspar was favoured by an increased liquidus temperature of the magma in case of extensive pre-eruptive water degassing at depth. Thus, the lack of alkali feldspar in material from the 1994 explosive eruption implied no pre-eruptive magma degassing.

A decade later, petro-geochemical investigations provided geobarometric information on deeper roots of the magma feeding system of Merapi. By studying the volatile (H_2O – CO_2 – S – Cl – F) content of crystal melt inclusions in

explosive scoria and dome samples, Nadeau et al. (2013b) inferred melt entrapment conditions as deep as 19–26 km and found that the proportions of dissolved volatiles in the melt inclusions were quite similar to the composition of volcanic gases collected during quiescent degassing in 2004 and immediately after the 2006 eruption. They thus suggested that, during explosive eruptions at least, Merapi magma could rise from great depth and fast enough to degas in approximate closed system conditions. Preece et al. (2014) further studied both melt inclusions and clinopyroxene (Cpx) hosts from the 2006 and the 2010 eruptive products, analysing H₂O–CO₂–Li–B–Be with SIMS and Cl–S–F with EMP. Geobarometry suggested that Cpx crystals had last equilibrated at depths of up to 20 km, the greatest depths being inferred for the 2010 pumice. By contrast, their melt inclusions had re-equilibrated at variable depths of ~10 to 0.6 km in the plumbing system. Some melt inclusions that were enriched in Li (<68 ppm) and B (<84 ppm) suggested the presence of a high-salinity (Cl-rich) brine in the upper crust beneath Merapi, in line with the conclusions reached by Nadeau et al. (2013b, 2016). Later, Erdmann et al. (2016) conducted phase equilibrium experiments on samples representing resident and recharge magmas from the 2010 eruption to quantify the pressure, temperature and water conditions of these magmas and the H₂O/CO₂ ratio of the related volatile phase. They calculated that the magma residing beneath Merapi prior to the eruption was emplaced at 4.5–9 km depth (100–200 MPa), had a temperature of 925–950 °C and contained 3–4 wt% H₂O; its equilibrium gas phase had H₂O/H₂O + CO₂ = 0.5–0.6. By contrast, the recharge magma that triggered the eruption was hotter (950–1000 °C) and richer in water (4–5 wt%), with H₂O/H₂O + CO₂ = 0.8 in its volatile phase. These information on the 2010 eruptive crisis obtained from petro-geochemical studies and laboratory experiments agree well with those derived from contemporaneous geophysical signals such as volcano-tectonic earthquakes (VT), long period (LP) and very long period (VLP) seismic events (Jousset et al. 2013).

11.5 Merapi Hydrothermal System

Hydrothermal systems are common features of active volcanoes such as Merapi. As already mentioned, evidence exists that magmatic gases emanating from Merapi can interact with meteoric groundwater or a hydrothermal system present in the volcanic pile or below. For example, a continuous survey of Woro fumarole temperatures in 2000–2001 showed variations from 200 to 500 °C that correlate with rainfall and seismic activity (Richter et al., 2004) and thus reflect the interactions or mixing between rising magmatic fluids and meteoric groundwater. Furthermore, a statistical correlation was established between high-frequency seismic clusters, ultra-long period (ULP) seismic signals and fumarole temperature: on 54 occasions a temperature rise of about 5 °C was found to occur a few minutes after ULP signals and simultaneously with high-frequency seismic clusters which were attributed to magma degassing. The existence of a salty brine in Merapi's hydrothermal system was advocated by Nadeau et al. (2013b). Based on a higher CO₂/Cl ratio in the volcanic gases than in crystal melt inclusions, they suggested that the magmatic volatile phase was exsolved from the magma as a supercritical fluid and subsequently separated into a high-salinity brine ponding at depth, and a lower-salinity vapor released as fumarolic emissions at the summit. Alternative explanations for the greater relative abundance of CO₂ in fumarolic gases than in melt inclusions include the pre-entrapment loss of poorly soluble CO₂ from the melt (inclusions) or a gaseous CO₂ addition due to magma-limestone interaction in the crustal basement. Vapor-brine separation would however remain the simplest mechanism to explain the higher CO₂/Cl ratio in volcanic gases than in melt inclusions.

A study of soil CO₂ degassing was conducted on Merapi during 2 inter-eruptive periods in 2002 and 2007 (Toutain et al. 2009). The research revealed high CO₂ soil concentrations, with the same δ¹³C signature as the fumarolic gases, along the concentric, hydrothermally altered rims of former crater structures in the

summit area, and low concentrations elsewhere and at the base of the volcano. Sub-surface soil permeability thus appeared to exert a main control on the transfer of heat and magma-derived gas across the summit part of Merapi: gas flow occurs preferentially through the fractures and former crater rim structures that intersect the massive and sealed lava dome blocks constituting the summit of the volcano. The total flux of diffuse soil CO₂ was estimated at 200–230 tons/day, i.e. of the same order as the volcanic plume CO₂ output during quiescent periods. More recently, a combination of electrical resistivity tomography, self-potential and CO₂-flux mapping was applied to image the shallow hydrothermal system of Merapi (Byrdina et al. 2017). Hydrothermal activity was delineated from the summit (2930 m asl) down the south slope of the volcano. Diffuse CO₂ flux at the summit in 2013 was found to be only 20 tons/day, ten times less than in 2007 (Toutain et al. 2009), likely reflecting the post-2010 rest in volcanic activity and the associated drop in volatile supply from depth (Allard et al. 2017). Such rare periods of reduced activity at Merapi are thus characterised by lower soil temperatures, lower CO₂ flux and a likely enhanced influx of meteoric groundwater into the hydrothermal system.

11.6 Magma-Limestone Interaction and CO₂ Degassing

At Merapi, interaction of magma with limestone in the crustal basement (see Deegan et al. 2023, Chap. 10) was first hypothesised by Brouwer (1928, 1945), based on the presence of trachyte, phonolite and vesicular calc-silicate skarn inclusions in the erupted lavas. Subsequently, such a process was further advocated by Allard (1980) from the δ¹³C signature of the volcanic gases and by Clocchiatti et al. (1982) following a detailed study of Merapi's calc-silicate xenoliths. Geochemical evidence of such an interaction was provided by Chadwick et al. (2007) who reported a negative correlation between Ca and Fe–Mg in plagioclase crystals having higher ⁸⁷Sr/⁸⁶Sr ratios

(0.70568–0.70627) than local basaltic rocks (<0.70574). Abundant calc-silicate skarn inclusions were found to have ⁸⁷Sr/⁸⁶Sr ratios ranging from 0.70584–0.70786, suggesting that limestone was partly assimilated by the magma, generating zones of endo- and exoskarns and liberating CO₂ (Whitley et al. 2019, 2020).

Decarbonation experiments were subsequently conducted by heating and pressurising limestone and Merapi's basaltic andesite in a reaction vessel (Deegan et al. 2010, 2023, Chap. 10; Blythe et al. 2015). The results showed rapid decarbonation, degassing and vesiculation of the original limestone, as well as physical mingling and chemical mixing of the two materials. The resulting melt was enriched in Ca and in ⁸⁷Sr/⁸⁶Sr, supporting the idea that the vesiculated calc-silicate xenoliths were the result of magma-limestone interactions.

Magma-limestone interaction was further advocated by Troll et al. (2012, 2013a) to explain the anomalously high δ¹³C of –2.4‰ in volcanic CO₂ (compared to a background average value of –4.1 ± 0.3‰ in 1994–2005) that they measured soon after the moderately explosive 2006 eruption, itself preceded by the 2006 M6.4 Yogyakarta earthquake. This interaction was also supported by higher δ¹⁸O in feldspar from the 1994, 1998, 2006 and 2010 eruptions (Troll et al. 2013b), further suggesting that explosive activity could be enhanced by the magmatic assimilation of limestone and CO₂ production that would over-pressurise the shallow plumbing system (cf. Handley et al. 2018). This interpretative model however remained a matter of debate, as the monotonous composition of Merapi lavas, including the 2006 and 2010 ones, restricts the possible extent of pure limestone assimilation prior to eruptions (e.g. Costa et al. 2013), whereas Borisova et al. (2013) documented that the radiogenic isotope record of the 2010 eruption would possibly indicate rather pervasive limestone assimilation. The average δ¹³C of the volcanic CO₂ and its broad steadiness over time, combined with the measured ³He/⁴He (6.6 R_a) and CO₂/³He ratios, led Allard (2013) to argue that magma-limestone interaction in the crust beneath Merapi was of second-order influence,

on average, compared to the deeper mixed contribution of mantle-derived and subducted sedimentary carbon and other volatiles, but Troll et al. (2013b) argued that considerable crustal volatile additions are required to lower the helium isotope values from the regional volcanic average of ca 8 R_a (see Halldórsson et al. 2013 and references therein, and discussion in Deegan et al. 2023, Chap. 10). More recently, $\delta^{13}\text{C}$ values as low as -29.3‰ were measured in situ in calcite from calc-silicate xenoliths, providing further evidence for magma-carbonate rock interaction, decarbonisation reactions, and the generation of carbonate melt beneath Merapi (Whitley et al. 2019). Xenoliths of endo- and exoskarn in Merapi lavas were taken to show that such decarbonisation reactions could affect eruption intensities, and the discovery of cubanite (CuFe_2S_3) in skarn xenoliths suggest that the skarnification process may be related with skarn-type mineralization beneath the volcano (Whitley et al. 2020).

11.7 Volcanic Gas Composition and Eruptive Activity

11.7.1 Pre-eruptive Gas Changes and Eruption Style

The extensive data set collected and analysed by CVGHM over the 1999–2010 period (Humaida et al. 2017) permits detailed examination of the relations between volcanic gas composition and eruptive events at Merapi. Here, the composition of volcanic gases from Woro are shown for the 1999–2010 average and for the 2001, 2006, and 2010 eruption (Fig. 11.3; Table 11.2) and in terms of $\text{CO}_2/\text{H}_2\text{O}$, $\text{S}_{\text{tot}}/\text{H}_2\text{O}$, $\text{HCl}/\text{H}_2\text{O}$ and $\text{H}_2/\text{H}_2\text{O}$ ratios over the 1999–2010 period (Fig. 11.5). The 2001 eruption, which lasted from January to March and peaked on 10 Feb. 2001, was purely effusive; it consisted of dome extrusion and block-and-ash flows resulting from the gravitational collapse of the dome, typical of the standard activity of Merapi (Global Volcanism Program 2001). The 2006 eruption, which lasted from April to July and peaked on 14 June

2006, displayed features similar to the 2001 eruption but also a few St-Vincent-type explosions and related pyroclastic flows, with an eruptive plume reaching up to 9 km in height (Global Volcanism Program 2007; Ratdomopurbo et al. 2013). The 2010 eruption was the most powerful explosive (VEI-4) eruption since 1872, with a column reaching over 18 km in height (Global Volcanism Program 2011; Surono et al. 2012; Preece et al. 2016). In addition to lava and pumiceous clasts, it generated column-collapse pyroclastic flow and ash fall deposits.

Prior to these three events, Woro volcanic gases varied proportionally to the differences in eruption style and magnitude. Before the 2001 eruption, Woro volcanic gases were slightly richer in H_2O and poorer in $\text{CO}_2\text{--S}_{\text{tot}}\text{--HCl}$ compared to their average composition over the whole 1999–2010 period (Fig. 11.5). By contrast, before the 2006 and 2010 eruptions, and most especially in October 2010 (Fig. 11.6), they became significantly to strongly enriched in both CO_2 and S_{tot} relative to H_2O and HCl . From August to October 2010 (Fig. 11.6), the $\text{CO}_2/\text{H}_2\text{O}$ ratio increased from 0.1–0.2 to 0.6–2.7; CO_2/HCl increased from 20.8–31.0 to 52.2–115.7; and $\text{CO}_2/\text{S}_{\text{tot}}$ increased from 6.0–11.0 to 8.6–12.3. In greater detail as regards sulphur, the CO_2/SO_2 ratio markedly increased from 9.4–19.0 to 24.1–115.6, whereas the $\text{CO}_2/\text{H}_2\text{S}$ ratio gradually decreased from 16.6–26.4 to 13.4–13.9. All such changes point to the increasing contribution of a CO_2 -rich gas phase derived from deeper magma prior to the major 2010 explosive eruption. By contrast, such a deep contribution was more modest before the 2006 eruption and was lacking before the 2001 eruption. This comparison thus shows that the explosivity of a given eruption at Merapi is well reflected in the chemical composition of the pre-eruptive volcanic gases and, especially, their CO_2 content, though other factors may influence eruption style and effusive-explosive transitions (e.g. Preece et al. 2016; Carr et al. 2020).

As verified on many other volcanoes (e.g. Allard et al. 2005; Aiuppa et al. 2007, 2017a, b; Aiuppa 2015), increasing $\text{CO}_2/\text{H}_2\text{O}$, $\text{CO}_2/\text{S}_{\text{tot}}$ and CO_2/HCl ratios in volcanic gases prior to or

Table 11.2 Gas composition of Woro fumaroles

| Woro | 1999–2010 | Dec. 2000 | Jan. 2006 | Oct. 2010 |
|---------------------|-----------|-----------|-----------|-----------|
| H ₂ O | 82.5 | 79.2 | 51.0 | 23.3 |
| CO ₂ | 10.3 | 4.8 | 16.1 | 62.6 |
| N ₂ | 4.0 | 1.5 | 29.7 | 3.0 |
| NH ₃ | 0.92 | b/l | 0.04 | 2.64 |
| SO ₂ | 0.80 | b/l | b/l | 2.60 |
| H ₂ S | 0.66 | 0.70 | b/l | 4.67 |
| HCl | 0.69 | 2.89 | 1.90 | 0.54 |
| H ₂ | 0.249 | 0.620 | 0.010 | b/l |
| O ₂ + Ar | 0.27 | 0.31 | 1.18 | 0.43 |
| CO | 0.02 | b/l | b/l | 0.19 |
| CH ₄ | 0.08 | b/l | 0.10 | 0.03 |

Data were collected and analysed by the Indonesian Center of Volcanology and Geological Hazard Mitigation (CVGHM) and compiled by Humaida et al. (2017)

Compositions are provided as an average for the whole 1999–2010 period and, specifically, for the 2001, 2006, and 2010 eruptions. All results are in mol%; b/l = below limit of detection. See also Fig. 11.3

during an eruption constitute the most straightforward index of the rise of deeply derived magmatic gas because CO₂ usually degasses much earlier than H₂O, S and Cl from silicate melts at high pressure (e.g. Holloway and Blank 1994). The higher temperature of deeper magma also favors water disproportionation into H₂ and O₂, both of which in turn react with S to produce SO₂ and H₂S (Delmelle and Stix 2000). Note that before the 2010 eruption, CVGHM measured an increase of the SO₂/H₂S ratio from September 2009 to April 2010 (maximum of 22.9), then a decrease of this ratio to 0.1 in October 2010.

11.7.2 Dome Growth and Gas Composition

During the 2001 and 2006 eruptions, the volume of the lava dome was estimated daily by CVGHM staff and volumetric changes were converted into growth rates (Fig. 11.5). Similar calculations could not be realised during the 2010 eruption for safety reasons. The 2001 eruption had an average dome growth rate of about 50,000 m³/day (maximum: 70,000 m³/day), while the 2006 eruption displayed a twice higher average dome growth rate (100,000 m³/day, with a maximum of 170,000 m³/day).

The higher extrusion rate in 2006 than in 2001 correlates with differences in volcanic gas composition, in particular with a higher CO₂/H₂O ratio in 2006 (0.15–0.53) than in 2001 (0.04–0.06). As expected, HCl/H₂O, HCl/CO₂, and HCl/S_{tot} ratios display a reversed trend. Hydrochloric acid, the prevalent halogen compound in volcanic gases, generally outgasses at low pressure from magmas (Webster and Mandeville 2007). Over the 1999–2010 decade, the molar amount of HCl in Woro gases averaged about 0.68%. In comparison, HCl in Woro gases (Fig. 11.3) and the HCl/H₂O (Figs. 11.5, 11.6), HCl/CO₂, and HCl/S_{tot} (Fig. 11.7) ratios increased prior to the 2001 eruption, to a slighter extent before the 2006 eruption, and lowered before the 2010 event. Thus, there exists a reverse relationship between the relative HCl concentration in Woro volcanic gases and the eruption intensity. This opposite behaviour of HCl with respect to both CO₂ and S_{tot} in terms of gas precursors at Merapi agrees with data for the solubility of Cl in different melts (Carroll and Webster 1994; Webster et al. 1999; Signorelli and Carroll 2000; Carroll 2005; Alletti et al. 2007). In particular, the fluid/melt partitioning coefficient of Cl increases at low pressures and low temperatures, i.e. during conditions typical for quiet lava effusions, and decreases under the

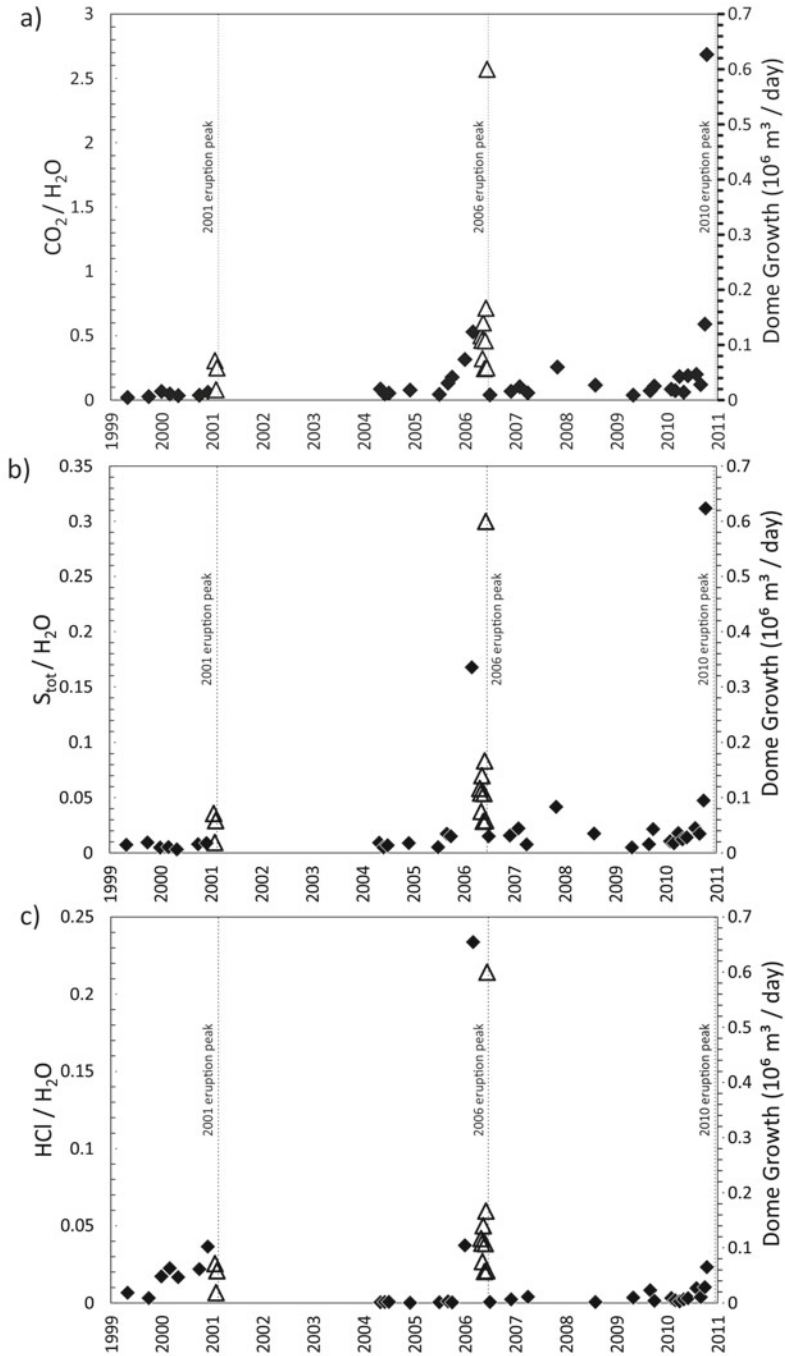
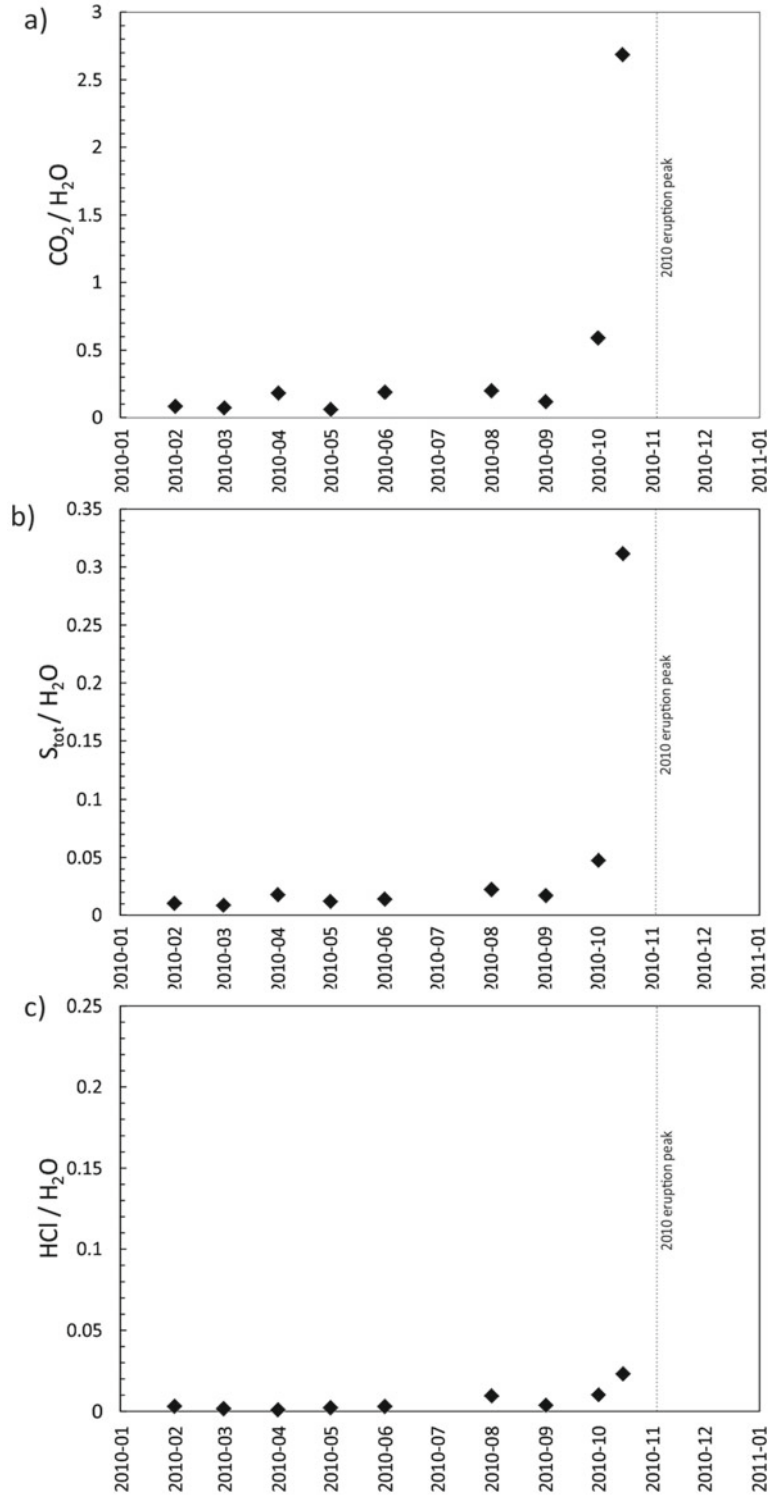


Fig. 11.5 Water-normalised concentration of CO_2 , S_{tot} , and HCl in volcanic gases from the Woro field from 1999 to 2011 (black diamonds). The values are compared to the rate of dome growth for the 2001 and the 2006 eruptions on the right-hand side vertical scale (white triangles). Data from Humaida et al. (2017)

Fig. 11.6 Water-normalised concentration of **a** CO₂, **b** S_{tot}, and **c** HCl in volcanic gases from the Woro field prior to the 2010 eruption. The 2010 eruption climax is identified. Data from Humaida et al. (2017)



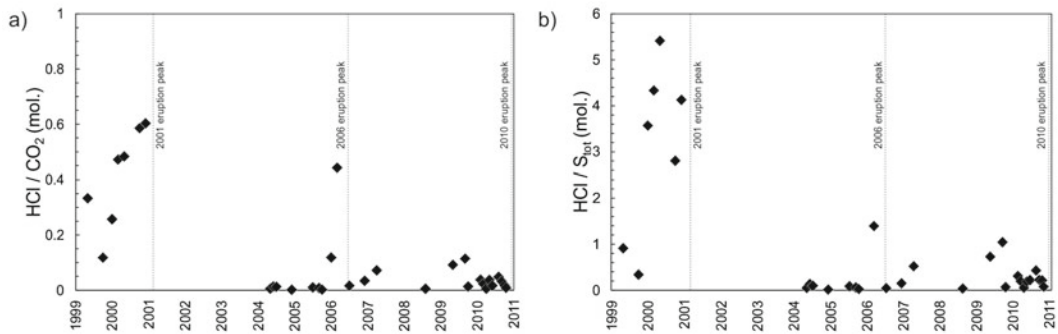


Fig. 11.7 a HCl/CO₂ and b HCl/S_{tot} ratios in Woro volcanic gases from 1999 to 2011. The 2001, 2006 and 2010 eruptions are identified. Data from Humaida et al. (2017)

higher pressure conditions controlling explosive eruptions. High HCl/H₂O, HCl/CO₂, and HCl/S_{tot} ratios in volcanic gases before an eruption at Merapi can thus be considered a reassuring indication of a low-to-moderate explosivity of the forthcoming event.

11.7.3 Volcanic Activity and Trace Metals in Gases

In 1991, tube-sampled sublimates and fumarole encrustations were collected on Merapi when blue-coloured molybdenum-rich encrustations (“Mo-blue”) were observed to cover 300 m² of fumarolic areas. These encrustations consisted of Mo oxides/hydroxides deposited on substrates of cristobalite-alunogen-anhydrite (Kavalieris 1994). The mixture contained 3 wt% Mo but also hosted 1.64 wt% Pb as PbSO₄ (anglesite), thousands of ppm As–Zn–W–Bi–Tl–Cs, hundreds of ppm Cd–Ti–Sn–Rb, and tens of ppm Sb–In–Au–Ag–Te. The presence of Mo-blue on Merapi was correlated with shallow seismicity, increased SO₂ flux and increased fumarole temperatures. Red and green-coloured encrustations consisted of Pb–Na–K–Al sulphates formed at less than 400 °C. In 2004, during quiescent degassing, encrustations collected by O. Nadeau and A. E. Williams-Jones at the Gendol field also hosted both Mo-blue and deep green sublimates which, using X-ray diffraction, were identified as ilsemanite (Mo₃O₈·nH₂O) and shcherbinaite (V₂O₅), respectively (Fig. 11.8).

Volcanic gases collected soon after the 2006 eruption were found to display Fe/Cu, Ni/Cu and Co/Cu ratios similar to those measured in sulphide melt inclusions of mafic scoria, i.e. in typical recharge magma (Nadeau et al. 2010). By contrast, gas samples from quiescent degassing in 2004 displayed different ratios between chalcophile elements. It was thus proposed that recharge mafic magmas that are injected into the shallower feeding system of Merapi and trigger explosive eruptions are sulphide-saturated, so that their magmatic volatile phase is able to extract and dissolve the metal-rich sulphide melt. Based on the study of Cu–Zn–Pb in melt inclusions and thermodynamic modelling, more work by the same group further suggested that this mafic volatile phase subsequently percolated through- and partitioned its Cu–Zn–Pb into the resident magma (Nadeau et al. 2013a). Based on condensates and tube sublimates collected at the Woro field in 2004 and 2006 and on the compilation of global volcanic gas compositions and fluid inclusions from world-class porphyry Cu (Au–Mo) deposits, Nadeau et al. (2016) concluded that mafic magma recharges of the shallow magmatic-hydrothermal system of Merapi may trigger fracturing of the overlying rock column, lithostatic-to-hydrostatic pressure transitions, flash boiling and adiabatic cooling of the supercritical volatile phase, and finally chalcophile/siderophile metal mineralization. It was shown that Merapi volcanic gases are indeed enriched in S–Cl–Pb–Cu–Zn during and after

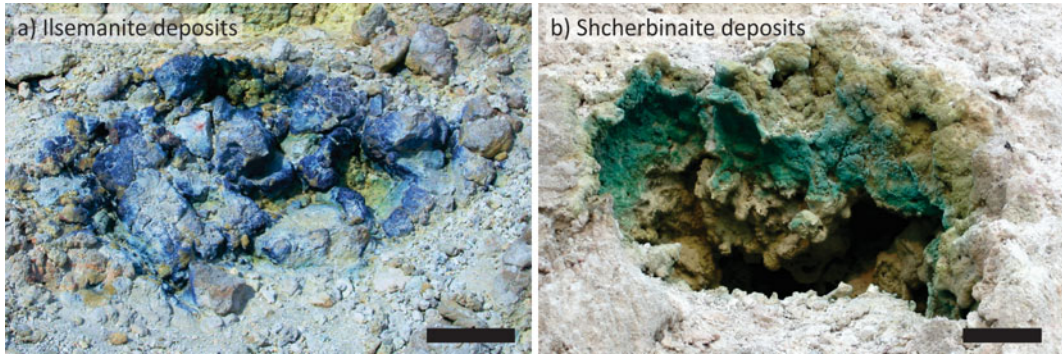


Fig. 11.8 Extinct fumaroles from the Gendol field at Merapi during a phase of quiescent degassing in 2004. **a** “Mo-blue”, or ilsemanite ($\text{Mo}_3\text{O}_8 \cdot n\text{H}_2\text{O}$), is found as encrustations around fumaroles upon temperature rises

but disappears after rainy seasons. **b** Green shcherbinaite (V_2O_5) is also found around fumaroles at Merapi. Scale bars are approximately 10 cm

explosive eruptions but become enriched in Mo–REE–Au–U, as well as in large ion lithophile (LILE) and high field strength (HFSE) elements, during the subsequent periods of quiescent degassing and magmatic differentiation (Fig. 11.9).

More broadly, the importance of deep mafic injections into the shallow resident magma reservoir of Merapi upon its eruptive behaviour was highlighted in a detailed chemical and radiocarbon study of lavas erupted over the past 2000 years (Gertisser and Keller 2003b). It was shown that periods of high eruptive activity, lasting several hundred years, were triggered and sustained by the supply of deep mafic magma to the plumbing system. These phases of high eruptive activity alternated with periods of lower activity, lasting about 150 years on average, during which the emplaced magma is evolving towards more felsic compositions. At a much shorter timescale, the analysis of mafic and felsic melt inclusions from undated scoria and lava, on the one hand, and of volcanic gases collected in 2004 and 2006 on the other hand, showed that the two magmas did not mix efficiently but that the volatile phase derived from the mafic magma transferred mobile elements, such as S and Cu, to the felsic magma (Nadeau et al. 2013a, b).

11.8 Volatiles at the Roots of the System

Compared to the previous low- and medium-K rock series at Merapi, the more recent high-K series is enriched in light rare earth elements (LREE) and LILE over heavy rare earth elements (HREE) and HFSE (Gertisser and Keller 2003a; Gertisser et al. 2023, Chap. 6). This, the higher $^{87}\text{Sr}/^{86}\text{Sr}$, $^{206}\text{Pb}/^{204}\text{Pb}$, $^{207}\text{Pb}/^{204}\text{Pb}$ and $^{208}\text{Pb}/^{204}\text{Pb}$ ratios, the lower $^{143}\text{Nd}/^{144}\text{Nd}$ and the lack of change in $\delta^{18}\text{O}$ in these rocks, led the authors to conclude that the increased K content of Merapi lavas tracked a higher contribution of subducted continental sediments to the mantle wedge of the Sunda arc, rather than the assimilation of crustal material upon magma ascent. As also inferred from by H–C–S–N isotopic data for Merapi volcanic gases (Allard 1983, 1986, 2013), hydrated and carbonated sediments subducted beneath Java thus represent a deep source of volatiles for the magmatic-hydrothermal system and gas emissions of the volcano.

Petrography and geobarometry studies conducted on the basaltic-andesite and co-magmatic enclaves, as well as on gabbroic/dioritic enclaves and amphibole megacrysts, both revealed textural

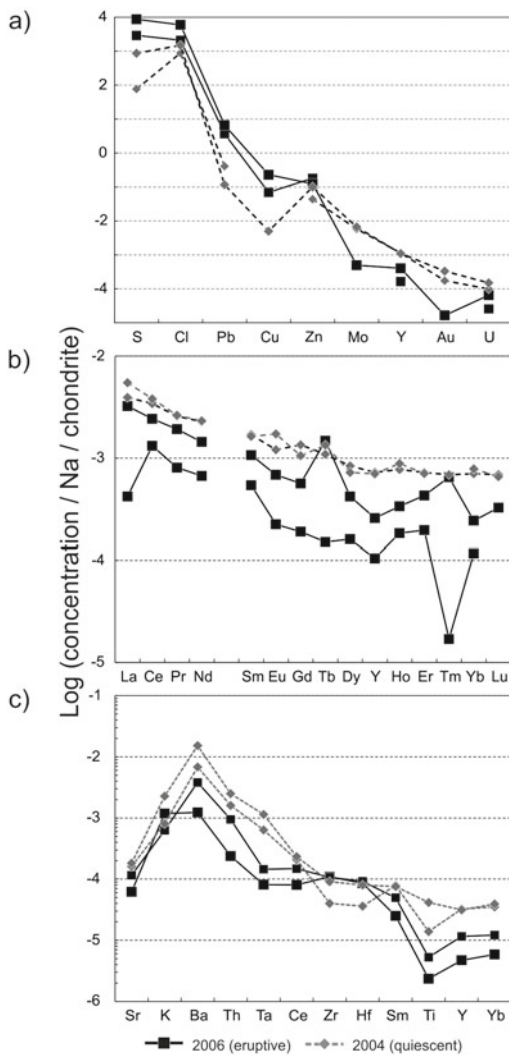


Fig. 11.9 Sodium- and chondrite-doubly-normalised trace element plots for Merapi volcanic gas condensates. **a** Metals and ligands with economic interest. **b** Rare earth elements. **c** Large ion lithophile and high field strength elements. All samples were collected from the Woro fumarolic field during quiescent degassing in 2004 and immediately after the eruption in 2006 (Nadeau et al. 2016)

relationships suggestive of mingling and mixing of distinct magmas and witnessed magma reaction with the surrounding wall rock (Chadwick et al. 2013; Troll et al. 2013b; Troll and Deegan 2023, Chap. 8). Combined with the results of geobarometry, these data indicate the existence of a multi-chamber magmatic system extending throughout the 25 km thick arc crust down to the

mantle beneath Merapi, in agreement with seismic imaging (Koulakov et al. 2016). This multi-chamber feeding system is affected by mafic recharge, magma mixing, fractional crystallisation, crystal accumulation and probably differential gas transfer, even though it remains uncertain whether a free volatile phase already exists at mantle and deep crustal magma ponding levels.

A 3D seismic velocity structural imaging of the subduction zone beneath Central Java showed the subducted slab dipping to the north, from nearly horizontally over the 0–150 km depth and at 70° at >250 km (Luehr et al. 2013, 2023, Chap. 5). Merapi, Sumbing and Lawu volcanoes are located at the edge of a south-dipping, low-velocity anomaly extending at 45° from the volcanic areas down to the subducted slab at 100 km. This anomaly was interpreted to result from the presence of 13–25% of fluids originating from the dehydration of the slab or from melts created by the presence of fluids. A 3D model of S-wave velocity was developed for the upper crust based on the analysis of seismic ambient noise data recorded by 100+ stations in 2004 (Koulakov et al. 2016). The low-velocity anomaly of Luehr et al. (2013) could be observed south of Merapi in the deeper crust and was interpreted as a volatile/melt pathway connecting the subducting slab to the volcanic system (see Luehr et al. 2023, Chap. 5). Therefore, even though the resolution of seismic imaging does not permit an accurate delineation of the Merapi feeding system, convergent lines of evidence suggest that a free volatile phase is present in the deep roots of the system.

11.9 Synthetic Models

Two synthetic models were derived from the reviewed literature for the magmatic-hydrothermal control of Merapi's degassing and eruptive activity (Fig. 11.10). A first model for the subduction zone was adapted mainly from Koulakov et al. (2016) (Fig. 11.10a). In this model the ultimate source of Merapi volcanic gases reside in the mantle and in subducted sediments (Gertisser and Keller 2003a; Allard 1986,

2013; Allard et al. 2011), as fluid release from the subducted slab drives metasomatism and partial melting of the mantle. Based on the findings of numerous authors (e.g. Chadwick et al. 2013; Costa et al. 2013; Jousset et al. 2013; Nadeau et al. 2013b; Preece et al. 2014; Deegan et al. 2021; Troll and Deegan 2023, Chap. 8), a multi-level magma plumbing system in the arc crust connects Merapi to the underlying mantle wedge. Volatiles are transferred from deep mafic magmas to shallower more felsic magmas, without necessary magma mixing, and the resident shallow magma is fluxed by a CO₂-H₂O-rich deep volatile phase derived from mafic magma (e.g. Blundy et al. 2010; Vigouroux et al. 2008; Hall-dórsson et al. 2013; Nadeau et al. 2013a).

The second model illustrates the cyclic nature of hydrothermal and eruptive activity at Merapi (Fig. 11.10b, c). During phases of low eruptive activity and quiescent degassing, the magma evolves predominantly through fractional crystallisation (e.g. Gertisser and Keller, 2003b) and volatiles are exsolved through second boiling. The gases are dominated by H₂O of magmatic origin (e.g. Allard 1986; Humaida et al. 2017) and CO₂ from magmatic and sedimentary sources (e.g. Allard 1980, 2013; Chadwick et al. 2007; Deegan et al. 2010; Troll et al. 2012; Carr et al. 2020). The injection of deeper derived, CO₂ and S-rich mafic magma is able to promote explosive eruptions (e.g. Surono et al. 2012; Subandriyo et al. 2023, Chap. 12) before which volcanic gases at the surface become greatly enriched in both CO₂ and S_{tot} (Surono et al. 2012; Humaida

et al. 2017). As the shallow plumbing system is replenished with volatile-rich mafic magma, pressure increases, the magmatic-hydrothermal system opens and depressurises down to a hydrostatic regime (Nadeau et al. 2016).

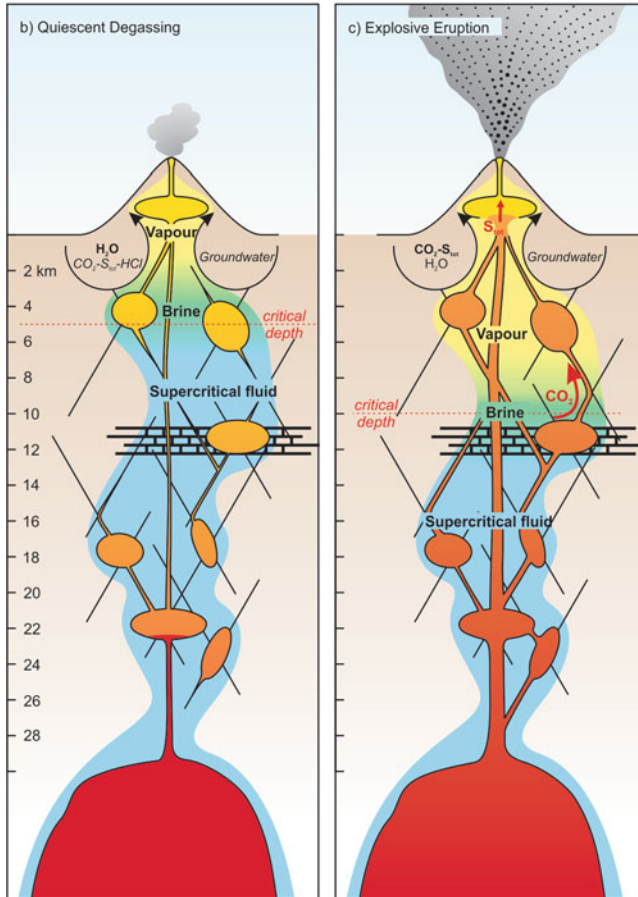
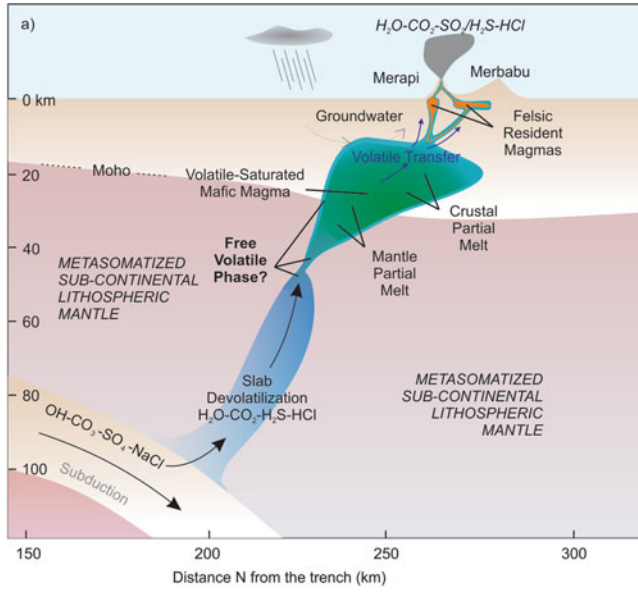
11.10 Regional Seismicity, Volcanism and Degassing

The temporal/causal links between the activity of Merapi and regional tectonics deserve a wide interest. In 2001, Woro fumarole temperatures were noticed to increase from 435 to 460 °C just after an M6.3 earthquake located about 50 km south of the volcano and at 130 km depth (Richter et al. 2004). In 2006, while a new volcanic crisis had already begun, another M6.4 earthquake occurred 50 km south of Merapi, but this time at less than 30 km depth. In the next 3 weeks, the eruptive activity, the magma extrusion rate and associated pyroclastic flows were increasing by a factor of 2 (Walter et al. 2007). This inspired Walter et al. (2007) to develop a theoretical model of stress transfer between earthquakes and the volcano, which suggested that seismic activity induced by dynamic (not static) stress changes could affect the eruptive behavior of the volcano.

During the 20th and the beginning of the twenty-first century, Merapi experienced long periods of slow magma extrusion rate (<0.1 m³/s) interrupted every few years by weeks- to months-long episodes of high magma extrusion rates (1–

Fig. 11.10 a Subduction zone model for the tectonic setting of Merapi, adapted mainly from Koulakov et al. (2016). The ultimate source of Merapi volcanic gases is a mixture of volatiles derived from the mantle wedge and from the sediments subducted beneath Central Java (Allard 1980, 1986; Gertisser and Keller 2003a; Deegan et al. 2021). Slab dehydration drives metasomatism and partial melting of the mantle wedge. A complex magmatic-hydrothermal plumbing system extends throughout the whole arc crust beneath Merapi (e.g. Chadwick et al. 2013; Costa et al. 2013; Jousset et al. 2013; Preece et al. 2014; Troll and Deegan 2023, Chap. 8). Volatiles are transferred from deep mafic magmas to shallower, more felsic magmas, without necessary mixing of these endmembers (Nadeau et al. 2013a). Two shallow reservoirs exist under Merapi, one of which may be feeding other nearby volcanoes (Koulakov et al. 2016). **b-c** Schematic representation of the cyclic nature of eruptive activity at Merapi,

adapted mainly from Nadeau et al. (2016). Javanese limestone is present in the mid- and upper crust (Brouwer 1928; Chadwick et al. 2007; Troll et al. 2012; Carr et al. 2018, 2020). During phases of low eruptive activity and quiescent degassing (**b**), magma evolves predominantly through fractional crystallisation (Gertisser and Keller 2003b) and volatiles are exsolved through second boiling. The gases are dominated by H₂O of magmatic origin (Humaida et al. 2017) and CO₂ from magmatic and sedimentary sources (Allard 1986). Explosive eruptions (**c**) are triggered by the injection of CO₂-S-rich mafic magma (e.g. Surono et al. 2012). If magma reacts with limestone (e.g. Chadwick et al. 2007, 2013; Deegan et al. 2010; Troll et al. 2012; Whitley et al. 2019, 2020), CO₂ is generated, internal pressure increases and opens the system, causing a pressure transition from a lithostatic to a hydrostatic regime (Nadeau et al. 2016). Volcanic gases are enriched in both CO₂ and S_{tot}



4 m³/s). In a study by Carr et al. (2018), the May–July 2006 eruption was taken to represent an episode of high extrusion rate and was studied by constructing a numerical model of magma ascent in a volcanic conduit. The model was intended to verify previous alternatives that the 2006 eruption resulted from either a change in dynamic stress following the M6.4 local earthquake (e.g. Walter et al. 2007) or from magma–limestone interaction and CO₂ pressurization of the magmatic system (e.g. Troll et al. 2013b; Carr et al. 2020). Calculations showed that a pressure rise of 5–7 MPa was needed to twice increase the magma extrusion rate and that such a pressure rise could have resulted by fluxing and dehydrating the melt with about 0.1 wt% CO₂. The delay of 3 days between the 2006 earthquake and the increase in magma extrusion rate was explained by the time taken to produce CO₂ by interaction with magma (1–2 days) and that taken by the magma to ascend from the storage zone to the surface (40 h). The reconciliation of these results and concepts shows how external (earthquake, regional stress changes, magma–limestone interaction) and internal (devolatilisation, overpressure) processes can interplay and produce complex feedback loops. With regards to the 2010 explosive eruption, TerraSAR-X satellite radar data was used to observe the lava dome resurging just after the cataclysmic eruption. A 200 m × 40 m wide fracture that opened in this dome during a discrete explosion on 18 Nov. 2013 was identified as aligned along a NNW–SSE structural direction controlling Merapi and close to the N–W direction of regional tectonic structures. Walter et al. (2015) thus proposed that this fracturing and the related explosion might be related to a larger volcano-tectonic system.

11.11 Volatiles and Triggering Mechanism of the 2010 Eruption

Together with CVGHM scientists, collaborating researchers from Indonesia, France, USA, Italy, Singapore and Norway contributed to document

and interpret the geophysical and geochemical precursors of the October–November 2010 eruption (e.g. Surono et al. 2012; Subandriyo et al. 2023, Chap. 12). Prior to the eruption, volcanic gases were collected at the Woro field on 26 May 2010, in September 2010 and, ultimately, on 20 October 2010 (less than one week before the first violent explosion on 26 October 2010). The gas temperature rose from 460 °C in May to 575 °C in October and this change was accompanied by the already described enrichments of CO₂, SO₂ and H₂S in the volcanic emissions. It is noteworthy that the relative molar content of CO₂ increased by a factor 6 between mid-September (10%) and 20 October 2010 (63%). As previously argued, such a remarkable change is consistent with early, separate gas transfer from deeply derived uprising volatile-rich magma, although CO₂ production through magma–limestone interaction may have contributed. Given the evidence of magma mixing in the 2010 eruptive products, it has become clear that CO₂-rich mafic magma was being injected upward into the more evolved resident magma and that this, along with possible magma–limestone interaction, caused the violent eruption (e.g. Surono et al. 2012; Borisova et al. 2013; Subandriyo et al. 2023, Chap. 12). The cumulative release of 0.44 Mt of SO₂ throughout the whole eruption, measured by satellite remote sensing, implies a degassed dense magma volume of ~0.12 km³, at least 3–5 times larger than the amount of magma erupted (Surono et al. 2012). Such a discrepancy, commonly observed for other major explosive eruptions (e.g. Westrich and Gerlach 1992), strongly suggests that a free CO₂- and S-rich volatile phase coexisted with the uprising magma prior to the onset of the eruption, indicating that this magma was already volatile-saturated at depth in the plumbing system.

Costa et al. (2013) compared the pre-eruptive conditions of the 2006 and 2010 eruptions by using geochemistry and petrological relationships. Both eruptions recorded open-system magmatic processes, including mixing of shallow and deeper magmas and carbonate assimilation. The main difference in the products from the two events was the presence of reaction rims around amphibole only in 2006, implying a

slower magma ascent than in 2010 (see Preece et al. 2023, Chap. 9). Using five different geothermobarometers, Costa et al. (2013) identified 3 different crystallisation (or magma ponding) levels beneath Merapi: at 30 ± 3 km, 13 ± 2 km and at <10 km. At 30 km the magma was inferred to contain $\geq 4\text{--}6$ wt% H_2O and ≥ 0.15 wt% SO_2 at a temperature of 1050 °C. The 13 ± 2 km zone roughly stands at the base of the limestone column beneath Merapi and might be a locus for possible magma-limestone interaction. There, the magma hosted $4\text{--}6$ wt% H_2O and was inferred to supply the pre-eruptive CO_2 enrichment observed in Woro volcanic gases. At <10 km, the new magma was increasingly degassing and sustained enhanced gas release at the surface. Costa et al. (2013) concluded that the 2006 and 2010 eruptions were controlled by similar processes but that the 2010 eruption simply involved a more massive injection of deep, volatile-rich magma. This resulted in a greater CO_2 overpressure that contributed to its faster ascent rate and enhanced explosivity during the eruption. Jousset et al. (2013) and Preece et al. (2014) came to similar conclusions using different methods, but the question remains as to why in 2010 a much larger amount of magma was segregated from depths.

Genareau et al. (2015) proposed an interesting approach to characterise changing fluid pressure during the course of the 2010 eruption, based on the changes in lithium (Li) concentrations in erupted glasses and crystals (measured with secondary ion mass spectrometry). They found that Li was more concentrated in the groundmass glass of dome-collapse material from the initial (26 October 2010) explosion than in glass and plagioclase from the climatic (5 November 2010) explosions. This pattern was interpreted as reflecting a higher fluid pressure in underground magma at the onset of the eruption (26 October) than towards its end when the new magma had already reached an advanced stage of degassing. The transition from explosive to effusive activity observed during the 2010 eruption was also driven mainly by gases according to Preece et al. (2016). Their conclusion was based on a quantitative textural analysis of feldspar microlites in

the groundmass of scoria and pumice from the initial explosions, scoriaceous dome material from effusive activity, and scoria and pumice from the sub-Plinian column collapse. Again, the main triggering mechanism of the 2010 eruption appeared to be the influx of hotter or more mafic magma into a dome-plugged subvolcanic magma chamber.

11.12 Atmospheric Impacts

It is now well established that major explosive eruptions from Merapi-like arc volcanoes are capable of affecting the climate, at regional or even global scale, by injecting gaseous aerosols and ash particles into the stratosphere (e.g. Robock 2000). Sulphate aerosols formed by conversion of gaseous SO_2 and H_2S are able to backscatter part of the sunlight radiation and hence to cool down the lower atmosphere, while halogen gases such as the HCl and HF can catalyse the destruction of ozone in the stratosphere (e.g. Millard et al. 2006).

Merapi has been selected more than once in the past to represent arc volcanoes in persistent degassing, in particular on occasion of the 1990–2000 United Nations International Decade for Natural Disaster Reduction. Its gas emissions during standard activity are moderate enough to affect only its proximal environment. This has been verified for its modest average SO_2 emission rate (123 ± 57 tons/day; Humaida et al. 2017), quite typical for andesitic arc volcanoes, and for its average HCl and HF discharge of about 35 and 0.6 tons/day, respectively (Allard et al. 2000; 2011). In a few days, the VEI-4 November 2010 eruption of Merapi injected 0.44 Mt of SO_2 and likely massive co-amounts of HCl and HF at up to 18.3 km altitude in the atmosphere (Surono et al. 2012). The documented atmospheric effects of this eruption include a heating of the lower tropical stratosphere, an increase in stratospheric equator-to-pole temperature gradient, and an enhanced Arctic polar vortex (Zuev et al. 2017). This strengthening of the polar vortex in turn resulted in a strong ozone depletion event in the Arctic stratosphere.

11.13 Summary and Outlook

In this chapter, we have reviewed the main advances made in our knowledge and understanding of volcanic/magmatic degassing at Merapi in the past four decades, since the pioneering work of French gas volcanologists in the late 1970s to early 1980s. The remarkable efforts of the VSI then the Indonesian CVGHM in developing a routine survey of volcanic gas compositions and SO₂ flux at Merapi (in complement to observational and geophysical monitoring), combined with the numerous geochemical, petrological and experimental research studies conducted by international groups in collaboration with Indonesian colleagues, have permitted to document various aspects of the volcano degassing behaviour, amongst which: (1) the source(s) and supply rate of its emitted magmatic volatiles, (2) their interactions with the hydrothermal system, (3) temporal relationships between volcanic gas composition, eruptive style and petrological-textural features of the erupted solid products, (4) gas precursors of 2010-type major explosive eruptions, and (v) P–T–redox volatile constraints on the magma feeding system and magma ponding levels down to mantle depth. The behaviour of metals in gases from Merapi was reviewed as the metals are relevant to the environment and economies and are present in high concentrations in Merapi gas emissions. The role of volatile-saturated, deep mafic recharge of the shallow plumbing system was addressed, along with the potential assimilation of limestone in the basement and consequent CO₂ degassing. Large-scale geophysical measurements and subduction-scale models now allow putting Merapi and its gas emissions into the geodynamic context of the central Sunda arc; the existing links between regional seismicity, eruption behaviour and volcanic degassing were thus reviewed. The latest lessons from the 2010 centennial eruption were addressed at the end.

In combination with geophysical signals, volcanic gas monitoring at Merapi has most of the time allowed CVGHM to adequately predict

volcanic eruptions and allow timely evacuation from the volcano surroundings. Direct gas sampling having been prevented after the 2010 eruption, Merapi's volcanic plume emissions have been monitored since mid-2015 with a permanent MultiGAS station installed at the summit. Automatic survey of Merapi gas emissions at high temporal resolution will indeed be a key step ahead to detect precursory gas signals of a new magma recharge but also to minimise the risks to fieldwork operators. As a reminder, the extraordinary CO₂ signal preceding the VEI-4 eruption in early November 2010 was detected by sampling of the Woro gases just one week prior to the first explosion on 26 October. It has now become widely accepted that the triggering mechanism of this 2010 paroxysmal eruption was essentially the rapid injection of a great amount of deep, gas-rich magma into Merapi's shallow plumbing system. Important unresolved questions, however, are what mechanism promoted the upraise of this greater amount of magma and how long time ahead such a process can be predicted.

Acknowledgements The contribution of the authors listed below and the collaboration with the Indonesian Center of Volcanology and Geological Hazard Mitigation (CVGHM) were central in the production of this review and are thus deeply acknowledged. The chief editors of this special publication on Merapi volcano, namely R. Gertisser, V. R. Troll, T. Walter, I. G. M. A. Nandaka and A. Ratdomopurbo are thanked for their invitation to write this chapter. Constructive reviews by A. Aiuppa, R. Gertisser and V. R. Troll are greatly appreciated.

References

- Aiuppa A (2015) Volcanic-gas monitoring. In: Schmidt A, Fristad KE, Elkins-Tanton LT (eds) *Volcanism and global environmental change*. Cambridge University Press, pp 81–96
- Aiuppa A, Fischer TP, Plank T, Robidoux P, Di Napoli R (2017a) Along-arc, inter-arc and arc-to-arc variations in volcanic gas CO₂/S_T ratios reveal dual source of carbon in arc volcanism. *Earth Sci Rev* 168:24–47
- Aiuppa A, Moretti R, Federico C, Giudice G, Gurrieri S, Liuzzo M, Papale P, Shinohara H, Valenza M (2007) Forecasting Etna eruptions by real time evaluation of volcanic gas composition. *Geology* 35:1115–1118

- Aiuppa A, Bitetto M, Francofonte V, Velasquez G, Bucarey Parra C, Giudice G, Liuzzo M, Moretti R, Moussallam Y, Peters N, Tamburello G, Valderama OA, Curtis A (2017b) A CO₂-gas precursor to the March 2015 Villarrica volcano eruption. *Geochem Geophys Geosyst* 18:2120–2132
- Allard P (1980) Proportions of ¹³C and ¹²C isotopes of carbon emitted at high temperature by a growing andesitic dome: Merapi, Indonesia. *C R Hebd Séances Acad Sci Ser D* 291:613–616
- Allard P (1983) The origin of hydrogen, carbon, sulfur, nitrogen and rare gases in volcanic exhalations; evidence from isotope geochemistry. In: Tazieff H, Sabroux JC (eds) *Forecasting volcanic events*. Elsevier, New York, pp 337–386
- Allard P (1986) Isotope geochemistry and origins of water, carbon and sulfur in volcanic gases: rift zones, continental margins and island arcs. Ph.D. thesis, University Paris VII, France, 390 p
- Allard P (2013) Isotopic and mass balance constraints on the origin(s) of carbon dioxide emissions from Merapi volcano, central Java, Indonesia. Abstract, IAVCEI Scientific Assembly, Kagoshima, Japan, 20–24 July 2013, IP2-3J-O10
- Allard P, Tazieff H (1979) Phenomenology and thermal mapping of the principal fumarole zones of Merapi volcano, Indonesia. *C R Hebd Séances Acad Sci Ser D* 288:747–750
- Allard P, Burton M, Murè F (2005) Spectroscopic evidence for a lava fountain driven by previously accumulated magmatic gas. *Nature* 433:407–410
- Allard P, Badrudin M, Carbonnelle J, Dajlevic D, Le Guern F, Pardyento L, Rouyer JL, Sabroux JC (1984) Geochemistry of gaseous emissions from an arc volcano in permanent activity: Merapi (Indonesia). In: Abstract, CNRS-PIRPSEV meeting, Clermont-Ferrand, France, 17–19 Dec 1984, p 53
- Allard P, Carbonnelle J, Dajlevic D, Métrich N, Sabroux JC (1995) Volatile source and magma degassing budget of Merapi volcano: evidence from high-temperature gas emissions and crystal melt inclusions. In: Abstract, Merapi decade volcano international workshop, UNESCO-VSI, Yogyakarta, Indonesia, 5–9 Oct 1995
- Allard P, Carbonnelle J, Dajlevic D, Le Bronec J, Morel P, Robe MC, Maurenas JM, Faivre-Pierret R, Martin D, Sabroux JC, Zettwoog P (1991) Eruptive and diffuse emissions of CO₂ from Mount Etna. *Nature* 351:387–391
- Allard P, Métrich N, Sabroux J-C (2011) Volatile and magma supply to standard eruptive activity at Merapi volcano, Indonesia. *Geophys Res Abstr* 13: EGU2011–13522
- Allard P, Métrich N, Carbonnelle J (2000) Magma degassing budget of Merapi volcano. In: Abstract, IAVCEI General Assembly, Bali, Indonesia, 18–22 July 2000
- Allard P, Aiuppa A, Tamburello G, Moussallam Y, De Napoli R, Liuzzo M, Bitetto M, Bani P, Budi-Santoso A, Sumarti S, Subandriyo J (2017). Post-paroxysmal magma degassing at Merapi volcano, Java (Indonesia): continuous survey and implications. In: Abstract, 13th IAVCEI-CCVG workshop, Ecuador, 24 Sept–3 Oct 2017
- Alletti M, Baker DR, Freda C (2007) Halogen diffusion in a basaltic melt. *Geochim Cosmochim Acta* 71:3570–3580
- Baker DR, Alletti M (2012) Fluid saturation and volatile partitioning between melts and hydrous fluids in crustal magmatic systems: the contribution of experimental measurements and solubility models. *Earth Sci Rev* 114:298–324
- Beauducel F, Cornet FH (1999) Collection and three-dimensional modeling of GPS and tilt data at Merapi volcano, Java. *J Geophys Res* 104(B1):725–736
- Bernard A, Symonds RB, Rose WI (1990) Volatile transport and deposition of Mo, W and Re in high temperature magmatic fluids. *Appl Geochem* 5:317–326
- Blank JG, Brooker RA (1994) Experimental studies of carbon dioxide in silicate melts; solubility, speciation, and stable carbon isotope behavior. *Rev Mineral* 30:157–186
- Blundy J, Cashman KV, Rust A, Witham F (2010) A case for CO₂-rich arc magmas. *Earth Planet Sci Lett* 290:289–301
- Blythe LS, Deegan FM, Freda C, Jolis EM, Masotta M, Misiti V, Taddeucci J, Troll VR (2015) CO₂ bubble generation and migration during magma–carbonate interaction. *Contrib Mineral Petrol* 169:42
- Borisova AY, Martel C, Gouy S, Pratomo I, Sumarti S, Toutain J-P, Bindeman IN, de Parseval P, Metaxian J-P, Surono (2013) Highly explosive 2010 Merapi eruption: evidence for shallow-level crustal assimilation and hybrid fluid. *J Volcanol Geotherm Res* 261:193–208
- Brouwer HA (1928) Production of trachyte and phonolite from pyroxene andesitic magma associated with limestone. *J Geol* 36:545–548
- Brouwer HA (1945) The association of alkali rocks and metamorphic limestone in a block ejected by the volcano Merapi (Java). *Proc K Ned Akad Wet* 48:166–189
- BudhieWijatna A, Sudarmadji S, Hendrayana H (2013) Tracing the origin of spring water by using environmental isotopes in the southern slope of Mount Merapi, Indonesia. *ASEAN Eng J* 2:118–130
- Burgisser A, Alletti M, Scaillet B (2015) Simulating the behavior of volatiles belonging to the C–O–H–S system in silicate melts under magmatic conditions with the software D-compress. *Comp Geosci* 79:1–14
- Byrdina S, Friedel S, Vandemeulebrouck J, Budi-Santoso A, Suhari, Suryanto W, Rizal MH, Winata E, Kusdaryanto (2017) Geophysical image of the hydrothermal system of Merapi volcano. *J Volcanol Geotherm Res* 329:30–40
- Carr BB, Clark AB, de'Michieli Vitturi M (2018) Earthquake induced variations in extrusion rate: a numerical modeling approach to the 2006 eruption of Merapi volcano (Indonesia). *Earth Planet Sci Lett* 482:377–387

- Carr BB, Clark AB, de'Michieli Vitturi M (2020) Volcanic conduit controls on effusive-explosive transition and the 2010 eruption of Merapi volcano (Indonesia). *J Volcanol Geotherm Res* 392:106767
- Carroll MR, Webster JD (1994) Solubilities of sulfur, noble gases, nitrogen, chlorine, and fluorine in magmas. *Rev Mineral* 30:231–279
- Carroll MR (2005) Chlorine solubility in evolved alkaline magmas. *Ann Geophys* 48:619–631
- Cashman KV, Sparks RSJ, Blundy JD (2017) Vertically extensive and unstable magmatic systems: a unified view of igneous processes. *Sci* 355
- Chadwick JP, Troll VR, Ginibre C, Morgan D, Gertisser R, Waight TE, Davidson JP (2007) Carbonate assimilation at Merapi Volcano, Java, Indonesia: insights from crystal isotope stratigraphy. *J Petrol* 48:1793–1812
- Chadwick JP, Troll VR, Waight TE, van der Zwan FM, Schwarzkopf LM (2013) Petrology and geochemistry of igneous inclusions in recent Merapi deposits: a window into the sub-volcanic plumbing system. *Contrib Mineral Petrol* 165:259–282
- Clocchiatti R, Joron JL, Kerinec F, Treuil M (1982) Quelques données préliminaires sur la lave du dôme actuel du volcan Mérapî (Java, Indonésie) et sur ses enclaves. *C R Acad Sci Paris* 295:817–822
- Costa F, Andreastuti S, Bouvet de Maisonneuve C, Pallister JS (2013) Petrological insights into the storage conditions, and magmatic processes that yielded the centennial 2010 Merapi explosive eruption. *J Volcanol Geotherm Res* 261:209–235
- Deegan FM, Troll VR, Freda C, Misiiti V, Chadwick JP, McLeod CL, Davidson JP (2010) Magma-carbonate interaction processes and associated CO₂ release at Merapi volcano, Indonesia: insights from experimental petrology. *J Petrol* 51:1027–1051
- Deegan FM, Troll VR, Gertisser R, Freda C (2023) Magma-carbonate interaction at Merapi volcano, Indonesia. In: Gertisser R, Troll VR, Walter TR, Nandaka IGMA, Ratdomopurbo A (eds) Merapi volcano—geology, eruptive activity, and monitoring of a high-risk volcano. Springer, Berlin, Heidelberg, pp 291–321
- Deegan FM, Whitehouse MJ, Troll VR, Geiger H, Jeon H, le Roux P, Harris C, van Helden M, González-Maurel O (2021) Sunda arc mantle $\delta^{18}\text{O}$ value revealed by intracrystal isotope analysis. *Nat Commun* 12:3930
- Delmelle P, Stix J (2000) Volcanic gases. In: Sigurdsson H, Houghton B, McNutt SR, Rymer H, Stix J (eds) *Encyclopedia of volcanoes*, 1st edn. Academic Press, pp 803–815
- Edmonds M, Woods AW (2018) Exsolved volatiles in magma reservoirs. *J Volcanol Geotherm Res* 368:13–30
- Erdmann S, Martel C, Pichavant M, Bourdier J-L, Champallier R, Komorowski J-C, Cholik N (2016) Constraints from phase equilibrium experiments on pre-eruptive storage conditions in mixed magma systems: a case study on crystal-rich basaltic andesites from Mount Merapi, Indonesia. *J Petrol* 57:535–560
- Gantes M, Sabroux JC, Vitter G (1983) Chemical sensors for monitoring volcanic activity. In: Tazieff H, Sabroux JC (eds) *Forecasting volcanic events*. Elsevier, New York, pp 409–424
- Gauthier PJ, Condomines M (1999) ²¹⁰Pb-²²⁶Pb Ra radioactive disequilibria in recent lavas and radon degassing: inferences on the magma chamber dynamics at Stromboli and Merapi volcanoes. *Earth Planet Sci Lett* 172:111–126
- Genareau K, Cronin SJ, Lube G (2015) Effects of volatile behaviour on dome collapse and resultant pyroclastic surge dynamics: Gunung Merapi 2010 eruption. *Geol Soc Lond Spec Publ* 410:199–218
- Gerlach TM (1982) Interpretation of the Merapi field gas chromatograph data. *Bull Volcanol* 45:249–251
- Gertisser R, Keller J (2003a) Temporal variations in magma composition at Merapi volcano (Central Java, Indonesia): magmatic cycles during the past 2000 years of explosive activity. *J Volcanol Geotherm Res* 123:1–23
- Gertisser R, Keller J (2003b) Trace element and Sr, Nd, Pb, O isotope variations in medium-K and high-K volcanic rocks from Merapi volcano, Central Java, Indonesia: evidence for the involvement of subducted sediments in Sunda arc magma genesis. *J Petrol* 44:457–489
- Gertisser R, del Marmol M-A, Newhall C, Preece K, Charbonnier S, Andreastuti S, Handley H, Keller J (2023) Geological history, chronology and magmatic evolution of Merapi. In: Gertisser R, Troll VR, Walter TR, Nandaka IGMA, Ratdomopurbo A (eds) Merapi volcano—geology, eruptive activity, and monitoring of a high-risk volcano. Springer, Berlin, Heidelberg, pp 137–193
- Giggenbach WF (1996) Chemical composition of volcanic gases. In: Scarpa R, Tilling RI (eds) *Monitoring and mitigation of volcano hazards*. Springer, Heidelberg, pp 221–256
- Giggenbach WF (1992) Isotopic shifts in waters from geothermal and volcanic systems along convergent plate boundaries and their origin. *Earth Planet Sci Lett* 113:495–510
- Giggenbach WF, Tedesco D, Sulistiyo Y, Caprai A, Cioni R, Favara R, Fischer TP, Hirabayashi J-I, Korzhinsky M, Martini M, Menyailov I, Shinohara H (2001) Evaluation of results from the fourth and fifth IAVCEI field workshops on volcanic gases, Vulcano Island, Italy and Java, Indonesia. *J Volcanol Geotherm Res* 108:157–172
- Global Volcanism Program (2001) Report on Merapi (Indonesia). In Wunderman R (ed) *Bulletin of the global volcanism network* 26. Smithsonian Institution. <https://doi.org/10.5479/si.GVP.BGVN200101-263250>
- Global Volcanism Program (2007) Report on Merapi (Indonesia). In Wunderman R (ed) *Bulletin of the global volcanism network* 32. Smithsonian Institution. <https://doi.org/10.5479/si.GVP.BGVN200702-263250>

- Global Volcanism Program (2011) Report on Merapi (Indonesia). In Wunderman R (ed) Bulletin of the global volcanism network 36. Smithsonian Institution. <https://doi.org/10.5479/si.GVP.BGVN201102-263250>
- Halldórsson SA, Hilton DR, Troll VR, Fischer TP (2013) Resolving volatile sources along the western Sunda arc, Indonesia. *Chem Geol* 339:263–282
- Hammer JE, Cashman KV, Voight B (2000) Magmatic processes revealed by textural and compositional trends in Merapi dome lavas. *J Volcanol Geotherm Res* 100:165–192
- Handley HK, Reagan M, Gertisser R, Preece K, Berlo K, McGee LE, Barclay J, Herd R (2018) Timescales of magma ascent and degassing and the role of crustal assimilation at Merapi volcano (2006–2010), Indonesia: constraints from uranium-series and radiogenic isotopic compositions. *Geochim Cosmochim Acta* 222:34–52
- Holloway JR, Blank JG (1994) Application of experimental results to C–O–H species in natural melts. *Rev Mineral* 30:187–230
- Humaida H, Sutaningsih NE, Sumarti S, Cahyono H, Bayu Aji A, Nurnusanto I, Sulistiyo Y, Sukarnen, Hartiyatun S, Damayanti AS, Widyono RL, Apriyanti T, Suryono, Suryatmaji, Hidayat H, Riyan A, Widodo S (2017) Data Geokimia Gunung Api Indonesia. Balai Penyelidikan dan Pengembangan Teknologi Kebencanaan Geologi, Pusat Vulkanologi dan Mitigasi Bencana Geologi, Badan Geologi, Kementerian Energi dan Sumber Daya Mineral, pp 652–732
- Joussot P, Budi-Santoso A, Jolly AD, Boichu M, Suroño DS, Sumarti S, Hidayati S, Thierry P (2013) Signs of magma ascent in LP and VLP seismic events and link to degassing: an example from the 2010 explosive eruption at Merapi volcano, Indonesia. *J Volcanol Geotherm Res* 261:171–192
- Kavalieris I (1994) High Au, Ag, Mo, Pb, V and W content of fumarolic deposits at Merapi volcano, central Java, Indonesia. *J Geochem Explor* 50:479–491
- Kern C, Deutschmann T, Werner C, Sutton AJ, Elias T, Kelly PJ (2012) Improving the accuracy of SO₂ column densities and emission rates obtained from upward-looking UV-spectroscopic measurements of volcanic plumes by taking realistic radiative transfer into account. *J Geophys Res* 117:D20302. <https://doi.org/10.1029/2012JD017936>
- Koulakov I, Maksotova G, Jaxybulatov K, Kasatkina E, Shapiro NM, Luehr B-G, El Khrepy S, Al-Arifi N (2016) Structure of magma reservoirs beneath Merapi and surrounding volcanic centers of Central Java modeled from ambient noise tomography. *Geochem Geophys Geosyst* 17:4195–4211
- Le Cloarec M-F, Gauthier PJ (2003) Merapi Volcano, central Java, Indonesia: a case study of radionuclide behavior in volcanic gases and its implications for magma dynamics at andesitic volcanoes. *J Geophys Res* 108(B5):2243. <https://doi.org/10.1029/2001JB001709>
- Le Guern F, Bernard A (1982) A new method for sampling and analyzing volcanic sublimates—Application to Merapi volcano. *J Volcanol Geotherm Res* 12:133–146
- Le Guern F, Biccocchi P, Nohl A, Tazieff H (1979) Analyse directe des gaz volcaniques. *C R Acad Sci* 288:867–870
- Luehr B-G, Koulakov I, Rabbel W, Zschau J, Ratdomopurbo A, Brotopuspito KS, Fauzi P, Sahara DP (2013) Fluid ascent and magma storage beneath Gunung Merapi revealed by multi-scale seismic imaging. *J Volcanol Geotherm Res* 261:7–19
- Luehr BG, Koulakov I, Suryanto W (2023) Crustal structure and ascent of fluids and melts beneath Merapi: Insights from geophysical investigations. In: Gertisser R, Troll VR, Walter TR, Nandaka IGMA, Ratdomopurbo A (eds) Merapi volcano—geology, eruptive activity, and monitoring of a high-risk volcano. Springer, Berlin, Heidelberg, pp 111–135
- Mason E, Edmonds M, Turchyn AV (2017) Remobilization of crustal carbon may dominate volcanic arc emissions. *Science* 357:290–294
- Millard GA, Mather TA, Pyle DM, Rose WI, Thornton B (2006) Halogen emissions from a small volcanic eruption: modeling the peak concentrations, dispersion, and volcanically induced ozone loss in the stratosphere. *Geophys Res Lett* 33:L19815
- Müller M, Hördt A, Neubauer FM (2002) Internal structure of Mount Merapi, Indonesia, derived from long-offset transient electromagnetic data. *J Geophys Res* 107(B9):2187. <https://doi.org/10.1029/2001JB000148>
- Nadeau O (2019) Sources of fluids in Archean hydrothermal stockwork-disseminated gold deposits of Abitibi, Canada: insights from Duquesne, Dolodau, Lac Shortt and Canadian Malartic. *Ore Geol Rev* 111:102975
- Nadeau O, Stevenson R, Jébrak M (2018) Interaction of mantle magmas and fluids with crustal fluids at the 1894 Ma Montviel alkaline-carbonatite complex, Canada: insights from metasomatic and hydrothermal carbonates. *Lithos* 296–299:563–579
- Nadeau O, Stix J, Williams-Jones AE (2016) Links between arc volcanoes and porphyry-epithermal ore deposits. *Geology* 44:11–14
- Nadeau O, Williams-Jones AE, Stix J (2010) Sulphide magma as a source of metals in arc-related magmatic hydrothermal ore fluids. *Nat Geosci* 3:501–505
- Nadeau O, Williams-Jones AE, Stix J (2013a) Magmatic-hydrothermal evolution and devolatilization beneath Merapi volcano, Indonesia. *J Volcanol Geotherm Res* 261:50–68
- Nadeau O, Williams-Jones AE, Stix J (2013b) The behaviour of copper, zinc and lead during magmatic-hydrothermal activity at Merapi volcano, Indonesia. *Chem Geol* 342:167–179
- Preece K, Gertisser R, Barclay J, Berlo K, Herd RA, Edinburgh Ion Microprobe Facility (2014) Pre- and syn-eruptive degassing and crystallisation processes of the 2010 and 2006 eruptions of Merapi volcano, Indonesia. *Contrib Mineral Petrol* 168:1061
- Preece K, Gertisser R, Barclay J, Charbonnier SJ, Komorowski J-C, Herd RA (2016) Transitions

- between explosive and effusive phases during the cataclysmic 2010 eruption of Merapi volcano, Java, Indonesia. *Bull Volcanol* 78:54
- Preece K, van der Zwan F, Hammer J, Gertisser R (2023) A textural perspective on the magmatic system and eruptive behaviour of Merapi volcano. In: Gertisser R, Troll VR, Walter TR, Nandaka IGMA, Ratdomopurbo A (eds) *Merapi volcano—geology, eruptive activity, and monitoring of a high-risk volcano*. Springer, Berlin, Heidelberg, pp 265–289
- Priatna P, Kadarsetia E (2007) Characteristics of volcanic gas correlated to the eruption activity: case study in the Merapi volcano, periods of 1990–1994. *J Geol Indon* 2:235–246
- Ratdomopurbo A, Beauducel F, Subandriyo J, Nandaka IGMA, Newhall CG, Suharna, Sayudi DS, Suparwaka H, Sunarta (2013) Overview of the 2006 eruption of Mt. Merapi. *J Volcanol Geotherm Res* 261:87–97
- Ratdomopurbo A, Poupinet G (2000) An overview of the seismicity of Merapi Volcano (Java, Indonesia); 1983–1994. *J Volcanol Geotherm Res* 100:193–214
- Richter G, Wassermann J, Zimmer M, Ohnberger M (2004) Correlation of seismic activity and fumarole temperature at the Mt. Merapi volcano (Indonesia) in 2000. *J Volcanol Geotherm Res* 135:331–342
- Robock A (2000) Volcanic eruptions and climate. *Rev Geophys* 38:191–219
- Sheppard SM, Epstein S (1970) D/H and $^{18}\text{O}/^{16}\text{O}$ ratios of minerals of possible mantle or lower crustal origin. *Earth Planet Sci Lett* 9:232–239
- Siebert L, Cottrell E, Venzke E, Andrews B (2015) Earth's Volcanoes and their eruptions: an overview. In: Sigurdsson H (ed) *The encyclopedia of volcanoes*, 2nd edn. Academic Press, pp 239–255
- Signorelli S, Carroll MR (2000) Solubility and fluid-melt partitioning of Cl in hydrous phonolitic melts. *Geochim Cosmochim Acta* 64:2851–2862
- Siswoidjoyo S, Suryo I, Yokoyama I (1995) Magma eruption rates of Merapi volcano, central Java, Indonesia during one century (1890–1992). *Bull Volcanol* 57:111–116
- Sparks RSJ (1978) The dynamics of bubble formation and growth in magmas: a review and analysis. *J Volcanol Geotherm Res* 3:1–37
- Subandriyo, Gertisser R, Aisyah N, Humaida H, Preece K, Charbonnier S, Budi-Santoso A, Handley H, Sumarti S, Sayudi DS, Nandaka IGMA, Wibowo HE (2023) An overview of the large-magnitude (VEI 4) eruption of Merapi in 2010. In: Gertisser R, Troll VR, Walter TR, Nandaka IGMA, Ratdomopurbo A (eds) *Merapi volcano—geology, eruptive activity, and monitoring of a high-risk volcano*. Springer, Berlin, Heidelberg, pp 353–407
- Sumarti S, Rinekso K, Yulianto, Sulistiyo Y (2007) Gas Vulkanik Gunung Merapi: Erupsi Juni 2006. Badan Geologi, Pusat Vulkanologi dan Mitigasi Bencana Geologi, Yogyakarta, Indonesia, pp 283–292
- Surono JP, Pallister J, Boichu M, Buongiorno MF, Budisantoso A, Costa F, Andreastuti S, Prata F, Schneider D, Clarisse L, Humaida H, Sumarti S, Bignami C, Griswold J, Carn S, Oppenheimer C, Lavigne F (2012) The 2010 explosive eruption of Java's Merapi volcano—A '100-year' event. *J Volcanol Geoth Res* 241–242:121–135
- Symonds RB (1993) Scanning electron microscope observations of sublimes from Merapi Volcano, Indonesia. *Geochem J* 27:337–350
- Symonds RB, Rose WI, Reed MH, Lichte FE, Finnegan DL (1987) Volatilization, transport and sublimation of metallic and non-metallic elements in high temperature gases at Merapi Volcano, Indonesia. *Geochim Cosmochim Acta* 51:2083–2101
- Symonds RB, Rose WI, Bluth GJ, Gerlach TM (1994) Volcanic-gas studies: methods, results and applications. *Rev Mineral* 30:1–66
- Toutain J-P, Sortino F, Baubron J-C, Richon P, Surono SS, Nonell A (2009) Structure and CO₂ budget of Merapi volcano during inter-eruptive periods. *Bull Volcanol* 71:815–826
- Troll VR, Deegan FM (2023) The magma plumbing system of Merapi: the petrological perspective. In: Gertisser R, Troll VR, Walter TR, Nandaka IGMA, Ratdomopurbo A (eds) *Merapi volcano—geology, eruptive activity, and monitoring of a high-risk volcano*. Springer, Berlin, Heidelberg, pp 233–263
- Troll VR, Chadwick JP, Jolis EM, Deegan FM, Hilton DR, Schwarzkopf LM, Blythe LS, Zimmer M (2013a) Crustal volatile release at Merapi volcano; the 2006 earthquake and eruption events. *Geol Today* 29:96–101
- Troll VR, Deegan FM, Jolis EM, Harris C, Chadwick JP, Gertisser R, Schwarzkopf LM, Borisova AY, Bindeman IN, Sumarti S, Preece K (2013b) Magmatic differentiation processes at Merapi volcano: inclusion petrology and oxygen isotopes. *J Volcanol Geotherm Res* 261:38–49
- Troll VR, Hilton DR, Jolis EM, Chadwick JP, Blythe LS, Deegan FM, Schwarzkopf LM, Zimmer M (2012) Crustal CO₂ liberation during the 2006 eruption and earthquake events at Merapi volcano, Indonesia. *Geophys Res Lett* 39:L11302
- Vigouroux N, Wallace PJ, Kent AJR (2008) Volatiles in high-K magmas from the western Trans-Mexican volcanic belt; evidence for fluid fluxing and extreme enrichment of the mantle wedge by subduction processes. *J Petrol* 49:1589–1618
- Voight B, Sukhyar R, Wirakusumah AD (2000) Introduction to the special issue on Merapi volcano. *J Volcanol Geotherm Res* 100:1–8
- Wallace PJ, Plank T, Edmonds M, Hauri EH (2015) Volatiles in magmas. In: Sigurdsson H (ed) *The Encyclopedia of volcanoes*, 2nd edn. Academic Press, pp 163–183
- Walter TR, Subandriyo J, Kirbani S, Bathke H, Suryanto W, Aisyah N, Darmawan H, Jousset P, Luehr BG, Dahm T (2015) Volcano-tectonic control of Merapi's lava dome splitting: The November 2013 fracture observed from high resolution TerraSAR-X data. *Tectonophysics* 639:23–33

- Walter TR, Wang R, Zimmer M, Grosser H, Lühr B, Ratdomopurbo A (2007) Volcanic activity influenced by tectonic earthquakes: Static and dynamic stress triggering at Mt. Merapi. *Geophys Res Lett* 34: L05304
- Webster JD, Kinzler RJ, Mathez EA (1999) Chloride and water solubility in basalt and andesite melts and implications for magmatic degassing. *Geochim Cosmochim Acta* 63:729–738
- Webster JD, Mandeville CW (2007) Fluid immiscibility in volcanic environments. *Rev Min Geochem* 65:313–362
- Westrich H, Gerlach TM (1992) Magmatic gas source for the stratospheric SO₂ cloud from the June 15, 1991, eruption of Mount Pinatubo. *Geology* 20:867–870
- Whitley S, Gertisser R, Halama R, Preece K, Troll VR, Deegan FM (2019) Crustal CO₂ contribution to subduction zone degassing recorded through calc-silicate xenoliths in arc lavas. *Sci Rep* 9:8803. <https://doi.org/10.1038/s41598-019-44929-2>
- Whitley S, Halama R, Gertisser R, Preece K, Deegan FM, Troll VR (2020) Magmatic and metasomatic effects of magma-carbonate interaction recorded in calc-silicate xenoliths from Merapi volcano (Indonesia). *J Petrol* 61(4):egaa048
- Zimmer M, Erzinger J (2003a) Continuous H₂O, CO₂, ²²²Rn and temperature measurements on Merapi volcano, Indonesia. *J Volcanol Geotherm Res* 125:25–38
- Zimmer M, Erzinger J (2003b) Geochemical monitoring on Merapi volcano, Indonesia. In: Zschau J, Küppers A (eds) Early warning systems for natural disaster reduction. Springer, Berlin, Heidelberg, pp 511–514
- Zuev VV, Zueva E, Savelieva ES (2017) The role of the Mt. Merapi eruption in the 2011 Arctic ozone depletion. *Atm Env* 166:327–333



An Overview of the Large-Magnitude (VEI 4) Eruption of Merapi in 2010

12

Subandriyo, Ralf Gertisser, Nurnaning Aisyah, Hanik Humaida, Katie Preece, Sylvain Charbonnier, Agus Budi-Santoso, Heather Handley, Sri Sumarti, Dewi Sri Sayudi, I Gusti Made Agung Nandaka, and Haryo Edi Wibowo

Abstract

The VEI 4 eruption in 2010 was the worst volcanic disaster at Merapi in 80 years. The unusual size and dynamics of the eruption, the

rapid acceleration of events and the large number of evacuees posed significant challenges for the management of the volcanic crisis and post-eruption recovery. The first indications of Merapi's reawakening were observed in the seismic monitoring record about one year before the eruption. The eruption commenced on 26 October 2010, with initial explosions and associated pyroclastic density currents (PDCs) directed towards the south flank of Merapi. Subsequently, the intensity of the eruption accelerated with rapid lava dome growth and increasing PDC runout, culminating in a climactic eruption phase on 5 November, where blast-like, high-energy PDCs destroyed areas on Merapi's south flank and PDCs reached ~16 km in the Gendol valley. After 5 November, the eruption waned, leading to reductions of the exclusion zone from mid-November 2010 and successive lowering of the alert level from early December 2010. The 2010 eruption was fed by basaltic andesite magma similar to other recent Merapi eruptions, but was driven by a larger than normal influx of deep, volatile-rich magma that replenished the shallower magma system within the carbonate-dominated upper crust beneath Merapi at relatively short timescales. During and after the eruption, lahars swept down almost all major valleys, causing considerably larger impact than after previous eruptions. As a result of the eruption, nearly 400,000 people were displaced from their

Subandriyo (✉) · N. Aisyah · H. Humaida · A. Budi-Santoso · S. Sumarti · D. S. Sayudi · I G. M. A. Nandaka

Balai Penyelidikan Dan Pengembangan Teknologi Kebencanaan Geologi (BPPTKG), Jl. Cendana 15, Yogyakarta 55166, Indonesia
e-mail: jsubandriyo@gmail.com

R. Gertisser (✉)
School of Geography, Geology and the Environment, Keele University, Keele ST5 5BG, UK
e-mail: r.gertisser@keele.ac.uk

K. Preece
Department of Geography, Swansea University, Swansea SA2 8PP, UK

S. Charbonnier
School of Geosciences, University of South Florida, Tampa, FL 33620-5201, USA

H. Handley
Department of Applied Earth Sciences, University of Twente, 7514 AE Enschede, The Netherlands

School of Earth, Atmosphere and Environment, Monash University, Clayton, VIC 3800, Australia

H. E. Wibowo
Department of Geological Engineering, Faculty of Engineering, Universitas Gadjah Mada, Yogyakarta 55281, Indonesia

Center for Disaster Studies, Universitas Gadjah Mada, Yogyakarta 55281, Indonesia

homes and accommodated in temporary or permanent residences. Tourist activities and sand quarrying of PDC and lahar deposits facilitated post-eruption recovery. Mitigation measures, including strengthening of the volcano monitoring system, establishment of a disaster risk reduction forum, strengthening of community capacity, and preparation of contingency plans for local governments based on hazard scenarios, were all part of the disaster risk reduction strategy that saved many lives during the 2010 eruption crisis.

Keywords

2010 eruption · Eruption chronology · Pyroclastic density currents · Geochemistry · Petrology · Eruption impact · Recovery · Disaster management · Risk reduction strategy

12.1 Introduction

With a Volcano Explosivity Index (VEI) of 4, the catastrophic eruption in 2010 was the largest eruption of Merapi since 1872 and the deadliest since 1930 (Siebert et al. 2011; Surono et al. 2012; Jousset et al. 2013a), causing 398 casualties. The eruption had a significant impact on the natural environment, built infrastructures and the population in the vicinity of Merapi (Fig. 12.1), and posed major challenges during crisis management and post-disaster recovery. Compared with Merapi's activity in the past few decades (e.g. Voight et al. 2000), the 2010 eruption was unusual in many respects. Following a rapid increase in seismicity and ground deformation, the eruption began on 26 October with partially laterally directed explosions at the summit. These were not preceded by lava dome extrusion, which frequently characterised previous Merapi eruptions. A few days later, a dome extruded within the newly formed summit crater over a period of less than a week, growing at unprecedented rates of $25 \text{ m}^3 \text{ s}^{-1}$ (Surono et al. 2012; Pallister et al. 2013). During the climactic eruption phase on 5

November, this dome was rapidly destroyed in a series of explosions generating blast-like, high-energy pyroclastic density currents (PDCs) and contemporaneous valley-confined PDCs, of which at least one travelled $\sim 16 \text{ km}$ beyond the summit along the Gendol valley, more than twice the distance of the largest flows in 2006 and other recent eruptions (Voight et al. 2000; Charbonnier and Gertisser 2008; Charbonnier et al. 2013; Komorowski et al. 2013). Both phenomena, as well as associated valley-derived, unconfined (overbank) flows and accompanying ash-cloud surges, caused widespread devastation on Merapi's south flank and the large number of casualties (Surono et al. 2012; Charbonnier et al. 2013; Cronin et al. 2013; Jenkins et al. 2013; Komorowski et al. 2013; Lerner et al. 2021). In a later phase on 5 November, collapse of a subplinian convective eruption column produced PDCs rich in pumice and scoria. This was followed by renewed lava dome extrusion, at a rate of $35 \text{ m}^3 \text{ s}^{-1}$ (Pallister et al. 2013), exceeding the already unusually high rates of the previous (pre-climax) dome extrusion phase. The eruption intensity declined on 8 November (Surono et al. 2012; Komorowski et al. 2013; Pallister et al. 2013).

This chapter provides an overview of the 2010 eruption compiled by an international team of experts who worked on various aspects of the eruption and its crisis management. After a summary of the chronology of the 2010 eruption crisis (Sect. 12.2), the chapter reviews the volcano monitoring record (Sect. 12.3) and the volcanic deposits of the eruption (Sect. 12.4). The petrology and geochemistry of the eruptive products are described in Sect. 12.5 and used to shed light on the pre-eruptive magma plumbing system and the magmatic processes leading up to the eruption. This is followed by a description of the eruption's impact on the environment, infrastructures and population as well as the recovery after the disaster (Sect. 12.6). The management and disaster risk reduction strategy of the 2010 volcanic crisis is covered in Sect. 12.7, followed by a conclusion section (Sect. 12.8).

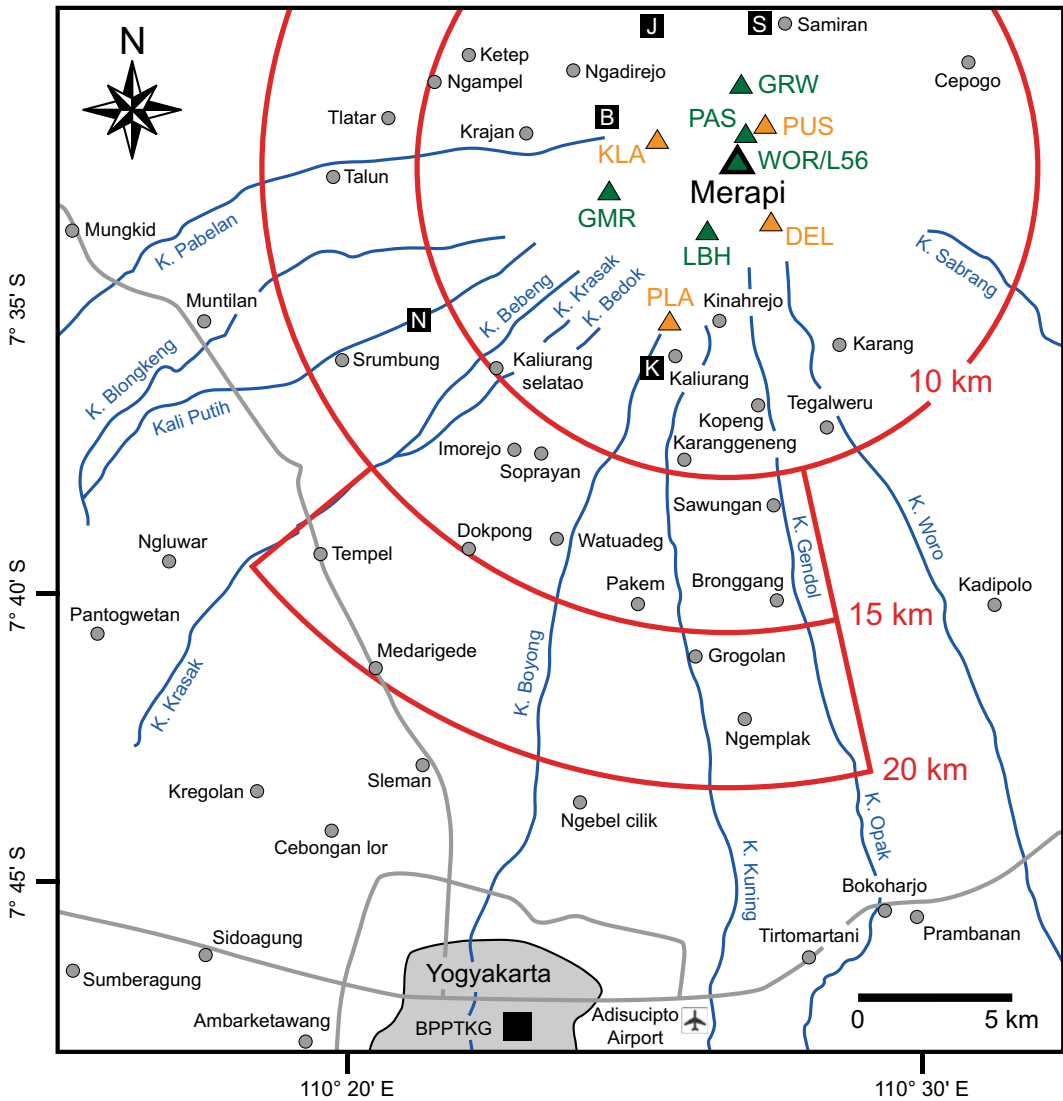


Fig. 12.1 Map of Merapi volcano and its surroundings, showing some of the larger towns and villages (grey circles), the city of Yogyakarta (grey area) and Adisucipto International Airport, the BPPTKG head office in Yogyakarta (black square), volcano observation posts (labelled black squares: K = Kaliurang; N = Ngepos; B = Babadan; J = Jrahah; S = Selo), main river valleys (blue), and major roads (light grey). Permanent short-period seismic

stations are shown by orange triangles (PUS; DEL; PLA; KLA) and temporary broadband seismic stations are indicated by green triangles (LBH; GMR; GRW; PAS; WOR/L56). The red arcs at distances of 10, 15 and 20 km from the summit of Merapi show evacuation zones in effect at different times during the 2010 eruption crisis. See text for details. After Surono et al. (2012) and Jousset et al. (2013a)

12.2 Eruption Chronology

For the purpose of this chapter, the chronology and main phenomena of the 2010 eruption are grouped into four phases: (1) Reawakening of Merapi and volcanic unrest, (2) Beginning of the eruption and pre-climactic activity, (3) Climactic eruption phase, and (4) Post-climactic activity and end of the eruption (Fig. 12.2). These are closely aligned with the eruption phases proposed by Suroño et al. (2012) and the eruption stages put forward by Komorowski et al. (2013) (Fig. 12.2). The latter provides a detailed framework for linking the volcanic deposits to eruption chronology (see Sect. 12.4).

12.2.1 Reawakening of Merapi and Volcanic Unrest

After the 2006 eruption, Merapi stayed in a resting phase for 42 months until signs of renewed activity began in October 2009 (Fig. 12.2). As in previous eruptions, the first substantial indication of Merapi's reawakening and continuing unrest was increased seismic activity, with various seismic signals, as previously identified at Merapi, associated with different processes and events, including (1) volcano-tectonic (VT—VTA = deeper VT earthquakes, 2.5–5 km below the summit; VTB = shallower VT earthquakes, <1.5 km below the summit), (2) multiphase (MP), (3) low-frequency (LF) or long period (LP), (4) very-long period (VLP), (5) tremor, (6) rockfall (RF), and (7) pyroclastic flow (PF) types (e.g. Ratdomopurbo 1995; Ratdomopurbo and Poupinet 2000; Jousset et al. 2013b). The rise in activity leading up to the 2010 eruption was signalled by the appearance of a swarm of shallow VT earthquakes (<1 km depth) on 31 October 2009. The largest VT events had a magnitude of 3.0 on the Richter Scale and were felt by the inhabitants around Merapi; further VT earthquakes were detected on 31 October 2009, 9 December 2009, 1 February 2010, and 10 June 2010 (Fig. 12.2). In September 2010, the seismic activity

increased significantly, marking the start of the 2010 eruption crisis phase (Fig. 12.2). The increase in VT earthquakes was accompanied by shortening of the slope distances (i.e. the distance between a base station on the lower slopes of the volcano and a reflector at the summit, as determined by electronic distance measurements (EDM)), particularly on the southern baselines from Kaliurang (see Aisyah et al. 2018). Felt VT earthquakes with a magnitude 2.5 and 2.2 on the Richter scale occurred on 12 and 13 September 2010, respectively. The first of the two earthquakes was followed by a large rockfall that was heard from several volcano observation posts. The daily number of MP and VT earthquakes increased sharply on 19 September 2010, and shortening of the southern baselines reached up to 0.5 m from 3 April 2009 to 19 September 2010, and 3 cm on 20 September alone. Considering the increase in seismicity and the gradual shortening of the slope distance, the alert level was upgraded on 21 September 2010 from level I (NORMAL) to level II (WASPADA; Engl.: Advisory) on the four-level alert system (Fig. 12.2).

From mid-October 2010, all monitoring data revealed a significant increase in volcanic activity. The daily numbers of VT and MP earthquakes increased to 56 and 579, respectively on 17 October, while the cumulative energy of both types of earthquakes reached 27.9×10^9 J on 20 October. On that day, rockfall activity increased to 87 events per day. This number was still relatively low compared to earlier eruptions between the 1990s and 2006, which involved rockfalls from the destruction of older domes. By 21 October, the southern baselines had contracted by up to 1.643 m since 3 April 2009. The concentration of CO₂ gas in the summit fumaroles also increased significantly, reflecting accumulation of high magmatic pressure in the upper conduit, and raising the possibility that the expected eruption could be explosive and not preceded by lava dome extrusion. The further increase in volcanic unrest prompted the Center of Volcanology and Geological Hazard Mitigation (CVGHM) to raise the alert level to level III (SIAGA; Engl.: Watch) on 21 October 2010 (Fig. 12.2).

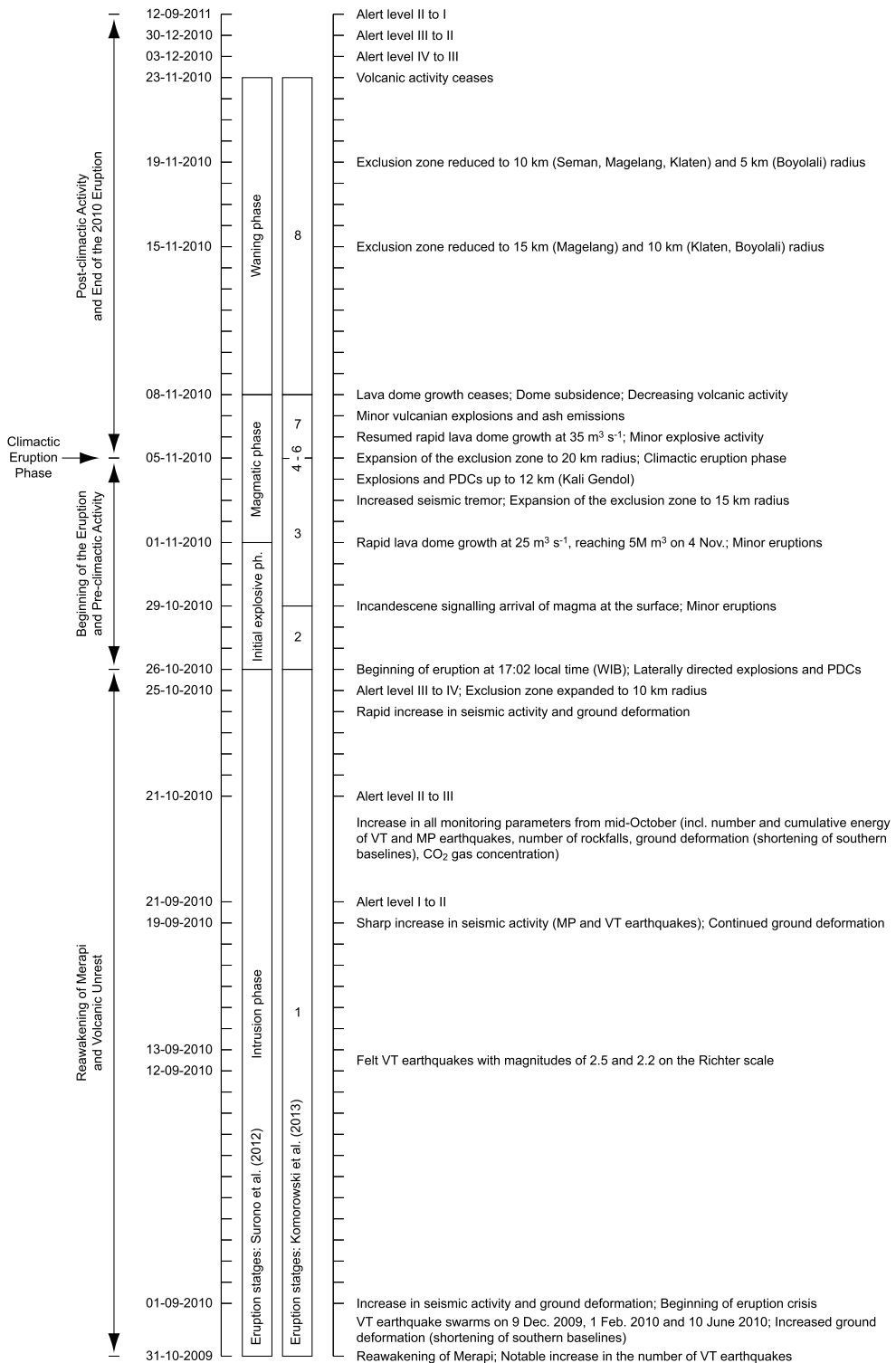


Fig. 12.2 Chronology and main phenomena of the 2010 eruption from the first signs of reawakening in October 2009 to September 2011, when the alert level was lowered to level I (NORMAL). Also shown are the eruption phases and stages proposed by Suroño et al. (2012) and Komorowski et al. (2013)

On 24 October, the number of VT and MP earthquakes significantly increased to 80 and 588, respectively, and the cumulative energy of VT and MP earthquakes reached 62.5×10^9 J. Rockfalls occurred frequently, with 194 events recorded, suggesting that the old 2006 lava dome became unstable. The concentration of CO₂ gas in the summit fumaroles also continued to increase. The following day, on 25 October, the numbers of VT, MP and rock-fall events continued to increase to 222, 624 and 454, respectively, and the cumulative seismic energy of VT and MP earthquakes reached 75.8×10^9 J. The southern baselines shortened by up to 0.551 m in only one day since 24 October, suggesting that at this point, the activity of Merapi was at a critical phase where an eruption could occur any time. Therefore, at 06:00 local time (WIB) on 25 October, CVGHM decided to raise the alert to the highest level IV (AWAS; Engl.: Warning). A restricted zone with a radius of 10 km from the summit was recommended, and 70,000 residents had to be evacuated from the restricted zone (Figs. 12.1, and 12.2).

High seismicity and rapid shortening of the southern baselines continued on 26 October. The number of VT, MP and rockfall events were 232, 397 and 269, respectively, and the total energy reached 94.8×10^9 J until the onset of the eruption. The shortening of the southern baselines was rapid at up to 0.744 m in only 4 h.

12.2.2 Beginning of the Eruption and Pre-Climactic Activity

The eruption began at 17:02 (local time (WIB) = UTC + 7 h) on 26 October (Fig. 12.1). The initial explosive phase, which was categorised as a magmatic eruption, lasted for about two hours (Table 12.1). It destroyed the 2006 lava dome and the southern rim of the summit, forming a large crater open to the south (Fig. 12.3a, b). Pyroclastic density currents from laterally directed explosions reached up to 6.8 km in Kali Gendol and Kali Kuning and caused as many as 35 casualties in the restricted zone in Kinahrejo, including Mbah Marijan, a local traditional figure.

The number of VT and MP events decreased after the initial explosions, and the quiescence continued until 28 October. As all the EDM reflectors were broken as a result of the 26 October events, ground deformation data could no longer be obtained along the established baselines. Further smaller eruptions occurred on 29 October, 31 October and 1 November. Incandescence, signalling arrival of magma at the surface, was initially observed on 29 October (Komorowski et al. 2013). Growth of a new lava dome within the 26 October summit crater was first detected by Interferometry Satellite Aperture

Table 12.1 Eruptive activity and phenomena observed at the beginning of the 2010 eruption on 26 October

| Time (WIB) | Eruptive activity and phenomena | Duration |
|---------------------|--|----------|
| 17:02 | Pyroclastic flow (PDC) ^a | 9 min |
| 17:18 | Pyroclastic flow (PDC) | 4 min |
| 17:23 | Pyroclastic flow (PDC) | 5 min |
| 17:30 | Pyroclastic flow (PDC) | 2 min |
| 17:37 | Pyroclastic flow (PDC) | 2 min |
| 17:42 | Large pyroclastic flow (PDC) | 33 min |
| 18:00–18:45 | Loud noise heard at the Jarakah and Selo volcano observation posts | 45 min |
| 18:10, 18:15, 18:25 | Thumping sounds occurred 3 times | < 1 min |
| 18:16 | Pyroclastic flow (PDC) | 5 min |
| 18:21 | Large pyroclastic flow (PDC); ‘flames’ and an ash column up to 1.5 km above Merapi observed from the Selo volcano observation post | 33 min |
| 18:54 | Activity begins to decline | – |

^a PDC—Pyroclastic density current

Radar (InSAR) on 1 November (Pallister et al. 2013; Kubanek et al. 2015; Kelfoun et al. 2017). Partial collapse of the growing dome led to several PDCs over the next few days.

At 11:00 local time (WIB) on 3 November, the amplitude of seismic tremors suddenly increased, marking the beginning of a short sub-Plinian eruption phase. With PDCs reaching more than 10 km runout distance, the restricted zone was enlarged to 15 km radius from the summit at 16:05 (WIB) on that day (Figs. 12.1, and 12.2). At 18:46 (WIB), further large PDCs occurred in the Gendol valley, reaching 9 km from the summit. At that time, the KLA (Klatakan) seismic station, located 2 km west of Merapi's summit (Fig. 12.1), was damaged by PDCs or falling rocks and stopped transmitting a signal. With PDCs reaching distances of up to 12 km in Kali Gendol on 4 November, CVGHM expanded the radius of the danger zone to 20 km that evening (Figs. 12.1 and 12.2). At that time, the volume of the lava dome had increased to ~ 5 million m^3 (Fig. 12.3c), suggesting a time-averaged growth rate of $\sim 25 \text{ m}^3 \text{ s}^{-1}$ ($2.160 \times 10^6 \text{ m}^3/\text{day}$) since 1 November (Surono et al. 2012; Pallister et al. 2013). This significantly exceeded the highest extrusion rates observed during the previous dome-forming eruption in 2006 ($0.285 \times 10^6 \text{ m}^3/\text{day}$) (Ratdomopurbo et al. 2013) and Merapi's long-term (100 year) average ($0.003 \times 10^6 \text{ m}^3/\text{day}$) (Siswowardjyo et al. 1995).

12.2.3 Climactic Eruption Phase

The eruptive activity reached its peak on 5 November (Fig. 12.2). The largest pyroclastic events occurred at 00:01 (WIB) and lasted for about 27 min. It included a sequence of several laterally directed dome explosions that produced high-energy PDCs and retrogressive gravitational dome collapses that removed the growing and older lava domes at the summit, and generated PDCs reaching a distance of ~ 16 km in the Gendol valley (Surono et al. 2012; Budi-Santoso et al. 2013; Charbonnier et al. 2013; Komorowski et al. 2013) (Fig. 12.3d). An unsustained

convective column reached a height of 17 km above the summit, producing PDCs rich in scoria and pumice clasts. A cumulative SO_2 emission of $\sim 0.44 \text{ Tg}$ (Surono et al. 2012), obtained by satellite observation, was used to estimate a volume of ~ 120 million m^3 of degassing magma at depth. The events at the peak of the eruption caused damage to the DEL (Deles) and PUS (Pusunglondon) seismic stations (Fig. 12.1). Due to the magnitude of the eruption and seismic energy, the vibrations were also recorded by the IMG (Imogiri) seismic station ~ 40 km south of Merapi (see Budi-Santoso et al. 2023, Chap. 13). The sound of the eruption could be heard more than 60 km away.

12.2.4 Post-Climactic Activity and End of the 2010 Eruption

The eruptive activity gradually decreased after 5 November (Fig. 12.2). Rapid lava dome extrusion resumed over a period of ~ 11 h on 6–7 November at an unprecedented rate of $35 \text{ m}^3 \text{ s}^{-1}$ and was accompanied by minor explosive activity. When dome growth ceased on 8 November, the new lava dome had a volume of $\sim 1.5 \times 10^6 \text{ m}^3$ (Pallister et al. 2013) (Fig. 12.3e). Subsequent activity was characterised by dome subsidence, and minor vulcanian explosions and ash emissions.

On 15 November, CVGHM recommended reducing the radius of the restricted zone to 15 km from the summit in the Magelang district and to 10 km in the Klaten and Boyolali districts, while the zone for the Sleman district, as the most impacted area, was kept at 20 km radius from the summit (Fig. 12.2). Reduction of the radius of the restricted zone continued on 19 November, with the hazard zone reduced to 10 km from the summit in the Sleman, Magelang and Klaten districts, and to 5 km in the Boyolali district (Fig. 12.2). With continued waning of the eruptive activity, as indicated by decreasing seismicity, the alert level was downgraded to level III on 3 December 2010, and subsequently to level II on 30 December 2010 (Fig. 12.2).

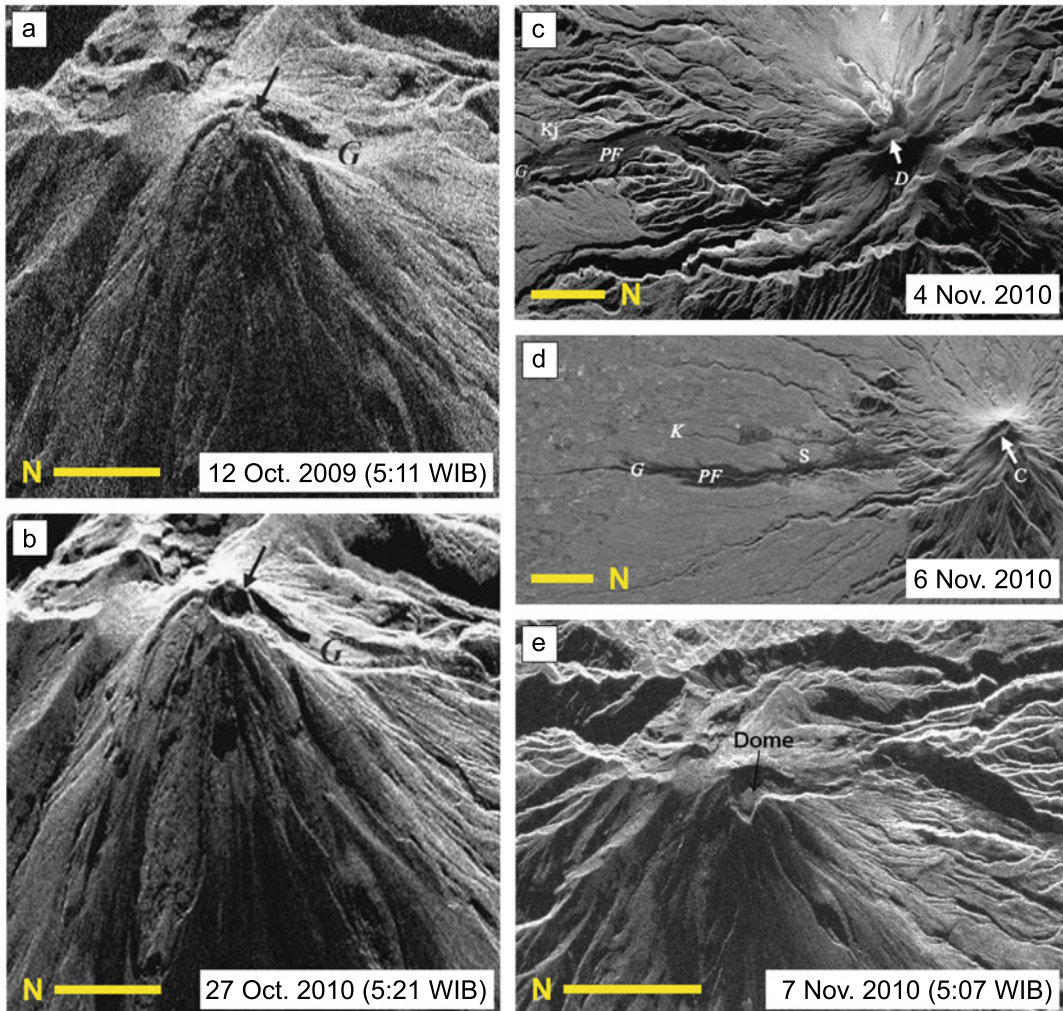


Fig. 12.3 **a** RADARSAT-2 Synthetic Aperture Radar (SAR) base reflectivity image of 12 October 2009 at 5:11 (WIB), with arrow indicating the remnants of the 2006 lava dome and ‘G’ denoting Kali Gendol. **b** TerraSAR-X image from 27 October 2010 at 5:21 (WIB), with arrow showing the deepened summit crater produced by the initial explosions of the 2010 eruption on 26 October. ‘G’ indicates Kali Gendol. **c** TerraSAR-X image from 4 November 2010. ‘D’ marks the large ($\sim 5 \times 10^6 \text{ m}^3$) lava dome, first detected on 1 November, ‘PF’ denotes pyroclastic flow (PDC) deposits from the 26 October to 4 November activity, and ‘Kj’ shows the location of Kinahrejo. **d** RADARSAT-2 SAR base

reflectivity image from 6 November 2010. ‘C’ indicates the empty summit crater, ‘PF’ shows channelised and overbank pyroclastic flow (PDC) deposits and ‘S’ are dilute PDC (surge) deposits in and around Kali Gendol (‘G’), both formed during the climactic eruption phase on 5 November. ‘K’ shows the location of Kali Kuning. **e** RADARSAT-2 SAR base reflectivity image from 7 November 2010 at 5:07 (WIB), showing the new lava dome that had grown to $\sim 1.5 \times 10^6 \text{ m}^3$ in the previous 11 h. In each image, the scale bar (yellow) is 2 km; the north direction is indicated by the position of ‘N’ relative to the scale bar. After Surono et al. (2012) and Pallister et al. (2013)

These decisions were crucial, given that the large number of refugees reached nearly 400,000 people (Mei and Lavigne 2013; Mei et al. 2013). After lowering of the alert level, some of the

refugees were able to return to their homes, except for people whose houses were severely damaged by the eruption. Lahars occurred continuously in all of the rivers around the flanks

during the rainy season from November 2010 to April 2011 (de B elizal et al. 2013). The alert level was downgraded to level I on 12 September 2011 after most of the lahar events had finished (Fig. 12.2). This means that from the first early warning issued on 20 September 2010 to the return to normal conditions, the 2010 Merapi disaster crisis lasted for about 1 year.

12.3 The Volcano Monitoring Record of the 2010 Eruption

As outlined in the previous section, indications of the eruption were clearly shown by the monitoring data. The daily seismicity gradually increased and was accompanied by felt earthquakes from 8 months prior to the eruption on 26 October 2010. The deformation of the summit area, which had been monitored by EDM, showed shortening of the slope distance for one year prior to eruption, and significantly accelerated about 2 weeks before the eruption. About five days before the eruption, volcanic gas concentrations increased. Below, the main characteristics of the seismic, deformation and gas-geochemical monitoring data of the 2010 eruption are presented and discussed.

12.3.1 Seismicity

The most prominent seismic features leading up to the 2010 eruption were the high seismic intensity and energy (Fig. 12.4). The maximum daily number of VT, MP, and RF earthquakes reached 242, 624 and 454, respectively. Excluding RF earthquakes, these numbers exceeded what occurred during previous eruptions. Leading up to the 2010 eruption, the maximum number of VT earthquakes was around 6 times higher, and the number of MP earthquakes was around 3 times higher, compared to the period prior to the 2006 eruption. Similarly, the value of seismic energy of the 2010 eruption was greater than the previous eruption in 2006 (Fig. 12.5). The cumulative seismic energy released through VT and MP earthquakes during the year prior to the 2010

eruption reached 7.5×10^{10} J. Compared to previous eruptions, the energy from 1992 to 2006 never exceeded 2.5×10^{10} J. This considerably higher amount of energy was the most important seismic feature of the 2010 eruption, consistent with its highly explosive character. Along with deformation and gas emission measurements, this observation gave an early identification of the impending large eruption and underpinned the decision making for the evacuation of a larger than usual area. An increase was also observed in the continuous seismic signals (Fig. 12.4). The accelerated rate of seismic energy was clearly reflected in the RSAM and MRSAM values for the frequency bands other than 1–3 Hz, and offered an opportunity to test the Failure Forecasting Method (Voight 1988) used to predict volcanic eruptions. MRSAM values of the 3–5 Hz frequency band gave the best results, where during the six days before the onset of eruption, the model consistently pointed to the eruption time with an accuracy of ~ 4 h (Budi-Santoso et al. 2013).

Rapid magma migration from depth was a further important feature in the lead-up to the eruption. Most deep VT events with focal depths from 2.5 to 5 km occurred before 17 October 2010, the date when VLP events were also recorded at the summit and at several distal broadband seismic stations and linked to inertial displacement of material such as magma or gas (Jousset et al. 2013b). After this date, deep VT events diminished, while shallow activity (<1.5 km) increased (Fig. 12.6). This indicated migration of magma towards the surface, with calculated ascent rates of 1 mm/s or 86 m/day during deep intrusion, 6 mm/s or 520 m/day during aseismic intrusion, and 3 mm/s or 260 m/day during shallow intrusion. These values were considered plausible given the different stress constraints corresponding to these different zones. According to Hidayat et al. (2000), the average magma ascent velocity ranged from 0.2 to 0.5 mm/s or 17 to 43 m/day during pre-eruptive activity of Merapi in the 1990s.

An additional important feature of the 2010 seismic data was the emergence of large LF earthquakes at a depth of several hundred metres below the summit on 23–24 October, about three

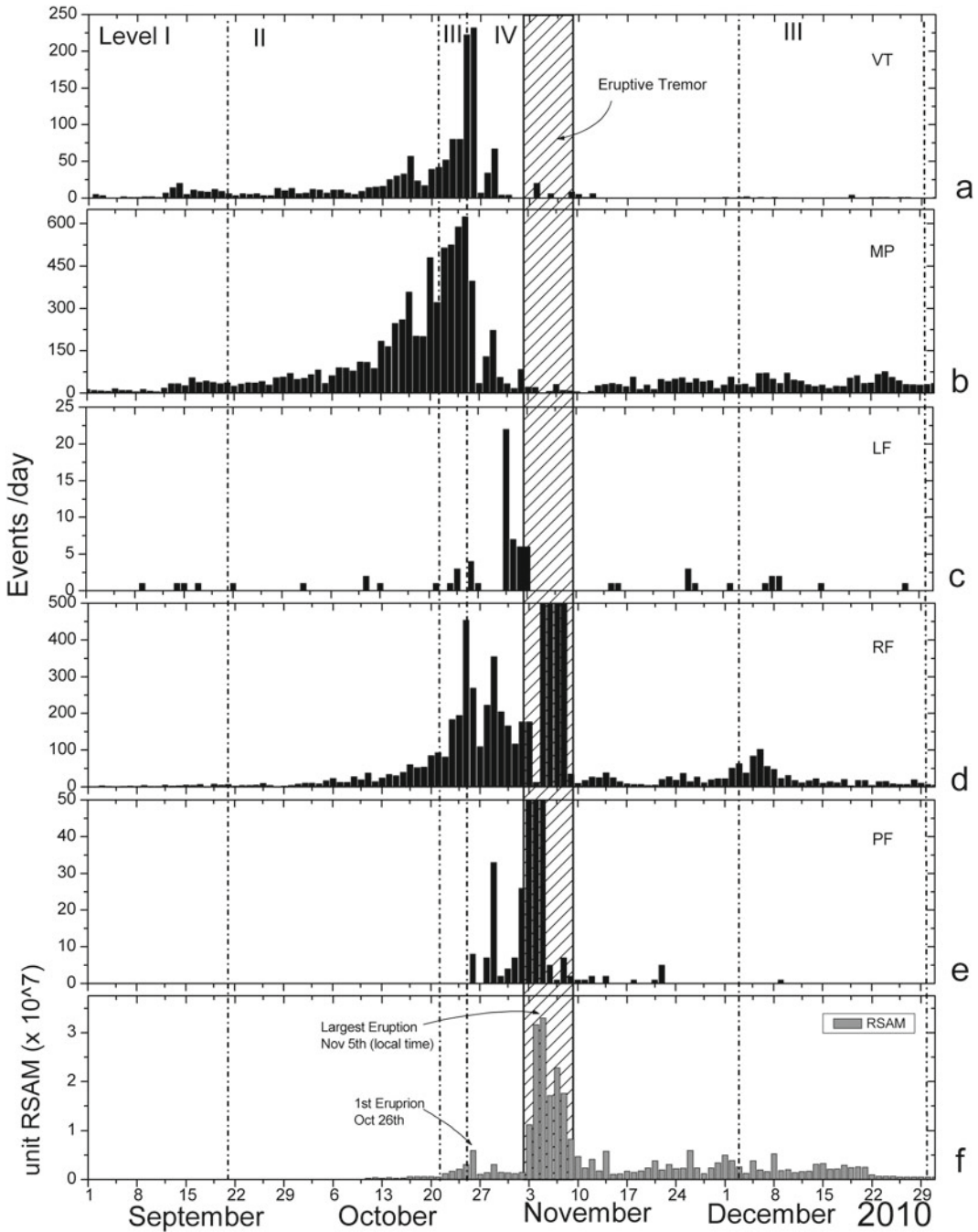


Fig. 12.4 Seismicity at Merapi from September to December 2010. **a** Volcano-tectonic (VT) earthquakes. **b** Multiphase (MP) earthquakes. **c** Low-frequency (LF) earthquakes. **d** Rockfalls (RF). **e** Pyroclastic flows (PF). **f** Real-time seismic amplitude measurements (RSAM). After Suroño et al. (2012)

days before the eruption (Figs. 12.4 and 12.6), which confirmed that a large bulk volume of gas was involved in the eruption. However, these

events were saturated on the short period stations and therefore not considered as LF events by the observers at the time.

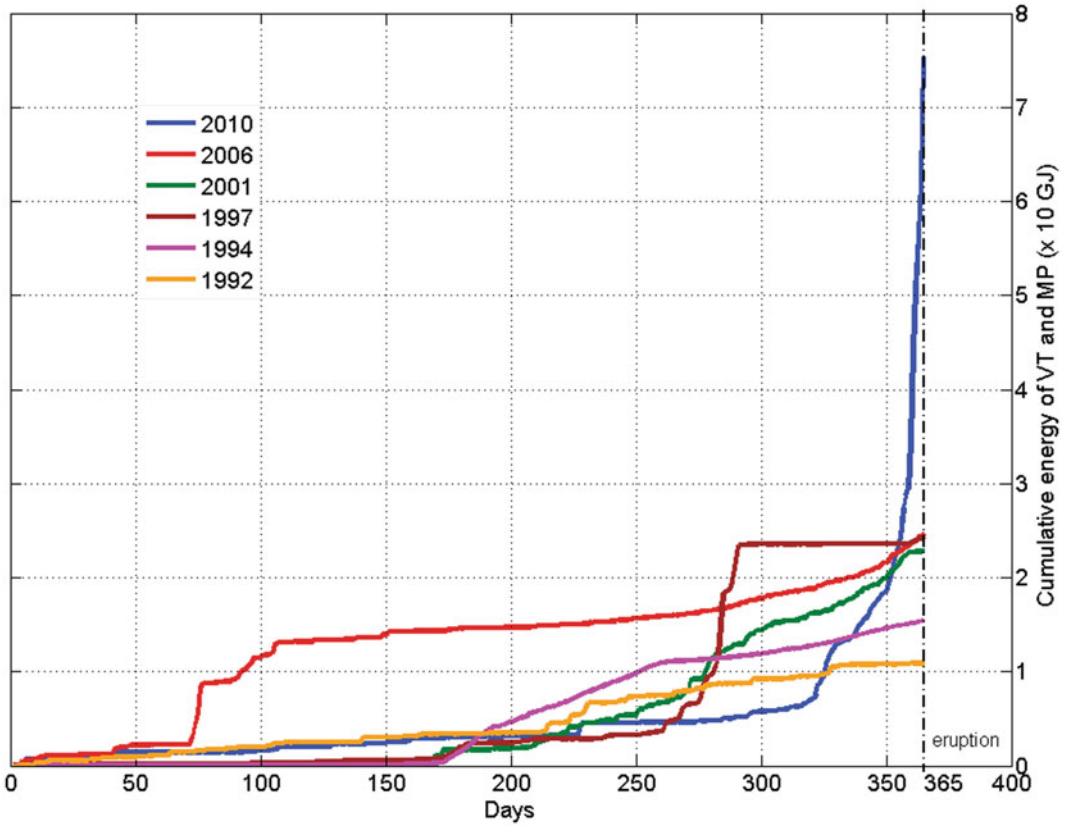
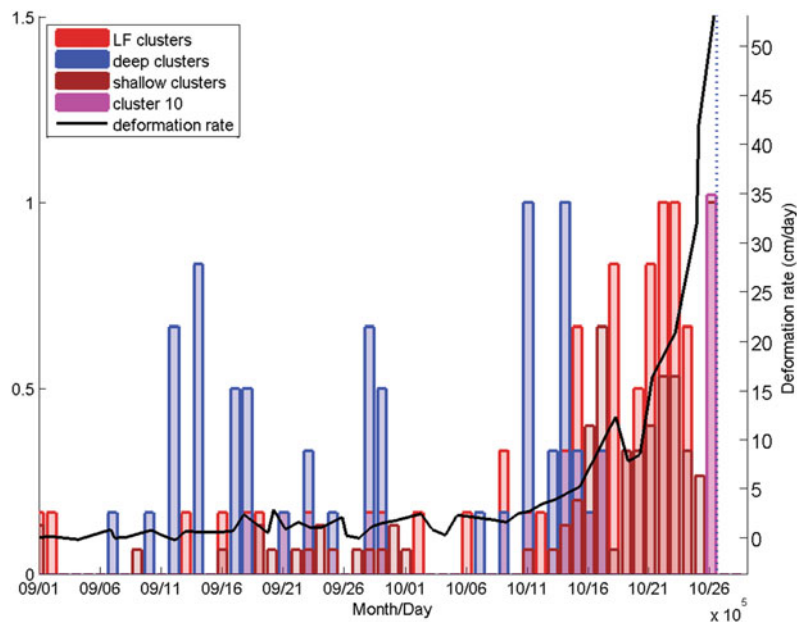


Fig. 12.5 Comparison of the cumulative energy release of VT and MP earthquakes in the year prior to the eruptions from 1992–2010. After Budi-Santoso et al. (2013)

Fig. 12.6 Daily number of events for each group of earthquake clusters during September and October 2010. The values (left axis) are normalised by their maximum. The deformation rate of reflector RK4 obtained by EDM is superimposed as a black line. The rapid increase in the deformation rate approximately on 18 October 2010 corresponds to the strong increase of shallow earthquake events and the vanishing of deep earthquakes



12.3.2 Ground Deformation

Ground deformation prior to the 2010 eruption was characterised by uniaxial displacement and long-term creep (Aisyah et al. 2018). A large change of slope distance was detected by daily distance measurements using EDM only from the southern volcano observation post (Kaliurang) to the south summit area; changes of slope distance from the other directions were minimal (Surono et al. 2012; Aisyah et al. 2018). The rate of contraction of the southern baselines accelerated up to the first explosions on 26 October.

Changes of slope distance of the baselines from April 2009 are shown in Fig. 12.7. The change of slope distance data was divided into 11 (T1 to T11) periods based on the contraction rate of the southern baseline Rk4-KAL (Kaliurang) (Fig. 12.7a), the slope distance of which decreased by 1.64 m from April 2009 to 21 October 2010. By contrast, shortening of baselines from the Babadan post (BAB) amounted to only 0.02 to 0.05 m for the same period (Fig. 12.7a, b). Larger contractions were observed using the reflectors closer to the summit, with a much larger contraction of baseline Rk4-KAL, compared to the other flanks. Baselines Rk1-KAL, Rk2-KAL, and Rk3-KAL on the south flank also exhibited significant contractions (−1.43 m, −0.58 m, and −0.59 m, respectively). Contractions of EDM lines accelerated from 21 to 26 October 2010, when baseline Rk4-KAL was shortened by 3.73 m on 26 October, while baselines Rk3-KAL, Rk2-KAL, and Rk1-KAL decreased by 3.23 m, 2.07 m, and 1.10 m, respectively. Unlike the contraction of the southern and north-western baselines, baselines Rj1-JRK (Jrakah) and Rb5-BAB were shortened only from April 2009 to August 2010 (T1 and T2), changing to extension from August to October 2010 (T3 to T7; Fig. 12.7b). Measurements at the Rs1-SEL (Selo) baseline indicated shortening until April 2010, after which no measurements were documented (Fig. 12.7b).

The contraction rate increased linearly during periods T4 to T6, from 0.03 m/day between 24 September and 15 October (T4 and T5) to 0.05 m/day between 15 and 20 October (T6)

(Fig. 12.7). On 20 October, the contraction rate increased exponentially, reaching 0.95 m/day on 26 October, the start date of the eruption. As before, the contraction of the north-western baseline Rb5-BAB was considerably less than that of the southern baseline Rk4-KAL, although the contraction rate gradually increased from T2 to T7 (Fig. 12.7). The CVGHM upgraded the alert level from level II to level III on 21 October and distance measurements of the north-western and northern baselines using EDM were discontinued. The dominant contraction of the southern baselines indicated surface deformation in an asymmetrical pattern, with a large movement of the summit area towards the south flank and minor movement of the summit area in other directions.

12.3.3 Gas Geochemistry

One of the manifestations of the activity of Merapi is the presence of solfataras or fumaroles in the summit area. The concentration of solfataras or fumarole gas emissions changes during an increase in activity. Merapi is a H₂O-rich volcano, with the volcanic gases mainly composed of H₂O—a typical feature of subduction zone volcanoes (Shinohara et al. 2008)—followed by CO₂, SO₂, H₂S and the minor gaseous components hydrogen (H₂), carbon monoxide (CO), hydrogen chloride (HCl), hydrogen fluoride (HF), and helium (He) (Le Guern et al. 1982; Sumarti and Suryono 1994; Delmelle and Stix 2000). The characteristics of the volcanic gas emissions of the explosive 2010 eruption were different from previous effusive eruptions, with the most significant changes prior to the 2010 eruption observed in the volcanic gas concentrations of H₂O and CO₂ (Fig. 12.8). During the repose period between the 2006 eruption and 2009, volcanic gas compositions fluctuated. In November 2007, the concentration of H₂O dropped to 75 mol.% from >90 mol.% and was accompanied by increases in other gas species, such as CO₂ and SO₂, which reached concentrations of 19.2 mol.% and 3.0 mol.%, respectively. After 2009, the composition returned to

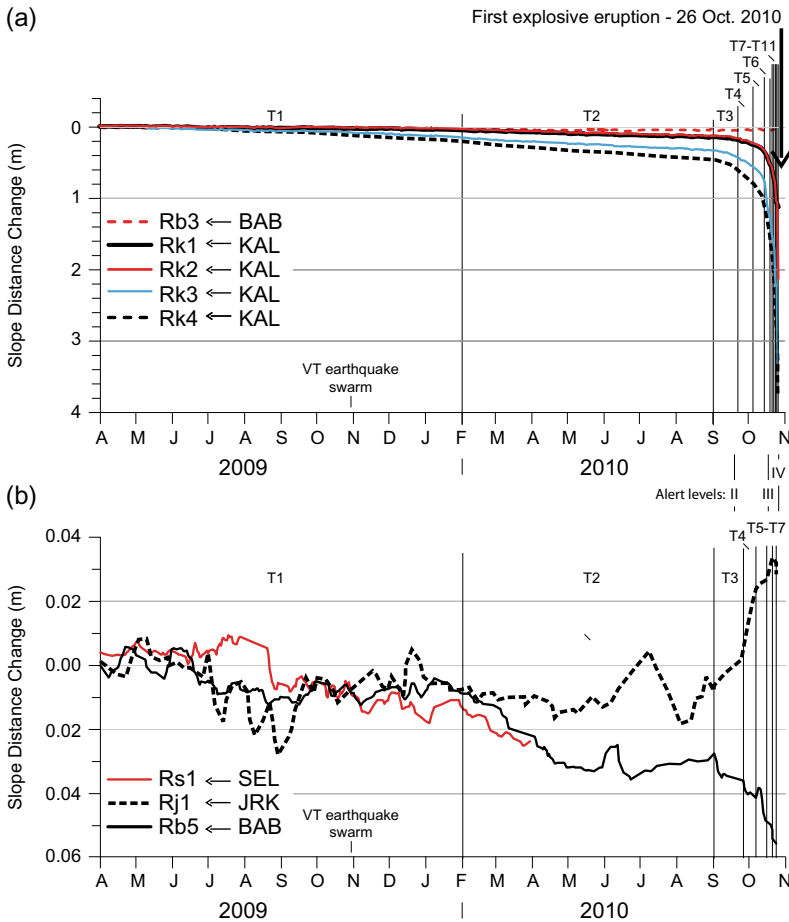


Fig. 12.7 **a** Change of slope distance (i.e. the distance between a base station on the lower slopes of the volcano and a reflector (R) at the summit, as determined by EDM) at the southern baselines (Rk1/Rk2/Rk3/Rk4-KAL), and the north-western baseline (Rb3-BAB) between April 2009 and October 2010. **b** Change of slope distance at the north-western (Rb5-BAB), northern (Rj1-JRK) and north-eastern (Rs1-SEL) baselines. For the configuration of the EDM network in 2010, see Aisyah et al. (2018).

Deformation changes, observed since the beginning of 2009, were divided into 11 (T1 through T11) periods based on the contraction rate of the Rk4-KAL baseline. The volcano-tectonic (VT) earthquake swarm on 31 October 2009 and the dates of alert level changes are also shown. Abbreviations: BAB = Babadan; JRK = Jarakah; KAL = Kaliurang; SEL = Selo. After Aisyah et al. (2018)

normal (background) levels until March 2010. In April 2010, the concentration of H₂O decreased, and CO₂ increased, before the gas emissions returned to normal levels in March 2010. In June 2010, H₂O levels decreased again to 77.7 mol.% and CO₂ rose to 14.2 mol.%, and gas concentrations remained at a higher-than-normal level afterwards. Significant changes in gas concentrations were observed in October 2010, when H₂O concentrations were as low as 59 mol.%,

and CO₂ and H₂S increased to 35 mol.% and 2.5 mol.%, respectively (Fig. 12.8).

During the 2010 eruption, explosive eruption phases were characterised by a significant increase in H₂S/H₂O ratios, which were not detected during the effusive eruption phase. This observation was due to the dominance of H₂S among the sulphur compounds (Fig. 12.9a). As H₂S is a stable sulphur compound at higher pressure and temperature (Delmelle and

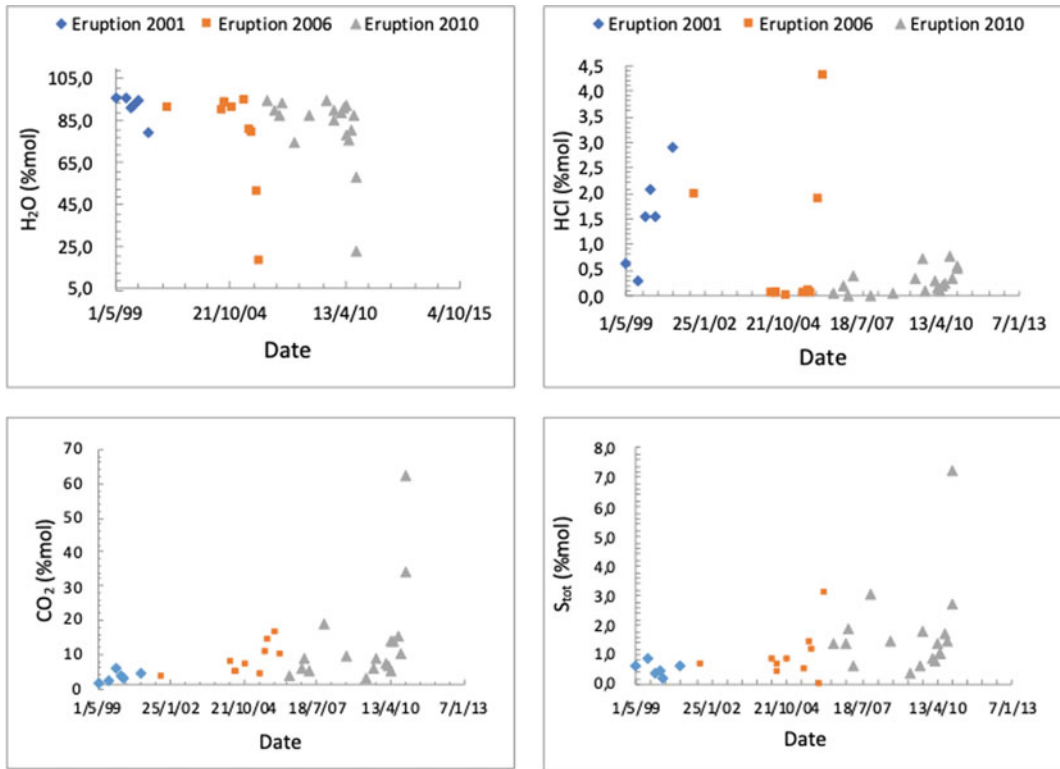


Fig. 12.8 Changes in gas composition at the Woro fumarole field at Merapi’s summit prior the 2001 and 2006 effusive eruptions and the explosive eruption of 2010

Stix 2000), the higher observed H₂S/H₂O ratios during explosive eruption phases likely reflects fresh magma input from depth characterised by higher H₂S (and CO₂) concentrations (relative to SO₂, HCl and H₂O) compared to magma stored in a shallower part of the magma plumbing system. The large variation in SO₂/H₂O may have been due to different gas sources in general (Shinohara et al. 2011), including deep as well as shallow magma sources, which release gas generally dominated by SO₂ (Delmelle and Stix 2000). Emitted CO₂/H₂O ratios, which are proportional to the bubble fraction in the melt (e.g. Botcharnikov et al. 2004), also significantly increased during the 2010 explosive eruption compared to the effusive eruptions in 2001 and 2006. The strong increase in the CO₂ emission prior to the 2010 eruption is distinctly negatively correlated with the emission of H₂O and a CO₂/H₂O ratio of 0.83, while the effusive eruptions in

2001 and 2006 were characterised by CO₂/H₂O ratios of 0.14 and 0.11, respectively (Fig. 12.9b).

Changes in gas ratios leading up to the 2010 eruption were observed from August/September 2010 to October 2010. CO₂/SO₂ increased from 9.4–19.0 to 24.1–115.6, CO₂/HCl from 20.8–31.0 to 52.8–115.7, and CO₂/H₂O from 0.1–0.2 to 0.6–2.7. Combined, these changes in gas concentrations indicated migration of magmatic fluid to shallower levels in October 2010. Such an interpretation is in line with seismic, particularly LP, events (Jousset et al. 2013b) and decreasing CO₂/H₂S ratios from 16.8–26.4 to 13.4–13.9, which suggested that the new magma from depth carried a volatile-rich phase of CO₂ and H₂S (relative to SO₂ and HCl) that was rapidly released at the surface.

During the effusive eruption phase in 2010, the growth rate of the lava dome showed a positive correlation with the CO₂/H₂O ratio and HCl

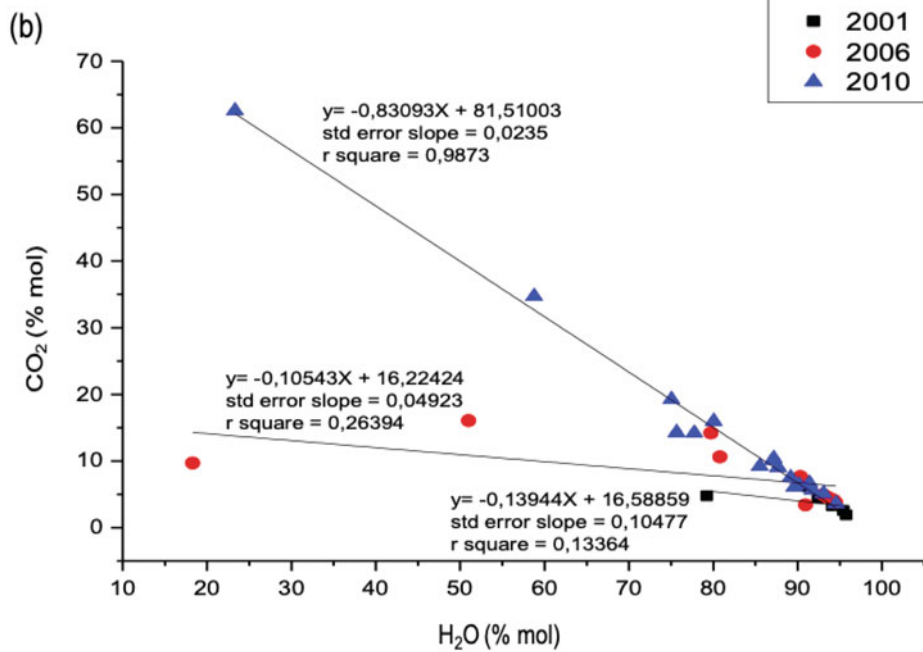
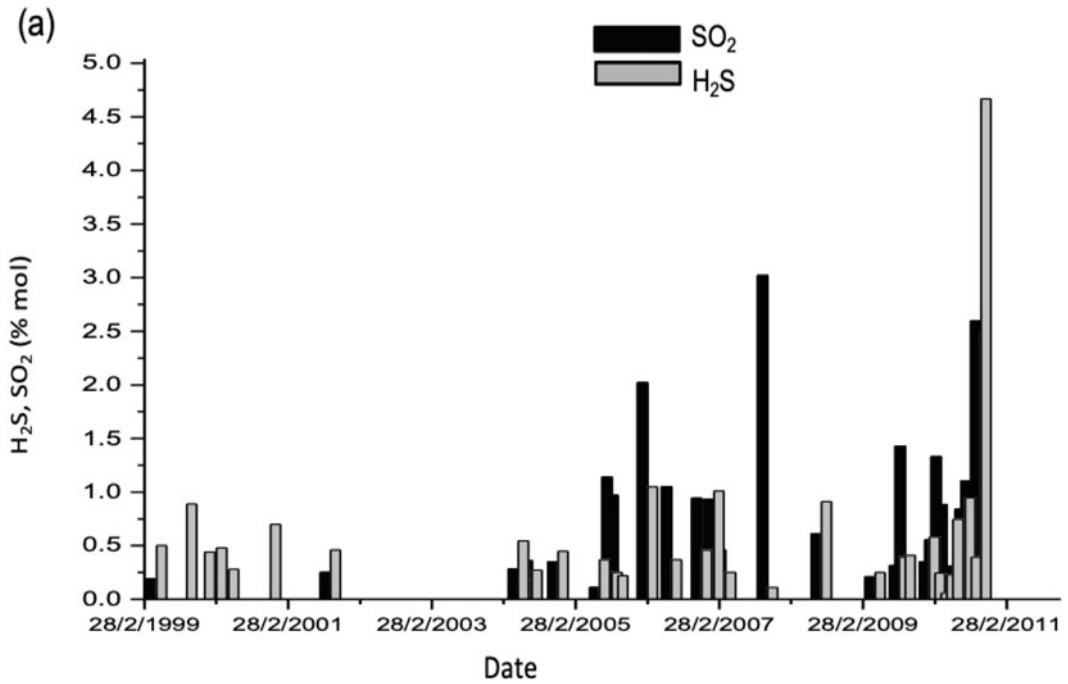


Fig. 12.9 **a** Merapi gas H₂S and SO₂ concentrations (mol.%) prior to the 2001 and 2006 effusive eruptions, and the explosive eruption in 2010. **b** Concentrations (mol.%) of CO₂ and H₂O prior to the 2001, 2006 and 2010 eruptions

concentration of the emitted gases. Typically, the HCl concentration during dome extrusion is higher than during explosive eruptions or eruption phases due to the complexity of the Cl degassing behaviour of the melt as magma rises towards to the surface, and other factors, including differentiation of the magma, melt composition, temperature and pressure (e.g. Carroll and Webster 1994).

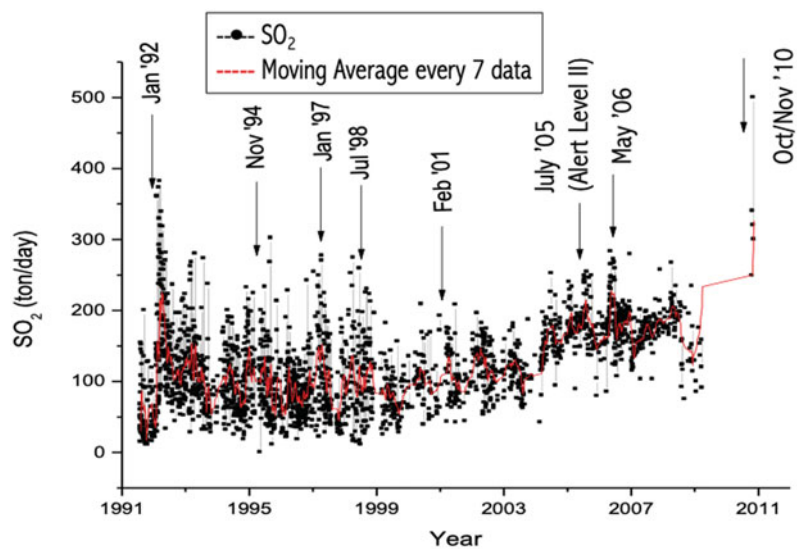
SO₂ emissions and their variations that have been routinely measured at Merapi provide insights into the behaviour of the volcano over longer periods of time. Since 1991, monitoring of SO₂ emissions was conducted from the fumaroles in the summit area and the former Gendol and Woro fumarole fields, using a correlation spectrometer (COSPEC) and differential optical absorption spectroscopy (DOAS), complemented by satellite remote sensing during explosive activity. Measurements were made almost daily when the weather permitted, especially in the dry season. Results indicate that SO₂ emissions averaging >100 tons/day coincide with an increase of activity at Merapi and that before every eruption, the SO₂ gas emission of Merapi increases (Fig. 12.10). Prior to the eruption in early 1992, a sharp increase from an average of 50 tons/day to >200 tons/day was observed, with a maximum SO₂ gas emission >300 tons/day, similar to the

eruptions in November 1994, January 1997 and July 1998. Long-term variations in the SO₂ concentration at Merapi are noticed, for example, between 1991 and 1998, when the SO₂ concentration decreased slightly. By contrast, from 1999 to 2010, the trend changed to a significant increase of the SO₂ concentration in the emitted gases (Fig. 12.10).

12.3.4 Physical Processes Prior to the Eruption

The topography of the summit area of Merapi prior to the 2010 eruption was dominated by the lava dome that extruded after the large dome collapse events in June 2006 (Ratdomopurbo et al. 2013). Therefore, the state of a shallow part of the conduit allowed higher pressure to build up than during the 2006 eruption (Aisyah et al. 2018). The location of the pressure source was estimated at 2 km beneath the crater (see Aisyah et al. 2018). Magma began to inject into the shallow reservoir at a depth of 2 km below the summit in April 2009, and the pressure of the reservoir increased to 150–200 MPa on 15 October 2010 (Fig. 12.11a). VT earthquakes were clustered (Budi-Santoso et al. 2013) below and above the shallow magma reservoir. The

Fig. 12.10 SO₂ emissions of Merapi from 1991 to 2010



increase in VT earthquakes was reflected by an increase in pressure of the shallow reservoir, causing inflation of the ground around the summit and movement of a block south-eastward. The block corresponds to one of the biggest lava domes which filled the east part of the large Mesdjidlanama crater in 1911 (East Dome). Inflation of the shallow reservoir increased the instability of the East Dome, the base of which corresponded to a deeper discontinuity.

Magma injection continued on 15 to 20 October 2010, increasing the pressure of the shallow reservoir to 200–250 MPa (Fig. 12.11b), and causing inflation of the ground around the summit and south-eastward movement of the 1911 lava dome. Magma injection accelerated on 20 October 2010 resulting in an estimated increase in pressure to 400–450 MPa (Fig. 12.11c). The acceleration continued until immediately before the onset of the explosive eruption on 26 October (Fig. 12.11d), when the pressure reached 450–500 MPa, about 4 times higher than in 2006. The explosivity of the 26 October events at the onset of the eruption, with ballistic bombs ejected up to 2 km and PDCs reaching 6.8 km from the summit, is therefore inferred to have been caused by a highly pressurised shallow magma reservoir (Aisyah et al. 2018).

12.4 Volcanic Deposits of the 2010 Eruption

During the multistage 2010 eruption, distinct volcanic deposit types were formed as the eruption progressed (Fig. 12.12). Following a description of types, volume and distribution of the 2010 volcanic deposits, we use the detailed framework of eruption stages proposed by Komorowski et al. (2013) to link the volcanic deposits to the eruption chronology, before discussing the generation, dynamics and significance of high-energy PDCs, which may well represent the first, well-documented examples of blast-like PDCs at Merapi (Komorowski et al. 2013; see Gertisser et al. 2023a, Chap. 1).

12.4.1 Types, Volume and Distribution of the 2010 Volcanic Deposits

Volcanic deposits of the 2010 eruption were associated with a range of volcanic phenomena, including vertical and directed explosions, eruption column or fountain collapse, lava dome extrusion, dome explosion, dome collapse, rockfalls and tephra (ash) fall (Surono et al.

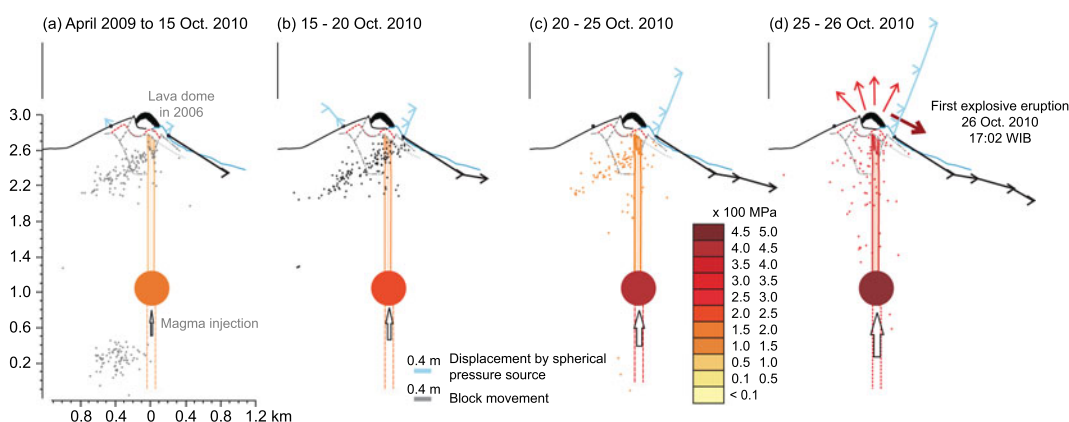


Fig. 12.11 Ascent and storage of magma and block movement prior to the 2010 eruption. Dots represent hypocentres of volcano-tectonic (VT) earthquakes, light blue vectors show displacement caused by a spherical pressure source and black vectors display southward

block movement. The thick dark red arrow shows the southward directed explosions on 26 October 2010, while the thinner red arrows indicate explosive eruption phases between 26 October and 5 November 2010

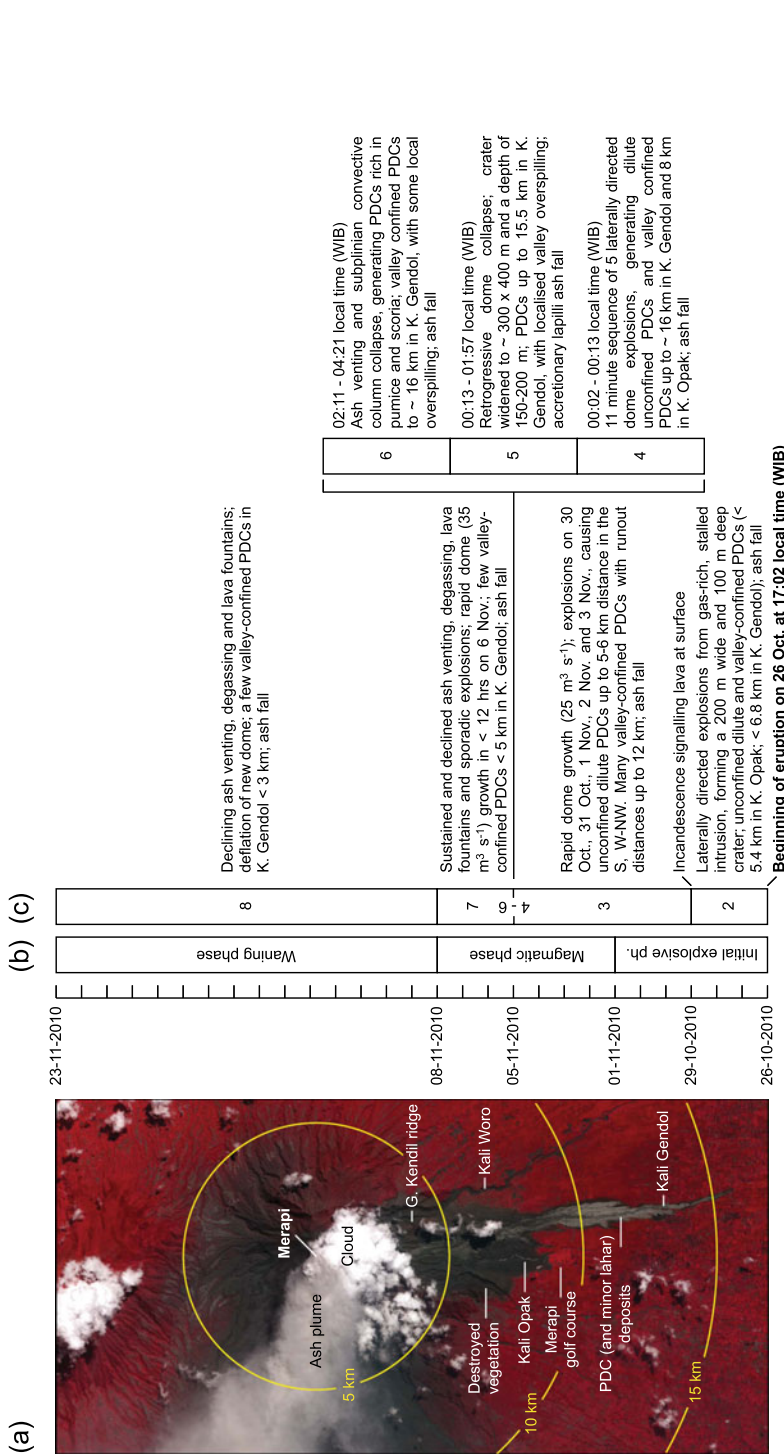


Fig. 12.12 a ASTER false-colour satellite image from 15 November 2010, showing pyroclastic density current (PDC) deposits filling the valleys of Kali Gendol and Kali Opak on Merapi's south flank (light grey). Fluvial erosion of the deposits in Kali Gendol had already set in, producing lahars. The dark grey area north of the Merapi Golf course was affected by dilute unconfined PDCs, causing almost total devastation. PDCs also fill the valley of Kali Woro. The bright red areas were unaffected by PDCs and consist of healthy vegetation. An ash plume is drifting away from the volcano to the west, causing ash fall in the dull red to grey area on Merapi's western slopes. *Source* NASA Earth Observatory (Digital Globe—November 2010). **b-c** Eruption timeline, with eruption stages since the beginning of the eruption on 26 October 2010 based on **(b)** Surono et al. (2012) and **(c)** Komorowski et al. (2013). The latter includes a description of the eruptive activity and deposits at each stage

2012; Charbonnier et al. 2013; Cronin et al. 2013; Komorowski et al. 2013; Preece 2014; Preece et al. 2016). Lahars occurred during and immediately after the eruption from remobilisation of primary pyroclastic deposits mainly during Indonesia's rainy season and continued for several years (de B elizal 2013).

As during other recent Merapi eruptions, generation of PDCs was ubiquitous, with PDCs having been produced during all eruption stages (Charbonnier et al. 2013; Cronin et al. 2013; Komorowski et al. 2013; Preece 2014; Preece et al. 2016). However, due to the complexity of the 2010 eruption, the PDCs were characterised by marked differences in deposit characteristics, distribution and dynamics, and included: (1) massive, concentrated and block-rich valley-confined PDCs or block-and-ash flows (BAFs) that formed by gravitational lava dome failure, (2) lobate overbank PDC deposits resulting from overspilling of the massive, concentrated and block-rich valley-confined PDCs onto interfluvial areas and into adjacent valleys (fast and slow overspill flows; Lerner et al. 2021), (3) dilute unconfined PDCs or surges that formed by detachment from valley-confined massive, concentrated and block-rich PDCs and by laterally directed explosions from a gas-rich, shallow intrusion or cryptodome (low-energy detached surges; Lerner et al. 2021), (4) pumice-rich PDCs generated by the collapse of explosive, pumice-rich eruption columns, and (5) unconfined, turbulent high-energy PDCs, distinct from the dilute unconfined PDCs or surges described above, which were among the most striking volcanic phenomena of the eruption (high-energy surges; Lerner et al. 2021).

The 2010 eruption was considerably larger than other recent and historical Merapi eruptions. Initial estimates (Surono et al. 2012) suggested a bulk deposit volume of $\sim 40\text{--}80 \times 10^6 \text{ m}^3$, consisting of $\sim 30\text{--}60 \times 10^6 \text{ m}^3$ of juvenile material and an additional $\sim 10\text{--}20 \times 10^6 \text{ m}^3$ of non-juvenile material derived from the summit. Based on field studies and a multi-temporal dataset of high-resolution satellite imagery, Charbonnier et al. (2013) determined a bulk PDC deposit volume of $\sim 36.3 \times 10^6 \text{ m}^3$, which is at

the lower end of the range proposed by Surono et al. (2012) and similar to the $\sim 40 \times 10^6 \text{ m}^3$ estimated by Bignami et al. (2013), based on synthetic aperture radar (SAR) data. Both estimates do not include deposits other than those on the south flank and must therefore be regarded as minimum values. They are slightly lower than the PDC bulk volume estimates of $\sim 41 \times 10^6 \text{ m}^3$ (Komorowski et al. 2013) and $48.6 \times 10^6 \text{ m}^3$ (Cronin et al. 2013). According to Charbonnier et al. (2013), the total volume is distributed between valley-confined deposits (50.2%), overbank deposits (39.3%), as well as surges and fallout tephra (10.5%). An estimated >70% of the deposits were generated on 4–5 November, and only 28.1% and 0.9% formed prior to and after 5 November, respectively. Solikhin et al. (2015) proposed a bulk PDC deposit volume of $\sim 45 \times 10^6 \text{ m}^3$ in the south, south-west, west and north-west sectors, and a bulk tephra-fall deposit volume of $\sim 18\text{--}21 \times 10^6 \text{ m}^3$. The authors estimated that the Gendol and Opak catchments on the south flank contained about 10–15% of the total tephra-fall and 65–70% of the PDC deposit bulk volume. Overall, the published estimates of the bulk volume of the 2010 deposits range from $\sim 36.3\text{--}80 \times 10^6 \text{ m}^3$. These estimates indicate a bulk deposit volume at least ~ 4 times (and possibly up to ~ 9 times) larger than, for example, that of the preceding eruption in 2006 ($\sim 8.7 \times 10^6 \text{ m}^3$; Charbonnier and Gertisser 2011). About $5 \times 10^6 \text{ m}^3$ of the juvenile material erupted in 2010 was derived from the main 2010 lava dome that formed over several days prior to its destruction on 5 November (Surono et al. 2012; Komorowski et al. 2013; Pallister et al. 2013).

With the significantly larger bulk deposit volume compared to previous eruptions has come a much wider distribution of the 2010 pyroclastic deposits (Fig. 12.13). The 2010 PDC deposits covered an estimated area between $\sim 22.3 \text{ km}^2$ (Charbonnier et al. 2013) and $\sim 33.9 \text{ km}^2$ (Cronin et al. 2013) or, when areas outside the south flank are considered, $\sim 35 \text{ km}^2$ (Solikhin et al. 2015). The high-energy PDCs generated on 5 November spread over $\sim 22 \text{ km}^2$ with a runout distance of ~ 8.4

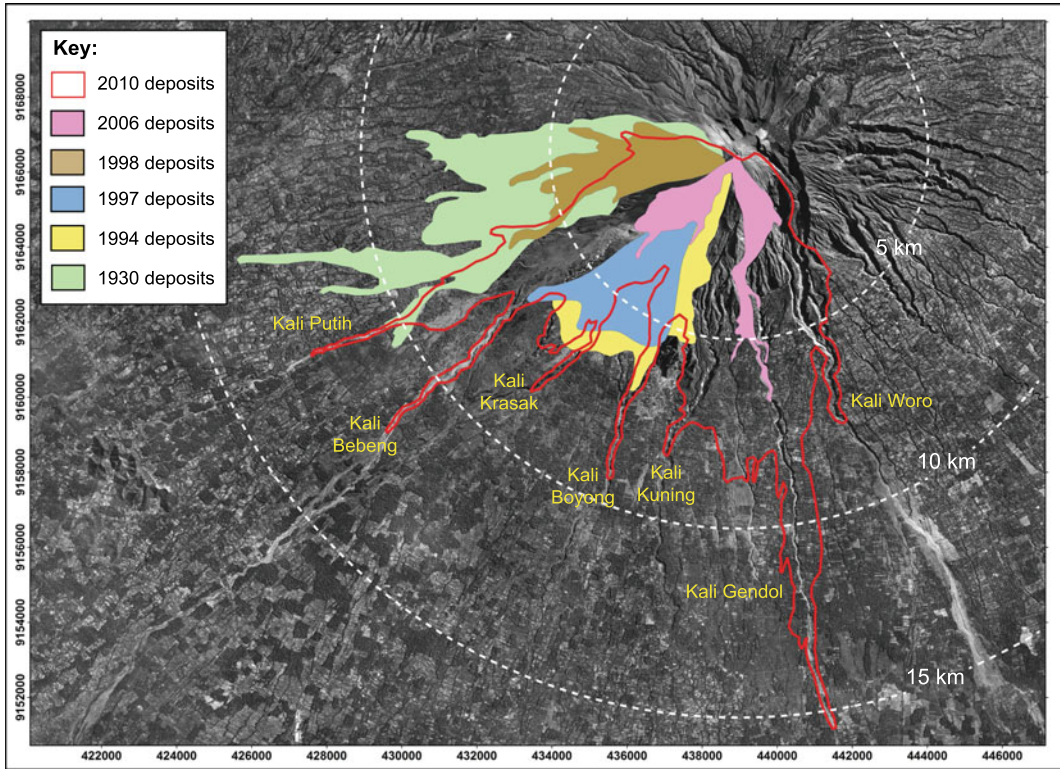


Fig. 12.13 Areas covered by PDC deposits from the 2010 and other recent Merapi eruptions since 1994 as well as from the most devastating historical eruption in 1930.

Circles mark areas within 5, 10 and 15 km radius from the summit of Merapi. The map coordinates are in UTM metres. After Gertisser et al. (2011)

km (Komorowski et al. 2013), while tephra fall deposits covered an area of 1300 km² (Solikhin et al. 2015). The majority of the PDC deposits inundated areas on Merapi's south flank, where they reached a runout distance of ~15.5 to 16.1 km in Kali Gendol on 5 November (Charbonnier et al. 2013; Cronin et al. 2013; Komorowski et al. 2013), approximately twice as long as during the previous eruption in 2006 (Charbonnier and Gertisser 2008). In other valleys, such as Kali Opak, PDC runout distances were typically <10 km. The large volume, significantly exceeding that of previous recent and historical Merapi BAFs, has been regarded as one of the controlling factors explaining the long runout distances reached by the 2010 PDCs (Cronin et al. 2013), although other causes, such as previous valley infilling and reduction in channel capacity, PDC generation mechanisms at the source or the transport regime, where currents

produce a near-frictionless basal region by air lubrication (Lube et al. 2019), may have also played a role.

12.4.2 Volcanic Deposits Linked to Eruption Chronology

Most of the deposits described in this section are from the most affected area on Merapi's south flank. Correlated stratigraphic sections of the 2010 deposits, linked to the eruption stages of Komorowski et al. (2013) (Fig. 12.12), are shown in Fig. 12.14.

The first eruption deposits were related to partially laterally (southward) directed explosions on 26 October, which generated dilute PDCs (surges) that spilled over the upper Gendol valley and propagated towards Kinahrejo (Gertisser et al. 2011; Charbonnier et al. 2013; Cronin

(a)

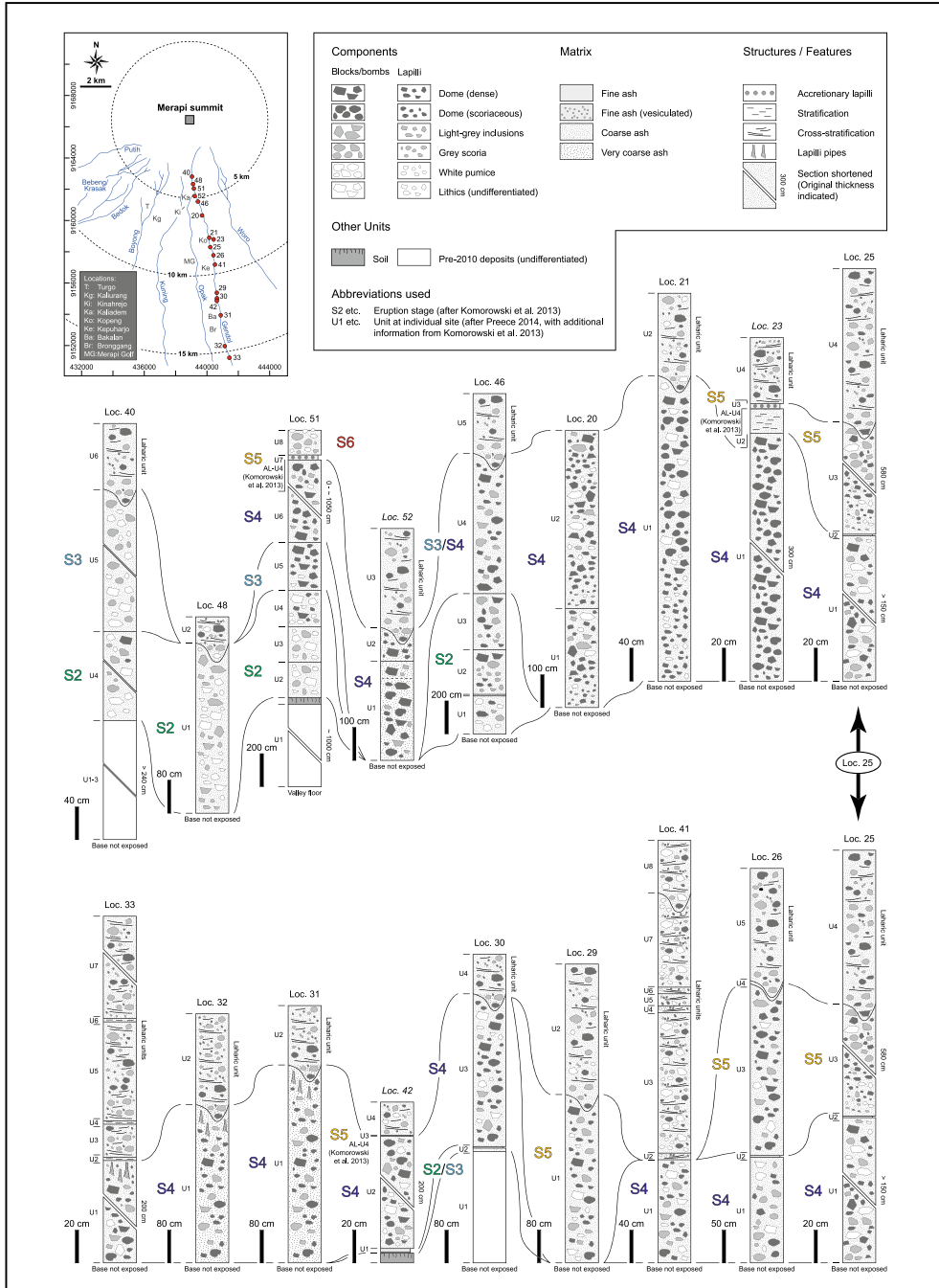


Fig. 12.14 a Correlated stratigraphic sections of the 2010 eruption deposits in the Gendol river valley (Kali Gendol), arranged from N (locality 40) to S (locality 33). Stratigraphic sections on interfluve areas adjacent to the main valley are indicated in italics. **b** Correlated stratigraphic sections of predominantly unconfined 2010

Merapi deposits in the southwestern and southern sector of the volcano, arranged from W (locality 49) to E (locality 22). Eruption stages (e.g. S4) after Komorowski et al. (2013). Detailed descriptions of the stratigraphic sections (including individual units; U) can be found in Preece (2014). After Preece et al. (2016)

(b)

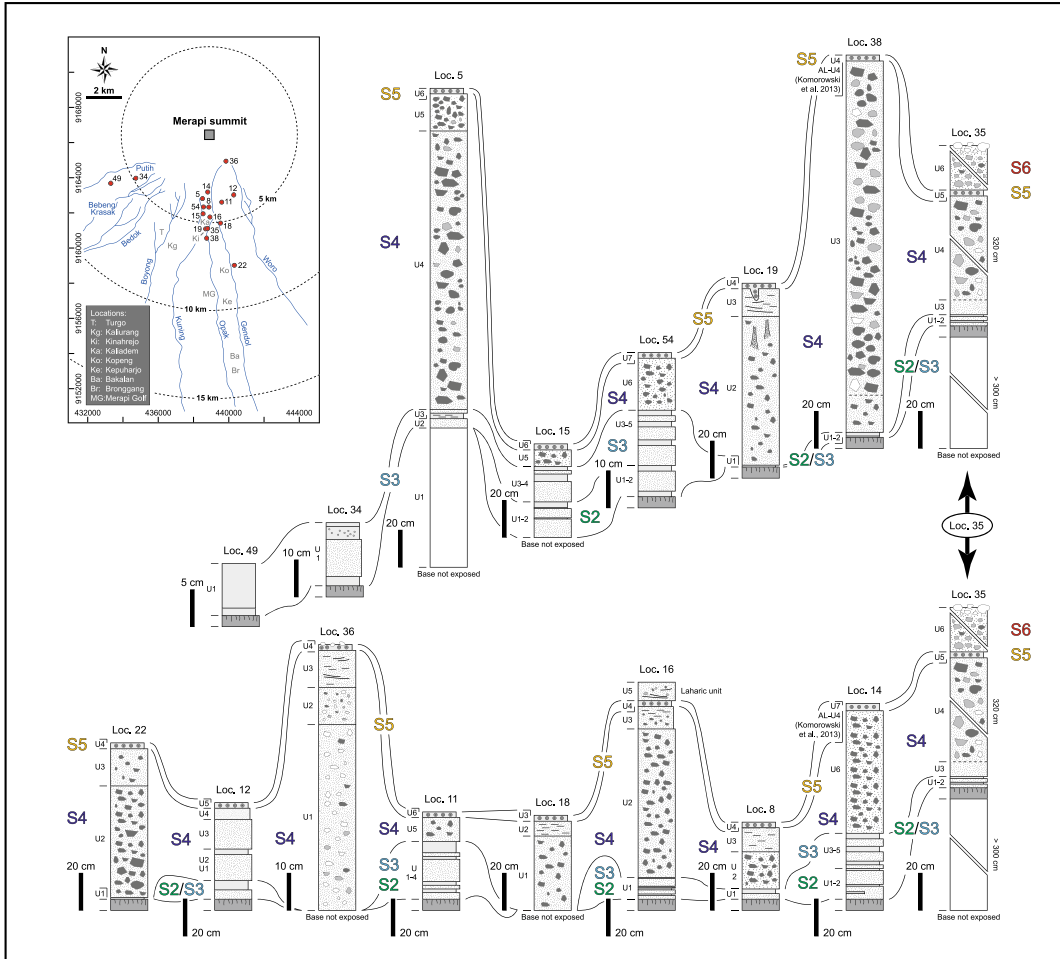
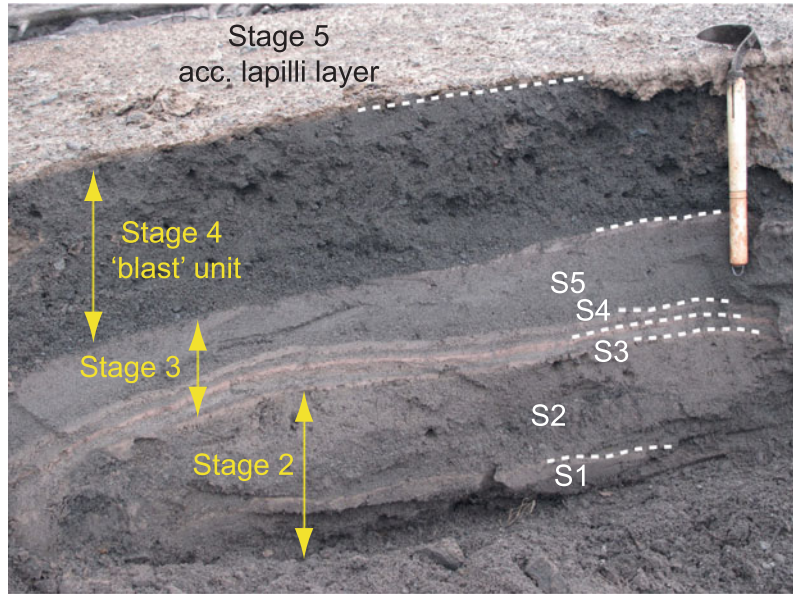


Fig. 12.14 (continued)

et al. 2013; Komorowski et al. 2013), and to subsequent explosive activity and partial lava dome collapse prior to the eruption climax on 5 November that affected a similar area (eruption stages 2 and 3; Komorowski et al. 2013). In and around Kinahrejo, up to 5 dilute PDCs occurred during these two stages, with each of these emplacing a unit consisting of two layers (Fig. 12.15). Typically, the lower layer is composed of massive, grey-coloured or ‘salt and pepper’ coarse ash to fine lapilli, comprised of scoriaceous, pumiceous or dense clasts (Charbonnier et al. 2013; Cronin et al. 2013; Komorowski et al. 2013; Preece 2014; Drignon et al.

2016; Preece et al. 2016). The upper layer is usually a brown-orange or grey coloured fine ash, which is often stratified. The coarser basal layer is interpreted to have formed via emplacement of the dilute PDC, with the upper fine ash layer emplaced due to ash settling from the accompanying ash cloud. Although valley-confined stage 2 and stage 3 PDCs or BAFs, such as those in the Gendol river valley (Kali Gendol), were buried by subsequent flows, some were already exposed a few weeks after the eruption due to fluvial erosion (Fig. 12.16). Correlation between valley-confined and unconfined PDC deposits (Fig. 12.14) was aided by

Fig. 12.15 Section on Merapi's south flank north of Kinahrejo (see Fig. 12.13) composed of 5 surge units formed during stages 2 and 3, all with a coarser lower layer and a fine ash upper layer. Above the surges is the stage 4 high energy PDC unit, topped by stage 5 accretionary lapilli-bearing ash. Scraper for scale (length: 35 cm). See text for further details. After Preece (2014)



stratigraphic position and comparable clast componentry, including the presence of non-juvenile, hydrothermally altered and accidental lithics, as well as light grey dense crystalline clasts, abundant grey scoria and occasional white pumice. The presence of scoriaceous and pumiceous clasts in at least two depositional units related to the 26 October deposits and pumice levees in unconfined and valley-confined PDC deposits near the base of the 2010 eruption sequence (Charbonnier et al. 2013; Komorowski et al. 2013; Preece 2014; Drignon et al. 2016; Preece et al. 2016), and the energetic nature of the surges (Cronin et al. 2013), suggests that fresh (juvenile) magma had already been involved in the initial explosions.

At the climax of the eruption, a series of deposits was produced over a period of a few hours in the early hours (local time; WIB) of 5 November (eruption stages 4, 5 and 6; Komorowski et al. 2013). During the most intense eruption phase, corresponding to eruption stage 4 (Komorowski et al. 2013), a series of paroxysmal dome explosions and collapses occurred in a matter of minutes (Fig. 12.12). These produced high-energy, dilute PDC (surge) deposits, valley-confined BAFs and associated overbank deposits (Fig. 12.16), which were generated via the

breakout of confined flows onto interfluvial areas (Charbonnier et al. 2013; Cronin et al. 2013; Komorowski et al. 2013). The high-energy PDC deposits have bi-partite layering (Fig. 12.17a), with the lower layer coarser than the upper one. The lower layer is clast-supported, fines-depleted, consisting mostly of lapilli, but may also contain blocks or bombs, sometimes up to ~20 cm in diameter, replaced distally by coarse ash. The upper unit is composed of fine to coarse ash, which sometimes has wavy cross- and planar-stratification (Fig. 12.17b). Lapilli pipes are often present, originating from the top of the lower unit (Preece 2014). Komorowski et al. (2013) identified two high-energy PDC units (termed U1 and U2) produced by two paroxysmal explosions, both with bi-partite layering (U1-L1, U1-L2, U2-L1 and U2-L2). Both units are similar and were distributed over a similar area, although Unit 2 is typically finer grained, thinner, and outcrops are less abundant. While the two paroxysmal explosions generated these unconfined dilute PDC deposits, channelling of the basal, high particle concentration portion of the PDCs resulted in emplacement of valley-confined BAFs and unconfined (overbank) flows. The valley-confined BAFs are massive, poorly sorted and often reversely graded (Charbonnier et al. 2013). They



Fig. 12.16 Valley-confined and overbank PDC (block-and-ash flow; BAF) deposits and some of their features. **a** BAF deposits filling the Gendol river valley (Kali Gendol); view north from Kaliadem towards Merapi. **b** Buried by subsequent flows from stage 4/5, stage 2 and stage 3 BAF deposits were already exposed in Kali Gendol a few weeks after the eruption due to fluvial erosion. The valley side is approximately 15 m high. Photograph taken near Kaliadem. **c** Partly eroded and still hot BAF deposits in the medial reaches of Kali Gendol around Kepuharjo. **d** Fumarole pipe at the surface of a BAF deposit, formed from continued degassing of the hot

deposit following emplacement. Hammer for scale. **e** Reversely graded BAF deposit from stage 4/5 near Kopeng. **f** Randomly orientated friction marks (Schwarzkopf et al. 2001) on a block within the 2010 BAF deposits, resulting from tumbling and sliding of blocks during flow transport. Field of view is 40 cm wide. **g** Vast area on the western side of Kali Gendol near Kepuharjo covered by overbank PDC deposits. **h** Close-up of overbank PDC deposits near Kepuharjo, illustrating their poorly sorted nature, with clasts up to a few decimetres in size. For locations, see Fig. 12.14. *Photo credit* R. Gertisser, K. Preece

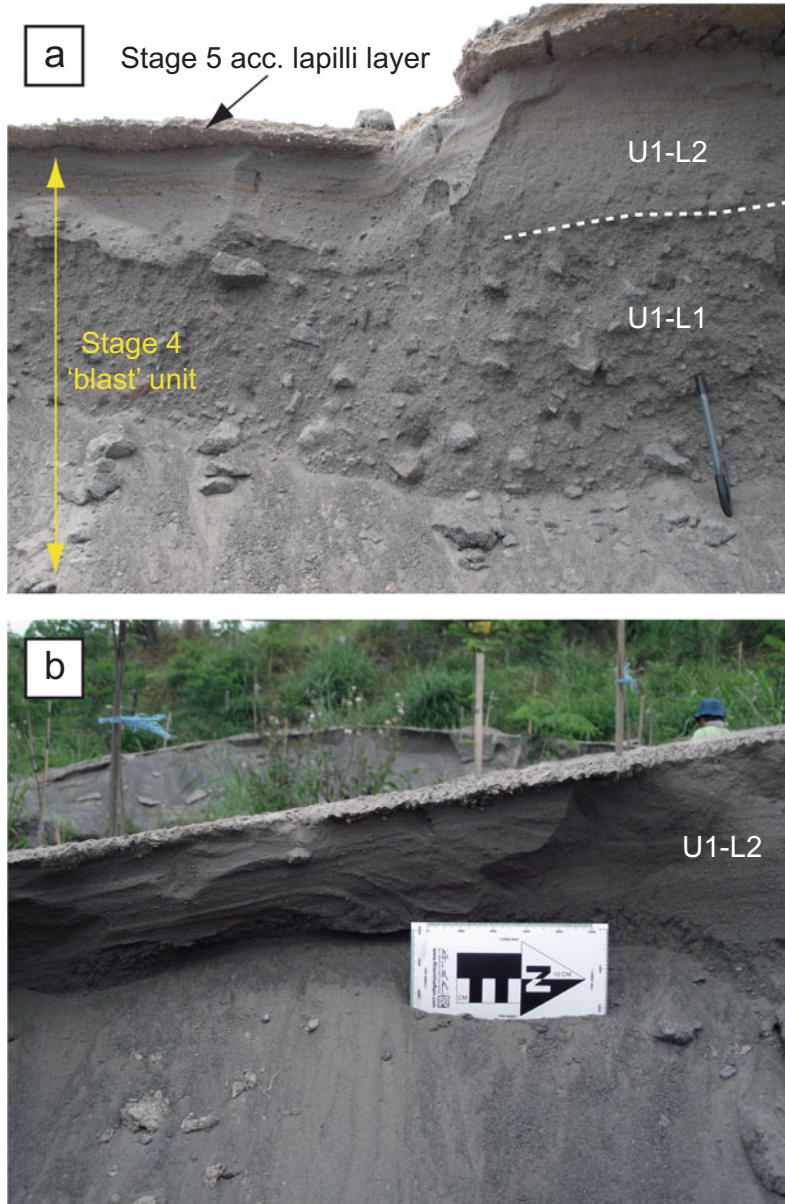


Fig. 12.17 **a** Stage 4 high-energy PDC unit with bi-partite layering, characterised by a coarse lower layer and a finer grained upper layer. The lower and upper layers correspond to units U1-L1 and U1-L2 of Komorowski et al. 2013. The unit is overlain by stage 5 accretionary lapilli-bearing ash.

Pen for scale (length: 15 cm). **b** Upper layer of high-energy PDC deposit (unit U1-L2; Komorowski et al. 2013) showing cross stratification. Photo scale (length: 12 cm). Both photographs were taken around Kinahrejo. For location, see Figs. 12.1 and 12.14. *Photo credit* K. Preece

may contain lapilli pipes formed via post-depositional gas escape, carbonised plant material, are frequently encrusted with sublimates, and may be oxidised towards the top. The deposits from the climactic phase of the eruption are almost

monolithological, in that their componentry is dominated by dark grey to black, dense fragments of the fast growing, pre-climax lava dome (Fig. 12.18a) that was destroyed by the cataclysmic explosions (stage 4; Komorowski et al.

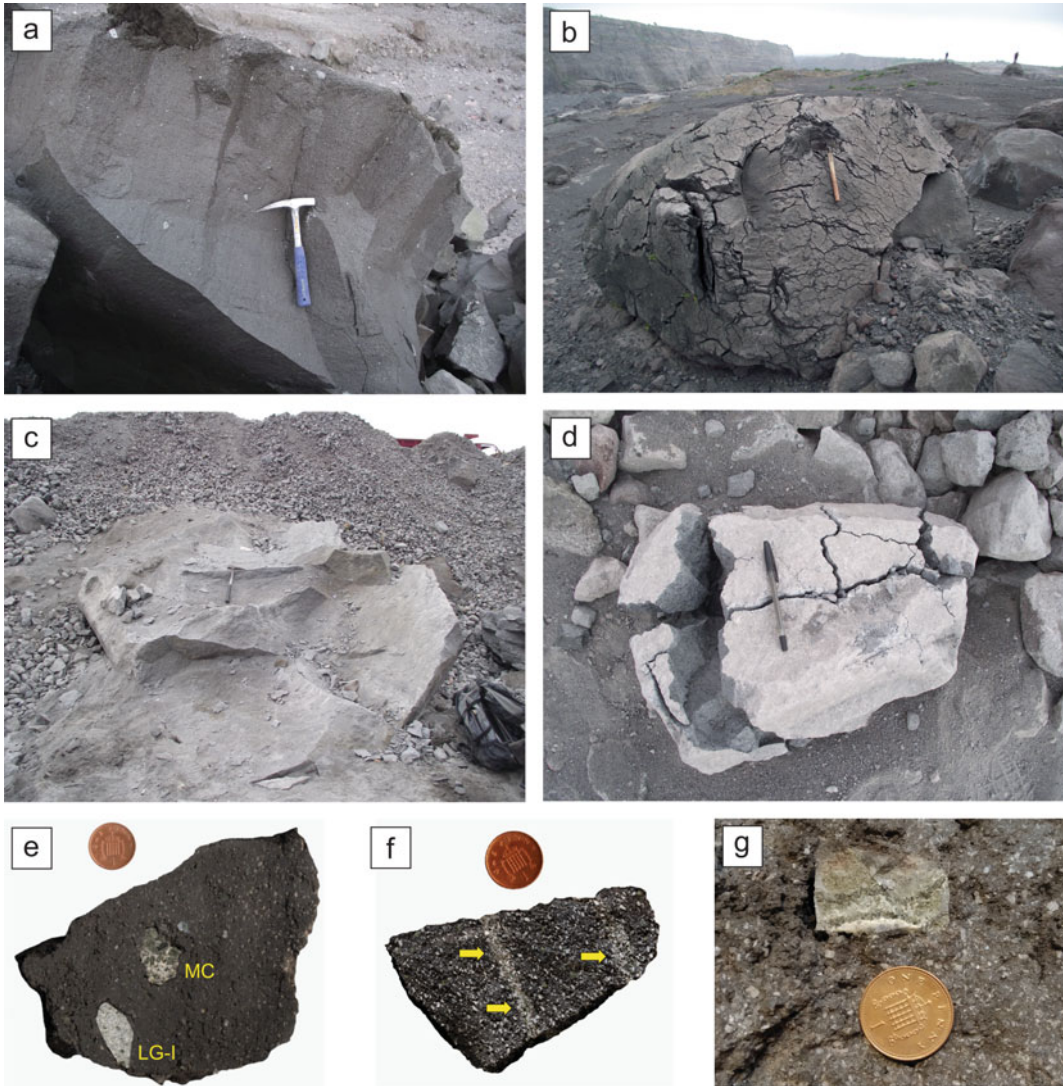


Fig. 12.18 Characteristic lithologies of stage 4 deposits in Kali Gendol and adjacent areas (see Fig. 12.14). **a** Dark dense fragment of the main 2010 lava dome, the principal component of stage 4 PDC deposits. Hammer for scale (length: 28 cm). **b** Rare lava dome block with breadcrust texture. Scraper for scale (length: 35 cm). **c** Highly crystalline block of light grey dense basaltic andesite. Hammer for scale (length: 40 cm). **d** Prismatic jointed

block of light grey dense basaltic andesite. Pen for scale (length: 15 cm). The light grey dense basaltic andesite also occurs as **e** inclusions (LG-I), and **f** streaks or bands within the 2010 dome lava, along with inclusions of **e** plutonic xenoliths (magmatic cumulates; MC) and **g** crustal carbonate (calc-silicate) xenoliths. Coin for scale (diameter: 2 cm). *Photo credit* R. Gertisser, K. Preece

2013) on 5 November. Dark grey to black scoriaceous fragments and rare blocks with breadcrust texture from the same lava dome also occur within the stage 4 PDC deposits, along with blocks (up to several metres in diameter) of light grey dense rock fragments (Fig. 12.18b, c). Many of the latter

are prismatic jointed, signifying that they were hot at the time of eruption, and therefore originate from the eruption (Fig. 12.18d). Light grey dense crystalline material has also been found as abundant inclusions within the juvenile dome material (Fig. 12.18e). These inclusions range in size from

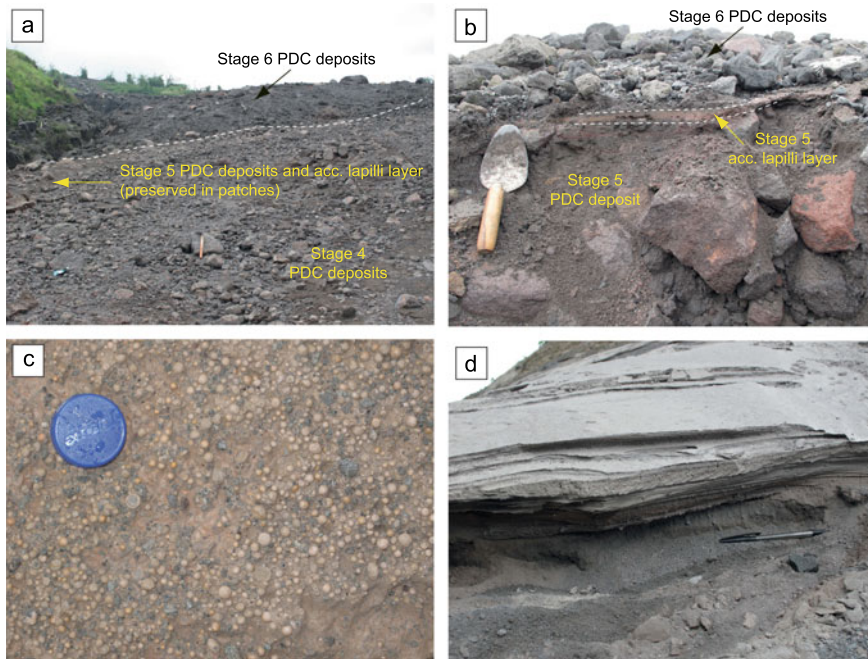


Fig. 12.19 Stage 5 and 6 deposits and their lithological characteristics. **a** Stage 5 and 6 deposits, emplaced stratigraphically above stage 4 flows around Kinahrejo. Scraper for scale (length: 35 cm). **b** Overbank deposits around Kinahrejo, including stage 5 red-pink PDC and accretionary lapilli-bearing ash layer below stage 6 PDC (scoriaceous and pumiceous flow) deposits. Trowel for scale (length: 20 cm). **c** Close-up of the distinctive orange

accretionary lapilli-bearing ash layer stratigraphically above the stage 4 high-energy PDC deposits north of Kinahrejo. Bottle lid for scale (diameter: 4 cm). **d** Dilute PDC (surge) layers north of Gunung Kendil containing poorly vesicular pumice lapilli. Pen for scale (length: 15 cm). For locations, see Figs. 12.1, 12.12 and 12.14. *Photo credit K. Preece*

a few millimetres to a several centimetres and have angular shapes, indicating brittle deformation of the light grey material, although occasionally it forms wavy bands through the dome material, indicating ductile behaviour (Fig. 12.18f). The light grey dense material has been interpreted to originate from a ‘plug’ of cooled, rigid magma that resided at shallow depth within the magmatic system and was partially re-heated, fragmented and incorporated the juvenile 2010 magma (Preece 2014; Preece et al. 2016). Other inclusions within the 2010 dome rocks comprise plutonic xenoliths or magmatic cumulates (Fig. 12.18e), which are composed of coarse-grained plagioclase, amphibole and clinopyroxene and interpreted to originate deep within the Merapi system (see Troll and Deegan 2023, Chap. 8), along with calc-silicate xenoliths (e.g. Preece 2014; Whitley et al. 2019, 2020; Deegan et al. 2023, Chap. 10). Formed by interaction of the 2010 magma with the

surrounding crustal carbonate rocks underlying the volcano, the calc-silicate inclusions are dominated by wollastonite and diopside, giving them a characteristic green and white colour (Fig. 12.18g).

Later on 5 November, during eruption stage 5 of Komorowski et al. (2013), the volcanic activity consisted of a series of retrogressive summit dome collapses followed by a brief eruptive lull of less than 15 min (Fig. 12.12). The summit collapses produced BAFs consisting of variable components, including dense and scoriaceous 2010 lava dome clasts, light grey dense clasts, as well as variable non-juvenile lithics (Fig. 12.19a, b). The deposits often have a distinctive reddish-pink colour. The eruptive lull at the end of stage 5 allowed for the deposition of a layer consisting of orange-pink coloured fine ash with abundant accretionary lapilli (Fig. 12.19b, c). This accretionary lapilli layer formed a distinctive marker

horizon across the southern flanks of Merapi either stratigraphically above the stage 5 BAFs in the valleys or above the stage 4 ‘directed blast’ deposits on interfluvial areas.

The last phase at the eruption climax on 5 November 2010 consisted of ash venting and recurrent fountain collapses (stage 6; Komorowski et al. 2013) (Fig. 12.12), generating PDCs rich in grey scoriaceous or white pumiceous clasts, deposited stratigraphically above stage 5 deposits in Kali Gendol and the adjacent interfluvial areas (Fig. 12.19a, b) (Komorowski et al. 2013; Preece 2014; Preece et al. 2016). Stage 6 deposits related to fountain collapse also contain minor amounts of juvenile lava dome fragments as well as various non-juvenile lithics. Where the stage 5 orange-pink accretionary lapilli-rich ash layer had been preserved, stage 6 deposits were readily identified in the field above this distinct marker horizon. Scattered on the surface of the scoria-rich flow deposits in and around Kali Gendol are abundant conspicuous juvenile white pumice clasts, interpreted to be associated with stage 6 Vulcanian to sub-Plinian fountain-collapse pumice-rich PDCs on 5 November, some of which may have reached distances of up to ~16 km in the Gendol valley (Komorowski et al. 2013). Juvenile white pumice lapilli were also found on the ridges north of Kinahrejo, where it was dispersed on the surface of the stage 5 accretionary lapilli-rich ash layer, scattered around the surface near to the Kinahrejo ‘Forest Gate’, as well as being found in reworked deposits in Kali Putih on the southwest flank of Merapi. Another type of poorly vesicular and low-K (see below) white pumice lapilli were discovered distributed on top of proximal dilute PDC deposits on a ridge north of Gunung Kendil and in Kali Putih (Preece 2014) (Fig. 12.19d).

After the climactic eruption phase on 5 November, the activity was characterised by ash venting, sporadic explosions and lava fountains (eruption stages 7 and 8; Komorowski et al. 2013). Renewed rapid lava dome growth in less than 12 h on 6 November was associated with occasional valley-confined PDCs with runout distances up to 5 km, directed towards Kali Gendol (Komorowski et al. 2013). Declining ash venting,

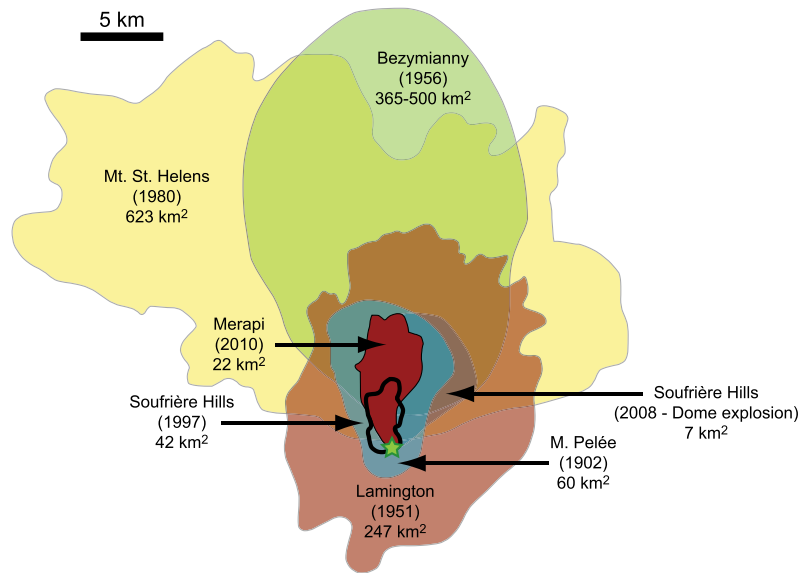
intermittent explosions and lava fountains, deflation of the new dome, and a few valley-confined PDCs with runout distances of less than 3 km in Kali Gendol continued until 23 November (Komorowski et al. 2013). Rain-triggered, syn-eruptive lahars also occurred during this period.

12.4.3 Generation, Dynamics and Significance of High-Energy Pyroclastic Density Currents

The recognition of high-energy PDCs is regarded as one of the most significant findings related to the 2010 volcanic deposits of Merapi. Interpreted as blast-like PDCs (Komorowski et al. 2013), the deposits of the high-energy PDCs generated during the peak of the eruption on 5 November and their impact on infrastructures, buildings and trees are strikingly similar to those from historical ‘directed blasts’ from Montagne Pelée, Martinique (1902), Mount Lamington, Papua New Guinea (1951), Bezymianny, Russia (1956), Mount St. Helens, USA (1980) and Soufrière Hills, Montserrat (1997) (e.g. Taylor 1958; Tanguy 1994, 2004; Clarke and Voight 2000; Sparks et al. 2002; Belousov et al. 2007, 2020). However, both the volume of magma ($>5 \times 10^6 \text{ m}^3$) and the devastated area of the Merapi high-energy PDCs (Fig. 12.20) were smaller than those of these historical volcanic blasts (Komorowski et al. 2013).

While the exact generation mechanism of the 2010 high-energy PDCs has been discussed controversially (Cronin et al. 2013; Komorowski et al. 2013), there is agreement that the high-energy PDCs on 5 November 2010 formed by explosive disintegration of a rapidly growing, unstable lava dome, favoured by rapid ascent of deeper, volatile-rich magma underneath a plugged conduit which limited degassing and induced significant pressurisation in the upper conduit prior to 5 November (Surono et al. 2012; Costa et al. 2013; Cronin et al. 2013; Jousset et al. 2013b; Komorowski et al. 2013; Preece 2014; Drignon et al. 2016; Kushnir et al. 2016, 2017;

Fig. 12.20 Areas devastated by the 2010 Merapi high-energy PDCs, other historical directed blasts and a smaller directed lava dome explosion at Soufrière Hills volcano, Montserrat. After Komorowski et al. (2013)



Preece et al. 2016; Carr et al. 2020). According to Komorowski et al. (2013), the asymmetric collapse phase of the blast was short-lived and transformed into a channelised blast phase downslope, where the dynamics of the unsteady, stratified, gravity-driven currents was strongly influenced by the topography along the flow path. The currents reached heights of ~ 330 m and travelled at velocities of ~ 100 m/s within the first 3 km from the summit. Flow momentum was maintained by the morphology of the upper southeastern slopes, which led to channelling of the currents into a deep valley (Kali Gendol) towards a major constriction downslope leading to a venturi effect after the currents were deflected by the Gunung Kendil ridge (Fig. 12.12). This resulted in increased current velocities and high particle concentrations, promoting avulsion of the currents across ridges and interfluvial areas into adjacent valleys, and generating high dynamic pressures (Jenkins et al. 2013; Komorowski et al. 2013). In total, a ~ 3 – 4 km wide area between Kali Kuning and Kali Woro, extending to the Merapi Golf course ~ 8.4 km from the summit, was affected by the 2010 high-energy PDCs (Komorowski et al. 2013).

The occurrence of high-energy PDCs related to directed explosions or blasts at the source are uncommon at Merapi. Grandjean (1931a, b, c)

suggested that such currents, referred to as Peléean-type, occurred during the 1930 eruption, which wiped out villages on the volcano's western slopes and caused about 1369 fatalities (Siebert et al. 2011). The idea of directed blast-generated PDCs was not accepted indisputably though at the time (Kemmerling 1932; Escher; 1933; Neumann van Padang 1933) and, as such, the 2010 eruption is the first, where unequivocal blast-like, high-energy PDC deposits were identified in Merapi's recent history (Komorowski et al. 2013). Moreover, the 2010 high-energy PDC deposits were the first to be studied comprehensively immediately after deposition using a modern volcanological approach, providing unparalleled insights into generation, transport and depositional mechanisms as well as their impact on the surrounding area and environment (Jenkins et al. 2013; Komorowski et al. 2013). High-energy PDCs generated by laterally directed dome explosions, as observed in 2010, may be a hitherto underestimated hazard of future eruptions at Merapi that pose challenges for eruption forecasts and prediction. The events in 2010 have highlighted that such currents can be associated with rapidly growing or pressurised domes and may occur repeatedly during multistage eruptions (Komorowski et al. 2013).

12.5 Geochemistry and Petrology of the 2010 Eruptive Products

In this section, we classify the 2010 eruptive products based on bulk rock geochemistry, document their petrography and mineral chemistry, and discuss magma storage and the pre-eruptive magmatic processes and their timescales, based on a range of petrological, geochemical and isotopic data.

12.5.1 Rock Types and Classification

The 2010 deposits contain a range of juvenile lithologies, which formed at different stages of the eruption and include clasts of grey scoria lapilli, white pumice lapilli, volcanic ash and dark lapilli to block-size clasts of dense to scoriaceous dome rock of the pre-5 November lava dome (Charbonnier et al. 2013; Komorowski et al. 2013; Preece 2014; Drignon et al. 2016; Preece et al. 2016). The volumetrically most significant juvenile component in the 2010 deposits from the pre-5 November lava dome is macroscopically similar to other recent Merapi domes (Fig. 12.18a) and contains inclusions of various lithologies (Fig. 12.18e, g).

In the total alkali versus silica (TAS) diagram (Fig. 12.21a), the 2010 rocks are classed as basaltic trachyandesite and trachyandesite, while in the K_2O versus SiO_2 classification diagram (Fig. 12.21b), they fall into the high-K basaltic andesite and andesite fields. All 2010 eruptive products contain between 52.6 and 58.1 wt.% SiO_2 , on a volatile-free basis (Preece 2014; Preece et al. 2016) (Fig. 12.21c). Most juvenile components have ~ 54.5 – 55.7 wt.% SiO_2 , similar to the 2006 products and those from other twentieth century dome eruptions (Gertisser et al. 2012b) and fall within the high-K group that has dominated the eruptive products of Merapi since ~ 1900 ^{14}C y BP (Gertisser and Keller 2003; Gertisser et al. 2012b, 2023b, Chap. 6). The light grey dense inclusions in the dome rocks generally have less SiO_2 -rich compositions (~ 52.6 – 55.0 wt.% SiO_2) and the ash sampled from surge and fall deposits is generally more

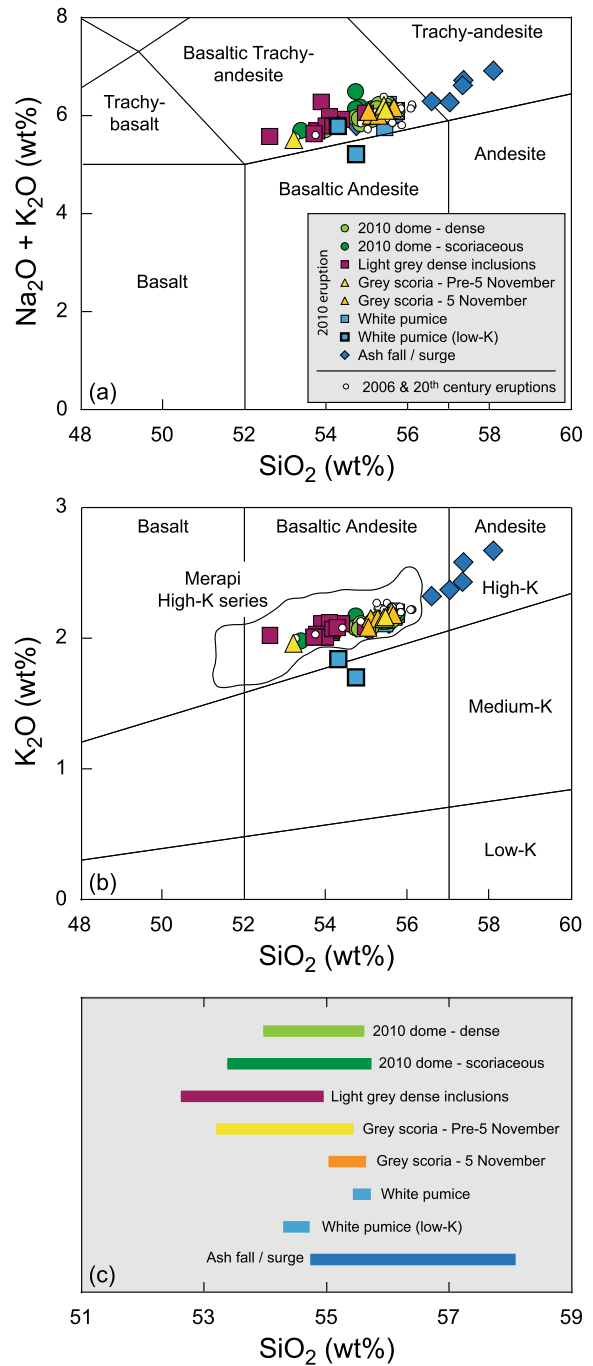
SiO_2 -rich (55.1–58.1 wt.% SiO_2), extending into the trachyandesite and high-K andesite field, respectively (Fig. 12.21a). Selected bulk-rock major element analyses of the 2010 eruptive products are presented in Table 12.2.

12.5.2 Petrography and Mineral Chemistry

The magmatic products of the 2010 eruption, including the 2010 dome lava and light grey dense inclusions, are seriate to porphyritic, with phenocrysts (2000–500 μm ; size range following Preece 2014) and microphenocrysts (500–50 μm) set in a groundmass that may be predominantly crystalline (microlites < 50 μm) or contain abundant glass (Fig. 12.22a–c). The mineral cargo typically includes plagioclase (and alkali) feldspar, clinopyroxene, orthopyroxene, amphibole, which may be megacrystic, Fe-Ti oxides and accessory apatite. Coarse-grained plutonic xenoliths (magmatic cumulates) in the pre-5 November dome are dominated by plagioclase, clinopyroxene and amphibole (Fig. 12.22d). Additionally, cristobalite and biotite are present in the light grey inclusions in the 2010 lava dome (Fig. 12.22e, f) (Costa et al. 2013; Preece 2014). There are large variations in mineral size, textures and compositions as summarised below from Preece (2014), with additional data from Costa et al. (2013) and Li et al. (2021), as indicated.

Feldspar is always present as phenocrysts, microphenocrysts and microlites. Phenocrysts and microphenocrysts are wide ranging in composition between $An_{25}Ab_{70}Or_5$ and $An_{91}Ab_9Or_{<1}$ (Fig. 12.23a-I). Phenocrysts may be normally, reversely or oscillatory zoned, have sieve-textured cores or have very high-An (up to An_{91}) unzoned cores, with lower-An rims. Rims often contain ~ 40 – 50 mol.% An. Microlites are generally more albitic but may contain up to ~ 84 mol.% An. Plagioclase microlites are often mantled by alkali element-rich rims of anorthoclase and more K-rich alkali feldspar (sanidine). Microlite compositions range from $An_1Ab_{41}Or_{58}$ (alkali feldspar) to $An_{84}Ab_{16}Or_{<1}$ (plagioclase) (Fig. 12.23a-II). Microlites from all

Fig. 12.21 **a** Total alkali versus SiO₂ (TAS) and **b** K₂O versus SiO₂ classification diagrams (Le Maitre et al. 2002) for the 2010 eruptive products. The dashed outline in **b** denotes the compositional field of the Merapi high-K series, as defined by Gertisser et al. (2012b). **c** SiO₂ range of the different lithologies erupted in 2010. All analyses are recalculated to 100 wt%, free of volatiles. *Data sources* 2010 eruption (Preece 2014; Preece et al. 2014); 2006 and twentieth century eruptions (Gertisser et al. 2012b; Preece et al. 2013)



lithologies possess a similar overall range of compositions, however white pumice microlites are generally more albitic and those from the light grey inclusions are predominantly alkali-rich.

Clinopyroxene is present as phenocrysts, microphenocrysts and microlites in all 2010 products, and orthopyroxene is a common microphenocryst and microlite phase. Crystals of anhedral to subhedral orthopyroxene are

Table 12.2 Selected whole-rock major element analyses of the 2010 eruptive products. Compiled from Preece (2014)

| Sample | M11-80 | M13-41 | M11-130 | M13-29 | M13-23 | M13-43 | M11-85 | M13-7 |
|---|--------|--------|---------|--------|--------|--------|--------|-------|
| Type ^a | A | B | C | D | E | F | G | H |
| SiO ₂ | 54.87 | 54.67 | 53.38 | 55.43 | 54.84 | 55.45 | 53.81 | 56.41 |
| TiO ₂ | 0.71 | 0.74 | 0.79 | 0.72 | 0.72 | 0.70 | 0.79 | 0.54 |
| Al ₂ O ₃ | 18.98 | 19.19 | 19.14 | 19.22 | 19.35 | 19.24 | 18.60 | 19.72 |
| Fe ₂ O ₃ ^T | 7.41 | 8.03 | 8.48 | 7.76 | 7.77 | 7.62 | 8.33 | 6.01 |
| MnO | 0.19 | 0.19 | 0.20 | 0.19 | 0.19 | 0.19 | 0.18 | 0.14 |
| MgO | 2.31 | 2.50 | 2.80 | 2.37 | 2.38 | 2.33 | 2.99 | 1.63 |
| CaO | 7.86 | 8.15 | 8.70 | 7.88 | 8.03 | 7.84 | 8.18 | 7.16 |
| Na ₂ O | 3.89 | 4.04 | 3.62 | 3.94 | 3.99 | 4.04 | 3.49 | 4.08 |
| K ₂ O | 2.12 | 2.08 | 2.00 | 2.16 | 2.07 | 2.16 | 1.67 | 2.39 |
| P ₂ O ₅ | 0.32 | 0.31 | 0.30 | 0.30 | 0.32 | 0.30 | 0.28 | 0.30 |
| LOI | 0.02 | 0.40 | -0.26 | 0.33 | 0.01 | 0.27 | 0.78 | 1.55 |
| Total | 98.68 | 100.30 | 99.15 | 100.30 | 99.67 | 100.14 | 99.10 | 99.93 |

^a Sample type: A = 2010 dome—dense; B = 2010 dome—scoriaceous; C—Light grey dense inclusions; D = Grey scoria—pre-5 November; E = Grey scoria—5 November; F = White pumice; G = White pumice (low-K); H = Ash fall/surge

sometimes rimmed by clinopyroxene. Phenocrysts may be zoned, commonly with oscillatory or sectoral zoning (Costa et al. 2013; Li et al. 2021) or unzoned and often host silicate melt inclusions, as well as inclusions of magnetite, plagioclase and apatite. Clinopyroxene phenocrysts are classed as augite and diopside ($Wo_{39-50}En_{36-46}Fs_{10-19}$), following the scheme of Morimoto (1988) (Fig. 12.23b-I), with between 0.4 and 8.9 wt% Al₂O₃, although the majority contain between 1.5 and 2.5 wt% and have Mg# 61–85, with most between 75 and 85 (Mg# = $100 \times Mg / (Mg + Fe^{2+})$). Orthopyroxene phenocrysts are classed as enstatite ($Wo_{0.2-0.3}En_{57-70}Fs_{27-39}$) (Fig. 12.23b-I). Microphenocrysts and microlites generally have more variable compositions compared to the phenocrysts. They are usually augite and diopside ($Wo_{40-50}En_{35-45}Fs_{13-21}$) (Fig. 12.23b-II), with 0.8–7.6 wt% Al₂O₃ and Mg# 65–81, with most between Mg# 70–80. Less common pigeonite, and crystals with higher Fe content, classed as hedenbergite ($Wo_{49-50}En_{8-21}Fs_{29-41}$) and containing 1.2–2.6 wt% Al₂O₃ and Mg# 19–47, also occur (Fig. 12.23b-II). Hedenbergite crystals were exclusively found in the dome lava, near a calc-silicate xenolith and were bright green when viewed in plane-polarised

light. Orthopyroxene microlites ($Wo_{0.5-9}En_{45-81}Fs_{16-53}$) are enstatite and ferrosilite (Fig. 12.23b-II). Orthopyroxene microphenocrysts and microlites contain between 0.2 and 3.6 wt% Al₂O₃ and have Mg# from 54 to 94, although the majority have Mg# ~65–75. The crystals with orthopyroxene cores and clinopyroxene rims plot within the same Wo-En-Fs space as the other pyroxene crystals.

Amphibole is present in all samples as phenocrysts (Fig. 12.23c-I) and microphenocrysts (Fig. 12.23c-II) but is absent as groundmass microlites. Amphibole is titanian magnesiohastingsite, following the classification of Leake et al. (1997), based on 23 oxygens with with Fe²⁺/Fe³⁺ estimation assuming 13 cations except Ca, Na and K. Crystals may be homogeneous in composition or zoned, often with rims of higher Al₂O₃ and MgO, and lower SiO₂, K₂O and FeO compared to the cores (see also Costa et al. 2013). The overall range of Al₂O₃ content is 10.0–14.9 wt%, with Mg# ranging between 49 and 58, with a cluster at ~62–68. Of the crystals with Mg# >68, 70% are phenocrysts from the white pumice, with the rest being phenocrysts from the light grey inclusions. More than 55% of the crystals with Mg# <62 are dense dome

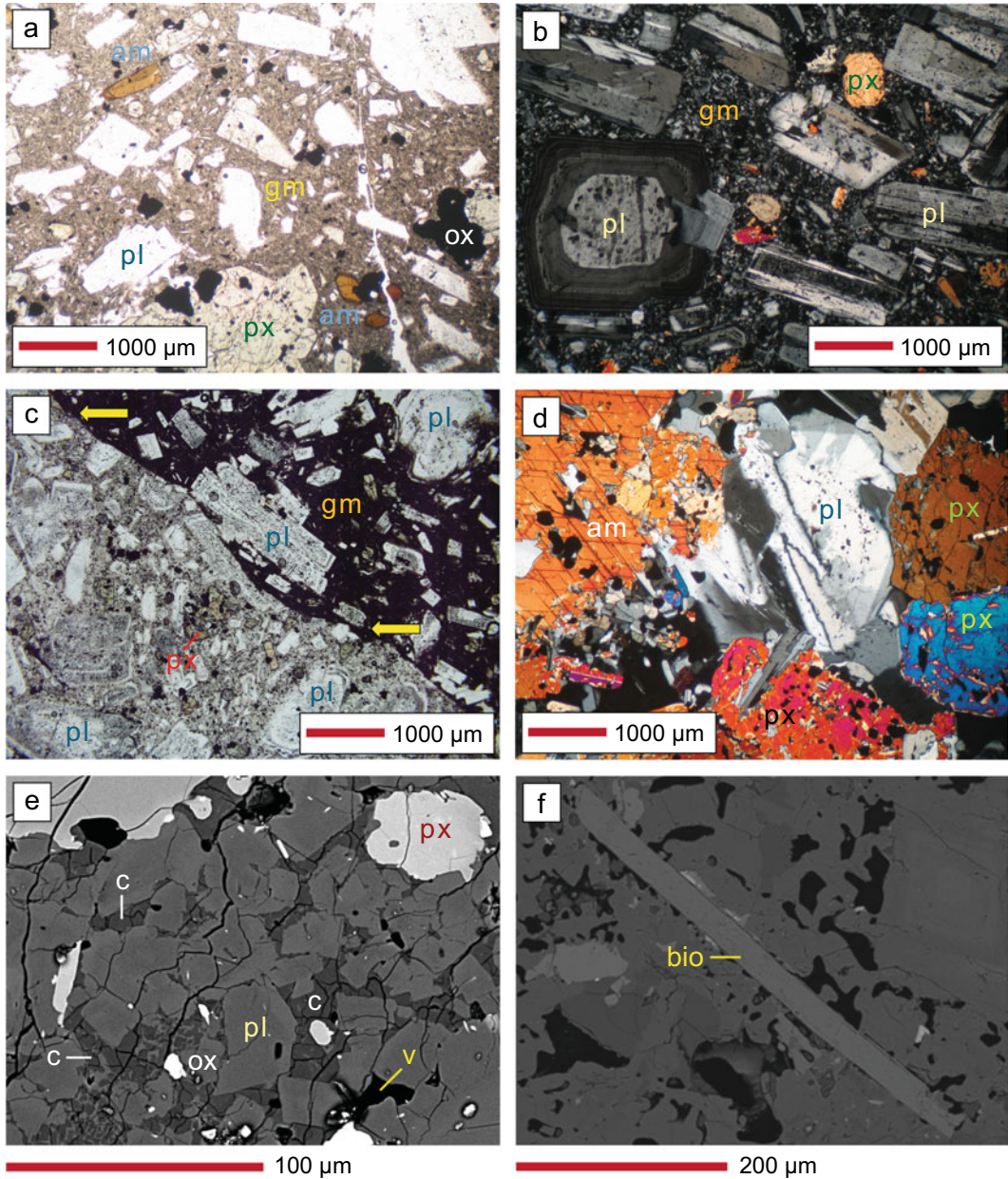


Fig. 12.22 Photomicrographs and backscattered electron (BSE) images of Merapi 2010 eruptive products. **a** Basaltic andesite of the 2010 lava dome, characterised by plagioclase, pyroxene (both clino- and orthopyroxene, Ti-magnetite and amphibole (both fresh and with breakdown rims) in a moderately crystalline groundmass (PPL). **b** Light-grey dense basaltic andesite inclusion containing complexly zoned plagioclase crystals, amphibole (rare and always with pronounced breakdown rims) and coarse grained, crystalline groundmass (X Nicols). **c** Contact relationship between light-grey dense inclusion (lower

left) and 2010 dome lava (upper right) (X Nicols). **d** Coarse-grained plutonic xenolith (magmatic cumulate) consisting of plagioclase, clinopyroxene and amphibole (X Nicols). **e-f** BSE images of the light-grey dense inclusions in the 2010 lava dome: **e** Highly crystalline, micro-vesicular groundmass with plagioclase, pyroxene, Ti-magnetite and abundant cristobalite. **f** Late-stage biotite. Abbreviations used: am = amphibole, pl = plagioclase, px = pyroxene, ox = oxide (Ti-magnetite), c = cristobalite, bio = biotite, gm = groundmass, v = vesicles

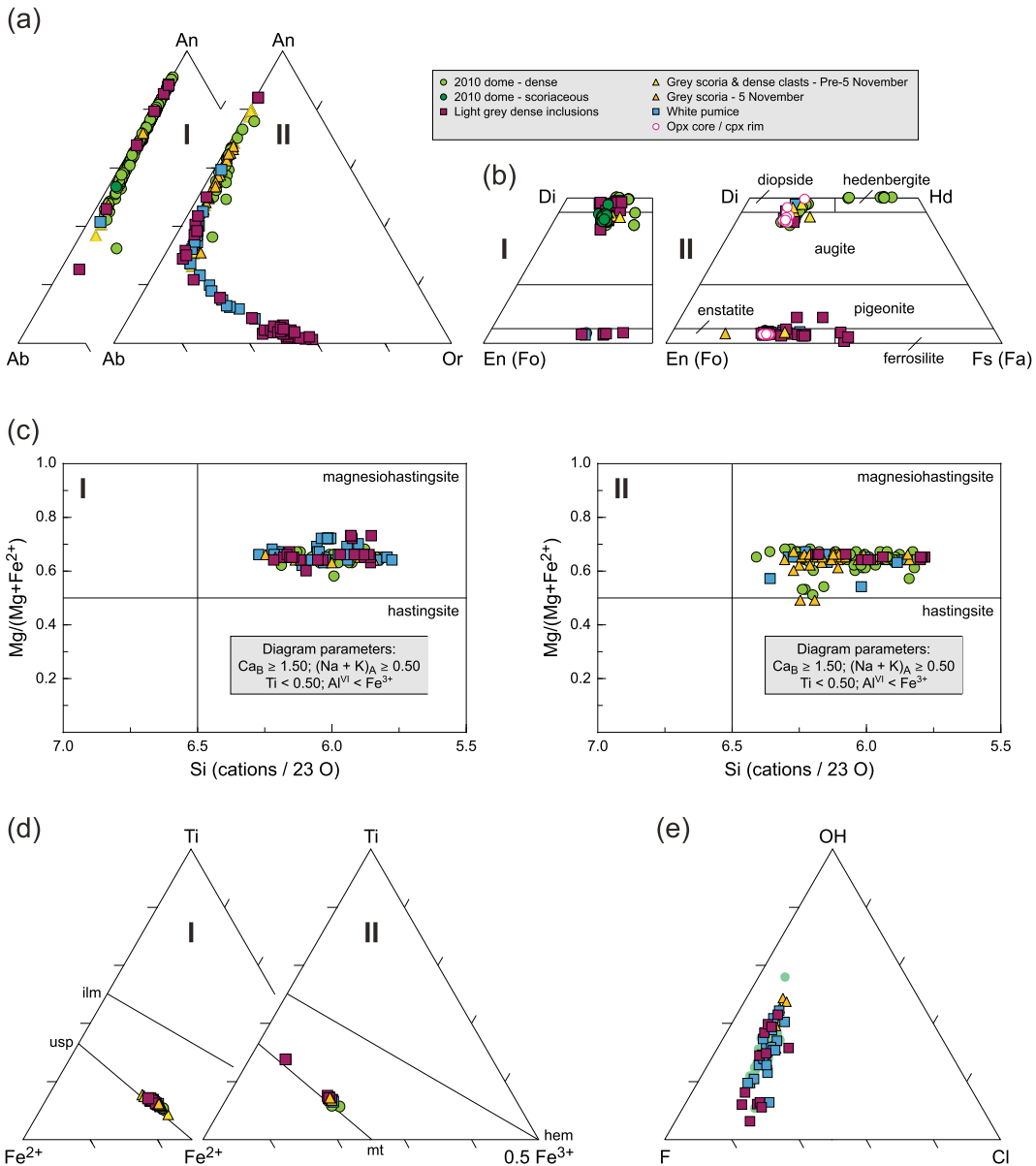


Fig. 12.23 Mineral compositions of phenocrysts, microphenocrysts and microlites from various 2010 eruptive products. **a** (I) Feldspar phenocrysts and microphenocrysts; (II) feldspar microlites. **b** (I) Pyroxene phenocrysts; (II) pyroxene microphenocrysts, microlites and crystals with opx cores/cpx rims. **c** (I) Amphibole phenocrysts; (II) amphibole microphenocrysts. **d** (I) Fe-Ti oxide microphenocrysts; (II) Fe-Ti oxide microlites. **e** Ternary OH-F-Cl plot of apatite compositions. *Data source* Preece (2014)

microphenocrysts. Amphiboles may be surrounded by breakdown reaction rims, composed of anhydrous minerals plagioclase, pyroxene (or olivine) and Fe-Ti oxides. However, amphiboles from 2010 frequently do not possess breakdown reaction rims.

Fe-Ti oxides are present in all samples as anhedral and irregularly shaped microphenocrysts (Fig. 12.23d-I) and microlites (Fig. 12.23d-II), as well as inclusions within clinopyroxene phenocrysts. All Fe-Ti oxides are titanomagnetite. Crystals range in ulvöspinel

content from 18–59 mol.%, although most range from ~22 to 35 mol.% (Fig. 12.23d). Titanomagnetite is often exsolved to various extents showing trellis-type exsolution, consisting of ilmenite lamellae parallel to the {111} planes of the titanomagnetite host (Buddington and Lindley 1964; Haggerty 1993). Rare pyrrhotite inclusions have also been observed within magnetite, amphibole and clinopyroxene hosts.

Apatite crystals occur in trace amounts (<1 vol.%) as inclusions within clinopyroxene, plagioclase and amphibole phenocrysts or as microphenocrysts or groundmass microlites. Crystals are F-rich (2.8–5.4 wt% F, with the majority containing ~3–4 wt% F) and contain 0.6–1.4 wt% Cl (Fig. 12.23e). Data obtained by Li et al. (2021) also suggest the presence of apatite crystals with lower F contents (1.1–2.3 wt%), a similar range of Cl concentrations (0.4–1.2 wt%), and H₂O concentrations of 0.4–1.0 wt%. Some CO₂-rich apatite inclusions in amphibole, with concentrations up to 1.6 wt%, were also found.

The presence of biotite in the 2010 eruption products—a mineral that has not previously been observed at Merapi—was noted by Costa et al. (2013) and Preece (2014). Preece (2014) documented biotite within the light grey inclusions (Fig. 12.22f), alongside a crystalline silica phase, cristobalite. Biotite contains 0.5–3.8 wt% F, 0.1–0.3 wt% Cl, between 11.9 and 15.6 wt% FeO, with Mg# 63–70, and has been interpreted as a late-stage magmatic phase that crystallised from highly evolved residual melt resulting from extensive groundmass crystallisation in the light grey inclusions (Preece 2014). Cristobalite is observed to fill small vesicles and is pervasive within the groundmass, often with ‘fish-scale’ cracked morphology or a microbotryoidal texture (Fig. 12.22e).

12.5.3 Magma Storage and Magmatic Processes

The crystallisation depths of magma involved in the 2010 eruption were determined using multiple approaches, including thermobarometry,

thermodynamic modelling, volatiles in melt inclusions, pumice glass and apatite crystals, experimental petrology and fluid inclusion barometry (Costa et al. 2013; Erdmann et al. 2014, 2016; Preece 2014; Preece et al. 2014; Drignon et al. 2016; Whitley et al. 2020; Li et al. 2021) that complemented geophysical investigations (Budi-Santoso et al. 2013; Saepuloh et al. 2013). Further insights into the pre-eruptive processes operating in the magma plumbing system were gleaned from mineral-scale elemental and oxygen isotopic variations (Borisova et al. 2013, 2016; Costa et al. 2013; Preece 2014; Preece et al. 2014; Erdmann et al. 2014) and major element, trace element and volatile concentrations in melt inclusions (Preece 2014; Preece et al. 2014) and apatite crystals (Li et al. 2021) that document a complex interplay of closed-system and open-system magmatic processes, including magma replenishment and mingling/mixing, assimilation of limestone and magmatic degassing. Bulk rock major element, trace element, and isotope (Sr, Nd, Pb, O, U-series) geochemistry have highlighted the similarity between the 2010 rock compositions and those of previous eruptions (Borisova et al. 2013; Preece 2014; Drignon et al. 2016; Preece et al. 2016; Handley et al. 2018), suggesting that similar processes and magma types drive eruptions at Merapi and that most Merapi magmas are potentially capable of producing explosive eruptions (Costa et al. 2013). Groundmass textures, glass and microlite compositions of the 2010 eruptive products (Preece 2014; Drignon et al. 2016; Preece et al. 2016) record the tapping of magma from depths of several kilometres, the final stages of magma ascent towards the surface, and the processes closest to the onset of and during eruption, as described in Preece et al. (2023, Chap. 9).

Based on application of different geothermobarometry and MELTS modelling, Costa et al. (2013) proposed at least three crystallisation zones at depths of (1) 30 ± 3 km, as evidenced by some amphibole compositions and high-Al clinopyroxene as well as by the presence of H₂O- and CO₂-rich apatite in amphibole and geobarometrical calculations that indicate comparable

crystallisation depths (Li et al. 2021), (2) 13 ± 2 km, where other amphiboles, high-Al clinopyroxene and high-An plagioclase crystallised, with very An-rich plagioclase linked to assimilation of limestone or, alternatively, to crystallisation from hydrous mafic magma (Preece 2014; Borisova et al. 2016), and (3) less than 10 km, where extensive crystallisation produced low-Al clinopyroxene, orthopyroxene and more Ab-rich plagioclase. Erdmann et al. (2014) concluded that amphibole crystallised at pressures of 200–800 MPa, corresponding to depths between ~ 9 and 28 km, assuming crustal densities of 2.242 and 2.9 g/cm³ at depths above and below 10 km (Widiyantoro et al. 2018). Preece et al. (2014) presented geobarometrical calculations that show that clinopyroxene crystallised at depths of up to ~ 20 km, with the greatest depths associated with phenocrysts from white pumice. This is consistent with results from amphibole barometry (Preece 2014), which also indicated that the greatest amphibole crystallisation depths are from white pumice samples. Preece et al. (2014) further suggested that melt inclusions equilibrated during shallower storage and/or ascent, at depths of ~ 0.6 – 9.7 km, based on H₂O and CO₂ contents (see also Li et al. 2021). H₂O concentrations range from up to 3.94 wt% in grey scoria and up to 3.91 wt% in white pumice to <3.62 wt% in dense dome clasts, while CO₂ concentrations are generally <200 ppm but reach up to 695 ppm and, in some cases, up to 3000 ppm in white pumice. The presence of an exsolved brine phase was proposed based on the occurrence of melt inclusions enriched in Li and B, that show uniform buffered Cl concentrations (Preece et al. 2014). In a subsequent study, Erdmann et al. (2016) presented phase equilibrium experiments to infer crystallisation at more than 100–200 (± 75) MPa in a shallow magma storage zone, corresponding to depths of more than 4.5 to ~ 9 (± 3) km. This is broadly consistent with results from pumice glass water concentration measurements (Drignon et al. 2016) that indicate tapping of magma from depths of several kilometres. Fluid inclusion barometry in calc-silicate xenoliths also record low pressures of less than ~ 100 MPa, indicating that the fluid

inclusions formed at shallow crustal depths or re-equilibrated during ascent (Whitley et al. 2020).

Despite the variations in the published models, there is an emerging consensus of the existence of multiple distinct or more continuous interlinked magma storage and crystallisation zones throughout the entire crust beneath Merapi prior to the 2010 eruption. Deeper and mid-crustal crystallisation were dominated by distinct types of amphiboles, high-Al clinopyroxene, and high-An plagioclase, while a more feldspar-dominated crystallisation regime existed at shallow crustal levels, where more Ab-rich plagioclase crystallised alongside low-Al clinopyroxene and, possibly, orthopyroxene. The shallow, uppermost crystallisation region at 10 km or less is thought to have consisted of a largely degassed and highly crystalline mush (Costa et al. 2013). This region is also located within the carbonate dominated upper crust beneath Merapi, where crustal carbonate assimilation plays an important role (Deegan et al. 2023, Chap. 10), although this process may extend to slightly deeper levels in the model of Costa et al. (2013). There have been suggestions that there were higher than usual rates of crustal carbonate assimilation and associated CO₂ addition to the volcanic system that may have contributed to the unusual explosivity of the 2010 eruption (Borisova et al. 2013; Costa et al. 2013), although U-series and radiogenic isotopic data (Handley et al. 2018) did not support such an interpretation. Multiple lines of evidence point towards interaction between degassed magma stored at shallower levels and hotter, deeper, more volatile-rich magma during the 2010 eruption (Surono et al. 2012; Costa et al. 2013; Preece 2014; Preece et al. 2014). In a general model, it may be envisaged that interaction between magma stored in various parts of the plumbing system plays a fundamental role in determining the eruptive behaviour of Merapi. Typical dome forming eruptions may predominantly be fed by the shallower crystal-rich or mush zones, in which magmas may have reacted intensively with carbonate country rock. Crystal mush rejuvenation may be triggered by reheating and remelting that result from small volumes of ascending hotter magma from depth that are partially or fully

stalled by the crystal-rich or mush zones that formed during previous intrusions into the shallow plumbing system (Costa et al. 2013). By contrast, a larger influx of deep magma that replenishes the shallower magma system at relatively short timescales and associated CO₂ fluxing (e.g. Caricchi et al. 2018) may be a controlling factor driving larger scale, explosive eruptions as in 2010. In such a scenario, the shallower crystal-rich magma system may get disrupted and eventually overwhelmed by the arrival of deep magma. This process may be capable of intensifying limestone assimilation (Costa et al. 2013), although there is little isotopic evidence for the latter when comparing the 2006 and 2010 eruptions (Handley et al. 2018). Subsequent processes include rapid magma ascent, accompanying closed-system degassing and, as inferred for the 2010 eruption, accumulation of ascending magma beneath a plugged conduit that builds up pressure in the uppermost conduit (Costa et al. 2013; Komorowski et al. 2013; Preece 2014; Preece et al. 2016). The light grey dense material in the 2010 dome rocks has been interpreted to originate from such a plug of cooled, rigid magma that resided at very shallow depth within the magmatic system and was partially reheated, fragmented and incorporated into the 2010 magma (Preece 2014; Preece et al. 2016, 2023, Chap. 9). If such a model is correct, magma replenishment and interaction with shallower crystal mush may exert important control on the continuum of eruption styles at Merapi that range from effusive, dome-forming eruptions to larger magnitude explosive eruptions.

12.5.4 Timescales of Magmatic Processes

An understanding of the timescales associated with the dynamic processes in the pre-and syn-eruptive 2010 magma system is fundamental to improved hazard assessment and interpretation of geophysical and geochemical monitoring signals. Based on Fe–Mg diffusion zoning in clinopyroxene, Costa et al. (2013) suggested that the inferred influx of hot and volatile-rich magma

from depth into the shallower magma storage zones occurred up to 1.6–2.7 years before the eruption, while Borisova et al. (2016) presented ¹⁸O diffusion data in plagioclase to propose a time span for plagioclase crystallisation prior to the 2010 eruption of up to 34 years. These results are broadly in line with those of a detailed study of U-series disequilibrium (Handley et al. 2018), where ²²⁶Ra and ²¹⁰Pb excesses ((²²⁶Ra/²³⁰Th) and (²¹⁰Pb/²²⁶Ra) > 1) observed in plagioclase separates from the 2010 eruption indicate that a proportion of the plagioclase grew within the decades before the eruption. However, none of these processes, which may have significantly predated the eruption, left an obvious signal in the monitoring record and, in the latter cases, may partly record processes associated with previous eruptive events. At the time of eruption, the 2010 samples were depleted in ²¹⁰Po, a nuclide that partitions efficiently into an exsolving volatile phase and is almost completely lost during eruption, relative to ²¹⁰Pb ((²¹⁰Po/²¹⁰Pb) < 1), but variably degassed, with the degree of degassing strongly related to sample texture and eruption phase (Handley et al. 2018). ²¹⁰Po ingrowth calculations (Handley et al. 2018) suggested that initial intrusion into the shallower magma system occurred several weeks to a few months prior to the initial explosions on 26 October 2010, which broadly coincides with the increase of various monitoring parameters (see Fig. 12.1).

The 2010 samples show a wide range in initial (²¹⁰Pb/²²⁶Ra) activity ratios within a single eruption at Merapi, comparable to the range of ratios of the preceding eruption in 2006 and those reported for the time between 1981 and 1995 (Gauthier and Condomines 1999). They are largely characterised by ²¹⁰Pb deficits ((²¹⁰Pb/²²⁶Ra) < 1) that have been interpreted to result from degassing of the intermediate nuclide ²²²Rn over ~ 0–3 years before eruption, a time span that is slightly less than for samples from the dome-forming 2006 eruption (Handley et al. 2018). A rock sample representing the onset of the 2010 eruption on 26 October (Stage 2) shows a significant ²¹⁰Pb deficit ((²¹⁰Pb/²²⁶Ra)₀ = 0.79). This is followed by a change to near equilibrium (²¹⁰Pb/²²⁶Ra)₀ values for samples

extruded during the rapid dome growth and destruction period between the 29 October to 4 November (stage 3) and emplaced in stage 4, which includes a sample of the light grey dense inclusions in the main 2010 lava dome. The white pumice sample erupted during the latest stages of the climactic phase of 5 November (stage 6) lies within uncertainty of the stage 4 emplaced samples with a ^{210}Pb deficit of 0.92. Samples from the climactic phase of the eruption therefore have smaller ^{210}Pb deficits than the analysed light grey dense crystalline inclusion ('plug') sample and the samples from the 2006 eruption, which also supports faster ascent and less time for degassing during the main phases of the 2010 eruption. The longer-term magma degassing processes described here, caused by changes in the subsurface conditions, may potentially be detectable through soil radon emission monitoring.

12.6 Eruption Effects, Impact and Recovery

The 2010 eruption had profound effects on the natural environment, built infrastructures and population, as well as all aspects of community livelihood (see also Lavigne et al. 2023, Chap. 2).

The morphology of the summit area of Merapi has seen continuous changes over the past years, decades and centuries. Explosive activity has produced craters and deep depressions, or breaches, at the top of the volcano or in the crater walls, which formed repeatedly by explosive activity or partial edifice collapses. Collapses have removed portions of the uppermost, often hydrothermally altered and weakened volcanic edifice, and have been promoted by dome growth and associated phenomena which may exert strain on the summit crater walls (e.g. Beauducel et al. 2000; Voight et al. 2000; Ratdomopurbo et al. 2013; Solikhin et al. 2015).

The 2010 eruption produced a large summit crater open to the SE (Fig. 12.24a), towards the headwaters of Kali Gendol, in an area previously occupied by the pre-2010 dome area and the remains of the 2006 lava dome, removing and

incising lava domes and flows that were emplaced during the twentieth century (Solikhin et al. 2015). The initial explosions on 26 October produced a 200 m wide and 100 m deep crater with a horseshoe-shaped morphology, which was enlarged (350 × 400 m wide) during the 5 November paroxysm (Surono et al. 2012; Komorowski et al. 2013; Solikhin et al. 2015). In total, the summit area of Merapi lost some 10–19 × 10⁶ m³ of material (Kubanek et al. 2015; Solikhin et al. 2015). New lava domes grew rapidly inside the newly formed and enlarged crater. The earlier, pre-5 November dome was completely destroyed by laterally directed dome explosions and retrogressive gravitational collapse on 5 November (Komorowski et al. 2013), while the later lava extrusion on 6 November produced a dome ~200 m in diameter that, since then, has seen further morphological changes by subsequent lava extrusion and short explosive events (e.g. Darmawan et al. 2023, Chap. 15). The downslope extension of the crater, the Gendol breach (Fig. 12.24a), is a SE-NW trending summit scar that originally formed during the 1872 eruption (Ratdomopurbo et al. 2013) and opens the upper SE slope of Merapi towards Kali Gendol. The canyon of the Gendol breach was notably lengthened and deepened during the 2010 eruption, forming a major pathway for future dome related PDCs (Gertisser et al. 2011; Solikhin et al. 2015). Since 2010, the steep, hydrothermally altered and unstable crater and canyon walls have been subject to rockfalls and landslides, while the unconsolidated eruption deposits and the exposed hydrothermally altered wall rocks have continued to feed lahars (Solikhin et al. 2015).

The PDCs generated throughout the 2010 eruption were highly destructive, devastating an area of 22 km² on the densely populated southern flank of Merapi (Jenkins et al. 2013; Komorowski et al. 2013). The ground was scoured, and vegetation and soil stripped by PDCs down to 1300 m elevation (Solikhin et al. 2015). Trees were felled and uprooted, splintered, abraded on the upstream side and lightly charred up to distances of ~6 to 7 km by the passage of the high-energy PDC of 5 November. North of Kinahrejo, the orientation of



Fig. 12.24 Impact of the 2010 eruption. **a** Summit crater, open to the SE, formed during the 2010 eruption, with its downslope extension, the Gendol breach. **b** Ridges north of Kinahrejo with scoured soil and blown down trees. Tree orientation indicates flow direction from Kali Gendol towards Kinahrejo. **c** Remnants of house in Kinahrejo, destroyed by Stage 4 ‘blasts’. Walls remained partly

standing as they were partially protected by local topography. **d** House destroyed by overbank deposits in Wukirsari near Bakalan, Lower K. Gendol. **e** Overturned and burnt car in Kinahrejo, covered by Stage 4 lapilli and blocks. **f** Bridge over Kali Opak on Merapi’s south flank destroyed by lahars. For locations, see Figs. 12.1 and 12.14. *Photo credit* R. Gertisser, K. Preece

blown down trees indicates flow direction from Kali Gendol towards Kinahrejo (Fig. 12.24b). Unburnt vegetation frequently occurred at the

base of the 5 November deposits (Komorowski et al. 2013). PDCs damaged or destroyed more than 2200 buildings along their flow paths up

to ~16 km from the source (Jenkins et al. 2013; Komorowski et al. 2013). About 150 buildings (and other objects) were damaged by PDCs associated with the early phases of the eruption; with most buildings destroyed by high-energy and overbank PDCs of 5 November (Jenkins et al. 2013) (Fig. 12.24c–e).

Using empirical damage data and calculations of material and structural resistance to lateral force, Jenkins et al. (2013) estimated dynamic pressures associated with the 5 November high-energy PDCs that exceeded 15 kPa at more than 6 km from the source and rapidly decreased towards the end of the PDC runout over a distance of less than 1 km. Temperatures of the high-energy PDCs were low, reaching ~200–300 °C, based on observed thermal damage to buildings and vegetation as well as medical observations (Jenkins et al. 2013; Komorowski et al. 2013; Baxter et al. 2017). This temperature range was subsequently confirmed by charcoal surface reflectance, which suggested a minimum temperature of 240–320 °C; a few charcoal fragments yielded temperatures up to 450 °C (Trolese et al. 2018). Charring temperatures were similar in proximal and distal high-energy PDC deposits, and significantly lower than those of the destroyed dome rock at source, indicating a rapid decrease in PDC temperature soon after its inception (Trolese et al. 2018).

Fatalities were caused over the entire length of the 2010 PDC runouts. Few people were killed directly by high-energy PDCs in proximal areas, due to the evacuation efforts by the Indonesian authorities (Suroño et al. 2012; Komorowski et al. 2013). Most fatalities occurred more than 12 km from the volcano, as people were evacuating and caught in overbank PDCs and surges that spilled into villages after they were discharged from nearby Kali Gendol (Jenkins et al. 2013; Komorowski et al. 2013). At these distances, PDC dynamic pressures and temperatures were relatively low, causing little structural damage, apart from the village of Bakalan that was completely buried and destroyed by the overbank PDCs (e.g. Charbonnier et al. 2013). Fatalities occurred both outside and inside of buildings, partly because of building design that

allowed PDCs to rapidly enter buildings (Jenkins et al. 2013; Komorowski et al. 2013).

At a greater distance from Merapi, the 2010 eruption led to major air traffic disruptions due to ash emissions (Picquout et al. 2013; Lavigne et al. 2023, Chap. 2). Adisucipto International Airport in Yogyakarta closed for a period of 15 days between 5 and 20 November, followed by a period of one month during which air traffic operations returned to pre-eruption levels. Other airports in Java, including Jakarta's Soekarno-Hatta International Airport were also affected by air traffic disturbances. Consequently, several airlines suspended their flights from and into Yogyakarta, while others adapted to the situation by transferring their flights to other airports. The Merapi crisis in 2010 revealed that, at the time, Indonesia had no suitable alternative means of transport to deal with airport closure during volcanic eruptions (Picquout et al. 2013).

Impact on the physical environment, built infrastructures and population continued for several years after the eruption (de Bézizal et al. 2013; Thouret et al. 2023, Chap. 17). Rain-induced lahars, including hyperconcentrated stream and debris flows, became a major hazard, with lahar occurrences in almost all major drainages. Lahar impact after the 2010 eruption was considerably larger than after previous eruptions due to the significantly larger volume of pyroclastic deposits (~36.3–80 × 10⁶ m³) on the flanks of the volcano. The first lahars associated with the 2010 eruption were syn-eruptive and hot, with 45 events recorded between 27 October and 3 December 2010. During the 2010–2011 rainy season, a total of 240 lahar occurrences were recorded (de Bézizal et al. 2013), notably in the Putih, Gendol, Boyong, Ladon and Apu river valleys, increasing to 429 events by March 2014. Lahar runouts exceeded 15 km and even reached Yogyakarta ~25 km south of Merapi on three occasions. Lahar filling of downstream river channels, followed by overbank flow into surrounding fields and villages, as well as riverbed and riverbank erosion, caused considerable damage. In total, 14 Sabo dams and 21 bridges were destroyed (Fig. 12.24f), affecting the road network on Merapi's southern and western flanks (de Bézizal et al. 2013). 860 houses were damaged

by burial with sediment, failure of walls and lahar infiltration into buildings, with the scale of damage related to building quality (de B elizal et al. 2013; Jenkins et al. 2015). Weak masonry houses were destroyed by dilute lahars that travelled at low velocities (<3 m/s) and generated low dynamic pressures (<5 kPa), while stronger rubble stone buildings were able to resist higher lahar velocities (<6 m/s) and dynamic pressures (<20 kPa) (Jenkins et al. 2015). The number of direct fatalities remained very low, but more than 3000 people lost their home after the first rainy season following the eruption due to the damaging effects of lahars (Global Volcanism Program 2013).

Many areas on Merapi's south flank that were affected by PDCs have remained largely uninhabitable. Nearly 400,000 people were displaced from their homes as a result of the eruption (Mei et al. 2013; Lavigne et al. 2023, Chap. 2). After the eruption, temporary dwellings (Indon. = *huntara*) were constructed outside the danger zone, supported by the Indonesian government, NGOs and the private sector, among others. The largest of these settlements contained more than 1000 households (Maly and Nareswari 2015). Although some residents stayed in these temporary settlements, the launch of a housing reconstruction programme (Rekompak—REhabilitasi dan ReKONstruksi Masyarakat dan Permukiman berbAsis Komunitas; Engl.: Community-Based Settlement Rehabilitation and Reconstruction) led to building of permanent homes, particularly in collective resettlement areas (Indon. = *huntap*). After completion in 2014, more than 80% of the 2000 new houses built within the framework of the ReKompak project in the most affected Cangkringan District, Sleman Regency were constructed in these collective resettlement areas (Maly and Nareswari 2015; Mei et al. 2016). The existing houses, infrastructures and facilities in two of these settlements, Huntap Kuwang and Huntap Plosokerep, were still in decent conditions, meeting the needs of the local community (Mei et al. 2016). While most residents appeared to be satisfied with their living conditions (Mei et al. 2016), further research is required to understand more fully understand the perception of residents in different settlements regarding their

ability to complete or extend their homes, support of community livelihood and continued occupation of the sites (Maly and Nareswari 2015).

In the Kaliadem-Kinahrejo area, facilities and activities for attracting day-trippers and visitors to the area sprang up soon after the eruption and currently still exist there (see also Lavigne et al. 2023, Chap. 2). These include food stalls and souvenir shops, a small museum, displays of items damaged during the 2010 eruption, designated visitor sites, such as the bunker in Kaliadem where two people perished during the 2006 eruption, and activities including guided adventure tours across the area destroyed by the 2010 eruption (Fig. 12.25a–e). As after every eruption of Merapi, sand quarrying activities of PDC and lahar deposits have increased in the valleys around the volcano after the 2010 eruption, particularly in, but not limited to the Gendol valley (Fig. 12.25f). Such deposits have been a substantial natural resource that has supported the local economy and regional development (e.g. de B elizal et al. 2011, 2013; Lavigne et al. 2023, Chap. 2). The Sleman District alone had mining tax revenues of 63 and 600 million IDR in 1999 and 2007, respectively (Ikhsan et al. 2010). At the same time, sand quarrying puts the people who mine the deposits at risk (de B elizal et al. 2011), as demonstrated in 2016 and 2017, when several trucks were swept down Kali Bebeng on Merapi's south-west flank, and at least eight miners were killed, and eight others injured following a landslide. It also has negative environmental and ecological effects, and necessitates sediment disaster management efforts, together with regulated sustainable sediment resource management and measures to stabilise riverbeds to reduce riverbed degradation (Ikhsan et al. 2010). By contrast, riverbed exploitation by sand extraction may, at least initially, reduce the probability of lahar events and reduce the potential for PDCs to spill over valley margins due to increased channel capacity. This, however, is offset by morphological changes to the generally steep riverbanks that may allow PDCs to spread over wider areas and the potential hazards associated with the failure of Sabo dams, triggered by uncontrolled sand extraction near to such structures.



Fig. 12.25 Recovery after the 2010 eruption. **a** Food stalls and souvenir shops catering for visitors in Kaliadem in February 2011. **b** The bunker in Kaliadem, where two people died during the Merapi eruption in 2006, has attracted visitors ever since. **c** Display of a damaged minivan in Kinahrejo. **d** 'Batu Alien' (Alien Rock), one of the tourist attractions on Merapi's south flank following

the 2010 eruption. **e** Adventure tour using off-road vehicles for tourists in Kaliadem. **f** Block and sand mining of the 2010 PDC and lahar deposits in Kali Gendol has turned into a profitable post-disaster business. For locations, see Figs. 12.1 and 12.14. *Photo credit* R. Gertisser, K. Preece

12.7 Managing the 2010 Volcanic Crisis

12.7.1 The Role of the National Disaster Management System in Indonesia

After the earthquake and tsunami disaster in Aceh in 2004, Indonesia considered it important to manage disasters with a new paradigm that prioritised risk management. Consequently, Law No. 24/2007 on Disaster Management was issued and, subsequently, the Indonesian National Board for Disaster Management (Badan Nasional Penanggulangan Bencana; BNPB) was formed based on Presidential Regulation No. 8/2008. Consisting of an organisational structure that includes a chairperson, a steering committee, and a disaster management implementer element, BNPB has the function of coordinating the implementation of disaster management in a planned, integrated, and comprehensive manner. As one of the steering elements in the National Disaster Management System, CVGHM under the Geological Agency of the Indonesian Ministry of Energy and Mineral Resources has been authorised to provide recommendations related to geological hazard mitigation at national, provincial and district/city level. Formally, BNPB has been a focal point of government agencies at the central level. Meanwhile, the disaster management focal point at the provincial and district/city level has been the Regional Disaster Management Agency. To strengthen the implementation of disaster management in Indonesia, forums for disaster risk reduction were formed at the national and local level. At a national level, a National Platform was formed, which consists of elements of civil society, the business world, universities, the media, and international institutions. At a local level, these included the Merapi Forum, the Yogyakarta Disaster Risk Reduction Forum, and the East Nusa Tenggara Disaster Risk Reduction Forum. A strategic step related to the 2010 Merapi eruption was the decision of BNPB to declare the eruption crisis as a national disaster because of its wide-ranging impact,

covering both the Central Java Province and the Yogyakarta Special Region. This meant that the central government took responsibility for all impacts of the eruption.

12.7.2 Vulnerability Before the 2010 Eruption

In 2006, two disasters struck the Central Java Province and the Yogyakarta Special Region; the 27 May 2006 Bantul earthquake and the eruption of Merapi that peaked on 14 June 2006. Both disasters provided important lessons for the community and stakeholders in disaster management. For example, the public became more rational in understanding geological disasters and government officials were able to increase their knowledge and skills in disaster management. Participation of non-governmental organisations (NGOs) seemingly became more real and an important factor in disaster management. These aspects were important factors of strength when facing the threat of the impending 2010 eruption. During the 2006 eruption crisis, the status of activity was lowered from alert level IV to alert level III on 12 June 2006, two days before the peak of the eruption on 14 June, when a large PDC reached as far as 7 km in Kali Gendol (e.g. Charbonnier and Gertisser 2008), highlighting the challenges not only of raising but also of lowering alert levels related to volcanic activity. Coincidentally, the traditional leader, Mbah Marijan, whose house was located a few hundred metres west of the Gendol valley in Kinahrejo, survived and was not affected by the large 14 June PDC. However, Mbah Marijan's refusal to be evacuated during the 2006 eruption crisis, which attracted widespread media interest, critically influenced the peoples' perception of the incident and understanding of the volcano. Accordingly, inhabitants on Merapi's southern slopes, particularly in Kinahrejo, believed more in the supernatural power associated with the eruption than the scientists. This led to further challenges four years later, when faced with the 2010 eruption crisis.

With the issuance of Law No. 24/2007 on Disaster Management, there has been a strong legal basis in Indonesia to carry out disaster management, alongside the implementation of effective and sustainable planning to facilitate efforts to reduce disaster risk at Merapi. In these disaster risk reduction efforts, the adopted threat factor is routinely assumed to be a larger than predicted future eruption, based on the assessment of volcanic and related hazards. Moreover, to this day, the settlements on the slopes of Merapi are characterised by a high population density of 900–1900 inhabitants/km², with 60,000 inhabitants living in the most vulnerable disaster-prone area III (Indon.: Kawasan Rawan Bencana (KRB) III), which is located closest to the summit of Merapi and frequently affected by PDCs (CVGHM 2002, 2011). Inhabitants on the slopes of Merapi are socially, economically and culturally vulnerable (e.g. Mei and Lavigne 2012; Bakkour et al. 2015; Lavigne et al. 2015), and a strong bond between the volcanic environment and social life exists because Merapi, like other volcanoes, is regarded as a place full of blessings of natural resources, which encourages people to live near the volcano (e.g. Kelman and Mather 2008; Holmberg 2023, Chap. 3). Mystical beliefs (e.g. Schlehe 1996; Dove 2008) continue to be held by some people around Merapi, as shown by traditional ceremonies that take place at a certain time every year, even though they are considered as touristic events by some. Social, economic and cultural vulnerability of people living in disaster-prone areas have been important challenges or threat factors for risk reduction efforts, and mystical beliefs were, at times, an impediment for evacuations at critical points in time.

12.7.3 Disaster Risk Reduction Strategy

Successful volcanic disaster mitigation requires long-term hazard assessment, short-term prediction for early warning, and refugee management in times of crises. Appropriate early warning can only be achieved through various volcano

monitoring data. Early warnings and recommendations issued by CVGHM must be understood by decision makers and the population, and implemented with concrete actions for disaster risk reduction. Therefore, the disaster risk reduction strategy before the 2010 eruption comprised four pillars: (1) Strengthening of the volcano monitoring system, (2) Formation of a disaster risk reduction (DRR) forum, (3) Strengthening of community capacity through disaster management training and information dissemination, and (4) Preparation of contingency plans for local governments based on hazard assessment as a threat scenario. This strategy continues to be applied up to the present time.

12.7.3.1 Strengthening of the Volcano Monitoring System During the 2010 Eruption Crisis

Before 2010, the Merapi volcano monitoring system consisted of seismic, deformation and geochemical monitoring, meeting the volcanic monitoring standards recommended by the International Association of Volcanology and Chemistry of the Earth's Interior (IAVCEI) (see Budi-Santoso et al. 2023, Chap. 13). In the face of the 2010 eruption, additional monitoring was carried out through the volcano observation posts around Merapi that had also been equipped with meteorological instruments to measure rainfall, wind speed, humidity and air temperature. Furthermore, visual monitoring was conducted using CCTV cameras installed at Gunung Plawangan, Kaliurang and Deles on the south to southeast slopes (see Budi-Santoso et al. 2023, Chap. 13).

The seismic monitoring system at Merapi in 2010 consisted of nine seismic stations (Fig. 12.1). These included four permanent Mark Products L-4 short-period stations (DEL, KLA, PLA, PUS) and five additional temporary broadband seismic stations. The latter comprised one Streckeisen STS-2 seismometer installed at station LBH, and four Guralp CMG-40 T seismometers installed prior to 2010 at stations GMR, GRW, PAS and WOR (Fig. 12.1), as part of the EU-funded MIAVITA (Mitigate and Assess risk from Volcanic Impact on Terrain and

human Activities) project (Thierry et al. 2008; Surono et al. 2012; Budi-Santoso et al. 2013; Jousset et al. 2013b) This broadband seismic network operated from July 2009; station L56 (Fig. 12.1) was installed in September 2010. A broadband station installed ~40 km south of Merapi at Imogiri, used as a reference for regional seismic activity, was replaced prior to the 2010 eruption by a short-period seismic station (CRM), as part of the MIAVITA project (Surono et al. 2012; Budi-Santoso et al. 2013; Jousset et al. 2013b). All seismic data were sent in real-time to BPPTKG (Balai Penyelidikan dan Pengembangan Teknologi Kebencanaan Geologi) in Yogyakarta (Fig. 12.1) using wireless transmission. During the peak of the 2010 eruption, three of the broadband stations (GMR, PAS, L56) and three of the four short-period stations (DEL, KLA, PUS) were destroyed and, therefore, the remaining broadband stations were included in the routine monitoring at the time. The remaining short-period station (PLA) was saturated on 4–5 November and individual events were indistinguishable. Therefore, seismic activity recorded at the distal seismic station (CRM) was crucial during the peak of the eruption, illustrating the importance of both proximal and distal seismic stations in the volcano monitoring network of Merapi (Surono et al. 2012; Budi-Santoso et al. 2013; Jousset et al. 2013b).

Deformation monitoring at Merapi was conducted via temporal measurements using EDM, and real-time measurements, using a tiltmeter platform consisting of three electronic tiltmeter stations at the summit and data acquisition using digital telemetry (e.g. Surono et al. 2012). EDM was used to measure the slope distance between several benchmarks, located at the Kaliurang, Babadan, Jarakah and Selo volcano observation posts as well as Deles (Fig. 12.1), and fixed targets (reflectors) around the summit of Merapi (Budi-Santoso et al. 2013; Aisyah et al. 2018). The reflectors south of the summit used in 2010 were moved to a lower elevation of 2400–2600 m on the 1911 lava flow, following the destruction of reflectors installed near Geger Buaya during the 2006 eruption. During the main eruption phases, ground-based geodetic

measurements were complemented by satellite data, providing insights into morphological changes at the summit, lava dome growth and PDC distribution, although cloud cover restricted data exploitation from optical satellite-based sensors (e.g. Surono et al. 2012; Pallister et al. 2013).

Geochemical monitoring prior to the 2010 eruption was carried out by regular measurements of gas composition from several fixed points of the solfatara in the Woro crater area. Gas samples were taken using the Giggenbach sampling method (Giggenbach 1975), followed by spectrophotometric and volumetric analysis. In 2009, a mini-DOAS instrument was also installed through the MIAVITA collaboration to measure gas emissions remotely from the Babadan observation post, although measurements carried out during the 2010 eruption from Babadan as well as from Ketep and Yogyakarta were challenging (Surono et al. 2012). Ground-based gas monitoring during the 2010 eruption was complemented by satellite data, which were particularly useful for the provision of real-time SO₂ emission measurements and ash cloud dispersal (Surono et al. 2012).

12.7.3.2 Formation of a Disaster Risk Reduction Forum: The Merapi Forum

In order to implement disaster risk reduction measures, the strategy for Merapi has been to establish a Disaster Risk Reduction (DRR) forum, the so-called Merapi Forum (see also Lavigne et al. 2023, Chap. 2). Since its inception in 2006, the Merapi Forum has been a collaborative forum between CVHGM and four local governments, supported by local and international NGOs, including the Early Recovery Assistance United Nations Development Programme (ERA-UNDP) and the Center for Disaster Management Study at the Universitas Pembangunan Nasional Veteran Yogyakarta in the framework of disaster risk reduction at Merapi. The five objectives of the cooperation have been (1) the application of Merapi risk analysis and maps, (2) the development of an early warning system, (3) the construction of a radio and web communication

system, (4) the preparation of contingency plans in each district, and (5) the strengthening of community capacity through disaster management training programmes. Used for the development of an early warning system, sirens were installed successfully in four locations, namely at the Kaliurang, Ngepos, Babadan and Jrahah volcano observation posts, and sounded as an order for evacuation for residents who live in the disaster-prone areas of Merapi. This was in addition to sirens that have been used since at least the early 1990s to warn people in the fields or in river valleys of impending danger. As not all public communication equipment around Merapi was covered by the mobile phone network, radio communication, which had long been used to connect the Yogyakarta headquarters with the villages on the slopes of Merapi, was still required. In 2008, the Merapi Forum established a VHF radio communication network that could reach all disaster-prone areas simultaneously. Additionally, standard procedures for the delivery of information through radio communication were formulated as a reference for the delivery of information on Merapi hazards.

12.7.3.3 Strengthening of Community Capacity Through Disaster Management Training and Information Dissemination

To reduce the risk from a future eruption of Merapi as in 2010, a disaster management training programme, aiming at strengthening the capacity of the community to overcome the socio-cultural vulnerability on the slopes of Merapi, has been a top priority. Implementation of the programme has been two-fold; under normal circumstances, disaster management training is carried out, while during a volcanic crisis, dissemination is done directly in the community. Disaster management training targets comprise aspects of knowledge, awareness and behaviour of the community in order to be safe from disasters. Subjects covered include knowledge of the sources of threats, early warning systems, understanding maps of

disaster-prone areas, and simulations of evacuation. In a volcanic crisis, dissemination is carried out for people living in disaster-prone areas, covering aspects such as the latest developments in the activity of Merapi, hazard estimation, and recommendations related to disaster risk reduction. Typically, a dissemination session lasts for about 2 h and is attended by 50–100 people.

After the volcanic earthquake swarm in October 2009 (Fig. 12.2), CVGHM held a disaster management training event on 16–17 December 2009 funded by ERA-UNDP. Among the 35 participants were the heads and community leaders of villages in disaster-prone areas in the Boyolali and Klaten regencies. Similar training events were held in the Magelang and Sleman districts on 22–23 December 2009. The trainees were chosen by the village heads and community leaders based on their involvement and responsibility for the community in case of an evacuation. Based on a survey of refugees during the 2010 eruption crisis, people received direct evacuation orders from the village head (54%), sirens (16%), radio/telephone communication equipment (19%) or neighbours (11%) (Mei et al. 2013).

With the beginning of the 2010 eruption and the shift to alert level II on 21 September 2010 (Fig. 12.2), dissemination of information in the disaster-prone area began. Between 29 September and 24 October 2010, people living in the most vulnerable areas, spread over 21 villages, were targeted. The last information dissemination event, which was attended by 35 residents, was held in Kinahrejo at the home of Mbah Marijan on 24 October 2010. The session failed to influence the participants to evacuate immediately, as they followed the orders of Mbah Marijan who refused to evacuate. Eventually they all fell victim to the first PDC at 17.02 WIB on 26 October 2010 (Fig. 12.2). In the aftermath of the eruption, Sri Sultan Hamengku Buwono X, the Sultan of the historic Yogyakarta Sultanate, appointed Mbah Marijan's son, Mas Asih, as Mbah Marijan's successor as caretaker of Merapi. This change may be regarded as the end of the era where a charismatic figure had been the mystical symbol of Merapi and the

beginning of an era in which the new caretaker is required to communicate with official institutions that observe the volcano's activity and in which the public is encouraged to accept science-based explanations rather than interpretations of dreams or irrational theories (Pajar Hatma 2012). The appointment of the new caretaker is symbolically interpreted as support for a modern mindset as opposed to support for a traditional mystical perspective.

12.7.3.4 Preparation of Contingency Plans

Contingency plans are important for local governments dealing with disasters in their regions and used to detect any gaps between the capacity and the magnitude of the threat, so that the appropriate strategy can be determined. The preparation of contingency plans for local governments has become a programme for the Merapi Forum involving various NGOs. Prior to the 2010 eruption crisis, contingency planning was carried out in four districts around Merapi (Sleman, Magelang, Klaten and Boyolali regencies) and completed in 2009. As a basis for the contingency plan, a scenario of a large eruption of Merapi directed towards the south was used, similar to the VEI 3 eruption in 1961. Following the guidelines, the eruption hazard scenario prepared on 8 June 2008 was based on (1) a maximum threat scenario to achieve optimal preparedness, (2) the history of Merapi eruptions, and (3) the experience and intuition of those involved in dealing with disasters at Merapi. In the completed scenario, the approximate runout distances and directions of the PDCs in the southern sector were estimated at 12 km in Kali Gendol, 10 km in Kali Woro, and 8 km in Kali Kuning and Kali Boyong. In addition, based on the history of the eruptions from 1872 to 2001, it was inferred that 90% of the PDCs followed the direction of the crater opening, which, since the 2006 eruption, was open to the south. Furthermore, it was estimated that 12,660 people in the Sleman Regency, 32,987 people in the Magelang Regency, 4420 people in the Klaten Regency, and 2540 people in the Boyolali Regency would have to be evacuated. When the 2010 eruption

eventually happened, it caused 398 victims due to PDCs and evacuation of nearly 400,000 people, the largest ever evacuation at Merapi because of an eruption that is thought to have saved 10,000–20,000 lives (Surono et al. 2012).

12.7.4 International Collaboration

The role of international cooperation was important to reduce the disaster risk at Merapi in 2010. For example, within the framework of the EU-funded MIAVITA project (2008–2012), coordinated by BRGM (Bureau de Recherches Géologiques et Minières—Risks Division, France), several broadband seismic stations were installed at Merapi (Sect. 12.7.3.1) and a programme of disaster management training was implemented for residents in the village of Tlogolele (Boyolali Regency) in the disaster-prone area on 2–4 July 2009. Following the issue of alert level III on 21 October 2010 (Fig. 12.2), the World Organization of Volcano Observatories (WOVO) at Nanyang Technological University (Singapore), offered to aid hazard assessment by modelling PDCs using the Titan2D Geophysical Mass-Flow Simulation Software developed at the State University of New York at Buffalo, and analysed SO₂ exposure in the atmosphere based on OMNI satellite imagery. Close collaboration with the Volcano Disaster Assistance Program (VDAP) of the United States Geological Survey (USGS) began when the activity of Merapi entered a critical phase on 25 October 2010 and the alert level was raised to level IV (Fig. 12.2). A crucial role of this cooperation was the provision of satellite imagery information to monitor the growing lava dome following the initial eruptions on 26 October 2010. The rapid growth of the lava dome before the peak of the eruption on 5 November 2010, was an important piece of information that formed the basis for the decision to expand the danger area from 10 to 15 km and, subsequently, to 20 km from the summit of Merapi (Figs. 12.1 and 12.2). This decision was of strategic importance to reduce the possibility of casualties caused by PDCs. Collaboration with the Sakurajima Volcano Observatory (SVO),

Japan began on 9 November 2010 and included petrological analysis and prediction, installation of infrasonic stations to detect explosive eruptions, and sampling and analysis of volcanic ash.

12.7.5 Reflection and Lessons Learned

Mitigation of volcanic risk depends on the ability of short-term predictions for early warning, rapid evacuation of people from hazardous areas, and land-use planning to reduce the risk of impending eruptions. A fundamental question related to volcanic hazard assessment and risk reduction is the long-term estimation of volcanic activity, which is critical for preparing contingency plans, disaster preparedness plans and land use planning strategies (e.g. Blong 1984; Scott 1989; Tilling 1989; MIAVITA Team 2012; Martí Molist 2017).

The disaster risk reduction strategy for the 2010 Merapi eruption was implemented precisely and comprehensively. Strengthening of the monitoring systems, data analysis, and accurate short-term predictions allowed early warnings in a manageable time window for preparedness and evacuation during the critical 35-day-long period between 20 September 2010, when the alert level was raised to level II, and 25 October 2010, when the alert level was raised to the highest level (level IV) (Fig. 12.2).

A mid-term assessment, which was represented in the eruption hazard scenario, proved helpful in preparing contingency plans for each district around Merapi. As a minimum, local governments were able to assess the resources they have and the magnitude of the threats they might face. However, the 2010 eruption exceeded the estimated danger as described in the eruption hazard scenario, which was based on a VEI 3 eruption and PDCs travelling as far as 12 km towards Kali Gendol. With a VEI of 4, the 2010 eruption was significantly larger than anticipated and PDC reached distances of ~16 km in Kali Gendol.

Even though the early warning given was relatively accurate and the disaster risk reduction strategy before the eruption was considered

appropriate, there were still many direct casualties (398) related to PDCs, total losses of >40 trillion IDR (>4.5 billion US\$) due to damage to infrastructures, livestock, agriculture and housing, and nearly 400,000 refugees.

Several factors caused casualties by PDCs during the 2010 eruption, which occurred in two stages. At the immediate onset of the eruption on 26 October, as many as 35 casualties were caused when residents refused to be evacuated, even though the alert level was at the highest level (level IV). The refusal of people to evacuate was due to strong local beliefs, exemplified by Mbah Marijan's attitude as a local figure, and the fact that they had remained unharmed during the previous eruption in 2006, which affected the same area. Further victims occurred when the eruption peaked on 5 November 2010. During a 1.5-h-long period of continuous PDCs on 3 November, the danger zone was expanded to a radius of 15 km, and on 5 November, the danger zone was expanded further to a radius of 20 km. Based on information from the government of the Sleman Regency, some people did not believe that the PDCs could reach more than 10 km. Further casualties were caused by confusion among the people as to where to go following a sudden evacuation order.

Along Kali Gendol, several Sabo dams were built to control lahars and volcanic sediment, and to inhibit PDCs. However, when PDCs hit a Sabo dam, additional hazards may result from rapid valley infilling by pyroclastic material or detachment of the hot ash cloud from the denser basal avalanche of the current (e.g. Charbonnier and Gertisser 2008, 2011; Lube et al. 2011; Gertisser et al. 2012a). Several people were unaware that to avoid the PDCs, they had to move away from the riverbank. This resulted in 49 deaths on both sides of the Sabo dam in Bronggang, ~15 km south of Merapi (Fig. 12.1). Overall, the fast changes in threats, which led to rapid changes of the size of the danger zone, was the main cause of the large number of casualties. These sudden changes did not give the community and the government enough time to prepare all matters related to massive evacuations.

The main reason for the number of refugees reaching 400,000 people was the increased displacement after the expansion of the danger zone to a radius of 20 km on 5 November 2010, based on refugee development data from BNPB. On 6 November 2010, there were additional 100,000 refugees in the western sector, namely in the Magelang Regency, which were mainly due to ash fall that affected this area because of the prevailing winds at the time. In the Boyolali (north), Klaten (east) and Sleman regencies (south), the number of refugees increased by 60,000. Refugee numbers continued to increase sharply until they reached a peak of 399,403 people, spread over more than 600 refugee barracks on 14 November 2010. Unplanned refugees contributed to this increase due to panic that was triggered by news issued by spiritual figures through television media stating that Merapi would erupt even more severely, affecting areas as far as 35 km away from the volcano, and that the Palace of Yogyakarta (Kraton) would disappear. To address this issue, BNPB held a closed emergency meeting at the Center for Disaster Management and Operations for Mt. Merapi, Yogyakarta on 15 November 2010, which was attended by all stakeholders. On this occasion, BNPB reported that the seismic activity had declined since 5 November and that a larger eruption was unlikely based on the amount of tephra already produced and on a comparison with historical eruption records. This was key to reducing public panic and controlling evacuations.

With the implemented strategic approach, there was an unavoidable risk of loss, including damage to immovable infrastructures and settlement sites and ecological losses in disaster-prone areas. Therefore, to reduce the risk of an impending eruption of Merapi, the Geological Agency issued the several recommendations in its rehabilitation and reconstruction programme:

- A map of the hazardous areas around Merapi should be used as a reference for spatial planning policies based on disaster mitigation. Subsequently, the Ministry of Public Works proposed Merapi as a National Strategic Area

(Indon.: Kawasan Strategis Nasional; KSN) to guide spatial planning, establishing Mount Merapi National Park through Presidential Regulation No. 70/2013. This step is regarded as a law enforcement map of the disaster-prone areas at Merapi that forms the basis for changing land use plans. When preparing detailed land use plans, local governments are required to refer to this Presidential Regulation.

- The area directly affected by the 2010 eruption was declared a restricted area for settlement. Utilisation of the area can be by cultivation such as plantations, agriculture, animal husbandry and tourism, as long as there are no accommodation facilities.
- People who were victims of the Merapi eruption in 2010, and whose homes were directly affected, had to be relocated to safer places. For people who still reside in parts of disaster-prone area (KRB) III that were not directly affected by the 2010 eruption, risk reduction efforts should be undertaken through social engineering (i.e. sustainable disaster management training) within a conceptual framework of living in harmony with Merapi.

12.8 Summary

The 2010 eruption of Merapi was the volcano's largest since 1872, differing markedly from other eruptions in the recent past. The eruption had clear precursors in the seismic, deformation and volcanic gas monitoring record. The earliest indications of renewed activity were observed about one year before the beginning of the eruption on 26 October 2010, demonstrated by a volcanic earthquake swarm and an increase in the rate of summit deformation. The 2010 eruption crisis lasted for about 3 months between September and November 2010. Early warning levels were gradually increased from alert level II on 20 September to alert level IV on 25 October, allowing about 35 days for mitigation measures to reduce disaster risk and save human lives. The runout distances of PDCs exceeded estimates

based on anticipated hazard scenarios, leading to crucial decisions to expand the danger area to a radius of 15 km on 3 November and to 20 km on 4 November 2010 before the climax of the eruption on 5 November, when PDCs propagated ~16 km down Kali Gendol. Despite the impact of the eruption that caused 398 casualties and considerable damage to infrastructures, it is estimated that the early warnings issued saved tens of thousands of lives. Apart from the remarkably long PDC runout, notable and in many respects unusual volcanic phenomena of the 2010 eruption included: (1) the lack of lava dome extrusion at the onset of the eruption, (2) the occurrence of powerful explosions that were directed laterally and focused to the south on 26 October and, particularly, during the paroxysmal phase on 5 November, when high-energy PDCs destroyed an area of up to 8.4 km from source on Merapi's south flank, (3) exceptionally high rates of lava dome extrusion and growth prior to and after the 5 November paroxysm, and (4) the generation of pumice-rich PDCs from collapse of short but sustained eruption columns. The 2010 eruption was driven by essentially the same basaltic andesite magma type as other recent Merapi eruptions. Multiple lines of evidence suggest that the exceptional magnitude of the eruption might have been caused by the arrival of deep, volatile-rich magma that disrupted and overwhelmed a shallower crystal-rich magma system, followed by rapid ascent, accompanying closed-system degassing and accumulation of ascending magma beneath a plugged conduit that builds up pressure in the uppermost conduit.

Acknowledgements The authors thank and respect Samsul Maarif, former Head of BNPB, Surono, former Head of the Center of Volcanology and Geological Hazard Mitigation (CVGHM; Indon.: Pusat Vulkanologi dan Mitigasi Bencana Geologi, PVMBG) and the Geological Agency, Ministry of Energy and Mineral Resources, and Raden Sukhyar, former Head of the Geological Agency, Ministry of Energy and Mineral Resources, for the management of the 2010 eruption crisis and the post-disaster rehabilitation and reconstruction phase. In addition, we gratefully acknowledge all staff members and volunteers of CVGHM, the Center for Research and Development of Geological Disaster

Technology (Indon.: Balai Penyelidikan dan Pengembangan Teknologi Kebencanaan Geologi, BPPTKG), and those in the Indonesian disaster management agencies and forums for disaster risk reduction, who were involved in the management of the eruption crisis that saved many lives. We are also grateful for fruitful discussions on various aspects of the 2010 eruption with a large number of colleagues in Indonesia and elsewhere, many of whom have contributed to this book. Philippe Jousset and Franck Lavigne are thanked for their detailed and constructive formal reviews that gave substantial input into this work and helped clarify the ideas presented in this chapter.

References

- Aisyah N, Iguchi M, Subandriyo BA, Hotta K, Sri Sumarti S (2018) Combination of a pressure source and block movement for ground deformation analysis at Merapi volcano prior to the eruptions in 2006 and 2010. *J Volcanol Geotherm Res* 357:239–253
- Bakkour D, Enjolras G, Thouret J-C, Kast R, Mei ETW, Prihatminingtyas B (2015) The adaptive governance of natural disaster systems: insights from the 2010 mount Merapi eruption in Indonesia. *Int J Disaster Risk Reduct* 13:167–188
- Baxter PJ, Jenkins S, Seswandhana R, Komorowski J-C, Dunn K, Purser D, Voight B, Shelley I (2017) Human survival in volcanic eruptions: thermal injuries in pyroclastic surges, their causes, prognosis and emergency management. *Burns* 43:1051–1069
- Beauducel F, Cornet F-H, Suhanto E, Duquesnoy T, Kasser M (2000) Constraints on magma flux from displacements data at Merapi volcano, Java, Indonesia. *J Geophys Res Solid Earth* 105(B4):8193–8203
- Belousov A, Voight B, Belousova M (2007) Directed blasts and blast-generated pyroclastic density currents: a comparison of the Bezymianny 1956, Mount St Helens 1980, and Soufrière Hills, Montserrat 1997 eruptions and deposits. *Bull Volcanol* 69:701–740
- Belousov A, Belousova M, Hoblitt R, Patia H (2020) The 1951 eruption of Mount Lamington, Papua New Guinea: devastating directed blast triggered by small-scale edifice failure. *J Volcanol Geotherm Res* 401:106947
- Bignami C, Ruch J, Chini M, Neri M, Buongiorno MF, Hidayati S, Sayudi DS, Surono (2013) Pyroclastic density current volume estimation after the 2010 Merapi volcano eruption using X-band SAR. *J Volcanol Geotherm Res* 261:236–243
- Blong RJ (1984) *Volcanic hazards: a source book on the effects of eruptions*. Academic Press, Sydney and London, p 424
- Borisova AY, Gurenko AA, Martel C, Kouzmanov K, Cathala A, Bohrson WA, Pratomio I, Sumarti S (2016) Oxygen isotope heterogeneity of arc magma recorded in plagioclase from the 2010 Merapi eruption (Central Java, Indonesia). *Geochim Cosmochim Acta* 190:13–34

- Borisova AY, Martel C, Gouy S, Pratomo I, Sumarti S, Toutain JP, Bindeman IN, de Parseval P, Metaxian JP, Surono (2013) Highly explosive 2010 Merapi eruption: evidence for shallow level crustal assimilation and hybrid fluid. *J Volcanol Geotherm Res* 261:193–208
- Botcharnikov RE, Behrens H, Holtz F, Koepke J, Sato H (2004) Sulfur and chlorine solubility in Mt. Unzen rhyodacitic melt at 850 °C and 200 MPa. *Chem Geol* 213:207–225
- Buddington AF, Lindsley DH (1964) Iron-titanium oxide minerals and synthetic equivalents. *J Petrol* 5:310–357
- Budi-Santoso A, Lesage P, Dwiyono S, Sumarti S, Subandriyo S, Jousset P, Metaxian JP (2013) Analysis of the seismic activity associated with the 2010 eruption of Merapi volcano, Java. *J Volcanol Geotherm Res* 261:153–170
- Budi-Santoso A, Beauducel F, Nandaka IGMA, Humaida H, Costa F, Widiwijayanti C, Iguchi M, Métaxian J-P, Rudianto I, Rozin M, Sulistiyani, Nurdin I, Kelfoun K, Byrdina S, Pinel V, Fahmi AA, Laurin A, Rizal MH, Dahamna N (2023) The Merapi volcano monitoring system. In: Gertisser R, Troll VR, Walter TR, Nandaka IGMA, Ratdomopurbo A (eds) *Merapi volcano—geology, eruptive activity, and monitoring of a high-risk volcano*. Springer, Berlin, Heidelberg, pp 409–436
- Caricchi L, Sheldrake TE, Blundy J (2018) Modulation of magmatic processes by CO₂ flushing. *Earth Planet Sci Lett* 491:160–171
- Carr BB, Clarke AB, de' Michieli Vitturi M (2020). Volcanic conduit controls on effusive-explosive transitions and the 2010 eruption of Merapi volcano (Indonesia). *J Volcanol Geotherm Res* 392:106767
- Carroll MR, Webster JD (1994) Solubilities of sulfur, noble gases, nitrogen, chlorine, and fluorine in magmas. *Rev Mineral* 30:231–280
- Charbonnier SJ, Gertisser R (2008) Field observations and surface characteristics of pristine block-and-ash flow deposits from the 2006 eruption of Merapi volcano, Java, Indonesia. *J Volcanol Geotherm Res* 177:971–982
- Charbonnier S, Gertisser R (2011) Deposit architecture and dynamics of the 2006 block-and-ash flows of Merapi volcano, Java, Indonesia. *Sedimentology* 58:1573–1612
- Charbonnier SJ, Germa A, Connor CB, Gertisser R, Preece K, Komorowski J-C, Lavigne F, Dixon T, Connor L (2013) Evaluation of the impact of the 2010 pyroclastic density currents at Merapi volcano from high-resolution satellite imagery, field investigations and numerical simulations. *J Volcanol Geotherm Res* 261:295–315
- Clarke AB, Voight B (2000) Pyroclastic current dynamic pressures from aerodynamics of tree or pole blow-down. *J Volcanol Geotherm Res* 100:395–412
- Costa F, Andreastuti S, Bouvet de Maisonneuve C, Pallister JS (2013) Petrological insights into the storage conditions, and magmatic processes that yielded the centennial 2010 Merapi explosive eruption. *J Volcanol Geotherm Res* 261:209–235
- Cronin SJ, Lube G, Dayudi DS, Sumarti S, Subrandiyo S, Surono (2013) Insights into the October–November 2010 Gunung Merapi eruption (Central Java, Indonesia) from the stratigraphy, volume and characteristics of its pyroclastic deposits. *J Volcanol Geotherm Res* 261:244–259
- CVGHM (Center of Volcanology and Geological Hazard Mitigation) (2002) Merapi volcano hazard map. Bandung
- CVGHM (Center of Volcanology and Geological Hazard Mitigation) (2011) Revised Merapi volcano hazard map. Bandung
- Darmawan H, Putra R, Budi-Santoso A, Humaida H, Walter TR (2023) Morphology and instability of the Merapi lava dome monitored by unoccupied aircraft systems. In: Gertisser R, Troll VR, Walter TR, Nandaka IGMA, Ratdomopurbo A (eds) *Merapi volcano—geology, eruptive activity, and monitoring of a high-risk volcano*. Springer, Berlin, Heidelberg, pp 457–472
- de Bézilal É, Lavigne F, Robin AK, Sri Hadmoko D, Cholik N, Thouret J-C, Sawudi DS, Muzani M, Sartohadi J, Vidal C (2013) Rain-triggered lahars following the 2010 eruption of Merapi volcano, Indonesia: a major risk. *J Volcanol Geotherm Res* 261:330–347
- de Bézilal É, Lavigne F, Grancher D (2011) Quand l'aléa devient la ressource: l'activité d'extraction des matériaux volcaniques autour du volcan Merapi (Indonésie) dans la compréhension des risques locaux. *Cybergeo: Eur J Geogr* [online] 525. <http://journals.openedition.org/cybergeo/23555>
- Deegan FM, Troll VR, Gertisser R, Freda C (2023) Magma-carbonate interaction at Merapi volcano, Indonesia. In: Gertisser R, Troll VR, Walter TR, Nandaka IGMA, Ratdomopurbo A (eds) *Merapi volcano—geology, eruptive activity, and monitoring of a high-risk volcano*. Springer, Berlin, Heidelberg, pp 291–321
- Delmelle P, Stix J (2000) Volcanic gases. In: Sigurdsson H, Houghton BF, McNutt SR, Rymer H, Stix J (eds) *Encyclopedia of volcanoes*. Academic Press, pp 803–816
- Dove MR (2008) Perception of volcanic eruption as agent of change on Merapi volcano, Central Java. *J Volcanol Geotherm Res* 172:329–337
- Drignon MJ, Bechon T, Arbaret L, Burgisser A, Komorowski J-C, Martel C, Miller H, Yaputra R (2016) Preexplosive conduit conditions during the 2010 eruption of Merapi volcano (Java, Indonesia). *Geophys Res Lett* 43:11595–11602
- Erdmann S, Martel C, Pichavant M, Kushnir A (2014) Amphibole as an archivist of magmatic crystallization conditions: problems, potential, and implications for inferring magma storage prior to the paroxysmal 2010 eruption of Mount Merapi, Indonesia. *Contrib Mineral Petrol* 167:1016

- Erdmann S, Martel C, Pichavant M, Bourdier J-L, Champallier R, Komorowski J-C, Cholik N (2016) Constraints from phase equilibrium experiments on pre-eruptive storage conditions in mixed magma systems: a case study on crystal-rich basaltic andesites from Mount Merapi, Indonesia. *J Petrol* 57:535–560
- Escher BG (1933) On a classification of central eruptions according to gas pressure of the magma and viscosity of the lava. *Leidsche Geol Med* 6:45–49
- Gauthier PJ, Condomines M (1999) ^{210}Pb - ^{226}Ra radioactive disequilibria in recent lavas and radon degassing: inferences on the magma chamber dynamics at Stromboli and Merapi volcanoes. *Earth Planet Sci Lett* 172:111–126
- Gertisser R, Keller J (2003) Trace element and Sr, Nd, Pb and O isotope variations in medium-K and high-K volcanic rocks from Merapi Volcano, Central Java, Indonesia: evidence for the involvement of subducted sediments in Sunda Arc magma genesis. *J Petrol* 44:457–486
- Gertisser R, Charbonnier SJ, Troll VR, Keller J, Preece K, Chadwick JP, Barclay J, Herd RA (2011) Merapi (Java, Indonesia): anatomy of a killer volcano. *Geol Today* 27:57–62
- Gertisser R, Cassidy NJ, Charbonnier SJ, Nuzzo L, Preece K (2012a) Overbank block-and-ash flow deposits and the impact of valley-derived, unconfined flows on populated areas at Merapi volcano, Java, Indonesia. *Nat Hazards* 60:623–648
- Gertisser R, Charbonnier SJ, Keller J, Quidelleur X (2012b) The geological evolution of Merapi volcano, Central Java, Indonesia. *Bull Volcanol* 74:1213–1233
- Gertisser R, Troll VR, Nandaka IGMA (2023a) The scientific discovery of Merapi: from ancient Javanese sources to the 21st century. In: Gertisser R, Troll VR, Walter TR, Nandaka IGMA, Ratdomopurbo A (eds) *Merapi volcano—geology, eruptive activity, and monitoring of a high-risk volcano*. Springer, Berlin, Heidelberg, pp 1–44
- Gertisser R, del Marmol M-A, Newhall C, Preece K, Charbonnier S, Andreastuti S, Handley H, Keller J (2023b) Geological history, chronology and magmatic evolution of Merapi. In: Gertisser R, Troll VR, Walter TR, Nandaka IGMA, Ratdomopurbo A (eds) *Merapi volcano—geology, eruptive activity, and monitoring of a high-risk volcano*. Springer, Berlin, Heidelberg, pp 137–193
- Giggenbach WF (1975) A simple method for collecting and analysis of volcanic gas samples. *Bull Volcanol* 39:132–145
- Global Volcanism Program (2013) *Volcanoes of the world*, v 4.9.4 (17 Mar 2021), Venzke E (ed) Smithsonian Institution. Downloaded 27 Apr 2021. <https://doi.org/10.5479/si.GVP.VOTW4-2013>
- Grandjean JB (1931a) Korte mededeeling over de uitbarsting van den Merapi op 18 December 1930. *De Mijningingenieur* 12(1):4–6
- Grandjean JB (1931b) De uitbarsting van den Merapi in 1930. *De Mijningingenieur* 12(4):47
- Grandjean JB (1931c) Bijdrage tot de kennis der Gloedwolken van den Merapi van Midden-Java. *De Mijningingenieur* 12(12):20–25
- Haggerty SE (1993) Oxide textures—A mini-atlas. In: Lindsley DH (ed) *Oxide minerals: petrologic and magnetic significance*. *Rev Mineral* 25:303–321
- Handley HK, Reagan M, Gertisser R, Preece K, Berlo K, McGee LE, Barclay J, Herd R (2018) Timescales of magma ascent and degassing and the role of crustal assimilation at Merapi volcano (2006–2010), Indonesia: constraints from uranium-series and radiogenic isotopic compositions. *Geochim Cosmochim Acta* 222:34–52
- Hidayat D, Voight B, Langston C, Ratdomopurbo A, Ebeling C (2000) Broadband seismic experiment at Merapi volcano, Java, Indonesia: very-long-period pulses embedded in multiphase earthquakes. *J Volcanol Geotherm Res* 100:215–231
- Holmberg K (2023) Merapi and its dynamic ‘disaster culture’. In: Gertisser R, Troll VR, Walter TR, Nandaka IGMA, Ratdomopurbo A (eds) *Merapi volcano—geology, eruptive activity, and monitoring of a high-risk volcano*. Springer, Berlin, Heidelberg, pp 67–87
- Ikhsan J, Fujita M, Takebayashi H (2010) Sediment disaster and resource management in the Mount Merapi area, Indonesia. *Int J Eros Control Eng* 3:43–52
- Jenkins S, Komorowski J-C, Baxter PJ, Spence R, Picquout A, Lavigne F, Surono (2013) The Merapi 2010 eruption: an interdisciplinary impact assessment methodology for studying pyroclastic density current dynamics. *J Volcanol Geotherm Res* 261:316–329
- Jenkins S, Phillips JC, Price R, Feloy K, Baxter PJ, Hadmoko DS, de Bézal E (2015) Developing building-damage scales for lahars: application to Merapi volcano, Indonesia. *Bull Volcanol* 77:75
- Jousset P, Pallister P, Surono (2013a) The 2010 eruption of Merapi volcano. *J Volcanol Geotherm Res* 261:1–6
- Jousset P, Budi-Santoso A, Jolly AD, Boichu M, Surono, Dwiyono S, Sumarti S, Hidayati S, Thierry P (2013b) Signs of magma ascent in LP and VLP seismic events and link to degassing: an example from the 2010 explosive eruption at Merapi volcano, Indonesia. *J Volcanol Geotherm Res* 261:171–192
- Kelfoun K, Gueugneau V, Komorowski J-C, Aisyah N, Cholik N, Merciecca C (2017) Simulation of block-and-ash flows and ash-cloud surges of the 2010 eruption of Merapi volcano with a two-layer model. *J Geophys Res Solid Earth* 122:4277–4292
- Kelman I, Mather TA (2008) Living with volcanoes: the sustainable livelihoods approach for volcano-related opportunities. *J Volcanol Geotherm Res* 172:189–198
- Kemmerling GLL (1932) De controverse uitgesloten gloedwolken (nuées ardentes d’explosion dirigée) of lawinen-gloedwolken (nuées ardentes d’avalanche). *De Ingenieur* 47:129–137
- Paroxysmal dome explosion during the Merapi 2010 eruption: processes and facies relationships of associated high-energy pyroclastic density currents. *J Volcanol Geotherm Res* 261:260–294

- Kubanek J, Westerhaus M, Schenk A, Aisyah N, Brotopuspito KS, Heck B (2015) Volumetric change quantification of the 2010 Merapi eruption using TanDEM-X InSAR. *Remote Sens Environ* 164: 16–25
- Kushnir ARL, Martel C, Bourdier J-L, Heap M, Reuschlé T, Erdmann S, Komorowski J-C, Cholik N (2016) Probing permeability and microstructure: unravelling the role of a low-permeability dome on the explosivity of Merapi (Indonesia). *J Volcanol Geotherm Res* 316:56–71
- Kushnir ARL, Martel C, Champallier R, Wadsworth FB (2017) Permeability evolution in variably glassy basaltic andesites measured under magmatic conditions. *Geophys Res Lett* 44:10262–10271
- Lavigne F, Morin J, Surono M (2015) Atlas of Merapi volcano. Laboratoire de Géographie Physique, Meudon, France, 58 color plates. Online Publication (hal-03010922)
- Lavigne F, Mei ETW, Morin J, Humaida H, Moatty A, de Bézal E, Sri Hadmoko D, Grancher D, Picquout A (2023) Physical environment and human context at Merapi volcano: a complex balance between accessing livelihoods and coping with volcanic hazards. In: Gertisser R, Troll VR, Walter TR, Nandaka IGMA, Ratdomopurbo A (eds) *Merapi volcano—geology, eruptive activity, and monitoring of a high-risk volcano*. Springer, Berlin, Heidelberg, pp 45–66
- Le Guern F, Gerlach TM, Nohl A (1982) Field gas chromatograph analyses of gases from a glowing dome at Merapi volcano, Java, Indonesia, 1977, 1978, 1979. *J Volcanol Geotherm Res* 14:223–245
- Le Maitre RW (ed), Streckeisen A, Zanettin B, Le Bas MJ, Bonin B, Bateman P, Bellieni G, Dudek A, Efremova J, Keller J, Lameyre J, Sabine PA, Schmidt R, Sørensen H, Woolley AR (2002) Igneous rocks. A classification and glossary of terms. In: *Recommendations of the International Union of Geological Sciences subcommission on the systematics of igneous rocks*. University Press, Cambridge
- Leake BE, Woolley AR, Arps CES, Birch WD, Gilbert MC, Grice JD, Hawthorne FC, Kato A, Kisch HJ, Krivovichev V, Linthout K, Laird J, Mandarino J, Maresch WV, Nickel EH, Rock NMS, Schumacher JC, Smith DC, Stephenson NCN, Ungaretti L, Whittaker EJW, Youzhi G (1997) Nomenclature of amphiboles: report of the subcommittee on amphiboles of the International Mineralogical Association Commission on new minerals and mineral names. *Mineral Mag* 61:295–321
- Lerner GA, Jenkins SF, Charbonnier SJ, Komorowski J-C, Baxter PJ (2021) The hazards of unconfined pyroclastic density currents: a new synthesis and classification according to their deposits, dynamics, and thermal and impact characteristics. *J Volcanol Geotherm Res* 107429. <https://doi.org/10.1016/j.jvolgeores.2021.107429>
- Li W, Costa F, Nagashima K (2021) Apatite crystals reveal melt volatile budgets and magma storage depths at Merapi volcano, Indonesia. *J Petrol* 62:egaa100
- Lube G, Breard ECP, Jones J, Fullard L, Dufek J, Cronin SJ, Wang T (2019) Generation of air lubrication within pyroclastic density currents. *Nat Geosci* 12:381–386
- Lube G, Cronin SJ, Thouret J-C, Surono (2011) Kinematic characteristics of pyroclastic density currents at Merapi and controls on their avulsion from natural and engineered channels. *Geol Soc Am Bull* 123:1127–1140
- Maly E, Nareswari A (2015). Housing relocation after the 2010 eruption of Mt. Merapi, Indonesia. In: 7th i-Rec conference: reconstruction and recovery in urban contexts. London, 6–8 July 2015
- Marti Molist J (2017) Assessing volcanic hazard: a review. Oxford Handbooks Online. <https://doi.org/10.1093/oxfordhb/9780190699420.013.3>
- Mei ETW, Lavigne F (2013) Mass evacuation of the 2010 Merapi eruption. *Int J Emerg Manag* 9:298–311
- Mei ETW, Lavigne F, Picquout A, de Bézal E, Brunstein D, Grancher D, Sartohadi J, Cholik N, Vidal C (2013) Lessons learned from the 2010 evacuations at Merapi volcano. *J Volcanol Geotherm Res* 261:348–365
- Mei ETW, Fajarwatia A, Hasanatia S, Saria IM (2016) Resettlement following the 2010 Merapi volcano eruption. *Procedia Soc Behav Sci* 227:361–369
- Mei ETW, Lavigne F (2012) *Pengungsian Penduduk Selama Erupsi Gunung Merapi 2010*, dalam *Buku Erupsi Gunung Merapi 2010 vol 2*, Yogyakarta
- MIAVITA Team (2012) *Handbook for volcanic risk management—Prevention, crisis management, resilience*. Orléans, France, 204 pp. <https://reliefweb.int/report/world/handbook-volcanic-risk-management-prevention-crisis-management-resilience>
- Morimoto N (1988) Nomenclature of pyroxenes. *Mineral Petrol* 39:55–76
- Neumann van Padang M (1933) De uitbarsting van den Merapi (Midden Java) in de jaren 1930–1931. *Vulkanol Seismol Med* 12:1–117
- Pajar Hatma IJ (2012) Dinamika Pola Pikir Orang Jawa Di Tengah Arus Modernisasi. *Humaniora* 24:133–140
- Pallister JS, Schneider DJ, Griswold JP, Keeler RH, Burton WC, Noyles C, Newhall CG, Ratdomopurbo A (2013) Merapi 2010 eruption—Chronology and extrusion rates monitored with satellite radar and used in eruption forecasting. *J Volcanol Geotherm Res* 261:144–152
- Picquout A, Lavigne F, Mei ETW, Grancher D, Cholik N, Vidal CM, Hadmoko DS (2013) Air traffic disturbance due to the 2010 eruption of Merapi volcano. *J Volcanol Geotherm Res* 261:366–375
- Preece K, Gertisser R, Barclay J, Berlo K, Herd RA, Facility EIM (2014) Pre- and syn-eruptive degassing and crystallisation processes of the 2010 and 2006 eruptions of Merapi volcano, Indonesia. *Contrib Mineral Petrol* 168:1061
- Preece K, Gertisser R, Barclay J, Charbonnier SJ, Komorowski J-C, Herd RA (2016) Transitions between explosive and effusive phases during the cataclysmic 2010 eruption of Merapi volcano, Java, Indonesia. *Bull Volcanol* 78:54

- Preece K, van der Zwan F, Hammer J, Gertisser R (2023) A textural perspective on the magmatic system and eruptive behaviour of Merapi volcano. In: Gertisser R, Troll VR, Walter TR, Nandaka IGMA, Ratdomopurbo A (eds) *Merapi volcano—geology, eruptive activity, and monitoring of a high-risk volcano*. Springer, Berlin, Heidelberg, pp 265–289
- Preece K (2014) Transitions between effusive and explosive activity at Merapi volcano, Indonesia: a volcanological and petrological study of the 2006 and 2010 eruptions. Ph.D. thesis, University of East Anglia, Norwich, UK
- Preece K, Barclay J, Gertisser R, Herd RA (2013) Textural and micro-petrological variations in the eruptive products of the 2006 dome-forming eruption of Merapi volcano, Indonesia: implications for sub-surface processes. *J Volcanol Geotherm Res* 261:98–120
- Ratdomopurbo A, Beauceul F, Subandriyo J, Nandaka IGMA, Newhall CG, Suharna, Sayudi DS, Suparwaka H, Sunarta (2013) Overview of the 2006 eruption of Mt. Merapi. *J Volcanol Geotherm Res* 261:87–97
- Ratdomopurbo A, Poupinet G (2000) An overview of the seismicity of Merapi volcano (Java, Indonesia), 1983–1994. *J Volcanol Geotherm Res* 100:193–214
- Ratdomopurbo A (1995) Etude sismologique du volcan Mérapi et formation du dôme de 1994. Ph.D. thesis, University of Joseph Fourier, Grenoble, France
- Saepuloh A, Urai M, Aisyah N, Sunarta WC, Subandriyo JP (2013) Interpretation of ground surface changes prior to the 2010 large eruption of Merapi volcano using ALOS/PALSAR, ASTER TIR and gas emission data. *J Volcanol Geotherm Res* 261:130–143
- Schlehe J (1996) Reinterpretations of mystical traditions. Explanations of a volcanic eruption in Java. *Anthropos* 91:391–409
- Schwarzkopf LM, Schmincke H-U, Troll VR (2001) Pseudotachylite on impact marks of block surfaces in block-and-ash flows at Merapi volcano, Central Java, Indonesia. *Int J Earth Sci* 90:769–775
- Scott WE (1989) Volcanic-hazards zonation and long-term forecasts. In: Tilling RI (ed) *Volcanic hazards*, vol 1. Short Courses in geology, pp 25–49
- Shinohara H, Aiuppa A, Giudice G, Gurrieri S, Liuzzo M (2008) Variation of H₂O/CO₂ and CO₂/SO₂ ratios of volcanic gases discharged by continuous degassing of Mount Etna volcano, Italy. *J Geophys Res Solid Earth* 113:B09203
- Shinohara H, Matsushima N, Kazahaya K, Ohwada M (2011) Magma-hydrothermal system interaction inferred from volcanic gas measurements obtained during 2003–2008 at Meakandake volcano, Hokkaido, Japan. *Bull Volcanol* 73:409–421
- Siebert L, Simkin T, Kimberly P (2011) *Volcanoes of the world*. University of California Press, Berkeley
- Siswawidjono S, Suryo I, Yokoyama I (1995) Magma eruption rates of Merapi volcano, Central Java, Indonesia during one century (1890–1992). *Bull Volcanol* 57:111–116
- Solikhin A, Thouret J-C, Liew SC, Gupta A, Sayudi DS, Oehler J-F, Kassouk Z (2015) High spatial-resolution imagery helps map deposits of the large (VEI 4) 2010 Merapi volcano eruption and their impact. *Bull Volcanol* 77:20
- Sparks RSJ, Barclay J, Calder ES, Herd RA, Luckett R, Norton GE, Pollard L, Robertson RA, Ritchie L, Voight B, Young SR, Woods AW (2002) Generation of a debris avalanche and violent pyroclastic density current: the Boxing Day eruption of 26 December 1997 at the Soufrière Hills volcano, Montserrat. In: Druitt T, Kokelaar BP (eds) *The eruption of Soufrière Hills volcano, Montserrat, from 1995–1999*. Geol Soc London Mem 21:409–434
- Sumarti S, Suryono (1994) Chemistry model of Merapi volcano, Technical Report, The fifth field workshop on volcanic gases in Indonesian volcanoes, Volcanological Survey of Indonesia, Bandung, pp 96–111
- Surono JP, Pallister J, Boichu M, Buongiorno MF, Budisantoso A, Costa F, Andreastuti S, Prata F, Schneider D, Clarisse L, Humaida H, Sumarti S, Bignami C, Griswold J, Carn S, Oppenheimer C, Lavigne F (2012) The 2010 explosive eruption of Java's Merapi volcano—A '100-year' event. *J Volcanol Geotherm Res* 241–242:121–135
- Tanguy J-C (1994) The 1902–1905 eruptions of Montagne Pelée, Martinique: anatomy and retrospection. *J Volcanol Geotherm Res* 60:87–107
- Tanguy J-C (2004) Rapid dome growth at Montagne Pelée during the early stages of the 1902–1905 eruption: a reconstruction from Lacroix's data. *Bull Volcanol* 66:615–621
- Taylor GA (1958) The 1951 eruption of Mount Lamington, Papua. *Austr Bur Mineral Res Geol Geophys* 38:1–117
- Thierry P, Jousset P, Le Cozannet G (2008) MIAVITA: mitigate and assess risk from volcanic impact on terrain and human activities. In: Abstract—IAVCEI General Assembly, 17–22 Aug 2008, Reykjavik, Iceland
- Thouret J-C, Aisyah N, Jenkins SF, de Belizal E, Sulistiyani, Charbonnier S, Sayudi DS, Nandaka IGMA, Mainsant G, Solikhin A (2023) Merapi's lahars: characteristics, behaviour, monitoring, impact, hazard modelling and risk assessment. In: Gertisser R, Troll VR, Walter TR, Nandaka IGMA, Ratdomopurbo A (eds) *Merapi volcano—geology, eruptive activity, and monitoring of a high-risk volcano*. Springer, Berlin, Heidelberg, pp 501–552
- Tilling RI (1989) Volcanic hazards and their mitigation: progress and problems. *Rev Geophys* 27:237–269
- Trolese M, Giordano G, Komorowski J-C, Jenkins SF, Baxter PJ, Cholik N, Raditya P, Corrado S (2018) Very rapid cooling of the energetic pyroclastic density currents associated with the 5 November 2010 Merapi eruption (Indonesia). *J Volcanol Geotherm Res* 358:1–12
- Troll VR, Deegan FM (2023) The magma plumbing system of Merapi: the petrological perspective. In: Gertisser R, Troll VR, Walter TR, Nandaka IGMA,

- Ratdomopurbo A (eds) Merapi volcano—geology, eruptive activity, and monitoring of a high-risk volcano. Springer, Berlin, Heidelberg, pp 233–263
- Voight B (1988) A method for prediction of volcanic eruptions. *Nature* 332:125–130
- Voight B, Constantine EK, Siswamidjono S, Torley R (2000) Historical eruptions of Merapi volcano, Central Java, Indonesia, 1768–1998. *J Volcanol Geotherm Res* 100:69–138
- Whitley S, Gertisser R, Halama R, Preece K, Troll VR, Deegan FM (2019) Crustal CO₂ contribution to subduction zone degassing recorded through calc-silicate xenoliths in arc lavas. *Sci Rep* 9:8803
- Whitley S, Halama R, Gertisser R, Preece K, Deegan FM, Troll VR (2020). Magmatic and metasomatic effects of magma-carbonate interaction recorded in calc-silicate xenoliths from Merapi volcano (Indonesia). *J Petrol* 61:egaa048
- Widiyantoro S, Ramdhan M, Métaxian J-P, Cummins PR, Martel C, Erdmann S, Nugraha AD, Budi-Santoso A, Laurin A, Fahmi AA (2018) Seismic imaging and petrology explain highly explosive eruptions of Merapi volcano, Indonesia. *Sci Rep* 8:13656



The Merapi Volcano Monitoring System

13

Agus Budi-Santoso, François Beauducel,
I Gusti Made Agung Nandaka, Hanik Humaida,
Fidel Costa, Christina Widiwijayanti,
Masato Iguchi, Jean-Philippe Métaxian,
Indra Rudianto, Much Rozin, Sulistiyani,
Ilham Nurdin, Karim Kelfoun, Svetlana Byrdina,
Virginie Pinel, Ali Ahmad Fahmi,
Antoine Laurin, Mochammad Husni Rizal,
and Nabil Dahamna

Abstract

Merapi volcano has the most advanced and comprehensive monitoring system in Indonesia. Monitoring at the volcano started in 1920, when the Dutch East Indies government established the *Vulkaanbewakingsdienst*. Since then, monitoring, initially carried out visually, evolved rapidly using bespoke monitoring equipment and modern technology, and with intensive cooperation with scientists and institutions from abroad. At present, BPPTKG (Balai Penyelidikan dan Pengembangan

Teknologi Kebencanaan Geologi) in Yogyakarta has the mandate for hazard mitigation and the task of monitoring and providing early warnings to save local communities at risk from eruptions of Merapi. In carrying out its duties, BPPTKG manages a monitoring network consisting of various techniques, including seismic, deformation, gas and temperature monitoring, visual observations and attempts to improve monitoring techniques and methods, data handling and ways to provide early warning information. One of the fundamental recent changes in the Merapi monitoring sys-

A. Budi-Santoso (✉) · I G. M. A. Nandaka (✉) ·
H. Humaida · I. Rudianto · M. Rozin · Sulistiyani ·
I. Nurdin
Balai Penyelidikan dan Pengembangan Teknologi
Kebencanaan Geologi, CVGHM, Geological
Agency of Indonesia, Jl. Cendana No. 15,
Yogyakarta 55166, Indonesia
e-mail: agus.budi@esdm.go.id

I G. M. A. Nandaka
e-mail: agung.nandaka@esdm.go.id

F. Beauducel · J.-P. Métaxian
Institut de Physique du Globe de Paris, Université de
Paris, 1 rue Jussieu, 75005 Paris, France

F. Costa · C. Widiwijayanti
Earth Observatory of Singapore (EOS), Nanyang
Technological University, 50 Nanyang Avenue,
Singapore 639798, Singapore

M. Iguchi
Disaster Prevention Research Institute, Sakurajima
Volcano Research Center, Kyoto University,
1722-19 Sakurajima-Yokoyama, Kagoshima
891-1419, Japan

K. Kelfoun
Université Clermont-Auvergne, Laboratoire Magmas
et Volcans, CNRS, OPGC et IRD, Campus les
Cézeaux, 6 avenue Blaise Pascal, 63178 Aubières,
France

S. Byrdina · A. A. Fahmi · A. Laurin · M. H. Rizal ·
N. Dahamna
Institut de Recherche pour le Développement (IRD),
Paris, France

V. Pinel
Institut des Sciences de la Terre, Université Savoie
Mont Blanc, 27 rue Marcoz, 73000 Chambéry,
France

tem has been the transition in data processing from off-line-based to real-time, on-line-based techniques. Although the current Merapi monitoring system is presently at its most advanced, monitoring and anticipating changes in eruption styles, particularly those with weak precursors, such as phreatic eruptions, remain challenging.

Keywords

Merapi volcano · Research and monitoring · International partnership · Modelling

13.1 Introduction

As one of the most active and hazardous volcanoes in Indonesia, monitoring of Merapi volcano has always been a priority of the Indonesian authorities. Since 1920, when systematic observations were essentially carried out visually through volcano observation posts, volcano monitoring at Merapi has developed through time using specific monitoring equipment and modern technology, capitalising on technical and scientific advances and international collaborations. Today, Merapi is the volcano with the most modern and extensive monitoring system in Indonesia, which, uniquely for Indonesia's volcanoes, includes five volcano observation posts. The Merapi volcano monitoring system is operated by BPPTKG (Balai Penyelidikan dan Pengembangan Teknologi Kebencanaan Geologi) in Yogyakarta, informally also known as the Merapi Volcano Observatory. Significant improvements of the monitoring network and advances in volcano monitoring at Merapi were made since the later parts of the twentieth century and have continued after the devastating eruption in 2010. This chapter describes the development of the Merapi monitoring system and offers insights into future challenges.

13.2 Volcano Monitoring at Merapi: 1920–2010

Monitoring of volcanic activity at Merapi officially began when the Dutch East Indies administration established the *Vulkaanbewakingsdienst* in 1920, which, from 1922, was called *Vulkanologisch Onderzoek*. The Merapi monitoring activity was initially carried out visually from an observatory post at Maron, about 6 km west of the summit of Merapi (see also Gertisser et al. 2023, Chap. 1). There were also periodic investigations around the volcano's crater, including temperature measurements and morphological observations. In 1924, seismic activity monitoring began with a Wiechert mechanical seismograph. Later, in 1955, an Akashi seismograph began to be used. This electromagnetic seismograph could be placed in a more appropriate location using a cable connection. In 1978, the National Volcanological Agency became the *Direktorat Vulkanologi*, also known as the Volcanological Survey of Indonesia (VSI). Currently, BPPTKG, a technical implementation unit of the Center for Volcanology and Geological Hazards Mitigation (CVGHM; formerly of VSI) under the Geological Agency, both located in Bandung, and the Ministry of Energy and Mineral Resources of Indonesia, located in Jakarta, carries out the monitoring of Merapi.

During the late 1970s to 1980s, the monitoring capabilities rapidly increased along with the rise of research collaborations with other countries. In 1977, an experimental network of nuclear magnetic resonance sensors was installed by the French *Commissariat à l'Énergie Atomique* (CEA) geophysical laboratory. In 1982, remote sensing techniques began to be applied in geochemical monitoring in the form of SO₂ emission measurement through observatory stations using COSPEC (CORrelation SPECTroscopy). In the same year, wireless technology was used in seismic monitoring using analog radio frequency modulation. Through collaboration with the

Volcano Disaster Assistance Program (VDAP) of the United States Geological Survey (USGS), 6 short-period seismometers were installed around the volcano at distances to the crater ranging from 0 to 6 km and equipped with VHF radio transmissions. Ground deformation methods also began to be applied at Merapi at that time. The measurement of slope distance between the summit and observatory stations using infrared light, also known as EDM (Electronic Distance Measurement), was carried out in 1988. In 1990, a real-time, remotely controlled visual camera was developed and installed on the summit crater rim by CEA to monitor lava dome growth, but it was destroyed by a cliff landslide 3 years later.

In 1993, ground deformation monitoring was strengthened by the first continuous tiltmeter stations and repeated measurements of GPS benchmarks, used at almost the same time through collaboration with the USA and France. During the 1990s and 2000s, collaborators from Germany installed broadband digital seismometers, continuous GPS, and shallow borehole tiltmeters on the volcano flank. Through research collaboration with scientists from France and Germany in particular, various less standard monitoring methods, such as magnetic, micro-gravimetric, kinematic GPS (Global Positioning System), radar, infrasound, self-potential, radon, temperature, oxygen fugacity and multigas measurements were also experimentally applied at Merapi with the benefit of many innovative scientific outcomes.

The development of the Merapi monitoring system has been driven in part by international collaborations (Table 13.1) that have been of mutual benefit to both local and foreign scientists. Indonesian scientists and technicians have benefitted from transferring technology and knowledge from abroad through joint field activities, workshops, and technical training. As a result, Indonesian volcanologists have successfully adapted several monitoring techniques and methods, including, among others, digital seismic monitoring, lahar early warning systems, GPS-based deformation monitoring and gas monitoring.

The development of the monitoring network at Merapi over time is shown in Fig. 13.1. In 2010, BPPTK (Balai Penyelidikan dan Pengembangan Teknologi Kegunungapian), the predecessor organisation of BPPTKG, added 2 seismic stations; one at the Woro solfatara field near the summit and another one at Imogiri, 47 km south of Merapi. In addition, BPPTK also reinstalled the seismic stations at Pasarbubar, Grawah, Gemer and Labuhan. Before the 2010 eruption, the monitoring network at Merapi consisted of 11 seismic stations, 2 tiltmeter stations, 2 temperature stations, 10 EDM reflectors and 17 GPS benchmarks (Fig. 13.2).

The **seismic** network prior to the 2010 eruption consisted of 11 stations, 4 with analog transmission using Mark Product L4C and L22 short-period seismometers, and 7 with digital transmission using Guralp CMG 40TD broadband seismometers (Suroño et al. 2012; Budi-Santoso et al. 2013; Jousset et al. 2013). Seismic monitoring using a broadband seismometer began in 1997 when the Indonesia-Germany MERAPI (Mechanism Evaluation, Risk Assessment, and Prediction Improvement) project installed 3 monitoring stations around the slopes of Merapi. Meanwhile, this project added 2 additional stations at Merapi in 1998 (Ohrnberger et al. 2000).

The geodetic network for **EDM** (electronic distance measurement) was installed at the summit and its surrounding slopes in 1988 (Young et al. 2000), in cooperation with the United States Geological Survey (USGS) and Pennsylvania State University (Table 13.1). The slope distances from benchmarks located around the flanks of Merapi to the reflectors at the summit were measured daily, if possible. The EDM instrument used at Merapi was a Distomat Wild D3000 with 3 to 5 mm + 1 ppm precision and a Theodolite T2 with 1-mm precision and a change in angle at 30 s and 1000 m. In 2005, BPPTKG improved the network by adding 11 single mirror prism reflectors scattered around the summit (Nandaka et al. 2019). In addition, a Leica TPS1200 Series exhibiting a 2 mm + 2 ppm precision with an integrated

Table 13.1 List of international collaborations at Merapi since 1980

| No. | Country | Institutions involved | Project name | Period (year) | Program/objectives |
|-----|---------|--|---|---------------------------------|--|
| 1 | USA | USGS (VDAP), Pennsylvania State University | International assistance to prevent volcanic eruptions from becoming volcanic disasters | 1982–2010 | To improve the monitoring system. Ground deformation (EDM survey, real-time tilt monitoring, geodetic network, seismic monitoring (analog/digital), crisis response, scientific collaboration, training program |
| 2 | France | d'Etat à la Prévention des Risques Majeurs | Natural disasters in Indonesia. The French-Indonesian cooperation in volcanology | 1986–2010 | Bilateral cooperative program to increase knowledge about explosive volcanism, methodological developments, training French & Indonesian volcanologists promotes technological transfers |
| | | IRD, IPGP, and other universities | DOMERAPI (dynamics of an arc volcano with extruding lava domes, Merapi) | 2013–2016 (extended until 2023) | To study from the magma reservoir to eruptive processes. GPS telemetry real-time, online analysis modelling and visualization (WEBOBS), continuous gas measurement, pyroclastic flow modelling |
| 3 | Japan | Disaster Prevention Research Institute (DPRI)-Kyoto University, Sakurajima Volcano Observatory (SVO) | Study of prediction and mitigation of natural disaster in Eastern Asia | 1991–1993, 1994–1999 | To improve the monitoring system including ground deformation monitoring, infrasonic monitoring and to improve the capacity of the volcanologist through the training program |
| | | Japan International Cooperation Agency (JICA) | SATREPS science and technology research partnership for sustainable development | 2014–2019 | An integrated study on mitigation of multimodal disasters caused by the ejection of volcanic products. Real-time GPS measurement, weather radar, pyroclastic flow and lahar modelling, telemetry tiltmeter, infrasonic |
| 4 | Germany | GFZ—GeoForschungsZentrum (coordinator) | MERAPI—mechanism evaluation, risk assessment, prediction improvement | 1995–2000 | Interdisciplinary monitoring of a high-risk volcano as a basis for an early warning system |
| | | | MERAMEX (MERapi AMphibious experiments) | 2004 | Seismic tomography (to study a volcanic arc system as part of an active continental margin) |

(continued)

Table 13.1 (continued)

| No. | Country | Institutions involved | Project name | Period (year) | Program/objectives |
|-----|--------------------------------|--|---|----------------------------|--|
| 5 | European Union, United Kingdom | Bureau de Recherches Géologiques et Minière (BRGM France), Le Centre national de la recherche scientifique (CNRS-France), University of Cambridge (UK) | MIAVITA (mitigate and assess risk from volcanic impact on terrain and human activities) | 2008–2013 | Risk mapping and socio-economic analysis. To develop integrated tools and cost-effective methodologies to mitigate risks from various volcanic hazards |
| 6 | Singapore | EOS (Earth Observatory of Singapore) | WOVODAT | 2010–2015 (2017 extension) | Database of volcanic unrest, workshop, and training program |

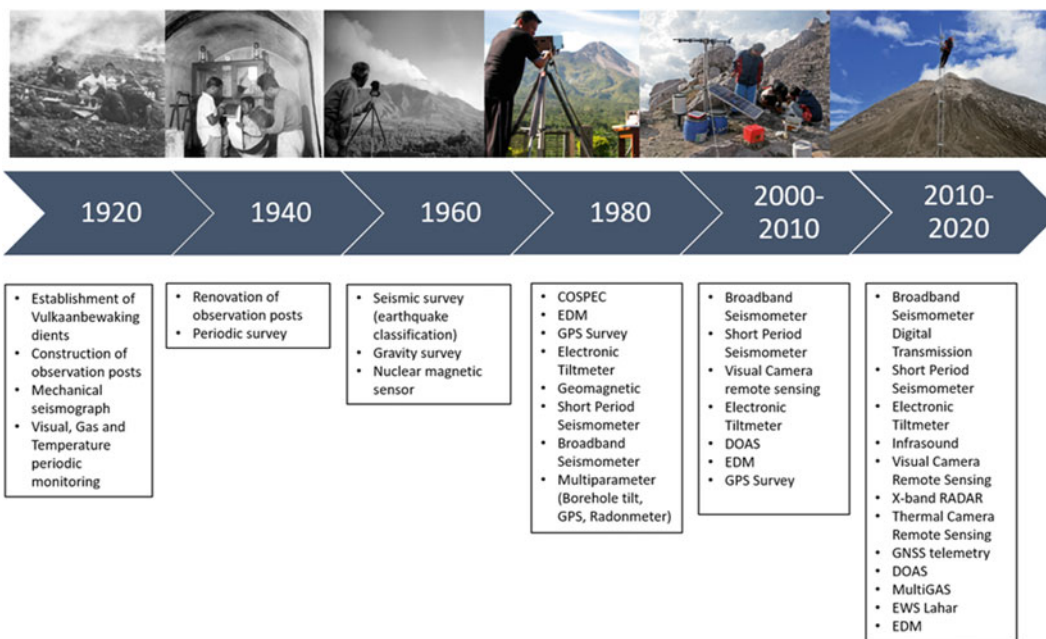


Fig. 13.1 A brief timeline of the monitoring techniques and instrument types operated around Merapi volcano

measuring angle and a distance measuring tool was used for the measurements.

Electronic **tiltmeters** were used for monitoring the deformation of Merapi from 1990 onwards in collaboration with countries including the USA, Japan, France and Germany (Table 13.1). The Indonesia–US and Indonesia–Japan collaborations used the Applied Geomechanics 700 and 800 platform tiltmeters mainly for monitoring lava dome deformation (Nandaka

et al. 2019). The tilt sensor was mounted on a large, stable rock at the summit of Merapi, and the data were sent every 15 min via a radio transmitter to BPPTKG. Meanwhile, in 1990, as part of a cooperation between Indonesian and French scientists, 5 units of tilt pendulums were installed on the south slope as far as 5 km from the summit (Beauducel et al. 2000). In 1995, scientists from Indonesia and Germany tested borehole tiltmeters at 4 multi-parameter stations

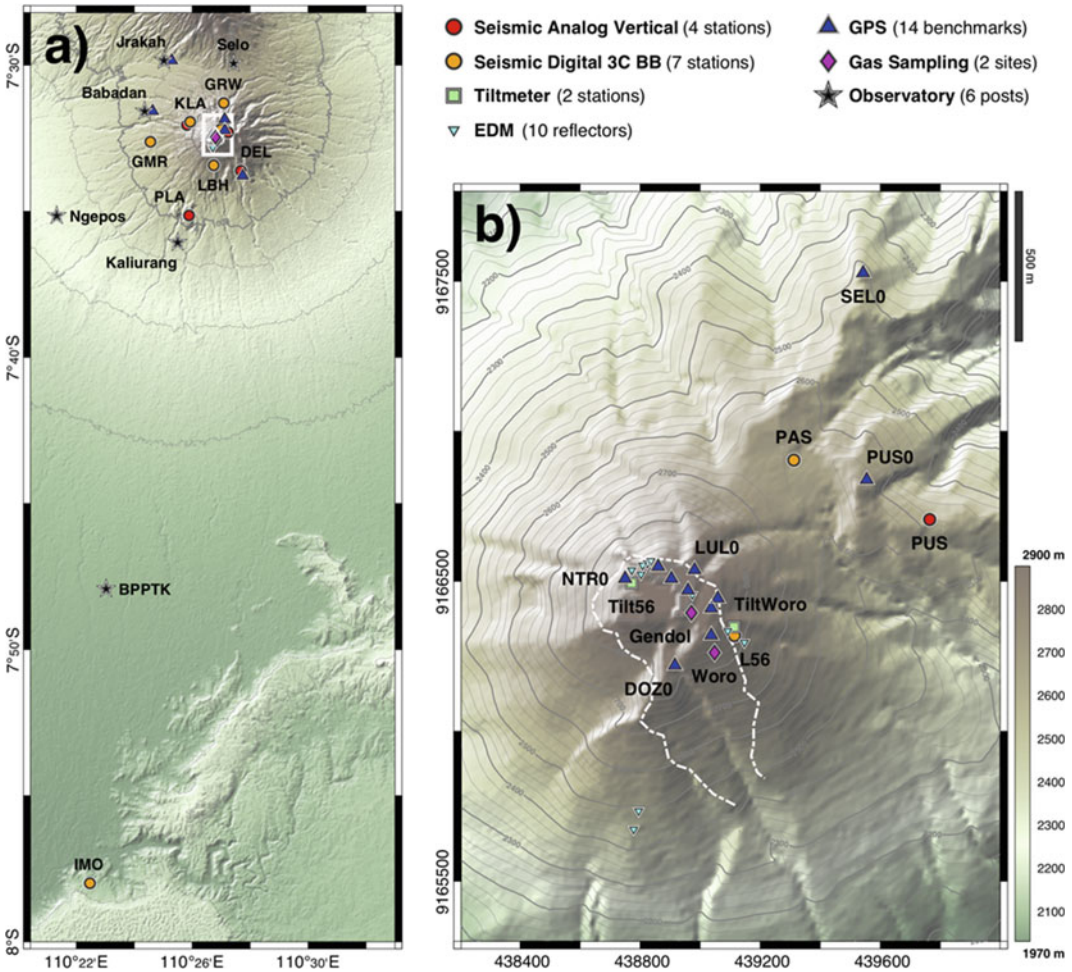


Fig. 13.2 Network map of monitoring instruments operating until the 2010 eruption: **a** Regional scale (Yogyakarta and Merapi). **b** Merapi summit area. Dashed line indicates the new post-2010 eruptive crater rim.

Background DEM from SRTM1/NASA (acquisition 2000) and Rupa Bumi/Badan Informasi Geospasial (BIG) (acquisition 1993/1994)

surrounding the flank of Merapi. The tiltmeters were part of multi-parameter monitoring stations with a Radon Detector, meteorological equipment and GPS for position control and ground displacement. Each station comprised 2 to 3 borehole tiltmeters buried 3–4 m deep to reduce regional effects (Rebscher et al. 2000). Before the eruption of 2010, there were 2 tiltmeter stations using Applied Geomechanics 701-2A model sensors installed at the summit. These sensors sent surface slope data to BPPTKG at 5-min intervals (Surono et al. 2012; Ratdompurbo et al. 2013).

Static and rapid static **GPS** measurement surveys of 14 benchmark points started in 1993 and were conducted using 2 or 3 receivers simultaneously (Sercel mono frequency 1993–1999, Sercel Scorpio dual frequency 1999–2006, Trimble 4000SSE Geodetic 2006–2010). The measurement campaigns were performed at least once a year (Beauducel and Cornet 1999; Beauducel et al. 2000). In addition, a kinematic survey of 50 points (geodetic nails) located on the crater rim area was installed in 1999 and conducted once or twice a year to analyse the

near-field deformation in three dimensions (Beauducel et al. 2006). Meanwhile, 2 experiments using GPS were carried out within the framework of the Indonesian-German collaborative project MERAPI (Table 13.1). The GPS campaign covered 19 points around Merapi, conducted once or twice a year. This project also built four GPS monitoring stations located in multiparameter stations around the slopes of Merapi, with a reference station located inside the BPPTKG building in Yogyakarta (Rebscher et al. 2000).

Temperature measurements were obtained through telemetry and direct in-situ measurements at two temperature monitoring stations at the summit, namely the Gendol and Woro solfataras fields, where both soil and air temperatures were measured. Direct temperature measurements were conducted almost every month using a digital K-type thermocouple, measuring the temperature of the fumaroles up to 1300 °C with high accuracy and precision. During the 2006 eruption crisis, the temperature at the Gendol and Woro solfataras fields reached ~800 °C and 500 °C, respectively (Sumarti et al. 2007).

Gas and condensate sampling for **geochemical** analysis were carried out every month in the summit area, which showed a high degree of gas activity. Prior to the 2006 eruption, gas sampling was conducted at the Gendol and Woro solfataras fields, using the Giggenbach method (Giggenbach and Goguel 1989). The samples were then analysed in the laboratory to obtain the composition of volcanic gas components (Surono et al. 2012). From July 2000 to January 2001 there was a gas station for continuous monitoring of H₂O, CO₂, and Rn concentrations at the Woro fumarole (Zimmer and Erzinger 2003). SO₂ emissions had been monitored using COSPEC since the early 1980s. Due to several difficulties in COSPEC operation, DOAS (Differential Optical Absorption Spectroscopy), adapted from Galle et al. (2003), was introduced in 2006. A comparison of measurements between COSPEC and DOAS showed that the values from the two methods were not significantly different (Humaida 2008).

Visual observations, such as direct inspection of the summit, taking photographs and video

through digital camera and video surveillance (CCTV-Closed-circuit TeleVision) and morphological analysis were conducted at five observatory posts. In 1992, a Celestron telescope was installed at Ngepos Observatory (12 km from the summit) to monitor the lava dome. Prior to the 1996 and 1997 eruption crises, visual observation played an important role in calculating lava dome volume and growth rate (Voight et al. 2000). Towards the 2006 crisis, a Canon Powershot S2 camera was installed at the Kaliurang observatory. Photographs were taken every morning when the weather was clear. Although some limitations appeared due to the weather condition, the outline envelope of the dome morphology could be identified and used to estimate volume changes (Ratdomopurbo et al. 2013). In 2007, for the first time, CCTV was installed by BPPTKG at Plawangan hill to monitor Merapi volcano from the south.

13.3 The Merapi Monitoring Network After 2010

Following the 2010 eruption, the Merapi monitoring network and observation system has continued to improve, using a multidisciplinary and multiparameter approach, and including both ground-based and remote sensing techniques. Among the in-situ measurements, continuous measurements, generally transmitted to BPPTKG by a radio network, sequential measurements, and punctual repetition measurements are distinguished. Among the continuous data, a distinction is made between ‘fast’ data acquisition with a sampling rate of 100 Hz (seismic sensors, inclinometers, infrasound) and ‘slow’ data acquisition with a sampling rate on the order of every second to several minutes (GPS/GNSS, ground temperature, radon, stereo visual imagery, thermal images, time series of gas composition and flux). Periodic measurements are those that are made regularly, with a sampling rate greater than once a day, such as EDM (conducted by a human operator) or satellite images (automatic but also requires human data processing). Punctual repetition

measurements essentially correspond to gas flux and composition data (UV camera, DOAS, multi-gas). Figure 13.3 shows the network map of permanent monitoring instruments and radio transmission as in 2020.

13.3.1 Real-Time Instruments

Analog Short-Period Seismometers—The network of short-period seismometers used began in 1982 with 6 seismometers installed around Merapi. These instruments use L4C Mark Product sensors with a natural frequency of 1 Hz. Most seismometers were installed in a concrete building with a ± 50 cm thick foundation. Further seismometers were planted in a hole as deep as ± 60 cm on top of a concrete slab as thick as ± 15 cm. Data transmission often uses an analog system where the output in the form of a voltage is converted into an audio frequency magnitude through a VCO (Voltage Converter Oscillator) and then sent to BPPTKG using a very high frequency (VHF) Monitron radio. The power system at the field station usually consists of 2 70 Ah battery units and 2 solar panels with 80 W power. At the receiving station, the audio signal is converted back to voltage using a discriminator which is then displayed in a seismograph and digitally stored through the Guralp CMG-DM16R8 digitizer. Nine short-period seismic stations with 10 Hz natural frequency geophones use digital transmissions and a PSN-ADC 16-bit digitizer. These seismic stations are specifically used for lahar monitoring (see Thouret et al. 2023, Chap. 17). Currently, there are 19 short-period seismic stations, 5 stations using 1 Hz seismometers, and 14 stations using 10 Hz geophones in operation.

Digital Broadband Seismometers—Most broadband seismic stations currently use the Guralp CMG-40TD instrument with a natural frequency of 30 s-50 Hz. Five stations use Guralp CMG-60TD instruments, which also have a natural frequency of 30 s-50 Hz, and were installed within the cooperation with the French Institut de Recherche pour le Développement (IRD) (Table 13.1). Seismometers were planted

at a depth of ± 60 cm below the ground surface and placed above a ± 15 cm thick concrete slab. The sensors were also covered with an isothermal container material. The seismometers are equipped with the Guralp EAM-0003 communication module and the data are transmitted through TCP-IP protocol using the UBNT RocketM5 5 GHz radio (Métaxian et al. 2020). In total, there are currently 23 broadband seismic stations deployed, 21 of them are installed within a 6 km radius from the crater. Two further broadband seismometers were installed on the slopes of Merbabu volcano north of Merapi, and at Imogiri, 47 km to the south.

Seismic Antenna—To locate emergent onset seismic signals such as rockfalls, a small aperture array composed of 5 stations was installed close to the summit at the site of Pasarububar in November 2013 (Fig. 13.4). This network, which is called MEA (MERapi Antenna, stations MEA01 to MEA05), has an aperture of 280 m. The shortest distance between the sensors is 90 m and the longest is 280 m. The MEA network is composed of Guralp CMG-6TD stations. Sensors have flat response characteristics from 30 s to the Nyquist frequency (50 Hz). Four short-period vertical sensors (Mark-Product 1 Hz) were installed in 2015 around station MEA05. These sensors are connected by cable to a digitizer. This very small aperture array has a cross shape geometry with an aperture of 80 m (Métaxian et al. 2020).

GNSS (Global Navigation Satellite System)—The 2010 eruption destroyed the entire network of GPS benchmarks located in the summit area of Merapi (see Fig. 13.1b), and the new crater topography formed during the 2010 eruption does not allow kinematic field measurements anymore. As early as 2011, the Indonesia-Japan project (Table 13.1) installed 3 new permanent GPS stations using Leica GR10 receivers and AR10 antennas, 1 Hz sampling, and real-time radio transmission at 2–3.5 km distance from the summit (Nakamichi et al. 2019). The fourth station was installed on the roof of the BPPTKG building in Yogyakarta, as a reference station 30 km from Merapi. The 1-h data file is downloaded hourly and processed using the Leica

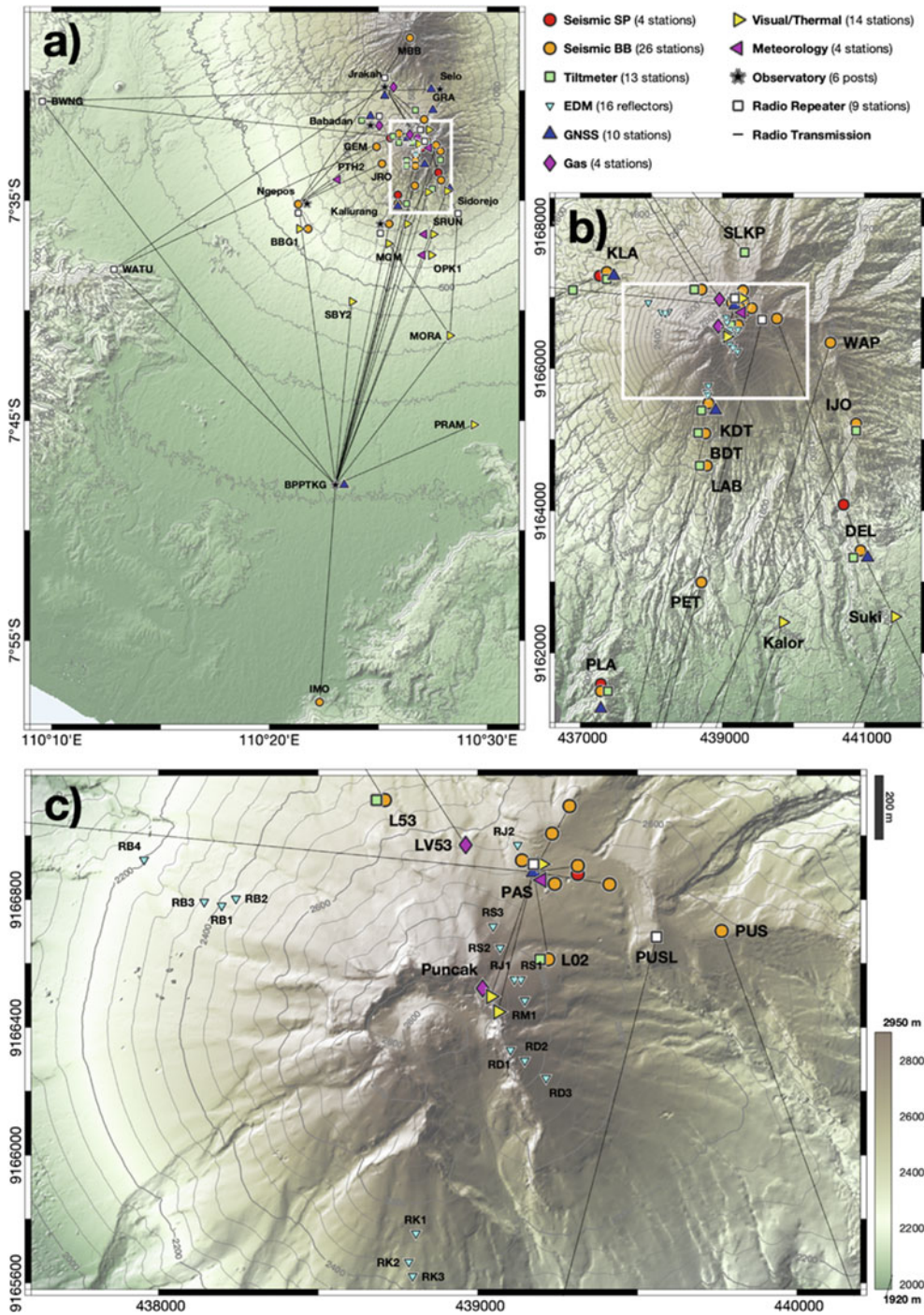


Fig. 13.3 Network map of monitoring permanent instruments and radio transmission in 2020. Background DEM from SRTM1/NASA (acquisition 2000) and stacking of DEM computed from Pléiades satellite images (acquisitions 2019)

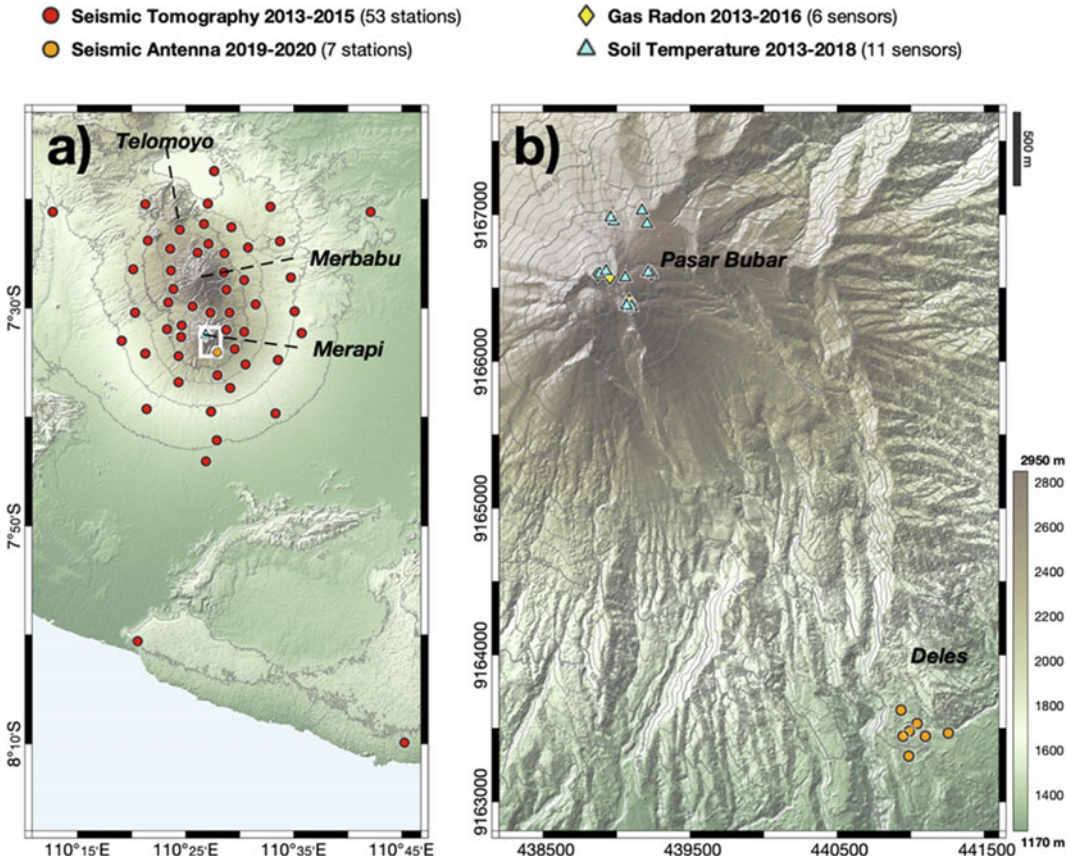


Fig. 13.4 The DOMERAPI project network map of temporary experiments during the period from 2013 to 2019: **a** Central Java and Yogyakarta. **b** Merapi

Spider software. In 2013, in collaboration with scientists from France (Table 13.1), BPPTKG installed 5 additional permanent stations, one at Pasarbubar (500 m from the crater), and 4 around the Merapi edifice at a distance of 5–6 km from the summit. In 2018, another station was installed 1 km south of the summit, but it was too exposed to ballistics, and was destroyed twice. The newest station was installed 2 km south of the summit in 2020. Data of the 10 stations are hourly transmitted through Wifi and processed in parallel with GipsyX/JPL and Spider/Leica software. The results are processed by the WebObs/IPGP system (see Sect. 13.4.3), and subsequently imported into the BPPTKG database.

EDM—To measure the horizontal deformation of the summit area, 12 reflector prisms are

used around the summit. Measurements take place at 6 positions on the slope (see Fig. 13.3) using the Leica Total Station TCR-1200. Thirteen reflector units were installed in 2011 and 3 more units were installed in 2014. Unfortunately, 4 units cannot be measured anymore because the rock on which the reflector was installed failed due to erosion. EDM measurements are taken daily as long as the weather allows them.

Tiltmeters—Deformation monitoring is also carried out through the measurement of surface slope changes. At present, there are 15 tiltmeter stations installed on the cliffs around the summit and the slopes of Merapi. The two tiltmeter models used are the Applied Geomechanics A701-2 high gain biaxial platform model with a resolution of $0.1 \mu\text{rad}$ and a 0.46° range, and a borehole model produced by the Institut de

Physique du Globe de Paris (IPGP) (Table 13.1). The sensor was installed 60–100 cm below the ground surface and placed above a 15 cm thick slab of concrete. Data from the sensor is transmitted using a Ubiquiti Rocket M5 device.

Visual/Thermal Stereo Cameras—Visual monitoring at Merapi is carried out through 7 Digital Single Lens Reflex (DSLR) cameras, 25 Internet Protocol (IP) cameras, and 3 thermal cameras. Most DSLR cameras use Nikon or Canon models with 200–400 mm focal length. This type of camera is primarily used at observation stations and the summit. Currently, there are 2 locations at the summit of Merapi where a DSLR camera is installed. IP cameras were installed at various locations, including the observatory posts, the slopes and summit of Merapi, and several rivers to monitor lahars. IP cameras use various commercial models (Axis, Hikvision, SPC, Infinity), with 0–30 times optical zoom capabilities. Meanwhile, thermal cameras were installed at 3 different locations, including one on the south slope, using an Axis-Q1921 model, and 2 on the southeast slope and at the summit, using Optris-Pi450 models (Kelfoun et al. 2021).

Differential Optical Absorption Spectroscopy (DOAS)—Measurements of SO₂ flux of the volcanic plume are carried out daily. DOAS provides an absorbance spectrum of the sunlight crossing the plumes. In 2014, a scanning DOAS instrument, built at the University of Cambridge with Ocean Optics spectrometers, was installed at the observation station of Babadan (see Fig. 13.2a), which is 4.5 km from the Merapi summit. This station is the best location for a DOAS instrument given its short distance to Merapi, the good sight of the summit, and prevailing wind direction.

The Volcanic Gas Monitoring System (VOGAMOS)—VOGAMOS is a continuous telemetry volcanic gas monitoring system designed by BPPTKG to measure the concentration of CO₂. The field system is placed on locations of volcanic gases in the solfatar/fumarole area. In 2018, VOGAMOS at Merapi was installed above the 1953 lava on the northwest side of the summit. The CO₂ gas

sensor used is of the K33 BLG type, made by a CO₂ detector with a measurement range of up to 30% volume of gas. In addition, the instrument is equipped with humidity and temperature sensors, measuring both air temperature and ground temperature. The data are sent to BPPTKG every 5 min, using a microcontroller system and a Bell 202 VHF-modem radio. Meanwhile, the receiving device is made on a web-based system so that users can easily access it via the internet/intranet network.

Multi-component Gas Analyzer System (Multi-GAS)—In September 2015, BPPTKG, in collaboration with a team from INGV-Palermo University (Italy), installed Multi-GAS equipment on the summit of Merapi. This work is within the scope of the DOMERAPI project (Table 13.1), linking conduit processes to an effusive or explosive transition, and aiming to increase the knowledge of carbon degassing from volcanic areas. Multi-GAS is an INGV custom-made instrument for the real-time detection of concentrations of H₂O, CO₂, SO₂, H₂, and H₂S in volcanic plumes at a rate of 0.1–1 Hz. The instrument used at Merapi consist of several gas sensors, namely CO₂ sensors (range: 0–3000 ppm), SO₂ sensors (range: 0–200 ppm), H₂S sensors (range: 0–100 ppm), and H₂ sensors (range: 0–20 ppm). It is also equipped with sensors to measure temperature, pressure, and humidity. Power consumption is 180 mA/h during standby and 750 mA/h during the measurement operation. Multi-GAS takes measurements four times a day, namely at 00.00, 06.00, 12.00, and 18.00 local time. Each measurement takes about 30 min, and the data is then sent to the BPPTKG office via radio telemetry, where the data can be processed, using the Ratio Calc software (Tamburello 2015).

Satellite Imagery—Monitoring using satellites has been more intensively used at Merapi since the commencement of the DOMERAPI project in 2013. The aim is to support and increase remote sensing data, particularly Synthetic Aperture Radar (SAR) data, for volcanic monitoring and, more generally, for geological hazard assessment in Indonesia. Even though satellite monitoring is still episodic, the data is

increasingly useful by revisiting satellite time. The satellite data can be used to map the surface (e.g. eruptive deposits, faults, landslides, dome evolution), observe topographic changes, and detect precursors for surface displacement. In particular, SAR provides valuable information, even in cloudy conditions, for eruption detection, volcanic monitoring, and lahar assessment complemented by field observations due to its wide-area coverage. At Merapi, SAR data from Sentinel-1 are used that are obtained above the volcano every 12 days on the descending path of 76 and every 6 days on the ascending path of 127. Since mid-2017, Sentinel-1 data have been automatically downloaded on the local server at BPPTKG. Interferograms and coherence images are then produced using a New Small Baseline Subset (NSBAS) technique processing chain, and automatically integrated into WebObs (see Sect. 13.4.3) to enable rapid and significant detection of potential signal changes (Pinel et al. 2021).

Meteorological Stations—Five volcano observation posts, namely Kaliurang, Ngepos, Babadan, Jrahah and Selo (Fig. 13.2), are equipped with a tipping bucket rain gauge and a weather station PCE-Instruments product that records meteorological conditions, such as wind direction, wind speed, air temperature, relative humidity and air pressure. Meteorological data are reported regularly, especially during the rainy season. Furthermore, after the 2010 eruption, BPPTKG, in cooperation with the USGS and the National Disaster Agency of Indonesia (BNPB), built lahar monitoring stations for early warning purposes.

Data Transmission System—All monitoring data are transmitted to BPPTKG in Yogyakarta, primarily using the wireless transmission that requires a clear line of sight between the field and receiver stations. Not all stations can send the data directly to BPPTKG; therefore, repeater stations were built to connect the field station to the receiver office. All observation posts (Kaliurang, Ngepos, Babadan, Jrahah, and Selo) also function as repeater stations (see Fig. 13.3a). Besides these, there are 2 other repeater stations around Merapi, initially built inside the disaster-

prone area. In 2017, BPPTKG moved the repeater stations outside the immediate hazard zone to a secure location. Along with the increasing need for extensive data transmissions, a fibre optics line was established between BPPTKG and the observation posts at Kaliurang and Ngepos in 2018.

13.3.2 Temporary Experiments

Merapi's volcanic activity attracts the attention of scientists and researchers, who implement tools and conduct experiments of innovative approaches. Numerous such investigations have been undertaken at Merapi, some of which are highlighted here (see Table 13.1).

In 1994, the GeoForschungsZentrum in collaboration with the Volcanological Survey of Indonesia and other institutions in Indonesia and Germany launched an interdisciplinary monitoring program, called the MERAPI project (Mechanism Evaluation, Risk Assessment, and Prediction Improvement), supplementing several ongoing national and international activities at this volcano (see Lühr et al. 2023, Chap. 5). This project intended to contribute to the development of prediction and warning strategies on various time scales, including intermediate and short-term prediction of volcanic events, as well as an early warning at various time scales (Zschau et al. 2003). As part of this project, a structural investigation to image the seismic velocities below Merapi was conducted using an active seismic experiment in 1997 and 1998. The model was built based on a layered 1-D depth profile of the P-velocity, which was derived from first break travel times. At the near-surface region, the velocity ranged from a few hundred m/s and more than 3×10^3 m/s at a maximum depth of 300 m (Maercklin et al. 2000).

In 2004, The MERapi AMphibious EXperiment (MERAMEX) was carried out to study not only Merapi but also the tectonic structure of Central Java and the relationship between subduction and arc volcanism (see Lühr et al. 2023, Chap. 5). A temporary seismological network

was installed in a dense grid at about 10–20 km spacing around Merapi, deploying 106 continuous short-period seismometers, 14 broadband stations, 9 Ocean Bottom Hydrophones (OBH), and 5 Ocean Bottom Seismometers (OBS) (Wagner et al. 2007).

In 2013, a collaboration between Indonesian and French research teams launched a project called ‘DOMERAPI, the dynamics of an arc volcano with extruding lava domes, Merapi (Indonesia): from the magma reservoir to eruptive processes’. The DOMERAPI project proposed a multidisciplinary approach, integrating petrological, geochemical, and geophysical methods to improve the understanding of dome-forming type volcano processes and their interactions with eruptive dynamics. During the DOMERAPI project, a seismograph network was deployed using 46 three-components seismometers (Nanometrics Taurus digitizer equipped with Guralp CMG-40 T seismometers) for 18 months (from October 2013 to April 2015) across the Merapi-Merbabu complex to record the local and regional seismic activity (Fig. 13.4a). Data of recorded local and regional earthquakes were combined with data of the permanent seismographic network of the Indonesian Agency for Meteorology, Climatology, and Geophysics (BMKG) to provide constraints on hypocentre estimates by extending spatial coverage. Body wave seismic tomography was performed by using P- and S-wave arrival time data. A magma reservoir at ≥ 10 to 20 km below mean sea level was imaged for the first time (Widiyantoro et al. 2018). To image the summit hydrothermal system, geophysical mapping was performed at the Merapi summit that included a field campaign of self-potential, CO₂ diffuse flux mapping, and the set up of three Radon-222 probes (Fig. 13.4b). Two multi-parameters stations were also installed at the summit (Métaxian et al. 2014), in addition to a seismic antenna network to analyse low-frequency signals such as long-period, multi-phase, and tremor earthquakes (Fig. 13.4b). The system consists of 5 Guralp CMG-6TD (with 30-s response) sensors and one Sercel L4C (Métaxian et al. 2020).

13.4 Data Handling and Monitoring Tools

The monitoring room at BPPTKG is dedicated to displaying the monitoring data from Merapi (Fig. 13.5). The officers at the observation posts are also monitoring the same view because they are connected to the BPPTKG via Wireless Local Area Network (WLAN) and fibre optic networks. Several application systems are used to manage the monitoring data into an informative display. Having many monitoring assets and various complex monitoring data is difficult without the help of an application system. For multiple purposes, BPPTKG uses several application systems that were integrated into a web portal called Cendana15. Several other application systems result from collaborative research with scientists from France, Singapore and Japan, such as WebObs, WOVodat, and the Support System for Decision Making (SSDM) (Table 13.1). Figure 13.6 shows the flow of data from the different data sources to these application systems to produce public information.

13.4.1 Cendana15: Integrated Collaborative Work Management Application

BPPTKG created Cendana15, an Integrated Collaborative Work Management Application in 2015, and it was first used in 2019. The address of the BPPTKG office in Yogyakarta inspired the name of this application. Cendana15’s main function is to serve as a database, semi-automated or interactive visualisation, and a data processing tool for Merapi monitoring data. Furthermore, the application aids in the administration of the office. Cendana15 helps users to quickly examine and handle monitoring data for hazard assessment and decision-making.

Cendana15 offers a variety of cloud-based applications and services related to task management, data storage services, computing services, and data visualisation in real-time to



Fig. 13.5 The Merapi monitoring room at BPPTKG office (photograph taken in 2020). The telemetry data, such as seismic, deformation, gas, and visual data from

remote cameras, are monitored from this room. An essential instrument is the seismic drum recorder VR65 which has been in use since 1982

support Merapi's monitoring infrastructure. It is implemented on local servers and managed internally by BPPTKG and is constantly improved to provide a more reliable monitoring ecosystem. By early 2021, there were 10 critical service applications on the Cendana15 platform: Monitoring Network Management System, Data Visualization System, Charting System, Data Entry System, File Management System, Media Gallery System, Information Broadcasting System, Laboratory Information Management System, Performance Accountability System, and API (Application Programming Interfaces) Monitoring. The aim and function of certain key features or applications in Cendana15 are briefly described below.

The Monitoring Network Management System (Monmas) was built to manage more than 1500 assets spread over 100 locations. These assets include sensors, benchmarks, reflectors, repeater stations, and other instruments. Network

routing generally becomes complicated because it involves various network hardware such as routers, gateways, firewalls, or switches. The general purpose of this application is to help operators quickly identify problems in network traffic based on problem identification provided by the system.

The Data Visualisation System (Davis) was built to provide a visualisation tool for various monitoring data through a cloud-based interface. The goal is to apply appropriate methodologies drawn from standards and best practices for data visualisation that is easy, accessible, understandable, and fast to use. Figure 13.7 shows an example of how users can simply interact with hypocentre data. Davis serves to monitor data through a cloud-based Application Programming Interface (API) called BPPTKG Monitoring API (BMA) as an entry point that defines the interaction between several services intermediaries. Meanwhile, the Chart Builder System (CBS) has

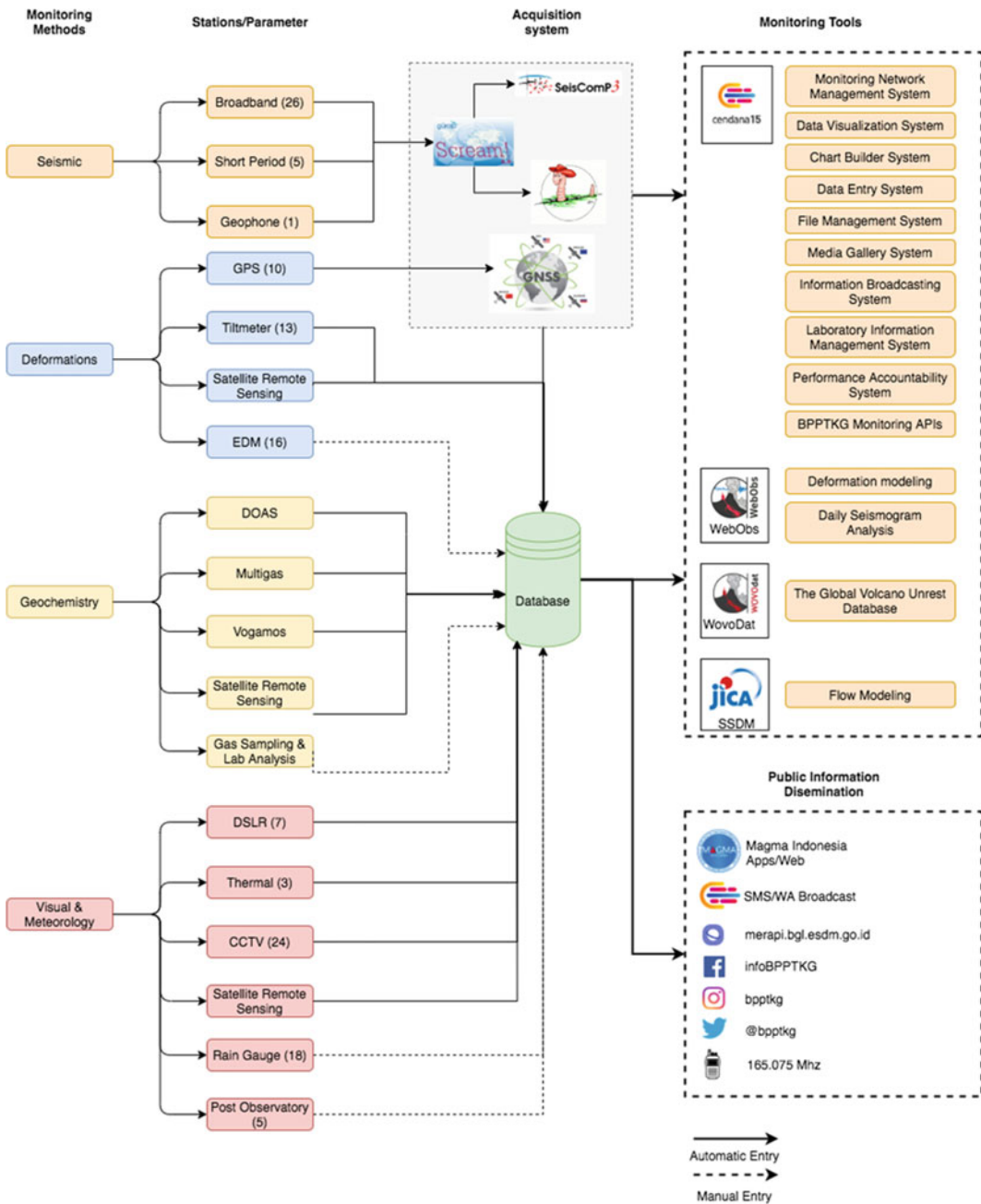


Fig. 13.6 Schematic diagram of the Merapi volcano monitoring data flow, illustrating how multi-parameter monitoring datasets are gathered from the field, processed,

archived, and disseminated through various data management systems, such as WebObs, WOVODat, Cendana-15, MAGMA Indonesia, and social media platforms

a function to generate real-time and interactive data charts. In addition, CBS produces static charts with a standard layout suitable for presentations or scholarly works.

The Data Entry System (DES) is a web-based application that is mainly used to monitor input data obtained from direct observations or measurements. Its purpose is to help organise data

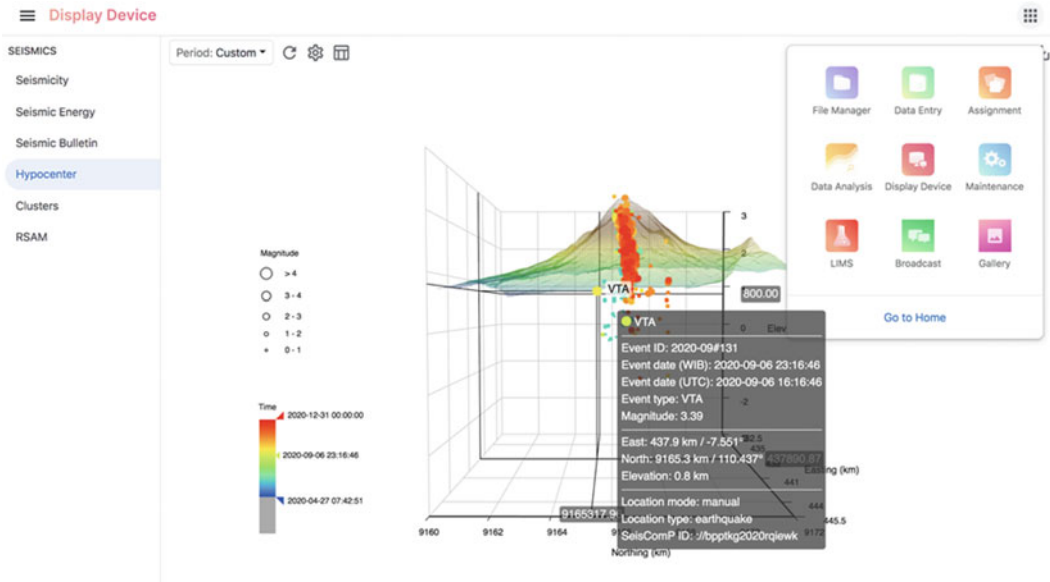


Fig. 13.7 Hypocentre plot on Cendana15 Data Visualization. Users can interact with the data by, for example, selecting the data period by dragging the time to the

colour legend or by simply rotating the plot. On the same page, users can view other data (left menu) or go to other Cendana15 applications (right menu)

and reduce the complexity of data storage and management. DES has 3 sub-applications to input specific data types: Daily Report, EDM, and Sampling applications. The Daily Report application has the task to enter data on visual observations, weather, visibility, and volcanic events such as rockfalls, plume height, plume colour, pyroclastic flows, explosions and lava extrusions. Using the Daily Report, users can enter the appropriate attributes for each monitoring data. The EDM application has the task of inputting distance measurement data between a reflector and the benchmark. Once data is sent to the server, other service features can access the data, enabling instant visualisation and automatic calculation of metrics such as linear regression, slope distance change, and data rate. Finally, the Sampling application allows users to enter various gas concentration data values obtained from on-site gas sampling measurements. All 3 sub-applications have external APIs that enable other applications to access the data or integrate it with other systems.

The File Management System (FMS) feature is a cloud-based file storage service, allowing

users to upload important documents, spreadsheets, presentations, images, videos, or other files related to monitoring data on the server.

The Media Gallery System (MGS) was created to make it easier to access and manage image and video data. This web-based application has a layout consisting of two views, the left-side navigation pane, and the main view. The main view displays a live CCTV view of various stations in the form of a grid. There is a folder explorer on the left side panel, which allows users to find photos or videos easily. It also provides a search menu that filters photos and videos by recording time and station location.

BPPTKG provides information on Merapi to the public using various modes of communication, including direct contact at offices and observation posts, via telephone, website, social media, radio communication, and text messages via mobile phones. The Information Broadcasting System (IBS) is a web-based application to broadcast text and multimedia messages via smartphones or other gadgets. Until now, this application has been used to send important or urgent messages to stakeholder officials related to

the disaster management of Merapi, ranging from governors to regents and village heads.

The BPPTKG Monitoring Application Programming Interface (BMA) is a web service that provides endpoints for querying various Merapi monitoring data, including, among others, seismicity, deformation, geochemistry, and weather. In addition, BMA provides API endpoints to enable data processing in the cloud and other utilities. BMA is the brain of the Cendana15 platform in charge of building and integrating all application software. BMA web service helps users easily query Merapi monitoring data, calculate specific metrics, and develop applications based on this service. For example, a Data Visualization System provides visualisation tools for various data monitoring via the web using BMA as the data provider. The File Manager built by BMA offers essential file management services, including the upload, search, backup, and quick access. Each user has a separate drive so they can manage their files. It also allows user administration to create special drives dedicated to specific user groups. In addition, File Manager integrates well with other services on the Cendana15 platform and is also often used as a collaboration tool. For example, the user can send survey data from the field so that other users can quickly download and process the data.

13.4.2 The WOVodat Platform

An important component for increasing the usefulness and usage of the data collected by the monitoring networks is to be able to store it in a consistent and organised manner. This includes data standardisation and organisation to allow efficient data finding and data analyses. Such capability helps the challenging task faced by volcanologists during volcanic crises to better analyse and interpret the current unrest in question, using background knowledge on past eruptions, and thus better hazard assessment and implementation of timely mitigation actions. During a volcanic crisis, early warning issued by the volcano observatory in the form of an alert level is critical. Incorrect decision-making and

improper response in terms of timing and recommendations could lead to fatalities and socio-economic losses. Therefore, a good data management platform allowing readiness for data access and analysis is a key to successful crisis response. The Merapi monitoring infrastructure includes a modified version of the WOVodat platform (Newhall et al. 2017), which is described below and shown in the schema of Fig. 13.6.

Managing volcano monitoring data is a complex task, as it includes operational instrumentation in the field, data transmission, data processing, data archiving, and data analysis. In addition, a comprehensive volcano monitoring system consists of multi-parameter datasets acquired from various methods (e.g. geophysical, geodetic, chemical) with various levels of data (e.g. raw data, processed data, model results), and covering different spatio-temporal scales during normal and unrest periods. The WOVodat standalone platform (Newhall et al. 2017; Costa et al. 2019) was installed at BPPTKG in 2014, and the schema and structure were adjusted to cater for the specific needs of BPPTKG (e.g. additional tables for bulletin/report, more attributes for image table), with additional features, including interactive data analytics tools (Fig. 13.8). This platform serves to archive and manage various data of Merapi activity since 1983, which include monitoring 'processed' data and metadata, unrest chronology, and alert level. The data are archived in a hierarchical MySQL database with an open-source online interface for users to submit, query, visualise, and mine data, aiming at an efficient and systematic data archiving system. This allows interactive retrieval and display of historical and current data, including synchronised time plots of changes in various parameters. In 2017, the WOVodat analytics tool dashboard was installed. This graphical user interface allows users to perform data queries, preparation/manipulation, visualisation, and analysis using various statistical algorithms available in the drop-down menu (Fig. 13.8).

Diagnostic on what the volcano might do next relies largely on data availability, both current

WOVOdat-Analytics Tools: Online Machine Learning Plugin for WOVOdat

Merapi Earthquake counts

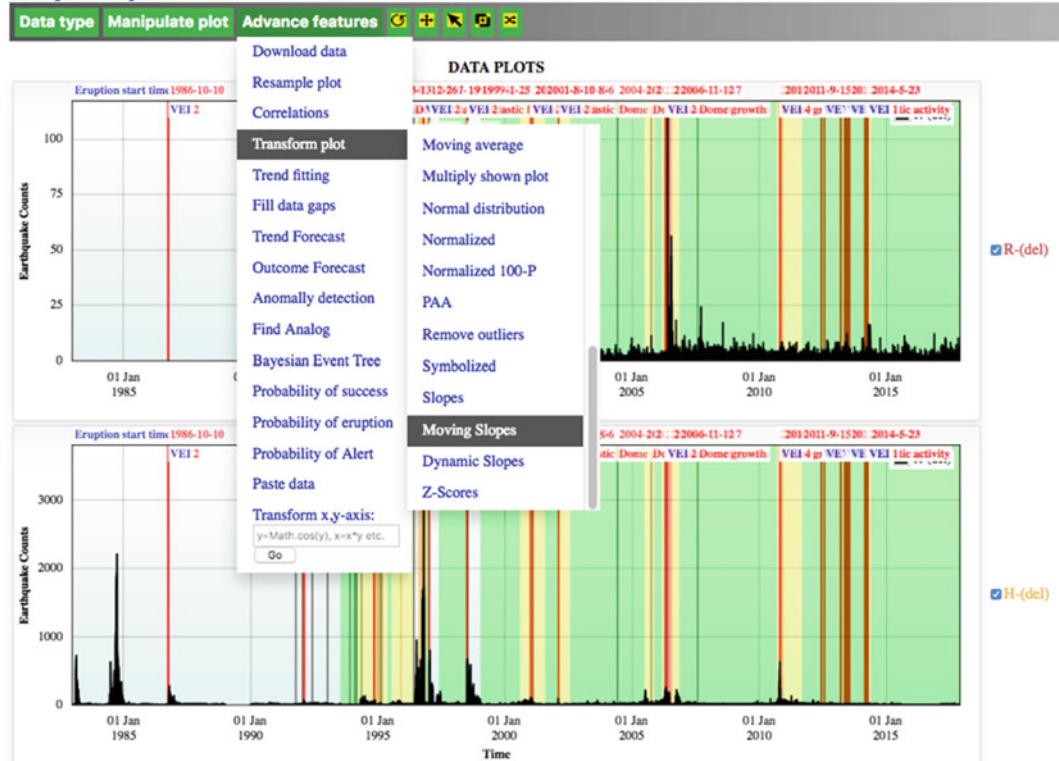


Fig. 13.8 Time series plot of Merapi daily earthquake counts for regional tectonic (R) and Multiphase (H) earthquake types (black bars) recorded by the Deles (DEL) seismic station between 1983 and 2017. Red vertical lines mark the onset of magmatic eruptions and volcano alert levels are displayed in the background colour shades green (normal level), yellow (Waspada/advisory), orange (Siaga/watch), and red

(Awas/warning). The online user interface of the WOVOdat analytics tools currently operational at Merapi Volcano Observatory (BPPTKG) allows users to interactively access, manipulate and visualise selected monitoring datasets into a time series plot. The interactive tools also enable users to perform statistical data analysis that can be selected from the list of statistical algorithms available in the drop-down menu

and past monitoring data, and the capability to analyse them. The frequent unrests at Merapi were dominated by dome-forming eruptions and provided a wealth of data that permit the study of unrest processes. Comparative studies between eruptions explore details of the unrest patterns and use the knowledge of previous unrest periods to evaluate the ongoing unrest and to forecast its further course. In 2017, in preparation for future crises and to improve decision-making, we examined the historical alert level changes of the 5 past eruptions of Merapi between 1996 and 2010. This includes alert changes from normal-to-advisory (1–2), advisory-to-watch (2–3), and

watch-to-warning (3–4). We created an inference system based on past unrest data that includes daily earthquake counts, deformation, and gas monitoring. These time-series data were analysed using the WOVOdat analytics tools (e.g. Bayesian inference) to detect changes of behaviour of each data type (‘evaluative indicators’) within 10 days prior to the onset of alert. The evaluative indicators obtained were then used as the basis of creating input variables and membership functions of a Fuzzy Inference System based on the Mamdani model (Mamdani and Assilian 1975), which yields two output variables: the alert level change and eruptive

style (effusive or explosive). For validation, we tested the robustness of this approach with the Merapi 2010 eruption crisis (VEI 4 eruption; Subandriyo et al. 2023, Chap. 12). Using the multi-parameter monitoring data of the 2010 unrest, we obtained a consistent result that reflected the corresponding escalating unrest and timing of the progressive alert change. A fuzzy inference system obtained from this study was then used to infer alert issuance at the Merapi crisis in 2018–2019 (Budi-Santoso et al. 2018).

The time series data using machine learning algorithms, represented into symbols similar to a DNA sequence, was also recently investigated. This is based on the Symbolic Aggregate Approximation and uses the position-penalised Sørensen-Dice similarity coefficient (Fajiculay et al. 2018). Our analysis was focused on the seismicity patterns of Merapi hybrid earthquake counts between 1983 and 2017. The dataset included 28 unrest episodes, and 21 eruptions, ranging from phreatic to VEI 4. The seismic data are transformed to $\log(y + 1)$, normalised to a range of 0–1, using Piecewise Aggregate Approximation with a bin of 6 days. The transformed y-axis was then divided into bins and integrated into 7 equiprobable regions which are given symbols from A to G. The approach was also used for synthetic data with the same distribution as the Merapi multiphase earthquake counts generated using Markov Chain Monte Carlo (MCMC) methods. Different levels of noise were introduced to the synthetic data to investigate the extent to which DNA-like precursors can match regions before eruptions. Initial results show that a pattern made of the precursory seismic sequence 60 days before the 1996 VEI 3 eruption (dome extrusion and explosive) also occurred in 7 other eruptions, with a sequence match better than 40%. There were two false positives with sequence match >40%, and 13 unmatched eruptions with a sequence match <40%. The low match includes 10 events that were phreatic eruptions and thus the analysis shows that in addition to being able to identify characteristic unrest patterns before eruption, it may also be possible to distinguish different eruptive styles.

13.4.3 The WebObs System

The WebObs system (Beauducel et al. 2020a) has been developed and used in the French volcano observatories for the past 20 years. The system is an open-source web-based tool that performs integrated, centralised, and automated real-time volcano monitoring from heterogeneous data sources. Functionalities answer most of the needs of any operational observatory in terms of network technical management, real-time data processing, visualisation, first-order modelling, and some early-warning alerts.

WebObs was installed at BPPTKG in the framework of the DOMERAPI project in 2013, but only to manage data from the French cooperation networks (seismic antenna, GNSS, bore-hole tiltmeters, DOAS, weather station). In 2017, BPPTKG installed its own WebObs to manage seismological data, GNSS, tilt, and satellite imaging. Because BPPTKG already developed its own network management and data visualisation systems, only partial use of WebObs capabilities is achieved at present. Since WebObs is a collaborative and open-source system, some of the functionalities have been developed or improved based on BPPTKG's specific needs and feedback, as described below.

Seismic Chart, Bulletin and Catalogue—For the continuous and high-frequency seismic data flux, WebObs proposes an innovative combination of a digital strip chart paper for multiple data streams, a manual and semi-automatic detection and classification of events, and a bulletin with dynamic graphs of event types: hourly/daily/moving histograms, cumulated number of events, cumulative seismic moment, and a Gutenberg-Richter diagram. The system accepts SEED and Earthworm data flux protocols and some basic filtering (median/trend removal, low/high/bandpass or bandstop Butterworth/Bessel/Chebyshev N-order filters). The catalogue is linked to external earthquake databases (local QuakeML or any web-service FDSN compatible) and raw data access in miniSEED format (FDSN dataselect, seedlink, arlink protocols). The objective of these tools is to construct and update a human-controlled earthquake bulletin, offering

the possibility to visually detect and/or check automatically triggered events, and to classify the type from a customised list. The system offers a synthetic view of up to 15 simultaneous channels at different time scales, an efficient way to immediately detect and recognize the origin of events (Fig. 13.9). The seismic bulletin named ‘main courante’ (handtrail) can be linked to multiple strip charts called ‘sefran’ (a graphical interface to operate seismic data in WebObs), allowing for example one strip chart with volcano stations and one for the regional tectonic activity. Sefran includes a broom-wagon process that fills up the gaps due to real-time data packet loss. The bulletin automatically creates an entry into a local earthquake catalog on the SeisComp3 database (<https://www.seiscomp.de/seiscomp3/>), with automatic event location using the Earthworm module (<http://folkworm.ceri.memphis.edu/ew-dist/>). Routine operators must daily complete the preliminary phase pickings and adjust and validate each earthquake location. Results are synchronised through the WebObs seismic bulletin. A specific WebObs process makes hypocentre maps at different timescales, operating the earthquake catalogue at customizable geographic scales with vertical cross-sections, magnitude, and quality filters, depth or time colour scale, and possible time series of earthquake location, depth, and magnitude.

GNSS—GNSS data are processed hourly through the analysis software GipsyX Precise Point Positioning (PPP) solutions (Bertiger et al. 2020). WebObs imports the data and proposes enhanced processing and graphs that include tectonic trend correction, absolute or relative velocity referencing (using one or more stations as reference) per station, summary time series plots of the three components (East, North, Up), principal component analysis, customisable baselines between pairs of stations, velocity vector maps, particle motion maps, and source modelling using an isotropic or complex point of inflation/deflation through exhaustive grid search to determine the spatial probability of a source and volume variation (Beauducel et al. 2020b).

Finally, time series of the best model parameters using different periods of integration are used for trend estimation. From a large number of parameters, it is possible to model only the horizontal components, to add an a priori target location to plot displacement amplitudes versus distances from the target, and to constrain the source location using a Gaussian-shape distance probability function. The output product of the time series source modelling offers a unique and novel way to follow possible volume variations at depth during the unrest. When sufficient stations are operational, the tool is sensitive to deep or shallow sources of deformation of less than 10^5 m^3 . BPPTKG experienced several cases of clear precursors a few days before Merapi explosions, such as inflation of a well-constrained source. The volume approximated by the method allows good anticipation of possible magma to erupt. When only syn-eruptive signals are detected, generally as deflation, results can be used to confirm the order of magnitude of erupted magma.

Tiltmeter—Tilt data are processed using a similar tool as GNSS, including data time series, trend estimations, vector maps, and isotropic point source modelling. It is possible to add an a priori target location to plot tilt amplitudes vs. distances from the target. Data are filtered using a moving median filter to exclude outliers. Source modelling results can be compared to GNSS modelling as all-time windows are the same.

Other Time Series and Import/Export—Other specific time series plots are performed by WebObs, including EDM baselines, data from multi-gas and meteorological stations, seismic helicoders, and satellite imagery (InSAR and visual). All the WebObs automatic and routine processing procedures produce data export as standard text files that are updated hourly. Some of these data are imported into the BPPTKG database and then used to update the data visualisation system. A project is under consideration to use WebObs outputs to feed the WOVodat platform with enhanced results like deformation source modelling time series.

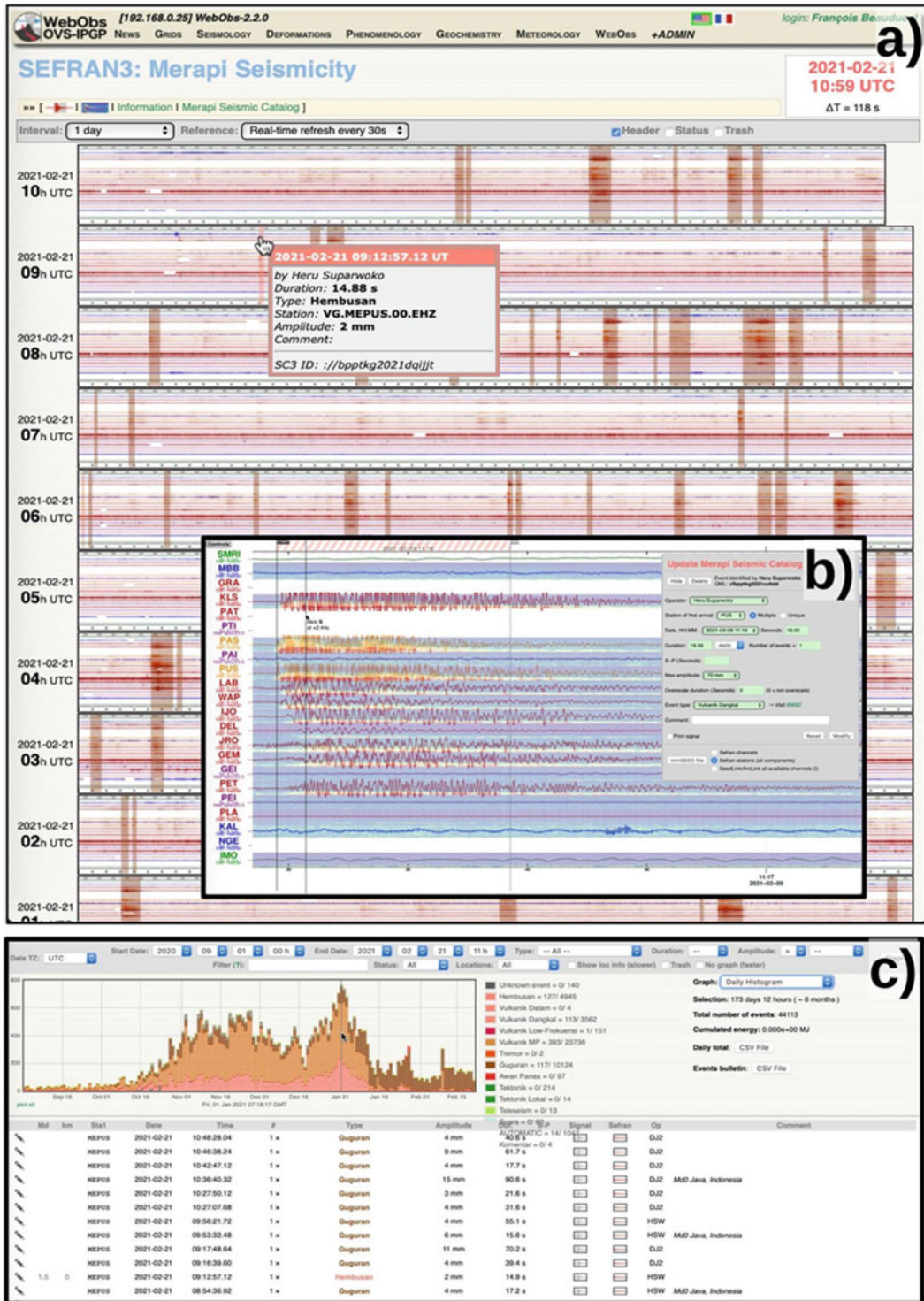


Fig. 13.9 WebObs seismic multi-channel strip chart ‘sefran’ and semi-automatic bulletin system used daily at BPPTKG: **a** Real-time main page showing the last hours of activity and identified events (manual and automatic). **b** Single event picking/editing and type classification manual form (with spectrogram transparency). **c** Bulletin of events and statistical graphs with filtering options (date, type, duration, amplitude). The system is linked to the located events catalogue (SeisComp3) and automatically exported into the Cendana-15 database

13.4.4 Support System for Decision Making (SSDM)

The Support System for Decision Making (SSDM) is a system to evaluate volcanic hazards caused by eruptions. This system was developed during the project 'Integrated study on mitigation of multimodal disasters caused by the ejection of volcanic products' that started in 2014 under SATREPS (Science and Technology Research Partnership for Sustainable Development), a cooperation between Indonesia and Japan in volcanology (Iguchi et al. 2019a). The SSDM comprises a database, simulation engines, monitoring devices, interfaces including a user interface, and a job controller. Four types of databases are stored in the system: (1) Digital Elevation Model (DEM) derived from ALOS2 or other satellite and parameters for simulation, (2) scenario of occurrence of phenomena, (3) monitoring data and processed data, and (4) pre-analysis hazard maps.

The database, including the Merapi monitoring data through time, is the core of the database and is essential to provide the initial conditions of the simulations. The project added GPS/GNSS, digital seismograms, tilt, and infrasonic microphones data to the SSDM database. The project installed the X-band Multi-Parameter (MP) in 2016 at the roof of Merapi Volcano Museum about 8 km south of the Merapi summit. The radar could estimate spatial distribution not only of rainfall in catchments but also of volcanic ash clouds (Fig. 13.10a). The radar captures precipitation distribution for lahar modelling and volcanic ash dispersion modelling in the range of 30 km from the Merapi summit.

Simulation engines are the main feature of SSDM. The engines performed the modelling process and controlled all the servers (Shimomura 2018). The SSDM considers an event chain, such as the recurrence of pyroclastic flows, the transition of pyroclastic flow to lahar, and the recurrence of lahars. The thickness of deposits is obtained by simulation for the first event. Then, the DEM is modified for the simulation of the second event, considering the simulated thickness of the deposit by the first event.

Change of the thickness by the event chain can be simulated, modifying the DEM step-by-step. The event chain is described in the scenario database. In addition, the event chain can be enriched by examining many disaster cases such as past eruptions and lahars.

SSDM creates many pre-analyses of hazard maps in the database based on various scenarios (Fig. 13.10b). A relevant hazard map must be chosen from the database, considering the monitoring data. In the case of Merapi, the seismicity of volcano-tectonic (VT) within a 12 month-interval is applicable to forecast the potential volume of eruptive material (Iguchi et al. 2019b). The relationship between the volume of pyroclastic material and the cumulative seismic energy released in past events at Merapi volcano is calculated by Iguchi et al. (2019b) based on the empirical formula:

$$\log_{10} V_p = 2 \log_{10} E_s - 13.7 \quad (13.1)$$

where V_p is a volume of pyroclastic material and E_s is seismic energy.

Based on Eq. 13.1, the potential volumes of the 1994, 1997, 1998, 2001 and 2006 eruptions, estimated from the seismic energy, were less than $2 \times 10^7 \text{ m}^3$. However, the volume of pyroclastic material in the 2010 eruption reached $2 \times 10^8 \text{ m}^3$ (Iguchi et al. 2019b).

13.4.5 MAGMA Indonesia

MAGMA Indonesia (Multiplatform Application for Geohazard Mitigation and Assessment in Indonesia) is a multiplatform (web-based and mobile phone) application that contains integrated geological disaster information and recommendations for volcanoes, earthquakes, tsunamis, and landslides. The Center for Volcanology and Geological Hazard Mitigation (PVMBG) created MAGMA Indonesia in 2015 using cutting-edge open-source technology. The main goal of MAGMA Indonesia is to convert data into information and recommendations that society can understand through a single-window approach (quasi-real-time and interactive). MAGMA

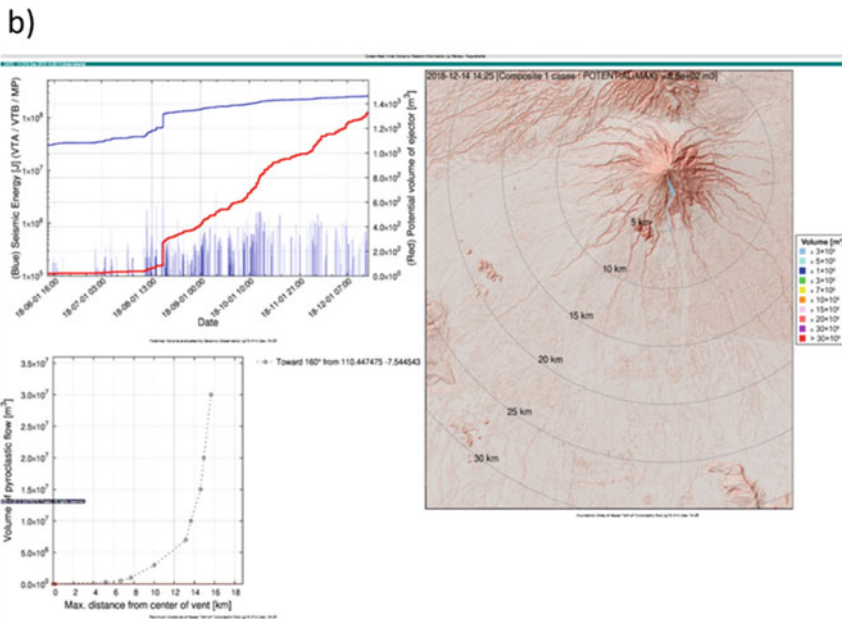
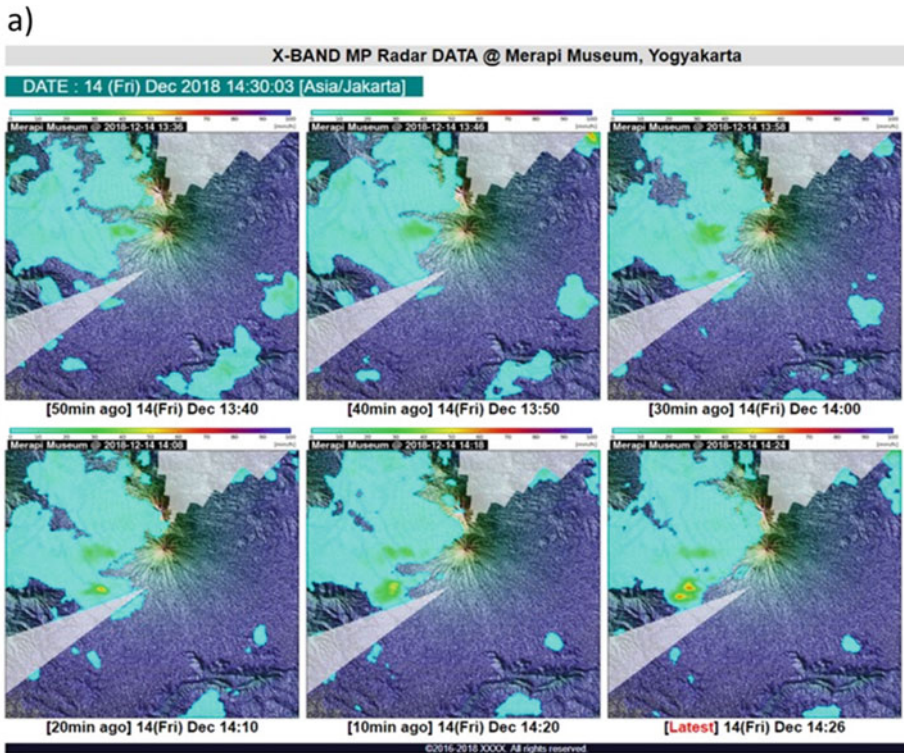


Fig. 13.10 Visualisation of the SSDM system at Merapi. **a** X-band Merapi radar data at Museum Gunung Merapi. The green colour indicates rainfall events in the northwest part of the volcano. **b** Quasi-real time volcanic hazard information on Merapi volcano. The left-top graph shows the real-time cumulative seismic energy (summation of VTA, VTB, and MP) in Joule. The left-bottom graph

shows the volume of pyroclastic flow evaluated by seismic observation and the maximum distance of the basal part of a pyroclastic flow from the centre of the vent. The map on the right shows the inundation area of the basal part of pyroclastic flow based on potential volume ejected by the volcano

Indonesia is the manifestation of the government's active participation in efforts to mitigate geological disasters in Indonesia (VSI-PVMBG 2020). MAGMA Indonesia can be accessed through <https://magma.esdm.go.id/> or downloaded via Google Play with the keyword MAGMA Indonesia.

Currently, MAGMA Indonesia provides the following volcano information:

1. MAGMA-VAR (Volcanic Activity Report) contains information on visual and instrumental observations such as meteorological conditions, visual, seismicity, alert level (status), and volcanic recommendations.
2. Volcanic Disaster Prone Areas Map.
3. VONA (Volcano Observatory Notice for Aviation) contains volcanic ash information for aviation safety. It issues reports on changes in volcanic activity, both increases, and decreases, providing a description of the nature of the unrest or eruption, potential or current hazards, and likely outcomes.
4. VEN (Volcano Eruption Notice) contains information about a volcano's eruption, such as eruptive time, visual and instrumental observations, and eruption recommendation.

13.5 Perspectives

13.5.1 Deep Magma Reservoir Monitoring

The present networks are well adapted to monitor the activity of the volcano. However, the stations' extent is still limited when attempting to constrain the location and some parameters related to deep magma sources below 10 km, particularly from seismic and deformation data. Still, monitoring the deep active sources is essential for mid-term eruption anticipation and sometimes short-term forecasting. Indeed, during an episode of new magma intrusion and migration towards the surface, an open volcanic system like Merapi gives limited geophysical signs during the shallow magma transit phase, as observed before the new

lava dome extrusion in 2018 (BPPTKG Internal Report 2018 (unpublished)). Estimating the volume of magma that migrated earlier from a deep reservoir is sometimes the only way to evaluate the potential volume of magma that will reach the surface. Therefore, one perspective is to extend the seismic and GNSS networks with new stations located at further distances between 6 and 10 km from the summit.

13.5.2 Modelling of Common Physical Parameters from Multidisciplinary Methods

One of the main challenges of volcanology today is integrated modelling, taking into account simultaneously all physical and chemical processes involved. Joint modelling is still unusual and often limited to two or three physical parameters (e.g. deformation, temperature, gravity) and most models are only constrained by a unique type of observation. We believe that any advance towards joint modelling will help reproduce the complexity of natural processes better, as volcano monitoring needs a quantitative approach to make robust forecasting. The joint modelling includes integrating geophysical and geochemical analysis of the eruptive products such as volcanic ash and rock samples.

13.5.3 Machine Learning

An extensive range and number of instruments need to be installed to acquire many valuable datasets in volcano monitoring. Furthermore, with the need for quick and accurate decision-making, it is problematic to rely solely on analyst officers' ability for rapid data analysis and interpretation. Machine learning can help to improve the situation and offer more excellent capabilities over more conventional algorithms. Therefore, machine learning in volcano monitoring has become necessary and applied at several volcanoes (Hibert et al. 2017; Malfante et al. 2018; Titos et al. 2019).

Machine learning at Merapi has been applied for several purposes. In one case, the random forest algorithm on RSAM (Real-time Seismic Amplitude Measurement) data was used for various frequency bands to automatically classify the type of earthquake events, such as deep and shallow earthquakes as well as multiphase, low frequency, rockfall, and pyroclastic flow-related events (Ramadan 2019). The training data test shows the best result with an average accuracy of 82%, when 1000 decision trees and 1.4 s of computation time are used.

In another case, automatic image classification for DSLR camera photos was performed, using the K-nearest neighbour (KNN) algorithm (Afif 2020). By extracting 27 features, the images were classified into two different categories, namely clear and foggy photos. The result reaches the best accuracy of 90%, with only 1 ms computation time for each 8 MB photo file.

In addition, fuzzy logic methods have been applied to determine the activity level status and eruption style for the 1992, 1997, 1998, 2001, 2006, and 2010 eruptions, based on earthquake events, deformation, and geochemical data (Budi-Santoso et al. 2018). An accuracy of over 60% was obtained in terms of determining the activity level status of almost all eruptions except for that in 1998. However, the style of the eruption was only predicted for the 1998, 2006 and 2010 eruptions with over 60% accuracy. Several aspects can be optimised to increase the prediction accuracy, for example, by improving the degree of truth as an extension of valuation and by applying weighting to the used parameters.

The applications of machine learning in volcanology are still very broad. However, we believe that ultimately machine learning will help solve many complexities, including extracting valuable information from monitoring data, and shorten the time and improve the accuracy of early warning decision-making.

13.5.4 Crisis Management

In general, volcanic activity increases before an eruption occurs. The increase of volcanic activity

allows an early warning system to be given sequentially in alert level status. However, before an eruption, volcanic activity can vary in behaviour patterns and speed of escalation. At Merapi, a slight increase in volcanic activity preceded some eruptions. For example, in the case of the 2006 and several previous eruptions, the average period of increasing alert levels has been approximately one month. The gradual change of alert level allows residents and local governments to adjust preparedness efforts according to the activity status level.

However, the case was different for the 2010 eruption. The increase in volcanic activity took place more rapidly. Status Awasi (Level IV) was given only five days after determining Status Siaga (Level III). Significantly, the first eruption occurred only 35 h after Status Awasi was given. The implication of this short delay between status determination and the eruption onset posed several challenges. For example, the evacuation process, which usually starts after Status Awasi (Level IV), became more challenging. Despite these constraints, the local government successfully evacuated around 20,000 vulnerable residents on 26 October 2010 (Mei et al. 2013).

As a hindsight eruption forecast, we applied the Failure Forecast Method (FFM) to the RSAM (Real-time Seismic Amplitude) data of the 2010 eruption. As early as 6 days before the eruption, we were able to obtain a prediction of the eruption time with an accuracy of fewer than 4 h (Budi-Santoso et al. 2013). These results potentially allow us to raise the alert level to the highest level early. Unfortunately, the FFM results are not accurate in all cases, and the asymptotic FFM time cannot always be interpreted as the eruption time. Therefore, making alert-level decisions only with the results from the FFM method is risky and can lead to repeated false alarms. The future challenges we face are how to improve the FFM method further and then correlate the results with other observation data to minimise inaccurate information or misinterpretation that may lead to inappropriate early warnings.

In conclusion, we have learned that the main challenge in volcano monitoring in general, and specifically at Merapi, is the rapid detection of

any changes in the observed monitoring signals, an understanding of how they evolve leading up to an eruption, the interpretation of the possible outcome and hazard phenomena, and allowing timely warnings that provide reasonable time for the community and stakeholders to handle and respond to potential hazards.

Continued efforts to improve volcano monitoring at Merapi include:

1. Strengthening the sensitivity of the monitoring system to capture weak symptoms usually hidden by noise.
2. Physical modelling to provide conclusive information of the observed data in terms of hazards, such as the potential magma volume extruded before magma reaches the surface. Aside from that, combining several geophysical and geochemical parameters into a unique physical model can enhance the weak anomalies of data observation.
3. Strengthening the ability to monitor data analysis by applying advanced data analysis techniques. Machine learning techniques allow bringing up data anomalies more firmly by minimising noise, pattern recognition, or multi-parameter correlation analysis. In some cases, it is helpful to implement Failure Forecast Method (FFM) techniques for predicting eruption onset.
4. Integration and automation of multi-parameter data analysis (e.g. geophysics, geodetic, geochemical, petrological), using the recently developed machine-learning algorithm for rapid evaluation and better decision making.

Acknowledgements After a lengthy period and facing numerous challenges, we are pleased to have completed and present this chapter on the Merapi monitoring system. We would like to express our gratitude to Andiani, the Head of CVGHM for the support in completing the Merapi monitoring chapter. We also appreciate the help of our colleagues at BPPTKG in Yogyakarta and particularly of our colleagues, the Merapi observers, who supplied the resources and data for this work. Finally, we want to convey our heartfelt gratitude to Silvana Hidalgo, Richard Herd, Ralf Gertisser and Thomas Walter for their detailed and constructive comments and suggestions that helped improve this chapter.

References

- Afif R (2020) *Pemodelan Pemilahan Citra Gunung Merapi Secara Otomatis Pada BPPTKG Yogyakarta, Program Studi Informatika—Program Sarjana Fakultas Teknologi Industri Universitas Islam Indonesia 2020*
- Beauducel F, Cornet FH (1999) Collection and three-dimensional modeling of GPS and tilt data at Merapi volcano, Java. *J Geophys Res* 104(B1):725–736
- Beauducel F, Cornet FH, Suhanto E, Duquesnoy T, Kasser M (2000) Constraints on magma flux from displacements data at Merapi volcano, Java. *J Geophys Res* 105(B4):8193–8204
- Beauducel FM, Agung Nandaka M, Cornet FH, Diament M (2006) Mechanical discontinuities monitoring at Merapi summit using kinematic GPS. *J Volcanol Geotherm Res* 150:300–312
- Beauducel F, Lafon D, Béguin X, Saurel J-M, Bosson A, Mallarino D, Boissier P, Brunet C, Lemarchand A, Anténor-Habazac C, Necessian A, Fahmi AA (2020a) WebObs: the missing link between research and real-time monitoring for volcano observatories. *Front Earth Sci* 8:48. <https://doi.org/10.3389/feart.2020.00048>
- Beauducel F, Peltier A, Villié A, Suryanto W (2020b) Mechanical imaging of a volcano plumbing system from GNSS unsupervised modelling. *Geophys Res Lett* 47:e2020bGL089419
- Bertiger W, Bar-Sever Y, Dorsey A, Haines B, Harvey N, Hemberger D, Heflin M, Lu W, Miller M, Moore AW, Murphy D, Ries P, Romans L, Sibois A, Sibthorpe A, Szilagyi B, Vallisneri M, Willis P (2020) GipsyX/RTGx, a new toolset for space geodetic operations and research. *Adv Space Res* 66:469–489
- Budi-Santoso A, Lesage P, Dwiyono S, Sumarti S, Subandriyo S, Jousset P, Metaxian J-P (2013) Analysis of the seismic activity associated with the 2010 eruption of Merapi Volcano, Java. *J Volcanol Geotherm Res* 261:153–170
- Budi-Santoso A, Rudianto I, Widolaksone R, Sulistiyani, Fajiculay E, Win NTZ, Widwijayanti C, Costa F (2018) Fuzzy inference system for Merapi alert level decision making. In: *Abstract—Cities on volcanoes 10 conference, 2–7 Sept 2018, Napoli, Italy. Miscellanea INGV No. 43. ISSN 2039-6651, p 64*
- Costa F, Widwijayanti C, Win NTZ, Fajiculay E, Espinosa-Ortega T, Newhall C (2019) WOVODat—The global volcano unrest database aimed at improving eruption forecasts. *Disaster Prev Manag* 28:738–751
- Fajiculay E, Budi-Santoso A, Sulistiyani Wi NTZ, Widwijayanti C, Costa F (2018) Anticipating volcanic eruptions using DNA-like precursors through machine learning. In: *Abstract—Cities on volcanoes 10 conference, 2–7 Sept 2018, Napoli, Italy. Miscellanea INGV No. 43. ISSN 2039-6651, p 67*
- Galle B, Oppenheimer C, Geyer A, McGonigle AJ, Edmonds M, Horrocks L (2003) A miniaturised ultraviolet spectrometer for remote sensing of SO₂ fluxes: a new tool for volcano surveillance. *J Volcanol Geotherm Res* 119:241–254

- Gertisser R, Troll VR, Nandaka IGMA (2023) The scientific discovery of Merapi: from ancient Javanese sources to the 21st century. In: Gertisser R, Troll VR, Walter TR, Nandaka IGMA, Ratdomopurbo A (eds) *Merapi volcano—geology, eruptive activity, and monitoring of a high-risk volcano*. Springer, Berlin, Heidelberg, pp 1–44
- Giggenbach WF, Goguel RL (1989) Collection and analysis of geothermal and volcanic water and gas discharges. NZ DSIR Chemistry Report 2401, pp 1–82
- Hibert C, Provost F, Malet J-P, Maggi A, Stumpf A, Ferrazzini V (2017) Automatic identification of rock-falls and volcano-tectonic earthquakes at the Piton de la Fournaise volcano using a Random Forest algorithm. *J Volcanol Geotherm Res* 340:130–142
- Humaida H (2008) SO₂ emission measurement by DOAS (differential optical absorption spectroscopy) and COSPEC (correlation spectroscopy) at Merapi volcano (Indonesia). *Indon J Chem* 8:151–157
- Iguchi M, Nakamichi H, Miyamoto K, Shimomura M, Nandaka IGMA, Budi-Santoso A, Aisyah N (2019b) Forecast of the pyroclastic volume by precursory seismicity of Merapi volcano. *J Disaster Res* 14:51–60
- Iguchi M, Nakada S, Miyamoto K (2019a) Special issue on integrated study on mitigation of multimodal disasters caused by ejection of volcanic products: Part 2. *J Disaster Res* 14:5–5
- Jousset P, Budi-Santoso A, Jolly AD, Boichu M, Surono DS, Sumarti S, Hidayati S, Thierry P (2013) Signs of magma ascent in LP and VLP seismic events and link to degassing: an example from the 2010 explosive eruption at Merapi volcano, Indonesia. *J Volcanol Geotherm Res* 261:171–192
- Kelfoun K, Budi-Santoso A, Latchimy T, Bontemps M, Nurdien I, Beaucecel F, Fahmi A, Putra R, Dahamna N, Laurin A, Rizal MH, Sukmana JT, Gueugneau V (2021) Growth and collapse of the 2018–2019 lava dome of Merapi volcano. *Bull Volcanol* 83:8
- Lühr BG, Koulakov I, Suryanto W (2023) Crustal structure and ascent of fluids and melts beneath Merapi: insights from geophysical investigations. In: Gertisser R, Troll VR, Walter TR, Nandaka IGMA, Ratdomopurbo A (eds) *Merapi volcano—geology, eruptive activity, and monitoring of a high-risk volcano*. Springer, Berlin, Heidelberg, pp 111–135
- Maercklin NC, Riedel C, Rabbel W, Wegler U, Luehr B-G, Zschau J (2000) Structural investigation of Mt. Merapi by an active seismic experiment. *DGG-Mitt Spec Issue IV/2000*:13–16
- Malfante M, Dalla Mura M, Metaxian J-P, Mars JJ, Macedo O, Inza A (2018) Machine learning for volcano-seismic signals: challenges and perspectives. *IEEE Signal Process Mag* 35(2):20–30
- Mamdani EH, Assilian S (1975) An experiment in linguistic synthesis with a fuzzy logic controller. *Int J Man Mach Stud* 7:1–13
- Mei ETW, Lavigne F, Picquout A, de Bézilaz E, Brunstein D, Grancher D, Sartohadi J, Cholikh N, Vidal C (2013) Lessons learned from the 2010 evacuations at Merapi volcano. *J Volcanol Geotherm Res* 261:348–365
- Métaxian J-P, Budi Santoso A, Caudron C, Cholikh N, Labonne C, Poiata N, Beaucecel F, Monteiller V, Fahmi AA, Rizal MH, Nandaka IGMA (2020) Migration of seismic activity associated with phreatic eruption at Merapi volcano, Indonesia. *J Volcanol Geotherm Res* 396:106795
- Métaxian JP, Surono, Widiyantoro S, Domerapi Consortium (2014) The Domerapi project. Dynamics of an arc volcano with extruding lava domes, Merapi (Indonesia): from the magma reservoir to eruptive processes. In: Abstract—Cities on volcanoes 8 conference, 9–13 Sept 2014, Yogyakarta, Indonesia
- Nakamichi H, Iguchi M, Triastuty H, Kuswandarto H, Mulyana I, Rosadi U, Gunawan H, Santika G, Aisyah N, Budi-Santoso A (2019) A newly installed seismic and geodetic observational system at five Indonesian volcanoes as part of the SATREPS project. *J Disaster Res* 14:6–17
- Nandaka IGMA, Suharna Y, Putra R, Sulistiyani S (2019) Overview of Merapi volcanic activities from monitoring data 1992–2011 periods. *J Disaster Res* 14:18–26
- Newhall CG, Costa F, Ratdomopurbo A, Venezky DY, Widiwijayanti C, Win NTZ, Tan K, Fajiculay E (2017) WOVodat—An online, growing library of worldwide volcanic unrest. *J Volcanol Geotherm Res* 345:184–199
- Ohmberger M, Wassermann J, Budi EN, Gossler J (2000) Continuous automatic monitoring of Mt. Merapi's seismicity. *DGG-Mitt (IV)*:103–108
- Pinel V, Beaucecel F, Putra R, Sulistiyani S, Nandaka GMA, Nurnaning A, Budi Santoso A, Humaida H, Doin M-P, Thollard F, Laurent C (2021). Monitoring of Merapi volcano, Indonesia based on Sentinel-1 data. EGU General Assembly 2021, online, 19–30 April 2021, EGU21-10392. <https://doi.org/10.5194/egusphere-egu21-10392>
- Ramadan I (2019) Klasifikasi Jenis Gempa Gunung Merapi Menggunakan data Rsam (real-time seismic amplitude measurement) Dengan Algoritma Random Forest, Program Studi Teknik Informatika Fakultas Teknik Industri Universitas Pembangunan Nasional “Veteran”, Yogyakarta
- Ratdomopurbo A, Beaucecel F, Subandriyo J, Nandaka IGMA, Newhall CG, Suharna, Sayudi DS, Suparwaka H, Sunarta (2013) Overview of the 2006 eruption of Mt. Merapi. *J Volcanol Geotherm Res* 261:87–97
- Rebscher D, Westerhaus M, Körner A, Welle W, Subandriyo, Brodscholl A, Kumpel H-J, Zschau J (2000) Indonesian-German Multiparameter stations at Merapi volcano. *DGG-Mitt (IV)*:93–102
- Shimomura M (2018) Operating manual of IGIS-MSD simulator
- Subandriyo S, Gertisser R, Aisyah N, Humaida H, Preece K, Charbonnier S, Budi-Santoso A, Handley H, Sumarti S, Sayudi DS, Nandaka IGMA, Wibowo HE (2023) An overview of the large-magnitude (VEI 4) eruption of Merapi in 2010. In: Gertisser R, Troll VR, Walter TR, Nandaka IGMA, Ratdomopurbo A (eds) *Merapi volcano—geology, eruptive activity, and monitoring of a high-risk volcano*. Springer, Berlin, Heidelberg, pp 353–407

- Sumarti S, Rinekso K, Yulianto Y, Sulistiyo Y (2007) Gas Vulkanik Erupsi Merapi Juni 2006. In: Edisi Khusus Merapi 2006 Laporan Dan Kajian Vulkanisme Erupsi. Pusat Vulkanologi dan Mitigasi Bencana Geologi, Yogyakarta, pp 283–292
- Surono JP, Pallister J, Boichu M, Buongiorno MF, Budisantoso A, Costa F, Andrestuti S, Prata F, Schneider D, Clarisse L, Humaida H, Sumarti S, Bignami C, Griswold J, Carn S, Oppenheimer C, Lavigne F (2012) The 2010 explosive eruption of Java's Merapi volcano—A '100-year' event. *J Volcanol Geotherm Res* 241–242:121–135
- Tamburello G (2015) Ratiocalc: Software for processing data from multicomponent volcanic gas analyzers. *Comput Geosci* 82:63–67
- Thouret J-C, Aisyah N, Jenkins SF, de Belizal E, Sulistiyani, Charbonnier S, Sayudi DS, Nandaka IGMA, Mainsant G, Solikhin A (2023) Merapi's lahars: characteristics, behaviour, monitoring, impact, hazard modelling and risk assessment. In: Gertisser R, Troll VR, Walter TR, Nandaka IGMA, Ratdomopurbo A (eds) Merapi volcano—geology, eruptive activity, and monitoring of a high-risk volcano. Springer, Berlin, Heidelberg, pp 501–552
- Titos M, Bueno A, García L, Benítez MC, Ibañez J (2019) Detection and classification of continuous volcano-seismic signals with recurrent neural networks. *IEEE Trans Geosci Remote Sens* 57(4):1936–1948
- Voight B, Young KD, Hidayat D, Subandrio PMA, Ratdomopurbo A, Suharna P, Sayudi DS, LaHusen R, Marso J, Murray TL, Dejean M, Iguchi M, Ishihara K (2000) Deformation and seismic precursors to dome-collapse and fountain-collapse nuées ardentes at Merapi Volcano, Java, Indonesia, 1994–1998. *J Volcanol Geotherm Res* 100:261–287
- VSI-PVMBG (2020) MAGMA Indonesia. <https://magma.vsi.esdm.go.id/>
- Wagner D, Koulakov I, Rabbel W, Luehr B-G, Wittwer A, Kopp H, Bohm M, Asch G, Scientists MERAMEX (2007) Joint inversion of active and passive seismic data in Central Java. *Geophys J Intern* 170:923–932
- Widiyantoro S, Ramdhan M, Métaxian J-P, Cummins PR, Martel C, Erdmann S, Nugraha AD, Budi-Santoso A, Laurin A, Fahmi AA (2018) Seismic imaging and petrology explain highly explosive eruptions of Merapi volcano, Indonesia. *Sci Rep* 8:13656
- Young KD, Voight B (2000) Ground deformation at Merapi Volcano, Java, Indonesia: distance changes, June 1988–October 1995. *J Volcanol Geotherm Res* 100:233–259
- Zimmer M, Erzinger J (2003) Continuous H₂O, CO₂, ²²²Rn, and temperature measurements on Merapi volcano, Indonesia. *J Volcanol Geotherm Res* 125:25–38
- Zschau J, Sukhyar R, Purbawinata MA, Lühr BG, Westerhaus M (2003) The Merapi-project—Interdisciplinary monitoring of a high-risk volcano as a basis for an early warning system. In: Zschau J, Küppers A (eds) Early warning systems for natural disaster reduction. Springer, Berlin, Heidelberg, pp 527–532



Thomas R. Walter

Abstract

Monitoring and assessing eruption hazard at Merapi volcano are challenging due to steep slopes, the harsh environment at the summit, and hazardous access during both volcanic crises and quiescent intervals. While passive remote sensing techniques often fail due to cloud coverage, active sensing techniques are increasingly used and bridge fields from mapping to geophysical studies. In particular, synthetic aperture radar (SAR) remote sensing and interferometric products are highly valuable at Merapi and similar volcanoes elsewhere, allowing views of the summit, crater, and dome, even when these are covered by dense rain or ash clouds. SAR and interferometric SAR (InSAR) permit assessment of eruption precursors, quantifying rapid geomorphological changes that occur during dome growth and fracturing, such as those in 2010, 2013–14, and 2018. Radar sensing also allows precisely mapping of volcanic deposits, lahars and damage, monitoring subtle ground displacements, and generating high-resolution digital elevation models. This chapter reviews the benefits of radar investi-

gations conducted at Merapi volcano and discusses future directions.

Keywords

Merapi · Satellite remote sensing · Synthetic aperture radar · Volcano monitoring

14.1 Introduction

Volcano remote sensing has a >30-year-long history of successful topographic, dynamic, compositional, and geometric observations (e.g. Francis and Rothery 2000). Satellite remote sensing offers the opportunity to acquire and analyse long time-series data of active volcanoes and provides a high resolution that allows mapping of topographic changes, identifying millimetre-scale deformations, tracing the outlines and features of growing and collapsing lava domes, and assessing the hazards associated with pyroclastic density currents (PDCs) and lahars. The sensors that have been used at Merapi and other volcanoes can be broadly categorised into passive and active technologies.

Passive techniques rely on the reflection (e.g. sunlight) or emission (e.g. thermal infrared) of energy, whereas active techniques emit an electromagnetic signal that is commonly echoed from the ground before it is recorded at the instrument again. Passive remote sensing satellites

T. R. Walter (✉)
GFZ German Research Centre for Geosciences,
Telegrafenberg, Potsdam, Germany
e-mail: twalter@gfz-potsdam.de

(e.g. SPOT, MODIS, AQUA, Terra, Landsat, and Sentinel-2) have been applied to volcanoes with great success, with several applications for Merapi volcano (Gerstenecker et al. 2005; Thouret et al. 2010, 2015; Kadavi et al. 2017; Darmawan et al. 2018a, b). In recent years, passive systems have also been transported by unmanned aerial vehicles (James et al. 2020) to gain insights into steep volcano summit regions (Darmawan et al. 2023, Chap. 15). While these passive sensors have wide applicability and high resolution, they are useful only during daylight hours and are obscured or useless under cloudy conditions.

Radar technologies (Fig. 14.1) are active techniques that illuminate the Earth's surface with electromagnetic waves in the microwave spectrum. Radar can penetrate even a dense cloud cover, can operate day and night and is largely independent of meteorological conditions. Depending on the wavelength of the radar sensor used, the signals can penetrate vegetation, provide textural information, show atmospheric attenuations, and even allow the detection of millimetre-scale ground motions. At Merapi volcano, in particular, radar sensing technologies have been used, both routinely and experimentally, from the ground using Doppler radar (Voge et al. 2008) and from satellites using synthetic aperture radar

(SAR) systems for the monitoring of deformation, lava dome growth, crater depth, deposition of materials and other purposes (Saepuloh et al. 2011, 2013; Bignami et al. 2012, 2013; de Michele et al. 2013; Pallister et al. 2013; Chua et al. 2015; Kubanek et al. 2015; Solikhin et al. 2015a, b; Walter et al. 2015). As summarised in this chapter, satellite-based radar sensing has led to a variety of experimental studies that have explored new approaches and tools for feature extraction and volcanic plume detection and have combined interdisciplinary data (de Michele et al. 2013; Saepuloh et al. 2013; Kadavi et al. 2017). Consequently, Merapi volcano has become a testing laboratory for radar sensing technologies. To this aim, Merapi is particularly challenging due to intense volcanic activity, steep topography, rapid material removal and deposition, dense vegetation, hydrometeorological conditions and land use. Studies of this volcano, in turn, are particularly rewarding, as any improvement in monitoring its volcanic activity and its processes may lead to a better understanding of related hazards and development of new risk mitigation strategies.

This chapter is organised as follows. First, it reviews the SAR geometry and SAR techniques used. After describing the amplitude and phase analysis methods, selected case studies at Merapi

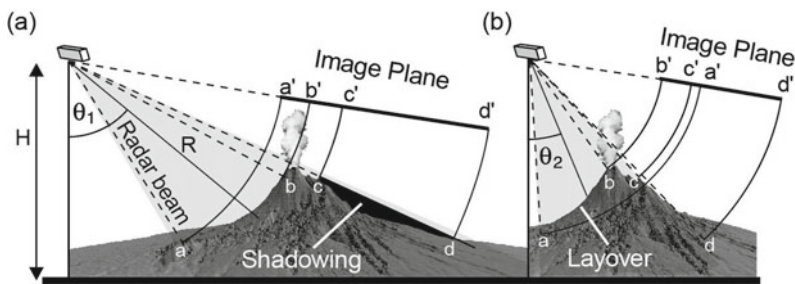


Fig. 14.1 Imaging geometry of a radar system adapted and redrawn from Carn (1999). The system includes a radar sensor at a height (H) with a slant range (R) and radar look angle (θ) between the nadir vertical and the slant range vector. Distortion in radar imagery leads to shadowing (left image; **a**) and layover (right image; **b**). Shadowing gives a region of zero backscatters on the resulting image [c' , d'], whereas layover causes high backscatter [a' , b' on the right

image]. Layover results when echoes received from low-lying areas reverse the terrain sequence in the image; hence, terrain [a , b , c , d] becomes [b' , c' , a' , d'] in the image. Different satellites may have different look angles so that the effects of shadowing and layover differ. In a side-looking radar system, a descending orbit means that the satellite looks to the west, and in ascending orbit, the satellite looks to the east

are outlined. This chapter provides the reader with an overview of the varied and important information that is relevant to monitoring processes and hazards at the volcano, such as topographic measurements, material transfer, dome growth, pyroclastic material deposition, lahar monitoring, and surface displacements associated with compaction, cooling, and eruption cycles, and the detection of eruption plumes.

14.2 Synthetic Aperture Radar

14.2.1 SAR Geometry

Synthetic aperture radar (SAR) is based on a microwave remote sensing instrument that allows mapping the scattering properties of the surface (Bamler 2000) and monitoring volcanoes (Meyer et al. 2015; Lu and Dzurisin 2018). Generally, SAR sensors are side-looking; where the geometry and the surface characteristics affect the received backscattered signal (Francis and Rothery 2000). The echoes of the radar signal are measured and, after processing, allow derivation of a high-resolution image (Wadge et al. 2011). The illumination is accomplished by the emission, echoing, and reception of the radar signal so that no other external energy source (such as sunlight) is required to monitor the target volcano. Especially useful in tropical environments such as that at Merapi volcano and its surroundings, the system can be used day and night and even when clouds are present (Carn 1999; Pinel et al. 2014). The ground pixels that are scattered back in the electromagnetic signal are usually several square metres in size and contain amplitude and phase values. These two values are exploited and analysed in many different ways. While the amplitude image bears some visual similarity to a digital shaded relief map and can be interpreted as such (Carn 1999), the phase image is not interpretable on its own. This is because the signal contains a contribution from random scattering, which is why current strategies mostly concentrate on the detection of changes in phase values, such as those applied in coherence

analysis (Lu and Freymueller 1998), or in interferometric SAR applications and related time-series analysis (Pepe and Calo 2017).

The geometry of a SAR image is commonly described by the azimuth (equivalent to the flight track of the satellite) and range (equivalent to the viewing direction, which is measured perpendicular to the flight track). As the available SAR satellites have near-polar paths (with common azimuth directions that are rotated 5–10° from north), they orbit the Earth at altitudes of 500–800 km alternating from north to south (called descending orbits) and from south to north (called ascending orbits), with orbital periods that are commonly 1–2 h.

The range direction is perpendicular to the orbit, so that SAR satellites illuminate the surface of the volcano from either easterly or westerly directions but never from the north or south. While the viewing direction oblique to the ground has many technical advantages (i.e., solving common left–right ambiguity problems), the disadvantages are shadowing and foreshortening (Fig. 14.1a) and layover (Fig. 14.1b) effects. As seen in the raw SAR amplitude images of Merapi and because of this geometric distortion, the brighter flanks appear to be shorter than the darker flanks. To a degree, this geometric distortion is corrected during the *terrain correction* processing step. When a certain change is to be investigated on the ground, two images are selected from before and after the event. During so-called coregistration, these images, referred to as the primary/replica images (or primary/secondary images; however, some authors still use the inappropriate terminology master/slave), are shifted, rotated, and warped until they exactly overlies each other. Then, the changes and characteristics of the phase and amplitude values are investigated for different purposes and applications.

14.2.2 Satellite SAR Systems

The observation and monitoring of volcanoes, especially Merapi, have a long history and have been conducted by different satellites as SAR

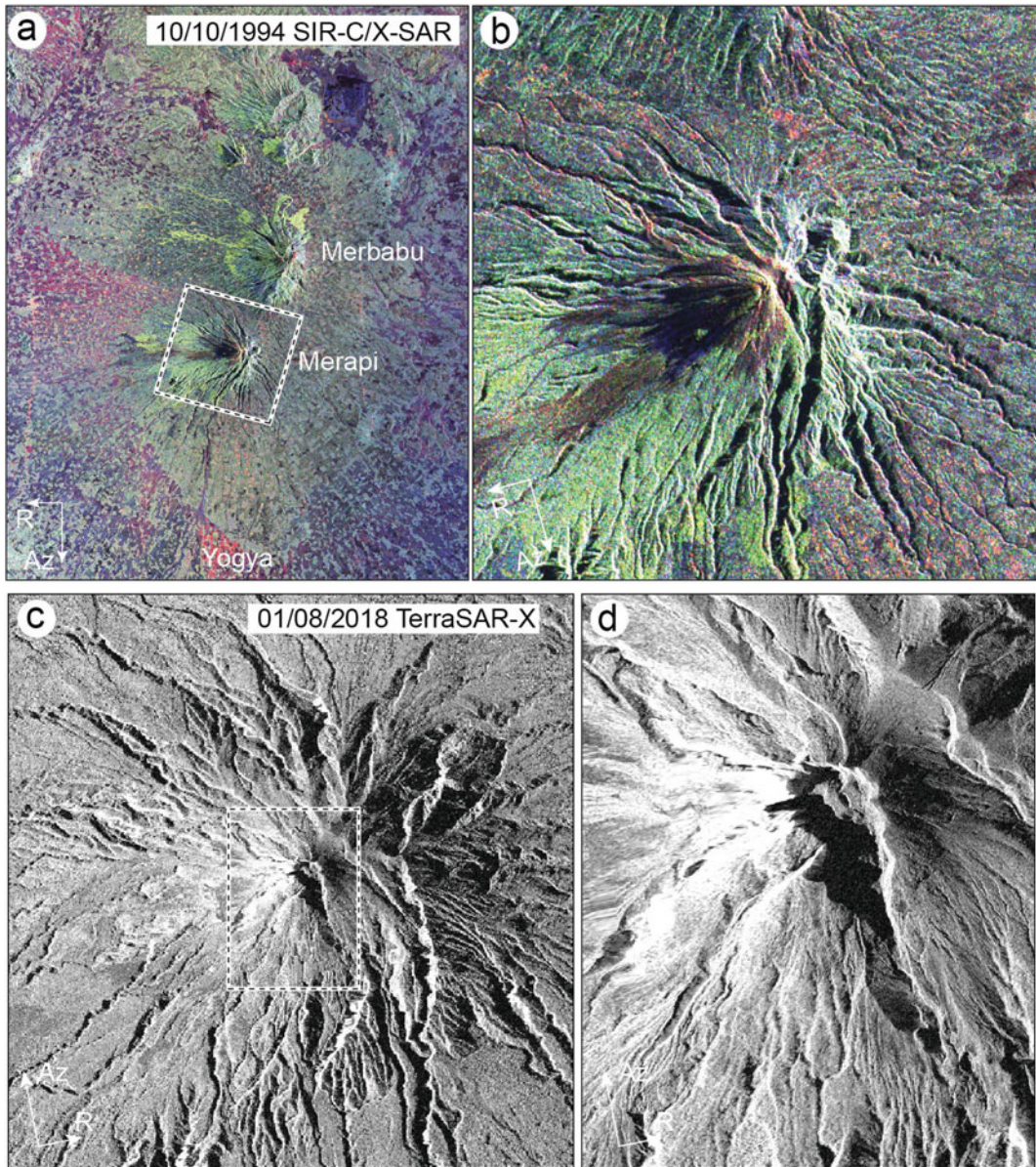


Fig. 14.2 Radar system imaging at Merapi volcano has been achieved for three decades. **a** The radar image shows the 10 October 1994 acquisition by the Spaceborne Imaging Radar-C/X-Band synthetic aperture radar (SIR-C/X-SAR) aboard the space shuttle *Endeavour*. **b** A magnified view of the dashed box indicates eruption deposits toward the southwest. A combination of different

radar wavelengths allows texture analysis. Images are shown in radar coordinates. **c** A high-resolution radar image 24 years later was acquired by the TerraSAR-X satellite in spotlight mode, providing a geolocated view with an area similar to that shown in **(b)**. **d** A magnified view of the dashed box showing the deep valley directing new deposits to the southeast

carriers. An early experiment carried out was the shuttle imaging radar (SIR) system (Fig. 14.2), which, for the first time, allowed mapping of geological and tectonic features (Sabins 1983;

Mouginis-Mark 1995). The SIR mission was special (Fig. 14.2a, b), as it used different acquisition parameters and facilitated the worldwide refinement of radar data analysis (MacKay

et al. 1998) by exploring different wavelengths (C-band (7.5–3.8 cm) and X-band (3.8–2.4 cm)) and vertical and horizontal polarisation. The incidence angles were found highly relevant for separating the contrasts between eruption deposits, lava flow units, and vegetation (Mouginis-Mark 1995). Depending on the applications and demands, various space agencies then developed and launched a new fleet of SAR sensors; examples are the Japanese JERS-1, ALOS, Canadian RADARSAT 1 and 2, and European ERS1/2 and Envisat missions, all of which have been used worldwide for volcano observations (Rowland et al. 1994; Massonnet et al. 1995; Wadge and Haynes 1998).

Another breakthrough for the SAR technique was propelled by two main developments in the past 5–10 years. (1) Next-generation radar systems are available, some with advanced temporal and spatial resolutions. Examples are the Italian Cosmo Skymed (CSK) and the German TerraSAR-X/TanDEM-X (TSX/TDX) missions (a TSX image is shown in Fig. 14.2c, d). (2) The first truly free online access to data and processing tools was pushed by the European Space Agency's (ESA) Copernicus program that followed the Earth monitoring initiative. Therefore, SAR systems are now considered to be complementary and, in some cases, even superior to common optical sensors for operational monitoring of volcanoes. A particular strength is that SAR systems can be used in many ways at any one time, such as observing volcanoes by change detection applications (Meyer et al. 2015), measuring surface deformation signals associated with eruptions and material compaction (Dzurisin 2003), and mapping material types (Solikhin et al. 2015a, b). In the following Sect. 14.3, the applications at Merapi are reviewed by grouping the studies into those that focus on the amplitude signal and those that focus on the phase information in the backscattered signal.

Although SAR systems have helped researchers to better understand a range of volcanic processes and hazards, with unique all-weather capabilities and monitoring of changes on the ground, these systems also have several limitations (Meyer et al. 2015), especially in a

steep and rapidly evolving terrain. Geometric limitations also limit the use of SAR and interferometric products at Merapi (Kubaneck et al. 2015). The upper eastern and western flanks of Merapi remain difficult to monitor for most steep-incidence SAR systems. Moreover, the deep crater and south-directed ravine that evolved after the 2006 and 2010 eruptions remain partly invisible in radar satellite views, so the details of activities may remain hidden. Spatial resolutions, although approaching those of optical satellites (e.g. TerraSAR-X spotlight mode at a 1–2 m resolution), may not be high enough to assess all activities and changes. For true operational monitoring of volcanoes, the temporal sampling of satellite SAR systems is often limited, with some having only a few observations per month. The repeat cycles vary from 35 days for ERS and Envisat satellites, 42 days for ALOS-1, 12 days for the Sentinel-1 satellites, 11 days for TerraSAR-X, and 6 days for the constellation Sentinel-1A and 1B. Thus, short-term changes, precursors and hazards are not well imaged by the limited temporal sampling provided by spaceborne radars. Another limitation arises from the large data volumes and consequently intense processing and computational demands, which is why attempts to simplify analysis and exploit amplitude-based data derivatives and phase-based data are required (Meyer et al. 2015).

14.3 SAR Applications at Merapi

Remote sensing by SAR is well suited to study the steep topography of Merapi, a volcano with spontaneous eruptions, changing hazards, and dangerous field access to the dome and deposition sites. Earlier attempts to precisely measure the topography were challenging; campaigns of light detection and ranging (LiDAR) measurements were blurred by summit clouds, and photogrammetric and drone-based approaches (see also Darmawan et al. 2023, Chap. 15) were challenged by steam, clouds and high winds (Darmawan et al. 2018a, b). Thanks to the SAR methods applied at Merapi volcano, its eruption

processes and related hazards are now much better understood.

14.3.1 Amplitude Methods and Analysis

One way of monitoring Merapi volcano with a SAR system is determining the amplitude component of the pixels. The amplitude is a representation of the echoed radar signal that is recorded at the satellite. The amplitude can be regarded as an intensity value that depends on the ground geometry, such as the local slope, and allows the study of volcanic deposits (Arnold et al. 2017). Moreover, the amplitudes depend on the surface roughness of the ground and on the material-dependent dielectric constant (Wadge et al. 2011), which is why they are applied for mapping new deposits on Merapi (Saepuloh et al. 2010). The dielectric constant can be viewed as the degree of polarisation of a given material (Adams et al. 1996). Comparisons of different regions in an image or different records (acquisitions) of the same region can be used to monitor variations in the scatterers. Therefore, these measurements can distinguish different materials, deposits, and their changes in time and space. Considering a large set of pixels from a given

image, subtle changes in radar amplitudes can be retrieved, even when phase-based techniques (see below) fail. Therefore, amplitude-based methods can be used effectively even inside the crater of Merapi volcano, as was done during the large volcano explosivity index (VEI)-4 2010 eruption (Surono et al. 2012), during the VEI-2 2013 dome-splitting eruption (Walter et al. 2015), and during the 2018 dome extrusion (see below and Darmawan et al. 2023, Chap. 15).

The value of SAR amplitude images has received increased attention since these images successfully contributed to interpretations during the 2010 eruption (Fig. 14.3). The timely delivery of these data products by space agencies and the near-real-time analysis were important for consideration in rapid assessment and early warning (Pallister et al. 2013). The main activity phase of this major eruption lasted 12 days (26 Oct–7 Nov 2010). Because single satellites often make one pass only every 1–2 weeks, comparative analysis of different SAR satellites was important to increase the temporal resolution. Based on SAR amplitude images, the eruption rates could be estimated and compared to the long-term rates. The long-term time-averaged eruption rate for Merapi is $0.04 \text{ m}^3 \text{ s}^{-1}$ for the period 1890–1992 (Siswowardjyo et al. 1995), although it strongly fluctuates with periods of

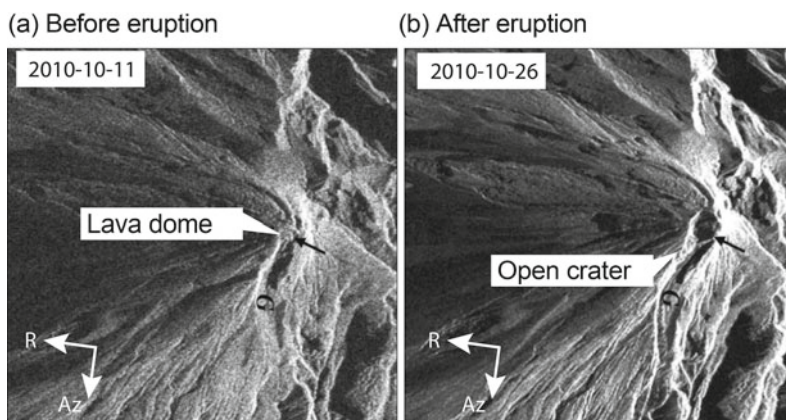


Fig. 14.3 Amplitude images **a** before and **b** after the 2010-10-26 eruption acquired in descending orbit by SAR systems Radarsat-2 and TerraSAR-X, respectively. A lava dome was identified before the explosive eruption, which

became the location of a deep ravine after the eruption. After Pallister et al. (2013). Az—Azimuth, R—Range direction of the SAR system

high eruption rates interrupted by intervals of apparently lower eruption rates (Gertisser et al. 2012). The SAR amplitude data suggested that rates of dome growth from 1 to 6 November 2010 were orders of magnitude higher at approximately $25\text{--}35\text{ m}^3\text{ s}^{-1}$ for the 1–4 November dome (Pallister et al. 2013) and ten times greater than those during the 2006 eruption (Ratdomopurbo et al. 2013).

The assessments of lava dome extrusion rates, in particular, have great relevance for several reasons. Extrusion rates are important to understand explosions from gas-charged, fresh magma, which may lead to PDCs from vertical eruptive columns, minor and directed explosions, and destabilisation and collapse of a new dome (Hartmann 1935; Fink and Anderson 2000; Voight 2000; Boudon et al. 2015). High extrusion rates may lead to destabilisation of a dome by localised and high shear strain in its carapace as well as in the weak core. During hydrothermal activity, fracture networks may temporarily seal again and cause incomplete degassing, possibly triggering spontaneous explosions (Darmawan et al. 2018a, b; Heap et al. 2019).

Several examples of such explosions occurred in the period from 2012–2014 and were monitored by SAR amplitude images (Walter et al. 2015), revealing that spontaneous explosions, commonly less than 2 km high, originated from open deep fissures on the dome carapace. This process was illustrated by comparing high-resolution SAR amplitude data from before and after the 18 November 2013 explosion. The explosion exhibited no defined edifice-wide deformation but occurred following periods of intense rain (Darmawan et al. 2018a, b) and led to a fissure that was 200 m long and up to 60 m deep. By generating a composite map from two or more SAR images, researchers could identify pixels representing amplitude increases and decreases (Fig. 14.4). Similarly, also the 2018 lava dome extrusion was captured by the SAR amplitude method and allowed the identification of lateral growth and flow-like structures as they developed (Fig. 14.5).

Thus, by comparing the SAR amplitude imagery, profound changes in reflectivity and

properties can be determined. From this view, small-scale features and lineaments can also be mapped. Lineaments may form due to different processes, such as faulting, fracturing, diking, or other lithologic or geomorphologic contrasts, and can be particularly helpful to characterise structural changes and evolving volcanic landscapes. As the backscattering of the SAR system is strongly topography- and lithology-dependent, lineaments may be extracted using edge-detection approaches (Saepuloh et al. 2015a, b; Walter et al. 2015). For instance, the 2013 explosions that led to the splitting of the dome may have indicated such profound lineament changes. Edifice-wide lineament identification may allow interpretation of general structural and volcanic-tectonic processes (Walter et al. 2015). Similarly, the 2010 eruption led to changes in the density of linear features, as observed on the southern flank of Merapi (Saepuloh et al. 2013, 2015a, b). As the 2010 lava dome was destroyed, a deep crater formed and channelled new magmatic material southward (Walter et al. 2013), gradually infilling the Gendol drainage system (Surono et al. 2012); the structural changes were identified in the SAR data (Saepuloh et al. 2015a, b). However, cautious interpretations are needed in such SAR amplitude image studies, as side-looking SAR satellites with polar orbits will always “see” north–south-trending linear features more clearly than east–west-trending features, which is why north–south lineaments might be overrepresented.

Tracking the locations of pixels in SAR amplitude image frames furthermore allows detection and the quantification of surface displacements. The pixel offset (PO) method identifies pixels (or groups of pixels) that are affected by large displacements. The range offset (RO) method exploits this approach in the radar range direction. This is commonly achieved by cross-correlations of moving subwindows of a SAR amplitude image stack, similar to the method of calculating pixel offsets in optical images (Pinel et al. 2014) that had already been applied to Merapi volcano (Walter et al. 2013). For the cross-correlation function, the chosen subwindow dimension needs to be significantly larger than the

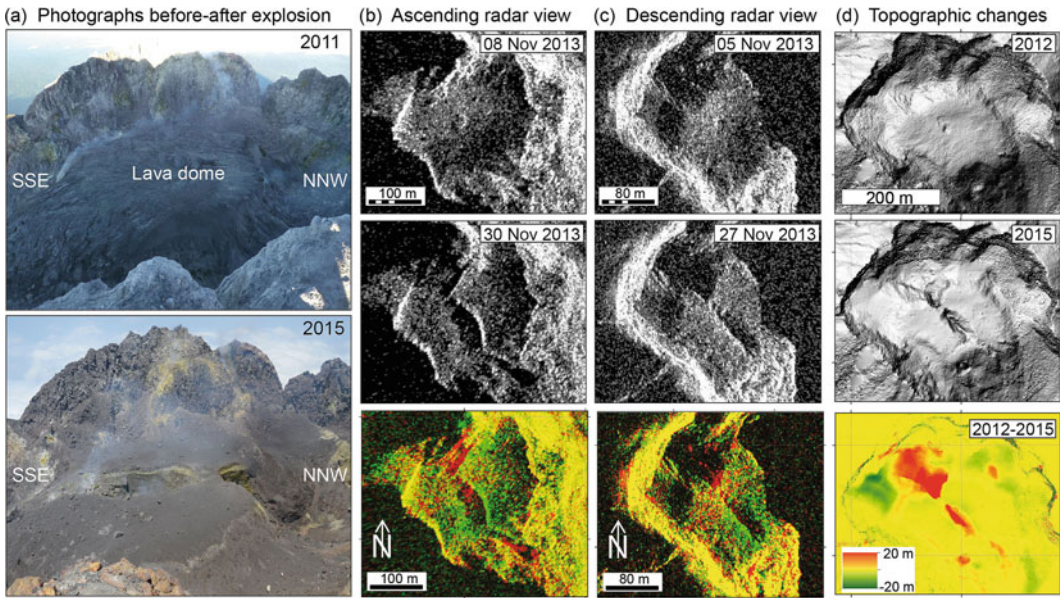


Fig. 14.4 Analysis of SAR data acquired before and after explosions reveals structural changes. **a** Photographs acquired from the eastern crater rim show the flat-topped lava dome in 2011 and the split dome in 2015. **b** Ascending radar view using high-resolution spot TerraSAR-X data before and after the dome-splitting explosions and a composite change map. **c** Same as **(b)** but for the descending radar view geometry (after

Walter et al. 2015). The range direction of the SAR system is from the left for the ascending SAR system **(b)** and from the right for the descending SAR system **(c)**. **d** Topographic changes derived from drone data are shown by shaded relief maps before and after the explosion episode, and the difference map shows the amount of material loss and gain by a scale ± 20 meters (after Darmawan et al. 2018a, b)

expected displacements, and the correlation peak is searched for in the corresponding subwindows in the primary image and the secondary image. This approach theoretically allows the identification of subpixel movements. The accuracy of the PO technique depends on coregistration, coherence, speckling, and other path effects of the radar signal and allows detection of decimetre to metre displacements (Pinel et al. 2014). At Merapi volcano, the displacements associated with PO analyses may allow tracking the growth of lava domes (Fig. 14.5e).

Time series of SAR amplitudes at selected points depict temporal surface changes on the growing lava dome (Saepuloh et al. 2015a, b); the power return to the sensor, σ^0 , is written as follows:

$$\sigma^0 = (4k^4 h_0^2 \cos^4 \theta_i) |\alpha|^2 \omega \quad (14.1)$$

where k is the wavenumber, h_0 is the surface roughness, θ is the angle of incidence from the

mean normal direction to the surface, α is proportional to the polarisation state and ω is the roughness height spectral density of the surface topography. Surface roughness strongly influences the backscattering intensity and may enable time-series analysis in the dome area for monitoring purposes. Applying this approach to a dataset of ALOS/PalSAR images, the growth of a NW–SE elongated dome was identified in the summit area, indicating an elliptically shaped extrusion of new volcanic material that was growing parallel to pre-existing fracture zones (Saepuloh et al. 2013). The gradual changes in backscattering intensity data can be particularly valuable if combined with interferometric methods (Saepuloh et al. 2013).

For decades, SAR sensors have been capable of measuring different polarisation states, while the phase information is preserved so that these systems transmit and receive both vertically and horizontally polarised microwave signals. While the polarity of the SAR data has little effect on

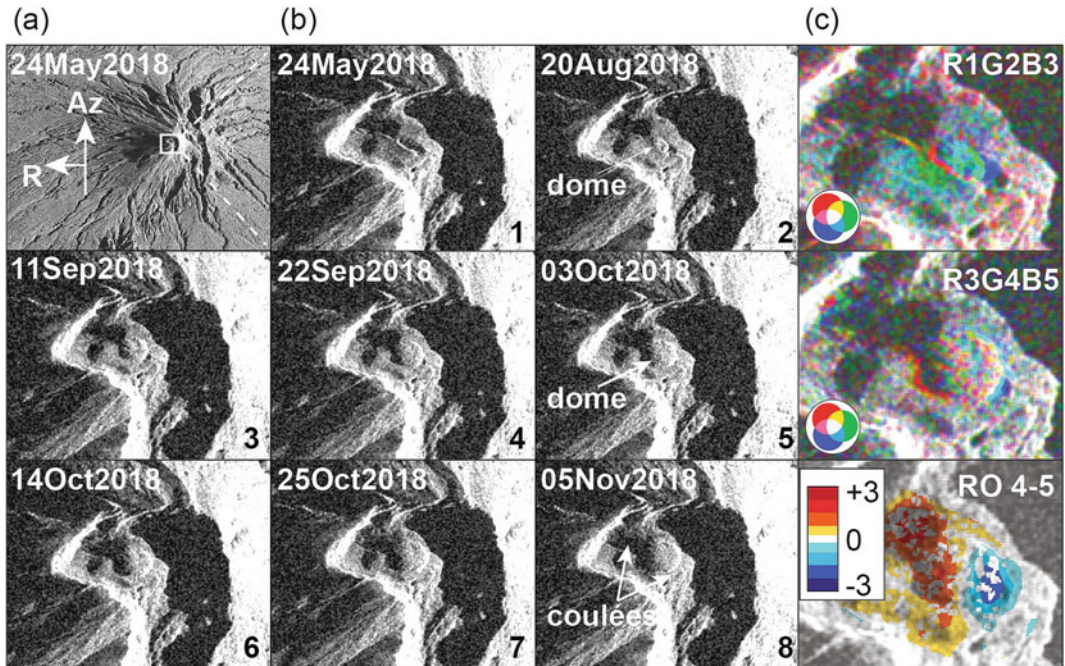


Fig. 14.5 SAR amplitude imagery allows monitoring dome growth. **a** A TerraSAR-X scene in radar coordinates; the white box indicates the summit crater area. **b** Magnified views of the summit crater area for eight SAR images (labelled 1 to 8) acquired before (24 May 2018) and during the dome growth episode. **c** Change detection by composite mapping. The red (R), green (G), and blue (B) channels are indicated for three images (R1G2B3 indicates red = 1st image, green = 2nd image,

and blue = 3rd image). Note the growth of the dome. The lower right image shows a range offset (RO) displacement map (shown by a scale ± 3 meters) associated with extrusion of the lava dome for images 4 and 5; blue indicates movement to the right, and red indicates movement to the left. All images are from TerraSAR-X track58, spot_092, descending view, radar coordinates, flipped E-W; Az—Azimuth is north, R—Range is west

deformation assessments, it may be highly sensitive for identifying surface characteristics. Radar microwave signals, especially in a polarisation state, interact in complex ways with scattering objects (lava dome rocks, ash, or vegetation), and such interactions depend on the shape/roughness and electrical characteristics of these objects. Consequently, the details of objects, their structure, and electrical characteristics can be inferred from SAR backscatter. Discriminating lava flows, for instance, with their different textures and roughness, is effectively accomplished using cross-polarised data (Zebker and Vanzyl 1991). Therefore, distinguishing different types of lava provides important support for scientists mapping in the

field (Pinel et al. 2014; Le et al. 2015). The effects of the relative radar polarisation on the SAR amplitudes were investigated at Merapi to identify the types of material (Saepuloh et al. 2015a, b; Solikhin et al. 2015a, b), such as deposits from PDCs and tephra falls (Solikhin et al. 2015a, b).

Therefore, SAR amplitude methods are highly valuable and contain important information that contributes to a better understanding of Merapi volcano and its hazards. While the above methods effectively allow the detection and mapping of new activity, the shape, topography, and volume are more quantitatively accessible by considering phase differencing methods, as detailed in the following section.

14.3.2 Phase Differencing Methods and Analysis

The interferometric SAR (InSAR) technique is probably the most widely known SAR method (Lu and Dzurisin 2018) and has been applied to solve several problems and questions at Merapi volcano. InSAR exploits the phase information of SAR data according to

$$\begin{aligned} \phi_{InSAR} = & \phi_{ref} + \phi_{topo} + \phi_{def} + \phi_{atm} \\ & + \phi_{orbit} + \phi_{bs} + \phi_{noise} \end{aligned} \quad (14.2)$$

where the phase of an interferogram (ϕ_{InSAR}) is described as the sum of the reference phase ϕ_{ref} , the topography phase ϕ_{topo} , the deformation ϕ_{def} and phase contributions arising from the atmosphere ϕ_{atm} , orbit ϕ_{orbit} , backscattering conditions ϕ_{bs} , and other noise (Hooper et al. 2004). Assuming that a satellite uses a wavelength $\lambda = 5.6$ cm (e.g., ESA satellites), a 2.8 cm movement in the line-of-sight direction would cause a difference in the interferometric phase of 2π , and the cycle is graphically represented by one fringe.

Along with the interferogram, the spatial coherence is measured. Coherence is a quality factor and a byproduct of InSAR processing (Zebker and Villasenor 1992) but by itself also contains important information for mapping changes at volcanoes (Rosen et al. 1996). As the coherence includes both amplitude and phase values, the InSAR pixels that are credible are separated from those that are not. Coherence has a range from 0 (noise) to 1 (credible) and is described by the cross-correlation factor between the complex reflectivity functions of the coregistered primary and secondary images. Coherence measures used alone have been investigated for volcanic monitoring purposes elsewhere (Rosen et al. 1996; Lu and Freymueller 1998). At Merapi, coherence has been assessed for detecting changes and mapping deposits (Solikhin et al. 2015a, b) and for determining interferometric quality (Bignami et al. 2013; Saepuloh et al. 2013).

The InSAR technique is particular challenging at Merapi volcano for several reasons, such as poor coherence, dense vegetation and land use on the flanks, strong geometric distortion of the steep edifice, atmospheric disturbance in the tropical environment, frequent material deposition, effects on backscattering characteristics, and a lack of major displacements. An excellent case for testing the validity of the retrieved ground displacement data is a comparison to the dormant Merbabu volcano, only ~ 10 kms to the north. Both Merapi and Merbabu have similar morphologies, heights, and weather so that artefacts arising from topography and a layered or turbulent atmosphere can be effectively explored (Pamungkas et al. 2014); this comparison allows the study of signals correlated at these two neighbouring edifices, which is better explained by atmospheric phase delays than by true volcanic-tectonic deformation (Chaussard and Amelung 2012).

An InSAR time series was created from a large set SAR images acquired between 2007 and 2011 at Merapi volcano (Chaussard and Amelung 2012) and other volcanoes in Indonesia (Fig. 14.6). The time-series approach significantly improved data quality compared to simple two-pass interferograms but was still not able to reveal major deformation associated with magma chamber pressurisation at Merapi. No precursory edifice-wide inflation was detected before the 2007, 2008, and 2010 eruptions (Chaussard and Amelung 2012). The lack of edifice-wide deformation may be due to the absence of a large shallow storage zone, the detection threshold of the SAR methods (InSAR ~ 3 cm/year and InSAR time series ~ 0.3 cm/year), and the poor data quality in the steep terrain and densely vegetated volcano flanks. In a holistic study, the analysis of deformation rates showed that other active volcanoes of the archipelago, in fact, did show inflation/deflation episodes (Chaussard and Amelung 2012; Chaussard et al. 2013), motivating further explorations at Merapi. Testing whether and how volcanoes inflate before eruptions and deflate during and after eruptions is relevant for monitoring and understanding

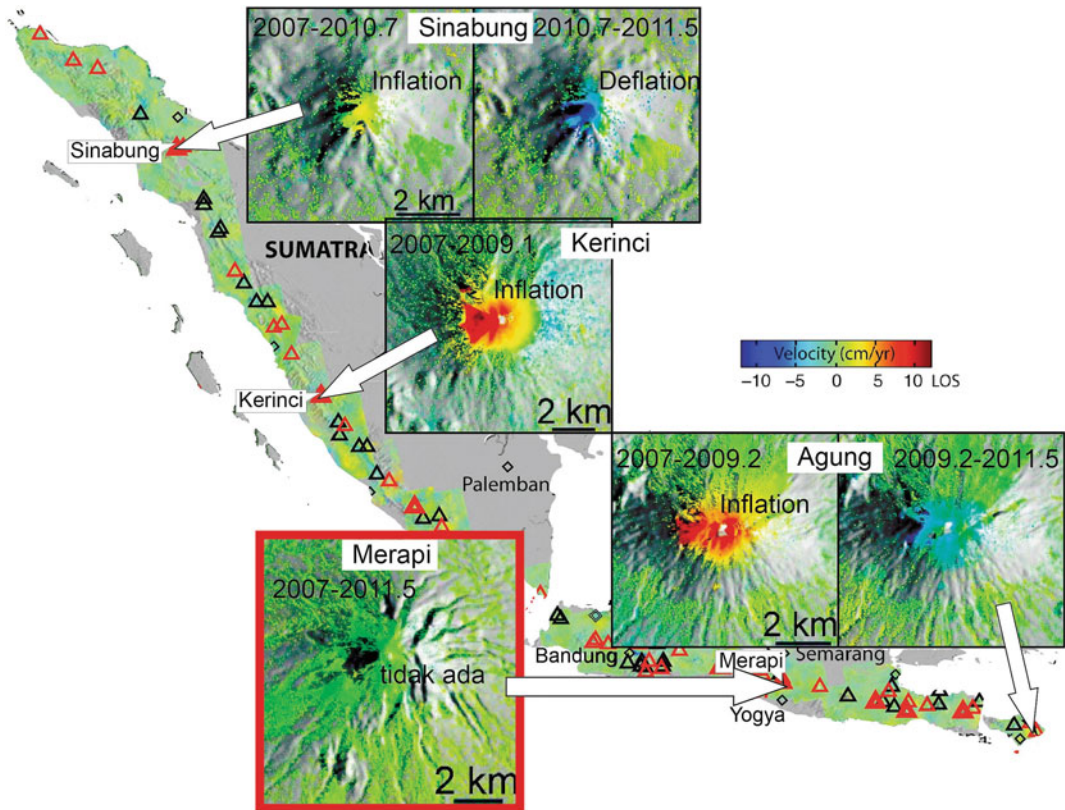


Fig. 14.6 Mean displacement maps compiled for the West Sunda arc, Indonesia, from InSAR time series of ALOS data for the period 2007–2011, provided by Falk Amelung and modified after (Chaussard and Amelung 2012; Chaussard et al. 2013). The insets show deforming volcanic centres with inflation (in red) and deflation

cycles (in blue). At Merapi (red box), no such deformation (in green) and no cycles are identified (Chaussard and Amelung 2012; Chaussard et al. 2013), even though the data covered the “hundred-year event” (Surono et al. 2012)

hazard processes. In- and deflations are possibly associated with the crustal magma plumbing system and/or a cyclic shallow hydrothermal zone or magma reservoir.

Therefore, the InSAR studies at Merapi could not add further constraints on the alleged shallow reservoirs at depths of 2 and 8.5 km (Beauducel and Cornet 1999; Ratdomopurbo and Poupinet 2000). Although the InSAR techniques used are highly valuable, they sometimes remain inconclusive, such as the very proximal deformation signal preceding the 2010 eruption that was identified by ground-truthing methods (electro-optical distant measurement (EDM)) and agreed with conduit pressurisation (Surono et al. 2012), which remained undetected in one study

(Chaussard and Amelung 2012) but was weakly identified in another study (Saepuloh et al. 2013).

Interferograms spanning the later eruption from 18 November 2013 indicate for the first time that deformation occurred on the upper and outer flanks of Merapi (Fig. 14.7), seen by a rather small scale fringe pattern identified at the highest crests of the western crater rim (Fig. 14.7). Therefore, at present, InSAR may stimulate future research in these areas and allow the refinement of dedicated ground-based networks. At time of this writing, the apparent lack of deformation seems to end, as ground truthing reported major deformations on the western flank of Merapi. This flank movement is distinguished by InSAR and pixel offset records, using

different satellites in X and C band from the European, German, Canadian, Spanish, and Italian space agencies, prompted by the International Charter “Space and Major Disasters” (Activation ID:685). These preliminary products show that motion of the upper and western flanks started in mid-2020, which is the first major and large scale displacements recorded by InSAR and highlights that a new episode of flank motion has initiated at Merapi volcano.

The above examples demonstrate that both two-pass InSAR and time series allow the measurement of subtle ground displacements, but validation and correct interpretation remains challenging at Merapi. SAR processing enables the construction of a digital elevation model and the investigation of volume changes associated with material deposition or erosion; in this regard, the comparison of two different digital elevation models is of particular relevance. To derive a digital elevation model (DEM) from radar satellite, two or more SAR images are required that were acquired from slightly different positions. This concept was used onboard the Shuttle Radar Topographic Mission (SRTM) project; during which a SAR signal was sent from the shuttle, and the echoes were received at

the shuttle as well as an attached 60 m-long. For radar satellites, the generation of DEMs is currently realised by either repeat-pass InSAR processing or tandem satellite constellations. While the former technique depends on the stability of the backscattering and travel path conditions during the radar acquisitions (Zebker and Villasenor 1992), the latter method allows the development of DEMs and the assessment of topographic changes due to lava dome activity at Merapi (Kubanek et al. 2015). Using Cosmo Skymed satellite data, the PDC volume of the 2010 eruption was determined (Bignami et al. 2013), and the value obtained was comparable to those from independent observations (Charbonnier et al. 2013; Komorowski et al. 2013). Some of these deposits also showed localised compaction after deposition (Fig. 14.8). By using data acquired by the German TanDEM-X radar satellite mission, DEM monitoring was realised associated with the 2010 Merapi eruption (Fig. 14.9). Given the flight path of two similar satellites in close formation, bistatic images were acquired simultaneously from two “viewpoints”, so that the limitations of repeat-pass surveys were overcome, and the phase formula was simplified to

Ascending track, 08 Nov - 30 Nov 2013

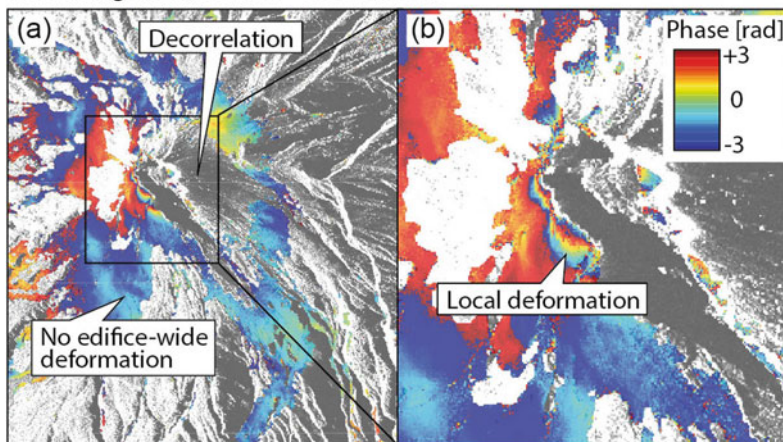


Fig. 14.7 Two-pass interferograms at Merapi often allow identification of proximal fringes that are possibly related to surface deformation. Here, an interferogram spanning 8–20 November 2013 is shown, which includes the 18 November 2013 eruption (Walter et al. 2015). In these

data, the inner crater is incoherent due to the deposition of new materials associated with the 18 November 2013 eruption. The range direction of the SAR system is from the left for the ascending SAR system shown

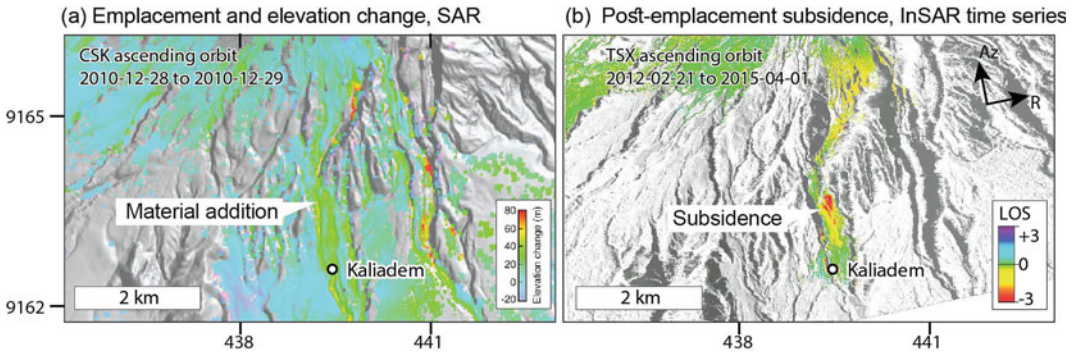


Fig. 14.8 SAR systems allow identification of elevation changes associated with eruption product deposition and determination of postdepositional subsidence. **a** Elevation changes from Cosmo Skymed X-band radar data acquired before and after a 2010 pyroclastic density current to the south of Merapi volcano (after Bignami et al. 2013).

Areas of material addition are identified in ravines near Kaliadem. **b** InSAR time-series analysis derived from SBAS processing of TerraSAR-X data (after Manzo and Walter 2014). Az—Azimuth, R—Range direction of the SAR system

$$\phi_{InSAR} = \phi_{ref} + \phi_{topo} + \phi_{noise} \quad (14.3)$$

Using this approach, the formation of the 200 m-deep summit crater, as well as changes in the lava dome, were analysed, and the results provided topographic details (Kubanek et al. 2015), as shown in Fig. 14.9. The 2010 eruption resulted in a volume loss of $6 \times 10^6 \text{ m}^3$ on 26 October 2010 and then a loss of $10 \times 10^6 \text{ m}^3$ on 4–5 November 2010, providing results that agreed well with independent assessments (Palister et al. 2013).

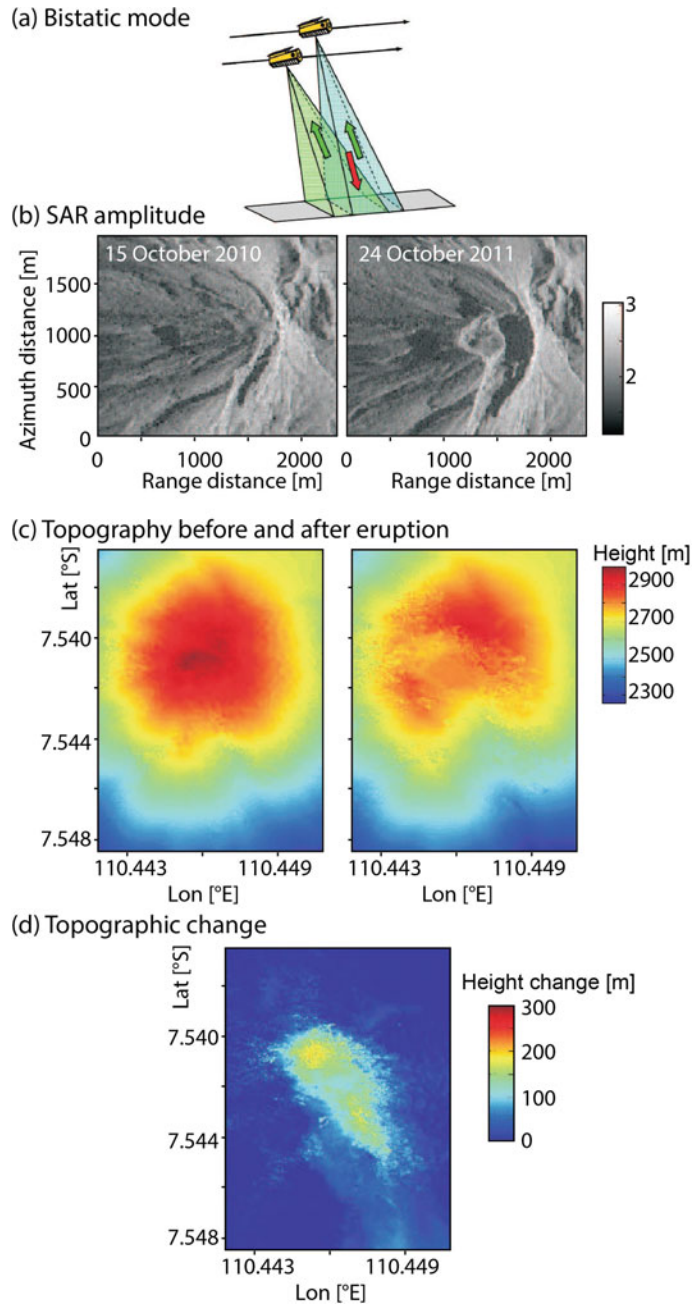
14.3.3 Other Applications of SAR Systems

Merapi volcano has been the site of several other experimental studies exploiting SAR amplitude and interferometry approaches. Shifts in SAR pixels may not necessarily be related to movements of the ground, as a study at Merapi volcano demonstrated (de Michele et al. 2013). Satellite SAR sensors may also be used to monitor degassing and eruption plumes (Schneider and Hoblitt 2013; Bredemeyer et al. 2018). The two-way travel path between the SAR satellite and the ground can be strongly affected by the atmosphere, which can effectively result in image defocusing, pixel misregistration, or both. Studies

at Merapi volcano demonstrated that a Doppler anomaly in the Radarsat-2 data was associated with the 2010 eruption (de Michele et al. 2013). The effect was determined from an elliptically shaped, approximately 3 km-wide pixel shift exceeding 10 m in the azimuth direction that was interpreted as being related to a delay in the echoed signal (de Michele et al. 2013). While radio waves are generally known to be (slightly) affected by atmospheric distortions, the 2010 Merapi case was unprecedented in terms of the clarity and scale of the anomaly and was explained by the presence of a 6–12 km-high ash plume. Additionally, in InSAR products, path effects related to atmospheric refractivity may be determined, which are often attributed to the distribution of water (H_2O) vapour in the atmospheric column. A study from a continuously degassing volcano suggested that the gas plume, which contained abundant water vapour and thus produced variations in the atmospheric water vapour content above and downwind of the volcano, could be monitored by short-wavelength X-band SAR systems (Bredemeyer et al. 2018). From this approach, many new opportunities may be provided to monitor the gas and eruption plumes at Merapi in the future.

Other effects, such as damage related to volcanic eruptions, are accessible by SAR (Plank 2014). Both the 2006 earthquake south of Merapi

Fig. 14.9 Digital elevation monitoring through SAR. **a** Bistatic mode of the TanDEM-X mission. **b** A close view of SAR amplitudes in the summit area of Merapi before and after the 2010 eruption. **c** The digital elevation model before and after the 2010 eruption. **d** Topographic changes due to the eruption show a deep crater that is open to the southeast. Modified after (Kubanek et al. 2015)



(Poland 2010) and the 2010 eruption at Merapi (Yulianto et al. 2013) revealed the capability of SAR and InSAR for exploring damaged areas. A tectonic earthquake of magnitude $M_w = 6.4$, which occurred on 26 May 2006 south of Merapi, damaged or destroyed 400,000 buildings and killed $\sim 6,000$ people, mainly in an area of

volcaniclastic material deposition with high peak ground accelerations (Walter et al. 2008). The same area was found to be subject to subsidence and coherence loss during the earthquake (Poland 2010), leading to speculation about whether the changes observed in SAR were indicative of earthquake site effects. The 2010

eruption also had very large impacts on land use and infrastructure (Yulianto et al. 2013). In total, approximately 12,300 buildings were estimated to have been damaged by this eruption (Yulianto et al. 2013), which was approximately 30 times less than the number of buildings damaged by the 26 May 2006 earthquake (Walter et al. 2008).

14.4 Summary and Outlook

Radar sensing of Merapi volcano has become a widely used method and has contributed to very different domains for understanding the volcano, ranging from change detection to deformation, plume and deposit analysis, and damage assessment:

- InSAR allows identification of pre-eruptive deformation (or lack of deformation) and inferences regarding the deeper plumbing system and the absence of a shallow magma reservoir (Chaussard and Amelung 2012);
- InSAR facilitates the identification of near-summit deformation (Saepuloh et al. 2013);
- SAR change analysis and pixel offsets are used to monitor the extrusion of new dome material (Walter et al. 2013; Saepuloh et al. 2015a, b);
- SAR coherence and polarimetric SAR enable the mapping of pyroclastic deposits on the

flanks of Merapi and their characterisation (Saepuloh et al. 2015a, b; Solikhin et al. 2015a, b);

- SAR allows the mapping of structural and tectonic lineaments (Saepuloh et al. 2015a, b; Walter et al. 2015);
- Bistatic modes and InSAR permit the determination of volume changes and material loss and addition and the mapping of topography associated with eruptive episodes (Bignami et al. 2012; Kubanek et al. 2015);
- SAR doppler anomalies allow the detection and the transport assessment of eruption plumes (de Michele et al. 2013);
- Radar sensing offers a suite of unique methods that constrain the physics and geology of Merapi from depth to the surface and beyond (Fig. 14.10). SAR systems and data from Merapi volcano have been available for more than 20 years, and Merapi is one of the best explored and tested volcanoes worldwide in this regard;
- SAR allows building damage evaluations relevant for risk assessment (Poland 2010; Yulianto et al. 2013).

The focus of satellite-based SAR sensing at Merapi volcano has been long on experimental tests for research and development purposes. Systematic monitoring has been conducted only temporarily, such as during the 2010 eruption

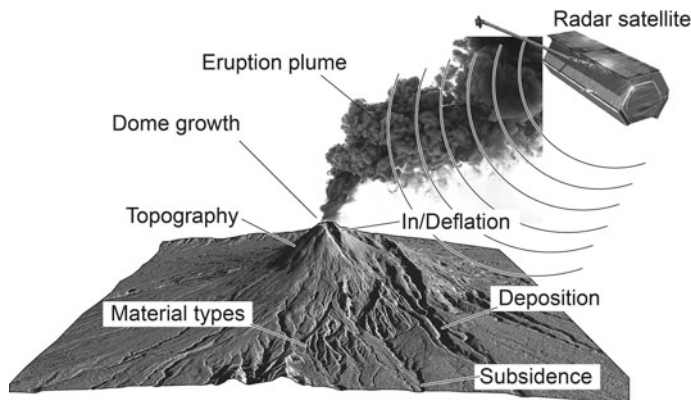


Fig. 14.10 Radar image of Merapi volcano and examples of various SAR and InSAR applications, including topographic measurements, detection of dome growth,

eruption plume, inflation and deflation associated with eruption cycles, depositional area and thickness measurements, and subsidence of deposited materials

crisis (Surono et al. 2012; Pallister et al. 2013), and became now implemented in a systematic monitoring plan (Budi-Santoso et al. 2023, Chap. 13). Space agencies have been shown to support volcanic monitoring efforts by increasing the number of acquisitions, eventually allowing observations of the volcano summit from multiple satellite missions and different viewing geometries (Pallister et al. 2013; Elliot et al. 2016). SAR systems complement existing ground-based monitoring networks deployed for large eruptions and then may be one of the last functioning data streams allowing views into the active crater (Surono et al. 2012); they may even help to identify sudden changes and define evacuation needs (Pallister et al. 2013). Therefore, testing the opportunities from available data streams and planning for possible routine implementation are timely.

As routine implementations have been costly and data access limited until a few years ago, few volcano observatories worldwide have invested in remote sensing analyses; rather, they have relied on freely available services provided by others. Merapi volcano has been a laboratory volcano where novel methods have been tested under “real-life” and dynamic situations. Current developments in new satellite technologies and data science may allow more routine monitoring of the volcano and the entire volcanic arc of Indonesia. Progress in this regard is currently seen on two fronts.

First, the freely available data and processing tools motivate researchers worldwide to investigate SAR data. In particular, with the availability of new-generation satellites (Sentinel-1A/1B) from the ESA and initiatives to share user-friendly processing software (e.g. the Sentinel Application Platform), the broad applicability of SAR systems is within reach of a wide and growing community. As a result, routine processing of interferograms and provision of InSAR time series are becoming feasible, such as those offered by the MOUNTs system (<https://www.mounts-project.com>, Valade et al. 2019) or the Miami InSAR map viewer (<https://insarmaps.miami.edu>). With access to nearly unlimited and free data, SAR data can be

obtained by an expanding community. Future missions are planned and will be implemented shortly; thus, SAR observations at Merapi are expected to provide increased temporal and spatial resolutions and will continue to change the views that scientists and decision-makers have regarding this volcano.

Second, routine and automatic processing, along with modern strategies in data sciences, aids in the processing and even in the interpretation of the data (Anantrasirichai et al. 2019; Valade et al. 2019). This perspective on SAR systems is related to the automatic exploitation of information. This expression may refer not only to automatic processing but also to the detection of amplitude decorrelations, lineaments, reflectivity, ground changes, and deformation. As the data volume steadily increases, data science, the definition of training databases, and the design of artificial intelligence systems are expected to play greatly expanded roles in monitoring Merapi volcano using SAR systems.

Radar remote sensing has been applied for different purposes at Merapi volcano. Merapi is part of the Indonesian archipelago, a volcanic arc with at least 76 historically active volcanoes. Due to the large number of possible geohazards including earthquakes, tsunamis, landslides, and volcanic activity (Cummins and Meilano 2017) and the location of the archipelago at tropical latitudes that often experience hydrometeorological hazards, remote sensing is particularly relevant.

SAR systems nowadays provide essential information for the volcano observatory (BPPTKG) operating also ground-based instruments, conducting field activities at high elevations and perennially cloud-covered summit areas, maintaining instrumentation and connections during all seasons and episodes of volcanic unrest, and promptly communicating hazards and risks. Although Merapi is one of the best instrumented and monitored volcanoes, its steep topography, difficult access, cloud coverage, frequent explosions (many are steam-driven), heavy rainfall, and vandalism of instruments are specific challenges. As was vividly demonstrated during the 2010 eruption, many of the instruments failed during the extended eruptions because of ash

coverage on solar panels and communication devices and other maintenance difficulties in the process of an ongoing eruption. Therefore, satellite remote sensing has become increasingly valuable for eruption responses (Pallister et al. 2013).

In addition to volcanic hazard assessment, radar sensing may be useful for a wide range of fundamental scientific problems. In this work, the success of radar sensing at Merapi volcano is outlined, and the sensor capabilities for the morphological, volcanological, and structural aspects interpreted from radar data are reviewed. The chapter not only describes technical approaches but also provides an overview of the geoscientific applications of these methods, which are potentially applicable at volcanoes worldwide and may contribute to a much greater understanding of volcanism in general.

Acknowledgements This work summarises the benefits of satellite synthetic aperture radar data that are provided by various space agencies, namely, the German Aerospace Centre DLR, the Canadian Space Agency, the European Space Center (ESA), and NASA's Space Radar Laboratory. In particular, the DLR team supported the collection of a large set of high-resolution spotmode TerraSAR-X data acquired at Merapi volcano for further research. Discussions and collaborations with colleagues at the Department of Research and Development on Technology for Geological Disaster (BPPTKG), Gadjah Mada University (UGM), and research centres in France, Germany, and the USA are appreciated.

References

- Adams RJ, Perger WF, Rose WI, Kostinski A (1996) Measurements of the complex dielectric constant of volcanic ash from 4 to 19 GHz. *J Geophys Res: Solid Earth* 101(B4):8175–8185
- Anantrasirichai N, Biggs J, Albino F, Bull D (2019) A deep learning approach to detecting volcano deformation from satellite imagery using synthetic datasets. *Remote Sens Environ* 230:111179
- Arnold DWD, Biggs J, Anderson K, Vargas SV, Wadge G, Ebmeier SK, Naranjo MF, Mothes P (2017) Decaying lava extrusion rate at el reventador volcano, ecuador, measured using high-resolution satellite radar. *J Geophys Res-Sol Earth* 122 (12):9966–9988
- Bamler R (2000) Principles of synthetic aperture radar. *Surv Geophys* 21(2–3):147–157
- Beauducel F, Cornet FH (1999) Collection and three-dimensional modeling of GPS and tilt data at Merapi volcano Java. *J Geophys Res* 104(1):725–736
- Bignami C, Ruch J, Chini M, Neri M (2012) Volcanic product detection after the 2010 Merapi eruption by using Vhr Sar Data. In: 2012 IEEE international geoscience and remote sensing symposium (Igarss), pp 1337–1340
- Bignami C, Ruch J, Chini M, Neri M, Buongiorno MF, Hidayati S, Sayudi DS, Surono (2013) Pyroclastic density current volume estimation after the 2010 Merapi volcano eruption using X-band SAR. *J Volcanol Geotherm Res* 261:236–243
- Boudon G, Balcone-Boissard H, Villemant B, Morgan DJ (2015) What factors control superficial lava dome explosivity? *Sci Rep* 5:14551
- Bredemeyer S, Ulmer FG, Hansteen TH, Walter TR (2018) Radar path delay effects in volcanic gas plumes: the case of Lascar volcano Northern Chile. *Remote Sens* 10(10):1514
- Budi-Santoso A, Beauducel F, Nandaka IGMA, Humaida H, Costa F, Widiwijayanti C, Iguchi M, Métaixian J-P, Rudianto I, Rozin M, Sulistiyani, Nurdin I, Kelfoun K, Byrdina S, Pinel V, Fahmi AA, Laurin A, Rizal MH, Dahamna N (2023) The Merapi volcano monitoring system. In: Gertisser R, Troll VR, Walter TR, Nandaka IGMA, Ratdompurbo A (eds) *Merapi volcano—geology, eruptive activity, and monitoring of a high-risk volcano*. Springer, Berlin, Heidelberg, pp 409–436
- Carn SA (1999) Application of synthetic aperture radar (SAR) imagery to volcano mapping in the humid tropics: a case study in East Java Indonesia. *Bull Volcanol* 61(1–2):92–105
- Charbonnier SJ, Germa A, Connor CB, Gertisser R, Preece K, Komorowski JC, Lavigne F, Dixon T, Connor L (2013) Evaluation of the impact of the 2010 pyroclastic density currents at Merapi volcano from high-resolution satellite imagery, field investigations and numerical simulations. *J Volcanol Geotherm Res* 261:295–315
- Chaussard E, Amelung F (2012) Precursory inflation of shallow magma reservoirs at west Sunda volcanoes detected by InSAR. *Geophys Res Lett* 39:L21311
- Chaussard E, Amelung F, Aoki Y (2013) Characterization of open and closed volcanic systems in Indonesia and Mexico using InSAR time series. *J Geophys Res-Sol Earth* 118(8):3957–3969
- Chua KM, Wan Q, Liew SC, Thouret JC (2015) Persistent scatterer InSAR for monitoring active volcanoes: measuring deformation at Merapi using ALOS PAL-SAR Data. In: 2015 IEEE 5th Asia-Pacific conference on synthetic aperture radar (Apsar), pp 859–861
- Cummins PR, Meilano I (2017) Geohazards in Indonesia: earth science for disaster risk reduction. *Geol Soc Lond Spec Publ* 441, p 221
- Darmawan H, Putra R, Budi-Santoso A, Humaida H, Walter TR (2023) Morphology and instability of the Merapi lava dome monitored by unoccupied aircraft

- systems. In: Gertisser R, Troll VR, Walter TR, Nandaka IGMA, Ratdomopurbo A (eds) *Merapi volcano—geology, eruptive activity, and monitoring of a high-risk volcano*. Springer, Berlin, Heidelberg, pp 457–472
- Darmawan H, Walter TR, Brotopuspito KS, Subandriyo NIGMA (2018a) Morphological and structural changes at the Merapi lava dome monitored in 2012–15 using unmanned aerial vehicles (UAVs). *J Volcanol Geoth Res* 349:256–267
- Darmawan H, Walter TR, Troll VR, Budi-Santoso A (2018b) Structural weakening of the Merapi dome identified by drone photogrammetry after the 2010 eruption. *Nat Hazard Earth Sys* 18(12):3267–3281
- de Michele M, Raucoules D, Wegmuller U, Bignami C (2013) Synthetic aperture radar (SAR) doppler anomaly detected during the 2010 Merapi (Java, Indonesia) Eruption. *IEEE Geosci Remote S* 10(6):1319–1323
- Dzurisin D (2003) A comprehensive approach to monitoring volcano deformation as a window on the eruption cycle. *Rev Geophys* 41(1):1001
- Elliot JR, Walters RJ, Wright TJ (2016) The role of space-based observation in understanding and responding to active tectonics and earthquakes. *Nat Commun* 7:13844
- Fink JH, Anderson SW (2000) *Lava domes and Coulees*. Academic Press, pp 307–319
- Francis P, Rothery D (2000) Remote sensing of active volcanoes. *Annu Rev Earth Planet Sci* 28:81–106
- Gerstenecker C, Laufer G, Steineck D, Tiede C, Wrobel B (2005) Validation of digital elevation models around Merapi Volcano, Java Indonesia. *Nat Hazards Earth Syst Sci* 5(6):863–876
- Gertisser R, Charbonnier S, Keller J, Quidelleur X (2012) The geological evolution of Merapi volcano, Central Java Indonesia. *Bull Volcanol* 74(5):1213–1233
- Hartmann MA (1935) Die Ausbrüche des G. Merapi (Mittel- Java) bis zum Jahre 1883. *N Jahrb Mineral* 75:127–162
- Heap MJ, Troll VR, Kushnir ARL, Gilg HA, Collinson ASD, Deegan FM, Darmawan H, Seraphine N, Neuberger J, Walter TR (2019) Hydrothermal alteration of andesitic lava domes can lead to explosive volcanic behaviour. *Nat Commun* 10:5063
- Hooper A, Zebker H, Segall P, Kampes B (2004) A new method for measuring deformation on volcanoes and other natural terrains using InSAR persistent scatterers. *Geophys Res Lett* 31(23)
- James MR, Carr BB, D'Arcy F, Diefenbach AK, Dietrich HR, Fornaciari A, Lev E, Liu EJ, Pieri DC, Rodgers M, Smets B, Terada A, von Aulock FW, Walter TR, Wood KT, Zorn EU (2020) Volcanological applications of unoccupied aircraft systems (UAS): Developments, strategies, and future challenges *Volcanica* 3(1):67–114
- Kadavi PR, Lee WJ, Lee CW (2017) Analysis of the pyroclastic flow deposits of Mount Sinabung and Merapi using Landsat imagery and the artificial neural networks approach. *Appl Sci* 7(9):935
- Komorowski JC, Jenkins S, Baxter PJ, Picquout A, Lavigne F, Charbonnier S, Gertisser R, Preece K, Cholik N, Budi-Santoso A, Suroso (2013) Paroxysmal dome explosion during the Merapi 2010 eruption: Processes and facies relationships of associated high-energy pyroclastic density currents. *J Volcanol Geotherm Res* 261:260–294
- Kubanek J, Westerhaus M, Schenk A, Aisyah N, Brotopuspito KS, Heck B (2015) Volumetric change quantification of the 2010 Merapi eruption using TanDEM-X InSAR. *Remote Sens Environ* 164:16–25
- Le TT, Atto AM, Trouve E, Solikhin A, Pinel V (2015) Change detection matrix for multitemporal filtering and change analysis of SAR and PolSAR image time series. *ISPRS J Photogramm Remote Sens* 107:64–76
- Lu Z, Dzurisin D (2018) Radar monitoring of volcanic activities. In: Singh R, Bartlett D (eds) *Natural hazards: earthquakes*. Taylor & Francis, Volcanoes and Landslides, pp 421–446
- Lu Z, Freymueller JT (1998) Synthetic aperture radar interferometry coherence analysis over Katmai volcano group Alaska. *J Geophys Res-Sol Earth* 103 (B12):29887–29894
- MacKay ME, Rowland SK, Mougini-Mark PJ, Garbeil H (1998) Thick lava flows of Karisimbi volcano, Rwanda: insights from SIR-C interferometric topography. *Bull Volcanol* 60(4):239–251
- Massonnet D, Briole P, Arnaud A (1995) Deflation of Mount Etna monitored by spaceborne radar interferometry. *Nature* 375:567–570
- Meyer FJ, McAlpin DB, Gong W, Ajadi O, Arko S, Webley PW, Dehn J (2015) Integrating SAR and derived products into operational volcano monitoring and decision support systems. *ISPRS J Photogramm Remote Sens* 100:106–117
- Mougini-Mark PJ (1995) Preliminary observations of volcanoes with the SIR-C radar. *Bull Volcanol* 33:934–941
- Pallister JS, Schneider DJ, Griswold JP, Keeler RH, Burton WC, Noyles C, Newhall CG, Ratdomopurbo A (2013) Merapi 2010 eruption-chronology and extrusion rates monitored with satellite radar and used in eruption forecasting. *J Volcanol Geotherm Res* 261:144–152
- Pamungkas AM, Osawa T, Adnyana A (2014) Monitoring of Merapi volcano deformation using interferometry synthetic aperture radar (InSAR) technique. *J Environ* 1:1–9
- Pepe A, Calò F (2017) A review of interferometric synthetic aperture RADAR (InSAR) multi-track approaches for the retrieval of earth's surface displacements. *Appl Sci* 7(12):1264
- Pinel V, Poland MP, Hooper A (2014) Volcanology: lessons learned from synthetic aperture radar imagery. *J Volcanol Geotherm Res* 289:81–113
- Plank S (2014) Rapid damage assessment by means of multi-temporal SAR—a comprehensive review and outlook to Sentinel-1. *Remote Sens* 6(6):4870–4906

- Poland M (2010) Localized surface disruptions observed by InSAR during strong earthquakes in Java and Hawai'i. *Bull Seism Soc Am* 100(2):532–540
- Ratdomopurbo A, Beauducel F, Subandriyo J, Nandaka IGMA, Newhall CG, Suharna SDS, Suparwaka H, Sunarta, (2013) Overview of the 2006 eruption of Mt Merapi. *J Volcanol Geotherm Res* 261:87–97
- Ratdomopurbo A, Poupinet G (2000) An overview of the seismicity of Merapi volcano (Java, Indonesia), 1983–1994. *J Volcanol Geotherm Res* 100(1–4):193–214
- Rosen PA, Hensley S, Zebker HA, Webb FH, Fielding EJ (1996) Surface deformation and coherence measurements of Kilauea volcano, Hawaii, from SIR-C radar interferometry. *J Geophys Res-Planet* 101 (E10):23109–23125
- Rowland SK, Smith GA, Mouginsmark PJ (1994) Preliminary Ers-1 Observations of Alaskan and Aleutian Volcanoes. *Remote Sens Environ* 48(3):358–369
- Sabins FF (1983) Geologic interpretation of space shuttle radar images of Indonesia. *AAPG Bull* 67:2076–2099
- Saepuloh A, Aisyah N, Urai M (2015a) Detecting surface structures after large eruption of Mt. Merapi in 2010 using ALOS/PALSAR data. *Procedia Earth Plan Sci* 12:84–92
- Saepuloh A, Koike K, Omura M, Iguchi M, Setiawan A (2010) SAR—and gravity change-based characterization of the distribution pattern of pyroclastic flow deposits at Mt. Merapi during the past 10 years. *Bull Volcanol* 72(2):221–232
- Saepuloh A, Urai M, Aisyah N, Sunarta WC, Subandriyo JP (2013) Interpretation of ground surface changes prior to the 2010 large eruption of Merapi volcano using ALOS/PALSAR, ASTER TIR and gas emission data. *J Volcanol Geotherm Res* 261:130–143
- Saepuloh A, Urai M, Widiwijayanti C, Aisyah N (2011) Observing 2006–2010 Ground Deformations of Merapi Volcano (Indonesia) Using Alos/Palsar and Aster Tir Data. *IEEE Int Geosci Remote Sens Symp*:1634–1637
- Saepuloh A, Wikantika K, Urai M (2015b) Observing lava dome roughness on synthetic aperture radar (SAR) data case study at Mt. Sinabung and Merapi—Indonesia. In: 2015b IEEE 5th Asia-Pacific conference on synthetic aperture radar (Apsar), pp 645–648
- Schneider DJ, Hoblitt RP (2013) Doppler weather radar observations of the 2009 eruption of Redoubt volcano, Alaska. *J Volcanol Geotherm Res* 259:133–144
- Siswamidjono S, Suryo I, Yokoyama I (1995) Magma eruption rates of Merapi volcano, Central Java, Indonesia during one century (1890–1992). *Bull Volcanol* 57(2):111–116
- Solikhin A, Pinel V, Vandemeulebrouck J, Thouret JC, Hendrasto M (2015a) Mapping the 2010 Merapi pyroclastic deposits using dual-polarization synthetic aperture radar (SAR) data. *Remote Sens Environ* 158:180–192
- Solikhin A, Thouret JC, Liew SC, Gupta A, Sayudi DS, Oehler JF, Kassouk Z (2015b) High-spatial-resolution imagery helps map deposits of the large (VEI 4) 2010 Merapi volcano eruption and their impact. *Bull Volcanol* 77:20
- Surono JP, Pallister J, Boichu M, Buongiorno MF, Budisantoso A, Costa F, Andreastuti S, Prata F, Schneider D, Clarisse L, Humaida H, Sumarti S, Bignami C, Griswold J, Carn S, Oppenheimer C, Lavigne F (2012) The 2010 explosive eruption of Java's Merapi volcano—a '100-year' event. *J Volcanol Geotherm Res* 241–242:121–135
- Thouret JC, Gupta A, Lube G, Liew SC, Cronin SJ, Surono (2010) The 2006 pyroclastic deposits of Merapi volcano, Java, Indonesia: high-spatial resolution IKONOS images and complementary ground based observations. *Remote Sens Environ* 114 (9):1949–1967
- Thouret JC, Kassouk Z, Gupta A, Liew SC, Solikhin A (2015) Tracing the evolution of 2010 Merapi volcanic deposits (Indonesia) based on object-oriented classification and analysis of multi-temporal, very high resolution images. *Remote Sens Environ* 170:350–371
- Valade S, Ley A, Massimetti F, D'Hondt O, Laiolo M, Coppola D, Loibl D, Hellwich O, Walter TR (2019) Towards global volcano monitoring using multisensor Sentinel missions and artificial intelligence: the MOUNTS monitoring system. *Remote Sens* 11 (13):1528
- Voge M, Hort M, Seyfried R, Ratdomopurbo A (2008) Automatic classification of dome instabilities based on Doppler radar measurements at Merapi volcano, Indonesia: Part II. *Geophys J Intern* 172(3):1207–1218
- Voight B (2000) Structural stability of andesite volcanoes and lava domes. *Phil Trans Roy Soc Lond* 358 (1770):1663–1703
- Wadge G, Cole P, Stinton A, Komorowski JC, Stewart R, Toombs AC, Legendre Y (2011) Rapid topographic change measured by high-resolution satellite radar at Soufriere Hills volcano, Montserrat, 2008–2010. *J Volcanol Geotherm Res* 199(1–2):142–152
- Wadge G, Haynes M (1998) Cover—radar images growth of Soufriere hills volcano Montserrat. *Int J Remote Sens* 19(5):797–800
- Walter TR, Ratdomopurbo A, Subandriyo AN, Brotopuspito KS, Salzer J, Luhr B (2013) Dome growth and coulée spreading controlled by surface morphology, as determined by pixel offsets in photographs of the 2006 Merapi eruption. *J Volcanol Geoth Res* 261:121–129
- Walter TR, Subandriyo J, Kirbani S, Bathke H, Suryanto W, Aisyah N, Darmawan H, Jousset P, Luehr BG, Dahm T (2015) Volcano-tectonic control of Merapi's lava dome splitting: the November 2013 fracture observed from high resolution TerraSAR-X data. *Tectonophysics* 639:23–33
- Walter TR, Wang R, Luehr BG, Wassermann J, Behr Y, Parolai S, Anggraini A, Gunther E, Sobiesiak M, Grosse H, Wetzel HU, Milkereit C, Brotopuspito PJKS, Harjadi P, Zschau J (2008) The 26 May 2006 magnitude 6.4 Yogyakarta earthquake south of Mt. Merapi volcano: Did lahar deposits amplify

- ground shaking and thus lead to the disaster? *Geochem Geophys Geosyst* 9(5):Q05006
- Yulianto F, Sofan P, Khomarudin MR, Haidar M (2013) Extracting the damaging effects of the 2010 eruption of Merapi volcano in Central Java, Indonesia. *Nat Haz* 66(2):229–247
- Zebker HA, Vanzyl JJ (1991) Imaging radar polarimetry: a review. *Proc IEEE* 79(11):1583–1606
- Zebker HA, Villasenor J (1992) Decorrelation in interferometric radar echoes. *IEEE Trans Geosci Remote Sens* 30(5):950–959



Morphology and Instability of the Merapi Lava Dome Monitored by Unoccupied Aircraft Systems

15

Herlan Darmawan, Raditya Putra,
Agus Budi-Santoso, Hanik Humaida,
and Thomas R. Walter

Abstract

Episodic growth and collapse of the lava dome of Merapi volcano is accompanied by significant hazards associated with material redeposition processes. Some of these hazards are preceded by over-steepening of the flanks of the dome, its destabilisation, fracturing and gravitational collapse, producing lethal pyroclastic density currents. With the emergence of unoccupied aircraft systems (UAS), these changes occurring high up at Merapi can now be monitored at unprecedented levels of detail. Here we summarise the use of UAS at Merapi to better understand the evolution of the lava dome following the 2010 eruption. Systematic UAS overflights and photogrammetric surveys were carried out in 2012, 2015, 2017, 2018 and 2019, allowing identification of the

progression of major structures and a three-stage morphological evolution of the dome. We first highlight the significant morphological changes associated with steam-driven explosions that occurred in the period 2012–2014. A large open fissure formed and split the dome into two parts. In the years 2014–2018, hydrothermal activity dominated and progressively altered the dome rock. Lastly, in May–June 2018, a series of steam-driven explosions occurred and was followed by dome extrusion in August 2018, initially refilling the formerly open fissure. This work demonstrates the importance of reactivating pre-existing structures, and summarises the unique contribution realised by high resolution photogrammetric UAS surveys.

Keywords

Merapi · Lava dome · Unoccupied aircraft systems · Photogrammetry · Volcano monitoring

H. Darmawan (✉)
Laboratory of Geophysics, Department of Physics,
Faculty of Mathematics and Natural Sciences,
Universitas Gadjah Mada, Yogyakarta 55281,
Indonesia
e-mail: herlan_darmawan@mail.ugm.ac.id

R. Putra · A. Budi-Santoso · H. Humaida
Center of Volcanology and Geological Hazard
Mitigation, Geological Agency, Ministry of Energy
and Mineral Resources, Jalan Diponegoro 57,
Bandung 40122, Indonesia

T. R. Walter
GFZ German Research Center for Geosciences,
Telegrafenberg, Potsdam, Germany

15.1 Introduction

Lava domes often form above a volcanic conduit and in the summit region of a steep sided volcano due to cooling of viscous silicic magma extrusion (Calder et al. 2015). The extrusion of lava domes is associated with gradual and/or sudden changes of the morphology, may develop rockfalls and an

apron, cause over-steepening of the slope of the dome, and even trigger large-scale gravitational instability that can promote dome collapse. However, the collapse of an active lava dome is hazardous and difficult to monitor, as it can involve the flanks (i.e. a dome flank collapse) or even the inner core and the conduit (i.e. a dome sector collapse) to produce hot avalanches or pyroclastic density currents (PDCs). Due to the hazardous nature of the Merapi lava dome, Unmanned Aircraft System(s) (UAS) have become efficient to support the observation and the monitoring of geomorphological changes, to map structural lineaments and quantify volumetric changes, as well as to identify hydrothermal processes (Darmawan et al. 2018a, b). Therefore, UAS (other designations and common acronyms for UAS are: UAV, RPAS or simply *drones*) have become an essential tool for volcano monitoring in general (James et al. 2020) and for Merapi volcano in particular.

UAS have major advantages to standard airborne photogrammetric surveys and satellite imagery, as they are low cost, extremely high resolution and temporally highly flexible. Therefore, UAS have been used in different domains at volcanoes (James et al. 2020; Jordan 2019), including eruption volume estimations (Favalli et al. 2018), topographic change detection and geomorphic studies (Müller et al. 2017; Darmawan et al. 2020a; Wahyudi et al. 2020), gas and spectroscopic measurements (McGonigle et al. 2008), effusive eruption monitoring and large distance surveys exceeding 100 km range (Nakano et al. 2014), ash cloud imaging (Gomez and Kennedy 2018), and many other purposes such as sampling and carrying of specific instrumentations (Jordan 2019; James et al. 2020). Especially at explosive and dome-building volcanoes, the use of UAS is sharply gaining importance, as vividly demonstrated, during the eruption crisis at Gunung Agung (Syahbana et al. 2019), as well as during various episodes at Merapi (Darmawan et al. 2017; 2018a, b), mapping topographic changes at the flanks of Colima (Walter et al. 2018) or detecting rapid growth and collapse at the domes of Santiaguito (Zorn et al. 2020) and Fuego (Watson et al. 2017).

UAS have been systematically used at Merapi in the past decade by a number of organisations, institutes and scientists, including the National Institute of Aeronautics and Space (LAPAN), the Gadjah Mada University in Yogyakarta (UGM), the Geological Agency of Indonesia, and the Centre for Volcanology and Geological Hazard Mitigation (CVGHM), contributing to the general understanding of this well-studied volcano.

Merapi is a steep-sided dome building volcano that is frequently subjected to dome collapse producing PDCs due to gravitational failure and gas overpressure (Voight et al. 2000) and hosts a complex plumbing system at depth (e.g. Widiyantoro et al. 2018; Troll and Deegan 2023, Chap. 8). UAS were used to map deposits of major explosions on the lower flanks of the volcano and for post-disaster analysis (Rokhmana and Andaru 2016; Malawani et al. 2020), to map and monitor changes of the morphology and structure at the summit of Merapi (e.g. Darmawan et al. 2018a, b), and to assess the degree of hydrothermal activity (Heap et al. 2019). In this chapter, we review repeat measurements performed at the summit of Merapi to better understand the volcanic activity and associated landscape in the decade following the 2010 eruption.

The typical 4–6 year-long eruption cycle and dome building activity at the summit of Merapi (Voight et al. 2000) rapidly changed and ceased after the devastating 2010 eruption (Surono et al. 2012). Short term regrowth of the dome occurred immediately after the eruption, followed by a quiet and cooling-dominated phase for most of the years 2011 and 2012. Then a small steam-driven explosion occurred on 15 July 2012, which initiated a lasting series of explosions on 22 July 2013, 18 November 2013, 10 March 2014, 27 March 2014, and 20 April 2014. Heights of the eruptions were generally below 2000 m above the summit. The 18 November 2013 event was the biggest explosion in this series and formed a NW–SE oriented open fissure that dissected the lava dome into two parts as identified by synthetic aperture radar satellite (Walter et al. 2015). Afterwards, the activity has been dominated by

progressive hydrothermal alteration that weakened the dome structure and several rock falls that occurred in the period between 2014 and 2017 (Darmawan et al. 2018b). These rapid changes in activity were of very small scale, so that UAS provided the only detailed accounts to monitor them.

The value of an UAS is linked to the ability to cover areas that are otherwise beyond the reach of traditional observations. At Merapi, UAS are found useful especially in the steep and difficult-to-access summit crater and the regions between the lava dome and the deep crater. UAS overflights and photogrammetric records allowed us to track the renewed unrest that began in May 2018 after only very short precursory activity (BPPTKG 2018) and continued with steam-driven explosions in June 2018, which was then followed by new lava dome growth in August 2018. The morphology of the new dome gradually expanded due to continuous magma extrusion, steepening its slope that eventually were outflowing and collapsing to produce small volume PDCs (Kelfoun et al. 2021). We summarise the insights drawn from UAS surveys and compare the results with independent observations. We see strong evidence for a control of earlier structures on the Merapi lava dome, identify different stages of activity during the period 2012–2019, and systematically track the evolution of the lava dome, its morphology and instability.

15.2 Methods

15.2.1 Unoccupied Aircraft Systems (UAS)

A number of attempts were made before successful and systematic UAS overflights could be realised, exploring the performance (and failure) of kites, helikites, helium filled balloons, multi-copters and fixed wing UAS; many of these attempts ended in a crash of the device due to wind turbulence or other difficulties. Certainly, the requirements for UAS measurements at the lower flanks of Merapi are different from those

high up at the summit. UAS used at the lower flanks of the volcano, for many applications, can be small scale consumer drones (Jordan 2019). UAS used at the Merapi summit, in turn, are commonly of two types; (i) fixed-wing drones with a long reach that can be launched from large lateral and vertical distance (Rokhmana and Andaru 2016) and (ii) UAS that the pilot has to carry up to the summit, involving a 3–4 h car drive from Yogyakarta and a 3–4 h climb. The UAS used by us for the monitoring of the 2012–2019 dome activity at the summit involved different types, small and large, and with different specifications.

The fixed-wing UAS used in 2012 was a ~3 m-wide Skywalker 1680 V6 styrofoam UAS, which took off ~3 km from the summit, ascended to the programmed altitude and flew along a predefined path. The UAS carried a Canon S100 digital camera recording high quality images. The other and smaller UAS we carried up to the summit crater rim. These were standard consumer quadcopters, which were either DJI Phantom or DJI Mavic models. These included a Phantom 2, carrying a GoPro HERO 3 + camera and a H3-3D gimbal to reduce shaking (used in 2015), a Phantom 3 (used in 2017), a Phantom 4 (used in 2018) and a Mavic platinum quadcopter (used in 2019) for the recent flights.

To achieve high quality UAS records, we had to consider the weather conditions such as cloud, fog, wind, and fumarole activity. Therefore, every flight required very careful planning and spontaneous decision making. Launch sites were either on the upper eastern rim of the summit crater, or on lower elevations on the south flank of Merapi for the fixed-wing UAS (Fig. 15.1). The UAS flew at heights of 100–500 m above the dome, covered the Merapi summit area, and captured geotagged aerial images with intervals of 1–2 images/second on average. Thus, during each flight, hundreds of close-range nadir aerial images could be collected. These images were then analysed either for simple photo documentation or for three-dimensional (3D) point cloud reconstruction as described in the following section.

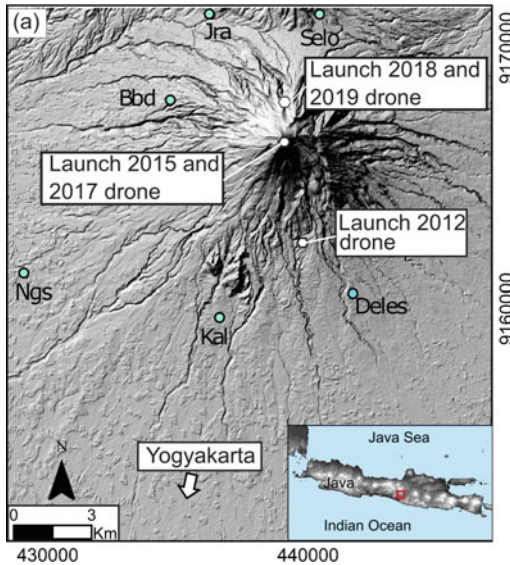


Fig. 15.1 Map of Merapi with drone launch sites

15.2.2 Photogrammetry and Structure From Motion (SfM)

To reconstruct the topography model of the Merapi lava dome, we applied the structure from motion (SfM) algorithm (Szeliski 2010), as implemented in the Agisoft Metashape Professional software. Some blurred and bad visibility images had to be removed before data processing as they can produce noise and outliers during 3D reconstruction. The 3D reconstruction using the SfM algorithm consisted of three main steps. First we applied the ground point detection and key point matching. After all objects were identified and matched, in the second step, we solved the intrinsic and extrinsic camera parameters, reconstructed a 3D scene, projected the identified objects into a 3D coordinate system and produced a 3D sparse point cloud. Then, by calculating the depth map of each camera frame, a 3D dense point cloud was generated in the third step. The generated 3D point clouds of the 2012, 2015, 2017 and 2019 aerial images collected over Merapi were compared to each other (using the Cloud Compare software) and then interpolated to produce high resolution digital elevation

models (DEMs) of the volcano summit. In addition, we also produced high resolution aerial photomosaic images of the Merapi lava dome. The repeat UAS surveys hence provide a sort of a time series of DEMs and orthomosaics (Derrien et al. 2020). These data were used to investigate the morphological and structural evolution of the Merapi lava dome from 2012 to 2019.

The data were represented and further analysed in the open-source geographical information system QGIS, allowing comparison of the DEMs and orthomosaics between the different episodes, before and after explosion, and delineation of the changes in the area. Using the GIS system, we also manually traced lineaments as identified by morphology or photographs. While results of the 2012, 2015 and 2017 flights were in part described in previous studies (Darmawan et al. 2018a; b; Heap et al. 2019), the latest results from 2018 and 2019 are new and reported here for the first time.

15.3 Repeat Surveys of the Summit of Merapi Using Unoccupied Aircraft Systems

We conducted the first successful UAS photogrammetry campaign at the Merapi summit on 26 April 2012, just a few months before the 15 July 2012 explosion. Then, we repeated the UAS flight campaign after the 2012–2014 explosion series, on 6 October 2015 and again on 2 September 2017. The new episode of lava dome growth that started on 18 August 2018 was first imaged by our drone on 23 September 2019.

15.3.1 Drone Flight 2012: Morphology and Structure of the Merapi Lava Dome

High resolution DEMs and aerial photomosaics derived from the 2012 UAS data mapped the morphology and structures of the lava dome and

provided the first and very important base map (Fig. 15.2), which also served as a reference for later surveys. The morphology of the 2012 lava dome was relatively flat-topped in shape and contained a large number of fissures and/or fractures (Fig. 15.2a, c). The dome had an E-W diameter of 154 m, and a N-S diameter of 145 m. The flat-topped surface area of the dome was estimated at 24,300 m², with abundant NW–SE

trending lineaments interpreted as fissures, fractures and other structural heterogeneities (Darmawan et al. 2018a). The lineaments had a mean azimuth of N135°E and an average density of 4 lineaments/m² (Fig. 15.2b). Lineaments at the dome margins were observed at preferred radial direction with respect to the centre of the dome, with a resolved common length ranging between 5 and 50 m.

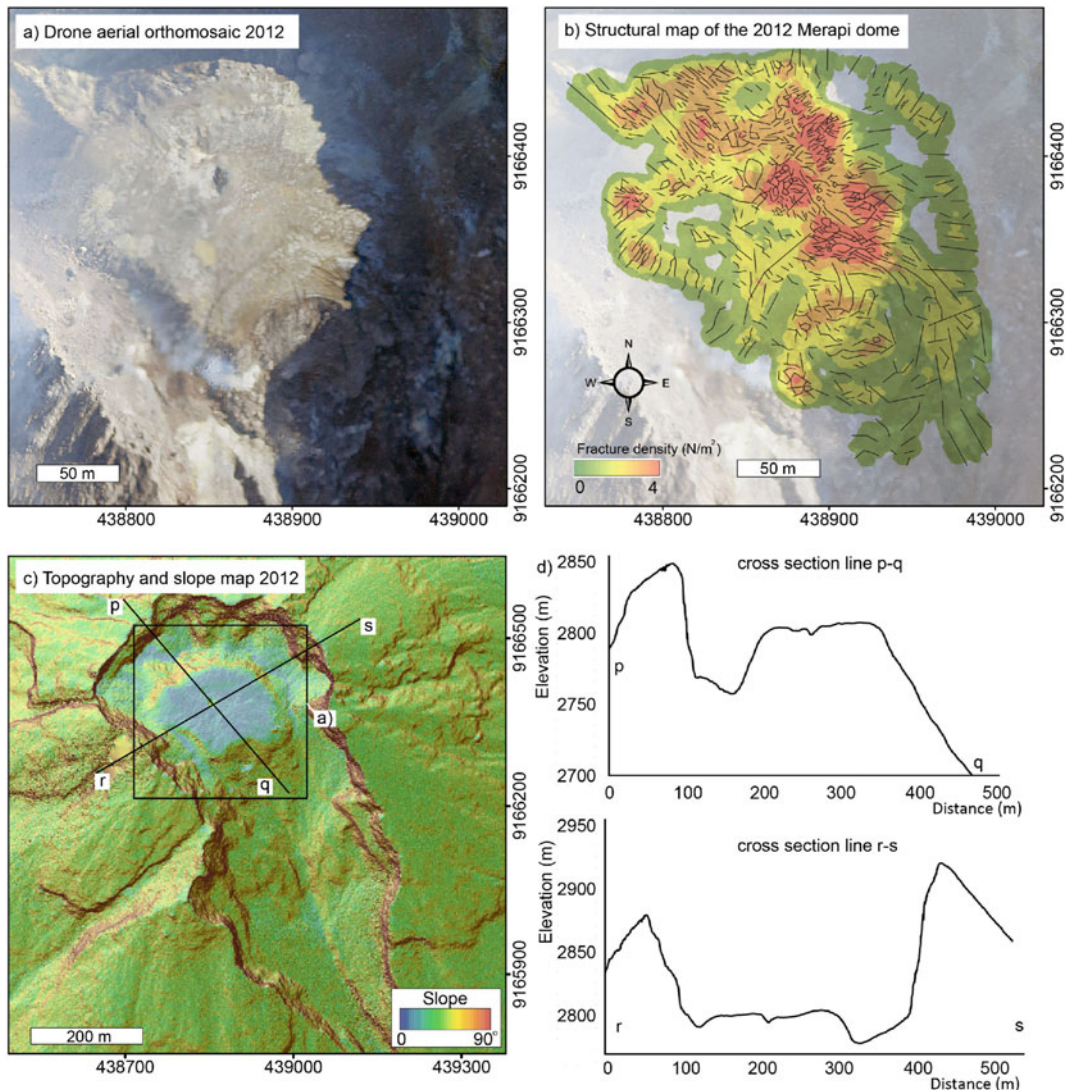


Fig. 15.2 a High-resolution aerial orthomosaic of the Merapi dome in 2012, showing detailed morphology. b Lineament distribution concentrating in the middle of the 2012 dome with NW–SE azimuth and 4 fractures/m².

c and d Slope map and topography profile indicating that the top of the 2012 Merapi dome was relatively flat, with a small depression in the middle, and steep sided with slopes $\sim >40^\circ$

More detailed topographic analysis of the dome revealed not only a flat-topped plateau but also a slightly convexly curved morphology at the top, forming a 50–70 m area that was slightly bowl shaped (Fig. 15.1), possibly associated with intense cooling of the dome since it had formed in 2010. A deep, possibly old vent was expressed with a maximum depth of 6 m and a diameter of 10 m, located approximately at the centre of the dome (Fig. 15.1c, d). The eastern, western and northern margins of the dome were steeply inclined with slopes of 43.8°, 32.2°, 42.9°, respectively, surrounded by blocky talus material forming the dome's apron (Fig. 15.1c, d). The southern part of the lava dome was steeply inclined at 40° or even more, with a blocky appearance, and showed sites of intense degassing (as seen by white steam in the imagery) especially in the western area of the southern flank. As the southern slope was steep and unbuttressed, it represented the sector of the dome most prone to instability and gravitational collapses (Darmawan et al. 2020b, c). A small-scale localised horseshoe shaped structure can be delineated on the southern dome sector.

15.3.2 Drone Flight 2015: Changes Associated with Steam-Driven Explosions

A series of steam-driven explosions that occurred between 2012 and 2014 partially split the carapace of the dome, as observed by satellite radar observations (Walter 2023, Chap. 14). The explosions were monitored by the Merapi Volcano Observatory staff (BPPTKG), describing (a) the first explosion on 15 July 2012, which ejected at the NE part of the dome, (b) a second explosion on 22 July 2013, which removed part of the NE dome again, and (c) the largest explosion on 18 November 2013, which was associated with a new NW–SE trending fissure that split the dome into two parts. This was followed by smaller explosions on 10 March 2014, 27 March 2014, and 20 April 2014. The changes due to these explosions are concentrated around

the fissure area, so that our high resolution UAS data provided more detailed records.

The following UAS dataset was acquired in October 2015 (one year after the 2012–2014 eruptions) and allowed quantification of the morphological changes associated with the explosion series in much greater detail. The NW–SE trending open fissure could be mapped at centimetre-scale resolution from our DEM and aerial orthomosaic (Fig. 15.3). The surface of the lava dome was covered by boulders and angular blocks with diameters of up to ~7 m, and by volcanic tephra accumulating to a thickness of ~3 m as determined by the difference of the two DEMs (Fig. 15.3a). The open fissure did not display signs of an displacement but was fractured with a mean azimuth of N135°E, which is consistent with the azimuth of the lineament as observed in the first UAS survey conducted in 2012 (Fig. 15.3b). The actively degassing area at the southern part of the dome evolved to a crescent-like or horseshoe-shaped structure, open to the south (Figs. 15.1b and 15.3b). The structure, first identified in the 2012 aerial image, has deepened up to 8 m depth and delineated a destabilising block (Darmawan et al. 2018b).

The main NW–SE trending fissure was steeply inclined, often vertical and had a maximum depth of ~33 m, a width of 28 m, and a length of ~95 m (Fig. 15.3c, d). The deepest part of the open fissure was found to be located at the depression already identified in the 2012 UAS data, representing remnants of an older vent (Fig. 15.3 d). This underlines the structural importance of earlier structures (here: a pre-existing vent) and their possible relevance for understanding later stages of dome building activity.

15.3.3 Drone Flight 2017: Changes Associated with Hydrothermal Activity

Following the 2012–2014 explosions, the activity of the Merapi dome was dominated by almost 4 years of degassing activity and virtual absence

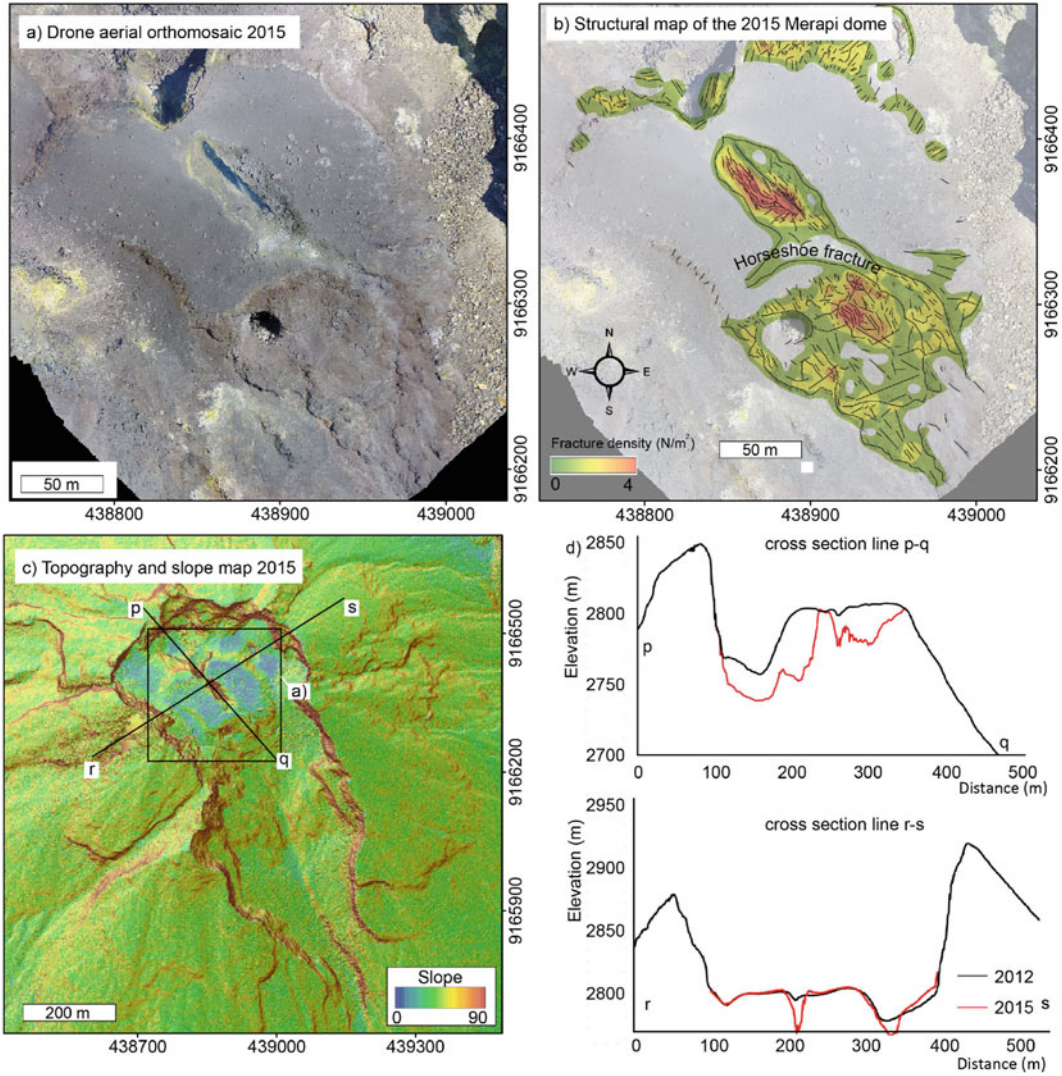


Fig. 15.3 **a** High resolution orthomosaic of the 2015 Merapi dome clearly showing the significant changes of the Merapi dome due to the 2012–2014 steam explosions. **b** Open fissures formed in the middle of the Merapi dome

with abundant NW–SE oriented fractures that were already identified in our 2012 UAS orthomosaic data. **c** and **d** Slope map and topography profiles suggesting that the fissure is near vertical and ~33 m deep

of large explosions (Fig. 15.4), as also confirmed by volcano observatory records. The UAS overflight carried out in 2017 showed intense and ongoing hydrothermal activity, but no major morphological changes except for small scale rock falls. A comparison of the 2017 and the earlier 2015 UAS dataset helped to identify rockfalls at steep cliffs often at a location that was also characterised by strong steaming and yellowish colourisation associated with

hydrothermal activity (Fig. 15.4c), further described in Heap et al. (2019) and in Darmawan et al. (2022). Moreover, five fractures with diameters of 0.3–1.3 m and located at the crescent-like structure were found to have intensified their degree of degassing and yellowish colourisation (Fig. 15.4c), although the plume and hydrothermal colourization can be influenced by the time of the day of the survey and atmospheric condition. Therefore,

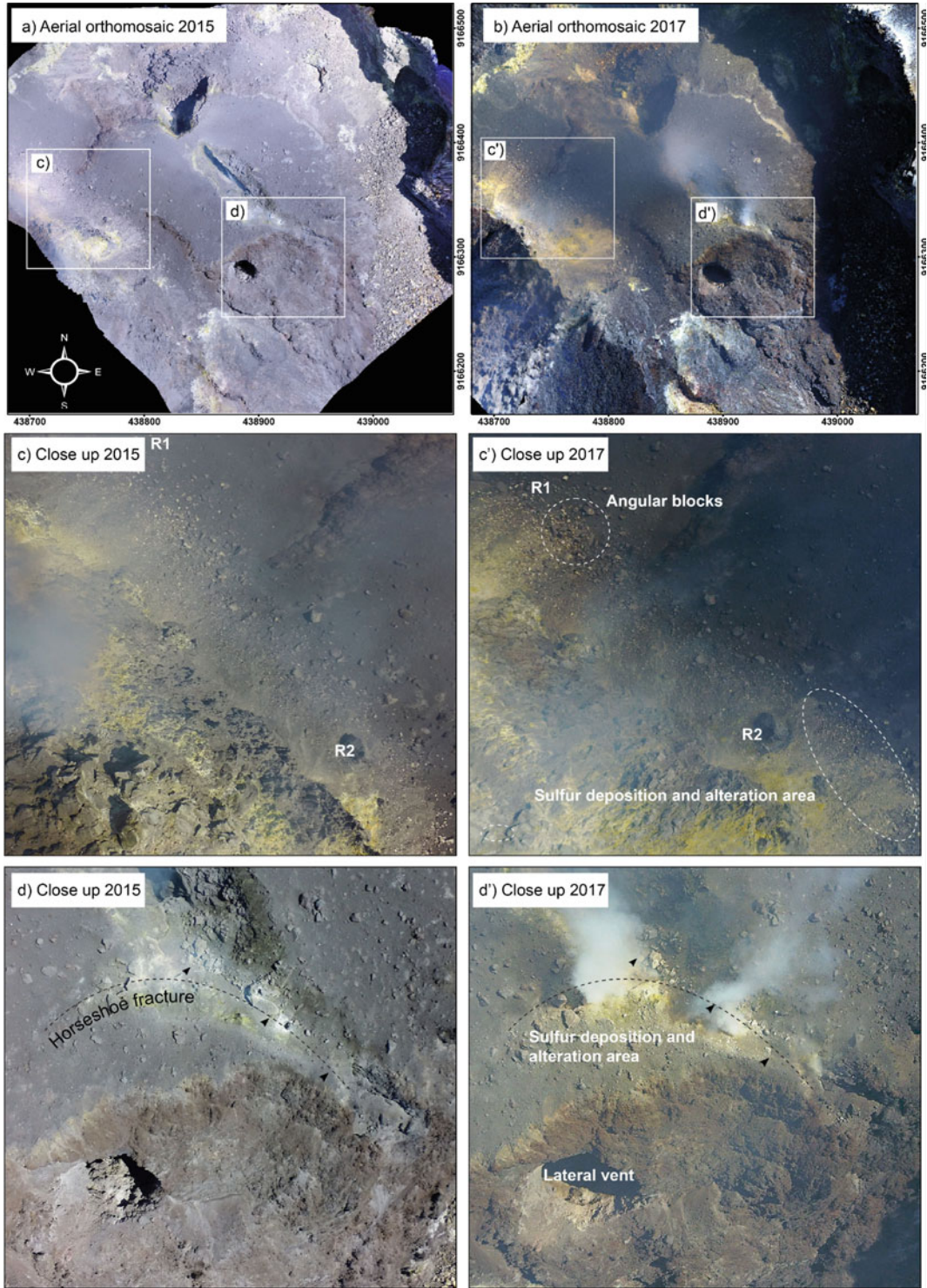


Fig. 15.4 Progressive hydrothermal alteration of the Merapi lava dome between **a** 2015 and **b** 2017. **c** and **c'** Zoomed images at the western cliff area showing evidence of hydrothermal alteration that weakens the rock and

triggers rock falls (red circle). **d** and **d'** Hydrothermal alteration also progressively occurred at the fractures of the southern part of the dome, which is indicated by the yellowish rock colour (black arrow)

hyperspectral analysis may be a better technique to document such activity (Kereszturi et al. 2018). As hydrothermal alteration can weaken the rock strength, we have speculated that the degassing and associated hydrothermal alteration can progressively trigger gravitational dome failure in the future (Darmawan et al. 2018b).

15.3.4 Drone Flight 2019: Changes Associated with a New Dome Growth Episode

After ~ 4 years of quiescence, a new series of steam-driven explosions occurred between May and June 2018. The first explosion occurred in the morning of 11 May 2018, when hikers were enjoying the sunrise at Merapi summit (as reported by BPPTKG), underlining the high-risk potential of the volcano. Fortunately, no victims were reported as the volcanic ejecta were dominated by fine grained tephra. Further explosions followed on 21, 22 and 23 May and on 1 June 2018, with maximum eruption column heights up to ~ 7 km above the summit. As the eruptions were getting more energetic, the alert level was raised to level 2 (Waspada) on a scale from 1 to 4.

The UAS data obtained by BPPTKG in August 2018 allowed us to illustrate the initiation of dome growth that started soon after the steam-driven explosions. The main dome growth started precisely inside the NW–SE trending open fissure that formed more than 4 years before and was most pronounced at a location where the NW–SE trending fissure was widest and where UAS data already showed a vent location as early as 2012 (see also Fig. 15.2). The morphology of the new dome during early emplacement was first elongated along this NW–SE trending fissure, with a length of ~ 55 m, a width of ~ 18 m, and an area cover of ~ 800 m² (Fig. 15.5). Continuous magma extrusion gradually changed the morphology of the lava dome as shown by a cross section determined by further UAS surveys on 12 August 2018 and 9 April 2019 (Fig. 15.6). The outline of the dome changed from being confined inside the fissure to a symmetric shape

with a blocky surface that consisted of some lava dome lobes. Comparison of the 2018 and 2019 UAS data further showed that during the first dome emplacement episode, the elevation of the dome was $\sim 2,860$ m, which then gradually increased to $\sim 2,875$ m and covered the entire surface area of the formerly flat-topped dome mapped in 2012 and 2015.

The final morphology of the new dome emplacement was half spherical (red polygon in Fig. 15.5), almost symmetrical, with blockier surface texture. Closer observations indicate, however, a rather episodic nature of dome emplacement, as it consisted of several individual lava lobes that piled up, possibly shear lobes and some crease structures, each hosting abundant and characteristic lineaments, allowing the different lobes to be distinguished (Fig. 15.5). By April 2019, the dimension of the new dome extrusion was $\sim 170 \times 160$ m, covering an area of 24,700 m² (Fig. 15.5b, d).

Several forms of mass wasting continued to be detectable by UAS data. Small gravitational collapses firstly occurred at the north-eastern part of the dome already in 2018, causing some debris at the northeast side of the crater infilling the depression between the dome and the crater wall (Fig. 15.6). Later collapses occurred predominantly in southerly directions. A major collapse, evident in 2019 UAS data (Fig. 15.5), was characterised by a crescent-like structure located at the steep southern flank part of the Merapi lava dome, which suggests continued dome instability due to gravitational instability at this site (Darmawan et al. 2020b). We note that this is the site of previous instability and crescent-like fracturing identified already in the 2012, 2015 and 2017 data. The instability can even be identified by simple camera monitoring networks operated on the southern flank that show the occurrence of rock falls (Fig. 15.7). As the rocks are falling and colliding, they break into smaller pieces within seconds that increase their velocity up to ~ 90 m/s (Darmawan et al. 2020c), further fragmenting to produce small (granular or pyroclastic) flows. Such short-term changes are beyond the ‘eyes’ of our campaign UAS surveys.

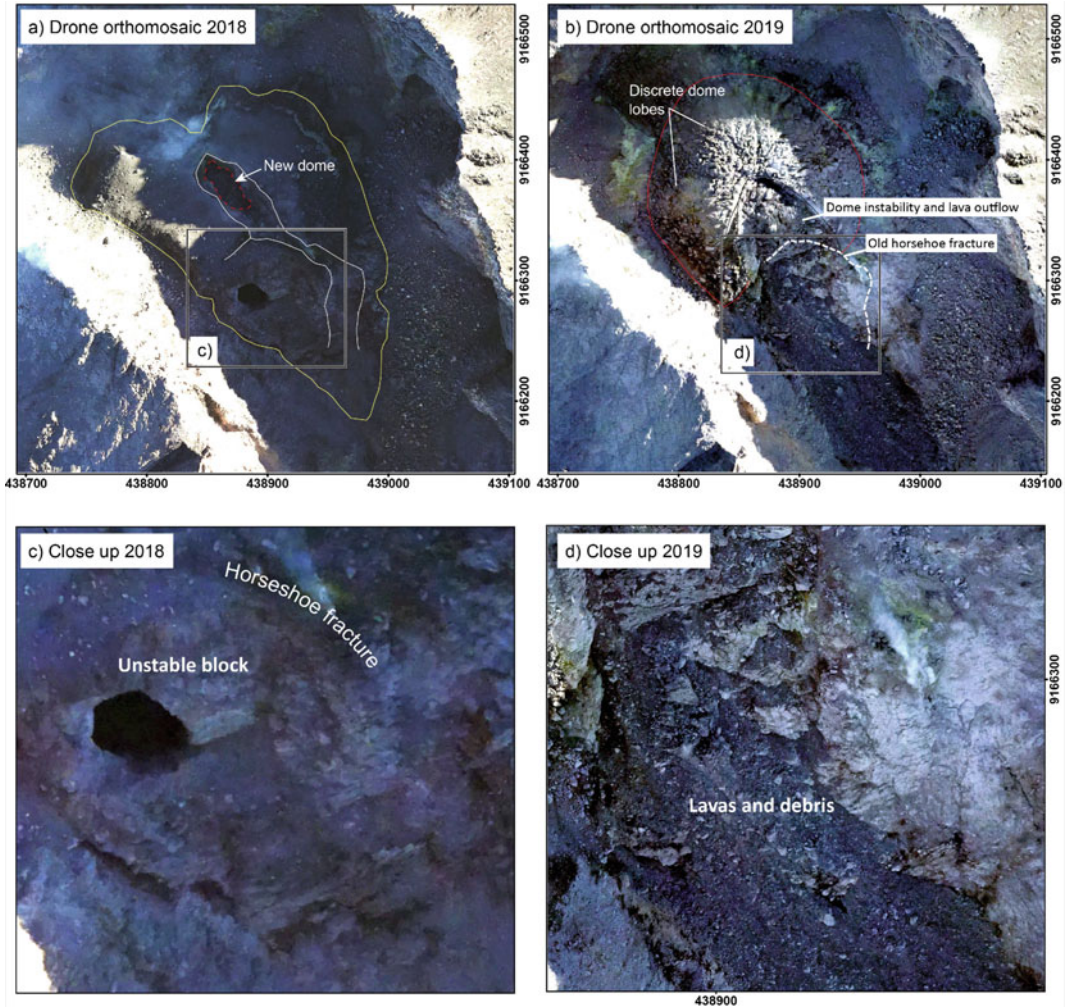


Fig. 15.5 **a** Morphology of the new lava dome, identified by our UAS camera on 12 August 2018, showing that the dome has an elongated shape and grew at the fissure area. **b** One year later, the dome has a half spherical, relatively symmetrical shape, and our UAS camera

observed a collapse area at the southeastern part of the dome, which is delineated by a horseshoe-shaped structure. **c** and **d** Close-up view of the southern part of the dome showing an unstable block in 2018 that collapsed in 2019, possibly caused by hydrothermal alteration

15.4 Monitoring Lava Dome Building Activity and Morphological Changes in the Summit Area of Merapi Using Repeat Unoccupied Aircraft Systems Surveys

UAS based photogrammetric data allow observation at high resolution, showing details of morphological and structural features of the lava

dome of Merapi volcano. Here we reviewed findings from repeat UAS surveys conducted by us in the summit region of the volcano and compared these to independent observations made by the volcano observatory (BPPTKG).

We find evidence for a structural memory, whereby older dome structures further evolve, affect or even control the later development of the lava dome (Darmawan et al. 2022). This structural influence involves (i) a small explosion vent that is also the location of the later NW–SE

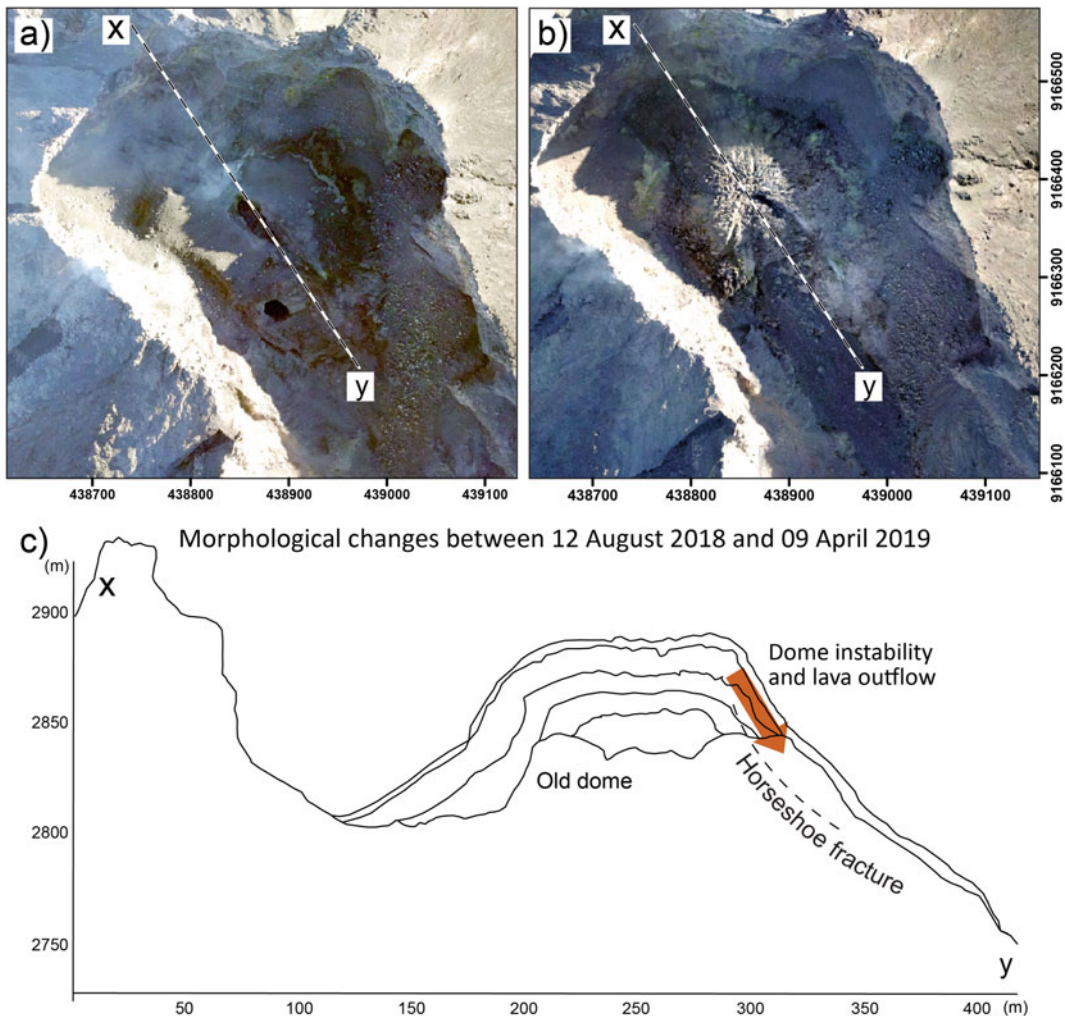


Fig. 15.6 Aerial images of Merapi summit that were acquired between **a** August 2018 and **b** April 2019, illustrating the evolution of the Merapi lava dome growth due to continuous magma extrusion. **c** Cross sections of line x - y during dome emplacement record the

morphological changes in a NW (left) to SE (right) direction. The initial dome filled the fissure area in August 2018, gradually expanded symmetrically, and finally filled in the crater of Merapi

trending fissure, (ii) the widest section of the NW–SE trending fissure that is also the site of the new dome growth initiation, (iii) a crescent-like fracture that is also the location of a later dome collapse and lava extrusion, and (iv) fumarole activity at steep flanks that are also the sites of later rock falls. We therefore conjecture that reactivation of pre-existing structures play an important role for the evolution of the lava dome, which is also consistent with observations made elsewhere (Watts et al. 2002; Ashwell et al. 2018).

The morphology of the Merapi dome has changed significantly due to several geological processes between 2012 and 2019. Prior to the 2012–2014 steam-driven explosions, the dome morphology was controlled by dome emplacement, cooling and volumetric expansion causing radial fractures at the dome margin and a flat-topped plateau dissected by NW–SE oriented lineaments. Between 2012 and 2014, the dome morphology changed due to six steam-driven explosions that commonly occur during the rainy

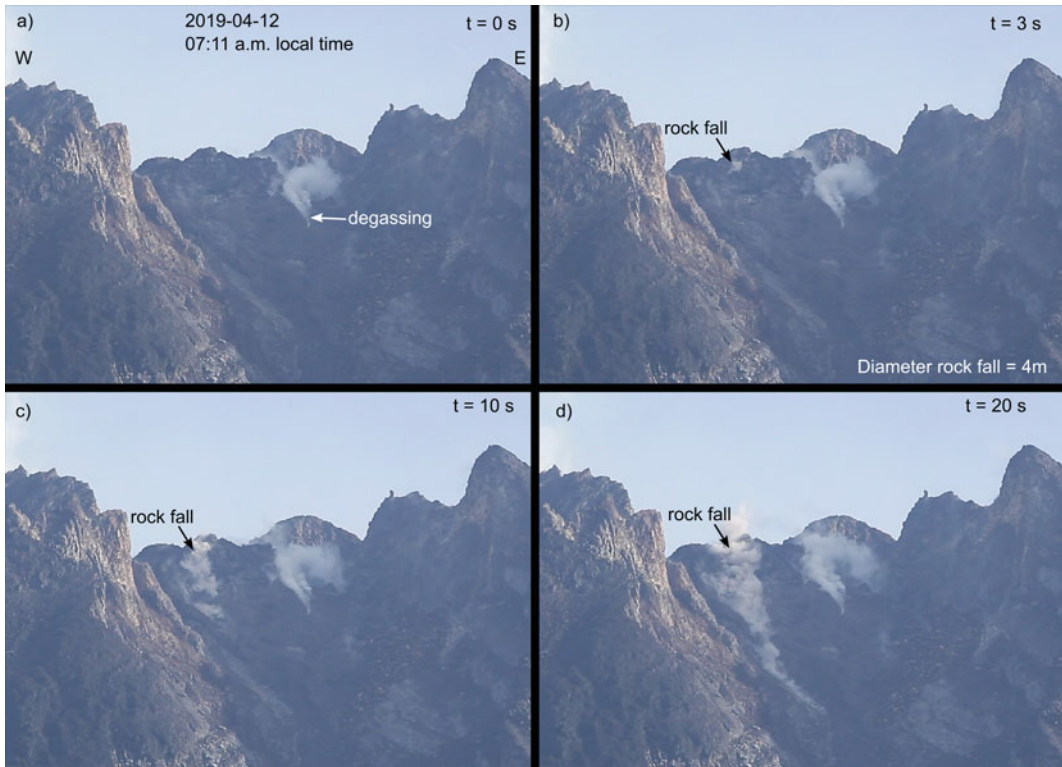


Fig. 15.7 Mechanism of a discrete rockfall of the lava lobe at the Merapi lava dome recorded by our high-resolution camera on 12 April 2019. **a** and **b** In the first 3 s, the rock was subjected to gravitational free fall. **c** Within 10 s, it then collided and broke into several rock

fragments. **d** The velocity of the rockfall was terminated over a sandy area (~ 200 m from the summit) in the next 10 s. Rockfalls occurred frequently as magma continuously extruded in the southeastern part of the dome

season. The explosions opened a large NW–SE oriented and open fissure that dissected the dome into two parts. As the UAS data reveal the presence of larger blocks closer to the fissure, and as no major displacement was found in association with its formation (Walter et al. 2015), it can be speculated that it is rather an elongated eruption fissure than a structure associated with strong deformation. The location of the NW–SE trending open fissure is confined to the sites of NW–SE oriented fractures identified in the 2012 UAS dataset, suggesting a structural control of the pre-existing fractures.

Steam-driven explosions might be caused by interaction between rainwater and the hot dome interior. UAS data at Merapi provided the necessary DEM resolution to study how rainwater may accumulate and possibly percolate through

the identified fractures, where it interacts with the hot dome interior, causing shallow hydrothermal gas overpressure and steam-driven explosions (Darmawan et al. 2018a). The NW–SE trending fissure at the Merapi dome is possibly related to a regional tectonic trend seen in the volcanic chain of Merapi—Merbabu—Telomoyo—Ungaran (Walter et al. 2015; Bronto et al. 2023, Chap. 7; Harijoko et al. 2023, Chap. 4). The NW–SE oriented lineaments mapped from our 2012 UAS data were identified previously (Beauducel et al. 2000), suggesting that this trend at Merapi is relevant in the long-term. Strong contrasts in seismic velocities also suggest a significant role of vertical heterogeneities at depth (Widiyantoro et al. 2018; Luehr et al. 2023, Chap. 5).

The activity of the Merapi dome was relatively calm and dominated by hydrothermal

activity in the period between 2015 and 2017. The UAS data added constraints to the study of the interaction between hydrothermal fluids and dome rocks that may strongly alter intact rocks, changing their porosity and permeability (Heap et al. 2019) by replacing the host rock minerals with secondary minerals and progressively reducing the strength of the dome rock (Pola et al. 2012; Wyering et al. 2014; Mayer et al. 2016). The location of hydrothermal activity was highly expressed at the structures of the Merapi dome, such as at the open NW–SE trending fissure and at the crescent-like structure described above. We hypothesised before that structural weakening at the crescent-like structure can trigger partial collapse at the southern dome sector without any significant seismic precursor in the future. Factor of safety analysis based on UAS data acquired at the southern dome sector suggests that intense rainfall at Merapi summit can further trigger this effect (Darmawan et al. 2018b). Indeed, this site was then also the location of collapses of the new dome that occurred in 2018–2019, as shown by 2019 UAS data (Fig. 15.5) and terrestrial photogrammetry datasets (Darmawan et al. 2020b, c).

The summary of the findings in this chapter are based entirely on drone-based photogrammetry, digital elevation modelling and analysis of the changes that occurred between UAS surveys. We note that, as UAS become more efficient, they may be able to carry instruments for measuring temperature (Zorn et al. 2020), gases become detectable and quantifiable (Liu et al. 2019), magnetic instruments may be deployed and picked up (Ohminato et al. 2011) and many further possibilities will arise (Jordan 2019; James et al. 2020). In addition, the use of more efficient image analysing methods such as classifiers, principal component analysis (Müller et al. 2021) and data science will further improve our ability to interpret data and understand volcanoes (Kereszturi et al. 2018).

In this regard, the use of UAS may allow much improved monitoring of hazards associated with dome building activity. Additionally, during periods of quiescence, the effects of hydrothermal

activity may be assessed using drone data. Hydrothermal activity and alteration will not only weaken the dome rock as the altered minerals accumulate and (Heap et al. 2019). This is potentially detectable in UAS imagery, as suggested by Kereszturi et al. (2018). The effects of hydrothermal alteration are important for hazard assessment, as they are associated with a possible reduction of rock strength, porosity and permeability, which can trigger superficial gas overpressure and may lead to a phreatic eruption (Stix and de Moor 2018). The full meaning of these alteration effects and possible interactions are still not fully understood at Merapi and elsewhere. However, we speculate that these may contribute to the explanation of the series of steam-driven explosions that suddenly occurred at Merapi between 11 May and 1 June 2018, possibly displaying a systematic change that occurs prior to renewed magmatic activity phases.

The UAS data presented have revealed details of a new dome growth episode, initiating at the open fissure in August 2018. The morphology of the new lava dome was first elongated, and strongly confined to and controlled by the open fissure. Of interest is that with continued extrusion of magma, this pre-defined direction waned. The dome grew endogenously in a relatively symmetric horizontal direction with an extrusion rate of 2200 m³/day and a low intensity of degassing as recorded by time lapse camera of the observatory (see published BPPTKG YouTube channel video; <https://www.youtube.com/c/BPPTKGCHANNEL>). The episode of dome growth reached its maximum volume of ~0.5 10⁶ m³ (BPPTKG 2019) and was in more depth investigated by Kelfoun et al. (2021), suggesting that total eruption volume may be much higher. The volume seen was affected by frequent gravitational collapses to the south, so that the erupted volume was estimated between 0.85 and 1.25 × 10⁶ m³, twice as large as the volume of the lava dome (Kelfoun et al. 2021). Exogenous extrusion may also occur during endogenous dome expansion, as indicated by our 2019 drone aerial images that recorded a blocky surface consisting of discrete lava lobes (Fig. 15.5b).

The endogenous-exogenous dome extrusion is quite common at dome-building volcanoes worldwide, such as Unzen volcano, Japan (Nakada et al. 1995; Kaneko et al. 2002), Soufrière Hills Volcano, Montserrat (Hale 2008), and the Santiaguito lava dome, Guatemala (Rhodes et al. 2018). We infer that endogenous—exogenous mechanisms were possible due to changes in magma rheology during dome growth. Exogenous domes will cool faster and become more viscous, whereas endogenous domes may stay insulated and retain a lower viscosity to outgas more efficiently and deflate (Kennedy et al. 2016).

As the dome continuously grows due to magma extrusion, it develops fractures, discrete dome lobes and oversteepening on its sides. Therefore, this mechanism of instability is characteristic for Merapi-type gravitational dome collapses (Voight et al. 2000), where the new UAS data suggest a strong control of pre-existing structures. In other words, by UAS surveys of the dome morphology and structural analysis, the processes and styles of later dome-building activity can be better understood.

15.5 Summary and Outlook

The morphology of the Merapi lava dome has significantly changed from 2012 to 2019. During this period, the dome underwent several profound morphological and structural changes, including (i) formation of a deep NW–SE trending fissure during the 2012–2014 steam-driven explosions, (ii) a period of hydrothermal activity and alteration, and (iii) renewed activity, initiated by explosions in 2018 followed by dome extrusion located inside the NW–SE trending fissure. Processes and hazards related to these morphological and structural changes and how they evolve can be well investigated by using UAS. The UAS data reveal that structures develop and evolve, possibly controlling later activity, sites of eruptions, flank instability and associated hazards. Moreover, with developing methods of the aircrafts, including the possibility to carry new sensors, and improved image

analysis and data science, it can be expected that the geomorphological and structural analysis of Merapi volcano and our understanding of associated hazards will significantly improve in the future.

Acknowledgements We appreciate support and suggestions by our colleagues in the office and in the field. We especially thank Professor Kirbani Sri Brotopuspito (†2019) for his vision and support of unconventional methods early during their development. We will miss him.

References

- Ashwell PA, Kennedy BM, Edwards M, Cole JW (2018) Characteristics and consequences of lava dome collapse at Ruawahia, Taupo Volcanic Zone, New Zealand. *Bull Volcanol* 80:43
- Beauducel F, Cornet FH, Suhanto E, Duquesnoy T, Kasser M (2000) Constraints on magma flux from displacements data at Merapi volcano, Java Indonesia. *J Geophys Res Solid Earth* 105(B4):8193–8203
- BPPTKG (2018) Diskusi Scientific forum: Kajian Erupsi Freatik G. Merapi 11 Mei 2018. In: BPPTKG website, Yogyakarta
- BPPTKG (2019) Laporan Aktivitas Gunung Merapi Tanggal 25–31 Januari 2019. In: BPPTKG website, Yogyakarta
- Bronto S, Rahardjo W, Asmoro P, Ratdomopurbo A, Adityarani M, Permatasari A (2023) The Godean debris avalanche deposit from a sector collapse of Merapi volcano. In: Gertisser R, Troll VR, Walter TR, Nandaka IGMA, Ratdomopurbo A (eds) *Merapi volcano—geology, eruptive activity, and monitoring of a high-risk volcano*. Springer, Berlin, Heidelberg, pp 195–231
- Calder ES, Lavallée Y, Kendrick JE, Bernstein M (2015) Lava dome eruptions. In: Sigurdsson H (ed) *The encyclopedia of volcanoes*, 2nd edn, chap 18. Academic Press, Amsterdam, p 343–362
- Darmawan H, Walter TR, Richter N, Nikkoo M (2017) High resolution digital elevation model of Merapi summit in 2015 generated by UAVs and TLS. V. 2015. GFZ Data Services. <https://doi.org/10.5880/GFZ.2.1.2017.003>
- Darmawan H, Walter TR, Brotopuspito KS, Subandriyo NIGMA (2018a) Morphological and structural changes at the Merapi lava dome monitored in 2012–2015 using unmanned aerial vehicles (UAVs). *J Volcanol Geotherm Res* 349:256–267
- Darmawan H, Walter TR, Troll VR, Budi-Santoso A (2018b) Structural weakening of the Merapi dome identified by drone photogrammetry after the 2010 eruption. *Nat Hazards Earth Syst Sci* 18:3267–3281
- Darmawan H, Mutaqin BM, Wahyudi HA, Wibowo HE, Haerani N, Suryayadi M, Syarifudin S,

- Asriningrum W (2020a) Topography and structural changes of Anak Krakatau due to the December 2018 catastrophic events. *Indones J Geogr* 52:402–410
- Darmawan H, Yuliantoro P, Suryanto W, Rakhman A, Budi Santoso A (2020b) Deformation and instability at Merapi dome identified by high resolution camera. *IOP Conf Ser Earth Environ Sci* 500:012008
- Darmawan H, Yuliantoro P, Rakhman A, Budi Santoso A, Humaida H, Suryanto W (2020c) Dynamic velocity and seismic characteristics of gravitational rockfalls at the Merapi lava dome. *J Volcanol Geotherm Res* 404:107010
- Darmawan H, Troll VR, Walter TR, Deegan FM, Geiger H, Heap MJ, Seraphine N, Harris C, Humaida H, Müller D (2022) Hidden mechanical weaknesses within lava domes provided by buried high-porosity hydrothermal alteration zones. *Sci Rep* 12(1):3202. <https://doi.org/10.1038/s41598-022-06765-9>
- Derrien A, Peltier A, Villeneuve N, Staudacher T (2020) The 2007 caldera collapse at Piton de la Fournaise: new insights from multi-temporal structure-from-motion. *Volcanica* 3:55–65
- Favalli M, Fornaciari A, Nannipieri L, Harris A, Calvari S, Lormand C (2018) UAV-based remote sensing surveys of lava flow fields: a case study from Etna's 1974 channel-fed lava flows. *Bull Volcanol* 80:29
- Gomez C, Kennedy B (2018) Capturing volcanic plumes in 3D with UAV-based photogrammetry at Yasur Volcano—Vanuatu. *J Volcanol Geotherm Res* 350:84–88
- Hale AJ (2008) Lava dome growth and evolution with an independently deformable talus. *Geophys J Int* 174:391–417
- Harijoko A, Marliyani GI, Wibowo HE, Freski YR, Handini E (2023) The geodynamic setting and geological context of Merapi volcano in Central Java, Indonesia. In: Gertisser R, Troll VR, Walter TR, Nandaka IGMA, Ratdomopurbo A (eds) *Merapi volcano—geology, eruptive activity, and monitoring of a high-risk volcano*. Springer, Berlin, Heidelberg, pp 89–109
- Heap MJ, Troll VR, Kushnir ARL, Gilg HA, Collinson ASD, Deegan FM, Darmawan H, Seraphine N, Neuberg J, Walter TR (2019) Hydrothermal alteration of andesitic lava domes can lead to explosive volcanic behaviour. *Nat Commun* 10:5063
- James M, Carr B, D'Arcy F, Diefenbach A, Dietterich H, Fornaciari A, Lev E, Liu E, Pieri D, Rodgers M, Smets B, Terada A, von Aulock F, Walter T, Wood K, Zorn E (2020) Volcanological applications of unoccupied aircraft systems (UAS): developments, strategies, and future challenges. *Volcanica* 3:67–114
- Jordan BR (2019) Collecting field data in volcanic landscapes using small UAS (sUAS)/drones. *J Volcanol Geotherm Res* 385:231–241
- Kaneko T, Wooster MJ, Nakada S (2002) Exogenous and endogenous growth of the Unzen lava dome examined by satellite infrared image analysis. *J Volcanol Geotherm Res* 116:151–160
- Kelfoun K, Budi-Santoso A, Latchimy T, Bontemps M, Nurdien I, Beauceul F, Fahmi A, Putra R, Dahamna N, Laurin A, Rizal MH, Sukmana JT, Gueugneau V (2021) Growth and collapse of the 2018–2019 lava dome of Merapi volcano. *Bull Volcanol* 83:8
- Kennedy BM, Wadsworth FB, Vasseur J, Ian Schipper C, Mark Jellinek A, von Aulock FW, Hess K-U, Kelly Russell J, Lavallée Y, Nichols ARL, Dingwell DB (2016) Surface tension driven processes densify and retain permeability in magma and lava. *Earth Planet Sci Lett* 433:116–124
- Kereszturi G, Schaefer LN, Schleiffarth WK, Procter J, Pullanagari RR, Mead S, Kennedy B (2018) Integrating airborne hyperspectral imagery and LiDAR for volcano mapping and monitoring through image classification. *Int J Appl Earth Obs Geoinf* 73:323–339
- Liu EJ, Wood K, Mason E, Edmonds M, Aiuppa A, Giudice G, Bitetto M, Francofonte V, Burrow S, Richardson T, Watson M, Pering TD, Wilkes TC, McGonigle AJS, Velasquez G, Melgarejo C, Bucarey C (2019) Dynamics of outgassing and plume transport revealed by proximal unmanned aerial system (UAS) measurements at Volcán Villarrica, Chile. *Geochem Geophys Geosyst* 20:730–750
- Luehr BG, Koulakov I, Suryanto W (2023) Crustal structure and ascent of fluids and melts beneath Merapi: insights from geophysical investigations. In: Gertisser R, Troll VR, Walter TR, Nandaka IGMA, Ratdomopurbo A (eds) *Merapi volcano—geology, eruptive activity, and monitoring of a high-risk volcano*. Springer, Berlin, Heidelberg, pp 111–135
- Malawani MN, Handayani T, Bariq JM, Lukafiardi R (2020) Morphological changes due to anthropogenic interferences in Gendol River Valley, Merapi Volcano. *Forum Geogr* 33:209–218
- Mayer K, Scheu B, Montanaro C, Yilmaz TI, Isaia R, Aßbichler D, Dingwell DB (2016) Hydrothermal alteration of surficial rocks at Solfatara (Campi Flegrei): petrophysical properties and implications for phreatic eruption processes. *J Volcanol Geotherm Res* 320:128–143
- McGonigle AJS, Aiuppa A, Giudice G, Tamburello G, Hodson AJ, Gurrieri S (2008) Unmanned aerial vehicle measurements of volcanic carbon dioxide fluxes. *Geophys Res Lett* 35:L06303
- Müller D, Walter TR, Schöpa A, Witt T, Steinke B, Gudmundsson MT, Dürig T (2017) High-resolution digital elevation modeling from TLS and UAV campaign reveals structural complexity at the 2014/2015 Holuhraun Eruption Site, Iceland. *Front Earth Sci* 5:59
- Müller D, Bredemeyer S, Zorn E, De Paolo E, Walter TR (2021) Surveying fumarole sites and hydrothermal alteration by unoccupied aircraft systems (UAS) at the La Fossa cone, Vulcano Island (Italy). *J Volcanol Geotherm Res* 413:107208
- Nakada S, Miyake Y, Sato H, Oshima O, Fujinawa A (1995) Endogenous growth of dacite dome at Unzen volcano (Japan), 1993–1994. *Geology* 23:157–160
- Nakano T, Kamiya I, Tobita M, Iwahashi J, Nakajima H (2014) Landform monitoring in active volcano by

- UAV and SFM-MVS technique. *Int Arch Photogramm Remote Sens* 40:71–75
- Ohminato T, Kaneko T, Koyama T, Watanabe A, Takeo M, Iguchi M (2011) Upward migration of the explosion sources at Sakurajima volcano, Japan, revealed by a seismic network in the close vicinity of the summit crater. AGU Fall Meeting 2011, Abstract ID V41H-07
- Pola A, Crosta G, Fusi N, Barberini V, Norini G (2012) Influence of alteration on physical properties of volcanic rocks. *Tectonophysics* 566–567:67–86
- Rhodes E, Kennedy BM, Lavallée Y, Hornby A, Edwards M, Chigna G (2018) Textural insights into the evolving lava dome cycles at Santiaguito lava dome Guatemala. *Front Earth Sci* 6:30
- Rokhmiana CA, Andaru R (2016) Utilizing UAV-based mapping in post disaster volcano eruption. 6th Insat Ann Eng Sem (InAES):202–205
- Stix J, de Moor JM (2018) Understanding and forecasting phreatic eruptions driven by magmatic degassing. *Earth Planets Space* 70:83
- Surono JP, Pallister J, Boichu M, Buongiorno MF, Budisantoso A, Costa F, Andreastuti S, Prata F, Schneider D, Clarisse L, Humaida H, Sumarti S, Bignami C, Griswold J, Carn S, Oppenheimer C, Lavigne F (2012) The 2010 explosive eruption of Java's Merapi volcano-A '100-year' event. *J Volcanol Geotherm Res* 241–242:121–135
- Syahbana DK, Kasbani K, Suantika G, Prambada O, Andreas AS, Saing UB, Kunrat SL, Andreastuti S, Martanto M, Kriswati E, Suparman Y, Humaida H, Ogburn S, Kelly PJ, Wellik J, Wright HMN, Pesicek JD, Wessels R, Kern C, Lisowski M, Diefenbach A, Poland M, Beauducel F, Pallister J, Vaughan RG, Lowenstern JB (2019) The 2017–19 activity at Mount Agung in Bali (Indonesia): intense unrest, monitoring, crisis response, evacuation, and eruption. *Sci Rep* 9:8848
- Szeliski R (2010) Computer vision: algorithms and applications, p 979
- Troll VR, Deegan FM (2023) The magma plumbing system of Merapi: the petrological perspective. In: Gertisser R, Troll VR, Walter TR, Nandaka IGMA, Ratdomopurbo A (eds) Merapi volcano—geology, eruptive activity, and monitoring of a high-risk volcano. Springer, Berlin, Heidelberg, pp 233–263
- Voight B, Constantine EK, Siswoidjoyo S, Torley R (2000) Historical eruptions of Merapi volcano, Central Java, Indonesia, 1768–1998. *J Volcanol Geotherm Res* 100:69–138
- Wahyudi SA, Putra H, Darmawan H, Suyanto I, Meilano I, Irzaman EM, Djamal M, Yasin M, Aminah NS, Perdinan AR, Srigutomo W, Suryanto W (2020) Topography changes and thermal distribution at the Kelud crater after the 2014 Plinian eruption. *Indones J Geogr* 52:411–417
- Walter TR (2023) Radar sensing of Merapi volcano. In: Gertisser R, Troll VR, Walter TR, Nandaka IGMA, Ratdomopurbo A (eds) Merapi volcano—geology, eruptive activity, and monitoring of a high-risk volcano. Springer, Berlin, Heidelberg, pp 437–455
- Walter TR, Salzer J, Varley N, Navarro C, Arámbula-Mendoza R, Vargas-Bracamontes D (2018) Localized and distributed erosion triggered by the 2015 Hurricane Patricia investigated by repeated drone surveys and time lapse cameras at Volcán de Colima, Mexico. *Geomorphology* 319:186–198
- Walter TR, Subandriyo J, Kirbani S, Bathke H, Suryanto W, Aisyah N, Darmawan H, Jousset P, Luehr BG, Dahm T (2015) Volcano-tectonic control of Merapi's lava dome splitting: the November 2013 fracture observed from high resolution TerraSAR-X data. *Tectonophysics* 639:23–33
- Watson M, Chigna G, Wood K, Richardson T, Liu E, Schellenberg B, Thomas H, Naismith A (2017) On the use of UAVs at active volcanoes: a case study from Volcan de Fuego, Guatemala. AGU Fall Meeting 2017, Abstract ID NH31C-03
- Watts RB, Herd RA, Sparks RSJ, Young SR (2002) Growth patterns and emplacement of the andesitic lava dome at Soufrière hills volcano, Montserrat. *Geol Soc Lond Mem* 21:115–152
- Widiyantoro S, Ramdhan M, Metaxian JP, Cummins PR, Martel C, Erdmann S, Nugraha AD, Budi-Santoso A, Laurin A, Fahmi AA (2018) Seismic imaging and petrology explain highly explosive eruptions of Merapi volcano Indonesia. *Sci Rep* 8:13656
- Wyering LD, Villeneuve MC, Wallis IC, Siratovich PA, Kennedy BM, Gravley DM, Cant JL (2014) Mechanical and physical properties of hydrothermally altered rocks, Taupo volcanic zone, New Zealand. *J Volcanol Geotherm Res* 288:76–93
- Zorn E, Walter T, Johnson BJ, Mania R (2020) UAS-based tracking of the Santiaguito lava dome Guatemala. *Sci Rep* 10:8644



Assessing the Pyroclastic Density Current Hazards at Merapi: From Field Data to Numerical Simulations and Hazard Maps

Sylvain J. Charbonnier, Karim Kelfoun,
Christina Widiwijayanti, Dewi Sri Sayudi,
and Raditya Putra

Abstract

Merapi is considered as the most active and the most frequently eruptive volcano in Indonesia and is responsible for more than 5200 casualties since the eighteenth century, mainly caused by pyroclastic density currents (PDCs). Although eruptions are predominated by gravitational dome-collapse events and small explosions of VEI < 3, some PDCs associated with larger explosive events repeatedly reached distances up to 15–20 km from the summit during the last 200 years. PDC hazard mapping in Indonesia is traditionally based on the maximum extent of PDCs as derived from previous eruptions. The potential hazard of

long-runout, widespread high-energy PDCs able to spread across densely populated interfluvial (non-valley) and distal regions is now considered the most challenging component of the PDC hazard mapping at Merapi. PDC hazard modelling approaches have developed and diversified in several ways and can be subdivided into either deterministic (i.e. scenario-based) or probabilistic types. The depth-averaged modelling approach seems to be suitable for the simulation of flows and surges generated by dome collapses, the most common type of PDCs at Merapi. However, regardless of the modelling approach chosen, simulation results should always be interpreted carefully and, if integrated into a hazard plan, done with expert advice. In doing this, the use of well-constrained geological data, validation metrics and statistical approaches such as those described here can provide valuable insight and assist in the PDC hazard analysis process. Outcomes of such modelling efforts could provide the basis for establishing an interpretation framework and defining the ‘best practices’ to conduct rigorous PDC hazard assessments. Such guidelines could be widely distributed to correctly inform and advise geological surveys worldwide about the breadth and depth of understanding of methodologies and procedures currently available for undertaking robust PDC hazard assessments at other active volcanoes like Merapi.

S. J. Charbonnier (✉)
School of Geosciences, University of South Florida,
4202 East Fowler Avenue, Tampa, FL 33620, USA
e-mail: sylvain@usf.edu

K. Kelfoun
Laboratoire Magmas et Volcans, Université
Clermont Auvergne, CNRS, IRD, OPGC,
Clermont-Ferrand, France

C. Widiwijayanti
Earth Observatory of Singapore, Nanyang
Technological University, 50 Nanyang Avenue,
N2-01b-30b, Singapore 639798, Singapore

D. S. Sayudi · R. Putra
Balai Penyelidikan Dan Pengembangan Teknologi
Kebencanaan Geologi, CVGHM, Geological
Agency of Indonesia, JL. Cendana No. 15,
Yogyakarta 55166, Indonesia

Keywords

Merapi · Pyroclastic density currents · Numerical modelling · Volcanic hazards · Hazard maps

16.1 Pyroclastic Density Current (PDC) Hazards at Merapi

For the past two centuries, the activity of Merapi has been dominated by periods of lava extrusion forming summit domes that lasted for several months (e.g. Voight et al. 2000; Ratdomopurbo et al. 2013). The extrusion phase is then followed by rock-falls and dome-collapse events, mainly due to gravitational slope instability and fragmentation of the growing lava dome or coulee. Material breaks off from the unstable lava dome, causing an avalanche of material down on the Merapi slope (Voight et al. 2000) which generates dome-collapse pyroclastic density currents (PDCs) ('awan panas guguran', in Indonesian) that usually affect a relatively narrow sector on the volcano flank. These dome growth episodes occur on average every 3–5 years (Newhall et al. 2000) that seldom alternated with small explosive phases ($VEI \leq 2$). However, directed blasts also occurred at Merapi, e.g. in 1930 and 2010 (Kemmerling 1931; Berthommier et al. 1992; Voight et al. 2000; Komorowski et al. 2013). In 1930, these unusually large dome-collapse PDCs with a lateral explosive component (Kemmerling 1931; Voight et al. 2000) reached a runout distance of 13.5 km (Neumann van Padang 1933; Hartmann 1935). Significant explosive eruptions with $VEI > 3$ involved removal of the summit domes (e.g. 1768, 1822, 1849, 1872, 1930, and 2010) and generated column-collapse PDCs ('awan panas letusan', in Indonesian), tephra falls, and lahars (Voight et al. 2000; Thouret et al. 2000; Suroño et al. 2012). Such column-collapse PDCs, caused by collapse of a near vertical eruption fountain, are capable of affecting a much broader sector or multiple sectors on the volcano flanks (Voight et al. 2000; Gertisser et al. 2012). Historical Merapi explosive eruptions that produced column-collapse PDCs

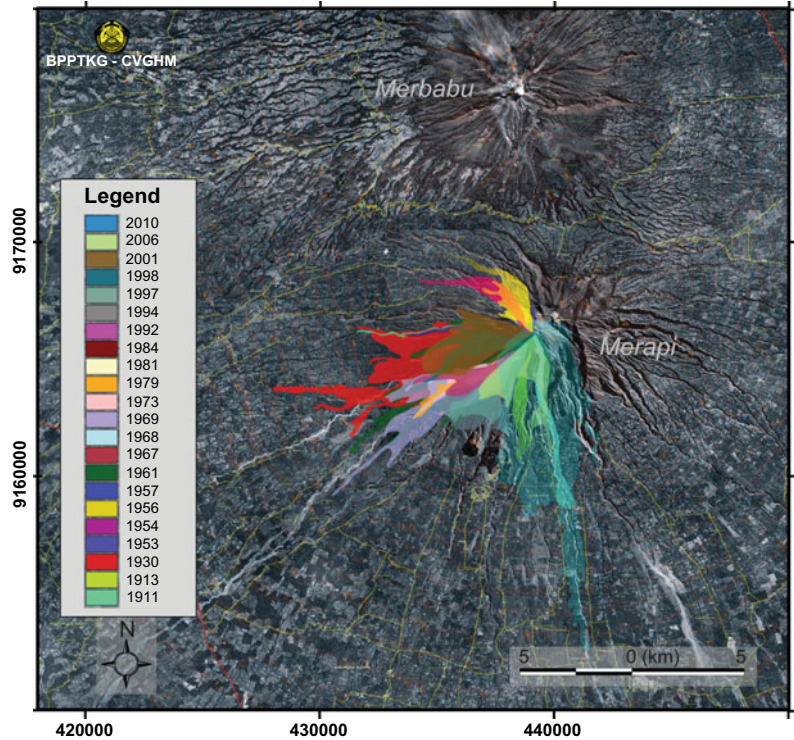
occurred several times in the twentieth century (e.g. 1934, 1969, and 1972, Suryo and Clarke 1985; CVGHM 2006).

Chronologically, the eruptive scenario can differ from one eruption to another, as a sequence of processes including lava dome extrusion, dome collapse, and explosion. The new lava dome typically forms in the summit area and can partially or entirely become unstable, collapse or being disrupted during explosive events, whereas some domes remain and become parts of the summit morphology (Ratdomopurbo et al. 2013). These intermittent processes between dome building and removal shape the summit morphology of Merapi and further control the prevailing direction of the following dome growth and PDCs.

Merapi is known for its "Merapi-type" *nuée ardentes* that generally involve small-volume, low-energy PDCs that are generated by relatively simple gravitational collapse of a lava flow or dome (Bardintzeff 1984; Voight et al. 2000). PDCs at Merapi typically originate from dome collapse, column-collapse, and lateral blasts, although the latter are relatively rare compared to the other two types of events. PDC deposits are mainly deposited in the mid and lower slopes at elevations between 700 and 1000 m above sea level. Thicker block-and-ash flow (BAF) deposits are confined to the valleys, whereas pyroclastic fall and surge deposits dominate the interfluvial areas. Between 300 and 700 m elevation, PDCs are inter-bedded with lahar and tephra deposits. Some scarce pyroclastic surge deposits have also been found more distally on the south flank at ~200 m elevation, ~22 km from the summit (Hadisantono et al. 2002; Newhall et al. 2000). Post-eighteenth century eruptions have produced PDC deposits that have predominantly covered the northwest, west, south, and southeast flanks with runout distances exceeding 10 km (Fig. 16.1; Purbo-Hadiwijoyo and Suryo 1980; Thouret et al. 2000; Voight et al. 2000).

Following the study of Thouret et al. (2000), the eruptive activity at Merapi during the twentieth century is composed of several important events that should be highlighted as background reference to better understand the various

Fig. 16.1 Overlay of Merapi PDC deposit coverage from the 1911 to 2010 eruptions. Figure modified from CVGHM (2016)



mechanisms capable of generating significant PDC hazards at Merapi. The three selected events are as follow:

- (1) In 1930–1931, a VEI 3 eruption began with lava dome extrusion followed by a series of large PDCs that reached runout distances of 13.5 km in the Putih and Blongkeng river valleys (Fig. 16.1). This energetic PDCs killed 1369 people and were possibly influenced by vertical explosions or a lateral blast (Voight et al. 2000). The volume of the eruption products was estimated as $26 \times 10^6 \text{ m}^3$ (Siswawidjono et al. 1995);
- (2) The dome collapse event of 22 November 1994, killed 64 people and burned dozens of others. A striking feature of this PDC event was the unexpectedly large and destructive ash-cloud surge component that resulted from the detachment of the valley-confined BAFs (Abdurachman et al. 2000; Kelfoun et al. 2000);
- (3) The multi-stage VEI 4 eruption of October–November 2010 began with a strong

explosion and was followed by a series of intermittent explosions and fast dome extrusion, the greatest so far in the twenty-first century, causing 386 fatalities and 400,000 evacuees (BNPB 2011). This eruption destroyed most of the 2006 lava dome and has formed a new 400 m diameter crater with a southward opening towards the Gendol valley. The eruption culminated on 5 November 2010 with an explosion column as high as 17 km (Surono et al. 2012). The PDCs were predominantly directed towards Gendol river valley (up to 16 km) but also entered other river valleys in the southwest, south, and southeast sectors (Fig. 16.1; Sayudi et al. 2010).

The population density around Merapi is very high with $\sim 350,000$ people living within volcanic hazard zone areas and ~ 5 million within a 30 km radius from the summit (BPS 2011). Merapi is also considered as the most active and the most frequently erupting volcano in Indonesia, responsible for more than 5200 fatalities

since the eighteenth century, mainly caused by PDC events (Siebert et al. 2010; Surono et al. 2012). Although eruptions are predominated by lava dome forming type of events and small explosions of VEI < 3, some PDCs repeatedly reach up to 10 km from the summit (Voight et al. 2000). Currently, the closest settlements are only ~4 km away from the summit on the southeast and north flanks, which make them prone to even small-sized PDCs (Ratdomopurbo et al. 2013).

16.2 Hazard Assessment of Pyroclastic Density Currents at Merapi

16.2.1 Field Data Acquisition and Processing

Detailed descriptions of pristine PDC deposits at Merapi are relatively rare, due to the high tropical erosion rates and reworking of primary pyroclastic deposits during the annual Indonesian rainy season between October and April. Therefore, most of these descriptions are related to the recent Merapi eruptions only (Boudon et al. 1993; Abdurachman et al. 2000; Kelfoun et al. 2000; Schwarzkopf et al. 2005; Charbonnier and Gertisser 2008; Lube et al. 2011; Charbonnier et al. 2013). When available, such field studies immediately after flow emplacement often allow to decipher the relationship between individual flow deposits and the eruption record, as well as to unravel the origin and emplacement mechanisms of the associated flows. The survey of the entire extent of the deposits, from proximal to distal reaches, carried out either directly from field-based methods (GPS, ground surveys) or indirectly via remote sensing tools (using any kind of available satellite products) enables the construction of a detailed map and the recognition of different types of deposits related to the generation and emplacement of the related flow events (e.g. Charbonnier and Gertisser 2008; Charbonnier et al. 2013; Solikhin et al. 2015). Interpretation of deposit surface features and morphologies, often coupled with density and

componentry/lithological analyses of surface particle assemblages, allow to relate such variations to the source materials involved in individual pyroclastic-flow-forming events and varying modes of transport and deposition of the different flows (e.g. Schwarzkopf et al. 2005; Lube et al. 2011). Other surface characteristics, such as superelevation at bends (used to derive local flow velocity), the distribution and orientation of friction or impact marks on block surfaces, presence of degassing pipes, erosional features observed at valley margins, zones of singed, broken or downed trees (used to derive local flow direction), as well as local temperature measurements, are also crucial for reconstructing the local dynamics of the associated flows and the effects of changing slope, channel morphology and local topographic features (e.g. Kelfoun et al. 2000; Schwarzkopf et al. 2002; Charbonnier and Gertisser 2008; Komorowski et al. 2013).

Intense erosion of the pristine PDC deposits after one or more rainy seasons following a Merapi eruption gives the opportunity to perform a detailed study of the sedimentological, stratigraphical, granulometrical and componentry characteristics of the different deposits. The distribution of the collected samples along the flow paths is controlled strongly by the distribution and availability of erosive channels and primary deposits. Identification of different depositional units, their stratigraphic correlations and longitudinal and lateral facies variations all provide crucial information about: (1) the distribution, volumes and sedimentological characteristics of the different units; (2) flow types and mobility as inferred from associated deposits; and (3) changes in the dynamics of the different flows and their material during emplacement (e.g. Charbonnier and Gertisser 2011; Lube et al. 2011; Komorowski et al. 2013). Results of such field studies obtained after the 2006 and 2010 Merapi eruptions (e.g. Charbonnier and Gertisser 2011; Lube et al. 2011; Charbonnier et al. 2013; Cronin et al. 2013; Komorowski et al. 2013) show that complex, local-scale variations in flow dynamics and deposit architectures are apparent and that the major factors controlling the propagation of the main flows and their potential hazards for

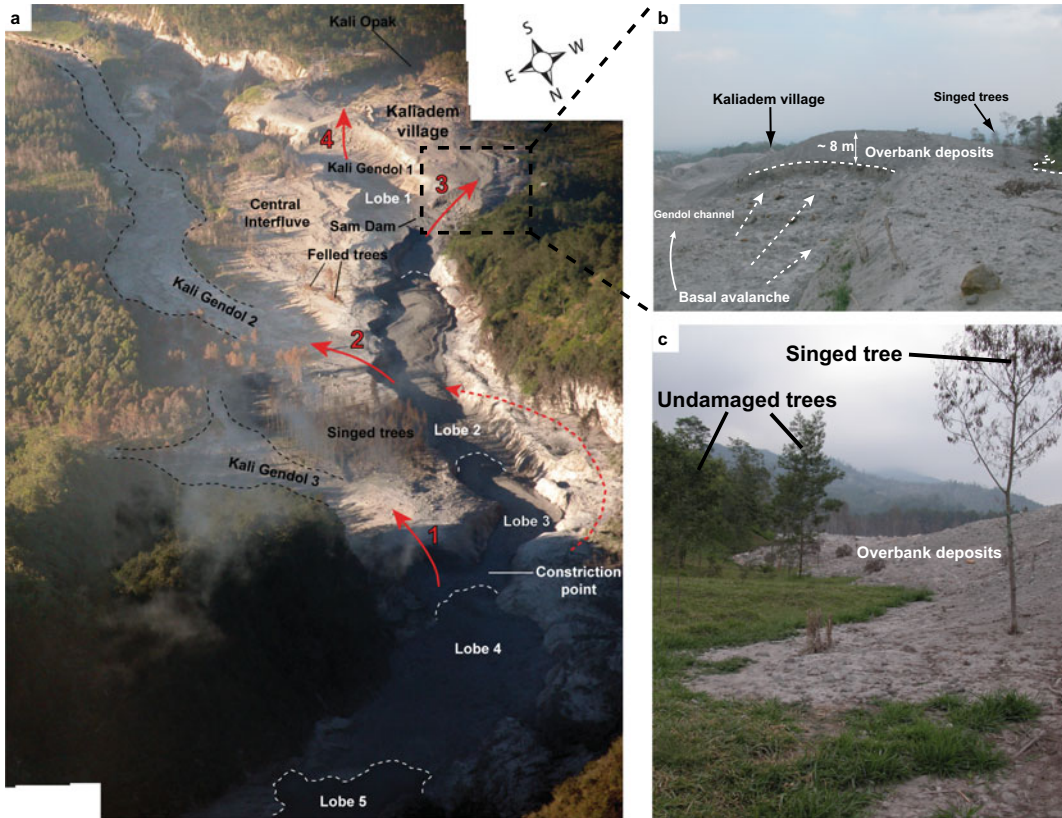


Fig. 16.2 **a** Photograph from the summit showing the four main sites of basal avalanche overspill (red arrows) and generation of overbank pyroclastic flows on the southern flank during the 2006 Merapi eruption. The front of each PDC lobe (white dashed line) in the main Gendol channel are also shown. **b** View of the third overspill site in the Kaliadem area showing wedge-shaped overbank pyroclastic-flow deposits issued from the basal avalanche that overspilled the valley margins and partly buried the

village. Note the concentration of coarse clasts at the foot of the valley wall. **c** Picture taken at the back of the wedge-shaped overbank deposits emplaced during the third overspill of the 14 June block-and-ash flows in the Kaliadem area, 4.8 km from the summit. Note the sharp boundary between the marginal coarse-grained deposits/singed tree and the fresh grass/undamaged trees. Modified from Charbonnier (2009)

avulsion and decoupling were driven by: (1) the rapid emplacement of several voluminous PDCs, associated with the steady infilling of the receiving landscape after the two first phases of the eruption; (2) longitudinal changes in channel capacity following increased sinuosity in the valley and decreased containment space; and (3) the effects of varying source mechanisms (gravitational dome collapse, vertical or lateral dome explosions and column collapse) and source materials involved during individual PDC-forming events. Results also emphasise the potential hazard of long-runout, voluminous concentrated PDCs at Merapi through the

recognition of overbank pyroclastic flows (Fig. 16.2). Due to their potential to spread across densely populated interfluve (non-valley) and distal regions (e.g. Gertisser et al. 2012), these overbank flows are now considered as one of the most hazardous parts of the PDC system (see Sect. 16.3).

Moreover, some PDC deposits and the widespread devastating impact of associated high-energy PDCs on trees and buildings during the 2010 Merapi eruption show striking similarities with those from historical volcanic blasts (Montagne Pelée, Martinique; Bezymianny, Russia; Mount St. Helens, USA; Soufrière Hills,

Montserrat) (see Subandriyo et al. 2023, Chap. 12). Using data from stratigraphical and sedimentological analyses as well as high resolution satellite imagery to map eruptive units and flow direction from the pattern of extensive tree blowdown, Komorowski et al. (2013) provided field evidence of the first unequivocal blast-like deposits in Merapi's recent history. In addition to these blast-like deposits, two other types of PDC deposits have been identified after the 2010 eruption based on lithofacies variations (stratification, grain size, grain shape, sorting, fabric and composition): (1) deposits from block-poor concentrated PDCs emplaced from sedimentation of high-energy stratified dilute PDCs from dome explosions (i.e. surge-derived PDCs; Druitt et al. 2002) and (2) deposits from dilute detached PDCs from the main valley-confined block-rich concentrated PDCs that propagated 50–400 m laterally from them in distal areas (see Subandriyo et al. 2023, Chap. 12). The latter type of deposits has also been observed and described (and often termed 'surge' deposits) in previous field studies at Merapi after the 1984, 1994 and 1998 eruptions (e.g. Boudon et al. 1993; Abdurachman et al. 2000; Kelfoun et al. 2000; Bourdier and Abdurachman 2001; Schwarzkopf et al. 2005). The occurrence of substantial interfluvial deposits suggests that the generation of such unconfined PDCs that escape the valley confines is a common process at Merapi. Associated flow decoupling processes have been proven to be a common feature during PDC emplacement at Merapi as the initial solid–gas mixture evolves during transport with time, space, and current thickness (e.g. Bourdier and Abdurachman 2001; Cronin et al. 2013; Komorowski et al. 2013).

Finally, Jenkins et al. (2013) conducted an inter-disciplinary impact assessment of the 2010 Merapi PDCs by combining remote, field, laboratory and GIS data to reconstruct their spatial and temporal dynamics and main hazard characteristics (see Subandriyo et al. 2023, Chap. 12). Empirical damage data and calculations of material and structural resistance to lateral force were used to estimate approximate dynamic pressures associated with the 5 November paroxysm. Their findings show that dynamic

pressures exceeded 15 kPa more than 6 km from source and rapidly attenuated over a distance of less than 1 km at the end of the PDC runouts (see Fig. 7 in Jenkins et al. 2013). Such detailed quantitative data can be used to support numerical PDC and impact modelling and risk assessment at dome-forming volcanoes like Merapi.

16.2.2 Numerical Models of PDCs and Their Approaches

PDCs are formed by particles and gases of various characteristics (grain sizes, densities, temperature, etc.) transported with a certain velocity. The basic concept of numerical simulation is to solve balance equations of mass, momentum and energy according to simplified physical laws that model the real physics of these currents. A variety of approaches exists, depending on the degree of simplification of the physics and on the way chosen to solve the equations:

- (1) As the topography and the volume of the currents are fundamental in their emplacement, some approaches assume that the velocities of the currents can be neglected, and that the system of equations can be reduced to volume conservation. This approach is used by the code PFz (see below);
- (2) For the kinetic approach, spreading and pressure stresses are neglected. The flow front trajectories are simulated, considering the PDC as a rigid block that moves on a complex topography (e.g. Sheridan and Malin 1983; Beget and Limke 1988; McEwen and Malin 1989; Rossano et al. 2004; Saucedo et al. 2005);
- (3) In Discrete Element Methods (DEM) and Smoothed-Particles Hydrodynamics (SPH) models (e.g. Haddad et al. 2010; Cagnoli and Piersanti 2017), currents are divided in volumes that interact together and with the topography according to physical laws;
- (4) In the multiphase approach (e.g. Wohletz et al. 1984; Valentine et al. 1992; Neri and Macedonio 1996; Neri et al. 2003; Darteville et al. 2004; Esposti Ongaro et al. 2008, 2012),

all the phases present (different size classes of particles, gases of various compositions) can be taken into account. The space is divided in meshes that exchange mass, momentum and energy (Eulerian frame);

- (5) To decrease the computation time, other approaches consider that the vertical variations of properties can be neglected and therefore simplify the equation in 2D, with a depth-averaged formulation of the problem. DAN-3D is a SPH model that uses a depth-averaged formulation (McDougall and Hungr 2004; Hungr and McDougall 2009; Salvatici et al. 2016). Yamashita and Miyamoto (1993) and Itoh et al. (2000) also used a depth-averaged model but in an Eulerian frame as well as the codes Titan2D and VolcFlow detailed below.

The PFz Model

The PFz model is a statistically constrained simulation model for block-and-ash flows (BAFs) to estimate potential deposit areas (PFz) by adapting methodology from Iverson et al. (1998) for lahars. The predictive equations for BAFs are calibrated with data from several volcanoes (Widiwijayanti et al. 2009) and given by $A = (0.05-0.1) \times V^{2/3}$, $B = (35-40) \times V^{2/3}$, where A is cross-sectional of deposit area, B is planimetric area and V is deposit volume. The planimetric area is simply the deposit map area, and the cross-section area embodies the lateral limits and average thickness of the deposit as measured normal to the thalweg (Iverson et al. 1998). The proportionality coefficients are obtained from regression analyses and comparison of simulations to mapped deposits. The statistical uncertainty of the predictive equations, which imply a factor of two or more in predicting A or B for a specified V, is superposed on the uncertainty of forecasting V for the next BAF to enter a particular valley. Multiple impacted zones, produced by simulations using a selected range of volumes, also accommodate these uncertainties. The resulting maps show graphically that the potential for BAF deposition is highest nearest to the volcano sources and along valley thalwegs, and decreases with distance from

source and lateral distance from the thalweg (Widiwijayanti et al. 2009).

For practical use in hazard assessment, Widiwijayanti et al. (2009) used the program LaharZ (Schilling 1998) to predict and map a range of BAF inundation areas for a specified range of V, and display a gradation of hazard. The model does not explicitly consider dynamics aspects, which can be an important limitation. Pyroclastic surge impacts must be extended beyond BAF hazard zones. This model focuses on BAFs caused by the collapse and disintegration of lava dome material rather than on PDCs associated with fountain- or column-collapse. In May–July 2006, the PFz model was used to generate deposit maps for expected BAF events at Merapi volcano to aid risk assessment during the volcanic crisis of 2006 (see Sect. 16.2.3).

Depth-Averaged Models: Titan2D and VolcFlow

In the depth-averaged approach the equations are solved in 2D, the physical properties being integrated in the third dimension. The depth-averaged approximation requires that the flow length is much greater than its depth, that vertical displacements are negligible and that the physical properties are constant or vary according to an imposed law along the direction of integration.

Two depth-averaged codes have been used for the simulation of PDCs at Merapi volcano: Titan2D (e.g. Patra et al. 2005) and VolcFlow (e.g. Kelfoun and Druitt 2005). They use different numerical schemes for the resolutions of the equations, but their approach and equations used are similar. In the depth-averaged form, the mass (1) and momentum balance equations can be written as follow:

$$\frac{\partial h}{\partial t} + \frac{\partial}{\partial x}(hu_x) + \frac{\partial}{\partial y}(hu_y) = 0 \quad (16.1)$$

$$\begin{aligned} \frac{\partial}{\partial t}(hu_x) + \frac{\partial}{\partial x}(hu_x^2) + \frac{\partial}{\partial y}(hu_xu_y) \\ = gh \sin \alpha_x - \frac{1}{2} \frac{\partial}{\partial x}(gh^2 \cos \alpha_x) + \frac{T_x}{\rho} \end{aligned} \quad (16.2)$$

$$\begin{aligned} & \frac{\partial}{\partial t}(hu_y) + \frac{\partial}{\partial x}(hu_xu_y) + \frac{\partial}{\partial y}(hu_y^2) \\ & = gh \sin \alpha_y - \frac{1}{2} \frac{\partial}{\partial y}(gh^2 \cos \alpha_y) + \frac{T_y}{\rho} \end{aligned} \quad (16.3)$$

Equation 16.1 means that the variation of the current thickness, h , at a given location, changes according to the thickness variation in space around this location and the velocity $\mathbf{u} = (u_x, u_y)$ of the current: if a current that thickens to the North moves to the South, the thickness will increase at a given space with time. Equations 16.2 and 16.3 calculate the momentum balance in the x and y directions taking into account to forces of the current weight of a slope α , of the pressure gradient and of the resisting stresses $\mathbf{T} = (T_x, T_y)$. The current is considered to be of constant density, ρ , in time and space.

The advantage of Titan2D is that it can use adaptive meshes: where the topography is covered by PDCs, meshes are smaller. This allows high-resolution simulations with a relative low number of meshes, accelerating the calculation time.

PDCs are thought to be composed of two parts. A dense part formed by large blocks and particles that follows the river drainages and a more dilute part, formed by small particles maintained in suspension by turbulent gases. A new version of VolcFlow has been developed especially for the simulation of pyroclastic density currents (Kelfoun 2017). Unlike Titan2D and the previous version of VolcFlow, it couples two fluids: one for the concentrated part, one for the dilute part. Exchange laws allow the concentrated part to form the dilute part or, inversely, the dilute part to form a deposit or a concentrated current by sedimentation. The dilute part is simulated by a set of equations similar to Eqs. 16.1–16.3, adding a fourth equation to simulate the density variation of the dilute part along the emplacement. However, due to the depth-averaged approach, no vertical variation of density can be simulated by the model.

16.2.3 Deterministic Versus Probabilistic PDC Hazard Modelling Approaches

PDC hazard modelling and mapping approaches have developed and diversified in a number of ways. Methods can be subdivided into either deterministic (i.e. scenario-based) or probabilistic types. Deterministic PDC hazard mapping typically defines the areas that are inundated once specific eruptive conditions (i.e. PDCs generation mechanisms) have been assumed and according to a limited number of specific past or foreseen events (e.g. Widiwijayanti et al. 2009; Charbonnier and Gertisser 2012). Probabilistic approaches are often the preferred technique as they are able to incorporate uncertainty in the physical phenomena by using numerous multiple computer runs as in a ‘Monte Carlo’ simulation approach (e.g. Wadge 2009; Tierz et al. 2016). This methodology, by varying input parameters across likely ranges, explores the effect of modifying key, but uncertain, variables. In some cases, probabilistic PDC hazard mapping allows to represent the likelihood of PDC invasion, or the distribution of a specific hazard variable associated with the current (e.g. velocity, dynamic pressure, temperature, solid concentration).

An Example of Deterministic PDC Hazard Mapping

Widiwijayanti et al. (2009) used the PFz model to forecast the hazards of future BAF events on the southern flank of Merapi in 2006. They used the following two empirical relationships, $A = 0.05 V^{2/3}$, $B = 35 V^{2/3}$, to calibrate their model against typical BAFs at Merapi. BAF hazard zones were graded from high to low, which represented a potential volume range of $0.5\text{--}4 \times 10^6 \text{ m}^3$. The authors were also concerned that the breadth of their simulated BAF deposits could be too small, particularly if early deposits filled the channel to cause subsequent overbank BAF flowage and deposits of broad

lateral extent. Therefore, they estimated an “overbank pyroclastic flow (PF) zone”, by using an arbitrary coefficient A of 0.15, a volume of $4 \times 10^6 \text{ m}^3$, and an arbitrary coefficient B of ~ 100 , sufficient to enable the simulation to run out fully to distal areas. Thus, their philosophy was to use their initial hazard zones to indicate the runout potential for BAFs of specified volumes, and to use the overbank PF zone to conservatively indicate the potential breadth of future BAF deposits. They also estimated ash-cloud surge limits, which extended beyond the overbank PF zone (see Fig. 5 in Widiwijayanti et al. 2009). Soon after their maps were delivered to Indonesia, several large BAFs occurred. On 14 June 2006, the largest BAFs occurred and reached distances of $\sim 6.5 \text{ km}$ from the summit in the Gendol valley, damaged many buildings in Kaliadem/Bebeng, and killed two persons in a bunker near Kaliadem (see Sect. 16.3.1). PFz modelling results show that the boundary of actual deposits matches rather well with the simulated overbank PF inundation zone, whereas the maximum runout is consistent with the simulation for $V = 1 \times 10^6 \text{ m}^3$, similar to some deposit volumes from valley-confined BAFs generated on 14 June 2006.

Charbonnier and Gertisser (2012) used a numerical geophysical mass flow modelling approach to forecast the hazards of future BAF events on the southern flank of Merapi after the 2006 eruption. Sensitivity analyses of the two models (Titan2D and VolcFlow), coupled with high-resolution field-based data, were used to produce a series of simulations based on a range of possible input parameters. A graduated zone of inundation probability for future gravitational dome-collapse events was developed from the combination of inundation areas derived from these simulations (Fig. 16.3). These simulations provide seven scenarios that can be further interpreted as seven hazard levels of progressively decreasing risk based on the likelihood of impact (Fig. 16.3). Results show that the sensitivity of the Titan2D and VolcFlow models, in particular for the area covered by the resulting deposits and runout distances of the simulated

flows, are highly dependent on the choice of the initial volume and the flow mechanical properties (Coulomb frictional law for Titan2D and pseudoplastic law for VolcFlow). The most likely scenario (hazard level 7) is based on the simulation of a single, discrete collapse of a small portion ($\sim 0.5 \times 10^6 \text{ m}^3$) of a new lava dome to the south. The worst-case scenario (hazard level 1) is based on the simulation of a sustained collapse of a significant portion ($>6.0 \times 10^6 \text{ m}^3$) of a new lava dome to the south, where the material is shed as several pulses. These scenarios are only suitable for BAF hazard assessment generated by gravitational dome collapses, and they do not consider hazards associated with voluminous explosive PDCs generated by column collapses and/or directed blasts, like those that occurred during the 2010 eruptive activity.

An Example of Probabilistic PDC Hazard Mapping

Recently, Charbonnier et al. (2016) proposed to assess the uncertainty in PDC hazard mapping at Merapi using a fully probabilistic approach. The resulting probabilistic maps benefit from: (1) a new flow database compiled from the past 100 years of activity at Merapi; (2) statistical/stochastic sampling of input parameters including vent locations, flow volumes and mechanical properties (basal friction angles for Titan2D and constant retarding stresses for VolcFlow); (3) a new digital elevation model (DEM) of Merapi volcano of 2 m spatial resolution and post-2010 eruption topography; and (4) new computational capacities at the University of South Florida to perform up to 64 runs in parallel. Using the Latin Hypercube Sampling method, 1024 starting points for 1024 flow simulations were computed inside the 2010 crater (Fig. 16.4a). A ‘Pareto 2’ probability density function was used to fit the distribution of 25 flow volumes from the database, ranging between 10^5 m^3 and 10^8 m^3 (Fig. 16.4b). Sampling and coupling of 1024 flow volumes with their appropriate flow rheology were performed by using bins of volumes (V) with uniform basal friction angle (BFA) and constant retarding stress (CRS) distributions as follow: (1) if $10^5 < V < 10^6 \text{ m}^3$, BFA is uniformly sampled

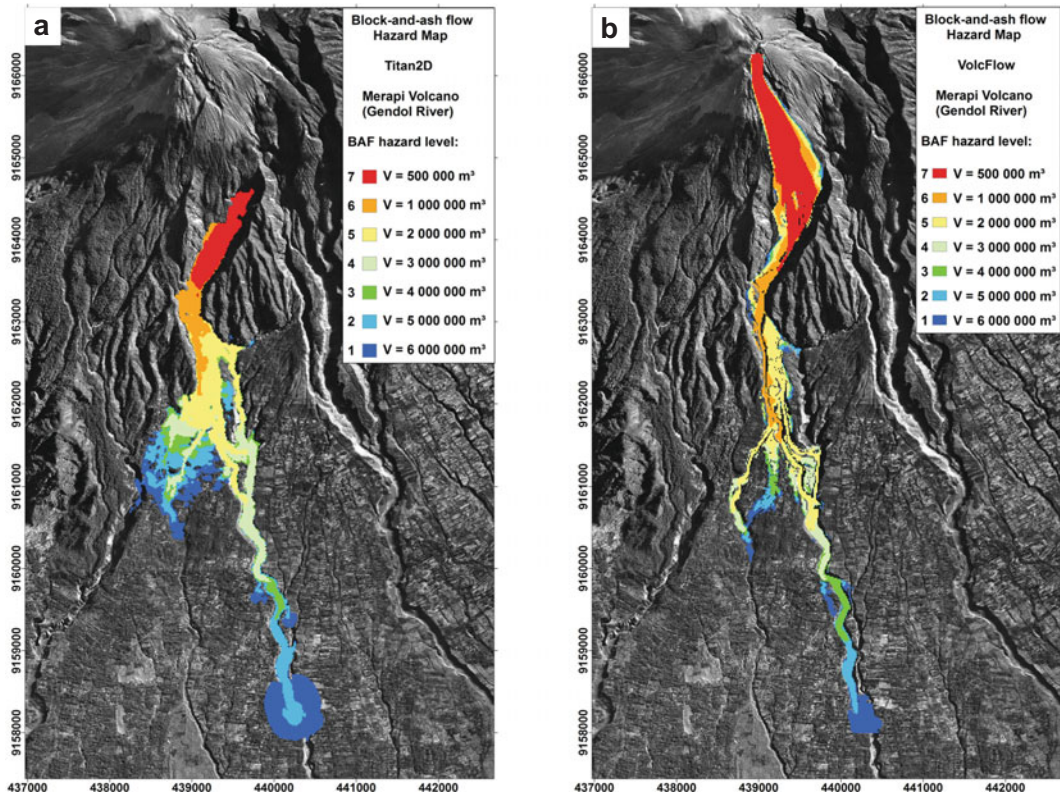


Fig. 16.3 Block-and-ash flow hazard maps of the southern flank of Merapi produced with **a** the Titan2D model and **b** the VolcFlow model. Graduating colours

(from blue to red) are used to represent scenarios of increasing hazard levels (from 1 to 7). Modified from Charbonnier and Gertisser (2012)

between 25° and 15°, CRS is uniformly sampled between 10 and 7.5 kPa; (2) if $10^6 < V < 10^7 \text{ m}^3$, BFA is uniformly sampled between 15° and 8°, CRS is uniformly sampled between 7.5 and 5 kPa; and (3) if $10^7 < V < 10^8 \text{ m}^3$, BFA is uniformly sampled between 8° and 5°, CRS is uniformly sampled between 5 and 3 kPa (Fig. 16.4c).

Compilations of the 1024 Titan2D simulations and 1024 VolcFlow simulations were used to compute two probabilistic maps of PDC inundation (exceeding 1 m) using two different flow rheologies (i.e. Coulomb frictional with Titan2D and pseudoplastic with VolcFlow) over a 2 m DEM of the southern flank of Merapi (Fig. 16.5a, b). Due to the excessive computational resources and time used by the VolcFlow code, the ensemble runs had to be performed over a smaller sample of the DEM, cropped in the East–West

direction to cover only the southern flank of the volcano (see Fig. 16.5b). One striking difference between the two maps is the extensive lateral spreading of the Titan2D simulations outside of the main river channels, between 5 and 10 km from the summit. Such significant lateral spreading results in shorter runout distances reached by the Titan2D simulated flows compared to the VolcFlow ones of similar initial volumes, which therefore show much smaller probabilities of flow inundation (<0.01) in the distal area (from 10 to 15 km from the summit). Differences of probability outcomes using two different flow rheologies highlight inherent sources of model uncertainties related to: (1) complex rheological behaviour of PDCs over natural terrain; (2) digital topography accuracy (DEM); and (3) input parameter estimation.

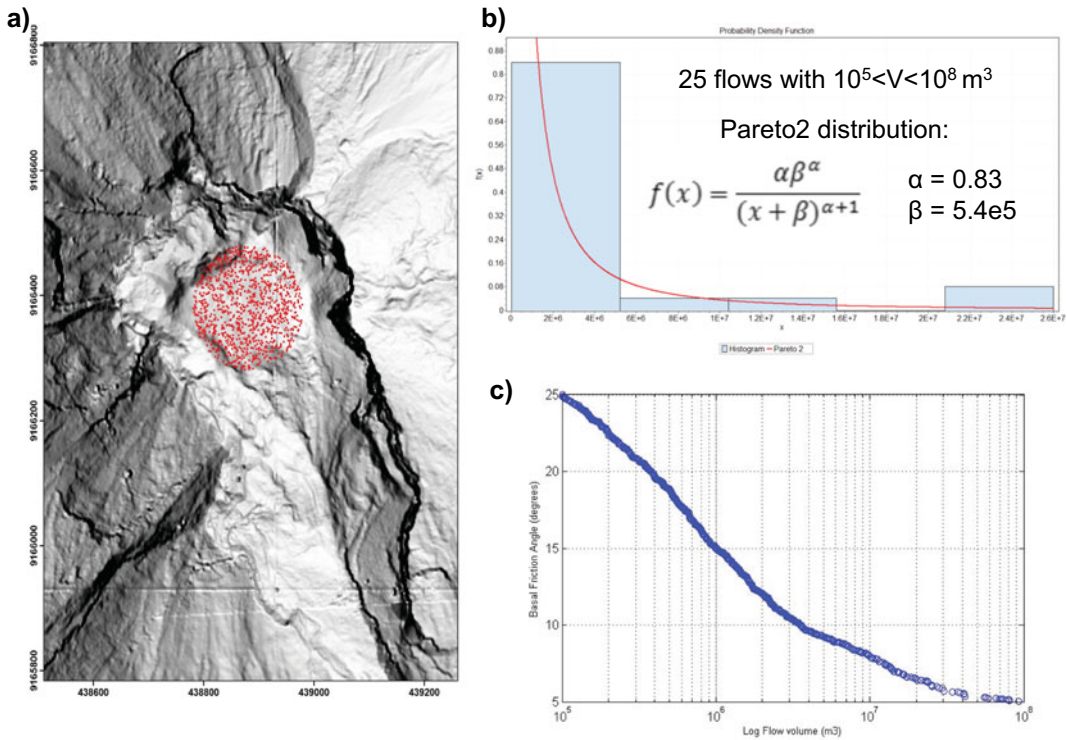


Fig. 16.4 a Distribution of the 1024 starting points (red dots) inside the 2010 crater. b ‘Pareto 2’ probability density function used to fit the distribution of the 25 flow

volumes selected. c Plot showing the 1024 couples of flow volumes and basal friction angles sampled for the Titan2D ensemble runs

16.2.4 The Merapi Volcanic Hazard Map

The Merapi volcanic hazard map (*Kawasan Rawan Bencana (KRB) Gunungapi*, in Indonesian) is maintained by the Center for Volcanological Hazard Mitigation (CVGHM) of the Geological Agency of Indonesia. The first hazard map of Merapi was published by Pardyanto et al. (1978). This map was generated based on previous literature studies focused on the behaviour and characteristics of Merapi eruptions. The hazard map was divided into three different zones that reflect the various hazards induced by an eruption: (1) The forbidden or closed zone is the area situated closest to the hazard source, which is affected by pyroclastic flows, and therefore should be permanently abandoned; (2) the first danger zone is the area that was impacted by historical eruption products, even though not

specifically affected by pyroclastic flows, during paroxysmal activity this area can be impacted by ballistics; (3) the third danger zone comprises the areas situated in or close to the valleys originating from the summit, and potentially inundated by lahars. This zone is divided into the alert zone and the abandoned zone. The first comprises areas with high topography (e.g. hills, which can be served as evacuation area in the case of a lahar event).

After the release of the Indonesian National Standard (BSN 1998) procedure to prepare volcanic hazard maps, the 1978 hazard map was revised in 2002 (Fig. 16.6a). The volcanic hazard map of 2010 is a revised version of the 2002 one and considers the area directly impacted by the PDCs of the 2010 eruption (Fig. 16.6b). The 2010 hazard map served as guidance to identify the particular hazard level of an area, as well as zones that can be impacted by various eruptive

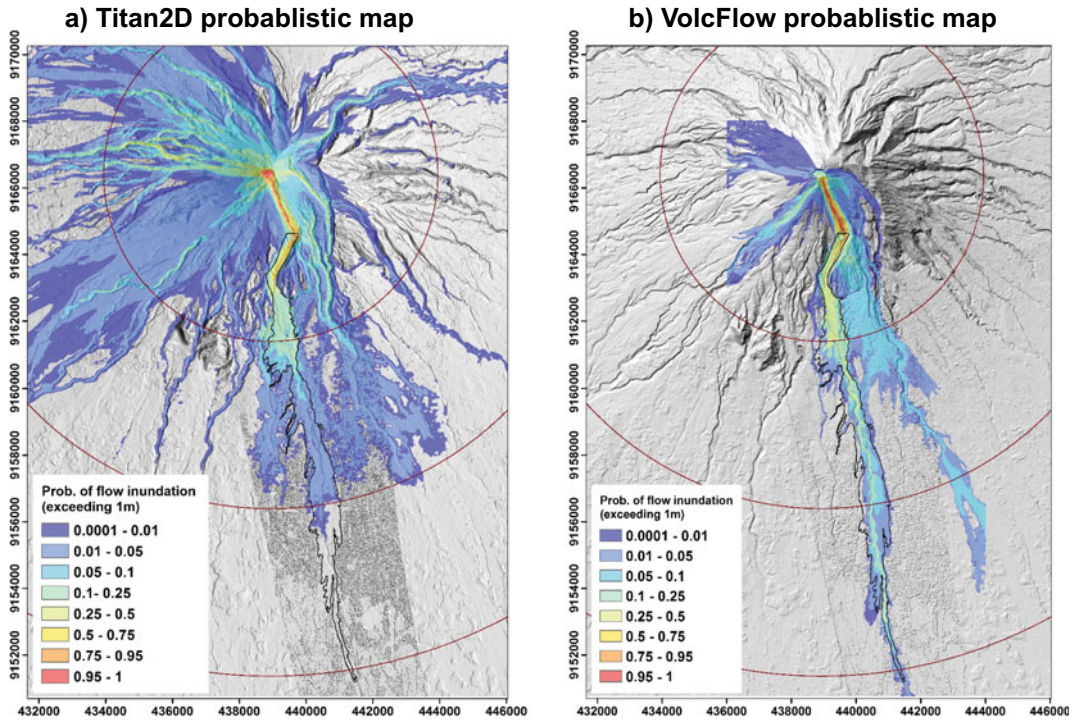


Fig. 16.5 Probabilistic maps of flow inundation (exceeding 1 m) on the southern flank of Merapi volcano using **a** Titan2D with a Coulomb frictional rheology and **b** VolcFlow with a pseudoplastic rheology. Red circles

show distance from summit at 5 km intervals. Black outline shows the inundation area of the 2010 concentrated PDCs

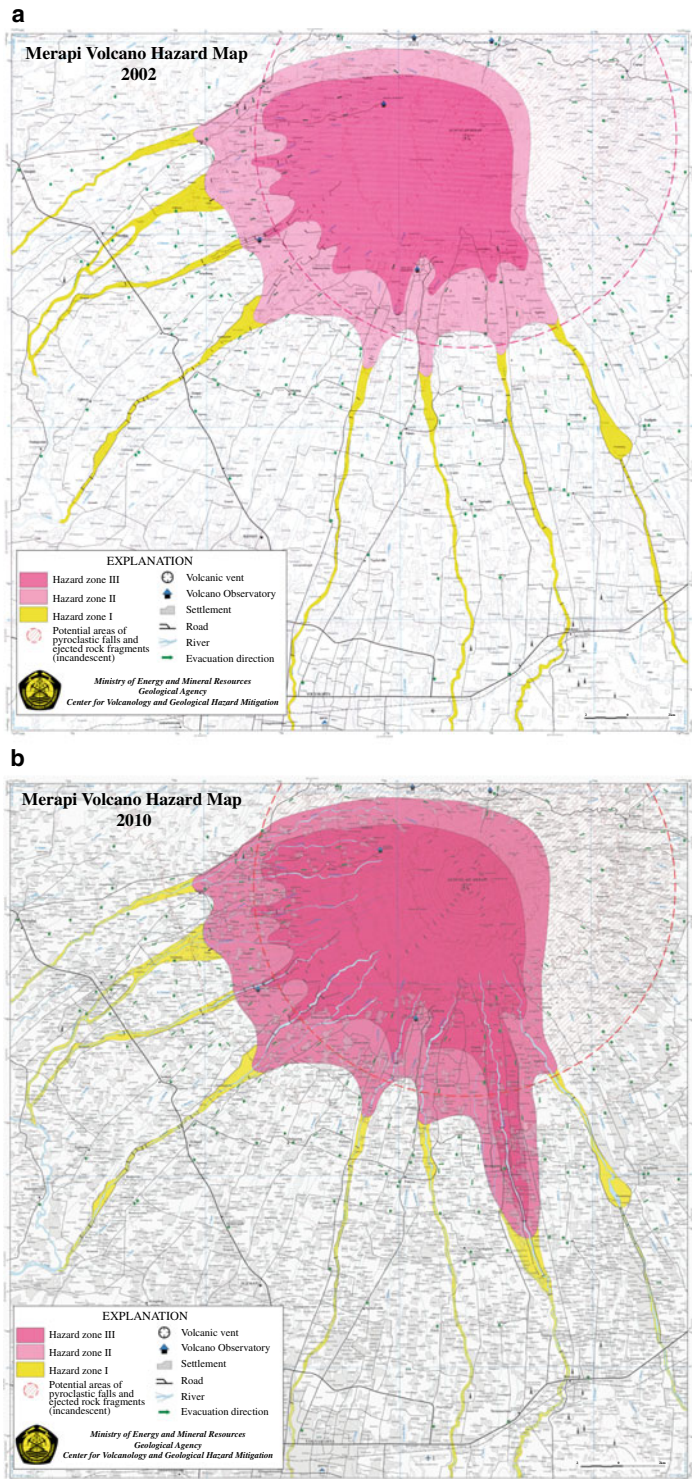
products when volcanic activity occurs. This map details the kind and type of volcanic hazards, hazard zones, direction of evacuation, locations of evacuation shelters and disaster relief posts. The map is based on a compilation of various information including geomorphology, geology, eruptive history, coverage of previous eruptive products, research, and field studies (Hadi-santonio et al. 2002). The different types of Merapi eruptive products that pose risk to people, property, and infrastructures consist of PDC, pyroclastic falls (including volcanic bombs and other ejected rock fragments), and lahars. Since lava flows rarely reach the lower slopes at Merapi, they may not directly endanger people. Terms and criteria for the different Merapi volcanic hazard zones are standardised and referred to the Indonesian National Standard (BSN 1998). Accordingly, the current Merapi volcanic hazard map (Fig. 16.6b) is divided into three levels: Hazard zone I, Hazard zone II, Hazard zone III,

and an additional zone potentially affected by pyroclastic falls and ejected rock fragments (incandescent) (Sayudi et al. 2010).

Hazard Zone I

Hazard zone I are areas potentially affected by lahars and possibly affected by high-energy PDCs (Fig. 16.6). In case of a significant eruption, these areas are also potentially affected by pyroclastic falls and ejected rock fragments (incandescent). During heavy rain, tephra falls and PDC deposits in the river valleys can be reworked and potentially trigger lahars. Lahars can escape from river valleys and inundate residential areas, farms, and infrastructures. People living in hazard zone I should increase their awareness when an eruption or heavy rain occurs, by paying attention to the development of the volcanic activity, which is communicated by CVGHM, stay away from the watershed and escape to the evacuation sites. In case of a large-

Fig. 16.6 Merapi volcanic hazard maps of **a** 2002 and **b** 2010, showing changes in hazard zone-II and hazard zone-III. The volcanic hazard map of 2010 is a revised version of 2002 and considers the area directly impacted by PDCs during the 2010 eruption. Figures modified from Hadisantono et al. (2002) and Sayudi et al. (2010)



scale lahar event, an evacuation plan is made, and dissemination and exercises about lahar disaster management need to be performed.

Hazard Zone II

Hazard zone II consists of two parts: (a) Mass flows consisting of pyroclastic flows, lava flows, and lahars; and (b) Ejecta in the form of volcanic tephra falls and ejected rock fragments (incandescent). In hazard zone II the community is required to evacuate, if there is an increase in volcanic activity in accordance with the recommendation of the CVGHM until this area is declared safe again. The commands for 'evacuation', 'remain in place', and 'the situation is safe again', are decided by the local government in accordance with the regulations. The boundaries of hazard zone II are based on eruptive deposits older than 100 years, including those from past VEI 3 and VEI 4 eruptions.

In the event of a major eruption, the highest risk level of hazard zone II covers several river valleys on the north, west, south and southeast slopes (Fig. 16.6). Based on the eruptive history of Merapi, the boundary of hazard zone II for PDC hazards can reach as far as 17 km or more from the summit. Changes in channel and ridge morphology due to sand mining may lead to future expansion of threats. In the case of large-scale lava dome collapses, these topographic changes may extend the lateral spreading of PDCs which could reach the current settlements. Large scale lahars can occur when rainfall accumulation reaches more than 40 mm within 2 h. After the 2010 eruption, thirteen rivers around Merapi have already experienced large-scale lahar events. The potential zone affected by lahars are between 600 and 450 m elevation above sea level in the southern sector of the volcano. On the western flanks, the slopes are generally more significant than on the southern flank (~10–11% for most rivers) and the area that could potentially be affected by lahars lies between 700 and 500 m elevation above sea level at a distance between 11 and 13 km from the summit (Hadasantono et al. 2002).

Pyroclastic Falls and Ejected Rock Fragments (Incandescent)

The hazard area including potential pyroclastic falls is determined by considering the volcano's eruptive behaviour without any assumption of wind direction, and the zone is described by a circular shape (Fig. 16.6). The distribution limit of the ejecta is based on tephra deposits older than 100 years at a distance of 6–18 km from the summit with a thickness of 6–24 cm and a maximum clast size of 1–4 cm. The diameter of the area potentially affected by heavy ash fall in the hazard zone II has been determined using the exponential thinning function based on Fierstein and Nathenson (1992), using a mathematical model which is suitable for any shape of isopach. The height of the eruption column is inferred from the distance where 2 segments of the thickness lines intersect (Sparks et al. 1991), while the dispersion index is determined based on Walker (1973). An area with a 10 km radius from the summit is thus obtained and defined as the area that could potentially be affected by ejecta and heavy ash fall (Andreastuti 1999). During the 2010 eruption, heavy ash fall and incandescent ejecta with grain sizes of 2–6 cm spread over a radius of 10 km. To anticipate major eruptions such as the 2010 events, the radius of the hazard zone from pyroclastic falls and ejecta of incandescent rock is defined at 10 km from the vent but can be expanded for larger eruptions.

Hazard Zone III

Hazard zone III is an area that is located closest to the summit and frequently affected by PDCs, lava flows, rock falls and ejected rock fragments (incandescent), and heavy ash falls (Fig. 16.6). Due to the high levels of vulnerability, permanent settlement is not allowed. The hazard zone III boundary was delineated based on deposits from historical eruptions during the past ~100 years (1900–2010), and considered dome-collapse events, explosive eruptions, morphological changes around the summit area, geological structure of the summit area, and present

dome location (if any). This zone encompasses the most vulnerable areas affected by any eruption, regardless of the type and scale of the eruption. A typical eruption at Merapi ranges between VEI 1 and VEI 3, with a maximum PDC runout of 8 km, while for large VEI 4 eruptions, PDCs can reach 15 km or more (Fig. 16.1; Siebert et al. 2010). In the event of intensified activity towards an explosive eruption, people living in hazard zone III are prioritised to be evacuated first.

Conditional Validity

The volcanic hazard map is applicable only in case of a typical eruption, where the following conditions are met: (1) the eruption occurs at the central vent/crater; (2) the eruption involves a vertical eruption column; (3) there is no occurrence of any caldera-forming events; and (4) there is no substantial morphological changes at the summit.

Map Revision

The volcanic hazard map will be revised when: (1) eruptions are greater than the anticipated range of a typical eruption (VEI > 3); or (2) in case of a new and major development in volcanology.

Recommendation

- (1) The Merapi volcanic hazard map is to be used as guidance by the local government authority (Pemerintah Daerah, in Indonesian) in disaster risk reduction efforts and as a basis for land use planning;
- (2) CVGHM coordinates with the National Disaster Management Agency (BNPB), the Government of the Central Java Province, the Special Province of Yogyakarta, the Magelang District, the Boyolali District, and the Klaten and Sleman Regencies on the current Merapi volcanic activity; and
- (3) At the time of high intensity rain, people who live in the riverbank area on the slope of Merapi need to be aware of the possibility of lahar occurrence.

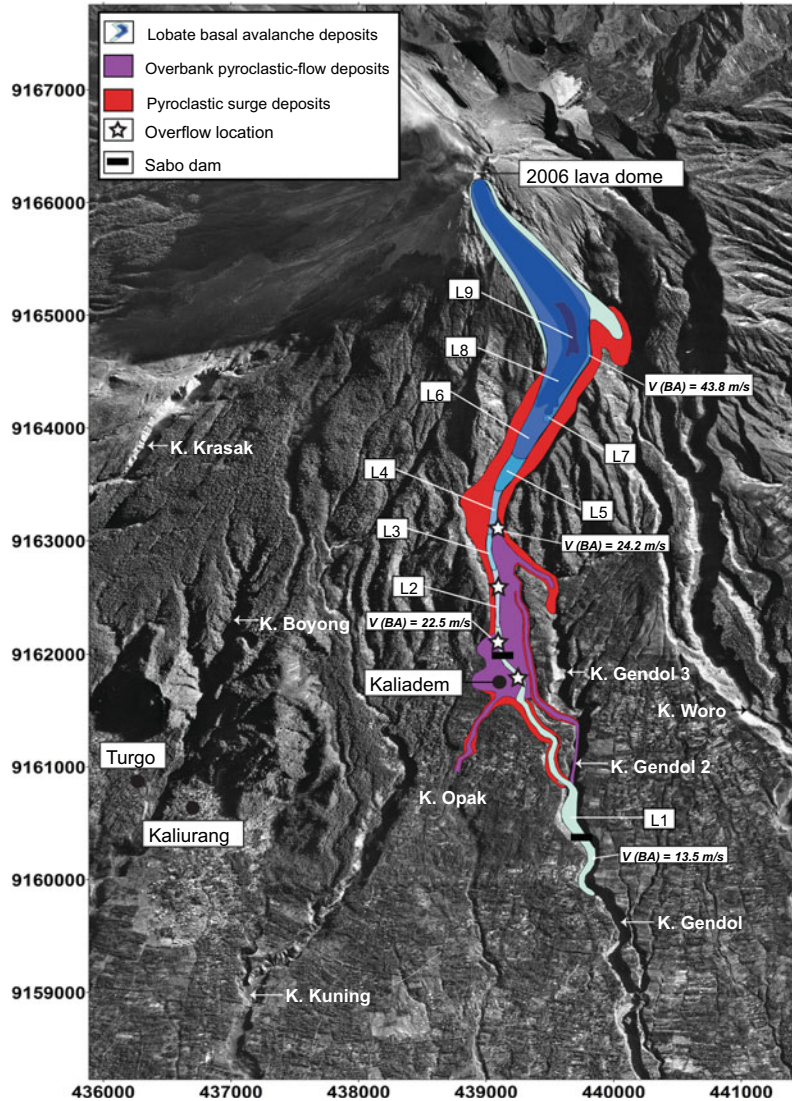
16.3 Case Study 1: Field Data Acquisition and Numerical Simulations of the 2006 PDCs

16.3.1 Summary of the 2006 Eruptive Events

The 2006 eruptive events of Merapi volcano began in July 2005 when seismicity and deformation in the summit area increased and a new lava dome extruded in April 2006 (BGVN 2007). Due to the particular location of the active lava dome, and the presence of a topographic barrier to the south of the new dome, the rockfalls and BAFs of May 2006 were mainly directed towards the south-western flank of Merapi with runout distances of typically less than 4 km (BGVN 2007; Charbonnier and Gertisser 2008). In June 2006, the main BAF activity shifted to the southern and south-eastern flanks of Merapi, with flows entering the upper Woro drainage and, predominantly, the Gendol river valley (BGVN 2007; Charbonnier and Gertisser 2008, 2011). Most of the flows in early June extended less than 5 km from the source. On 14 June, the activity peaked with two sustained dome-collapse events that generated BAFs with runout distances of 5 (14 June a.m.) and 7 km (14 June p.m.), respectively (BGVN 2007; Charbonnier and Gertisser 2008, 2011). The largest of these caused two fatalities and partial burial of the village of Kaliadem ~5 km from the summit (Fig. 16.7). After 14 June, both the number of dome-collapse events and the extent of BAFs decreased (L2–L9 in Fig. 16.7). The activity of Merapi eventually dropped to background levels in early July 2006 (BGVN 2007).

Valley-confined basal avalanche deposits (Fig. 16.7) were exposed in the main Gendol River valley, herein referred to as Kali (Indon. = river) Gendol 1, and formed nine ~100 m wide, overlapping lobes that were in part exposed for tens to hundreds of metres along their flow axis (L1–L9 in Fig. 16.7). Runout distances of individual lobes ranged from 2 to 7 km from the summit. These lobes represented a record of successive flows generated during and after the major

Fig. 16.7 Geological map of the June 2006 block-and-ash flow deposits that fill the Gendol river valley and adjacent areas on the southern flank of Merapi. Minimum velocities calculated at four locations for the Basal Avalanche (V(BA)) of the 14 June p.m. flow (L1) are also shown. Modified from Charbonnier and Gertisser (2012)



pyroclastic-flow-forming events on 14 June, with individual volumes varying between 0.08 and $2.7 \times 10^6 \text{ m}^3$ (Table 4 in Charbonnier and Gertisser 2011). The overbank pyroclastic-flow deposits outcropped mainly within an area of 0.5 km² between 3.5 and 5 km from the summit (Fig. 16.7). The June 2006 BAF deposits also had associated thin deposits from a dilute ash-cloud surge above the basal avalanche. These deposits were mostly restricted to valley margins and outer banks, ~ 1 km to the west and east at their maximum extent (Fig. 16.7). In total, the June 2006

BAF deposits covered an area of ca 1.4 km², equally distributed between basal avalanche (35.2%), overbank (28.1%) and ash-cloud surge deposits (36.7%). Their overall volume was $8.7 \times 10^6 \text{ m}^3$, with 89% of this volume accounting for basal avalanche deposits ($7.8 \times 10^6 \text{ m}^3$), 9.2% for overbank deposits ($0.8 \times 10^6 \text{ m}^3$) and only 1.8% for ash-cloud surge deposits ($0.15 \times 10^6 \text{ m}^3$). More than half of the total volume (54%) was deposited during the emplacement of the two major flows of 14 June (Charbonnier and Gertisser 2011).

16.3.2 Numerical Simulations of the 2006 Block-And-Ash Flow Events

In the first case, a single, discrete (~ 1 min) collapse of a small portion ($\sim 1.0 \times 10^6$ m³) of the 2006 lava dome to the south was simulated, where the material was shed as one pulse and generated one of the post-14 June, short- to medium-runout BAF (SM-BAFs). Due to its average values of runout distance, area covered and volume of the associated deposits within the whole range of SM-BAF deposits recognised in the field (Charbonnier and Gertisser 2008, 2011), the characteristics of lobe 5 (Fig. 16.7) were taken as a reference for evaluation of the SM-BAF simulation results.

The second example is a simulation of a sustained (~ 300 s) collapse of a significant portion ($> 1.0 \times 10^6$ m³) of the 2006 lava dome to the south, where the material was shed as several pulses and generated one of the long-runout BAFs (L-BAFs) that occurred on 14 June 2006. Due to its complete stratigraphic record and reconstitution of its deposit architecture from an extensive field-based study (Charbonnier 2009; Charbonnier and Gertisser 2011), the characteristics of the 14 June p.m. BAF were taken as a reference for the evaluation of the L-BAF simulation results.

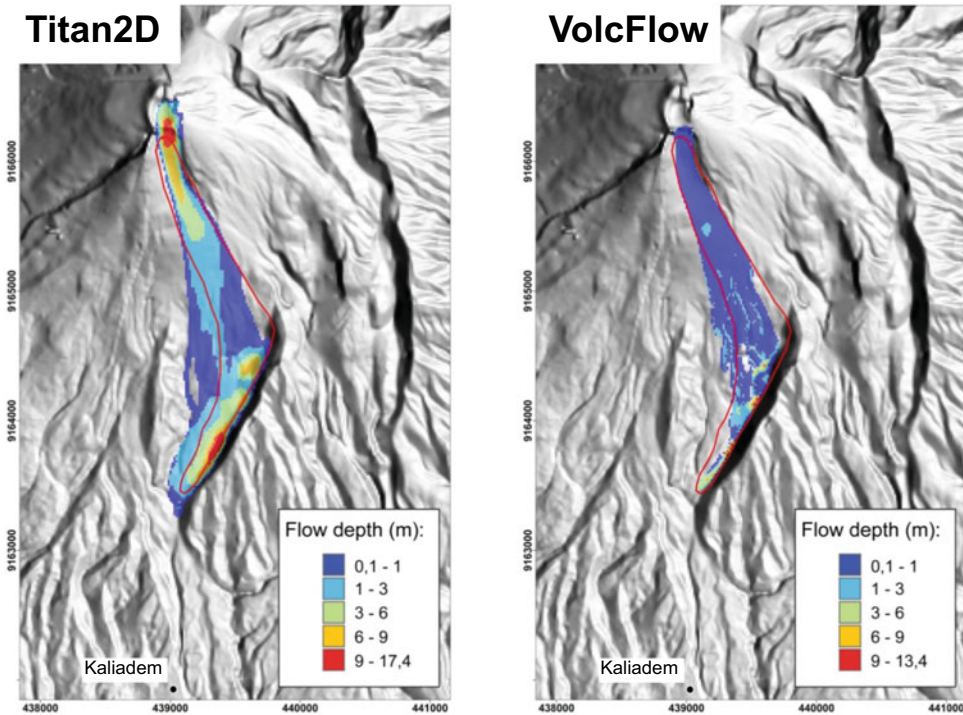
Numerical simulations of the 2006 BAFs were performed using two different rheological behaviours: a frictional (Mohr–Coulomb) behaviour with the Titan2D model, (e.g. Patra et al. 2005) and a pseudoplastic behaviour using a constant retarding stress in addition to a collisional stress component (VolcFlow model, e.g. Kelfoun and Druitt 2005). The different processing steps required to reduce uncertainties in objectively defining the different input parameters and to correctly evaluate the output variables of both models are detailed in Charbonnier and Gertisser (2012). Validation of results is discussed on the basis of best-fit values of three validation metrics based on the comparison of the areas inundated (see Charbonnier et al. 2018 for details).

16.3.2.1 Simulations of Short-to Medium-Runout 2006 Block-And-Ash Flows (SM-BAF)

Comparing the areas inundated by both models, spreading occurs for simulated flows with both models just after flow generation and before they reach the first topographic obstacle on the southern flank (Fig. 16.8). However, only the constant retarding stress model (VolcFlow) leads to a minor deposition of ~ 1 m thick deposits on open slopes $> 30^\circ$. Once the flows are channelled along the Kendil hill in the proximal Gendol valley, spreading only occurs during the depositional phase of the Titan2D simulation. This leads to final deposits that are not entirely channelled by the local drainage system but affect the whole valley floor on more than 200 m width (Fig. 16.8). Such a widespread distribution of SM-BAF deposits has not been observed in the field. By contrast, a striking feature is that the VolcFlow model is able to simulate deposit morphologies similar to the lobe 5 deposits, including a steep, lobate front with a convex morphology and comparable lateral extent and thickness distribution (Fig. 16.8). All these features are absent in the frictional model, which forms a uniform pile of deposits with greater thickness towards the centre and a relatively flat frontal region. Even if significant differences in model validation results are apparent, best-fit values (i.e. confidence or probability of safety in model results) are overall pretty high (all $> 50\%$). VolcFlow, using a pseudoplastic rheology, generally shows a better fit and higher model precision (R_{MP}) than Titan2D using a Coulomb frictional model.

16.3.2.2 Simulations of Long-Runout 2006 Block-And-Ash Flows (L-BAF)

The footprint of the inundated area by Titan2D is in close agreement with the extent of the 14 June p.m. mapped BAF deposits (Fig. 16.9). However, the complete filling of the easternmost river valley, K. Gendol 3, down to the junction with K. Gendol 2 (see Fig. 16.7 for location) and the

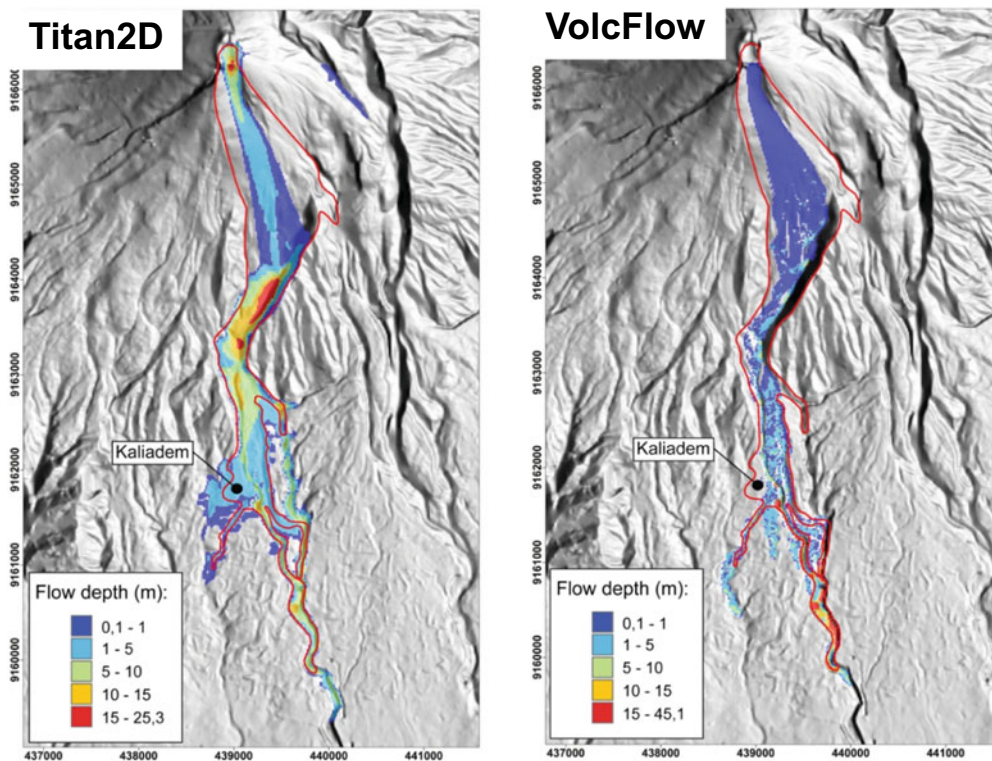


| Metric | Jaccard Fit (R_j) | | Sensitivity (R_{MS}) | | Precision (R_{MP}) | |
|----------|-----------------------|----------|--------------------------|----------|------------------------|----------|
| | Titan2D | VolcFlow | Titan2D | VolcFlow | Titan2D | VolcFlow |
| Best-fit | 54.4% | 68.3% | 92.4% | 80.6% | 59.0% | 82.9% |

Fig. 16.8 Simulation results for the SM-BAF case study. Footprints of the flow inundations and best-fit values obtained for three validation metrics are shown. Red outline is the area inundated by lobe 5. See text for explanation

widespread inundation of the Kaliadem interflue area beyond the extent of the actual deposits (Fig. 16.9) are features that were not observed for the 14 June p.m. deposits. The inundation area produced by VolcFlow is also close to that mapped in the field, in particular with the partial infilling of the upper part of K. Gendol 3 only. However, discrepancies are observed with: (1) the limited extent of the simulated deposits on the Kaliadem interflues; (2) the widespread filling of the Opak river to the southwest; ~650 m beyond the extent of the actual deposits; and (3) the overspill of the southern margin of the Opak valley, producing overbank pyroclastic flows that propagated ~550 m further to the south (Fig. 16.9). One of the most

striking features is the ability of both models to reproduce some of the local features (run-up onto obstacles and superelevation along the outside of bends) that characterise the 14 June deposits. The simulated flows slow and thicken when encountering a break in slope and a channel constriction. A change in channel width affects the flow thickness by a factor equal to that of the width change. Comparison between the distribution of the overbank deposits produced by the Titan2D L-BAF simulation and that mapped in the field illustrates the capacity of the model to simulate overbank pyroclastic flows. At each computation time-step where the simulated flow reached the four main sites of basal avalanche overspill identified in the field (red arrows and numbers in



| Metric | Jaccard Fit (R_J) | | Sensitivity (R_{MS}) | | Precision (R_{MP}) | |
|----------|-----------------------|----------|--------------------------|----------|------------------------|----------|
| Model | Titan2D | VolcFlow | Titan2D | VolcFlow | Titan2D | VolcFlow |
| Best-fit | 72.3% | 53.8% | 71.0% | 60.6% | 73.2% | 50.8% |

Fig. 16.9 Simulation results for the L-BAF case study. Footprints of the flow inundations and best-fit values obtained for three validation metrics are shown. Red

outline is the area inundated by the 14 June p.m. flow. See text for explanation

Fig. 16.2), the Titan2D model was able to reproduce the avulsion processes and trigger the development of overbank pyroclastic flows that entered the surrounding valleys (first K. Gendol 2 and 3 and then K. Opak). These correlations are not so obvious with the VolcFlow model, which lead to lower best-fit values (i.e. lower confidence in the model results) observed for the three validation metrics (Fig. 16.9).

16.3.2.3 Evaluation of Simulation Results

The results obtained in both simulations highlight the benefit of using well-constrained

geological data and key model output parameters, in this case total inundated area, to evaluate the performance and accuracy of a numerical model regarding the simulation of BAFs. The lower (but still high) best-fit values ($> 50\%$) obtained indicate that there is more than 50% chance that a BAF similar to these two 2006 BAF events will hit a location given a simulated hit. However, model results should be interpreted carefully and, if integrated into a hazard plan, done with expert advice. In doing this, the use of well-constrained geological data and validation metrics such as those described here allow the model user to calibrate and tune model-specific

input parameters in order to obtain a best-fit flow simulation with the highest model sensitivity and model precision. Careful use of such tools can provide valuable insight and assist in the PDC hazard analysis process.

16.4 Case Study 2: Field Data Acquisition and Numerical Simulations of the 2010 Pyroclastic Density Currents

16.4.1 Chronology of the Eruption

The eruption of 2010 occurred after two months of enhanced levels of all monitored parameters (e.g. seismicity, ground deformation; Aisyah et al. 2010; Subandriyo et al. 2023, Chap. 12). The first eruptive phase began on 26 October. After a short period of relative calm, a lava dome appeared on 29 October, as evidenced by incandescence. On 1 November, several PDCs reached a distance of 9 km on the southern flank. The dome growth was then extremely rapid for Merapi during the period 1–4 November and was associated with several explosions (Suroño et al. 2012; Pallister et al. 2013) that destroyed the active lava dome. By 4 November, the new summit lava dome had been rebuilt to a volume of $\sim 5 \times 10^6 \text{ m}^3$ (see Subandriyo et al. 2023, Chap. 12).

The activity peaked on 5 November with a series of dome explosions and retrogressive collapses that destroyed the new dome (Komorowski et al. 2013). The PDCs generated reached 16 km on the south flank and destroyed an area of about 22 km^2 . Another eruptive phase caused the retrogressive collapse of a large part of the summit. This was followed by a sub-Plinian phase that produced a convective plume that rose up to 17 km in height. Post-eruption images of the summit show a new, roughly circular crater with a diameter of $\sim 400 \text{ m}$, breached to the southeast (see Gertisser et al. 2023, Chap. 6; Subandriyo et al. 2023, Chap. 12).

From 5 to 8 November, the activity changed to intense degassing, and, after 8 November,

seismic activity gradually started to decrease in intensity. Satellite data indicated that dome growth ceased by 8 November, following a brief 12 h-long pulse at a remarkable rate of $\sim 35 \text{ m}^3 \text{ s}^{-1}$ (Suroño et al. 2012; Subandriyo et al. 2023, Chap. 12).

16.4.2 The Two-Layer Model

For this eruption, surges were particularly devastating and must be simulated. The depth-averaged model used, a recent version of VolFlow, couples two distinct parts: a concentrated part (here a block-and-ash flow; BAF) and a dilute part (the ash-cloud surge). Each part is simulated by a depth-averaged approach. Details and analysis of our two-layer model are described in detail in Kelfoun (2017) and Kelfoun et al. (2017). The concentrated flow is simulated by solving the system of the three governing equations (Eqs. 16.1–16.3 in Sect. 16.3.2): mass, and momentum equations in x and y . As the dilute current can be affected by strong density variation, a fourth equation of volume balance is added in the system for the simulation of the surge.

The physical behaviour of the concentrated part (deposit and concentrated pyroclastic flows) is approximated by a predominantly plastic rheology with an additional term related to the square of the velocity u which can take into account particle collisions or rock dismantling (Kelfoun et al. 2009; Charbonnier and Gertisser 2012). This rheology allows the formation of deposits of realistic thickness, extension and velocity with levee morphologies (Kelfoun 2011). The resistive stress \mathbf{T} (Eqs. 16.2 and 16.3) of a plastic flow is given by:

$$\mathbf{T} = -T_0 \frac{\mathbf{u}}{\|\mathbf{u}\|} - a_1 \rho_d \|\mathbf{u}\| \mathbf{u} \quad (16.4)$$

where T_0 is the yield strength, ρ_d is the concentrated flow density, and a_1 is a parameter that relates the velocity squared of the concentrated flow to the stress exerted.

Pyroclastic surges are considered to move in a predominantly turbulent mode (Wright et al. 1980) and their resistive stress is given by:

$$\mathbf{R} = -a_2 \rho_s \|\mathbf{v}\| \mathbf{v} \quad (16.5)$$

where a_2 is a parameter that relates the turbulent stress to the velocity squared of the surge, ρ_s is the surge density and \mathbf{v} its velocity.

Other laws describe the mass exchanges between the concentrated and the dilute currents. The particles of the flow can separate out to form the dilute current and, inversely, the dilute current can form either a basal concentrated flow or a deposit by sedimentation (Kelfoun 2017; Kelfoun et al. 2017).

16.4.3 Emplacement of the 5 November Pyroclastic Density Currents

This section describes the emplacement of the 5 November 2010 PDCs based on the numerical model detailed in Kelfoun et al. (2017). Following the collapse, a concentrated flow is formed and accelerates rapidly on the steep slope of the summit to reach a velocity of 50 m/s. The high velocity leads to the strong generation of a surge that reaches rapidly about 100 m/s. The surge acquires its own momentum and, once it has left the flow, its density decreases laterally by sedimentation. To the north of the Kendil ridge (all the locations are shown on Fig. 16.10), the flow curves to the southwest, following the Gendol valley. The surge initially follows the same path but, because its thickness increases with time, it becomes thick enough to overflow the Kendil ridge and move southward. A part of the surge detaches from the flow and moves around the east flank of the Kendil ridge to enter the Woro valley. The surge that follows the Gendol valley becomes increasingly thicker because it is continuously being generated by the underlying concentrated part. In areas where PDCs leave the Kendil ridge and reach an open area where the Gendol valley is shallower, the concentrated part overflows the Gendol drainage basin to spread out on the

interfluves. Part of the mass is channelized in the tributaries of the Opak valley and then flows along this valley for 3 kms. As the surge is no longer channelized by the hilly topography, it can now spread out, covering a large arc-shaped sector from the Kuning valley in the west to the Woro valley in the east, and reaching 8 km from the summit to the south along the Opak and Gendol valleys. The concentrated flow reaches runout distances of 6 and 15 km in the Opak and Gendol valleys, respectively.

A comparison between the simulations and the field data (Fig. 16.11) shows a good correspondence between both. The flow deposit shows similar characteristics: (1) the overall shape of the area covered by the concentrated flow; (2) the overflow into the Opak valley to the south of the Kendil ridge; and (3) the runout in the Gendol and the Opak valleys. The large overbank deposits mapped in the southern part of the Gendol valley are not reproduced but they were formed during another eruptive phase, which is not simulated here (stage 5; Komorowski et al. 2013). The thickness of one unit, nearly constant at ~ 5 m from the Kendil ridge to the deposit front, is compatible with reality. For the surge, its density is close to the value estimated (~ 5 kg/m³, Jenkins et al. 2013) as well as its thickness. The overall shape of the surge deposits corresponds to the real deposits, with a similar thickness over the whole area, and the isopachs elongated southward to form lobes that follow the main drainage basins. The surge trajectories generally coincide with the directions of the blown-down trees (Komorowski et al. 2013), and the total volume of the surge deposits fits with the field data.

16.4.4 Evaluation of Simulation Results

The depth-averaged approach seems to be adapted for the simulation of flows and surges generated by dome collapses. The model needs to be tested with other well constrained eruptions and efforts must be made towards a better understanding of the physics of these currents, in

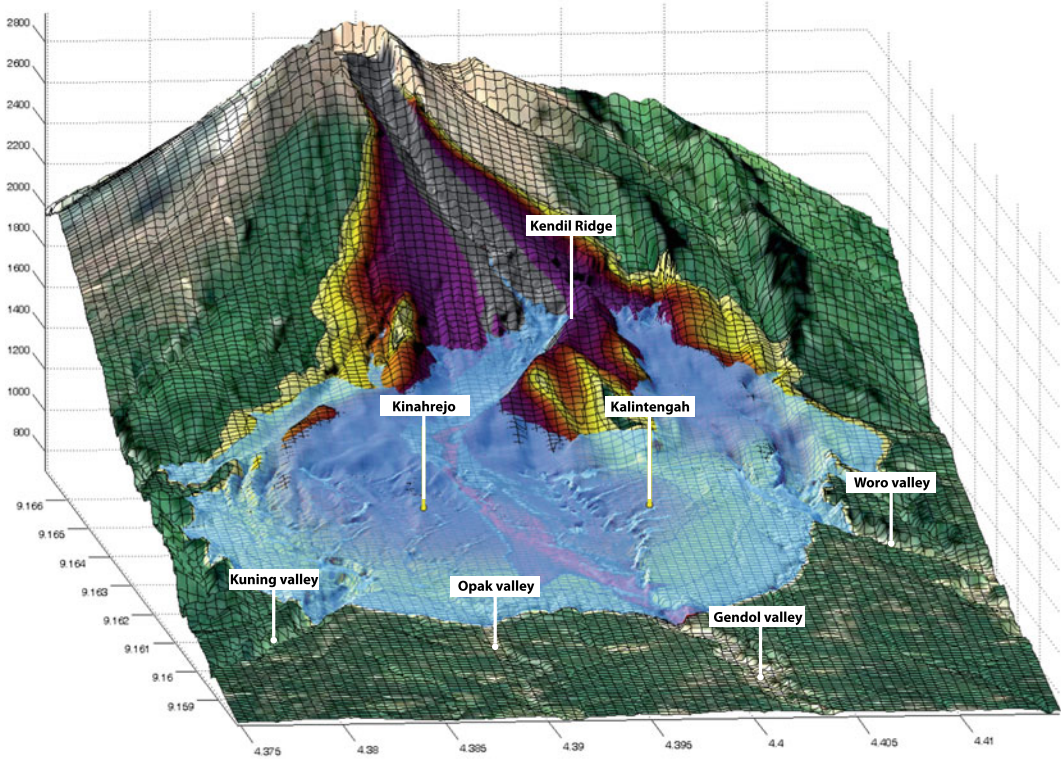


Fig. 16.10 3D view of the two-fluid simulation of the 5 November 2010 PDCs 5 min after the dome collapse. The blue part is the surge, yellow to purple is the surge deposits and grey to red is the flow

particular the mass exchanges between the concentrated and dilute currents. Nevertheless, this new model gives promising perspectives for the understanding of pyroclastic current emplacements and for future estimation of related hazards and impacts on the population, the infrastructure, and the environment.

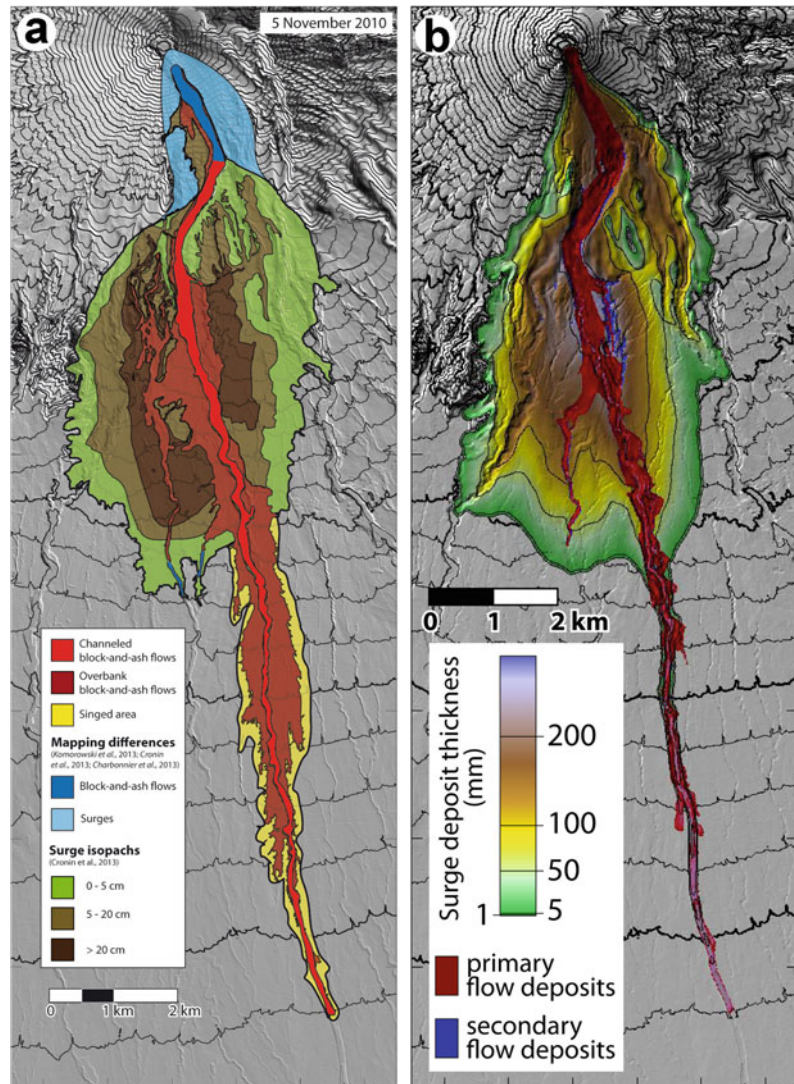
16.5 Towards an Integration of Numerical Modelling Results into Hazard Maps

The assessment and zoning of PDC-related hazards have been traditionally defined on the basis of the recognized extent of pyroclastic flow and surge deposits of historical age, or of prehistoric deposits (e.g. Crandell et al. 1984; Scott 1989). This technique is limited for active volcanoes in tropical environments like Merapi in that deposit

preservation is often poor, particularly for surges and blasts. Additionally, differences in summit topography, edifice heights and channel topography at the time prior to eruption may be unknown but could greatly affect the potential extent of future PDCs (e.g. the 2006 and 2010 eruptions). Thus, computer models based on current topography were first recognized as useful to check deposit-based hazard boundaries, and with more sophisticated development, have become a primary technique for mapping PDC hazards around active volcanoes (e.g. Cole et al. 2015).

Despite significant progress, assessments of PDC hazards are still influenced by a remarkable amount of uncertainty. The physical complexity of PDC-related processes implies that there are substantial uncertainties that cannot be neglected, stemming from the intrinsic natural variability of such processes (aleatory variability) and from our

Fig. 16.11 Map and thickness of the 5 November 2010 deposits from the field work of Charbonnier et al. (2013), Cronin et al. (2013) and Komorowski et al. (2013). **b** Map and thickness of simulated flow and surge deposits with VolcFlow (after Kelfoun et al. 2017)



lack of knowledge or available data (epistemic uncertainty). The quantification and communication of the diverse uncertainty sources affecting hazard assessments appear to be a principal future challenge.

Few recent studies have tried to fully account for uncertainties in modelling the hazard posed by PDCs. Dalbey et al. (2008) applied the Titan2D model (coupled with Polynomial Chaos Quadrature) to produce probability maps, conditional upon the occurrence of PDCs within a given volume range, at Volcán de Colima (Mexico). Bayarri et al. (2009) and Spiller et al.

(2014) developed a Bayesian emulator for the Titan2D simulator to produce hazard curves (Tonini et al. 2015) at a few locations around Soufrière Hills volcano in Montserrat. These hazard curves are conditional upon the occurrence of PDCs or applicable to a given time window. Nonetheless, the physical assumptions at the basis of Titan2D equations make it suitable only to simulate dense PDCs. More recently, Sandri et al. (2018) proposed a novel multi-volcano Probabilistic Volcanic Hazard Assessment (PVHA) of PDCs over the city of Napoli and its surroundings, in the next 50 years, by

combining the probability of PDC invasion from each volcano (assuming that they erupt independently), Somma-Vesuvius and Campi Flegrei. They model PDC invasion with the energy cone model (Malin and Sheridan 1982), accounting for flows of different mobility, and use the Bayesian Event Tree for Volcanic Hazard (BET_VH, Marzocchi et al. 2010) to incorporate other volcano-specific information such as the probability of eruption or the spatial variability in vent opening probability. A major limitation of using a simple model like the energy cone is that it cannot capture some physical processes relevant for hazard assessment such as PDC channelization (e.g. Tierz et al. 2016), relevant for the dense, basal part of PDCs. Results from these previous studies imply that the absolute validation of a model is presently impossible, despite continuous progress in the experimental validations of models at different spatial and temporal scales (e.g. Dufek 2016). Simplified 1D/2D flow models and statistically based representations of the flows could be adapted to Monte Carlo simulations to investigate model sensitivity to input parameters, such as flow volume and vent location, and to produce probabilistic hazard maps (e.g. Wadge 2009; Tierz et al. 2016). Alternatively, multidimensional and multiphase flow models are becoming increasingly effective in representing the complex behaviour of PDC phenomena and enable simulations that include remarkable details on specific scenario conditions (e.g. Esposti-Ongaro et al. 2008). However, at this time, they cannot yet be readily adapted to Monte Carlo simulations due to the excessive computing time required.

In terms of PDC hazard mapping, the risk is that hazard zones may be incautiously defined, with the margin of error dangerously disproportionate to our ability to forecast reliably PDC inundation limits. Hazard maps have traditionally been based on the maximum extent of PDCs as derived from previous eruptions. In most cases these were based on the extent of deposits from prehistoric eruptions within the geological record. However, studies of PDC-forming eruptions in the past few decades have highlighted that PDC deposits, particularly those of dilute

PDCs, leave deposits that are only a few centimetres thick and are likely to be quickly removed by erosion (e.g. Komorowski et al. 2013). Another factor is that the topography of a volcano changes dramatically with time. Removal and deposition of vast amounts of materials can occur during the tens of thousands of years represented by the base data for map construction. This changed topography is a major uncertainty in the comparison of past deposits with a prediction of areas of future inundation (e.g. Sheridan et al. 2010). Finally, the volumes, styles of emplacement, and source starting locations are poorly known in many cases. This leads to a large uncertainty in initial conditions. Thus, hazard maps solely based on the geological record may provide only a limited perspective and should be treated with extreme caution as they are likely to seriously underestimate the true extent of future PDCs (e.g. Cole et al. 2015).

The current Merapi hazard map is based on a compilation of various pieces of information, including geomorphology, geology, eruptive history, coverage of previous eruptive products, research, and field studies (Hadisantono et al. 2002). However, the current map does not integrate results from recent numerical modelling studies. Recent efforts have been made to promote the use of numerical models of PDCs for hazard assessment (e.g. Ogburn and Calder 2017). Validation and benchmarking exercises can inform users of the uncertainties, strengths and weaknesses of different models for their use in research and hazard management (e.g. Gueugneau et al. 2021). In particular for the generation of PDC hazard maps, model choices need to be defensible for each set of flow scenarios considered. Benchmarking can also constrain the circumstances under which each model performs best. Outcomes of such community-wide efforts could provide the basis for establishing an interpretation framework and defining the 'best practices' to conduct rigorous PDC hazard assessments. Such guidelines could be widely distributed to correctly inform and advise geological surveys worldwide about the breadth and depth of understanding of methodologies and procedures currently available for

undertaking rigorous PDC hazard assessments and formats of those assessments at other active volcanoes like Merapi.

Acknowledgements Field work following the 2010 eruption was funded through the National Science Foundation (NSF) RAPID grant 1114852. SJC thanks Laura Connor for her assistance with the Titan2D and VolcFlow probabilistic modelling. The authors would like to thank our Indonesian colleagues at the Center of Volcanology and Geological Hazard Mitigation (CVGHM) at the Merapi Volcano Observatory, Yogyakarta, for fruitful discussions about the 2006 and 2010 eruptions and PDC hazard assessment at Merapi volcano. We also thank the editor Ralf Gertisser and reviewer Lucia Capra for their constructive comments.

References

- Abdurachman EK, Bourdier JL, Voight B, Kelfoun K (2000) Nuées ardentes of 22 November 1994 at Merapi Volcano, Indonesia. *J Volcanol Geotherm Res* 100:345–361
- Andreastuti SD (1999) Stratigraphy and geochemistry of Merapi volcano, Central Java, Indonesia: implication for assessment of volcanic hazards. PhD thesis, The University of Auckland, New Zealand
- Aisyah N, Sumarti S, Sayudi DS, Budi-Santoso A, Muzani M, Dwiyono S, Sunarto, Kurniadi (2010) Aktivitas G. Merapi period September–December 2010 (Erupsi G. Merapi 26 October–7 November 2010), *Bull Berkala Merapi* 07/03
- Badan Nasional Penanggulangan Bencana (BNPB), Indonesia (2011) Rencana aksi rehabilitasi dan rekonstruksi wilayah pasca bencana erupsi Gunung Merapi di Provinsi D.I. Yogyakarta dan Provinsi Jawa Tengah 2011–2013 (The action plan of post-disaster rehabilitation and reconstruction of Merapi volcano eruption in Yogyakarta and Central Java Provinces, 2011–2013). BAPPENAS and BNPB, Jakarta, p 205
- Badan Pusat Statistik (BPS), Indonesia (2011) Population of Indonesia—result of population census 2010. BPS No. 04110.1202, p 706
- Badan Standardisasi Nasional (BSN), Indonesia (1998) SNI 13, 4689-1998, Penyusunan peta kawasan rawan bencana gunung api (Preparation of maps of volcanic hazard-prone areas), Badan Standardisasi Nasional, p 23
- Bardintzeff JM (1984) Merapi Volcano (Java, Indonesia) and Merapi-type Nuées Ardentes. *Bull Volcanol* 47 (3):433–446
- Bayarri M, Berger JO, Calder ES, Dalbey K, Lunagomez S, Patra AK, Pitman EB, Spiller ET, Wolpert RL (2009) Using statistical and computer models to quantify volcanic hazards. *Technometrics* 51(4):402–413
- Beget JE, Limke AJ (1988) Two-dimensional kinematic and rheological modelling of the 1912 pyroclastic flow, Katmai, Alaska. *Bull Volcanol* 56:148–160
- Berthommier P, Bahar I, Boudon G, Camus G, Gourgaud A, Lajoie J, Vincent P-M (1992) Le Merapi et ses eruptions: importance des mecanismes phreatomagmatiques. *Bull Soc Geol Fr* 5:635–644
- BGVN (2007) Smithsonian Institution, Washington DC, 32:2
- Boudon G, Camus G, Gourgaud A, Lajoie J (1993) The 1984 nuée ardente deposits of Merapi volcano, Central Java, Indonesia: stratigraphy, textural characteristics, and transport mechanisms. *Bull Volcanol* 55:327–342
- Bourdier JL, Abdurachman E (2001) Decoupling of small-volume pyroclastic flows and related hazards at Merapi volcano, Indonesia. *Bull Volcanol* 63 (5):309–325
- Cagnoli B, Piersanti A (2017) Combined effects of grain size, flow volume and channel width on geophysical flow mobility: three-dimensional discrete element modelling of dry and dense flows of angular rock fragments. *Solid Earth* 8:177–188
- Charbonnier SJ, Gertisser R (2008) Field observations and surface characteristics of pristine block-and-ash flow deposits from the 2006 eruption of Merapi Volcano, Java, Indonesia. *J Volcanol Geotherm Res* 177:971–982
- Charbonnier SJ (2009) The dynamics and hazards of small-volume pyroclastic flows: a case study of the 2006 eruption of Merapi volcano, Java, Indonesia. PhD Dissertation, Keele University, United Kingdom, p 347
- Charbonnier SJ, Gertisser R (2011) Deposit architecture and dynamics of the 2006 block-and-ash flows of Merapi Volcano, Java, Indonesia. *Sedimentology* 58 (6):1573–1612
- Charbonnier SJ, Gertisser R (2012) Evaluation of geophysical mass flow models using the 2006 block-and-ash flows of Merapi Volcano, Java, Indonesia: towards a short-term hazard assessment tool. *J Volcanol Geotherm Res* 231–232:87–108
- Charbonnier SJ, Germa A, Connor CB, Gertisser R, Preece K, Komorowski JC, Lavigne F, Dixon TH, Connor LJ (2013) Evaluation of the impact of the 2010 pyroclastic density currents at Merapi volcano from high-resolution satellite imagery analysis, field investigations and numerical simulations. *J Volcanol Geotherm Res* 261:295–315
- Charbonnier SJ, Connor CB, Connor LJ, Ogburn S, Calder E, Gertisser R (2016) Validation of depth-averaged models for pyroclastic density currents (PDCs): examples from Merapi and Soufriere Hills volcanoes. Abstract, Uncertainty in Geoscience Workshop, Buffalo, USA, 15–18 March 2016
- Charbonnier SJ, Connor CB, Connor LJ, Sheridan MF, Oliva-Hernandez JP, Richardson JA (2018) Modeling the October 2005 lahars at Panabaj (Guatemala). *Bull Volcanol*: 80:4
- Cole PD, Neri A, Baxter PJ (2015) Hazards from pyroclastic density currents. In: Sigurdsson H, Houghton B, McNutt SR, Rymer H, Stix J (eds) *The encyclopedia of volcanoes*, 2nd ed. Academic Press, New York, pp 943–956

- Crandell DR, Booth B, Kazumadinata K, Shimozuru D, Walker GPL, Westercamp D (1984) Source book for volcanic hazards zonation. UNESCO, p 97
- Cronin SJ, Lube G, Sayudi DS, Sumarti S, Suroño S (2013) Insights into the October–November 2010 Gunung Merapi eruption (Central Java, Indonesia) from the stratigraphy, volume and characteristics of its pyroclastic deposits. *J Volcanol Geotherm Res* 261:244–259
- CVGHM (2006) In: Ratdomopurbo et al. (eds) *Prekursor erupsi gunung Merapi (Precursors of Merapi eruptions)*. Geological Agency, Energy and Mineral Resources Department, p 87
- CVGHM (2016) *Erupsi Merapi 2010 (2010 Merapi eruption)*. Badan Penyelidikan dan Pengembangan Teknologi Kebencanaan Geologi (BPPTKG), Geological Agency, Energy and Mineral Resources Department, vol 1, p 231
- Dalbey K, Patra AK, Pitman EB, Bursik MI, Sheridan MF (2008) Input uncertainty propagation methods and hazard mapping of geophysical mass flows. *J Geophys Res* 113:B05203
- Darteville S, Rose WI, Stix J, Kelfoun K, Vallance JW (2004) Numerical modelling of geophysical granular flows: 2. Computer simulations of plinian clouds and pyroclastic flows and surges. *Geochem Geophys Geosys* 5(8):1–36
- Druitt TH, Calder ES, Cole PD, Hoblitt RP, Loughlin SC, Norton GE, Ritchie LJ, Sparks RS, Voight B (2002) Small-volume, highly mobile pyroclastic flows formed by rapid sedimentation from pyroclastic surges at Soufrière Hills volcano, Montserrat: an important volcanic hazard. In: Druitt TH, Kokelaar BP (eds) *The eruption of Soufrière Hills volcano, Montserrat, from 1995 to 1999*. *Mem Geol Soc London*, vol 21, pp 263–280
- Dufek J (2016) The fluid mechanics of pyroclastic density currents. *Ann Rev Fluid Mech* 48:459–485
- Esposti Ongaro T, Neri A, Menconi G, de Michieli VM, Marianelli P, Cavazzoni C, Erbacci G, Baxter PJ (2008) Transient 3D numerical simulations of column collapse and pyroclastic density current scenarios at Vesuvius. *J Volcanol Geotherm Res* 178:378–396
- Esposti Ongaro T, Clarke AB, Voight B, Neri A, Widiwijayanti C (2012) Multiphase flow dynamics of pyroclastic density currents during the May 18, 1980 lateral blast of Mount St. Helens. *J Geophys Res* 117:535–538
- Fierstein J, Nathenson M (1992) Another look at the calculation of fallout tephra volumes. *Bull Volcanol* 54:156–167
- Gertisser R, Cassidy NJ, Charbonnier SJ, Nuzzo L, Preece K (2012) Overbank block-and-ash flow deposits and the impact of valley-derived, unconfined flows on populated areas at Merapi volcano, Java, Indonesia. *Nat Haz* 60:623–648
- Gertisser R, del Marmol M-A, Newhall C, Preece K, Charbonnier S, Andreastuti S, Handley H, Keller J (2023) Geological history, chronology and magmatic evolution of Merapi. In: Gertisser R, Troll VR, Walter TR, Nandaka IGMA, Ratdomopurbo A (eds) *Merapi volcano—geology, eruptive activity, and monitoring of a high-risk volcano*. Springer, Berlin, Heidelberg, pp 137–193
- Haddad B, Pastor M, Palacios D, Muñoz-Salinas E (2010) A SPH integrated model for Popocatepetl 2001 lahar (Mexico): sensitivity analysis and runout simulation. *Eng Geol* 114:312–329
- Hadisantono RD, Andreastuti SD, Abdurrachman EK, Sayudi DS, Nurnusanto I, Martono A, Sumpena AD, dan Muzani M (2002) *Peta Kawasan Rawan Bencana, Jawa Tengah dan Daerah Istimewa Yogyakarta*; Bandung: Pusat Vulkanologi dan Mitigasi Bencana Geologi
- Hartmann MA (1935) Die Ausbrüche des G. Merapi (Mittel-Java) bis zum Jahre 1883. *Neues Jahrb Für Mineral* 75:127–162
- Hungr O, McDougall S (2009) Two numerical models for landslide dynamic analysis. *Comp Geosc* 35:978–992
- Itoh H, Takahama J, Takahashi M, Miyamoto K (2000) Hazard estimation of the possible pyroclastic flow disasters using numerical simulation related to the 1994 activity at Merapi Volcano. *J Volcanol Geotherm Res* 100:503–516
- Iverson RM, Schilling SP, Vallance JW (1998) Objective delineation of lahar-inundation hazard zones. *Geol Soc Amer Bull* 110:972–984
- Jenkins S, Komorowski J-C, Baxter PJ, Spence R, Picquout A, Lavigne Suroño F (2013) The Merapi 2010 eruption: an interdisciplinary impact assessment methodology for studying pyroclastic density current dynamics. *J Volcanol Geotherm Res* 261:316–329
- Kelfoun K, Legros F, Gourgaud A (2000) A statistical study of trees damaged by the 22 November 1994 eruption of Merapi volcano (Java, Indonesia): relationships between ash-cloud surges and block-and-ash flows. *J Volcanol Geotherm Res* 100:379–393
- Kelfoun K, Druitt TH (2005) Numerical modelling of the emplacement of Socompa rock Avalanche, Chile. *J Geophys Res* 110:B12202
- Kelfoun K, Samaniego P, Palacios P, Barba D (2009) Testing the suitability of frictional behaviour for pyroclastic flow simulation by comparison with a well-constrained eruption at Tungurahua volcano (Ecuador). *Bull Volcanol* 71(9):1057–1075
- Kelfoun K (2011) Suitability of simple rheological laws for the numerical simulation of dense pyroclastic flows and long-runout volcanic avalanches. *J Geophys Res* 116:B08209
- Kelfoun K (2017) A two-layer depth-averaged model for both the dilute and the concentrated parts of pyroclastic currents. *J Geophys Res*. <https://doi.org/10.1002/2017JB014013>
- Kelfoun K, Gueugneau V, Komorowski JC, Aisyah N, Cholik N (2017) Simulation of block-and-ash flows and ash-cloud surges of the 2010 eruption of Merapi volcano with a two-fluid layer model. *J Geophys Res* 122. <https://doi.org/10.1002/2017JB013981>

- Kemmerling GLL (1931) Beshouwigen over de her-nieuwde werking van den Merapi der Vorstenlanden van December 1930. Tijdschr Kon Ned Aardr Genoot 48(2):712–743
- Komorowski J-C, Jenkins S, Baxter PJ, Picquout A, Lavigne F, Charbonnier S, Gertisser R, Preece K, Cholik N, Budi-Santoso A, Surono (2013) Paroxysmal dome explosion during the Merapi 2010 eruption: processes and facies relationships of associated high-energy pyroclastic density currents. *J Volcanol Geotherm Res* 261(1):260–294
- Lube G, Cronin SJ, Thouret Surono J-C (2011) Kinematic characteristics of pyroclastic density currents at Merapi and controls on their avulsion from natural and engineered channels. *Geol Soc Am Bull* 123(5–6):1127–1140
- Malin MC, Sheridan MF (1982) Computer-assisted mapping of pyroclastic surges. *Science* 217:637–640
- Marzocchi W, Sandri L, Selva J (2010) BET_VH: a probabilistic tool for long-term volcanic hazard assessment. *Bull Volcanol* 72:705–716
- McEwen AS, Malin MC (1989) Dynamics of Mount St. Helens' 1980 pyroclastic flows, rockslide-avalanche, lahars, and blast. *J Volcanol Geotherm Res* 37:205–231
- McDougall S, Hungr O (2004) A model for the analysis of rapid landslide motion across three-dimensional terrain. *Can Geotech J* 41:1084–1097
- Neri A, Macedonio G (1996) Numerical simulation of collapsing volcanic columns with particles of two sizes. *J Geophys Res* 101:8153–8174
- Neri A, Esposti Ongaro T, Macedonio G, Gidaspow D (2003) Multiparticle simulation of collapsing volcanic columns and pyroclastic flows. *J Geophys Res* 108:2202
- Newhall C, Bronto S, Alloway B, Banks NG, Bahar I, del Marmol MA, Hadasantono RD, Holcomb RT, MCGeehin J, Miksic JN, Rubin M, Sayudi SD, Sukhyar R, Andreastuti SD, Tilling RI, Torley R, Trimble D, Wirakusumah AD (2000) 10,000 years of explosive eruptions of Merapi Volcano, Central Java: archaeological and modern implications. *J Volcanol Geotherm Res* 100:9–50
- Neumann van Padang M (1933) De uitbarsting van den Merapi (Midden Java) in de jaren 1930–1931. *Vulkanol Seismol Med* 12:1–116
- Ogburn SE, Calder ES (2017) The relative effectiveness of empirical and physical models for simulating the dense undercurrent of pyroclastic flows under different emplacement conditions. *Front Earth Sci* 5:83
- Pallister JS, Schneider DJ, Griswold JP, Keeler RH, Burton WC, Noyles C, Newhall CG, Ratdomopurbo A (2013) Merapi 2010 eruption—chronology and extrusion rates monitored with satellite radar and used in eruption forecasting. *J Volcanol Geotherm Res* 261:138–146
- Pardiyanto L, Reksowirogo LD, Mitrohartono FXS, Hardjowarsito SH (1978) Volcanic hazard map, Merapi volcano, central Java (1/100 000), Geol. Survey of Indonesia, II, 14, Ministry of Mines, Bandung
- Patra AK, Bauer AC, Nichita CC, Pitman EB, Sheridan MF, Bursik MI, Rupp B, Webber A, Stinton AJ, Namikawa LM, Renschler CS (2005) Parallel adaptive simulation of dry avalanches over natural terrain. *J Volcanol Geotherm Res* 139:1–22
- Purbo-Hadiwijoyo MM, Suryo I (1980) Distribution pattern of the Merapi volcanic debris, South Central Java. In: V.S.I. (ed), *Volcanologi Merapi*, pp 276–290
- Ratdomopurbo A, Beauducel F, Subandriyo J, Agung Nandaka IGM, Newhall CG, Suharna, Sayudi DS, Suparwaka H, Sunarta (2013) Overview of the 2006 eruption of Mt. Merapi. *J Volcanol Geotherm Res* 261:87–97
- Rossano S, Mastrolorenzo G, De Natale G (2004) Numerical simulation of pyroclastic density currents on Campi Flegrei topography: a tool for statistical hazard estimation. *J Volcanol Geotherm Res* 132:1–14
- Salvatici T, Di Roberto A, Di Traglia F, Bisson M, Morelli S, Fidolini F, Bertagnini A, Pompilio M, Hungr O, Casagli N (2016) From hot rocks to glowing avalanches: Numerical modelling of gravity-induced pyroclastic density currents and hazard maps at the Stromboli volcano (Italy). *Geomorphology* 273:93–106
- Sandri L, Tierz P, Costa A, Marzocchi W (2018) Probabilistic hazard from pyroclastic density currents in the Neapolitan area (Southern Italy). *J Geophys Res* 123:3474–3500
- Saucedo R, Macias JL, Sheridan MF, Bursik MI, Komorowski JC (2005) Modelling of pyroclastic flows of Colima Volcano, Mexico: implications for hazard assessment. *J Volcanol Geotherm Res* 139:103–115
- Sayudi DS, Aisyah N, Juliani Dj, Muzani M (2010) Peta Kawasan Rawan Bencana Gunungapi Merapi, Jawa Tengah dan Daerah Istimewa Yogyakarta 2010 (Merapi Hazard Map, Central Java and Yogyakarta Special Region Provinces). Center for Volcanology and Geological Hazard Mitigation (CVGHM), Bandung
- Schilling SP (1998) LAHARZ: GIS programs for automated mapping of lahar-inundation zones. US Geol Survey, Open-file Report 98–638
- Schwarzkopf LM, Schmincke H-U, Troll VR (2002) Friction marks on blocks from pyroclastic flows at the Soufriere Hills volcano, Montserrat: implications for flow mechanisms: comment. *Geology* 30:190–190
- Schwarzkopf LM, Schmincke H-U, Cronin SJ (2005) A conceptual model for block-and-ash flow basal avalanche transport and deposition, based on deposit architecture of 1998 and 1994 Merapi flows. *J Volcanol Geotherm Res* 139:117–134
- Scott WE (1989) Volcanic-hazards zonation and long-term forecasts. In: Tilling RI (Ed.) *Volcanic hazards short course presented at 28th International geology congress AGU, Washington DC*, pp 25–49
- Siswowardjoyo S, Suryo I, Yokoyama I (1995) Magma eruption rates of Merapi volcano, Central Java, Indonesia, during one century (1890–1992). *Bull Volcanol* 57:111–116

- Sheridan MF, Malin MC (1983) Application of computer-assisted mapping to volcanic hazard evaluation of surge eruption: Vulcano, Lipari, and Vesuvius. *J Volcanol Geotherm Res* 17:187–202
- Sheridan MF, Patra AK, Dalbey K, Hubbard B (2010) Probabilistic digital hazard maps for avalanches and massive pyroclastic flows using TITAN2D. *Geol Soc Am Spec Paper* 464:1–11
- Siebert L, Simkin T, Kimberly P (2010) *Volcanoes of the World*, 3rd ed. University of California Press, p 568
- Spiller ET, Bayarri M, Berger JO, Calder ES, Patra AK, Pitman EB, Wolpert RL (2014) Automating emulator construction for geophysical hazard maps. *SIAM/ASA J Uncert Quant* 2(1):126–152
- Solikhin A, Thouret J-C, Liew SC, Gupta A, Sayudi DS, Oelher J-F, Kassouk Z (2015) High-spatial-resolution imagery helps map deposits of the large (VEI 4) 2010 Merapi volcano eruption and their impact. *Bull Volcanol* 77(20)
- Sparks RSJ, Bursik MI, Ablay GJ, Thomar RME, Carey SN (1991) Sedimentation of tephra fall deposits. *Bull Volcanol* 54:685–695
- Subandriyo, Gertisser R, Aisyah N, Humaida H, Preece K, Charbonnier S, Budi-Santoso A, Handley H, Sumarti S, Sayudi DS, Nandaka IGMA, Wibowo HE (2023) An overview of the large-magnitude (VEI 4) eruption of Merapi in 2010. In: Gertisser R, Troll VR, Walter TR, Nandaka IGMA, Ratdomopurbo A (eds) *Merapi volcano—geology, eruptive activity, and monitoring of a high-risk volcano*. Springer, Berlin, Heidelberg, pp 353–407
- Surono JP, Pallister J, Boichu M, Buongiorno MF, Budisantoso A, Costa F, Andreastuti S, Prata F, Schneider D, Clarisse L, Humaida H, Sumarti S, Bignami C, Griswold J, Carn S, Oppenheimer C, Lavigne F (2012) The 2010 explosive eruption of Java's Merapi volcano—a '100-year' event. *J Volcanol Geotherm Res* 241–242:121–135
- Suryo I, Clarke MCG (1985) The occurrence and mitigation of volcanic hazards in Indonesia as exemplified at the Mount Merapi, Mount Kelud and Mount Galunggung volcanoes. *Q J Eng Geol Lond* 18:78–98
- Tierz P, Sandri L, Costa A, Zaccarelli L, Di Vito MA, Sulpizio R, Marzocchi W (2016) Suitability of energy cone for probabilistic volcanic hazard assessment: Validation tests at Somma Vesuvius and Campi Flegrei (Italy). *Bull Volcanol* 78(11):79
- Thouret J-C, Lavigne F, Kelfoun K, Bronto S (2000) Toward a revised hazard assessment at Merapi volcano, Central Java. *J Volcanol Geotherm Res* 100:479–502
- Tonini R, Sandri L, Thompson MA (2015) PyBetVH: A Python tool for probabilistic volcanic hazard assessment and for generation of Bayesian hazard curves and maps. *Comp Geosci* 79:38–46
- Valentine GA, Wohletz KH, Kieffer SW (1992) Effects of topography on facies and compositional zonation in caldera-related ignimbrites. *Geol Soc Am Bull* 104:154–165
- Voight B, Constantine EK, Sismowidjoyo S, Torley R (2000) Historical eruptions of Merapi Volcano, Central Java, Indonesia, 1768–1998. *J Volcanol Geotherm Res* 100:69–138
- Wadge G (2009) Assessing the pyroclastic flow hazards from dome collapse at Soufriere Hills Volcano, Montserrat. In: Thordarsson T, Self S, Larsen G, Rowlands SK, Hoskuldsson A (eds) *Studies in volcanology: the legacy of George Walker*. *Geol Soc Lond Spec Pub*, vol 2, pp 211–224
- Walker GPI (1973) Explosive volcanic eruptions, a new classification scheme. *Geologische Rundsch* 62:431–446
- Widiwijayanti C, Voight B, Hidayat D, Schilling SP (2009) Objective rapid delineation of areas at risk from block-and-ash pyroclastic flows and surges. *Bull Volcanol* 71:687–703
- Wohletz KH, McGetchin TR, Sandford MT, Jones EM (1984) Hydrodynamic aspects of caldera-forming eruptions: numerical models. *J Geophys Res* 89:8269–8285
- Wright JV, Smith AL, Self S (1980) A working terminology of pyroclastic deposits. *J Volcanol Geotherm Res* 8(2–4):315–336
- Yamashita S, Miyamoto K (1993) Model of pyroclastic flow and its numerical simulation, sediment problems—strategies for monitoring, prediction and control. *IAHS Publ* 217:67–74



Merapi's Lahars: Characteristics, Behaviour, Monitoring, Impact, Hazard Modelling and Risk Assessment

Jean-Claude Thouret, Nurnaning Aisyah, Susanna F. Jenkins, Edouard de Bélizal, Sulistiyani, Sylvain J. Charbonnier, Dewi Sri Sayudi, I Gusti Made Agung Nandaka, Guérolé Mainsant, and Akhmad Solikhin

Abstract

Lahar is an Indonesian term, and Merapi volcano is arguably one of the most renowned lahar producers worldwide. Frequent and voluminous lahars at Merapi result from a combi-

nation of four factors: (1) large volumes of pyroclastic debris, in particular dome growth and collapse block-and-ash flows (BAF); (2) high frequency of eruptions; (3) abundant rainfall with intensities and durations regularly exceeding critical thresholds, and (4) a dense drainage network incising the steep summit topography. The majority of Merapi's lahars are rain triggered, occurring for two to four years after moderate, magmatic BAF-producing eruptions; however, during large eruptions, liquefaction of BAF deposits in the river channels can also cause lahars. Merapi lahars have moderate sediment concentrations of 20–50 vol.%, mean velocities between 2.5 and 7.5 m/s, moderate peak discharges ($< 600 \text{ m}^3/\text{s}$), and runout distances rarely exceeding 20 km. Beyond 20 km, hyperconcentrated flows and muddy floods propagate across the ring plain and through the city of Yogyakarta (637,000 people). Post-2010 lahar damage assessments revealed that most weak masonry buildings on Merapi can be destroyed by dilute lahars with low velocities c. 3 m/s and dynamic pressures $< 10 \text{ kPa}$. At least 372,000 of the 1,300,000 people living within a 30 km radius of Merapi's summit are located in the path of potentially harmful flows conveyed by radial rivers. Despite limited resources, lahar monitoring at Merapi has considerably improved since the 2010 eruption. Warning systems

J.-C. Thouret (✉)
Université Clermont-Auvergne, Laboratoire Magmas
Et Volcans, CNRS, OPGC Et IRD, Campus les
Cézeaux, 6 avenue Blaise Pascal, 63178 Aubière,
France
e-mail: j-claude.thouret@uca.fr

N. Aisyah · Sulistiyani · D. S. Sayudi ·
I G. M. A. Nandaka
BPPTKG, Merapi Volcano Observatory, Center of
Volcanology and Geologic Hazard Mitigation
CVGHM, Yogyakarta, Indonesia

A. Solikhin
CVGHM, Bandung, Indonesia

S. F. Jenkins
Earth Observatory of Singapore EOS, Nanyang
Technological University, Singapore, Singapore

E. de Bélizal
Laboratoire Mosaïques, Université Paris-Nanterre,
UMR LAVUE 7218 CNRS, Nanterre, France

S. J. Charbonnier
School of Geosciences, USF University of South
Florida, 4202 E Fowler Avenue, Tampa, USA

G. Mainsant
Laboratoire Magmas Et Volcans, Now at Institut
Supérieur de L'Aéronautique Et de L'Espace,
Université Clermont-Auvergne, Toulouse, France

based on 24 lahar monitoring stations have been implemented, supporting efficient evacuations when lahars did occur. Building on previous, semi-empirical, operational hazard-zone maps following the 2010 eruption, we present the first FLO-2D lahar simulations over LiDAR-derived topography. A risk mapping assessment encompassing physical and socio-economic factors at the village scale along rivers likely to be affected by lahars and BAFs provides a risk map for future lahars at Merapi.

Keywords

Lahar · Debris flow · Hyperconcentrated flow · Hazards · Merapi volcano · Lahar behaviour · Monitoring · Impacts · Modelling · Risk

17.1 Introduction

Nearly 60% of people in Indonesia live on the central island of Java and an estimated 10% of Javanese are exposed to disasters induced by eruptions from any of the 22 historically active (since 1600 CE) Javanese volcanoes (Amri et al. 2016). Merapi volcano, located in the most densely populated area of Central Java (Fig. 17.1) is the most iconic volcano of Java and arguably Indonesia, and one of the most active and dangerous volcanoes in the world. The slopes and ring plain of Merapi contain two world class temples (the eighth–tenth century Buddhist Borobudur and the Hindu Prambanan temples), and many other historic stupas and temples built during the Sailendra and Sanjaya dynasties more than one thousand years ago. The black and grey stones of these temples are andesite rocks from the lava domes of the volcano. Volcaniclastic blocks and sand, deposited by Merapi’s numerous lahars and pyroclastic density currents (PDCs), are easily found in the riverbeds and banks draining the volcano, and extracted by temple builders. As many as 1.3 million people are exposed to frequent volcanic and flood threats within a radius of 30 km from the summit of Merapi. Population density on the volcano slopes (above 200 m in elevation) ranges between 600 and 1500 per km²

(Table 17.1). The south and west flanks of Merapi, the most prone to volcanic hazards from the summit dome, are part of the Yogyakarta plain, a fertile region of land replenished by nutrients derived from ashfalls. Merapi lies 28 km north of the city of Yogyakarta (population c. 637,000 in 2017), capital of the densely populated “special territory” of Yogyakarta (> 3,600,000 inhabitants in 2014), which is highly valued in Indonesian culture, history and economic life.

Merapi comprises a collection of large summit domes which, except for a few large (VEI 4) Plinian eruptions (e.g. 1872, 1930–31, 2010), have successively grown and collapsed during the available eruptive activity record spanning the past 200 years (e.g. Newhall et al. 2000; Voight et al. 2000; Gertisser et al. 2012). Merapi’s most common eruptions are of moderate magnitude (VEI ≤ 3), and typically produce block-and-ash flows (BAFs) and rockslide avalanches that result either from magmatic or gravity-driven dome collapses. These BAFs emplace typically homogeneous, semi-vesicular, block-and-ash flow deposits of mainly basaltic andesite composition, which are the primary material for lahar initiation. This chapter provides an overview of the typical characteristics, dynamics and impacts of Merapi’s lahars, as well as current efforts to monitor and model the threat to surrounding populations.

17.1.1 Terminology and Scope

Lahar is an Indonesian generic term for rapidly flowing mud-rock slurries, other than normal streamflows, that initiate on volcano flanks (Smith and Lowe 1991; Vallance 2000; Iverson 2014). As they are water saturated, both liquid and solid interactions influence their behaviour and distinguish them from volcanic debris avalanches or from jökulhlaups triggered by subglacial volcanism (Björnsson 1975, 2002). Two broad categories of lahars can be defined using sediment concentration, grain-size distribution, bulk density, and rheological properties (Pierson and Costa 1987; Jakob and Hungr 2005; Pierson 2005; Vallance and Iverson 2015):

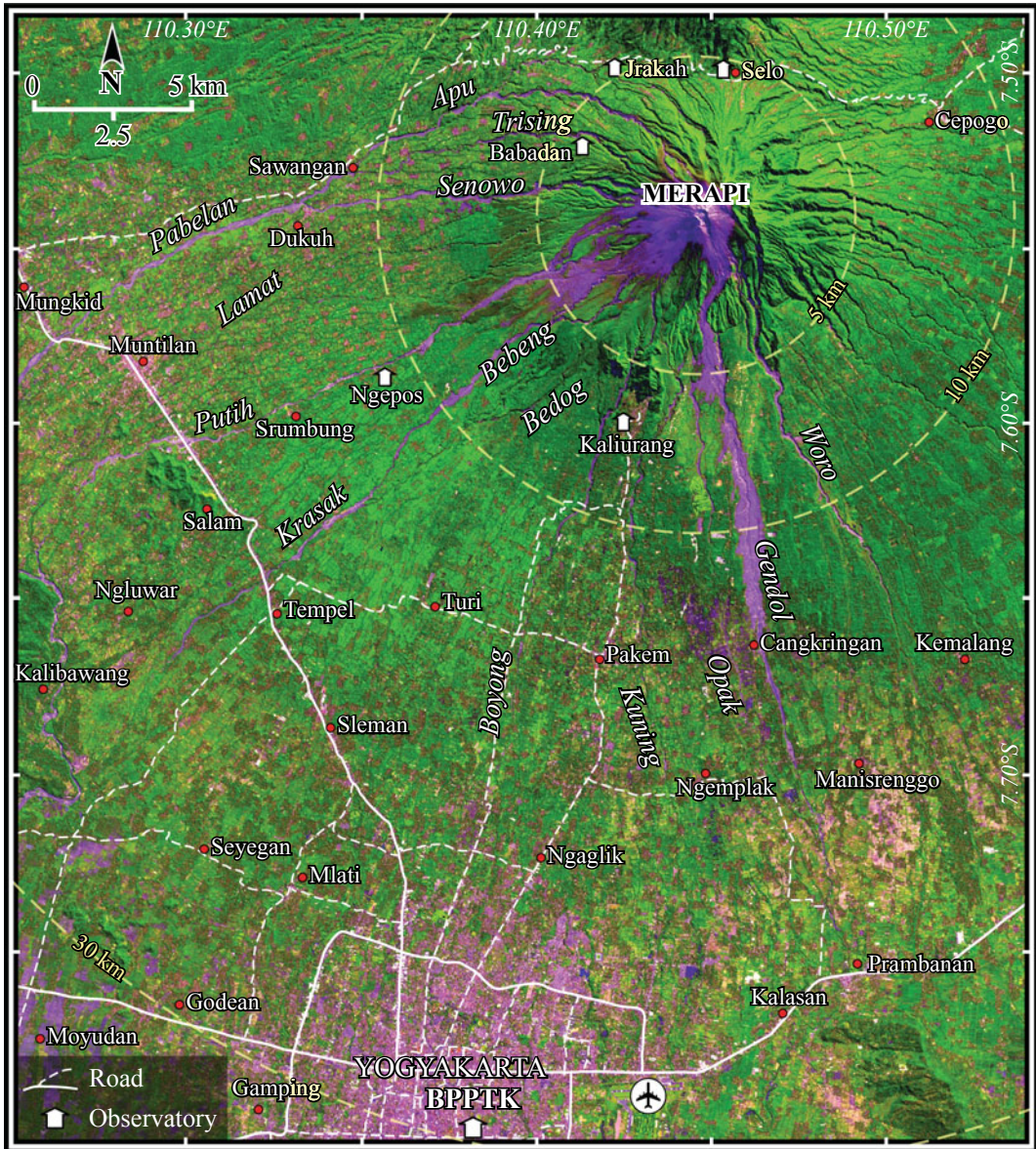


Fig. 17.1 The 13 June 2012 ASTER image shows Merapi volcano and its ring plain to the west and south including the principal rivers, the city of Yogyakarta, towns, roads, in the south and west ring plain as well as the six volcano Observatories. Purple areas indicate valleys filled by the 2010 pyroclastic deposits and 2011–12 lahar deposits (Solikhin 2015; Solikhin et al.

2015a). Pyroclastic and lahar deposits stored in valleys (purple areas) are still available for potential lahars and floods along the south and west drainages. Ongoing dome growth since August 2017 above the Gendol breach will deliver debris from dome collapses towards the uppermost Gendol valley

1. Debris flows (DFs) are mixtures of debris and water with high sediment concentrations that move downslope due to gravity as surging sediment slurries (Vallance 2000). DFs

with density ranging between 1800 and 2400 kg/m³ comprise a solid phase of at least 60 vol% (> 80 wt%), thoroughly mixed with water. The solid component includes mostly

Table 17.1 Population at risk, population density and growth around Merapi, based on Thouret et al. (2000) and updated with the 2012 Indonesian Census

| Zone of interest | Number of villages | Area (km ²) | Population 1995 ^a | Population 2012 | Population density/km ² | Population growth per year |
|-------------------------|--------------------|-------------------------|------------------------------|-----------------|------------------------------------|----------------------------|
| Elevation > 500 m | 89 | 374.5 | 258,200 | 360,400 | 962 | 1.66 |
| Forbidden zone KRB3 | 32 | 186.4 | 79,100 | 110,400 | 592 | 1.66 |
| First danger zone KRB1 | 37 | 100.3 | 114,800 | 151,900 | 1514 | 1.43 |
| Second danger zone KRB2 | 138 | 661.2 | 631,900 | 655,900 | 992 | 0.21 |
| Total elevation > 200 m | 296 | 1322.4 | 1,083,400 | 1,278,600 | 967 | 0.90 |

Source BPS (2017). Elevations < 200 m are not considered

^aAfter Lavigne et al. (2000a, b), Lavigne and Thouret (2000), BPS (2017), and unpublished BPTTKG surveys

gravel and boulders with sand, while silt and clay proportions remain low. A threshold of 3 wt% of silt and clay mineral fraction helps distinguish non-cohesive from cohesive DFs (Scott 1988). DFs show some cohesive behaviour (Major 1997; Major and Iverson 1999) as clay mineral fraction, in particular swelling clay, contributes to the development of cohesive strength (Bardou et al. 2007).

- Hyperconcentrated flows (HCFs) are two-phase flows intermediate in sediment concentration between normal streamflows and DFs with density ranging between 1300 and 1800 kg/m³. HCFs transport between 20 and 60 vol% (40 and 80 wt%) of sediment (Pierson 2005). HCFs exhibit non-Newtonian behaviour and have less internal cohesion, so that particle–particle interactions and frictional behaviour prevail in them (Mulder and Alexander 2001).

Lahar initiation mechanisms include direct transformation from debris avalanches, rapid melting of snow and ice during eruptions, outbreaks of volcanically-impounded lakes, rainfall on fresh tephra deposits (Pierson and Major 2014), and outbursts of groundwater (Wörni et al. 2012; Johnson et al. 2018). Post-eruptive, secondary lahars are more frequent and protracted at Merapi than syn-eruptive, primary lahars. As Merapi usually produces frequent

PDCs in a wet tropical climate, post-eruptive lahars have prevailed over time (Van Bemmelen 1949; Suwa and Nishimura 1992; Lavigne et al. 2000a,b; Thouret and Lavigne 2005). Lahars occurred for 2–4 years after the 1984, 1992, 1994, 1998, and 2006 eruptions, and exceptionally for 6 years after the 2010 Merapi eruption. These protracted threats may be triggered long after a large eruption, for instance as many as 10–15 years after the 1980 Mt. St-Helens event (Major 2000) and the VEI 6 Pinatubo eruption in 1991 (Pierson and Major 2014). Once initiated, lahars usually exhibit more than one flow regime along one river channel, e.g. from HCF to DF and back again (Vallance 2000). An individual lahar pulse can be broken down into three successive segments in time and space: (1) the ‘head’ or front is characterised by the densest slurry reaching the highest flow height and peak velocity, (2) the ‘body’, representing the bulk of the lahar, is characterised by packets or pulses driven by variations in particle entrainment (sediment bulking) and dilution and/or deposition (debulking), and (3) the ‘tail’ represents the recessional limb of the slurry having the lowest sediment concentration due to dilution (Pierson 1986; Manville et al. 2013).

A natural hazard impact can be defined as direct or indirect, and tangible or intangible, and is usually regarded as a loss to an environment or a society (Hausmann and Swiss Re 1998). Here,

we use impact as a collective term that includes the direct and indirect actions and consequences that lahars or DFs bear on valuables: buildings, infrastructure and networks or lifelines. We further distinguish the physical effects (e.g. land or building burial), the direct and indirect processes (e.g. loading or capillarity rise), and the ultimate damage as collapse and/or the removal of valuables, e.g. a building, dam, bridge or a vehicle. Direct loss deals with the physical effects of the hazard on individuals (death or injury) or infrastructure (reduction in functionality, failure and/or removal). Indirect loss, often underestimated, concerns the effect on society's functionality via damage to utility services or local business, the loss of revenue and jobs, the failure of networking activities, and increases in living costs and insurance. Intangible losses are defined as the psychological or cultural effects of the disasters, but they remain beyond the scope of this chapter.

17.1.2 Population at Risk

The region around Merapi supports more than 300 villages above 200 m in elevation, making the population the most exposed to the "expected annual fatality risk" from volcanic threats in Java with the exception of Semeru, East Java (e.g. Pan et al. 2015). Between 1976 and 1995, the population on a surface area of c. 390 km² of Merapi flanks and the Yogyakarta ring plain at risk from PDCs and lahars from Merapi doubled to approximately 440,000 (Thouret et al. 2000). The same area now hosts almost 1,300,000 people (BPS 2017; Table 17.1). It is estimated that 185,000 people live within 10 km distance from the Merapi summit while a record number of 1.278 million, as of 2012, live in a 30 km radius (Table 17.1). The highest recorded death toll from Merapi occurred during the 1672 eruption, which killed at least 3000 people (Dove 2008), and the total number of deaths since the sixteenth century is estimated to be around 7000 people (Thouret et al. 2000). Taking the historical, voluminous eruptions of Merapi into consideration, should a larger than VEI 4 event (e.g.,

similar to 1872) occur in the future, with hazards such as flank failure or voluminous PDCs produced by a Plinian eruption, a population > 3.5 million might be at risk in, and beyond, the special territory of Yogyakarta, from direct debris avalanche, PDC and tephra fall hazards, and subsequent lahars. Following the VEI 4 2010 eruption, hundreds of people did not return to the affected areas within the first month after impact, and the majority of villagers have since rebuilt homes at the margins of affected valleys and at the outskirts of the forbidden zone despite the National disaster management agency (BNPB) recommendations. Potential impacts from volcanic eruptions include building damage or destruction, respiratory and health issues related to ash inhalation, or death or burns from being caught in a PDC or lahar flow, and food shortage due to damage to crops and disruption to the air and road networks, not to mention indirect dire consequences on daily activities, business and transportation.

Pyroclastic density current and lahar deposits may also have positive effects on people's livelihood and hazard knowledge (de Bézizal 2013). Quarries in Merapi valleys are the core of both manual and industrial activities for building material purposes, which have steadily grown over the past three decades. As the quarries take place in the most lahar-prone channels, the workers have long acquired knowledge about lahar initiation timing and processes. A spontaneous, community-based monitoring of the river conditions was developed immediately after the 2010 eruption, with lookout stations installed in the upstream reaches of each valley. Depending on their location, villages along the rivers can be warned using radio transmitters and cell phones 15 to more than 30 min before a reported lahar might reach the quarries. Another economic motivation for villagers on Merapi, who were displaced but returned to villages declared unfit for dwelling, is the flux of tourists visiting disaster-prone areas (Naspiah et al. 2017). Resident income has increased owing to car and motorcycle rental, as well as small restaurants and shops for lucrative 'Volcano tour and exploration' tourism in all areas affected by the 2010 eruption.

17.2 Merapi, Java's Largest Lahar Producer

Merapi is one of the most prolific lahar producers in SE Asia. At least 25 of the 63 reported eruptions since 1672 CE have produced source deposits for syn-eruptive lahars, but many more post-eruptive, rain-triggered lahars occurred for years after each event (Table 17.2). Following the 22 November 1994 eruption, 31 rain-triggered lahar events were recorded in the Kali (River) Boyong between December 1994 and May 1996. Following the 2010 VEI 4 eruption, as many as 270 lahar events were triggered in 17 valleys between 2011 and 2012 (de B elizal et al. 2013; Fig. 17.2). The combined lahar deposits cover about 390 km² on the flanks and surrounding ring plain of the volcano. Lahar impacts have represented major concerns for the local authorities dedicated to hazard mapping, early warning, and disaster risk reduction.

Lahars have long been identified as the most frequent, if not most deadly, hazard at Merapi. During the Dutch colonial period, Merapi's lahars were already identified as a major threat and a critical geomorphic process in shaping Indonesian composite volcanoes and their ring plains (Van Bemmelen 1949; Verstappen 1988). They have been thoroughly studied since the end of the twentieth century, when seismic and acoustic sensors were installed (Lavigne et al. 2000b), following early video film footage and discharge measurements (Suwa and Nishimura 1992; Suwa and Sumaryono 1996). Knowledge on Merapi's lahars has then been developed through research papers dealing with flows (Lavigne et al. 2000a, b, 2007; Lavigne and Thouret 2003; de B elizal et al. 2013; Mainsant 2014; Wibowo et al. 2015; Solikhin et al. 2015a,b) and/or PDCs (Abdurachman et al. 2000; Charbonnier and Gertisser 2008, 2009; Thouret et al. 2010, 2015; Komorowski et al. 2013; Charbonnier et al. 2013), and hazard and risk assessments at Merapi (Thouret et al. 2000; Voight et al. 2000; Mei et al. 2013; Jenkins et al. 2015; Lavigne et al. 2015; Hadmoko et al. 2018). The role of lahars has also been highlighted in geological studies of Merapi

volcano based on PhD research projects (e.g. Berthommier 1990; Lavigne 1998; Solikhin 2015; Solikhin et al. 2015a; Wibowo 2016) and collated in special Journal issues (Voight et al. 2000; Newhall et al. 2000; Gertisser et al. 2012; Solikhin et al. 2015a,b). Knowledge about lahar behaviour at Merapi has steadily grown over the past decade based on in situ geophysical flow measurements, providing researchers with better inputs for accurate flow models (Widiwijayanti and Voight 2009; Charbonnier et al. 2013, 2018a, b; Mainsant 2014). At the same time, surveys on lahar hazard knowledge and risk perception (Dove 2008; Mei and Lavigne 2012; Lavigne et al. 2015) have better assessed coping strategies of people who regularly extract PDC and lahar material after each of the sizeable eruptions (de B elizal et al. 2013).

The common, low magnitude eruptions were always followed by 'secondary' rain-triggered lahars, while large eruptions (e.g. 1930–31, 1975–76) have also triggered primary, syn-eruptive lahars (Table 17.2). The historical activity record indicates that the average time interval between eruptions is 2–6 years (Newhall et al. 2000; Voight et al. 2000; Siebert et al. 2010; Gertisser et al. 2012). Despite a few large-magnitude eruptions (VEI \geq 3), most events fall in VEI 2 range and have occurred on average once per decade since 1861 (Gertisser et al. 2023, Chap. 6). Dome growth and collapse, which commonly produce 1–10 million m³ of BAF deposits readily available for rain-triggered lahars, have prevailed during the past 140 years (Voight et al. 2000). One such example was the small-magnitude 2006 eruption that taught us important lessons on hazards linked to PDC and lahar overbank flows on the south flank. In the wake of the 2006 overbank flows, subsequent avulsion in the hitherto off-hazard tributaries was recognised for the first time as the most severe hazard at Merapi. Overbank flow processes appeared to be linked to Sabo (check) dams (e.g. upstream of Kaliadem), and narrow bends in the Kali Gendol (Charbonnier and Gertisser 2008, 2009; Thouret et al. 2010; Lube et al. 2011).

Table 17.2 Primary (syn-eruptive) and post-eruptive, rain-triggered lahars at Merapi volcano since the seventeenth century (data from Lavigne et al. 2000a, b, 2015; Thouret et al. 2000; Voight et al. 2000; Lavigne 2001; Lavigne and Thouret 2003; Charbonnier and Gertisser 2008; Thouret et al. 2010; Mei and Lavigne 2012; de Bézilal et al. 2013). Eruptive events without recorded lahars have been discarded. Fatalities and injured and displaced people also refer to the effects of PDCs, lahars and tepihra fall from large eruptions (**bold** when VEI 3–4) on local population. River abbreviations, from NW to SE: Ld Ladon; Jw Juweh; Ap Apu; Tr Trising; Se Senowo; Pa Pabelan; La Lamat; Bl Blongkeng; Pu Putih; Ba Batang; Be Bebung; Kr Krasak; Bo Boyong; Ku Kuning; Op Opak; Ge Gendol; Wo Woro

| Eruption | | | | | | | | | | | | | | |
|--|---------------|--|--------------------------|---------------|-------------------|------------------|-----------------------------------|--------------------------|-------------------|----------------|------------------------------------|--|------------------------|----------------------------|
| Primary (Pr) and post-eruptive (post) lahars | | | | | | | | | | | | | | |
| Year | Magnitude VEI | Pyroclastic deposit volume (m ³ × 10 ⁶) | PDC runout distance (km) | PDC direction | Year | Number of events | Affected rivers | Max runout distance (km) | Maximum depth (m) | Velocity (m/s) | Peak discharge Q m ³ /s | Damage to property | Fatalities and injured | Affected, displaced people |
| 1672 | | | | | | | all | Pr | | | | | 3000? | |
| 1822–1823 | | | | | Dec 1822 | | | Pr | | | | 4 villages | 100 | |
| 1832 | | | | | Dec 1832–1835 | | | Pr | | | | 50 ha farmland | 32 | |
| 1849 | | | | | Sept | | | Post | | | | > 100 s h | 100's | |
| 1871–1872 | 4 or 5 | | | | April 1872 | | Bl | Post | | | | 3 villages | 200 | |
| 1887–1889 | | | | | Oct. 1888 | | Tr, Se | Post | | | | 1 village | | |
| 1902–04 | | | | | | | | Post | | | | 3 villages | 16 PDC & 45 | 3000 |
| 1920–1921 | 2 | 5 | 5.5 | W | Oct 1920 | | West and SW | Post | | | | 1 village | 5 and 35 | 1000 |
| 1930–1931 | 3 | 26 | 13 | S – SW | Dec. 1930–1931 | 33 | Ba West to SW | Pr | | | | 10 s houses 4 bridges, 340 ha farmland | 1369 (PDCs + LHs) | 13,000 |
| | | | | | Apr 1931–Feb 1932 | 162 | Se, Pa, La Bl, Ba, Be, Kr, Bo, Ku | Pr, Post | | | | 42 villages several bridges | | |
| 1953–1954 | 2 | 20 | 7 | W–NW | 1954 | 1 | Pa | Post | 2 m | | | 6 villages | 64 & 57 (PDCs) | 3000 |
| 1961 | 3 | 29.4 | 12 | SW | Nov 1961–1963 | | Se, Pa, Bl Bl, Ba | Pr | > 5 m | | | 10 villages, 95 h, 1 bridge | 6 & 7 (PDC + LHs) | 8000 |

(continued)

Table 17.2 (continued)

| Eruption | | Primary (Pr) and post-eruptive (post) lahars | | | | | | | | | | | | |
|-----------------|---------------|--|--------------------------|---------------|--------------------------|------------------|---|--------------------------|-------------------|----------------|--------------------------------|--|------------------------|----------------------------|
| Year | Magnitude VEI | Pyroclastic deposit volume ($m^3 \times 10^6$) | PDC runout distance (km) | PDC direction | Year | Number of events | Affected rivers | Max runout distance (km) | Maximum depth (m) | Velocity (m/s) | Peak discharge Q (m^3/s) | Damage to property | Fatalities and injured | Affected, displaced people |
| 1969 | 2 | 12.6 | 13.3 | SW | Jan-Feb., Apr 1969 | 44 | 8 valleys NW to SE Be, Pu, BI | Pr, Post | > 5 m | | | 26 villages, 13 bridges, 370 ha farmland | 3 PDCs & LHs | |
| 1972–1974, 1975 | 2 | 6.5 | 7 | SW | 1970–1971 | 21 | Se, Pu, La Ba, Be, Kr, Bo, Ku, Op, Ge, Wo | Post | > 5 m | | | 75 + 134 h, 1 bridge, 30 ha farmland | 9 | |
| Nov-Dec 1976 | 2 | 1.2 | 3.5 | SW | 1972–1973 Nov. 1974–1975 | 17 21 65 | Pu, Be, Kr, Bo, Ku Kr | Post | > 5 m | | | 323 h, 3 bridges, 330 ha farmland | 29 | |
| 1979 | 2 | | | SW | 1980–3 | | BI, Pu, Ba, Be, Kr, Bo, Ku | Pr, Post | | | | | | |
| June 1984 | 2 | 7 | 7 | SW | 1984–1990 | 203 | Pu | Post | | | 100–1000 Max 2000 | | | |
| 1992 | 2 | 3 | 4 | SW | 1992–1993 | 9 | Pu | Post | | | | | | |
| Nov. Dec. 1994 | 2 | 3.5 | 6 | S | Dec. 1994–March 1995 | 42 | Be, Bo | Pr, Post 13 | | 3.4 – 15 m/s | 360 minimum: 33 | 27 trucks, 1 bridge, houses, farmland | 66 & 500 (PDCs + LHs) | 6026 |
| Jan-July 1997–8 | 2 | | | | 1997–1998 | | | Post | | | | farmland | 6 & several | 6000 |
| Dec-Feb 2000–1 | 1 | | | SW | 2001 | | | Post | | | | farmland | 2 | |
| 2006 | 1–2 | 13.3 | 7 | SE | 2006–2009 | ? | Ge | Post < 8 | | | | 1 village, farmland | 2 | 22,253 |

(continued)

Table 17.2 (continued)

| Eruption | | Primary (Pr) and post-eruptive (post) lahars | | | | | | | | | | | | |
|-------------------|---------------|--|--------------------------|---------------|------------------------|-----------------------|---------------------|--------------------------|-------------------|----------------|------------------------------------|-----------------------------|------------------------|----------------------------|
| Year | Magnitude VEI | Pyroclastic deposit volume (m ³ × 10 ⁶) | PDC runout distance (km) | PDC direction | Year | Number of events | Affected rivers | Max runout distance (km) | Maximum depth (m) | Velocity (m/s) | Peak discharge Q m ³ /s | Damage to property | Fatalities and injured | Affected, displaced people |
| 2010 ^a | 4 | 30 – 60 Total 74–84* | 17 | NW–W–SW–S–SE | Oct. 2010–Jan. 2012 | 45 primary LHs | All rivers NW to SE | Pr, Post > 20 | | 3.5–7.53 | 1800 | 860 houses, 21 bridges | 341 & 368 | 3000 affected 400,000 |
| 2011–2014 | | | | | May–Jun 2011, Feb 2014 | 282 post-eruptive LHs | All rivers NW to SE | Post > 20 | 1.6–5 m | 1.5–16 | 473 minimum 10–40 | 21 bridges 14 check dams | 3 & 15 | X |
| 2015 – 2017 | | | | | Jan, March 2017 | 5 | Pa, Se | Post | | | | 1 car, 4 trucks | | |

^a The estimated volume of 2010 PDC and tephra-fall deposits varies between 74 and 84 million m³ (Solikhin et al. 2015a, b, using high-spatial resolution imagery and in situ GNSS measurements), and 150 million m³ as estimated by Suroño et al. (2012)

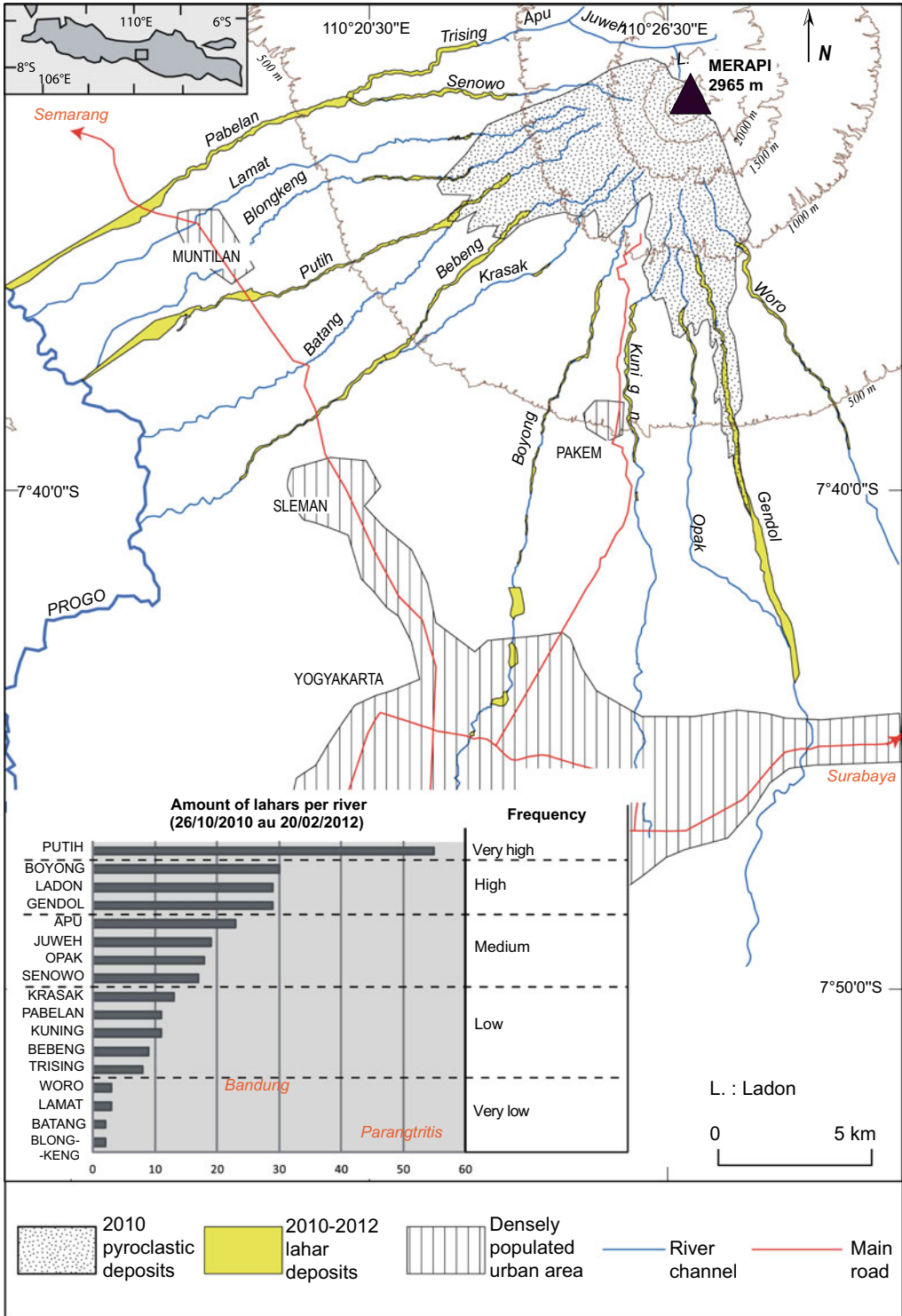


Fig. 17.2 Sketch map showing the drainage network and 2010 deposits around Merapi (after de Bézilal et al. 2012). The extent of pyroclastic deposits from the 2010 eruption and post-eruptive lahars is shown in grey and yellow-

green, respectively. Inset diagram displays the number of lahar events for each of the 17 rivers over two years after the eruption. Densely populated urban areas are outlined

Lahars at Merapi prior to the 2010 eruption were defined as brief events, with small to moderate volumes (10^4 – 10^5 m³) associated with runout distances rarely exceeding 15 km (Lavigne et al. 2000a, b; Thouret et al. 2000; Lavigne and Thouret 2003). However, large volume lahars (e.g. in 1969, 1976) destroyed bridges and heavily damaged houses when they spilled over river banks on the lower slopes of the volcano. At least 100 people were killed, about 80 villages and 1500 houses destroyed, and several thousand hectares of tilled land flooded by 17 post-eruption lahars during the twentieth century (Table 17.2). Sabo dams and dykes that were erected along the river channels since the late 1970s (particularly on the west flank where the lahar threat had prevailed prior to 2006) have slowed lahars (Lavigne and Thouret 2003). Lahar-related damage and human casualties at Merapi have therefore been reduced during the late part of the twentieth century. However, the attention of engineers and risk management personnel has been drawn to the negative effects of such dams as these civil protection works can also favour decoupling of pyroclastic flows followed by overbank runout of hot dilute ash-cloud surges, as in the 2010 eruption (Lube et al. 2011).

17.2.1 Lahar Triggering at Merapi

Lahars at Merapi can be triggered in two ways: (1) Primary lahars are produced by liquefaction of channelled pyroclastic flows and runoff on surge-mantled slopes close to valley margins. Since 1672, at least 23 historical eruptions have reportedly triggered primary, syn-eruptive lahars. (2) An overwhelming majority of Merapi lahars are post-eruptive and rain triggered for the 1–6 years after eruptions, as pyroclastic material can be easily remobilised in steep catchments between 1100 and 2000 m asl at distances between 0.8 and 4.5 km from the summit (Table 17.2). Each year, Merapi lahars with discharges between 100 and 2000 m³/s are triggered during the rainy season in at least 13 rivers that drain the NW, W, SW, S and SE flanks. These lahars can flow with average velocities of

5–7 m/s at 1000 m asl and inundate areas of the extensive ring plain below 600 m asl, reaching 15–25 km from the summit (Fig. 17.2).

Owing to the frequent deposition of pyroclastic material and erosional effects of lahars and hyperconcentrated or streamflows, Merapi stands amongst the composite volcanoes that exhibit the highest erosion rates measured in drainage basins under a humid climate globally (Major et al. 2000; Pierson and Major 2014). Lavigne (2004) calculated huge sediment yields exceeding 1.5×10^5 m³ km⁻² yr⁻¹ in the Kali Boyong catchment on the south flank of Merapi. Greater volumes of sediment have only been estimated at Semeru in 2000, Pinatubo during the first rainy season after the 1991 eruption and at Chaitén, Chile, after the 2008–09 events (Janda et al. 1996; Major et al. 2016). Estimates of aggradation/erosion rates based on high-spatial resolution satellite-, terrestrial Laser (Light) detection and ranging (LiDAR) scanner- and drone-based DEMs have been computed over different time intervals between 30 years and one rainy season, for example at Semeru (Thouret et al. 2014) and on Montserrat (Jones et al. 2017). At Merapi and Semeru, the sediment yield derives from similar sources, namely PDC deposits, rockfalls from lava domes, and pre-existing material from the riverbed and banks (together with daily tephra fall at Semeru). Based on seven month-long (1994–1995) surveys in the Kali Boyong catchment following the 22 November 1994 dome collapse and BAFs at Merapi, Lavigne (2001, 2004) determined four sediment sources delivered to lahars: (1) 85% of the total yield from mostly BAF deposits, (2) 7% from daily rockfalls sourced at the lava dome, (3) 7% from pre-existing alluvial and lahar deposits removed from the riverbeds and banks, and (4) 1% from ash-cloud surge deposits. Prevailing erosion processes resulted from entrenchment and lateral migration and widening of river channel banks and retreat of tributary headwalls and knickpoints in fresh PDC deposits, providing a source of material for lahars. Figure 17.3 shows to which extent the sedimentation/erosion budget was estimated and how sediment was successively removed by

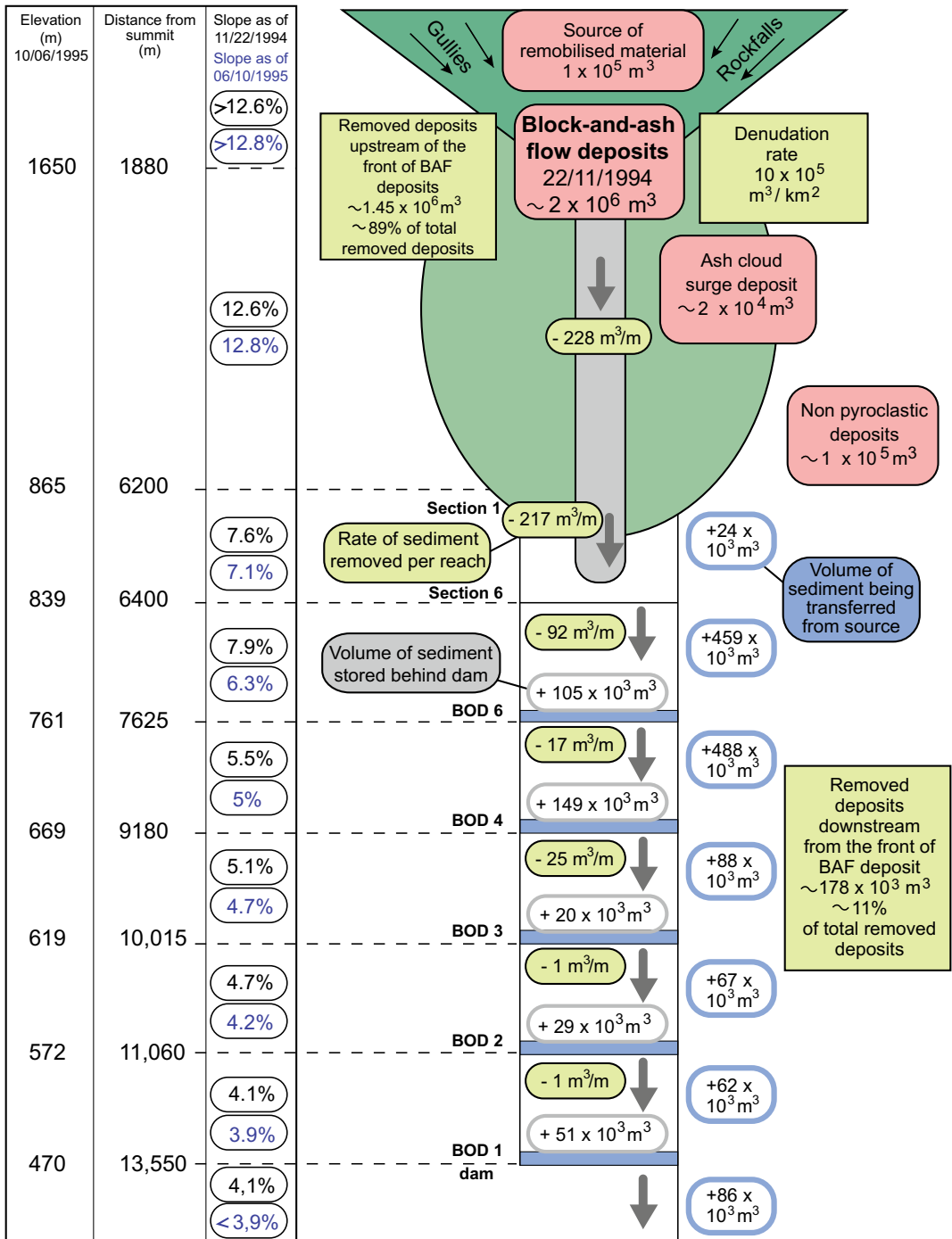


Fig. 17.3 Sketch diagram showing how sediment was removed, stored at Sabo (check) dams, and transferred along the c.14 km-long Kali Boyong channel over seven months following the 22 November 1994 BAF-producing eruption at Merapi (after Lavigne 1998, 2001). This is a

contribution to estimating the balance between aggradation, by BAF deposits, and degradation, by lahars, at active volcanoes, despite sediment storage at Sabo (check) dams

lahars, temporarily stored by check dams, and transferred down valley along the 14 km-long channel of Kali Boyong (Lavigne 2001).

17.2.2 Why is Merapi Prone to Producing Lahars?

Lahar triggering processes are due to at least three main factors:

1. Several millions of cubic metres of pyroclastic deposits (e.g. 6.7×10^6 in 2006 and $36.3 \times 10^6 \text{ m}^3$ in 2010; e.g. Charbonnier and Gertisser 2008, 2009; Thouret et al. 2010; Solikhin et al. 2015a, b) have been emplaced by frequent dome-collapse PDCs (Table 17.2). Dome growth and collapse has regularly shed voluminous pyroclastic deposits onto the upper flanks of Merapi, particularly on the W, NW and SW flanks prior to 2006 and on the S and SW flanks since 2006 (Gertisser et al. 2012). This supply of unconsolidated materials has been rapidly mobilised by runoff from local (orographic) or regional (monsoon) rainstorms, which commonly last 1–3 and several hours, respectively (Lavigne et al. 2000a, b; Lavigne and Thouret 2003; Wibowo et al. 2015).
2. High rainfall amounts of 2–2.8 m/year (perhaps as high as 4 m/year in the altitudinal belt 1000–2000 masl; JICA 1979) and long-lasting (30–90 min) rainfall intensity (20–40 mm/h on average) occur during the rainy season from October to April. Five rain gauges between 1160 and 1600 m asl measured between 300 and 700 mm/month of rain and a maximum monthly and daily intensity of 75 and 100–115 mm, respectively (Wardoyo et al. 2013). Rainfall with an average intensity of c. 20–30 mm/10 min (Lavigne and Thouret 2000) or 40 mm for 2 h in the Kali Putih catchment (Kusumarwadani et al. 2017) typically triggers post-eruptive lahars. Using X-MP radar and the Sabo Work Agency network during the rain-triggered 17 February 2016 lahar, Syarifuddin et al. (2017) measured an average rainfall intensity of 36.58 mm/h for 1 h in the upper catchment of Kali Gendol, and an accumulated rainfall amount of 42 mm in 2 h. The critical rainfall threshold of 40 mm in 2 h proposed by Lavigne and Thouret in (2003) was confirmed by the calculations of Kusumarwadani et al. (2017). Legono and Rahardjo (2017) claimed that rainfall duration, intensity, cumulative and antecedent rainfall play the major role in lahar triggering. Based on recorded rainfall data at the Gunung Maron station located c.1450 m asl on the west side of upper Kali Putih, the authors show that a rainfall intensity of 40 mm/hour, a cumulative rainfall of 72 mm, and a duration of 1.8 h will initiate a lahar. Such critical rainfall parameters can be used for warning and evacuation, but Legono and Rahardjo (2017) aptly recommend further investigation and caution in using lahar rainfall-related thresholds, as local rainfall characteristics are highly variable. Besides these thresholds, high levels of soil water saturation, a slope of at least 8°, and a minimum water depth of 3 cm for runoff are equally important for the lahar triggering process.
3. The drainage pattern is dense with a 220 km length of major rivers across a 720 km² catchment area, yielding an average drainage density of 0.32 km/km² on the volcano's WNW, W, S and SE flanks. Many creeks whose slope gradients range between 8 and 14% cut down in the steep slopes (30°) of the summit Merapi cone; in particular lahars are initiated between 1200 and 2200 m asl from steep catchment headwalls showing numerous landslide scars. An additional contributing factor stems from the fast growth of elementary drainage (rills and gully networks) on tephra cover, as shown by remote sensing (Thouret et al. 2015). Spatial analysis of a time series of high-spatial resolution Pléiades and GeoEye images following the 2010 eruption has revealed that first-order drainage elements started incising the pristine tephra cover on the valley margins of the Gendol valley (Merapi's south flank) as early as two years after the event. A few months after the eruption, the top surface of the tephra cover

had hardened, inhibiting infiltration and favouring overland flow before vegetation regrowth, but creek incision took place within two rain seasons as soon as the tephra top surface was cut by runoff.

17.2.3 Lahar Activity Following the 2010 VEI 4 Eruption

The current lahar threat around Merapi derives from the large (VEI 4) 26 October–8 November 2010 eruption (Subandriyo et al. 2023, Chap. 12). The 2010 eruption totally changed the narrow spatial distribution of pyroclastic material prior to 2006; the 2010 volume of pyroclastic materials from PDCs and tephra fallout was more than ten times larger than the 2006 dome-collapse BAF deposits that used to mantle the upper west flank (Newhall et al. 2000; Hadisantono et al. 2002; Schwarzkopf et al. 2005; Charbonnier and Gertisser 2008, 2009). A summary of this eruption is given in Subandriyo et al. (2023, Chap. 12), while eruption reports can be found in Surono et al. (2012), Cronin et al. (2013), Komorowski et al. (2013), Charbonnier et al. (2013) and Jenkins et al. (2013). As many as 2300 houses were destroyed or severely damaged, and 376 people lost their lives, while financial losses were estimated at Rp 7.1 trillion (approximately US\$ 781 million; Aspinall et al. 2011). Every watershed located downstream of the active summit dome was covered by the 2010 pyroclastic deposits except catchments extending on the east and north flanks (Figs. 17.1, 17.2). Lahars thus remain one of the major ongoing threats at this time of writing (April 2020). The source is 56–63 million m³ of PDC deposits that covered the south and west flanks of the volcano, while 75% of this volume mantled an area of c. 26 km² in the Gendol-Opak catchment to the south, where PDCs reached an exceptional runout distance of 16 km from the summit (e.g. Solikhin et al. 2015a, b). Pyroclastic density currents travelled a mere 3–4 km towards the NW, West, and the SW, but tephra-fall deposits mantled the W and SW flanks with a volume of 18–21 million m³

(Solikhin et al. 2015a). Syn-eruption lahars occurred in October 2010 on all flanks, and then prevailed ever since on the south slope, where about a quarter of the erupted PDC material has remained in the uppermost catchment of Kali Opak and Kali Gendol.

More than 280 lahar events occurred between October 2010 and May 2011, and 108 from 2012 to 2013 in 17 rivers draining the WNW, W, S and SE Merapi flanks (Fig. 17.2; de Bézizal et al. 2013; Lavigne et al. 2015). Intense rainfall episodes on thick and poorly consolidated 2010 PDC and tephra deposits generated lahars during and just after the end of the eruption, and endangered people living in the vicinity of river banks. The first lahars occurred on 27 October 2010 and were channelled through Kali Boyong and Kuning draining the SW and S flanks (de Bézizal et al. 2013). Lahars were triggered in the western and southern catchments shortly after the eruption; approximately two lahars per week were recorded in Kali during the 2010–2011 monsoon season. This was mainly due to runoff on the wide expanse of fresh tephra-fallout deposited on the west flank of the volcano. The 3 January 2011 voluminous lahar (about 1.5 million m³) inundated an area of c. 0.28 km² in and around Kali Putih. BNPB (the Indonesian National Board for Disaster Management) reported that this lahar destroyed 65 houses and damaged a further 118 in Jumoyo and four neighbouring villages, as well as two bridges on the main Magelang-Yogyakarta highway (Figs. 17.2, 17.4; Sect. 17.4.3). More than 2000 people were evacuated from the villages located on the banks of Kali Putih while minor damage also occurred along Kali Krasak.

The southern catchments (Kali Boyong, Opak-Gendol, and Woro) produced more than 60 large but less frequent lahars (Fig. 17.2). On 1 May 2011, additional lahars (about 1 million m³) spilled out from the lowermost, narrow, and winding Kali Gendol, and inundated ~0.16 km² on the west bank of the valley (Figs. 17.2, 17.4; Sect. 17.4.3). This lahar buried Ngerdi with ~2 m of mud, destroyed 40,000 m² of crops and damaged 51 houses (de Bézizal et al. 2013). These overbank lahars occurred along the

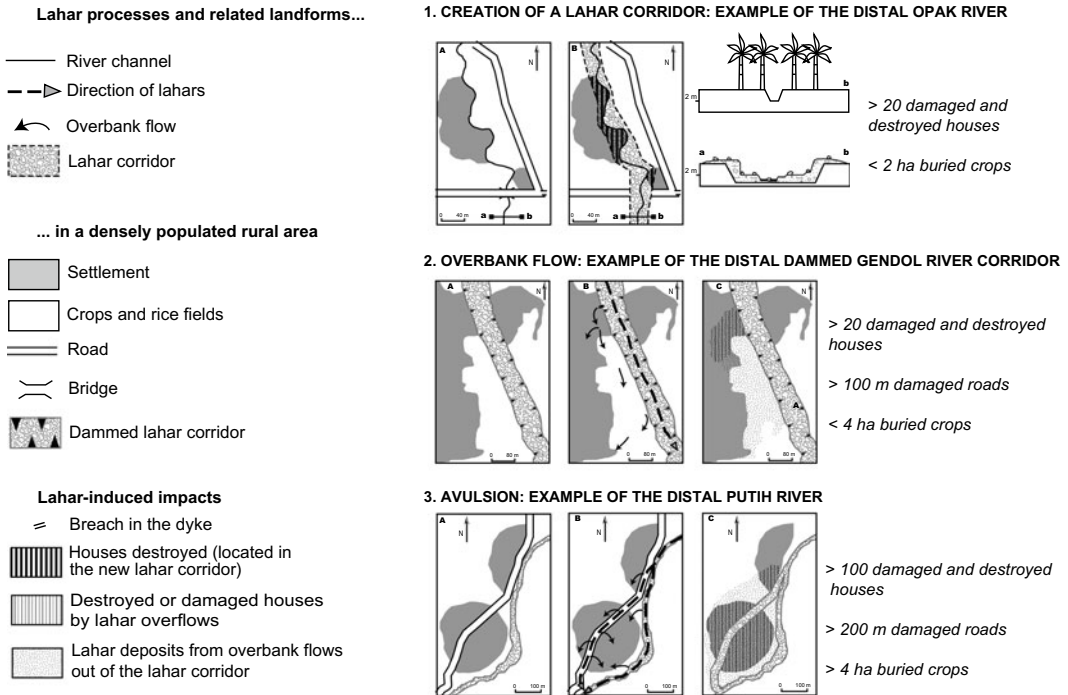


Fig. 17.4 Sketch diagrams showing how lahars form “corridors” (elongated fans adjacent to river banks) and how lahar overspills (overbanks) and avulsions occur

along three valleys at Merapi, including their effects on houses, roads and crops (after de B elizal 2012)

most sinuous part of the river course where tributaries of Kali Gendol cross gentle slopes (< 2%) down valley from the confluence with Kali Opak (Fig. 17.4). These inundation areas are shown in maps derived from the 15 November 2010 and 10 June 2011 SPOT5 images along Kali Putih and Krasak (at distances of 18 and 15 km from Merapi, respectively), and Kali Gendol (19 km from Merapi) (Fig. 17.2).

The frequency of lahars has strongly decreased after 2012: a large part of the 2010 PDC deposits had already been removed by lahars and transported downstream, while material extraction by sand mining also contributed to sharply shrinking the supply of pyroclastic material. In 2014–2015, approximately 20 lahars were counted in Kali Gendol and Kali Apu, and one further lahar occurred in Kali Bebeng in November 2016. The post-2010 lahars reached the ring plain of the volcano, as far as the Progo river draining the west flank of Merapi toward

the south (Fig. 17.2). Southward, three HCFs reached the inner city of Yogyakarta in 2010 and 2011, without causing any casualties as they were very dilute. The long runout distances of the 2011 lahars raised the issue of risk in areas that had been considered safe for decades. Lahars were usually confined to river channels, but overbank flows 10–15 km downstream along Kali Putih, Kali Gendol, Kali Pabelan and Kali Boyong damaged several villages and continued until 2016, threatening other villages near river channels more than 20 km from the summit.

As the lahars flowed on gentle slopes, they disrupted the local hydrographic network, causing channel widening and bank erosion, which, coupled with incision and/or aggradation, led to landscape changes after each event. Figure 17.4 depicts how lahars form “corridors”, i.e. elongated fans adjacent to river banks, and how lahar overbank flows and avulsions occur along three valleys around Merapi, including their effects on

houses, roads and crops. Once lahars reached the distal 3° slopes with wide and shallow valley channels, they spilled over banks and generated heavy damage over urban areas and rice fields; a few hamlets of the Jumoyo and Sirahan villages along Kali Putih showed a destruction rate exceeding 50% and the Yogyakarta-Semarang road—one of the main south-north roadway on Java Island—was cut for weeks, leading to major road traffic disturbances. One of the piers of the Magelang bridge across Kali Pabelan was swept 950 m downstream by a lahar in March 2011 (de B elizal et al. 2013). For two years after the 2010 eruption, lahars threatened the people living on the slopes and ring plain of the volcano, where 860 houses were damaged, 14 check dams buried and 21 bridges swept away. However, lahars did not cause many casualties (3 killed and 15

injured people according to reports gathered by de B elizal et al. 2013) due to an effective community-based early warning system.

17.3 Lahar Monitoring and Warnings at Merapi

The lahar monitoring system at Merapi pursues the twofold purpose of lahar dynamics research and early warning. A total of 24 lahar monitoring stations were gradually established by the Merapi Volcano Observatory (*Balai Penyelidikan dan Pengembangan Teknologi Kebencanaan Geologi*, BPPTKG) from November 2010 until 2012 in cooperation with the Volcano Disaster Assistance Program (VDAP, USGS), and with funding from the National Disaster Management Agency

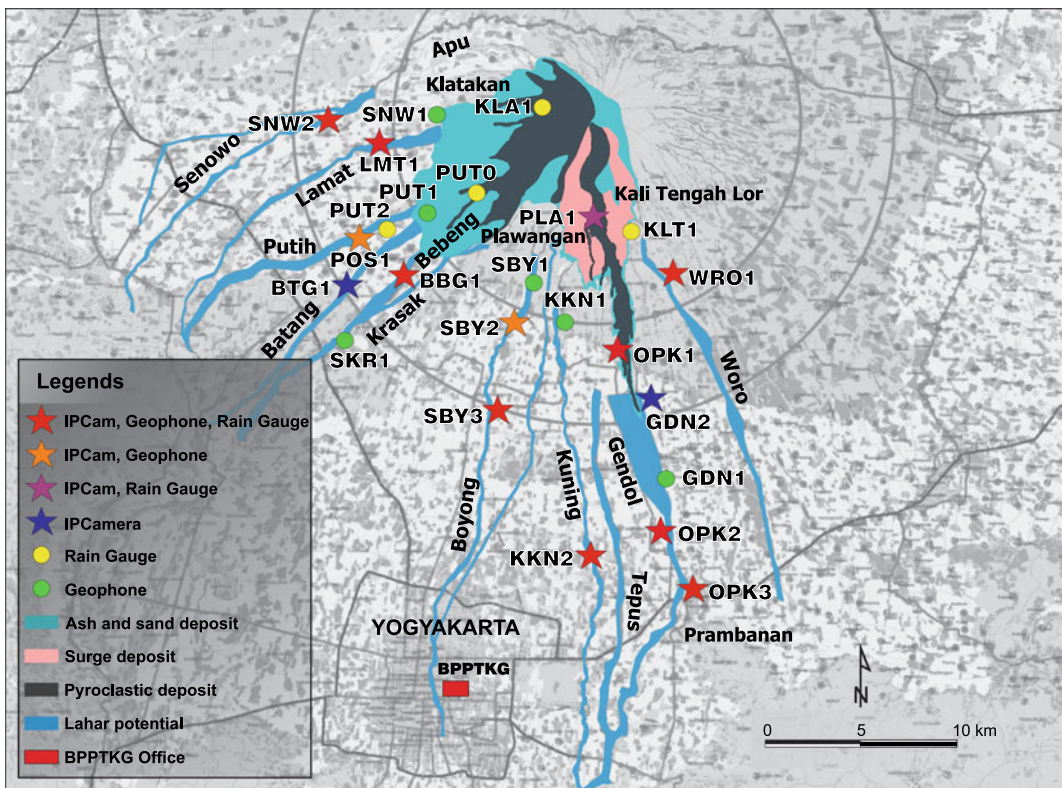


Fig. 17.5 Map showing the distribution of the lahar stations and corresponding river names. Gendol river has the largest number of stations compared to other drainages: six monitoring stations were installed in or near the Gendol channel due to higher lahar hazards and

risk since the 2010 eruption. Data from all monitoring stations are transmitted to the BPPTKG office in Yogyakarta. Grey rectangles indicate the distribution of populated settlements

Table 17.3 Location of the monitoring stations operated by BPPTKG (CVGHM) along the thirteen rivers draining the west, south and south-east flanks of Merapi (see Fig. 17.5 for the spatial location)

| No | River Name | Code of station | Longitude East | Latitude South | Elevation (m) | Village | District | Regency |
|----|-------------|-----------------|----------------|----------------|---------------|---------------|-------------|----------|
| 1 | Gendol | GDN1 | 110.4638 | -7.6628 | 463 | Glagaharjo | Cangkringan | Sleman |
| 2 | Gendol | GDN2 | 110.4710 | -7.6860 | 344 | Pencar | Ngemplak | Sleman |
| 3 | Opak | OPK1 | 110.4500 | -7.6236 | 661 | Pager Jurang | Cangkringan | Sleman |
| 4 | Opak | OPK2 | 110.4834 | -7.7331 | 173 | Tulung | Kalasan | Sleman |
| 5 | Opak | OPK3 | 110.4895 | -7.7532 | 204 | Bokoharjo | Prambanan | Klaten |
| 6 | Kali Tengah | KLT1 | 110.4577 | -7.5818 | 1163 | Balerante | Kemalang | Klaten |
| 7 | Kuning | KKN1 | 110.4270 | -7.6240 | 653 | Sidorejo | Pakem | Sleman |
| 8 | Kuning | KKN2 | 110.4411 | -7.7257 | 165 | Tirto Martani | Kalasan | Sleman |
| 9 | Woro | WRO1 | 110.4702 | -7.5971 | 907 | Sidorejo | Kemalang | Klaten |
| 10 | Boyong | SBY1 | 110.4250 | -7.5930 | 967 | Kaliurang | Pakem | Sleman |
| 11 | Boyong | SBY2 | 110.4140 | -7.6240 | 649 | Kemiri | Pakem | Sleman |
| 12 | Boyong | SBY3 | 110.3963 | -7.6598 | 159 | Purwobinangun | Pakem | Sleman |
| 13 | Plawangan | PLA1 | 110.4315 | -7.5857 | 1276 | Kaliurang | Pakem | Sleman |
| 14 | Klatakan | KLA1 | 110.4321 | -7.5323 | 1635 | Babadan | Muntilan | Magelang |
| 15 | Senowo | SNW1 | 110.3823 | -7.5339 | 774 | Kajangsoko | Dukun | Magelang |
| 16 | Senowo | SNW2 | 110.3339 | -7.5387 | 580 | Talun Lor | Muntilan | Magelang |
| 17 | Lamat | LMT1 | 110.3430 | -7.5529 | 674 | Wates | Dukun | Magelang |
| 18 | Putih | PUT0 | 110.3926 | -7.5707 | 920 | Ngepos | Srumbung | Magelang |
| 19 | Putih | PUT1 | 110.3721 | -7.5771 | 729 | Dam Setiabudi | Srumbung | Magelang |
| 20 | Putih | PUT2 | 110.3549 | -7.5853 | 608 | Ngepos | Srumbung | Magelang |
| 21 | Batang | BTG1 | 110.3413 | -7.6043 | 501 | Kalibening | Srumbung | Magelang |
| 22 | Bebeng | BBG1 | 110.3629 | -7.6047 | 592 | Kamongan | Srumbung | Magelang |
| 23 | Krasak | SKR1 | 110.3400 | -7.6290 | 446 | Sudimoro | Srumbung | Magelang |
| 24 | Kaliurang | KAL1 | 110.4247 | -7.601 | 869 | Kaliurang | Pakem | Sleman |

(BNPB) (Fig. 17.5; Table 17.3; Hardjosuwarno et al. 2013; Sulistiyani et al. 2018a, b). BPPTKG, one of the units of Centre for Volcanology and Geological Hazard Mitigation (CVGHM), whose task is to mitigate volcanic hazards at Merapi, developed the lahar monitoring system by adding sensors and increasing the number of real-time monitoring parameters.

17.3.1 Monitoring Instrumentation

Each of the main rivers around Merapi includes one to three monitoring stations, with BPPTKG and Sabo Work Agency rain gauges

implemented at about 1000 to 1600 m asl in order to detect the rainfall intensity as close as possible to the uppermost catchments where lahars initiate (Fig. 17.5, Table 17.3; see also Kusumarwadani et al. 2017 and Syarifuddin et al. 2017). For the purpose of early warning, monitoring of lahars at Merapi uses four non-contact sensors: geophones (natural frequency 10 Hz) and short period seismometer (natural frequency 1 Hz) to monitor ground vibrations induced by lahar flows, high definition closed-circuit television CCTV cameras to validate and investigate the size of these flows, and tipping-bucket rain gauges (0.5 and 1 mm/count resolution) to measure the rainfall intensity. Seismometers and

geophones are buried 1 m in depth near the channel, rain gauges installed on a pole 2 m above the ground while the CCTV cameras are hung on top of triangle towers 30 m high, and footage transmitted to BPPTKG in real time mode. Seismometer or geophone outputs are amplified and converted, then transmitted using radio with a 100 Hz sampling rate. Data from the field stations are transmitted to Yogyakarta using the wireless connection. Lahar monitoring stations thus include two sub-systems, i.e. instruments in the field and a receiver.

17.3.2 Warning System

The main purpose of lahar flow monitoring is to provide early warning to the stakeholders and people living around Merapi about timely lahar occurrence. The information and early warnings are delivered using various methods, such as radio communications, Short Messages System (SMS), e-mail, and through a website. When the real-time amplitude measurement (RSAM) value and rainfall intensity exceeds a certain amount, the system sends the information through the aforementioned methods. Real-time CCTV footage is displayed on the BPPTKG website (www.merapi.bgl.esdm.go.id). If the RSAM value exceeds 5000 counts, the instrument will trigger the warning system. However, false alarms can also be adversely delivered, because sand mining and tectonic events can also be recorded with the same number of counts. Examples of lahar events recorded by Boyong and Putih river stations are described in Sect. 17.4.2. Overall, the seismic amplitude and frequency characteristics, and visual or camera confirmation, can be used to refine the design of existing early warning systems.

As a result, BPPTKG has proposed a new design using criteria and thresholds from lahar characteristics (Sulistiyani et al. 2018a). If the seismic data across the 10.1–20 Hz frequency bands exceeds the amplitude of 5000 counts, the system will deliver the first warning. Then, if the amplitude value exceeds 1000 counts in the next 5 min, it can be inferred that the event is a real

lahar flow and the system provides an alarm. For the large lahar events, the maximum amplitude envelope exceeds 5000 counts and keeps growing over time.

17.4 Lahar Behaviour and Dynamics at Merapi

At Merapi, methods exploited to study lahars have resembled those carried out on other voluminous lahar producing volcanoes (e.g. Pinatubo, Ruapehu, Colima, and Semeru). These methods include geology, sedimentology, mapping using field surveys and remote sensing data, DEM analysis and morphometric characteristic of channels, statistical and shallow water depth-averaged models, and geophysical instruments. Here, we present information gleaned from: (i) direct measurement; (ii) remote sensing, DEMs and channel morphometry, and (iii); the lahar monitoring system at Merapi, providing two examples of the 2010 and 2014 lahar case studies where multiple measurement methods were considered together in order to estimate lahar behaviour and dynamics.

17.4.1 Direct Measurement

Direct measurements of lahar propagation include sampling material inside flows or analysing video camera recordings (e.g. Lavigne et al. (2000a,b) at Merapi (Indonesia), Doyle et al. (2010, 2011) at Semeru (Indonesia), Cole et al. (2009), Cole (2011) and Lube et al. (2012) at Mt. Ruapehu (New Zealand), Okano et al. (2012) at Mt. Yakedake (Japan), and Vázquez et al. (2016) at Volcán Colima (Mexico)). Sampling using buckets or hatches carved in the channel bed help collect the flow mixture at frequent time intervals, which help in analysing the particle size, density and sediment concentration of lahars as well as the water chemistry in order to trace their origin (Cronin et al. 1996; Lube et al. 2012). Video recordings allow the flow velocity and stage and the transport of large blocks to be measured, and surficial instabilities

such as rolling waves and hydraulic jumps to be recorded (Lavigne and Thouret 2003; Doyle et al. 2010; Starheim et al. 2013; Wibowo et al. 2015). Combined with hydraulic characteristics of lahar/debris flows recorded in channels, rheological tests using flow material in laboratory devices (Major and Pierson 1992; Dumaisnil et al. 2010) aim to describe lahar behaviour.

17.4.2 Sedimentological and Hydraulic Analysis

Hydraulic and rheological flow characteristics explain why lahars are amongst the most erosive mass flows (Table 17.4). At Merapi, they cause damage at distances between 15 and 25 km down valley, i.e. beyond the range of 5–15 km usually attained by PDCs on similar composite volcanoes. Sedimentological analyses of the lahar deposits in several rivers at Merapi found two thirds of clast-supported and matrix-supported debris-flow deposits, and one third of HCF deposits, and streamflow deposits. The stratigraphic succession of massive and stratified beds observed immediately after any given lahar event indicates that the sediment concentration varies widely over time and space during a single lahar event. Sedimentation rate varies from 3 to 4.5 cm/min during relatively long-lived, slow surges to as much as 20 cm/min during short-lived, fast surges (Lavigne and Thouret 2003). These results indicate that the sediment load fluctuates during lahar flow, further demonstrating that lahars are transient sediment–water flows with unsteady properties. Some lahars and pulses within an event can be transient without depositing any material for a long-time interval at a particular location. However, lahars follow topography and so the areas likely to be damaged can be identified relatively easily. Impacted areas can be extensive on flattish land below 300 m asl across the Merapi ring plain, and the velocity of lahars and their ability to entrain debris makes them spill over from a dense network of shallow riverbeds.

Debris-flow phases at Merapi typically last from a few minutes to 10 min, and are often

restricted to the lahar front. Debris flow surges are sometimes preceded, and always followed, by long HCF phases. As a result, mean sediment concentration of the lahars remains low, between 20 and 50 vol% (Table 17.4). Besides, transient streamflow phases (sediment concentration < 20 vol%) can occur between two debris-flow surges. The transition zone between the two debris flow or HCF types may fluctuate within the flow itself. Grain-size distribution, physical composition of sediments, shear stress, yield stress, and water temperature each play a role. Low sediment load and frequent transient flows along the Merapi channels may result from at least four factors: (1) several breaks-in-slope along the channel increase the deposition rate of sediment and hinder the bulking capacity of the lahars; (2) the source material is mainly composed of coarse debris from “Merapi-type” BAFs. Consequently, the remobilization of coarse debris by HCFs is more difficult and clast deposition is accelerated; (3) variations of rainfall intensity over time and space, that are common during tropical monsoon rainfall, influence the sediment load variations of the lahars; and (4) confluence of tributaries with the main valleys can create obstacles, slowing down the moving flows, and inducing temporary damming, followed by sudden release of pulses of coarse material.

17.4.3 Remote Sensing, DEM and Channel Morphometry Analysis

The behaviour and complex overbank mechanisms of PDCs and lahars involves many parameters, such as flow depth, volume and dynamics, flow grain size, source mechanism, and the topography and geometry of the flow-confining valley (Lavigne et al. 2000a, b; Lube et al. 2011; Andrews and Manga 2011; Charbonnier et al. 2013; de Bélizal et al. 2013; Solikhin et al. 2015a). Changes in channel capacity and geometry, and river gradient are critical in terms of hazard assessment for people and villages located near the river banks and down valley. Along Merapi's river network, the

Table 17.4 Hydraulic, physical and rheological characteristics of lahars at lahar-producing volcanoes of Java, including Merapi. Symbols: pLH primary lahars (other are rain triggered), DF debris-flow behaviour, HCF Hyperconcentrated-flow behaviour, FF Flash floods. Reference number: 1—Vallance (2000); 2—Neall (1976); 3—Thouret et al. (1998); 4—Arguden and Rodolfo (1990); 5—Lavigne and Suwa (2004); 6—Dumaisnil et al. (2010), Doyle et al. (2010, 2011), Thouret et al. (2014); 7—Maruyama et al.; 8—Jitousouno et al. (1996); 9—Shimoda et al.; Lavigne et al. (2000a, b), Lavigne and Thouret (2003); 10—de Bézal et al. (2013), BPPTKG (Unpubl. data), this chapter; 11—Solikhin et al. (2015a, b), BPPTKG (Unpubl. data), this chapter; 12—Mainsant (2014); 13—Wibowo et al. (2015). See additional references and Table 1 in Thouret et al. (2020)

| Indonesian volcano Ref. no | Event date | Type, occurrence | Surface km ² | Volume 10 ⁶ m ³ | Velocity m/s | Depth m | Peak discharge m ³ /s | Runout distance km | Mobility ΔH/L | Froude number | Solid concentration vol. % | Density kg/m ³ | Total runoff 10 ⁶ m ³ | Specific sediment yield 10 ⁵ m ³ /km ² /yr |
|----------------------------|-------------------------|----------------------|-------------------------|---------------------------------------|----------------|---------------|----------------------------------|--------------------|---------------|---------------|----------------------------|---------------------------|---|---|
| Galunggung, 1,2 | 1822 | pLH | > 100 | > 0.11 | | | | 10–30 | | | | | | |
| Kelut 2,3,4 | 1585,1919 1990,2014 | pLH | 131 | 0.131 30 (1990) | 4–11 (1990) | 3–7 (1990) | | 24–40 | | | | | | |
| Semeru, 5,6 | 2000–2004 | HCF | | 0.05–0.5 | 1.0–5.0 | 0.6–3.5 | 50–500 | 25–35 | 0.07 | 1–1.7 | 31–64 | 1,980 - 2,100 | | 2.7 C. Lengkong 1 yr |
| Semeru 5,6 | 2008 | HCF, DF | | 0.011–0.11 | 3–6 | 0.5–2 | 25–250 | 20–25 | 0.07 | | 28–44 | 1,460 - 1,670 | | 10 ³ –10 ⁵ C. Lengkong over 10 to 30 yr |
| Semeru 5,6 | 2008 | HCF, DF | | 0.011–0.11 | 2.9–4.3 | 0.5–2 | 25–250 | 20–25 | 0.07 | | 26–48 Max 68 | 1,460 - 1,670 | | |
| Merapi 7 | 1976 | DF, HCF, FF | 31.7 K. Krasak | 0.0026–1.18 | | | 580– 1100 | | | | | | | 3.0 (Gendol) 5.94 (Woro) |
| Merapi 8 | 1984 | DF | | 0.0050–5.0 | | | 100–800 Max 2000 | | | | | | 114.9 for 5 years Aver. 5–15 | 1–6 |
| Merapi 9 | Nov. 1994– June 1995 | HCF, DF | K. Boyong 10.5 | 0.028–0.278 | 3.4–15 | 0.5–3.4 | 33–360 | 20–30 | 0.1 | 1.7–3.33 | 12–62 Average < 40 | | | 1.5 K. Boyong (1 year) |
| Merapi 10,11 | May–June 2011 | HCF, DF, FF | > 100 | 0.01–1.5 | 3.5– 7.53 | 1–4.5 | 10–400 | 15–25 | 0.08 | | HCF 20–40 DF > 50 | | | |
| Merapi 12 | 16 Feb. 2012 | HCF, 4 packets | 14.6 | 0.01 | 1.5–16 | 1.5–4 | 10–300 | 15–20 | 0.09 | | < 40 | | | |
| Merapi 13 | 28 Feb. 2014 | HCF, DF 4 packets | 10.6 | c. 0.012 | 4.1–12 | 1–7 | 10–473 | 15–20 | 0.11 | | HCF < 40 DF > 50 | | | |

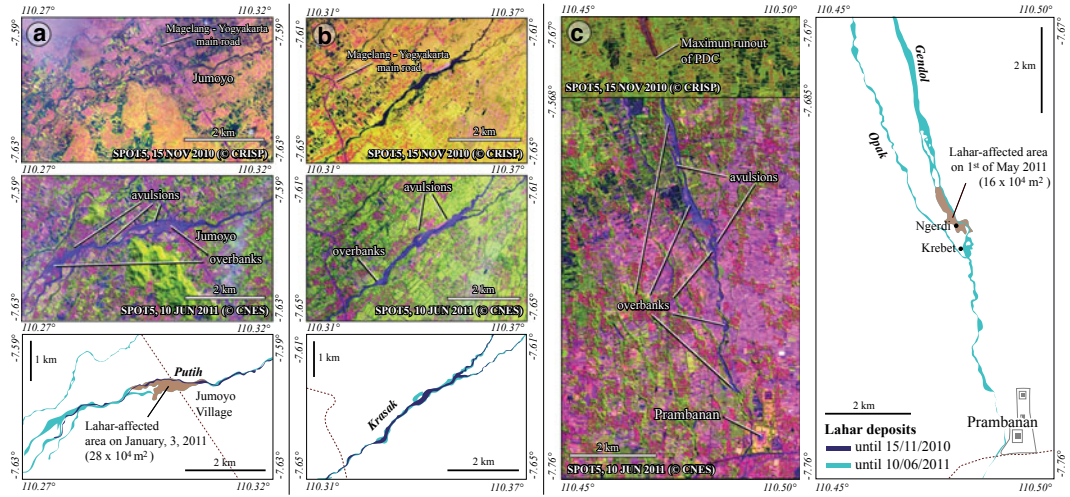


Fig. 17.6 Comparison between enlarged excerpts from the 15 November 2010 and 10 June 2011 SPOT5 images shows the extent of lahar deposits and highlighting the effects of the 2011 lahar events along **a** Kali Putih, **b** Kali

Krasak, and **c** Kali Opak and Gendol rivers (after Solikhin et al. 2015a; see also de Bélizal et al. 2013; Thouret et al. 2015)

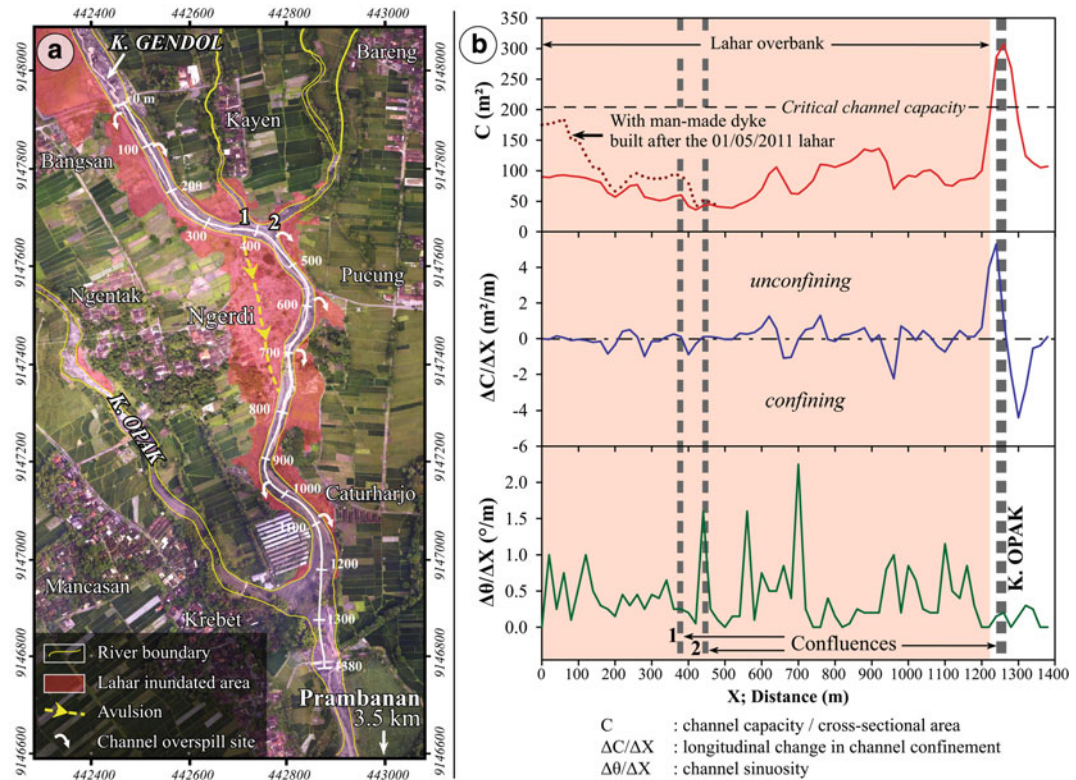


Fig. 17.7 a Low-altitude photograph of the Gendol valley near the village of Ngerdi (19.5 km from Merapi summit) showing the 1 May 2011 lahar deposits. **b** Three morphometric indices have been computed: channel capacity (C in m^2), longitudinal change in channel

confinement ($\Delta C/\Delta X$ in m^2/m), and channel sinuosity ($\Delta\theta/\Delta X$ in degree/metre). Channel overspill sites (white arrow) occur where the channel sinuosity is high (>1 degree/metre) (after Solikhin et al. 2015a)

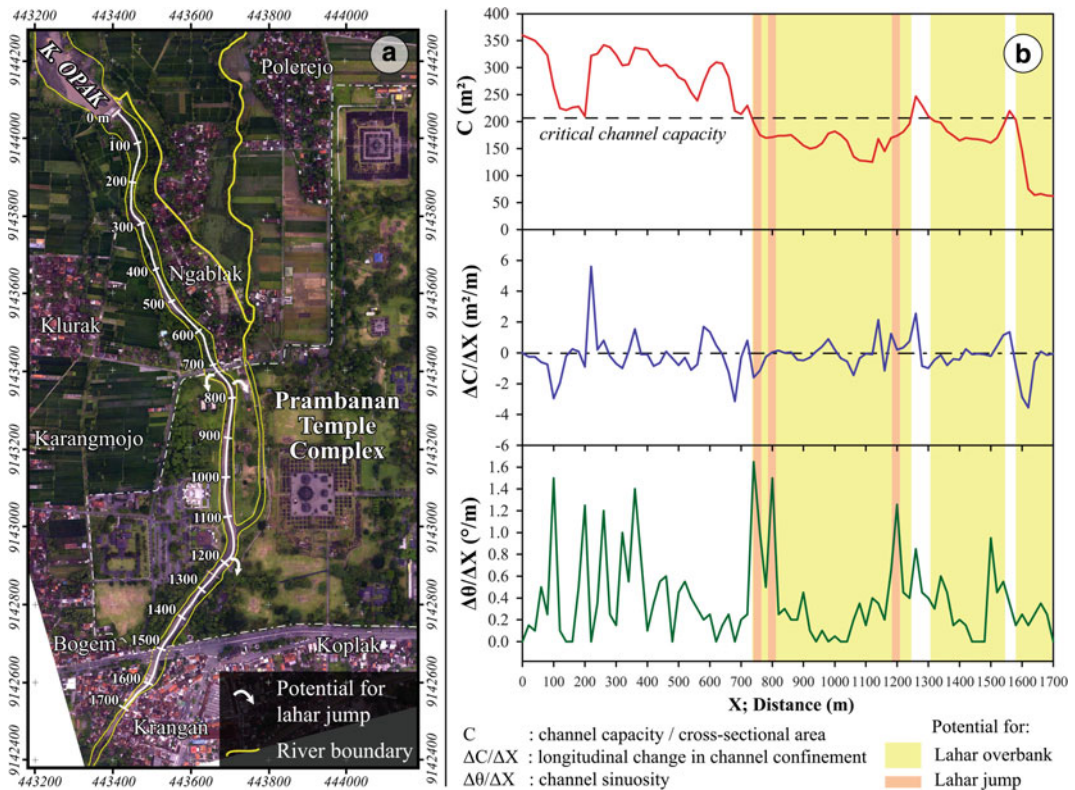


Fig. 17.8 Potential areas of future lahar overbanking in the vicinity of historic assets down the Opak Valley. **a** Low-altitude photograph of the Opak-Gendol valley near the Prambanan temple (25 km from Merapi summit) and white arrows indicating potential sites for lahar overbank and avulsion. **b** Value profiles of three computed indices: channel capacity (C in m^2),

longitudinal change in channel confinement ($\Delta C/\Delta X$ in m^2/m), and channel sinuosity ($\Delta\theta/\Delta X$ in degree/metre), indicating the potential lahar overbank flow zone beyond 750 m down valley from the 0 point in (a) and three potential sites for lahar to spill out of the channel (after Solikhin et al. 2015a)

construction of check dams and dykes also plays a role in overbank PDC and lahar behaviour, as this process strongly depends on the geometry of the confining valley (Figs. 17.8, 17.9 and 17.10). Solikhin et al. (2015a) explored the relationships between the topography of the Gendol valley, the morphology of river channels, and the PDC/lahar overbank process using the deposit map (Fig. 17.2), the longitudinal profile (Figs. 17.4, 17.6, 17.7), and a high-spatial resolution DEM. Factors that favour flow overspill from the river channel include the channel cross-sectional area or capacity (C), the longitudinal rate of channel confinement ($\Delta C/\Delta x$), and the channel sinuosity ($\Delta\theta/\Delta x$) where x is the travel distance (Fig. 17.7b; Lube et al. 2011).

A clear correlation exists between the channel capacity and the width of areas characterised by overbank flow deposits (Fig. 17.7) for which any reduction in channel capacity would lead to wider affected areas. The case study of the May 2011 lahar that spilled over the village of Ngerdi for a distance of 1400 m down Kali Gendol (Figs. 17.6c, 17.7a) allowed characterisation of geometric parameters for the river channel where lahars inundated an area of $\sim 0.16 \text{ km}^2$ mostly on the west bank (Fig. 17.7a). Figure 17.7 illustrates the pre-eruption valley cross sections with longitudinal distance at a 20-m spacing between the upper check dam in Bangsan village (point zero, 19 km from the summit) and the lower check dam (end point) 100 m downstream

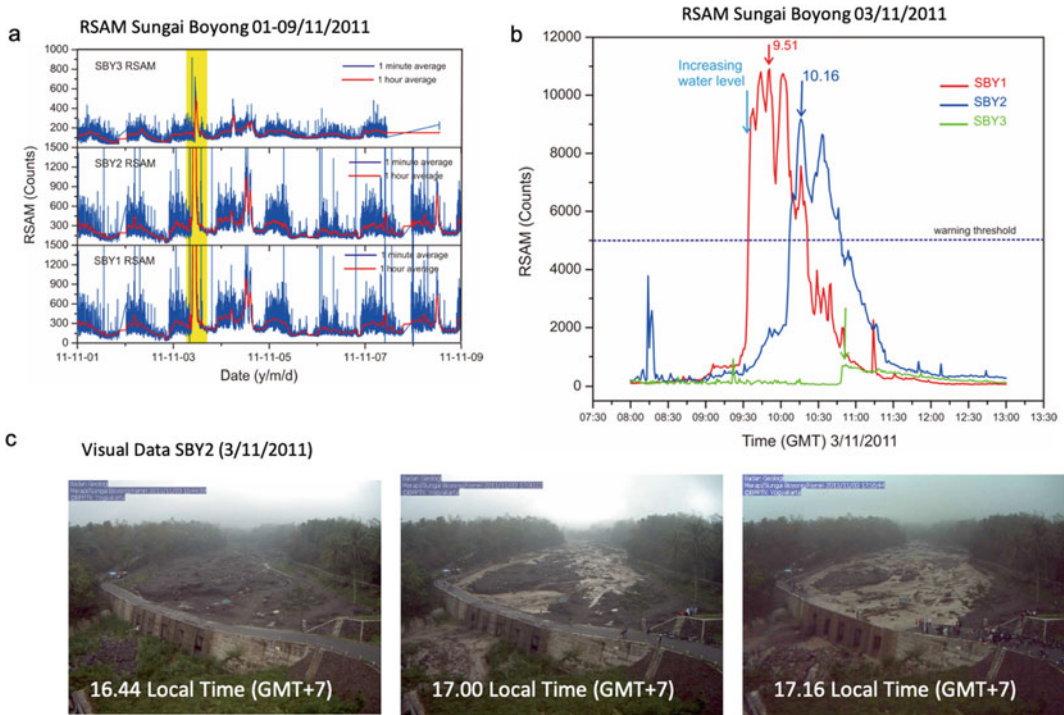


Fig. 17.9 3 November 2011 lahar event at Kali Boyong stations. **a** The RSAM data recorded at SBY1, SBY2 and SBY3 on 01–09 November 2011. The yellow band shows the lahar events on November 3, 2011. The red line indicates the average 1-h moving window **b** RSAM graphs of 3 November 2011 recorded by SBY1 stations (red), SBY2 (blue), and SBY3 (green). The peak amplitude was observed at 09:51 UTC at SBY1 station and

10:16 UTC at SBY2 station. The black dashed line indicates the warning threshold for lahars, i.e. 5000 counts. **c** Visual observation from CCTV Camera at SBY2 stations. Image captured at 09:44 UTC shows no lahar flowing as yet, while at 10:00 UTC the flow increased in the river channel. At 10:16 UTC the entire channel was flooded when the maximum amplitude was reached (after Nandaka et al. 2013)

from the confluence of Kali Gendol and Kali Opak (20 km from the summit). Figure 17.7a shows the mapped extent of the lahar overbank at a distance of 1210 m down from the zero point. In the lahar inundation areas (red zone in Fig. 17.7a), the wetted channel cross section was always less than 210 m², which was defined as the critical channel capacity. However, no overbank lahar occurred 1300 m downstream from the initiation point although the channel capacity drops below 210 m² (Fig. 17.7b). This may be due to the distance from source and a capacity expansion in the upper stream, which resulted in a decrease in lahar volume and velocity. Another factor is that sufficient material was lost to overbank flow so that the peak discharge of the

lahar fell below the channel capacity farther downstream and thus remained confined.

Dykes were built using lahar deposits along the riverbank from the zero point up to 450 m distance, in order to protect the villages. Although up to 100 m² has been added to the channel cross section, the engineered dykes are ineffective as the capacity of the channel remains lower than the 210-m² critical wetted cross section of the 1 May 2011 lahar. The capacity curve C (Fig. 17.7b) reaches its minimum at the distance of 350–450 m, where the lahar avulsion occurred (Fig. 17.7a). The red line channel capacity shows the flow cross-sectional area (defined by the high-water marks of the lahar) exceeding the bank-full cross-sectional area of the channel on the right,

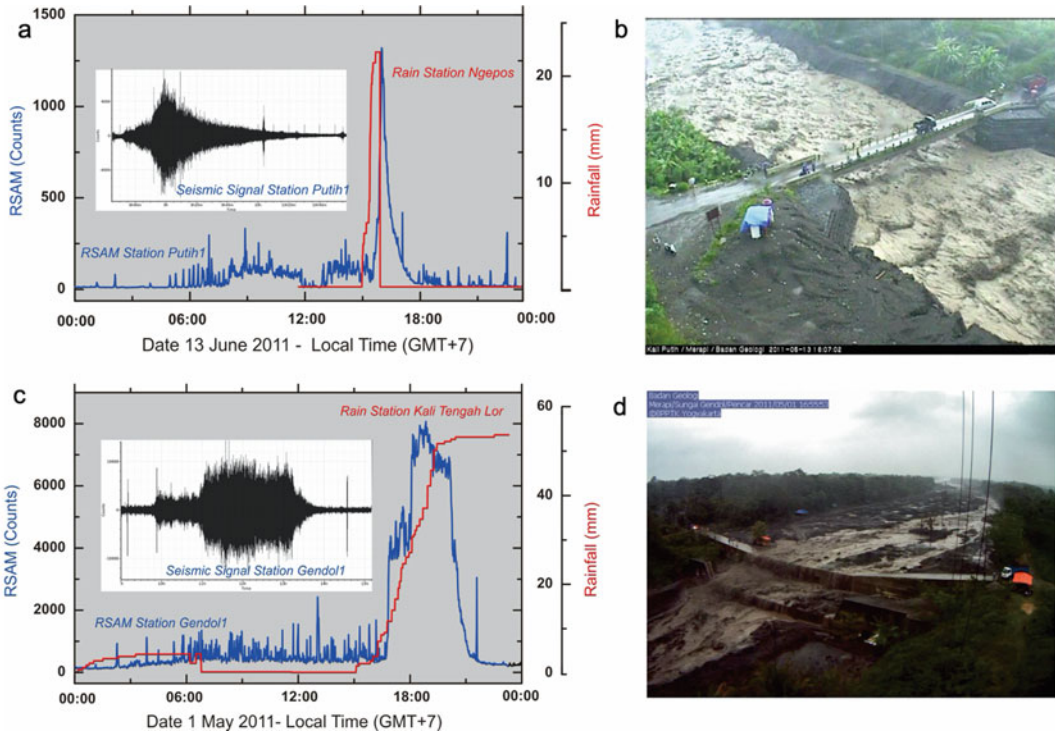


Fig. 17.10 a-d Examples of lahar signals recorded at Merapi. Lahar signals recorded at **a** the PTH1 station (Kali Putih) on 13 June 2011 and **c** at the GDN1 station (Kali Gendol) on 1 May 2011. The black line indicates the time series data of the seismic signal; the blue line shows the 1-min RSAM data, and the red line shows rainfall

intensities (between 22 and 56 mm/hour during 60 and 240 min, respectively) both from Ngepos and Kali Tengah Lor rain gauges. **b, d** Snapshots taken from PTH1 and GDN1 station CCTV cameras. Note surface flow instabilities in image **b** (after Nandaka et al. 2013)

east margin. This suggests that overbanking occurred at that point because the flow cross section reached a transient peak (maximum stage height) due to an abrupt change in channel geometry such as sudden constriction and probably a hydraulic jump coupled with a bend. For the channel segments with capacities less than 210 m^2 , the longitudinal change in channel confinement, $\Delta C/\Delta X$, with distance is less than $4 \text{ m}^2/\text{m}$ and mostly less than $1 \text{ m}^2/\text{m}$, with no significant negative minima (Fig. 17.7b). The curve for $\Delta\theta/\Delta X$ (Fig. 17.7b) has seven maxima where channel sinuosity increases above one degree/metre, three of which exceed 1.5 degree/metre at distances of 450, 550, and 700 m from the zero point. High channel sinuosity, and hence potential for flow acceleration in outer

bends may lead to overbank/avulsion processes due to flow superelevation.

Computation of channel geomorphological parameters from the DEM is also useful to anticipate sites of future lahar overflows (Fig. 17.8). To be completed, such an approach must be combined with a study of lahar flow characteristics. The May 2011 Ngerdi village case study helped apply morphometric indices to the area containing Prambanan temple, as runout lahars may threaten the valley farther down Kali Opak. In this area, three spots were found where channel sinuosity exceeds one degree/metre and channel capacity was below 210 m^2 (Fig. 17.8). These spots are potential sites for future lahar overbank flows if the lahar volume and velocity are equal to or greater than the May 2011 Ngerdi event.

However, the evolution of the lower and middle reaches of the river systems at Merapi can hinder sediment transportation, which may not feed further lahar overbank flow. Material extraction from valley-confined PDC deposits is a fast process that takes place along all reaches as soon as the deposits have cooled down. Over the past 50 years, many check dams have been erected across the majority of the river channels on the west and south flanks, holding sediment mass at least temporarily and altering the behaviour of sediment transportation down valley (e.g. Fig. 17.3). This has two profound implications, according to the results based on geomorphological surveys and investigations on sediment transport along the Gendol-Opak catchment by Gob et al. (2016). Firstly, the expected sediment wave, subsequent to the massive PDC input in 2010, was not recorded down valley. Sediment travelled a few kilometres and never reached the lower reaches. Clastic aggradation occurred during the eruption, followed by a rapid incision by lahar tails and floods over four years, but the sediment was trapped by numerous dams across the middle and lower valley reaches. A series of flash floods swept away these reaches, but peak discharges and sediment transport rates never reached the values that lahars exhibited in the upper reaches. Secondly, Gob et al. (2016) stressed the fact that the middle and low reaches of the valleys, instead, show clear indication of bed incision and signs of river entrenchment, which may destabilise dam foundations. Overall, these valley reaches seem disconnected from the upper catchment where the sediment production occurs. This is at odds with the results of studies carried out on volcanoclastic aprons elsewhere, where engineering protection is missing. We cannot conclude, therefore, that the evolution of river systems at Merapi may hinder most lahars in the near future, as in case of massive PDC and tephra production, the middle and lower reaches may be re-connected to the upper valleys.

17.5 Geophysical Measurements

The lahar monitoring system at Merapi is but one example among several experimental devices devoted to studying flow behaviour and dynamics in natural channels at active volcanoes such as Semeru, Colima, Ruapehu, and elsewhere; a broad array of geophysical sensors, including ultrasonic or laser radars recording flow stages (Doyle et al. 2010, 2011; Iverson et al. 2010, 2011;), in and near river channels measure a series of lahar characteristics (Itakura et al. 2005; Coviello et al. 2018). Measured parameters include: mean and peak front and surface velocities, mean and peak discharges, depth range, sediment concentration, surface instability, temperature and pH. In turn, these parameters help infer important characteristics of lahars such as Froude number, density, dynamic viscosity and bulking capacity (Pierson et al. 1990; Doyle et al. 2010, 2011). Basal normal stress and shear stress can be measured by load cells, and two load cells are used to infer changes in sediment concentration. Pore pressure sensors measure the pressure of the interstitial flow fluid, which can increase due to turbulence, but can also decrease with fluid dilatation due to collisional phenomena (Cole et al. 2009).

Over the past two decades, diverse seismic sensors have been used to record ground vibrations generated by lahars and debris flows: (1) seismometers, (2) acoustic devices such as geophones, microphones, hydrophones, and (3) accelerometers (Bänziger and Burch 1990; Itakura et al. 1997; Suwa et al. 2000; Lavigne et al. 2000b; Huang et al. 2004, 2007; Arattano and Marchi 2008; Cole et al. 2009). A few studies have focused specifically on lahars by means of seismic survey and frequency analysis to determine flow dynamics and kinematics (Zobin et al. 2009; Cole et al. 2009; Cole 2011; Vázquez et al. 2016; Coviello et al. 2018). The signal duration, frequency composition, apparent velocity, and correlations between them are the most significant and discriminant parameters.

The amplitude and frequency band signals generated by lahar/debris flow events are often determined by (1) the type of particle motion, (2) the distribution and size of particles, (3) properties of the interstitial fluid, and (4) the geometry and nature of the channel (Huang et al. 2004; Cole et al. 2009).

The succession of phases within a lahar event can also be recognised using seismic records (Cole et al. 2009; Doyle et al. 2010, 2011; Coviello et al. 2018). The front is defined by high velocity and an increased flow height, which generates relatively low seismic activity. The head phase, behind the front, shows a rapid increase in sediment concentration with corresponding intense seismic activity. The body phase is marked by seismic activity lower than the head phase, while a further decrease in seismic energy reflects the lahar tail. Seismic analysis of the propagation of lahars led several authors to similar conclusions: lahar fronts generate signals between 10 and 30 Hz (in some cases due to the accumulation of large blocks at the flow front), while lahar tails trigger frequency signals between 60 and 80 Hz. Common variations in frequency depend on the flow composition and dynamics. HCFs, instead, generate higher frequency bands between 100 and 300 Hz (Marcial et al. 1996; Lavigne et al. 2000b; Huang et al. 2004, 2007). The characteristics of the three components of a signal, i.e. north, east and vertical, may suggest the flow type and its dominant regime or rheology. Different mechanical models of flows can explain the differences in the spectral composition of lahars illustrated by seismic signals (Cole et al. 2009; Zobin et al. 2009; Vázquez et al. 2016). These innovative and promising studies show the advantage of passive flow recording to define particle–particle and particle-bed interactions, and eventually flow regimes.

17.5.1 Early Experimental Measures

Not only has real-time monitoring of lahars at Merapi improved early warning delivery, but it has provided some clues on lahar flow

characteristics. Lahar-related seismic signals have been processed to identify flow characteristics such as impulse signal, duration, maximal amplitude, and inferred flow velocity. Early geophysical measurements were conducted in situ along three rivers that conveyed lahars on the W and SW flanks after the 1984 eruption (Suwa and Nidhimura 1992; Suwa and Sumaryono 1996) and the 1994 events (Lavigne et al. 2000a).

Rainfall intensity/duration that triggered lahars were derived from weather radar and telemetered rain gauges of the former Sabo Technical Centre. Lahar dynamics were monitored using new non-contact detection instruments installed on the slopes of the volcano, including real time seismic amplitude measurements (RSAM; Endo and Murray 1991), seismic spectral amplitude measurement (SSAM) and acoustic flow monitoring (AFM) devices. Calibration of these systems was accomplished by field measurements of flow velocities and discharge, contemporaneously with instrumental monitoring (see Fig. 13 in Lavigne et al. 2000a) and non-contact lahar sensors operated by BPPTKG and involving RSAM, SSAM and AFM systems (see Fig. 14 in Lavigne et al. 2000a). The various systems have advantages and disadvantages relative to each other and against competing technologies, but the multiple-system approach has demonstrated its effectiveness. The RSAM system was able to capture data for 8 lahars, and together with SSAM, they offer the advantage of being connected to the Merapi operative seismic system. They are not actually “lahar sensors” but techniques for analysing data from conventional seismic sensors and telemetry.

More than 50 rain-triggered lahars were generated in the Boyong, Bebeng and Bedok valleys during the first rainy season following the BAF deposits of 22 November 1994. The 1994–1995 lahars were relatively short events, ranging between 30 and 90 min. As many as 90% of the lahars were observed at Kaliurang village between 13:00 and 17:30 pm owing to predominant afternoon rainfalls. The mean velocity of lahar fronts ranged between 1.1 and 3.4 m/s, whereas the peak flow velocities varied from 11–15 m/s, under the Gardu Pandang viewpoint

location at Kaliurang, to 8–10 m/s at a Section 500 m downstream from this site. Peak discharges recorded in various events ranged from 33 to 360 m³/s, with the maximum peak discharge 360 m³/s on 20 May 1995.

Instrumental thresholds were proposed to improve the lahar warning system along Kali Boyong: These non-contact instruments possess obvious advantages to the breaking-wire class of lahar sensors that require field maintenance after each significant lahar and provide no protection in the instance of multiple flow pulses. Thus, lahars recognised by 10-min RSAM values exceeding 400 units, one-minute SSAM signals exceeding 80 units on the higher frequency band, or AFM ground velocities greater than 400 mV on the low-gain band, can be considered as hazardous.

17.5.2 Signal Characteristics

At Merapi, several river channels were equipped with more than one lahar station, enabling us to calculate the intervening velocity of flows from the RSAM data. Lahar velocity is an important

piece of information; once a lahar can be detected upstream and the velocity computed at one station, then early warning can be delivered to settlements exposed down valley. Sulistiyani et al. (2018a, b) applied the Arratano and Marchi (2008) method to the pairs of stations installed along the Putih, Boyong, and Senowo rivers (Tables 17.3, 17.6). Flow velocities have been calculated using cross-correlation methods and the correlation function has been used to identify the pattern and structure of signals. RSAM datasets obtained from Kali Boyong, Putih, and Senowo stations have been plotted on the same time intervals to observe similarities. The cross-correlation calculation results show that flow velocities along Kali Putih range between 3.50 and 7.53 m/s (with reliable correlation coefficients of 0.81–0.99; Table 17.6). Lahars reach higher velocities in Kali Putih than in Kali Boyong and Senowo. Kali Boyong has the steepest slope gradient, followed by Senowo and Putih, but the Kali Putih riverbed contains a smaller size range of volcanic material, thus reducing riverbed roughness.

Physical parameters of the 2011 lahar flows recorded at GDN2 (Kali Gendol) and SBY1

Table 17.5 Physical parameters of lahar flows as recorded at GDN1 (Kali Gendol) and SBY1 (Kali Boyong) stations

| Parameters | K. Gendol GDN2 Station | | | | | | K. Boyong SBY1 Station | |
|--|------------------------|------------------|---------------------|---------------|---------------------|--------------|------------------------|---------------|
| | 21 February 2011 | 28 February 2011 | 14 April 2011 | 23 April 2011 | 1 May 2011 | 6 May 2011 | 8 March 2011 | 14 April 2011 |
| Start time (UTC) | 10:04:00 | 09:05:00 | 09:28:00 | 05:19:09 | 09:36:31 | 09:14:00 | 09:52:18 | 08:08:59 |
| Duration (minutes) | 167 | 91 | 142 | 66 | 295 | 86 | 68 | 170 |
| Max Amplitude (Count) | 17.952 | 18.253 | 19.400 ^a | 182.14 | 19.400 ^a | 18.703.53 | 20.861.66 | 16.621.16 |
| Dominant frequency (Hz) | 17 | 15 | 11 | 9.5 | 10.4 | 14.8 | 8.70 | 10.67 |
| Rainfall intensity at Kaliurang (mm/h) | 25 | 230 | 97 | 80 | 265 | 27 | 22 | 112 |
| LH flow pulses | Single pulse | Multi pulse | Multi pulse | Multi pulse | Multi pulse | Single pulse | Single pulse | Single pulse |
| Flow type | HCF | HCF | DF | DF | DF | HCF | DF | DF |

^a saturated amplitude

Table 17.6 Velocity of lahar flows recorded in the Putih, Boyong and Senowo stations in 2011. Maximum velocity was 7.53 m/s, minimum was 2.29 m/s, average velocity was 4.12 m/s

| No | Date | River name | Station name | Distance (m) | Elevation difference (m) | Correlation coefficient | Velocity (m/s) |
|----|-----------------|------------|--------------|--------------|--------------------------|-------------------------|----------------|
| 1 | 2 March 2011 | K. Putih | PTH1-PTH2 | 2080 | 121 | 0.81 | 3.50 |
| 2 | 4 March 2011 | | PTH1-PTH2 | | | 0.99 | 7.53 |
| 3 | 8 Mar 2011 | | PTH1-PTH2 | | | 0.99 | 7.00 |
| 4 | 11 Mar 2011 | | PTH1-PTH2 | | | 0.96 | 7.00 |
| 5 | 3 November 2011 | | PTH1-PTH2 | | | 0.98 | 5.00 |
| 6 | 4 March 2011 | K. Boyong | SBY1-SBY2 | 4400 | 318 | 0.82 | 3.86 |
| 7 | 8 March 2011 | | SBY1-SBY2 | | | 0.78 | 2.93 |
| 8 | 14 April 2011 | | SBY1-SBY2 | | | 0.97 | 2.82 |
| 9 | 3 November 2011 | | SBY1-SBY2 | | | 0.97 | 2.29 |
| 10 | 8 March 2011 | K. Senowo | SNW1-SNW2 | 3950 | 194 | 0.85 | 2.93 |
| 11 | 17 March 2011 | | SNW1-SNW2 | | | 0.90 | 3.33 |
| 12 | 19 March 2011 | | SNW1-SNW2 | | | 0.93 | 3.33 |
| 13 | 21 March 2011 | | SNW1-SNW2 | | | 0.93 | 3.49 |
| 14 | 22 March 2011 | | SNW1-SNW2 | | | 0.72 | 3.19 |
| 15 | 23 March 2011 | | SNW1-SNW2 | | | 0.74 | 3.67 |

(Kali Boyong) stations are shown in Table 17.5. The 2011 lahar flows recorded at GDN1 (Gendol) and SBY1 (Boyong) stations lasted between 30 min and 5 h, and they were often recorded between 13:00 and 17:00 pm local time due to more frequent daytime rainfall events. Figures 17.9 and 17.10 show seismic and visual analysis of the CCTV camera videos acquired during the 11 March, 1 May and 13 June 2011 lahar events. The lahar signals can be divided into the following four phases: (a) before the flow arrival, (b) once the first flow pulse propagates, (c) after the flow pulse, and (d) during the second flow pulse.

According to the classification distinguishing single-pulse and multi-pulse events (SPE and MPE) proposed by Vázquez et al. (2016) at Volcán de Colima, Sulistiyani et al. (2018b) determined that Merapi lahars also show SPE and MPE based on recording seismic signals and visual data observations, as previously shown by Doyle et al. at Semeru in 2010 and 2011 (Table 17.5). Based on the available dataset, the maximum seismic amplitude was correlated with the magnitude of the flow. The amplitude

envelope was calculated with a Hilbert transform algorithm using the Seismic Analysis Code on the filtered signals. The frequency contents were analysed using simple Fast Fourier Transform (FFT). The dominant frequency of lahars ranged between 8 and 11 Hz at the Boyong station and the prevailing frequency of the lahar pulse recorded at the GDN1 station ranges between 9.5 and 17 Hz, pointing to DF fronts with higher solid concentration than DF bodies and HCFs (Table 17.5). According to publications on lahar seismic signals, this frequency range is similar to that delivered by coarse, boulder-rich DF fronts (e.g. Cole et al. 2009; Coviello et al. 2018), whereas DF bodies and HCFs show higher frequencies.

Based on these seismic signal analyses, compared and validated with CCTV footage, two categories of flows were identified at Merapi: (1) Lahars having coarse and highly concentrated fronts are detected owing to a small increase in the seismic signal before the main peak. The turbulent flow bodies show surface instabilities typical of debris flows enriched with block-rich peak discharges; and (2) lahars showing no

boulder-rich fronts and less concentrated bodies with low seismic frequency and weak surface instabilities are attributed to HCFs.

17.5.3 Recent Geophysical Measurements in the Kali Gendol Valley

Using an array of geophysical instruments installed in and near river channels on the south flank of Merapi, in particular the Kali Gendol valley after the 2010 eruption, Mainsant (2014) and Wibowo et al. (2015) measured lahar dynamics in order to define their hydraulic and physical characteristics.

The dataset analysed by Mainsant (2014) was acquired at a study site about 10 km from the summit on the edge of Kali Gendol channel near Kepuharjo. Two stations were implemented 275 m apart in a linear reach of the 60 m-wide, N-S trending channel with a slope of 3.3°: (1) *Sabo Up* (upstream) on a 50 m wide dam at 655 m asl and (2) *Sabo Down* (downstream) on a 30 m wide dam at 639 m asl (Fig. 17.11A). The seismometer was installed at the *Sabo Up* site 6 m from the edge on the east channel bank and 12 m above the bed. AFM geophones were located at both sites on the east bank (Fig. 17.11A). Figure 17.11B shows the geophysical dataset: seismic envelopes of the three-component seismic signal, its spectrogram, sediment concentrations sampled at both sites, pore pressure, and vibrations recorded by the upstream AFM. The 16 February 2012 front arrived at the stations in the afternoon with a velocity of 1.5 m/s. Pore pressure measurements revealed the arrival of the lahar front, followed by irregular fluctuations during flow propagation (Fig. 17.11B(a)). Four packets, separated by dotted lines, were defined by abrupt changes in waveform envelopes of signals (Fig. 17.11B(f)) and pore pressure measurements (Fig. 17.11B(e)).

For packet 1, the sediment concentration was relatively stable at the *Sabo down* site. For packet 2, the sediment concentration increased at *Sabo down* but remained stable at *Sabo up*. At the beginning of lahar from packet 2 onward, the

sediment concentration values were similar, i.e. c. 20% at the two stations. Packet 3 shows a decrease in sediment concentration at both upstream and downstream sites, but with larger values for the last one. The last packet 4 was defined by a low and relatively stable sediment concentration for both sites. The sediment concentration also decreased at the downstream site, equaling the upstream value (< 10%) indicating that the lahar tail mainly consisted of water. Average values of sediment concentration were under 40 vol%, suggesting HCF type (Fig. 17.11B(b)).

Figure 17.12 shows the spectrogram and envelopes of the three-component seismometer. AFM recording at *Sabo up* showed a sudden increase in vibrations, which indicated lahar arrival, identified by the amplitude increase of the signal (Fig. 17.12a, b). Then, vibration variations varied in accordance with pore pressure fluctuations at the same site. However, the signal merged with ambient noise before the end of flow. About 45 min after the front arrival, the signal/noise ratio tends to 1 while the AFM sensor records a significant propagation of the flow. The spectrogram shows a relatively low frequency band (between c.5 and 75 Hz) of a shallow and concentrated lahar, which remains stable for packets 1 and 2 (Fig. 17.12c). Packet 3 shows a slow drop of seismic energy and frequencies (between 5 and 50 Hz). Then the lahar tail merges with the relatively large background noise at low frequencies (< 10 Hz). Envelopes of the three components clearly mark a lower energy in the direction perpendicular to the channel during the passage of lahar (Fig. 17.12d).

In the case of Semeru, bulking and debulking phases were defined by the difference between the inflow and outflow discharges (Doyle et al. 2011). Discharge flow calculation being impossible at Merapi, Mainsant (2014) defined these phases using the difference between incoming and outgoing sediment concentration. Both concentrations were similar during packet 3–4 (Fig. 17.11B(d)), so the bulking-debulking ratio tends to 1. This ratio began to decrease for packet 3 because the outgoing sediment concentration was about two times larger than the incoming, so bulking dominated this phase. However, these

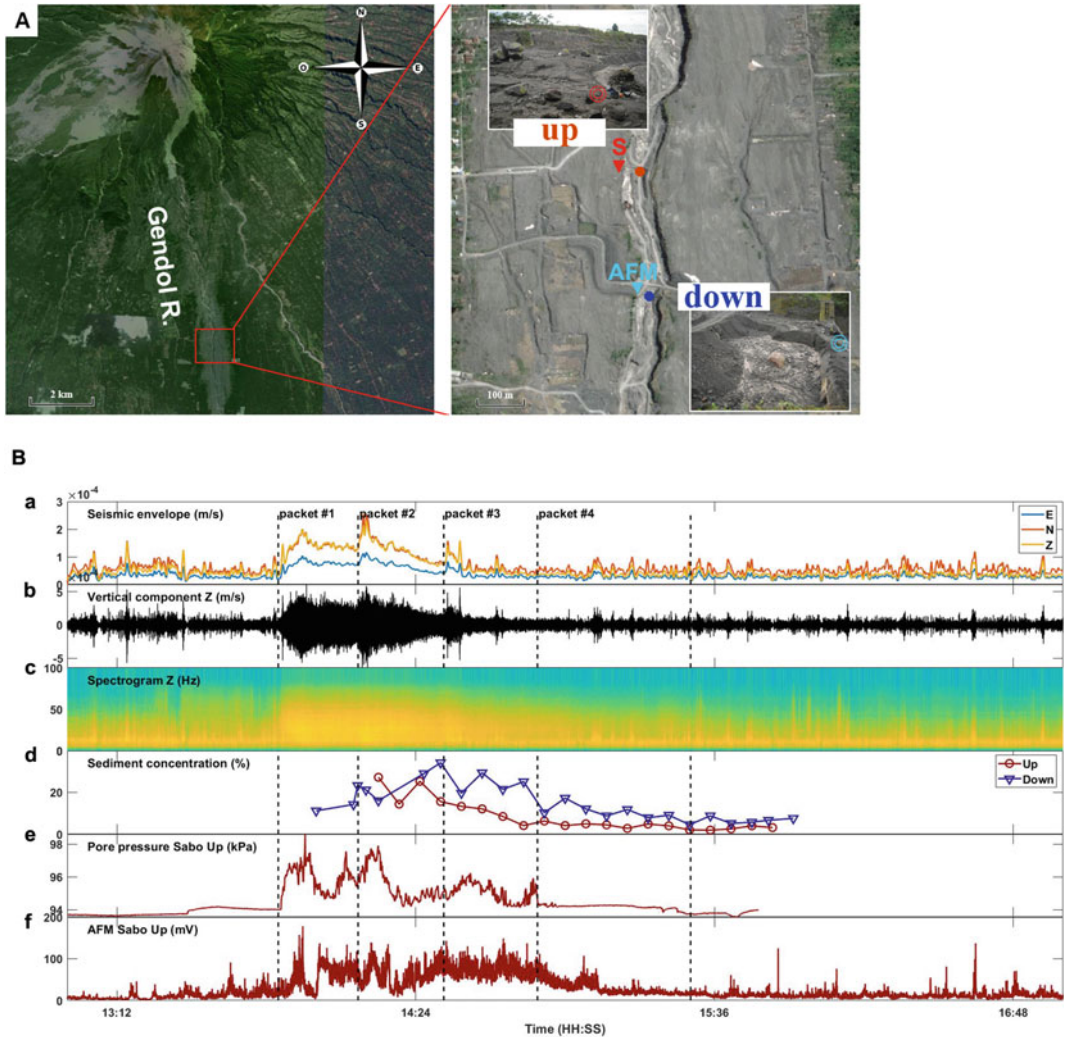


Fig. 17.11 Geophysical measurements of lahars in Kali Gendol valley at Merapi. **A** Red rectangle to locate the two stations on the Google Earth image, termed Sabo dam down (Manggong site, blue point) and Sabo dam up (Kepuh site, red point) at 275 m distance; double circles inside the two pictures indicate sensors buried in the channel (3 components seismometers S and AFM geophone at up and down sites respectively). **B** Dashed lines outline different packets or pulses within the 16 February 2012 lahar. **a** Envelope components from

seismometer (S): perpendicular to the channel (\perp), parallel to the channel (\parallel) and vertical (Z). **b** Vertical component of the signal generated by the lahar flow. Red: signal envelope process by a cutoff frequency with low pass filter 0.025 Hz. **c** Spectrogram of the vertical component of the signal. **d** Sediment concentration in % of both sites (at *up* and *down* sites). **e** Pore pressure in kPa (at *up* site). **f** AFM vibrations at *up* site (vertical component Z, in mV) (after Mainsant 2014)

behavioural changes were not reflected by a clear change in the frequency and directional response of the seismic signal (Figs. 17.11B(a) and 17.12b). The lahar tail (packet 4) was marked by a sediment concentration decrease of the two sites and a convergence towards low values

(between 5 and 13%). The increase in seismic amplitude was correlated with the concentration of the sediment.

Two important differences stem from the Semeru and Merapi seismic datasets (Fig. 17.12 b). First, in the case of Merapi, there are no

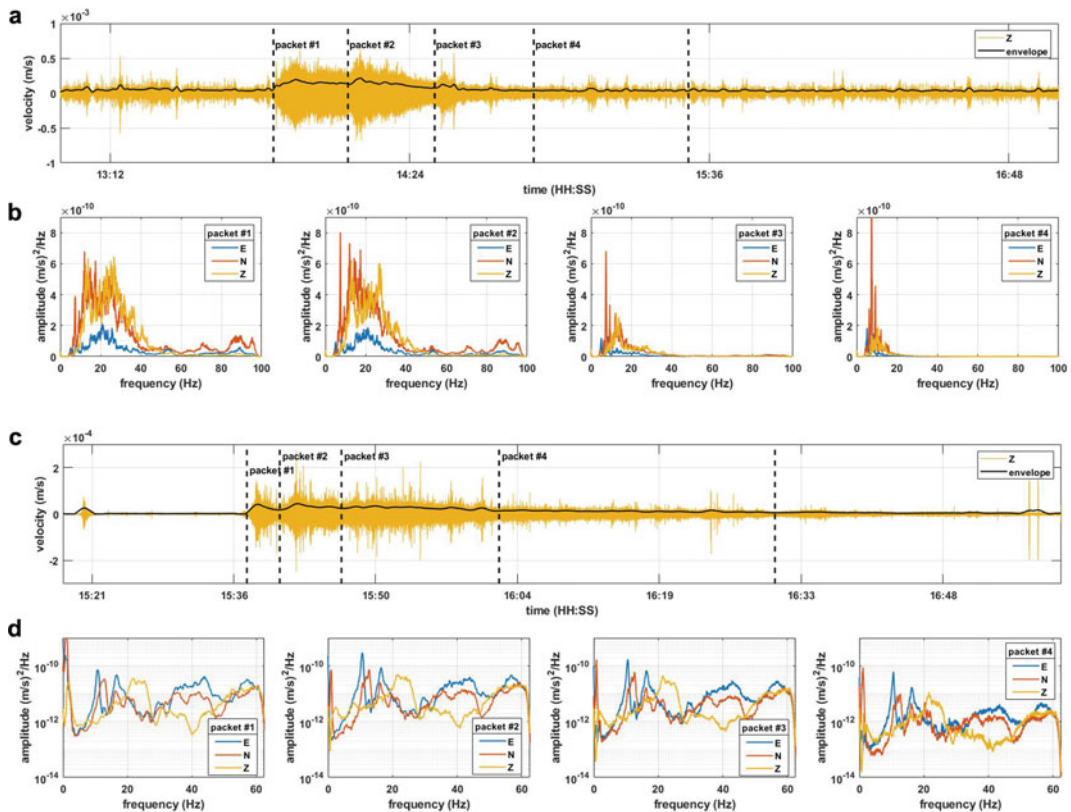


Fig. 17.12 **a** Seismic signals of the three components, perpendicular, parallel and vertical, of the 16 February 2012 Merapi lahar. Vertical black dotted lines indicate different lahar packets or pulses. **b** Spectra of three signal components (E, N and Z) for each packet of signal responses (1–4). **c** Seismic signals of the three components, perpendicular, parallel and vertical, of the 12

March 2008 Semeru lahar (modified from Doyle et al. 2010). Dotted lines indicate different lahar packets or pulses. **d** Spectra of three signal components (E, N and Z) for each packet of signal responses (1–4). Seismometers have been oriented with respect to channel geometry (after Mainsant 2014)

preferential frequency bands as distinct peaks. The dominant frequency band exhibits homogeneous amplitudes and extends between c. 10 and 40 Hz (Fig. 17.12a, b). Second, peak vibrations at Merapi, although similar in frequency (about 12 Hz and 16 Hz; Fig. 17.12b), were not oriented perpendicular to the channel as at Semeru, but parallel. This may be related to the difference in sedimentary concentrations and/or to local site-specific effects on amplification or damping of particular frequencies or directions. The 5 March 2008 lahar event at Semeru (Doyle et al. 2010) exhibited solid concentrations between 40 and 60%, while they remain under 40% for the Merapi event. This difference may play an

important role on flow regimes: a turbulent regime with collisional processes for Semeru lahars, and a laminar regime for Merapi lahars. Further studies are required to validate this hypothesis.

17.5.4 Combining Measurements: 28 February 2014 Lahar Event

The interpretation of lahar dynamics remains challenging without performing in situ observations using multi-parameter stations and video images of the flow in motion (Doyle et al. 2010,

2011; Starheim et al. 2013). Wibowo et al. (2015) combined video shooting and seismic data acquisition to analyse lahar dynamics in the upper reaches of the Kali Gendol catchment (4.6 km from the summit at 1090 m asl) during the 28 February 2014 event. Although the frequency of lahars in Kali Gendol had decreased in 2014 due to the shrinking supply of unconsolidated material, it increased instantly after the 13 February 2014 Kelud eruption, which deposited ashfall thicknesses between 2 mm to the west of Merapi (Yogyakarta and Magelang) and 5 mm to the east of Merapi (Sleman and Klaten), some 200 km away from Kelud. A key point is that rain-triggered lahar activity can be initiated in a distal system due to landscape destabilisation by an influx of distal ash erupted from another volcano. Within 30 days of the Kelud eruption, there had been 19 lahar events at Merapi. The first major event during this period, the 28 February 2014 lahar, was observed in the upper reach of the Kali Gendol catchment by a station that included a datalogger and two seismic geophones installed 76 m apart and parallel to the river channel, completed by an automatic camera on the east bank and a manual video on the west bank of the river. Two rain gauges were mounted at 1100 m asl on the SW and SE flanks of the volcano.

The 28 February 2014 lahar was triggered at 14:11 pm at the summit area and arrived at the observation site with an average velocity of 4.1 m/s, following rainfall coming from the eastern part of the volcano (Wibowo et al. 2015). The rainfall intensity was 24 mm for 67 min, but this value cannot be considered as a threshold since most of the lahar flows in this catchment were initiated further upstream, between 1500 and 2000 m asl (see Sect. 17.2.2). Four lahar flow phases were identified. The first phase, 13 min. long, was recognised as an HCF, which reached a maximum depth of 1.6 m with a maximum velocity of 5 m/s and discharge of 40 m³/s (Table 17.4). The second phase was attributed to a 3-min peak of debris flow, which reached a maximum depth of 7 m, a mean velocity of 16 m/s, and a maximum discharge of 473 m³/s. The third 6-min-long phase was

identified as the lahar body characterised by an irregular decrease of the flow stage (from 4 to 1 m), velocity (from 12 to 4 m/s), and discharge (from 80 to less than 10 m³/s). The fourth phase was a 72-min. long lahar tail, which was indicated by a slow decrease of the flow stage (< 0.1 m), velocity (< 0.4 m/s), and discharge (< 0.10 m³/s) until it reached the usual low river stage at the end of lahar. The transport of visible boulders was concentrated at the peak of the debris flow phase, which was able to transport boulders weighing more than 20 tons. The seismic signals of the two geophones (upstream and downstream) showed the same frequency for the HCF flow (150–240 Hz). However, for the debris flow phase, the geophone responses were different; the upstream geophone recorded a frequency range between 10 and 50 Hz with a peak frequency at 20 Hz, whereas the frequency range from the downstream geophone recorded a frequency between 10 and 150 Hz, with peak frequency at 70 Hz.

Direct sampling of sediment concentration during the event was impossible because the lahar flow was 6 m deep at a velocity of 16 m/s. However, based on the discharge and number of visible boulders, different lahar phases have been distinguished, including streamflow, HCF, debris flow front and peak, debris flow of lahar body, and HCF of lahar tail, as Mainsant (2014) observed in the same valley and Doyle et al. (2010, 2011) at Semeru. This lahar with one peak discharge only was followed by two major pulses, but previous lahars in the same river in 2011 also exhibited irregular and multi-peaked discharges (de B elizal et al. 2013, and Sect. 17.4.2). Most of the transported boulders were forced to touch the riverbed at the upstream station due to a waterfall, but these boulders floated farther downstream due to buoyancy and dispersive pressure effects of the viscous flow. This transport process produced a higher frequency seismic signal at the downstream site (5–150 Hz) compared to the seismic signal recorded at the upstream site (5–50 Hz), confirmed by the result of video analysis during the debris flow phase at the downstream station. However, debris flows have often been interpreted in the literature by having a relatively low

seismic frequency range (Cole et al. 2009). The location of seismometers with respect to channel morphology may play a role; given that seismic responses vary according to the channel morphology, geophysical parameters must take seismic directionality and flow regimes into account for interpreting the seismic frequency ranges of different lahar pulses (Doyle et al. 2010, 2011; Mainsant 2014; Coviello et al. 2018).

17.6 Lahar Impact

Lahars account for about a quarter of all historical volcanic fatalities globally since the seventeenth century, and are the largest cause of fatal volcanic incidents > 15 km from the volcano, with fatalities recorded as far as 100 km away (Brown et al. 2017). Lahars can bury, wash away, damage or destroy structures, abrade critical infrastructure such as water turbines or infill sediment traps polluting any drinking supplies. A review of the impact of lahar on critical infrastructure (Wilson et al. 2014) found documented lahar damage for buildings, bridges, roads, vehicles, railways, water intakes, hydro-electricity facilities, and computers. For example, lahars damaged water intake systems used for energy site cooling during and after the 1980 Mt. St Helens eruption (Pierson 1986), and water pipes and well heads were damaged or buried following lahars at Soufriere Hills Volcano, Montserrat in 1995 (CDERA 1997) and at Mayon in 2002 (GVP Global Volcanism Program 2002). Large lahar deposits or fast-moving flows can scour or bury agriculture. However, thin lahars can bring valuable nutrients to agriculture areas. The deposition of large quantities of sand by lahars provides economic resources that fund large mining efforts, as seen at Merapi following the 2010 eruption (Ikhsan et al. 2010; de B elizal et al. 2013). A well-recognised downside of mining such deposits is that the increased numbers of people, trucks and equipment in lahar inundated areas cause concerns for hazard and risk management.

Large, energetic lahars can move or destroy buildings, bridges and other structures, and

modify the drainage network on a volcano, as at Merapi after the 2010 eruption (de B elizal et al. 2013; Jenkins et al. 2015). Yulianto et al. (2013) calculated that the post-2010 lahars affected 133.31 ha of settlements, 92.32 ha of paddy fields, 235.60 ha of dry farming, 570.98 ha of plantations, 380.86 ha of bare land, and 0.12 ha of forested areas. In total, 12,276 buildings were estimated to have been damaged. The extent to which a structure has been damaged will depend upon lahar characteristics such as the velocity, depth, density, viscosity, sediment concentration and grain size, as well as the setting, orientation and integrity of the structure being impacted. A number of studies have been dedicated to assessing likely lahar dynamics (e.g. Rodolfo et al. 1996; Lavigne and Thouret 2003; W orni et al. 2012), but few have concentrated on the physical responses of buildings and infrastructure to lahars (e.g. Zuccaro and De Gregorio 2013; Ettinger et al. 2016; Jenkins et al. 2015; Hadmoko et al. 2018; Thouret et al. 2020).

Studies on the impacts of recent lahars, such as Nevado del Ruiz, Colombia, 1985 (Pierson et al. 1990), Pinatubo, Philippines, 1991 (Major et al. 1996), Sarno, Italy, 1998 (Zanchetta et al. 2004), and Chait en, Chile, 2008–2009 (Pierson et al. 2013) provide valuable insights into the range of damage that a lahar may cause. However, detailed data on damage from lahars are scarce (Blong 1984), often because damage is total, either through structural collapse or burial, or because the redirection of a channel during or following a lahar can threaten investigator safety and inhibit detailed studies (Jenkins et al. 2015). Post-impact damage surveys were carried out for Merapi by Jenkins et al. (2015) and Hadmoko et al. (2018). Jenkins et al. (2015) identified the different levels of damage sustained by buildings during the 9 January 2011 lahar in Kali Putih (Fig. 17.13), using remote sensing and field studies to evaluate modes of failure and calculate the approximate ranges of impact pressure sustained by buildings in the impact area. The authors used these data to develop quantitative relationships between lahar characteristics and the probability of failure for building types around Merapi. They found that most weak

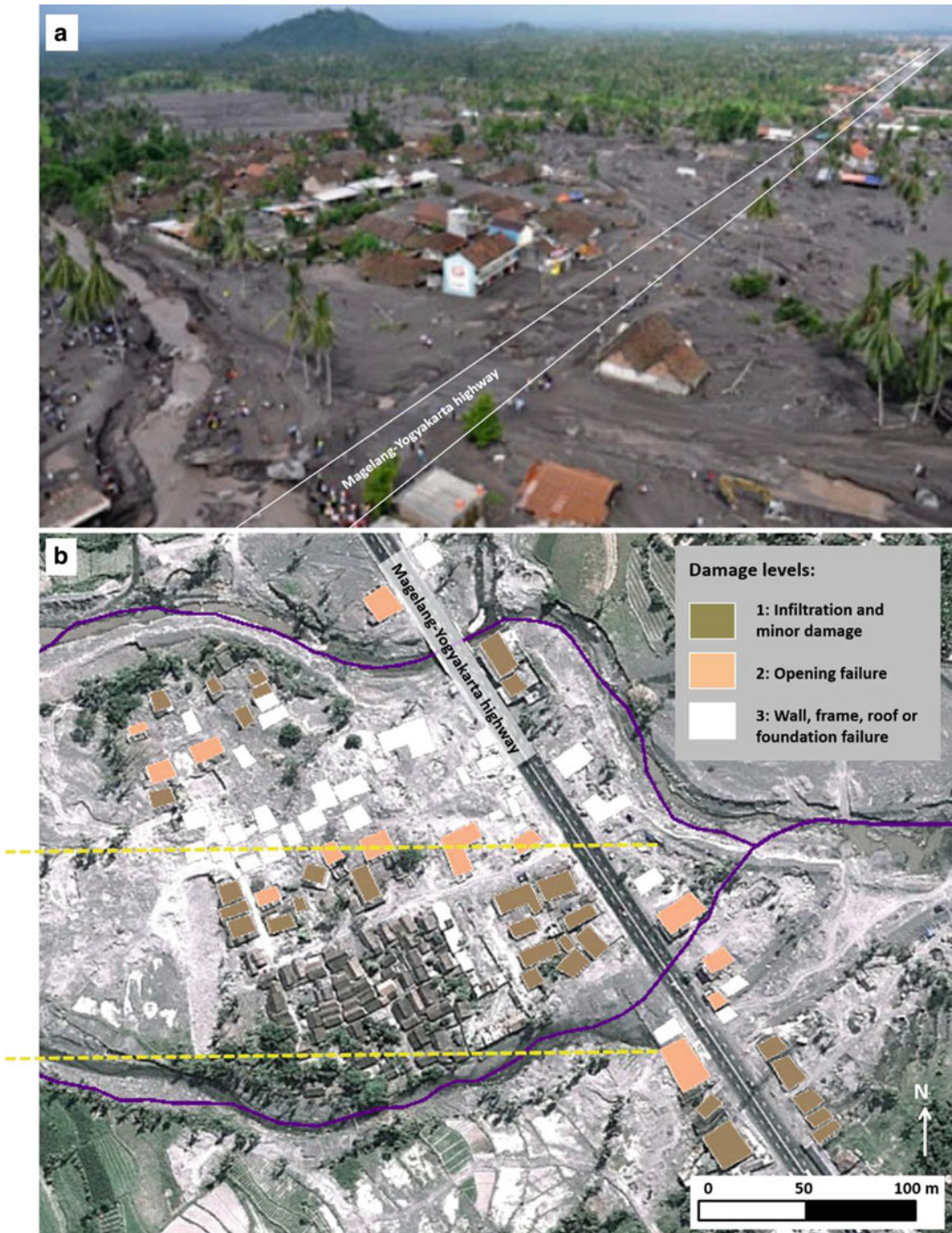


Fig. 17.13 **a** Aerial image of Gempol village, along K Putih river 17 km away from Merapi summit, taken shortly after the 11 June 2011 lahar impact and before the main highway had been cleared of deposit (photo credit: Jakarta Post). **b** Google Earth satellite image acquired

5 months later showing the main axis of damage (buildings in white: Jenkins et al. 2015) as a result of lahar not following a split in pre-existing river channels. The lahar flowed from right to left in both images

Table 17.7 A comparison of damage states/levels proposed by Jenkins et al. (2015) and Hadmoko et al. (2018) for buildings impacted by the 2011–2012 lahars along Kali Putih

| Damage states (Jenkins et al. 2015) | | | Damage levels (Hadmoko et al. 2018) | |
|-------------------------------------|---|---|-------------------------------------|--|
| Description | Criteria | Consequence | Description | Criteria |
| No damage | – | – | No damage | No sign of damage visible |
| Minor | Infiltration into building under door and through gaps not produced by lahar, e.g. cracks or ventilation grills | Damage to contents of building | Very slight damage | Minor damage to doors and windows visible; no crack/s in the walls |
| Moderate | Window glass failure; possible weak door and window frame failure | Deposition of sediment inside building; significant damage to contents | Slight damage | Minor damage to doors and windows visible; cracks and potholes in walls; no damage to the structure |
| Major | Loss of parts of external and/or internal walls and infill panels Burial by sediment | Significant internal deposits Building likely unsafe for occupancy Potentially irreversible damage or costly clean-up | Moderate damage | Some damage visible as in previous two levels; cracks evident in some of the side walls with a large hole on one side; minor damage to the structural cracks; roof intact |
| | | | Severe damage | Some damage visible as in previous three levels; wall collapsed on several sides of the building; severe damage to the structure (cast pillars bent and partially broken); minor roof damage |
| Complete | Wall, frame, roof or foundation failure Burial by sediment | Building unsafe for occupancy; building may have to be demolished Potentially irreversible damage or costly clean-up | Very heavy damage | Some damage visible as in previous four levels; walls collapsed on almost all sides; severe damage to structure; roof severely damaged; building remains standing |
| | | | Destroyed | Building completely destroyed, with only the foundation remaining |

See also Prasetyo et al. (2018) for an approach based on Sentinel1, ALOS Palsar and Landsat imagery

masonry buildings would be destroyed by dilute lahars with relatively low velocities (c. 3 m/s) and pressures (c. 5 kPa), while the majority of stronger rubble stone buildings may be expected to withstand higher velocities (up to 6 m/s) and pressures (up to 20 kPa). Hadmoko et al. (2018) covered a larger temporal domain for Kali Putih valley (November 2010 to April 2012) and included damage collected from local government reports. Both studies categorised the buildings into different classes that reflected their vulnerability to lahars and assigned damage

levels to each of the identified buildings (Table 17.7). Hadmoko et al. (2018) further assessed the impact of lahars on Sabo dams, an important feature around Merapi designed to capture sediment and reduce flow runout and sediment concentration.

Buildings at the periphery of the lahars, where velocities and dynamic pressures were lower, were partially or completely buried in metres of sand or silt with some damage to walls, doors and windows (Jenkins et al. 2015; Fig. 17.14). Closer to the main flow axis, boulders and high



Fig. 17.14 Lahar impacts in the Kali Putih river valley. **a** Interior of a large building in Sirahan showing the inundation lines from the flow and deposit (red dashed lines); some damage was caused to the building exterior, and the building has since been emptied (Photo credit: S. Jenkins). **b** A destroyed building showing failure of the masonry infill walls within a reinforced concrete frame and some remaining deposit inside; flow direction was

right to left (modified from Jenkins et al. 2015). **c** Annotations of the damage caused to Gejungan I Sabo dam in the upper Putih river following the 2010 eruption of Merapi (modified after Hadmoko et al. 2018). A classification of Sabo dams based on four types of reported damage states (Fujita classification) is given in Wardoyo et al. (2013)

dynamic pressures resulted in buildings either being completely removed and washed downstream, or structurally damaged beyond repair, and buried in the deposit (Jenkins et al. 2015; Hadmoko et al. 2018; Figs. 17.13, 17.14). Sabo dams were compromised or collapsed due to vertical and lateral erosion of the dam, while cracking and weakening was caused by the large boulders colliding with the Sabo walls (Hadmoko et al. 2018; Fig. 17.14C; see Wardoyo et al. 2013 for a classification of damaged dams).

A building-damage scale was hence developed, which categorises likely lahar damage levels and, through theoretical calculations of expected building resistance to impact, approximates ranges of impact pressures. Jenkins et al. (2015) applied this preliminary damage scale to a large lahar in the Putih valley that occurred on 9 January 2011, and inundated and caused extensive building damage in the village of Gempol, 16 km southwest of Merapi (Fig. 17.13). The scale was applied remotely using public satellite images and through field studies to categorise damage and estimate impact pressures and velocities within the village. Results were compared with those calculated independently from Manning’s calculations for flow velocity and depth within Gempol village using an estimate of flow velocity at one upstream site. The results of this calculation showed reasonable agreement

with an average channel velocity (2.5–6 m/s) derived from travel time observations. The calculated distribution of flow velocities across the area of damaged buildings was consistent with the new damage scale (Table 17.7). The complementary results, even given the basic nature of the tools and data, suggest that the damage scale provides a valid representation of the failure mode that is consistent with estimates of the flow characteristics.

At the large scale of Merapi and the “Second danger zone (KRB 1)” (see below), Fig. 17.15 displays the extent and typology of the actual damage (as of 2010–11) and potential damage (as of 2012), as well as threatened strategic assets along 13 radial rivers as far as 30 km away from Merapi summit (de Bélizal 2012).

17.7 Revised Lahar-Prone Maps and Modelling Lahar Inundation Extent and Impact

Early hazard-zone maps for lahars and PDCs, drawn by Pardyanto et al. (1978) and the Japanese–Indonesian Cooperation Agency (JICA 1979), and Suryo and Clarke (1985), were revised in 2002 (Hadisantono et al. 2002). The 2002 hazard-zone or KRB map of Merapi was divided into three different regions based on

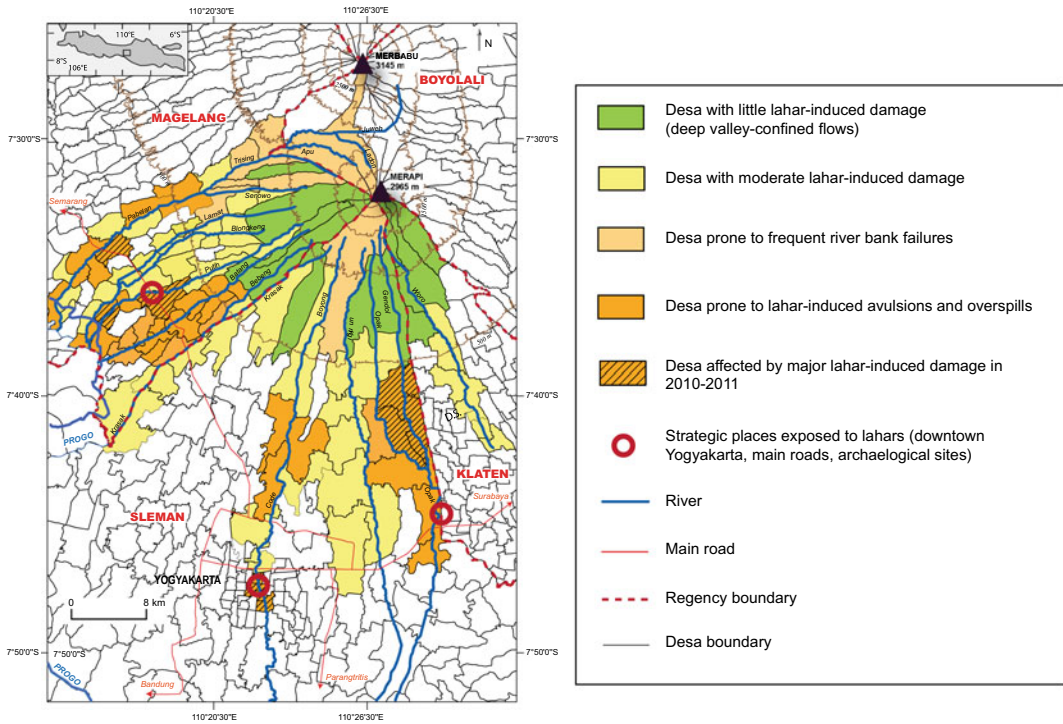


Fig. 17.15 Map showing actual and potential lahar damage at the scale of each of the *desa* (villages) along all drainages impacted by the 2010 eruption. This map has

been drawn by de Bélizal (2013) for the situation in the two years following the large 2010 event

hazard types, termed danger zones: “Forbidden zone (KRB 3), “First danger zone (KRB 2)” and “Second danger zone (KRB 1)” that collectively hosted at least 359,000 inhabitants in 2012. The 2002 hazard map outlined danger zones with the purpose of providing first-order prevention measures and mitigation policies, which proved to be useful ahead of moderate block-and-ash flow-forming, ‘Merapi-type’ eruptions. These maps did not permit accurate mapping of PDCs and lahar extent, in particular in areas subjected to overbank flow and avulsion following a large eruption such as the 2010 event. Thus, BPPTKG updated these maps immediately after the 2010 eruption taking into account the wide extent of areas affected by PDCs, lahars, and tephra fallout (Sayudi et al. 2010). Noticeable changes in summit morphology observed after the 2006 and 2010 eruptions were also taken into consideration. Thus, the revised KRB 1 and 2 zones include PDC- and lahar-prone areas based on the

most recent, large magnitude event, and extended to 17–18 km along the Gendol and Opak rivers. The revised KRB map also indicates evacuation routes, shelters, the road network, public facilities, and Merapi observatory posts.

At the time of map revision, and still now, the key zones are the ‘First Danger Zone’ (KRB 2) that considers uppermost catchments where lahars commonly initiate and converge down valley, and KRB 1, the “Second Danger Zone”, where experts thought that only lahars and tephra fall would affect the lowermost valleys. KRB1 narrows down the valley along the 13 radial drainage that cross the lowermost slopes of Merapi in the NW, W, S, and SE directions (Figs. 17.1, 17.2). These arteries are known to have conveyed lahars 15 to 25 km from the summit and partially affected the cities of Yogyakarta to the south and Magelang to the west (Lavigne et al. 2000a; Rachmawati and Budiarti 2016). In 2010, KRB 1, in particular the

south catchment, was actually affected by exceptional long-runout PDCs, and KRB 2 hosted the bulk of valley-confined PDC deposits that became the source for lahar material once the 2010 eruption unfolded and during the following rain seasons.

17.7.1 LAHARZ Modelling

Following the October–November 2010 crisis response, BPPKTG used LAHARZ simulations to generate a few large-scale (1:10,000 and 1:2000 scale) operational maps and risk assessments for a few critical river systems. The simulations delineated areas potentially affected by lahars along the valley network around Merapi after the 2010 event, in order to guide decision makers,

especially in the case of overbank flow events, and for the purpose of risk management and contingency planning. The lahar operational maps encompass several characteristics, including drainage morphology, overbank areas, road networks around valley channels, evacuation routes, settlements around the drainage network, and public facilities (Fig. 17.16). LAHARZ simulations (Schilling 2014) required three main inputs:

- (1) A Digital Elevation Model (DEM) that reflects the post-2010 topography. In early 2011, CVGHM (BPPTKG) conducted a LiDAR aerial survey to obtain a high-spatial resolution DEM of the 12 river valleys with < 1 m spatial resolution, which provided detailed geomorphic features suitable for simulations;

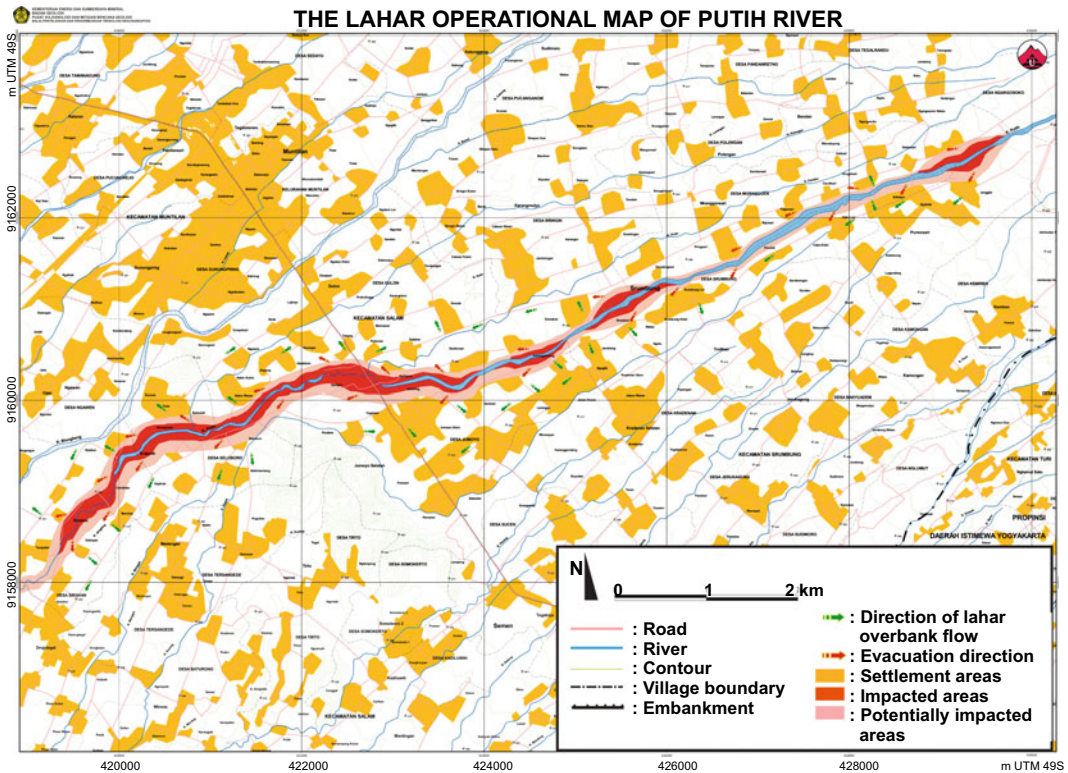


Fig. 17.16 Part of the LH operational map generated by BPPTK (CVGHM) in 2011 showing actually impacted and potentially impacted areas along the Putih river valley together with the principal exposed assets. Red areas

along Kali Putih channel were actually impacted in 2010–2011. Pink area represents the predicted maximum extent of lahars with a volume of 3.4 million m³ using LAHARZ simulations

- (2) Lahar volumes between 1 and 3.4 million m³ were estimated from volumes of pyroclastic deposits from past eruptions, which were collected by field surveys in all relevant rivers (Table 17.4);
- (3) Initial source locations were taken as the upstream boundary of the actual depositional area. These parameters were obtained from lahar events recorded in late 2010 and early 2011.

LAHARZ simulations compute the valley cross-sectional and planimetric areas of valley inundation as function of the recorded lahar volumes (Iverson et al. 1998). The planimetric area delineates hazard zones prone to lahar inundation, while the cross-sectional areas express the average extent of valley inundation and lateral spread perpendicular to riverbeds. The simulation results were then validated with the actual lahar inundation map from field surveys, especially across overbank flow areas (e.g. Figures 17.4, 17.6, 17.13 and 17.16).

Several potential lahar overbank areas were identified from the simulation results, the largest of them with a width of 310 m along the Gendol-Opak valley in the hamlet of Ngentak, village of Sindumartani, at a distance of c. 17 km from the summit. The maximum simulated overbank areas along Kali Putih, Boyong-Code, Pabelan, Woro, and Krasak were 285 m, 260 m, 230 m, 219 m, and 112 m in width, respectively. Lahar overbanks were mostly caused by the reduced volume capacity of the Gendol-Opak channel due to voluminous PDC deposits and lahar deposits that successively accumulated during the post-2010 eruption rainy season. In contrast to the Gendol-Opak case, the overbank lahar areas along Kali Putih were influenced by shallowing riverbeds and the morphological characteristics of the bends (Fig. 17.16; Sect. 17.4.3). Changes in channel slope gradient, sinuosity, and retaining embankment walls highly influence the lateral extent of lahar flows. Lee et al. (2015) also used Landsat imagery and LAHARZ to simulate lahars for several rivers around Merapi. Using GIS, they found almost 56% similarity between the detected and simulated zones, but

LAHARZ is a simple topography-filling model, which does not simulate dynamic flow interactions with channels.

For this chapter, we have updated hazard-zone area maps based on lahar simulations using the FLO-2D model with a LiDAR digital terrain model (DTM).

17.7.2 New Developments in Lahar Modelling Using the FLO2D Code

FLO-2D (FLO-2D Software Inc 2019; O'Brien et al. 1993) is based on depth-averaged continuum flow equations. Assuming that lahar thickness is much smaller than its length, it is possible to integrate the 3D mass and momentum balance equations over depth to obtain the depth-averaged continuum flow equations (Savage and Hutter 1989). This code models lahar rheology using a shear stress relationship. Details about the code itself can be found in O'Brien et al. (1993) while some details about how to apply this code to simulate lahars can be found in Charbonnier et al. (2018b). Two separate case studies are investigated here for the emplacement of: (1) three debris flows in the Gendol and Putih catchments; (2) three HCFs in the Gendol and Putih catchments. The debris flows and the HCFs separately exhibited the same rheology and sediment concentration (i.e. all debris flows were the same and all HCFs were the same), but they each had three different volumes/discharges corresponding to small-, moderate- and large-volume events; having the same rheology and sediment concentration but with three different volumes/discharges corresponding to small-, moderate- and large-volume events. FLO-2D includes various input parameters: (1) a DTM of the study area; (2) an inflow hydrograph based on measured rainfall accumulation and water and sediment discharge values (i.e. flow volume); (3) a range of Manning roughness coefficients; (4) rheological parameters; (5) laminar flow resistance; and (6) an extended Froude number, a dimensionless value defined as the ratio of kinetic energy to potential energy that also

accounts for the effect of gravity. All simulations were performed over the post-2010 LiDAR DTM (courtesy of BPTTKG) topography after smoothing and resampling of the grid to 4 m spatial resolution. Inflow hydrographs for each simulation are shown in Fig. 17.17a. Peak

discharge rates vary from 160 m³/s (small-volume events) to 480 m³/s (large-volume events) for both DF and HCF simulations while peak sediment volumetric concentrations (attained after ~ 30 min.) are set at 60 vol.% and 40 vol.% for debris flow and HCF simulations,

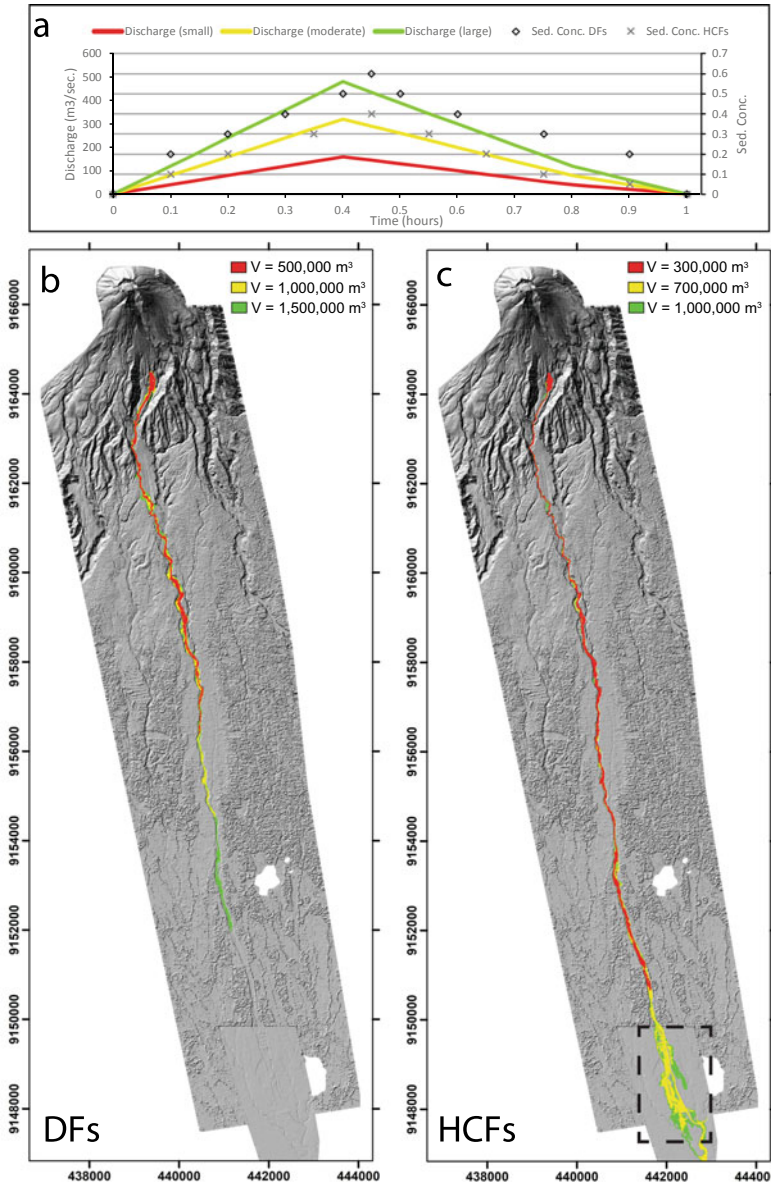


Fig. 17.17 FLO-2D simulation results for the Gendol catchment. **a** Inflow hydrographs for the three lahar events considered: small-volume (red), moderate-volume (yellow) and large-volume (green). Sediment volumetric concentrations for the debris flow (DF) and

hyperconcentrated flow (HF) simulations are also shown. **b** Inundation map of the three simulated DFs. **c** Inundation map of the three simulated HCFs. Dashed black rectangle shows the overbank area in the distal part of the Opak-Gendol catchment

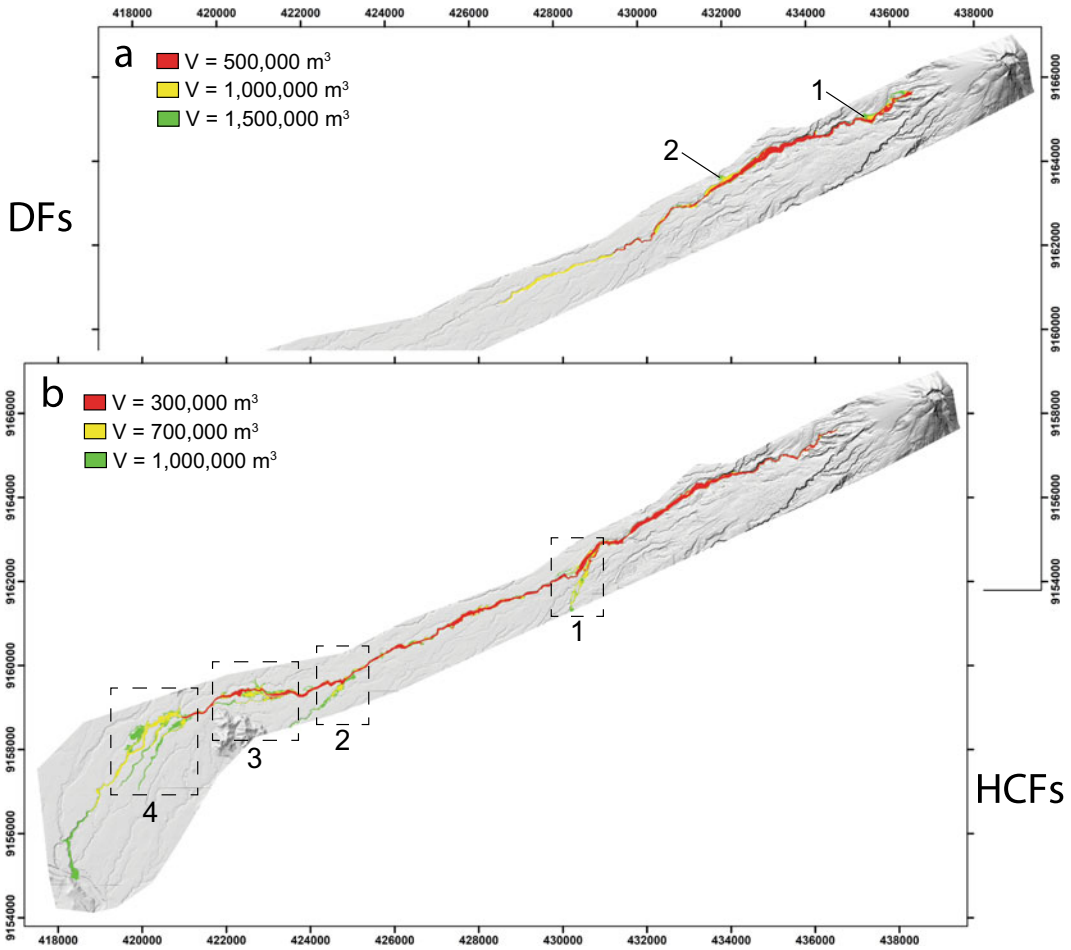


Fig. 17.18 FLO-2D simulation results for the Putih catchment. **a** Inundation map of the three simulated DFs. Numbers correspond to the location of minor overspills.

b Inundation map of the three simulated HCFs. Dashed black rectangles and numbers show the major overbank areas along the Putih catchment (see text for explanation)

respectively. Total flow volumes vary between $0.3 \times 10^6 \text{ m}^3$ (small-volume events) to $1.5 \times 10^6 \text{ m}^3$ (large-volume events). Following Charbonnier et al. (2018b), the Manning roughness coefficients vary with channel geometry and roughness between 0.03 to 0.08, the laminar flow resistance is set at 400, the extended Froude number at 0.9 and two different rheological parameters were used to simulate the differences in yield strengths and viscosities of debris flows versus HCFs. Inundation maps for the Gendol and Putih catchments are shown in Figs. 17.17 and 17.18, respectively.

FLO-2D model results in the Gendol catchment (Fig. 17.17b-c) highlight the contrasting

behaviour of debris flows compared to HCFs. Runout distances of the three simulated debris flows (Fig. 17.17b) do not exceed 15 km and flows are confined to the main river channel only. In contrast, runout distances of the three simulated HCFs (termed hyperconcentrated flow HF in Fig. 17.17) vary between 16 km (small-volume event) to > 20 km (moderate- to large-volume events) and major overspills from both sides of the main river channel occur between 17 to 19.5 km runout distances (dashed black rectangle area in Fig. 17.17c), flooding the interfluvial area between the Opak and Gendol river channels with < 1 m thick water-rich HCFs. Similar overbank flow processes were observed in this

area during the 1 May 2011 lahar event (see Sect. 17.5.2 and Figs. 17.4, 17.5). FLO-2D simulations performed in the Kali Putih catchment emphasise the contrasting internal dynamics between debris flows and HCFs; runout distances of the three simulated debris flows (Fig. 17.18a) do not exceed 13.5 km and flows are mostly confined to the main river channel, except for two proximal locations (1 and 2 in Fig. 17.18a) where minor overflows (< 250 m width) occur along the northern bank of the river. In contrast, runout distances of the three simulated HCFs vary between 19.5 km (small-volume event) to 24.5 km (large-volume events) and major overbank flows occur at 4 locations (dashed black areas 1–4 in Fig. 17.18b), mostly along the southern bank of the river. Overbank flow area 3 in Fig. 17.18b is located between 17 to 18 km runout distance from the summit and matches well the area affected by the 3 January 2011 lahar event of similar volume in Jumoyo and neighbouring villages along the main Magelang-Yogyakarta highway (see Sect. 17.6 and Figs. 17.6A, 17.13). Simulated flow velocities in this location are 5–10 m/s and flow depths are < 2 m.

These first FLO-2D modelling results at Merapi highlight the fact that while debris flows are mostly confined in the main river channels, impacted areas of large-volume ($> 1 \times 10^6 \text{ m}^3$) HCFs on flattish land below 300 m across the Merapi ring plain can be extensive and dangerous; they can spill over from the dense network of shallow riverbeds and inundate populated interfluvies.

17.8 Assessment of Lahar Risk

Disaster risk has been defined as the potential loss of life, injury, and damage of assets for a system, society or a community in a specific period of time. It has been probabilistically determined as a function of hazard, exposure, vulnerability and capacity to cope with disaster consequences (UNDRR 2002). Disaster risk assessment is needed for planning, strategising, and implementation of disaster risk management.

Several indicators can describe the parameters of hazard, exposure, vulnerability and capacity, where each indicator can be assigned with a weight. Hence, the risk can be assessed using the following equation:

$$R = w(H + E + V - C)$$

R is risk, H is hazard, E is exposure, V is vulnerability, C is capacity and w is indicator weight (Bollin et al. 2003). This equation and indicators used by BPPTKG are one of the methods available to assess risk at Merapi following the 2010 eruption.

The indicator weight is determined by a multi-criteria decision method, termed Analytical Hierarchy Process (AHP) that uses hierarchical structures to represent a problem and then develop priorities for alternatives based on the judgement of the user (Saaty 1990). The indicators selected to measure risk index are listed in Fig. 17.19 and ranked by colour-coded categories; hazard, exposure, vulnerability and capacity. Each indicator has been weighted according to its relevance and importance to hazard; the value for each indicator has been obtained by multiplying the weight of the indicator by the scoring index in a matrix. The scoring index transforms each value of an indicator into a scaled value, simply by assigning the value of 1, 2 or 3 according to the low, medium, high risk category of the indicator (Bollin et al. 2003). The local area risk index was computed as the sum of all the indicator values. The risk index for each area has been displayed in a risk map that aims at identifying and quantifying the main risk characteristics (exposure, vulnerability, and capacity measures) associated with hazards from Merapi activity. Finally, three categories or levels of risk have been determined: low, medium and high (Fig. 17.20) at the scale of each of the hamlets and villages along the drainage network on Merapi.

BPPTKG has applied this risk evaluation methodology at the village scale for both lahar and PDC hazards since 2009, which was then released as the ‘Merapi risk map’. The large eruption in 2010 caused severe damage to the

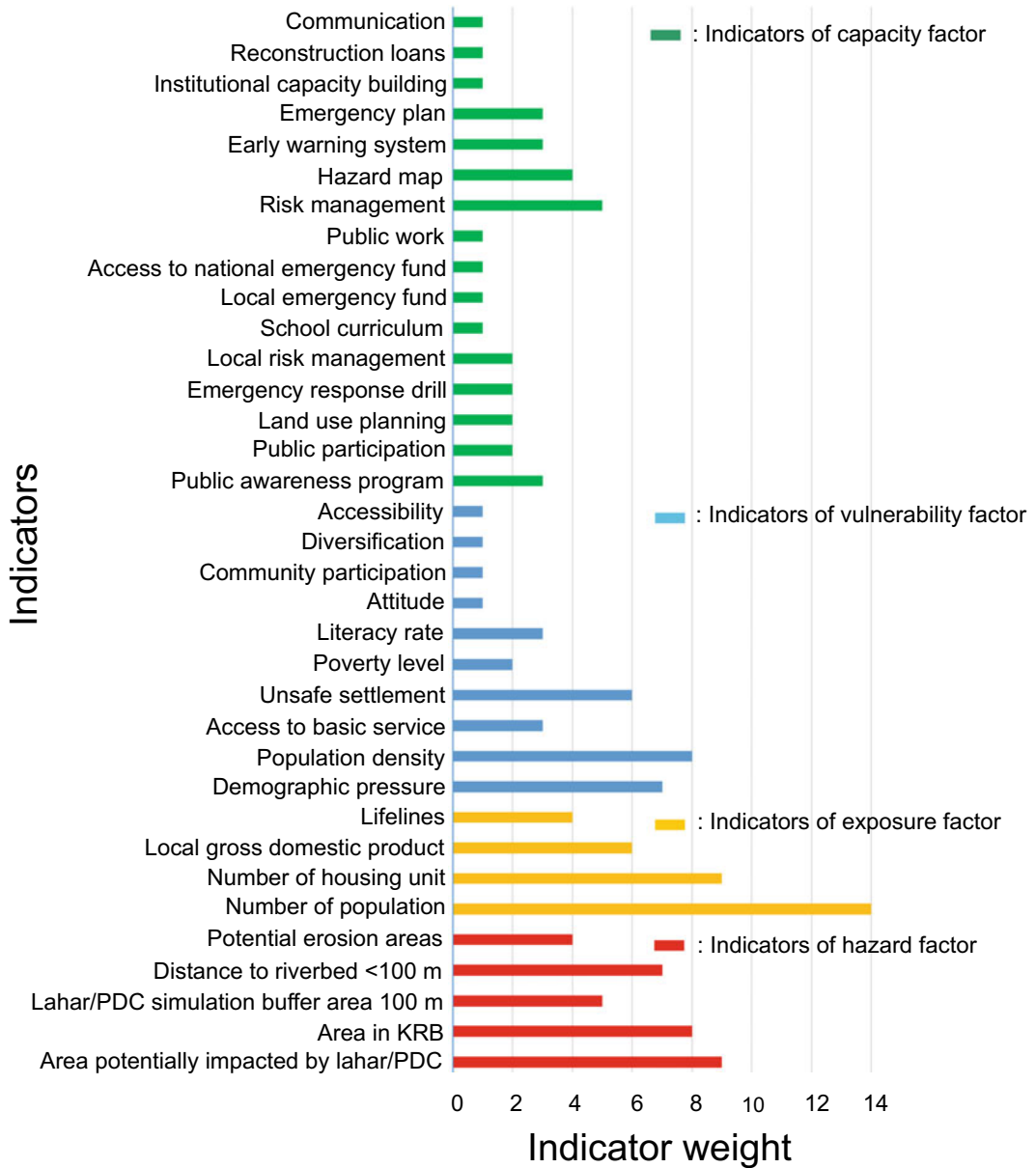


Fig. 17.19 List of risk indicators together with their respective weight (BPKTTG, Unpubl. data). Risk indicators are ranked according to four colour-coded categories of factors; hazard, exposure, vulnerability and capacity. Numbers between 0 and 14 along the x-axis express the value of each indicator, which has been obtained by

multiplying the weight of each indicator by the scoring index in matrix cells. The scoring index transforms the value of an indicator into a scaled value according to the low-, medium-, and high-risk category of the indicator. The local area risk index was computed as the sum of all the indicator values

villages located on the west and south Merapi flanks. Therefore, the 2010 event has not only changed the extent of hazard zones, but it has altered other risk characteristics, namely

exposure, vulnerability, and capacity of the communities living on the volcano. Due to significant changes in the four main risk factors, the Merapi risk map was therefore revised in 2012 at

RISK INDEX MAP OF MERAPI VOLCANO

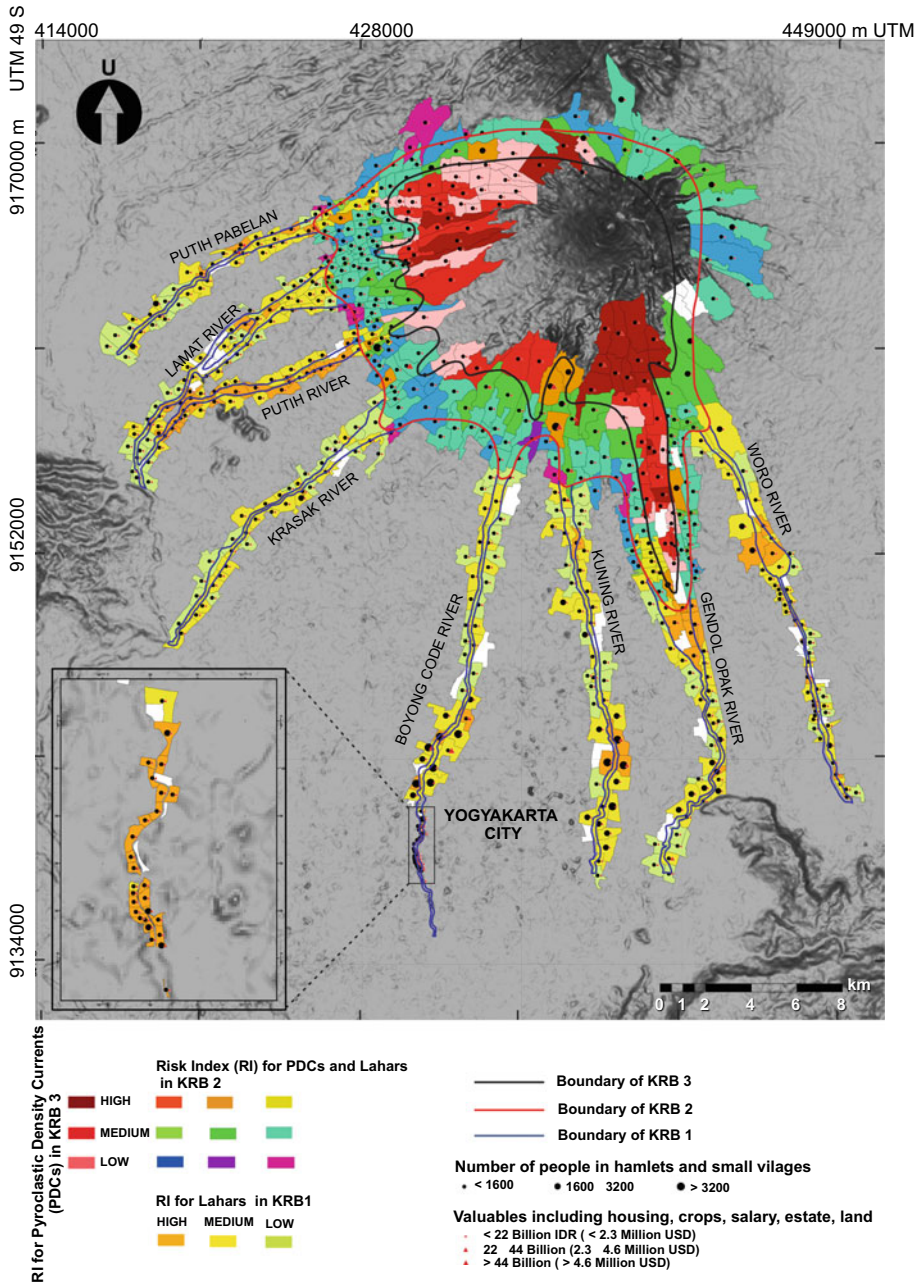


Fig. 17.20 Merapi risk map based on lahar and PDC hazards and risk indicators (see text), released by BPPTK (CVGHM) in 2012. The risk index, which incorporates population number and local GDP, has been broken down into three categories: low, medium and high at the scale of each of the *dusun* (hamlets and sub-villages) forming a

village. The risk index for PDCs (with three coloured rectangles, vertical distribution) has been applied to KRB zone 3. The risk Index applies to both PDC and lahars (with nine coloured rectangles) has been applied to KRB 2 zone. The risk Index for lahars (with three coloured rectangles) has been applied to KRB zone 1

the scale of sub-villages or hamlets (termed *dusun*) (Fig. 17.20). The risk assessment was carried out for a total of 727 *dusun*, 12% of those located in the KRB 3, 32% in the KRB 2, and 56% in the KRB 1 zones. The indicator method applied to the different KRB zones has been slightly different owing to different pertinent hazards; indicators for risk assessment are concerned only with PDC hazard in the KRB 3 zone, with both PDC and lahar hazards in the KRB 2 zone, and with lahar hazard only in the KRB 1 zone. The hazard indicators in KRB 1 consider the intensity of lahar impacts during the past 100 years, as well as the potential inundation areas obtained from lahar simulations using LAHARZ and probabilistic assessment. As a result, KRB 1 includes 74 *dusun* (19%) at high risk, 181 (47%) at medium risk, and 99 (25%) at low risk from lahar hazard. Villages at high-risk have been severely impacted by historically large, disastrous lahars along the Kali Putih, Boyong-Code, Kuning, and Gendol-Opak rivers.

17.9 Summary

From the combination of observations, field surveys, long-lived monitoring stations and temporary geophysical measurements, Merapi lahar characteristics, dynamics, behaviour and impacts can be summarised as follows:

1. Typically, lahars occur for 2 to 4 years after each Merapi eruption, in particular for rain-triggered lahars as they remobilize tephra and voluminous PDC deposits. After VEI 4 or greater eruptions, lahars can continue for up to a decade. They initiate in upper catchments that divide the west and south flanks of the volcano owing to two types of rainfall of local or regional origin, which last over 60 min with a threshold above 20 mm/hour. Merapi's flows exhibit specific characteristics: low to medium sedimentation concentrations (20–50 vol.%), low to medium velocities (2.5 to 7.5 m/s) and moderate discharges (rarely exceeding 600 m³/s), so that runout distances hardly exceed 15 to 20 km.
2. Beyond this distance, lahars transform downstream into HCFs and muddy floods across the ring plain. Although lahars propagate at moderate average velocities over relatively short distances on the volcano flanks, they often spill over river banks or dykes and avulse towards a dense network of small creeks across the gentle (< 3°) slopes of the ring plain.
3. Large, energetic lahars can move or destroy buildings, bridges and other structures, and modify the drainage network on a volcano, as shown after the 2010 Merapi eruption. The different states/levels of damage sustained by buildings during the January 2011 lahar in the Putih river have been identified using remote sensing and field studies to evaluate modes of failure and calculate the approximate range of impact pressures sustained by buildings in the impact area. Quantitative relationships between lahar characteristics and the probability of failure have been developed for building types around Merapi. Most weak masonry buildings would be destroyed by dilute lahars with relatively low velocities (c. 3 m/s) and pressures (c. 5 kPa), while the majority of stronger rubble stone buildings may be expected to withstand higher velocities (up to 6 m/s) and pressures (up to 20 kPa).
4. Flow mobility, volume and momentum strongly influence the runout distance and inundated area (Rickenmann 1999, 2005; de Haas et al. 2015). Runout distance is rather limited around Merapi owing to specific characteristics of lahars and riverbeds, but inundated areas are widespread (> 300 km²) due to the potential for overbank flows and avulsions across the ring plain. Both runout distance and inundated area are pivotal parameters to forecast the extent of damage (Toyos et al. 2007; Bettella et al. 2012; Han et al. 2017a, b).
5. Lahars are unsteady flows that move in a pulsating way, forming packets with each having variations of flow properties along the length of the surge, which exert erosion and aggradation that fluctuate in space and time (Doyle et al. 2010, 2011). Such mass flows

erode their channels by cutting debris away from the banks and the base. Undercutting of banks can cause vital problems in populated areas, as witnessed for lahars following the 2010 Merapi eruption.

5. Unsteady and pulsating lahar behaviour depends on bulking/debulking; as the flow volume, flow density and grain size distribution changes, so too does its erosion power through pressure changes (Manville et al. 2013). Sediment bulking will increase volume and peak discharge by a factor of three to ten relative to initial values. In contrast, sediment debulking will decrease the pressure, and less concentrated flow pulses or tails will induce incision of the deposit and undercutting of structures such as bridges. This leads to burial followed by incision, which occurred with each of the lahar packets during the 90-min flow at Semeru in 2008 (Doyle et al. 2010), for three to five hours along the Putih and Gendol rivers in 2011 (Table 17.5), and for as long as 16 h at Ruapehu in 2007 (Manville and Cronin 2007; Cole et al. 2009).
6. Channel morphology plays a role in runout distance and flooding area. Three geometric parameters of the channel-bed system determine how confined lahars can spill over banks and avulse to induce widespread impacts: reduced channel capacity, change in the longitudinal rate of channel confinement, and change in channel sinuosity. Overspill not only induces hazards for areas adjacent to the river channel, but also for secondary channels beyond the main valley, leading to further threats due to flow avulsion, e.g., immediately after the 2006 and 2010 Merapi eruptions.
7. Uncertainties remain in: (i) understanding the complex lahar behaviour despite progress being made over the past 20 years, (ii) forecasting lahar-prone areas based on (iii) the need for improved lahar models and validation of their outputs, and (iv) risk assessment, as this involves risk communication and accounts for social and cultural aspects, which are beyond the scope of this chapter.

Uncertainties also remain in current and future material supply rate for lahar initiation. At the time of writing, almost ten years after the large 2010 eruption, pyroclastic debris stored in the west drainage at Merapi became too depleted to be remobilised by large ($> 10^5 \text{ m}^3$) lahars. However, pyroclastic debris stored in the upper catchment and reaches of Kali Gendol-Opak and its tributaries can trigger large lahars under long-lasting, intense rainfall. The growth of the summit dome since August 2018 (estimated volume of $475,000 \text{ m}^3$ as of March 2019, BPPTKG) has generated small rock avalanches, including BAFs channelled 0.5–2 km down valley through the Gendol breach. However, the rate of growth of the intra-crater dome has declined since February 2019 to as little as $1,300 \text{ m}^3/\text{day}$. After September 2019, the dome growth came to an end, and a large part was destroyed by recent eruptions until March 2020. As a result, the volume of BAF deposits, and consequently lahars, decreased drastically at the end of 2019.

8. Strategies to mitigate damage and loss from Merapi lahars, however, have been adopted in the vicinity of lahar-prone valleys. They include: (1) land use planning using the revised KRB map to avoid hazards, (2) engineered protection structures to modify hazards, e.g., along the post-2010 Kali Gendol channel, (3) a warning system based on 24 lahar monitoring stations, which might enable evacuations, and (4) efficient evacuations when lahars do occur, although large expanses of habitat still remain at risk across the ring plain and in Yogyakarta. We emphasise that engineered protection structures, although desirable in general, can lead to counterproductive effects. Although this may be controversial, check dams in confined and sinuous channels should be removed to widen and deepen the valley, curved banks should be straightened, and valley-filling sediments should be removed in order to decrease the chances for avulsion from large-volume lahars.

Acknowledgements We are indebted to a number of colleagues who have acquired a huge dataset on lahars and pyroclastic density currents at Merapi and Indonesian volcanoes: F. Lavigne, A. Solikhin, K. Abdurachman, G. Lube, J.N. Procter, S.J. Cronin, and C. Dumaisnil. Funding for JCT research was obtained from the French National Agency for Research (ANR) Laharisk, RiskAdapt and Domerapi projects, and the French Centre of Spatial Studies CNES. This research was financed by the French government IDEX-ISITE initiative 16-IDEX-0001 (CAP 20-25). We thank R. Gertisser, Chief Editor, for his patience and advice, and V. Manville for his constructive and valuable comments.

References

- Abdurachman KE, Bourdier JL, Voight B (2000) Nuées ardentes of 22 November 1994 at Merapi volcano, Java, Indonesia. *J Volcanol Geotherm Res* 100(1-4):345–361
- Amri RM, Yulianti G, Yunus R, Wiguna S, Adi AW, Ichwana AN, Randongkir RE, Septian RT (2016) RBI—Risiko Bencana Indonesia. Badan Nasional Penanggulangan Bencana, Direktorat Pengurangan Risiko Bencana, 218 p
- Andrews BJ, Manga M (2011) Effects of topography on pyroclastic density current runout and formation of coignimbrites. *Geology* 39(12):1099–1102
- Arattano M, Marchi L (2008) Systems and sensors for debris-flow monitoring and warning. *Sensors* 8(4):2436–2452
- Arguden AT, Rodolfo KS (1990) Sedimentologic and dynamic differences between hot and cold laharc debris flows of Mayon Volcano, Philippines. *Geol Soc Am Bull* 102:865–876
- Aspinall W, Auker M, Hincks T, Mahony S, Nadim F, Pooley J, Sparks RSJ, Syre E (2011) Volcano hazard and exposure in GFDRR priority countries and risk mitigation measures—GFDRR volcano risk study. NGI Report 3:20100806. Bristol University Cabot Institute and NGI Norway for the World Bank, Bristol.
- Bänziger R, Burch H (1990) Acoustic sensors (hydrophones) as indicators for bed load transport in a mountain torrent. *IAHS (Int Assoc Hydrol Sci) Publ* 193:207–214
- Bardou E, Bowen P, Boivin P, Banfil P (2007) Impact of small amounts of swelling clays on the physical properties of debris-flow-like granular materials. Implications for the study of alpine debris flows. *Earth Surf Process Landf* 32(5):698–710
- Berthommier P (1990) Etude volcanologique du Merapi (Centre Java). Téphrostratigraphie et chronologie—produits éruptifs. PhD thesis, Université Blaise Pascal, Clermont-Ferrand, France
- Bettella F, Bisantino T, D'Agostino V, Gentile F (2012) Debris-flow runout distance: laboratory experiments on the role of Bagnold, savage and friction numbers. In: De Wraichen D, Brebbia CA, Mambretti D (eds) *Monitoring, stimulation, prevention and remediation of dense and debris flows*. WIT Press, pp 27–36
- Björnsson H (1975) Subglacial water reservoirs, jökulhlaups and volcanic eruptions. *Jökull* 25:1–14
- Björnsson H (2002) Subglacial lakes and jökulhlaups in Iceland. *Global Planet Change* 35:255–271
- Blong RJ (1984) *Volcanic hazards: a sourcebook on the effects of eruptions*, 1st edn. Academic Press, Australia, p 424
- Bollin C, Cárdenas C, Hahn H, Vasta KH (2003) Disaster risk management by communities and local Governments. *Natural Disaster Network, Inter-American Development Bank, Regional Policy Dialogue*, p 90
- BPS (Badan Pusat Statistics, Indonesia Statistics) (2017) *Census results, Population, Jakarta*. <http://www.bps.go.id>
- Brown SK, Jenkins SF, Sparks RSJ, Odbert H, Auker MR (2017) *Volcanic fatalities database: analysis of volcanic threat with distance and victim classification*. *J Appl Volcanol* 6(15):1–20
- CDERA (Caribbean Disaster Emergency Response Agency) (1997) *Montserrat volcano situation report number 3*. Department of Humanitarian Affairs
- Charbonnier S, Gertisser R (2008) Field observations and surface characteristics of pristine block-and-ash flow deposits from the 2006 eruption of Merapi Volcano, Java, Indonesia. *J Volcanol Geotherm Res* 177:971–982
- Charbonnier SJ, Gertisser R (2009) Numerical simulations of block-and-ash flows using the Titan2D flow model: examples from the 2006 eruption of Merapi Volcano, Java, Indonesia. *Bull Volcanol* 71:953–959
- Charbonnier SJ, Germa A, Connor CB, Gertisser R, Preece K, Komorowski JC, Lavigne F, Dixon TH, Connor LJ (2013) Evaluation of the impact of the 2010 pyroclastic density currents at Merapi volcano from high-resolution satellite imagery analysis, field investigations and numerical simulations. *J Volcanol Geotherm Res* 261:295–315
- Charbonnier SJ, Macorps E, Connor CB, Connor LJ, Richardson JA (2018a) How to correctly evaluate the performance of volcanic mass flow models used for hazard assessment? In: Thouret J-C (ed) *Hazard and risk mapping—The Arequipa—El Misti case study and other threatened cities*. Presses Universitaires Blaise Pascal, Clermont-Ferrand, pp 15–20
- Charbonnier SJ, Connor CB, Connor LJ, Sheridan MF, Oliva Hernández JP, Richardson JA (2018b) Modeling the October 2005 lahars at Panabaj (Guatemala). *Bull Volcanol* 80:4
- Cole SE (2011) *Geophysical investigation into the internal dynamics of moving lahars*. PhD thesis, Massey University, Palmerston North, New Zealand
- Cole S, Cronin SJ, Sherburn S, Manville V (2009) Seismic signals of snow-slurry lahars in motion: 25 September 2007, Mt. Ruapehu, New Zealand. *Geophys Res Lett* 36:L09405

- Coviello V, Capra L, Vázquez R, Márquez-Ramirez V-H (2018) Seismic characterisation of hyperconcentrated flows in a volcanic environment. *Earth Surf Process Landf* 43(10):2219–2231
- Cronin SJ, Neall VE, Lecointre JA, Palmer AS (1996) Unusual “snow slurry” lahars from Ruapehu volcano, New Zealand, September 1995. *Geology* 24 (12):1107–1110
- Cronin SJ, Lube G, Dayudi DS, Sumarti S, Subrandiyo S (2013) Insights into the October–November 2010 Gunung Merapi eruption (Central Java, Indonesia) from the stratigraphy, volume and characteristics of its pyroclastic deposits. *J Volcanol Geotherm Res* 261:244–259
- de Bézal E (2012) Les corridors de lahars du volcan Merapi (Java, Indonésie): des espaces entre risque et ressource. Contribution à la géographie des risques au Merapi. PhD thesis, Université Paris 1 Panthéon-Sorbonne, Paris, France
- de Bézal E (2013) Les impacts des lahars du volcan Merapi (Java, Indonésie) après l'éruption de 2010. Lahar-related impacts after the 2010 eruption of Merapi volcano (Java, Indonesia). *Géomorph Relief Proc Environ* 4:463–480
- de Bézal E, Lavigne F, Hadmoko DS, Degeai JP, Dipayana GA, Mutaqin BW, Marfai MA, Coquet M, Le Mauff B, Robin AK, Vidal C, Cholikh N, Nurnaning A (2013) Rain-triggered lahars following the 2010 eruption of Merapi volcano, Indonesia: a major risk. *J Volcanol Geotherm Res* 261:330–347
- de Haas T, Braat L, Leuven JRFW, Lokhorst IR, Kleinhans MG (2015) Effects of debris flow composition on runout, depositional mechanisms, and deposit morphology in laboratory experiments. *J Geophys Res Earth Surf* 120:1949–1972
- Dove M (2008) Perception of volcanic eruption as agent of change on Merapi volcano, Central Java. *J Volcanol Geotherm Res* 172:329–337
- Doyle EE, Cronin SJ, Cole SE, Thouret J-C (2010) The coalescence and organization of lahars at Semeru, Indonesia. *Bull Volcanol* 72(8):961–970
- Doyle EE, Cronin SJ, Thouret J-C (2011) Cycles of bulking and debulking in lahars at Semeru, Indonesia. *Geol Soc Am Bull* 123:1234–1246
- Dumaisnil C, Thouret J-C, Chambon G, Doyle EE, Cronin SJ (2010) Hydraulic, physical and rheological characteristics of rain-triggered lahars at Semeru volcano, Indonesia. *Earth Surf Process Landf* 35:573–590
- Endo ET, Murray TL (1991) Real-time seismic amplitude measurement (RSAM), a volcano monitoring and prediction tool. *Bull Volcanol* 53:533–545
- Ettinger S, Mounard L, Magill C, Yao-Lafourcade A-F, Thouret J-C, Manville V, Negulescu C, Zuccaro G, De Gregorio D, Nardone S, Uchichoque JAL, Arguedas A, Macedo L, Manrique NM (2016) Building vulnerability to hydro-geomorphic hazards: Estimating damage probability from quantitative vulnerability assessment using logistic regression. *J Hydrol* 541:563–581
- FLO-2D Software Inc (2019) FLO-2D ProModel. <https://www.flo-2d.com>
- Gertisser R, Charbonnier S, Keller J, Quidelleur X (2012) The geological evolution of Merapi volcano, Central Java, Indonesia. *Bull Volcanol* 74:1213–1233
- Gertisser R, del Marmol M-A, Newhall C, Preece K, Charbonnier S, Andreastuti S, Handley H, Keller J (2023) Geological history, chronology and magmatic evolution of Merapi. In: Gertisser R, Troll VR, Walter TR, Nandaka IGMA, Ratdomopurbo A (eds) Merapi volcano—geology, eruptive activity, and monitoring of a high-risk volcano. Springer, Berlin, Heidelberg, pp 137–193
- Gob F, Gautier E, Virmoux C, Grancher D, Tamisier V, Primanda KV, Wibowo SD, Sarrazin C, de Bézal E, Ville A, Lavigne F (2016) River responses to the 2010 major eruption of the Merapi volcano, Central Java, Indonesia. *Geomorphology* 273:244–257
- GVP (Global Volcanism Program) (2002) Report on Mayon (Philippines). In: Wunderman R (ed) *Bull Glob Volc Network* 27:4
- Hadisantono RD, Andreastuti S, Abdurachman E, Sayudi D, Nurnusanto I, Martono A (2002) Volcanic hazard map of Merapi volcano, Central Java and Yogyakarta special province. Scale 1:50,000. Center for Volcanology and Geological Hazard Mitigation, Bandung
- Hadmoko DS, de Belizal E, Mutaqin BW, Dipayana GA, Marfai MA, Lavigne F, Sartohadi J, Worosuprojo S, Starheim CCA, Gomez C (2018) Post-eruptive lahars at Kali Putih following the 2010 eruption of Merapi volcano, Indonesia: occurrences and impacts. *Nat Hazards* 94:419–444
- Han Z, Li L, Huang J, Chen G, Xu L, Tang C, Zhang H, Shang Y (2017a) Numerical simulation for run-out extent of debris flows using an improved cellular automaton model. *Bull Eng Geol Environ* 76:961–974
- Han Z, Chen J, Xu P, Zhan J (2017b) A well-balanced numerical scheme for debris flow run-out prediction in Xiaojia Gully considering different hydrological designs. *Landslides* 14:2105–2114
- Hardjosuwarno S, Sukatja CB, Yunita FT (2013) Early warning system for Lahar in Merapi. Global assessment report on disaster risk reduction. <https://www.unisdr.org/we/inform/publications/50053>
- Huang C-J, Shieh C-L, Yin H-Y (2004) Laboratory study of the underground sound generated by debris flows. *J Geophys Res* 109:F01008
- Huang C-J, Yin H-Y, Chen C-Y, Yeh C-H, Wang C-L (2007) Ground vibrations produced by rock motions and debris flows. *J Geophys Res* 112:F02014
- Ikhsan J, Fujita M, Takabayashi H (2010) Sediment disaster and resource management in the Mount Merapi area, Indonesia. *Int J Erosion Control Eng* 3 (1):43–52
- Itakura Y, Inaba H, Sawada T (2005) A debris-flow monitoring devices and methods bibliography. *Nat Hazards Earth Syst Sci* 5:971–977
- Itakura Y, Kamei N, Takahama J, Nowa Y (1997) Real time estimation of discharge of debris flow by an

- acoustic sensor. In: 14th IMEKO (International Measurement Confederation) world congress, Tampere, Finland, vol XA, pp 127–131
- Iverson RM (2014) Debris flows: behaviour and hazard assessment. *Geol Today* 30:15–20
- Iverson RM, Schilling SP, Vallance JW (1998) Objective delineation of lahar-inundation hazard zones. *Geol Soc Am Bull* 110:972–984
- Iverson RM, Logan M, LaHusen RG, Berti M (2010) The perfect debris flow? Aggregated results from 28 large-scale experiments. *J Geophys Res* 115:F03005
- Iverson RM, Reid ME, Logan M, LaHusen RG, Godt JW, Griswold JP (2011) Positive feedback and momentum growth during debris-flow entrainment of wet bed sediment. *Nat Geosci* 4:116–121
- Jakob M, Hungr O (2005) Debris flows hazards and related phenomena. Springer, Berlin, Heidelberg, p 739
- Janda RJ, Daag AS, Delos Reyes PJ, Newhall CG, Pierson TC, Punongbayan RS, ... Umbal JV (1996) Assessment and response to lahar hazard around Mount Pinatubo, 1991 to 1993. Fire and mud: eruptions and lahars of Mount Pinatubo, Philippines, pp 107–140
- Jenkins SF, Komorowski J-C, Baxter PJ, Spence R, Picquout A, Lavigne F, Suroño (2013) The Merapi 2010 eruption: an interdisciplinary impact assessment methodology for studying pyroclastic density current dynamics. *J Volcanol Geotherm Res* 261:316–329
- Jenkins SF, Phillips JC, Price R, Feloy K, Baxter PJ, Hadmoko DS, De Bélizal E (2015) Developing building-damage scales for lahars: application to Merapi volcano, Indonesia. *Bull Volcanol* 77:1–17
- JICA (Japanese–Indonesian Cooperation Agency) (1979) Master plan for land conservation and volcanic debris control in the area of Mt. Merapi. Japan International Cooperation Agency, p 153
- Johnson PJ, Valentine GA, Stauffer PH, Lowry CS, Sonder I, Pulgarin BA, Santacoloma CC, Agudelo A (2018) Groundwater drainage from fissures as source for lahars. *Bull Volcanol* 80:39
- Jones R, Manville V, Peakall J, Froude MJ, Odbert HM (2017) Real-time prediction of rain-triggered lahars: incorporating seasonality and catchment recovery. *Nat Hazards Earth Syst Sci* 17:2301–2312
- Jitousono T, Shimokawa E, Tsuchiya S, Haryanto, Djamil H (1996) Debris flow following the 1984 eruption with pyroclastic flows in Merapi volcano, Indonesia. Proc Workshop “Erosion Control Through Volcanic Hydrological Approach”, Yogyakarta, Indonesia, p 131–162
- Komorowski JC, Jenkins S, Baxter PJ, Picquout A, Lavigne F, Charbonnier SJ, Gertisser R, Preece K, Cholik N, Budi-Santoso A, Suroño (2013) Paroxysmal dome explosion during the Merapi 2010 eruption: processes and facies relationships of associated high-energy pyroclastic density currents. *J Volcanol Geotherm Res* 261:260–294
- Kusumawardani R, Kurniadhi R, Mukhlisin M, Legono D (2017) Rainfall threshold for triggering debris flows on Merapi Volcano area, Yogyakarta, Indonesia. *AIP Conf Proc* 1818:020027
- Lavigne F (1998) Les lahars du volcan Merapi, Java central: dynamique, budget sédimentaire et risques associés. PhD thesis, Université Blaise Pascal, Clermont-Ferrand, France
- Lavigne F (2001) Evolution géomorphologique de la vallée Boyong à la suite de l'éruption du 22 novembre 1994 du volcan Merapi, Java, Indonésie. *Géomorph Relief Proc Environ* 3:159–174
- Lavigne F (2004) Rate of sediment yield following small-scale volcanic eruptions—a quantitative assessment at the Merapi and Semeru stratovolcanoes, Java, Indonesia. *Earth Surf Process Landf* 29(8):1045–1058
- Lavigne F, Suwa H (2004) Contrasts between debris flows, hyperconcentrated flows and stream flows at a channel of Mount Semeru, East Java, Indonesia. *Geomorph* 61(1–2):41–58
- Lavigne F, Thouret J-C (2000) Les lahars: dépôts, origines et dynamique. *Bull Soc Géol Fr* 1741(5):545–557
- Lavigne F, Thouret J-C (2003) Sediment transportation and deposition by rain-triggered lahars at Merapi Volcano, Central Java, Indonesia. *Geomorphology* 49(1–2):45–69
- Lavigne F, Morin J, Suroño M (2015) Atlas of Merapi volcano. Laboratoire de Géographie Physique, Meudon, France, 58 color plates. Online Publication (hal-03010922)
- Lavigne F, Thouret J-C, Hadmoko DS, Sukatja B (2007) Lahars in Java: initiations, dynamics, hazard assessment and deposition processes. *Forum Geogr* 21:17–32
- Lavigne F, Thouret J-C, Voight B, Suwa H, Sumaryono A (2000a) Lahars at Merapi volcano: an overview. *J Volcanol Geotherm Res* 100:423–456
- Lavigne F, Thouret J-C, Suwa H, Voight B, Young K, Lahusen R, Marso J, Sumaryono A, Sayudi DS, Dejean M (2000b) Instrumental lahar monitoring at Merapi volcano, Central Java, Indonesia. *J Volcanol Geotherm Res* 100:457–478
- Legono D, Rahardjo PA (2017) Lahar flow disaster, human activities, and risk mitigation on volcanic rivers: case study of rivers on Mount Merapi slopes, Indonesia. In: Tsutsumi D, Laronne JB (eds) Gravel-bed rivers: processes and disasters, 1st edn. Wiley-Blackwell, pp 549–565
- Lube G, Cronin SJ, Thouret J-C, Suroño (2011) Kinematic characteristics of pyroclastic density currents at Merapi and controls on their avulsion from natural and engineered channels. *Geol Soc Am Bull* 123(5–6):1127–1140
- Lube G, Cronin SJ, Manville V, Procter JN, Cole SE, Freundt A (2012) Energy growth in laharc mass flows. *Geology* 40(5):475–478
- Mainsant G (2014) Etude géophysique des lahars. Rapport post-doc AXA, Laboratoire Magmas et Volcans, Université Clermont-Auvergne, p 89
- Major JJ (1997) Depositional processes in large-scale debris-flow experiments. *J Geol* 105:345–366

- Major JJ, Pierson TC (1992) Debris flow rheology: experimental analysis of fine-grained slurries. *Water Resour Res* 28(3):841–857
- Major JJ, Janda RJ, Daag AS (1996) Watershed disturbance and lahars on the east side of Mount Pinatubo during the mid-June 1991 eruptions. In: Newhall CG, Punongbayan R (eds) *Fire and mud: eruption and lahars of Mount Pinatubo, Philippines*. University of Washington Press, Seattle, pp 885–920
- Major JJ, Iverson RM (1999) Debris-flow deposition: effects of pore-fluid pressure and friction concentrated at flow margins. *Geol Soc Am Bull* 111:1424–1434
- Major JJ, Pierson TC, Dinehart RL, Costa JE (2000) Sediment yield following severe volcanic disturbance: a two-decade perspective from Mount St. Helens. *Geology* 28:819–822
- Major JJ, Bertin D, Pierson TC, Amigo A, Iroumé A, Ulloa H, Castro J (2016) Extraordinary sediment delivery and rapid geomorphic response following the 2008–2009 eruption of Chaitén volcano, Chile. *Water Resour Res* 52(7):5075–5094
- Manville V, Cronin SJ (2007) Break-out lahar from New Zealand's Crater Lake. *Eos* 88(43):441–442
- Manville V, Major JJ, Fagents SA (2013) Modeling lahar behaviour and hazards. In: Fagents SA, Gregg TKP, Lopes RMC (eds) *Modeling volcanic processes*. Cambridge University Press, pp 300–330
- Marcial S, Melosantos AA, Hadley KC, LaHusen RG, Marso JN (1996) Instrumental lahar monitoring at Mount Pinatubo. In: Newhall CG, Punongbayan R (eds) *Fire and mud: eruption and lahars of Mount Pinatubo, Philippines*. University of Washington Press, Seattle, pp 1015–1022
- Mei ETW, Lavigne F (2012) Influence of the institutional and socio-economic context for responding to disasters: case study of the 1994 and 2006 eruptions of the Merapi volcano, Indonesia. *Geol Soc Lond Spec Publ* 36:171–186
- Mei ETW, Picquout A, Lavigne F, Grancher D, Cholikh N, Sartohadi J, De Bézilal E (2013) Lessons learned from the 2010 evacuations at Merapi volcano. *J Volcanol Geotherm Res* 261:348–365
- Mulder T, Alexander J (2001) The physical character of subaqueous sedimentary density flows and their deposits. *Sedimentology* 48:269–299
- Nandaka A, Sulistiyani, Sulistio A, Sampurno A, Nurudin, Miswanto, Kusdaryanto (2013) Multiparameter Lahar monitoring and warning at Merapi volcano, Java, Indonesia. Abstract, SEDIMER Workshop, 30–31 July 2013, Universitas Gadjah Mada, Yogyakarta, Indonesia
- Naspiah BG, Oekan SA, Munandar S (2017) Economic rationality of residents living in the area prone to Merapi volcanic disaster. *Kom Int J Indon Soc Cult* 9(2):203–215
- Neall VE (1976) Lahars-global occurrence and annotated bibliography: publications of the geology department. *Victoria Univ Wellington* 5:1–18
- Newhall CG, Bronto S, Alloway B, Banks NG, Bahar I, Del Marmol MA, Hadisantono RD, Holcomb RT, McGeehin J, Miksic JN, Rubin M, Sayudi SD, Sukhyar R, Andreastuti S, Tilling RI, Torley R, Trimble D, Wirakusumah AD (2000) 10,000 years of explosive eruptions of Merapi Volcano, Central Java: archaeological and modern implications. *J Volcanol Geotherm Res* 100:9–50
- O'Brien J, Julien P, Fullerton W (1993) Two-dimensional water flood and mudflow simulation. *J Hydraul Eng* 119(2):244–261
- Okano K, Suwa H, Kanno T (2012) Characterisation of debris flows by rainstorm condition at a torrent on the Mount Yakedake volcano, Japan. *Geomorphology* 136(1):88–94
- Pan H, Shi P, Ye T, Xu W, Wang J (2015) Mapping the expected annual fatality risk of volcano on a global scale. *Int J Disaster Risk Reduc* 132:52–60
- Pardiyanto L, Reksowirogo LD, Mitrohartono FXS, Hardjowarsito SH (1978) Volcanic hazard map. Merapi Volcano, Central Java. Geological Survey of Indonesia, Bandung (1 sheet, scale 1:100,000)
- Pierson TC (1986) Flow behaviour of channelised debris flows, Mount St. Helens, Washington. In: Abrahams AD (ed) *Hillslope processes*, 1st edn. Routledge, London, pp 269–296
- Pierson TC (2005) Hyperconcentrated flow–transitional process between water flow and debris flow. In: Jakob M, Hungr O (eds) *Debris-flow hazards and related phenomena*. Springer, Berlin, Heidelberg, pp 159–208
- Pierson TC, Costa JE (1987) A rheologic classification of subaerial sediment-water flows. *Geol Soc Am Rev Eng Geol* 7:1–12
- Pierson TC, Major JJ (2014) Hydrogeomorphic effects of explosive volcanic eruptions on drainage basins. *Ann Rev Earth Planet Sci* 42:469–507
- Pierson TC, Janda RJ, Thouret J-C, Borrero CA (1990) Perturbation and melting of snow and ice by the 13 November 1985 eruption of Nevado del Ruiz, Colombia, and consequent mobilization, flow and deposition of lahars. *J Volcanol Geotherm Res* 41(1–4): 17–66
- Pierson TC, Major JJ, Amigo A, Moreno H (2013) Acute sedimentation response to rainfall following the explosive phase of the 2008–2009 eruption of Chaitén volcano, Chile. *Bull Volcanol* 75:723
- Prasetyo Y, Pratiwi R, Bashit N (2018) The impacts analysis of pre and post Merapi Mount eruption on residential areas using Sentinel 1, ALOS Palsar and Landsat satellite images combination in 2009–2015. *IOP Conf Ser Earth Environ Sci* 165:012022
- Rachmawati R, Budiarti CV (2016) Use of space and the need for planning in the disaster-prone area of Code River, Yogyakarta, Indonesia. *Indon J Geogr* 48(2):178–190
- Rickenmann D (1999) Empirical relationships for debris flows. *Nat Hazards* 19:47–77
- Rickenmann D (2005) Runout prediction methods. In: Jakob M, Hungr O (eds) *Debris-flow hazards and related phenomena*. Springer, Berlin, Heidelberg, pp 305–324

- Rodolfo KS, Umbal JV, Alonso RA, Remotigue CT, Paladio-Melosantos ML, Salvador JHG, Evangelista D, Miller Y (1996) Two years of lahars on the western flank of Mount Pinatubo: initiation, flow processes, deposits, and attendant geomorphic and hydraulic changes. In: Newhall CG, Punongbayan R (eds) *Fire and mud: eruption and lahars of Mount Pinatubo, Philippines*. University of Washington Press, Seattle, pp 989–1013
- Saaty TL (1990) How to make a decision: the analytic hierarchy process. *Eur J Oper Res* 48:9–26
- Savage SB, Hutter K (1989) The motion of a finite mass of granular material down a rough incline. *J Fluid Mech* 199:177–215
- Sayudi DS, Aisyah N, Juliani DJ, Muzani M (2010) Peta Kawasan Rawan Bencana Gunungapi Merapi, Jawa Tengah dan Daerah Istimewa Yogyakarta 2010 (Merapi Hazard Map, Central Java and Yogyakarta Special Region Provinces). Center for Volcanology and Geological Hazard Mitigation (CVGHM), Bandung
- Schilling SP (2014) Lahar_z_py: GIS tools for automated mapping of lahar inundation hazard zones. *US Geol Surv Open File Rep* 2014-1073, p 78
- Schwarzkopf LM, Schmincke HU, Cronin SJ (2005) A conceptual model for block-and-ash flow basal avalanche transport and deposition, based on deposit architecture of 1998 and 1994 Merapi flow. *J Volcanol Geotherm Res* 139:117–134
- Scott KM (1988) Origins, behaviour, and sedimentology of lahars and lahar-runout flows in the Toutle-Cowlitz river system. *US Geol Survey Prof Paper* 1447-A, p 74
- Siebert L, Simkin T, Kimberly P (2010) *Volcanoes of the world*, 3rd edn. University of California Press, Berkeley
- Smith GA, Lowe DR (1991) Lahars: volcano-hydrologic events and deposition in the debris-flow-hyperconcentrated flow continuum. In: Fisher RV, Smith GA (eds) *Sedimentation in volcanic settings*. SEPM Society for Sedimentary Geology 45, pp 60–70
- Solikhin A (2015) *Geology, tectonics and post-2001 eruptive activity interpreted from high-spatial resolution satellite imagery: the case study of Merapi and Semeru volcanoes, Indonesia*. PhD thesis, Université Clermont-Auvergne, Clermont-Ferrand, France
- Solikhin A, Thouret J-C, Liew SC, Gupta A, Sri Sayudi D, Oehler J-F (2015a) Deposits and effects from the 2010 pyroclastic density currents and lahars at Merapi Volcano: Mapped and analyzed from high-spatial resolution imagery. *Bull Volcanol* 77:20
- Solikhin A, Pinel V, Vandemeulebrouck J, Thouret J-C, Hendrasto M (2015b) Mapping the 2010 Merapi pyroclastic deposits using dual-polarization synthetic aperture radar (SAR) data. *Rem Sens Environ* 158:180–192
- Starheim CCA, Gomez C, Davies T, Lavigne F, Wassmer P (2013) In-flow evolution of lahar deposits from video-imagery with implications for post-event deposit interpretation, Mt. Semeru, Indonesia. *J Volcanol Geotherm Res* 256:96–104
- Subandriyo, Gertisser R, Aisyah N, Humaida H, Preece K, Charbonnier S, Budi-Santoso A, Handley H, Sumarti S, Sayudi DS, Nandaka IGMA, Wibowo HE (2023) An overview of the large-magnitude (VEI 4) eruption of Merapi in 2010. In: Gertisser R, Troll VR, Walter TR, Nandaka IGMA, Ratdomopurbo A (eds) *Merapi volcano—geology, eruptive activity, and monitoring of a high-risk volcano*. Springer, Berlin, Heidelberg, pp 353–407
- Sulistiyani S, Nandaka A, Nurudin (2018a) Merapi's lahar early warning system 2011-2012 period. *Proceedings, International Association for Hydro-Environment Engineering and Research (IAHR)-Asia Pacific Division (APD) Congress: Multi-Perspective Water for Sustainable Development, IAHR-APD 2018a*, pp 1311–1316
- Sulistiyani S, Nandaka A, Nurudin (2018b) Seismic lahar characteristics of Merapi volcano post 2010 Eruption. *EAGE-HAGI 1st Asia Pacific Meeting on Near Surface Geoscience and Engineering*, Abstract No. 45159
- Surono P, Jousset J, Pallister M, Boichu MF, Buongiorno A, Budisantoso F, Costa S, Andreastuti F, Prata D, Schneider L, Clarisse H, Humaida S, Sumarti C, Bignami J, Griswold S, Carn C, Oppenheimer C, Lavigne F (2012) The 2010 explosive eruption of Java's Merapi volcano—a “100-year” event. *J Volcanol Geotherm Res* 241–242:121–135
- Suryo I, Clarke MCG (1985) The occurrence and mitigation of volcanic hazards in Indonesia as exemplified at the Mount Merapi, Mount Kelut and Mount Galunggung volcanoes. *Quat J Eng Geol* 18:79–98
- Suwa H, Nishimura K (1992) Debris flows and topographic change in River Bebeng on the slope of Mount Merapi, Indonesia. *Annual meeting of the Japanese Geomorphological Union, Japan, 1992*. *Chikei Trans* 13(3):233–234
- Suwa H, Sumaryono A (1996) Sediment discharge by storm runoff from a creek on Mount Merapi. *J Jpn Soc Eros Control Eng* 48:117–128
- Suwa H, Yamakoshi T, Sato K (2000) Relationship between debris-flow discharge and ground vibration. In: Wiczorek GF, Naeser ND (eds) *Proceedings of 2nd International conference on debris-flow hazards mitigation: mechanics, prediction, and assessment*. Balkema, pp 311–318
- Hausmann P, Swiss Re (1998) *Floods—an insurable risk?* Swiss Reinsurance Company, Zurich, p 48
- Syarifuddin M, Oishia S, Legonoc D, Hapsarid RI, Iguchi M (2017) Integrating X-MP radar data to estimate rainfall induced debris flow in the Merapi volcanic area. *Adv Water Resour* 110:249–262
- Thouret J-C, Lavigne F (2005) Hazards and risks at Gunung Merapi, Central Java: a case study. In: Gupta A (ed) *The physical geography of Southeast Asia*. Oxford University Press, pp 275–299
- Thouret J-C, Abdurachman KE, Bourdier J-L, Bronto S (1998) Origin, characteristics, and behaviour of subsequent lahars of the 1990 eruption at Kelud, East Java (Indonesia). *Bull Volcanol* 59:460–480

- Thouret J-C, Lavigne F, Kelfoun K, Bronto S (2000) Toward a revised hazard assessment at Merapi volcano, Central Java. *J Volcanol Geotherm Res* 100:479–502
- Thouret J-C, Gupta A, Lube G, Liew SC, Cronin SJ, Surono (2010) The 2006 pyroclastic deposits of Merapi Volcano, Java, Indonesia: high-spatial resolution IKONOS images and complementary ground based observations. *Rem Sens Environ* 114:1949–1967
- Thouret J-C, Oehler J-F, Solikhin A, Gupta A, Procter J (2014) Aggradation and erosion at persistently active volcanoes: the Semeru case study, Indonesia. *Bull Volcanol* 76:857
- Thouret J-C, Kassouk Z, Gupta A, Liew SC, Solikhin A (2015) Tracing the evolution of 2010 Merapi volcanic deposits (Indonesia) based on object-oriented classification and analysis of multi-temporal, very high resolution images. *Rem Sens Environ* 70:350–371
- Thouret J-C, Antoine S, Magill C, Mead S (2020) Lahars and debris flows: characteristics and impacts. *Earth Sci Rev* 201:103003
- Toyos G, Oramas Dorta D, Oppenheimer C, Pareschi MT, Sulpizio R, Zanchetta G (2007) GIS-assisted modelling for debris-flow hazard assessment based on the events of May 1998 in the area of Sarno, Southern Italy: I. Maximum Run-out. *Earth Surf Proc Landf* 32:1491–1502
- UNDRR (United Nations Office for Disaster Risk Reduction) (2002) Regional report of the 2002 world disaster reduction campaign in Latin America and the Caribbean: disaster reduction for sustainable mountain development, p 20
- Vallance JW (2000) Lahars. In: Sigurdsson H, Houghton B, McNutt SR, Rymer H, Stix J (eds) *Encyclopedia of volcanoes*, 1st edn. Academic Press, San Diego, pp 601–615
- Vallance JW, Iverson R (2015) Lahars and their deposits. In: Sigurdsson H, Houghton B, McNutt SR, Rymer H, Stix J (eds) *Encyclopedia of volcanoes*, 1st edn. Academic Press, San Diego, pp 649–664
- Van Bemmelen RW (1949) *The geology of Indonesia*, vol 1A. Government Printing Office, The Hague
- Vázquez R, Suriñach E, Capra L, Arámbula-Mendoza R, Reyes-Dávila G (2016) Seismic characterisation of lahars at Volcán de Colima, Mexico. *Bull Volcanol* 78:8
- Verstappen HT (1988) Geomorphological surveys and natural hazard zoning, with special reference to volcanic hazards in Central Java. *Zeitschr Geomorph Suppl* 68:81–101
- Voight B, Constantine EK, Siswoidjuyo S, Torley R (2000) Historical eruptions of Merapi volcano, central Java, Indonesia, 1768–1998. *J Volcanol Geotherm Res* 100:69–138
- Wardoyo W, Legono D, Jayadi R, Fathani TF (2013) Analysing sediment transport mechanism and related hydraulic structure damage after Mt. Merapi Eruption in Gendol River. *J Basic Appl Sci Res* 3(1):849–855
- Wibowo SB (2016) *Approches multiscalaires de l'érosion du volcan Merapi, Indonésie. Contribution à la compréhension du déclenchement et de la dynamique des lahars*. PhD Thesis, Laboratoire de Géographie Physique, Université Paris 1 Sorbonne, Meudon, France
- Wibowo SB, Lavigne F, Mourot P, Métaxian JP, Zeghdoudi M, Virmoux C, Cosmas BS, Hadmoko SD, Mutaqin BW (2015) Analyse couplée d'images vidéo et de données sismiques pour l'étude de la dynamique d'écoulement des lahars sur le volcan Merapi, Indonésie. *Géomorph Relief Proc Environ* 21(3):251–266
- Widiwijayanti C, Voight B, Hidayat D, Schilling SP (2009) Objective rapid delineation of areas at risk from block-and-ash pyroclastic flows and surges. *Bull Volcanol* 71:687–703
- Wilson G, Wilson TM, Deligne NI, Cole JW (2014) Volcanic hazard impacts to critical infrastructure: A review. *J Volcanol Geotherm Res* 286:148–182
- Wörni R, Huggel C, Stoffel M, Pulgarín B (2012) Challenges of modeling current very large lahars at Nevado del Huila Volcano, Colombia. *Bull Volcanol* 74(2):309–324
- Yulianto F, Sofan P, Rokhis Khomarudin M, Haidar M (2013) Extracting the damaging effects of the 2010 eruption of Merapi volcano in Central Java, Indonesia. *Nat Hazards* 66:229–247
- Zanchetta G, Sulpizio R, Pareschi MT, Leoni FM, Santacroce R (2004) Characteristics of May 5–6, 1998 volcanoclastic debris flows in the Sarno area (Campania, southern Italy): relationships to structural damage and hazard zonation. *J Volcanol Geotherm Res* 133(1–4):377–393
- Zobin VM, Plascencia I, Reyes G, Navarro C (2009) The characteristics of seismic signals produced by lahars and pyroclastic flows: Volcán de Colima, Mexico. *J Volcanol Geotherm Res* 179(1–2):157–167
- Zuccaro G, De Gregorio D (2013) Time and space dependency in impact damage evaluation of a sub-Plinian eruption at Mount Vesuvius. *Nat Hazards* 68(3):1399–1423



Merapi: Evolving Knowledge and Future Challenges

18

I Gusti Made Agung Nandaka, Ralf Gertisser,
Thomas R. Walter, Valentin R. Troll,
and Antonius Ratdompurbo

Abstract

Despite the significant progress in our understanding of Merapi and its activity, as demonstrated by the contributions in this book, fundamental scientific questions about the volcano have remained unanswered and there are significant challenges that lie ahead. In this final chapter, we provide a scientific outlook

for Indonesia's most intensely studied and best monitored volcano and explore some of these open questions and upcoming challenges. These comprise open issues regarding the geology, volcanic history, petrogenesis, eruptive activity, volcano monitoring, early warning system, emergency planning, volcanic crisis management, social and communication changes, international collaboration, and the volcano's current status of activity following the large-magnitude eruption in 2010.

I G. M. A. Nandaka (✉)
Balai Penyelidikan dan Pengembangan Teknologi
Kebencanaan Geologi (BPPTKG), Yogyakarta,
Indonesia
e-mail: agung.nandaka@esdm.go.id

R. Gertisser
School of Geography, Geology and the
Environment, Keele University, Keele, UK

T. R. Walter
GFZ German Research Centre for Geosciences,
Telegrafenberg, Potsdam, Germany

V. R. Troll
Department of Earth Sciences, Section for Natural
Resources and Sustainable Development, Uppsala
University, Uppsala, Sweden

Centre of Natural Hazards and Disaster Science,
Uppsala University, Uppsala, Sweden

Istituto Nazionale Di Geofisica e Vulcanologia,
Rome, Italy

Faculty of Geological Engineering, Universitas
Padjadjaran (UNPAD), Bandung, Indonesia

A. Ratdompurbo
Geological Agency, Ministry of Energy and Mineral
Resources, Bandung, Indonesia

Keywords

Merapi · Scientific challenges · Outlook ·
Future hazards

18.1 Introduction

Over the past decades, our understanding of Merapi volcano (Fig. 18.1) and its activity has increased significantly through research conducted by the Center of Volcanology and Geological Hazard Mitigation (CVGHM) and BPPTKG (Balai Penyelidikan dan Pengembangan Teknologi Kebencanaan Geologi), including their preceding organisations, and through collaborations with Indonesian academic scientists, university research, and collaborative international research programmes. These research efforts have made Merapi the most intensely studied and best



Fig. 18.1 Aerial photo of Merapi volcano (foreground). New Merapi forms the highest peak of the volcanic edifice. The heavily vegetated parts to the right (east) of the New Merapi cone are the remnants of ‘Old Merapi’ and the ‘Proto-Merapi’ edifice of Gunung (G.) Bibi (see

Gertisser et al. 2023a, Chap. 6). Merbabu volcano can be seen immediately north of Merapi and Ungaran volcano is visible in the far distance. Photo credit: Igan Sutawijaya, CVGHM

monitored volcano in Indonesia and, at the same time, helped to considerably advance the discipline of volcanology. Many findings and technical advances developed and tested at Merapi were transferred to volcanoes elsewhere, especially in respect of our understanding of dome-forming eruptions at andesite volcanoes and pyroclastic density currents (PDCs), but also with regard to petrology, geochemistry, and assessment and mitigation of direct and indirect volcanic hazards. The contributions in this book demonstrate the scientific progress at Merapi that has been made to date, covering results from both the geosciences, such as geology, petrology, geochemistry, geophysics, and physical volcanology, and the social sciences, and provide state-of-the-art information on volcano monitoring, assessment of volcanic hazards, and risk mitigation. These advances highlight that Merapi is both an ‘experimental volcano’, where new techniques and ideas have been tested and developed for application worldwide, and a ‘high-risk volcano’, where robust and innovative monitoring helps saving lives. Despite

the scientific achievements, many fundamental scientific questions, both of an academic and an applied nature, still remain open and pose significant future challenges. This final chapter, written from the editors’ perspective, provides a scientific outlook and explores some of the future challenges we are facing at Merapi due to its frequent eruptions and varied styles of activity. This includes an update on, and the lessons learnt from, Merapi’s last major eruption in 2010 and the development since then up to the status of activity at the time of writing in early 2022.

18.2 Geology and Volcanic History

Building on the pioneering work by Kemmerling (1921), Hartmann (1935) and, in particular, van Bemmelen (1949), who recognised that the Merapi volcanic complex consists of a partly destroyed older edifice (Old Merapi) and an active stratocone (New Merapi), significant progress has been made in the interim 70 years

which greatly advanced our modern understanding of the geological evolution of Merapi (see Gertisser et al. 2023a, Chap. 6). Nevertheless, one of the major events in the volcano's history, the postulated collapse of Old Merapi, has remained elusive both in terms of the exact process as well as its exact age (cf. Camus et al. 2000; Newhall et al. 2000; Gertisser et al. 2012, 2023b, Chap. 1; Bronto et al. 2014, 2023, Chap. 7). Many authors agree that there is little geological evidence for a 'catastrophic outburst' of Merapi in AD 1006 that led to the collapse of the western flank of the old Merapi edifice, as originally suggested by van Bemmelen (1949). Similarly, the role of Merapi and its eruptions in the demise of the early Mataram kingdom in Central Java continues to be debated, with a combination of moderate to large explosive eruptions and associated political or social turmoil remaining possibilities (see Holmberg 2023, Chap. 3). The important recent discovery of a large debris avalanche deposit (Bronto et al. 2023, Chap. 7) contributes to the long-standing debate on the history of sector collapses at Merapi on the one hand and to the large sector collapse that defines the end of the Old Merapi stage on the other, but requires robust radiometric dating of the deposit. While correlation of pyroclastic deposits and abundant radiocarbon dates provide a robust stratigraphic framework for the past few thousand years of activity at Merapi (e.g. Andreastuti et al. 2000; Camus et al. 2000; Newhall et al. 2000; Gertisser et al. 2012, 2023a, Chap. 6), difficulties remain in the unique identification of earlier historical and especially pre-historical eruption deposits in the field. This issue may be partly improved upon by petrological-geochemical investigations and high precision radiocarbon and other radiometric dates, particularly of earlier historical deposits, such as those described by Bronto et al. (2023, Chap. 7) and Gertisser et al. (2023a, Chap. 6) in this book, but detailed further work on many deposits in the field remains to be established. Further questions exist about the completeness of the stratigraphic record, given the complicating rapid lateral facies variations, the frequent burial and reworking of primary pyroclastic deposits in

the tropical climate of Central Java, and the interfingering of older pyroclastic deposits from Merapi and Merbabu volcanoes. Since Merbabu is located immediately north of Merapi, distinguishing between the different sources for some deposits is not at all trivial and requires improved geochemical fingerprinting of the eruptive products from the Merbabu system versus those from older Merapi tephra. The application of radiometric dating methods other than the radiocarbon method is still in its infancy at Merapi and only a few reliable K–Ar ages exist to date (Gertisser et al. 2012, 2023a, Chap. 6). The lack of absolute age information limits our current knowledge of particularly the volcanic edifices of 'Old Merapi' and 'Proto-Merapi', including Gunung Bibi (Camus et al. 2000; Newhall et al. 2000; Gertisser et al. 2012, 2023a, Chap. 6), and thus provides an opportunity for future research to place tighter constraints on the earlier geological evolution of Merapi.

18.3 Petrogenesis, Magma Plumbing System and Magmatic Processes

Magma generation and differentiation, the architecture of the magma plumbing system, and the magma storage and crystallisation conditions have been intensively studied at Merapi, using petrological, geochemical and geophysical approaches (see summaries in Deegan et al. 2023, Chap. 10; Gertisser et al. 2023b, Chap. 1; Luehr et al. 2023, Chap. 5; Preece et al. 2023, Chap. 9; Troll and Deegan 2023, Chap. 8). A consensus seems to have gradually emerged over the past two decades that both mantle source contamination by subducted sediment and crustal contamination by carbonate rock in the subvolcanic basement are important factors controlling the geochemical and isotopic characteristics of the Merapi magmas and eruptive products. However, the relative significance of these at times contrasting, but for some parameters also complementary petrogenetic processes, e.g. in the generation of the distinctly more K₂O-rich magmas erupted over the past ~1900 ¹⁴C

years and the subtle K_2O variations within this magmatic series, is still not fully resolved (e.g. Gertisser et al. 2023a, Chap. 6; Deegan et al. 2023, Chap. 10). Regarding Merapi's magma plumbing system, a complex magma storage system has been proposed, where magmas are stored in magma storage zones or reservoirs at different levels throughout the upper mantle and the crust. The deep structure of Merapi over a depth range of more than 100 km has been highlighted by large-scale seismic experiments (e.g. Luehr et al. 2023, Chap. 5) and is supported by unusual amphibole megacrysts that come from a deep storage system (Troll and Deegan 2023, Chap. 8). Ascent of hot, volatile-rich magma from this depth, and recharge and interaction with magma stored in mush-rich regions at lower- to mid-crustal levels may be a key feature in driving the ultimate surface eruptions at Merapi. A high heat flux may keep intra-crustal mush-rich magmatic systems and reservoirs at relatively warm storage conditions (e.g. Chadwick et al. 2013) that may be a factor for the near steady-state eruptive behaviour of Merapi and its apparent 'hyperactive' nature. Large volumes of hot, volatile-rich replenishing magma may overwhelm the shallower mush-rich magma storage zones, lead to the crystal-rich andesite magmas that commonly erupt from Merapi and will, at times, cause larger than normal eruptions at Merapi when larger pulses of recharge magmas are migrating through the plumbing system, as proposed for the 2010 eruption (e.g. Costa et al. 2013; Preece et al. 2014; Subandriyo et al. 2023, Chap. 12). Recurrent magma replenishment and associated mixing of more evolved and lesser evolved magma parcels, each with a somewhat different degree of fractional crystallisation and assimilation history, may also explain the relatively uniform basaltic andesite bulk-rock compositions that characterise the volcanic edifice as well as the, at times, subtle shifts towards more or less SiO_2 -rich bulk-rock compositions (e.g. Gertisser and Keller 2003a; Chadwick et al. 2013). Detailed crystal-scale petrological, geochemical and isotopic studies are needed to unravel the precise histories and timescales of the various

magma parcels and the relative roles of the various differentiation processes each magma batch would have experienced. In this context magma-country rock interaction may be a process that warrants more in-depth investigation as it has the potential to change not only magma chemistry, but also eruptive behaviour (e.g. Troll et al. 2012; Whitley et al. 2019; Deegan et al. 2023, Chap. 10). The frequent occurrence of calc-silicate xenoliths in the Merapi eruptive products is testimony to ongoing and intense reactions that would release considerable quantities of extra volatiles (mainly CO_2 , but also H_2O), which could explain the short lived explosive, i.e. irregular, behaviour that Merapi volcano displays every so often. This may be compounded by deep plutonic rocks that break down when ascending to shallow levels (e.g. large amphibole megacrysts), providing an additional source of H_2O that contributes to the gas budget of the shallow magma system under Merapi (cf. Peters et al. 2017; Troll and Deegan 2023, Chap. 8) and may further complicate the eruptive pattern of the volcano.

18.4 Eruptions and Transitions in Eruptive Style

Lava dome extrusion and dome-collapse PDCs have dominated the activity of Merapi in the 20th and early twenty-first centuries, but much larger explosive eruptions have occurred in the pre-historical and older historical periods (e.g. Newhall et al. 2000; Voight et al. 2000; Gertisser et al. 2012, 2023b, Chap. 1) and most recently in 2010 (Fig. 18.2). This suggests that the common dome-forming or 'Merapi-type' eruptions may be interrupted by much larger explosive eruptions at relatively short timescales. Equally, abrupt transitions between effusive and explosive phases can occur during individual eruptions and at short notice, as recently observed during the large-magnitude eruption in 2010 and thereafter (Surono et al. 2012; Komorowski et al. 2013; Preece et al. 2016, 2023, Chap. 9; Heap et al. 2019; Subandriyo et al. 2023, Chap. 12).

Fig. 18.2 Example of explosive activity at Merapi during the waning phase of the 2010 eruption (10 November 2010). The ash column is about 3000–4000 m high and the photograph was taken 6.5 km south-east of Merapi from the village of Deles



Such eruptive behaviour, with sudden shifts between effusive and often erratic explosive activity, is not unusual at dome-forming andesite volcanoes, as demonstrated recently at other Indonesian volcanoes such as Kelud in 2014 (Cassidy et al. 2016, 2019; Deegan et al. 2019) and Semeru in late 2021 and early 2022 (Global Volcanism Program 2013). A common feature of eruptions at these volcanoes is the occurrence of PDCs, which may be produced by dome failure, vertical eruption column/fountain collapse or, less commonly, by directed explosions (Gertisser et al. 2023b, Chap. 1). The PDC generation mechanisms determine the type of current produced, the area affected and runout distance and, hence, the effects of PDCs in proximal areas up to ~ 10 km or, occasionally, more from the source. Detailed field studies of the 1984, 1994, 1998, 2006 and 2010 PDC deposits have been made at Merapi, validating and improving numerical simulations used as a hazard assessment tool (Charbonnier et al. 2023, Chap. 16). The same holds for lahars, which may be regarded as the most significant hazardous volcanic phenomenon at Merapi in distal areas beyond the limits of primary PDC deposition (Thouret et al. 2023, Chap. 17). Although the results of numerical simulations obtained so far have provided the basis for defining hazard zonation of the main areas at risk from PDCs and lahars at

Merapi and important progress has been made, many aspects still require further investigation. These unresolved aspects include the, at times, unusual long runout distance of PDCs (e.g. Kelfoun and Gueugneau 2022), such as those generated at the peak of the 2010 eruption, the potential wider areas that may be affected by eruption column or fountain collapse PDCs, and the effects of valley sinuosity, channel capacity and the effects of Sabo dams on both PDC and lahar dynamics. These aspects are all still relatively poorly understood and not fully accounted for in current hazard assessment tools.

Large eruptions that are similar to, or even exceed the intensity and magnitude of the 2010 events pose a particular challenge, especially if they occur over extended periods. Understanding the changes in the magma plumbing system leading to variations in the style, magnitude, and duration of future eruptions and to effusive-explosive transitions at various timescales is thus of critical importance. Comprehensive petrological studies are available for individual recent to historical eruptions prior to the two most recent twenty-first century eruptions in 2006 and 2010 (cf. Gertisser 2023a, Chap. 6; Troll and Deegan 2023, Chap. 8), but are sparser for older eruption events. Here, on the one side, future research may help to develop a petrological monitoring procedure that focuses on the eruptive products

themselves, aiming to tie in pre-eruptive magmatic processes with the monitoring signals detected at the surface during the course of an eruption (e.g. Re et al. 2021). On the other side, a wealth of information can also still be gleaned from detailed petrological-geochemical studies of eruptions and eruption sequences in the stratigraphic record of both ‘Old Merapi’ and ‘New Merapi’ (e.g. Andreastuti et al. 2000; Newhall et al. 2000; Gertisser et al. 2012, 2023a, Chap. 6), which have been far less intensely studied than the more recent eruptions of the last decades and several of these older eruptive events remain essentially unstudied at this point in time.

A hazard at Merapi, not to be underestimated, is a large flank or sector collapse of the volcanic edifice, which may have occurred already several times in the volcano’s history (van Bemmelen 1949; Newhall et al. 2000; Bronto et al. 2023, Chap. 7; Gertisser et al. 2023a, Chap. 6). A flank collapse at Merapi may range from a smaller collapse of parts of the summit region, as occurred during the 2006 eruption (Charbonnier and Gertisser 2008; Ratdomopurbo et al. 2013) or most recently after the 2018 lava dome extrusion (e.g. Darmawan et al. 2022, 2023, Chap. 15), to a large event of the size of the recently discovered Godean debris avalanche deposit (Bronto et al. 2014, 2023, Chap. 7). Areas most at risk from a flank collapse are the volcano’s southern and western flanks. A large flank collapse, which may affect areas several tens of kilometres away from Merapi, is considered extremely unlikely, however, and there are no indications for an event of such magnitude to occur in the near future. At some volcanoes, large flank collapses were associated with significant changes in magma compositions before and after the collapse event (see Gertisser et al. 2023a, Chap. 6). At Merapi, the observed shift from medium-K to high-K type magmas coincides roughly with the inferred date of a flank collapse at the end of the Old Merapi stage, as proposed by Newhall et al. (2000). However, given the uncertainty about the exact date of this event (e.g. Bronto et al. 2023, Chap. 7; Gertisser et al. 2023a, Chap. 6), and the attribution of the compositional change to deep processes at the

magma source (Gertisser and Keller 2003b; Gertisser et al. 2023a, Chap. 6), a potential causal link between such a collapse events and precursory processes in the magma plumbing system, or the post-collapse readjustment of the latter, remain to be more fully explored in a dedicated future study.

18.5 Volcano Monitoring

The volcanic activity of Merapi was closely watched since the arrival of the first settlers, though systematic instrumental monitoring only started much more recently (see Gertisser et al. 2023b, Chap. 1). Since the 1980s, computerised monitoring has been used at Merapi with the main aim of recognising eruption precursors and the most common ‘Merapi-type’ eruptions, characterised by PDCs caused by lava dome failure, are now recognised by preceding volcanic-tectonic (VT) earthquakes and subsequent multiphase (MP) earthquakes. These usually reflect pre-eruptive magma ascent to the surface. From the experience of the last decades, it appears that larger explosive eruptions are associated with multiparameter monitoring data exceeding average baseline intensities of the precursors of the more common ‘Merapi-type’ eruptions (e.g. Surono et al. 2012; Budi-Santoso et al. 2013; Jousset et al. 2013; Subandriyo et al. 2023, Chap. 12). Anticipating a possible eruption scenario may therefore become yet more accurate with the development and deployment of technically advanced volcano monitoring systems (Budi-Santoso et al. 2023, Chap. 13). In these systems, observables and data are increasingly interpreted by novel numerical and statistical decision-support tools, replacing more traditional approaches that have been strongly influenced by the training and experience of the individual volcanologists involved. Following the 2010 eruption, possible scenarios considered by BPPTKG include a Plinian or sub-Plinian eruption of VEI 4 or above (e.g. Subandriyo et al. 2023, Chap. 12), as observed in 1872 and also in 2010, in addition to the classic VEI 2 to VEI 3 ‘Merapi-type’ eruptions. By contrast, the classic ‘Merapi-type’

eruptions are indicated by the formation of a new lava dome, such as occurred since 2018 (Global Volcanism Program 2019, 2021a; Darmawan et al 2022, 2023, Chap. 15), but, as might be inferred from the post-2010 activity (see below), short-lived phreatic or small Vulcanian explosions may possibly become more frequent at Merapi (e.g. Heap et al. 2019). Anticipating and detecting these varied eruption scenarios presents a continued challenge and highlights the need to reevaluate and improve the monitoring strategy and early warning system at Merapi.

This is compounded by the realisation that increased technological surveillance also brings a new set of vulnerabilities. During the 2010 eruption, almost all monitoring stations were destroyed and only one seismic station remained operational during the later parts of the eruption. As a result, remote sensing data were used to help understand the behaviour of the volcano and international experts were called in to contribute to the effort at the time. For instance, satellite radar data acquired through the International Charter for Space and Major Disasters (RADARSAT-2 and TerraSAR-X) were used together with optical and spectral data (ASTER, GeoEye 1 and WorldView-2) to monitor the magma extrusion rate and lava dome growth during the 2010 eruption (Pallister et al. 2013; Subandriyo et al. 2023, Chap. 12), which, at the time, provided valuable near real-time information about the type of eruption and hazard magnitude. With these technologically advanced monitoring systems, instrumental stations at greater distances away from Merapi were increasingly deployed and the use of remote satellite data has become more pertinent, and it is expected that future large eruptions may be closely watched with more distal and remote instrumentation that is increasingly developed at the moment.

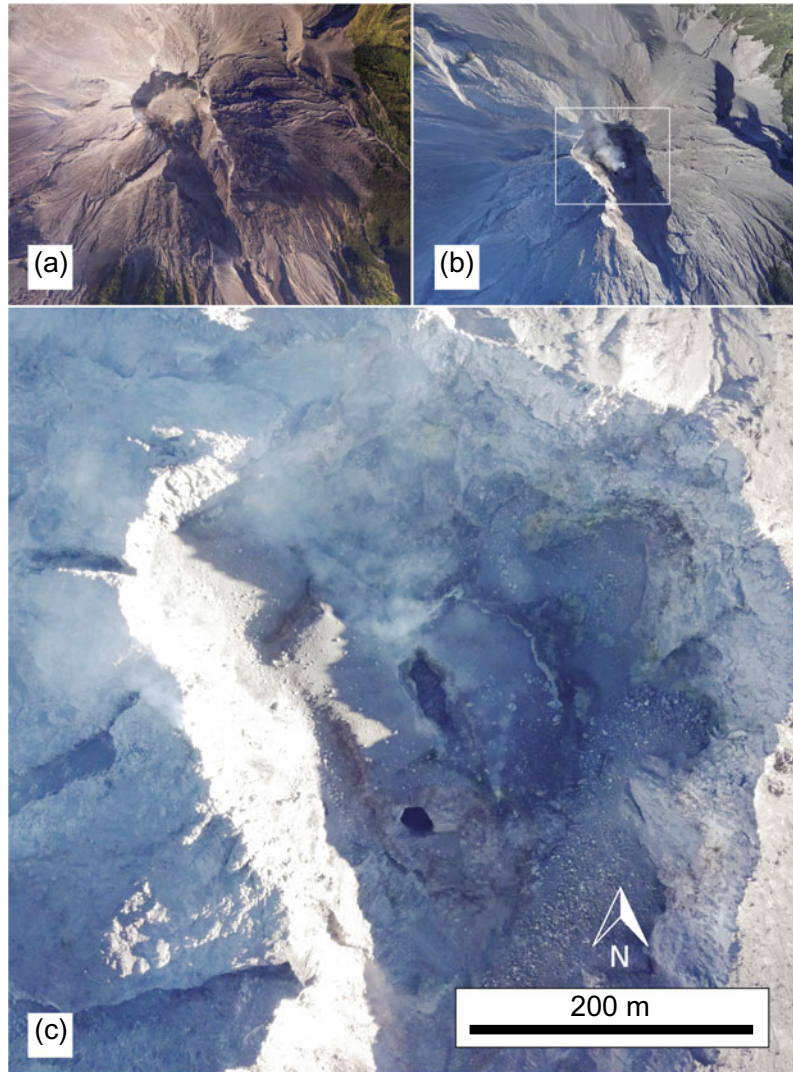
One of such new developments to monitor morphological changes at the summit of Merapi is the use of unmanned aerial vehicles (UAVs) (Darmawan et al. 2022, 2023, Chap. 15), which are more effective than terrestrial laser scanning (TLS) in areas with steep topography such as volcano craters and volcanic domes (Fig. 18.3).

UAV data acquisition is relatively simple, as UAVs are easy to carry in a backpack and can be launched from a safe distance away from, for example, the active lava dome.

Advances in our understanding of PDC and lahar behaviour has also benefited from technological advances, especially from increases in available computational power, and from the development of numerical simulation codes, which now allow PDC and lahar simulation in near-real time, taking into account morphological and topographical background data. This is of critical importance prior to and especially during crisis management, as PDC simulations based on the ejected volume of magma during an eruption may provide important information about potentially affected areas, and allow evacuation scenarios to be assessed quantitatively. Several computer models and numerical simulations for PDCs and lahars have been successfully implemented and used at Merapi, comprising Titan2D (Charbonnier and Gertisser 2009, 2012; Widwijayanti et al. 2009; Charbonnier et al. 2023, Chap. 16), VolcFlow, a code using a two-fluid layer models (Kelfoun et al. 2017; Charbonnier et al. 2023, Chap. 16), a PDC simulation model developed by Itoh et al. (2000), and LaharZ for simulating lahars (e.g. Thouret et al. 2023, Chap. 17).

In addition to technological advances and use of high precision instruments in volcano monitoring, there is also a need for improved data processing, analysis and documentation capabilities. The often simultaneous occurrence of multiple volcanic hazards at Merapi requires integrated mitigation strategies to reduce the disaster risk caused by volcanic eruptions. This strategy must account for PDC and lahar as well as volcanic ash fall disaster mitigation, and integrate and automate multi-parameter analysis of geophysical, geodetic, geochemical, and petrological data. Several new data analysis tools have been developed and partly been implemented at Merapi (Budi-Santoso et al. 2023, Chap. 13), including: (i) WebObs, an online data system developed in collaboration with French scientists, which is particularly useful for processing deformation data to calculate quasi real-time

Fig. 18.3 UAV images of the summit area of Merapi in **a** 2012 and **b**, **c** 20 August 2018. **c** Close-up of the summit crater recorded on 20 August 2018, showing the extrusion of a new lava dome (dark colour) in the crater



pressures and magma volumes based on GNSS, tiltmeter, and EDM data, (ii) WOVOdat, a database that allows a comparison of current monitoring data with those from previous eruptions for more accurate eruption forecasting (Newhall et al. 2017; Costa et al. 2019), and (iii) SSDM (Shimomura 2015), a support system for decision making, developed together with scientists from Japan to build event chain hazard scenarios. This set of improved data processing systems is very promising for mitigation purposes but, in practice, its usefulness remains to be proven when Merapi erupts again on a large scale. In the meantime, recently developed machine-learning

algorithms for rapid evaluation and better decision making are being contemplated to continue to further improve volcano monitoring at Merapi even in the current absence of a larger eruption, as an event of the magnitude of the 2010 eruption may recur in the decades ahead and therefore has to be anticipated.

18.6 Early Warning System

Monitoring data are the main basis for providing volcanic alert level information, while information on the geological and eruptive history is

crucial for making hazards maps (e.g. Budi-Santoso et al. 2023, Chap. 13; Gertisser et al. 2023a, Chap. 6; Subandriyo et al. 2023, Chap. 12). At Merapi, there are 4 alert levels starting from the lowest level 1 (Normal) to level 2 (Waspada; Engl.: Advisory), level 3 (Siaga; Engl.: Watch), and level 4 (Awasi; Engl.: Warning). The alert level is based on the monitoring data changes and the potential hazard (Fig. 18.4). Each alert level has different recommendations that will be reported to the local government and the National Disaster Management Agency. At the highest level (level 4), evacuation advice is given to areas that are potentially at risk from the eruption. A hazard map of Merapi consists of three hazard zone categories (zones 1, 2 and 3; e.g., Charbonnier et al. 2023, Chap. 16; Lavigne et al. 2023, Chap. 2). Hazard zone 3 includes the most vulnerable areas most likely exposed to PDCs when Merapi erupts. Delineation of zone 3 is an area that has been hit by PDCs in the past 100 years. Hazard zone 2 is an area that has been affected historically by PDCs based on

geological and stratigraphic research, while hazard zone 1 is an area that is threatened particularly by lahars. The Merapi hazard map was first published in 1978 (Pardiyanto et al. 1978) and was revised twice in 2002 and 2011 (CVGHM 2002, 2011). This was because there were new areas that were affected by PDCs, such as the more distal areas of the Gendol river valley (Kali Gendol) that were reached by PDCs at the peak of the 2010 eruption (e.g. Charbonnier et al. 2013; Komorowski et al. 2013; Subandriyo et al. 2023, Chap. 12), and other emerging geological evidence that supported changes to be made to the hazard map. Such updates of the existing hazard map are essential for progressively improved emergency planning and volcanic crisis management, and will continue to be necessary based on the fluctuating status of activity of Merapi volcano, the changing location(s) of the summit lava dome(s), and the morphology of the summit region of Merapi, which are all crucial factors in determining PDC direction and other hazards such as smaller collapses of the crater

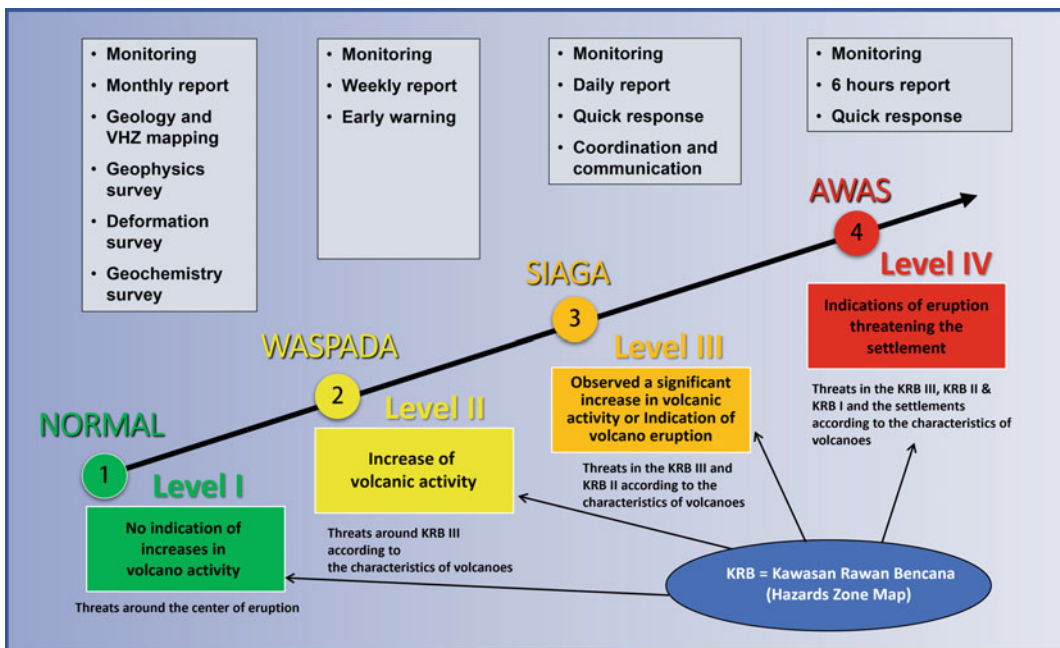


Fig. 18.4 The four volcanic alert levels applied by CVGHM to all volcanoes in Indonesia, with activity responses at each level

walls and uppermost parts of the Merapi cone (e.g. Charbonnier and Gertisser 2008; Ratdomopurbo et al. 2013; Bronto et al. 2023, Chap. 7; Darmawan et al. 2022, 2023, Chap. 15).

18.7 Emergency Planning and Volcanic Crisis Management

Among all stakeholders who are part of the Merapi disaster management, CVGHM, through its unit BPPTKG, is the only institution that has the authority for monitoring Merapi and for issuing early warnings. Recommendations by CVGHM volcanologists have direct impact on the disaster management and will inform the evacuation management of several hundred thousands of people who live in the different hazard zones, as required. The latest crisis management during the 2010 eruption of Merapi has been regarded as successful in saving up to 20,000 lives (Surono et al. 2012; Lavigne et al. 2023, Chap. 2; Subandriyo et al. 2023, Chap. 12). However, the eruption still caused nearly 400 fatalities, indicating that there are a number of issues that require close attention (Mei et al. 2013). Particular challenges include the response to erratic explosive events, such as the phreatic eruptions that occurred after the 2010 eruption (see below), which are difficult to predict in the volcano monitoring data. Equally, during the course of an eruption, eruptive style and intensity can vary significantly, and transitions between effusive and explosive phases may occur at very short timescales (e.g. Walter et al. 2007; Troll et al. 2012; Preece et al. 2016; Subandriyo et al. 2023, Chap. 12), imposing significant challenges for crisis and evacuation management, as most recently seen in 2010 (Surono et al. 2012; Lavigne et al. 2023, Chap. 2; Subandriyo et al. 2023, Chap. 12). The 2010 eruption also demonstrated the need for careful preparation and a coordinated response to larger than normal eruptions at Merapi that may last longer and may even be more intense than the catastrophic events of 2010. The issue is magnified further by increasing population pressure in the areas around

Merapi, the need to protect an increasingly technology dependent infrastructure and the requirement for larger numbers or sizes of emergency shelters, supply chains and other basic elements of a volcanic emergency plan (e.g. UNDRO 1985). This is especially pertinent when combined with other external factors, e.g. complications similar to the current COVID-19 pandemic or possible extreme weather events due to climate change.

18.8 Social and Communication Changes

Social and communication changes impact emergency planning and volcanic crisis management by the authorities. A prosperous agricultural life at Merapi is supported by the landscape, topography and the fertile volcanic soil produced by volcanic ash deposited around the volcano, and a high annual rainfall between 2000 and 4500 mm per year (Lavigne et al. 2000). The fertile soil supports various plant types, and the southern and western slopes of Merapi are particularly famous for salak (snake fruit) farming. Rocks and sand deposited in the river valleys around Merapi from PDCs and lahars are sought-after building materials and many people are involved in sand mining and selling it to various cities in Central Java (e.g. Holmberg 2023, Chap. 3; Lavigne et al. 2023, Chap. 2; Subandriyo et al. 2023, Chap. 12). Unfortunately, uncontrolled mining raises a new threat to the environment causing, for example, the loss of pristine river valleys and changes to the morphology of the landscape. The latter poses a new threat, as PDCs may travel along the morphological tracks produced, possibly leading to a wider distribution of such currents over larger areas. The 2010 eruption caused a change in the livelihoods of many residents, especially for the farmers on the southern slope of Merapi, who turned to other professions, including small traders and tour guides, providing facilities for the tourism industry (e.g. Lavigne et al. 2023, Chap. 2; Subandriyo et al. 2023, Chap. 12). Tourism around Merapi has grown and

developed significantly due to the combined natural beauty of the volcanic environment and the relatively cool temperatures on the volcano's slopes compared to the surrounding plains. In 2017, the Merapi Volcano Museum in Yogyakarta reached 260,000 visitors, 3000 of whom were foreign tourists (Museum Gunung Merapi 2018). After the 2010 eruption, residents on the south slope of the volcano developed a new type of tourist activity, called the 'Volcano Lava Tour', where visitors can hire open cars to explore the area destroyed by the 2010 eruption. Currently, there are at least 700 vehicles operating on these 'lava tours'. In addition, according to information from the Merapi National Park, on average 200–300 people climb Merapi each week, with ascents typically taking the northern route to the summit from Selo (Fig. 18.5). At weekends or during national holidays, the number of climbers can reach 1500–2000 people per day, causing a considerable volcanic risk,

especially as the number of unpredictable steam-driven explosions can be high. For safety reasons, climbing Merapi in recent years has, at times, only been permitted up to 2650 m elevation (Pasarbubar), and since 2018, it has not been permitted to climb Merapi for leisure at all.

The rapid development of information technology and digital communication provides new challenges and prospects for disaster communication. As of January 2022, Indonesia has a total of 204.7 million internet and 191.4 million social media users out of a population of 277.7 million (Digital 2022 Indonesia). The large number of users accessing social media means that disaster information can be disseminated quickly and widely. However, the ease of receiving and sharing such information means that users are also often flooded by digital information and there is a danger of people spreading hoaxes, false information, or news from unreliable or untrusted sources. Another issue is that the



Fig. 18.5 Trailhead of the northern climbing route to the summit of Merapi at New Selo at 1,800 m a.s.l. From there the summit can be reached by a several hour-long

climb along a relatively steep hiking trail up to the crater rim on the summit of the volcano

national disaster communication in Indonesia may become increasingly dependent on social media platforms developed and operated in other countries (e.g. Twitter, Facebook, WhatsApp). CVGHM has therefore introduced, and continues to develop, a smart phone-based application that can be used to report geological disasters and to obtain information about volcanic activity, eruptions, earthquakes and landslides.

During a volcanic crisis, the BPPTKG Media Center plays an important role in the dissemination of the current condition of the volcano, providing answers to questions by the public and, importantly, countering hoaxes. For example, during the volcanic crisis in May 2018, the Center publicised correct volcano facts and information to reduce the spread of misguided information. In such a context, it is important that the disseminated information is updated regularly, that citizens' questions are answered quickly and correctly, and that a response is given to flawed or faulty information that is circulating in social media in times of crisis.

Moreover, we must be aware that there will be a generation change when Merapi erupts next. Children who experienced the 2010 eruption are now becoming adults with a mindset and behaviour that are different from their parents and that will affect their specific responses to a disaster. Nowadays, people living near Merapi are aware of the previous volcanic eruption. Before 2010, the residents still held their beliefs and trusted their local leaders more than official authorities, in part refusing to evacuate when advised to do so by the government, based on the volcanologists' recommendations (Mei et al. 2013; Troll et al. 2021). After the 2010 events, however, public trust in the government and volcano experts has increased due to practical successes and continued educational efforts, and has now become very high compared to previous generations (Lavigne et al. 2023, Chap. 2; Subandriyo et al. 2023, Chap. 12).

18.9 International Collaboration

Merapi volcano combines several factors that make it a key site for research and collaboration (e.g. Budi-Santoso et al. 2023, Chap. 13; Gettisser et al. 2023b, Chap. 1). It is one of the most active volcanoes of Indonesia and it is located in the vicinity of (and threatens) a major metropolitan area. For this reason, it is being closely watched from a long-established and highly experienced volcano observatory, which has, by now, become one of the major field sites for teaching and research at universities and research centres in Yogyakarta and beyond. This high-risk situation, together with the extensive studies and monitoring efforts, have made Merapi a nucleus for novel ideas and hypotheses, most of which were derived from national and international collaborative networks. The success of these long-term collaborative projects between different scientists, institutions, and countries, including mutual agreements and memoranda of understanding between diverse consortia, are a shining example of modern scientific practice, and a feature that will hopefully be widely continued in the decades to come. This international interest and world-wide research network has allowed a number of Indonesian students to be invited to Europe (e.g. France and Germany) to study for their collaborative Masters or doctorate degrees, supported by institutional exchange and national academic exchange programs, which will strengthen the internationalisation of research at Merapi and increase the bonds within these networks for the future. Several European scientists have had the opportunity for extended research stays in Indonesia, and the continuity of these close international collaborations is considered essential for further technical and scientific developments at Merapi and other volcanoes in the region.

18.10 Post-2010 Activity and Current Status of Merapi

After the catastrophic events in October–November 2010 and the end of lava dome growth in the later stages of the 2010 eruption (Subandriyo et al. 2023, Chap. 12), the activity of Merapi volcano gradually returned to background levels. This background activity has subsequently been interrupted by minor eruptions and renewed lava dome extrusion, accompanied by rockfalls and small PDCs with runout distances up to 3 km from minor dome collapses (Global Volcanism Program 2013; Kelfoun et al. 2021; Darmawan et al. 2022). By the time of writing in early 2022, there has not been a major eruption at Merapi since the large-magnitude eruption in 2010.

The post-2010 activity has provided valuable monitoring data and important insights into

Merapi's varied and changing eruptive behaviour, which has been documented by fluctuations in seismicity, as recorded by the seismic network at Merapi (Fig. 18.6). In brief, two main post-2010 episodes of volcanic activity can be distinguished: (i) a period of small-scale phreatic explosions from 2012 to 2014 (Fig. 18.7) and again in 2018, and (ii) a new magmatic dome-forming episode from 2018 onward (Fig. 18.3b, c).

During the period of small-scale phreatic explosions, at least six minor, short-lived phreatic eruptions occurred between 2012 and 2014, producing vertical eruption columns between 100 and 2000 m above the summit (Fig. 18.7). Eruptive volumes were relatively small and estimated at $<50,000 \text{ m}^3$ for a single event. Another phreatic eruption that occurred after nearly four years of quiescence on 11 May 2018 produced a vertical eruption column up to 5 km

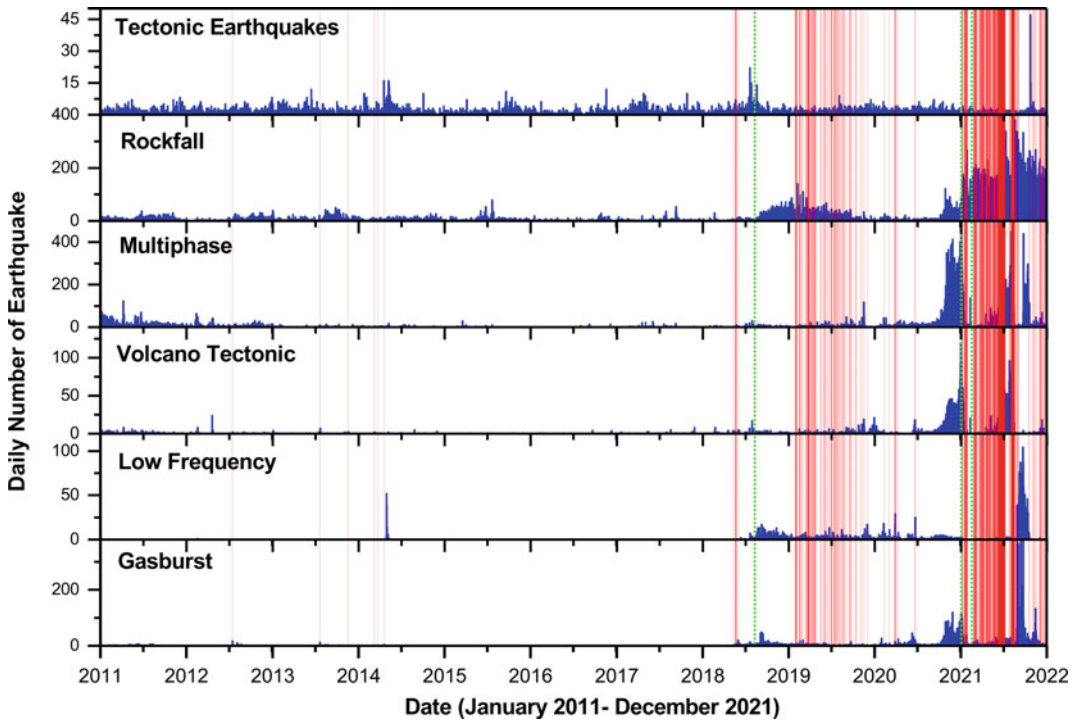


Fig. 18.6 Seismicity of Merapi between 2011 and early 2022. In red colour are the eruptions and PDCs, while the green colour indicates lava dome extrusion. Extrusion of a new lava dome on top of the remnants of the 2010 dome commenced on 11 August 2018. The south-west lava dome started to extrude on 31 December 2020, as

indicated by incandescence at the summit, and was first observed on 7 January 2021. On 17 February 2021, the two domes were noted to be active simultaneously in the summit area, and so there are currently two active domes, the south-west dome and the new dome in the centre of the 2010 summit crater

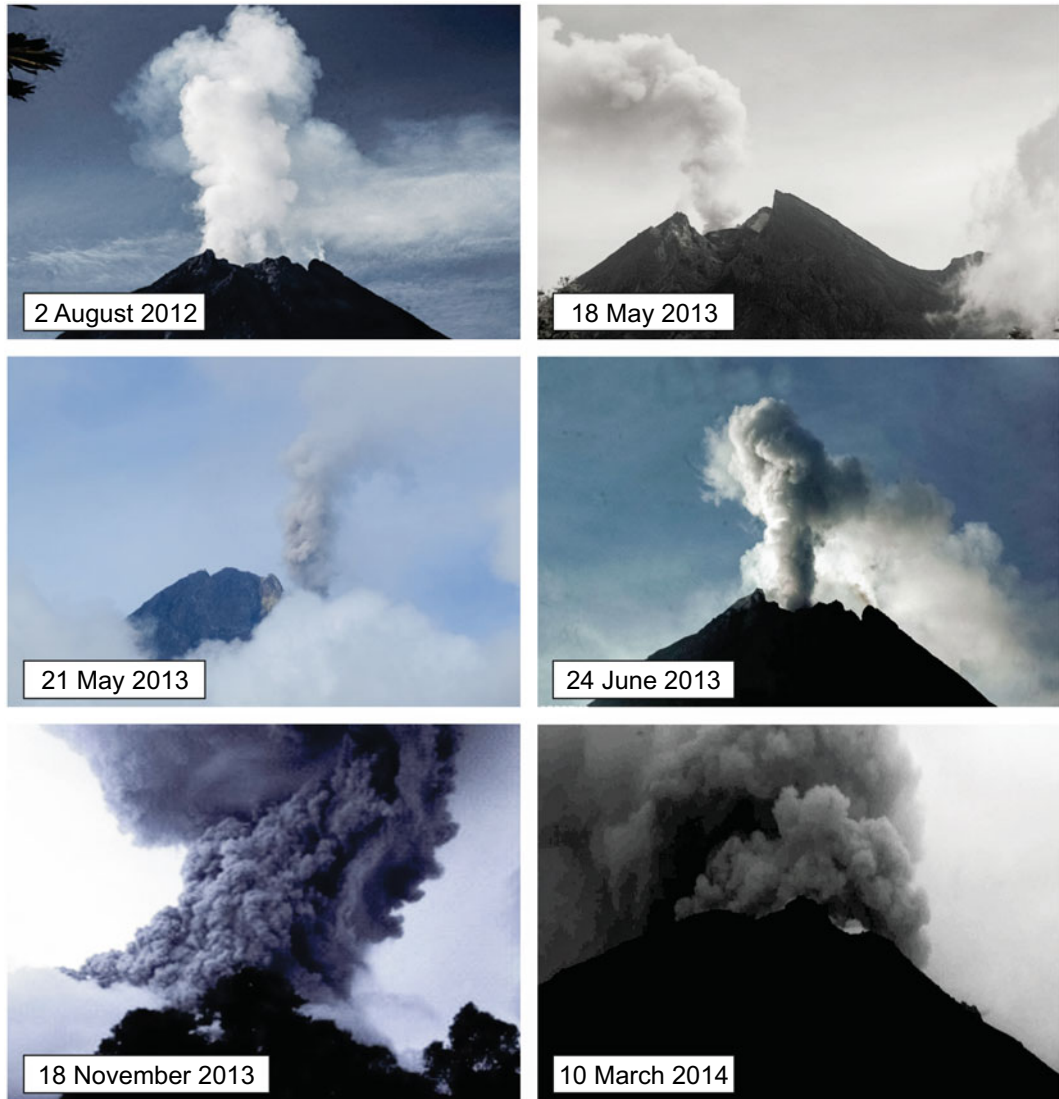


Fig. 18.7 Images of small, predominantly phreatic eruptions of recent Merapi events during the 2012–2014 period

above the summit and caused light ashfall in Yogyakarta and in the south-east sector of the volcano. Twelve further phreatic eruptions were recorded by BPPTKG in 2018 after the event of 11 May, with up to three eruptions per day (Global Volcanism Program 2018). Common features of these eruptions were the very weak to almost no precursors and a lack of significant pre-eruptive changes in various monitoring parameters, including seismicity, deformation (EDM, tilt and GPS data), and temperature and

volcanic gas emissions, as determined by regular sampling at the solfataras on Merapi's summit. These observations suggest that there was no major new magma supply from depth associated with these sporadic eruptions, but, instead, they might have been triggered by gas accumulation in the shallow conduit (e.g. Heap et al. 2019). With no obvious early warning signs, such minor activity at Merapi remains extremely difficult to forecast and continues to pose a threat particularly to mountain climbers around the volcano's

summit and villages that are located on the slopes of Merapi less than 3 km away from the summit.

A small Vulcanian-type explosion on 1 June 2018 signalled the beginning of a new magmatic episode though. The eruption was accompanied by a rumbling sound that was heard for several minutes, and a hot volcanic bomb—the first sign of a clear magmatic eruption for several years—burned trees some 2 km from the summit on the north-west flank of Merapi. Seismicity and shallow earthquakes started to increase after July 2018 and were accompanied by increasing surface deformation. On 11 August 2018, a new lava dome was first seen at the summit, marking a return to typical ‘Merapi-type’ activity after the eruption in 2010. The new dome piled up on top of the 2010 lava dome and grew at a relatively low rate between 1000 and 6200 m³ per day during August to November 2018 (Global Volcanism Program 2019). By the end of 2018, the lava dome had a volume of 389,000 m³, increasing to a maximum of 475,000 m³ on 4 July 2019, with the volume of the dome balanced by magma extrusion and dome growth on the one

hand versus partial dome destruction by rock falls, rock avalanches, small block-and-ash flows and explosions on the other hand (Global Volcanism Program 2019, 2020a; Kelfoun et al. 2021, Darmawan et al. 2022, 2023, Chap. 15). Activity further increased in September 2019, causing fifteen explosive eruptions in the following ten months (Budi-Santoso et al. 2019, 2020). Incandescence in the summit area, indicating the arrival of new magma at the surface, was first noted on 31 December 2020, and rock avalanches continued up to 1.5 km towards the western and north-western flanks. Incandescent rock avalanches were first reported on 4 January 2021, and extrusion of a new dome in the south-western part of the summit at the bottom of the 1997 dome was confirmed on 7 January 2021 (Global Volcanism Program 2021a). A large number of PDCs, accompanied by a significant explosion with an ash plume of ~12 km altitude and ash fall in the areas surrounding Merapi, occurred on 27 January 2021 (Global Volcanism Program 2021a; Fig. 18.8). On 17 February 2021, two domes were noted in the summit area,



Fig. 18.8 Eruptive activity of Merapi in 2021. On 27 January 2021, 58 PDCs occurred at Merapi, which was the highest observed number of daily PDC events in 2021. The photograph shows people watching a small PDC at

07:29 (WIB) on 27 January 2021 from the village of Pakem about 8 km south of Merapi. Photo credit: Noer Cholik, BPPTKG

comprising the dome that extruded in the south-western part of the summit on 31 December 2020 and a new dome in the centre of the 2010 summit crater. This has led to the remarkable situation of two simultaneously growing, spatially separate active lava domes at Merapi. Both domes continued to grow during 2021 and in early 2022 (Fig. 18.9). Incandescent rock avalanche and block-and-ash flow activity with runout distances of up to 2–3 km remained high, particularly on the south-west flank but occasionally also down Kali Gendol, and was interrupted sporadically by minor explosions, producing ash fall in the surrounding area (Global Volcanism Program 2021b). By early January 2022, the south-west dome had an estimated volume of 1,670,000 m³, while the central summit dome reached a volume

of more than 3 million m³. Due to the continued high seismic activity and frequent rockfalls, rock avalanches and small block-and-ash flows, particularly from the south-west dome, the alert level has remained elevated at level 3 and the public has continued to be advised to stay outside a zone of 3–5 km from the summit (Global Volcanism Program 2021b). The location and extrusion direction of the south-west dome requires a reevaluation of the areas threatened by Merapi's ongoing activity and the sequence of the recent events highlights once more that Merapi is in constant activity and change.

Past eruptions and recent developments have shown that Merapi's eruptive behaviour can change rapidly and with little advance warning. Anticipating such changes in activity and

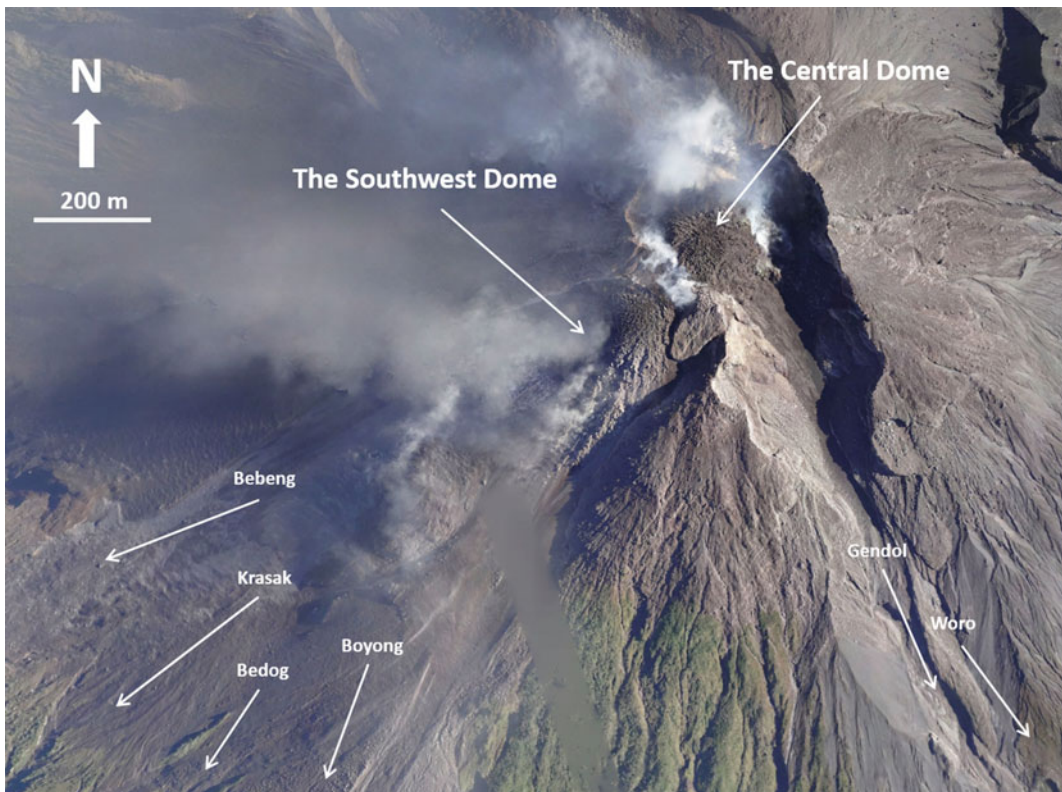


Fig. 18.9 UAV image from 16 September 2021, showing the presence of the two lava domes at the summit of Merapi: the central and the south-west dome. This is a rather unusual situation and for the first time since the

recorded modern Merapi monitoring history commenced are there two simultaneously growing, active lava domes in the summit region of Merapi volcano

mitigating the risk to the population on the slopes of Merapi therefore remain among the highest priority challenges that lie ahead.

References

- Andreastuti SD, Alloway BV, Smith IEM (2000) A detailed tephrostratigraphic framework at Merapi Volcano, Central Java, Indonesia: implications for eruption predictions and hazard assessment. *J Volcanol Geotherm Res* 100:51–67
- van Bemmelen RW (1949) *The geology of Indonesia, vol 1A: General geology*. Government Printing Office, The Hague
- Bronto S, Ratdomopurbo A, Asmoro P, Adityarani M (2014) Longsoran rakasa Gunung Api Merapi Yogyakarta—Jawa Tengah (Gigantic landslides of Merapi volcano, Yogyakarta—Central Java). *J Geol Sumb Min* 15:165–183
- Bronto S, Rahardjo W, Asmoro P, Ratdomopurbo A, Adityarani M, Permatasari A (2023) The Godean debris avalanche deposit from a sector collapse of Merapi volcano. In: Gertisser R, Troll VR, Walter TR, Nandaka IGMA, Ratdomopurbo A (eds) *Merapi volcano—geology, eruptive activity, and monitoring of a high-risk volcano*. Springer, Berlin, Heidelberg, pp 195–231
- Budi-Santoso A, Lesage P, Dwiyo S, Sumarti S, Subandriyo S, Jousset P, Metaxian J-P (2013) Analysis of the seismic activity associated with the 2010 eruption of Merapi Volcano, Java. *J Volcanol Geotherm Res* 261:153–170
- Budi-Santoso A, Widyo-Laksono R, Putra R, Aisyah N, Humaida H, Rudianto I, Rahmadi N, Rozin M, Nurdin I, Suparwoko H, Triyono T, Sopari A, Yulianto Y, Trimujianto T, Nurmanaji A (2019) *Aktivitas Vulkanik Gunung Merapi Periode September-Desember 2019*. *Bul Merapi* 24(03/Edisi Desember 2019):1–12
- Budi-Santoso A, Humaida H, Aisyah N, Putra R, Widyo-Laksono R, Sayudi DS, Subandriyo S, Julianto J, Triguri I, Rozin M, Rudianto I, Rahmadi N, Nurdin I, Suparwoko H, Triyono T, Sopari A, Yulianto Y, Trimujianto T, Nurmanaji A (2020) Data Peman-taan G. Merapi Menjelang Status Siaga 5 November 2020. *Bul Merapi* 25(03/Edisi Desember 2020):1–18
- Budi-Santoso A, Beauducel F, Nandaka IGMA, Humaida H, Costa F, Widiwijayanti C, Iguchi M, Métaxian J-P, Rudianto I, Rozin M, Sulistiyani, Nurdin I, Kelfoun K, Byrdina S, Pinel V, Fahmi AA, Laurin A, Rizal MH, Dahamna N (2023) The Merapi volcano monitoring system. In: Gertisser R, Troll VR, Walter TR, Nandaka IGMA, Ratdomopurbo A (eds) *Merapi volcano—geology, eruptive activity, and monitoring of a high-risk volcano*. Springer, Berlin, Heidelberg, pp 409–436
- Camus G, Gourgaud A, Mossand-Berthommier P-C, Vincent PM (2000) Merapi (Central Java, Indonesia): an outline of the structural and magmatological evolution, with a special emphasis to the major pyroclastic events. *J Volcanol Geotherm Res* 100:139–163
- Cassidy M, Castro JC, Helo C, Troll VR, Deegan FM, Muir D, Neave DA, Mueller SP (2016) Volatile dilution during magma injections and implications for volcano explosivity. *Geology* 44:1027–1030
- Cassidy M, Ebmeier SK, Helo C, Watt SFL, Caudron C, Odell A, Spaans K, Kristianto P, Triastuty H, Gunawan H, Castro JM (2019) Explosive eruptions with little warning: experimental petrology and volcano monitoring observations from the 2014 eruption of Kelud, Indonesia. *Geochem Geophys Geosyst* 20:4218–4247
- Chadwick JP, Troll VR, Waight TE, van der Zwan FM, Schwarzkopf LM (2013) Petrology and geochemistry of igneous inclusions in recent Merapi deposits: a window into the sub-volcanic plumbing system. *Contrib Mineral Petrol* 165:259–282
- Charbonnier SJ, Gertisser R (2008) Field observations and surface characteristics of pristine block-and-ash flow deposits from the 2006 eruption of Merapi Volcano, Java, Indonesia. *J Volcanol Geotherm Res* 177:971–982
- Charbonnier S, Gertisser R (2009) Numerical simulations of block-and-ash flows using the TITAN2D flow model: examples from Merapi Volcano, Indonesia. *Bull Volcanol* 71:953–959
- Charbonnier S, Gertisser R (2012) Evaluation of geophysical mass flow models using the 2006 block-and-ash flows of Merapi Volcano, Java, Indonesia: Towards a short-term hazard assessment tool. *J Volcanol Geotherm Res* 231–232:87–108
- Charbonnier SJ, Germa A, Connor CB, Gertisser R, Preece K, Komorowski J-C, Lavigne F, Dixon T, Connor L (2013) Evaluation of the impact of the 2010 pyroclastic density currents at Merapi volcano from high-resolution satellite imagery, field investigations and numerical simulations. *J Volcanol Geotherm Res* 261:295–315
- Charbonnier SJ, Kelfoun K, Widiwijayanti C, Sayudi, DS, Putra R (2023) Assessing the pyroclastic density current hazards at Merapi: From field data to numerical simulations and hazard maps. In: Gertisser R, Troll VR, Walter TR, Nandaka IGMA, Ratdomopurbo A (eds) *Merapi volcano—geology, eruptive activity, and monitoring of a high-risk volcano*. Springer, Berlin, Heidelberg, pp 473–500
- Costa F, Andreastuti S, Bouvet de Maisonneuve C, Pallister JS (2013) Petrological insights into the storage conditions, and magmatic processes that yielded the centennial 2010 Merapi explosive eruption. *J Volcanol Geotherm Res* 261:209–235

- Costa F, Widiwijayanti C, Nang TZW, Fajiculy E, Espinosa-Ortega T, Newhall C (2019) WOVodat—the global volcano unrest database aimed at improving eruption forecasts. *Disaster Prev Manag* 28:738–751
- CVGHM (Center of Volcanology and Geological Hazard Mitigation) (2002) Merapi Volcano Hazard Map. Bandung
- CVGHM (Center of Volcanology and Geological Hazard Mitigation) (2011) Revised Merapi Volcano Hazard Map. Bandung
- Darmawan H, Troll VR, Walter TR, Deegan FM, Geiger H, Heap MJ, Seraphine N, Harris C, Humaida H, Müller D (2022) Hidden mechanical weaknesses within lava domes provided by buried high-porosity hydrothermal alteration zones. *Sci Rep* 12:3202
- Darmawan H, Putra R, Budi-Santoso A, Humaida H, Walter TR (2023) Morphology and instability of the Merapi lava dome monitored by unoccupied aircraft systems. In: Gertisser R, Troll VR, Walter TR, Nandaka IGMA, Ratdomopurbo A (eds) Merapi volcano—geology, eruptive activity, and monitoring of a high-risk volcano. Springer, Berlin, Heidelberg, pp 457–472
- Deegan FM, Troll VR, Geiger H (2019) Forensic probe of Bali's great volcano Eos 100. <https://doi.org/10.1029/2019EO115211>
- Deegan FM, Troll VR, Gertisser R, Freda C (2023) Magma-carbonate interaction at Merapi volcano, Indonesia. In: Gertisser R, Troll VR, Walter TR, Nandaka IGMA, Ratdomopurbo A (eds) Merapi volcano—geology, eruptive activity, and monitoring of a high-risk volcano. Springer, Berlin, Heidelberg, pp 291–321
- Digital 2022 Indonesia (2022) Digital 2022 - Indonesia. <https://datareportal.com/reports/digital-2022-indonesia>. Accessed 17 Feb 2022
- Gertisser R, Keller J (2003a) Temporal variations in magma composition at Merapi Volcano (Central Java, Indonesia): magmatic cycles during the past 2000 years of explosive activity. *J Volcanol Geotherm Res* 123:1–23
- Gertisser R, Keller J (2003b) Trace element and Sr, Nd, Pb and O isotope variations in medium-K and high-K volcanic rocks from Merapi Volcano, Central Java, Indonesia: evidence for the involvement of subducted sediments in Sunda Arc magma genesis. *J Petrol* 44:457–486
- Gertisser R, Charbonnier SJ, Keller J, Quidelleur X (2012) The geological evolution of Merapi volcano, Central Java, Indonesia. *Bull Volcanol* 74:1213–1233
- Gertisser R, del Marmol M-A, Newhall C, Preece K, Charbonnier S, Andreastuti S, Handley H, Keller J (2023a) Geological history, chronology and magmatic evolution of Merapi. In: Gertisser R, Troll VR, Walter TR, Nandaka IGMA, Ratdomopurbo A (eds) Merapi volcano—geology, eruptive activity, and monitoring of a high-risk volcano. Springer, Berlin, Heidelberg, pp 137–193
- Gertisser R, Troll VR, Nandaka IGMA (2023b) The scientific discovery of Merapi: from ancient Javanese sources to the 21st century. In: Gertisser R, Troll VR, Walter TR, Nandaka IGMA, Ratdomopurbo A (eds) Merapi volcano—geology, eruptive activity, and monitoring of a high-risk volcano. Springer, Berlin, Heidelberg, pp 1–44
- Global Volcanism Program (2013) Volcanoes of the World, v 4.10.5 (27 Jan 2022) Venzke E (ed) Smithsonian institution. Downloaded 16 Feb 2022. <https://doi.org/10.5479/si.GVP.VOTW4-2013>
- Global Volcanism Program (2018) Report on Merapi (Indonesia). In: Crafford AE, Venzke E (eds) Smithsonian Inst Bull Glob Volc Netw 43:7
- Global Volcanism Program (2019) Report on Merapi (Indonesia). In: Crafford AE, Venzke E (eds) Smithsonian Inst Bull Glob Volc Netw 44:4
- Hartmann M (1935) Die Ausbrüche des G. Merapi (Mittel-Java) bis zum Jahre 1883. *Neues Jahrb Mineral Geol Paläontol* 75:127–162
- Heap MJ, Troll V, Kushnir ARL, Gilg H, Collinson A, Deegan F, Darmawan H, Seraphine N, Neuberg J, Walter T (2019) Hydrothermal alteration of andesitic lava domes can lead to explosive volcanic behaviour. *Nat Comms* 10:5063
- Holmberg K (2023) Merapi and its dynamic 'disaster culture'. In: Gertisser R, Troll VR, Walter TR, Nandaka IGMA, Ratdomopurbo A (eds) Merapi volcano—geology, eruptive activity, and monitoring of a high-risk volcano. Springer, Berlin, Heidelberg, pp 67–87
- Itoh H, Takahama J, Takahashi M, Miyamoto K (2000) Hazard estimation of the possible pyroclastic flow disasters using numerical simulation related to the 1994 activity at Merapi Volcano. *J Volcanol Geotherm Res* 100:503–516
- Jousset P, Budi-Santoso A, Jolly AD, Boichu M, Surono DS, Sumarti S, Hidayati S, Thierry P (2013) Signs of magma ascent in LP and VLP seismic events and link to degassing: an example from the 2010 explosive eruption at Merapi volcano, Indonesia. *J Volcanol Geotherm Res* 261:171–192
- Kelfoun K, Gueugneau V, Komorowski J-C, Aisyah N, Cholik N, Merciecca C (2017) Simulation of block-and-ash flows and ash-cloud surges of the 2010 eruption of Merapi volcano with a two-layer model. *J Geophys Res Solid Earth* 122:4277–4292
- Kelfoun K, Budi-Santoso A, Latchimy T, Bontemps M, Nurdien I, Beauducel F, Fahmi A, Putra R, Dahamna N, Laurin A, Rizal MH, Sukmana JT, Gueugneau V (2021) Growth and collapse of the 2018–2019 lava dome of Merapi volcano. *Bull Volcanol* 83:8
- Kelfoun K, Gueugneau V (2022) A unifying model for pyroclastic surge genesis and pyroclastic flow fluidization. *Geophys Res Lett* 49:e2021GL096517
- Kemmerling GLL (1921) De hernieuwde werking van den vulkan G. Merapi (Midden Java) van den begin Augustus 1920 tot en met einde Februari 1921. *Vulkanol Seismol Med* 3:1–30
- Komorowski J-C, Jenkins S, Baxter PJ, Picquout A, Lavigne F, Charbonnier S, Gertisser R, Preece K,

- Cholik N, Budi-Santoso A, Surono (2013) Paroxysmal dome explosion during the Merapi 2010 eruption: processes and facies relationships of associated high-energy pyroclastic density currents. *J Volcanol Geotherm Res* 261:260–294
- Lavigne F, Thouret JC, Voight B, Suwa H, Sumaryono A (2000) Lahars at Merapi volcano, Central Java: an overview. *J Volcanol Geotherm Res* 100:423–456
- Lavigne F, Mei ETW, Morin J, Humaida H, Moatty A, de Bélizal E, Sri Hadmoko D, Grancher D, Picquout A (2023) Physical environment and human context at Merapi volcano: A complex balance between accessing livelihoods and coping with volcanic hazards. In: Gertisser R, Troll VR, Walter TR, Nandaka IGMA, Ratdomopurbo A (eds) *Merapi volcano—geology, eruptive activity, and monitoring of a high-risk volcano*. Springer, Berlin, Heidelberg, pp 45–66
- Luehr BG, Koulakov I, Suryanto W (2023) Crustal structure and ascent of fluids and melts beneath Merapi: Insights from geophysical investigations. In: Gertisser R, Troll VR, Walter TR, Nandaka IGMA, Ratdomopurbo A (eds) *Merapi volcano—geology, eruptive activity, and monitoring of a high-risk volcano*. Springer, Berlin, Heidelberg, pp 111–135
- Mei ETW, Lavigne F, Picquout A, de Bélizal E, Brunstein D, Grancher D, Sartohadi J, Cholik N, Vidal C (2013) Lessons learned from the 2010 evacuations at Merapi volcano. *J Volcanol Geotherm Res* 261:348–365
- Museum Gunung Merapi (2018) *Kunjungan Museum Gunung Merapi Tahun 2017 Didominasi oleh Golongan Pelajar*. Museum Gunung Merapi, Yogyakarta, Indonesia
- Newhall CG, Bronto S, Alloway B, Banks NG, Bahar I, Del Marmol MA, Hadisantono RD, Holcomb RT, McGeehin J, Miksic JN, Rubin M, Sayudi SD, Sukhyar R, Andreastuti S, Tilling RI, Torley R, Trimble D, Wirakusumah AD (2000) 10,000 years of explosive eruptions of Merapi Volcano, Central Java: archaeological and modern implications. *J Volcanol Geotherm Res* 100:9–50
- Newhall C, Costa F, Ratdomopurbo A, Venezky DY, Widiwijayanti C, Win NTZ, Tan K, Fajiculay E (2017) WOVodat—an online, growing library of worldwide volcanic unres. *J Volcanol Geotherm Res* 345:184–199
- Pallister PS, Schneider DJ, Griswold JP, Keeler RH, Burton WC, Noyles C, Newhall CG, Ratdomopurbo A (2013) Merapi 2010 eruption—chronology and extrusion rates monitored with satellite radar and used in eruption forecasting. *J Volcanol Geotherm Res* 261:144–152
- Pardyanto L, Reksowirogo LD, Mitrohartono FXS, Hardjowarsito SH (1978) Volcanic hazard map. Merapi Volcano, Central Java. Geological Survey of Indonesia, Bandung (1 sheet, scale 1:100,000)
- Peters STM, Troll VR, Weis FA, Dallai L, Chadwick JP, Schulz B (2017) Amphibole megacrysts as a probe into the deep plumbing system of Merapi volcano, Central Java Indonesia. *Contrib Mineral Petrol* 172:16
- Preece K, Gertisser R, Barclay J, Berlo K, Herd RA, Facility EIM (2014) Pre- and syn-eruptive degassing and crystallisation processes of the 2010 and 2006 eruptions of Merapi volcano Indonesia. *Contrib Mineral Petrol* 168:1061
- Preece K, Gertisser R, Barclay J, Charbonnier SJ, Komorowski J-C, Herd RA (2016) Transitions between explosive and effusive phases during the cataclysmic 2010 eruption of Merapi volcano, Java Indonesia. *Bull Volcanol* 78:54
- Preece K, van der Zwan F, Hammer J, Gertisser R (2023) A textural perspective on the magmatic system and eruptive behaviour of Merapi volcano. In: Gertisser R, Troll VR, Walter TR, Nandaka IGMA, Ratdomopurbo A (eds) *Merapi volcano—geology, eruptive activity, and monitoring of a high-risk volcano*. Springer, Berlin, Heidelberg, pp 265–289
- Global Volcanism Program (2020a) Report on Merapi (Indonesia) In: Bennis KL, Venzke E (eds) *Smithsonian Inst Bull Glob Volc Netw* 45:4
- Global Volcanism Program (2020b) Report on Merapi (Indonesia) In: Bennis KL, Venzke E (eds) *Smithsonian Inst Bull Glob Volc Netw* 45:10
- Global Volcanism Program (2021a) Report on Merapi (Indonesia) In: Crafford AE, Venzke E (eds) *Smithsonian Inst Bull Glob Volc Netw* 46:3
- Global Volcanism Program (2021b) Report on Merapi (Indonesia) In: Crafford AE, Venzke E (eds) *Smithsonian Inst Bull Glob Volc Netw* 46:9
- Ratdomopurbo A, Beauducel F, Subandriyo J, Nandaka IGMA, Newhall CG, Suharna SDS, Suparwaka H, Sunarta (2013) Overview of the 2006 eruption of Mt Merapi. *J Volcanol Geotherm Res* 261:87–97
- Re G, Corsaro RA, D’Orlando C, Pompilio M (2021) Petrological monitoring of active volcanoes: a review of existing procedures to achieve best practices and operative protocols during eruptions. *J Volcanol Geotherm Res* 419:107365
- Shimomura M (2015) Development of Integrated GIS-MSD (Multimodal Sediment Disaster) Simulator. Abstract, Workshop ‘Integrated Study on Mitigation of Multimodal Disasters Caused by Ejection of Volcanic Products’, SATREPS (Science and Technology Research Partnership for Sustainable Development), Yogyakarta, Indonesia, pp 9–10
- Subandriyo, Gertisser R, Aisyah N, Humaida H, Preece K, Charbonnier S, Budi-Santoso A, Handley H, Sumarti S, Sayudi DS, Nandaka IGMA, Wibowo HE (2023) An overview of the large-magnitude (VEI 4) Eruption of Merapi in 2010. In: Gertisser R, Troll VR, Walter TR, Nandaka IGMA, Ratdomopurbo A (eds) *Merapi volcano—geology, eruptive activity, and monitoring of a high-risk volcano*. Springer, Berlin, Heidelberg, pp 353–407
- Surono JP, Pallister J, Boichu M, Buongiorno MF, Budisantoso A, Costa F, Andreastuti S, Prata F, Schneider D, Clarisse L, Humaida H, Sumarti S, Bignami C, Griswold J, Carn S, Oppenheimer C, Lavigne F (2012) The 2010 explosive eruption of

- Java's Merapi volcano—a '100-year' event. *J Volcanol Geoth Res* 241–242:121–135
- Thouret J-C, Aisyah N, Jenkins SF, de Belizal E, Sulistiyani, Charbonnier S, Sayudi DS, Nandaka IGMA, Mainsant G, Solikhin A (2023) Merapi's lahars: characteristics, behaviour, monitoring, impact, hazard modelling and risk assessment. In: Gertisser R, Troll VR, Walter TR, Nandaka IGMA, Ratdomopurbo A (eds) *Merapi volcano—geology, eruptive activity, and monitoring of a high-risk volcano*. Springer, Berlin, Heidelberg, pp 501–552
- Troll VR, Hilton DR, Jolis EM, Chadwick JP, Blythe LS, Deegan FM, Schwarzkopf LM, Zimmer M (2012) Crustal CO₂ liberation during the 2006 eruption and earthquake events at Merapi volcano, Indonesia. *Geophys Res Lett* 39:L11302
- Troll VR, Deegan FM, Seraphine N (2021) Ancient oral tradition in Central Java warns of volcano-earthquake interaction. *Geol Today* 37:100–109
- Troll VR, Deegan FM (2023) The Magma plumbing system of Merapi: The petrological perspective. In: Gertisser R, Troll VR, Walter TR, Nandaka IGMA, Ratdomopurbo A (eds) *Merapi volcano—geology, eruptive activity, and monitoring of a high-risk volcano*. Springer, Berlin, Heidelberg, pp 233–263
- UNDRO (Office of the United Nations Disaster Relief Coordinator) (1985) *Volcanic emergency management*. United Nations, New York, p 426
- Voight B, Constantine EK, Siswoidjoyo S, Torley R (2000) Historical eruptions of Merapi volcano, Central Java, Indonesia, 1768–1998. *J Volcanol Geoth Res* 100:69–138
- Walter TR, Wang R, Zimmer M, Grosser H, Lühr B, Ratdomopurbo A (2007) Volcanic activity influenced by tectonic earthquakes: Static and dynamic stress triggering at Mt Merapi. *Geophys Res Lett* 34:L05304
- Whitley S, Gertisser R, Halama R, Preece K, Troll VR, Deegan FM (2019) Crustal CO₂ contribution to subduction zone degassing recorded through calc-silicate xenoliths in arc lavas. *Sci Rep* 9:8803
- Widiwijayanti C, Voight B, Hidayat D, Schilling SP (2009) Objective rapid delineation of areas at risk from block-and-ash pyroclastic flows and surges. *Bull Volcanol* 71:687–703